GEOPHYSICAL
EXPLORATION

By

C. A. HEILAND, Sc.D.

Professor of Geophysics
Colorado School of Mines

New York
PRENTICE-HALL, INC.
1940

PREFACE

THIS BOOK is intended as a comprehensive survey of the entire field of geophysical exploration. The author has endeavored to present the subject in broad perspective, emphasizing the relations, differences, common features, and, above all, the fundamentals of geophysical methods.

The material is divided into two parts of six chapters each. The first part, written in elementary language, addresses those desiring an insight into the working principles and geological applications of geophysical methods. It is intended for individuals in executive and geologic advisory capacity and for persons not directly concerned with field or laboratory operations.

The second and major portion is written for the technical student of geophysics. It presents the subject from an engineering point of view, striving at a balanced discussion of theory, field technique, laboratory procedure, and geological interpretations. The author has aimed at a presentation that will enable the geophysicist to get an insight into the geologist's reasoning in selecting geophysical methods and in interpreting geophysical data, and that will acquaint the geologist with the mathematical and physical approach to instrument and interpretation problems.

Certain compromises were unavoidable if a volume of practical size was to be arrived at. It is not possible to cover the ground in such detail as a specialist, working with a particular method, may deem advisable. Geophysical exploration changes rapidly; processes once in the limelight have been discarded; others, seemingly forgotten, have been revived. In this book the fundamental or methodical significance of a given method is its chief criterion for inclusion. This has been followed even at the risk of describing "older" methods. Field, office, and laboratory procedures are so changeable and so subject to personal preferences that the discussion of such procedures is confined to a few examples illustrative of method but not of detail. Since there is a limit to the number of geophysical surveys that can be illustrated, a choice was made on the basis of distinctness of response to subsurface conditions, and not on the basis of survey date.

The necessity for elementary treatment has occasioned a certain breadth in the mathematical discussions, possibly at the expense of rigor and elegance. In many cases formulas are given without derivation. The

description of procedures and instruments used in geophysical science is limited to those having a direct bearing on geophysical exploration. A chapter on the history of geophysical exploration was abandoned in favor of a few historical references. The material is arranged in methodical rather than historical order.

A table of symbols precedes each major chapter dealing with methods that represent a geophysical entity. This applies to gravitational, magnetic, seismic, and electrical methods (Chapters 7 through 10). In these chapters the discussion follows a uniform plan. First is an outline of fundamentals, followed by a description of rock properties and rock-testing methods. Instruments and instrument theory, as well as corrections and interfering factors, are reviewed next. The treatment is concluded in each case with a derivation of the fundamental interpretation equations and a description of surveys made on known geologic conditions.

Various individuals and organizations have assisted in the preparation of this book. Specific acknowledgment is made on the following page.

<div style="text-align: right;">C. A. HEILAND</div>

ACKNOWLEDGMENTS

CONTENTS

PART I

I

INTRODUCTION

I. SIGNIFICANCE OF GEOPHYSICAL EXPLORATION

Gᴇᴏᴘʜʏꜱɪᴄᴀʟ ᴇxᴘʟᴏʀᴀᴛɪᴏɴ may be defined as *prospecting for mineral deposits and geologic structure by surface measurement of physical quantities.*

Geophysical exploration does not rely on magic or on any other supernatural procedure. It makes use of phenomena which can be interpreted fully through the fundamental laws of physics, measured, and verified by anyone as long as suitable instruments are used. A psychological reaction of the individual does not enter. Therein lies the difference between geophysical exploration and the "divining rod" whose scientific merits have never been established. There may be persons who can "sense" the presence of subsurface geologic anomalies; however, if they are so distinguished, they should have no need to surround their ability with a veil of mysterious devices. Experience has shown that the divining rod, contrary to geophysical instruments, will rarely give identical indications at the same place or for different operators.

Geophysical exploration may be considered an *application of the principles of geophysics to geological exploration.* Derived from the Greek ἡ γῆ and ἡ φύσις, the word *geophysics* means "physics" or "nature" of the earth. It deals with the composition and physical phenomena of the earth and its liquid and gaseous envelopes; it embraces the study of terrestrial magnetism, atmospheric electricity, and gravity; and it includes seismology, volcanology, oceanography, meteorology, and related sciences.

The foundation to the development of most geophysical exploration methods was laid by geophysical science. In the past century systematic efforts were begun in all parts of the world to study earth's phenomena, such as gravity, magnetism, earthquakes, and volcanism. Such studies were expected to give information in regard to the constitution of the earth's interior. Magnetic and gravitational surveys were organized by government and state agencies, and observatories for recording meteorologic, oceanographic, and earthquake phenomena were established.

Practically every geophysical exploration method has been developed

from corresponding procedures in geophysical science. While the objects of these earlier studies were the broad regional features, present geophysical methods aim at the location of *local* geologic structures and mineral deposits. This development resulted from a substantial increase in accuracy and reliability of field methods. It has been coincident with the advances made in physics generally and in electricity in particular and received its impetus from the need for raw materials during and after the World War. Geophysical *exploration* may be called the application of the principles of geophysical *science* to (commercial) problems of *smaller geologic scale*.

Experience has demonstrated that most subsurface structures and mineral deposits can be located, provided that *detectable differences in physical properties exist.* The main properties exhibited by the more common rocks and formations are: *density, magnetism, elasticity,* and *electrical conductivity.* This entails four major geophysical methods: gravitational, magnetic, seismic, and electrical.

II. GEOPHYSICS AS A TOOL FOR DETERMINING GEOLOGIC STRUCTURE; EXCEPTIONS; INDIRECT MINERAL LOCATION

The first objective of geophysical exploration is the location of geologic structures; as a rule, information regarding the occurrence of specific minerals is obtained only in an indirect manner.

The geophysicist measures, at the earth's *surface*, anomalies in physical forces which must be interpreted in terms of *subsurface* geology. In many cases he has to be content with a general statement that a given area is structurally high or low (as in oil exploration), or that a zone of good or poor conductivity exists (as in mining). In some instances, however, an appreciation of the geologic possibilities and a background of experience obtained by working in similar areas makes it possible to interpret surface anomalies more specifically. Assume, for example, that an iron ore deposit has been traced by magnetic instruments. When surveying adjacent properties, one would, therefore, be justified in attributing large magnetic anomalies to the same ore. In a different area, however, large magnetic anomalies may result from entirely different geologic bodies, such as intrusions of igneous rocks or contact-metamorphic zones.

Other definite geophysical indications are: gravity minima on salt domes, magnetic highs on basement uplifts, seismic refraction travel-time curves typical of salt domes, electrical indications characteristic of sulfide ore bodies, and so on. In such cases interpretation of findings in terms of definite mineral deposits has been very successful. On the other hand, a geophysicist unacquainted with geologic possibilities may carry interpre-

tative analogies too far into unknown territory. Failures resulting from such procedure are forceful reminders that geophysics does not locate specific deposits, but furnishes only a physical indication which must be interpreted conservatively in geologic terms.

In this connection a word may be said about the present status and future possibilities of methods for direct location of oil, gold, or water. At present there is no established direct means for finding oil; it is located indirectly by mapping geologic structures which, from experience, are expected to be *favorable* for the accumulation of oil. Gold in placer channels may be located indirectly by tracing magnetic black sand concentrations, provided that the geologic association of gold with black sand has been established. Water is difficult to locate; the indications require careful interpretation in the light of the electrical characteristics and disposition of near-surface beds. On the other hand, recent developments along the line of direct methods indicate definite possibilities. The best chances for direct oil location are in the fields of electrical prospecting and soil and gas analysis. Electrical induction methods show promise of success in locating placer gold concentrations and water.

As indicated above, the greater number of applications of geophysical methods are of an indirect nature. If a mineral, rock, or formation does not have any distinguishing physical properties, another mineral or geologic body may be utilized which has such properties and bears a known relation to the ineffective body. The location of oil by the mapping of structures which provide a trap for oil (anticlines, salt domes, faults, and buried hills), and the location of ore bodies by determining associated structure are examples of indirect procedure.

III. MAJOR FIELDS OF GEOPHYSICAL EXPLORATION

Since geophysical exploration is the determination of subsurface geologic structure by means of surface physical measurements, it is applicable in industrial fields where a knowledge of geologic conditions is essential. It is understood that such applications are advisable only where structures and ore bodies are not exposed, as most geophysical measurements are more expensive than surface geological surveying.

At present the greatest use of geophysical prospecting is made in oil exploration. In this country relatively few oil areas exist where geologic structure is exposed at the surface; in the majority of cases, the deeper formations are concealed by (frequently unconformable) younger strata. This is particularly true for the entire Gulf coast, the Midcontinent, the Great Plains, Western Canada, and a part of California. The Gulf coast has seen the most extensive geophysical activity because conditions exist-

ing there are virtually ideal for geophysical exploration. At present seismic and gravitational methods for mapping oil structures dominate the field; electrical well-logging is widely used for the purpose of correlating formations by their resistivity and for identification of oil sands. It has been estimated that the oil industry spends between 15 and 20 million dollars annually for geophysical field work and laboratory research.

Compared with the oil industry, the mining industry has made relatively little use of geophysical exploration although there have been more published accounts of mining surveys. Various reasons account for this lack of geophysical activity. (1) The small size of the average ore body makes it impossible to cover systematically township after township, as in oil surveying. (2) Large industrial groups capable of financing extensive research and exploration programs are few. (3) In mining areas geology is frequently known from outcrops, so that a determination of subsurface structure so important in oil exploration is less necessary. (4) Structural relations and dispositions of ore bodies are usually complex, making interpretation of geophysical data more difficult. (5) Many geophysical methods are adversely affected by the rugged topography prevalent in mining districts. (6) Seismic methods, at present most prominent in oil exploration, have found little application in mining because dynamo- and contact-metamorphic agencies have obliterated original differences in elasticity between formations. (7) Transportation in mining regions is difficult and inadequate. In spite of these handicaps, the application of geophysics in mining is often more fascinating to the geophysicist than in oil because of the greater variation in method and procedure. Not only may structural investigations be made, but the ore itself may produce indications; further, associations of the sought but ineffective mineral with noncommercial but physically effective minerals may be utilized. Generally speaking, the planning and execution of a geophysical survey in mining and oil are quite different; further details are presented in Chapter 5.

A third major field for geophysical work is that of engineering, encompassing civil engineering, engineering geology, and allied fields such as military, structural, gas, and pipe-line engineering, and the like. Geophysics is being applied to problems involved in dam-site and tunnel investigations, determination of foundation conditions in highway and railroad construction, location of construction materials for highway and railroad work, water location, detection of corrosion and leakage in gas and water pipes, investigation of building and road vibrations, and so on. Military engineering has utilized geophysics in similar ways; Chapter 6 covers these topics in more detail.

2

METHODS OF GEOPHYSICAL EXPLORATION

I. CLASSIFICATION

GEOPHYSICAL methods may be broadly classified under two headings: major and minor (see Tables 1 and 2). There are four major geophysical methods: gravitational, magnetic, seismic, and electrical.

In the *gravitational* methods, measurements are made of anomalies in gravity attraction produced by differences in densities of formations and structures. In the *magnetic* method, measurements are made of anomalies in the earth's magnetic field due to geologic bodies of different degrees of para- or dia-magnetism. In either case, the reactions of geologic bodies are permanent, spontaneous, and unchangeable; the operator cannot control the depth from which they are received.[1]

In the other two major methods, energy is applied to the ground for the purpose of producing a measurable reaction of geologic bodies. This gives the possibility of spacing transmission and reception points in such a manner that the depth range can be controlled. In the *seismic* method, energy is supplied by dynamite explosions, and the travel times (time interval between firing of the shot and reception of elastic impulses) of refracted and reflected waves are measured.

In one group of the *electrical* methods energy is applied galvanically, and the distribution of the potential or the electromagnetic field resulting from conductive bodies is measured. These are known as potential and electromagnetic (electromagnetic-galvanic) methods. In another group, known as electromagnetic-inductive methods, the primary energy is applied inductively to the ground and the distortions of the electromagnetic field are determined.

---

[1] If only one geologic body is present, this limitation may be overcome by varying the position of the receiving units in a horizontal direction away from the axis of the geologic body. Thereby, a variation of the anomaly with distance is introduced and, for one geologic body at least, enough equations may be established so that direct depth determinations may be made. Horizontal changes of distance may be supplemented by vertical changes in distance, with observations from scaffolds and aircraft. In practice, these methods are of limited value when a plurality of geologic bodies exists.

TABLE 1

SUMMARY OF THE FOUR MAJOR GEOPHYSICAL METHODS

Method	Field	Geologic Application	Action and Control
I. Gravitational			No Depth Control — Spontaneous Action
A. Torsion balance	Oil	Anticlinal structures; buried ridges; salt domes; faults; intrusions	
B. Pendulum C. Gravimeter		Salt domes; buried ridges; major structural trends	
II. Magnetic	Oil, mining	Anticlinal structures; buried ridges; intrusions; faults; iron ore, pyrrhotite, and assoc. sulfide ores; gold placers	
III. Electrical A. Self-potential	Mining	Sulfide ore bodies	
B. *Galvanic* application of primary energy — 1. Potential distribution of secondly field measured: (a) Equipot., potential profile (b) Resistivity (c) Pot.-drop ratio	Mining, civil eng., oil	General stratigraphic and structural conditions; bedrock depth on dam sites; ground water; oil structures; sulfide ore bodies; highway problems; elec. logging	Control of Depth of Penetration — Reaction to Energizing Fields
2. Electromagnetic field meas.	Mining	Sulfide ore bodies	
C. *Inductive* application of primary energy	Oil, mining	Faults; anticlinal, etc., structure; sulfide ore bodies	
IV. Seismic A. Refraction	Oil, civil eng.	Salt domes; anticlinal etc., structures; faults; foundation & highway problems	
B. Reflection	Oil	Low-dip structures; buried ridges; faults	

Some of the minor geophysical exploration or detection methods make use of the elastic properties of the surface soil (dynamic soil testing) and of the water and atmospheric air (acoustic detection).   Other methods involve the detection of thermal effects (geothermal well testing), the detection of gases, and the mapping of radioactive radiations (see Table 2).

TABLE 2
SUMMARY OF MINOR GEOPHYSICAL METHODS

Methods		Field	Application
Utilizing elastic properties	Acoustic	Mining, civil engineering	Mine safety; pipe leak detection
		Military engineering	Sapper, submarine, airplane detection; sound ranging
		Navigation	Echo depth sounding; iceberg location
	Dynamic vibration tests	Structural; civil engineering	Earthquake & vibration-damage tests of buildings, ground, & road beds
	Strain gauging	Mining, Civil engineering	Mine safety Tests of structures
Utilizing thermal effects	Geothermal	Oil exploration	Structural correlation of wells; cementation problems
	Thermal detection	Military Navigation	Airplane location Iceberg location
Gas detection		Oil Mining Military Civil engineering	Location of oil (?) Mine safety Poisonous gases Gas leaks
Radioactivity measurements		Mining Oil	Radioactive ores Well logging

In the following sections, a summary of both major and minor geophysical methods is presented, with special reference to general principles involved, instruments used, corrections applied, and interpretation procedure.

II. GRAVITY METHODS

General.   Variations in the gravitational field may be mapped by the pendulum, gravimeter, and torsion balance.   The pendulum and gravimeter measure relative gravity, whereas with the torsion balance, the

variations of gravity forces per unit horizontal distance, also known as "gradients" of gravity are determined. Since the gravitational effects of geologic bodies are proportional to the contrast in density between them and their surroundings, gravity methods are particularly suitable for the location of structures in stratified formations. As there is generally an increase of density with depth, the uplift of deeper formations will result in placing formations of greater density in the same horizontal level as lighter and younger formations.

Pendulum methods. It is well known that a pendulum may be used to determine not only time but gravity as well. Gravity pendulums are kept as constant as possible in length so that variations in period indicate changes in gravity only. To obtain the necessary accuracy, the pendulum period must be determined to within 1/10,000,000 of a second. By using an inverted pendulum (Lejay-Holweck type, see Fig. 2-1), the sensitivity of the period to gravity variations may be increased 1000 to 2000 times.

The most common method for securing the necessary accuracy in pendulum observations is the "coincidence" or beat method whereby the gravity pendulum is compared with a chronometer or another pendulum of nearly equal period. If the interval between successive coincidences of the two time pieces is measured with an accuracy of 1 millisecond, gravity is determined with an accuracy of 1 milligal.[2] Comparisons of field pendulums with the reference time piece are usually made by electrical wire or radio transmission. Corrections are applied on observed periods for the "rate" of the comparison time piece, air temperature and density, pendulum amplitude and flexure of the support.

FIG. 2-1. Lejay-Holweck pendulum (schematic). *P*, Pin; *Q*, quartz rod; *E*, elinvar spring; *D*, diaphragm; *A*, arresting device.

Gravimeters. Pendulum, or "dynamic" methods of measuring gravity have been superseded recently by "static" or "gravimeter" methods in which gravity is compared with an elastic spring force. Mechanically simplest are the Threlfall and Pollock instrument (in which a thin horizontal quartz bar is suspended from a horizontal torsion wire), the Hartley gravimeter (containing a horizontal, hinged beam suspended from two helical springs), the Lindblad-Malmquist and the Askania gravimeters in which the masses are suspended directly from a spring or springs, with

"Gal" (after Galileo), acceleration unit of 1 centimeter per second squared.

arrangements for electrical or similar means of magnifying the displacement. An increase in mechanical sensitivity may be attained by providing "astatizing" mechanisms which involve the application of a labilizing force nearly equal and opposite to the elastic restoring force. Examples are the Ising gravimeter, in which a vertical quartz rod is suspended in inverted position from a taut horizontal quartz fiber, gravimeters using bifilar and trifilar suspensions, the Truman-Humble gravimeters and the Thyssen gravimeter (Figs. 2-2 and 2-3), astatized by a rigidly attached inverted pendulum.

Corrections on gravity values observed with pendulums and gravimeters. The following corrections must be applied on relative gravity values: (1) a correction for normal variations of gravity (planetary effect); (2) terrain correction; (3) free-air and Bouguer (elevation) correction. The planetary correction is due to the variation of gravity with latitude. The effect of terrain is calculated from elevations along radial lines and concentric circles around the station. Elevation is allowed for by a reduction to sea level (free-air correction) to which the influence of the rocks between station and sea level is added (Bouguer reduction).

Interpretation of gravity anomalies. Gravity anomalies may be represented by contours (isogams) or profiles in connection with geologic sections. Their interpretation is largely qualitative and is given in terms of structural highs and lows or presence or absence of heavier or lighter bodies (see Fig. 2-3).

FIG. 2-2. Gravimeter, lowered to ground through floor of passenger car (Thyssen).

If some information is available about the subsurface section and dimensions and nature of geologic bodies to be expected, more quantitative interpretation methods may be applied by calculating their attraction and by varying the assumptions regarding dimensions, shape, differences in density, and depth until a reasonable agreement between field curves and theoretical curves is obtained. This method of interpretation is of a trial and error nature and generally referred to as indirect interpretation.

The Eötvös torsion balance. Contrarily to the beam in an *ordinary* balance, the beam in a *torsion* balance revolves in a horizontal plane and is deflected from a position corresponding to the torsionless condition of the suspension wire by the unbalance of horizontal forces acting on it. For the sake of illustration, two types of torsion balance beams may be distinguished. In the beam of the first type (see Fig. 2-4a) two masses are at the ends of the beam and at the same level. The beam is deflected by forces resulting from horizontal differences of the horizontal compo-

nents of gravity.   These forces are frequently referred to as "horizontal directing forces" or "curvature values" since they are related to the curvature of the equipotential surfaces of gravity.   If a spherical equipotential surface be so placed that its apex coincides with the beam center, the
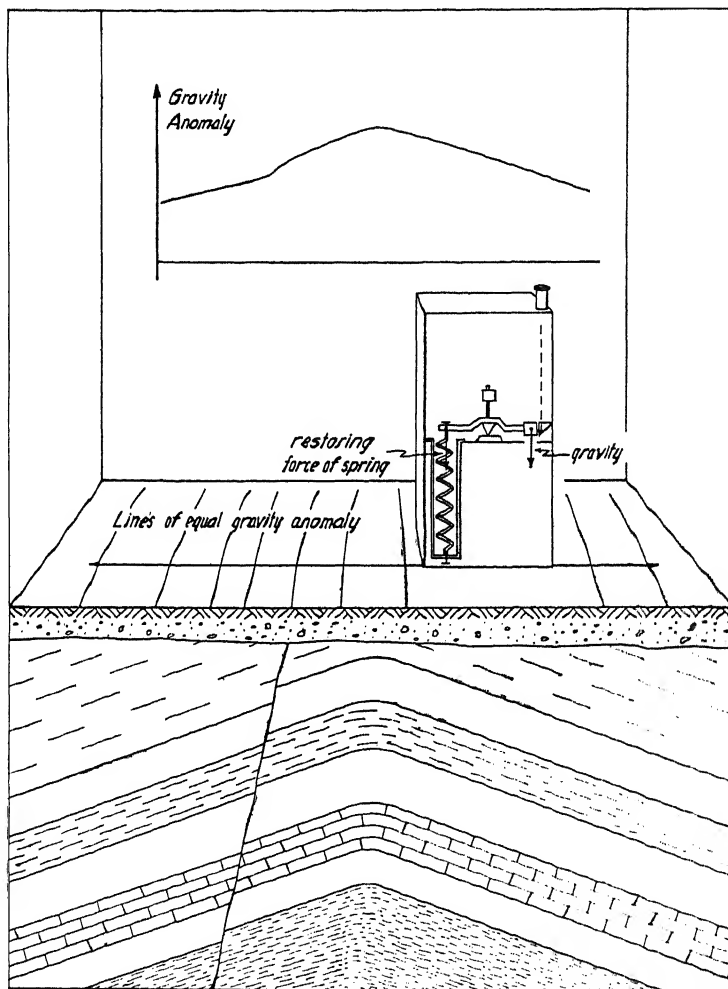
FIG. 2-3. Gravimeter on traverse across anticline (schematic).

horizontal components of the gravity forces (which at all points are at right angles to the equipotential surface) all point to the axis of rotation and no deflection of the beam takes place.   When this surface is curved in a different manner, the horizontal components no longer point in a radial direction; they tend to turn the beam into the direction of minimum

curvature of the equipotential surfaces (see Fig. 2-5). Hence, the deflection is proportional to the deviation of the equipotential surface from the spherical shape and the deviation of the beam from the direction of minimum curvature.

In the second type of beam the two weights are attached to its ends at different levels (Fig. 2-4b). In addition to the above "horizontal direct-
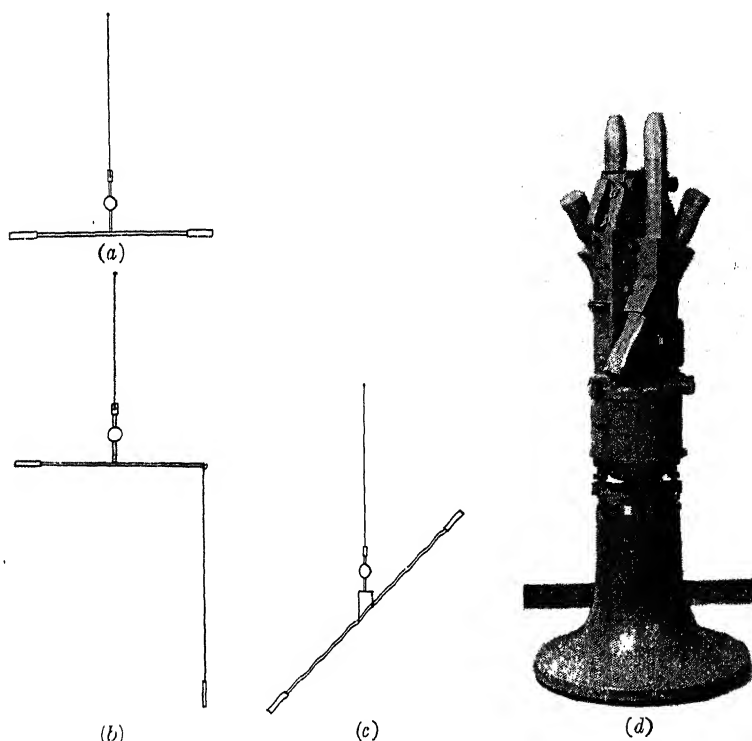
Fig. 2-4. Eötvös torsion balance. (a) Beam of the first kind; (b) beam of the second kind; (c) tilt beam; (d) Askania double tilt-beam balance (*American Askania Corp.*).

ing forces," this beam is affected by the difference in direction of the gravity forces on the upper and lower weights, which increases with the convergence of the equipotential surfaces passing through the weights, that is, with the rate of change, or "gradient," of gravity (see Fig. 2-6). The torsion balance is so sensitive that one may detect convergences of equipotential surfaces of the order of $1/100,000$ of an arc-second, which corresponds to a horizontal variation of gravity of 10^{-9} gals^3/cm.

[3] See footnote on p. 10.

In practice, only a beam of the second type is used. The gradients and curvature values may be resolved into their north and east components. Hence the torsion balance beam is affected by four unknown quantities, to which is added a fifth, the zero or torsionless position of the beam. As the deflection of the beam depends on its azimuth, the action of gravity forces on it may be changed by rotating the entire instrument in a different direction. To determine the five unknown quantities, five azimuths are therefore required. To shorten the observation time (20 to 30 minutes in each position), two beams are mounted side by side in antiparallel arrangement. The second beam adds its torsionless position as sixth unknown, so that three positions separated by angles of 120° are required to determine all quantities. In present practice, double beam instruments of the second Eötvös type are used exclusively, arranged either for visual observation of the beam deflection or with full automatic recording mechanism. Most recent torsion balances carry beams suspended at an angle of 45° (see Fig. 2-4c and d). Calculation of gradients and curvatures proceeds in accordance with formulas or nomographs based on the fundamental theory of the instrument.

FIG. 2-5. Action of torsion-balance beam of first kind in gravity field characterized by cylindrical equipotential surface.

Corrections on torsion balance results. Torsion balance results must be provided with a number of corrections. Most important is the terrain correction, which is obtained from elevations measured around the instrument in a number of radial directions and along suitably selected concentric circles. In rugged terrain, topographic corrections may become involved and inaccurate, which limits the usefulness of the torsion balance to fairly level country. A second (planetary) correction results from the variation of gravity with latitude. Finally, it is often desirable to correct for regional geologic structure. In torsion balance measurements underground, allowance must be made for mass deficiencies due to tunnels, drifts, and so on.

Interpretation. In plan view, gradients are represented as arrows point-

ing in the direction of maximum change of gravity (see Fig. 2-6); curvature values are plotted as straight lines through the station, the length of the line being in proportion to the deviation of the equipotential surface from spherical. Torsion balance results may also be plotted in the form of curves along profiles at right angles to the strike (see Fig. 2-6). Relative gravity may be calculated from gradients, and points of equal relative gravity may be connected by "isogams."

Torsion balance interpretation may be qualitative or quantitative. In the former, gradients are given preference over curvature values. The
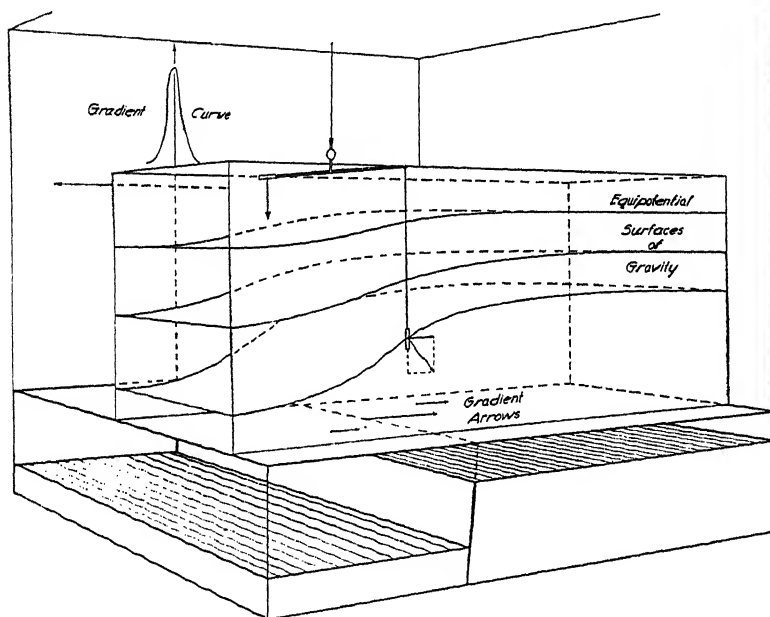
FIG. 2-6. Convergence of equipotential surfaces of gravity caused by subsurface fault and reaction of torsion balance beam of the second kind.

largest gradients occur above such portions of subsurface geologic features as are characterized by the greatest horizontal variation of density, for example, on flanks of anticlines, synclines, edges of salt domes, igneous intrusions, buried escarpments, and faults. Quantitative interpretation is usually of an indirect nature; geologically plausible assumptions are made about subsurface mass dispositions; their gravity anomalies are calculated and compared with the field findings. Discrepancies between the two are reduced step by step by modifying the assumptions regarding depth, shape, and density of the subsurface bodies.

III. MAGNETIC METHODS

General. In common with gravitational methods, magnetic prospecting utilizes a natural and spontaneous field of force, with fields of geologic bodies superimposed upon a normal terrestrial field. Coulomb's law, which controls the attraction of magnetic bodies, is identical in form with Newton's law; integral effects of all bodies within range are observed and depth control is lacking. One important difference is that the gravitational fields of geologic bodies do not depend on the earth's gravitational field, whereas magnetic bodies frequently owe their magnetization to the magnetic field of the earth. For this reason, magnetic anomalies are often subject to change with latitude. Moreover, rocks may have magnetism of their own whose direction may or may not coincide with that induced by the terrestrial magnetic field. An important factor in the interpretation of magnetic methods is that rock magnetism, contrary to rock density, is of a bipolar nature.

In gravity methods, total field vector and the horizontal gradients of the vector or of its horizontal components, are observed. In magnetic prospecting, measurements of the total vector are the exception rather than the rule; it is usually resolved into its horizontal and vertical components. Experience has shown that the vertical component exhibits the clearest relation between magnetic anomalies and disposition of geologic bodies, at least in northern and intermediate magnetic latitudes. Therefore, measurements of the magnetic vertical intensity are preferred and are supplemented occasionally by horizontal intensity observations for greater completeness in the evaluation of the anomalies.

Magnetic fields are generally expressed in gauss;[4] in magnetic exploration it is more convenient to use 1/100,000 part of this unit, called the gamma (γ). The accuracy requirements in magnetic prospecting are less than in gravity work; hence, it is a comparatively easy matter to design instruments suitable for magnetic exploration.

The magnetic anomalies of geologic bodies are dependent on their magnetic "susceptibility" and "remanent" magnetism, properties which vary much more widely than their densities. Rocks and formations fall into two natural groups: igneous rocks and iron ores are strongly magnetic, whereas sedimentary rocks are generally weak in magnetization. The magnetic characteristics of rocks are affected by numerous factors such as: magnetite content, grain size, lightning, heat, contact metamorphism, mechanical stresses, disintegration and concentration, and also by structural forces which may alter the disposition of magnetic formations in the course of geologic periods.

---

[4] Simplest definition is lines per square centimeter (in air). See also footnote on p. 295.

Magnetic instruments.   Most widely used in magnetic prospecting are the Schmidt magnetometers.   In the Schmidt vertical intensity magnetometer (see Figs. 2-7 and 2-8), a magnetic system is suspended on a knife-edge at right angles to the magnetic meridian; its center of gravity is so arranged that the system is approximately horizontal in the area under test.   Deflections from this position are measured with a telescope and scale arrangement, expressed in scale divisions, and are then multiplied by a scale value to give relative vertical intensities.

In the Schmidt horizontal magnetometer, a magnetic system is suspended in the magnetic meridian and its center of gravity is so adjusted that the system stands approximately vertical in the area under survey and is deflected by the horizontal force.   The methods of taking the readings and applying corrections are the same as for the vertical magnetometers, except that for large anomalies of vertical intensity a correction for vertical intensity variations is required.

In the Hotchkiss superdip, a magnetized needle is suspended on a horizontal pivot and provided with a counter arm so that both the position and the sensitivity of the needle may be controlled.   The system may be used at right angles to the direction of the inclination so that it will then measure variations in total intensity.

The instruments described above furnish the high degree of accuracy required in oil exploration.   In mining exploration, however, simpler devices are often quite satisfactory.   The earliest instrument of this kind is the Swedish mining compass in which a magnetic needle is suspended on a jewel and

American Askania Corp.
Fig. 2-7. Schmidt-Askania magnetometer.

a stirrup so that it can rotate about a horizontal and vertical axis.   Another early instrument is the dial compass which is a combination of a compass and sun dial.   Extensive use has been made of the dipneedle, which is a magnetic needle capable of rotation about a horizontal axis and is essentially a vertical-intensity instrument.

Corrections.   The following corrections are required in magnetic exploration: (1) correction for temperature of instrument, arising from the fact that the magnets used for comparison with the earth's magnetic field lose their strength with an increase in temperature; (2) a "base" correction

which allows for errors of closure when checking back to a base station; (3) a correction for daily variation which may be determined by visual observation or recording of a second magnetometer; (4) a planetary correction, which eliminates the normal variations of the earth's magnetic field with latitude.
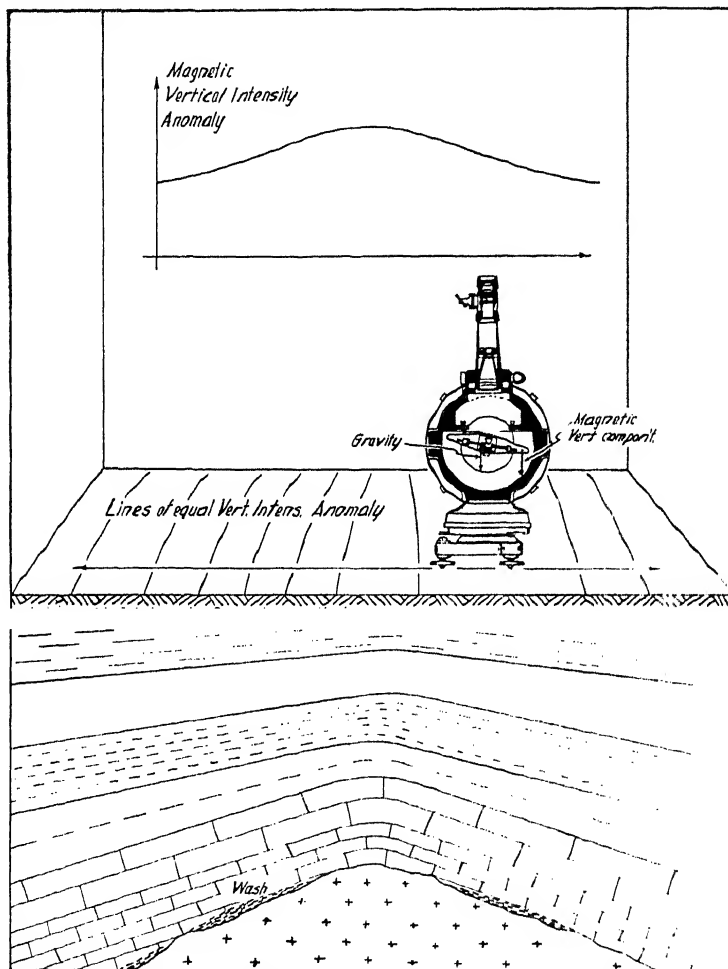
FIG. 2-8. Vertical magnetometer on traverse across buried granite ridge.

Fences, bridges, pipe lines, tanks, derricks, well casings, and the like, are a serious handicap to magnetic exploration and must be kept at sufficient distance, as it is difficult to correct for them.

Interpretation. Magnetic results are generally represented in the form of lines of equal magnetic anomaly ("isanomalic" lines[5]) or in the form

[5] The name " " as applied to magnetic lines is a misnomer.

of curves for profiles at right angles to the assumed strike (see Fig. 2-8). Interpretation of magnetic anomalies is usually qualitative. Depth determinations are the exception rather than the rule, because magnetic anomalies may be due not only to variations in the relief of a magnetic formation but also to changes in magnetization; moreover, the ratio of induced and remanent magnetization is frequently subject to unpredictable variations. In the interpretation of magnetic data in oil exploration, magnetic anomalies ranging from fifty to several hundred gammas may be assumed to result from variations in topography and composition of igneous or metamorphic basement rocks or from igneous intrusions. Anomalies of lesser magnitude are usually due to variations in the magnetization and structural arrangement of sedimentary rocks. Magnetic anomalies observed in mine exploration are of large magnitude and result in most cases from igneous rocks or magnetic ore bodies.

In quantitative interpretation magnetic effects of assumed bodies are calculated, compared with the field curves, and assumptions changed until a geologically reasonable agreement is obtained. Direct methods of interpretation are applicable when the magnetic anomaly is simple and arises from one geologic body only; in that case, approximate calculations of depth may be made directly from the anomaly curves by assuming that the magnetic bodies are equivalent to single poles, magnetic doublets, single magnetized lines, and line doublets.

The pole and line theories make no assumptions regarding the origin of the magnetic poles and may, therefore, be applied irrespective of whether geologic bodies are normally or abnormally polarized. On the other hand, where the magnetization is sufficiently homogeneous and the remanent magnetization small, the magnetic anomalies may be attributed to induction in the earth's magnetic field. In that case the so-called "induction theory" is applied. This theory relates the magnetic effects to the strength and direction of the earth's magnetic field and therefore to the magnetic latitude in which geologic bodies occur.

Considerable help may be derived in the interpretation of magnetic anomalies from the use of model experiments. In underground magnetic exploration it is necessary to measure both horizontal and vertical intensities, since magnetized bodies may occur not only below but also above the plane of observation. Depths of magnetized bodies may be determined by observations on scaffolds, in balloons, and in airplanes.

IV. SEISMIC METHODS

General. Seismic methods are in the category of "indirect" geophysical methods, in which the *reactions* of geologic bodies to physical fields are measured. Since the depth of penetration of such fields depends upon the spacing of transmission and receiving points, variations of physical

properties with depth may be measured by noting how certain physical quantities change in horizontal direction.   Seismic methods are therefore well adapted to depth determination of horizontal formation boundaries. In seismic exploration a charge of dynamite is fired at or near the surface and the elastic impulses are picked up by vibration detectors, likewise at the surface.   The time which elapses between generation and reception of the elastic impulses (''travel time'') is measured by recording also the instant of the explosion and time marks (usually at 1/100 sec. interval).

The simplest form of seismic exploration is the "fan shooting" method, which has for its objective the determination of the nature of the media occurring between the shot point and a number of detectors set up in a circle around it.   A second important seismic method is the "refraction method," in which travel times of first arrivals are observed along a profile.   The variation of this travel time with distance or the "travel time curve" makes it possible to determine true velocities and depths of the refracting formations.   A third, and now the most important, method of seismic prospecting is the "reflection method," in which the time required for an elastic impulse to travel to and from a reflecting bed is measured.   From the travel times it is possible to make a direct calculation of the depths of the reflecting sufaces but not an evaluation of the elastic wave speeds within the reflecting formations.

Seismic equipment.   Seismic equipment falls into two groups, that used at the shot point and that used at the receiving points.   For the generation of elastic impulses, dynamite is employed, although weights dropped from scaffolds or towers and unbalanced flywheel machines have been applied to generate nonperiodic and periodic impulses (see Chapter 12). The dynamite is set off by special electric blasting caps, and the break in the firing circuit is transmitted by wire or radio to the recording truck. Seismic shot holes are drilled by special rotaries, spudders, or centrifugal pumps.   In reflection work a special detector is set up at the shot hole for transmitting the time elapsed between the firing of the shot and the arrival of the wave at the surface.

The equipment at the receiving points consists of as many vibration detectors as there are receiving points (6 or 12), connected to as many amplifiers and a recording camera in a specially designed truck.   The function of this equipment is to detect, amplify, and record the ground vibrations on rapidly moving photographic paper (see Figs. 2-9, 2-10, and 2-11).   The detectors, also referred to as "geophones," phones, or pickups, record the vertical component of the vibration and are constructed like microphones.   "Inductive" detectors are built like moving coil dynamic microphones, "reluctance" detectors like phonograph pickups and "capacitive" detectors like condenser microphones and "piezo-electric" detectors

like crystal microphones.   At present the inductive and reluctance types predominate.   The amplifiers have usually three to four stages, are either straight transformer or resistance–impedance coupled, and include automatic volume control and amplitude expanding circuits to offset the decrease of (reflection) amplitude with depth.   Recording units are coil galvanometers, bifilar oscillographs, or unifilar string galvanometers.

Fan shooting.   In this method receivers are grouped at equal distances along the circumference of a circle, at the center of which the shot is fired. This gives the arrangement the appearance of a fan.   An area is covered with a series of overlapping fans for the purpose of determining the char-
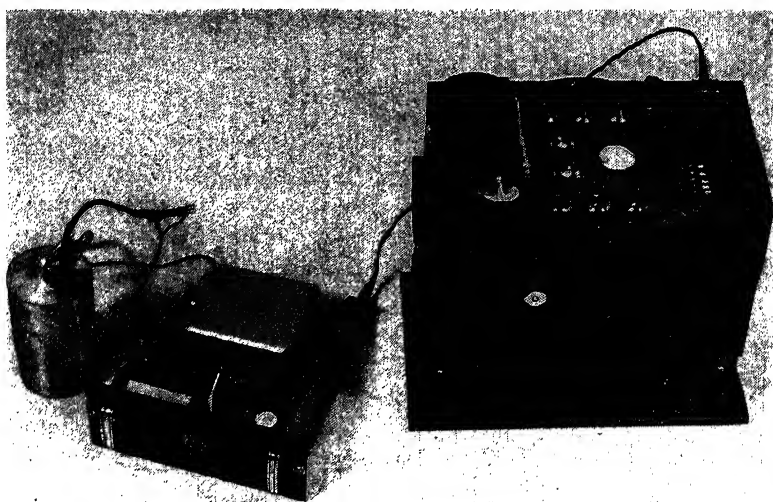
Heiland Research Corp.

FIG. 2-9. Representative seismic recording channel.   From left to right: detector; three-stage self-contained amplifier; six-element camera with six electromagnetically damped galvanometers and timing mechanism.

acter of a medium intervening between shot point and receiving points. A salt dome or other high speed medium will appear as a reduction of the normal travel time for the particular distance and area, or as a time "lead."   By plotting these leads for each fan line a salt dome, anticline, or the like can be outlined rapidly.   Usually, fan-shooting indications are detailed by other geophysical methods.   In mining, the method has been applied to the location of gold placer channels which appear as time *lags* instead of leads.

Refraction methods.   In refraction shooting, travel times (of first impulses) are determined and plotted as functions of the distance of receptors arranged in a profile.   If the medium between source and reception

points is homogeneous in horizontal and vertical direction, the arrival times will be proportional to distance, and therefore the travel time curve will be a straight line, its slope giving the velocity in the medium.   If the ground is horizontally stratified and if a high speed medium occurs beneath a low speed medium, only the first part of the travel time curve will give the speed in the upper medium.   From a certain distance on, waves that have taken a "detour" through the lower high-speed medium will overtake and therefore arrive ahead of the wave through the upper medium (see
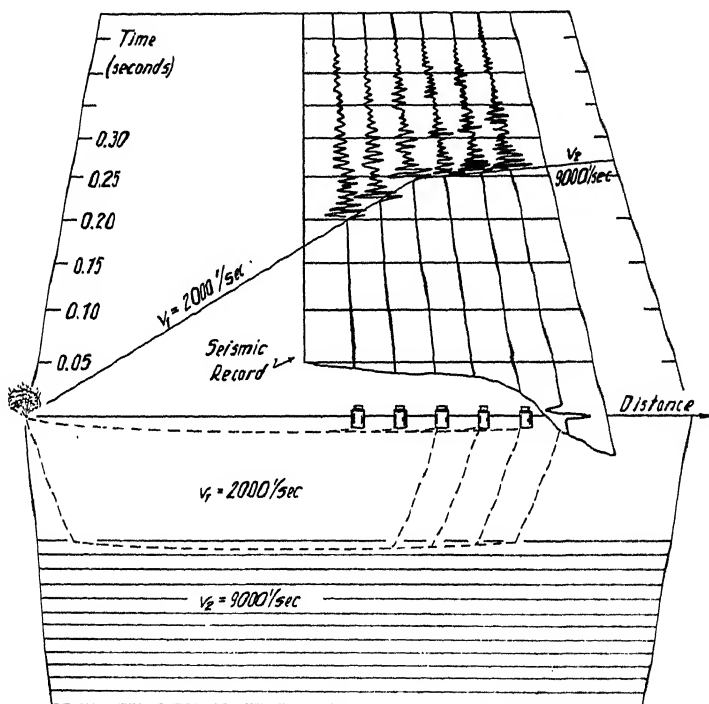
FIG. 2-10. Wave path, schematic record, and travel-time curve in single-layer refraction problem.

Fig. 2-10).   The simultaneous arrival of the two waves will be indicated by a break in the travel time curve; the slope of the second part of the travel time curve will correspond to the velocity in the lower medium. From these two velocities and the abscissa of the break in the travel time curve, the depth of the interface may be calculated.

If more than one interface exists, depths are calculated from the corresponding breaks and velocities.   In the case of dipping beds the slopes of the travel time curve no longer give a true but only an apparent velocity. Compared with the horizontal bed, an up-dip profile shows a greater ap-

parent velocity in the second part of the travel time curve, and the intercept moves toward the shot point. If the profile is down dip, the apparent velocity is less than the true velocity, and the intercept moves away from the shot point. Dip and depth may be obtained from 2 profiles (perpendicular to strike), one up and the other down the dip. To determine strike and dip, it is necessary to shoot two up- and down-dip profiles at right angles to each other. Interpretation of refraction data may be simplified where considerable velocity contrasts exist, so that the rays may be assumed to be perpendicular to the interfaces. This leads to simplified field technique, widely used in mining exploration and weathered-layer reflection correction, known as "method of differences." It involves forward and reverse shooting of a refraction profile with one receptor set out at the end of the forward profile away from the rest of the units. This location serves as the shot point for the reverse profile with the other receptors in the same location. In most refraction problems interpretation is based on the assumption of straight wave paths, that is, uniform velocity within each medium. In areas with great thicknesses of unconsolidated formations, a continuous depth-increase of velocity occurs and manifests itself in a curved travel time diagram. In that case special interpretation methods are used.

Reflection methods. Reflection impulses, or "echoes," always appear in a seismic record after the first arrivals. Since there is no way of differentiating between a later refraction impulse and a reflection in a single record a multiplicity of receivers is used in a number of shot distances. In a six- or twelve-receiver record, reflection impulses stand out by their almost simultaneous arrival (see Fig. 2-11). Important factors controlling the appearance of reflections in a seismogram are the placement (depth) of the charge and the distance between the shot point and receiver locations.

Depths are calculated from reflection records by timing the reflections for a mean receptor distance, and multiplying the time by one-half of the average velocity. This is true for nearly vertical incidence. For greater distances a "spread correction" is applied. Although reflection rays are curved, it is usually satisfactory to calculate depths on the basis of straight ray propagation. If beds are dipping, at least two profiles must be shot up and down dip. For the determination of dip and strike, two profiles at an arbitrary angle with each other, shot up and down dip, are required.

Relative depth determination may be made by plotting travel time only. For absolute depth determinations the average velocity must be known. It may be determined by recording reflections from known depths, by shooting in wells, or by surveying a long reflection profile at

the surface.　If squares of travel times are plotted against squares of distances, the square of the average velocity follows from the slope of
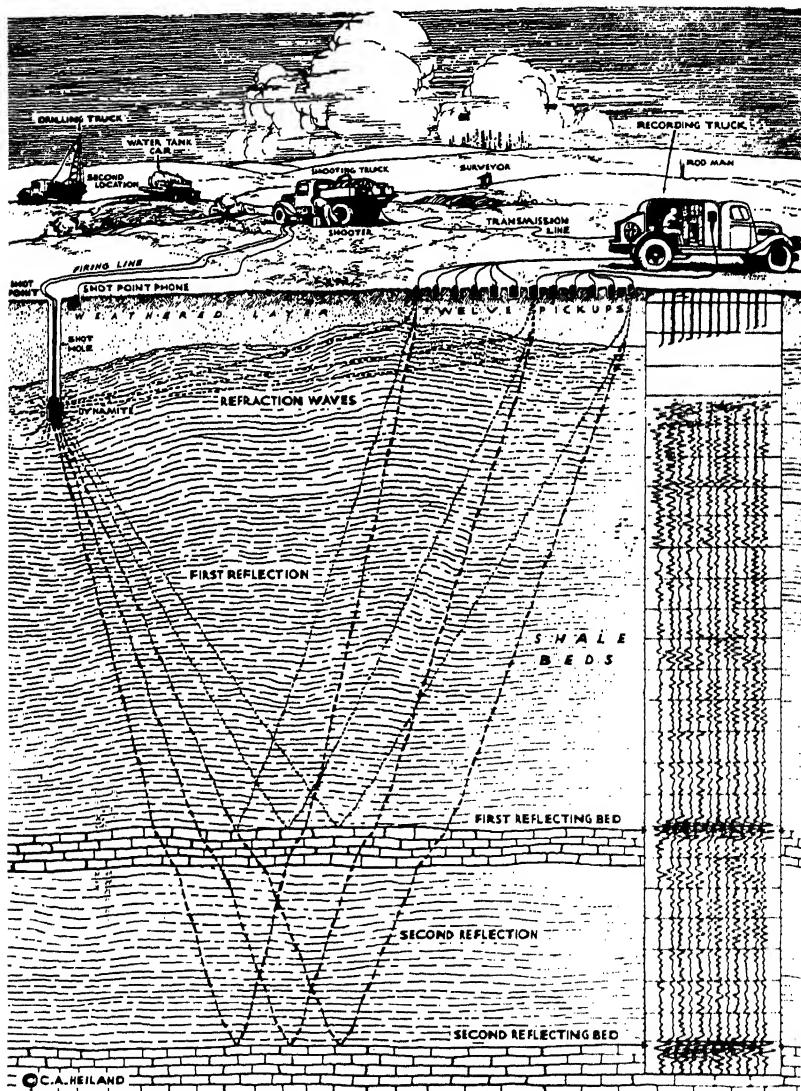
Heiland Research Corp.

Fig. 2-11. Wave paths, record, and arrangement of seismic reflection party.

such curve.　Because of the delay affecting primarily the return ray in the low-velocity surface zone, a "weathered layer" correction must be applied.　Data for this correction are obtained by the refraction procedure

described above. Elevations are considered by a topographic correction to shot datum; by reducing to a regional datum, variations in the geology of surface beds may be allowed for. Sometimes it is necessary to make corrections for horizontal velocity variations.

In practice, reflection technique is applied as correlation shooting, continuous profiling, or dip shooting. Correlation shooting consists of placing individual reflection locations from one-half to one mile apart and correlating reflection depths through that distance. In continuous profiling, there is an overlap of reflection profiles, whereas in dip shooting, profiles are shot in opposite directions. It may be necessary to use dip shooting on horizontal, but discontinuous beds to avoid errors due to miscorrelation. The reflection method is at present the most accurate method of determining depths of formations in oil exploration.

V. ELECTRICAL METHODS

General. Mineral deposits and geologic structures may be mapped by their reaction to electrical and electromagnetic fields. These are produced by either direct or alternating current, except where ore bodies spontaneously furnish their own electrical field (self-potential methods). Electrical energy may be supplied to the ground by contact or by induction. The field of the electrical currents so produced may likewise be surveyed by contact or by induction. In respect to surveying procedure and the field measured, three main groups of electrical methods may be distinguished: (1) self-potential, (2) surface-potential, and (3) electromagnetic methods. Frequently the first two groups are combined into one group of potential methods; the electromagnetic methods are usually subdivided into galvanic-electromagnetic and inductive-electromagnetic in respect to the manner in which the primary field is applied.

Four frequency bands may be used in connection with alternating current electrical prospecting: (1) low frequencies of from 5 to about 100 cycles; (2) the audio-frequency range of from 200 to 1000 cycles; (3) high frequencies of from 10 to 80 kilocycles; and (4) radio frequency of from 100 kilocycles to several megacycles. The low-frequency range is applied in most potential methods; the audio-frequency range is used in some potential and most electromagnetic methods; the high-frequency range in the high-frequency electromagnetic methods; and radio frequency in the radio methods of electromagnetic prospecting. The application of high and radio frequencies is limited owing to their lack of depth penetration; of greatest importance are the audio frequencies and the low frequencies. In a number of respects, electrical methods are similar to seismic methods; comparable to the refraction methods are the resistivity and the potential-

drop–ratio methods; inductive methods as applied to the mapping of horizontal beds are comparable to reflection methods but lack their resolving power.

In electrical prospecting, three kinds of current conduction are significant: (1) electronic conduction in solids (metallic minerals and ores); (2) electrolytic conduction (by ions); (3) dielectric conduction (by displacement current). Conductivity of rock minerals plays a part only in metallic ores; in most igneous and sedimentary formations "mineral" conductivities are insignificant. Their conductivity is a function of the pore volume and of the conductivity and amount of the water filling the pores. For all practical purposes it is sufficient to assume that sodium chloride is the only substance in solution.

Self-potential method. The self-potential method is the only electrical method in which a natural field is observed; its causes are spontaneous electrochemical phenomena. These phenomena occur on ore bodies and on metallic minerals and placers; they are produced by corrosion of pipe lines and on formation boundaries in wells by differences in the conductivity of drilling fluid and formation waters. Ore bodies whose ends are composed of materials of different solution pressure and are in contact with solutions of different ion concentration, act as wet cells and produce an electrical field which can be detected by surveying equipotential lines or potential profiles.

To prevent interference from electrode potentials set up by contact of metallic stakes with moist ground, nonpolarizable electrodes are used. These consist of porous pots filled with copper sulphate into which a copper rod is immersed. For the mapping of equipotential lines, a high-resistance milliammeter is connected to two nonpolarizable electrodes. One is kept stationary and the other is moved until the current vanishes. At that point the electrodes are on an equipotential line.

Potential profiles are run by measuring potential differences between successive electrode locations (see Fig. 2-12). Interpretation of self-potential surveys is qualitative; the negative potential center may be taken with sufficient accuracy to be the highest location of an ore body. Approximate depth determinations can be made by observing the distance from the point of maximum potential to the half-value point in the potential curve. Interpretative advantages are often gained by plotting the results in the form of current-density curves which are obtained from the potential curve by graphical differentiation.

Equipotential-line and potential-profile methods. When a source of electrical energy is grounded at two points, an electrical field is produced. Distortions of this field result from the presence of bodies of different conductivity; good conductors will attract the lines of flux, and vice versa.

As it is difficult to survey these lines of flux, lines of equal potential, that is lines along which no current flows, are mapped instead. In practice power is supplied to two grounded electrodes from an alternating current generator. Two types of primary electrodes may be used: (1) point elec-
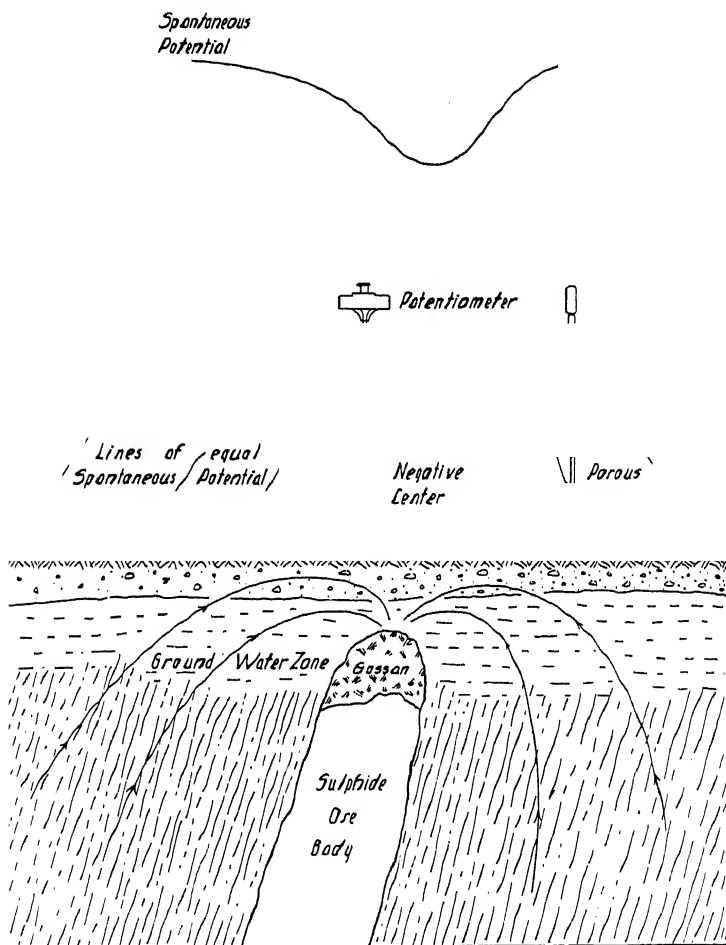

FIG. 2-12. Self-potential mapping (schematic).

trodes, so laid out that their base line is in the direction of strike, (2) line electrodes laid out at right angles to the strike. Equipotential lines are surveyed with one fixed and one moving probe which are connected to an audio amplifier with head phones. Greater detail is obtainable by the

use of so-called "compensators," which measure the voltage between the search electrodes in terms of generator voltage and phase, or split it up into one component which is in phase and another which is 90° out of phase with the generator voltage. Interpretation of equipotential-line methods is largely empirical and makes use of the displacement of the lines from their normal position. More quantitative interpretation is possible by comparing the field results with laboratory experiments made on small scale models. Because of the fact that in stratified ground the conductivity is generally better in the direction of the bedding planes than at right angles thereto, it is possible to use equipotential-line methods for structural and stratigraphic investigations. Since an equipotential line near one electrode will be elliptical instead of circular, the direction of the major axis indicates the direction of strike.

Resistivity methods. Equipotential-line methods, while useful for the mapping of vertical or steeply dipping geologic bodies, are not suited to the investigation of horizontally stratified ground. Conversely, resistivity methods are applicable to depth determinations of horizontal strata and the mapping of dipping formations.

In resistivity procedures not only the potential difference between two points but also the current in the primary circuit is observed. The ratio of potential difference and current, multiplied by a factor depending on electrode spacing, gives the resistivity of the ground. True resistivities are observed in homogeneous ground only; the presence of horizontal or vertical boundaries in the range of the instrument gives what is known as "apparent" resistivity. The arrangement in most frequent use is the four-terminal Wenner-Gish-Rooney method (see Fig. 2-13). Resistivity methods may be applied in two ways: (1) with constant electrode separation (that is, constant depth penetration), called resistivity "mapping"; (2) with fixed center point and progressively increasing electrode separation, called resistivity "sounding," whereby the apparent resistivity is observed as a function of electrode separation and therefore of depth. A modification of the resistivity mapping method is used in electrical logging.

Interpretation of resistivity data may be qualitative and quantitative. The qualitative method uses the appearance of the curves and is applied primarily in resistivity mapping, a drop in apparent resistivity indicating the approach of bodies of better conductivity, and vice versa. In resistivity sounding, the horizontal variation of apparent resistivity is interpreted in terms of the equivalent vertical variation of resistivity; however, the curves do not have sharp breaks at formation boundaries. Structural correlations are sometimes possible by comparing curves through a series of locations. When only one or two formation boundaries are effective, direct depth determinations are possible by comparing the field data with

"type" curves calculated for given conductivity ratios and for various possible depths.

Potential-drop–ratio methods.   The essential feature of the resistivity methods previously discussed is a determination of the potential difference between two points at the surface and a measurement of the current in the external circuit.   In potential-drop–ratio methods current measurements in the external circuit are not made and the potential drops in two successive ground intervals (represented by three stakes arranged in a
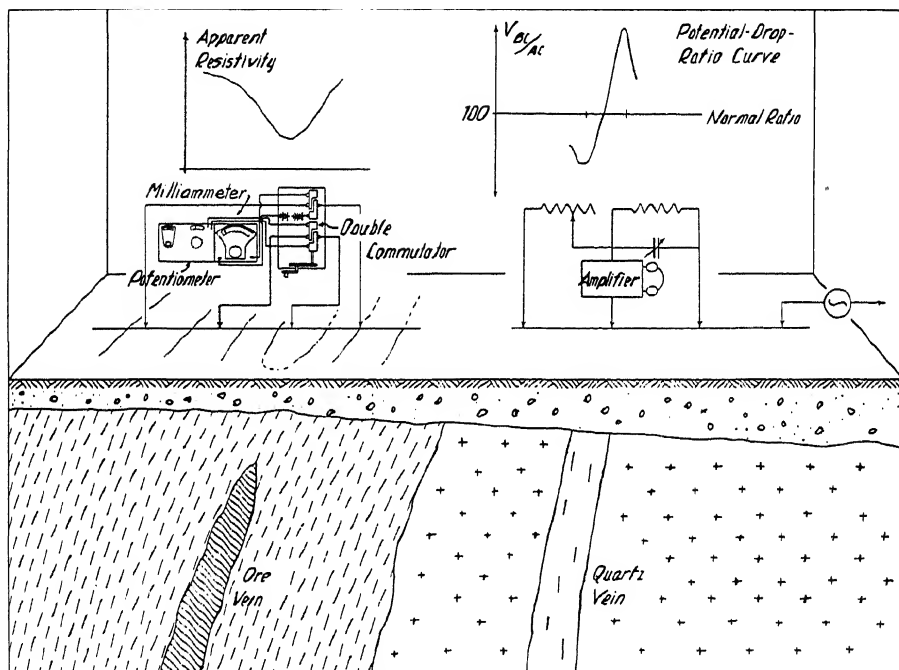
Fig. 2-13. Resistivity and potential-drop-ratio mapping (schematic).

straight line, radiating from one of the power electrodes) are compared. The potential-drop-ratio method is best suited for the location of vertical formation boundaries (faults, dikes, veins, and the like).   The arrangement used for the comparison of the potentials is a modified A.C. Wheatstone bridge; the two external stakes are connected to two resistors (with condensers in series or parallel) whose center tap connects through the indicating instrument to the center stake.   When this arrangement is moved across a vertical formation boundary, a potential-drop ratio greater than one is obtained when proceeding from a medium of lower resistivity toward a medium of greater resistivity, and vice versa (see Fig. 2-13).

Other potential methods. Surface potential measurements may be made not only with continuous direct or alternating current but also by the use of transients, such procedure being known as "Eltran." The electrode arrangement is similar to the resistivity method. In the primary circuit, impulses are applied to the ground and the time change of the potential between two stakes (usually placed outside the two current stakes) is measured with an amplifier and cathode-ray oscillograph.
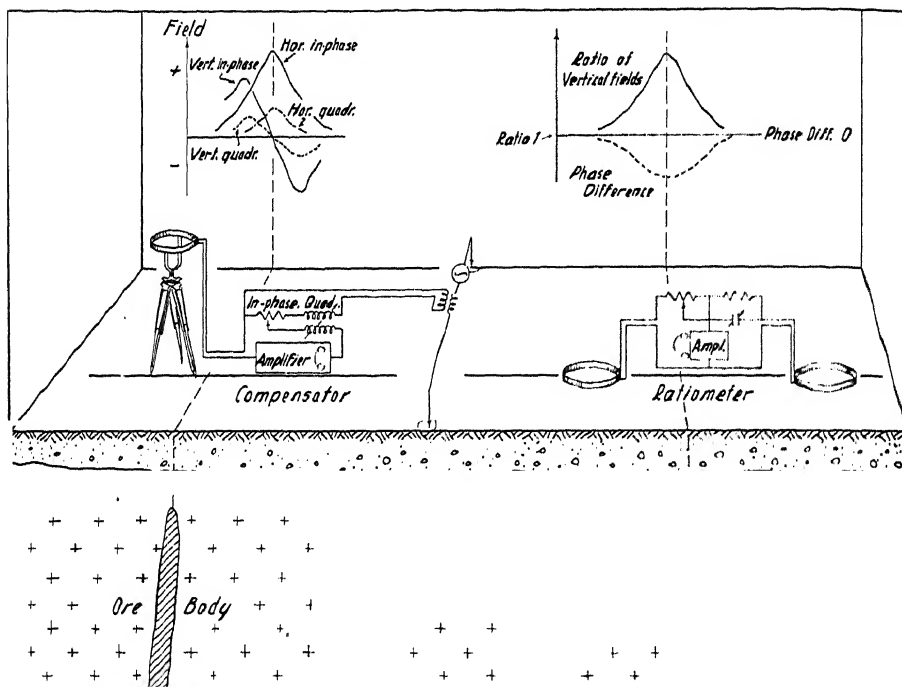
Fig. 2-14. Semiabsolute and relative electromagnetic prospecting methods (schematic).

Electromagnetic-galvanic methods. Electromagnetic methods of electrical prospecting differ from potential methods in that the electromagnetic field of ground currents and not their surface potential (electrical field) is measured. They fall into two major groups: (1) electromagnetic-"galvanic" methods in which the primary energy is supplied by contact as in the potential methods; (2) electromagnetic-"inductive" methods in which the ground is energized by inductive coupling (with insulated loops). To supply electrical energy to the ground by contact, line electrodes or point electrodes are used. Line electrodes are laid out at right angles to the strike, point electrodes parallel with the strike.

Numerous methods are available for measuring the electromagnetic field. The simplest procedures involve a determination of direction only or of the absolute values of the horizontal and vertical components by using a vacuum-tube voltmeter in the output circuit of an amplifier connected to a reception frame. A determination of the in-phase and quadrature components of the field is possible by the use of the compensators previously described (see Fig. 2-14). These are connected by a pair of leads to the source of the primary power and thus determine the electromagnetic field in terms of the current and phase of the primary circuit. Finally, the *ratios* of field intensities and their phase *differences* at successive points may be measured by dual coil arrangements and "ratiometer" bridges (see Fig. 2-14).

Interpretation of results obtained with the electromagnetic-galvanic method is both qualitative and quantitative. In approximation, lines of equal direction of the field vector (in horizontal projection) may be assumed to represent flux lines which are attracted by bodies of good conductivity, and vice versa. If the current is concentrated in a good conductor and flows along its strike, then the horizontal component will have a maximum above the current concentration. The vertical component will be zero at a location immediately above the concentration and will have a maximum and minimum, respectively, on either side of the concentration, their distance being equal to twice the depth.

Indications are also obtained from induction currents concentrated along the edges of a subsurface body. Therefore, in the case of an ore body of some width, the horizontal intensity will show not merely a maximum over the center but a maximum and minimum, respectively, over the edges. This, strictly speaking, comes under the heading of electromagnetic-inductive methods described in the next paragraph.

Electromagnetic-inductive methods. In inductive procedures power is supplied to the ground by insulated loops which will cause induction currents to flow in subsurface conductive bodies. An advantage of inductive methods is the ease with which power may be transferred into the ground when the surface formations are poor conductors. Since currents induced in the subsurface conductors are dependent on frequency, interpretative advantages may be gained by regulating the frequency.

However, there are limitations to this procedure. Too low frequencies will reduce the strength of the induced currents, while too high frequencies lack depth penetration and cause interference from near-surface noncommercial conductors and from topography. Frequencies usually applied in mining, range from 250 to 1000 cycles; in structural exploration the range is from 25 to 200 cycles. The other extreme is represented by the high-frequency methods using several tens of kilocycles which have been

practically abandoned on account of the limitations mentioned. In inductive methods a horizontal or vertical loop may be employed. The former afford the most effective coupling with horizontal subsurface conductors and are used in the form of long cables and rectangular or circular loops. Theoretically vertical loops would be more suitable for steeply dipping bodies, but they are difficult to handle. For the measurement of the electromagnetic field, the same procedures are used as described before in connection with the electromagnetic-galvanic methods.

Interpretation methods in electromagnetic-inductive exploration depend to some extent on the purpose of the survey and the general shape and disposition of the subsurface conductor. In wide and steeply dipping conductive bodies the electromagnetic field is due primarily to currents flowing along the edges. Hence, the horizontal component will show a maximum and minimum, respectively, over the edges; a minimum in the vertical component will occur over the center. Depth calculations of the equivalent current concentrations are based on the relations discussed before in connection with electromagnetic-galvanic methods.

Inductive methods, using separate measurements of the in-phase and out-of-phase components, have great interpretative advantages. The in-phase component is largely due to the field-supplying loop, while the out-of-phase components result from the induced subsurface current concentrations. In horizontally stratified ground, interpretation is usually based on the out-of-phase components. If a very good conductor occurs in horizontal position, the surface anomaly is largely due to the reflection of the primary cable on the conductor, with a phase change of 180°. Depth determinations of this conductor are, therefore, possible by locating the "image" of the primary cable from the trend of the horizontal intensity curve. Attempts have also been made to determine resistivities of subsurface formations and their variation with depth by using a horizontal circular loop of gradually increased radius. The quadrature component in this case depends on resistivity and frequency, depth penetration being controlled by the radius of the loop. As in most other electrical methods, interpretation of results obtained with inductive methods is aided greatly by model experiments.

Radio methods. Since radio methods employ frequencies still higher than the high-frequency–inductive methods, they are subject to the same limitations. In one group of radio methods the effect of subsurface conductors on the emission characteristics of a transmitter is observed. In a second group a receiving arrangement is employed in addition to the transmitter, and the variation of field intensity with location is measured. This will give some idea of the absorption, interference, and reflection that the waves may have undergone along their path from the trans-

mitter to the receiver. In the catagory of radio methods belong the so-called "treasure finders." These are portable instruments for the location of shallow metallic objects, pipe lines, and the like.

VI. GEOPHYSICAL WELL TESTING

Geophysical well-testing methods may be divided into four groups: (1) electrical testing methods, known as "electrical logging"; (2) temperature measurements; (3) seismic measurements; and (4) miscellaneous measurements of radioactivity, rock magnetism, opacity of drilling fluid, and so on.

Electrical logging methods. Electrical logging methods fall into two groups: (a) methods calling for the application of an electrical field, which furnish the resistivities of the formations traversed; and (b) methods in which spontaneous electrical potentials are observed. The latter will give data regarding the porosity of formations. Numerous arrangements have been proposed for the determination of resistivities in wells. The system most widely used is the Schlumberger procedure. Three electrodes are lowered into the well and the fourth is the casing at the surface (see Fig. 2-15). Current is supplied to the casing and the lowest electrode, and the potential difference between the two other electrodes is recorded. The resistivities thus obtained are *not* true formation resistivities but *apparent* resistivities which are functions of the electrode spacing and of the absolute resistivities involved. Electrical logging makes possible the correlation of formations by their resistivity parameters, and the location of water- and oil-bearing strata. In some wells it has been found that the resistivities are a true indication of the productivity of oil sands.

In the second group of electrical coring methods spontaneous potentials are observed. These are of two types: (1) electrofiltration potentials (caused by movement of fluids through porous formations), and (2) concentration potentials (caused by difference in ion concentration of drilling fluid and formation water). Spontaneous potential records are valuable in connection with resistivity logs. A high resistivity may mean a limestone or an oil sand, but high porosity will eliminate the limestone from the picture.

Temperature measurements. It is generally known that there is an increase in temperature with depth of penetration into the earth's crust. However, this temperature variation with depth is not uniform; it depends not only on the local geologic and stratigraphic conditions but also on the presence or absence of heat developed by physical and chemical actions of the formation fluids. As the heat conductivity of beds is greater in the bedding planes than at right angles thereto, uplifts of sedimentary beds and salt domes will generally result in a rise of well temperatures.

Chemical and physical processes responsible for changes of the normal temperature gradient are: the transformation of anhydrite to gypsum; the oxidation of sulfides; the influx of water, oil, and gas into the hole; and the heat developed by the setting of cement behind the well casing.
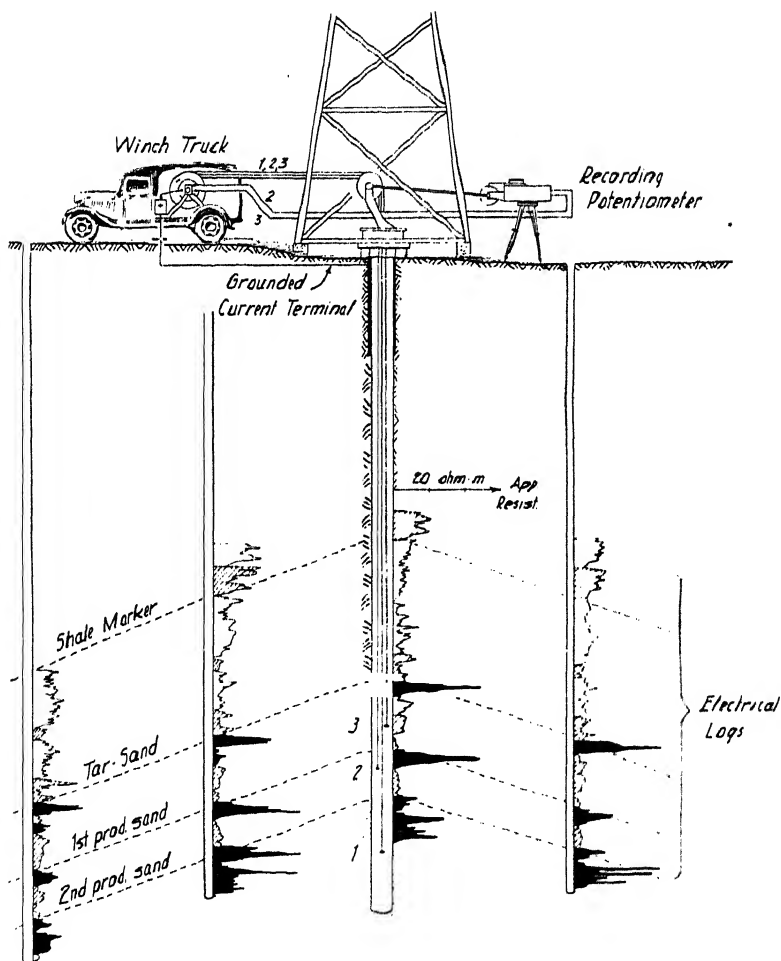

FIG. 2-15. Electrical logging arrangement (schematic).

It is clear, therefore, that temperature measurements in wells will furnish valuable information in connection with the location of oil, gas, and water-bearing strata, cementation problems, and so on. Correlation of temperature curves obtained in a series of wells will give valuable clues to geologic structure.

Seismic measurements. Seismic measurements in wells are made for two purposes: (a) to supplement surface refraction data, and (b) to obtain average velocity data for reflection shooting. In both applications a vibration detector is lowered into the well to the depth desired and shots are fired at the surface. In wells drilled into or near the edge of salt domes, it is thus possible to obtain valuable information in regard to presence of overhang and the behavior of strata along the flanks. In order to make absolute depth determinations in reflection shooting, it is desirable to know the velocity of seismic waves at right angles to the bedding, which is likewise determined by firing several shots at or near the well at the surface, with a detector lowered to various depths.

Miscellaneous measurements. The radioactivity of strata traversed by the well may be determined by lowering a small ionization chamber to the desired depth. Magnetic well investigations are generally confined to determinations of core orientation. Acoustic measurements are made in deep wells for the location of gas and water flows. Gas detectors, when used in connection with shallow holes, permit of locating leaks in gas mains.

VII. MISCELLANEOUS GEOPHYSICAL METHODS

Radioactivity methods. Application of radioactivity methods rests on the fact that zones of shattering in the earth's crust, such as faults and fissures, will allow passage and accumulation of radioactive disintegration products. Owing to the limited penetration power of radioactive gases and radiations, the depth range of these methods is limited. It does not appear to be necessary for the channels of radioactive products to remain open. If they have become mineralized, it is nevertheless possible to locate them by increased activity; hence, there is a possibility of locating sulfide and other veins by measurement of radioactivity. Some shallow oil deposits emit radioactive radiations because oil is an absorbent of radon. It goes without saying that radium ore, such as pitchblende and the other uranium compounds, may be located by radioactivity measurements.

Radioactivity methods fall into two groups: in the first the relative content of radon in the surface soil is determined; in the second the penetrating radiation of radioactive disintegration products is measured.

Hydrocarbon (soil and gas) analysis. Oil seepages and gas emanations have served for decades as indications of oil deposits. These macroscopic examination methods have been supplemented recently by microscopic procedures for determining small amounts of hydrocarbon in the soil air and in the soil itself. The air from shallow holes is pumped into a gas

detector which may be of the hot filament type or which may indicate the amount of carbon dioxide liberated on combustion of the hydrocarbons contained in the air. These detectors do not differentiate between methane and the heavier hydrocarbons. In soil analysis methods, on the other hand, the soil samples are degassed and the gases passed through an analytical apparatus, where their constituents are separated by low-temperature distillation and combustion into methane, ethane, and the heavier hydrocarbons. Soil samples may also be extracted by suitable solvents, and their content in socalled pseudohydrocarbons (soil waxes, and the like) may be determined. Several of the known oil fields have been found to be characterized by a corona or halo pattern of the significant heavy hydrocarbons. The pseudohydrocarbons and methane appear to follow a similar, though less regular, trend, methane being possibly least significant, since its distribution may be affected by near-surface decomposition processes.

Dynamic ground tests, strain gauging, vibration tests. Building sites may be tested by setting them into forced vibration and measuring their amplitudes at any desired points by vibration recorders as functions of frequency, thereby determining their natural frequency and damping. Experience appears to indicate that the former frequently coincide with their predominant response frequency to earthquake vibrations. Hence, any structure to be built on such ground should be so designed that resonance between structure and ground is avoided.

Strain gauging is a comparatively new field of geophysics. Its purpose is the measurement of small displacements between adjacent portions of ground in underground openings such as tunnels, mine shafts, and the like. Continuous recording of strains in subsurface openings and of their fluctuations with time makes it possible to predict roof and wall failures and to guard against them.

The purpose of vibration tests is to determine the magnitude and characteristics of vibrations set up in buildings by traffic, mine operations, blasting, and so on, by one or more vibration recorders set up at various distances from the source of the disturbance or in various stories of the building. Results of such tests have played no unimportant part in settling disputes arising from damage claims in connection with industrial operations.

Acoustic methods. Acoustic methods are concerned with the transmission and reception of audible sounds in the air, in water, and in the ground. Their purpose is communication, position finding, sound ranging, direction finding, echo sounding, and, indirectly, the collection of data for noise prevention. For communication or signaling, transmitters of suitable frequency and directional characteristic are required, depending

on the medium.   Position finding is the procedure of determining one's
location by distance measurements from two acoustic sources of known
coordinates or, as in radio-acoustic position finding, from one source
transmitting a simultaneous radio and acoustic impulse.   Conversely,
sound ranging is the location of a source of unknown position by acoustic
triangulation, that is, by recording sound impulses on receivers of known
positions.   By direction finding is meant the determination of the direc-
tion of sound by a rotatable base with two receivers (binaural hearing)
or with multiple receivers equipped with electrical delay networks to
balance their phase differences (compensators).   Echo sounding is identi-
cal in principle with reflection shooting described on page 24, except that
because of the homogeneous character of the medium of propagation
(usually water) the devices may be so made as to indicate or record depth
directly.   Noise prevention extends into the fields of architecture, building
construction, industrial activity, vehicle traffic, and sound insulation of
military conveyances.

Military and peacetime applications of acoustic methods are numerous
and are covered in Chapters 6 and 12 in greater detail.

3

MEASUREMENT PROCEDURES IN GEOPHYS-
ICAL EXPLORATION

I. SIGNIFICANCE AND MEASUREMENT OF PHYSICAL QUANTITIES INVOLVED

IN GEOPHYSICAL EXPLORATION geologic bodies are located by surface observation of their physical fields. What type of physical field is selected as being the most characteristic of a subsurface body depends entirely upon what rock property is most characteristic of that body. The choice of which field parameter is used, in turn, is determined by four factors: (1) distinctiveness of response; (2) ease and rapidity of field determination; (3) accuracy; and (4) freedom from interference (of surface or subsurface origin).

Notwithstanding the widely varying nature of physical fields observed, there is a definite similarity in the parameters measured by various methods. Broadly interpreted, geophysical methods fall into two groups: (1) methods in which the propagation of a field with time (and location) is observed; (2) methods in which the characteristics of stationary and quasi-stationary fields are measured. Virtually all seismic and certain electrical methods fall in the first group. Related in principle are those methods in which the variation of a field with time is observed. In this group fall the majority of the "recording" methods, such as the observation of time variations in gravity; of magnetic variations, of fluctuations in electric currents produced by corrosion of pipes, and so forth. There are some methods in which quantities related to time—for example, phase shift and frequency—are measured (A.C. potential and electromagnetic method and dynamic soil testing method); however, as they operate with quasi-stationary fields they are discussed in the following group.

Most geophysical exploration is concerned with stationary and quasi-stationary fields, such as in the gravitational, magnetic, self-potential, and other electrical prospecting methods. It is here that similarities in the selection of a suitable field parameter and method of observation may be most readily observed. In these methods we usually work with fields

38

which have a potential and are characterized by four parameters: (1) the potential itself; (2) the potential gradient, or field intensity; (3) the direction of the field; and (4) the field gradient and its direction (second derivatives of the potential).   Derivatives of the potential higher than the second are rarely, if ever, measured in geophysical exploration.   Interpretative experience indicates that the distinctiveness and therefore the resolving power of a method increases with the order of the potential derivative. However, accuracy requirements and the field difficulties also increase. Measurements of absolute potentials are rarely undertaken.   They probably would accomplish no useful purpose in gravitational and magnetic exploration.   Potential measurements in electrical prospecting actually involve a determination of potential difference, potential gradient or electrical field strength.

The first derivative of a potential is measured in most methods employing stationary or quasi-stationary fields.   In gravitational exploration, the first derivative of the gravity potential with respect to the vertical— that is, gravity—is determined in a number of ways, particularly by pendulums and gravimeters.   The horizontal derivative (horizontal gravity component), is not measured directly,[1] although there is no reason why instruments for this purpose could not be developed and perform a useful function.   In magnetic exploration, the derivatives of the magnetic potential in almost any desired direction can and have been measured. Instruments have been developed for the determination of the total intensity and its vertical and horizontal components.   However, the vertical component has been found to be of the greatest diagnostic value.   In electrical prospecting, potential difference and therefore electrical field strength is determined in the self-potential, the potential profile, and the resistivity methods.   Intensities of electromagnetic fields are observed in the electromagnetic, the inductive, and the high-frequency methods of electrical prospecting (although these fields do not derive from a potential).

As far as technique is concerned, simple conditions prevail when merely the *direction* of a field is observed.   This is done in magnetic exploration by measuring declination and inclination and in electrical prospecting by tracing equipotential lines and by observing the minimum-signal position of a reception coil.   However, direction observations are less readily interpreted than intensity measurements; hence, the latter are usually given preference.

Measurements of second derivatives of a field potential play an impor-

---

[1] This component may be obtained indirectly from torsion balance observations by graphical integration of curves representing the horizontal variation of curvature values.

tant part because of their greater resolving power. In practice this advantage is sometimes offset by increased difficulties in technique. The best-known example of this method is the torsion balance. Observations of second derivatives have been made in magnetic exploration by an adaptation of the earth inductor. In electrical prospecting it has been found advantageous to measure the *ratio* of fields in successive intervals rather than to measure their gradients. This advantage is due to the ease with which "ratio" bridges can be designed. Examples are the potential-drop-ratio method and the determination of the ratio of electromagnetic fields with dual coil arrangements.

As stated at the outset, preference is given to field parameters which can be measured with the greatest accuracy as well as ease and rapidity; hence, the tendency to measure physical fields relatively and not absolutely whenever possible. The terms "absolute" and "relative" are somewhat difficult to define in geophysical exploration, since most quantities, which by their nature can be determined absolutely, may with greater ease be observed relatively by reference to a fixed point or base station.

Absolute procedures include measurements of direction (magnetic inclination and declination, equipotential lines, dip and strike of induction coils), time and distance (seismic refraction and reflection measurements), and electric voltage (as in electrical potential methods).

Semiabsolute procedures are those which measure a physical parameter by comparison with another which is assumed to remain constant for a reasonable interval of time. Examples are: relative gravity measurements, made with the assumption that the pendulum length remains constant; magnetometer measurements, made by comparing the vertical intensity with the presumably constant gravity; the gravimeter, whose reliable functioning depends on the constancy of the elastic comparison force; and many others.

Relative procedures involve physical measurements by actual connection of the detecting unit with a similar unit located at a reference station or an adjacent ground interval. Examples are: the transmission of the oscillation of a reference gravity pendulum from a base station to a field station; the magnetic earth-inductor gradiometer; the potential-drop-ratio method; the comparison of electromagnetic fields with the amplitude and phase of the current in the generator circuit by compensator arrangements; and two-coil ratiometer bridges for a comparison of electromagnetic fields with respect to amplitude and phase at successive points. It is seen that by such procedures time variations of comparison parameters are virtually eliminated.

II. ARRANGEMENT OF OBSERVATION POINTS WITH RELATION TO GEOLOGIC OBJECTS

In geophysical exploration, the objects of detection are geologic structures or mineral deposits, and the detecting units are usually spread out along the earth's surface. This is done (1) to determine the variation of

TABLE 3

PROCEDURES OF MEASUREMENT IN GEOPHYSICAL EXPLORATION

Object	Detector	Measurement
Stationary.	Stationary; horizontal position varied, or multiple detectors used.	Gravitational, magnetic, seismic, electric surveying on land, in shallow water, and underground; radioactivity measurement, water- and gas-pipe leak detection, and corrosion surveying; model experiments in laboratory.
	Stationary; vertical position varied.	Scaffold or underground observations, well shooting at different levels; electrical and geothermal well surveying; vibration tests of structures at different stories.
	Moving; vertical and horizontal position varied.	Gravity and magnetic surveys on ships, floats, submarines; magnetic surveys in vehicles and aircraft; resistivity surveys from ships and floats; other electric surveys by aircraft; echo sounding from ships.
	Stationary; position not varied.	Determination of physical properties of rocks on outcrops or samples in laboratory; vibration tests on structures.
Moving.	Stationary or moving.	Acoustic and thermal submarine and airplane detection; iceberg location.
Measurement of variation of physical quantities with time.	Stationary; recording.	Recording of magnetic variations, of corrosion voltage fluctuations, and of traffic vibrations, sound ranging; strain gauging.

the physical quantities measured between points and to obtain a clue to the presence or absence of a geologic body; and (2) to determine the depth of a formation if it remains in horizontal position throughout the length of a profile. The first operation falls under the heading of geophysical *mapping*; the second is known as geophysical *sounding*. By far the greater portion of all geophysical work is done by means of surveying processes on land, in shallow water, underground, or on small-scale laboratory models

with miniature detecting units. As depth to geologic bodies is commercially a most desirable quantity, wells are used whenever possible. Examples are: seismic determination of average velocities; measurement of resistivity, temperature, and radioactivity in wells; and observations at different levels of mines. Although attempts have been made to survey from moving supports (automobiles, ships, floats, submarines, and planes) little has been accomplished along this line, since measurements on moving supports introduce a reduction in accuracy. The present trend in geophysics is more toward accuracy than speed. The use of moving objects and moving detectors plays a part in the military and oceanographic fields of geophysics. Stationary detectors for determining variations in physical effects of stationary objects are used in the recording of magnetic variations, corrosion voltages, traffic vibrations, strain gauging, sound ranging, and in small-scale laboratory investigations where model ore bodies may be used and detectors remain stationary. Table 3 gives a summary of these procedures.

4

GEOPHYSICAL METHODS IN OIL EXPLORATION

THE FOLLOWING CHAPTER is intended to assist the operator in the selection of the correct geophysical method when prospective oil territory is to be surveyed. It contains a discussion of (1) the general possibilities of geophysical methods, with chief reference to new areas where the expected type structure is unknown; (2) the choice of methods for specific types of structures; and (3) other nongeological considerations in the selection of methods.

If nothing whatever is known about the geology of an area, the most expedient procedure is to make a magnetic reconnaissance survey with widely spaced stations. This may be expected to indicate the topography of areas of the basement rocks, provided they are uniformly magnetized. After promising high areas have been located, the magnetic discoveries should be followed up (preferably by seismic-reflection methods) to determine whether the basement uplifts are accompanied by structure in the overlying sediments. In certain areas magnetic anomalies may also be caused by magnetic sediments. Cases have been known where salt domes have furnished magnetic indications, and where anticlines and faults could be traced by virtue of the presence of magnetic beds in the stratigraphic sections. If the basement rocks are not uniformly magnetized, a magnetic high may simply mean an area of greater magnetization or an area occupied by more magnetic rocks. In some instances it has been found that the magnetization was the reverse of that normally expected and that magnetic highs indicated structural lows.

Where magnetic anomalies have no structural significance, it is necessary to use other reconnaissance methods—for instance, the gravitational method. A survey made with pendulums or gravimeters can generally be depended upon to depict fairly accurately the major structural trends. In a few instances it has been found that gravity highs do not reflect geologic structure in the oil-bearing strata. In such cases the work has to be conducted by methods, such as seismic refraction or reflection, which rely only on the structure in the sedimentaries.

43

The refraction method has definite possibilities in virgin areas as a means of stratigraphic analysis of a section. As a means of finding salt domes, its use has decreased considerably on the Gulf coast in favor of gravity and reflection-seismic work. Some oil companies still retain the use of the refraction method for work preceding or accompanying reflection work if the section to be followed out does not exceed 6000 feet in depth. Beyond the distances required for such depth penetration (about seven miles) difficulties in transportation, handling of dynamite, and therefore operation costs generally increase out of proportion to the results achieved and detail of information obtained.

For detail, the reflection method is unquestionably the most widely used geophysical technique; it works best on low-dip structures but encounters difficulties with beds of complex faulting, folding, and steep dip. Compared with many other geophysical methods, it has the advantage of giving positive depth information. Because of the fact that several reflecting beds may be mapped in one area, this method gives data in regard to lateral variations of the thicknesses of formations and permits the following of unconformities.

As aptly expressed by Barton,[1] "Geophysical orientation in regard to an area is as necessary to the geophysicist as geological orientation is to the geologist." The geologist must acquire a knowledge of the general stratigraphy and regional structure of an area and must learn the relation of particular features to the regional geology before he can begin to evaluate the significance of local structure in respect to its potential productivity. Likewise, the geophysicist should first investigate the general magnetic, gravitational, seismic, and electric characteristics of an area from a regional point of view before he can begin to evaluate the local significance of geophysical anomalies. Moreover, the regional geological features must be correlated with the regional geophysical features. It often takes considerable time until certain magnetic and gravity anomalies, seismic velocities, reflection travel times, and electrical logging indications can be definitely tied up with specific formations or groups of formations. The geophysicist frequently must wait for the driller before he can complete his correlations.

The task of choosing methods for reconnaissance and for detail which will give the most reliable information at least expense is facilitated if it is definitely known what type of geologic structure will be encountered in a given area, and if geophysical measurements have been made on a known field. When geophysical methods were first introduced in oil prospecting, practically every method was first tried on known structure. In exploring

---

[1] A. E. Dunston, *et al.*, *The Science of Petroleum*, Oxford University Press (1938).

a new territory it is still advisable to start with, and work away from, known conditions. If the type structure to be encountered in a given area is known, a selection of the most advantageous method is much facilitated. In Fig. 4–1 a schematic representation of reconnaissance and
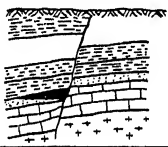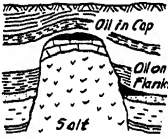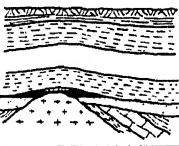
Location of Oil Structure			Reconn.	Choice for Detail	Method
Tectonic	Anticlines Domes Monoclines Terraces		1		Magnetic
			(1)		Gravimeter
				1	Reflection Seismic
			2		Refraction Seismic
				2	Torsion Balance
			3	3	Resistivity, Inductive
	Faults		1	1	Reflection Seismic
			2	(1)	Torsion Balance
			(2)		Magnetic
			3		Refraction Seismic
			(3)	2	Resistivity, Inductive
				(2)	Gas Survey
Salt	Salt Domes Salt Anticlines		1		Gravimeter
				1	Torsion Balance
			2		Refraction Seismic
				(1)	Reflection Seismic
				2	Resistivity, Inductive
Buried Ridge	Granite Ridges Other buried topographic features		1		Magnetic
			2		Gravimeter
				1	Torsion Balance
				2	Reflection Seismic
Volcanic	Intrusions Dikes		1		Magnetic
				1	Torsion Balance
				2	Reflection Seismic
Lens	Shoestrings etc.			1	Magnetic (?)
				2	Resistivity (?)
Direct Location	In Wells				Electrical Coring
	From Surface			1	Soil & Gas Analysis (?)
				2	Resistivity (?)

FIG. 4-1. Geophysical methods in oil exploration.

detail methods for definite geologic conditions is given. Oil structures are divided into the better-known types of tectonic, volcanic, salt, and buried-ridge structures, with schematic illustration of the geologic forms. It is seen that for the tectonic-type structure the magnetic method is first choice

for reconnaissance, provided it is expected that basement rocks are somewhat conformable to the structure in the sedimentaries, or provided some of the sedimentary beds are magnetic themselves. Second and third choices, respectively, in structure exploration are reflection-seismic and gravity methods. For detailed surveys, reflection work is first choice, torsion balance and gravimeter second.

The reflection method has had the most brilliant success in Oklahoma for mapping the Viola and Hunton (Ordovician) limestone topography and has been applied in most other petroliferous areas in the United States and abroad. There are comparatively few prospective oil territories that cannot be worked with reflection methods.

For general structural reconnaissance, gravimeter surveys to locate regional structural trends have been and are being conducted on a large scale along the coastal belt of the Gulf and in the northern parts of Texas and in the mid-continent. The torsion balance has successfully located or detailed general structure-type fields in Texas, Oklahoma, California, New Mexico and other states. For the fault-type of structure, magnetic methods are probably not recommendable for first place in reconnaissance surveying. Even if basement rocks are expected to be somewhat conformable to the oil-bearing series, they usually are too far away to furnish satisfactory information regarding faults—that is, faults of such throw as to be of importance in oil work. However, there are some faults which give a magnetic expression without apparent association with igneous rocks—the indication being directly above the fault plane. In the absence of a definite explanation for this phenomenon, magnetic methods should be relegated to second place for reconnaissance, while first place probably would be given to reflection and possibly torsion-balance methods, for both reconnaissance and detail. Applications of these two methods to the location of faults have been numerous in oil areas of this country and abroad.

In cases where oil occurrence is associated with volcanic intrusions or dikes, the magnetometer is first choice for reconnaissance and detail, and the torsion balance is second. Examples are the intrusions at Monroe and Richland, Louisiana; and Jackson, Mississippi; and the intrusive dikes in the Tampico region of Mexico.

There has been so much work done with geophysical methods in the salt-dome areas of the Gulf coast that the choice of methods in salt dome exploration is very definite, although the order of preference has undergone some changes during the past ten years. For domes down to 5000 to 6000 feet, refraction-seismic work was first choice, but the torsion balance and gravimeter are now more in favor, particularly for the deep domes and for detailing their crests. Reflection-seismic methods are best adapted for

detailing formations above and on the flanks of domes.   The same applies to the salt dome or salt anticline regions of Tehuantepec in Mexico, the northern and north central regions of Germany, Rumania, and other areas of similar geologic structure.

For the buried-ridge type of oil structure, magnetic methods are still first choice for reconnaissance surveying.   However, as pointed out before, care must be exercised in the interpretation of the results.   The magnetic method has been quite successful in general reconnaissance of the Amarillo buried mountains, the Nemaha granite ridge in Kansas and its extension into Oklahoma and Texas, and similar buried-ridge type structures. Pendulum, gravimeter, and reflection-seismic methods are second choice in reconnaissance for this type.   For detail, torsion balance ranks first, reflection-seismic methods second.   Extensive torsion-balance, pendulum, and gravimeter work has been done in the buried-ridge areas mentioned above in connection with magnetic surveys.   Very little has been accomplished by geophysical methods in location of oil pools controlled by porosity variations and not by structure, that is, the lensing type of deposit.   Magnetic work has been reported to be somewhat successful; resistivity methods also appear to be applicable.

As far as the direct location of oil is concerned, it has not been demonstrated beyond all doubt that this is possible by use of the methods available at present.   Indications by the "Eltran" method appear in some cases to be related to shallow stratigraphic conditions above deeper oil accumulations.   Eltran anomalies frequently coincide with hydrocarbon halos revealed by soil analysis methods.   To what extent these methods can be depended upon to furnish reliable oil indications in completely new areas remains to be seen.

The only place where indications can be obtained from the oil itself is underground, that is, by using the electrical logging method in wells. In fact, the resistivities recorded have in some cases been correlated with the productivity of formations.   The advantages of electrical logging are: (1) the increase in drilling speed as mechanical coring is eliminated or reduced to a minimum; (2) correlation of formations which may not have distinct petrographic or paleontological characteristics; (3) the possibility of locating water horizons; (4) continuity of the records; and (5) the ease with which electrical logging may be combined with other procedures, giving important physical data in a drill hole—such as measurement of temperature, side-wall sampling by bullets, and the like.

In geophysical oil exploration it is often impossible to select the most suitable method, since other factors—cost, time, terrain, permits, and secrecy—in addition to the geologic factors, must be considered.   Cost is of principal importance.   It determines whether the work can be done

at all, in view of the available appropriation and anticipated returns, and, if so, which method will be the most economical. Frequently the consideration of cost may lead to the adoption of geological surveying or shallow drilling, where applicable, to replace or at least reduce the geophysical work. Time may be another factor in view of competitive activities or expirations of leases and options, and it may readily lead to the selection of a faster but more expensive, in place of a slower and less expensive, method. Certain terrain conditions, such as swamps and water, will often eliminate some of the methods, for example, torsion balance, gravimeter and magnetometer, from consideration. Fortunately the most important reconnaissance and detail methods—seismic refraction and reflection—can be operated on both land and water. Rugged topography precludes the application of torsion balances, but seismic reflection work is still possible unless conditions are extreme. Adverse surface geologic conditions will handicap many methods, such as heterogeneous glacial beds in torsion balance work, igneous and metamorphic rocks in magnetic exploration, and high-speed surface formations in refraction and reflection shooting. Some types of surveys, for example, those with gravimeters and magnetometers, may be made along public roads without permits, while others requiring the most favorable terrain setups, as torsion balance and some reflection work, will necessitate going on private land. Remarkably free from this restriction is the refraction method, inasmuch as plots of ground for which permits are not obtained may be placed between shot and detector location. In respect to secrecy, operation of gravimeters or magnetometers is much more favorable than is torsion-balance or seismic exploration. Finally, restrictions in regard to the use of dynamite or patented processes may be decisive factors in the selection of a method.

Specific applications of geophysical methods to oil exploration problems will be found in Chapter 7 on pages 157-162, 272-286; in Chapter 8 on pages 422-433; in Chapter 9 on pages 499-501 and in Figs. 9-46, 9-74, 9-85, 9-92, 9-93; in Chapters 10, 11, and 12 on pages 706, 735-739, 752, 835-837, 856, 863-865, 869, 898-901, and in Figs. 10-122 and 10-123.

The role of geophysics in oil exploration is reflected in a statement by De Golyer who says:[2] "With good, not average, practice the cost of oil finding in the early twenties was 20 to 25 cents per barrel. Today on volume operation, the cost of oil finding for good practice is 10 to 12 cents per barrel." It is estimated that geophysics has been responsible for the discovery of over 5 billion barrels of crude oil to 1939.[3]

[2] E. De Golyer, Mining and Metallurgy, **20(391)**, 335 (1939).

[3] G. Egloff, Colo. School of Mines Mag., **29(6)**, 277 (1939).

GEOPHYSICAL METHODS IN MINING

SELECTING the correct geophysical method in mining is not so simple as in oil exploration because of the greater complexity and geologic variety of ore deposits. The choice is often facilitated by the fact that the *type* of ore body to be located is already known. Conditions prevailing in most mining areas (see page 6) eliminate the possibility of gravitational and seismic methods, so that the choice is likely to be magnetic or electrical exploration. Which of these is preferable depends much on the type of ore and its origin.

In the genetic classification of Fig. 5-1 mineral deposits are arranged largely in accordance with the scheme suggested by Lindgren. Geological and geophysical "type" locations, schematics of the geologic form, and suggestions as to choice of direct and structural geophysical methods are given for six groups: (I) *magmatic differentiation deposits*, which are formed by crystallization within magmas and occur, therefore, mostly in intrusive igneous rocks; (II) *heterogenetic solution deposits*, formed by infiltration of solutions from without, usually derived from adjacent igneous formations; (III) *autogenetic solution deposits*, originating from chemical concentration of rock substance; (IV) *sedimentation deposits*, such as salt, coal, and limestone; (V) *dynamo-metamorphic deposits*, formed by concentration and chemical transformation of rock substance in consequence of diastrophic forces; and (VI) *mechanical concentration deposits* in gravels, conglomerates, and the like.

Metal mining is concerned primarily with groups I-III and V-VI. Nonmetallic minerals are derived largely from deposits in group IV.

I. METAL MINING

Surprisingly enough the greatest number of geophysical methods are applicable to location of mechanical concentration (placer) deposits. They may be worked by magnetic methods where a definite relation between gold concentration and black-sand content can be established. For determination of depth to bedrock, resistivity and refraction-seismic

methods may be used.   Extensive magnetic surveys have been conducted on gold deposits of similar type in the Witwatersrand fields of South Africa, where the suboutcrop of the gold series could be traced by virtue
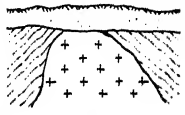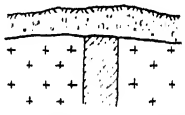
Deposit	Type Locality (Geophysical or Geological)	Geologic Form	Geophysical Method direct	struct.
I. Magmatic Differentiation Deposits				
Diamonds ⎱ in intrusives Platinum ⎰ Chromite	Arkansas Urals Quebec		— — —	magn. magn. magn.(?)
Magnetite	Kiruna, Urals, Colorado		magn. (grav.)	
Sulphide Ores	Nickel ores, Sudbury		elect. magn. (grav)	
II Heterogenetic Solution Deposits				
Contact-metamorphic: 400-800° Magnetite; Specl.Hem. Lead, Zinc Copper	New Mex., Saxony New Mex. New Mex., Arizona		magn. elect.	
100-500° Gold-Silver-Sulphides ⎱ Lead-Silver; Baryte Tungsten, Fluorite Siderite, Molybdenite Quartz & Pegmatite veins	Calif., Nevada, Canada Colo., Illinois N.Mex. Appal.Ontario, Brazil etc.		⎱ elect. — - elect. elect.	⎱ elect. elect., mag.
to 100° Lead - Zinc Ores	Missouri		magn. grav.	

Fig. 5-1a. Genetic classification of mineral deposits and applications of geophysical methods.

of its association with magnetic shales.   Reflection-seismic and electrical methods likewise hold promise in this area for structural investigations.

Much geophysical work has been done on the type of mineral deposits classified above in group II (heterogenetic solution deposits).   An example

is the application of magnetic methods to the mapping of contact-metamorphic iron ores. For the location of contact-metamorphic sulfides, electrical methods have been employed. Magnetic exploration may be of
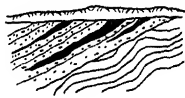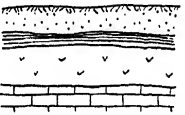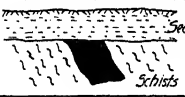
Deposit	Type Locality (Geophysical or Geological)	Geologic Form	Geophysical Method direct	struct.
III. Autogenetic Solution Deposits				
Residual weathering & sec. depos.: Limonite, Hematite, Manganese, Bauxite, Vanadium, Uranium SS	Alabama, Cuba, Arkansas, Colo.		magn. magn. magn.? — radioact.	magn. magn.
Native Copper deposits formed by zeolithization of lavas	Lake Superior (possibly in II ?)			magn.
IV. Sedimentation Deposits				
Inorganic: Minette, Salt, Potash, Gypsum, Limestone, Cement rocks	Clinton, Lorraine, Stassfurt, Carlsbad		magn. resist. seism.	magn. resist. seism.
Organic: Coal, Lignite			elect.	resist. seism.
V. Dynamo-metamorphic Deposits				
Magnetite	Kursk, Adirondacks, N.Y., N.J.		{ magn. { grav.	
Pyrrhotite	Ducktown		elect.	
VI. Mechanical Concentration Deposits				
Gold (also Tin and Platinum) Placers	Alaska, Br. Col., Calif., etc.		magn. (black sand)	elec. seism.
Gold-Conglomerates	Witwatersrand (Possibly in Group II)			magn. seis.(?)

FIG. 5-1b. Genetic classification of mineral deposits and applications of geophysical methods (concluded).

assistance for structural investigations (mapping of intrusives, contact zones, and the like).

Electrical methods have good possibilities in the direct or indirect location of deposits falling in the category of hot-water concentrations. Ex-

amples are: lead sulfides, iron and copper pyrites, cobalt ores associated with other sulfides, and gold-bearing quartz veins. It is often possible to trace the ore-bearing faults or fissures in which mineralized waters are circulating. This method has been applied on tungsten deposits in Colorado and fluorite deposits in Illinois. Magnetic prospecting will frequently furnish valuable structural information in such cases. In the Tri-State district referred to under group II, various methods were tried but no satisfactory way of locating the ore itself was found. Torsion balance measurements appeared to be capable of tracing chert zones associated with the ore and magnetic observations were used to outline highs in the underlying porphyry to which the major ore accumulations appeared to be related. The principal reason for the failure to locate the Tri-State ores directly is that zinc sulfide, unlike other sulfides, is a nonconductor of electricity.

Magmatic-differentiation deposits have been worked principally with magnetic and electrical methods. In part, these applications have been of an indirect nature, such as the location of diamond-bearing intrusions in Arkansas and of platinum ores in intrusive rocks in the Urals by magnetic methods. Chromite has been worked indirectly by its association with igneous rocks and with magnetite. Magnetite deposits of the magnetic-differentiation type have been surveyed primarily with the magnetometer, though torsion-balance and electrical methods have been applied occasionally. Much work has been done on nickel sulfide ores in the Sudbury district with electrical and magnetic methods.

Magnetite deposits of the dynamo-metamorphic type (group V) have been surveyed primarily with magnetic and gravity methods (Kursk). Magnetic exploration likewise has had some success in the location of sedimentary ores, such as iron (hematite) and manganese.

A moderate amount of geophysical work has been done on deposits resulting from concentration of rock substance (group III). Examples are: magnetic surveys of bauxite deposits, radioactive measurements on uranium and vanadium ores, and electrical prospecting for sulfide veins in intrusive rocks. Considerable attention has been given to the possibilities of geophysics in locating copper deposits in the lava flows of the Lake Superior region, but only the magnetic method was found to be successful for determining structural relations of the flows by tracing suboutcrops, faults, and the like.

II. MINING OF NONMETALLICS

Nonmetallic mining is chiefly concerned with mineral deposits formed by chemical precipitation and mechanical sedimentation in surface waters (group IV, Fig. 5–1). In discussing the applications of geophysics in this

field, a classification somewhat different from that customary in economic geology will be adopted.   Petroleum, natural gas, asphalt, and related bitumina will be excluded, and the remainder will be classed as follows: (a) coal, (b) sulfur, (c) salt, (d) nitrates, phosphates, potash, (e) building and road materials, (f) abrasives, (g) materials for various industrial uses, (h) gems and precious stones.

A. Coal, Including Anthracite and Lignite

In this group only anthracite and possibly lignite offer possibilities of direct geophysical location; virtually all other types of coal are amenable to indirect prospecting only.   Anthracite may be located directly by self-potential measurements or resistivity or other electrical methods.   Some anthracitic coals are conductive while some other varieties act as insulators.[1]

In stratigraphic and structural investigations of coal deposits, various methods are applicable.   For general reconnaissance, the magnetic method may be useful if the carboniferous strata are conformable with basement topography.   For the mapping of regional Paleozoic structure, extensive pendulum surveys were undertaken at one time in northern Germany. For detail, electrical resistivity methods have been used.   Examples are the Carboniferous syncline of Villanueva de Minas and Villanueva del Rio in Spain and the Saar coal basin.   Both refraction and reflection-seismic methods can render valuable service in the determination of the structure of Carboniferous areas, as demonstrated in Spain, in Silesia, and in Westphalia.   Under favorable conditions structural studies of the Carboniferous have been made by means of the torsion balance and the gravimeter.

Various geophysical methods have been tried on lignite deposits.   The success of electrical methods appears to depend greatly on the local stratigraphy and the water content of the lignite.   Seismic-refraction methods have possibilities for determining the thickness of lignite beds.   However, structural and stratigraphic investigations may be expected to be more successful as exemplified by Schlumberger's electrical surveys in the department of Landes, France, and by Edge-Laby's and Seblatnigg's torsion balance work on faults associated with lignite deposits in Australia and Germany respectively.

B. Sulfur

Geophysics has been applied on a large scale to the indirect location of sulfur deposits found in the cap rocks of salt domes on the Gulf coast.

---

[1] For details and bibliography see C. A. H., "Geophysics in the Non-Metallic Field," A.I.M.E. Geophysical Prospecting, 546–576 (1934).

Methods ordinarily used for the location of salt domes are applicable, especially gravimetric and seismic methods.

C. Salt

Salt is obtained commercially from salt brines, salt beds, or salt domes. The literature on the location of salt brines is meager and deals only with the type occurring in salt mines. As far as salt domes are concerned, the geophysical problem is the same as in oil exploration (see Chapter 4); for depth determinations of salt beds, seismic and electrical resistivity methods have been used.

D. Nitrates, Phosphates, Potash

It is doubtful whether any commercial geophysical work has been done on these deposits (owing to the abundant supply of nitrate in Chile, and of phosphate in the western United States). Since the commercially important potassium minerals occur with salt, the geophysical methods discussed in the preceding paragraph have found frequent application in the indirect location of potash deposits. Siñeriz' second report[2] contains numerous examples for depth determination of salt beds in Spain. Underground, it appears possible to differentiate between potash beds of different age by measurement of their penetrating radiation.

E. Building and Road Materials

Applications of geophysical methods in this branch of the nonmetallic field overlap with those in engineering and include cement materials, gravel, sand and clay, and building and road stone.

Cement materials possess a number of physical characteristics (for example: high elastic wave speed and density of gypsum, anhydrite, and limestone; electrical resistivity of lime, chalk, and the like) which indicate the best possibilities for electrical and seismic methods.

Electrical, seismic, and (in case of crystalline bedrock) magnetic methods are suitable for the location of gravel, sand, and clay. Further details are given in Chapter 6 under the heading of engineering applications.

A few geophysical surveys have been made for the location of building or road materials. Electrical exploration appears to hold the greatest possibilities, since resistivities of formations depend on their degree of alteration and moisture content. Magnetic methods are often applicable, since rocks preferable from the standpoint of roadbuilding (igneous rocks)

---

[2] J. G. Siñeriz, "La interpretacion geologica de las mediciones geofieieas applicadas a la prospeccion," Inst. Geol. y Minero Espana *Mem.* (1933).

are more magnetic than are sedimentary rocks, and basic (and more magnetic) igneous rocks are preferred to acidic rocks in regard to toughness and abrasive resistance. Seismic methods have good possibilities for the location of road materials as well as for determining their composition, alteration, and general nature.

F. ABRASIVES

Where deposits are of sufficient size, as in the cases of diatomaceous earth, quartz sand and sandstone, the application of seismic refraction and electrical resistivity is indicated.

G. MATERIALS FOR VARIOUS INDUSTRIAL USES

1. *Fluorspar.* As this mineral is usually found in fissure and fracture zones, indirect structural prospecting, or locating of such zones by resistivity or electromagnetic methods is suitable.

2. *Talc* and *soapstone.* One instance is known in the literature where talc formations could be located by an electromagnetic method, since they reacted as poor conductors in contrast with adjacent graphite deposits.

3. *Lithographic stone.* See road and building materials.

4. *Sand* (used as construction material, abrasive, for glass manufacture, molding, filtering, furnace lining, and so on). Provided an application of geophysics is at all economical compared with surface-geological methods, electrical-resistivity method will be most suitable for the delineation of sand lenses.

5. *Monacite sands.* In addition to resistivity and refraction surveys usable for the location of channels (see Chapter 6), radioactivity methods may be applied to sands of high thorium content.

6. *Serpentine.* Magnetic methods are best suited for reconnaissance, to be supplemented by electrical and possibly seismic measurements for detail.

7. *Barite.* Its high density makes the torsion balance or gravimeter applicable, provided that topography is suitable. Barite, being a poor conductor, may be located in more conductive rocks by surface-potential methods. When barite occurs with conductive minerals such as pyrite, almost any electrical method could be suited.

8. *Graphite.* This mineral may be readily located by most electrical methods. It produces strong self-potentials, usually of positive sign.

9. *Magnesite, feldspar, asbestos, mica.* The geologic occurrence of these minerals suggests that any application of geophysical methods (probably magnetic or electrical) would have to be of an indirect nature.

H. Gems and Precious Stones

A direct location of gems by geophysical methods is out of the question. In some instances a survey of the formation in which they occur may be of assistance.   Examples are the peridotite plugs in Arkansas and the blue-ground pipes in South Africa.   Where diamonds occur in sands and gravels of stream and beach deposits, methods discussed under the heading of engineering applications of geophysics may be useful for locating and tracing lenses or channels.

Specific applications of geophysical methods in mining are discussed in Chapter 7 on pages 162, 286-292; in Chapter 8 on pages 409-422; in Chapter 9 on pages 501-502 and Figs. 9-41, 9-49, 9-75; and in Chapter 10 on pages 675-681, 703-706, 739-741, 755-757, 771-773, and 802-805.

6

APPLICATIONS OF GEOPHYSICS IN ENGINEERING

Applications of geophysical methods in engineering are of fairly recent date. Although many engineering problems may be attacked by geophysics, developments have been slow for various reasons: (1) information on the possibilities of geophysics has not been readily available to engineers; (2) few engineering projects compare in commercial scope with oil and mining projects; (3) in near-surface engineering problems geophysical exploration has to complete with surface geology and drilling. It is unfortunately true that numerous engineering projects are still undertaken without consulting a geologist. With an increased appreciation of the advantage of geological advice, an increase in the number of applications of geophysics to engineering problems will undoubtedly follow.

Engineering applications of geophysics may be divided into two classes: (1) geological, and (2) nongeological.

I. GEOLOGICAL APPLICATIONS

These are concerned with: (a) foundation problems; (b) location of construction materials, and (c) water location.

A. Foundation Problems

As shown in Table 4, special problems in this category are: determination of depth to bedrock, of type of rock encountered in dam, aqueduct, canal, tunnel, shaft, harbor, bridge, railway, highway, tramway, subway, and other construction projects. Similar problems in the field of military engineering are tests of foundations for military roads, railroads, shelters, forts, and other underground mining operations. They are best attacked by seismic-refraction and electrical-resistivity and potential-drop-ratio methods. The seismic-refraction method is aided by the considerable velocity contrast existing between overburden and bedrock. Similar conditions prevail in electric potential surveys, since the resistivity of the

TABLE 4

GEOPHYSICAL AND PHYSICAL METHODS IN CIVIL AND MILITARY ENGINEERING

TYPE PROBLEM, GEOPHYSICAL OR PHYSICAL → CHOICE OF METHOD →	DEPTH TO AND CONSTITUTION OF ROCK 1 Potential Electric 2 Seismic Refraction	LOCATION OF BUILDING MATERIAL 1 Potential Electric 2 Seismic Refraction	LOCATION OF WATER 1 Potential Electric 2 Inductive Electric 3 Seismic Refraction	LOCATION OF PIPES AND OTHER METALLIC OBJECTS 1 Magnetic 2 Potential Electric 3 Electro-Magnetic 4 Radio	CORROSION SURVEYS 1 Self-Potential Electric 2 Potential Electric	SOUND DETECTION AND SOUND RANGING 1 Microphone or Geophone	STRAIN GAUGING, EARTHQUAKE AND VIBRATION DAMAGE 1 Strain Gauges 2 Dynamic Response Tests	GAS DETECTION Gas Detectors	THERMAL DETECTION
FOUNDATION AND HYDRAULIC — Earthworks, Dams, Aqueducts, Canals, Shafts, Tunnels, Rivers, and Harbors	X	X	X						
SANITARY — Water Supply, Sewerage, Irrigation, and Drainage	X	X	X	X	X	X			
TRANSPORTATION — Highway, Railway, Tramway, Subway	X	X	X	X					
STRUCTURAL — Bridges; Masonry, Timber, Steel, Concrete Structures	.	X					X		
PIPE LINE — Water, Oil, Gas, Steam, Air			X	X	X	X		X	X

CIVIL ENGINEERING

MILITARY ENGINEERING

LAND WARFARE	Military Roads, Railroads, Military Mining, Field Fortifications	×	×						
	Water Supply, Drainage			×					
	Sound Ranging, Listening Posts						×		
	Buried Explosives, Chemical Warfare				×	×		×	
MARINE	Submarine Signaling, Submarine Detection, Echo Sounding, Iceberg Location						×	×	×
AERIAL	Sound Ranging, Thermal Detection						×		×

overburden is usually lower than the resistivity of the more consolidated bedrock.   Both seismic velocities and electrical conductivities furnish valuable information on the type of rock encountered in dam, tunnel, or similar sites.   Additional information may be obtained by dynamic vibration tests which will give the natural frequency of a building site as well as the elastic moduli and bearing strengths of overburden and bedrock.

B. Location of Construction Materials

This application of geophysics is important in (1) foundation and hydraulic engineering in connection with the construction of dams, canals, tunnels, bridges, and the like; (2) sanitary engineering; (3) transportation engineering (railway, highway, tramway, and subway construction); (4) structural engineering; and (5) military engineering.   Electrical-resistivity, potential-drop-ratio and seismic-refraction methods are applicable; details were given previously in the section on nonmetallics in Chapter 5.

C. Location of Water

The location of water plays an important part in sanitary engineering in connection with water supply, sewage disposal, irrigation, and drainage problems.   In transportation engineering, determination of water levels and water-bearing fissures is essential for subway and tunnel construction. The same applies to military engineering.

Prospecting for water is one of the most difficult tasks in geophysical exploration.   It requires exceptional geologic ability on the part of the geophysicist.   In the ideal case, the geophysicist should be able to (1) locate the water, (2) determine its salinity, and (3) estimate yields.   At the present status of technique, he can rarely hope to predict yields, and he can make only approximate calculations of salinity when working away from wells of known water composition.   Hence, the geophysicist's task is narrowed down primarily to the location of water itself.

Underground waters may be divided as follows[1] in decreasing order of geophysical importance: (1) ground water proper, which includes waters derived from precipitation and "connate" water; (2) fissure water; (3) cavern water; (4) spring water; and (5) water issuing from leaks in water pipes.   Applications of geophysics to waters in the first group are controlled largely by the *geometric disposition of the reservoir*.   The following types are of importance: (*a*) horizontal (or stratigraphic) boundaries; (*b*) lateral confinement by vertical boundaries such as faults, dikes, or fracture zones; and (*c*) erosional boundaries of impervious rocks.

---

[1] See tabulation in C. F. Tolman, *Ground Water*, p. 265, McGraw-Hill (1937) and in Trans. Am. Geophys. Union (1937), Hydrology section, p. 575.

There are three general possibilities for the geophysical location of water: (1) direct, (2) structural, and (3) stratigraphic location.

1. *Direct location.* Water occurring in the form of thermal, saline, or radioactive springs may be located by temperature, electrical, or radio-activity measurements, or by its noise in escaping from pipe leaks. Brine accumulations in salt mines may be found by electrical-resistivity, inductive, or radio-transmission observations. Water occurring in caves and fissures is on the borderline between direct and stratigraphic location, as it is often difficult to decide whether the indication comes from the water as such or from an impregnated medium. Water filling large cavities in limestones or dolomites may be located directly by resistivity measurements or, if it is sufficiently conductive, by inductive or radio methods. Water which occupies fissures is often heavily mineralized and may thus be detected by inductive, resistivity, radioactivity, or radio measurements. Direct application of geophysics to the location of the ground-water table is limited to such special problems as the determination of the vertical moisture gradient by hygrometric observations in different depths and the calculation of the rate of motion of a ground-water stream in wells by salting the water and measuring the rate of motion of the surface potential peak due to the lateral motion of the salt-water front.

2. *Structural water location* involves the attempt to find locations *favorable* for its occurrence. It entails the mapping of certain formations which may or may not be aquifers and which may occur in synclines, troughs, or areas of general depression. Hence, virtually all major geophysical methods are applicable, depending upon whether differences in *density*, *magnetism, elasticity*, or *conductivity* occur on a stratigraphic or erosional boundary. For instance, water-bearing gravel channels and valley fills may be mapped by torsion-balance, seismic, or resistivity methods. The magnetometer may be applied for tracing channels in igneous or metamorphic rocks. If a reservoir is confined laterally by faults, gravitational, seismic, resistivity, or magnetic methods are applicable (if igneous dikes cut through the water-bearing strata). Key beds in large artesian basins have been surveyed by reflection-seismic methods.

In the location of fissure water the function of structural geophysical work is the mapping of fissures or faults. Gravitational, magnetic, seismic, or electrical methods apply, depending upon whether strata with differences in density, magnetic, elastic, or electric properties have been placed in juxtaposition by the faults.

3. *Stratigraphic water location* has for its objective a determination of the condition and depth of the *aquifer* itself. The choice of geophysical methods is here much more limited. Seismic methods are applicable under favorable circumstances as the elastic wave velocity is greater in moist than in dry, unconsolidated formations. More important and inex-

pensive are electrical methods. Their application rests on the fact that water in the pores of a rock changes its conductivity to such an extent that the conductivity of the mineral substance is virtually without effect. Hence, the following factors are effective: (1) porosity, (2) percentage of pores filled, and (3) electrolytic conductivity of the water. The latter depends very much on the degree of stagnation in a rock and complicates the geophysical picture, as the groundwater may be either a good or a poor conductor. Very pure waters are more difficult to locate than waters of fair conductivity. The former requires sensitive electrical-potential methods, while waters of high salinity, particularly connate waters, may also be found by inductive-electrical procedures.

It is further impossible to recognize water by a *specific* value of rock conductivity. The change brought about by the presence of water is not great enough to produce outstanding values; therefore, it would be difficult to select an arbitrary location in virgin territory and to determine the presence and depth of water from the geophysical response. However, where the presence of an aquifer has been established by wells, it is possible to correlate conductivities with water-bearing formations, their depth, type, and thickness, and to follow this type of indication into unknown territory until a complete change in character occurs. With resistivity methods, frequently a "typical" ground-water curve is obtained, which is discussed in greater detail in Chapter 10.

II. NONGEOLOGICAL APPLICATIONS

Though not directly geophysical but closely related to geophysics, since they involve similar techniques, these applications include: (a) dynamic vibration tests of structures, (b) strain gauging, (c) corrosion surveys, (d) pipe and metal location, (e) sound ranging and other acoustic detection methods, (f) gas detection, and (g) thermal detection.

A. Dynamic Vibration Tests of Structures

These tests involve a determination of natural frequency and damping characteristics of completed structures and of models of proposed structures to determine their seismic resistance to earthquakes and artificial vibrations by the free and forced vibration methods. Details are given in Chapter 12.

B. Strain Gauging

The purpose of these measurements is to determine the variations of elastic strains with time in structures and underground workings so that

zones of weakness may be found and failures predicted. In connection with subsidence investigations, mine workings have been thus tested to predict wall or roof failure; shafts and tunnels have been examined in areas of active faults and earthquakes; strain gauges have been installed in important structures, such as Boulder Dam; and like methods have been used on models of dams and other structures.

C. CORROSION SURVEYS

The purpose of these surveys is to follow the process of corrosion, chiefly on buried pipes, and to determine progress made by preventive measures, such as cathodic protection and coating. Two procedures of geophysical exploration are applicable: (1) self-potential surveys and recordings, and (2) resistivity measurements. By self-potential measurements along a pipe, the areas of ingress and egress of current and therefore the zones of greatest destruction of pipe material may be located. Recording fluctuations of spontaneous potentials issuing from buried pipes, gives information about occurrence and time variations of vagabondary currents producing corrosion. Resistivity measurements serve to find areas of high ground conductivity in which, according to experience, corrosion is greatest.

D. PIPE AND METAL LOCATION

Occasionally it is necessary to locate pipes of which the record has been lost. If the lost pipe is part of a network accessible elsewhere, it may be energized by contact and located by following the electromagnetic field surrounding it. Isolated pipes can be found by so-called "treasure finders," consisting of combined radio transmitters and receivers, described in more detail in Chapter 10. Magnetic prospecting can be applied in favorable cases. Methods for the location of buried ammunition and other war machinery, and procedures for the detection of metal and weapons on workers and visitors of mints and penal institutions belong in the same category and require the same or similar procedures.

E. SOUND RANGING AND OTHER ACOUSTIC DETECTION METHODS

As outlined at the end of Chapter 2, (page 37), acoustic detection methods are used for communication, direction finding and noise analysis, position finding, sound ranging, and echo sounding. Applications of these methods in the fields of civil and military engineering are numerous. Acoustic means of communication, particularly at supersonic frequencies, are widely used between surface vessels and submarines, and between submarines and shore stations. Radio-acoustic position finding is a valu-

able aid in navigation. Sound ranging is used in both the army and the navy for locating enemy guns and for determining the range of their own artillery. Direction finding and noise analysis applies in the detection of airplanes, submarines, and enemy sappers, and the location of pipe leaks in sanitary and pipe-line engineering. Echo sounding methods are currently applied in the merchant marine and the navy for measuring the depth to sea bottom. Occasionally they have been applied in the location of icebergs and in finding the depth to fish shoals. An electrical reflection method based on frequency modulation of ultrashort waves has made possible the airplane terrain-clearance indicator.

F. Gas Detection

Gas detection methods are applied in chemical warfare, in pipe-line engineering, and in mine safety work. Detectors have been constructed for both combustible and toxic gases and are used to find leaks in buried gas pipe lines, gases in manholes, mine openings, and the like.

G. Thermal Detection

Thermal-detection methods involve the location of objects by their heat radiation. During the war it was found that planes could be detected by the heat issuing from their exhaust pipes; icebergs have been located at appreciable distances by such detection methods.

PART II

7

GRAVITATIONAL METHODS

I. INTRODUCTION

Gravitational exploration falls in the category of "direct" geophysical procedures by which physical forces are measured at the earth's surface without application of an artificial extraneous field. The field of gravitation is present everywhere and at all times; it is due to the fundamental property of all matter to have mass. Since all masses, regardless of size, exert an attraction upon one another, any method designed to measure the gravitational field will invariably determine the influence of all masses within range and, therefore, lack the depth control possessed by the seismic and the electrical methods. Consequently, direct methods of interpretation (that is, determinations of the depths, dimensions, and physical properties of geologic bodies from surface indications) are rare and applicable only where essentially one single mass produces the gravitational anomaly.

The application of gravitational exploration methods is dependent on the existence of *differences in density* between geologic bodies and their surroundings. Because of the vertical differentiation of the earth's crust in regard to density (due to the general increase of density with depth and the effect of structural movements which have uplifted deeper and denser portions and have placed them in the same level as younger and lighter formations) there occur changes of density in horizontal direction which are essential for the successful application of gravitational methods. For the interpretation of gravity data, it is fortunate that densities remain constant for considerable distances in formations which had their origin in large depositional basins.

Although gravitational exploration is concerned with one field of force only, a number of characteristic parameters exist which lend themselves readily to accurate observation. The magnitude of the gravity vector is determined by measuring the oscillation period of a pendulum or the deflection of a mass suspended from a spring (gravimeter). It is not feasible to measure the absolute direction of the gravity vector in space.

SYMBOLS USED IN CHAPTER 7

a	distance, equatorial radius	a	coefficient
b	distance, breadth	b	coefficient
c	(spring) constant, polar radius	c	coefficient
d	deflection, distance, thickness	d	coefficient
e	distance	e	coefficient
f	frequency	f	focal length
g	gravity		
h	height, elevation, distance	h	humidity
i	dip		
k	gravitational constant		
l	length, thickness		
m	mass	m	coefficient
n	scale reading, coincidence interval	n	number
		o	coefficient
p	pressure	p	coefficient
q	quotient	q	coefficient
r	radius, distance	r	coefficient
s	distance	s	coefficient
t	time	t	coefficient
		u	coefficient
v	volume	v	coefficient
w	width	w	coefficient; weight
x	coordinate		
y	coordinate		
z	coordinate		
A	} earth's moments of inertia	A	astatization
B		B	buoyancy
C		C	constant, curvature value capacity
$\|B\|$	} terrain correction coefficients		
$\|C\|$			
D	depth	D	couple, moment
E	Young's modulus	E	voltage
E.U.	Eötvös unit		
F	force	F	flexure
G	couple per radian	G	gravity gradient
H	height, elevation	H	horizontal force
I	integral		
J	sectional moment of inertia		
K	moment of inertia	K	terrain correction
L	distance, length		

SYMBOLS USED IN CHAPTER 7

M	mass	$\mathbf{M}$	coefficient
N	restoring force	$\mathbf{N}$	coefficient
O	coefficient	$\mathbf{O}$	coefficient
P	porosity	$\mathbf{P}$	coefficient
Q	pyknometer weight		
R	radius, distance	$\mathbf{R}$	differential curvature
S	chronometer rate	$\mathbf{S}$	section, surface, area
T	period		
U	potential		
V	potential	$\mathbf{V}$	static magnification
W	potential	$\mathbf{W}$	weight
X	horizontal force		
Y	horizontal force		
Z	vertical force		
α	azimuth, amplitude	α	coefficient
β	angle	β	coefficient
γ	angle	γ_0	normal gravity
δ	density		
Δ	difference	Δ	torsion balance deflection
ϵ	scale value	ε	elasticity
ζ	elevation		
η	restoring force		
θ	angle	θ	temperature
ι	angle		
κ	labilizing force		
λ	angle		
μ	micron (10^{-4} cm)	μ	rigidity modulus
ν	scale interval		
ξ	angle		
π	3.1416	.	
ρ	radius, distance		
σ	water content		
Σ	sensitivity	Σ	sum
τ	torsion coefficient		
φ	deflection angle, latitude, phase		
Φ	angle		
χ	parallax		
ψ	angle		
ω	angular velocity, angular frequency		

However, differences in its direction between locations may be determined ("deflections of the vertical"). The Eötvös torsion balance is used for measuring the rate of change, or gradients, of gravity and of its horizontal components in horizontal direction. In more common terminology, this measures (1) the north gradient of gravity, (2) the east gradient of gravity, (3) the difference in the maximum and minimum curvatures, and (4) the direction of minimum curvature of an equipotential surface of gravity. For the measurement of the vertical gradient, various instruments have been suggested but they have not come into practical use. There are no methods in present use to measure the potential of gravity; the pendulum and gravity meters measure its first derivative and the torsion balance its second derivatives.

Instruments employed in pendulum exploration rather closely resemble those developed for scientific purposes. The development of a geologically useful gravimeter, attempted repeatedly since the turn of the century, is largely the result of the efforts of commercial geophysicists. On the other hand, the torsion balance, long known to physical science, has been adopted by exploration geophysicists in the form developed by Eötvös, with comparatively minor changes.

The pendulum and gravimeter have been used predominantly in oil exploration to outline large regional geologic features, to determine basement-rock topography, and to locate buried ridges. Owing to its greater accuracy and rapidity, the gravimeter is being used for more local problems of oil geology, for example, location of domes, anticlines, salt domes and general structure. Attempts have also been made to use the gravimeter in mining, primarily for large near-surface ore bodies, to supplement data secured by other geophysical methods.

The torsion balance has been used predominantly in oil exploration for the determination of general geologic structure, mapping of basement topography, and location of buried ridges, anticlines, domes, terraces, faults, volcanic dikes, intrusions, and salt domes. In mining exploration, the following problems have been attacked by the torsion balance: location of iron, copper, and lead ore bodies, faults, dikes, veins, meteors, lignite and barite deposits, and salt domes (exploration for sulfur and potash). Indirectly the torsion balance has been of use in mining in the determination of the thickness of the overburden, mapping of buried channels, and the like.

II. ROCK DENSITIES

A. DETERMINATION OF ROCK DENSITIES

A direct determination of formation densities *in situ* is possible from gravitational measurements if the dimensions and depth of a geologic

body are known from drilling or from other geophysical surveys, or these measurements may be made from a gravimeter traverse across a known topographic feature not associated with structure.[1] The prevalent procedure is to secure representative samples from outcrops, well cuttings, or underground workings, and to test them in the laboratory. Methods of rock-density determination do not differ much from standard physical methods of measuring densities of solids. Difficulties arise only with specimens from unconsolidated formations or with samples of large pore volumes or permeabilities.

1. *Measurement of weight and volume* is widely used for determining densities of surface strata in connection with torsion balance terrain corrections and is practically the only method available for this purpose. A comparatively large quantity of the sample is placed in a cylinder ranging in volume from 1000 to 2000 cc, taking precautions not to alter its pore volume. Cylinder and sample are weighed, and the weight of the empty cylinder is deducted. If mass of the sample is m grams and its volume is v cc, the density $\delta = m/v$. If a great number of determinations have to be made, it is of advantage to use a portable balance with horizontal arm graduated in density units, since the volume of the sample may be kept constant. If the rock sample is solid and of irregular shape, its volume is determined from the amount of water it displaces in a calibrated glass cylinder; for water-soluble samples, alcohol, machine oil, kerosene, toluol, or a saturated solution of the same substance is substituted. Air bubbles must be removed with a brush, by shaking the vessel, boiling the water, or by using an air pump.

2. *The pyknometer* is a small glass flask of precisely determined volume with a ground-in glass stopper extending into a fine capillary to provide an overflow for excessive liquid. It is useful for measuring densities of small specimens only. Determination of three weights is necessary: (1) of the specimen (m); (2) of the pyknometer filled with water (Q); (3) of the pyknometer with specimen (Q'). Then the density of the sample: $\delta = m/(Q + m - Q')$.

3. *Weighing in air and water* is a very common method of density determination. If the weight of a specimen in air is m_0 and under water it is m', the buoyancy $B = m_0 - m'$, and the density $\delta = m_0/B$. An ordinary balance may be adapted to this test by first balancing the sample on the balance in air and then suspending it in water with a fine wire or in a small pan. Allowance for the weight of this pan under water is made by a corresponding adjustment of the balance. Specimens soluble in water are weighed in some other liquid (see paragraph No. 1); the result is multiplied by the specific gravity of the liquid used. Powdered minerals

[1] This applies only to near-surface formations. See L. L. Nettleton, Geophysics, **4(3)**, 176–183 (1938).

and rocks are inclosed in a thin glass tube. Porous specimens are coated thinly with wax, shellac, or paraffin. Clays should be weighed in machine oil of high viscosity. To reduce interference due to surface irregularities, fairly large samples should be used, since the surface is proportional to the second power of the dimensions and the volume is proportional to the third power.
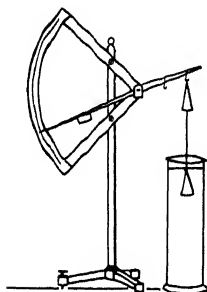
FIG. 7-1a. Schwarz balance for determining specific gravity (after Keilhack).

A number of balances have been designed for the determination of the density of rocks by the buoyancy method. Typical examples are the Schwarz and Jolly balance. The former (see Fig. 7-1a) is designed in the fashion of a letter scale and may be used for light and heavy samples, two ranges being provided by two lever arms and two graduations. In the Jolly balance (Fig. 7-1b) the two pans are suspended from a coil spring whose extension is read on a scale. If the specimen is placed in the upper pan and the index lowered h scale divisions, and is then placed in the lower pan corresponding to a reading of h' divisions, the density $\delta = h/(h - h')$.
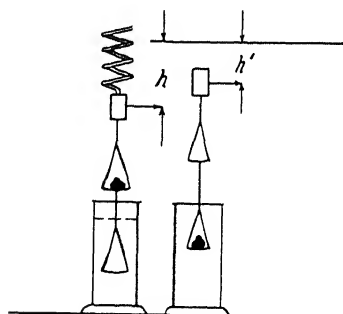
4. The *flotation method* is used for the determination of densities of very small mineral specimens. A specimen is first floated in a liquid of greater density which is then diluted until the specimen neither comes to the surface nor goes to the bottom. At that moment the density of the liquid as determined by a hydrometer is equal to the density of the specimen. Examples for heavy solutions are: bromoform ($CHBr_3$), $\delta = 2.9$; mercury-potassium-iodide (Thoulet's solution, $2HgI_2 \cdot$; barium-mercury-iodide ($HgI_2 \cdot 2BaI$), $\delta = 3.59$; and thalliumformiate, $\delta = 4.76$ at $90°C$.

FIG. 7-1b. Jolly balance

B. FACTORS AFFECTING FORMATION DE

In an evaluation of the applicability of gravitational methods to a g geologic problem, and in the calculation of the effects of geologic bodies of definite properties, it is necessary to make reasonable assumptions in regard thereto or to extrapolate from tabulated values when samples for the desired depth or locality are not available. In order to arrive at correct values, an evaluation of the influence of changes in chemical co

sition, depth of crystallization, porosity, depth of burial, moisture, and so on, is desirable.

1. *Densities of igneous rocks* generally increase with a decrease in SiO_2 content. For instance, the average density of granite is about 2.65, that of gabbro, 3.00; the density of quartz porphyry is 2.63, that of diabase, 2.95; the density of rhyolite is 2.50, that of basalt, 2.90. Holocrystalline igneous rocks solidified at greater depth generally have a higher density than effusive igneous rocks of the same chemical composition. Hence, the igneous rocks older than Tertiary are heavier than Tertiary and younger igneous rocks, as is seen from the tabulations in paragraph 2 following. The density of igneous rocks decreases with an increase in the amount of amorphous material. Igneous magmas solidified as volcanic glasses are generally lighter than magmas with more crystalline matter. For instance, the average density of basalt is 2.90; that of basaltic glass, 2.81; the density of rhyolite is 2.50, but that of rhyolite glass is 2.26.

2. *Mean densities of ore bodies as a function of mineral composition.* Although the density of most commercial minerals is high, its influence upon the mean density of an ore body is not always so great as may be expected because of irregular distribution or lack of concentration throughout the ore body. Table 5, which gives average quantities of commercial ore per 100 tons of mined material, illustrates the small contribution to the mean density of an ore body which may be expected from even the heavy minerals.

TABLE 5

AVERAGE QUANTITIES OF COMMERCIAL ORE PER 100 TONS OF MINED MATERIAL

Iron	25-45 tons	Copper	$1-2\frac{1}{4}$	tons
Manganese	10-25 "	Tin	0.5-1	
Chromium	10-25	Nickel	0.75-2.5	
Zinc	6-12 "	Mercury	0.7-1	
Lead	5-12 "	Silver	0.020-0.075	
		Gold	0.0008-0.0015	

Source: F. Beyschlag, P. Krusch, and J. H. L. Vogt, *Die Lagerstaetten der nutzbaren Mineralien und Gesteine,* Vol. 1, p. 216 (1914).

On the other hand, an association with (usually noncommercial) minerals may increase the mean density of an ore body; for example, if silver or zinc is associated with lead; copper and gold with pyrite; nickel with pyrrhotite, and so on. If the quantities of minerals present are well enough known, it is a simple matter to compute mean densities. For an ore body containing 75 per cent quartz and 25 per cent galena, the resultant density is $0.75 \times 2.6 + 0.25 \times 7.5$, or 3.82. The tests in Table 6 were run on ore samples containing quartz as gangue and containing

varying percentages of iron, copper, and zinc-sulfide ore whose mean density was 4.71.[2]

In some ores the densities are directly dependent on the iron, lead, or copper content; the mean density may then be computed from chemical analyses, as borne out by the correlation of analyses and densities in Table 7.[3]

3. Densities of sedimentary formations change with *porosity, moisture,* and *depth of burial.* The porosity of a rock is given by the ratio of volume weight and density. If δ_d is the dry volume weight ("bulk density"), and δ the density of the substance ("mineral density"), the porosity $P = 1 - \delta_d/\delta$. The density of the sample (powdered, if necessary) may be determined in a pyknometer and the volume weight by the method de-

TABLE 6

Sample No.	Per Cent Ore	Density
1	18.0	3.11
2	24.0	3.32
3	36.4	4.09
4	43.9	4.48

TABLE 7

Sample No.	Iron Content	Density	Sample No.	Iron Content	Density
1	14.33%	2.88	6	43.95%	3.78
2	24.45	3.20	7	47.50	3.92
3	31.10	3.37	8	49.25	4.01
4	31.15	3.37	9	62.35	4.73
5	36.25	3.56	10	63.95	4.83

TABLE 8

Igneous rocks (except pumistone) and metamorphics	1%	3%
Dynamo-metamorphosed sediments	1	10
Consolidated sediments	10	30
Unconsolidated sediments, mostly postcretaceous (except diatomaceous earth and peat)	25	60

scribed under paragraph A-1. Porosity of rocks depends on the degree of consolidation in the course of their geologic history as well as on weathering when exposed at the surface. Igneous rocks have smaller porosities than sedimentary rocks. Table 8 gives a tabulation of average values for *unweathered rocks.*

In the last group, shales and clays show the greatest variation. Immediately after deposition, muds may have porosities as high as 70 to 90 per cent, silts from 50 to 70 per cent, sands from 30 to 40 per cent. Moisture affects their bulk density considerably. Hedberg has determined porosities and densities of clays and sands from many localities.[4]

[2] After H. Reich, *Handbuch der Experimentalphysik,* Vol. XXV, pt. 3, p. 16 (1930).
[3] *Ibid.*
[4] H. D. Hedberg, "The effect of gravitational compaction on the structure of sedimentary rocks," A.A.P.G. Bull., **10(11)**, 1035–1072 (1926).

Weathering may produce appreciable changes in porosities and densities of surface formations, which may have to be allowed for in torsion-balance terrain corrections when they occur near the instrument.

Densities of formations undergo considerable change when their condition is disturbed artificially. Consideration of this effect is important in leveling torsion balance stations in hilly country. The volume weight of soil or clay may be reduced as much as 50 per cent, as shown in Table 9.[5]

TABLE 9

Rock	Bulk Density of	
	Rock in Situ	Fill
Trap	2.992	1.712
Granite	2.720	1.552
Sandstone	2.416	1.376

In the course of their geologic history, sediments are submerged to greater depth and subjected to gravitational pressure and diastrophic forces which bring about an expulsion of excess water, a dehydration of colloids, and a deformation and granulation of soft grains. This results in an apparent increase of density with geologic age. The effect of gravitational pressure on density and porosity may be determined for moderate pressure from experiments on sands, clays, and muds. Hedberg[6] calculated the variation of shale porosity to be expected with variations in overburden thickness. A number of other attempts have been made[7] to express changes in density with depth by a simple formula. However, it is doubtful whether such relations, based on observations in one area, are universally applicable for geophysical purposes, since the variable effects of diastrophism cannot be separated from those resulting from gravitational compaction. For instance, Hedberg's recent density-depth curves[8] (see Fig. 7-2) indicate a much smaller increase of density with depth than do the curves published earlier for the mid-continent. Hedberg concludes that it is best to use different expressions for the ranges 0 to 800, 800 to 6000, and 6000 to 10,000 feet,[9] but for practical convenience he gives the following approximation formula for the entire range (except the first 200 to 300 pounds): P (porosity) $= 40.22 \cdot 0.9998^p$ where p (the exponent) is pressure in pounds per square inch.

---

[5] After A. C. Lane, Geol. Soc. Amer. Bull., **33**, 353–370 (1922).

[6] *Loc. cit.*

[7] W. W. Rubey, Amer. Assoc. Petrol. Geol. Bull., **11**, 621–633, 1333–1336 (1927); U. S. Geol. Survey. Prof. Paper, **165A**, 1–54 (1930).

    L. F. Athy, Amer. Assoc. Petrol. Geol. Bull., **14**, 1–24 (1930), *ibid.*, Sidney Power Mem. Vol., 811–823 (1934).

[8] H. D. Hedberg, Am. J. Sci. **31(184)**, 241–287 (April, 1936), with very complete bibliography on the subject.

[9] Depth in feet and pressure in pounds per square inch are almost equal numerically.

The pores of rocks are usually not filled with air alone, but also with water, oil, and/or gas, of which, for geophysical purposes, water is the most important. It is difficult to estimate the percentage of pores filled; 50 per cent is probably a good average. Water content ranges from 20 to 60 per cent in moderate climates and is less in arid, greater in humid
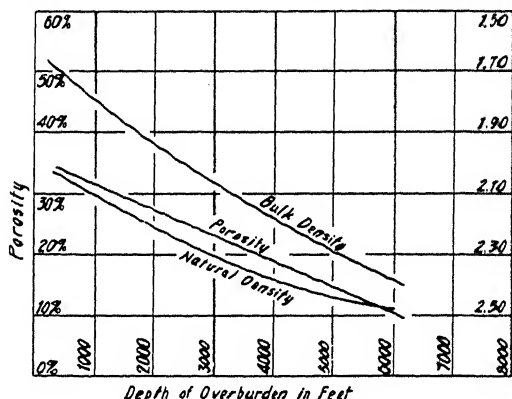
Fig. 7-2. Relation of shale porosity and density to depth, Venezuela (after Hedberg).

TABLE 10

Rock	Density δ	Wet Volume Weight δ_σ
Igneous rocks	2.80	2.80
Clays	2.69	2.51
Sandstones	2.67	2.35
Limestones	2.76	2.64

TABLE 11

Rock	Dry Volume Weight	Wet Volume Weight
Granite	2.58	2.60
Dolerite	2.89	2.90
Basalt	2.87	2.88
Serpentine	2.71	2.71
Schist	2.65	2.67
Shale	2.75	2.72
Sandstone	2.23	2.35
Permian and Triassic sandstone, av.	2.07	2.27
Eocene sandstone	1.86	2.18
Porous limes	1.91	2.20

climates. The wet volume weight (natural density) δ_σ may be computed from the mineral density δ, the pore volume P, and the water content of the pores σ:

$$\delta_\sigma = \delta - \frac{P}{100}\left(\delta - \frac{\sigma}{100}\right). \quad \text{Since } \delta_d = \delta(1 - P),$$

$$\delta_\sigma = \delta_d + \frac{P}{100} \cdot \frac{\sigma}{100}.$$

Table 10 illustrates the effect on density produced by a water content of 50 per cent in the more important types of rocks.[10]

Table 11 shows the difference between dry and wet volume weight (bulk density and natural density) based on actual determinations.[11]

C. TABULATIONS OF MINERAL AND ROCK DENSITIES

Tables 12 through 18, based on the work of many investigators, largely Reich,[12] show density values for (1) minerals, and (2) rocks and formations. They are divided into groups of metallic minerals, nonmetallic minerals, combustible minerals, rock-forming minerals, intrusive and extrusive igneous rocks, volcanic glasses, metamorphics, and sedimentary rocks.

TABLE 12
DENSITIES OF METALLIC MINERALS

MATERIAL	LOCALITY	INVESTIGATOR	DENSITY (δ)	REMARKS
Gold		Fuchs Brauns	15.6–19.4	
Silver		" "	10.5	
Bismuth		" "	9.7	
Copper		" "	8.7	
Sylvanite		" "	8.2	
Cinnabar		" "	8.1	
Uraninite		Reich	8.0–9.7	
Galena		Dana	7.4–7.6	
Argentite		Fuchs Brauns	7.2	
Wolframite		Reich	7.1–7.5	
Nagyagite		Fuchs Brauns	6.8–7.0	
Cassiterite		" "	6.8	
Wulfenite		" "	6.8	
Vanadinite		" "	6.9	
Antimony		" "	6.7	
Bismuthinite		" "	6.5	
Calomel		" "	6.5	
Anglesite		" "	6.4	
Smaltite			6.4–6.6	
Phosgenite		" "	6.2	
Polybasite		" "	6.1	
Arsenopyrite		Reich	6.0–6.2	
Crocoite		Fuchs Brauns	6.0	
Cobaltite		Dana	5.8–6.2	
Pyrargyrite		Fuchs Brauns	5.8	
Cuprite		" "	5.7–6.0	
Hornsilver		" "	5.6	
Proustite		" "	5.6	
Valentinite		" "	6.0	
Psilomelane		Reich	5.5–6.0	

[10] After J. Barrell, Journal of Geology, **22**, 214 (1914).
[11] After H. Reich, *op. cit.*, p. 13.
[12] *Ibid.*

TABLE 12—*Concluded*

DENSITIES OF METALLIC MINERALS

MATERIAL	LOCALITY	INVESTIGATOR	DENSITY (δ)
Chalcocite		Dana	5.5-5.8
Millerite		Fuchs Brauns	5.3
Senarmontite		" "	5.2
Magnetite		" "	4.9-5.2
Franklinite		" "	5.0-5.1
Bornite		" "	5.0
Pyrolusite		" "	4.7 5.0
Hematite		Reich	4.9-5.3
Pyrite		"	4.9-5.2
Tetrahedrite		Fuchs Brauns	4.7-5.0
Molybdenite		Dana	4.8
Markasite		Reich	4.7-4.9
Molybdenite		Fuchs Brauns	4.5-4.9
Stibnite		Dana	4.6
Antimonite		Reich	4.6-4.7
Pyrrhotite		Fuchs Brauns	4.5-4.6
Chromite		" "	4.5
Manganite		" "	4.3-4.4
Enargite		" "	4.3-4.5
Ilmenite		Reich	4.3-4.9
Smithsonite		Dana	4.3 4.5
Rutile		Reich	4.3
Chalcopyrite		Fuchs Brauns	4.1 4.3
Malachite		" "	4.0
Psilomelane		" "	3.7
Zincblende		Reich	3.9 4.2
Azurite		Fuchs Brauns	3.8
Spinel		" "	3.5 4.0
Atacamite		" "	3.8
Covellite		" "	3.8
Siderite		Reich	3.7 3.9
Realgar		Fuchs Brauns	3.4 3.6
Orpiment		" "	3.5
Sphalerite		Dana	3.5 4.0
Limonite		Reich	3.5 4.0
Titanite		Reich	3.5 3.6
Hypersthene		Fuchs Brauns	3.4 3.5
Pharmacosiderite		" "	2.9 3.0
Cobaltbloom		" "	2.9 3.0
Annabergite		" "	3.0 3.1
Cryolite		" "	2.9 3.0
Glauberite		" "	2.7 2.8
Vivianite		" "	2.6 2.7
Thenardite		" "	2.7
Kieserite		" "	2.5 2.6
Brucite		" "	2.3 2.4
Chrysocolla		" "	2.0 2.3
Gaylussite		" "	1.9
Thermonatrite		" "	1.6
Sassoline		" "	1.4

TABLE 13

DENSITIES OF NONMETALLIC MINERALS

Material	Locality	Investigator	Density (δ)	Remarks
Barite		Reich	4.3–4.7	
Corundum		"	3.9–4.0	
Fluorite		"	3.1–3.2	
Magnesite		"	2.9–3.1	
Anhydrite	Beienrode salt dome, Germany	Tuchel	2.9–3.0	
Kaolinite		Ross & Kerr	2.59	
Kaolin			2.5–2.6	
Bauxite		Fuchs Brauns	2.3–2.4	
Phosphate		Reich	2.2–3.2	
Kaolinite		"	2.2–2.6	
Gypsum	Beienrode salt dome, Germany	Tuchel	2.2	
Gypsum	.	Reich	2.2–2.4	
Salt	Gulf coast	Barton	2.16–2.22	Average
Impure salt	Malagash, Nova Scotia	Miller	2.16–2.21	
Salt	"	"	2.14–2.24	
Rock salt		Reich	2.1–2.2	
Older rock salt	Beienrode salt dome, Germany	Tuchel	2.1	
Younger rock salt	" "	"	2.1	
Kainite		Fuchs Brauns	2.1	
Graphite		Reich	2.1–2.3	
Graphite		Fuchs Brauns	1.9–2.3	
Sulfur		" "	1.9–2.1	
Sylvite		Reich	1.9–2.0	
Carnallite		Fuchs Brauns	1.6	Av. values
Carnallite		Tuchel	1.6–1.7	German salt
Potassium salt deposit	Beienrode salt dome, Germany	"	1.6	domes

TABLE 14

DENSITIES OF COMBUSTIBLE MINERALS AND
MISCELLANEOUS MATERIALS

Material	Locality	Investigator	Density (δ)	Remarks
Saltpeter		Fuchs Brauns	2.0	
Borax		" "	1.5–1.7	
Brick		Reich	1.5	
Anthracite		"	1.34–1.46	
Coal		"	1.26–1.33	
Lignite	Germany	Seblatnigg	1.2	
Lignite		Reich	1.10–1.25	
Asphalt		"	1.1–1.2	
Peat		"	1.05	
Ozokerite		Fuchs Brauns	0.94–0.97	
Ice		Ambronn	0.88–0.92	
Wood		Reich	0.7–1.0	
Petroleum		"	0.6–0.9	
Snow		Ambronn	0.125	

Table 15
DENSITIES OF ROCK-FORMING AND OTHER MINERALS

MATERIAL	LOCALITY	INVESTIGATOR	DENSITY (δ)
Zircon		Fuchs Brauns	4.6–4.7
Garnet		Reich	3.8 4.2
Topaz		Fuchs Brauns	3.5 3.6
Diamond		" "	3.5 3.6
Olivine		Reich	3.3 3.4
Epidote		"	3.3 3.5
Zoisite		"	3.3 3.4
Augite		"	3.2 3.6
Apatite		"	3.2
Andalusite		"	3.1 3.2
Tourmaline		"	3.1 3.2
Pyroxene & amphibole		"	3.0–3.5
Hornblende		Dana	3.0 3.3
Dolomite		Reich	2.85 2.95
Mica		"	2.8 3.0
Beryl		Fuchs Brauns	2.7
Chlorite		Reich	2.6 2.7
Calcite		"	2.6 3.8
Talc		"	2.6 2.8
Nephelite		"	2.58 2.64
Flint	Kansas	George	2.54
Quartz		Reich	2.5 2.65
Feldspars			
Oligoclase		Dana	2.66
Albite		Reich	2.61–2.64
Feldspar		"	2.5 2.8
Orthoclase		"	2.5 2.58
Serpentine		"	2.5 2.7
Leucite		"	2.45 2.5

Table 16
DENSITIES OF IGNEOUS ROCKS

MATERIAL	LOCALITY		DENSITY (δ)
1. *Intrusive Rocks*			
		Reich	2.99 3.08
Hornblende-gabbro			2.98 3.18
Pyroxenite			2.93 3.34
Gabbro			2.89 3.09
Olivine-gabbro			2.85 3.06
Nephelite-basalt		and	2.85 3.0
	Scotland	Phemister	
Igneous rocks		Barrell	2.8
Peridotite		Reich	2.78 3.37
Diorite		"	2.72 2.99
Norite		"	2.70 3.24
Essexite		"	2.69 3.14
Quartz-diorite		"	2.62 2.90
Syenite		"	2.60 2.95

Table 16—*Concluded*
DENSITIES OF IGNEOUS ROCKS

MATERIAL	LOCALITY	INVESTIGATOR	DENSITY (δ)	RE-MARKS
Anorthosite		Reich	2.64–2.94	
Granite		"	2.56–2.74	
Nephelite-syenite		"	2.53–2.70	
2. Extrusive Rocks				
(a) Older than Tertiary				
Diabase		Reich	2.73–3.12	
Melaphyre		"	2.63–2.95	
Porphyrite		"	2.62–2.93	
Porphyry		"	2.60–2.89	
Quartzporphyrite		"	2.55–2.73	
Quartzporphyry		"	2.55–2.73	
(b) Younger than Tertiary				
Picrite		Reich	2.73–3.35	
Basalt		"	2.74–3.21	
Andesite		"	2.44–2.80	
Dacite		"	2.35–2.79	
Trachyte		"	2.44–2.76	
Phonolite		"	2.45–2.71	
Rhyolite		"	2.35–2.65	
3. Volcanic Glasses				
Basaltic glass		Reich	2.75–2.91	
Andesite- and porphyrite glass		"	2.50–2.66	
Vitrophyre		"	2.36–2.53	
Obsidian		"	2.21–2.42	
Rhyolite glass		"	2.20–2.28	

TABLE 17
DENSITIES OF METAMORPHIC ROCKS

MATERIAL	LOCALITY	INVESTIGATOR	DENSITY (δ)	REMARKS
Eclogite		Reich	3.20–3.54	
Jadeite		"	3.27–3.36	
Pre-Cambrian	Hazeldean, Ont.	Miller	3.0	
Amphibolite		Reich	2.91–3.04	
Serpentine		"	2.80–3.10	
Pre-Cambrian	Leitrim, Ont.	Miller	2.8	
Chloritic slate		Reich	2.75–2.98	
Slate		Hedberg	2.7 –2.85	
Haelleflinta		Reich	2.70–2.86	
Phyllite		"	2.68–2.80	
Siliceous lime		"	2.67–3.11	
Quartzitic slate		"	2.63–2.91	
Marble		"	2.63–2.87	
Gneiss		"	2.50–3.0	
Granulite		"	2.57–2.73	
Schists		"	2.39–2.87	
Graywacke		"	2.6 –2.7	

TABLE 18

DENSITIES OF SEDIMENTARY ROCKS

MATERIAL	LOCALITY	INVESTIGATOR	DENSITY (δ)	REMARKS
		Soil, Clay, and Various Formations		
Clay, potash-bearing		Ross & Kerr	2.46	
Marl, Lower Triassic	Scotland	McLintock & Phemister	2.4	Keuper Marl
Jurassic formations		Tuchel	2.3 2.5	
Marl, Lower Triassic		"	2.3 2.5	
Clay, Basal Pennsylvanian	Fulton, Mo.	Hedberg	2.37	White flint clay
Clay, grey	Malagash, N. S.	Miller	2.15	
Overburden	Kassel, Germany	Seblatnigg	2.1	
Soil, stamped wet		Reich	2.1 2.2	
Tertiary formations		Tuchel	2.0 2.4	
Sediments	Gulf coast	Barton	1.9 2.05	From surface to 500 ft.
Sediments	" "	"	2.20	From 2000-4000 ft.
Sediments	" "	"	2.25	From 4000-8000 ft.
Sediments	" "	"	2.30	From 8000-12,000 ft. (average values at these depths)
Drift	Leitrim, Ont.	Miller	1.8	0-70 ft.
Clays & sands	Glasgow, Scotland	McLintock & Phemister	1.72	
Loam, sandy wet		Reich	1.7 2.2	
Soil, stamped dry		"	1.6 1.9	
Clay, Mio-Pliocene	Crossley, N. J.	Hedberg	1.66	
Alluvium, recent	Missouri River, St. Charles Co., Mo.	"	1.54	Air-dried
Soil		Reich	1.5 2.0	
Clay, Cretaceous	Richland Co., S. C.	Hedberg	1.51	Mittendorf white clay
Loess, Pleistocene	Collinsville, Ill.	"	1.43	
Clay, Miocene	Yorktown, N. J.	"	1.30	Yellow Alloway clay, depth 4'

TABLE 18—*Continued*

DENSITIES OF SEDIMENTARY ROCKS

Material	Locality	Investigator	Density (δ)	Remarks
Soil, loose dry		Reich	1.3	
Top soil, wet		"	1.2–1.7	
Top soil, dry		"	1.1–1.2	
Sands, Sandstones, and Conglomerates				
Carboniferous sandstone & ironstone	Glasgow, Scotland	McLintock & Phemister	2.38	
Black River, Chazy sandstone	Hazeldean, Ont.	Miller	2.7	
Sandstones		Barrell	2.67	
Sandstone	McLean Co., Ky.	Russel	2.64	
Sandstone		Reich	2.59–2.72	
Potsdam sandstone	Leitrim, Ont.	Miller	2.5	
Gravels & sand, compacted		Reich	2.5	
Conglomerate	Malagash, N. S.	Miller	2.35–2.38	
Sandstone, Triassic	Germany	Seblatnigg	2.35	
Sandstone	Malagash, N. S.	Miller	2.32–2.67	
Variegated sandstone		Tuchel	2.3	
Sandstone, Triassic	Beienrode salt dome, Germany	"	2.25	
Sandstone	Malagash, N. S.	Miller	2.25–2.45	
Quartz sand, wet		Reich	2.2–2.3	
Conglomerates		"	2.1–2.7	
Coarse gravel, dry		"	2.0–2.2	
Woodbine sand		Brankstone, Gealy & Smith	1.95	
Gravel, wet		Reich	1.9–2.1	
Sand, wet		"	1.7–1.9	
Sand, dry		"	1.4–1.7	
Shales				
Shale, Permian	Salina, Kan.	Hedberg	2.39	Wellington shale
Shale, Pennsylvanian	Fulton, Mo.	"	2.29	Cherokee shale (weathered)
Shale, Pennsylvanian	Independence, Kan.	"	2.31	Chanute shale
Shale, Pennsylvanian	Bonner Springs, Kan.	"	2.28	Weston shale

TABLE 18—*Concluded*

DENSITIES OF SEDIMENTARY ROCKS

MATERIAL	LOCALITY	INVESTIGATOR	DENSITY (δ)	REMARKS
Shale, Black, Commanchean	Falun, Kan.	Hedberg	2.12	From Mentor beds
Shale, Upper Cretaceous	Hamilton Co., Kan.		1.98	Graneros shale
Shale, Devonian	Hannibal, Mo.		2.32	Hamilton shale
Shale, black	Irvine Field, Ky.		2.57	
Shale, red	Malagash, N. S.	Miller	2.56	
Shale, red	Malagash, N. S.	Miller	2.50	
Chazy shale & sandstone	Leitrim, Ont.		2.5	At 200 ft.
Shale		Brankstone, Gealy & Smith	2.36	
Shales		Reich	2.3-2.6	
Shales, yellow	Malagash, N. S.	Miller	2.17-2.30	
Shales	Venezuela	Hedberg	2.0-2.45	Increasing with overburden
Shales, Tertiary	Beienrode salt dome, Germany	Tuchel	1.9	

Limestones and Dolomites

MATERIAL	LOCALITY	INVESTIGATOR	DENSITY (δ)	REMARKS
Anhydrite	Beienrode salt dome, Germany	Tuchel	2.9	
Dolomite	Leitrim, Ont.	Miller	2.8	
Dolomite, Beekmantown	Hazeldean, Ont.	"	2.8	
Limestones		Barrell	2.76	
Limestone	Leitrim, Ont.	Miller	2.7	At 588 ft.
Limestones		Reich	2.68-2.84	
Limestones	Kansas	George	2.67	
Cap rock	Gulf coast	Barton	2.6	Average
Shales & limestone	Leitrim, Ont.	Miller	2.6	At 158 ft.
Gypsum & anhydrite	Beienrode salt dome, Germany	Tuchel	2.6	
Shell limestone		"	2.4-2.6	
Limestone		Brankstone, Gealy & Smith	2.07	
Chalk		Reich	1.8-2.6	

III. GRAVITATIONAL CONSTANT; GRAVITY COMPENSATOR; GRAVITY MULTIPLICATOR

The mutual attraction of all masses is governed by Newton's law of gravitation which states that the attraction of two masses m_1 and m_2 is proportional to their product and inversely proportional to the square of the distance between them,

$$F = \frac{k \cdot 1}{}$$ (7-1)

where F and k are measured in dynes if m is in grams and r in centimeters. When $m_1 = m_2 = r = 1$, $F = k$; hence, k (called the *gravitational constant*)

is the force of attraction between two equal masses of **1** g. each at a distance of 1 cm. Its dimension in the C.G.S. system is $gr^{-1} \cdot cm^3 \cdot sec^{-2}$; although it is exceedingly small (about one 15 billionth part of gravity), it may be determined accurately from the force exerted by large masses upon small masses at a known distance.

The Cavendish torsion balance is generally used in making these measurements. The force may be determined statically (by measuring deflections) or dynamically, that is, by observing the period of oscillation of the balance beam under the influence of known masses. Fig. 7–3a shows arrangements of deflecting masses M in reference to the deflected beam of the length $2l$, carrying two small

Fig. 7–3a. Arrangements for the static and dynamic determination of the gravitational constant (after Heyl).

masses m at its ends. The angle of deflection, φ, is measured at great distances from the balance with telescope and scale. Sometimes the double deflection is observed by revolving the masses M about a horizontal axis to the other side of the small masses. For the single deflection, the gravitational constant follows from

$$k = \frac{\tau \varphi r^2}{2Mml},$$ (7-2)

where τ is the torsional coefficient of the wire, and r the distance between M and m. A correction is applied since, for very small distances, the mass of M may not be assumed to be concentrated in its center of gravity.[13]

[13] P. R. Heyl, "A Redetermination of the Newtonian constant of Gravitation," Proc. Natl. Acad. Sci., **13**(8), (Aug., 1927).

In the dynamic method the period of oscillation of the beam is determined with an arrangement shown in Fig. 7-3a and 7-3b.   The large masses are used first in the extension of the beam and second with their axis at right angles to the beam.   Heyl,[14] using masses of 66 kg each for the deflectors, a beam 20 cm long with platinum balls of 54 g each, and a scale distance of 3 m, obtained a difference in the two periods of oscillation in the two deflector positions of about 330 seconds.   The transits of the beam were
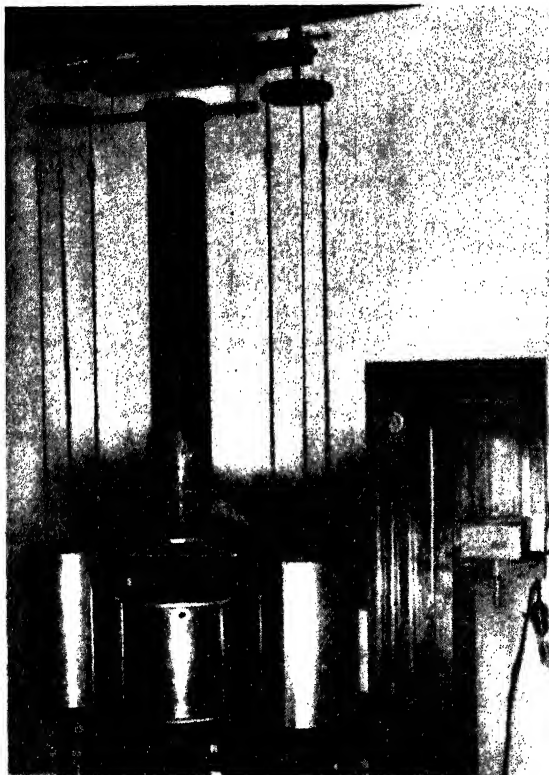
Fig. 7-3b. Torsion-balance arrangement for the determination of the gravitational constant (after Heyl).

recorded on a chronograph, with second signals from a Riefler clock. Heyl reduced the mean error of measurement to $\pm 0.002 \cdot 10^{-5}$ C.G.S., and obtained for k the value of

$$k = 6.664 \cdot 10^{-8} \text{ C.G.S.}$$

which is considered the most accurate value now available.

[14] *Loc. cit.*

It has been proved by a number of experiments that the gravitational constant does not change with the chemical or physical nature of the masses used. By the measurement of the gravitational constant, not only is the proportionality factor in Newton's law determined, but an experiment of greater physical significance is made. Since gravity is the earth's attraction upon a mass of 1 g, and since, from Newton's law, $M_E = (gR_m^2)/k$, (g is gravity, M_E the mass of the earth, and R_m its mean radius) it is seen that determination of the gravitational constant is equivalent to *weighing the earth*. As the earth's volume can be calculated, its mean density, δ_m, may be obtained from the gravitational constant:

$$\overline{\frac{1.0014}{k}}$$

where $g_{45} = 980.616$ cm·sec^{-2}, and $R_m = 6.371 \cdot 10^8$ cm. This relation yields 5.53 for the mean density of the earth.
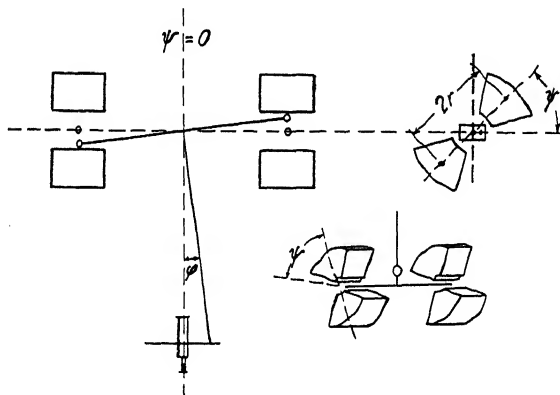
FIG. 7-4. Eötvös gravity compensator (adapted from Jung).

To increase the effect of gravitating masses upon the torsion balance, Eötvös[15] designed the gravity compensator and the gravity multiplicator. The instruments incorporate a regular torsion balance of the first type (curvature variometer), provided with four sector-shaped deflectors whose position may be changed by rotation about a horizontal axis (see Fig. 7–4). In vertical position the attraction of the deflectors is a minimum; when arranged in horizontal direction, it is a maximum. If the balance beam is in the center of the case, the attraction of the deflectors is zero because of their symmetrical disposition; however, if a small deflection, φ, is produced by an outside mass whose attraction is to be measured, the deflectors become effective since they are now unsymmetrically disposed

[15] R. v. Eötvös, "Untersuchungen ueber Gravitation und Erdmagnetismus," Ann. d. Phys. und Chem., **59**, 392 (1896).

with respect to the beam. If $\mathbf{D}$ is the couple produced by an outside mass (or by the "curvature" effect of the gravitational field), and $G \cdot \varphi$ is the couple produced by the gravity compensator, then $\tau \varphi = \mathbf{D} + G\varphi$. It is seen that τ, the torsional coefficient of the wire, is reduced to $\tau - G \equiv \tau'$ by the action of the deflectors and that the balance becomes more sensitive. The "apparent" torsion coefficient is given by

$$\tau' = \tau - \frac{kKM}{r^3} (1 + 3 \cos 2\psi), \qquad (7\text{-}4)$$

where K is the moment of inertia of the balance beam, M the deflector mass, r the distance from the beam and ψ the deflector angle from horizontal. The difference between the extreme values of τ (when ψ is 90° and 0°) is $6kKM/r^3$. With the arrangement used by Eötvös (very thin wires, $\tau = 0.15$, $M = 40$ kg, $r = 10$ cm, and $K = 20,000$ C.G.S.) it is possible even to overcompensate external gravity forces. The gravity compensator is applicable in gravitational model experiments not only with a curvature variometer but with a gradient variometer as well.

The gravity multiplicator is essentially a gravity compensator for "dynamic" measurements. The deflector positions are changed in synchronism with the beam oscillations and thereby the beam amplitude is gradually increased.

IV. PRINCIPLES OF GRAVITATION AS APPLIED IN GRAVITY MEASUREMENTS

As in all geophysical problems involving fields of force, the analysis of the gravitational field makes extensive use of two parameters, the field vector and the potential. The gravity field vector has the peculiarity that its three space components are very unequal; the horizontal components are small and the vertical component is almost equal to the total vector. The force of gravity, that is, the pressure which 1g mass exerts on its base, is measured in units of $g \cdot cm.sec^{-2}$, or dynes, and is numerically but not physically equal to the acceleration of gravity measured in units of $cm.sec^{-2}$, or "Gals."[16] Convenient practical units are the milligal, or 10^{-3} Gal, and the microgal, or 10^{-6} Gal. Gravity varies from 9.78 m·sec^{-2} at the equator to 9.83 m·sec^{-2} at the pole. Gravity anomalies rarely exceed 100 milligals.

The potential of the gravity field is frequently employed in its analysis since, contrarily to the vector, it is a scalar quantity. Its first negative derivatives with respect to the coordinates represent the components of gravity. The gravity potential at the earth's surface may be defined as

---

[16] Named after Galileo.

the work performed by a mass of 1 g in falling from space upon the earth. Since the gravity force g, in accordance with Newton's law, is $g = k(M/R^2)$ (M = earth's mass, R = earth's radius), and since work is the product of force and distance, the attraction potential $V = kM/R = 6.25 \cdot 10^{11}$ ergs. The gravity potential may also be defined as potential energy of the unit mass. Since the potential energy of a body of the weight $m \cdot g$ at an elevation h is $m \cdot h$ g and since, at the earth's surface, $g = kM/R^2$, $h = R$, and $V = kM/R$, the potential energy is $m \cdot V$. Actually the system to which this potential is referred is not stationary but rotates with the earth; hence, the potential of the centrifugal force, or $V' = \frac{1}{2}\omega^2(x^2 + y^2)$, must be added to the attraction potential. The total potential at the earth's surface is usually designated by the letter $U \equiv V + V'$; ω is the angular velocity of the earth's rotation, or $2\pi/86,164 \mathrm{sec}^{-1}$. For any point outside a heavy mass, the potential function with all its derivatives of arbitrary order is finite and continuous and controlled by Laplace's equation:

$$\frac{\partial^2 U}{\partial x^2} + \frac{\partial^2 U}{\partial y^2} + \frac{\partial^2 U}{\partial z^2} - 2\omega^2 = 0. \tag{7-5}$$

Points of equal value of U may be connected by "equipotential" ("level," or "niveau") surfaces. The potential gradient in this surface is zero, and no force component exists. Any equipotential surface is always at right angles to the force. The value of gravity can change arbitrarily on a niveau surface; hence, a niveau surface is not a surface of equal gravity. The ocean surface is an equipotential surface of gravity, since the surface of a liquid adjusts itself at right angles to the direction of gravity. The distance of successive equipotential planes is arbitrary and depends on their difference of potential. The difference in potential of two surfaces 1 cm apart is 980 ergs; conversely, the distance corresponding to unit (1 erg) potential difference is 1/980 cm. The interval h between successive planes is a constant and is inversely proportional to gravity, or $C = g \cdot h$, where h is the interval and g gravity.

Fundamentally, the aim of gravitational methods is to measure "anomalies" in the gravitational field of the earth. Since it is not possible[16a] to compensate the normal field by the technique of measurement (as shown in Chapter 8, a compensation of the normal terrestrial field is possible in magnetic instruments), its value must be computed for each point of observation and must be deducted from the observed gravity. The *theorem of Clairaut* makes it possible to calculate the normal distribution of gravity from the mass and figure and the centrifugal force at the surface

[16a] This applies to the total vector and its vertical component. Horizontal gravity components may be compensated (as in the gravity compensator, see p. 87).

of the earth, and to express this distribution as a simple function of lon-
gitude and latitude. The coefficients of the final equation may be deter-
mined from gravity measurements in different latitudes and longitudes,
leading to an empirical formula for the variation of the normal value of
gravity distribution at the surface. The only assumptions made in its
derivation are that the surface of the earth is a niveau surface, and that the
earth consists of concentric and coaxial shells on which arbitrary changes
of density may occur. Stokes and Poincaré showed later that the theorem
of Clairaut follows alone from the assumption that the earth's surface is a
niveau surface and that it is not necessary to assume a distribution of
density in concentric shells.

Referring to Fig. 7–5, consider[165] the potential at the point P' with the
coordinates x_1, y_1, z_1, due to a mass element dm with the coordinates $x, y,$
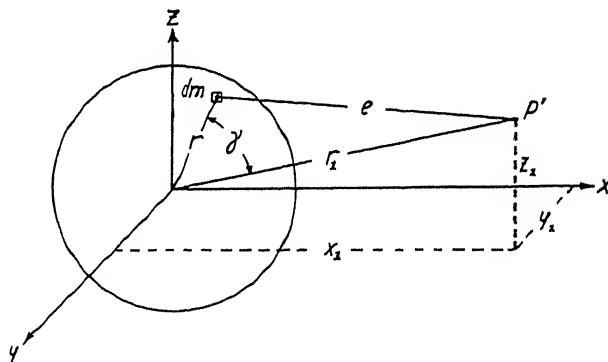
FIG. 7-5. Relation of outside point to mass element in spherical body.

and z. The distance of P' and of dm from the origin is r_1 and r, resp
the angle between them being γ. If the distance between P' and dm is e,
then $V = k(dm/e)$. Further,

$$- x)^2 + (y_1 - y)^2 +$$

$$\cos \gamma - \frac{xx_1 + yy_1 + zz_1}{rr_1}.$$

$$r =$$

and

[165] See also A. Prey, *Einfuehrung in die Geophysik*, p. 60 (1922).

Thus,

$$\frac{1}{e} = (r^2 + r_1^2 - 2rr_1 \cos \gamma)^{-\frac{1}{2}}, \qquad (7\text{-}6a)$$

which may be written

$$\frac{1}{e} = \frac{1}{r_1}\left[1 + \left(\frac{r^2}{r_1^2} - 2\frac{r}{r_1} \cos \gamma\right)\right]^{-\frac{1}{2}},$$

so that by series expansion and considering only terms up to the second order:

$$\frac{1}{e} = \frac{1}{r_1}\left[1 + \cos \gamma \frac{r}{r_1} + \frac{r^2}{r_1^2}\left(-\frac{1}{2} + \frac{3}{2}\cos^2 \gamma\right)\right]. \qquad (7\text{-}6b)$$

Substituting the value given above for $\cos \gamma$, the potential by multiplication with $k \int dm$ becomes:

$$V = \frac{k}{r_1}\int dm + \frac{kx_1}{r_1^3}\int x\, dm + \frac{ky_1}{r_1^3}\int y\, dm + \frac{kz_1}{r_1^3}\int z\, dm$$

$$+ \frac{kx_1^2}{2r_1^5}\int (2x^2 - y^2 - z^2)\, dm + \frac{ky_1^2}{2r_1^5}\int (2y^2 - z^2 - x^2)\, dm$$

$$+ \frac{kz_1^2}{2r_1^5}\int (2z^2 - x^2 - y^2)\, dm + \frac{3x_1y_1}{r_1^5}\int xy\, dm$$

$$+ \frac{3y_1z_1}{r_1^5}\int yz\, dm + \frac{3z_1x_1}{r_1^5}\int zx\, dm. $$

$$(7\text{-}7)$$

The integrals have to be extended over the mass of the whole earth. If we assume the latter to be concentrated in the center of gravity and make it the zero point of the system of coordinates,

$$\int dm = M, \qquad \int x\, dm = \int y\, dm = \int z\, dm = 0;$$

$$\int xy\, dm = \int yz\, dm = \int zx\, dm = 0.$$

The integrals involving the squares of the coordinates are not zero. Assuming that the earth is a three-axial ellipsoid of rotation with three

moments of inertia, A, B, and C, about the three principal axes, l_1, l_2, and l_3,

$$A = \int l_1^2 dm; \qquad B = \int l_2^2 dm; \qquad C = \int l_3^2 dm;$$

when $l_1 = \sqrt{y^2 + z^2}$; $l_2 = \sqrt{z^2 + x^2}$; $l_3 = \sqrt{x^2 + y^2}$; hence,

$$A = \int (y^2 + z^2) dm; \qquad B = \int (z^2 + x^2) dm; \qquad C = \int (x^2 + y^2) dm. \quad (7\text{-}8)$$

Substituting these values in (7-7),

$$V = \frac{kM}{r_1} + \frac{kx_1^2}{2r_1^5}(B + C - 2A) + \frac{ky_1^2}{2r_1^5}(C + A - 2B) + \frac{kz_1^2}{2r_1^5}(A + B - 2C).$$

If we drop subscripts, the location of any surface point may be written in geocentric coordinates:

$$x = r \cos \varphi \cos \lambda \quad \text{and} \quad x^2 = r^2 \cos^2 \varphi \cdot \tfrac{1}{2}(1 + \cos 2\lambda);$$

$$y = r \cos \varphi \sin \lambda \quad \text{and} \quad y^2 = r^2 \cos^2 \varphi \cdot \tfrac{1}{2}(1 - \cos 2\lambda);$$

$$z = r \sin \varphi \qquad \text{and} \quad z^2 = r^2 \sin^2 \varphi.$$

Hence, after combining terms containing φ and λ,

$$V = \frac{kM}{r} + \frac{k}{2r^3}\left(C - \frac{A + B}{2}\right)(1 - 3\sin^2 \varphi) + \frac{3k}{4r^3}\cos^2 \varphi \text{ co}$$

This is the potential of the attraction only. The potential of the centrifugal force must be added to it. Its three components are $C_x = x \cdot \omega^2$; $C_y = y \cdot \omega^2$; $C_z = 0$, when ω is the angular velocity. Thus, the resultant centrifugal force is $\omega^2 \sqrt{x^2 + y^2}$ and its potential is $V' = \frac{\omega^2}{2} \cdot (x^2 + y^2)$. In polar coordinates, $V' = \frac{\omega^2}{2} \cdot r^2 \cos^2 \varphi$. Then the total gravity potential, $V + V' \equiv U$, is

$$U = \frac{kM}{r} + \frac{k}{r^3}\left(C - \frac{A + B}{2}\right)(1 - 3\sin^2 \varphi)$$

$$\frac{3k}{4r^3}\cos^2 \varphi \cos 2\lambda (B - A) + \frac{\omega^2 r^2}{2}\cos^2 \varphi. \quad (7\text{-}9b)$$

This expression may be further simplified by confining the derivation to a *two*-axial ellipsoid, that is, by neglecting the deviation of the equator

from circular shape and by assuming that the two equatorial moments of inertia are equal. Thus, if $A \equiv B$, the final expression for the total potential is

$$U = \frac{kM}{r} + \frac{k}{2r^3}(C - A)(1 - 3\sin^2\varphi) + \frac{\omega^2 r^2}{2} \cdot \cos^2\varphi. \qquad (7\text{-}9c)$$

From this expression, the gravity may be obtained with sufficient approximation, by differentiation with respect to r:

$$g = -\frac{dU}{dr} = \frac{kM}{r^2} + \frac{3k}{2r^4}(C - A)(1 - 3\sin^2\varphi) - \omega^2 r \cos^2\varphi$$

or

$$g = \frac{kM}{r^2}\left[1 + \frac{3}{2Mr^2}(C - A)(1 - 3\sin^2\varphi) - \frac{\omega^2 r^3}{kM}\cos^2\varphi\right]. \qquad (7\text{-}10a)$$

The second and third terms in the first of the above equations are of the second order and are small. Therefore, another simplification may be made by letting $r \equiv a$, that is, by replacing the radius of the earth with the equatorial radius, a. For reasons which will be evident from what is to follow, it is convenient to express g in terms of U. Eq. (7-9b) may be written:

$$U = \frac{kM}{r}\left[1 + \frac{(C - A)}{2Mr^2}(1 - 3\sin^2\varphi) + \frac{\omega^2 r^3}{2kM}\cos^2\varphi\right].$$

By substituting a for r in the brackets,

$$U = \frac{kM}{r}\left[1 + \frac{(C - A)}{2Ma^2}(1 - 3\sin^2\varphi) + \frac{\omega^2 a^3}{2kM}\cos^2\varphi\right].$$

Using the abbreviated notation o for $(C - A)(1 - 3\sin^2\varphi)/2a^2M$ and p for $\omega^2 a^3 \cos^2\varphi/2kM$,

$$g = \frac{kM}{r^2}[1 + 3\mathrm{o} - 2\mathrm{p}]$$

and

$$U = \frac{kM}{r}[1 + \mathrm{o} + \mathrm{p}].$$

$$\left.\begin{array}{c}\\[2.5em]\\[2.5em]\end{array}\right\} \qquad (7\text{-}10b)$$

The r may be eliminated from the last two equations so that

$$g = \frac{U^2}{kM}\frac{1 + 3\mathrm{o} - 2\mathrm{p}}{(1 + \mathrm{o} + \mathrm{p})^2}.$$

The division gives $g = U^2 (1 + o - 4p)/kM$ or in the original notation

$$g = \frac{U^2}{kM} \left[1 + \frac{C - A}{2a^2 M} (1 - 3\sin^2\varphi) - \frac{2\omega^2 a^3}{kM} \cos^2\varphi \right]. \quad (7\text{-}10c)$$

Substituting $1 - \sin^2\varphi$ for $\cos^2\varphi$, and using the abbreviations $s_i \equiv (C - A)/2a^2 M$ and $t \equiv 2\omega^2 a^3/kM$,

$$g = \frac{U^-}{kM} [1 + s - t + \sin^2\varphi(t - 3s)],$$

for which

$$g_\varphi = \frac{U^2}{kM} [(1 + s - t)(1 + \sin^2\varphi(t - 3s))]$$

approximately. The neglected term, $\sin^2\varphi (4st - 3s^2 - t^2)$, is very small, since all terms in the brackets involve the square of the earth's mass in the denominator. As $g = V/r$ and $V = kM/r, 1/r = V/kM$; thus, $g = V^2/kM$. Therefore, the term before the bracket in eq. (7-10c) is the gravity at the equator (since a was previously substituted for r) or rather the portion of gravity due to attraction only. Since the term $(s - t)$ expresses the effect of inertia and centrifugal force upon the attraction, $V^2/kM \cdot (1 + s - t)$ represents the total equatorial gravity, g_a. Substituting g_a for $V^2 (1 + s - t)/kM$, and b' for $(t - 3s)$, we obtain a simple form for the gravity at any point at the surface, thus:

$$\underline{g_\varphi = g_a(1 + b' \sin^2\varphi)} \quad (7\text{-}11)$$

This equation represents gravity as a function of latitude. It will also be convenient to express the earth's radius, r, as a function of latitude. From (7-10b)

$$r = \frac{kM}{U} [1 + o + p].$$

Recalling the significance of the abbreviated notations o, p, s, and t, o may be expressed in terms of s, and p in terms of t: $o = s(1 - 3\sin^2\varphi)$ and $p = (t/4) \cdot \cos^2\varphi$. Thus, for r we have:

$$r = \frac{kM}{U} \left[1 + s - 3s\sin^2\varphi + \frac{t}{4} \cdot \cos^2\varphi \right].$$

Again substituting $(1 - \sin^2\varphi)$ for $\cos^2\varphi$:

$$r = \frac{kM}{U} \left[1 + s + \frac{t}{4} - \sin^2\varphi \left(3s + \frac{t}{4} \right) \right]$$

which may be written with the approximations used before:

$$r = \frac{kM}{U}$$

Since V is kM/r (the attraction potential), the total (attraction and centrifugal) potential at the equator would be

$$U = V\left(1 + s + \frac{t}{4}\right) = \frac{kM}{a}\left(1 + s + \frac{t}{4}\right).$$

Hence, a is $kM(1 + s + t/4)/U$, so that

$$r_\varphi \equiv a(1 - a' \sin^2 \varphi) \tag{7-12}$$

where a' is $t/4 + 3s$.

Resubstituting the values of the coefficients a' and b',

$$a' \equiv 3s + \frac{t}{4} = \frac{3(C - A)}{2a^2 M} + \frac{\omega^2 a^3}{2kM},$$

and

$$b' \equiv t - 3s = \frac{-3(C - A)}{2a^2 M} + \frac{2\omega^2 a^3}{kM}.$$

Their sum is

$$a' + b' = \frac{5}{4}t = \frac{5}{2}\cdot\frac{\omega^2 a^3}{kM},$$

or, substituting c' for $\omega^2 a^3/kM$,

$$a' + b' = \frac{5}{2}c' \tag{7-13}$$

This equation represents Clairaut's theorem. To determine the physical significance of the three coefficients, a', b', and c', use eq. (7-12) thus: $r = a(1 - a' \sin^2 \varphi)$. If φ is 90°, then r is the polar radius, or the minor axis, of the earth ellipsoid, which may be denoted by c. Hence, $c = a(1 - a')$, or

$$a' = \frac{a - c}{a}. \tag{7-14a}$$

The coefficient a' is the ratio of the difference of the polar and equatorial radii, divided by the equatorial radius. It is called the *flattening* (compression). In eq. (7-11), which expresses the variation of gravity with

latitude, the gravity at the pole becomes $g_c = g_a(1 + b')$, if $\varphi = 90°$. Therefore, the coefficient

$$b' = \frac{g_c - g_a}{g_a} \qquad (7\text{-}14b)$$

represents the ratio between the difference of polar and equatorial gravity and equatorial gravity, or the gravitational flattening. Finally, the coefficient

$$c' = \frac{\omega^2 a^3}{kM} = \frac{\omega^2 a}{kM/a^2} = \frac{\omega^2 a}{U/a} = \frac{\omega^2 a}{g_a} \qquad (7\text{-}14c)$$

indicates the ratio of the centrifugal force at the equator to the gravity at the equator. Therefore, the theorem of Clairaut may be stated as follows:

$$\text{geometric} + \text{gravitational flattening} = \frac{5}{2} \times \frac{\text{equatorial centrifugal force}}{\text{equatorial gravity force}}$$

Since this relation involves only surface quantities, the figure of the earth may be computed from a known surface distribution of gravity. From a number of carefully selected stations, gravity as a function of latitude, and thus the coefficient b', may be determined. The coefficient c' is computed from the known velocity of revolution of the earth. Thus, by applying Clairaut's theorem, the flattening may be calculated. With a more rigorous derivation involving spherical harmonics of higher order in (7-6b) and all moments of inertia in (7-8), Clairaut's theorem may be stated in more extended form. If the variation of gravity with longitude, in addition to its change with latitude, is considered,

$$g = g_0(1 + b' \sin^2 \varphi + b'' \cos^2 \varphi \cdot \cos 2\lambda + \cdots). \qquad (7\text{-}15a)$$

By a careful analysis of the distribution of gravity and by eliminating stations with large topographic effects and local anomalies, Berroth has computed the following values for the coefficients in (7-15a):

$$g = 978.046 \; [1 + 0.005296 \sin^2 \varphi$$
$$ {\scriptstyle \pm 4.4}$$
$$+ 0.0000116 \cos^2 \varphi \cos 2(\lambda + 10°) - 0.000007 \sin^2 2\varphi] \qquad (7\text{-}15b)$$

from which follows the flattening as a function of longitude (from Greenwich): $a' = 0.003358 + 0.000012 \cos 2(\lambda + 10°)$. The major axis of the elliptical equator is 10° west of Greenwich. The flattening in this meridian is 1/296.7, and at right angles thereto it is 1/298.9. The mean flattening is 1/297.8. The difference of the equatorial radii is only 150 ± 58 meters. Hence, the equator is practically a circle and is considered as such in all

problems in gravitational exploration involving calculations of normal gravity, normal gravity gradient, and so on.

Likewise, for many problems in geodesy and geophysical science it is desirable to use the same reference surface (namely, an ellipsoid of revolution) for both normal gravity and geodetic measurements. For this reason the International Association of Geodesy adopted at the Stockholm meeting of the International Geodetic and Geophysical Union in 1930 a formula not including a longitude term, based on an ellipsoid of revolution with a flattening of 1/297:

$$g = 978,049 \ (1 + 0.0052884 \sin^2 \varphi - 0.0000059 \sin^2 \qquad \text{(7-15c)}$$

This international gravity formula is now used in all gravity reductions by the U. S. Coast and Geodetic Survey.[17]

V. PENDULUM AND GRAVIMETER METHODS

A. THEORY OF THE PENDULUM ON FIXED AND MOVING SUPPORT

1. *Pendulum on fixed support.* A mathematical pendulum consists of a particle of mass suspended from a point by means of a massless, flexible, inextensible cord. In Fig. 7–6 let m be the mass, l the length of the cord, and θ the angle of deflection from its rest position. In the state of motion the inertia force $m \cdot l \cdot d^2\theta/dt^2$ balances the restoring force $-m \cdot g \cdot \sin \theta$ for sustained amplitudes; the weight component $m \cdot g \cdot \cos \theta$ and the centrifugal force $m \cdot l \cdot (d\theta/dt)^2$ are compensated by the tension of the suspension cord and need not be considered. Hence,

$$\frac{d^2\theta}{dt^2} + \frac{g}{l} \cdot \sin \theta = 0. \qquad \text{(7-16a)}$$

An exact evaluation of this expression leads to an elliptical integral. For small amplitudes, $\sin \theta \equiv \theta$ and

$$\frac{d^2\theta}{dt^2} + \omega^2\theta = 0 \qquad \text{(7-16b)}$$

where $\omega = \sqrt{g/l}$ is the natural angular frequency or the number of oscillations in 2π sec, so that with f as frequency and T as period, $\omega = 2\pi f = 2\pi/T$.

For finite amplitudes, equation (7-16b) does not apply. A solution of (7-16a) is possible by decreasing the order of the differential equation and considering the energy of motion, assuming again that no energy is con-

[17] Personal communication, courtesy of Admiral L. O. Colbert, Director, U. S. Coast and Geodetic Survey.

sumed by friction or damping.   The energy for the maximum amplitude, α, is $m \cdot g \cdot l(1 - \cos \alpha)$,[18] and is equal to the sum of the potential energy, $m \cdot g \cdot l(1 - \cos \theta)$, and the kinetic energy, $\frac{1}{2} m \cdot l^2 \cdot (d\theta/dt)^2$, for the position θ. Hence,

$$dt = \sqrt{\frac{1}{2\omega^2}} \cdot \frac{d\theta}{\sqrt{\cos \theta - \cos \alpha}} \qquad (7\text{-}16c)$$

The period T_α is twice the time required for the pendulum to swing from $\theta = \alpha$ to $\theta = -\alpha$. By substitution of $1 - 2 \sin^2 \theta/2$ for $\cos \theta$ and $1 - 2 \sin^2 \alpha/2$ for $\cos \alpha$,

$$T_\alpha = \frac{1}{\omega} \int_{-\alpha}^{\alpha} \frac{d\theta}{\sqrt{\sin^2 \frac{\alpha}{2} - \sin^2 \frac{\theta}{2}}} \qquad (7\text{-}16d)$$

By introducing the auxiliary angle ψ, so that $\sin \theta/2 = \sin \psi \sin \alpha/2$ and

$$d\theta = \frac{2 \sin \frac{\alpha}{2} \cos \psi \, d\psi}{\sqrt{1 - \sin^2 \frac{\alpha}{2} \sin^2 \psi}},$$

the period

$$T_\alpha = \frac{2}{\omega} \int_{-\frac{\pi}{2}}^{+\frac{\pi}{2}} \frac{d\psi}{\sqrt{1 - \sin^2 \frac{\alpha}{2} \sin^2 \psi}}. \qquad (7\text{-}16e)$$
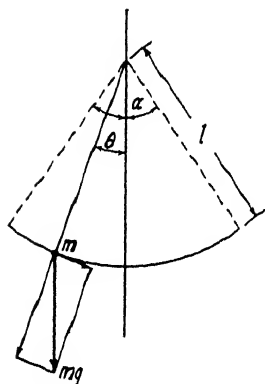
FIG. 7-6. Mathematical pendulum.

The elliptic integral has the form

$$\int_{-\frac{\pi}{2}}^{+\frac{\pi}{2}} \frac{d\psi}{\sqrt{1 - p^2 \sin^2 \psi}},$$

whose solution, (see B. O. Pierce, Table of Integrals, No. 524) is

$$\pi \left[1 + \left(\frac{1}{2}\right)^2 p^2 + \left(\frac{1 \cdot 3}{2 \cdot 4}\right)^2 p^4 + \left(\frac{1 \cdot 3 \cdot 5}{2 \cdot 4 \cdot 6}\right)^2 p^6 + \cdots \right]$$

so that the period

$$T_\alpha = \frac{2\pi}{\omega} \left(1 + \frac{1}{4} \sin^2 \frac{\alpha}{2} + \frac{9}{64} \sin^4 \frac{\alpha}{2} + \cdots \right). \qquad (7\text{-}16f)$$

If the period for small amplitudes is T_o,

$$T_\alpha = T_o \left(1 + \frac{1}{4} \sin^2 \frac{\alpha}{2} + \frac{9}{64} \sin^4 \frac{\alpha}{2} + \cdots \right), \qquad (7\text{-}16g)$$

[18] Partly after L. Page, *Theoretical Physics*, Van Nostrand (1928).

in which for most practical applications it is sufficient to use the angle for its sine so that the "amplitude reduction formula" is

$$T_a = T_o \left(1 + \frac{\alpha^2}{16} + \cdots\right). \qquad (7-16h)$$

For the physical pendulum of the mass M and the moment of inertia K,

$$K \cdot \frac{d^2\theta}{dt^2} = -Mgs \sin \theta$$

where s is the distance of the center of gravity from the axis of rotation (see Fig. 7-7). By comparison with equation (7-16a) it is seen that a physical pendulum, in which $K/Ms = l$ = reduced pendulum length, is isochronous with a mathematical pendulum; its period $T = 2\pi \sqrt{K/Mgs}$.

The reversible pendulum (Fig. 7-8) is a physical pendulum with two knife edges so placed that the period of oscillation about either axis is the same. Their distance is then equal to the length of the equivalent mathematical pendulum. It is for this reason that the reversible pendulum has been and is still being used for the precise determination of *absolute* gravity. The distance between knife edges may be measured by means of a vertical comparator. Determination of absolute gravity by means of the

Fig. 7-7. Physical pendulum.

reversible pendulum is a difficult procedure and requires a number of corrections: (1) for the flexure of the support, (2) for the effect of the surrounding air, (3) for the elastic tension and bending of the pendulum, (4) for changes in temperature, and (5) for the rate of the comparison chronometer.

Inverted or near-astatic pendulums have the advantage of smaller mass, greater periods, and greater sensitivity in period to variations in gravity. The best-known representative is the Lejay-Holweck pendulum.[19] If an ordinary pendulum is suspended from a spring instead of from a massless thread as in Fig. 7-9a, the restoring force of gravity is added to that of the spring. If its spring constant be designated by c_o (see pages 449 and 581), the equivalent spring constant of gravity (force per unit elongation) would be $mg \sin \theta/a$. Since $\sin \theta \approx a/r$, the resultant spring constant $c_r = c_o + mg/r$. It follows further from the equation for the elastic line that the equivalent axis of rotation is
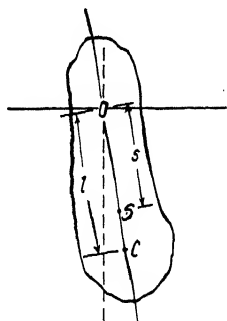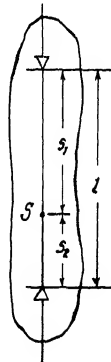
Fig. 7-8. Reversible pendulum.

[19] Comptes Rendues, **186**, 1827-1830 (1928); **188**, 1089-1091 (1929); **190**, 1387-1388 (1930); **192**, 1116-1118 (1931); **193**, 1399-1401 (1931); (1933).
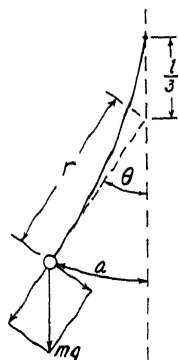
FIG. 7-9a. Suspended elastic pendulum.

located approximately one-third of the spring length from the point of suspension. Substituting, therefore, $\frac{2}{3}l$ for r and $3EJ/l^3$ for the spring constant c_o (where E is Young's modulus of elasticity and J the moment of inertia of the spring section), the resulting spring constant $c_r = 3EJ/l^3 + 3mg/2l$, so that by substitution into $\omega = \sqrt{c/m}$:

$$\omega = \sqrt{\frac{3EJ}{ml^3} + \frac{3g}{2l}} \qquad (7\text{-}17a)$$

In the inverted pendulum the action of gravity tends to drive the mass away from the rest position instead of toward it (Fig. 7-9b); hence,

$$\left. \begin{array}{l} \omega = \sqrt{\dfrac{3EJ}{ml^3} - \dfrac{3g}{2l}} \\[2em] \text{or} \\[1em] T = 2\pi\sqrt{\dfrac{2ml^3}{6EJ - 3mgl^2}} \end{array} \right\} \qquad (7\text{-}17b)$$

FIG. 7-9b. Inverted elastic pendulum.

The change of period with gravity is given by $dT = dg\, T_0 l/(2EJ - mgl^2)$. T becomes infinite when $m = 2EJ/l^2g$. In a derivation not involving the approximations made here, the factor is $\pi^2/4$ instead of 2.[20] Numerical evaluation of eq. (7-17b) shows that in order to obtain any advantage in sensitivity, the mass has to be made so large that the buckling strength of the spring is approached. This can be avoided by using a long bar and a short spring; in the Lejay-Holweck pendulum the length l is several times smaller than the distance L (see Fig. 7-10). With K as the moment of inertia of the pendulum mass, the period and its change with gravity

$$T = 2\pi\sqrt{\frac{K}{c_o - mgL}};$$
$$dT = \frac{dg}{2} \cdot \frac{T}{c_o - mgL} \qquad (7\text{-}17c)$$

FIG. 7-10. Lejay-Holweck pendulum.

With the dimensions used in the Lejay-Holweck pendulum, a change in period of $1 \cdot 10^{-5}$ seconds

[20] A. Graf, Zeit. Geophys., **10**(2), 76 (1934).

sponds to a change in gravity of 1 to 2 milligals. This inverted pendulum is therefore 1000 to 2000 times more sensitive than the ordinary gravity pendulum.

2. *Pendulum on moving support.* The theory of the pendulum on moving support is of equal importance for gravity measurements on vessels and floats and for land observations in connection with the elimination of the flexure of the pendulum support. Details of the theory are given in two publications by Vening Meinesz;[21] only the principal formulas are discussed here. On a moving support three factors alter the period of a pendulum: (1) horizontal accelerations, (2) vertical accelerations of the suspension point, (3) rotational movements of the apparatus.

When rotational movements are kept down by suspending the apparatus in gimbals, horizontal accelerations cause practically the only interference with the movement of the pendulum. This interference may be completely eliminated by swinging two pendulums simultaneously on the same support in the same vertical plane. By extension of eq. (7–16b) the equations for two pendulums may be written

$$\left.\begin{array}{l} \dfrac{d^2\theta_1}{dt^2} + \omega_1^2\theta_1 + \dfrac{d^2y}{dt^2}\cdot\dfrac{1}{l_1} = 0 \\[3mm] \dfrac{d^2\theta_2}{dt^2} + \omega_2^2\theta_2 + \dfrac{d^2y}{dt^2}\cdot\dfrac{1}{l_2} = 0, \end{array}\right\} \qquad (7\text{–}18a)$$

where y is the horizontal coordinate in the plane of oscillation of the pendulums, ω_1 and ω_2 their angular frequencies, θ_1 and θ_2 their amplitudes, and l_1 and l_2 their lengths. When an optical arrangement is provided whereby only the differences in the amplitudes of the two pendulums are recorded, the following equation is obtained for two isochronous pendulums ($\omega_1 = \omega_2$ and $l_1 = l_2$):

$$\frac{d^2\theta_1}{dt^2} - \frac{d^2\theta_2}{dt^2} + \omega^2(\theta_1 - \theta_2) = 0 \qquad (7\text{–}18b)$$

This relation is identical with the equation of motion of a single undisturbed pendulum. It holds for a "fictitious" pendulum with the elongation $\theta_1 - \theta_2$, the same length l and the same frequency ω as the original pendulums. A correction is required if the two pendulums are not isochronous. Denoting the period of the fictitious pendulum by T, that of the first original pendulum by T_1 and that of the second by T_2, the devia-

[21] F. A. Vening Meinesz and F. E. Wright, "The gravity measuring cruise of the U. S. Submarine S 21," Publ. U. S. Naval Observatory (Washington), Vol. XIII, App. I (1930); F. A. Vening Meinesz, "Theory and Practice of Pendulum Observations at Sea," Publ. Netherlands Geodetic Comm. (Delft, 1929).

tion from the isochronous condition may be expressed by an equation of the form $T = T_1 + \Delta T$, with

$$\Delta T = \frac{\omega_2 - \omega_1}{2\omega_2} \int_0^{2T} \frac{\alpha_2}{\alpha} \cdot \cos (\varphi_2 - \varphi), \qquad (7\text{--}18c)$$

where α_2 and α are the amplitudes of the second and of the fictitious pendulum, and φ_2 and φ, respectively, their phases. Since, in practice, the difference $T_2 - T_1$ is usually small compared with T', $\frac{(T_2 - T_1)^2}{T'}$ may be neglected. Letting $\omega_2/\omega_1 = 1$, $\omega_2 - \omega_1 = -\pi (T_2 - T_1)/T'^2$, and considering α_2, α, and $\cos (\varphi_2 - \varphi)$ as constant, we have from eq. (7–18c)

$$\Delta T = -(T_2 - T_1) \frac{\alpha_2}{\alpha} \cdot \cos (\varphi_2 - \varphi). \qquad (7\text{--}18d)$$

The Vening Meinesz pendulum apparatus is designed to record the movements of the fictitious pendulum by reflecting a light beam from one pendulum to the other. In addition, one pendulum is photographed separately to obtain T_2 for the above correction.

Vertical acceleration of a pendulum is equivalent to a change in the value of gravity and produces little change in period, provided the amplitude is kept reasonably constant during the observation. Relative movements of knife edge or slippage on bearings are negligible, provided the amplitude remains sufficiently constant. Rotation about a vertical axis does not affect the period. Rotation about a horizontal axis (inclination of the plane of oscillation) changes the gravity from g to $g \cos \beta$ if β is the angle of inclination. The resulting change in period is

$$\Delta T = \frac{T_1}{4} (\beta_{\text{const.}} + \tfrac{1}{2}\alpha_g), \qquad (7\text{--}18e)$$

where $\beta_{\text{const.}}$ is the constant tilt and α_g is the amplitude of oscillation of the gimbal frame about this position. *Acceleration* imparted to the pendulum in the plane of oscillation by *rotation* about both horizontal and vertical axes produces a change in period,

$$\Delta T = -\frac{T_1^2}{4T_g^2} \alpha_g^2, \qquad (7\text{--}18f)$$

so that by combination with eq. (7–18e)

$$\Delta T = \tfrac{1}{4} T_1 (\beta_{\text{const.}} + C\alpha_g^2),$$

where

$$C = \frac{1}{2} \left(1 - 2 \frac{T_1^2}{T_g^2} \right)$$

$$\left. \right\} \qquad (7\text{--}18g)$$

T_g (the period of oscillation of the frame in the gimbal suspension) and β (the tilt angle) are recorded separately by a highly damped pendulum in marine gravity apparatuses. Lastly, the customary reductions for amplitude, chronometer rate, temperature, and air pressure are applied.

B. Observation and Recording Methods; Pendulum Apparatus

The high accuracy required in pendulum observations is attained by using the "coincidence" or "beat" method. This method may be likened to a vernier. Two nearly equal periods are compared by observing which time "divisions" coincide. The gravity pendulum is compared with a chronometer (or an astronomic clock or reference pendulum) of very nearly the same (or double) period, and the number of chronometer seconds are measured which elapse between two subsequent coincidences, that is,
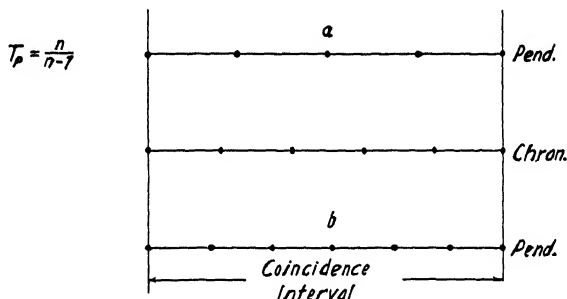
Fig. 7-11. Coincidence method.

between two successive instants when pendulum and chronometer are in phase." The pendulum may lag behind (Fig. 7-11a) or be ahead (Fig. 7-11b) of the chronometer. In case a, the pendulum makes $(n - 1)$ oscillations for n oscillations of the chronometer; in case b, $(n + 1)$ oscillations. The pendulum period is $T_p = \dfrac{n}{n - 1} \cdot T_o$ in the first case and $T_p = \dfrac{n}{n + 1} \cdot T_o$ in the second case. When the periods of the two time pieces are a small integer multiple of each other, that is, if the ratio $T_p/T_o = q$, the coincidence method is applicable if q is slightly less or greater than 1, or slightly less or greater than 2, and so on. Letting T_o (the period of the chronometer) equal *one* second, the following relations apply in the general coincidence case:

$$T_p = \frac{qn}{n \pm q}. \tag{7-19a}$$

By substituting $1/q \equiv \mathbf{v}$:

$$T_p = \frac{n}{\mathbf{v}n \pm 1},\qquad(7\text{-}19b)$$

where n is the coincidence interval. In these formulas the $\frac{\text{upper}}{\text{lower}}$ sign applies if $q \frac{>1}{<1}$ and $\mathbf{v} \frac{<1}{>1}$ (or $\gtrless$ any other integer). They may also be written

$$T_p = q \pm \frac{q^2}{n \mp q},\qquad(7\text{-}19c)$$

and, by substituting the reciprocal of q,

$$T_p = \frac{1}{\mathbf{v}} \pm \frac{1}{\mathbf{v}(\mathbf{v}n \pm 1)}.\qquad(7\text{-}19d)$$

Hence, for a half-second pendulum, compared with a full-second chronometer, $\mathbf{v} = 2$ and therefore

$$T_p = \frac{n}{2n \pm 1}$$

and

$$T_p = \frac{1}{2} \mp \frac{1}{4n \pm 2}.\qquad(7\text{-}19e)$$

If the pendulum swings slower than the chronometer,

$$dT = -\frac{1}{\mathbf{v}n - 1}\cdot dn,\quad\text{and}\quad dg = \frac{-2g}{T}\cdot dT.\qquad(7\text{-}19f)$$

If the pendulum is so made[22] that

$$n = \frac{1}{2\mathbf{v}}\left(\sqrt{8\mathbf{v}g + 1} + 1\right),\qquad(7\text{-}19g)$$

$dg = dn$ and *one millisecond change in coincidence interval* corresponds to *one milligal change* in gravity.

Coincidence intervals may be observed visually (stroboscopic method) or be recorded photographically. In the first method the gravity pendulum is observed only during a short interval when the reference pendulum or chronometer passes through its zero position. Therefore, the image of the gravity pendulum appears in the telescope every second with a dif-

[22] H. Schmehl, Zeit. Geophys., 5(1), 1-15 (1929).

ferent phase, that is, a different distance from the crossweb, and "coincidence" occurs when the pendulum image coincides with the crossweb. For observation of the flashes, light is shone intermittently through a diaphragm upon the pendulum mirror and thence to the telescope; the diaphragm is attached to the armature of an electromagnet actuated by the electric contact in the chronometer or astronomic clock. Light source, electromagnet, and telescope are all mounted in one box (flash box).

For photographic registration of coincidences, Martin[23] has described the arrangement shown in Fig. 7–12. The filament of an electric light bulb is projected by means of lens L_1 and mirror M on a slot placed in the focus of the pendulum lens, L_2. From the pendulum mirror the light is reflected and passes through a cylindrical lens to the photographic plate
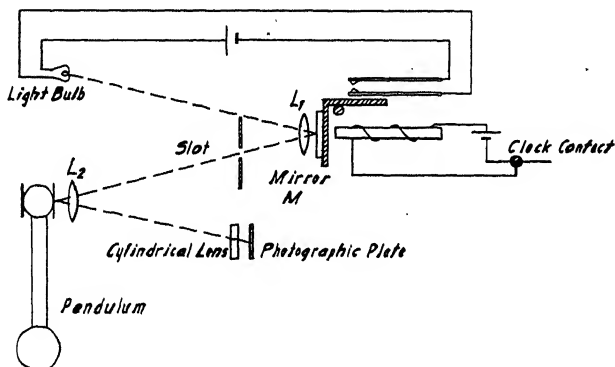
FIG. 7-12. Stroboscopic photography of pendulum by comparison with contact clock (after Martin).

which advances at a slow rate. The mirror M is fastened to the armature of an electromagnet actuated by the chronometer contact. The flashes so recorded (see Fig. 7–13) are arranged in a sine curve; one-half period is the coincidence interval. The photographic plates are evaluated with an accuracy of ± 0.01 mm; the error in determining the coincidence interval is ± 0.03 sec. By observing a sufficient number of coincidences (usually ten), and repeating the procedure after fifty intervals, the accuracy is increased to the point where the mean error of the result is ± 0.0001 (see Table 19). This corresponds to an error in T of $\pm\ 1.2 \cdot 10^{-8}$ sec., or 0.1 milligal in gravity.

In another photographic method, the pendulum oscillations are photographed directly on the same film with accurate time marks and (radio) time signals, transmitted by a chronometer or reference pendulum. The accuracy is increased if two pendulums, swung on the same support with

[23] Zeitschrift für Geophysik, 5(3/4), 148–151 (1930).

opposite phases, are photographed simultaneously. Since the passage of the pendulum through the rest position, with reference to a radio time signal, may be determined with an accuracy of about $2 \cdot 10^{-4}$ sec. and ten successive passages are observed at intervals of about 40 minutes, the period may be measured with an accuracy of about $\pm 2.10^{-8}$ seconds.
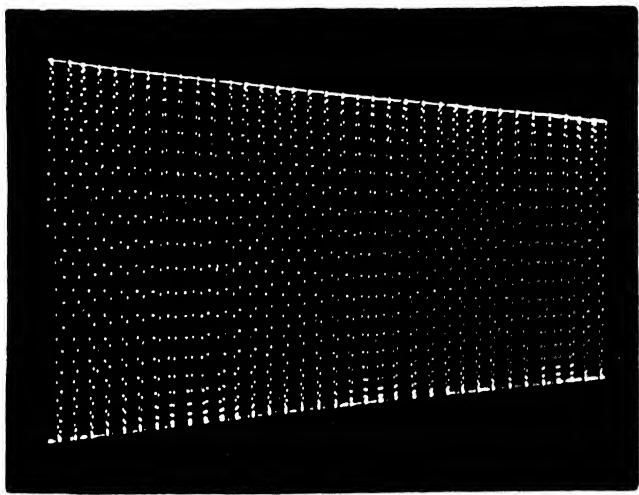
FIG. 7-13. Stroboscopic coincidence record (after Martin).

TABLE 19

EVALUATION OF STROBOSCOPIC COINCIDENCE RECORD[a]

					50 n		P Corr.	
0h 21m	6.92s	20h 58m	33.77s		2246.85	44.9370	0.0192	44.9178 se
	51.88	59	18.71		2246.83	44.9366	.0189	44.9177 "
22	36.82	21 0	3.65		2246.83	44.9366	.0186	44.9180 "
23	21.75		48.59		2246.84	44.9368	.0184	44.9184 "
24	6.69	1	33.53		2246.84	44.9368	.0181	44.9187 "
	51.65	2	18.46		2246.81	44.9362	.0178	44.9184 "
25	36.61	3	3.39		2246.78	44.9356	.0175	44.9181 "
26	21.54		48.32		2246.78	44.9356	.0172	44.9184 "
27	6.47	4	33.25		2246.78	44.9356	.0170	44.9186 "
	51.43	5	18.18		2246.75	44.9350	0.0167	44.9183 "

44.9182 se

[a] After Martin.

In the Vening Meinesz method, the coincidence record (Fig. 7-14) is obtained by interrupting the light beam twice during a full swing. In the actual record (see Fig. 7-15), more vibrations occur between successive passages than indicated in Fig. 7-14, since the difference in period between

the pendulum pair and the chronometer is very slight. If the period of chronometer and pendulum pair were exactly alike, the chronometer breaks would always occur at the same relative positions in the pendulum curves and the phase-lag-sine curve passing through the breaks would be a straight line. If the period of the pendulum pair is greater than the chronometer interval, the chronometer breaks occur at intervals less than a complete cycle (or $\frac{1}{2}$ cycle). The sine curve of the breaks is therefore an expression of the
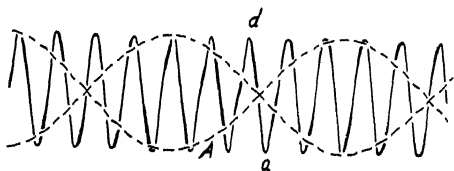
FIG. 7-14. Vening Meinesz pendulum record (schematic).
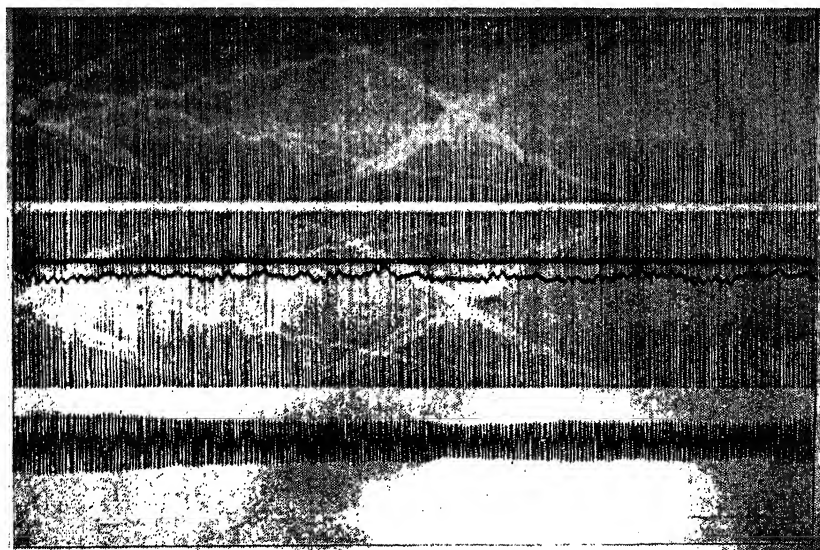
FIG. 7-15. Photographic record of Vening Meinesz pendulum apparatus. *Upper record:* First fictitious pendulum with marks of two chronometers. *Middle record:* Second fictitious pendulum with chronometer marks and record of air temperature and of auxiliary damped pendulum 1, recording the tilt angle. *Lower record:* Record of pendulum 2 recorded with reference to auxiliary damped pendulum 2. (The latter swings in the plane of oscillation of the regular pendulum while auxiliary damped pendulum 1 swings at right angles to that plane.)

receding movement of the pendulum vector whose angular velocity is the phase lag of the pendulum pair.

The evaluation of the record is made as follows. By an automatic mechanism a mark is left off every 60 seconds on the record (for instance, before A in Fig. 7–14). In determining the time of passage of the phase-lag

curve (or the coincidence time interval n) these 60-second markers are used as reference lines. Instead of the breaks themselves being counted, the excursions on the upper or lower side of the record, such as d or a in Fig. 7–14, may be used. If $\Delta\varphi$ is the angular phase lag of the pendulum pair for a complete cycle 2π, the number of oscillations required to complete the 360° cycle is $2\pi/\Delta\varphi$, and the period of the pendulum pair differs from that of the chronometer in the proportion $2\pi/2\pi - \Delta\varphi$; thus,

$$\frac{1}{2} \cdot \frac{2\pi}{2\pi -} \cdots = 0.5 + \frac{0.25}{n - 0.5} \qquad (7\text{-}20)$$

where $2n \equiv 2\pi/\Delta\varphi =$ the coincidence interval.

For absolute and relative determination of gravity, various forms of pendulums have been developed which are described in detail by Swick.[24] Two widely used forms are illustrated in Fig. 7-16. A is the Sterneck-type quartermeter pendulum. The top part is a stirrup holding a knife-edge made of agate or quartz and two mirrors. B is a more recent form known as the "rod" or "minimum" pendulum. In it the knife edge is so placed that a change in its position has a minimum effect on the period. In a physical pendulum the moment of inertia, $K = lMs$ (see page 99), may be considered as the sum of two moments, one with the radius of gyration s about the knife edge and the other with the radius of gyration r about the center of gravity so that $K = s^2M + r^2M$ and $l = (r^2 + s^2)s$. Hence follows by differentiation that

FIG. 7-16. (A) Sterneck pendulum; (B) Meisser bar pendulum.

$$dl = \frac{2r}{\quad} \cdots \frac{s^2}{\quad} \cdots ds. \qquad \cdot 21)$$

For the least change of period T and therefore of reduced pe　　　　ngth l with s, the factor of ds must be zero. This gives $s = r$ and therefore $l = 2s$. For "minimum" pendulums, (1) the reduced length must be twice the distance of the center of gravity from the knife edge, s; (2) the radius of gyration in reference to the center of gravity must be equal to the distance s. It is not difficult to do this for circular rods, since $r^2 = L^2/12 + R^2/4$, where L is the geometric length and R the radius.

[24] H. Swick, Modern Methods for Measuring the Intensity of （　　　U.S. and Geodetic Survey, Serial No. 150.

Pendulum apparatuses have gone through a process of slow development. Although they have been largely replaced by the gravimeter in geophysical exploration, they still retain a fairly important place for deep water marine exploration where it is impracticable to lower remote indicating gravimeters to ocean bottom. The pendulum apparatus for regional geodetic work on land generally consists of an evacuated receiver with one to four pendulums, a lens and prism arrangement for visual observation and recording, a flash box, and a chronometer or reference pendulum. The earlier representatives are the U.S. Coast and Geodetic Survey apparatus, the
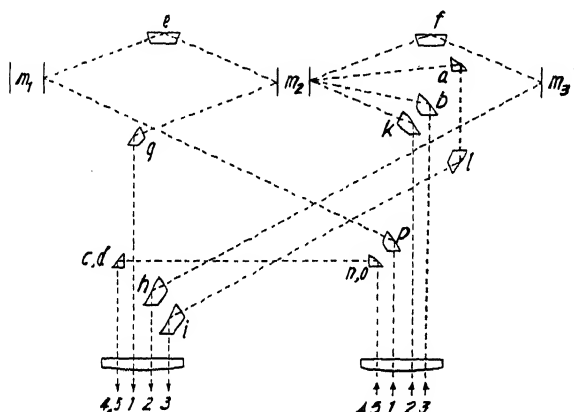
FIG. 7-17. Optical paths in Vening Meinesz pendulum apparatus. No. 1 records $\theta_1 - \theta_2$. No. 2 records $\theta_2 - \theta_3$. No. 3 records θ_2 (the prisms a and b are fastened to the *first* auxiliary pendulum, moving in a plane parallel to the plane of oscillation of the principal pendulums). No. 4 records air temperature (prism c is fastened to a temperature recording device). No. 5 records the position of the second auxiliary pendulum moving in a plane perpendicular to the plane of oscillation of the principal pendulums (prism d is fastened to this pendulum). The horizontal projections of the rays numbered 4 and 5 coincide; the other prisms have a height of 30 mm, but c, d, n, and o have a height of only 12 mm and are above one another. The prisms e, f, g, h, i, k, l, n, o, and p and the lenses are attached to the top plate of the apparatus.

Fechner-Potsdam pendulum, the Askania-Sterneck apparatus, the Meisser 4-pendulum instrument, the Numerov pendulum apparatus. Reference is made to the literature[25] for descriptions and illustrations of these types. Only the Vening Meinesz marine apparatus, the Askania 3-pendulum instrument, and the Brown gravity pendulum of the U.S. Coast and Geodetic Survey will be briefly described here.

In the *Vening Meinesz pendulum apparatus*, three pendulums are sus-

[25] H. Swick, *loc. cit.* A. Berroth, Handb. d. Phys., II(9), 447 (1926). H. Schmehl, Handb. Exper. Phys., 25(2), 216–238 (1931).

pended in the order m_1, m_2, m_3 (see Fig. 7–17) from left to the right, and an optical arrangement is provided to record *two* fictitious pendulums, one representing $\theta_1 - \theta_2$, the second $\theta_2 - \theta_3$. In addition, pendulum 2 is recorded independently with reference to a highly damped auxiliary pendulum in the plane of oscillation of the other pendulums. A fourth record is obtained from a second highly damped pendulum, which swings in a plane at right angles to the plane of oscillation of the regular pendulums, giving the angle of tilt β.[26] Altogether five pendulums are contained in the apparatus. The regular pendulums are as nearly isochronous as possible, the differences in periods not exceeding 50×10^{-7} sec. at normal pressure and temperature. In the damped pendulums, one unit is mounted inside the other, the outer pendulum being filled with oil. The entire pendulum apparatus is suspended in a frame in which it may be leveled by means of four screws. This frame, in turn, is suspended in gimbals.

Many desirable features of the Vening Meinesz pendulum apparatus have been incorporated in the *Askania three-pendulum apparatus*, shown in Fig. 7–18. The receiver is rigidly anchored with three leveling screws and clamps (4) to the base plate (3) and consists of a roughly rectangular case (1) with a hood (2), both made of duraluminum. An air-tight seal is provided between them so that a pressure of about 0.1 mm may be maintained inside for 6 to 7 hours. The three pendulums are arrested and released by three movements (10). During transportation from one station to another an additional mechanism (8) is provided, which secures the pendulum in three sockets; two of these are seen below the mirrors (14) while one of them has been taken out and is shown separately in front (11). Three impulse disks (7) are provided to start the pendulums at the desired time with a phase difference of 180°. The pendulums are of the invariable type, about 430 mm long and 26 mm around. The knife edge is located about 120 mm from the center. The upper surfaces of the pendulums are polished to act as mirrors, reflecting the light on the mirrors (14) through a lens (15) into a recording apparatus shown in the center of the picture. This apparatus may be used with time signals transmitted by radio from a pendulum located at a central station. If the latter is adjusted to match the field pendulums within $2 \cdot 10^{-3}$ seconds, coincidence intervals are around 120 seconds and are determined with an accuracy of 0.2 second. For a two-hour set, an accuracy of $\pm 0.6 \cdot 10^{-7}$ seconds and thus a mean error in gravity of only 0.2 milligal is claimed.

The Brown pendulum apparatus of the U.S. Coast and Geodetic Survey represents a considerable improvement over their earlier type. As in the latter, only one pendulum is used, housed in an air-tight receiver (Fig.

[26] See eq. (7–18e) and (7–18g).
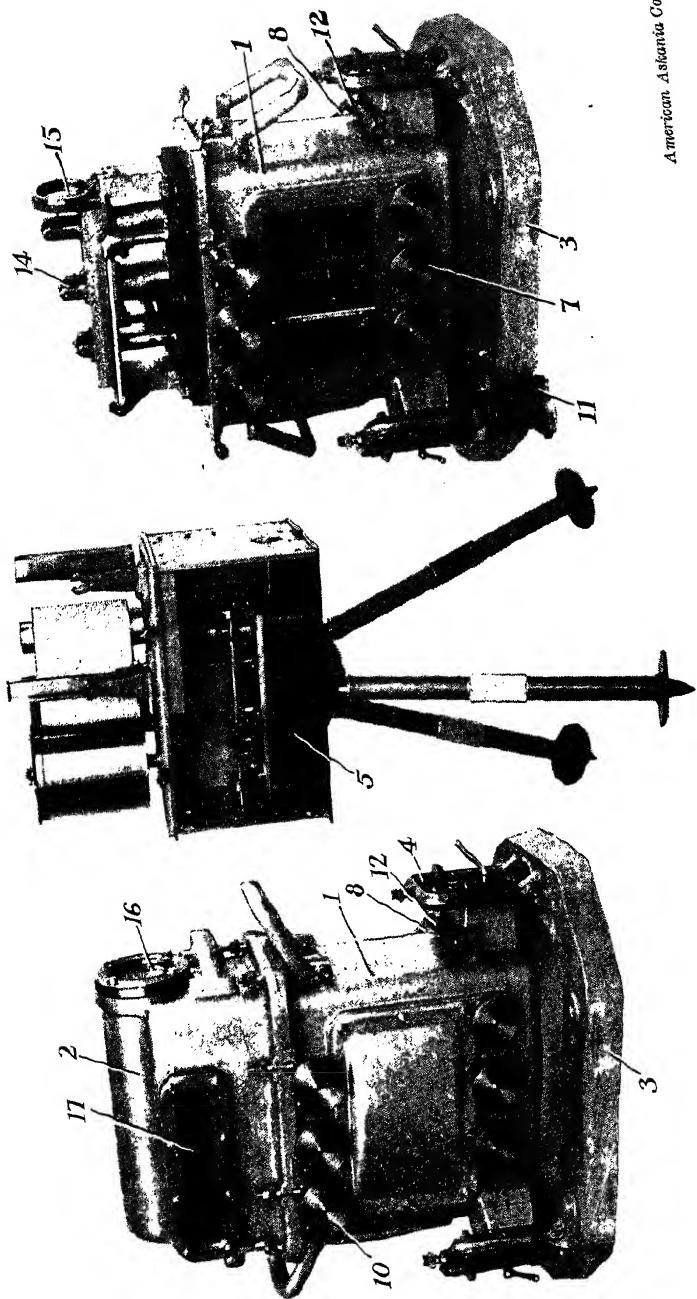
American Askania Corp.

g. 7-18. Askania three-pendulum apparatus.

111

7-19).   On top is a photo cell arrangement for the transmission of the pendulum oscillations.

U. S. Coast and Geodetic Survey

FIG. 7-19. Brown gravity apparatus.   Upper part contains recording device and photoelectric cell; lower (evacuated) part contains the (¼ m. invar pendulum.

The Lejay-Holweck pendulum apparatus is distinguished from other pendulum instruments by its small size and weight.   The pe

inclosed in an evacuated glass bulb not much larger than a radio tube (see Fig. 2–1), consists of a fused quartz rod 4 mm in diameter and 60 mm in length, extends into a pin, P, for observation or photoelectric recording, and is fastened at the bottom to an elinvar spring, E, which at the thinnest point has a thickness of only 0.02 mm. An ingenious arresting mechanism clamps the pendulum by a slight movement of the diaphragm, D. In this manner, the vacuum inside the tube is not disturbed. The period of this pendulum is about 6 to 7 seconds; the time required for a single observation is about 4 minutes. A 40- to 60-minute observation period gives better than one milligal accuracy in gravity.

C. Time-Determination and Time-Signal–Transmission Methods

For an accurate determination of the pendulum period some sort of a standard timepiece must be used, such as a contact chronometer, a contact clock (Riefler), or a gravity pendulum. None of these (with the possible exception of a well-protected gravity pendulum at a central station) retain a sufficiently constant rate and must be compared with absolute time standards. This comparison may be made (1) astronomically, with a zenith telescope, (2) by recording of observatory time signals transmitted by wire, or (3) by radio. The following discussion of time-determination and time-signal–transmission methods will include a description of procedures used for transmitting pendulum oscillations from a base to a field station or vice versa.

1. *Astronomic time determination* is now used in emergency cases only when reception of time signals is impossible. With a zenith telescope the time is determined when a star (or the sun) passes the astronomic meridian. At that instant the hour angle of the star is zero and its right ascension is equal to the local sidereal time; therefore, the "time correction" of the chronometer is right ascension minus chronometer time.

2. *Reception of observatory time signals.* In most of the U. S. Coast and Geodetic Survey pendulum work until about 1932 the telegraphic noontime signals of the U.S. Naval Observatory were used. They were recorded on a chronograph, together with the beats of the contact chronometer. Relays were employed throughout to save the contact points in the chronometers, since their time lag does not affect the chronometer rates as long as it remains the same in successive time signal observations. If the telegraph office is too far away from the pendulum room where the chronometers are located, a hack chronometer is compared with the stationary chronometers, then carried to the telegraph office, and afterwards compared with the stationary chronometers.

It is now the more common practice to record radio time signals on a chronograph together with the beats of the comparison chronometer.

A standard radio receiver and a variety of circuits and instruments may be used for recording. With chronographs, relays must be employed; an ordinary headphone receiver may be changed readily to a relay by attaching a bridge with an adjustable contact spring to its top. In some chronograph recorders thyratron arrangements have been applied (see Fig. 7-20).

3. *Reception of time signals from a central station.* With observatory time signal reception, a pendulum station requires 24 hours, since this is the interval at which these signals are usually transmitted. However, if a chronometer at a central station were connected by wire to the flash box at each field station, time comparisons could be made as frequently as desired. Berroth was the first to apply this method in a pendulum survey of a north German salt dome. For larger surveys, wire connection is impracticable and radio transmission is used instead. Transmitters range
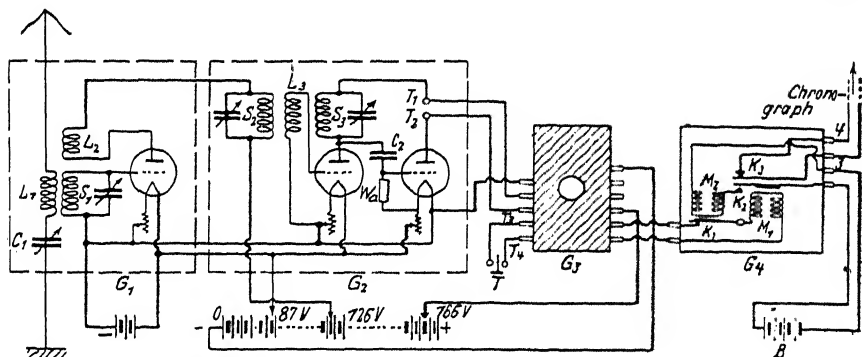
FIG. 7-20. Radio receiver with thyratron and mechanical relays for time recording (after Weber, Richter, and Geffcken). G_1, Detector circuit; G_2, amplifier circuit; G_3, thyratron; G_4, mechanical relay and circuit breaker.

in power from 50 to 200 watts and in wave length from 40 to 100 meters. In the transmission of chronometer beats, the contact circuit feeds through an input transformer into the grid of the modulator tube or operates a relay which controls the B-supply of the transmitter.

If a gravity pendulum is the time standard, capacitive or photoelectric transmission of its beats is employed. As shown in Fig. 7-21, the pendulum itself, or a pin fastened to its bob, is one plate of a condenser and passes the fixed plate when the pendulum goes through its zero position. This change in capacity may be made to control a transmitter in various ways. In the arrangement shown, the pendulum passage changes the tuning of a regenerative oscillator. The resulting changes in plate current are amplified and operate a relay, which in turn controls the B-supply of the transmitter. In the photoelectric method, the light beam reflected from the pendulum mirror is used to make contact. The light source and

the photo cell shown in Fig. 7–22 are in the focal plane of the lens attached to the front of the pendulum receiver. When the pendulum passes through the rest position, the photoelectric cell receives a light flash and passes current, which is amplified and operates the transmitter through a relay. Fig. 7–23 shows a photo cell connected to a four-stage resistance-coupled amplifier and a transmitter without relay.
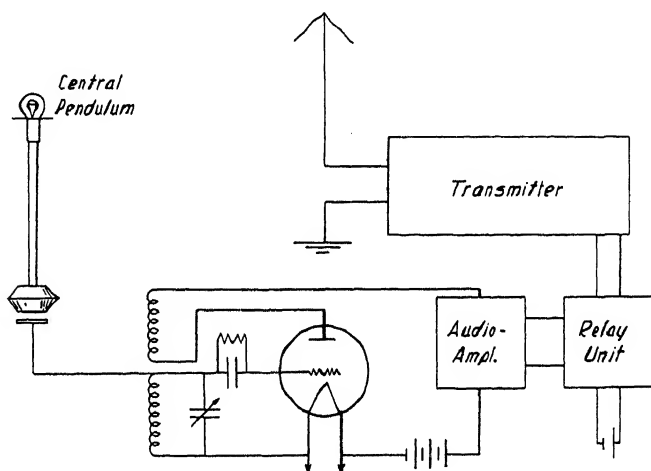
FIG. 7-21. Transmission of pendulum beats from central station by capacitive method (adapted from Mahnkopf).

Radio time signals may be picked up at the field stations by standard short-wave receivers provided with some sort of a recording device in the output stage so that the signals may be photographed on the same film with the oscillations of the field pendulums. A simple recording
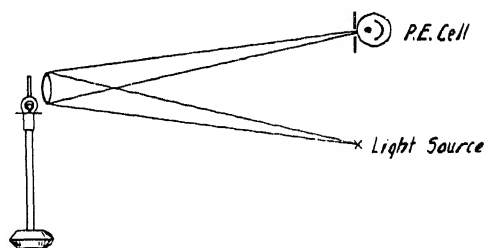
FIG. 7-22. Arrangement for photoelectric transmission of pendulum beats.

device may be made of a telephone receiver (2–4000 ohms) by removing the diaphragm and replacing it by a steel reed with a mirror. To reduce static and other interference, the reed should be tuned to the signal frequency. In the Askania mirror device (Fig. 7–24), an armature with mirror is so suspended between the poles of a horseshoe magnet that it adjusts itself parallel to the lines of force and is deflected as plate current passes through the coils fastened to the one pole piece. A regular oscillograph coupled to the output tube by a step-down transformer is likewise ap-
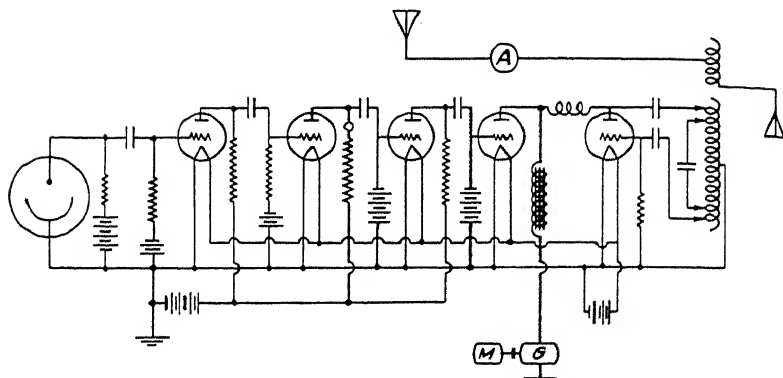
FIG. 7-23. Photoelectric cell, amplifier, and transmitter.

American Askania Corp.
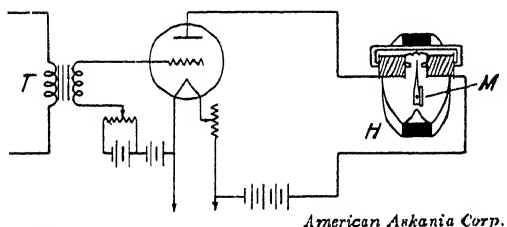
FIG. 7-24. Mirror device (Askania) in amplifier stage added to receiver. *T*, transformer; *H*, horseshoe magnet (end view); *M*, mirror.
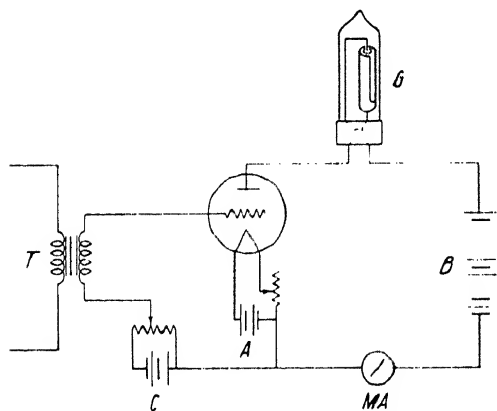
FIG. 7-25. Amplifier stage with recording glow tube. *T*, Transformer; *C*, bias battery; *A*, battery; *B*, B battery; *MA*, milliammeter; *G*, glow tube.

plicable. Any inertia in the recording system may be eliminated by a glow-tube oscillograph as shown in Fig. 7-25. Its cathode is a slotted cylinder. The length of the light glow in it is proportional to the current.

D. INSTRUMENT CORRECTIONS IN PENDULUM OBSERVATIONS

Corrections are required in pendulum observations because of (1) variations in the rate of the chronometer, (2) of period on amplitude, (3) temperature, (4) air pressure, and (5) flexure of the support.

1. The *correction for rate of the chronometer* is determined by comparing it with astronomical time determinations at least every 24 hours, or with radio time signals. The pendulum period reduced for the chronometer rate is

$$T_{\text{red.chron.}} = T_{\text{obs.}} + \frac{S}{86,400}\, T_{\text{obs.}}, \qquad (7\text{--}22a)$$

where S is the rate of the chronometer in seconds in sidereal time per sidereal 24 hour day (positive if losing, negative if gaining), so that the rate correction itself is $0.00001157\, ST$. The correction for chronometer rate on the coincidence interval n is

$$n_{\text{red.chron.}} = n - \frac{\dfrac{S}{86,400}\, n(2n-1)}{1 + \dfrac{S}{86,400}\, 2n}, \qquad (7\text{--}22b)$$

provided the pendulum swings more slowly than the chronometer does. For rates less than $2\frac{1}{2}$ seconds per day, equation $(7\text{--}22b)$ may be simplified to

$$n_{\text{red.chron.}} = n - \frac{S}{86,400}\, n(2n-1) \qquad (7\text{--}22c)$$

If $S < 2\frac{1}{2}$ sec., the effect is less than 0.1 milligal. No correction for chronometer rates and no time comparisons are necessary if measurements are made simultaneously on two field stations and if their flash boxes are connected to the same chronometer, or if radio time signals sent out by a central astronomical clock or pendulum are recorded simultaneously. Of course, rate corrections are likewise unnecessary when a gravity pendulum is used for radio transmission from a base station.

2. The *amplitude correction* follows from formula $(7\text{--}16h)$, so that the reduced period $T_{\text{red.}\,\alpha=0} = T(1 - \alpha^2/16 \cdots)$, in which α is the average amplitude during an observation. It may be considered as the arithmetic or geometric mean of the extreme amplitudes or may be obtained from "Borda's relation." If α_0 is the initial amplitude and α_f the final amplitude,

$$(a) \quad \alpha^2 = \left(\frac{\alpha_0 + \alpha_f}{2}\right)^2$$

or

$$(b) \quad \alpha^2 = \alpha_0 \alpha_f$$

$$(c) \quad \alpha^2 = \frac{\sin(\alpha_0 + \alpha_f)\,\sin(\alpha_0 - \alpha_f)}{2(\log_e \sin \alpha_0 - \log_e \sin \alpha_f)}$$

$$(7\text{--}23a)$$

which, for small angles, is

$$(d) \quad \alpha^2 = \frac{\alpha_0^2 - \alpha_f^2}{2(\log_e \alpha_0 - \log_e \alpha_f)}.$$

With the last expression, the arc correction is

$$-T\frac{1}{2.3 \times 32}\frac{\alpha_0^2 - \alpha_f^2}{\log_{10}\alpha_0 - \log_{10}\alpha_f}. \qquad (7\text{-}??)$$

If the effect of this reduction is to be less than 0.1 milligal, the amplitude must not exceed $1\frac{1}{4}°$. With a simplification permissible for such amplitudes, the reduced coincidence interval is

$$n_{\text{red. }\alpha=0} = n + \alpha^2 \cdot \frac{n(2n-1)}{16}. \qquad (7\text{-}23c)$$

The correction may be further reduced if referred to (*constant*) *average amplitude* α_m and a mean coincidence interval n_m:[27]

$$n_{\text{red. }\alpha_m} = n + \frac{\alpha_m n_m}{8}[2(\alpha_n - \alpha_m n_m) - (\alpha - \alpha_m)]. \qquad (7\text{-}23d)$$

3. In the *temperature correction* it is sufficient to assume a linear change of period with temperature. The change in length of invar pendulums ranges from 1.2 to 1.6 μ per meter and degree Centigrade. Quartz pendulums expand much less, while brass or bronze pendulums increase in length as much as 20 μ per meter and degree Centigrade. The reduced period is

$$T_{\text{red. temp.}} = T - c_\Theta(\Theta - \Theta_o), \qquad (7\text{-}24a)$$

where c_Θ is the "temperature coefficient," determined by experiment.[28] The correction on the coincidence interval is

$$n_{\text{red. temp.}} = n + c_\Theta'(\Theta - \Theta_o), \qquad (7\text{-}24b)$$

where the relation between c_Θ and c_Θ' is

$$c_\Theta' = \frac{1}{(2T_{\text{red.}} - 1)^2} \cdot c_\Theta, \quad \text{or} \quad c_\Theta' = (2n_{\text{red.}} - 1)^2 \cdot c_\Theta. \qquad (7\text{-}24c)$$

4. The *air-pressure correction* arises from the fact that the period of the pendulum is lengthened by the buoyancy of the air, by its hydrodynamic effect, and by its viscosity (interior friction). The buoyancy effect is the most important and depends not only upon the pressure of the air but also upon the amount of water vapor in it. That is, the buoyancy effect is less for saturated air than for dry air at the same pressure. For this reason a "hygrometer correction" has to be applied to the observed air pressure and the reduced air density is computed from the relation

$$\delta = \frac{p_b - 0.377 p_v \cdot h}{760[1 + 0.003665(\Theta - \Theta_o)]}. \qquad (7\text{-}25a)$$

[27] H. Schmehl, *loc. cit.*
[28] H. Schmehl and W. Jennie, Zeit. Instrumentenkunde, **49**: 8, 396–406, 1929.

where p_b is the manometer or barometer reading in millimeters, p_v the saturation pressure of water vapor, h the relative humidity in per cent. Then the period as reduced for air pressure is

$$T_{\text{red. air}} = T - \mathbf{c}_p(\delta - \delta_o), \qquad (7\text{-}25b)$$

where δ_o is the mean density of the air (constant) and $\mathbf{c}_p$ is the pressure coefficient to be determined by experiment.[29] The coincidence interval reduced for air pressure is

$$n_{\text{red. air}} = n + \mathbf{c}'_p(\delta - \delta_o), \qquad (7\text{-}25c)$$

where the relation of $\mathbf{c}'_p$ and $\mathbf{c}_p$ is given by

$$\mathbf{c}'_p = (2n_{\text{red.}} - 1)^2 \mathbf{c}_p, \quad \text{or} \quad \mathbf{c}'_p = \frac{1}{(2T_{\text{red.}})^2} \cdot \mathbf{c}_p. \qquad (7\text{-}25d)$$

5. The *flexure correction* is due to the fact that the vibrating pendulum produces oscillations of the receiver case, of the pillar, and of the surface soil. Rather complex coupled vibration phenomena arise and the period of the pendulum itself changes. Numerous methods have been suggested to correct for this influence or to eliminate it. Since the correction is of the order of 10 to $40 \cdot 10^{-7}$ on solid rock or cement and may increase to as much as $500 \cdot 10^{-7}$ sec. on marshy ground (Berroth), it must be determined accurately.

The displacement of the point of suspension of the pendulum is

$$y = \frac{Y}{\varepsilon}, \qquad (7\text{-}26a)$$

where Y is the horizontal tension produced by the pendulum and ε the elasticity of the support. The tension, Y, may be assumed to be equal to the restoring force. Hence, from equation (7-16a), $Y = Mgs \sin \theta / l$ and $\varepsilon y = Mgs \sin \theta / l$. Then the differential equation of motion,

$$\frac{d^2\theta}{dt^2} + \frac{g}{l} \sin \theta + \frac{1}{l} \frac{d^2 y}{dt^2} = 0,$$

is identical with the equation given for the Vening Meinesz pendulum (7-18a) and the "disturbed" pendulum length and the change in period are given by

$$l' = l\left(1 + \frac{Mgs}{\varepsilon l^2}\right)$$

$$\Delta T = T \frac{Mgs}{2\varepsilon l^2}. \qquad \Bigg\} \qquad (7\text{-}26b)$$

Since the flexure of the support produces an increase in period, the flexure correction (sometimes called only flexure), is always negative. Flexure is determined experimentally (1) by applying an external force (producing a deflection of the pendulum apparatus), or (2) from the displacement caused by the moving pendulum itself. Since (according to eq. [7–26a]) the elasticity of the support is given by the ratio of horizontal force and corresponding displacement, the horizontal stress may be applied statically to the pendulum receiver by weights and pulley and the resulting displacement may be measured by a micro-scope or an interferometer. The external impulses may also be produced periodically; then the forced oscillation amplitude of a light auxiliary pendulum (at rest at the beginning of the test) is measured.
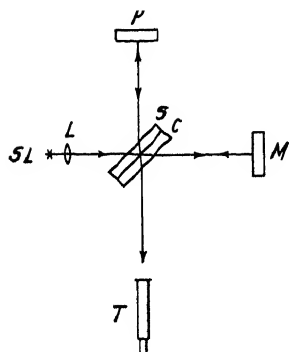
FIG. 7-26a. Interferometer (after Wright).

Methods employing external forces are now superseded by those making use of the effect of the oscillating pendulum itself. They measure the corresponding displacement of the receiver or the effects of the "driving" upon a companion pendulum. For making direct flexure observations, the pendulum apparatus is so set up that the pendulum swings to and fro in respect to the telescope of the flash box. A mirror, P (see Fig. 7-26a), is attached to the head of the pendulum receiver and an interferometer is placed between pendulum and flash box on an independent support. From a source, SL, of monochromatic light (sodium-chloride in an alcohol burner) the light beam travels through the lens, L, to the two plane-parallel glass plates, S and C. S is provided with a semireflecting backing of silver so that part of the light is reflected to the mirror, P,

FIG. 7-26b. Fringes and fringe displacements (after Wright).

and from it into the telescope, T, while another portion goes through the plates, S and C, to a stationary mirror, M, and thence into the telescope.

The glass plate, C, is a compensator to make the two light rays travel through exactly the same substances and the same thicknesses on their way to the telescope where they unite under conditions producing inter-ference. As shown in Fig. 7-26b, a number of dark and light bands appear, the former corresponding to a phase difference of one-half wavelength and the latter to a full-wave phase shift. When the pendulum mirror, P,

moves periodically, the distances traveled by both rays change and the fringes shift periodically. If light changes to darkness and back to light, the movement has been one fringe, the phase shift one wavelength, and the displacement of the mirror one-half wavelength, or 0.29 microns (since the wavelength of sodium light is 0.58 microns). The shift of the fringes dx, is expressed in terms of fringe width, x, and all observations are reduced to 5 mm arc (not semi-arc) of pendulum movement. The correction on the pendulum period is determined by measuring periods T and corresponding fringe shifts (F) under varying conditions of stability of the pendulum support so that the flexure "coefficient" $c_f = \Delta T / \Delta F$. Then the flexure correction

$$\Delta T_{\text{flexure}} = (F) \cdot c_f \cdot \alpha = \frac{dx}{x} \cdot \frac{(2\alpha)_{\text{av.}}}{(2\alpha)} \cdot c_f. \tag{7-27}$$

A set of flexure observations with calculations is reproduced in Swick's pamphlet.[30] The actual displacement of the pendulum support is very small; for firm ground and pillar it varies from 0.06 to 0.10 fringe width or 0.017 to 0.029 microns.

Twin-pendulum procedures give greater accuracy than the interferometer method in the determination of flexure. Observations may be started with the companion pendulum at rest or with both pendulums in opposite phases and identical amplitudes. The second method is more accurate, since theoretically the influence of flexure is completely eliminated. Only a small correction remains, because of the impossibility of keeping the amplitude and phase relations of the two pendulums constant throughout the entire observation period. If, in the first method, one pendulum is at rest at the time t_0 ($\alpha_2 = 0$ and $\varphi_2 - \varphi_1 = \pi/2$), and if at the time t the amplitude α_2 of the driven pendulum and the amplitude α_1 of the driving pendulum is observed, the effect of flexure on period and coincidence interval respectively is

$$\left.\begin{aligned} \Delta T_{\text{flex.}} &= \frac{\alpha_2}{\alpha_1} \cdot \frac{T^2}{\pi(t - t_0)} \\ \Delta n_{\text{flex.}} &= \frac{\alpha_2}{\alpha_1} \cdot \frac{n^2}{\pi(t - t_0)}, \end{aligned}\right\} \tag{7-28a}$$

provided the phase difference at the end of the observation period is still nearly 90°. If two pendulums swing against each other on the same support, the flexure corrections for *each* pendulum on period and coincidence interval are, at any instant t,[31]

---

[30] *Loc. cit.*
[31] H. Schmehl, Zeit. Geophys., 3(4), 157–160 (1927).

$$(\Delta T_1)_t = \mathbf{F}_T\left[1 + \left(\frac{\alpha_2}{\alpha_1}\right)_t \cdot \cos(\varphi_2 - \varphi_1)_t\right]$$

$$(\Delta T_2)_t = \mathbf{F}_T\left[1 + \left(\frac{\alpha_1}{\alpha_2}\right)_t \cdot \cos(\varphi_2 - \varphi_1)_t\right]$$

$$(\Delta n_1)_t = \mathbf{F}_n\left[1 + \left(\frac{\alpha_2}{\alpha_1}\right)_t \cdot \cos(\varphi_2 - \varphi_1)_t\right]$$

$$(\Delta n_2)_t = \mathbf{F}_n\left[1 + \left(\frac{\alpha_1}{\alpha_2}\right)_t \cdot \cos(\varphi_2 - \varphi_1)_t\right]$$

$$(7\text{-}28b)$$

in which $\mathbf{F}_T$ and $\mathbf{F}_n$, respectively, are approximate values of the flexure corrections obtained from equation (7-28a). The values of these corrections for the entire observation period are found by integration between the limits t_1 and t_2, reckoned from the time t_0 when the phase difference is exactly 180° and the amplitude ratio is $(\alpha_2/\alpha_1)_0$ and $(\alpha_1/\alpha_2)_0$:

$$\Delta T_1 = -\mathbf{F}\left\{1 - \left(\frac{\alpha_2}{\alpha_1}\right)_0 + \frac{1}{2}\left[\left(\frac{\alpha_2}{\alpha_1}\cos(\varphi_2 - \varphi_1)\right)_2 - \left(\frac{\alpha_2}{\alpha_1}\cos(\varphi_2 - \varphi_1)\right)_1\right]\right.$$

$$\left. + \frac{\mathbf{F}\pi^2}{T^4}(T_2 - T_1)\left[\left(\frac{\alpha_2}{\alpha_1}\right)_0(T_2 - T_1) + \mathbf{F}\left(1 - 3\left(\frac{\alpha_2}{\alpha_1}\right)_0^2\right)\right]\left[\frac{t_2^2 - t_1^2}{4} - \frac{t_2^3 - t_1^3}{6(t_2 - t_1)}\right]\right\}$$

$$(7\text{-}28c)$$

T_2 has the same equivalent as eq. (7-28c) with α_1/α_2 instead of α_2/α_1. The correction for the coincidence interval, with $n_m = (n_1 + n_2)2$, is

$$\Delta n_1 = \mathbf{F}_n\left\{1 + \frac{1}{2}\left[\left(\frac{\alpha_2}{\alpha_1}\cos(\varphi_2 - \varphi_1)\right)_2 + \left(\frac{\alpha_2}{\alpha_1}\cos(\varphi_2 - \varphi_1)\right)_1\right]\right.$$

$$\left. + \frac{\pi^2}{n^4}(t_2 - t_1)^2[n_{m_1} - n_{m_2}]\left[(n_{m_1} - n_{m_2})\left(\frac{\alpha_2}{\alpha_1}\right)_0 + \mathbf{F}_n\left(3\left(\frac{\alpha_2}{\alpha_1}\right)_0^2 - 1\right)\right]\right\}$$

$$(7\text{-}28d)$$

The n_2 has the same equivalent as eq. (7-28d) with α_1/α_2 instead of α_2/α_1 and $(n_{m_2} - n_{m_1})$ instead of $(n_{m_1} - n_{m_2})$.

The elimination of flexure by the simultaneous oscillation of two pendulums is so perfect that, although the flexure itself may be 20-50 × 10⁻⁷ seconds, the corrections seldom exceed -1×10^{-7} seconds, provided the phase differences do not deviate more than 30° from 180°.

6. *Examples of pendulum observations* have been published by various authors for different instruments and procedures. A complete set of U.S. Coast and Geodetic Survey observations has been reproduced by

Swick.[32] For the Potsdam apparatus, observations with the one-pendulum and twin-pendulum methods are found in Schmehl's publication;[33] Vening Meinesz has illustrated the application of his method by photographs of records and calculation examples.[34]

E. GRAVIMETERS

The pendulum methods discussed in the preceding section are sometimes referred to as "dynamic" gravity procedures since they involve the measurement of time. Other possibilities in the same category are: (1) the determination of the time and distance characteristics of free fall in vacuum; (2) a comparison of gravity with the centrifugal force of a rotating body by measuring the slope of a surface of mercury subjected to rapid rotation in a vessel. None of these methods has been perfected to the same degree of accuracy as that found in pendulum or gravimeter methods.

The term "gravimeter," or "gravity meter," is customarily applied to an instrument involving a *static* method of comparing gravity with an elastic force and a measurement of the deflection or position of certain "indicators" when gravity and comparison force are in equilibrium. In the barometric method, atmospheric pressure as measured with an aneroid (or boiling-point thermometer) is compared with the reading of a mercury barometer; in the volumetric method (Haalck gravimeter), both sides of a mercury barometer are connected to two vessels with the air under different pressure. In all remaining static gravity methods, the elasticity of springs is used for comparison with gravity.

The mechanical gravimeters fall into two groups: nonastatic and astatic. Gravimeters that are modifications of horizontal seismometers[35] may be called horizontal seismo-gravimeters, while those resembling vertical seismographs may be designated vertical seismo-gravimeters.

1. *Barometric method.* If atmospheric pressure is measured at different localities with an aneroid and a mercury barometer, discrepancies result because the mercury barometer is affected by variations in gravity. Since the aneroid does not give sufficient accuracy, the boiling point of water is measured instead to give atmospheric pressure. The barometric method was the first to make possible determinations of gravity on board ship and was perfected principally by Hecker. To obtain a mean error of ±40 milligals it is necessary to read the boiling point with an accuracy of 1/1000° C. and the barometer with an accuracy of 0.01 mm. How much

---

[32] *Loc. cit.*
[33] Schmehl, Zeit Geophys., *loc. cit.*
[34] *Loc. cit.*
[35] See page 580, Fig. 9-94.

the error could be reduced on land has probably not been determined. In any event, this method is not likely even to approach a modern gravimeter in accuracy.

2. *Volumetric method* (Haalck gravimeter[36]) is illustrated schematically in Fig. 7-27, where v and v' are the two volumes and z and z', respectively, are the positions of the mercury menisci. If p is the pressure in the volume v and p' is the pressure in the volume v', then the difference in pressure Δp must be equal to the weight of the mercury column so that $\Delta p = \Delta z \cdot \delta \cdot g$, where δ is the specific gravity of the mercury. To obtain sufficient sensitivity, use is made of vessels of greatly increased section, of a lighter liquid (toluol) on top of the mercury, and of small capillary tubes, C and C', for reading the menisci. The increase in the accuracy is proportional to the ratio of the sections of the vessel and the capillary (about 10,000 in the Haalck apparatus). A displacement of the menisci by about 1 mm corresponds to a change in gravity of one milligal. In the first experimental model, the mean error was ± 10 milligals. The lastest model is a quadruple apparatus, has an accuracy of about one milligal, is suspended in gimbals, and may be used on board ship.
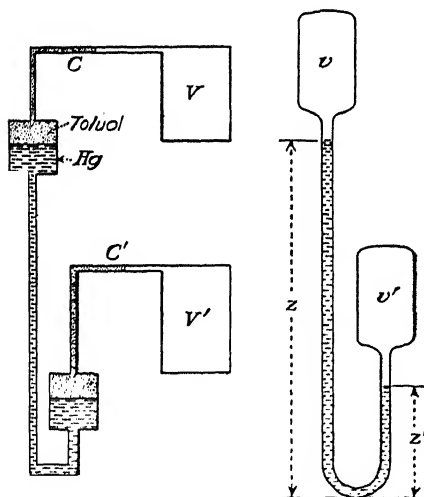
FIG. 7-27. Haalck gravimeter.

3. *Unastatized mechanical gravimeters* utilize the elastic force of springs and the torsion of wires for comparison with gravity. Mechanical, optical, or electrical means of magnification are applied to obtain the necessary accuracy of 1 in 10 million. In a spring gravimeter, the deflection, d, is inversely proportional to the square of its natural frequency, ω_0. Since the relation $\omega_0 = \sqrt{c/m}$ may be written[37] $\omega_0^2 = m \cdot g / d \cdot m$, the variation of deflection d and of the reading a with gravity (V = static magnification) is given by

$$\Delta d = \frac{\Delta g}{\omega_0^2} \quad \text{and} \quad \Delta a = V \frac{\Delta g}{\omega_0^2}. \tag{7-29}$$

[36] H. Haalck, Zeit. Geophys., **7**(1/2), 95-103 (1931); **8**(1/2), 17-30 (1932); **8**(5), 197-204 (1932); **9**(1/2), 81-83 (1933); **9**(6/8), 285-295 (1933); **11**(1/2), 55-74 (1935); **12**(1), 1-21 (1935). *Idem*, Beitr. angew. Geophys., **7**(3), 285-316 (1938).
[37] See page 581, eq. (9-83).

It is seen that for high (mechanical) sensitivity an increase in period (astatization) is of advantage. However, not all gravimeters are astatized.

The Threlfall and Pollock gravimeter[38] is one of the earliest examples of an unastatized gravimeter. It consists of a torsion wire about 0.0015 in. in diameter, supporting in the middle a quartz bar about 5 cm long and 0.018 g in weight, whose position is read by a microscope. One of the studs holding the wire is fixed; the other is rotated until the bar end coincides with the crossweb in the microscope (horizontal position). The corresponding stud position is read on an accurate dial.

The Wright gravimeter closely resembles the Threlfall-Pollock instrument, two tapering helical springs taking the place of the torsion wire. Between them a small boom with a mirror is adjusted to horizontal position by turning one of the studs supporting the springs. An illustration based on a patent drawing is given in the author's publication on gravimeters.[39] In the most recent type[40] measurements are made as follows: The springs are wound until the boom is horizontal, at which time the reading of the spring-supporting frame is recorded. Then the spring is unwound so that the boom passes through its vertical position and reaches a horizontal position on the other side. The corresponding reading is recorded; the difference between readings for the horizontal boom positions is a measure of gravity. Since the boom is used near the upsetting position, this instrument may be included in the group of astatic gravimeters. Accurate temperature and pressure control is required; the accuracy is about 1 milligal.

The Lindblad-Malmquist ("Boliden") gravimeter[41] consists of two springs carrying a light mass with two disk-shaped extensions (see Fig. 7-28a). The upper disks act as the variable condenser in an "ultramicrometer" circuit. Using a spacing of $2 \cdot 10^{-3}$ cm, the authors claim to have been able to detect displacements of the order of $3.5 \cdot 10^{-9}$ cm. A gravity change of one milligal corresponded to a displacement of about $5.5 \cdot 10^{-7}$ cm, so that variations of the order of 1/100 milligal would be detectable. Because of various interfering factors, however, the mean error in the field was 0.1 to 0.2 milligal for a single observation and 0.05 to 0.1 milligal for five to ten observations. The ultramicrometer circuit acts merely as an indicator, the deflections being compensated by electrostatic attraction between the upper plates. The distance between the lower plates is so adjusted that a potential difference of 10 volts corresponds to a gravity variation of 1 milligal.

[38] Phil. Trans. Roy. Soc. (A) **193**, 215-258 (1900); (A) **231**, 55-73 (1932).

[39] C. A. Heiland, A.I.M.E. Tech. Publ., 1049 (1939).

[40] F. E. Wright and J. L. England, Am. J. Sci., **35A**, 373-383 (1938).

[41] A. Lindblad and D. Malmquist, Ingen. Vetensk. Handl., No. 146, 52 pp. (Stockholm, 1938).

In the Hartley[42] gravimeter the mass is supported approximately from the center of a beam hinged on one end. The movement of the beam is transferred to two rocking mirrors that rotate in opposite directions when the beam is displaced. The main spring supporting the beam above the mass is made of an alloy of tungsten and tantalum, carries 99.9 per cent of the total load, is wound with high initial tension, and in extended position is about 10 cm long. A small additional spring is provided for compensating the beam deflections by rotation of a micrometer screw.

In the Gulf (Hoyt) gravimeter, Fig. 7-28b (U. S. Patent 2,131,737, Oct. 4, 1938) a spider weighing about 100 grams is suspended from a helical spring of rectangular section. A spring section whose width is much greater than its thickness produces a rotation of the suspended mass when the weight changes, this action being comparable with that of a bifilar suspension (see below). The dimensions may be so selected that a change of 0.1
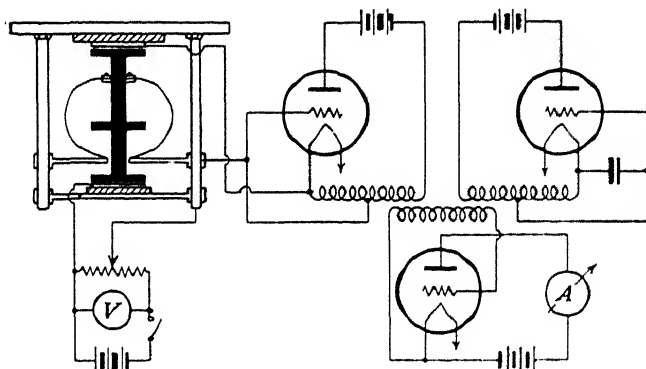
FIG. 7-28a. Lindblad-Malmquist gravimeter (schematic).

milligal produces a deflection of the order of 1 arc-second. Deflections are measured by a multiple reflection setup involving two semireflecting lenses. One of these is attached to the spider. Scale and light source are in the conjugate foci of the lens combination. Reading the tenth multiple reflection, a deflection of 1 arc-second corresponds to about 20 scale divisions.

In the Askania-Graf gravimeter[43] a mass is suspended freely from a helical spring. Its deflection is measured with an electrical displacement meter (presumably operating without amplifier) with a magnification of about $4 \cdot 10^4$. Temperature compensation and a double battery-operated thermostat is provided. The accuracy is of the order of 0.1 milligal. It

[42] Physics, **2**(3), 123-130 (March, 1932).
[43] A. Graf., Zeit. Geophys., **14**(5/6), 154-172 (1938).

follows from eq. (7–29) that a deflection of $2.5 \cdot 10^{-1} \mu$ is produced by a gravity anomaly of one milligal, since the natural frequency is 1 sec. This displacement, with a magnification of $4 \cdot 10^4$, gives a galvanometer deflection of 10 mm.

4. *Astatization of gravimeters* is equivalent to lowering their natural frequency. It involves the application of a negative restoring force in such a manner as to drive the mass away from its rest position and to aid any deflecting force.

While unastatized gravimeters are invariably vertical seismographs, the process of astatization makes it possible to utilize horizontal seismographs for gravity measurements. Virtually all horizontal seismo-gravimeters are inverted pendulums, analogous to the Wiechert astatic seismograph (Lejay-Holweck and the Ising gravimeters). Vertical seismographs may be astatized by attaching the suspension spring below the horizontal axis of the lever arm (Ewing), by using the spring at an angle of less than 90° with the beam (Berlage,[44] La-Coste[45]), by combining a horizontal pendulum with a vertical balance (Schmerwitz[46]), by fastening an inverted pendulum permanently to the center of the beam (Tanakadate, Thyssen), or by providing an additional
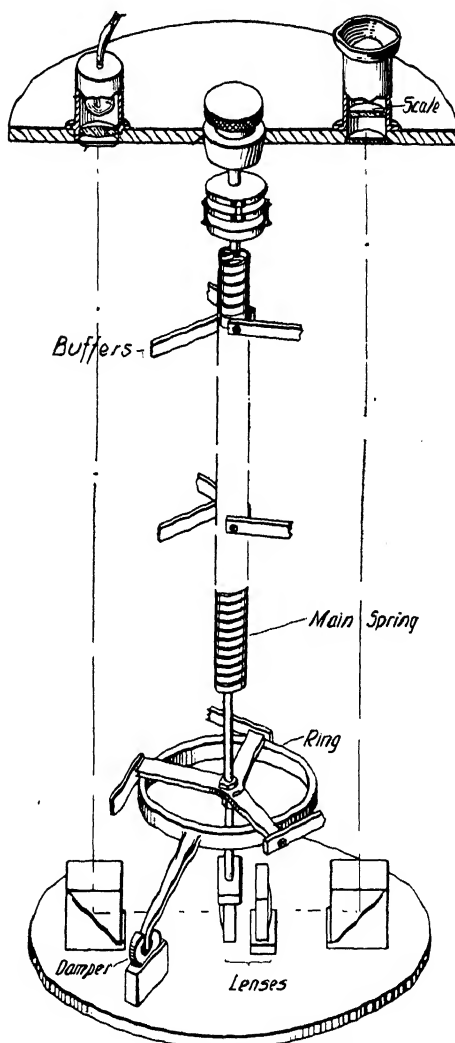
FIG. 7-28b. Gulf gravimeter (after Hoyt).

[44] H. P. Berlage, Jr., Handbuch der Geophysik, IV(2), 385.

[45] L. J. B. LaCoste, Physics, 5(3), 174-176 (1934); Seis. Soc. Amer. Bull., 25(2), 176-179 (April, 1935).

[46] Zeit. Geophys., 7(1/2), 95-103 (1931); Beitr. angew. Geophys., 4(3), 274-295 (1934).

"period" or "pull-back" spring through the axis of rotation (Truman, Mott-Smith). In vertical and horizontal seismo-gravimeters, the restoring and labilizing forces act in the vertical plane with rotation about a horizontal axis. It is also possible to produce a labilizing gravity moment with action in a horizontal plane and rotation about a vertical axis (bifilar suspension). The tendency of such a system to come to rest in the lowest position of the mass produces a horizontal torque. Bifilar systems may be astatized by "twisting" the bifilar suspension 180° (Fig. 7-30), or by addition of a helical spring ("trifilar" gravimeter, Fig. 7-31).

By astatization the sensitivity to gravity variations is greatly increased. If η is the (positive) restoring force and κ the (negative) labilizing force, then the resulting restoring force, N, is

$$N \equiv \eta - \kappa. \tag{7-30a}$$

If the system is to be stable, η must be greater than κ. The degree of astatization, A, may be defined[47] as the ratio of the labilizing force, κ, and the resultant force, N:

$$A = \kappa/N. \tag{7-30b}$$

The degree of astatization, A, increases, therefore, with the labilizing force and the difference between the restoring and the labilizing forces. Small differences in either may be observed with great accuracy. In some astatic systems differences in stabilizing force are the object of observation; in others it is differences in the labilizing force (inverted gravity pendulums). If the labilizing forces are held constant and changes in the stabilizing forces are observed, the resultant restoring force and the degree of astatization change in accordance with

$$\left. \begin{aligned} \frac{dN}{N} &= (A + 1)\frac{d\eta}{\eta} \\[2mm] \frac{dA}{A} &= -(A + 1)\frac{d\eta}{\eta}. \end{aligned} \right\} \tag{7-30c}$$

On the other hand, if changes in the labilizing forces are observed, the corresponding relations are

$$\left. \begin{aligned} \frac{dN}{N} &= -A\frac{d\kappa}{\kappa} \\[2mm] \frac{dA}{A} &= (A + 1)\frac{d\kappa}{\kappa}. \end{aligned} \right\} \tag{7-30d}$$

[47] G. Ising, A.I.M.E. Tech. Publ., 828 (August, 1937).

5. *Horizontal seismo-gravimeters* resemble in principle the well-known Wiechert astatic seismograph. In the Ising gravimeter a quartz fiber is stretched between the prongs of a fork-shaped support and forms the horizontal axis of rotation of an inverted quartz rod fused rigidly to the fiber (Fig. 7-29). The pendulum assembly is mounted on a heavy metal block hung from two leaf springs in such a manner that it can be turned slightly about an axis parallel to the fiber by tightening a spring attached to one side of the block. When the block is tilted at an angle φ, the pendulum is deflected from its vertical position by the angle θ. In the position of equilibrium,

$$\left.\begin{array}{c} \eta\theta = \kappa(\theta + \varphi) \\ \text{or} \\ \theta = \dfrac{\kappa}{\eta - \kappa} = A\varphi. \end{array}\right\} \quad (7\text{-}31a)$$

Assuming that the gravity at a (base) station is g_0 and that a tilt, φ, has produced the deflection, θ_0, the labilizing force at that station $\kappa_0 = \eta\theta_0/(\varphi + \theta_0)$. If, at another station with the gravity g_1, the same tilt angle is used, the labilizing force is $\kappa_1 = \eta\theta_1/(\varphi + \theta_1)$. Then the difference in gravity is $\Delta g = g(\kappa_1 - \kappa_0)/\kappa_0$ or, in terms of (small) deflection angles for constant tilts,

$$\Delta g = g\left[\frac{\theta_1}{\theta_0} \cdot \frac{\varphi + \theta_0}{\varphi + \theta_1} - 1\right]. \quad (7\text{-}31b)$$

The deflection of the inverted pendulum is read with a microscope, and the tilt of the block is measured with the micrometer screw that controls the tension of the tilt spring. In the instruments described in the published reports the mean error was 0.5 to 0.6 milligal.

The Lejay-Holweck pendulum with some modifications also could be used as a *static* gravimeter to operate like the Ising instrument.
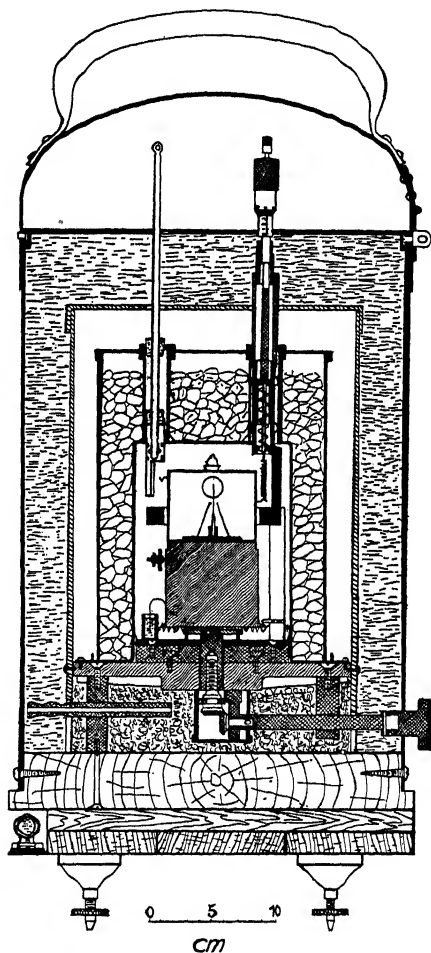
FIG. 7-29. Ising astatic gravimeter (section).

The Nørgaard gravimeter[48] has two inverted quartz pendulums leaning toward one another, with an index rod between them. The distance between the ends of the quartz rods is read with a microscope and is a measure of gravity. The entire system is immersed in water of constant temperature and is thus highly damped and insensitive to vibration. The mean error is about 0.3 milligal.

6. *Vertical seismo-gravimeters* fall into two groups: (1) instruments in which gravity changes produce rotations about a vertical axis (bifilar or trifilar suspensions); (2) gravimeters in which this rotation takes place in a vertical plane and about a horizontal axis. In the *bifilar* gravimeters, the restoring force is due to the torsion of the suspension wires (equivalent torsional coefficient τ) as well as to gravity, since the suspended mass is raised upon rotation. If $2a$ is the distance of the suspension points above, $2b$ the distance below, and d their vertical distance, the effect of gravity is given by the expression $mg \cdot ab/d$ and, therefore, the resulting restoring force is

$$N = \frac{mgab}{d'} + 2\tau, \qquad (7\text{-}32a)$$

where d' is the vertical distance corrected for a reduction in length which occurs because of the bending of the wires. With a moment of inertia K, the period of oscillation of a mass on bifilar suspension is

$$T = 2\pi \sqrt{K \Big/ \left(2\tau + \frac{ab}{d'} \cdot mg\right)}, \qquad (7\text{-}32b)$$

which, however, is much too short to give sufficient sensitivity to gravity variations. A bifilar system can be readily astatized by changing the sign of the second term in the denominator of eq. (7-32b), that is, by making gravity the labilizing force (reversing the suspension 180° as shown in Fig. 7-30). Then

$$T = 2\pi \sqrt{K \Big/ \left(2\tau - \frac{ab}{d'} \cdot mg\right)}. \qquad (7\text{-}32c)$$

With high astatizing factors this procedure increases the sensitivity to gravity variations about 1000-fold, which is an improvement of similar order as in the Lejay-Holweck pendulum, where gravity likewise acts as a labilizing force. Bifilar gravimeters have been constructed by Berroth,[49] Ising,[50] (Fig. 7-30), and Hart Brown.

Bifilar instruments with crossed wires appear to be inferior to the

[48] G. Nørgaard, Dansk Geodaetisk Inst. Medd., No. 10 (Kobenhavn, 1938).

[49] Zeit. Geophys., **8**(8), 366 (1932).

[50] *Loc. cit.*

trifilar gravimeters which are capable of the greatest sensitivity yet attained in such instruments. The trifilar gravimeter consists of a disk supported by a helical spring at its center and by three equally spaced wires at its circumference. It was first described by A. Schmidt.[51] Fig. 7-31 is a schematic showing only one of the suspension wires, fastened at the ceiling at C and attached to the disk at A. The vertical distance of C above the disk is $CB = d$, and its horizontal distance from the center is $OB = a$. The radius of the disk is $OA = r$ and the horizontal distance $AB = e$. When a disk deflection, φ, has been brought about by a torsion-head rotation, α, the suspension wire is deflected by the angle, β, from the vertical. The total weight, W, is so distributed that the coil spring bears a weight $W - w$ and the suspension wires each $w/2$ or $w/3$, depending upon whether two or three wires are used. If $w/2$ is resolved into its components, Q and H (see Fig. 7-31), it is seen that Q is ineffective and $H = w/2 \tan \beta = we/2d$. Its tangential component, $H \cos \psi$, produces the couple $2Hr \cos \psi$. In the triangle OAB, $e \cdot \sin (90 + \psi) = a \sin \varphi$. With $\cos \psi = a \sin \varphi/e$, the couple $D_2 = wra \sin \varphi/d$. It is opposed by the moment of torsion of the main coil, $D_1 = \tau(\alpha - \varphi)$. Thus in the equilibrium position,

$$\tau(\alpha - \varphi) - \frac{wra}{d} \sin \varphi = 0. \qquad (7\text{-}33a)$$

Small changes in the weight of the disk and hence in gravity will produce large deflections, since

FIG.

$$\frac{d\varphi}{dw} = \frac{\dfrac{ar}{d} \sin \varphi}{\dfrac{war}{d} \cos \varphi + \tau}. \qquad (7\text{-}33b)$$

It is seen that maximum sensitivity occurs when the denominator is zero or when $\cos \varphi = -\tau d/war$. As τ is small, the position of maximum sensitivity is very close to 90° from the position of zero deflection. With a trifilar gravimeter, Tomaschek and Schaffernicht[52] have recorded the
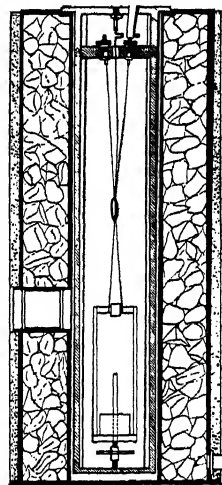
[51] Beitr. Geophys., **4**, 109–115 (1900).
[52] Zeit. Geophys., **9(3)**, 125–136 (1933).
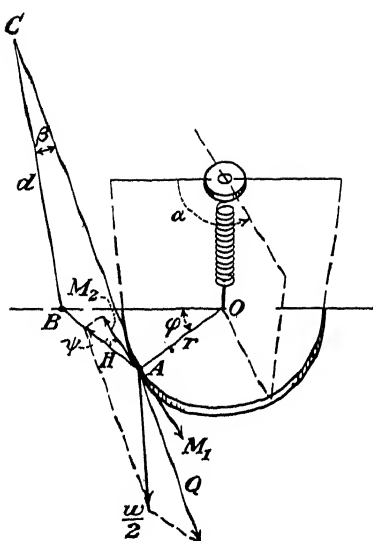
Fig. 7-31. Action of trifilar gravimeter.
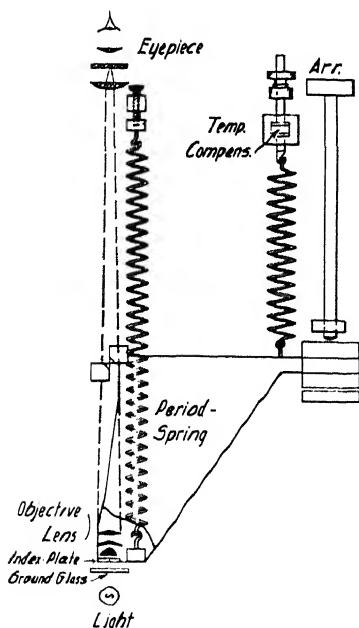
Fig. 7-32. Truman gravimeter.

changes in gravity brought about by the changes in attraction of the moon with an accuracy of about 0.001 milligal. A portable instrument for gravity exploration has not yet been developed.

The Truman gravimeter (see Fig. 7-32), used chiefly by the Humble Oil Company and associated companies, is similar in construction to a Ewing astatic vertical seismograph. The beam consists of a right triangle with the right angle at the axis of rotation. The mass is attached to the end of this triangle, and near it a vertical coil spring supports most of the mass and the beam. An astatizing spring is attached to the other corner of the triangle, approximately below the point of suspension. The accuracy is of the order of 0.5 milligal.[53]

The Thyssen gravimeter (Fig. 7-33) is likewise a beam-type vertical seismometer. The beam is horizontal and suspended in the center on a knife edge, the balancing spring being housed in a tube surrounded by a water jacket expanding downward with an increase in temperature to offset the increase in spring length. An astatizing arm is fastened to the center of the beam which is made of fused quartz and has a length of 15 to 20 cm. Two beams are arranged side by each in antiparallel arrangement as in a torsion balance. They are clamped by a mechanism operated from the top of the instrument and are read separately by the optical arrangement shown in the figure. The zero position is calculated from reversal readings. The mean error of one station is 0.25 milligal,

[53] A. B Bryan, Geophysics, **2**(4), 301 308 (Oct., 1937)

that of repeat stations about 0.5 milligal.[54]   The drift in one day is 1 to 1.5 milligals.

The Mott-Smith gravimeter[55] (Fig. 7–34) is essentially a torsion-wire gravimeter with astatization.   The torsion fiber (2) is made of fused quartz and carries a weight arm (1) to which is attached the pointer (3). A negative restoring force is supplied by a fiber (4) passing through the axis of rotation of the weighing arm.   Deflections of the system are read by a microscope.

Gravimeter readings are affected by temperature, air pressure, humidity, abrupt changes and slow drift of the base reading. These effects must be corrected for and be determined by experiment; furthermore, the sensitivity (scale value) of the instrument must be known.   The effect of temperature is complex, cannot always be calculated, and is generally determined by experiment. In most gravimeters some sort of temperature compensation and thermostat protection is provided.   If this were not done, the temperature effect would be tremendous.. In a spring gravimeter a change of 1° C. would produce an apparent change in gravity of 200 to 300 milligals.   In a volumetric gravimeter the same temperature change would correspond to an apparent gravity anomaly of 3000 to 4000 milligals.

Changes in air pressure affect some gravimeters, depending upon construction of the case and the weight of the moving member.   The buoyancy increases with barometric pressure, and its effect on the reading is determined by experiment.   Changes in humidity may produce large effects in gravimeters whose mass is small, since water condensation will
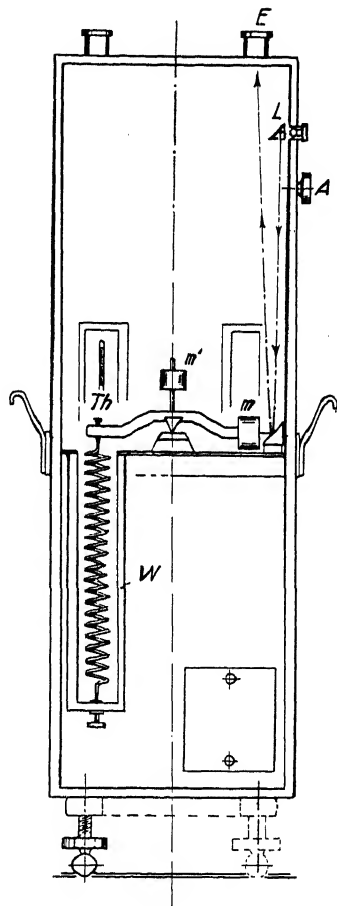
Fig. 7-33. Thyssen gravimeter (schematic).

[54] A. Schleusener, Zeit. Geophys., **10**(8), 369–377 (1934); Oel und Kohle, **2**(7), 313–318 (1934). St. v. Thyssen and A. Schleusener, Oel und Kohle, **2**(8), 635–650 (1935); Beitr. angew. Geophys., **6**(1), 1–13 (1936). St. v. Thyssen, Zeit. Geophys., **11**(3), 131–133 (1935) ; **11**(4/**5**), 212–220 (1935) ; Beitr. angew. Geophys., **5**(2), 178–181 (1935); **5**(3), 303–314 (1935); 7(3), 218–229 (1938). A. Berroth, Oil Weekly, **76**(13), 33–37 (March 11, 1935). F. Lubiger, Beitr. angew. Geophys., 7(3), 230–244 (1938).
[55] Geophysics, **2**(1), 21–32 (Jan., 1937).

produce large changes in equivalent mass.   In some instruments, calcium chloride in solid form or as supersaturated solution is used to keep the air dry.

Although the sensitivity of a gravimeter is proportional to the square of the period, determinations of scale values by period observations are not in use (except for qualitative observation while adjusting an instrument), since there are numerous other methods with which scale values can be determined more easily and accurately. Some gravimeters may be calibrated by tilting. For an inclination, φ, the effective gravity changes from g to $g \cos \varphi$; therefore, the apparent difference in gravity is
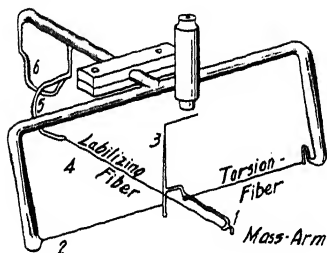
Fig. 7-34. Mott-Smith gravimeter (schematic).

$$\Delta g = g(1 - \cos \varphi) = 2g \sin^2 \frac{\varphi}{2} \approx g \frac{\varphi^2}{2}. \quad (7\text{-}34a)$$

Many gravimeters lend themselves readily to scale value determinations by addition of weights (see Fig. 7-35). If the total gravimeter mass is M, the apparent change in gravity produced by an addition of mass m is

$$\Delta g = \frac{dm}{M} \cdot g. \quad (7\text{-}34b)$$

Gravimeters with condenser plates may readily be calibrated electrostatically. If the two condenser plates have equal surfaces of S square centimeters at a distance of d centimeters, the apparent change in gravity brought about by a voltage difference, E, is
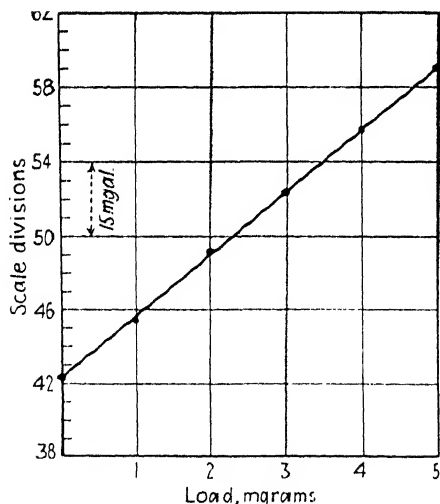
Fig. 7-35. Gravimeter calibration by addition of mass (after Schleusener).

$$\Delta g = \frac{SE^2}{8\pi d^2 M}. \quad (7\text{-}34c)$$

In terms of capacity $C = S/4\pi d$, which is more readily determined,[56] the apparent change in gravity is

$$\Delta g = 2\pi \frac{E^2 C^2}{SM}. \quad (7\text{-}34d)$$

[1] A. Lindblad and D. Malmquist, loc. cit.

Almost any kind of gravimeter may be calibrated by measuring the change in reading with elevation. A sufficient difference exists in most office buildings between basement and the highest floor (Fig. 7–36). From the formulas given in the next section for the "free air" reduction, the change in gravity with elevation is

$$\Delta g \text{ (in milligals)} = -\Delta h \text{ (in meters)} \cdot 0.3086. \qquad (7\text{–}34e)$$

Because of the elastic hysteresis of the suspension material, most gravimeters show a more or less appreciable "drift" of the zero position with time. Furthermore, abrupt changes in base position may result from mechanical changes in the moving systems. Both kinds of changes may
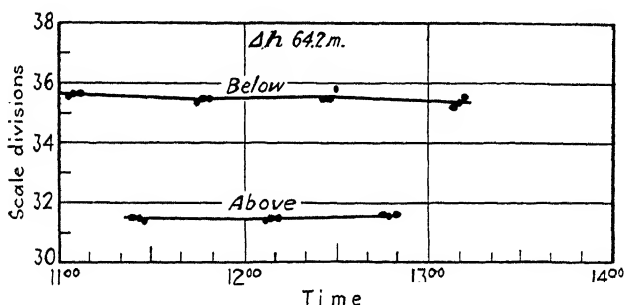
Fig. 7-36. Calibration of gravimeter on building (after Schleusener).

be corrected for by checking with a base station or a number of them at regular intervals.[57]

F. Corrections on Observed Gravity Values

In relative gravity determinations with pendulums, the values at a field station (g_a) are calculated from the base station values (g_p) as follows:

$$g_a = g_p \left(\frac{T_p}{T_a}\right)^2 \quad \text{and} \quad g_a = g_p \frac{n_p^2}{n_a^2} \frac{(2n_a - 1)^2}{(2n_p - 1)^2}, \qquad (7\text{–}35a)$$

where T, as before, is the period and n the coincidence interval. By series expansion, these equations take the more practical form:

$$\left. \begin{aligned} g_a &= g_p - 2g_p \frac{T_a - T_p}{T_p} + 3g_p \frac{(T_a - T_p)^2}{T_p^2} + \cdots \\ g_a &= g_p + 2g_p \frac{n_a - n_p}{n_p(2n_p - 1)} - g_p(4n_p - 3)\frac{(n_a - n_p)^2}{n_p^2(2n_p - 1)^2} + \cdots, \end{aligned} \right\} \qquad (7\text{–}35a)$$

[57] See, for instance, D. C. Barton and W. T. White, Am. Geophys., Union Trans., **18**, "Geodesy," 106–107 (1937).

in which the second order terms are usually neglected. The following corrections are then applied: (1) free-air correction (the symbol for gravity thus corrected is g_0); (2) Bouguer's reduction (the symbol for gravity thus corrected is g_0'); (3) terrain correction (the symbol for gravity supplied with all three corrections is g_0''); (4) isostatic correction; (5) correction for normal gravity (γ_0). The symbol for the fully corrected gravity anomaly is $\Delta g_0''$. Corrections (1) and (2) are generally combined; reductions (3) and (4) are combined only if pendulum observations are made for the purpose of geodetic investigations. In gravimeter exploration the isostatic correction is generally omitted, correction (5) is applied in the form of a latitude reduction, and provision is made for a base correction previously discussed.

1. *The free-air reduction.* In a gravity survey all stations must be reduced to sea level (or another reference level). The change of the gravity with elevation may be obtained with sufficient accuracy by differentiating the Clairaut equation (7–10a) with respect to r, so that the vertical gradient of gravity is

$$\frac{\partial^2 U}{\partial z^2} \equiv \frac{\partial g}{\partial z} = -g\left[\frac{2}{R} + \frac{3}{MR^3}\frac{(C-A)}{}(1 - 3\sin^2\varphi) + \frac{3\omega^2 R^2}{kM}\cos^2\varphi\right], \quad (7\text{-}36a)$$

where R (substituted for r) is the earth's radius. From eq. (7-36a), we have, with sufficient accuracy,

$$\left.\begin{aligned}\frac{\partial g}{\partial z} &= -\frac{2g}{R}(1 + 0.00071\cos 2\varphi)\\[6pt]&= -0.3086(1 + 0.00071\cos 2\varphi)\text{ milligals}\cdot\text{m}^{-1}\end{aligned}\right\} \quad (7\text{-}36b)$$

and gravity (in gals), as reduced to sea level, is

$$g_0 = g + 0.0003086\,(1 + 0.00071\cos 2\varphi)\,H_{\text{meters}}, \quad (7\text{-}36c)$$

where H is absolute elevation. Table 20 gives some values for the elevation correction in milligals ($\varphi = 45°$).

TABLE 20

Elevation H (Meters)	Free-Air Correcti (Milligals)
0	0
100	+30.9
200	+61.7
300	+92.6
400	+123.4
500	+154.3
600	+185.2
700	+216.0
800	+246.9
900	+277.7
1000	+308.6

The sign of the correction is positive; the effect of the latitude term is very small. In gravimeter surveys requiring an accuracy of ± 0.1 milligal, elevations must be determined with an accuracy of one foot, and free-air and Bouguer corrections are usually combined (see eq. [7-37b]).

2. *Bouguer's reduction* is concerned with the effect of the rocks between station level and sea level not included in the free-air reduction. It lessens the amount of the free-air correction and is calculated from the attraction of an infinite horizontal plate between station and sea level since the topographic correction (see paragraph 3) "fills up" all mass deficiencies to station level. The attraction of an infinite plate of thickness h and density δ is $\Delta g = 2\pi \cdot k \cdot \delta \cdot h$ (see eq. [7-40]). Since g is approximately equal to $kM/R^2 = \frac{4}{3} k\pi R \delta_m$, ($M$ = earth's mass; δ_m = mean density), $k = 3g/4\pi R \delta_m$. Thus,

$$= \frac{3}{2} \frac{\delta}{\delta_m} \cdot \frac{h}{R} \cdot g. \qquad (7\text{-}37a)$$

Therefore, Bouguer's reduction, combined with the free-air reduction, is

$$g_0'' = g + H_{\text{meters}} (0.0003086 - 0.0000421\delta) \text{ gals.} \qquad (7\text{-}37b)$$

The last coefficient in this equation is also used in the form $0.0128 \cdot \delta$ milligals per foot.

It follows from eq. (7-37b) that in Bouguer's reduction the attraction of a plate of 10 m thickness and 2.4 density corresponds to a gravity anomaly of about 1 milligal. Therefore, in the combined free-air and Bouguer's reductions, a difference in elevation of 1 m (for a density of 2.5) corresponds to a gravity anomaly of about 0.20 milligal. With the density variations encountered in practice, the correction varies between 0.06 to 0.08 milligal per foot. Surface densities are usually determined by trial and error as discussed on page 71.

3. *Terrain correction* is of appreciable value only in very hilly country. It may be computed from elevations obtained by leveling around the station and from contour maps. The surrounding terrain is divided into sectors bounded by radial lines from and concentric circles about the station. The effect of a sector with the notation employed in Fig. 7-37 is

$$\Delta g_s = k \cdot \delta \cdot \varphi (r_1 + \sqrt{r_2^2 + h^2} - \sqrt{r_1^2 + h^2} - r_2). \qquad (7\text{-}38a)$$

The derivation of this relation is given in the next section on interpretation of gravity anomalies. By selecting zones of suitable radii and dividing them into a predetermined number of compartments, eq. (7-38a) may be solved for h. Thus, the attraction of each compartment may be determined for unit elevation. A chart and tables for twelve zones ranging

in radius from 2 m to 22 km, each containing from four to sixteen compartments, have been published by Hammer.[58]

Another procedure uses so-called graticules, or correction diagrams, in which the attraction of each element is the same, regardless of distance or azimuth. They may be prepared for use in plan view (with contour lines) or in vertical section (with terrain profiles). A graticule for use with contour lines is calculated in the following manner:[59] As indicated in Fig. 7-37, the surrounding topography is assumed to be composed of masses which have the shape of cylindrical segments. Hence, the mass of such an element is $dm = \delta \cdot r d\varphi \cdot dr \cdot dh$. Since the potential of a mass element at the origin is $U = k \cdot dm/r$, the potential due to the entire topography surrounding the station is given by

FIG. 7-37. Terrain sectors.

$$U = k\delta \int_0^\infty \int_0^{2\pi} \int_0^h r dr \cdot d\varphi \cdot dh \qquad (7\ 38b)$$

The integration is here extended for distances from 0 to infinity. In practice the calculation is carried only to the point where the terrain effect is less than the probable error. The integration may be carried out by introducing a terrain angle $\psi = \tan^{-1} h/r$. Then the vertical component of the attraction follows from a differentiation of eq. (7 38b):

$$\Delta g \equiv \qquad\qquad (1 - \cos \psi)\, dr \cdot d\varphi. \qquad (7\ 38c)$$

The mass elements are now so dimensioned that within each of them the terrain angle may be assumed to be constant. If each mass e is bounded by the concentric radii r_m and r_{m+1} and by the angles and φ_{n+1},

$$\Delta g = -k\delta(1 - \qquad\qquad \int_{r_m}^{r_{m+1}} \int_{\varphi_n}^{\varphi_{n+1}} dr \cdot d\varphi, \qquad 38d)$$

which is

$$- r_m)(\varphi_{n+1}$$

[58] S. Hammer, Geophysics, 4(3), 184-194 (July, 1939).
[59] K. Jung, Zeit. Geophys., 3(5), 201-212 (1927).

The diagram must obviously be drawn at the reduced scale of $1:p$, which means that the scale must be considered in the calculation. The elements are so calculated that their effect remains the same regardless of distance and direction. In this case it is convenient to make $r_m - r_{m+1} = 4/\pi$ and $\varphi_n - \varphi_{n+1} = \pi/40$, so that the resultant constant for each mass element becomes 0.1. If the numerical value is substituted for the gravitational constant, the effect of each mass element as shown in Fig. 7–38 is

$$= -6.67 \cdot 10^{-3} \cdot \delta \cdot p \cdot (1 - \cos \psi) \text{ microgals.} \qquad (7\text{–}38e)$$

It is seen that the spacing of the concentric circles and of the angles is the same and that the effect is independent of azimuth. In application to
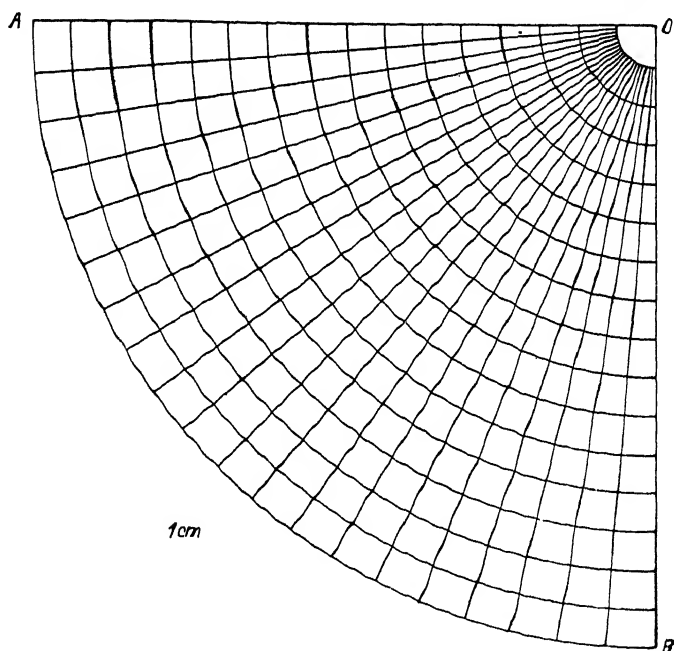
FIG. 7-38. Diagram (horizontal quadrant) for calculating terrain effect on gravity (after Jung). If ψ (terrain angle) $= \tan^{-1} h/r$, the effect of each field is $-6.67 \cdot 10^{-3} \cdot \delta \cdot p (1 - \cos \psi)$ microgals, where $1:p$ is the scale to which the diagram is drawn, and δ is density.

terrain calculation, the diagram of Fig. 7–38 is first completed for the three remaining quadrants. The surrounding terrain is surveyed by rod and alidade. When the above diagram is used, the elevations are most conveniently taken in the form of terrain angles. Lines of equal terrain angle are then drawn on transparent paper and superimposed on the diagram, and the number of elements is counted between two adjacent contour lines. The function $1 - \cos \psi$ is taken from the diagram in Fig.
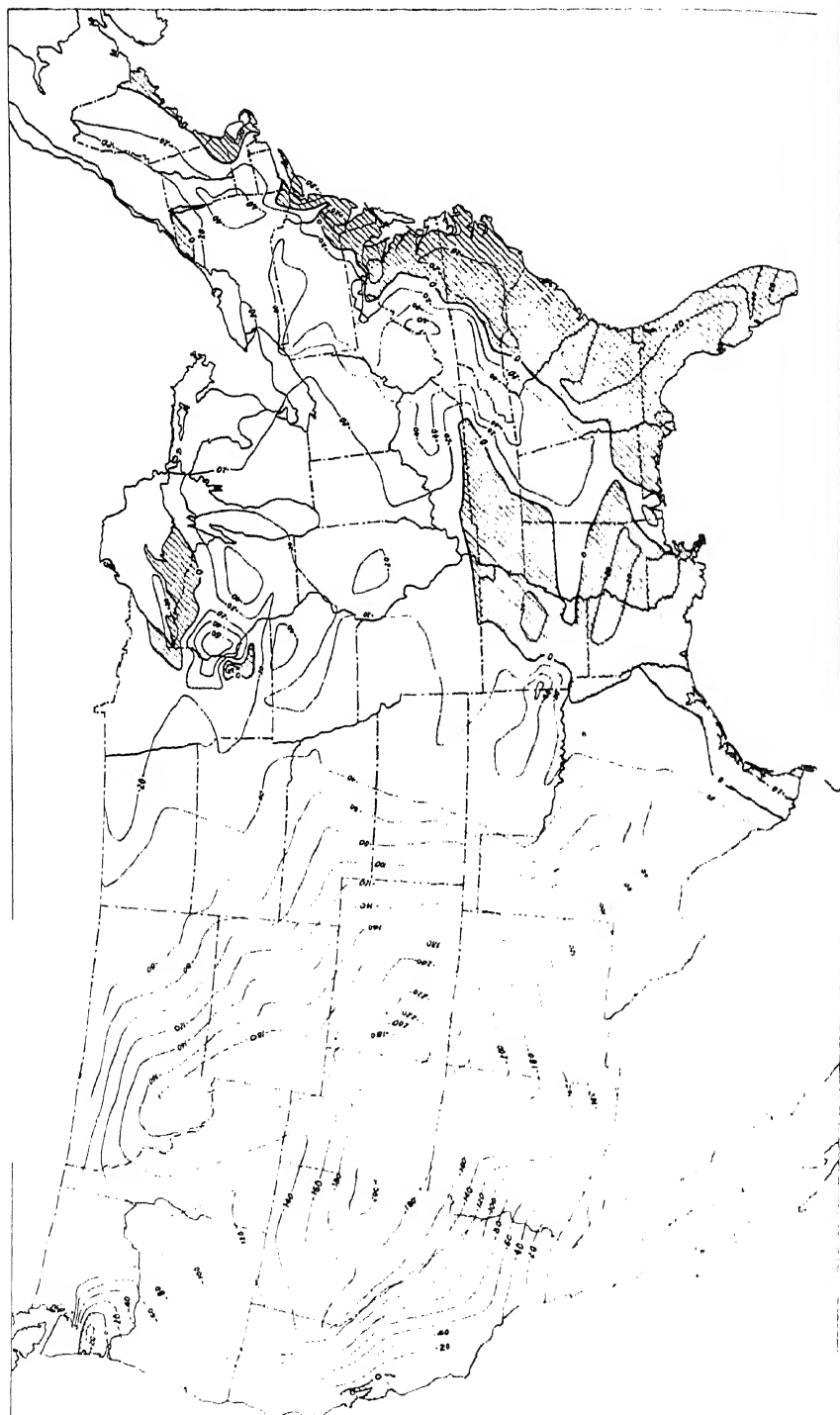
Fig. 7-40. Lines of equal Bouguer anomaly for the United States (U. S. Coast and Geod. Surv., Spec. Pub. No. 40).

U. S. Coast and Geodetic Survey

1 or 2 milligals; for less accurate work and large anomalies, 5 or 10 milligals. The results may also be represented as profile curves, preferably in conjunction with a geologic section (Δg curve).

G. Theory of Subsurface Effects; Methods of Interpretation

1. General procedure. in interpretation. The interpretation of gravity anomalies has as its objective the determination of density, shape, and depth of subsurface bodies. Theoretically this is an impossible task, as the number of unknowns is greater than the number of equations. In other words, an infinitely great number of mass arrangements may produce the same anomaly in the gravitational field. In practice, however, conditions are much more favorable. Some of the unknown quantities may be determined (1) by the application of another geophysical method, preferably one with depth control (seismic or electric); (2) by a consideration of the geological possibilities in the area. Even after some of the unknowns are thus determined, it still remains difficult to compute directly from the results the shape or depth of subsurface bodies. The "direct" method is applicable only (1) when geometrically regular forms are involved; (2) when the gravity anomaly is of regular shape; and (3) when only one disturbing body exists. The same considerations apply here as in the interpretation of torsion balance anomalies.[61]

Usually a tentative or qualitative interpretation is first made by consulting theoretical curves for a number of common geologic features, such as vertical steps, anticlines, cylinders, and the like. For routine interpretation it is of advantage to have an extensive file of such curves on hand not only for various subsurface bodies but for as many variables in each case as possible. Formulas and tables are given on pages 148–150 and 152–153, respectively, for such calculations and estimates. By consulting curves based on these and by considering the geologic possibilities, a fairly good picture of the subsurface conditions may generally be obtained.

This qualitative procedure may be supplemented by quantitative interpretation which likewise is an indirect and a trial-and-error method. Definite shapes, densities, and depths of subsurface bodies are assumed and their effects are calculated. The results are compared with the data obtained in the field, and the theoretical assumptions are changed until a satisfactory agreement is obtained. Naturally, the complexity of these computations increases with the number of geologic bodies which must be considered in the interpretation of any given anomaly.

For the calculation of subsurface effects, three methods are available:

(1) analytical methods, (2) graphical methods, and (3) integraphs. The first method is equivalent to a calculation, by the formulas given on pages 146–153, of the attraction of a body of given dimensions and depth. In the second method use is made of diagrams (graticules) described before in connection with the calculation of terrain anomalies. The geologic section is superimposed on these diagrams, and the anomaly is calculated by counting the number of elements included within the outline of the body. In the third method the area of the section of a geologic body and its effect is obtained mechanically by tracing the outline with integraphs of special design. In all of these methods considerable simplification in the calculation is possible by assuming that the geologic bodies are two dimensional instead of three dimensional, that is, that they have virtually an infinite extent in the strike direction. Regardless of whether analytical, graphical, or mechanical-integration methods are applied, the fundamental mathematics are the same in each method and differ only in such details of solution as lend themselves best to the application of each method. These relations will be discussed first before the analytical, graphical, and mechanical-integration methods are described in detail.

Fundamentally, the calculation of the gravitational effect of subsurface masses rests on Newton's law. Since the force of attraction, F, between two masses, m and m', is $F = kmm'/r^2$, the gravity anomaly or vertical component of the force may be obtained by letting $m' = 1$ and $Z \equiv \Delta g = F \cos \gamma$. Since $\cos \gamma = z/r$, the effect of a point mass on gravity is

$$\Delta g = km \frac{z}{r^3}. \qquad (7\text{–}39a)$$

For the calculation of the anomalies of all other types of masses it is more convenient to follow a different line of approach. It is based on the gravity potential of a mass element which is given by the expression $U = k \cdot dm/r$. Since $dm = \delta \cdot dv$, where δ is density and dv is element of volume, the potential is $U = k\delta \iiint_v (1/r) \, dv$ or

$$U = k\delta \iiint_v \frac{1}{r} \, dx \, dy \, dz$$

in rectilinear coordinates and

$$U = k\delta \iiint_v r \, dr \cos \varphi \, d\varphi \, d\alpha$$

$$(7\text{–}39b)$$

in polar spherical coordinates with φ as latitude and α as longitude, assuming the density to be constant throughout the volume.

Therefore, the anomaly in gravity is

$$\Delta g \equiv \frac{\partial U}{\partial z} = k\delta \iiint_v \frac{z}{r^3} \cdot dv$$

$$= k\delta \iiint_v \frac{z}{r^3} \, dx \, dy \, dz \qquad \left.\begin{array}{c} \\ \\ \\ \\ \end{array}\right\} \quad (7\text{-}39c)$$

in rectilinear coordinates, with $r = \sqrt{x^2 + y^2 + z^2}$, and

$$\Delta g = k\delta \iiint_v \frac{z}{r} \, dr \cos \varphi \, d\varphi \, d\alpha$$

in polar coordinates as above.

The gravity attraction of three-dimensional bodies derives from the "Newtonian" potential. This is not true for two-dimensional bodies, i.e. bodies which are much longer in one direction than in the other two. This direction of greatest extension is usually the strike; therefore, the attraction of such bodies is proportional to their section in a plane perpendicular to the strike. The attraction between masses in a plane derives from the "logarithmic" instead of the Newtonian potential. This follows also from eq. (7-39b) by carrying out the integration in the strike (y)-direction between the limits of + and − infinity. Therefore, while the Newtonian potential of a point mass is proportional $1/r$, the logarithmic potential of a line mass is proportional $2 \log_e 1/r$. The attraction in Newton's law is proportional $1/r^2$, but the attraction of two-dimensional bodies is proportional $1/r$:[62]

$$F = \frac{kmm'}{r} \, . \qquad (7\text{-}39d)$$

In the potential and gravity expressions a surface integral takes the place of the volume integral:

$$U = 2k\delta \iint_S \log_e \frac{1}{r} \, dS \quad \text{or} \quad = 2k\delta \iint_S \log_e \frac{1}{r} \, dx \, dz \qquad \left.\begin{array}{c} \\ \\ \\ \\ \end{array}\right\}$$

in rectilinear, and $\qquad (7\text{-}39e)$

$$U = 2k\delta \iint_S \log_e \frac{1}{r} \cdot r \, dr \, d\varphi$$

[62] This is also true for electrical and magnetic attractions which follow Coulomb's law. The attraction of a magnetic "line" is proportional $1/r$ while the attraction of a magnetic pole is proportional $1/r^2$.

in polar coordinates. Therefore, the anomaly in gravity is

$$\Delta g \equiv \frac{\partial U}{\partial z} = 2k\delta \iint_S \frac{z}{r^2}\, dS$$

or

$$= 2k\delta \iint_S \frac{z}{r^2}\, dx\, dz$$

in rectilinear and

$$= 2k\delta \iint_S \sin\varphi\, dr\, d\varphi$$

(7-39f)

in polar coordinates.

Calculations of torsion balance anomalies are likewise based upon these equations by forming the second partial derivatives with respect to the horizontal directions (in the case of the curvature values) and with respect to horizontal and vertical directions (in the case of the gradients) (see page 254).
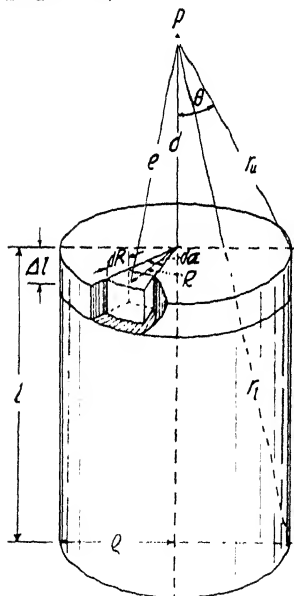
Fig. 7-41. Cylinder.

2. *"Analytical"* methods involve calculations of the anomalies produced by subsurface bodies and a substitution of their assumed dimensions and depths in the formulas derived below. For *three-dimensional* bodies, the gravity anomalies may frequently be estimated with sufficient accuracy by assuming them to be spherical, although it is, of course, understood that geologic bodies seldom have such simple geometric shapes. The effect of a sphere follows directly from eq. (7-39e), thus:

$$\Delta g = \frac{kMz}{r^3} = \frac{4}{3}\pi\delta kz \left(\frac{R}{r}\right)^3, \quad (7\text{-}40a)$$

with M as the mass and R the radius of the sphere.

A number of useful relations may be obtained by calculating the gravity anomaly due to a vertical cylinder, for a point in its axis (see Fig. 7-41).[6] Let the cylinder have the length l and the radius ρ and let d be the distance between its upper surface and the point P. Consider a mass element in a thin disk of the thickness Δl at a dis-

[63] F. R. Helmert, *Theorieen der hocheren Geodaesie*, Vol. 2, p. 144 (Leipzig, 1884).

tance R from the axis and a distance e from the point P at the surface so that

$$dm = \delta \cdot dl \cdot R \, d\alpha \cdot dR.$$

According to eq. (7–39b), its potential at P is

$$U = k\delta \iiint \frac{d\alpha \, dl R \, dR}{e},$$

which gives, for a circular disk of thickness Δl and radius ρ,

$$U = 2\pi k\delta\Delta l(\sqrt{d^2 + \rho^2} - d).$$

Hence, the gravity anomaly

$$\Delta g = -\frac{\partial U}{\partial d} = 2\pi k\delta\Delta l\left(1 - \frac{d}{\sqrt{d^2 + \rho^2}}\right). \qquad (7\text{–}40b)$$

With notation of Fig. 7–41:

$$\Delta g = 2\pi k\delta\Delta l\left(1 - \frac{d}{r_u}\right) = 2\pi k\delta\Delta l(1 - \cos\theta). \qquad (7\text{–}40c)$$

By additional integration, the potential of the entire cylinder is

$$U = k\delta \int_0^{2\pi} \int_d^{d+l} \int_0^{\rho} \frac{d\alpha \, dl R \, dR}{e},$$

and, therefore, its attraction, from eq. (7–40b), is

$$\Delta g = 2\pi k\delta \int_d^{d+l} dl\left(1 - \frac{d}{\sqrt{d^2 + \rho^2}}\right),$$

which gives

$$\Delta g = 2\pi k\delta[l + \sqrt{d^2 + \rho^2} - \sqrt{\rho^2 + (l+d)^2}]$$

and with notation as in Fig. 7–41

$$\Delta g = 2\pi k\delta[l - (r_l - r_u)]. \qquad (7\text{–}40d)$$

Equations (7–40c) and (7–40d) permit a number of interesting deductions for extreme cases.

If the radius of a thin disk becomes very large, $\cos\theta$ is zero. Therefore the gravity anomaly due to an infinite bed of thickness Δl, is

$$\Delta g = 2\pi k\delta\Delta l. \qquad (7\text{–}40e)$$

This formula is identical with that giving the attraction of the rock material between station and sea level in Bouguer's reduction (see page

137). It is significant that in formula (7-40e) *no effect of depth* is contained. The gravity method has, therefore, no resolving power; for very extended formations their attraction is proportional to thickness but not to depth.

It should be noted at this point that in all equations concerned with gravity anomalies of heavy bodies, the *difference* between the density of a body, δ', and that of the surrounding formation, δ_0, must be substituted in place of the absolute density, so that

$$\delta = \delta' - \delta_0. \tag{7-40f}$$

A few other extremes of formula (7-40d) are of interest. If a station is located on the upper surface of a cylindrical mass, the anomalous gravity is,

$$\Delta g = 2\pi k\delta[l - (r_1 - \rho)].$$

If the cylinder is very long compared with its radius, the gravity anomaly is

$$\Delta g = 2\pi k\delta\rho.$$

This indicates that for a very long cylinder the gravity effect depends only on its radius. In Special Publication No. 99 of the U. S. Coast and Geodetic Survey, tabulations are given for the effects of cylinders of varying lengths (or depths to bottom), l, and varying radii, ρ, for a station located at the center of the upper surface.

These tables may also be used (1) if the station is not located on the upper surface, but at a distance, d, above it; (2) if the station is located off the cylinder, but in the level of the upper surface; (3) if the station is both off the center and above the upper surface of the cylinder. In the first case the attraction of a second cylinder with $l_2 = d$ is subtracted from that of a cylinder of the length l_1. In the second case, if the distance between station and axis of the cylinder is R, anomalies of two cylinders are subtracted from each other. Thus, the effect of a hollow cylinder is obtained, whose thickness is equal to the diameter 2ρ of the cylinder wanted. Its effect is then multiplied by the ratio of the surfaces, (sought cylinder)/(surface ring), so that in abbreviated notation

$$[C_{(R+\rho)} - C_{(R-\rho)}]\left[\frac{\rho^2}{(R + \rho)^2 - (R - \rho)^2}\right], \tag{7-40g}$$

where $C_{(R+\rho)}$ is the attraction of the cylinder with the radius $R + \rho$, and $C_{(R-\rho)}$ is the attraction of the cylinder with the radius $R - \rho$. If the station is off center and above the cylinder, the procedures followed in the first and second cases are combined.

From eq. (7-40d) and by integrating between 0 and φ instead of between

0 and 2π, we obtain, for a cylindrical sector (Fig. 7-42a) with the central angle φ,

$$\Delta g = \varphi k \delta [l - (r_l - r_u)]; \quad (7\text{-}41a)$$

and, if the station is on the sector,

$$\Delta g = \varphi k \delta [l - (r_l - \rho)]. \quad (7\text{-}41b)$$

For a cylindrical compartment the gravity anomaly with notation as used in Fig. (7-42b) is

$$\Delta g = \varphi k \delta (r_3 + r_2 - r_1 - r_4),$$

Fig. 7-42. Cylindrical sectors and segments.

which follows from (7-41a) by subtraction of an inner from an outer sector.

Eq. (7-41c) has a wide application, since irregular three-dimensional masses may be divided up into such compartments. It may, therefore, be used for terrain corrections. Substituting for

$$r_1 : \sqrt{\rho_1^2 + d^2} \qquad r_3 : \sqrt{\rho_1^2 + (d + l)^2}$$
$$r_2 : \sqrt{\rho_2^2 + d^2} \qquad r_4 : \sqrt{\rho_2^2 + (d + l)^2},$$

and letting $d = 0$ and $l = h$, since the station is usually located level with the lower surface of the segment,

$$\Delta g = \varphi k \delta (\rho_1 + \sqrt{\rho_2^2 + h^2} - \sqrt{\rho_1^2 + h^2} - \rho_2),$$

which is identical with (7-38a).

Formula (7-41c) may also be used for computing the effect of irregular subterranean masses. In practice, however, formula (7-40d) is preferred in the form

$$\Delta g = 2\pi k \delta (\sqrt{\rho^2 + d^2} - \sqrt{\rho^2 + (l + d)^2} + l),$$

which may be written

$$\Delta g = 2\pi k \delta \rho \left(\sqrt{1 + \left(\frac{d}{\rho}\right)^2} - \sqrt{1 + \left(\frac{d}{\rho} + \frac{l}{\rho}\right)^2} + \frac{l}{\rho} \right). \quad (7\text{-}41d)$$

In this equation d/ρ and l/ρ are considered as variables[64] (see Fig. 7-43). To find the anomaly of a sector, the effect of a cylinder of given l/ρ and d/ρ ratio is obtained from the graph and multiplied by the outer radius, ρ_2. From it the effect of another cylinder is subtracted (likewise

[64] See F. E. Wright and F. A. Vening Meinesz, Bull. Naval Obs., **XIII**, app. 1 (1930).

obtained from the diagram and multiplied by ρ_1). This difference is finally multiplied by $\Delta\delta\varphi/2\pi$, to obtain the attraction of a compartment.

Calculation of the gravity anomalies of subsurface geologic features which are extended in the direction of strike (*two-dimensional* features) is based on the equations for the logarithmic potential, (7-39e) and (7-39f). For example, application of these formulas to the case of a
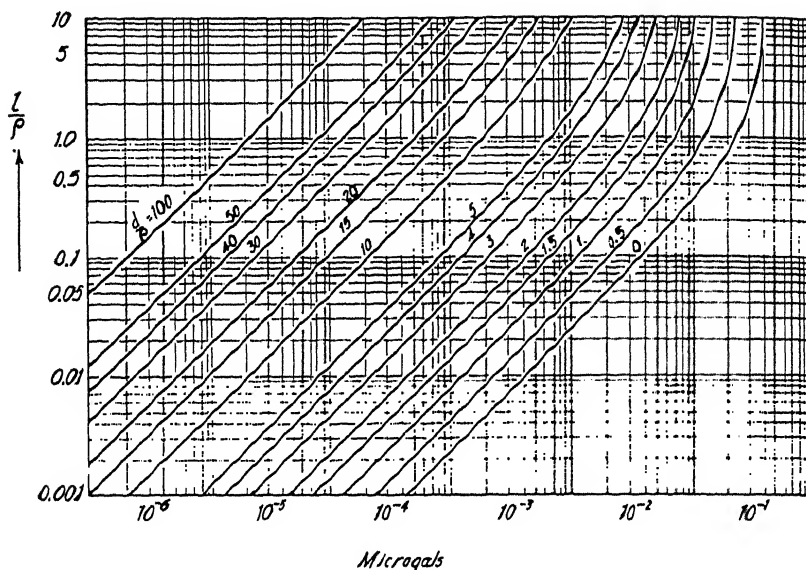
FIG. 7-43. Attraction of cylinders of various length/radius and depth/radius ratios (after Wright).

horizontal cylinder (Fig. 7-44a) gives directly $\Delta g/2k\delta = \mathbf{S}\cdot z/r^2 = \mathbf{S} \sin\varphi/r$; hence,

$$\Delta g = 2k\delta z\left(\frac{R}{r}\right)^2 = \frac{2\pi k\delta R^2 \sin\varphi}{r}. \tag{7-42a}$$

Rectangular prisms (Fig. 7-44b) represent in approximation such geologic bodies as vertical dikes, ore veins, or horizontally stratified formations. Their attraction may be calculated by integration of eq. (7-39f). If d is the depth to its upper surface, D the depth to the lower surface, x the distance of the station from the far face, x' the distance from the near face, and b the breadth:

$$\Delta g = 2k\delta \int_0^b \int_d^D \frac{z\cdot dx\,dz}{z^2 + (x-x')^2} = 2k\delta \int_0^b \log_e \sqrt{\frac{D^2 + (x-x')^2}{d^2 + (x-x')^2}} \qquad \text{or}$$

$$\Delta g = 2k\delta \left[x \log_e \sqrt{\frac{D^2 + x^2}{d^2 + x^2}} - (x - b) \log_e \sqrt{\frac{D^2 + (x - b)^2}{d^2 + (x - b)^2}} \right.$$

$$\left. + D \left(\tan^{-1} \frac{x}{D} - \tan^{-1} \frac{x - b}{D} \right) - d \left(\tan^{-1} \frac{x}{d} - \tan^{-1} \frac{x - b}{d} \right) \right].$$
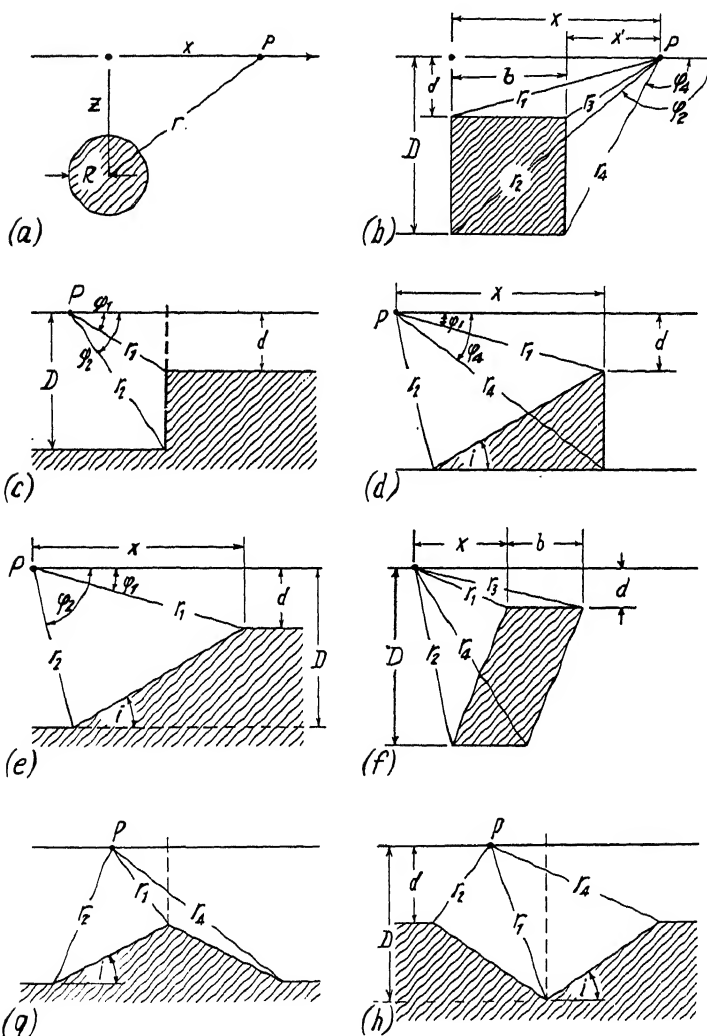
FIG. 7-44. Effects of two-dimensional bodies on gravity. (a) Cylinder, (b) rectangle, (c) step fault, (d) triangular prism, (e) slope, (f) inclined bed, (g) anticline, (h) syncline. In (d), (e) and (f), the distance x should extend to a point but halfway up the slope.

With $x - x' = b$, and

$$d^2 + x^2 = r_1^2 \qquad x = d \tan \varphi_1$$

$$D^2 + x^2 = r_2^2 \qquad x = D \tan \varphi_2$$

$$d^2 + (x - b)^2 = r_3^2 \qquad x - b = d \tan \varphi_3$$

$$D^2 + (x - b)^2 = r_4^2 \qquad x - b = D \tan \varphi_4,$$

the anomaly in gravity is

$$\Delta g = 2k\delta \left[x \log_e \frac{r_2 r_3}{\text{—} \text{—}} + b \log_e \frac{'4}{\text{—}} + D(\varphi_2 - \varphi_4) - \right.$$

If a vertical dike has a considerable extent in depth, $r_2 = r_4$ and $D(\varphi_2 - \varphi_4) = b$. The anomaly in gravity then becomes

$$\Delta g = 2k\delta \left[x \log_e \frac{r_3}{r_1} + b \left(\log_e \frac{r_4}{r_3} + 1 \right) - d(\varphi_1 - \varphi_3) \right]. \quad (7\text{-}42c)$$

It is seen that (contrary to the corresponding torsion balance anomalies) the attraction of a vertical dike cannot possibly be calculated without making some assumption about the depth to its lower end. Formula (7-42b) may be used to calculate the effect of a fault or buried escarpment (Fig. 7-44c). Then $r_3 = r_4$, $D\varphi_4 \doteq d\varphi_3$, and

$$\Delta g = 2k\delta \left(x \log_e \frac{r_2}{r_1} + D\varphi_2 - d\varphi_1 \right). \quad (7\text{-}42d)$$

At a station far removed from the edge, $r_2/r_1 \doteq 1$ and $\varphi_2 \approx \varphi_1 \doteq \pi$ so that $\Delta g = 2\pi k\delta(D - d)$. This is identical with the formula for an infinite disk or with Bouguer's formula. The Bouguer effect is twice as great as the gravity anomaly directly over the edge of the escarpment. If $x = 0$, then $\varphi_2 = \varphi_1 = \pi/2$ or

$$\Delta g = \pi k\delta(D - d). \quad (7\text{-}42e)$$

If the section of a horizontal two-dimensional prism is triangular (Fig. 7-44d), the gravity anomaly is

$$\Delta g = 2k\delta \left\{ - [x \sin i + d \cos i] \left[\sin i \log_e \frac{r_2}{r_1} + \cos i \right. \right.$$

$$\left. \left. - x \log_e \frac{r_4}{r_1} + D(\varphi_2 - \varphi_4) \right\}. \quad (7\text{-}43a)$$

Adding to this the effect of a vertical step $(7\text{–}42d)$, the following gravity anomaly for a slope (Fig. $7\text{–}44e$) is obtained:

$$\Delta g = 2k\delta\left\{- [x \sin i + d \cos i]\left[\sin i \log_e \frac{r_2}{r_1} + \cos i(\varphi_2 - \varphi_1)\right]\right.$$
$$\left. + D\varphi_2 - d\varphi_1\right\}. \quad (7\text{–}43b)$$

Above a very extended slope, $r_2/r_1 \doteq 1$, $\varphi_2 - \varphi_1 \doteq \pi$, $d\varphi_1 \doteq 0$ and $\cos i \approx 1$ so that

$$\Delta g = 2k\delta \left[- k(x \sin i + d) + D\varphi_2\right] \quad (7\text{–}43c)$$

By a subtraction of two slopes with identical dip, the effect of an inclined bed, ore vein, or the like (Fig. $7\text{–}44f$), can be calculated:

$$\frac{\Delta g}{2k\delta} = - [x \sin i + d \cos i]\left[\sin i \log_e \frac{r_2 r_3}{r_1 r_4} + \cos i(\varphi_2 - \varphi_1 + \varphi_3 - \varphi_4)\right]$$
$$+ b \sin i\left[\sin i \log_e \frac{r_4}{r_3} + \cos i(\varphi_4 - \varphi_3)\right] + D(\varphi_2 - \varphi_4) - d(\varphi_1 - \varphi_3).$$
$$(7\text{–}43d)$$

If the inclined formation has great depth, the same approximations as before may be introduced, namely, $r_2 = r_4$ and $D(\varphi_2 - \varphi_4) = b$, so that

$$\frac{\Delta g}{2k\delta} = - [x \sin i + d \cos i]\left[\sin i \log_e \frac{r_3}{r_1} + \cos i(\varphi_2 - \varphi_1 + \varphi_3 - \varphi_4)\right]$$
$$+ b \sin i\left[\sin i \log_e \frac{r_4}{r_3} + \cos i(\varphi_4 - \varphi_3)\right] + b - d(\varphi_1 - \varphi_3).$$
$$(7\text{–}43e)$$

For symmetrical anticlines and synclines (Fig. $7\text{–}44g$ and h) the anomalies are calculated by adding the attractions of two triangular prisms or slopes respectively.

3. In *graphical interpretation methods*, graticule diagrams are superimposed on structural maps or profiles. Gravity anomalies are obtained by counting the mass elements included within adjacent contours (three-dimensional diagrams), or (in profiles) within the outlines of the formations involved (two-dimensional diagrams). Construction of the former is based on the same analysis that is used in the preparation of terrain correction charts (see page 138) or the calculation of the effects of cylindrical compartments (see page 149). In application the scale of the geologic sections must be considered. The calculation of two-dimensional diagrams is based on formula $(7\text{–}39f)$ with polar coordinates. A vertical

subsurface quadrant is divided into compartments bounded by concentric circles with radii r_m and by angles φ_n. Then the effect of one compartment is

$$\frac{\partial U}{} \qquad\qquad -r_m)(\cos\varphi_{n+1} - \cos\varphi_n). \qquad (7\text{--}44a)$$

A diagram constructed in this manner is shown in Fig. 7–45. The effect of each field is $6.67\cdot10^{-3}\cdot\delta\cdot p$ microgals, where p is the scale of the
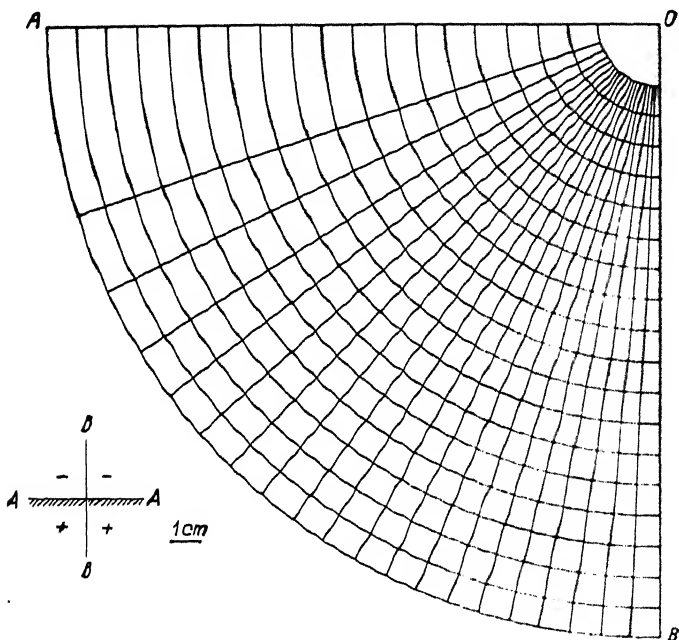
FIG. 7-45. Diagram for the calculation of attractions due to two-dimensional (after Jung). Unit effect: $6.67\cdot10^{-6}\cdot\delta\cdot p$ milligal; scale: $1:p$.

geologic section with which the diagram is used. For subsurface masses the anomaly is always positive, the diagram being inverted north of the station. For masses above the horizon the anomaly is negative. Masses in the horizon are ineffective; masses vertically below the station most effective.

4. *Integraphs.* Since the gravity anomalies of two-dimensional masses depend on their area (eq. [7 39f]), "planimeter" methods may be used to calculate the attraction of geologic features of irregular outline. However, the effect of area is also dependent on distance and vertical angle. The geologic section must be redrawn on distorted coordinates when used with

an *ordinary* planimeter (Below's method[65]). According to eq. (7-38c), the anomaly produced by an element $r\,dr\,d\varphi$, whose elevation appears at the angle ψ, is given by $\Delta g = -k\delta(1 - \cos\psi)\cdot\iint dr\cdot d\varphi$. If a new R, is substituted for $\sqrt{2r}$, the anomaly becomes

$$\Delta g = -\tfrac{1}{4}k\delta(1 - \cos\psi)\iint R\,dR\,d\varphi, \qquad (7\text{-}44b)$$

where $R\,dR\,d\varphi$ is an areal element whose attraction now is independent of distance and requires representation in a scale so distorted that $R = 1.4\,\sqrt{r}$ (Fig. 7-46). If the surface elevations are represented by lines of equal angle, ψ, terrain effects between adjacent contour lines may be determined by planimetering. The same method is adaptable to calculation of irregular subsurface masses represented by contours. For two-dimensional features it is necessary to distort both the radius and the angle scale. In formula (7-39f) the integral $\iint \sin\varphi\,d\varphi\,dr$ may be transformed

[65] K. Jung, *op. cit.*, 6 (2), 114–122 (1930).
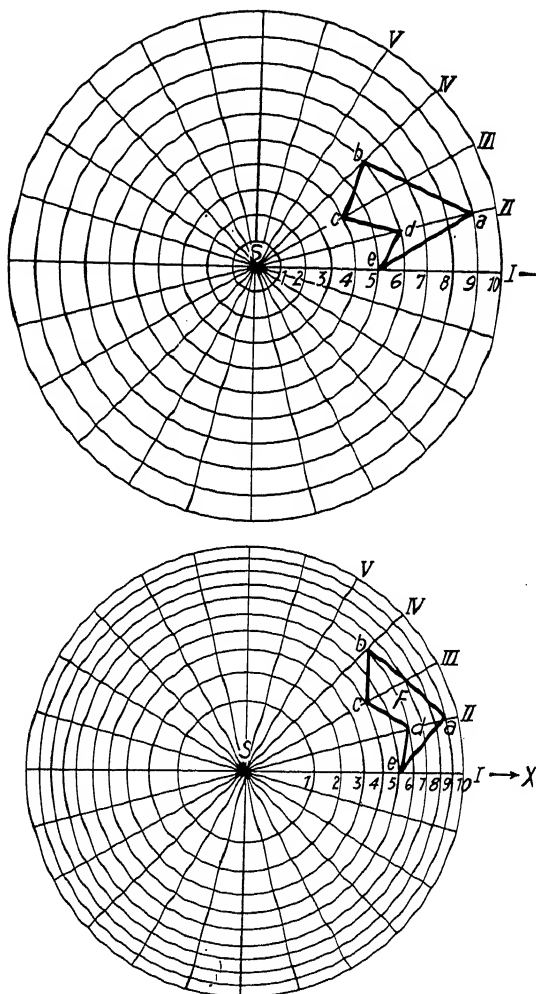
FIG. 7-46. Radial scale distortion for planimetric determinations of attractions due to three-dimensional masses (after Jung).

into a surface integral independent of distance and azimuth by the substitution $R = \sqrt{2r}$ and $\Phi = \cos\varphi$. Then $\iint \sin\varphi \, d\varphi \, dr \equiv \tfrac{1}{4} \iint R \, dR \, d\Phi$.

The resulting scale distortion may be seen in Fig. 7-47.
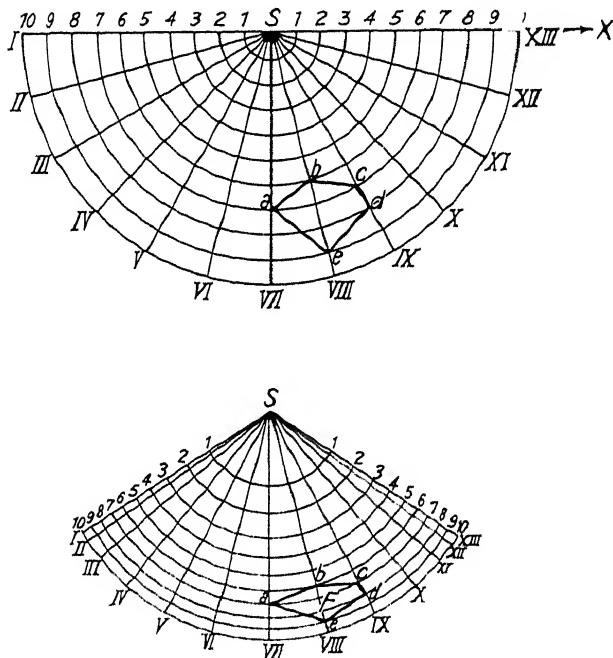
Fig. 7-47. Radial and vertical angle scale distortion for planimetric determinations of anomalies of two-dimensional masses (after Jung).

Scale distortion may be avoided by the use of a special integraph. If the double integral in eq. (7-39f) is reduced to a single integral, the attraction of a two-dimensional body may be written

$$= 2k\delta \int r \sin\varphi \, d\varphi. \qquad (7\text{-}44c)$$

The function of the integraph shown in Fig. 7-48 is to carry out the multiplication $d\varphi \times r \sin\varphi$. It consists of a finder, F, moving radially (distance r) on the arm, A, which in turn is rigidly coupled to the disk, D. The latter thus rotates by amounts $d\varphi$ when a section is traced. The finder, F, engages the bridge, B, which carries the roller, R. This roller is rotated by the disk, D, and transfers its reading to the scale, S. Because of the coupling of A and B, the distance of the roller from the center (station) is thus always $r \sin\varphi$ and is rotated by the amount of this

distance as lever arm, multiplied by the angular disk displacements $d\varphi$. Since the horizontal gravity component is given by $\iint \cos \varphi \, d\varphi \, dr$, its value for a given section may be obtained with the same integraph by simply interchanging the z and x axes.

(a)

(b)
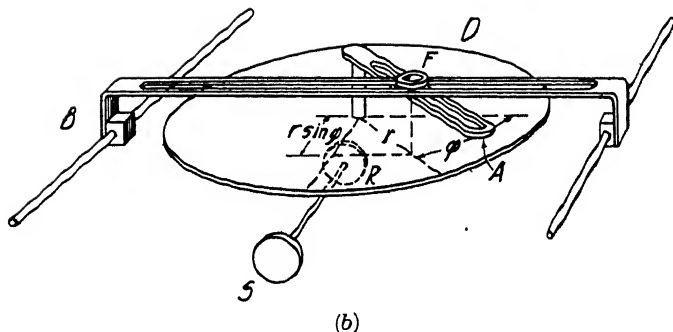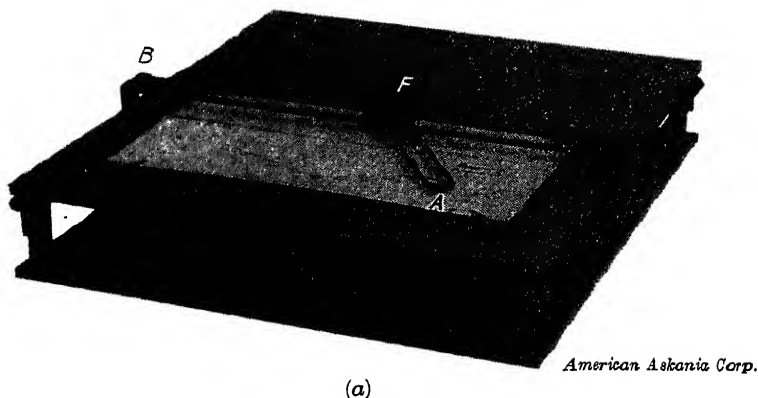
FIG. 7-48. Integraph for the calculation of horizontal and vertical components of gravity attraction of two-dimensional bodies.

H. RESULTS OF PENDULUM AND GRAVIMETER SURVEYS

The following short description of results of gravity surveys is not intended to convey the idea that a limited amount of such work has been done. Owing to the fact that in the earlier days of geophysical prospecting the pendulum method was less widely used than the torsion balance and because of the comparatively short length of time that gravimeters have been employed, not much data on results have found their way into the literature. Much information on gravity variations over known geologic structures has been accumulated in the course of calculations of relative gravity from torsion balance gradient observations. These in-

direct determinations of gravity, however, by the torsion balance are excluded from this section and discussed on pages 270–292 of this chapter.

Reference is made in this connection to Fig. 7–104, showing the gravity anomalies on salt anticlines in the Maros Valley in Hungary; to Fig. 7–108, in which the gravity results in the Solikamsk area (northern Urals) are given; to Fig. 7–109, illustrating the gravity anomalies in a portion of the Emba district in Russia; to Fig. 7–115, representing one of the earliest gravity surveys in oil exploration (Egbell anticline); and to Fig. 10–67, in which a gravity profile across the Grozny anticline is illustrated.
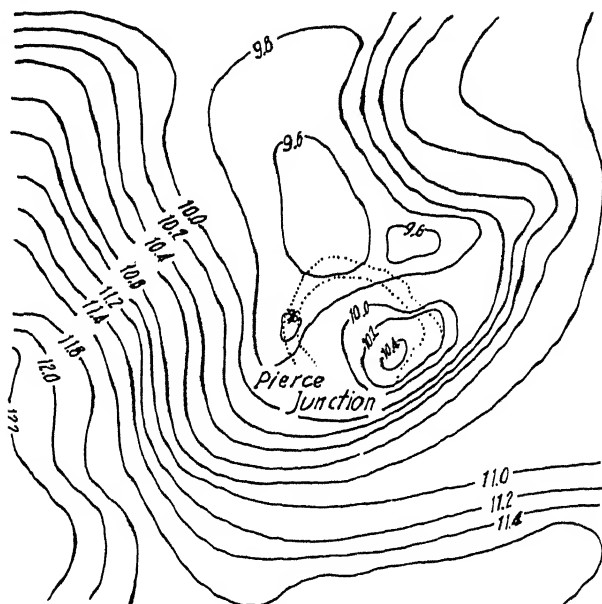
FIG. 7–49. Gravimeter survey of Pierce Junction field (after Skeeters).

Most gravimeter and pendulum work has probably been done in salt-dome exploration. Fig. 7–49 represents an example of a comparatively shallow dome, the gravity anomaly being about 1.0 to 1.4 milligals. The dome shown in Fig. 7–50a was reached at the indicated well location at a depth of 7200 feet, the anomaly along the apparent axis of the salt anticline being about 2 milligals, rising to the east and west to several milligals. One of the earliest pendulum surveys across a salt dome (Wietze, northern Germany) is illustrated in Fig. 7–105. Seismic and torsion balance data for the same dome are also shown. The possibilities of the gravimeter on nonsalt dome type of structures are demonstrated by the survey of the Ramsey field in Oklahoma,[65a] shown in Fig. 7–50b, which indicates an un-

[65a] J. F. Evans, Oil and Gas J., **38**(26), 37 (Nov. 9, 1939). Contour interval: 0.2 milligal.
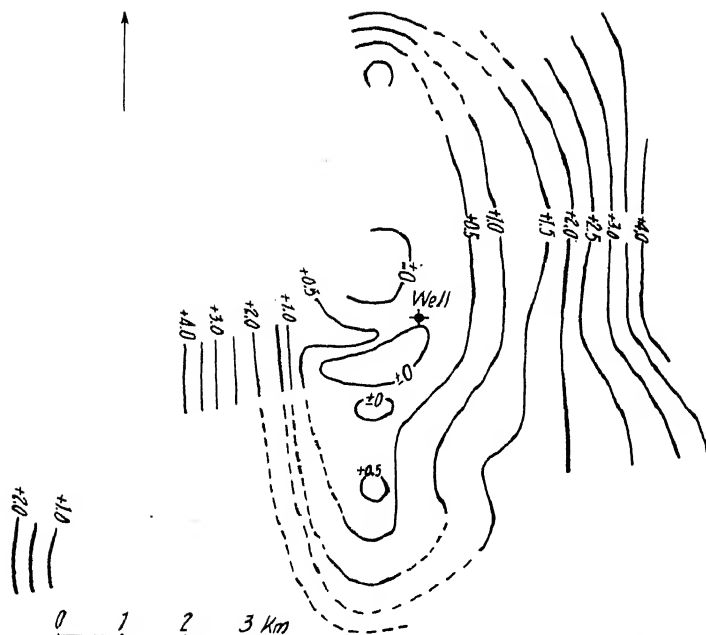
Fɪɢ. 7-50a. Gravimeter results on Schneeheide salt dome (Germany). Salt in well at depth of 7200 feet.
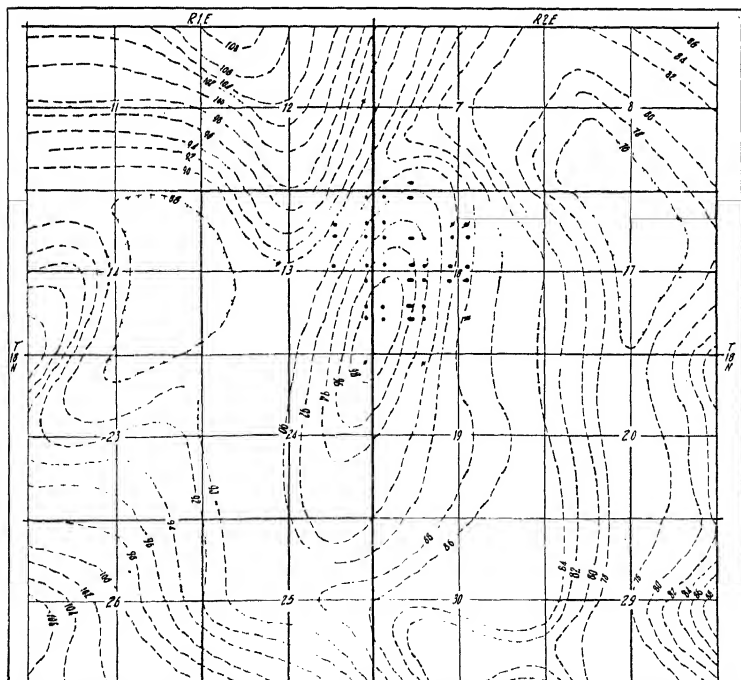
Fɪɢ. 7-50b. Gravimeter survey of Ramsey field, Oklahoma (after Evans).

usually good parallelism of production and gravity anomaly, after correcting the observed values for regional variation.

Fig. 7-51a shows a gravity (pendulum) survey of one of the most important oil regions of the world—the Apsheron Peninsula and adjacent portions of Azerbeijan near the Caspian Sea. The oil fields near Baku (Bibi Eibat, Balachany, and Surachany) are situated in a gravity trough extending along the peninsula with an anomaly from 100 to 130 milligals.
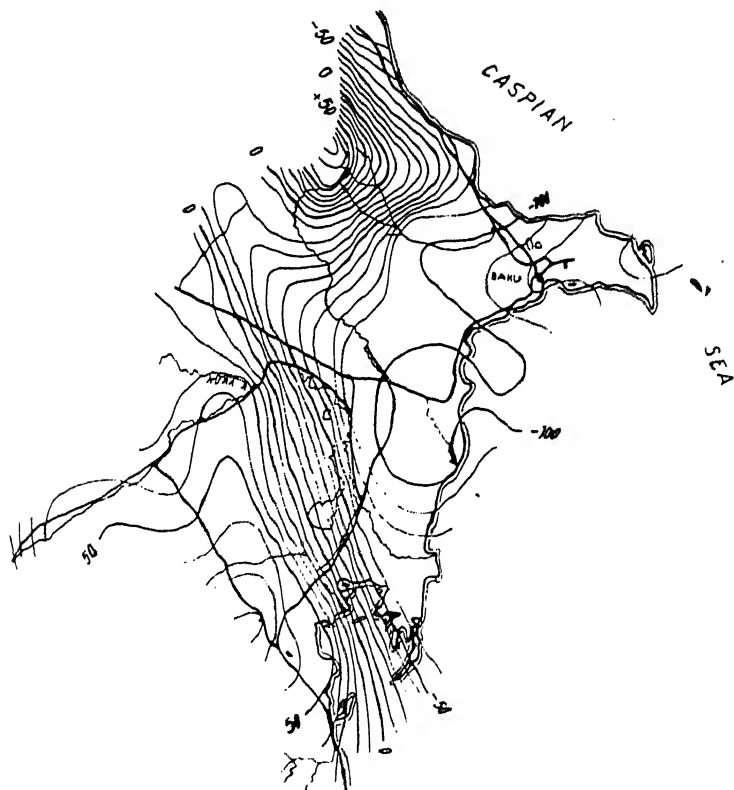
Fig. 7-51a. Pendulum observations of relative gravity in East Azerbaijan (southeast Caucasus) (after Se

Details of the anticlines on which these fields are situated are not.
The general trend of the strata from NW to SE is indicated by the steep gradient portion in the SW part of this area.

The gravity map of the Wichita and Arbuckle Mountain area shown in Fig. 7-51b is discussed at this time, although the greater portion of the gravity data was derived from torsion-balance observations. The gravity anomalies are caused largely by the crystalline basement rocks,

to which is probably added the influence of the old Ordovician land surface. The main features of the map are a series of maxima corresponding to the Arbuckle Mountains, the continuation of the Wichita Mountains (Walters Arch) and the Münster Arch.   A pronounced minimum is found between the Arbuckle Mountains on one side and the Wichita Mountains and their south-eastward continuation on the other, lending strong support to the theory first advanced on the basis of geologic evidence that the Arbuckle
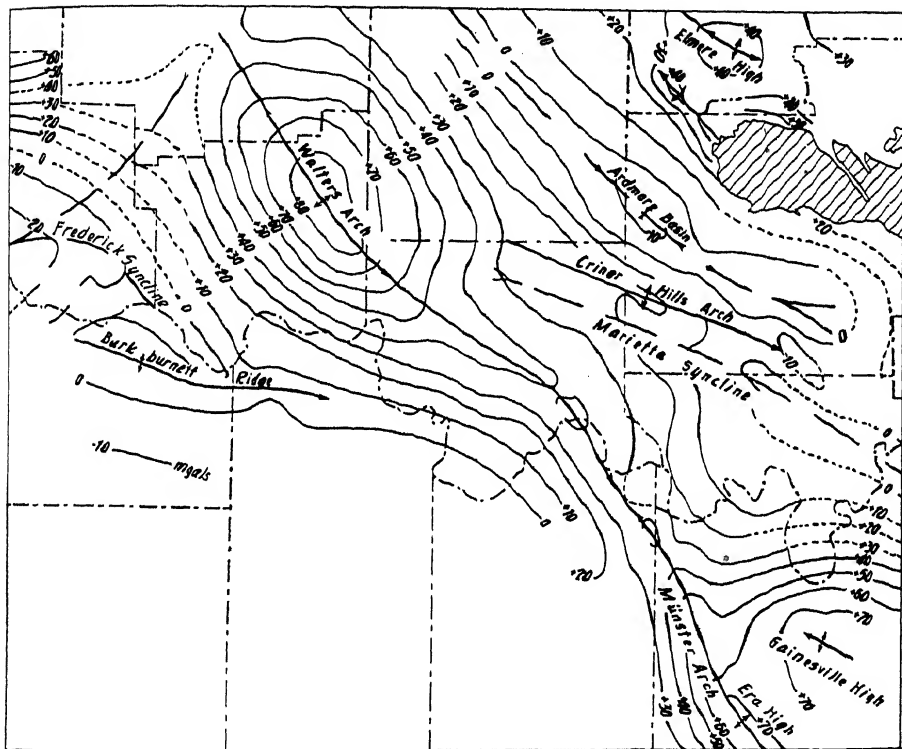
FIG. 7-51b. Gravimetric map of Wichita and Arbuckle mountains and of structural trends along the Oklahoma-Texas border (after Van Weelden).

and Wichita Mountains are separate systems separated by the Anadarko and Ardmore basins.[66]   A comparison of the gravity data with the results of magnetic surveys made in the same area is of interest (see page 431).

Where overburden is shallow and veins comparatively wide, gravimeter observations will give good results in ore prospecting.   Accuracy requirements are high and corrections for adjacent formations often necessary.

[66] A. Van Weelden, World Petrol. Congr. Proc., Sec. B. I., 174–176 (1934).
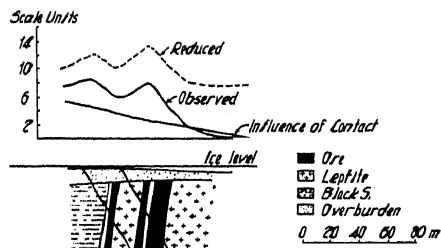
(a)
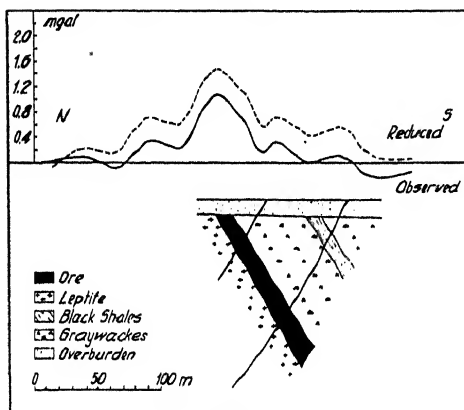
(b)

FIG. 7-52. Gravimeter observations (a) on Mensträsk Lake, and (b) at Lake Långsele, Skellefte district, Sweden (after Lindbladand Malmquist).

It is not believed that this method will give so distinct results as electrical prospecting, although it would be useful to segregate electrical anomalies due to noncommercial mineral disseminations from commercial ore indications. Fig. 7-52 shows the results of gravity measurements made on the ice at Mensträsk in Sweden. The ore bodies below the lake, discovered by electrical prospecting, consist of three parallel lenticular sulfide veins of steep north dip; the thickness of the southern vein is about 30 feet, that of the others from 10 to 13 feet. Leptite formation occurs in the south, black schists in the north. Owing to their difference in density (0.2), a correction was applied. The indications are shifted to the north with respect to the suboutcrop of the veins. This shift may partially result from the dip and partially from the effect of the contact. The shift above the southern ore body may be explained by the occurrence of an additional body to the north.

VI. TIME VARIATIONS OF THE GRAVITATIONAL FIELD

Variations of gravity with time may be divided into periodic and nonperiodic phenomena. The former are related to the position of sun and moon, the latter are caused by natural changes of geologic origin or by artificial mass transports. While magnetic variations are of the order of 10^{-3} to 10^{-4} of the normal terrestrial magnetic field, gravity variations represent only a 10 to 100 millionth part of normal gravity. As a rule they do not interfere with gravimeter exploration but may be recorded by stationary instruments. Observations of gravity variations are of scientific value in the analysis of geologic forces bringing about slow changes in

elevation (epirogenic movements). They are of practical importance in determining corrections for (torsion balance) coast stations, in ground subsidence problems, and in the investigation of subsurface mass displacements leading to earthquakes and volcanic eruptions. The following discussion deals not only with variations of gravity itself but also with related variations of torsion balance quantities and the deflection of the vertical.

A. Planetary (Lunar) Variations

Planetary variations of the gravitational field and the well-known "oceanic" and "bodily" tides are related phenomena. Tidal forces are due to the fact that the attractions of sun and moon at the earth's surface deviate in direction and intensity from those attractions effective at the earth's center. They would be present even if the earth did not rotate,

would be approximately constant for any given surface point, and would have but semimonthly or semiannual periods. The earth's rotation produces a migration of a double tidal bulge with a period of one-half lunar day, the maximum amplitudes occurring if the

FIG. 7-53. Tidal forces.

tide-generating body is in the zenith or nadir. Superposition of the semidiurnal, semimonthly, or semiannual periods brings about excessive or abnormally reduced tidal amplitudes, the more important of these being known as "spring" and "neap" tide.
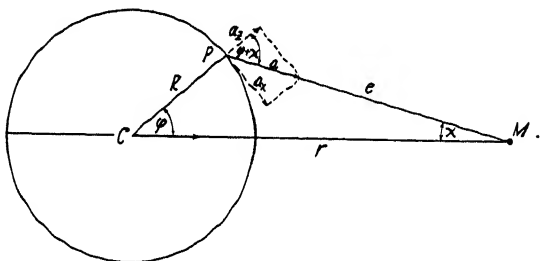
The variations in intensity and direction of gravity which can be calculated from the distance and mass of the sun and the moon are modified by the change of distance of a surface point from the earth's center, brought about by the bodily tide. The observed variations in the direction of the vertical (recorded with horizontal pendulums) are about $\frac{2}{3}$ to $\frac{4}{5}$ the theoretical values; the observed variations in gravity are about 1.2 times greater than the theoretical variations.

In Fig. 7-53, let M be a heavenly body (sun or moon) at a distance r from the earth's center, C, and at a distance e from a point P at the earth's surface in the latitude φ. The angle between r and e is the parallax of the star, or χ. If the star is in the zenith, the attraction on P is $-(kM/e^2)$ (negative in respect to gravity), and at C it is $-(kM/r^2)$. To deduct the latter from the former, it is convenient to resolve either force into its ver-

tical and horizontal components. For P the vertical component is then proportional to $\cos (\varphi + \chi)$ and for C, proportional to $\cos \varphi$. The horizontal component is proportional $\sin (\varphi + \chi)$ for P and proportional $\sin \varphi$ for C. The resultant deflection of the vertical, $\Delta\psi$, is equal to the difference of the horizontal components divided by gravity, so that

$$
\left.
\begin{aligned}
\Delta g_z &= -kM\left[\frac{\cos (\varphi + \chi)}{e^2} - \frac{\cos \varphi}{r^2}\right] \\
&= \frac{kM}{r^2}\left[\frac{\frac{R}{r} - \cos \varphi}{\left[1 - 2\frac{R}{r}\cos \varphi + \left(\frac{R}{r}\right)^2\right]^{\frac{3}{2}}} + \cos \varphi\right] \\
\Delta g_h &= kM\left[\frac{\sin (\varphi + \chi)}{e^2} - \frac{\sin \varphi}{r^2}\right] \\
&= \frac{kM}{r^2}\left[\frac{\sin \varphi}{\left[1 - 2\frac{R}{r}\cos \varphi + \left(\frac{R}{r}\right)^2\right]^{\frac{3}{2}}} - \sin \varphi\right] \\
\Delta\psi &= -\frac{\Delta g_h}{g} = -\frac{kM}{gr^2}\left[\frac{\sin \varphi}{\left[1 - 2\frac{R}{r}\cos \varphi + \left(\frac{R}{r}\right)^2\right]^{\frac{3}{2}}} - \sin \varphi\right]
\end{aligned}
\right\} \quad (7\text{-}45a)
$$

As the earth's radius, R, is $6.37 \cdot 10^3$ km and r for the moon $= 3.8 \cdot 10^5$ km and for the sun $= 1.5 \cdot 10^8$ km, it follows that R/r is $1.7 \cdot 10^{-2}$ for the moon and $4.3 \cdot 10^{-5}$ for the sun (and may, therefore, be neglected). Then

$$
\left.
\begin{aligned}
\Delta g_z &= -\frac{3kMR}{2r^3}\left(\cos 2\varphi + \frac{1}{3}\right) \text{ milligals} \\
\Delta g_h &= \frac{3kMR}{2r^3}\sin 2\varphi \text{ milligals, and} \\
\Delta\psi &= -\frac{3kMR}{2gr^3}\sin 2\varphi
\end{aligned}
\right\} \quad (7\text{-}45b)
$$

The coefficient $3kMR/2r^3$ is 0.0824 milligals for the moon and 0.0376 for the sun, and the coefficient $3kMR/2gr^3$ is 0.0173 arc-sec. for the moon and 0.0079 arc-sec. for the sun.

Tabulations of lunar and solar tide-components have been published by K. Jung.[66a] R. D. Wyckoff[67] calculated the total amplitude for the two principal lunar and solar semidiurnal, the principal lunar and solar diurnal, and the lunisolar diurnal tides for Pittsburgh, and found 0.167

[66a] Handb. Exper. Phys. **25**(2), 322 (1931).

[67] Trans. Amer. Geophys. Union, 17th Ann. M t., pt. I, 46-52, July,

milligals. Therefore, the maximum possible variation between the maximum and minimum of the curves would have been approximately 0.34 milligals. The theoretical values agreed well with the records of a stationary vertical seismo-gravimeter.

B. SECULAR (GEOLOGIC) VARIATIONS

In the course of geologic time, considerable changes in mass distribution occur near the earth's surface because of erosion, deposition of sediments, glaciation, removal of ice caps, orogenic and epeirogenic movements, faulting, volcanism, magma migrations, and the like. That some of these factors bring about changes in elevation has been definitely established. A well-known example is the uplift of Fennoscandia, whose postglacial rise is assumed to amount to a maximum of 275 m. Areas in which such movements occur are generally characterized by strong gravity anomalies, indicating incomplete isostatic compensation. Since the earth's crust tends to re-establish the isostatic equilibrium disturbed by geologic factors, it must be expected that the greatest gravity changes occur in areas of large gravity anomalies. However, definite proof of this appears to be scarce. Virtually the only corroborative material has been supplied by measurements in India in 1865–1873 and their repetition in 1903 and 1904. The observed differences average 54 milligals, which is equivalent to an increase in gravity by about 1½ milligals per year. Some authors have expressed doubt as to the accuracy of the earlier measurements, and confirmation of such gravity variations in other regions is urgently needed.

Subsurface mass displacements brought about by faulting, volcanic phenomena, and the like may also be expected to cause gravity variations. With an increase in the accuracy of recording gravimeters it is probable that useful information may be accumulated over a period of years in active earthquake regions and may lead to a solution of the problem of earthquake prediction. Combination of recording gravimeters with recording magnetometers and seismographs would be particularly useful. As is shown below, subsurface mass displacements can likewise be recorded by the torsion balance.

C. CHANGES IN WATER LEVEL (TIDES AND THE LIKE)

That changes in water level have a definite effect on the torsion balance has been shown both theoretically and by actual measurements.[68] If a torsion balance is set up on the edge of a quay having vertical walls, so that the center of gravity of the balance is 13 feet above water level

[68] K. Jung, Handb. Exper. Phys., **25**(3), 158 (1930). A. Schleusener, Beitr. angew. Geophys., **5**(4), 480–518 (1936).

at ebb tide, a rise in water level of 6.5 feet causes a change in gradient of the order of 90 Eötvös units;[69] however, this effect declines rapidly away from the edge and is only 1 Eötvös unit at a distance of 100 feet. The variation in the curvature values above the edge is 0. The maximum is observed about 10 feet from the edge; thence, the effect declines slowly and reaches 1 Eötvös unit about 1000 feet from the edge. These values may be calculated by applying the formula for the two-dimensional effect of a vertical step given on page 264. If the coast is sloping, the tide effects must be calculated by using the formula for an inverted sloping edge. The gradients and curvature effects are less in this case. The gravity anomalies directly above the edge follow from formula (7-42e). It is seen that, for the same conditions assumed in the calculation of the torsion balance
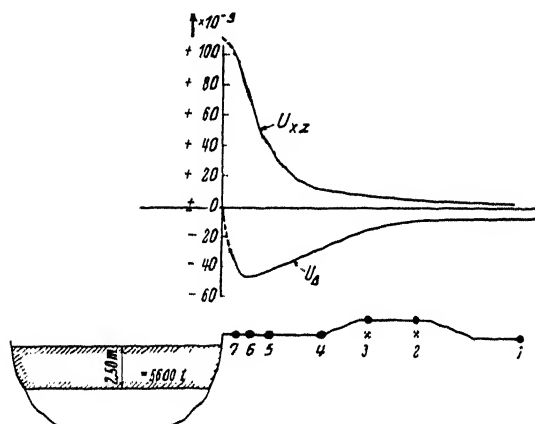
FIG. 7-54. Gravity gradients and curvature anomalies produced when the water level in a lock is raised by 8.2 feet (after Schleusener).

anomalies, the gravity anomaly at the edge is 0.05 milligal, which is within the limits of accuracy of present gravimeters.

Fig. 7-54 shows the gravity gradients, as well as the curvature values, for a water rise of about eight feet in a lock, all determined by a torsion balance, the distance of which from the edge ranged from 1 to 20 m. At 1 m distance the gradient reaches a maximum of about 100 E.U. At 3 m distance a maximum in the curvature occurs with 47 E.U., and at 20 m distance the gradient is 1 E.U. and the curvature 7 E.U. Deflections of the vertical may be calculated from an integration of the curvature variation; near the edge the deviation is $1.2 \cdot 10^{-2}$ arc-sec. Deobserved values for all quantities were in good agreement with values calculated from the theory.

[69] Eötvös unit = E.U. = $1 \cdot 10^{-9}$ Gal·cm^{-1}.

D. ARTIFICIAL MASS DISPLACEMENTS (MINING OPERATIONS) AND THE LIKE

There can be no doubt that mass displacements, brought about by the removal of commercial minerals (salt, coal, sulfur, ore), and rock formation underground, and by filling of subsurface cavities produce variations of gravity anomalies with time. Actual measurements of such variations are apparently lacking. The only information now available are some calculations concerning the maximum deflection of equipotential surfaces of gravity to be expected in such cases. For a coal seam 66 ft. in thickness, occupying a square 7.1 km wide, A. Schleusener[70] has calculated that the maximum deformation would amount to only 3.4 mm. In the Ruhr district where 4 billion tons of coal have been removed in an area of 1000 to 1500 square km., a drop of 3 mm of the niveau surfaces was calculated, assuming the average seam thickness to be 3 m. It should be observed that in these calculations the effect of refilling emptied pillars has not been considered. For a lignite open-pit mine of 50 m depth and 500 m breadth (200 m length), the maximum drop would be 2 mm and the maximum deflection of the vertical at the edge would be $0.77 \cdot 10^{-2}$ arc-sec., corresponding to a maximum curvature anomaly of about 140 E.U. at that point.

VII. DETERMINATION OF THE DEFLECTIONS OF THE VERTICAL

Deflections of the vertical, or "plumb-line deviations," are as the name indicates departures of the direction of gravity from some reference direction. As there is no absolute way of establishing a constant reference direction all over the earth, the direction of gravity is referred to an arbitrarily adapted standard. It is easier to visualize the attitude of these two directions by considering the surfaces to which they are perpendicular. The first is a niveau surface of gravity (a surface in which no gravity components exist), called a "geoid." This has no regular geometric shape and is affected by all visible and invisible irregularities in mass distribution. The second is an ellipsoid of revolution, also known as reference ellipsoid, since all accurate geodetic surveys are referred to it. The deviations in the direction of the perpendiculars to these planes are, therefore, the deflections of the vertical, that is, the deviation in the direction of actual gravity from that of normal gravity. The meridional deflection of the vertical is equal to the ratio of the horizontal gravity component in the meridian to gravity. It is frequently convenient to refer the deflection of the vertical to a point (P in Fig. 7–55) in which the directions of the normal and actual gravity are assumed to be identical. The magnitude

---

[70] Schleusener, Beitr. angew. Geophys., *loc. cit.*

of the gravity vectors is not defined by the direction of the niveau surface alone, but by the number of niveau surfaces per unit distance in the direction of gravity.

There are altogether four methods of determining deflections of the vertical. The first consists of a comparison of astronomic and geodetic measurements to establish a difference in the direction of the geoid and reference ellipsoid. The second measures the time variations of the direction of the vertical with horizontal pendulums. The third is based on field measurements of the horizontal component of gravity and is at present of theoretical significance only. The fourth is an indirect determi-
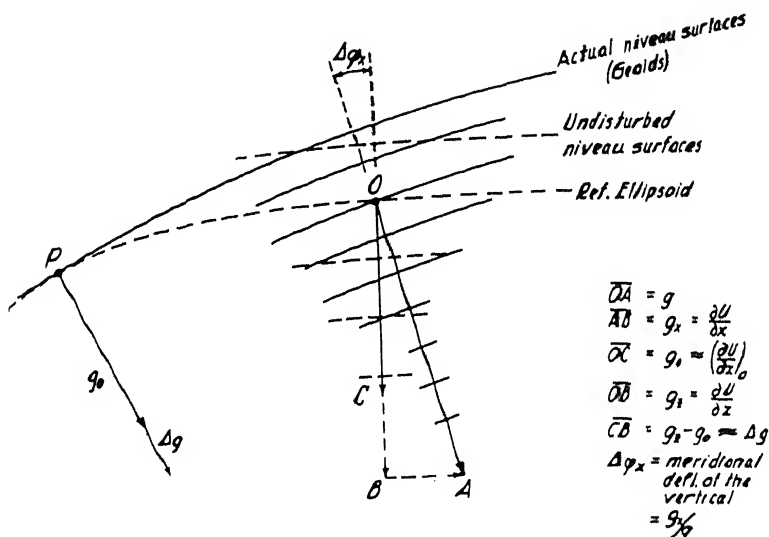
Fig. 7-55. Relations between deflection of vertical, geoid, reference ellipsoid and gravity comp

nation by integration from curvature values measured with the torsion balance. Only the first and last methods are discussed in this section.

In the astronomic or star observations, instruments used for the determination of longitude and latitude are set with their axes of revolution vertical, by means of accurate spirit levels which adjust themselves into a niveau surface of gravity. Therefore, astronomic observations give coordinates of a station on the geoid. If these coordinates, on the other hand, are determined by geodetic triangulation, the calculation of arcs, distances, and angles is based on the geometric figure of the reference ellipsoid. The difference of astronomic and geodetic latitude, therefore, gives the deflection in the meridian. From differences in astronomic and geodetic longitudes, deflections in the prime vertical may be obtained.

The accuracy is ±0.03 arc-sec. in the meridian and 0.10 arc-sec. in the prime vertical.

Much greater accuracy is obtainable by using torsion-balance observations. Since the torsion balance measures the rate of change of the horizontal gravity components in the directions of minimum and maximum curvature, differences in the horizontal gravity components may be obtained by integrating their variations with distance between stations. With division by gravity, the corresponding differences in the deflections of the vertical can be calculated. Since the torsion balance does not measure the vertical gravity gradient and furnishes the gradients of the horizontal components only in the combination $\partial^2 U/\partial y^2 - \partial^2 U/\partial x^2$, relative determinations are possible only when deflections of the vertical are known at two points, at the end of a torsion-balance traverse.[71] According to Oltay[72] a comparison of astronomic and geodetic deflection observations with torsion-balance measurements in the Hungarian plain gave an accuracy of $3 \cdot 10^{-3}$ arc-sec. per km.

In practice the determination of deflections of the vertical from torsion-balance observations is simplified when geologic bodies are essentially two-dimensional. In that case, the curvature values correspond to cylindrical niveau surfaces, which are fully defined by one radius of curvature, and a variation of the horizontal gravity component in only one (x') direction. Then the deflection of the vertical is

$$\Delta\varphi_{x'} = \frac{1}{a} \int \frac{\partial^2 U}{\partial x_1^2} \cdot dx' \qquad (7\text{–}46)$$

The integration is carried out numerically by using averages of curvatures between closely spaced stations or by integraphs. In this manner Schleusener[73] obtained an accuracy of about $1 \cdot 10^{-4}$ arc-sec. per meter of horizontal distance. The maximum deflections calculated from curvature values, reaching a maximum of 50 E.U., were of the order of $1 \cdot 10^{-2}$ arc-sec. Such deflections cannot be detected by the astronomic-geodetic method.

Observations of deflections of the vertical must be carefully corrected for the effects of near and distant topography. Terrain effects may be calculated by the use of diagrams composed of sectors bounded by radial lines and concentric circles, such as those calculated by Hayford[74] and Schleusener.[75] For the interpretation of anomalies in the deflection of the

[71] R. v. Eötvös, Verh. 15. Allg. Conf. Internat. Erdmess. (Budapest, 1908).

[72] K. Oltay, Geodet. Arb. d. R. v. Eötvös Geophys. Forsch. Inst., Vol. II (Budapest, 1927).

[73] Beitr. angew. Geophys., *loc. cit.*

[74] John F. Hayford, "The Figure of the Earth and Isostasy from Measurements in the U. S.," U. S. Department of Commerce (1909).

[75] *Loc. cit.*

vertical, graphical methods or integration machines are employed. Since deflection of the vertical is horizontal gravity component divided by gravity, diagrams and integraphs developed for the (vertical component of) gravity are applicable with 90° rotation of geologic section or diagram.

VIII. TORSION-BALANCE METHODS

A. Quantities Measured; Space Geometry of Equipotential Surfaces

The torsion balance measures the following physical quantities: (1) the "gradient," or rate of change of gravity, related to the convergence of equipotential surfaces and to the curvature of the vertical; (2) the so-called "curvature values," or "horizontal directing forces," which give the deviation of equipotential surfaces from spherical shape, and give the direction of the minimum curvature. The curvature values represent the north gradient of the east component of gravity and the difference of the east gradient of the east component minus the north gradient of the north component. From the previous discussion of gravity, gravity potential, and surfaces of equal potential,[76] it is seen that the distance between the latter is inversely proportional to the gravity. Hence, a convergence of equipotential surfaces corresponds to a horizontal change or a gradient of gravity. If the change between two points is uniform, $g' = g + (\partial g/\partial s) \cdot ds$ where $(\partial g/\partial s)$ is the gradient of gravity at right angles to a line of equal gravity (isogam). The gradient may be resolved into a north and east component so that

$$\frac{\partial g}{\partial s} = \sqrt{\left(\frac{\partial^2 U}{\partial x\, \partial z}\right)^2 + \left(\frac{\partial^2 U}{\partial y\, \partial z}\right)^2} \quad \text{and} \quad \tan \alpha = \frac{\frac{\partial g}{\partial y}}{\frac{\partial g}{\partial x}}. \quad (7\text{-}47a)$$

Gradients are expressed in Eötvös units — E.U. = 10^{-9} C.G.S. units or 10^{-9} Gals cm^{-1}. Isogams are usually drawn at intervals of 1 or $\frac{1}{2}$ milligal. A change in gravity by 1 milligal for 1 km distance corresponds to a gradient of about 10 E.U. If h and h', respectively, represent the spacings of two equipotential surfaces with the convergence ι between two points whose horizontal separation is ds, then $dh - dh' = dh = \iota ds$. If r is the radius of curvature of the vertical, $dh = \iota \cdot r$. Since $gdh = g'dh'$, $gdh = (g + (\partial g/\partial s) \cdot ds) \cdot (dh - \iota ds)$. Substituting $\iota = dh/r$, $gdh =$
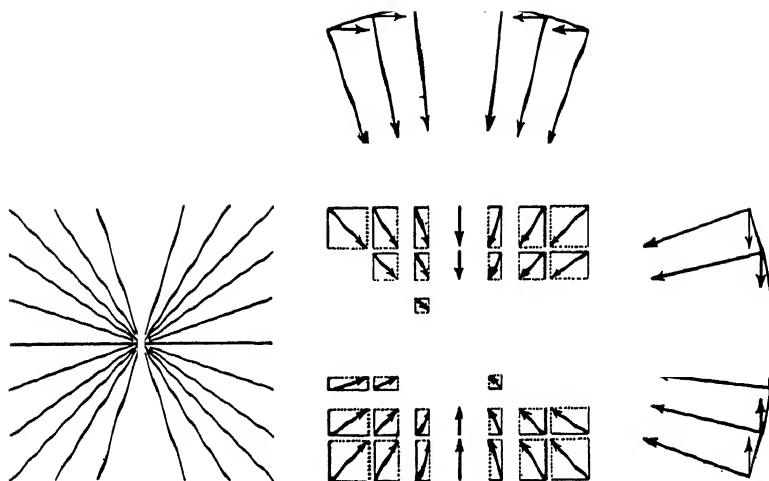
FIG. 7-56a. Horizontal gravity components and lines of force corresponding to a niveau surface with equal principal curvatures (after Rybar).
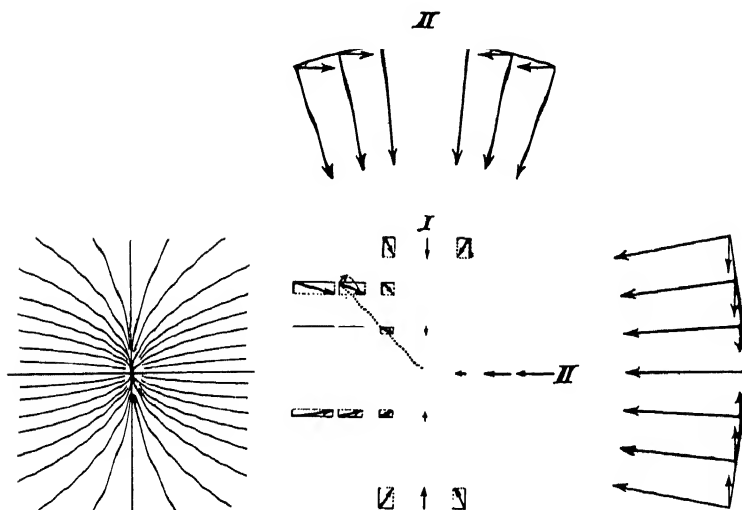
FIG. 7-56b. Horizontal gravity components and lines of force corresponding to a niveau surface with unequal principal curvatures (after Rybar).

$dh(1 - ds/r)$ $(g + (\partial g/\partial s) \cdot ds)$. Dividing by dh and ds, $0 = g/r - (ds/r) \cdot \partial g/\partial s$, so that, by neglecting second-order terms,

$$\frac{\partial g}{\partial s} \equiv \frac{g}{r} = \frac{\iota \cdot g}{dh}, \qquad (7\text{-}47b)$$

which states that the gradient of gravity is proportional to the curvature of the vertical or to the convergence of the equipotential surfaces. A torsion balance with a sensitivity of 1 E.U., in which dh (corresponding to the distance between weights) is of the order of 60 cm, can therefore still detect a convergence of equipotential surfaces of the order of 1/100,000 arc-sec.

In addition to the forces resulting from a convergence of equipotential surfaces, the torsion balance is affected by components resulting from the curvature conditions of a single equipotential surface. These surfaces, in turn, are customarily defined by the maximum and the minimum curvatures in two directions at right angles to each other. The torsion balance does not give these curvatures independently; it gives merely their difference. One E.U. corresponds to a difference in the principal curvature radii of about 4 km.

FIG. 7-57. Horizontal forces and directions of principal curva-

Fig. 7-56a illustrates the gravity field for a spherical surface. Since the principal curvatures are equal, the horizontal gravity components are equal at points of equal distance from the center. Their resultants point to the center and no beam deflection obtains. If the curvature in section I is less than in section II, as in Fig. 7-56b, the gravity components in the former are less than those in the latter. The resultant forces no longer point to the center, and give rise to a small couple tending to move the beam into the direction of least curvature. It is seen that the torsion balance indicates the deviation of a level plane from spherical shape. Let x' and y' (Fig. 7-57) be the directions of principal curvatures, x' making the angle λ with north (x direction). Assuming a linear variation which is permissible within the small dimensions of the instrument, the horizontal gravity components at any point $P(x, y)$ are

$$\Delta g_x \equiv \frac{\partial U}{\partial x} = x\left(\frac{\partial g_x}{\partial x}\right) + y\left(\frac{\partial g_x}{\partial y}\right)$$

$$\Delta g_y \equiv \frac{\partial U}{\partial y} = x\left(\frac{\partial g_y}{\partial x}\right) + y\left(\frac{\partial g_y}{\partial y}\right). \qquad (7\text{-}48a)$$

It will be convenient to introduce the following simplified notation for the components and their gradients in the xy as well as the $x'y'$ system:

$$\frac{\partial U}{\partial x} \equiv X \qquad \frac{\partial U}{\partial x'} \equiv X'$$

$$\left. \begin{array}{ll} \dfrac{\partial^2 U}{\partial x^2} \equiv \mathbf{a}; & \dfrac{\partial^2 U}{\partial x'^2} \equiv \mathbf{a}' \\[2mm] \dfrac{\partial^2 U}{\partial y^2} \equiv \mathbf{b}; & \dfrac{\partial^2 U}{\partial y'^2} \equiv \mathbf{b}' \\[2mm] \dfrac{\partial^2 U}{\partial x\,\partial y} \equiv \mathbf{c}; & \dfrac{\partial^2 U}{\partial x'\,\partial y'} \equiv \mathbf{c}' \end{array} \right\} \quad (7\text{--}48b)$$

$$\frac{\partial U}{\partial y} \equiv Y \qquad \frac{\partial U}{\partial y'} \equiv Y'$$

Hence, eq. (7–48a) may be written

$$\left. \begin{array}{l} X = \mathbf{a}x + \mathbf{c}y \\[1mm] Y = \mathbf{c}x + \mathbf{b}y. \end{array} \right\} \quad (7\text{--}48c)$$

The following relations, as obtained from Fig. 7–57 may be substituted in eq. (7–48c):

$$\begin{array}{ccc} X = X' \cos \lambda - Y' \sin \lambda & & x = x' \cos \lambda - y' \sin \lambda \\ & \text{and} & \\ Y = X' \sin \lambda + Y' \cos \lambda & & y = x' \sin \lambda + y' \cos \lambda \end{array}$$

Divide the resulting equations by $\sin \lambda$ and $\cos \lambda$, respectively, and form two new equations by adding and subtracting them. When divided by $(\cotan \lambda + \tan \lambda)$ the new equations have the form

$$\left. \begin{array}{l} X' = x' \{\mathbf{u}\} + y' \{\mathbf{v}\} \\[1mm] Y' = x' \{\mathbf{v}\} + y' \{\mathbf{w}\} \end{array} \right\} \quad (7\text{--}48d)$$

The coefficients are:

$$\mathbf{u} = \mathbf{a} \cos^2 \lambda + \mathbf{b} \sin^2 \lambda + \mathbf{c} \sin 2\lambda;$$

$$\mathbf{v} = \frac{\mathbf{b} - \mathbf{a}}{2} \sin 2\lambda + \mathbf{c} \cos 2\lambda;$$

$$\mathbf{w} = \mathbf{b} \cos^2 \lambda + \mathbf{a} \sin^2 \lambda - \mathbf{c} \sin 2\lambda,$$

so that eq. (7–48d) becomes

$$X' = x'(\mathbf{a} \cos^2 \lambda + \mathbf{b} \sin^2 \lambda + \mathbf{c} \sin 2\lambda) + y'\left(\frac{\mathbf{b} - \mathbf{a}}{2} \sin 2\lambda + \mathbf{c} \cos 2\lambda\right)$$

$$X' = x'\left(\frac{\mathbf{b} - \mathbf{a}}{2} \sin 2\lambda + \mathbf{c} \cos 2\lambda\right) + y'(\mathbf{b} \cos^2 \lambda + \mathbf{a} \sin^2 \lambda - \mathbf{c} \sin 2\lambda)$$

$$(7\text{--}48e)$$

Since in the $x'y'$ system the coefficient of y' in the first equation and the coefficient of x' in the second equation are zero, it follows that $\tan 2\lambda = -2c/(b - a)$ or, in regular notation,

$$\tan 2\lambda = \frac{2\dfrac{\partial^2 U}{\partial x\, \partial y}}{-\left(\dfrac{\partial^2 U}{\partial y^2} - \dfrac{\partial^2 U}{\partial x^2}\right)}. \tag{7-48f}$$

Hence, (7-48e) becomes

$$\left.\begin{aligned} X' &= x' \{\mathbf{a} \cos^2 \lambda + \mathbf{b} \sin^2 \lambda + \mathbf{c} \sin 2\lambda\} \\ Y' &= y' \{\mathbf{b} \cos^2 \lambda + \mathbf{a} \sin^2 \lambda - \mathbf{c} \sin 2\lambda\}. \end{aligned}\right\} \tag{7-48g}$$
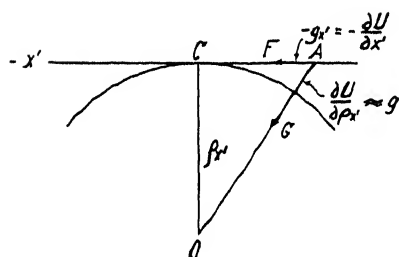
FIG. 7-58. Relations of gravity components and curvature of niveau surface.

In the x' plane of minimum curvature (see Fig. 7-58), $AG/AO = AF/AC$ or

$$\frac{g}{\rho_{x'}} = -\frac{\dfrac{\partial^2 U}{\partial x'^2}\cdot x'}{x'};$$

hence, $\partial^2 U/\partial x'^2 = -(g/\rho_{x'})$. Similarly, for the y' plane, $\partial^2 U/\partial y'^2 = -(g/\rho_{y'})$, so that the difference of the curvatures or the *deviation from the spherical shape* is

$$-g\left(\frac{1}{\rho_1} - \frac{1}{\rho_2}\right) = \frac{\partial^2 U}{\partial y'^2} - \frac{\partial^2 U}{\partial x'^2}, \tag{7-48h}$$

where the notations ρ_2 and ρ_1 (principal radii of curvature) have been used for $\rho_{x'}$ and $\rho_{y'}$.

The torsion balance does not indicate the quantity on the right side of this equation, since the directions $x'y'$ and the angle λ are unknown. However, it is seen by comparing eq. (7-48d) with eq. (7-48c) that the coefficients $\mathbf{a}'$ and $\mathbf{b}'$ defined in eq. (7-48b) are identical with the coefficients $\mathbf{u}$ and $\mathbf{w}$, so that

$$\mathbf{a}' = \mathbf{a} \cos^2 \lambda + \mathbf{b} \sin^2 \lambda + \mathbf{c} \sin 2\lambda$$

and

$$\mathbf{b}' = \mathbf{b} \cos^2 \lambda + \mathbf{a} \sin^2 \lambda - \mathbf{c} \sin 2\lambda.$$

By forming the difference of these two equations and substituting eq. (7-48f), we obtain $(\mathbf{b} - \mathbf{a})/(\mathbf{b}' - \mathbf{a}') = \cos 2\lambda$ or

$$\left(\frac{\cdot}{\cdot} - \frac{\cdot}{\cdot}\right) \cos 2\lambda = \qquad 1$$

so that eq. (7–48h) becomes

$$- g \left\{ \frac{.}{.} - \frac{.}{.} \right\} \cos 2\lambda = \frac{\partial^2 U}{\partial x^2} \qquad (7\text{–}48i)$$

B. THEORY OF TORSION BALANCE

The torsion balance measures horizontal and vertical gradients of horizontal gravity components but does not react to vertical changes in gravity. Its center of gravity is far enough below the point of suspension so that tilting effects are not noticeable; nor is it affected by gravity itself, since its action on the center of gravity is compensated by the tension of the suspension wire. The suspended lower weight will be deflected from the vertical, but this is too small to be measured. Horizontal forces alone are effective at both ends of the beam. For a given deflection the torsional moment of the wire and the moment of the horizontal forces are in equilibrium.

1. The *Eötvös curvature variometer* is identical in form with the instruments used by Cavendish, Heyl, and others for the determination of the gravitational constant (see Fig. 7–3). Its action in a field with parabolic lines of force was illustrated in Fig. 7–56b. It will be shown in the next paragraph that its deflections are proportional to the "curvature values" $\partial^2 U/\partial y^2 - \partial^2 U/\partial x^2$ and $\partial^2 U/\partial x \partial y$. It has not been extensively used, since curvature values are not too readily interpreted and are affected more by masses near the horizon than underneath the instrument. Consequently, terrain irregularities cause considerable interference. Eötvös built three types, two with one beam and one with three beams 120° apart. Separate curvature variometers are no longer used, since beams designed to give gravity gradients furnish the curvature values at the same time when they are set up in the requisite number of azimuths. Such instruments are known as gravity variometers of the second type, combined gradient and curvature variometers, or merely "gradient" variometers.

2. The *combined gradient and curvature variometer* is illustrated in Fig. 2–4 of Chapter 2. If the equipotential surfaces passing through the weights make an angle ι with one another, a horizontal component $\mathbf{H} = mg\iota$ is produced. Its moment $\mathbf{D_1} = lmg\iota$, where l is one half of the beam length and m the beam mass. Substituting eq. (7–47b).

$$\mathbf{D_1} = mhl \, \frac{\partial g}{\partial s}. \qquad (7\text{–}49a)$$

If the angle of the beam with north is α and that of the direction of maximum gradient is $(90 + \alpha)$,

$$\frac{\partial g}{\partial s} = \frac{\partial^2 U}{\partial y \partial z} \cos \alpha - \frac{\partial^2 U}{\partial x \partial z} \sin \alpha$$

and the "gradient" moment is

$$\mathbf{D}_1 = mhl \left(\frac{\partial^2 U}{\partial y \partial z} \cos \alpha - \frac{\partial^2 U}{\partial x \partial z} \sin \alpha \right), \tag{7-49b}$$

where $\partial^2 U / \partial x \partial z \equiv U_{xz}$ is the north gradient of gravity and U_{yz} is the east gradient.

For a derivation of the curvature effect, assume that the beam makes the angle α with the north direction and the angle β with the direction of mini-
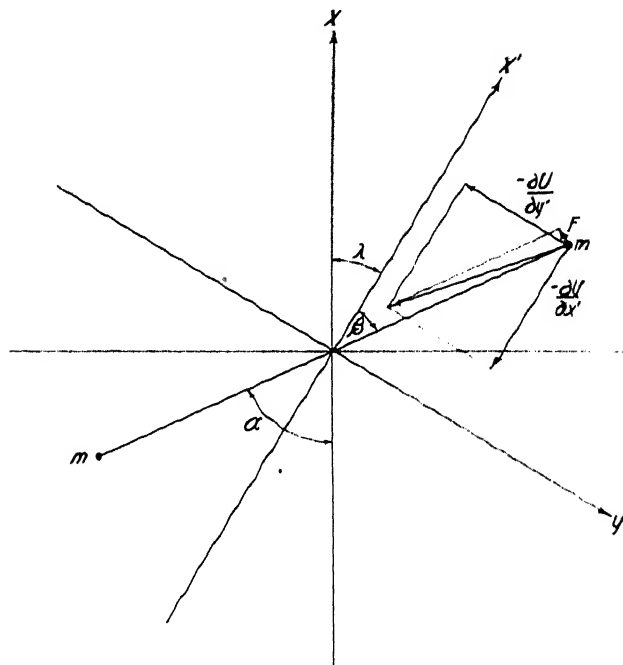
FIG. 7-59. Horizontal forces on balance beam, due to c   ons in niveau

mum curvature (Fig. 7-59). Then the component F at right angles to the beam is the projection of the resultant of $-\partial U/\partial x'$ and $-\partial U/\partial y'$ and its moment $\mathbf{D}_2 = 2mlF$. Since $F = (\partial U/\partial y') \cos \beta - (\partial U/\partial x') \sin \beta = (\partial^2 U/\partial y'^2)y' \cos \beta - (\partial^2 U/\partial x'^2)x' \sin \beta$, the moment $\mathbf{D}_2$ becomes, by substitution of $x' = l \cos \beta$, $y' = l \sin \beta$, and $2l^2m = K$, the moment of inertia of the beam,

$$\mathbf{D}_2 = \tfrac{1}{2}K \sin 2\beta \left(\frac{\partial^2 U}{\partial y'^2} - \frac{\partial^2 U}{\partial x'^2} \right). \tag{7-50a}$$

By combination of (7–48h) and (7–48i),

$$\frac{\partial^2 U}{\partial y'^2} - \frac{\partial^2 U}{\partial x'^2} = \frac{1}{\cos 2\lambda} \left(\frac{\partial^2 U}{\partial y^2} - \frac{\partial^2 U}{\partial x^2} \right),$$

so that by substituting $(\alpha - \lambda)$ for β and considering eq. (7–48f)

$$\mathbf{D_2} = K \left\lfloor \left(\frac{\partial^2 U}{\partial y^2} - \frac{\partial^2 U}{\partial x^2} \right) \tfrac{1}{2} \sin 2\alpha + \frac{\partial^2 U}{\partial x \partial y} \cos 2\alpha \right\rfloor, \qquad (7\text{–}50b)$$
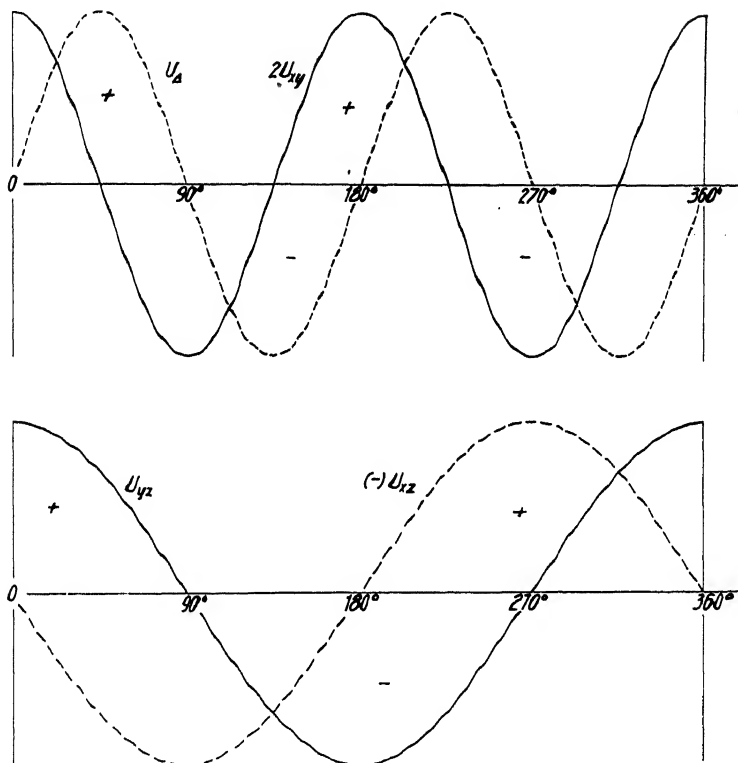
FIG. 7-60. Gradient and curvature effects on balance beam as functions of azimuth.

where $\partial^2 U/\partial y^2 - \partial^2 U/\partial x^2 \equiv U_\Delta$ is the so-called north and $2\,\partial^2 U/\partial x \partial y \equiv 2U_{xy}$ the east component of the curvature values. The equation indicates that the curvature effects are proportional to the double azimuth, while the gradient effects are porportional to the azimuth itself (see Fig. 7-60).

In the equilibrium position, $\tau \varphi = \mathbf{D_1} + \mathbf{D_2}$, where τ is the torsional coefficient of the wire and φ the angle of deflection. The beam deflection is measured by mirror (attached to the beam), graduated scale, and telescope, or by photographic recording. In both cases, an "autocollimation" method is applied with the "objective" lens in front of the balance-beam mirror. If n is the reading corresponding to a deflection φ, and n_0 (torsion-

less position) the reading corresponding to zero deflection, $n - n_0 = 2\varphi f$ (or $4\varphi f$ with double reflection, as in the small "Z"-bar and tilt-beam Askania balances). Then, $n - n_0 = 2f\dfrac{\mathbf{D_1 + D_2}}{\tau}$, or

$$n - n_0 = \frac{fK}{\tau} \sin 2\alpha \left(\frac{\partial^2 U}{\partial y^2} - \frac{\partial^2 U}{\partial x^2} \right) + \frac{fK}{\tau} \cos 2\alpha \cdot 2 \left. \frac{\partial^2 U}{\partial x \partial y} \right\}$$
$$\left. + \frac{2fmlh}{\tau} \frac{\partial^2 U}{\partial y \partial z} \cos \alpha - \frac{2fmlh}{\tau} \frac{\partial^2 U}{\partial x \partial z} \sin \alpha \right\} \quad (7\text{-}51a)$$

This is the *principal equation of the torsion balance of the second kind*. In the abbreviated notation previously referred to, and with the "instrument constants,"[77]

$$\mathbf{a} \equiv \frac{fK}{\tau} \quad \text{and} \quad \mathbf{b} \equiv \frac{2fmlh}{\tau},$$

the principal equation (see Fig. 7-60) is

$$n - n_0 = \mathbf{a}(U_\Delta \sin 2\alpha + 2U_{xy} \cos 2\alpha) + \mathbf{b}(\cos \alpha U_{yz} - \sin \alpha U_{xz}). \quad (7\text{-}51b)$$

This equation contains five unknown quantities: the four second derivatives of the gravity potential and n_0. They may be determined from five equations by observing beam deflections in five azimuths ($0°$, $72°$, $144°$, $216°$, and $288°$). Such observations take considerable time, owing to the long period of the beam. Since $T = 2\pi \sqrt{K/\tau}$, a beam with $K \approx 20,000$ C.G.S. units and $\tau \approx 0.5$ C.G.S. unit has a period of the order of 20 minutes. To reduce the observation time, Eötvös designed a double instrument with two beams in antiparallel arrangement, rotated together into the respective azimuths. This adds a sixth unknown (the torsionless position of the second beam). However, since two observations are made in each azimuth, six quantities may be obtained in three positions.

3. The *double gradient and curvature variometer* is usually so arranged that when the photographic or reading device is oriented toward north, the hanging weight of balance I is in the south, and $\alpha' = 180°$, $\alpha'' = 0$. Then $\mathbf{a'b'}$ are the constants for the first balance and $\mathbf{a''b''}$ for the second balance. The subscripts 1, 2, and 3 refer to the azimuths ($0°$, $120°$, $240°$). Then the general equations are, for beam II (az. α),

$$n'' - n_0'' = \mathbf{a''} (\sin 2\alpha \cdot U_\Delta + \cos 2\alpha \cdot 2U_{xy}) + \mathbf{b''} (\cos \alpha \cdot U_{yz} - \sin \alpha \cdot U_{xz})$$

and, for beam I (az. $\alpha + \pi$),

$$n' - n_0' = \mathbf{a'} (\sin 2\alpha \cdot U_\Delta + \cos 2\alpha \cdot 2U_{xy}) - \mathbf{b'} (\cos \alpha \cdot U_{yz} - \sin \alpha \cdot U_{xz}). \Big\}$$

$$(7\text{-}52a)$$

---

[77] The above symbols are customarily used for the instrument constants and are not identical with the quantities $\mathbf{a}$ and $\mathbf{b}$ defined by eq. (7-48b).

These equations indicate that in any azimuth the effect of curvatures is in the same direction and that of the gradients is in opposite direction for both beams. The following set of equations is then obtained for three positions:

Position 1

$$\alpha' = 180°: \qquad n_1' - n_0' = 2a'U_{xy} - b'U_{yz}$$

$$\alpha'' = 0°: \qquad n_1'' - n_0'' = 2a''U_{xy} - b''U_{yz}$$

Position 2

$$\alpha' = 300° \quad n_2' - n_0' = -a'\sin 60° \; U_\Delta - 2a'\cos 60° \; U_{xy}$$
$$+ b'\sin 60° \; U_{xz} + b' \cos 60° \; U_{yz}$$

$$\alpha'' = 120° \quad n_2'' - n_0'' = -a''\sin 60° \; U_\Delta - 2a''\cos 60° \; U_{xy}$$
$$- b''\sin 60° \; U_{xz} - b'' \cos 60° \; U_{yz}$$

Position 3

$$\alpha' = 60° \quad n_3' - n_0' = a'\sin 60° \; U_\Delta - 2a'\cos 60° \; U_{xy}$$
$$- b'\sin 60° \; U_{xz} + b' \cos 60° \; U_{yz}$$

$$\alpha'' = 240° \quad n_3'' - n_0'' = a''\sin 60° \; U_\Delta - 2a''\cos 60° \; U_{xy}$$
$$+ b''\sin 60° \; U_{xz} - b'' \cos 60° \; U_{yz}$$

The two torsionless position readings, n_0' and n_0'', are obtained from the arithmetic mean of the deflections

$$n_0' = \frac{n_1' + n_2' + n_3'}{3} \quad \text{and} \quad n_0'' = \frac{n_1'' + n_2'' + n_3''}{3}. \qquad (7\text{-}52b)$$

Two positions are therefore sufficient to calculate the other four unknowns. Combination of positions 2 and 3 is in most general use, but combinations 1 and 3, and 1 and 2 are equally suitable. With the notations $n_1' - n_0' = \Delta_1'$; $n_2' - n_0' = \Delta_2'$; $n_3' - n_0' = \Delta_3'$ and $n_1'' - n_0'' = \Delta_1''$; $n_2'' - n_0'' = \Delta_2''$; $n_3'' - n_0'' = \Delta_3''$, the equations for *positions* 2 and 3 are:

$$(1) \qquad \Delta_2' = \frac{-\sqrt{3}}{2} a'U_\Delta - a'U_{xy} + \frac{\sqrt{3}}{2} b'U_{xz} + \tfrac{1}{2}b'U_{yz}$$

$$(2) \qquad \Delta_2'' = \frac{-\sqrt{3}}{2} a''U_\Delta - a''U_{xy} - \frac{\sqrt{3}}{2} b''U_{xz} - \tfrac{1}{2}b''U_{yz}$$

$$(3) \qquad \Delta_3' = \frac{\sqrt{3}}{2} a'U_\Delta - a'U_{xy} - \frac{\sqrt{3}}{2} b'U_{xz} + \tfrac{1}{2}b'U_{yz}$$

$$(4) \qquad \Delta_3'' = \frac{\sqrt{3}}{2} a''U_\Delta - a''U_{xy} + \frac{\sqrt{3}}{2} b''U_{xz} - \tfrac{1}{2}b''U_{yz}$$

(5)   (2 + 4) $= \Delta_2' + \Delta_3'' = -2a'' U_{xy} - b'' U_{yz}$

(6)   (1 + 3) $= \Delta_2' + \Delta_3' = -2a' U_{xy} + b' U_{yz}$

(7)   (1 − 3) $= \Delta_2' - \Delta_3' = -\sqrt{3}\,a' U_\Delta + \sqrt{3}$

(8)   (2 − 4) $= \Delta_2'' - \Delta_3'' = -\sqrt{3}\,a'' U_\Delta - \sqrt{3}\,\cup\, \cup_{zz}.$

Multiplying (5) by a' and (6) by $-a''$ and adding,

$$U_{yz} = \frac{a''}{a'b'' + a''b'}\left[(\Delta_2' + \Delta_3') - \frac{a'}{a''}(\Delta_2'' + \Delta_3'')\right]. \qquad (7\text{-}52c)$$

Multiplying the same equations by b' and b'' respectively,

$$2U_{xy} = -\frac{b''}{a''b' + a'b''}\left[(\Delta_2' + \Delta_3') + \frac{b'}{b''}(\Delta_2'' + \Delta_3'')\right]. \qquad (7\text{-}52d)$$

Multiplying (7) by b'' and (8) by b' and adding,

$$U_\Delta = -\frac{b''}{\sqrt{3}\,(a'b'' + a''b')}\left[(\Delta_2' - \Delta_3') + \frac{b'}{b''}(\Delta_2'' - \Delta_3'')\right]. \qquad (7\text{-}52e)$$

Multiplying (7) by a'' and (8) by $-a'$ and adding,

$$U_{zz} = \frac{a''}{\sqrt{3}\,(a''b' + a'b'')}\left[(\Delta_2' - \Delta_3') - \frac{a'}{a''}(\Delta_2'' - \Delta_3'')\right]. \qquad (7\text{-}52f)$$

With the notations

$$0 = \frac{a''}{\sqrt{3}\,(a''b' + a'b'')} \qquad\qquad p = \frac{a''}{a'b'' + a''b'}\ (p = 0\sqrt{3})$$

$$q = \frac{b''}{\sqrt{3}\,(a''b' + a'b'')} \qquad\qquad r = \frac{b''}{a'b'' + a''b'}\ (r = q\sqrt{3}) \qquad (7\text{-}52g)$$

$$s = \frac{a'}{a''} \qquad\qquad\qquad\qquad t = \frac{b'}{b''}$$

formulas (7 52c) to (7 52f) may be written

$$U_{zz} = 0\,[(\Delta_2' - \Delta_3') - s(\Delta_2'' - \Delta_3'')]$$

$$U_{yz} = p\,[(\Delta_2' - \Delta_3') - s(\Delta_2'' - \Delta_3'')]$$

$$U_\Delta = -q\,[(\Delta_2' - \Delta_3') + t(\Delta_2'' - \Delta_3'')] \qquad (7\ 52h)$$

$$2U_{xy} = -r\,[(\Delta_2' + \Delta_3') + t(\Delta_2'' + \Delta_3'')].$$

In a similar manner, the following expressions are obtained for positions (1) and (2):

$$U_{zz} = \frac{a''}{\sqrt{3}\,(a''b' + a'b'')}\left[(2\Delta_2' + \Delta_1') - \frac{a'}{a''}(2\Delta_2'' + \Delta_1'')\right]$$

$$U_{yz} = \frac{a''}{a''b' + a'b''}\left[\Delta_1' - \frac{a'}{a''}\Delta_1''\right]$$

$$U_\Delta = -\frac{b''}{\sqrt{3}\,(a''b' + a'b'')}\left[(2\Delta_2' + \Delta_1') + \frac{b'}{b''}(2\Delta_2'' + \Delta_1'')\right]$$

$$2U_{xy} = \frac{b''}{a''b' + a'b''}\left[\Delta_1' + \frac{b'}{b''}\Delta_1''\right].$$

$$(7\text{-}52i)$$

For positions (1) and (3):

$$U_{zz} = -\frac{a''}{\sqrt{3}(a''b' + a'b'')}\left[(2\Delta_3' + \Delta_1') - \frac{a'}{a''}(2\Delta_3'' + \Delta_1'')\right]$$

$$U_{yz} = -\frac{a''}{a''b' + a'b''}\left[\Delta_1' - \frac{a'}{a''}\Delta_1''\right]$$

$$U_\Delta = \frac{b''}{\sqrt{3}\,(a''b' + a'b'')}\left[(2\Delta_3' + \Delta_1') + \frac{b'}{b''}(2\Delta_3'' + \Delta_1'')\right]$$

$$2U_{xy} = \frac{b''}{a''b' + a'b''}\left[\Delta_1' + \frac{b'}{b''}\Delta_1''\right].$$

$$(7\text{-}52j)$$

It may happen that for some reason one beam of the double variometer gets out of order. It is then possible to work with one beam only. However, more than three positions are required. For gradients only, observations are necessary in four positions, and for all derivatives five azimuths are required.

For observations in four azimuths, it is advisable to take the first reading in the azimuth N 45° E. and rotate the instrument by 90° intervals. Then, for beam I:

(position 1) $\alpha = 225°$: $= a'U_\Delta + b' \sin 45° \, U_{zz} - b' \sin 45° \, U_{yz}$
(position 2) $\alpha = 315°$: $= -a'U_\Delta + b' \sin 45° \, U_{zz} + b' \sin 45° \, U_{yz}$
(position 3) $\alpha = 45°$: $= a'U_\Delta - b' \sin 45° \, U_{zz} + b' \sin 45° \, U_{yz}$
(position 4) $\alpha = 135°$: $= -a'U_\Delta - b' \sin 45° \, U_{zz} - b' \sin 45° \, U_{yz}.$

For beam II:

(position 1) $\alpha = 45°$: $= a''U_\Delta - b'' \sin 45° \, U_{zz} + b'' \sin 45° \, U_{yz}$
(position 2) $\alpha = 135°$: $= -a''U_\Delta - b'' \sin 45° \, U_{zz} - b'' \sin 45° \, U_{yz}$
(position 3) $\alpha = 225°$: $= a''U_\Delta + b'' \sin 45° \, U_{zz} - b'' \sin 45° \, U_{yz}$
(position 4) $\alpha = 315°$: $= -a''U_\Delta + b'' \sin 45° \, U_{zz} + b'' \sin 45° \, U_{yz}.$

Hence, for balance I:

$$(1 + 2) = \Delta_1' + \Delta_2' = 2b' \,(0.707)U_{xz}$$

$$(2 + 3) = \Delta_2' + \Delta_3' = 2b' \,(0.707)U_{yz}$$

$$(3 + 4) = \Delta_3' + \Delta_4' = -2b' \,(0.707)U_{xz}$$

$$(4 + 1) = \Delta_4' + \Delta_1' = -2b' \,(0.707)U_{yz},$$

and for balance II:

$$(1 + 2) = \Delta_1'' + \Delta_2'' = -2b'' \,(0.707)U_{xz}$$

$$(2 + 3) = \Delta_2'' + \Delta_3'' = -2b'' \,(0.707)U_{yz}$$

$$(3 + 4) = \Delta_3'' + \Delta_4'' = 2b'' \,(0.707)U_{xz}$$

$$(4 + 1) = \Delta_4'' + \Delta_1'' = 2b'' \,(0.707)U_{yz}.$$

From beam I:

$$U_{xz} = \frac{\Delta_1' + \Delta_2'}{1.414b'} = \frac{-(\Delta_3' + \Delta_4')}{1.414b'}$$

$$U_{yz} = \frac{\Delta_2' + \Delta_3'}{1.414b'} = \frac{-(\Delta_1' + \Delta_4')}{1.414b'}, \qquad (7\text{-}53a)$$

and from beam II:

$$U_{xz} = \frac{\Delta_3'' + \Delta_1''}{1.414b''} = \frac{-(\Delta_1'' + \Delta_2'')}{1.414b''}$$

$$U_{yz} = \frac{\Delta_1'' + \Delta_1''}{1.414b''} = \frac{-(\Delta_2'' + \Delta_3'')}{1.414b''}. \qquad (7\text{-}53b)$$

In these equations

$$n_0' = \frac{n_1' + n_2' + n_3' + n_4'}{4}$$

and

$$n_0'' = \frac{n_1'' + n_2'' + n_3'' + n_4''}{4}.$$

Therefore, $U_{xz} = +(n_1 - n_2)/2b$ and $U_{yz} = \pm(n_3 - n_1)/2b$, where the upper signs are for beam I and the lower for beam II.

If only one balance beam is functioning and if both gradients and curvatures are desired, observations in five azimuths are required. Then for beam II:

(1)　　$\alpha = \quad 0°; \quad n_1'' - n_0'' = 2a''U_{xy} + b''U_{yz}$

(2)　　$\alpha = \quad 72°; \quad n_2'' - n_0'' = a'' \sin 36° \, U_\Delta - 2a'' \cos 36° \, U_{xy}$

$$+ b'' \cos 72° \, U_{yz} - b'' \sin 72° \, U$$

(3)　　$\alpha = 144°; \quad n_3'' - n_0'' = a'' \sin 36° \, U_\Delta + 2a'' \cos 72° \, U_{xy}$

$$- b'' \cos 36° \, U_{yz} - b'' \sin 36° \, U$$

(4)　　$\alpha = 216°; \quad n_4'' - n_0'' = a'' \sin 36° \, U_\Delta + 2a'' \cos 72° \, U_{xy}$

$$- b'' \cos 36° \, U_{yz} + b'' \sin 36° \, U.$$

(5)　　$\alpha = 288°; \quad n_5'' - n_0'' = a'' \sin 36° \, U_\Delta - 2a'' \cos 36° \, U_{xy}$

$$+ b'' \cos 72° \, U_{yz} + b'' \sin 72° \, U_{x}$$

For beam I reverse only the signs for gradients.

Hence, for beam II:

$$U_{xz} = \frac{1}{b} \left[\mathbf{M}(n_5 - n_2) + \mathbf{N}(n_4 - n_3) \right]$$

$$U_{yz} = \frac{1}{b} \left[\mathbf{P}(n_5 + n_2 - 2n_1) - \mathbf{O}(n_4 + n_3 - 2n_1) \right]$$

$$U_\Delta = -\frac{1}{a} \left[\mathbf{N}(n_5 - n_2) - \mathbf{M}(n_4 - n_3) \right]$$

$$2U_{xy} = -\frac{1}{a} \left[\mathbf{O}(n_5 + n_2 - 2n_1) - \mathbf{P}(n_4 + n_3 - 2n_1) \right],$$

$(7\text{-}54a)$

where

$$\mathbf{M} = \frac{\sin 72°}{2 - \cos 72° + \cos 36°} \text{ or } 0.38042$$

$$\mathbf{N} = \frac{\sin 36°}{2 - \cos 72° + \cos 36°} \text{ or } 0.23511$$

$$\mathbf{O} = \frac{1 + \cos 36°}{5(\cos 72° + \cos 36°)} \text{ or } 0.32361$$

$$\mathbf{P} = \frac{1 - \cos 72°}{5(\cos 72° + \cos 36°)} \text{ or } 0.12361.$$

With the foregoing coefficients, the instrument constants **a** and **b** may be combined for convenience in calculation. Equations (7-54a) contain

only readings n and no n_0. With deflections Δ from the torsionless position, the equations are:

$$U_{xz} = -\frac{1}{b}[0.2351(\Delta_3 - \Delta_4) + 0.3804(\Delta_2 - \Delta_5)]$$

$$U_{yz} = -\frac{1}{b}[0.7236(\Delta_3 + \Delta_4) + 0.2764(\Delta_2 + \Delta_5)]$$

$$U_\Delta = \frac{1}{a}[0.2351(\Delta_3 - \Delta_4) - 0.3804(\Delta_2 - \Delta_5)]$$

$$2U_{xy} = -\frac{2}{a}[0.1382(\Delta_3 + \Delta_4) + 0.3618(\Delta_2 + \Delta_5)]$$

(7–54b)

where the numerical factors represent combinations of trigonometric functions, as given before, and where

$$n_0 = \frac{}{5}.$$

4. *Horizontal gradiometers and similar instruments.* Because gradients are more readily interpreted than curvature values, and since the latter are very erratic in certain types of work (rugged topography, and irregular density distribution near the surface), a number of attempts have been made to design torsion balances which furnish the gradients alone or give them at least in fewer positions than are required to obtain both gradients and curvature values. This objective may be accomplished by balance beams of different designs or by suitable combinations of standard beams. In any beam with symmetrical mass distribution the influence of the curvatures is zero. If one of these masses is placed at a different elevation, the beam will be affected by the gradient forces alone. In the gradiometer of Shaw and Lancaster-Jones[78] three masses

G. 7-61. Gradiometer. R, Damping ring; ρ, arm; m, masses (after Lancaster-Jones).

[78] J. Sci. Instr., **49**(11/12), 1–20 (Nov. and Dec., 1932).

are spaced at angles of 120° (Fig. 7–61). All masses are equal and balanced. Since the moment of the curvature forces on each mass is $D_2 = m\rho F$ (ρ = radius arm), the sum of the three moments to be used in eq. (7–50b) would be zero for any value of α. This may be demonstrated readily for the position $\alpha = 0$:

$$\mathbf{D}_2' + \mathbf{D}_2'' + \mathbf{D}_2''' = \frac{3}{2}\, m\rho^2 \{U_\Delta \sin 60° - U_\Delta \sin 60°$$

$$+ 2U_{xy} - 2U_{xy} \cos 60° - 2U_{xy} \cos 60°\} = 0.$$

Therefore, formula (7–51b) for the standard balance reduces to

$$n - n_0 = \mathbf{b}\,(\cos \alpha \; U_{yz} - \sin \alpha \; U_{xz}), \tag{7–55}$$

where $\mathbf{b} = 2fm\rho h/\tau$ and which contains three unknowns. These may be determined in three azimuths so that when

$$\alpha = 0°, \qquad n_1 - n_0 = \mathbf{b}U_{yz};$$

$$\alpha = 120°, \qquad n_2 - n_0 = \mathbf{b}\left(-\frac{1}{2}\,U_{yz} - \frac{\sqrt{3}}{2}\,U_{xz}\right); \text{ and}$$

$$\alpha = 240°, \qquad n_3 - n_0 = \mathbf{b}\left(-\frac{1}{2}\,U_{yz} + \frac{\sqrt{3}}{2}\,U_{xz}\right).$$

Hence,

$$\left.\begin{array}{l} U_{xz} = \dfrac{1}{\sqrt{3}\,\mathbf{b}}\, [(n_3 - n_0) - (n_2 - n_0)] \text{ and} \\[2ex] U_{yz} = \dfrac{1}{\mathbf{b}}\,(n_1 - n_0) \end{array}\right\} \tag{7–55b}$$

where $\qquad n_0 = \frac{1}{3}(n_1 + n_2 + n_3).$

For four positions (0°, 90°, 180°, and 270°) the readings become

$$n_1 - n_0 = \mathbf{b}\,U_{yz}, \qquad n_3 - n_0 = -\mathbf{b}\,U_{yz},$$

$$n_2 - n_0 = -\mathbf{b}\,U_{xz}, \qquad n_4 - n_0 = \mathbf{b}\,U_{xz},$$

so that $n_3 - n_0 = n_0 - n_1$ and $n_2 - n_0 = n_0 - n_4$. The n_0 is thus half the sum of the opposing readings. Then

$$\left.\begin{array}{l} U_{xz} = \dfrac{1}{2\mathbf{b}}\,[(n_4 - n_0) - (n_2 - n_0)] \\[2ex] U_{yz} = \dfrac{1}{2\mathbf{b}}\,[(n_1 - n_0) - (n_3 - n_0)]. \end{array}\right\} \tag{7–55c}$$

If two balance systems are used in a gradiometer, only two azimuths are required.

In the Haalck torsion balance (see Fig. 7-62a) two standard beams are used at right angles to each other; only two azimuths are necessary to cancel the curvatures and to determine gradients. The arrangement is seen from the following scheme:

Fig. 7-62a. Haalck balance (gradiometer).

BALANCE I		BALANCE II	
	Reading		*Reading*
Azimuth 1, $\alpha = 0°$.	n_1'	$\alpha = 90°$.	n_1''
"　　 2, $\alpha = 180°$.	n_2'	$\alpha = 270°$.	n_2''

With formula (7-51b) (position 1):

(1) balance I: $n_1' - n_0' = \mathbf{a}' \cdot 2U_{xy} + \mathbf{b}' \cdot l$

(2) balance II: $n_1'' - n_0'' = \mathbf{a}'' \cdot -2U_{xy} + \mathbf{b} \qquad U_{xx}$,

(position 2):

(3) balance I: n_2' $\qquad\qquad + $

(4) balance II: $n_2'' - n_0'' = \mathbf{a}'' \cdot -2l \qquad \mathfrak{I}'' + U_{xx}$.

Subtracting equation (3) from (1),

$$U_{yz} = \frac{1}{2\mathbf{b}'} (n_1' - n_2'),$$

and subtracting equation 2 from 4, $\qquad\qquad$ (7-56)

Curvature values may be obtained by setting up the balance in three azimuths.

In *Hecker's* balance (Fig. 7-62b), four beams are used in such manner that two standard sets make an angle of 60° with each other. Only *two* azimuths are required to obtain *both* gradients and curvature values. The formulas for this instrument may be derived by substituting the values in Table 21 in eq. (7-51b).
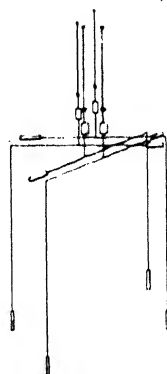
Fig. 7-62b. Hecker four-beam balance.

<center>TABLE 21</center>

POSITION	BALANCE I		BALANCE II		BALANCE III		BALANCE IV	
	Az.	Read.	Az.	Read.	Az.	Read.	Az.	Read.
1.......	0°	n_1'	60°	n_1''	180°	n_1'''	240°	n_1''''
2.......	180°	n_2'	240°	n_2''	0°	n_2'''	60°	n_2''''

Fig. 7-63 shows the Numerov[79] three-beam balance. With it, gradients may be determined in the 0° and 180° or 90° and 270° positions. An intermediate azimuth is required for curvatures. The beam azimuths and readings in these positions are shown in Table 22.

The equations for the six possible combinations (canceling the torsionless-position reading) are:[79a]

(1) From positions 1 and 2:

$$n_1' - \qquad\qquad \cdot bU_{yz} + $$
$$+ a\sqrt{3}$$
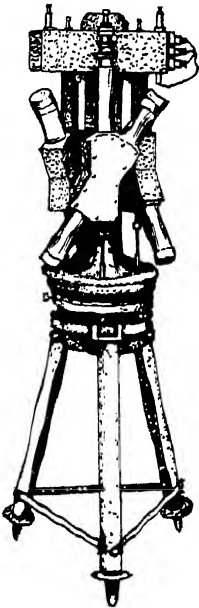
FIG. 7-63. Numerov - Askania three-beam balance.

$$-\frac{b}{2}(\sqrt{3}+1)U_{yz} + \frac{b}{2}(\sqrt{3}-1)U_{zz}$$

<center>TABLE 22</center>

POSITION	BALANCE I		BALANCE II		BALANCE III	
	Az.	Read.	Az.	Read.	Az.	Read.
1..........	0°	n_1'	120°	n_1''	240°	n_1'''
2..........	90°	n_2'	210°	n_2''	330°	n_2'''
3..........	180°	n_3'	300°	n_3''	60°	n_3'''
4..........	270°	n_4'	30°	n_4''	150°	n_4'''

[79] B. Numerov, Astron. Inst. Leningrad Bull., **30**, 103–108 (1932).
[79a] For simplicity, the constants a and b are here taken to be alike for all three beams.

(2) From positions 1 and 3:

$$n_1' - n_3' \equiv \Delta_{1-3}' = 2\mathbf{b}\,U_{yz}$$

$$n_1'' - n_3'' \equiv \Delta_{1-3}'' = -\mathbf{b}U_{yz} - \mathbf{b}\sqrt{3}\,U_{zz}$$

$$n_1''' - n_3''' \equiv \Delta_{1-3}''' = -\mathbf{b}U_{yz} + \mathbf{b}\sqrt{3}\,U_{zz}$$

(3) From positions 1 and 4:

$$n_1' - n_4' \equiv \Delta_{1-4}' = 4\mathbf{a}U_{xy} + \mathbf{b}U_{yz} - \mathbf{b}U_{xz}$$

$$n_1'' - n_4'' \equiv \Delta_{1-4}'' = -2\mathbf{a}U_{xy} + \mathbf{a}\sqrt{3}\,U_\Delta$$

$$\quad -\frac{\mathbf{b}}{2}\left(\sqrt{3}+1\right)U_{yz} - \frac{\mathbf{b}}{2}\left(\sqrt{3}-1\right)U_{xz}$$

$$n_1''' - n_4''' \equiv \Delta_{1-4}''' = -2\mathbf{a}U_{xy} - \mathbf{a}\sqrt{3}\,U_\Delta$$

$$\quad +\frac{\mathbf{b}}{2}\left(\sqrt{3}-1\right)U_{yz} + \frac{\mathbf{b}}{2}\left(\sqrt{3}+1\right)U_{xz}$$

(4) From positions 2 and 3:

$$n_2' - n_3' \equiv \Delta_{2-3}' = -4\mathbf{a}U_{xy} + \mathbf{b}U_{yz} - \mathbf{b}U_{xz}$$

$$n_2'' - n_3'' \equiv \Delta_{2-3}'' = 2\mathbf{a}U_{xy} - \mathbf{a}\sqrt{3}\,U_\Delta$$

$$\quad -\frac{\mathbf{b}}{2}\left(\sqrt{3}+1\right)U_{yz} - \frac{\mathbf{b}}{2}\left(\sqrt{3}-1\right)U_{xz}$$

$$n_2''' - n_3''' \equiv \Delta_{2-3}''' = 2\mathbf{a}U_{xy} + \mathbf{a}\sqrt{3}\,U_\Delta$$

$$\quad +\frac{\mathbf{b}}{2}\left(\sqrt{3}-1\right)U_{yz} + \frac{\mathbf{b}}{2}\left(\sqrt{3}+1\right)U_{xz}$$

(5) From positions 2 and 4:

$$n_2' - n_4' \equiv \Delta_{2-4}' = -2\mathbf{b}U_{xz}$$

$$n_2'' - n_4'' \equiv \Delta_{2-4}'' = -2\mathbf{b}\sqrt{3}\,U_{yz} + \mathbf{b}U_{xz}$$

$$n_2''' - n_4''' \equiv \Delta_{2-4}''' = +\mathbf{b}\sqrt{3}\,U_{yz} + \mathbf{b}U_{xz}$$

(6) From positions 3 and 4:

$$n_3' - n_4' \equiv \Delta_{3-4}' = 4\mathbf{a}U_{xy} - \mathbf{b}U_{yz} - \mathbf{b}U_{xz}$$

$$n_3'' - n_4'' \equiv \Delta_{3-4}'' = -2\mathbf{a}U_{xy} + \mathbf{a}\sqrt{3}\,U_\Delta$$

$$\quad -\frac{\mathbf{b}}{2}\left(\sqrt{3}-1\right)U_{yz} + \frac{\mathbf{b}}{2}\left(\sqrt{3}+1\right)U_{xz}$$

$$n_3''' - n_4''' \equiv \Delta_{3-4}''' = -2\mathbf{a}U_{xy} - \mathbf{a}\sqrt{3}\,U_\Delta$$

$$\quad +\frac{\mathbf{b}}{2}\left(\sqrt{3}+1\right)U_{yz} - \frac{\mathbf{b}}{2}\left(\sqrt{3}-1\right)U_{xz}$$

It is seen that from the diametrical positions 1–3 and 2–4, the gradients alone may be obtained, but that for curvatures an additional intermediate position is required.

Hence, for the gradients,

$$
U_{xz} = -\frac{1}{2b\sqrt{3}}(\Delta_{1-3}'' - \Delta_{1-3}'''), \quad \text{and}
$$

$$
U_{yz} = \frac{1}{2b}\cdot\Delta_{1-3}'
$$

or

$$
U_{xz} = -\frac{1}{2b}\cdot\Delta_{2-4}', \quad \text{and}
$$

$$
U_{yz} = -\frac{1}{2b\sqrt{3}}(\Delta_{2-4}'' - \Delta_{2-4}''').
$$

$(7\text{--}57a)$

From combinations 1, 3, 4, and 6, we have the following equations for the curvatures:

(1) $\quad U_\Delta = \dfrac{1}{2a\sqrt{3}}(\Delta_{1-2}'' - \Delta_{1-2}''') + \dfrac{b}{2a}(U_{xz} - U_{yz})$

$\quad 2U_{xy} = \dfrac{1}{2a}\cdot\Delta_{1-2}' - \dfrac{b}{2a}(U_{xz} + U_{yz})$

(3) $\quad U_\Delta = \dfrac{1}{2a\sqrt{3}}(\Delta_{1-4}'' - \Delta_{1-4}''') + \dfrac{b}{2a}(U_{xz} + U_{yz})$

$\quad 2U_{xy} = \dfrac{1}{2a}\cdot\Delta_{1-4}' + \dfrac{b}{2a}(U_{xz} - U_{yz})$

(4) $\quad U_\Delta = -\dfrac{1}{2a\sqrt{3}}(\Delta_{2-3}'' - \Delta_{2-3}''') - \dfrac{b}{2a}(U_{xz} + U_{yz})$

$\quad 2U_{xy} = -\dfrac{1}{2a}\cdot\Delta_{2-3}' - \dfrac{b}{2a}(U_{xz} - U_{yz})$

(6) $\quad U_\Delta = \dfrac{1}{2a\sqrt{3}}(\Delta_{3-4}'' - \Delta_{3-4}''') - \dfrac{b}{2a}(U_{xz} - U_{yz})$

$\quad 2U_{xy} = \dfrac{1}{2a}\cdot\Delta_{3-4}' + \dfrac{b}{2a}(U_{xz} + U_{yz})$

$(7\text{--}57b)$

Although it is not a gradiometer, the continuously rotating balance proposed by Kilchling[80] may be mentioned here. It consists of a single combined gradient and curvature balance, which is suspended from a

---

[80] K. Kilchling, Zeit. Geophys., **2**(4), 134–137 (1926); **3**(6), 281–285 (1927).

slowly rotated wire while a record is taken of the beam position with respect to the instrument case.   As the gradient effects are proportional to the single azimuth, and the curvature values proportional to the double azimuth, one revolution yields an irregular curve whose positive and negative portions have different amplitudes.   Evaluation is based on a determination of two equal ordinates of the same sign having an interval of π.   These ordinates are proportional to the gradients in the two directions.   Curvatures may be calculated from two pairs of equal but opposite ordinates of the interval π.   The total period of observation was intended to be 2 hours with a 40 minute wait period to allow the beams to come to rest.   Extensive experimentation with this balance did not show any superiority over the standard instrument.

   5. *Vertical gradiometers and similar instruments.*   The opinion has been expressed in the literature that a determination of the vertical gradient of gravity would be very desirable for a more complete interpretation of gravitational data.   However, the geologic importance of the vertical gravity gradient has possibly been overstressed since for two-dimensional geologic bodies it may be readily determined from the corrected curvature values.   Be that as it may, several attempts have been made to determine the vertical gravity gradient directly.   These date back to 1880 and were continued in subsequent years in connection with measurements of the gravitational constant and of the mean density of the earth.   Assume that in a sensitive balance the pans are replaced by a weight fixed to one end of the beam and by an equal weight suspended at a lower level on the other end (Fig. 7-64).   Compared with the weight positions in the same level, the beam is unbalanced because of the increase in weight of the suspended mass.   If the addition of a weight, Δm, is required to rebalance the beam, if the masses are m, and their difference in elevation is h, $(m + \Delta m)g = m(g + \partial g/\partial z \cdot h)$, and therefore

$$\Delta m = \frac{mh}{g} \cdot \frac{\partial g}{\partial z}. \qquad (7\text{-}58a)$$

In this manner Jolly found that with 5 kg (mercury) weights at a difference of elevation of 21 m, an addition of 31.69 mg was necessary to rebalance the beam, which gave 3.01×10^{-6} for $\partial g/\partial z$.

   The normal value of the vertical gravity gradient may be obtained (1) from Clairaut's theorem; (2) from the curvature of the reference ellipsoid.   Since in Clairaut's theorem, gravity is expressed as a function of the earth's radius, the vertical gravity gradient may be obtained by differentiation with respect to the radius, so that[81]

---

[81] See also F. R. Helmert, *Higher Geodesy*, Part 2, pp. 94-98, and formulas (7-36a) and (7-36b).

$$\frac{\partial g}{\partial z} = 3.086 \, (1 + 7.1 \cdot 10^{-4} \cdot \cos 2\varphi) \text{ microgals} \cdot \text{cm}^{-1}. \quad (7\text{-}58b)$$

The second method[82] uses Laplace's equation (7–5) and the curvatures of the reference ellipsoid in the meridian and the prime vertical, which are given by

$$\frac{1}{\rho_x} = -\frac{1}{g}\frac{\partial^2 U}{\partial x^2} \quad \text{and} \quad \frac{1}{\rho_y} = -\frac{1}{g}\frac{\partial^2 U}{\partial y^2},$$

so that

$$\frac{\partial g}{\partial z} = g\left(\frac{1}{\rho_x} + \frac{1}{\rho_y}\right) + 2\omega^2, \quad (7\text{-}58c)$$

where $2\omega^2 = 10.52$ E.U. For g, ρ_x, and ρ_y, their values as function of latitude must be used (see Fig. 7–73b). The vertical gravity gradients calculated from eq. (7–58c) agree with those obtained from (7–58b) to a tenth Eötvös.

Forty years after Jolly's experiments, Berroth[83] proposed to use a standard torsion balance for the measurement of vertical gravity gradients by suspending it on nearly horizontal wires. Deflections were to be measured in different azimuths and at different starting angles of the beam against the horizontal. Another design proposed by Schmerwitz[84] aims to increase the sensitivity of a regular balance by the addition of a horizontal pendulum, that is, by astatization (see page 127). A horizontal pendulum oscillating about a vertical axis is in labile equilibrium, but when it is tilted forward by an angle φ, it will assume a definite rest position. If the axis of revolution is then tilted sideways by the angle θ, a deflection $\psi = \theta/\varphi$ from the rest position results. When a horizontal pendulum is placed on a balance, as in Fig. 7–64, the deflection θ is due to an increase in weight of the suspended mass. The deflection ψ throws additional weight over to the right, the moment being $m'l' \sin \psi$. For an ordinary balance with (equal) lever arms L, beam mass M_0, and vertical distance of center of gravity from the axis of rotation d, the sensitivity $\Sigma = L/M_0 d$. With the horizontal pendulum,

$$\overline{} \approx \overline{\frac{}{M_0\, d\varphi - m'l'}}.$$

With a horizontal pendulum balance ($l' = 14$ cm, $m' = 100$ mg, suspended by two 17μ wires [Zoellner suspension] at an angle of about $2°$), a sensitivity of 10^{-3} mg per mm scale deflection could be obtained at a

[82] R. v. Eötvös, op. cit., p. 362.
[83] A. Berroth, Zeit. Instr., 40, 210–211 (1920).
[84] G. Schmerwitz, Zeit. Geophys., 7(1/2), 104 (1931).

scale distance of 2.5 m.   Accuracy of 1 Eötvös (1/3000 part of the normal gradient) would require that the apparent change in weight be determined to $1 \cdot 10^{-4}$ mg.   In that case it would be necessary to observe the vertical gradient in different azimuths, since gravity varies not only in vertical
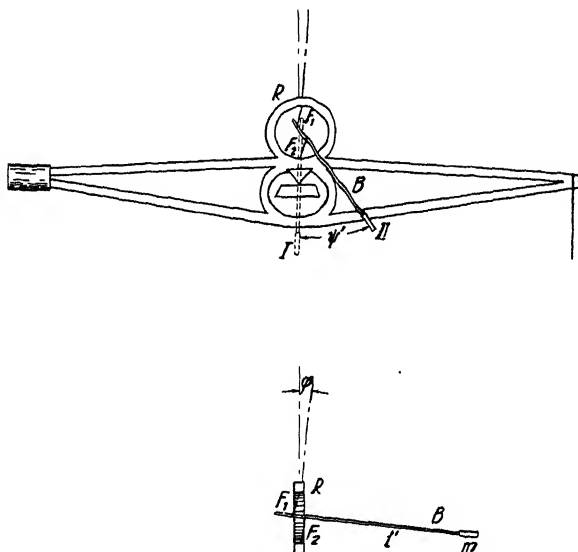
Fig. 7-64. Schmerwitz balance for determination of vertical gravity gradients.

but also in horizontal direction.   Thus, the action of all three gravity components on the beam is given by

$$\int dm[(g_x \cos \alpha + g_y \sin \alpha) \cdot z + g_z(x \cos \alpha + y \sin \alpha)].$$

C. Instrument Types, Instrument Constants

1. *Types.* Although numerous types of torsion balances have been proposed and designed, comparatively few have attained commercial sig-

nificance. A detailed description with instrument constants has been given by Jung.[35] In 1888 and 1890, respectively, Eötvös constructed the first curvature and combined curvature and gradient variometers for laboratory use. In 1898 he followed this with a combined *single* beam field instrument. Its dimensions and constants were (in round figures): m (single beam mass) $= 30$ g, h (distance of weights) $= 60$ cm, l ($\frac{1}{2}$ beam length) $= 20$ cm, K (moment of inertia) $= 21,000$, τ (torsional coefficient of suspension wire) $= 0.5$, d (thickness of wire) $= 40\mu$, L (length of wire) $= 56$ cm. These dimensions have been maintained by all designers of *large* visual and automatic torsion balances.
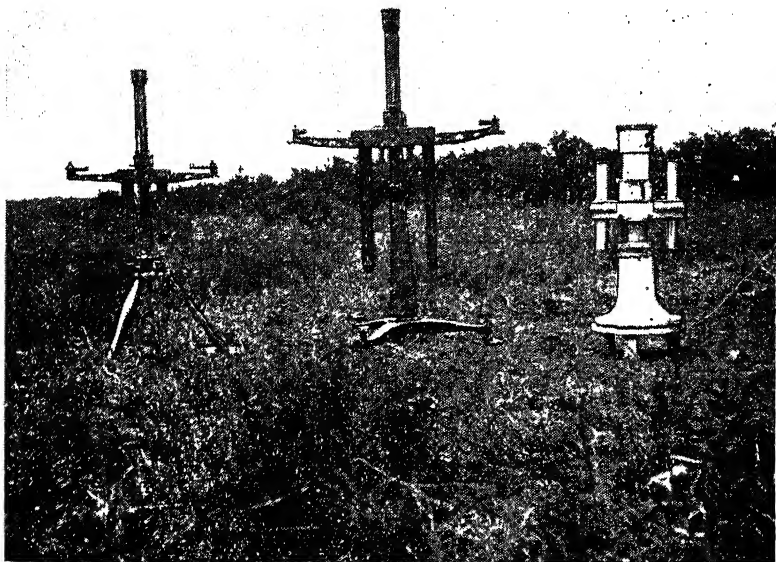
G. 7-65. From left to right: small Suess balance, large Suess balance, small Askania balance.

The single balance was replaced in 1902 by a double variometer (see Fig. 7-65) with visual observation. Most large instruments developed after that, such as the Fechner, Oertling, and Askania (see Fig. 7-66) balances, used photographic recording devices and automatic azimuth rotation. Repeated attempts were made to reduce the dimensions of the large torsion balance. Eötvös himself went to the extreme with an instrument in which $m = 1.4$ g, $h = 20$, $l = 5$, K only 90, and $\tau = 0.0046$; but this instrument was a failure. Similar in dimensions was the Tsuboi

---

[35] K. Jung, Handb. Exper. Phys., **25**(2), 103–123 (1930).

American Askania Corp.
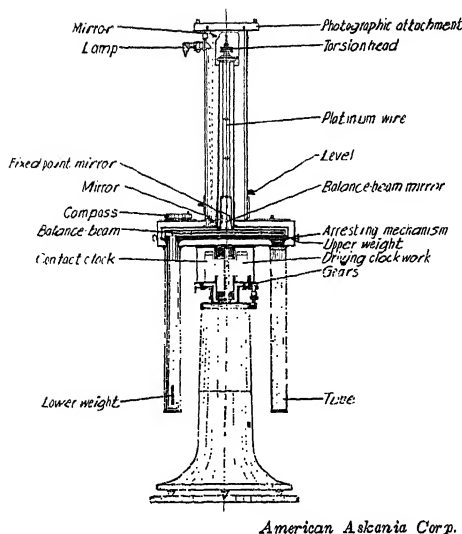
FIG. 7-66. Large Askania photographic recording torsion balance.

quartz balance with $m = 0.25$, $h = 20$, $l = 10$, $K = 66$, $d = 5\mu$, and $L = 20$. It was soon found that a geologically useful torsion balance cannot be decreased in dimensions beyond certain limits. For instance, the Eötvös-Suess small visual balance (Fig. 7-65) has the dimensions $m = 8$, $h - 30$, $l = 10$, $d = 20\mu$, $L = 40$ cm. Very effective in the reduction of overall dimensions was Schweydar's invention of the Z beam (Fig. 7-67). This balance has the following dimensions: $m = 22$, $h = 45$, $l = 20$, $d = 26\text{-}36\mu$, $L = 28$ cm, $K = 19,500$, $\tau = 0.23\text{-}0.47$. Other small balances in which a further reduction in dimensions has been at-

tempted (Gepege, Haff, Hecker, Rybar) have not been very successful.

The Z beam has recently been superseded by the tilt beam (Fig. 7-68),[86] with the following constants: $m = 40$ g, $h = 30$ cm, $l = 10$ cm, $K = 9150$, $d = 33\text{-}43\mu$, $\int dmhl = 13,800$. Torsion balances completely deviating in dimensions from those mentioned are: the Tangl balance (curvature variometer floated in water), Nikiforov's short-wire balance ($\tau = 16$, $L = 2$ cm), and the gravity gradiometer previously discussed.

2. *Constants.* The instrument constants m, h, l, $\mathbf{f}$, L are readily determined before assembly in the factory by measurement of lengths and weights; they are not subject to change, are usually given in the calibration certificate, and require no recalibration. More involved are the

American Askania Corp.

G. 7-67. Z-beam
skania balance.

determinations of K and τ. In an assembled instrument, K/τ may be obtained from oscillations and τ from deflections. More convenient is the independent determination of these constants before assembly.

[86] H. Imhof and A. Graf, Beitr. angew. Geophys., **4**(4), 426–436 (1934); Rev. Sci. Instr., **5**(10), 356–358 (1934).

The ratio K/τ follows directly from the (undamped) period $T = 2\pi \sqrt{K/\tau}$, which may be determined to a high degree of accuracy (1/100 of a second) by using a coincidence method. Since in most basement laboratories the gravity field is disturbed by adjacent walls and excavations, it is necessary to make period observations in two directions at right angles to each other $(\alpha_1,$ and $\alpha_2 = \alpha_1 + 90°)$ to eliminate such effects. Then the equations for two periods are

American Askania Corp.

FIG. 7-68. Balance beam of tilt-beam balance.

$$(1) \quad \frac{4\pi^2 K}{T_1^2} = \tau - (KU_\Delta \cos 2\alpha_1 - 2KU_{xy} \sin 2\alpha_1)$$

$$(2) \quad \frac{4\pi^2 K}{T_2^2} = \tau - (-KU_\Delta \cos 2\alpha_2 + 2KU_{xy} \sin 2\alpha_2). \qquad \Bigg\} \quad (7\text{-}59a)$$

Addition of the two equations gives

$$\frac{K}{\tau} = \frac{T_1^2 T_2^2}{2\pi^2(T_1^2 + T_2^2)}. \qquad (7\text{-}59b)$$

By observing the deflection of the beam due to a known mass at a known distance, τ can be determined independently from the equation

$$\tau\varphi = \frac{mMk}{\rho^2} Cl, \qquad (7\text{-}59c)$$

where φ is the deflection angle; C is a constant ($C = \dfrac{1}{\sqrt{1 + \dfrac{l_m^2}{4\rho^2}}}$, with

l_m = length of cylindrical mass m); ρ = the distance between center of gravity of m and M; and k = gravitational constant. Since ρ is difficult to measure, the mass M is used on a swivel and rotated from one side of the weight to the other. For equal deflections on both sides, the radius of the swivel arm is equal to ρ and

$$\tau = \frac{mMkl}{\rho^2 \sqrt{1 + \dfrac{l_m^2}{4\rho^2}}} \cdot \frac{2f}{n - n_0}. \qquad (7\text{-}59d)$$

The more common practice is now to determine both K and τ before the instrument is assembled. K is obtained by oscillating the beam on a calibrated wire with known τ. For this purpose an oscillation box is made, usually of wood, provided with extensions for the lower (and upper) parts of the beam and of sufficient capacity to keep air damping down. Observations are corrected for (wire) temperatures and amplitude of oscillations. Where large gravity anomalies exist, observations are made in two positions of the box. Wires are very thoroughly tested. The following characteristics are of practical importance: (1) torsional coefficient, (2) carrying capacity, (3) temperature coefficient, and (4) elastic hysteresis. The carrying capacity of a wire varies with the square of the diameter, while the torsional coefficient varies as the fourth power of the radius and inversely as the length:

$$\tau = \frac{\mu \pi r^4}{2l}, \tag{7-60a}$$

where r = radius, l = length, and μ = modulus of rigidity. For other wire sections (ribbons, and the like) the torsional coefficient is given by the relation

$$\tau = \frac{C \mu S^4}{l J_p}, \tag{7-60b}$$

where S = section, C a constant, and J_p the polar moment of inertia.

For a rectangular section, $J_p = (ab^3 + ba^3)/12$, where a and b are the sides of the rectangle. For ratios of $a/b = 1, 2, 3, 4$, and so on, the constant C takes the values 234×10^{-4} (for $a/b = 1$), 238, 249, and 260×10^{-4}. For thin ribbons in which the one dimension is less than one-third the other, the torsional coefficient is closely enough

$$\tau = \frac{\mu}{3l} \cdot ab^3 \left(1 - 0.63 \cdot \frac{b}{a}\right), \tag{7-60c}$$

in which the last term may be generally neglected. Ribbons have the advantage that for a given carrying capacity the torsional coefficient is less, but they are more difficult to obtain. In practice torsional coefficients of torsion balance wires are determined from oscillation observations with calibrated weights. For this purpose a specially built instrument is used, consisting essentially of an upright tube with torsion head above and observation window below, and provided with a heating coil and thermometer.

After a wire has been cut to length, provided with its clamps, and heat-treated, it is placed in the instrument with a mass of calibrated moment of

inertia K. The period is determined by reading the time required for ten complete swings and repeating five to six times. This gives an accuracy in T of better than $1/100$ of a second and a torsional coefficient $\tau = 4\pi^2 K/T^2$. The moment of inertia, K, is determined by calibration with a ring of calculated moment of inertia. If the mass of the ring is m, its outer radius R, and its inner radius r, its moment of inertia is $K_R = {}^2 - r^2)$. If T_1 is the period without the ring and T_2 with the ring,

$$T_1^2 = \frac{4\pi^2}{\tau}(K + K_R)$$

and

$$T_2^2 = \frac{4\pi^2}{\tau} \cdot K,$$

from which

$$K = K_R \frac{T_2^2}{T_1^2 - T_2^2}. \tag{7-60d}$$

The torsion coefficient changes with temperature, θ:

$$\tau_\theta = \tau_{20}[1 + \beta(\theta : -20°)], \tag{7-60e}$$

in which the temperature coefficient, β, of the torsional coefficient follows from period observations at different temperatures. In the field the variation of τ with temperature is disregarded, but in selecting torsion wires in the factory, wires with excessive temperature coefficients of τ are discarded. Equally undesirable are wires of excessive variation of the rest position, n, with temperature. If the reading is n_1 at a temperature θ_1, and n_2 at a temperature θ_2, the variation of n with θ is defined by $n_2 = n_1 - a(\theta_2 - \theta_1)$. The temperature coefficient a of a good wire should not exceed $3\text{--}5 \cdot 10^{-2}$ mm per degree C (referred to the same optical magnification as used in the field instrument). The temperature coefficient of a wire depends largely on the method of clamping and heat treatment.[87] Platinum wires are heat treated electrically under load; tungsten wires are annealed in an atmosphere devoid of oxygen. Fig. 7–69 illustrates the improvement brought about in a wire by heat treatment. Curve A is the zero shift of an untreated wire, curve B that of a wire tempered under load fifty times a day.

It should be noted that in a test instrument the change of the zero position with temperature is generally not the same as in a torsion balance

---

[87] Concerning the effect of annealing and baking on temperature coefficient, see N. N. Zirbel, Physics, **2**(3), 134–138 (March, 1932).
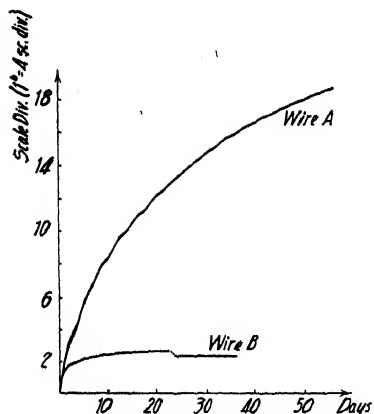
FIG. 7-69. Change of rest position of torsion wires with treatment (after Shaw and Lancaster-Jones).

since beam deflections are produced by convection currents in the narrow interior compartment. It has been found[88] that this effect can be nearly eliminated by determining an optimum transverse position of the beam in the interior compartment.

When a wire breaks in the field and a new wire is inserted, the coefficients o, p, q, and r, as well as s and t, are changed (see formula [7-52f]). If τ_1' is the torsion coefficient of a broken wire in balance I, τ_1'' the t.c. of a broken wire in balance II, τ_2' the t.c. of a new wire in balance I, and τ_2'' the t.c. of a new wire in balance II, the

new coefficients are:

$$
\left.
\begin{aligned}
U_{xz} &= \text{o } \frac{\tau_2'}{\tau_1'}\left[(\Delta_2' - \Delta_3') - \text{s } \frac{\tau_1'\tau_2''}{\tau_2'\tau_1''}(\Delta_2'' - \Delta_3'')\right] \\[2mm]
U_{yz} &= \text{p } \frac{\tau_2'}{\tau_1'}\left[(\Delta_2' + \Delta_3') - \text{s } \frac{\tau_1'\tau_2''}{\tau_2'\tau_1''}(\Delta_2'' + \Delta_3'')\right] \\[2mm]
U_{\Delta} &= -\text{q } \frac{\tau_2'}{\tau_1'}\left[(\Delta_2' - \Delta_3') + \text{t } \frac{\tau_1'\tau_2''}{\tau_2'\tau_1''}(\Delta_2'' - \Delta_3'')\right] \\[2mm]
2U_{xy} &= -\text{r } \frac{\tau_2'}{\tau_1'}\left[(\Delta_2' + \Delta_3') + \text{t } \frac{\tau_1'\tau_2''}{\tau_2'\tau_1''}(\Delta_2'' + \Delta_3'')\right]
\end{aligned}
\right\} \quad (7\text{-}61)
$$

and similarly for other beam positions. The replacement of a torsion wire must be done with great care to avoid kinking or overstraining the wire. Directions given by the manufacturers should be closely followed.[89]

3. *The sensitivity of a torsion balance* is a function of its geometric dimensions, of the torsional coefficient of the suspension wire, and of the optical magnification. According to eq. (7-51a), the angular deflection increases in the proportion K/τ for curvatures and in the proportion mhl/τ for gradients. The optical magnification is given by $2f/\nu$ for single and $4f/\nu$ for double reflection, where f is focal length and ν scale interval. Since the latter is generally so chosen that 1/10 division may still be

[88] C. A. Heiland, *Directions for the Askania Torsion Balance*, American Askania Corporation (Houston and Chicago, 1933). H. Imhof and A. Graf, *loc. cit.* A. Schleusener, Zeit. Geophys., **9(6/8)**, 301.

[89] For a description of steps necessary to readjust the beam after insertion of a new wire, see *Directions for the Askania Torsion Balance, op. cit.*

read conveniently, the sensitivity for curvatures is proportional $20fK/\nu\tau$ and for gradients $20fmhl/\nu\tau$, where for double reflection the factor 40 takes the place of 20. The reciprocal of the sensitivity is the "scale value" of the instrument,

$$\frac{\nu\tau}{20fmhl} \text{ (gradients)} \quad \text{and} \quad \frac{\nu\tau}{20fK} \text{ (curvatures)} \quad (7\text{-}62)$$

where 40f instead of 20f is used for double reflection.

4. *Calculation of instrument readings* of a standard torsion balance proceeds in accordance with formulas (7-52b) to (7-54b). A number of positions are generally repeated. Deflections are averaged in such a manner that the variation of the torsionless position with time is eliminated. In visual torsion balances, beam readings are entered against
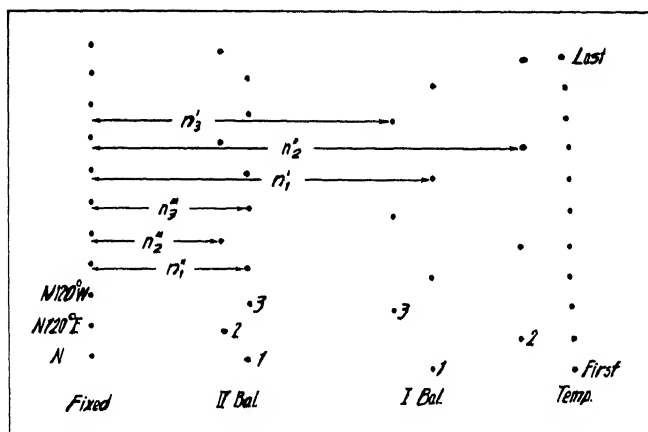
Fig. 7-70. Evaluation of torsion-balance record (large Askania balance).

azimuth, time, and temperature (see Fig. 7-71). Calculation is the same as in photographic balances. Fig. 7-70 illustrates a record taken with a recording balance. On the left is the fixed mirror record, then follows the record of the second balance, first balance, and temperature. For evaluation, a graduated scale is placed over the record and its 0-line aligned with the fixed-point line. Deflections for positions occupied are read for beams II and I, giving n_1'', n_2'', n_3'', n_1', n_2', and n_3', and so on, in scale divisions. These are entered for three positions in Table 23. The temperature record is not evaluated. The torsionless position is calculated by averaging successive readings in the following manner:

1. $n_0' = \quad n_1' + n_2' + n_3')$ 1. $n_0'' = \frac{1}{3}(n_1'' + n_2'' + n_3'')$

2. $n_0' =$ 2. $n_1'')$

3. $n_0' = \quad + n_1' + n_2')$ etc.   3. $\quad = \frac{1}{3}(n_3'' + n_1'')$ etc.

By this procedure a linear change of the zero position with time is eliminated. After that the differences $n_1' - n_0'$, $n_2' - n_0'$, $n_3' - n_0'$ and $n_1'' - n_0''$, $n_2'' - n_0''$, $n_3'' - n_0''$ (or Δ_1', Δ_2', Δ_3', and Δ_1'', Δ_2'', and Δ_3'') are

TABLE 23

CALCULATION OF THREE-POSITION TORSION BALANCE RECORD

Station No. 10

Location: Fort Bend County,　　Date: July 10, 1935
　　　　　Texas　　　　　　　　Observer: J. A. S.
　　　$\varphi = 29°$　　　　　　　1st Reading: 9 h., 55 min.
　　　　　　　　　　　　　　Notes: Instr. set due north

	BALANCE I						BALANCE II				
No.	n'	n_0'	Δ_1'	Δ_2'	Δ_3'	No.	n''	n_0''	Δ_1''	Δ_2''	Δ_3''
1	84.5	...	...	...	...	1	54.2	...	...	...	...
2	87.6	87.0	...	+0.6	...	2	52.1	52.1	...	0	...
3	89.0	87.4	...	...	+1.6	3	50.0	51.9	...	...	−1.9
1	85.5	87.6	−2.1	...	...	1	53.7	51.8	+1.9	...	...
2	88.4	87.9	...	+0.5	...	2	51.6	51.7	...	−0.1	...
3	89.8	88.1	...	...	+1.7	3	49.7	51.6	...	...	−1.9
1	86.0	88.2	−2.2	...	...	1	53.5	51.5	+2.0	...	...
2	88.7	88.3	...	+0.4	...	2	51.4	51.4	...	0	...
3	90.2	...	...	...	...	3	49.4	...	...	...	...
1	...	...	...	...	...	1	...	...	...	...	...
2	...	...	...	...	...	2	...	...	...	...	...
3	...	...	...	...	...	3	...	...	...	...	...
1	...	...	...	...	...	1	...	...	...	...	...
2	...	...	...	...	...	2	...	...	...	...	...
3	...	...	...	...	...	3	...	...	...	...	...
Mean Δ'			−2.2	+0.5	+1.7	Mean Δ''			+2.0	−0.1	−1.9

$$\Sigma = 0$$

$$\Delta_2' - \Delta_3' = -1.2 \qquad\qquad +\Delta_3' = +2.2$$

$$\Delta_2'' - \Delta_3'' = +1.8 \qquad\qquad '+\Delta_3'' = -2.0$$

Difference	×o	$= U_{xz}$		Difference	×p	
−3.0	+1.45	−4.4		+4.2	2.51	+10.5
Sum	×q	$= U_\Delta$		Sum	×r	
+0.6	−4.17	−2.5		+0.2	−7.21	−1.4

calculated and averaged. Their sum should equal zero. For three positions the differences $\Delta_2' - \Delta_3'$ and $\Delta_2'' - \Delta_3''$, and the sums $\Delta_2' + \Delta_3'$ and $\Delta_2'' + \Delta_3''$ are then calculated. Their sums and differences are multiplied

by factors o, p, q, and **r**, which gives gradients and curvatures, assuming that the factors s and t are equal to 1. When there are rapid changes of zero position with time, deflections are calculated by leaving out one in each set of deflections,

$$\quad\quad - \quad \Delta_2$$

$$\Delta_1 \quad - \quad \Delta_3$$

$$\Delta_1 \quad \Delta_2 \quad -,$$

Posn.	Time	Bal #1	Temp.	Correct	Mean	Value	Bal #2	Temp.	Correct	Mean	Value
1 60°20'	12·30	168.9	31.9				464.6				
2 180°20'	1 20	177.4	32.3		173.1	+4.3	462.1			465.0	−2.9
3 300°20'	2:10	173.1	32.7		173.3	−0.2	468.2			465.1	+3.1
4 60°20'	3.00	169.4	33.0		173.5	−4.1	465.0			465.1	−0.1
5 180°20'	3 50	178.0	32.8				462.1				
A 2'+3'	B 2'−3'	C 2"+3"	D 2"−3"	B−D	XZ		A−C	YZ	B+D	(—)	A+C	XY
+4.1	+4.5	+0.2	−6.0	+10.5		+3.9		−1.5		+4.3	
2:3'	(2:3')+1'	2:3"	(2:3")+1"	B−D	+10.55	1'−1"	+3.95	B+D	−1.55	1'+1"	+4.25
−0.4	−4.5	+6.2	+6.1	−10.6		−4.0		+1.6		−4.2	
Stat. No.	1001		Full Values		+14.35	+9.28		−6.51		+15.43
Date	6-20-29		Terr. Effects		+1.40	−0.60		0		+0.32
Obs. by	G/v		Topog. Values		+12.95	+9.88		−6.51		+15.11
Check by	H≡S		Norm. Value		+6.90	−0.90		+7.50		+1.20
Anomalies	R 31.2	λ N32°E	+6.05			+10.78		−14.01		+13.91

FIG. 7-71. Evaluation of torsion-balance readings (small Suess balance).

and completing the vacant spaces from

$$(-) + \Delta_2 \quad + \Delta_3 \quad = 0$$

$$\Delta_1 \quad + (-) + \Delta_3 \quad = 0$$

$$\Delta_1 \quad + \Delta_2 \quad + (-) = 0.$$

Several short cuts to calculations of torsion-balance quantities from records and readings have been suggested. One method uses nomographs[90] and another[91] employs charts for calculating gradients and curvatures from the differences $\Delta_2 - \Delta_3$ and the sums $\Delta_2 + \Delta_3$. Fig. 7–72 shows such charts calculated for a balance with the coefficients o = 1.59, p = 2.75, q = 2.93 and r/2 = 2.56. Chart I is for U_{zz} and U_Δ, Chart II

[90] A. Stepanoff and W. Ayvazoglou, U.S. Bur. Mines I. C., 6306 (July, 1930).

[91] M. M. Slotnick, Physics, **2**(3), 131-133 (March, 1932).

for U_{yz} and U_{xy}. Assume, as in the example given on the form, that $\Delta_3'' = -1.9$, $\Delta_2'' = -0.1$, $\Delta_3' = 1.7$, and $\Delta_2' = 0.5$. Then $\Delta_3'' - \Delta_2'' = -1.8$, $\Delta_3'' + \Delta_2'' = -2.0$, $\Delta_3' - \Delta_2' = 1.2$ and $\Delta_3' + \Delta_2' = 2.2$. Using Chart I, locate -1.8 on the left side of the $\Delta_3'' - \Delta_2''$ axis, go N to $+1.2$ on the $\Delta_3' - \Delta_2'$ axis, thence NE to the intersection with U_{xz} to find -4.8. Going SE, -1.7 is obtained on the U_Δ axis. On Chart II, locate -2.0
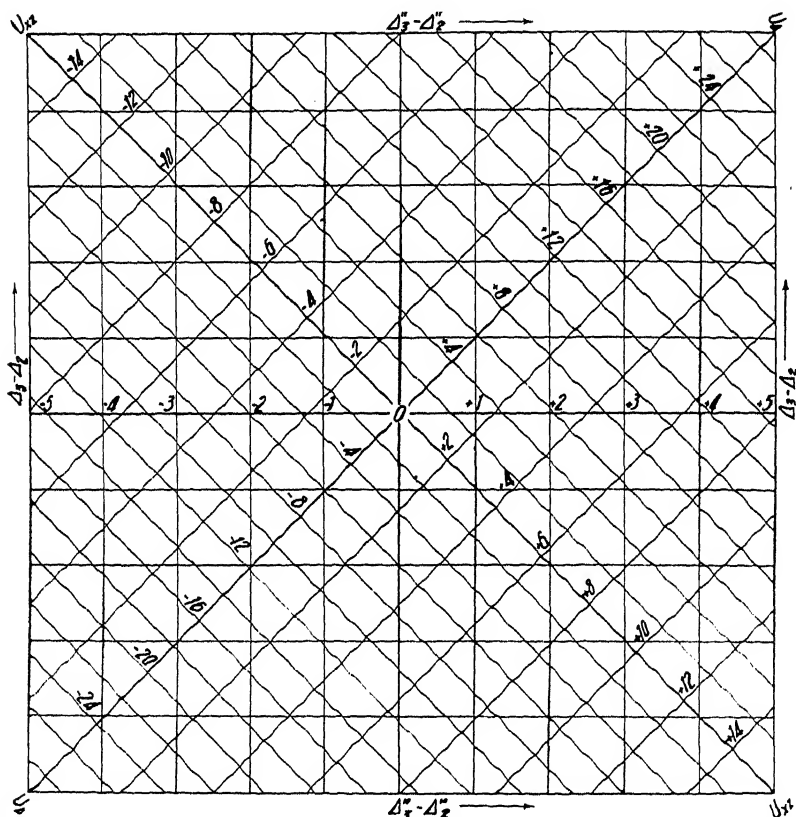
Fig. 7-72a. Torsion-balance calculation chart for U_{xz} and U_Δ (after Slotnick).

on the left side of the $\Delta_3'' + \Delta_2''$ axis, go N to 2.2 on the $\Delta_3' + \Delta_2'$ axis, thence SW to $+11.8$ for U_{yz} and SE to -0.5 for U_{xy}.

In connection with the form shown in Table 23, a second form is used for the terrain correction, which contains also additional columns for far terrain, planetary correction, and calculation of final results (see Table 32).

The following example is an illustration of calculations made for a station with very large gradients and curvature values, on which records

in three, four, and five positions were taken.	The formulas used in the calculation of the three-position record were

$$U_{xz} = \quad 1.26[(\Delta_2' - \Delta_3') - (\Delta_2'' - \Delta_3'') + 0.01044(\Delta_2'' - \Delta_3'')]$$

$$U_{yz} = \quad 2.18[(\Delta_2' + \Delta_3') - (\Delta_2'' + \Delta_3'') + 0.01044(\Delta_2'' + \Delta_3'')]$$

$$U_\Delta = -3.60[(\Delta_2' - \Delta_3') + (\Delta_2'' + \Delta_3'') - 0.01233(\Delta_2'' - \Delta_3'')]$$

$$2U_{xy} = -6.24[(\Delta_2' + \Delta_3') + (\Delta_2'' + \Delta_3'') - 0.01233(\Delta_2'' + \Delta_3'')],$$

where $o = 1.26$, $p = 2.18$, $q = 3.60$, and $r = 6.24$, $0.01044 = 1 - s$, and $0.01233 = 1 - t$.	These formulas are derived from the standard formulas
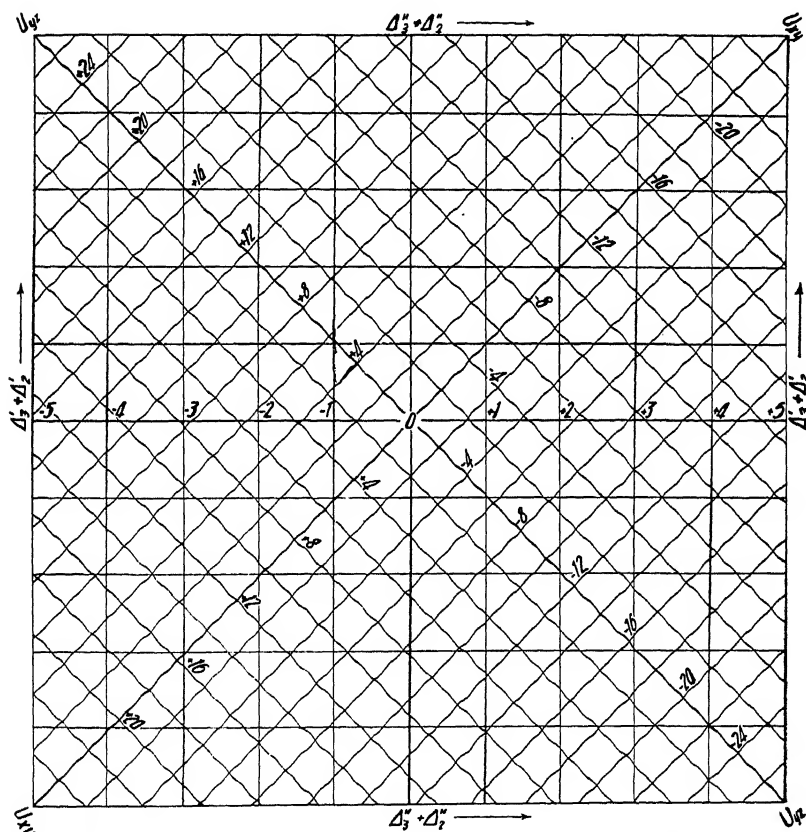
FIG. 7-72b. Torsion-balance calculation chart for U_{xy} and U_{yz} (after Slotnick).

(7-52h), which may be written $U_{xz} = o(\Delta_1 - s\Delta_2) = o(\Delta_1 - \Delta_2 + \Delta_2 - s\Delta_2)$, and so on, so that

$$U_{xz} = o[(\Delta_2' - \Delta_3') - (\Delta_2'' - \Delta_3'') + (1 - s)(\Delta_2'' - \Delta_3''$$

In the example (Table 24), $(\Delta_2'' - \Delta_3'')(1 - s)$ is designated as C_{zz}, $(\Delta_2'' - \Delta_3'') \cdot (1 - t)$ as C_Δ, and so on.

TABLE 24

CALCULATION OF THREE-POSITION TORSION-BALANCE RECORD
(LARGE DEFLECTIONS)

No.	n'	n_0'	Δ_1'	Δ_2'	Δ_3'	No.	n''	n_0''	Δ_1''	Δ_2''	Δ_3''
1	141.7	...	...	...	...	1	81.5	...	...	...	...
2	90.0	116.8	...	−26.8	...	2	34.5	53.6	...	−19.1	...
3	118.7	117.0	...	...	+1.7	3	44.9	53.7	...	...	−8.8
1	142.2	117.0	+25.2	...	...	1	81.7	53.7	+28.0	...	...
2	90.0	116.8	...	−26.8	...	2	34.6	53.8	...	−19.2	...
3	118.2	116.1	...	...	+2.1	3	45.0	53.7	...	...	−8.7
1	140.0	115.8	+24.2	...	...	1	81.6	53.9	+27.7	...	...
2	89.2	115.8	...	−26.6	...	2	35.2	54.0	...	−18.8	...
3	117.5	115.5	...	...	+2.0	3	45.2	54.0	...	...	−8.8
1	139.8	115.5	+24.3	...	...	1	81.5	54.0	+27.5	...	...
2	89.5	115.8	...	−26.3	...	2	35.2	54.0	...	−18.8	...
3	118.0	...	...	...	...	3	45.3	...	...	...	...
1	...	...	...	...	...	1	...	...	...	...	...
2	...	...	...	...	...	2	...	...	...	...	...
3	...	...	...	...	...	3	...	...	...	...	...
Mean Δ'			+24.6	−26.6	+1.9	Mean Δ''			+27.7	−19.0	−8.8

$$\angle = -0.1 \qquad \Sigma = -0.1$$

$$\Delta_2' - \Delta_3' = -28.5 \qquad\qquad \Delta_2' + \Delta_3' = -24.7$$

$$\Delta_2'' - \Delta_3'' = -10.2 \begin{cases} \times & (1-s) = C_{zz} \\ \times - & (1-t) = C_\Delta \end{cases} \qquad \Delta_2'' + \Delta_3'' = -27.8 \begin{cases} \times & (1-s) = C_{yz} \\ \times - & (1-t) = C_{xy} \end{cases}$$

Diff.	C_{zz}	Res.	$\times$o	$= U_{xz}$		Diff.	$-$	Res.	$\times$p	$-$
−18.3	−0.1	−18.4	1.26	−23.2		+3.1	−0.3	+2.8	2.18	+6.1
Sum	C_Δ	Res.	$\times$q	$= U_\Delta$		Sum		Res.	$\times$r	$2U_{xy}$
−38.7	+0.1	−38.6	−3.60	+139.0		−52.5	+0.3	−52.2	6.24	+325.7

In the calculation of the four-position record in Table 26, the numerical values in Table 25 were used.

TABLE 25

BEAM	b	$1.414b$	$m = \dfrac{1}{1.414\,b}$	$m' = \dfrac{1}{1.414\,b'}$
I	$0.2289 \cdot 10^9$	$0.3237 \cdot 10^9$	3.089	.....
II	$0.2318 \cdot 10^9$	$0.3278 \cdot 10^9$	.....	3.051

TABLE 26

CALCULATION OF FOUR-POSITION TORSION-BALANCE RECORD (FROM LARGE DEFLECTIONS)

	Beam II							Beam I					
No.	n'	n_0'	Δ_1'	Δ_2'	Δ_3'	Δ_4'	No.	n'	n_0'	Δ_1'	Δ_2'	Δ_3'	Δ_4'
1	62.5						1	99.5					
2	50.2	52.9		−2.7			2	92.1	99.9		−7.8		
3	54.0	53.3			+0.7		3	110.2	100.2			+10.0	
4	45.5	53.3				−7.8	4	97.6	100.3				−2.7
1	63.6	53.0	+10.6				1	101.0	100.3	+0.7			
2	50.0	52.9		−2.9			2	92.5	100.2		−7.7		
3	53.0	52.7			+0.3		3	110.1	99.9			+10.2	
4	44.8	52.6				−7.8	4	97.1	99.8				−2.7
1	62.9	52.5	+10.4				1	100.0	99.8	+0.2			
2	49.6	52.4		−2.8			2	92.1	99.9		−7.8		
3	52.6	52.5			+0.1		3	110.1	100.2			+9.9	
4	44.5	52.5				−8.0	4	97.3	100.5				−3.2
1	63.2	52.6	+10.6				1	101.5	100.8	+0.7			
2	49.8	52.6		−2.8			2	93.1	100.8		−7.7		
3	53.1						3	111.2					
4	44.4						4	97.5					
	$\Sigma =$	+0.2	+10.5	−2.8	+0.4	−7.9		$\Sigma =$	−0.1	+0.5	−7.8	+10.0	−2.8

$$\Delta_1' + \Delta_2' = -7.3m = -22.5 \quad \text{or} \quad -(\Delta_3' + \Delta_4') = -7.2m = -22.2$$
$$\Delta_2' + \Delta_3' = +2.2m = +6.8 \quad \text{or} \quad -(\Delta_1' + \Delta_4') = +2.3m = +7.1$$
$$= -(\Delta_1'' + \Delta_2'') = -7.7m' = -23.5 \quad \text{or} \quad = \Delta_3'' + \Delta_4'' = -7.5m' = -22.9$$
$$= -(\Delta_2'' + \Delta_3'') = +2.4m' = +7.3 \quad \text{or} \quad = \Delta_1'' + \Delta_4'' = +2.6m' = +7.9 \quad \text{II}$$

For five positions, calculations from deflections Δ with respect to the torsionless position, and from the readings n are possible. Both calculations are given in Tables 27 to 30. The following formulas were used for the calculations from deflections:

Balance I:

$$U_{zz} = -1.03\,(\Delta_4' - \Delta_3') - 1.66\,(\Delta_5' - \Delta_2')$$
$$U_{yz} = +3.16\,(\Delta_4' + \Delta_3') + 1.21\,(\Delta_2' + \Delta_5')$$
$$U_\Delta = +4.73\,(\Delta_4' - \Delta_3') - 2.93\,(\Delta_5' - \Delta_2')$$
$$2U_{xy} = -3.44\,(\Delta_4' + \Delta_3') - 9.02\,(\Delta_5' + \Delta_2')$$

Balance II:

$$U_{zz} = +1.01\,(\Delta_4'' - \Delta_3'') + 1.64\,(\Delta_5'' - \Delta_2'')$$
$$U_{yz} = -3.12\,(\Delta_3'' + \Delta_4'') - 1.19\,(\Delta_2'' + \Delta_5'')$$
$$U_\Delta = +4.69\,(\Delta_4'' - \Delta_3'') - 2.90\,(\Delta_5'' - \Delta_2'')$$
$$2U_{xy} = -3.40\,(\Delta_3'' + \Delta_4'') - 8.93\,(\Delta_2'' + \Delta_5'')$$

TABLE 27

CALCULATION OF FIVE-POSITION TORSION-BALANCE RECORD
(FROM Δ's)

PART 1

n''	n_0''	Δ_1''	Δ_2''	Δ_3''	Δ_4''	Δ_5''	n'	n_0'	Δ_1'	Δ_2'	Δ_3'	Δ_4'	Δ_5'
82.2	....	.....	....	....	....	....	124.0	....	.....	....	....	....	....
44.2	....	.....	....	....	....	....	79.2	....	.....	....	....	....	....
53.2	53.6			−0.4			95.2	99.3			−4.1		
66.9	53.4				+13.5		121.2	99.0				+22.2	
21.5	53.5					−32.0	76.7	98.9					−22.2
81.2	53.5	+27.7					122.5	98.8	+23.8				
44.6	53.5		−8.9				79.0	98.6		−19.6			
53.5	53.3			+0.2			94.3	98.6			−4.3		
66.6	53.4				+13.2		120.2	98.7				+21.5	
20.9	53.3					−32.4	76.7	98.7					−22.0
81.2	53.1	+28.1					123.5	98.8	+24.7				
44.1	53.1		−9.0				79.0	99.2		−20.2			
52.7	52.9			−0.2			94.5	99.1			−4.6		
66.5							122.1						
19.8							76.5						
Σ = 0		+27.9	−9.0	−0.1	+13.4	−32.2	Σ = −0.2		+24.3	−19.9	−4.3	+21.8	−22.1

BEAM II:
$\Delta_3'' + \Delta_4'' = +13.3$ $\quad \Delta_2'' + \Delta_5'' = -41.2$
$\Delta_4'' - \Delta_3'' = +13.5$ $\quad \Delta_5'' - \Delta_2'' = -23.2$

BEAM I:
$\Delta_3' + \Delta_4' = +17.5$ $\quad \Delta$
$\Delta_4' - \Delta_3' = +26.1$ $\quad \Delta_5' -$ $\quad -2.2$

Table 28 shows the calculation of gradients and curvature values for each beam from the sums and differences in Table 27, in accordance with the formulas given on page 184. The same numerical coefficients apply to the calculation of gradients and curvatures from the n's as from the Δ's. The calculation is shown in Tables 29 and 30. Table 31 contains a summary of results obtained for both beams combined or individually in three, four, and five positions.

5. *Operation of torsion balances.* First, an observation site that is flat, at least in the immediate vicinity, should be selected. Next, the differences of elevations on concentric rings are measured at eight or sixteen points, as described in the next section. Three wooden stakes are driven into the ground, and their tops are leveled and placed at an elevation such that the center of gravity of the beam is at a height for which the terrain correction has been calculated. A base plate is so laid on the wooden stakes that its north groove points north, and the differences in elevation for the inside terrain circles against it are determined. It is advantageous to set out a stake about ten feet north of the station site to facilitate orientation of the base plate, house, and instrument. After the hut is erected, the instrument

Table 28

CALCULATION OF FIVE-POSITION TORSION-BALANCE RECORD (FROM Δ's)

Part 2

$\Delta_3'' + \Delta_4''$ $+13.3$	$\times -3.12 =$ -41.5	$\Delta_2'' + \Delta_5''$ -41.2	-1.19 $+49.0$	U_{yz} $+7.5$	$\Delta_3' + \Delta_4'$ $+17.5$	$+3.16$ $+55.3$	$\Delta_2' + \Delta_5'$ -42.0	$+1.21$ -50.8	U_{yz} $+4.5$
$\Delta_3'' + \Delta_4''$ $+13.3$	-3.40 -45.2	$\Delta_2'' + \Delta_5''$ -41.2	-8.93 $+367.9$	$2U_{xy}$ $+322.7$	$\Delta_3' + \Delta_4'$ $+17.5$	-3.44 -60.2	$\Delta_2' + \Delta_5'$ -42.0	-9.02 $+378.8$	$2U_{xy}$ $+318.6$
$\Delta_4'' - \Delta_3''$ $+13.5$	$+1.01$ $+13.6$	$\Delta_5'' - \Delta_2''$ -23.2	$+1.64$ -38.0	U_{zz} -24.4	$\Delta_4' - \Delta_3'$ $+26.1$	-1.03 -26.9	$\Delta_5' - \Delta_2'$ -2.2	-1.66 $+3.7$	U_{zz} -23.2
$\Delta_4'' - \Delta_3''$ $+13.5$	$+4.69$ $+63.3$	$\Delta_5'' - \Delta_2''$ -23.2	-2.90 $+67.3$	U_Δ $+130.6$	$\Delta_4' - \Delta_3'$ $+26.1$	$+4.73$ $+123.5$	$\Delta_5' - \Delta_2'$ -2.2	-2.93 $+6.4$	U_Δ $+129.9$

pedestal is placed in position on the aluminum base plate.   This is followed
by the center piece, which in the automatic instruments is provided with
stops for three, four, and five positions and which must be set according to
the azimuths selected.   The upper part of the instrument containing the
beams is secured in place, and tubes for the hanging weights are attached
where necessary.

After the instrument has been assembled, it is carefully leveled.   In
automatic balances the driving clockwork is wound and engaged and the
upper part allowed to rotate until it reaches the first stop.   The compass

TABLE 29
CALCULATION OF FIVE-POSITION TORSION-BALANCE RECORD
(FROM n's)
PART 1

	BEAM II					BEAM I			
1	82.2	....	....	....	....	124.0	....	....	.....	....
2	....	44.2	....	....	....	.....	79.2	....	.....	....
3	....	....	53.2	....	....	.....	....	95.2	.....	....
4	....	....	....	66.9	....	.....	....	....	121.2	....
5	....	....	....	....	21.5	.....	....	....	.....	76.7
1	81.2	....	....	....	....	122.6	....	....	.....	....
2	....	44.6	....	....	....	.....	79.0	....	.....	....
3	....	....	53.5	....	....	.....	....	94.3	.....	....
4	....	....	....	66.6	....	.....	....	....	120.2	....
5 ·	....	....	....	....	20.9	.....	....	....	.....	76.7
1	81.2	....	....	....	....	123.5	....	....	.....	....
2	....	44.1	....	....	....	.....	79.0	....	.....	....
3	....	....	52.7	....	....	.....	....	94.5	.....	....
4	....	....	....	66.5	....	.....	....	....	122.1	....
5	....	....	....	....	19.8	.....	....	....	.....	76.5
.	81.5	44.3	53.1	66.7	20.7	123.4	79.1	94.7	121.2	76.6
.	n_1''	n_2''	n_3''	n_4''	n_5''	n_1'	n_2'	n_3'	n_4'	n_5'

needle is then released and the upper part, together with the turntable, is
turned clockwise until the side of the balance case is in the astronomic
meridian.   After the beams have been released, a visual instrument is
ready for observations in the first and all other azimuths at about 50-
minute intervals.   In an automatic instrument a plate must be inserted,
the recording clock wound, and a trial run made before the instrument
can be left to itself.   Further details are given in the author's torsion-
balance manual.[92]

[92] *Directions for the Askania Torsion Balance.*

TABLE 30

CALCULATION OF FIVE-POSITION TORSION-BALANCE RECORD (FROM n's)

PART 2

Beam II

$n_5'' - n_2''$	$+1.64$	$n_4'' - n_3''$	$+1.01$	U_{zz}		
-23.6	-28.7	$+13.6$	$+13.7$	-25.0		
$n_6'' - n_2''$	-2.90	$n_4'' - n_3''$	$+4.69$	U_Δ		
-23.6	$+68.4$	$+13.6$	$+63.8$	$+132.2$		
$n_6'' + n_2'' - 2n_1''$	$+0.53$	$n_4'' + n_3'' - 2n_1''$	-1.40	U_{xy}		
-98.0	-51.9	-43.2	$+60.5$	$+8.6$		
$n_6'' + n_2'' - 2n_1''$	-3.99	$n_4'' + n_3'' - 2n_1''$	$+1.52$	$2U_{xy}$		
-98.0	$+391.0$	-43.2	-65.7	$+325.3$		

Beam I

$n_5' - n_2'$	-1.66	$n_4' - n_3'$	-1.027	U_{zz}
-2.5	$+4.2$	$+26.5$	-27.2	-23.0
$n_6' - n_2'$	-2.93	$n_4' - n_3'$	$+4.74$	U_Δ
-2.5	$+7.3$	$+26.5$	$+125.6$	$+132.9$
$n_5' + n_2' - 2n_1'$	-0.540	$n_4' + n_3' - 2n_1'$	$+1.413$	U_{yz}
-91.1	$+49.2$	-30.9	-43.4	$+5.8$
$n_6' + n_2' - 2n_1'$	-4.032	$n_4' + n_3' - 2n_1'$	$+1.546$	$2U_{xy}$
-91.1	$+367.3$	-30.9	-47.8	$+319.5$

209

Table 31

Positions	Beam	U_{xz}	U_{yz}	U_Δ	$2U_{xy}$
3........	I & II	−23.2	6.1	139.0	325.7
5........	I ⎫ from Δ's.	−23.2	4.5	129.9	318.6
5........	II ⎭	−24.4	7.5	130.6	322.7
5........	I ⎫ from n's.	−23.0	5.8	132.9	319.5
5........	II ⎭	−25.0	8.6	132.2	325.3
4........	I	−22.5	6.8	.....	.....
		−22.2	7.1		
4........	II	−23.5	7.3	.....	.....
		−22.9	7.9		

D. Corrections

After torsion-balance readings have been calculated in the form of gradients and curvature values as shown in the preceding section, a number of corrections must be applied. These may be divided into corrections required for every station and corrections required only in special cases. In the first group fall (1) the planetary correction, and (2) the terrain correction; in the second are (3) corrections for regional effects, (4) corrections for coast effect, and (5) corrections for fixed masses other than terrain, underground openings, and so forth.

1. *Planetary corrections.* As in measurements of relative gravity with the pendulum or gravimeter, the normal or planetary variation of gravity must be considered in both gradients and curvature values. It is here again sufficient to consider the earth as an ellipsoid of revolution with a major (equatorial) axis and a minor (polar) axis.

The planetary variation in the gradient may be obtained by differentiation of formula (7–15b), disregarding the longitude term so that the planetary gradient is

$$(U_{xz})_{\text{norm.}} \equiv \left(\frac{\partial g}{\partial x}\right)_{\text{norm.}} = \frac{\partial g}{\rho_x \, \partial \varphi} \equiv \frac{\partial g}{R \partial \varphi}, \qquad (7\text{-}63)$$

where ρ_x is the radius of curvature of the meridional ellipse, which in this case is sufficiently close to the earth's radius so that after substitution of the numerical values from eq. (7–15b)

$$(U_{xz})_{\text{norm.}} = 8.16 \cdot 10^{-9} \cdot \sin \qquad (7\text{-}64)$$

The variation of gravity and gravity gradient with latitude is shown in Fig. 7–73a. It is seen that the north gradient is zero at the equator and the poles, is always directed toward the north or south pole, and has a maximum at 45° latitude. Under the conditions assumed (two-axial ellipsoid of revolution), there is no variation of gravity along the parallels of latitude, and hence no correction need be applied for planetary variation to the observed values of U_{yz}. If the instrument is oriented into the

magnetic meridian, a correction would, of course, be necessary. However, this can be avoided by allowing for the declination, and setting it in the direction of the astronomic meridian.

For calculating the planetary effect on curvature values, formula (7–48i) may be used, which relates the curvature U_Δ to the two principal radii of curvature of the equipotential surface.   The normal surface is assumed to be that of a two-axial ellipsoid of rotation, in which case the planes con-
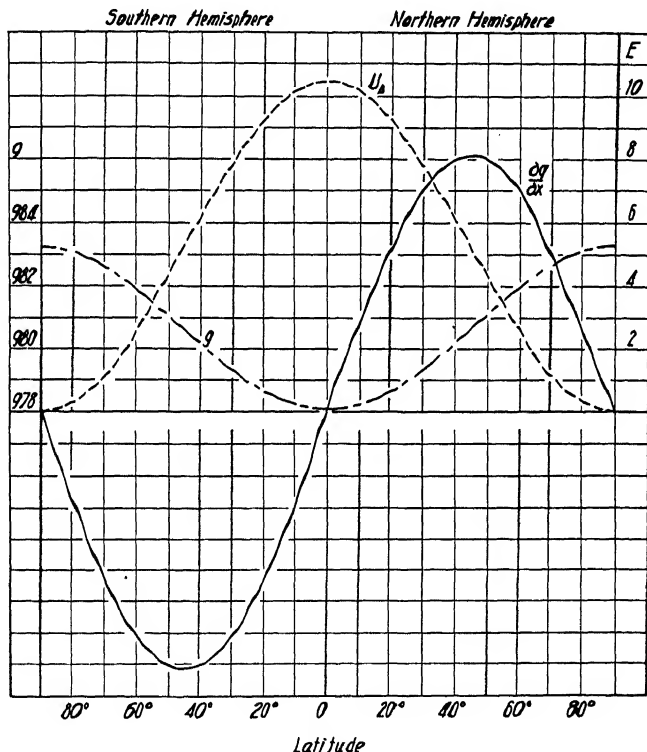
FIG. 7-73a. Planetary variation of gravity, gradients, and curvature values.

taining the principal radii of curvature are in the astronomic meridian and the prime vertical, so that $\lambda = 0$.   Hence $(U_\Delta)_{\text{norm.}} = -g\left(\dfrac{1}{\rho_y} \quad \dfrac{1}{\rho_x}\right)$ where ρ_x and ρ_y are the principal radii of curvature.   For the meridian ellipse the radius of curvature[93] in the latitude φ, is given by

$$\rho_x = \frac{a^2 c^2}{\left(a^2 \cos^2 \varphi + \right.}$$

[93] K. Jung, Handb. Exper. Phys., 25(3), 150 (1930).

with a as equatorial and c as polar radius, while the radius in the prime vertical is

$$\rho_y = \sqrt{a^2 \cos^2 \varphi + c^2 \sin^2 \varphi}$$
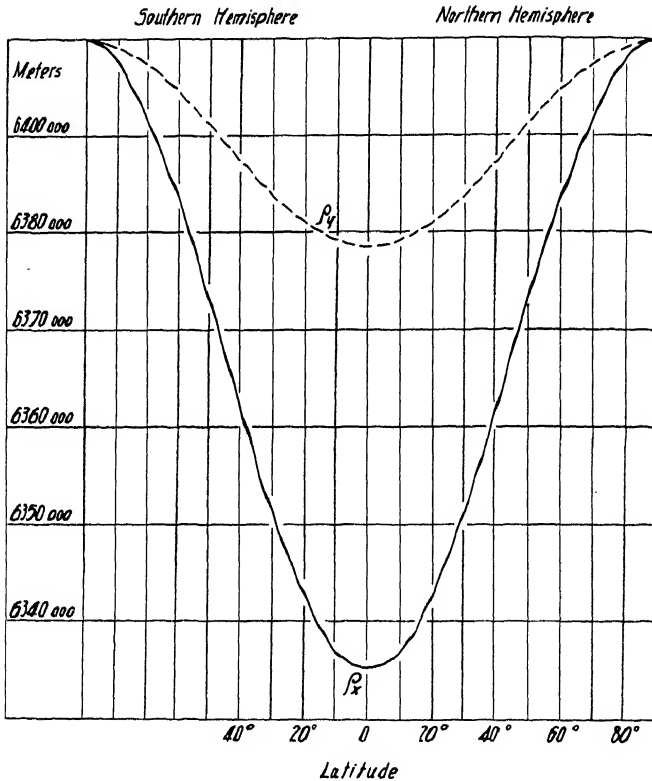
FIG. 7-73b. Planetary variation of curvature radii of reference ellipsoid in meridian and prime vertical.

The variation of these radii with latitude is shown in Fig. 7 73b. Therefore, with sufficient approximation

$$\frac{g}{a} \cdot \frac{a^{\sim} - c^{\sim}}{a^2} \cos^2$$

where the second factor is approximately twice the flattening, or $2 \cdot (a - c)/a$ (see eq. 7-14a). By substitution of the numerical value for the equatorial radius,

$$U_{\Delta})_{\text{norm.}} = 5.15 \cdot 10^{-9} (1 + \cos 2\varphi). \tag{7-65}$$

The planetary variation of the curvature value is shown in Fig. 7–73a. U_{xy} is zero, since λ was assumed to be zero. The maximum value of $(U_\Delta)_{\text{norm}}$ occurs at the equator; it is zero at both poles.

2. *Terrain corrections.* Since the torsion balance is a very sensitive instrument for the detection of certain types of subsurface mass irregularities, it is readily understood why it also reacts very perceptibly to the visible, that is, topographic masses around it. As it measures variations in gravity components rather than gravity itself, it is seen that it must be more sensitive to terrain variations than is the pendulum or the gravimeter. Finally, the variations of the *horizontal* gravity components (curvature values) are much more affected by terrain than are the variations of the *vertical* components (gradients).

In order to correct for terrain effects, it is necessary to know the shape of the topography surrounding the instrument. This is done for close distances (up to about 200 or 300 feet) by leveling. For greater distances, existing contour maps may be used with sufficient accuracy. It is customary to refer to the correction for the short distances as terrain or topographic correction and to the correction for the greater distances as cartographic correction.

It is obviously impossible to survey in detail all the small terrain irregularities around the instrument. As will be shown below, *any* method of terrain correction can do no more than substitute a more or less idealized surface for the actual terrain surface. Hence, the field survey need not be carried beyond the limits of accuracy inherent to the mathematical representation of terrain effects. The principal requirement is that the calculation of the terrain effects be within the limits of error with which gradients and curvature values can be read on the instrument and interpreted. Terrain effects are therefore calculated in flat country (oil exploration) with a probable error of several tenths to one E.U., while in hilly country (mining applications) the probable error is several to 5 or even 10 E.U. In any event, there is no need for carrying the accuracy of terrain surveys to extremes, since most analytical terrain methods are based on the assumption of uniform densities. This assumption is not always correct for the surface layer, to say nothing of the effect of a denser medium beneath the weathered layer.

Experience has shown that it is generally sufficient to smooth out the ground immediately adjacent to the instrument (out to 1.5 m radius) as much as possible and to measure elevations in eight azimuths from the setup, along circles whose radii depend on terrain and correction method used. In most terrain methods the radii are fixed; and, in very unfavorable terrain, elevations are determined in sixteen instead of eight azimuths.

Terrain correction procedures may be divided into (*a*) analytical, (*b*)

graphical, and (c) integraph methods. In the first, elevations measured in the field in predetermined azimuths and radii about the instrument are substituted in formulas with fixed coefficients for such azimuths and distances. In the second method, evaluation diagrams, or "graticules," are used which are superimposed upon a terrain contour map or upon terrain sections in predetermined azimuths. A count is made of the number of diagram "elements" which are included within adjacent contour lines, or between the terrain profile and a plane through the center of gravity of the balance beam. In the integraph methods, contour maps or terrain profiles are evaluated directly by specially constructed integraphs.

Terrain correction methods are numerous, and only those differing sufficiently in mathematical principles or procedure will be discussed.
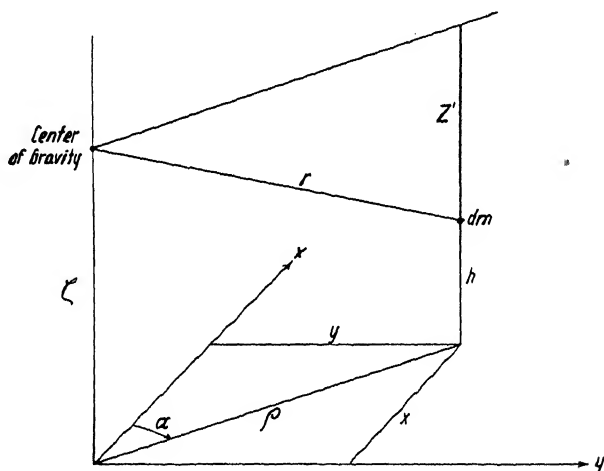
Fig. 7-74. Mass element in relation to center of gravity of torsion balance.

Their description will proceed in the order given above and will be concluded with a discussion of application and field practice.

(a) *Analytical methods.* The fundamental principle underlying not only the analytical but all other terrain-correction methods is to divide the surrounding terrain into sectors bounded by angles and concentric circles and to sum up their effects. The action of each sector is calculated in the analytical methods by assuming definite variations from one azimuth to another and from one circle to another. Within two successive circles all sectors have the same opening. (In the graphical methods the sectors are all different and so calculated in respect to azimuth and distance that they exert the same effect on the instrument.)

The action of each sector follows from the effect of a mass element dm (see Fig. 7-74). Since its gravity potential at the distance r is $U =$

$(k\,dm)/r$, the gradients and curvature values, or the second derivatives of the potential, are

$$U_\Delta = 3k \int dm.?$$

$$(7\text{-}66)$$

$$U_{yz} = 3k \int dm.\frac{yz'}{r^5}$$

Assume that the center of gravity of the balance beam is at a distance ζ and the mass element at an elevation h above ground. Then by substitution of $r = \sqrt{\rho^2 + (\zeta - h)^2}$ and $z' = \zeta - h$

$$U_{xz} = 3k \int dm \frac{x(\zeta - h)}{[\rho^2 + (\zeta - h)^2]^{5/2}} \qquad U_\Delta = 3k \int dm \frac{y^2 - z^2}{[\rho^2 + (\zeta - h)^2]^{5/2}}$$

$$U_{yz} = 3k \int dm \frac{y(\zeta - h)}{[\rho^2 + (\zeta - h)^2]^{5/2}} \qquad U_{xy} = 3k \int dm \frac{xy}{[\rho^2 + (\zeta - h)^2]^{5/2}}.$$

With polar coordinates $x = \rho \cos \alpha$ and $y = \rho \sin \alpha$:

$$U_{xz} = 3k \int dm \frac{\rho \cos \alpha(\zeta - h)}{[\rho^2 + (\zeta - h)^2]^{5/2}} \qquad -U_\Delta = 3k \int dm \frac{\rho^2 \cos 2\alpha}{[\rho^2 + (\zeta - h)^2]^{5/2}}$$

$$U_{yz} = 3k \int dm \frac{\rho \sin \alpha(\zeta - h)}{[\rho^2 + (\zeta - h)^2]^{5/2}} \qquad 2U_{xy} = 3k \int dm \frac{\rho^2 \sin 2\alpha}{[\rho^2 + (\zeta - h)^2]^{5/2}}.$$
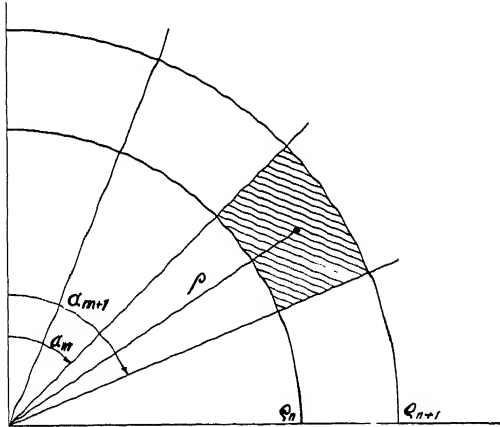
FIG. 7-75. Sectorial mass element.

For a sectorial mass element (Fig. 7-75), $d\rho \cdot \rho d\alpha \cdot dh \cdot \delta$ (δ = density) bounded by two concentric circles with the radii ρ_n and ρ_{n+1} and angles α_m and α_{m+1},

$$dm = \delta \int_{\alpha_m}^{\alpha_{m+1}} \int_{\rho_n}^{\rho_{n+1}} \int_0^h d\alpha \, d\rho \, dh. \qquad (7\text{-}67)$$

Extending the limits of integration over the entire surrounding topography,

$$
\left.
\begin{aligned}
U_{xz} &= 3k\delta \int_0^\infty \int_0^{2\pi} \int_0^h \frac{\rho^2 \cos\alpha\, d\alpha\, d\rho\, dh(\zeta - h)}{[\rho^2 + (\zeta - h)^2]^{5/2}} \\[2mm]
U_{yz} &= 3k\delta \int_0^\infty \int_0^{2\pi} \int_0^h \frac{\rho^2 \sin\alpha\, d\alpha\, d\rho\, dh(\zeta - h)}{[\rho^2 + (\zeta - h)^2]^{5/2}} \\[2mm]
-U_\Delta &= 3k\delta \int_0^\infty \int_0^{2\pi} \int_0^h \frac{\rho^3 \cos 2\alpha\, d\alpha\, d\rho\, dh}{[\rho^2 + (\zeta - h)^2]^{5/2}} \\[2mm]
2U_{xy} &= 3k\delta \int_0^\infty \int_0^{2\pi} \int_0^h \frac{\rho^3 \sin 2\alpha\, d\alpha\, d\rho\, dh}{[\rho^3 + (\zeta - h)^2]^{5/2}}
\end{aligned}
\right\}
\qquad (7\text{-}68a)
$$

In practice the integration of the effects of the concentric circles is not carried to infinity. The circles are calculated individually; the calculation is stopped when a circle exerts an influence of less than 0.1 E.U.; and all circles are added. Within each circle the effect of the elevation h is a function of azimuth, as shown further below. For the last integration the denominator in eq. (7-68a) is more conveniently written

$$
[\rho^2 + (\zeta - h)^2]^{-5/2} = \left[(\rho^2 + \zeta^2)\left(1 + \frac{h^2 - 2\zeta h}{\rho^2 + \zeta^2}\right) \right]^{-5/2}.
$$

For fairly gentle slopes not exceeding $8°$–$10°$, the last term is generally small and the above expression may be expanded in the form of a power series, so that after multiplication by $\int_0^h dh\,(\zeta - h) = \frac{1}{2}(2\zeta h - h^2)$ the series is

$$
\frac{1}{2}[(\rho^2 + \zeta^2)^{-5/2}]\left[2\zeta h - h^2 + \frac{5}{2}\frac{(h^2 - 2\zeta h)^2}{\rho^2 + \zeta^2} - \cdots \right] \qquad (7\text{-}68b)
$$

Only the first two terms of the last factor are considered. This approximation is made in *all* analytical terrain-correction methods. Carrying out the integrations $\int_0^h dh(\zeta - h)$ and $\int_0^h dh$, the four derivatives are:

$$
\left.
\begin{aligned}
U_{zz} &= -3k\,\frac{\delta}{2}\int_0^\infty \int_0^{2\pi} \frac{\rho^2 \cos\alpha\, d\alpha\, d\rho}{(\rho^2 + \zeta^2)^{5/2}}\,(h^2 - 2\zeta h) \\[2mm]
U_{yz} &= -3k\,\frac{\delta}{2}\int_0^\infty \int_0^{2\pi} \frac{\rho^2 \sin\alpha\, d\alpha\, d\rho}{(\rho^2 + \zeta^2)^{5/2}}\,(h^2 - 2\zeta h) \\[2mm]
-U_\Delta &= +6k\,\frac{\delta}{2}\int_0^\infty \int_0^{2\pi} \frac{\rho^3 \cos 2\alpha\, d\alpha\, d\rho}{(\rho^2 + \zeta^2)^{5/2}}\cdot h \\[2mm]
2U_{xy} &= +6k\,\frac{\delta}{2}\int_0^\infty \int_0^{2\pi} \frac{\rho^3 \sin 2\alpha\, d\alpha\, d\rho}{(\rho^2 + \zeta^2)^{5/2}}\cdot h
\end{aligned}
\right\}
\qquad (7\text{-}69)
$$

From this point on, various analytical terrain methods make different assumptions regarding the variation of h with azimuth and radius. For greater distances it is permissible to make no assumption whatever regarding a variation and to assume merely that the elevation measured in the field is representative of the mean elevation of a sector which is so bounded that the station at which the elevation is measured is *at its center*[94] (and not at its corners as assumed in other analytical methods).

The effect of each sector is then obtained by integration between the limits ρ_n and ρ_{n+1} and α_m and α_{m+1}. Considering that

$$\int_0^{2\pi} \zeta^2 \cos \alpha \, d\alpha = \int_0^{2\pi} \zeta^2 \sin \alpha \, d\alpha = \int_0^{2\pi} \zeta \cos 2\alpha \, d\alpha = \int_0^{2\pi} \zeta \sin 2\alpha \, d\alpha = 0$$

and that, therefore, the substitutions

$$h^2 - 2\zeta h \equiv h^2 - 2\zeta h - \zeta^2 \equiv H^2 \quad \text{and} \quad h - \zeta \equiv H \tag{7-70}$$

are permissible, the azimuthal effects of all sectors in a concentric ring are given by

$$\left.\begin{array}{l}
\displaystyle\int_0^{2\pi} \cos \alpha \, d\alpha \, H^2 = \frac{2\pi}{m} \sum_m H^2 \cos \alpha \equiv c' \\[3mm]
\displaystyle\int_0^{2\pi} \sin \alpha \, d\alpha \, H^2 = \frac{2\pi}{m} \sum_m H^2 \sin \alpha \equiv b' \\[3mm]
\displaystyle\int_0^{2\pi} \cos 2\alpha \, d\alpha \, H = \frac{2\pi}{m} \sum_m H \cos 2\alpha \equiv e' \\[3mm]
\displaystyle\int_0^{2\pi} \sin 2\alpha \, d\alpha \, H = \frac{2\pi}{m} \sum_m H \sin 2\alpha \equiv d'
\end{array}\right\} \tag{7-71}$$

where m is the number of azimuths (eight or sixteen) in which the elevations are measured.

Then the effect of one ring bounded by the radii ρ_n and ρ_{n+1} is

$$\left.\begin{array}{l}
\displaystyle U_{xz} = -3k \frac{\delta}{2} \int_{\rho_n}^{\rho_{n+1}} \frac{\rho^2 \, d\rho}{(\rho^2 + \zeta^2)^{5/2}} \cdot c' \\[4mm]
\displaystyle U_{yz} = -3k \frac{\delta}{2} \int_{\rho_n}^{\rho_{n+1}} \frac{\rho^2 \, d\rho}{(\rho^2 + \zeta^2)^{5/2}} \cdot b' \\[4mm]
\displaystyle -U_\Delta = 6k \frac{\delta}{2} \int_{\rho_n}^{\rho_{n+1}} \frac{\rho^3 \, d\rho}{(\rho^2 + \zeta^2)^{5/2}} \cdot e' \\[4mm]
\displaystyle 2U_{xy} = 6k \frac{\delta}{2} \int_{\rho_n}^{\rho_{n+1}} \frac{\rho^3 \, d\rho}{(\rho^2 + \zeta^2)^{5/2}} \cdot d'
\end{array}\right\} \tag{7-72}$$

[94] C. A. Heiland, A.I.M.E. Geophysical Prospecting, 554 (1929).

Coefficients for each ring resulting from the evaluation of these integrals and the expansion of the coefficients c', b', e', and d' in terms of elevations in eight and sixteen azimuths are given in the article referred to.[95]

As stated before, this procedure is permissible only for greater distances (cartographic correction). In the application of terrain methods to smaller distances, some variation of elevation between successive azimuths and radii must be assumed in order to arrive at a mean elevation of a sector. The simplest assumption has been made by Eötvös.[96] If the sector is bounded by angles α_1 and α_2 and by radii ρ' and ρ''; if the elevations h_1' and h_2' have been determined on the radius ρ' in the azimuths α_1 and α_2; and if the elevations h_1'' and h_2'' have been determined on the radius ρ'' in the same azimuths, the mean elevation is assumed to be given by

$$h = c_1 + c_2\alpha + c_3\rho\alpha + c_4\rho,$$

so that the coefficients

$$\left.\begin{aligned}
c_1(\alpha_2 - \alpha_1)(\rho'' - \rho') &= \rho''(\alpha_2 h_1' - \alpha_1 h_2') - \rho'(\alpha_2 h_1'' - \alpha_1 h_2'') \\
c_2(\alpha_2 - \alpha_1)(\rho'' - \rho') &= \rho''(h_2' - h_1') - \rho'(h_2'' - h_1'') \\
c_3(\alpha_2 - \alpha_1)(\rho'' - \rho') &= h_2'' - h_1'' - (h_2' - h_1') \\
c_4(\alpha_2 - \alpha_1)(\rho'' - \rho') &= \alpha_2(h_1'' - h_1') - \alpha_1(h_2'' - h_2').
\end{aligned}\right\} \quad (7\text{-}73)$$

The effect of each ring is calculated from integrals similar to those contained in eq. (7-72). However, Eötvös does not use the squares of the elevations as in eqs. (7-71) to represent the azimuthal variations but breaks off the power series of (7-68b) after the first term, which makes it possible to use the first powers of elevations. By considering only the first term in eq. (7-68b), eq. (7-69) therefore takes the following form for the gradients:

$$U_{zz} = -3k\delta \int_0^\infty \int_0^{2\pi} \frac{\rho^2 \cos\alpha\, d\alpha\, d\rho}{(\rho^2 + \zeta^2)^{5/2}} \cdot (h\zeta - Q),$$

where Q indicates a quadratic term $Q = h^2/2$. Because of this simplification, the formulas are applicable to *small elevations* and *gentle terrain* only.

In the Eötvös formulas given below, the innermost ring of 1.5-m radius is considered a plane with the inclination of ξ in the north and ι in the east directions. A quadratic term is included for the 5-m radius, which is generally negligible for the gentle terrain to which Eötvös' formula is applied. The radii are

ρ_1	ρ_2	ρ_3	ρ_4	ρ_5
1.5 m	5 m	20 m	50 m	100 m

Density is assumed to be 1.8 and ζ is 100 cm.

---

[95] *Ibid.*

[96] *Op. cit.*, 358.

$$U_{\cdot} = [5.77\ \xi]_{\rho_1}$$

$$+[0.00379\ \xi(h_1 + h_5) + 0.0061\ \xi(h_3 + h_7)$$

$$+ 0.0221\ \xi(h_2 + h_4 + h_6 + h_8) + 0.0160\iota(h_2 + h_6 - h_4 - h_8)$$

$$+ 0.13046(h_1 - h_5) + 0.09225(h_2 + h_8 - h_4 - h_6) + Q]_{\rho_2}$$

$$+[0.01173(h_1 - h_5) + 0.00831(h_2 + h_8 - h_4 - h_6)]_{\rho_3}$$

$$+[0.00108(h_1 - h_5) + 0.00077(h_2 \quad h_8 - h_4 \quad h_6)]_{\rho_4}$$

$$+[0.00028(h_1 - h_5) + 0.00020(h_2 \quad h_8 - h_4 \quad h_6)]_{\rho_5}$$

$$= [5.77\ \iota]_{\rho_1}$$

$$+[0.0379\ \iota(h_3 + h_7) + 0.0061\ \iota(h_1 + h_5)$$

$$+ 0.0221\ \iota\ (h_2 + h_4 + h_6 + h_8) + 0.0160\ \xi(h_2 + h_6 - h_4$$

$$- h_8) + 0.13046(h_3 - h_7) + 0.09225\ (h_2 + h_4 - h_6 - h_8)$$

$$+ Q]_{\rho_2} \tag{7-74}$$

$$+[0.01173(h_3 - h_7) + 0.00831(h_2 + h_4 - h_6 - h_8)]_{\rho_3}$$

$$+[0.00108(h_3 - h_7) \quad 0.00077(h_2 + h_4 - h_6 - h_8)]_{\rho_4}$$

$$+[0.00028(h_3 - h_7) \quad 0.00020(h_2 + h_4 - h_6 - h_8)]_{\rho_5}$$

$$-U_\Delta = [0.4826(h_1 - h_3 + h_5 - h_7)]_{\rho_2}$$

$$+[0.08194(h_1 - h_3 + h_5 - h_7)]_{\rho_3}$$

$$+[0.03181(h_1 - h_3 + h_5 - h_7)]_{\rho_4}$$

$$+[0.03077(h_1 - h_3 + h_5 - h_7)]_{\rho_5}$$

$$2U_{xy} = [0.4826(h_2 - h_4 + h_6 - h_8)]_{\rho_2}$$

$$+[0.08194(h_2 - h_4 + h_6 - h_8)]_{\rho_3}$$

$$+[0.03181(h_2 - h_4 + h_6 - h_8)]_{\rho_4}$$

$$+[0.03077(h_2 - h_4 + h_6 - h_8)]_{\rho_5}$$

These formulas have been simplified yet extended to more unfavorable terrain by Schweydar.[97] He eliminated the separate calculation of the innermost ring and developed two methods for calculating gradients for: (1) gentle terrain and elevations not exceeding the height above ground of the center of gravity of the instrument; (2) any topography. The first method follows Eötvös' procedure and considers only the first

[97] W. Schweydar, Zeit. Geophys., **1(1)**, 81–89 (1924); **4(1)**, 17–23 (1927).

and linear elevation term in the power series of eq. (7–68b); the second uses the squares of the elevations as in eq. (7–69). In both methods the variation of elevation with azimuth is represented by Fourier series. This makes the method more flexible and it is possible to apply the formulas to any desired number of azimuths. In any given azimuth, the variation of elevation is assumed to be linear between rings in the first method and quadratic in the second. In both methods the variation is assumed to be linear in the curvatures.

Considering the linear variation between rings first, the following proportion exists:

$$\frac{h_{n+1} - h_n}{\rho_{n+1} - \rho_n} = \frac{h_\rho - h_n}{\rho - \rho_n}.$$

Therefore the elevation is

$$h_\rho(\rho_{n+1} - \rho_n) = h_n \rho_{n+1} - h_{n+1}\rho_n - \rho(h_n - h_{n+1}).$$

Substituting this in eq. (7–68a), and considering in the expansion of eq. (7–68b) only the linear terms, the terrain effect of *one* ring between the radii ρ_{n+1} and ρ_n is

$$U_{xz} = \frac{3k\delta\zeta}{\rho_{n+1} - \rho_n}\left[I_3 \int_0^{2\pi} \cos\alpha\, d\alpha (h_n\rho_{n+1} - h_{n+1}\rho_n) \right.$$

$$\left. + I_1 \int_0^{2\pi} \cos\alpha\, d\alpha (h_n - h_{n+1}) \right]$$

$$U_{yz} = \frac{3k\delta\zeta}{\rho_{n+1} - \rho_n}\left[I_3 \int_0^{2\pi} \sin\alpha\, d\alpha (h_n\rho_{n+1} - h_{n+1}\rho_n) \right.$$

$$\left. + I_1 \int_0^{2\pi} \sin\alpha\, d\alpha (h_n - h_{n+1}) \right]$$

$$-U_\Delta = \frac{3k\delta}{\rho_{n+1} - \rho_n}\left[I_1 \int_0^{2\pi} \cos 2\alpha\, d\alpha (h_n\rho_{n+1} - h_{n+1}\rho_n) \right.$$

$$\left. - I_2 \int_0^{2\pi} \cos 2\alpha\, d\alpha (h_n - h_{n+1}) \right]$$

$$2U_{xy} = \frac{3k\delta}{\rho_{n+1} - \rho_n}\left[I_1 \int_0^{2\pi} \sin 2\alpha\, d\alpha (h_n\rho_{n+1} - h_{n+1}\rho_n) \right.$$

$$\left. + I_2 \int_0^{2\pi} \sin\alpha\, d\alpha (h_n - h_{n+1}) \right].$$

$$(7\text{--}75a)$$

The integral I_3 is the same as the integral in the gradients of formula (7–72), and integral I_1 is the same as the integral in the curvature expres-

sion of the same formula. They involve the second and third powers of ρ, while I_2 involves the fourth power:

$$I_3 = \int_{\rho_n}^{\rho_{n+1}} \frac{\rho^2 \, d\rho}{(\rho^2 + \zeta^2)^{5/2}} = \left[\frac{\rho^3}{3\zeta^2(\rho^2 + \zeta^2)^{3/2}} \right]_{\rho_n}^{\rho_{n+1}}$$

$$I_1 = \int_{\rho_n}^{\rho_{n+1}} \frac{\rho^3 \, d\rho}{(\rho^2 + \zeta^2)^{5/2}} = -\left[\frac{\rho^2 + \frac{2}{3}\zeta^2}{(\rho^2 + \zeta^2)^{3/2}} \right]_{\rho_n}^{\rho_{n+1}}$$

$$I_2 = \int_{\rho_n}^{\rho_{n+1}} \frac{\rho^4 \, d\rho}{(\rho^2 + \zeta^2)^{5/2}}$$

$$= -\left[\frac{\frac{4}{3}\rho(\rho^2 + \frac{3}{4}\zeta^2)}{(\rho^2 + \zeta^2)} \right]_{\rho_n}^{\rho_{n+1}} [\log_e (\rho + \sqrt{\rho^2 + \zeta^2})]_{\rho_n}^{\rho_{n+1}}.$$

$$(7\text{-}75b)$$

The integrals expressing the azimuth variation are represented by Fourier series of the form

$$h = a + b \sin \alpha + c \cos \alpha + d \sin 2\alpha + e \cos 2\alpha$$

so that the four coefficients are

$$\pi b = \int_0^{2\pi} h \sin \alpha \, d\alpha \qquad \pi d = \int_0^{2\pi} h \sin 2\alpha \, d\alpha$$

$$\pi c = \int_0^{2\pi} h \cos \alpha \, d\alpha \qquad \pi e = \int_0^{2\pi} h \cos 2\alpha \, d\alpha.$$

Like the coefficients in eq. (7-71), these are obtained from observations of elevations h in m azimuths on one circle:

$$b = \frac{2}{m} \sum h \sin \alpha \qquad d = \frac{2}{m} \sum h \sin 2\alpha$$

$$c = \frac{2}{m} \sum h \cos \alpha \qquad e = \frac{2}{m} \sum h \cos 2\alpha,$$

so that in eight azimuths

$$\begin{aligned}
b &= 0.25[0.707(h_2 + h_4 - h_6 - h_8) + h_3 - h_7] \\
c &= 0.25[0.707(h_2 - h_4 - h_6 + h_8) + h_1 - h_5] \\
d &= 0.25[h_2 - h_4 + h_6 - h_8] \\
e &= 0.25[h_1 - h_3 + h_5 - h_7].
\end{aligned}$$

$$(7\text{-}76)$$

For sixteen and thirty-two azimuths, the formulas are calculated in the same manner.[98] The final terrain formulas then take the following form in Schweydar's first method:

$$U_{xz} = \frac{\delta}{2}[2.36c_1 + 0.643c_2 + 0.239c_3 + 0.082c_4 + 0.0186c_5$$

$$+ 0.00467c_6 + 0.00187c_7 + 0.001204c_8 + 0.000803c_9$$

$$+ 0.0004284c_{10} \cdots]$$

$$U_{yz} = \frac{\delta}{2}[2.36b_1 + 0.643b_2 + 0.239b_3 + \cdots]$$

$$-U_{\Delta} = \frac{\delta}{2}[3.302e_1 + 1.962e_2 + 1.343e_3 + 0.844e_4 + 0.357e_5$$

$$+ 0.147e_6 + 0.0805e_7 + 0.0686e_8 + 0.0616e_9$$

$$+ 0.0472e_{10} \cdots]$$

$$2U_{xy} = \frac{\delta}{2}[3.302d_1 + 1.962d_2 + \cdots].$$

(7-77)

In these formulas the indexes of the Fourier coefficients refer to the following distances (in meters):

1	2	3	4	5	6	7	8	9	10
1.5	3	5	10	20	30	40	50	70	100 m

The formulas are calculated for an elevation of 90 cm of the center of gravity of the beam above the ground. The constants give the terrain *effects* in E.U. Formulas for other beam elevations are given in the Askania publication referred to previously.

Table 32 represents the calculation of a terrain correction in accordance with eqs. (7-76) and (7-77). Above are the ground elevations in reference to the height of the base plate (22.5) and the telescope axis of the alidade (125 cm). With formula (7-76), the coefficients **a**, **b**, **c**, and **d** are calculated and multiplied by the factors in (7-77) to obtain the effects of each ring, whose sum gives the gradients and curvatures. The form represented by Table 32 is used together with the form given on page 200 and contains also the calculation of final results with planetary and terrain corrections.

Schweydar's second method is applied when the elevations of the sur-

[98] C. A. Heiland, *Directions for the Askania Torsion Balance*; also A.I.M.E. Geophysical Prospecting, 533 (1929).

rounding terrain exceed the height of the center of gravity of the instrument above ground.   Then the first *two* terms in the series of formula

<div align="center">

TABLE 32

TERRAIN CORRECTION A

</div>

$4\mathbf{b} = 0.707(h_2 + \quad - h_6 - h_8) + h_3 - h_7 \qquad 4\mathbf{d} = h_2 - h_4 + h_6 - h_8$
$4\mathbf{c} = 0.707(h_2 -$

Density: 2.0   Plate = 22.5   Instrument = 125 cm

ρ	1.5	3	5	10	20 m	ρ	1.5	3	5	10	20 m
h	I	II	III	IV	V	h	I	II	III	IV	V
1	+0.7	+0.7	+7.0	+10.7	−4.0	1	21.8	21.8	118.0	114.3	129.0
2	+0.9	+1.1	+0.7	+5.0	+7.0	2	21.6	21.4	124.3	120.0	118.0
3	−1.2	−4.3	+1.6	+1.7	−5.2	3	23.7	26.8	123.4	123.3	130.2
4	−3.5	+2.7	+10.3	+0.3	+5.5	4	26.0	19.8	114.7	124.7	119.5
5	+0.3	−1.1	+1.6	+4.3	+0.2	5	22.2	23.6	123.4	120.7	124.3
6	+1.5	+3.2	+3.2	+3.8	+8.8	6	21.0	19.3	121.8	121.2	116.2
7	+1.5	+9.5	+0.7	+3.5	−6.0	7	21.0	13.0	124.3	121.5	131.0
8	+0.3	+8.3	+6.6	+5.8	−9.0	8	22.2	14.2	118.4	119.2	134.0
c	+0.6	+1.1	+0.3	+2.8	−4.0	e	+0.2	−1.4	+1.6	+2.5	+2.0
b	−1.5	−4.8	+0.4	−1.2	+2.4	d	+1.4	−1.7	−3.3	+0.7	+4.8

<div align="center">times</div>

c	2.36	0.643	0.239	0.082	0.0186	e	3.302	1.962	1.343	0.844	0.357
b						d					

<div align="center">equals</div>

c′	+1.4	+0.7	+0.1	+0.3	−0.1	e′	+0.7	−2.7	+2.2	+2.1	+0.7
b′	−3.5	−3.1	+0.1	−0.1	0	d′	+4.6	−3.3	−4.4	+0.6	+1.7

$$\mathbf{K}_{zz} = \text{Sum } c' \times \frac{\delta}{2} = +2.4 \qquad \mathbf{K}_\Delta = \text{Sum } e' \times -\frac{\delta}{2} = -3.0$$

$$\mathbf{K}_{yz} = \text{Sum } b' \times \frac{\delta}{2} = -6.6 \qquad 2\mathbf{K}_{xy} = \text{Sum } d' \times \quad \frac{\delta}{2} = -0.8$$

RECORDED	NEGATIVE CORRECTIONS			CORRECTED VALUES		
	Terrain	Topog.	Planet.			
−4.4	+2.4	—	+6.9	−13.7	U_{zz}	λ
+10.5	−6.6	—	—	+17.1	U_{yz}	$-2\frac{1}{2}°$
−2.5	−3.0	—	+7.9	−7.4	U_Δ	R
−1.4	−0.8	—	—	−0.6	$2U_{xy}$	7.4

(7–68b) are used, which leads to formula (7–69).   As shown in (7–70), it is then more convenient to use the squares of the differences, $(h - \varsigma)^2 \equiv H^2$.

Their variation with azimuth is again represented by Fourier series, so that the new coefficients (comparable with those given in [7–71]) are:

$$|\mathbf{B}| = \frac{2}{m} \sum_m H^2 \sin \alpha \quad \text{and} \quad |\mathbf{C}| = \frac{2}{m} \sum_m H^2 \cos \alpha \qquad (7\text{–}78)$$

Instead of introducing again a linear variation between two rings, it is now more convenient to assume a variation of their *squares* between *three* rings, so that

$$H^2 = c_1 + c_2\rho + c_3\rho^2.$$

The coefficients are determined from the variation of H^2 in one azimuth in three distances, ρ_n, ρ_{n+1}, and ρ_{n+2}, so that the gradients

$$\left.\begin{aligned}
U_{xz} &= -3k\,\frac{\delta}{2}\left[I_3 \int_0^{2\pi} c_1 \cos \alpha\,d\alpha \right.\\
&\qquad\qquad \left. + I_1 \int_0^{2\pi} c_2 \cos \alpha\,d\alpha + I_2 \int_0^{2\pi} c_3 \cos \alpha\,d\alpha \right]\\
U_{yz} &= -3k\,\frac{\delta}{2}\left[I_3 \int_0^{2\pi} c_1 \sin \alpha\,d\alpha \right.\\
&\qquad\qquad \left. + I_1 \int_0^{2\pi} c_2 \sin \alpha\,d\alpha + I_2 \int^{2\pi} c_3 \sin \alpha\,d\alpha \right],
\end{aligned}\right\} \qquad (7\text{–}79)$$

where the integrals I_1, I_2, and I_3 are as given in (7–75b) except that the limits are ρ_n and ρ_{n+2}. Substituting numerical values for the same distances as in the first method the gradient formulas of the second method are:

$$\left.\begin{aligned}
U_{zz} &= -\frac{\delta}{2}\big[172.9\,|\mathbf{C}|_1 + 11.64\,|\mathbf{C}|_2 + 17.92\,|\mathbf{C}|_3 + 3.020\,|\mathbf{C}|_4 \\
&\qquad + 1.454\,|\mathbf{C}|_5 + 0.031\,|\mathbf{C}|_6 + 0.1404\,|\mathbf{C}|_7 \\
&\qquad + 0.0399\,|\mathbf{C}|_8 + 0.0592\,|\mathbf{C}|_9 + 0.0152\,|\mathbf{C}|_{10}\big] \\
U_{yz} &= -\frac{\delta}{2}\big[172.9\,|\mathbf{B}|_1 + 11.64\,|\mathbf{B}|_2 + \cdots \big].
\end{aligned}\right\} \qquad (7\text{-}80)$$

These formulas hold for $\zeta = 0.9$ m. All elevation (differences) must be expressed in *meters*. The formulas for curvatures originally given do not change. Table 33 illustrates the calculation of terrain corrections for both curvatures and gradients (second Schweydar method) for very rugged terrain. Fig. 7–76 gives an idea of the magnitude of terrain effects under such conditions.

In concluding the discussion of analytical methods, brief reference should be made to a method for calculating the effects of remote terrain features

TABLE 33

TERRAIN CORRECTION B

$$4e = H_1 - H_3 + H_5 - H_7$$
$$4d = H_2 - H_4 + H_6 - H_8$$

$$4\,|C| = 0.707(H_2^2 - H_4^2 - H_6^2 + H_8^2) + H_1^2 - H_5^2$$
$$4\,|B| = 0.707(H_2^2 + H_4^2 - H_6^2 - H_8^2) + H_3^2 - H_7^2$$

Right portion (m)

$H^2 = (h-\zeta)^2$	1.5 I	3 II	5 III	10 IV	20 V	30 VI	40 VII	50 VIII	70 IX
1	0.828	0.856	1.99	2.99	23.0	49.0	22.1	0.4	0.0
2	.828	.865	5.62	6.00	50.4	32.5	54.8	47.6	42.3
3	.828	.865	2.59	2.62	16.0	47.6	86.5	158.8	219.0
4	.828	.865	2.96	3.24	9.0	16.0	70.6	47.6	33.6
5	.783	.783	6.60	7.40	29.2	59.3	86.5	123.2	43.6
6	.774	.757	6.97	7.73	28.1	0.1	25.0	25.0	88.4
7	.783	.757	0.37	0.06	12.3	0.1	0.0	49.0	9.0
8	.783	.783	0.30	0.21	0.0	0.1	0.5	0.8	15.2
m									
|C|	+0.013	+0.023	−1.86	−1.89	+0.85	−10.95	−23.2	−35.0	−22.3
|B|	+0.029	+0.061	+0.79	+0.92	+6.45	+9.12	+29.4	+39.7	+47.6
|C|, |B|	172.9	11.64	17.92	3.02	1.45	0.031	0.1404	0.0399	0.0592
C'	+2.3	+0.3	−33.3	−5.7	+1.2	−0.3	−3.3	−1.4	−1.3
B'	+5.0	+0.7	+14.2	+2.8	+9.4	+0.3	+5.5	+1.6	+2.8

$$K_{zz} = \Sigma\,|C|' \times -\tfrac{\delta}{2} = +41.5$$
$$K_{yz} = \Sigma\,|B|' \times -\tfrac{\delta}{2} = -42.3$$

Left portion

$-\zeta = 1$	1.5 I	3 II	5 III	10 IV	20 V	30 VI	40 VII	50 VIII	70 IX
	−0.91	−0.925	−1.41	−1.73	−4.8	−7.0	−4.7	−0.6	−0.1
	−.91	−.930	−2.37	−2.51	−7.1	−5.7	−7.4	−6.9	−6.5
	−.91	−.930	−1.61	−1.62	−4.0	−6.9	−9.3	−12.6	−14.8
	−.91	−.930	−1.72	−1.80	−3.0	−4.0	−8.4	−6.9	−5.8
	−.885	−.885	−2.57	−2.72	−5.4	−7.7	−9.3	−11.1	−6.6
	−.88	−.870	−2.64	−2.78	−5.3	−8.0	−5.0	−5.0	−9.4
	−.885	−.870	−0.61	−0.24	−3.5	+0.3	−0.1	+7.0	+3.0
	−.885	−.885	−0.55	−0.46	+0.2	+0.3	+0.7	+0.9	+3.9
m									
|C|	0	−0.3	−44	−65	−68	−202	−115	−153	+127
|B|	+0.1	+0.4	−68	−77	−240	−250	−117	−149	−352
d	3.302	1.962	1.343	0.844	0.357	0.147	0.081	0.069	0.062
C'	0	−0.6	−50.1	−54.9	−24.3	−29.7	−9.3	−10.6	+7.9
B'	+0.3	+0.8	−91.3	−64.9	−85.6	−37.0	−9.5	−10.3	−21.8

times ... equals

$$K_{\Delta} = \Sigma e' \times -\tfrac{\delta}{2} = +180.6$$
$$2K_{xy} = \Sigma d' \times -\tfrac{\delta}{2} = -319.3$$

Surface density $\delta = 2.0$

Fig. 7-76. Terrain effects and contours at Caribou, Colorado (compare with Fig. 7-119).

on gradients and curvatures from contour lines (*cartographic* correction). The procedure is illustrated in Fig. 7-77. The terrain is divided into elements bounded by successive contours (interval $d\rho$) and subtended by an angle $d\alpha$, so that the coordinates of the center of the element are ρ and α. Then the corresponding gradients and curvatures may be obtained from (7-69) by neglecting ζ compared with h so that

$$U_{xz} = -3k\frac{\delta}{2}h^2\frac{d\rho\cos\alpha\,d\alpha}{\rho^3}$$

$$U_{yz} = -3k\frac{\delta}{2}h^2\frac{d\rho\sin\alpha\,d\alpha}{\rho^3}$$

$$-U_\Delta = 3k\delta h\frac{d\rho\cos 2\alpha\,d\alpha}{\rho^2}$$

$$2U_{xy} = 3k\delta h\frac{d\rho\sin 2\alpha\,d\alpha}{\rho^2}$$

$$(7\text{-}81)$$

(b) *Graphical methods.* The essence of graphical terrain correction methods is that the influence of the terrain is evaluated not by measurements in fixed distances and azimuths but by the use of contour lines and

terrain profiles. For this purpose diagrams are used which contain the outlines of mass sectors of such dimensions that their effect on the instrument is identical regardless of distance or azimuth. Hence, the determination of terrain effects is accomplished by "counting" the number of "graticule" elements encompassed by the successive contours or the terrain profile. In the first case we speak of "horizontal" diagrams; in the second, of vertical diagrams. The construction and use of horizontal diagrams is based on the calculation of sector plans of such dimensions that for equal
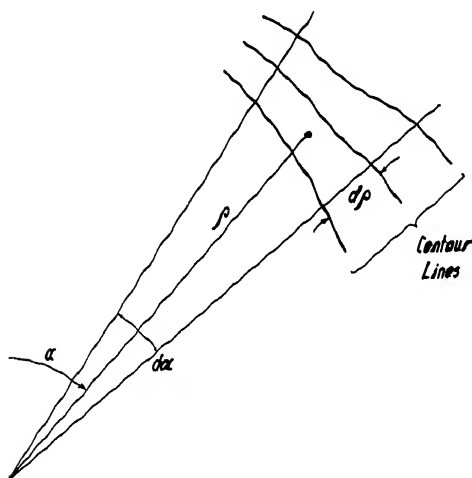
FIG. 7-77. Cartographic correction with contour lines.

elevation their effect on the instrument is equal. An approximation method (Numerov[99]) and a rigorous method (K. Jung[100]) have been developed.

Numerov's method of calculating terrain diagrams rests on eq. (7–69), which, for an element bounded by successive radii ρ_n and ρ_{n+1} and angles α_m and α_{m+1}, may be written in the following form, provided ζ^2 is negligible compared with ρ^2 in the denominator:

[99] Zeit. Geophys., 4(3), 129 (1928).
[100] Zeit. Geophys., 3(5), 201 (1927).

$$U_{xz} = 3k\delta(\zeta h - \tfrac{1}{2}h^2) \int_{\alpha_m}^{\alpha_{m+1}} \cos \alpha \, d\alpha \int_{\rho_n}^{\rho_{n+1}} \frac{d\rho}{\rho^3}$$

$$U_{yz} = 3k\delta(\zeta h - \tfrac{1}{2}h^2) \int_{\alpha_m}^{\alpha_{m+1}} \sin \alpha \, d\alpha \int_{\rho_n}^{\rho_{n+1}} \frac{d\rho}{\rho^3}$$

$$-U_\Delta = 3k\delta \cdot h \int_{\alpha_m}^{\alpha_{m+1}} \cos 2\alpha \, d\alpha \int_{\rho_n}^{\rho_{n+1}} \frac{d\rho}{\rho^2}$$

$$2U_{xy} = 3k\delta \cdot h \int_{\alpha_m}^{\alpha_{m+1}} \sin 2\alpha \, d\alpha \int_{\rho_n}^{\rho_{n+1}} \frac{d\rho}{\rho^2}$$

(7-82)

Carrying out the integration for a sector of constant elevation h,

$$\left. \begin{aligned} U_{xz} &= \frac{3}{2} k\delta(\zeta h - \tfrac{1}{2}h^2)(\sin \alpha_{m+1} - \sin \alpha_m)\left(\frac{1}{\rho_n^2} - \frac{1}{\rho_{n+1}^2}\right) \\[2mm] U_{yz} &= -\frac{3}{2} k\delta(\zeta h - \tfrac{1}{2}h^2)(\cos \alpha_{m+1} - \cos \alpha_m)\left(\frac{1}{\rho_n^2} - \frac{1}{\rho_{n+1}^2}\right) \\[2mm] -U_\Delta &= \frac{3}{2} k\delta h(\sin 2\alpha_{m+1} - \sin 2\alpha_m)\left(\frac{1}{\rho_n} - \frac{1}{\rho_{n+1}}\right) \cdot \\[2mm] 2U_{xy} &= -\frac{3}{2} k\delta h(\cos 2\alpha_{m+1} - \cos 2\alpha_m)\left(\frac{1}{\rho_n} - \frac{1}{\rho_{n+1}}\right) \end{aligned} \right\}$$

(7-83)

Assuming now that $\zeta h - \tfrac{1}{2}h^2 = \text{constant} = 1$; that $\delta = 1$; that the unit effect is 10^{-12} for gradients and 10^{-10} for curvatures; and further that

$$(\sin \alpha_{m+1} - \sin \alpha_m) = \text{const.} \qquad \text{and} \qquad \frac{1}{\rho_n^2} - \frac{1}{\rho_{n+1}^2} = \text{const.}; \quad (7\text{-}84)$$

it is possible to divide the entire surrounding topography into elements so dimensioned that regardless of distance and azimuth all produce the same effect. It is not necessary to construct separate diagrams for the east gradient and the northeast curvature. The north gradient and north curvature diagrams may be used for the purpose by rotation through 90° and 45°, respectively.

Fig. 7-78a shows a diagram for the calculation of terrain gradients. With the arrow north, the diagram is used for U_{xz}; with the arrow east, for U_{yz}. The unit effect of the five interior rings is 10^{-12}, that of the others 10^{-13} C.G.S. The diagrams are applicable from 50 to 500 m or 5 to 50 m; however, ζ must be expressed in the same units as h. If the elevation between two successive contour lines is h, the effect of the contour "strip" is

where $\mathbf{n}$ is the number of "compartments" (or dots) covered and δ the density. Fig. 7-78b is a diagram for the curvature values, likewise for 50 to 500 linear scale units. The unit effect of five inner rings is 10^{-10}; that of the outer rings, 10^{-11} C.G.S. The calculation of a "strip" of mean elevation h covering $\mathbf{n}$ dots proceeds in accordance with: effect $= \mathbf{n}\delta \cdot h$.

In the application of the Numerov diagrams, it must be remembered that they do not hold for very rugged terrain or for very short distances from the instrument, since ζ^2 is disregarded compared with ρ^2. A rigorous
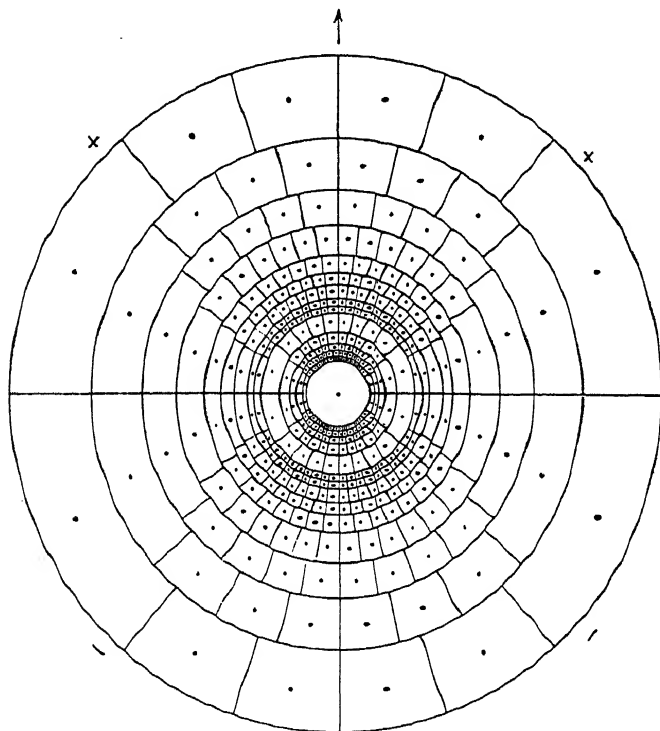
FIG. 7-78a. Numerov diagram for terrain gradients.

method has been proposed by Jung. Its only inconvenient feature is that lines of equal terrain angle (from the instrument) must be drawn about the station. This method was described before in connection with terrain corrections for gravity measurements (formulas [38c to 38e]).

The rigorous mathematical representation of the terrain variation is made possible by figuring all elevations in respect to the center of gravity of the instrument, which eliminates ζ from eqs. (7-68a). With the angle $\psi = \tan^{-1}(h/\rho)$, the gradients and curvatures due to one segment are
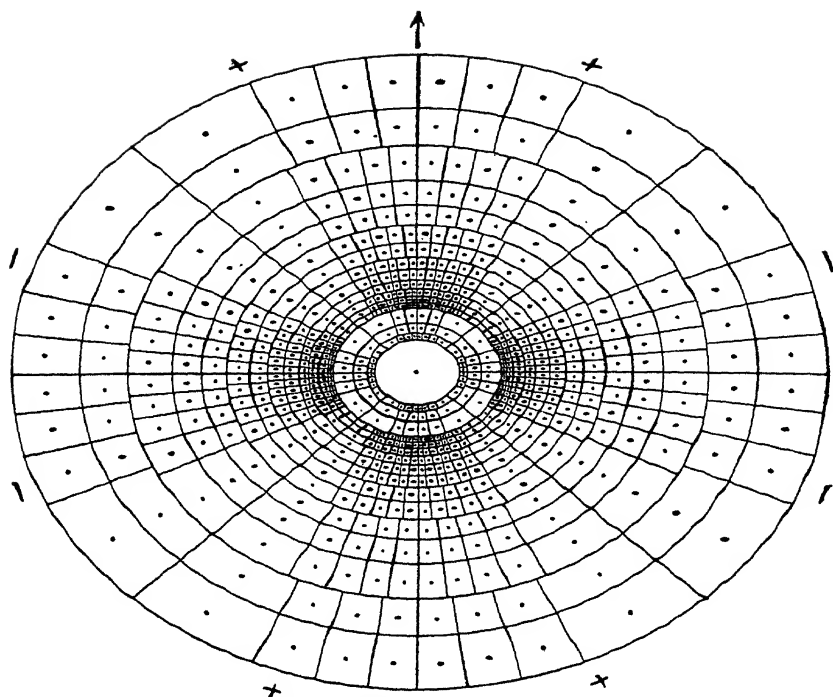
FIG. 7-78b. Numerov diagram for terrain curvatures.
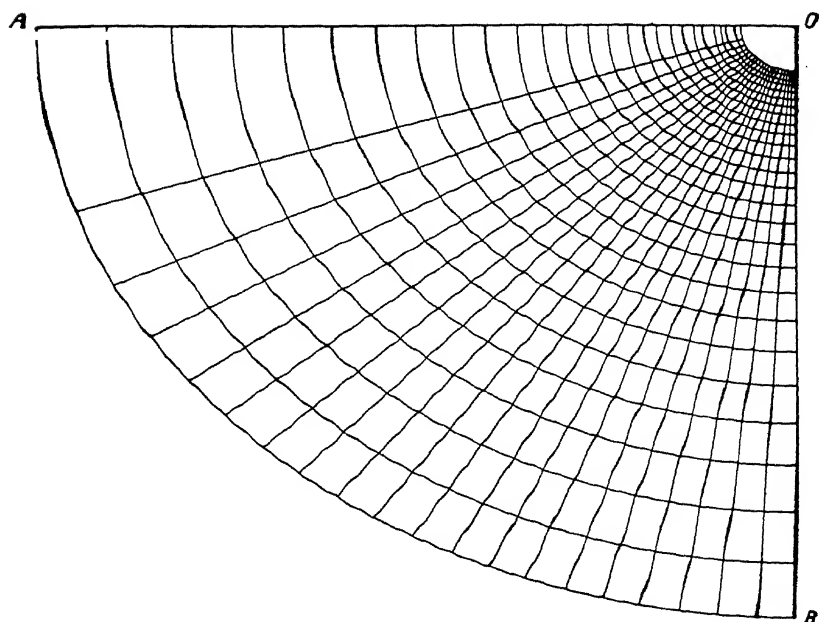
FIG. 7-79a. Jung diagram (D) for terrain gradients.

$$U_{xz} = -k\delta \int_{\rho_n}^{\rho_{n+1}} \int_{\alpha_m}^{\alpha_{m+1}} (1 - \cos^3 \psi) \frac{d\rho}{\rho} \cos \alpha \, d\alpha$$

$$U_{yz} = -k\delta \int_{\rho_n}^{\rho_{n+1}} \int_{\alpha_m}^{\alpha_{m+1}} (1 - \cos^3 \psi) \frac{d\rho}{\rho} \sin \alpha \, d\alpha$$

$$U_\Delta = k\delta \int_{\rho_n}^{\rho_{n+1}} \int_{\alpha_m}^{\alpha_{m+1}} (3 \sin \psi - \sin^3 \psi) \frac{d\rho}{\rho} \cos 2\alpha \, d\alpha$$

$$2U_{xy} = k\delta \int_{\rho_n}^{\rho_{n+1}} \int_{\alpha_m}^{\alpha_{m+1}} (3 \sin \psi - \sin^3 \psi) \frac{d\rho}{\rho} \sin 2\alpha \, d\alpha.$$

(7–85)

In these expressions the terms $1 - \cos^3 \psi \equiv G(\psi)$ and $3 \sin \psi - \sin^3 \psi \equiv K(\psi)$ may be obtained for any terrain profile from Fig. 7–39. Carrying out the integrations in eq. (7–85), the following equations are obtained

$$U_{xz} = -k\delta G(\psi) \log_e \frac{\rho_{n+1}}{\rho_n} (\sin \alpha_{m+1} - \sin \alpha_m)$$

$$U_{yz} = -k\delta G(\psi) \log_e \frac{\rho_{n+1}}{\rho_n} (\cos \alpha_{m+1} - \cos \alpha_m)$$

$$U_\Delta = \tfrac{1}{2}k\delta K(\psi) \log_e \frac{\rho_{n+1}}{\rho_n} (\sin 2\alpha_{m+1} - \sin 2\alpha_m)$$

$$2U_{xy} = -\tfrac{1}{2}k\delta K(\psi) \log_e \frac{\rho_{n+1}}{\rho_n} (\cos 2\alpha_{m+1} - \cos 2\alpha_m)$$

(7–86)

Again only two diagrams are necessary, since the N gradient diagram may be used by rotation through 90° for the E gradient, and the curvature diagram by rotation through 45°. The graticules shown in Figs. 7–79a and 7–79b were calculated by making

$$\log_e \frac{\rho_{n+1}}{\rho_n} = \text{const.} = 0.1, \quad \sin \alpha_{m+1} - \sin \alpha_m = \text{const.} = 0.05$$

and $\tfrac{1}{2}(\sin 2\alpha_{m+1} - \sin 2\alpha_m) = \text{const.} = 0.05$, so that for both diagrams the product of distance and azimuth factors is 0.005. Hence, for the curvature diagram C the unit effect is $0.333 \cdot 10^{-9} \cdot \delta \cdot K(\psi)$, and for the gradient diagram D the unit effect is $0.333 \cdot 10^{-9} \cdot \delta \cdot G(\psi)$. For calculating U_Δ, the C diagram is oriented with the M axis toward N, E, S, and W. The effects of the N and S quarters are negative and those of the E and W quarters positive when elevations are positive, and vice versa. For calculating $2U_{xy}$, the M lines are oriented NE, SE, SW, and NW. The NE and SW quarters are positive and the SE and NW quarters negative when elevations are positive. Diagram D, for calculating U_{xz}, is oriented

with B north and south and A east and west. For U_{xz}, A is north and south, and B east and west.
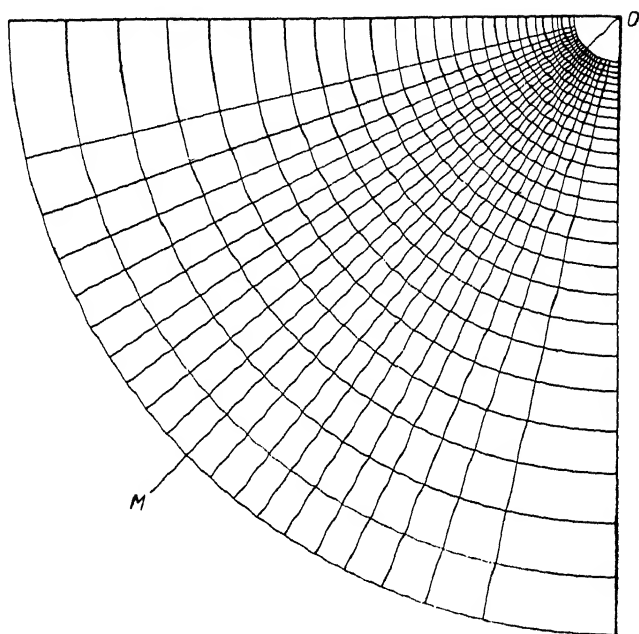
FIG. 7-79b. Jung diagram (C) for terrain curvatures.

The evaluation of lines of equal elevation becomes unnecessary in a method using vertical diagrams proposed by the author.[101] These diagrams are placed through the surrounding terrain in sixteen azimuths; the terrain profile is superimposed on the diagram; and a count is made of the number of elements which are included between the horizon (through the center of gravity of the instrument) and the terrain profile. The calculation of these diagrams is based on a determination of the effect of a segment of a spherical shell, such as that shown in Figs. 7-80 and 7-81. Substituting in eqs. (7-66) $r \sin \psi \cos \alpha$ for x, $r \sin \varphi \sin \alpha$ for y, and $r \cos \varphi$ for z, the equations

FIG. 7-80. Mass element in reference to torsion balance.

[101] A.A.P.G. Bull., 13(1), 39–74 (Jan., 1929).

are

$$U_{xz} = 3k \int dm \, \frac{\sin \varphi \cos \varphi \cos \alpha}{r^3}$$

$$U_{yz} = 3k \int dm \, \frac{\sin \varphi \cos \varphi \sin \alpha}{r^3}$$

$$U_\Delta = -3k \int dm \, \frac{\sin^2 \varphi \cos 2\alpha}{r^3}$$

$$2U_{xy} = 3k \int dm \, \frac{\sin^2 \varphi \sin 2\alpha}{r^3}.$$

(7-87)
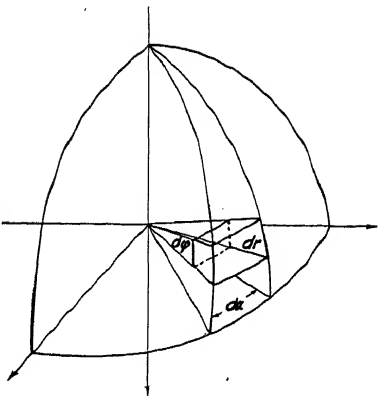
FIG. 7-81. Spherical shell mass-element.

Since the mass element $dm = \delta \cdot dr \cdot r d\varphi \cdot r \, \sin\varphi \cdot d\alpha$, the gradients and curvatures of *one element* are

$$U_{xz} = 3k\delta \int_{\alpha_m}^{\alpha_{m+1}} \int_{\varphi_p}^{\varphi_{p+1}} \int_{r_n}^{r_{n+1}} \frac{\cos \alpha \, d\alpha \sin^2 \varphi \cos \varphi \, d\varphi \, dr}{r}$$

$$U_{yz} = 3k\delta \int_{\alpha_m}^{\alpha_{m+1}} \int_{\varphi_p}^{\varphi_{p+1}} \int_{r_n}^{r_{n+1}} \frac{\sin \alpha \, d\alpha \sin^2 \varphi \cos \varphi \, d\varphi \, dr}{r}$$

$$U_\Delta = 3k\delta \int_{\alpha_m}^{\alpha_{m+1}} \int_{\varphi_p}^{\varphi_{p+1}} \int_{r_n}^{r_{n+1}} \frac{\cos 2\alpha \, d\alpha \sin^3 \varphi \, d\varphi \, dr}{r}$$

$$2U_{xy} = 3k\delta \int_{\alpha_m}^{\alpha_{m+1}} \int_{\varphi_p}^{\varphi_{p+1}} \int_{r_n}^{r_{n+1}} \frac{\sin 2\alpha \, d\alpha \sin^3 \varphi \, d\varphi \, dr}{r}.$$

These four equations may be reduced to two because the azimuthal differences (sin, cos) in the components can be taken care of by rotation of the diagrams. Then the effect of one mass element is

$$U_{xz} = k\delta \, (\sin \alpha_{m+1} - \sin \alpha_m)(\sin^3 \varphi_{p+1} - \sin^3 \varphi_p) \log_e \frac{r_{n+1}}{r_n}$$

$$U_\Delta = -\tfrac{1}{2}k\delta \, (\sin 2\alpha_{m+1} - \sin 2\alpha_m)(\cos^3 \varphi_{p+1} - \cos^3 \varphi_p$$

$$- 3 \cos \varphi_{p+1} + 3 \cos \varphi_p) \log_e \frac{r_{n+1}}{r_n}.$$

(7-88)

Evaluation of gradients and curvatures in eight sections, that is, in sixteen azimuths, does not require thirty-two but only six diagrams. Of these, the *GI* and the *CI* diagrams are reproduced in Figs. 7-82 and 7-83. Unit effect is $1 \cdot 10^{-10}$; scale is arbitrary; and assumed density is 1.0. Their application above and below the horizon is indicated in the scheme in Fig. 7-84.

of the diagrams in different azimuths are combined by vectorial addition to a vector of the azimuth α for gradients and another vector of the azimuth 2α for the curvatures. The justification for this procedure is seen by reference to formula (7–86), since the azimuth terms may be written in the form $2 \sin \dfrac{\Delta \alpha}{2} \dfrac{\cos \alpha}{(\sin \alpha)}$ for gradients and $2 \sin \Delta \alpha \dfrac{\cos 2\alpha}{(\sin 2\alpha)}$ for curvatures. The gradient and curvature vectors of the terrain may then be resolved into their x- and y-components to obtain the corrections for all four gradient and curvature components.

(c) *Planimeter and integraph methods.* If planimeters or integraphs are used, terrain effects are determined by outlining the terrain profile or terrain contours with the stylus of one of these instruments rather than by counting elements as in the graphical methods. Two procedures are applicable: (1) use of ordinary planimeters with contour lines or terrain profiles distorted in respect to horizontal azimuth or vertical angle and distance scale in such a manner that the effect of the mass area is independent of azimuth and distance; (2) use of special integraphs with contour lines or terrain profiles drawn to undistorted scale.

The first procedure was proposed by Below and has been described before in connection with the interpretation of gravity anomalies (page 155). Its applications have been worked out: (a) for the entire surrounding topography; (b) for small elevations at greater distance.[105] The relations that apply in the first case have been given in eq. 7–85. They contain integrals of the form $\int \dfrac{d\rho}{\rho}$ for both gradients and curvature values which express the effect of distance, and of the form $\int \dfrac{\sin \alpha \, d\alpha}{(\cos \alpha)}$ for gradients and $\int \dfrac{\sin 2\alpha \, d\alpha}{(\cos 2\alpha)}$ for curvatures which express the effect of azimuth. These integrals may be reduced to surface integrals of the form $\iint R \, dR \, d\Phi$ by the substitution $R \equiv \sqrt{2 \log_e \rho}$ and $\Phi \equiv \sin \alpha$, $\cos \alpha$, $\sin 2\alpha/2$ and $\cos 2\alpha/2$. These substitutions result in a diagram which is distorted in respect to both scale and azimuth (see Figs. 7–85 and 7–86). On such diagrams lines of equal elevation angle ψ are plotted and the area S between successive lines is determined with a planimeter so that for the gradients

$$\frac{\cos \alpha}{(\sin \alpha)} \frac{d\rho}{\rho} \, d\alpha \equiv \frac{1}{36} \iint R \, dR \, d\Phi \equiv \frac{1}{36} \, S$$

[105] K. Jung, Zeit. Geophys., **6(2)**, 114 (1930).
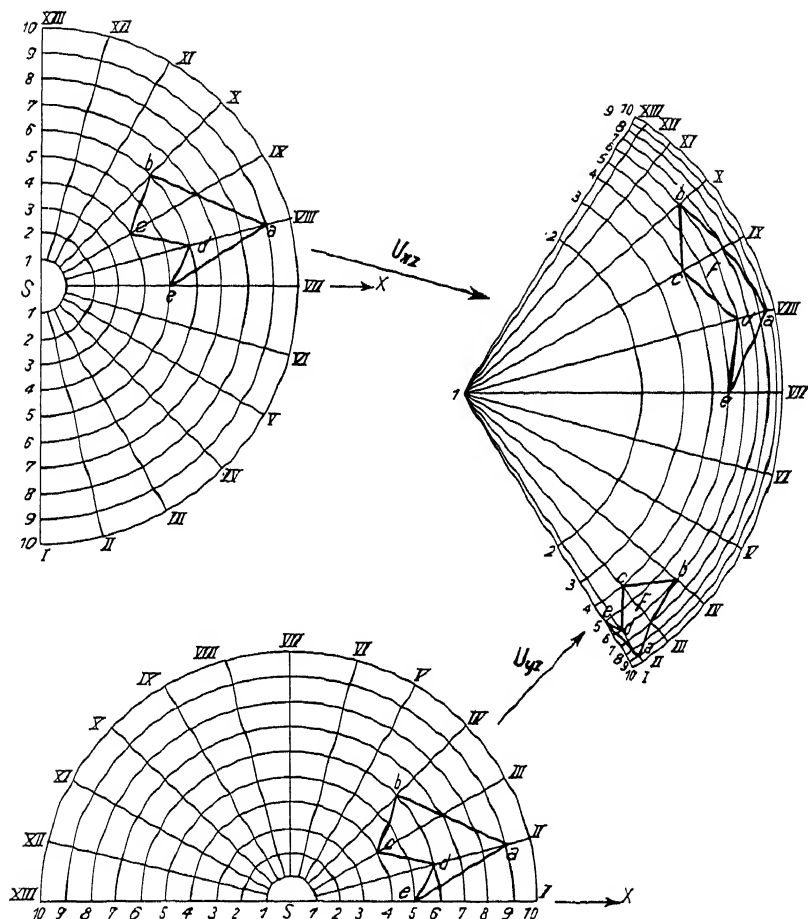
FIG. 7-85. Scale distortion for gradients in Below-Jung's planimeter terrain correction (after Jung).

and for the curvatures

$$\begin{matrix} \cos 2\alpha \\ (\sin 2\alpha) \end{matrix} \frac{d\rho}{\rho}\, d\alpha \qquad\qquad\qquad \frac{1}{36}$$

For small elevations at greater distances, when the square of the height of the instrument above the ground is negligible compared with the square of the distance, formulas 7–82, containing the integrals

$$\begin{matrix} \cos \alpha \\ (\sin \alpha) \end{matrix}\, d\alpha \int \frac{d\rho}{\rho^3}$$

for gradients and

$$\cos 2\alpha \atop (\sin 2\alpha)} \, d\alpha \, \frac{d\rho}{\rho^2}$$

for curvatures, apply. Hence, the substitutions $R \equiv 1/\rho$ for gradients and $R \equiv \sqrt{2/\rho}$ for curvatures, $\Phi \equiv \sin \alpha$, $\cos \alpha$ for gradients and $\Phi \equiv \sin 2\alpha$ and $\cos 2\alpha$ for curvatures may be made.
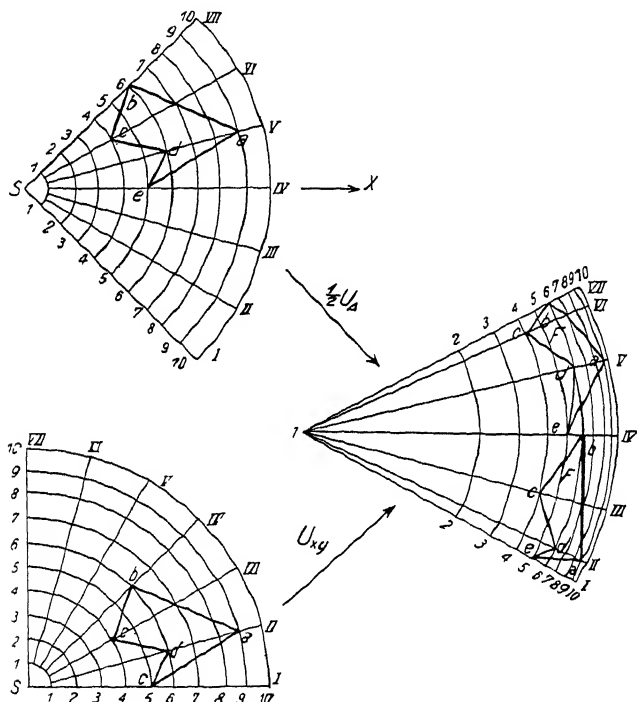
Fig. 7-86. Scale distortion for curvatures in Below-Jung's planimeter terrain correction (after Jung).

Distortions of diagrams may be avoided by the use of specially constructed integraphs. The Askania Werke have constructed a special integraph[106] for the evaluation of gravity and torsion anomalies which may also be applied to calculations of terrain effects. If the topography around the station has been represented by lines of equal elevation angle, the terrain effects which contain the double integrals $\iint \cos \alpha \atop (\sin \alpha)} \, d\alpha \, \frac{d\rho}{\rho}$ for gradients and $\iint \cos 2\alpha \atop (\sin 2\alpha)} \, d\alpha \, \frac{d\rho}{\rho}$ for curvatures may be written

[106] F. Kaselitz, Zeit. Geophys., **8**(3/4), 191 (1932). See also p. 269.

in the form of eq. 7–85. The general form of these integrals is $\iint \dfrac{d\rho}{\rho} \dfrac{\cos n\alpha}{(\sin n\alpha)}\, d\alpha$, which may be evaluated by the integraph as surface integral of the form $n \displaystyle\int \dfrac{d\rho}{\rho} \dfrac{\sin n\varphi(\rho)}{[\cos n\varphi(\rho)]}$ A more detailed discussion of this integraph is given in the following section on interpretation of torsion balance anomalies.

(d) *Field practice in terrain survey; preparation of station site.* The accuracy of a torsion balance may be enhanced considerably by a judicious selection of the station site. The location should be as flat as possible, at least to a distance of about 20 meters. Vicinity of ditches, bluffs, embankments, and houses should be avoided if possible. In forests it is advisable to set up the instrument in such a manner that large trees are symmetrically arranged with respect to it. If setups in rugged terrain have to be made, the site should be so selected that the effect on gradients is a minimum. The site should be leveled with a shovel to a radius of 3 to 5 m. In the filling of depressions, the dirt should be tightly tamped to preserve approximately the same density around the station. Leveling the immediate vicinity has the further advantage of avoiding difficulties in setting up the house.

After the site has been leveled, a plane table or transit is set up and the "far terrain" determined first (at 5, 10, 20, 30 m, and so on). On the plane table sheet, eight or sixteen azimuths are laid off. If a transit is used, it is advisable to mount a compass on top and to read the angles on it instead of on the horizontal circle. The instrument is set up over the station point. One man reads the elevations and takes them down, the other goes around the station and places the leveling rod where directed. A rope or chain with the proper measurements marked on it is used in obtaining distances. It is advisable to carry a rope 20 m long for the average terrain and an extension out to 100 m for more complicated terrains. The rope is laid out first in the north direction and the rod is placed at 5, 10, 20, 30 m, and so on. Then the rope is moved over to the next azimuth and the rod is placed at 30, 20, 10, 5 m, and so on.

In some terrains the use of ropes or chains may be impracticable. Some companies have trained their men to pace the distance accurately. In brush country it may be necessary to cut lines for the terrain survey (Fig. 7–87). The rod should be graduated in centimeters; it may be so made that differences in elevation may be read directly. For this purpose the rod is graduated both ways from zero, with red divisions below and black divisions above, red indicating positive elevations and black negative. The foot of the rod carries an adjustable shoe. Before elevations are taken, the rod is placed close to the telescope of the transit and so adjusted that the zero point coincides with the optical axis of the telescope.

After "far" terrain has been taken, three pegs are driven into the ground, and the aluminum base plate is laid on it and so oriented that the north mark is in the astronomic meridian. The "near" terrain (1.5 m and 3 m radii) is then taken by placing the leveling rod successively in the eight directions marked on the plate and leveling it with a carpenter's level. Distances to ground are read at 1.5 m and 3 m distances with a ruler (see Table 32).

The density of the surface soil is taken by filling a 1000 cc container and weighing it. If considerable contrast exists between the density of the surface weathered layer and the formation below, its density may
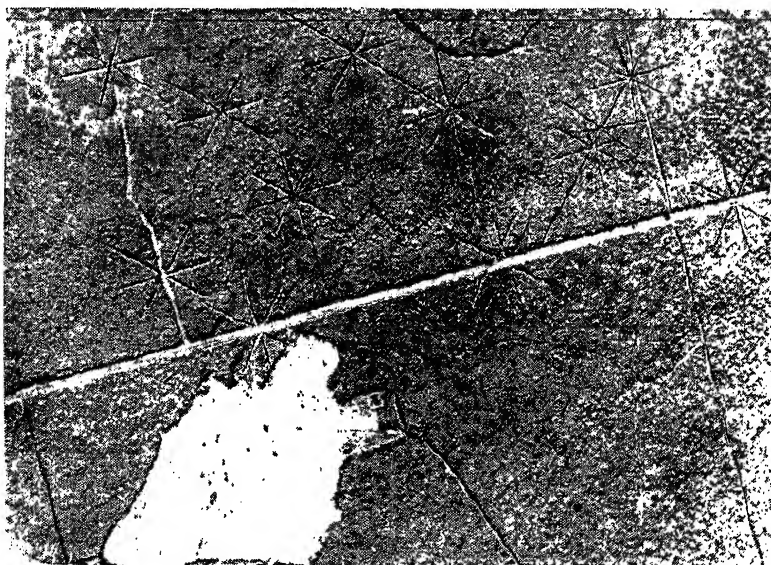
FIG. 7-87. Aerial photograph of torsion-balance stations in Mexico.

have to be determined separately. Further details on terrain field methods, selection of station, calculations, and the like are given in *Directions for the Askania Torsion Balance.* The brief directions given above apply to the Schweydar method and may be modified for other terrain methods. Different companies have adopted slightly different techniques in the field and in the calculations (use of nomographs, and so on), but the fundamentals of procedure are more or less the same. With calculation diagrams involving units of equal elevation angle it may be advisable to measure angles directly on the vertical circle of the transit or alidade.

3. *Correction for regional gradient.* In torsion balance surveys it happens that the gradient and curvature anomaly due to a structure or geologic body

is frequently superimposed upon a larger anomaly due to regional geologic structure or some other larger geologic body. Examples of such regional effects are monoclines, deep-seated intrusions, regional attitude of base-ment topography, geosynclines, and the like. When a local structure is superimposed on such regional features, it is possible that its effect is not immediately recognized in the gradient picture. For instance, in the case of an anticline or dome, the familiar reversal of gradients may not appear in the torsion balance map at all. It can be produced, however, by sub-tracting (vectorially) the effect of the regional geologic feature (see Fig. 7–93). It is impossible, however, to give general directions for the applica-tion of such correction. The magnitude and direction of the "regional" gradient depend entirely on distance, depth, and configuration of the regional geologic feature involved. The regional effect may be deter-mined (1) by field measurements and (2) by calculation. Where sufficient well-information is available to establish definitely the absence of local structure and the presence of nothing but regional effect, the regional gradient and its variation with distance may be determined from a suffi-cient number of torsion balance observations.

The regional gradient may also be derived from regional surveys with the gravity pendulum or gravimeter. If the geologic feature producing the regional gradient is definitely known, its effect may be calculated by the formulas and procedures given in the following section on interpreta-tion. An instructive example for the application of the regional gradient correction is given by D. C. Barton[107] for the Fox and Graham oil fields in Oklahoma. In mining exploration the "regional" feature to be elimi-nated is frequently of very restricted extent and often a geologic body which in the regular usage of the term would likewise be called a "local" structure, for example, a contact zone, a fault, an intrusion, or the like. What is considered a regional feature depends, in other words, entirely on what geologic feature is sought by the survey. The procedure of correcting for a regional gradient is, therefore, comparable in every detail with the subtraction of a "normal" value from magnetic anomalies.

4. *Correction for coast effect.* Coast effects are due to (1) the slope of the coastal shelf and (2) variations in water level (tides). The second of these has been discussed before (pages 165-166) in connection with time variations of gravity, and it need not be considered here. That fairly appreciable gravity anomalies accompany the continental shelf had been observed by Hecker. An analysis and theoretical explanation of the effect was given by Schiötz and Helmert.[108] Whereas above a buried slope of dense material the gravity anomaly rises gradually from its lowest

[107] A.I.M.E. Geophysical Prospecting, 458 (1929).
[108] Encycl. Math. Wiss., VI 1 (7), 143 (1906-1925).

to its highest value, a negative peak occurs over the foot and a positive over the upper edge of a continental shelf in isostatic equilibrium. For a slope of about 1° inclination, Helmert calculated a positive peak of 53 milligals above the upper edge of the shelf, dropping to about 25 milligals 100 km inland. Hence, a coastward gradient is produced along a wide zone which for the slope mentioned is of the order of 3 E.U., increasing to 5 and more units near the coast. For shelves of steeper slope the effect is correspondingly greater. Like other regional effects the coast effect may be determined by direct observation or calculation and may be deducted (vectorially) from the observed gradients.

FIG. 7-88. Lines of equal gradients in infinite rectangular tunnel section (after Meisser).

5. *Corrections for fixed masses* (other than terrain), *effects of underground openings* (tunnels and the like). Corrections for fixed masses other than terrain are required only in exceptional cases when setups near them cannot be avoided. Frequently it is sufficient to calculate their effects by assuming point masses, linear masses (trees), slabs, or parallelopipeds. The formulas given for these in the section on interpretation (pages 258–265) are applicable. If several fixed masses are present, it is often possible to reduce or virtually avoid a correction by setting up the instrument so that their effects are compensated. On gradients two or more equal masses in symmetrical disposition cancel; on curvatures three symmetrical, equal masses compensate.

In underground work a similar precaution reduces corrections for tunnel

sections appreciably. In the two planes of symmetry of a rectangular section the gradients are zero. However, the curvatures cannot be made zero. The effects of a tunnel of rectangular section, infinite in its longitudinal direction, on gradients and curvatures follow directly from the formulas for a vertical step given in the section on interpretation. Figs. 7–88 and 7–89 (after Meisser[109])
show the gradient and curvature distribution inside a tunnel which is infinite in the y' direction. With the notation of Fig. 7–90, $U_{y'z'}$ and $2U_{x'y'} = 0$ and

$$J_\Delta' = 2k\delta(\alpha \cdot$$

$$J_{x'z} = 2k\delta \log_e \frac{r_2}{r_1} \frac{r_3}{r}, \qquad (7\text{-}89)$$

if the center of gravity of the torsion balance is below the center of the section. When setting up an instrument in the center line of the tunnel so that its height above the tunnel floor can be varied (i.e. along the z axis), $x' = 0$, $U_{x'z} = 0$, and $U_\Delta' = 8k\delta \tan^{-1} h/a$.

If the tunnel section is not rectangular or nearly rectangular in section, it is advisable to use the graphical or integraph methods given in the interpretation section for two-dimensional features and to calculate the effect of the actual tunnel outline. In any event, the instrument should be set up as nearly in the center of the section as possible. Although the curvatures are not

FIG. 7-89. Lines of equal curvatures in infinite rectangular tunnel section (after Meisser).

zero, their variation with location is least and the correction (if curvatures are used at all) may be determined with fair accuracy. The tunnel outline can be measured with a device used in excavation, sometimes

[109] Zeit. Geophys., 6(1), 17–18 (1930).

called the "sunflower." It consists of a graduated arm rotatable about a horizontal axis, which is shifted until it makes contact with the tunnel wall, thus giving the distance of the wall at any vertical angle from the center of gravity of the torsion balance. The vertical angle of the arm may be read on a dial. If the tunnel is not straight, or if the shape of other subsurface cavities is to be determined, the sunflower may be provided with a vertical axis permitting the variation of section with horizontal azimuth to be obtained.

E. Graphical Representation of Torsion Balance Data

For convenience in interpretation, torsion balance results are plotted as vectors or as curves. The corrections discussed in the preceding section are applied to the instrument readings algebraically or vectorially. Geologic interpretation is based on the corrected values represented by vectors or by curves of gradient and curvature components in geologically significant directions (usually at right angles to the strike). For more qualitative interpretation or comparison with gravimeter or pendulum data, relative gravity is calculated from gradients and represented in the form of isogams.
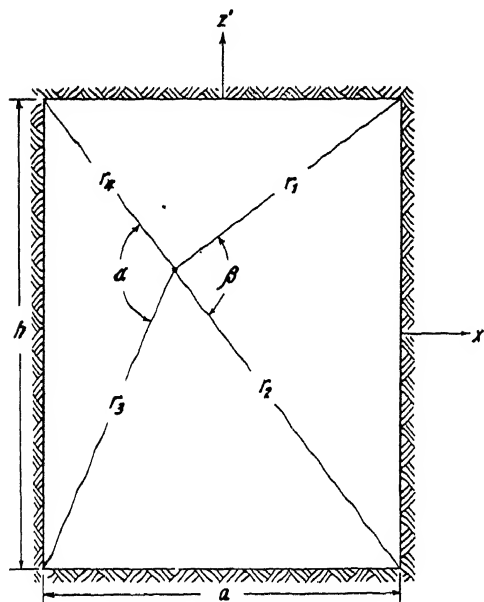
Fig. 7-90. Tunnel section.

1. In *vector representation*, the east gradient (see Fig. 7-91a), U_{yz}, is laid off to the east if it is positive and the north gradient, U_{xz}, to the north if it also is positive. The resultant vector is the total gradient dg/ds. Its azimuth, α, gives the direction of maximum change of gravity. In plotting curvature values, $-U_\Delta$ is laid off toward north and $2U_{xy}$ toward east. The resultant vector is the "differential curvature," R, and it makes the angle 2λ with north. Therefore, it must be replotted. In doing so, it is customary to shift the R line on itself so that the station

is in its center. The same procedure is recommended for gradients (Fig. 7–91c). Therefore;

$$\tan \alpha = \frac{U_{yz}}{U_{xz}} \qquad\qquad \tan 2\lambda = \frac{2U_{xy}}{-U_\Delta}$$

$$\frac{dg}{ds} = \sqrt{(U_{xz})^2 + (U_{yz})^2} \qquad \mathbf{R} = \sqrt{(U_\Delta)^2 + (2U_{xy})^2}$$

$$\left.\right\}\;(7\text{-}90a)$$

For plotting the vectors, the coordinate axes are drawn through the station in astronomic or magnetic directions, depending on how the instrument was set up in the field. Use of astronomic coordinates is pref-' erable. The scale is generally 1 mm per E.U. Replotting of curvatures may be avoided by using the diagram of Fig. 7–92. The radial lines
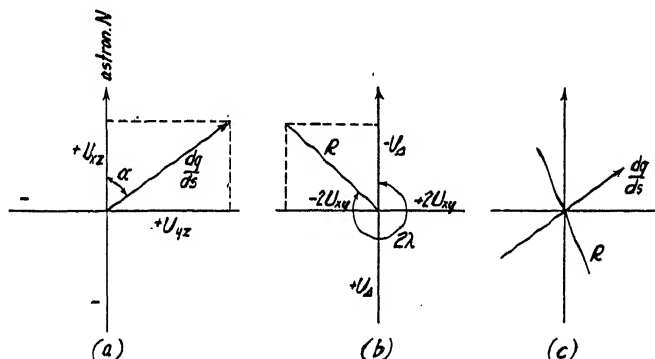
FIG. 7-91. Method of plotting gradients and curvatures.

divide each quadrant into 45° sectors, so that the resultant differential curvature, **R** (concentric circles) and its azimuth are obtained directly.

2. *Vectorial addition and subtraction of gradients and curvatures* is useful for visualizing the effects of (terrain, regional, and so on) corrections. In the case of gradients, vectorial subtraction is possible without difficulty. Fig. 7–93a shows the addition of two gradient vectors, Fig. 7–93b the subtraction of a regional gradient vector. For curvatures, vectorial addition and subtraction must be made by auxiliary vectors of twice the azimuth. In Fig. 7–93c, R_1 and R_2 are the original vectors to be added; R_1' and R_2' are the auxiliary vectors of double azimuth that combine to form the vector R_3'. This vector, when plotted at half its azimuth, gives R_3, representing the vectorial sum of R_1 and R_2. Subtraction of curvature values follows a similar procedure.

3. *A transformation of coordinates* may be desirable for changing observed

values from magnetic to astronomic directions, or, in certain interpretation problems, for referring different sets of vectors to a uniform system.
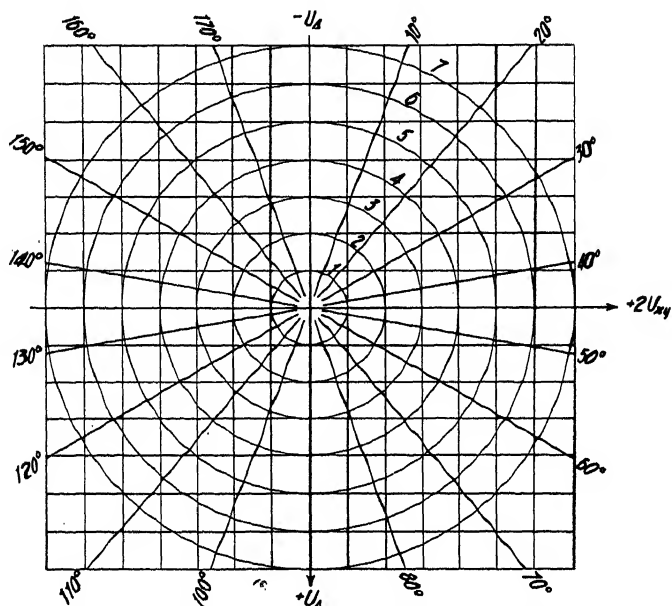
FIG. 7-92. Diagram for the calculation of curvature values.
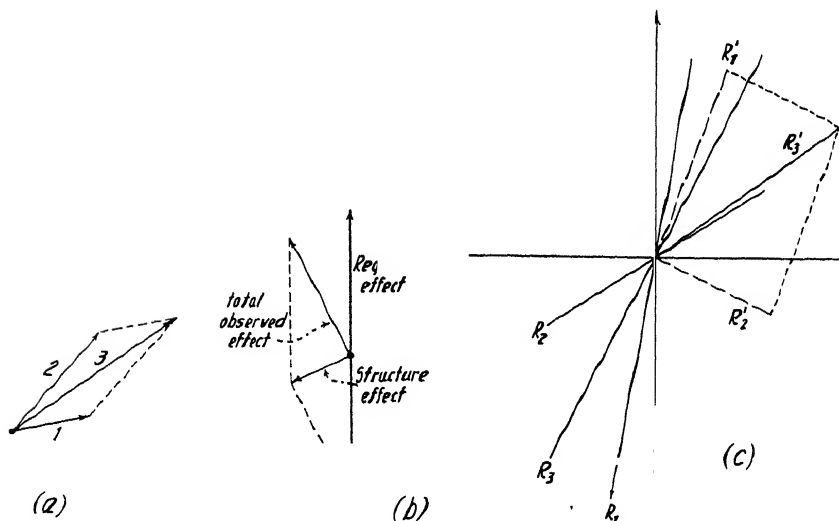
FIG. 7-93. Vectorial addition and subtraction of gradients and curvatures.

The transformations may be made analytically or graphically. If two systems, (x, y) and (x', y'), make the angle α with each other (positive

from north by east), the two sets of transformation equations for gradients and curvatures are:

$$U_{xz} = U_{x'z} \cos \alpha - U_{y'z} \sin \alpha$$

$$U_{yz} = U_{x'z} \sin \alpha + U_{y'z} \cos \alpha$$

$$U_{\Delta} = U_{\Delta'} \cos 2\alpha + 2U_{x'y'} \sin 2\alpha$$

$$= -U_{\Delta'} \sin 2\alpha \qquad \cos 2\alpha$$

and   (7–90b)

$$U_{x'z} = U_{xz} \cos \alpha + U_{yz} \sin \alpha$$

$$U_{y'z} = -U_{xz} \sin \alpha + U_{yz} \cos \alpha$$

$$U_{\Delta'} = U_{\Delta} \cos 2\alpha - 2U_{xy} \sin 2\alpha$$

$$2U_{x'y'} = U_{\Delta} \sin 2\alpha + 2U_{xy} \cos 2\alpha.$$

Graphical transformation follows a similar procedure as shown previously in Fig. 7–93, that is, single azimuth projection of components for gradients, double azimuth projection for curvatures.

4. *Conversion to curves.* Conversion of torsion balance data to curves frequently gives considerable interpretational advantages, particularly where these curves are used with geologic sections through "two-dimensional" geologic bodies. Therefore, field traverses and interpretation profiles are laid out at right angles to the strike when possible. Because of regional or other effects, the directions of gradient and curvature vectors may not coincide with the direction of the profile. In this case they should be projected on the profile, which may be done analytically or graphically. If in Fig. 7–94, φ is the azimuth of a gradient vector with reference to the profile direction x', and ψ is the azimuth of a curvature vector, the projected values are

$$\frac{g}{\partial x'} = \frac{\partial g}{\partial s} \cos \varphi \qquad \text{and} \qquad -U_{\Delta}' = \text{Rc os}! \qquad (7\text{–}90c)$$

In the corresponding graphical construction the gradient vector is projected upon the profile direction as shown. For the projection of the curvature, the construction of the auxiliary vector at twice the angle with the profile is again necessary.

For two-dimensional geologic features of virtually infinite extent in the y direction, the (corrected) gradient vectors make the angles of $0°$ or $180°$ with the profile direction. The corresponding angles of the curvatures are $0°$ or $90°$. If the subsurface feature is infinite in the y' direction, $\partial g/\partial y'$, $2U_{x'y'}$, and $\partial^2 U/\partial y_1^2 = 0$ and $-U_{\Delta'} = \partial^2 U/\partial x_1^2$. A gradient vector in the x' direction is then plotted as positive ordinate and a vector pointing

in the $-x'$ direction as negative ordinate. A curvature vector at $0°$ angle is plotted as positive ordinate $(\partial^2 U/\partial x_1^2)$ and a curvature making an angle of $90°$ with the profile as negative ordinate.

5. *Calculation of relative gravity, construction of isogams.* Since the horizontal gradient of gravity represents the *slope* of the gravity curve, it is possible to calculate the *difference* in gravity between two points when the rate is reasonably uniform and the distance between them is small. A number of procedures are in use to accomplish the "mechanical integration" of the gradient curve. For close spacings of stations and uniform gradients it is satisfactory to project the gradient vectors on the profile line, to average the projections at successive stations, and to multiply the average by the distance. If gradients are expressed in E.U. and distances in kilometers, the gravity anomaly is obtained in tenth milligals. Calculation of the projection of the vectors upon a line connecting the station is facilitated by the use of a graduated glass scale or transparent graduated paper. Gravity differences are added from station to station along closed loops, and the error of closing is distributed at the end. A least square adjustment of the entire net of stations can be made if desired.[110]

(a)

(b)

FIG. 7-94. Projection of gradients and curvatures on profile direction.

A second method of calculating gravity differences between stations is based on the construction of tangent polygons (Fig. 7-95b), with the assumption that the rate given by the gradient at one station prevails half way to the next. Between two stations, A and B, the projections of the vectors U'_{sz} and U''_{sz} are plotted as ordinates against unit distance. This procedure, beginning with A, gives the point D on the "Δg curve" for the half-way point E. Hence, the gradient for the second station, B, is plotted as ordinate against unit distance and the point F is obtained on the gravity curve. The procedure is again applied to several sets of stations arranged in closed loops or polygons. Three stations arranged

---

[110] D. C. Barton, A.A.P.G. Bull., **13**(9), 1168–1181 (Sept., 1929). I. Roman, A.I.M.E. Geophysical Prospecting, 486–503 (1932).

for simplicity at the corners of a triangle are shown in Fig. 7–95c. They happen to show a large error of closure which has been adjusted graphically as shown in Fig. 7–95d. The adjustment follows the rule that the *tangents* at the points B and C must be kept constant, and that the curve must close at A. When gravity differences have been so calculated, "isogams" may be plotted as shown in Fig. 7–95e.
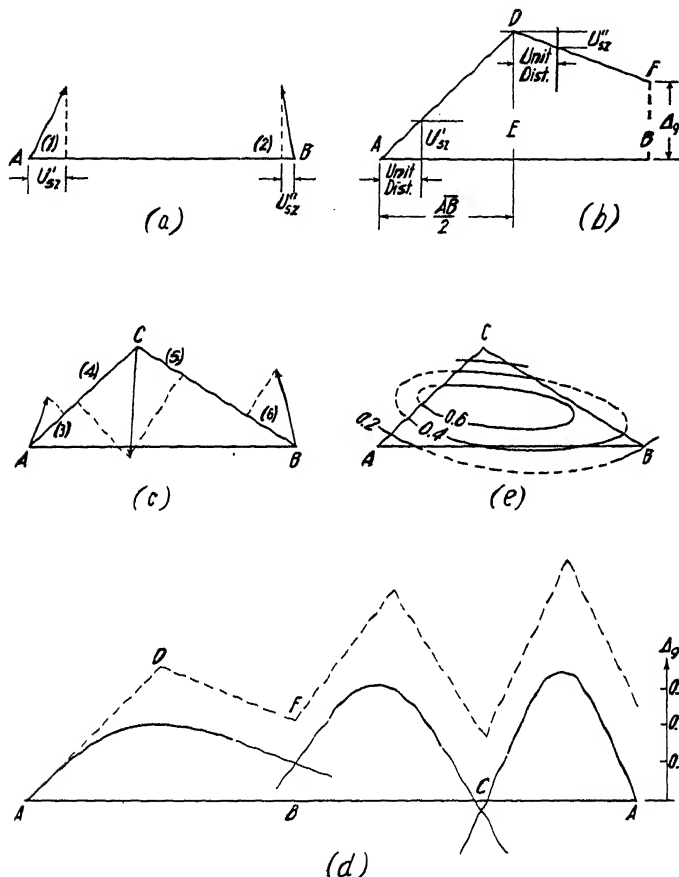
FIG. 7-95. Calculation of relative gravity from gradients in station triangle (after Jung).

A third procedure is based on a graphical integration of the gradient curve. Stations are arranged on straight lines, and projections of gradients are plotted as ordinates in a continuous gradient curve. The station lines should be so laid out that they close back to the original station. The gradient curve is then integrated numerically or by the use of an integraph (such as those designed by Abdank-Abakanovicz, Harbou,

and others) for tracing the curve $\int f(x)\,dx$, if the curve $y = f(x)$ is given. The error of closure in this method naturally depends much on how closely the integrated gradient curve approaches the true gradient variation. In any event, some sort of an adjustment of the errors of closure is required, as in the other two methods. In areas where gradients are very erratic and near-surface anomalies overshadow deeper effects, a better isogam picture may be obtained by arranging the stations in clusters of three or four, calculating the average vector for the center of gravity of the station polygon, and using this average vector for the isogam construction.[111]

F. THEORY OF SUBSURFACE EFFECTS, INTERPRETATION METHODS

1. *Interpretation methods.* Interpretation of torsion balance results is based on gradient and curvature maps, isogam maps, or gradient and curvature profile curves constructed as described in the last section. Whether all of these maps and curves or only some of them are used depends entirely on the nature of the geologic objects under survey. In oil exploration, a representation of torsion balance results in the form of a gradient, a curvature, and an isogam *map* is best suited for interpretation. If such a gravitational survey reveals definite geologic units (such as an anticline, a salt dome, or an intrusion), it is better to plot the results as *profile* curves, since they lend themselves better to quantitative analysis. Gradient profiles are usually more reliable than curvature profiles. In rugged country the latter are often disregarded entirely.

Interpretation methods are qualitative, semiquantitative, or quantitative, depending upon the nature of the survey, the complexity of the geologic situation (number of effective geologic bodies), and, generally, the amount of geologic information available. Naturally the first step in almost every torsion balance survey is preliminary interpretation by inspection. For this purpose gradient and isogam maps are most suitable. From the appearance of the indications it is possible to determine whether the geologic features mapped are extensive or of local significance, whether they are of three-dimensional proportions or extended in the direction of strike, whether they occur at great or at shallow depths, whether their outline is well defined or gradual, and so on. An observer acquainted with the regional geologic possibilities will be able to arrive rather rapidly at a preliminary interpretation of the geologic significance of the anomalies.

The reliability of these preliminary findings is enhanced considerably if local geologic or geophysical information is available from outcrops and

[111] J. Koenigsberger, A.A.P.G. Bull., **14**(9), 1222 (Sept., 1930).

wells, or from magnetic, seismic, and electric surveys. Even the preliminary interpretation of a torsion balance map requires close cooperation of the physicist and the geologist, or else the geologist must acquire a good working knowledge of the theory of subsurface effects (that is, he must be able to appreciate the physical possibilities), and the physicist must be familiar with the geologic possibilities to avoid misinterpretation of the results. In any event, it is advisable, wherever possible, to start a survey in an area where geologic information from outcrops, well records, or underground workings is available.

The preliminary interpretation of an isogam or a gradient map will often indicate the need for a revision of the map by allowing for a regional gradient. How this correction is applied depends entirely upon the geologic situation. It is a trial-and-error proposition and may require a considerable amount of work, which, however, more than pays for itself in the quantitative analysis. The qualitative interpretation of such a corrected gradient or isogam map has as its first objective a delineation of the areas which are structurally high and low or which represent occurrences of heavier and lighter masses. In this preliminary phase it is quite permissible to consider an isogam map as the equivalent of a geologic contour map. Subsequent quantitative analysis will then determine whether the gravity anomalies are due predominantly to one or several geologic features. It is evident that the deviation of the isogam map from the equivalent contour map increases with the number of effective geologic bodies or formations.

Further determination of the type of geologic body or structure producing a gravitational high or low is possible by estimating its outline, strike, dip, and approximate depth from the anomaly. The outline is given by stations characterized by the longest gradient arrows, by a crowding of the isogams, and by small curvature values (located between stations with different directions of the **R** lines). The strike of geologic bodies may be expected to be parallel with the trend of the isogams, at right angles to the gradient arrows, and parallel with (or at right angles to) the **R** lines. The dip of geologic bodies is frequently indicated by the isogam interval, the length of the gradient arrows, and the magnitude of the **R** lines (compare, for instance, Fig. 7–99h with Fig. 7–99i). Regional dip is indicated by uniform magnitude and direction of gradient arrows through considerable distances. An indication of depth may be obtained from the rapidity of changes in the gradient and curvature values in horizontal direction. The type of change in direction and the magnitude of gradients and curvatures in the direction of strike indicates to what extent geologic bodies may be considered two-dimensional. Fortunately, most forma-

tions and ore deposits are of two-dimensional character; they allow representation of the field findings by gradient (or curvature) curves, and a somewhat more quantitative interpretation. The following rules apply in semiquantitative interpretation of anomalies due to two-dimensional and some three-dimensional bodies:

(a) If but one density contrast is effective, the Δg curve is approximately parallel with the outline of the subsurface feature and the isogams represent approximately its surface contours.

(b) The gradient arrows point toward the highest point of the subsurface feature. Their magnitude is approximately proportional to the rate of change of subsurface density in horizontal direction. Maxima occur above points or areas of greatest dip; zero points occur above the lines of symmetry of anticlines, vertical dikes, and the like. When a gradient curve has only positive values, a subsurface feature rises in one direction only. The curve is symmetrical if there occurs a vertical face. Positive and negative values are observed in the gradient curve if the subsurface feature is limited across the strike. If the positive and negative gradient anomalies are symmetrical, the boundaries of the subsurface feature are vertical on both sides or dip equally in opposite directions. If the anomalies are unsymmetrical, the two boundaries dip equally in the same direction (inclined dike) or unequally in opposite directions (anticline with unequal flank dips).

(c) The (curvature) R lines are parallel with the strike of heavier subsurface features above them, but they are small and perpendicular to the strike beyond them (see, for instance, the curvature anomaly of a fault block in Fig. 7-99b). The magnitude of the lines depends in a general way on the *curvature* in the *outline* of the heavier masses below the surface; or, if the outlines are straight for short distances, on the rate of change in their direction. Hence, the curvature values are greatest above the center of a dike or plug-shaped mass, above the crest of an anticline, or above the trough of a syncline. Zero points of curvature values frequently occur above abrupt subsurface changes from light to heavy masses. They coincide sometimes with points of maximum gradient, and vice versa.

In semiquantitative interpretation, extensive use is made of "type" curves calculated for geologic features most frequently encountered, such as vertical and inclined faults, vertical and inclined dikes and slabs, symmetrical and asymmetrical anticlines and synclines, and so on. How these are calculated is further explained below. An extensive file of such curves for a variety of depths, dimensions, and dispositions of geologic bodies is of considerable help in a preliminary analysis of torsion balance data and reduces the work required for a quantitative analysis.

Contrary to semiquantitative analysis, quantitative analysis requires an evaluation of the anomalies by *calculation* in *each* particular case. The approach may be direct or indirect. The direct methods are applicable only where *one* geologic feature exists, where the geologic situation is simple, and where the geologic features have or approach the shape of simple geometric bodies. Direct methods make use of the *magnitude* of the anomalies in gradients, curvatures, and relative gravity at the points of symmetry or maximum anomaly; or they utilize the *abscissas* of zero, maximum, minimum, or half-value anomalies to calculate depth, dimensions, and disposition of geologic bodies. The application of direct methods of interpretation is confined largely to mining problems and to ore bodies of simple character. Its application in oil exploration problems is the exception rather than the rule.

Indirect interpretation methods are applicable in all interpretation problems. Their principle is as follows: From the results of qualitative and semiquantitative analysis the assumption is made that a gravitating body has a definite shape, depth, and density. The anomalies of this body are then calculated and the results of such calculations are compared with the field data. The assumed body is then changed with regard to its different parameters until a reasonable agreement between field data and calculated anomalies is secured. This is a trial-and-error method, and fairly laborious; however, it has been very successful when applied with patience and supplemented by geologic data. It is the only interpretation method that can be used when a number of geologic bodies or formations are effective. It is superior to qualitative analysis where sufficient geologic or geophysical information is available to limit the number of possible combinations of bodies capable of producing a given anomaly.

In all semiquantitative and quantitative torsion balance interpretation methods, it is necessary to know what type anomalies are produced by geologic bodies of a given shape, density, and depth. They may be calculated (1) analytically, (2) graphically, or (3) by integration machines. Regardless of calculation method, the fundamental relations are the same in all methods, but they differ depending upon whether they apply to two- or three-dimensional bodies and are derived from the expressions for the Newtonian and logarithmic gravity potentials given in eqs. (7-39b) and (7-39e). It was shown before that gravity was obtained from these potentials by differentiation with respect to z. Likewise, the horizontal gravity component would be obtainable by differentiation with respect to x. Therefore, the gravity gradients and curvature values follow by differentiation with respect to x and y, respectively, of the vertical (eqs.

[7–39c] and [7–39f]) and horizontal gravity components.   Then the gradients and curvatures are

(a) for *three-dimensional* bodies (v = volume):

$$\left. \begin{aligned}
U_{xz} &= 3k\delta \iiint\limits_{v} \frac{xz}{r^5}\, dv = 3k\delta \iiint\limits_{v} \frac{xz}{r^5}\, dx\, dy\, dz \\[2mm]
U_{yz} &= 3k\delta \iiint\limits_{v} \frac{yz}{r^5}\, dv = 3k\delta \iiint\limits_{v} \frac{yz}{r^5}\, dx\, dy\, dz \\[2mm]
U_{\Delta} &= 3k\delta \iiint\limits_{v} \frac{y^2 - x^2}{r^5}\, dv = 3k\delta \iiint\limits_{v} \frac{y^2 - x^2}{r^5}\, dx\, dy\, dz \\[2mm]
2U_{xy} &= 3k\delta \iiint\limits_{v} \frac{xy}{r^5}\, dv = 3k\delta \iiint\limits_{v} \frac{xy}{r^5}\, dx\, dy\, dz
\end{aligned} \right\} \quad (7\text{–}91a)$$

(b) for *two-dimensional* bodies (**S** = surface):

$$\left. \begin{aligned}
U_{x'z} &= 4k\delta \iint\limits_{S} \frac{xz}{r^4}\, \mathbf{dS} = 4k\delta \iint\limits_{S} \frac{xz}{r^4}\, dx\, dz \\[2mm]
U_{y'z} &= 0 \qquad 2U_{x'y'} = 0 \\[2mm]
-U_{\Delta}' &= 2k\delta \iint\limits_{S} \frac{x^2 - z^2}{r^4}\, \mathbf{dS} = 2k\delta \iint\limits_{S} \frac{x^2 - z^2}{r^4}\, dx\, dz
\end{aligned} \right\} \quad (7\text{–}91b)$$

or in *polar coordinates*:

$$\left. \begin{aligned}
U_{x'z} &= 2k\delta \iint\limits_{S} \frac{\sin 2\varphi}{r^2}\, \mathbf{dS} = 2k\delta \iint\limits_{S} \frac{\sin 2\varphi}{r}\, dr\, d\varphi \\[2mm]
-U_{\Delta}' &= 2k \iint\limits_{S} \frac{\cos 2\varphi}{r^2}\, \mathbf{dS} = 2k\delta \iint\limits_{S} \frac{\cos 2\varphi}{r}\, dr\, d\varphi.
\end{aligned} \right\} \quad (7\text{–}91c)$$

2. In *analytical methods of interpretation,* the above equations are used for calculating the anomalies of bodies of simple geometric shape.   To illustrate the development of these formulas, it is useful to begin with the simpler forms (point element, line element, spherical body, cylindrical body), although it is, of course, realized that geologic bodies occurring in nature never have such shapes and rarely approach them.

The gradients and curvatures of a *point element* are given by eqs. (7-66)

and (7–91a). In polar coordinates, $x = \rho \cos \alpha$, $y = \rho \sin \alpha$, $\rho = r \cos \varphi$, and $z = r \sin \varphi$, so that

$$
\left.
\begin{aligned}
U_{xz} &= 3kdm \frac{z\rho \cos \alpha}{r^5} = \frac{3}{2} kdm \frac{\sin 2\varphi \cos \alpha}{r^3} \\[2mm]
U_{yz} &= 3kdm \frac{z\rho \sin \alpha}{r^5} = \frac{3}{2} kdm \frac{\sin 2\varphi \sin \alpha}{r^3} \\[2mm]
U_\Delta &= -3kdm \frac{\rho^2 \cos 2\alpha}{r^5} = -3kdm \frac{\cos^2 \varphi \cos 2\alpha}{r^3} \\[2mm]
2U_{xy} &= 3kdm \frac{\rho^2 \sin 2\alpha}{r^5} = 3kdm \frac{\cos^2 \varphi \sin 2\alpha}{r^3}.
\end{aligned}
\right\} \quad (7\text{–}92a)
$$
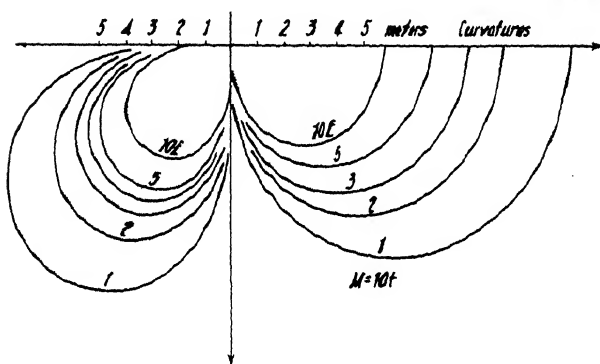
FIG. 7-96a. Effect of three-dimensional mass on gradients and curvature values (after Jung).

The following conclusions may be derived from these equations: The torsion balance anomalies of *three-dimensional* masses are (1) inversely proportional to the *cube* of the distance, other things (horizontal and vertical azimuths) being equal; (2) proportional to the single horizontal azimuth for gradients and the double horizontal azimuth for curvatures; (3) proportional to the sine of the double vertical angle for gradients and the square of the cosine of the single vertical angle for curvatures. By comparison with eqs. (7-91a) and (7-91c) it is noted that for two-dimensional features the effects are inversely proportional to the *square* of the distance and to the sine and cosine of the double vertical angle. For the anomaly of a sphere, the same formulas ([7-66], [7-91a], and [7-92a]) apply by substitution of the total mass, M, for the differential mass, dm.

K. Jung[112] has published a number of diagrams showing the effects of spherical masses on gradients and curvature values (see Fig. 7-96a). If C (= curvature) is an abbreviated notation for $-U'_\Delta/2k\delta$ and G (= gradient) for $U_{zz}/2k\delta$, then the depth, D, to the center of the sphere is

$$D = 2x_{G_{max.}} = 1.23x_{C_{max.}};$$

its radius is

$$R = 0.949\sqrt[3]{C_{max.}}\cdot D = 0.823\sqrt[3]{G_{max.}}\cdot D.$$

$$(7\text{-}92b)$$

For cylindrical disks, cones, and paraboloids of rotation[113] the curvatures and gradients for points on the axis are zero. Lancaster-Jones[114] has
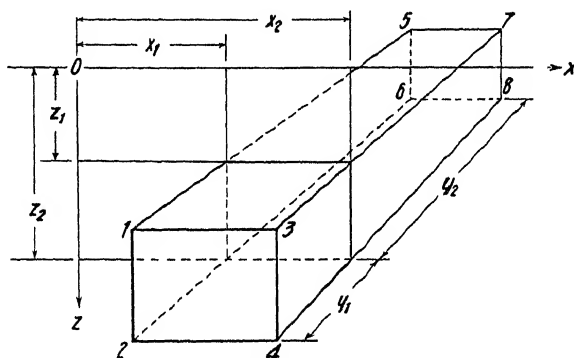
FIG. 7-96b. Rectangular unsymmetrical slab.

calculated the gradients and curvatures of a vertical line element and of a thin cylinder in order to arrive at a correction for the influence of trees in densely wooded country. For the development of graphical interpretation diagrams, the following relations for rectangular slabs are of importance. If in Fig. 7-96b z_1 is the depth to the upper surface, z_2 the depth to the lower, x_1 the distance to the south, and x_2 the distance to the north face of a rectangular slab whose extension in the strike is given by y_1 toward east and y_2 toward west, and if distances to the corners are indicated by numerals 1 to 4 in the east and by 5 to 8 in the west, integration of eq. (7-91a) results in

[112] Handb. Exper. Phys., **25**(3), 160-161.
[113] *Ibid.*
[114] A.I.M.E. Geophysical Prospecting, 508-509 (1929).

$$U_{xz} = k\delta \log_e \left[\frac{r_1 + y_1}{r_5 + y_2} \cdot \frac{r_6 + y_2}{r_2 + y_1} \cdot \frac{r_7 + y_2}{r_3 + y_1} \cdot \frac{r_4 + y_1}{r_8 + y_2} \right]$$

$$U_{yz} = k\delta \log_e \left[\frac{r_1 + x_1}{r_3 + x_2} \cdot \frac{r_4 + x_2}{r_2 + x_1} \cdot \frac{r_7 + x_2}{r_5 + x_1} \cdot \frac{r_6 + x_1}{r_8 + x_2} \right]$$

$$U_{xy} = k\delta \log_e \left[\frac{r_1 + z_1}{r_2 + z_2} \cdot \frac{r_6 + z_2}{r_5 + z_1} \cdot \frac{r_4 + z_2}{r_3 + z_1} \cdot \frac{r_7 + z_1}{r_8 + z_2} \right]$$

$$\begin{aligned}
-U_\Delta = k\delta &\left[\tan^{-1}\frac{y_2 z_2}{x_2 r_8} - \tan^{-1}\frac{x_2 z_2}{y_2 r_8} + \tan^{-1}\frac{y_1 z_1}{x_2 r_3} - \tan^{-1}\frac{x_2 z_1}{y_1 r_3} \right.\\
&+ \tan^{-1}\frac{y_2 z_1}{x_1 r_5} - \tan^{-1}\frac{x_1 z_1}{y_2 r_5} + \tan^{-1}\frac{y_1 z_2}{x_1 r_2} - \tan^{-1}\frac{x_1 z_2}{y_1 r_2}\\
&- \tan^{-1}\frac{y_1 z_1}{x_1 r_1} + \tan^{-1}\frac{x_1 z_1}{y_1 r_1} - \tan^{-1}\frac{y_2 z_2}{x_1 r_6} + \tan^{-1}\frac{x_1 z_2}{y_2 r_6}\\
&\left. - \tan^{-1}\frac{y_1 z_2}{x_2 r_4} + \tan^{-1}\frac{x_2 z_2}{y_1 r_4} - \tan^{-1}\frac{y_2 z_1}{x_2 r_7} + \tan^{-1}\frac{x_2 z_1}{y_2 r_7} \right].
\end{aligned} \quad \Bigg\} \quad (7\text{–}92c)$$

When the slab is symmetrically disposed in respect to the profile plane, $y \equiv y_1 = -y_2$, $r_1 = r_5$, $r_2 = r_6$, $r_3 = r_7$, and $r_4 = r_8$; the U_{xy} and U_{yz} components vanish and the gradients and curvatures become

$$\begin{aligned}
U_{xz} &= k\delta \log_e \left[\frac{r_1 + y}{r_1 - y} \cdot \frac{r_2 - y}{r_2 + y} \cdot \frac{r_3 - y}{r_3 + y} \cdot \frac{r_4 + y}{r_4 - y} \right]\\
U_\Delta &= 2k\delta \left[\tan^{-1}\frac{yz_1}{x_2 r_4} - \tan^{-1}\frac{x_2 z_2}{y r_4} - \tan^{-1}\frac{yz_1}{x_2 r_3} + \tan^{-1}\frac{x_2 z_1}{y r_3} \right.\\
&\qquad \left. + \tan^{-1}\frac{yz_1}{x_1 r_1} - \tan^{-1}\frac{x_1 z_1}{y r_1} - \tan^{-1}\frac{yz_2}{x_1 r_2} + \tan^{-1}\frac{x_1 z_2}{y r_2} \right].
\end{aligned} \quad \Bigg\} \quad (7\text{–}92d)$$

It is convenient to consider the gradients and curvatures due to a horizontal line of limited strike extent since this gives the possibility of deriving an approximate formula which will indicate when it is permissible to consider a three-dimensional feature as two-dimensional. If ρ is the radius vector from the station to the line of the section dS in the profile plane and if $\pm b$ is its extension at right angles thereto, then $U_{y'z}$ and $2U_{x'y'}$ are zero, and the gradient and curvature component follow from integration of eq. (7–91a) and series expansion of the expressions involving $r = b(1 + {}^{\prime\prime\backslash\frac{1}{2}}$

$$U_{x'z} = \frac{3}{2} k\delta \cdot dS \cdot \rho^2 \sin 2\varphi \int_{-b}^{+b} \frac{db}{r^5} = 4k\delta \cdot dS \cdot \frac{x'z}{\rho^4} \left[1 - \frac{3}{8} \left(\frac{\rho}{b} \right)^2 + \cdots \right]$$

$$-U_{\Delta'} = -3k\delta \cdot dS \int_{-b}^{+b} \frac{b^2 - \rho^2 \cos^2 \varphi}{r^5} db$$

$$= 2k\delta \cdot dS \cdot \frac{x^2 - z^2}{\rho^4} \left[1 + \frac{3}{2} \frac{\rho^2}{x^2 - z^2} \left(\frac{\rho}{b} \right)^2 + \cdots \right].$$

$$(7-92e)$$

When the extension of the line is $\pm \infty$, the second terms in the brackets vanish and the two-dimensional values as given in eq. (7–91b) remain. Hence, these terms indicate the error committed when limited features are considered two-dimensional. According to Jung[115] an error of 1 per
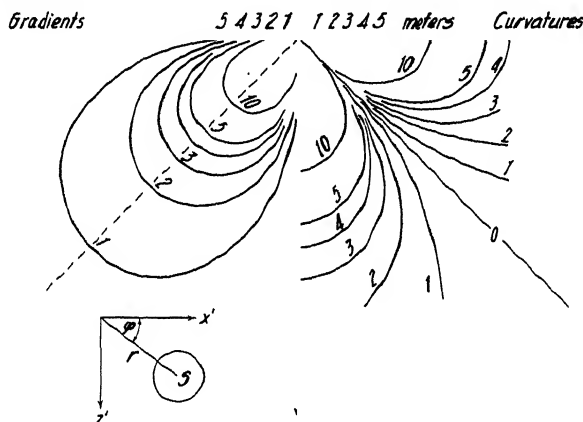
Fig. 7-97. Effect of two-dimensional mass (cylinder section) on gradients and curvature values (after Jung).

cent is produced in gradients when b is less than 2.5ρ, and the same error arises in curvatures when b is less than 12ρ. For gradient calculation it is therefore permissible to consider most geologic features of elliptical outline as two-dimensional in interpretation calculations.

As an example of a *two-dimensional* feature, consider the torsion balance anomalies due to a horizontal cylinder. These anomalies follow directly from eq. (7–91c) and are

$$U_{x'z} = 2k\delta R^2 \pi \frac{\sin 2\varphi}{r^2}$$

and

$$-U_{\Delta'} = 2k\delta R^2 \pi \frac{\cos 2\varphi}{r^2},$$

$$(7-93a)$$

[115] Handb. Exper. Phys., 25(3), 184 (1930).

where R is the radius of the cylinder. Fig. 7–97 illustrates the action of a horizontal cylinder in the form of lines of equal position for a given effect on gradients and curvatures. It is seen that the curvature is insensitive
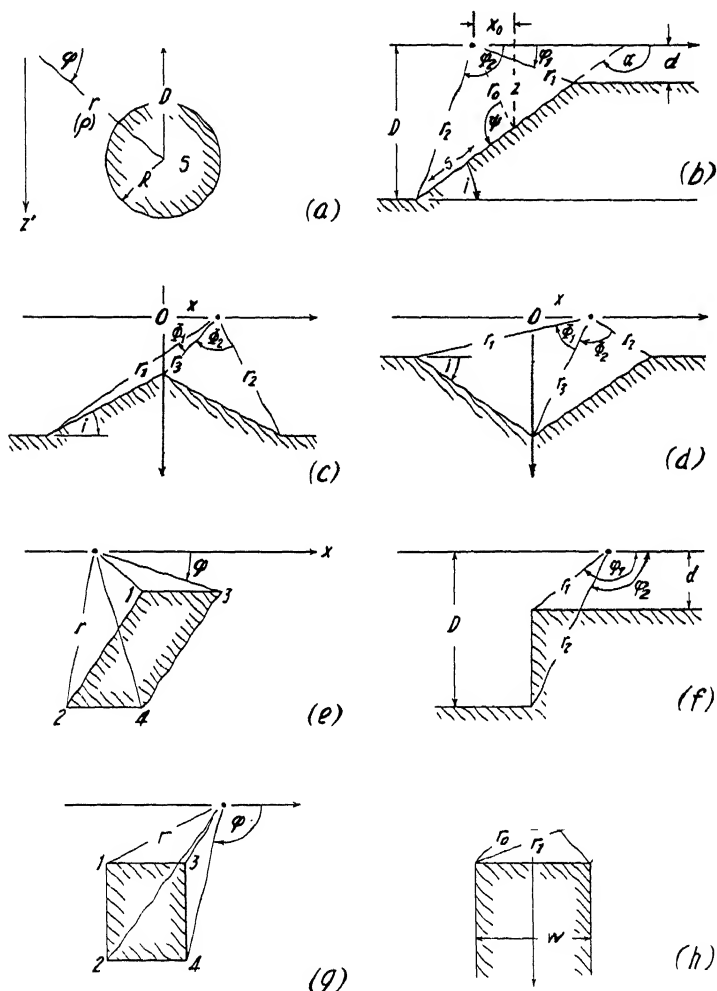
FIG. 7-98. Two-dimensional bodies: (*a*) cylinder, (*b*) slope, (*c*) symmetrical anticline, (*d*) symmetrical syncline, (*e*) inclined dike, (*f*) vertical step, (*g*) rectangular slab, (*h*) infinite vertical dike.

to masses 45° below the horizon and most sensitive to those directly beneath and in the horizon. The gradients, on the other hand, are insensitive to masses in the horizon and directly below, and most sensitive to

masses 45° below the horizon.   The gradient anomalies of two- and three-dimensional masses are therefore quite similar in respect to vertical angle and differ only in regard to distance power.   In the curvatures, an extensive strike dimension produces sensitivity in the vertical direction in addition to that in horizontal direction.   The depth to center, D, and radius may be determined, as in eq. (7–92b), from the relations[116]

$$\left.\begin{array}{l} D = x_{\mathrm{C}_o} = 1.73 x_{\mathrm{G_{max.}}} = 0.578 x_{\mathrm{C_{max.}}} \\[2mm] R = 0.564\sqrt{\mathrm{C_{max.}}}\cdot D = 0.700\sqrt{\mathrm{G_{max.}}}\cdot D, \end{array}\right\} \quad (7\text{–}93b)$$

where x_{C_o} is the abscissa of the point of zero curvature anomaly (see Fig. 7–99).

Other two-dimensional features are illustrated in Fig. 7–98, such as anticlines, synclines, inclined dikes, vertical steps, slabs, and vertical dikes.   Their anomalies may be calculated readily from those of a slope (Fig. 7–98b).   The calculation involves essentially the integration of formula (7–91b).   For the gradient this may be written, with the notation of Fig. 7–98b, $U_{x'z} = 2k\delta \int_d^D z\,dz \int_{x_0}^{\infty} \dfrac{2x\,dx}{r^4}$, where $x \equiv x_0$ on the sloping edge.   Using $r_0^2 = x_0^2 + z^2$, $\psi = \alpha - \varphi_0$, $r_0\,d\varphi_0 = ds \sin \alpha$, and $dz = ds \sin \alpha$, we have $U_{x'z} = 2k\delta \int_{\varphi_1}^{\varphi_2} d\varphi_0 \sin \alpha \sin \varphi_0 / \sin \psi$ or $U_{x'z} = k\delta\left[2 \sin^2 \alpha \dfrac{r_2}{r_1} - \sin 2\alpha(\varphi_2 - \varphi_1) \right]$.   Thus, with the dip angle $i = \pi - \alpha$, and similar analysis for the curvature,

$$U_{x'z} = 2k\delta \sin i\left[\sin i \log_e \frac{r_2}{r_1} + \cos i(\varphi_2 - \varphi_1) \right]$$

$$-U_{\Delta'} = 2k\delta \sin i\left[\sin i(\varphi_2 - \varphi_1) - \cos i \log_e \frac{r_2}{r_1} \right]. \qquad (7\cdot 93c)$$

For direct interpetation it is useful to know that the center between the extremes in the curvatures is situated above the center of the subsurface slope.   With this point as origin, the abscissas of the maximum gradient and curvature values are given by

$$x_{\mathrm{G}} \quad = \quad (D - d)^2$$

For complete depth and dip determinations, diagrams have been constructed by Jung.[117]

[116] Jung, Zeit. Geophys., **3**(6), 267-280 (1927).
[117] *Ibid.*
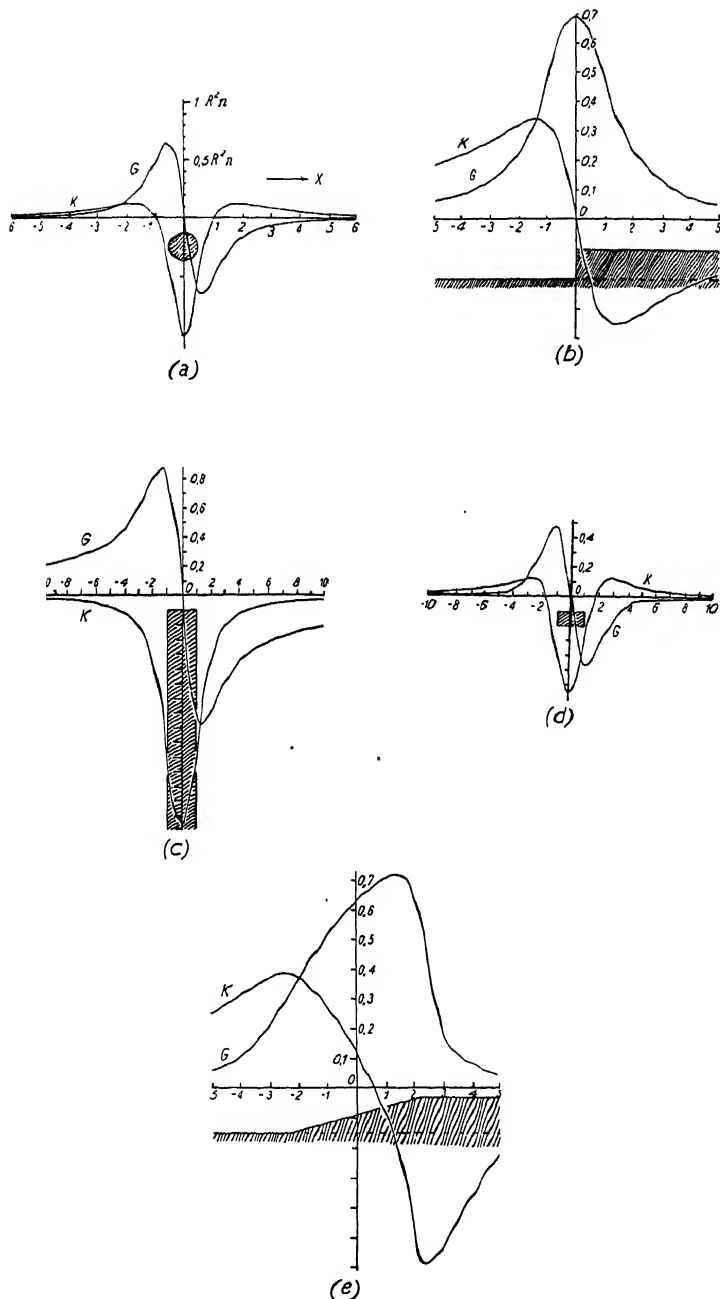
Fig. 7-99a-e. Gradients and curvatures for two-dimensional features (after Jung). (Fig. 7-99f-i on page 262.) G = Gradient, K = curvature value.

Above an extended slope (see Fig. 7-99) $\log_e \dfrac{r_2}{r_1} \doteq 0$ and $\quad - \varphi_1 \doteq$ so that

$$U_{x'z} \doteq k\delta\pi \sin 2i$$

$$- U_{\Delta'} \doteq 2k\delta\pi \sin^2 i. \tag{7-93d}$$
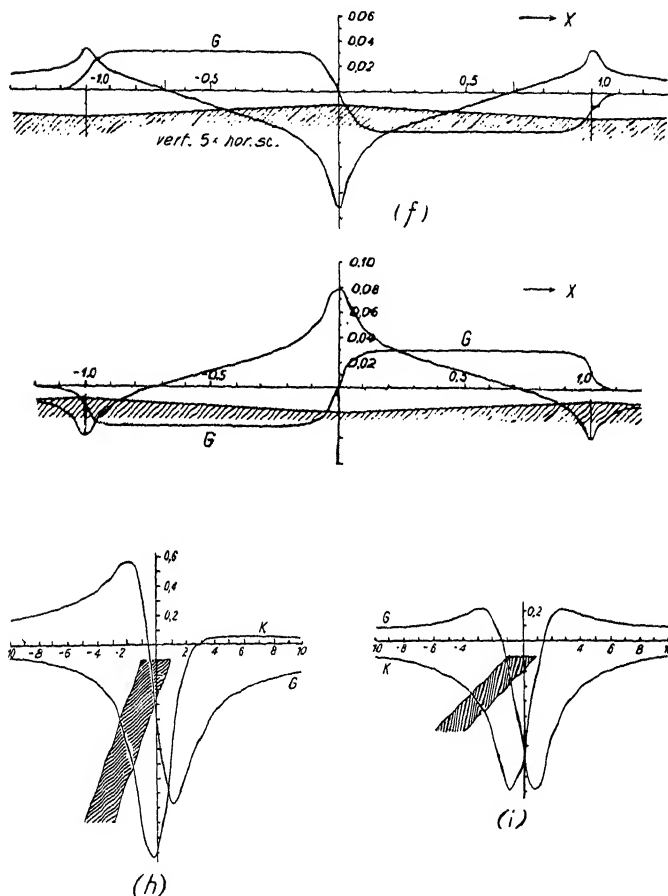
Fig. 7-99f–i. Gradients and curvatures for two-dimensional features, continued (after Jung). G=Gradient, K=curvature value.

For small angles $\sin i \approx i$; therefore, the gradient on extended slopes is

$$U_{x'z} \doteq 2k\delta\pi i = 7.3\delta i° \text{ E.U.}, \tag{7-93e}$$

which is a useful formula for correlating regional dip and regional gradient. In all these formulas, δ signifies, of course, *difference* in density. If i is expressed in radians, the coefficient in eq. (7-93e) is 419 E.U.

In the calculation of symmetrical anticlines, the curvatures due to two opposite slopes given by eq. (7–93c) are added and the gradients subtracted so that

$$\left.\begin{aligned}
U_{x'z} &= 2k\delta \sin i \left[\sin i \log_e \frac{r_1}{r_2} + \cos i(\Phi_1 - \Phi_2) \right] \\
-U_{\Delta'} &= 2k\delta \sin i \left[\sin i(\Phi_1 + \Phi_2) - \cos i \log_e \frac{r_1 r_2}{r_3^2} \right].
\end{aligned}\right\} \quad (7\text{–}93f)$$

For a symmetrical syncline,

$$\left.\begin{aligned}
U_{x'z} &= 2k\delta \sin i \left[\sin i \log_e \frac{r_1}{r_2} - \cos i(\Phi_1 - \Phi_2) \right] \\
-U_{\Delta'} &= 2k\delta \sin i \left[\sin i(\Phi_1 + \Phi_2) + \cos i \log_e \frac{r_1 r_2}{r_3^2} \right].
\end{aligned}\right\} \quad (7\text{–}93g)$$

It should be noted that in Figs. 7–98c and 7–98d Φ stands for *difference* in angle. K. Jung[118] and H. Shaw[119] have calculated a number of diagrams to assist in direct determinations of the characteristics of anticlines and synclines from gradients and curvature values.

To obtain the gradients and curvatures for an inclined dike as in Fig. 7–98e, two slopes (eq. [7–93c]) are deducted from each other, so that with the notation indicated in the figure,

$$\left.\begin{aligned}
U_{x'z} &= 2k\delta \sin i \left[\sin i \log_e \frac{r_2 r_3}{r_1 r_4} + \cos i(\varphi_2 - \varphi_1 - \varphi_4 + \varphi_3) \right] \\
-U_{\Delta'} &= 2k\delta \sin i \left[\sin i(\varphi_2 - \varphi_1 - \varphi_4 + \varphi_3) - \cos i \log_e \frac{r_2 r_3}{r_1 r_4} \right].
\end{aligned}\right\} \quad (7\text{–}93h)$$

Usually the depth extent of the dike is considerable, so that

$$U_{x'z} = 2k\delta \sin i \left[\sin i \log_e \frac{r_3}{r_1} + \cos i(\varphi_3 - \varphi_1) \right]$$

$$-U_{\Delta'} = 2k\delta \sin i \left[\sin i(\varphi_3 - \varphi_1) - \cos i \log_e \frac{r_3}{r_1} \right].$$

If the gradient at the origin ($x = 0$ above the center of the upper face) (see Fig. 7–99) is $G_0 = G_{max.} + G_{min.}$ and if the curvature $C_0 = C_{max.} + C_{min.}$, then $\cotan i = C_0/G_0$, and $G_0 = \frac{1}{2} \sin 2i\Phi_0$ ($\Phi_0 = \Phi$ for $x = 0$); $d = (w/2) \cotan \Phi/2$. For the last calculation, special diagrams

[118] *Ibid.*, **3**, 257–280 (1927); **5**, 238–252 (1929).
[119] H. Shaw, A.I.M.E. Geophysical Prospecting, 336–366 (1932).

using the distance between the extremes in gradients and curvatures have been constructed by Jung. The dip angle may also be calculated from the ratios of gradient maxima and minima. The direct interpretation of torsion balance anomalies of vertical and inclined dikes has been discussed in detail by H. Shaw.[120]

By letting $i = 90°$ in eq. (7-93c), the gradient and curvature anomalies of a step with a vertical face (fault, escarpment, or the like) are obtained. With the notation of Fig. 7-98f,

$$\left. \begin{array}{l} U_{x'z} = 2k\delta \log \dfrac{r_2}{r_1} \\[2mm] -U_{\Delta'} = 2k\delta(\varphi_2 - \varphi_1). \end{array} \right\} \quad (7\text{-}94a)$$

The upper and lower depths follow, therefore, from the amplitudes and abscissas of the extremes in gradients and curvatures, thus:

$$\left. \begin{array}{l} d \cdot D = (x_{C \text{ max.}})^2 = (x_{G_{\frac{1}{2}}})^{\frac{1}{2}} \\[2mm] \log_{10} \dfrac{d}{D} = 0.438 G_{\text{max.}} \end{array} \right\} \quad (7\text{-}94b)$$

The anomalies of a block with vertical faces, as in Fig. 7-98g, may be obtained by subtracting two faces, as in eq. (7-94a) or by letting $i = 90°$ in formula (7-93h). Then

$$\left. \begin{array}{l} U_{x'z} = 2k\delta \log_e \dfrac{r_2 r_3}{r_1 r_4} \\[2mm] -U_{\Delta'} = 2k\delta(\varphi_2 - \varphi_1 - \varphi_4 + \varphi_3). \end{array} \right\} \quad (7\text{-}94c)$$

For direct interpretation, it is helpful that the curvature at the symmetry point, $x = 0$, is equal to twice the angle subtended by the upper and lower edges. Hence, $C_{\text{max.}} = 2\varphi_0$, where $\varphi_0 = (\varphi_1 - \varphi_2)_{x=0} = (\varphi_4 - \varphi_3)_{x=0}$. The complete determination of depth and outline is possible by means of diagrams constructed by Jung.[121]

When the dike is of infinite depth extent, $r_4 \approx r_2$ and $\varphi_4 \approx \varphi_2$, so that with the notation of Fig. 7-98h,

$$\left. \begin{array}{l} U_{x'z} = 2k\delta \log_e \dfrac{r_2}{r_1} \\[2mm] -U_{\Delta'} = -2k\delta\Phi. \end{array} \right\} \quad (7\text{-}94d)$$

[120] Ibid.
[121] Zeit. Geophys., **3**, 257–280 (1927); **5**, 238–252 (1929).

Since $C_{max.} = \Phi_o$ and $x_{G\ max.} = r_o$, the depth and the width, according to Jung,[122] are

$$d = r_0 \cos \frac{\Phi_0}{2}$$

and

$$w = 2r_0 \sin \frac{\Phi_0}{2}.$$

$(7\text{--}94e)$

It is possible to approximate the outline of two-dimensional masses of irregular shape by using a polygon with straight sides and applying formula $(7\text{--}93c)$ repeatedly, as proposed by Matuyama and Higasinaka.[123] However, it is easier in such cases to use the graphical methods described in the following paragraphs.

3. *Graphical interpretation methods* make use of diagrams containing mass elements in section or plan view in such an arrangement that their effect on a station (0-point) is identical irrespective of distance or azimuth (see also pages 153 and 227). For three-dimensional subsurface features of moderate relief the diagrams calculated by Numerov, discussed on page 228 and illustrated in Figs. 7–78a and 7–78b, are applied in connection with subsurface contour maps, and strips bounded by successive contours are evaluated. Then the height of the instrument above ground ζ corresponds to the depth, D, of the effective geologic feature beneath the instrument. The mean "elevation" of a contour strip with respect to this point is $h = D - d$ where $d = (d_1 + d_2)/2$, or the mean of the depth values of two contours. δ is the density *contrast*. If $\mathbf{n}_c$ is the number of elements comprised by a contour strip in the curvature diagram and $\mathbf{n}_g$ the corresponding number in the gradient diagram, the effect of one strip, (subscript st), is

$$(U_{zz})_{st} = \tfrac{1}{2}\delta \cdot \mathbf{n}_g \cdot (D^2 - d^2)$$
$$(-U_\Delta)_{st} = \delta \cdot \mathbf{n}_c \cdot (D - d).$$

$(7\text{--}95a)$

For determinations of U_{yz} and $2U_{xy}$ the diagrams are rotated 90° or 45°, respectively, as in the terrain applications. For steep slopes of subsurface features the accuracy of horizontal (contour line) diagrams is insufficient, and vertical diagrams such as shown in Figs. 7–82 and 7–83 must be applied with geologic sections through the geologic body in a number of azimuths. Although the diagrams under discussion have been calculated

---

[122] *Ibid.*

[123] Japan. J. Astron. and Geophys., **7**, 47–81 (1930).

for sixteen azimuths, they may readily be modified for fewer directions by changing the azimuth factor in eq. (7–88). These diagrams are particularly suited for the calculation of salt domes, cap rocks, irregular ore bodies, mine cavings, and the like. Certain two-dimensional diagrams are applicable to such geologic features as domes or anticlines if a definite variation of strike extent with depth of the elements (Barton) is incorporated.

$U_{x'z}$
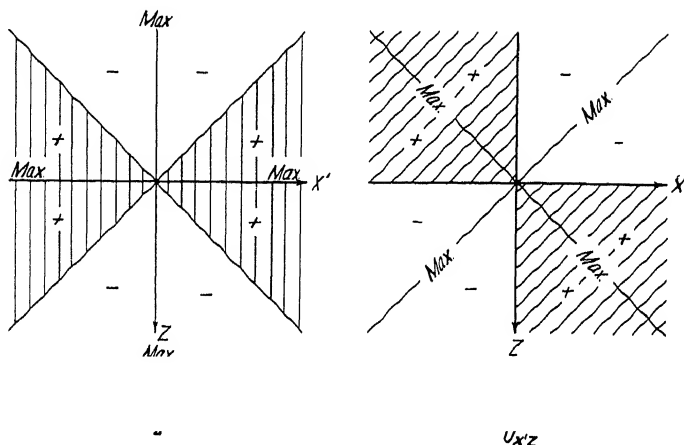
FIG. 7–100. Orientation of two-dimensional interpretation diagram (Fig. 7–79b) for gradients and curvatures (after Jung).

Diagrams for two-dimensional bodies are readily calculated, since their surface effects depend on section only. Calculations are a minimum with cylindrical coordinates. Integration of eq. (7–91c) gives

$$U_{x'z} = -k\delta \log_e \frac{'^{n+1}}{r_n} (\cos 2_{\iota} \quad - \cos$$

$$U_{\Delta'} = -k\delta \log_e \frac{r_{n+1}}{\sim} (\sin 2\varphi_{m+1} - \sin 2\varphi_m) \tag{7–95b}$$

for an element bounded by radii r_n and r_{n+1} and angles φ_m and φ_{m+1} (as in Fig. 7–79b). A comparison of these equations with the last two in eq. 7–86 shows that the curvature terrain diagram of Fig. 7–79b may be used for calculations of gradients *and* curvatures of two-dimensional masses. Eq. (7–95b) indicates 45° symmetry and therefore the orientation for gradients and curvatures differs by 45°, as shown in Fig. 7–100. The unit effect is $\frac{2}{3}$ E.U. For evaluating horizontal or nearly horizontal formations, it is more convenient to arrange the mass elements along horizontal lines and therefore base the calculations on formula (7–94c). In a form

better suited for determining the vertical boundaries of mass elements in a horizontal bed this may be written

$$
\left.
\begin{aligned}
U_{x'z} &= k\delta \log_e \left(\frac{x_1^2 + z_2^2}{x_1^2 + z_1^2} \cdot \frac{x_2^2 + z_1^2}{x_2^2 + z_2^2} \right) \\
-U_{\Delta'} &= 2k\delta \left(\tan^{-1}\frac{z_2}{x_1} + \tan^{-1}\frac{z_1}{x_2} - \tan^{-1}\frac{z_1}{x_1} - \tan^{-1}\frac{z_2}{x_2} \right).
\end{aligned}
\right\}
\quad (7\text{-}95c)
$$
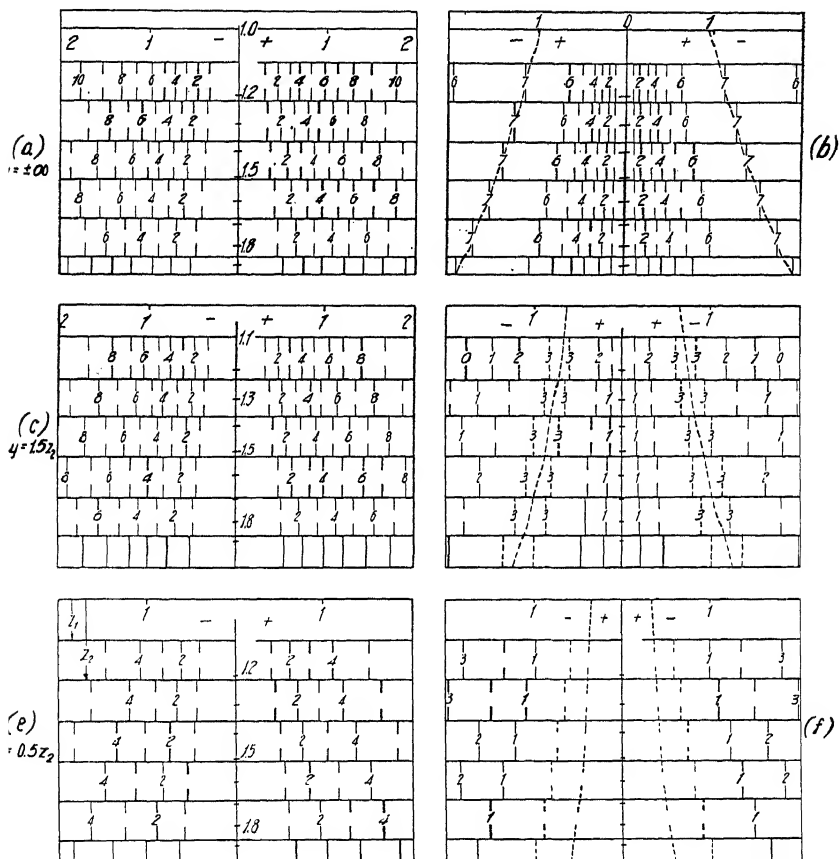
FIG. 7-101. Interpretation diagram for two-dimensional features (after Barton).

Diagrams based on these equations are shown in Figs. 7-101a and 7-101b.[124] In the calculation the vertical sequence of formation boundaries is determined by the assumption that $z_{n+1} = (10/9)z_n$. Therefore in semilogarithmic representation, as in the figure, the vertical formation interval is

[124] D. C. Barton, A.I.M.E. Geophysical Prospecting, 489 (1929).

constant which, however, necessitates a replotting of the geologic section to that scale. A limited strike extent proportional to depth (as in salt domes and anticlines) may be introduced as shown in Figs. 7–101c, d, e, and f. Calculations of the anomalies are then based on formulas (7–92d)

4. *Planimeter and integraph* methods may be used for the calculation of torsion balance anomalies from known or assumed outlines of a geologic body. Since, according to eq. (7–91c), the action of a two-dimensional feature depends not only on area but also on distance and vertical angle, the area to be evaluated must be replotted to suitable scale before a regular
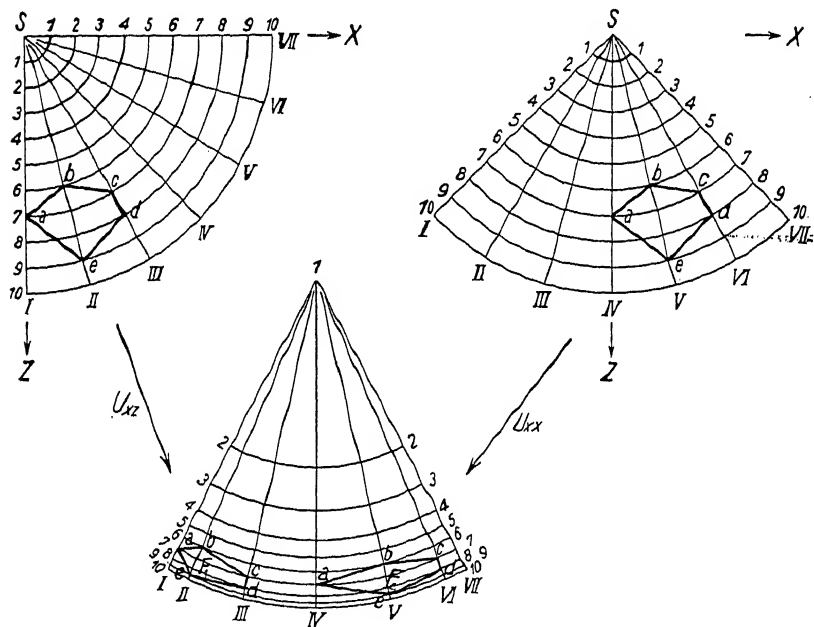
FIG. 7-102a. Scale distortion in Below-Jung planimeter interpretation method for two-dimensional bodies (after Jung).

planimeter can be applied to give the torsion balance anomaly (Below method,[125] see eq. [7–44b] and Figs. 7–46 and 7–47). To convert the double integral in eq. (7–91c) into a surface integral independent of azimuth and distance, the substitutions R for $\sqrt{2} \log_e \rho$, Φ for $\frac{1}{2} \sin 2\varphi$, and $\frac{1}{2} \cos 2\varphi$, respectively, are necessary so that the gradients and curvatures are proportional $\iint R \, d\Phi \, dR$ after the scale distortion has been accomplished, as shown in Fig. 7–102a.

A direct evaluation of gravity integrals *without scale distortion* is pos-

[125] Jung, Zeit. Geophys., **6**(2), 114–122 (1930).

sible with the instrument illustrated in Fig. 7–102b. It gives the surface integrals

$$\iint \begin{Bmatrix} \sin \mathbf{n}\varphi \\ \cos \mathbf{n}\varphi \end{Bmatrix} d\varphi\, dr \quad \text{and} \quad \iint \begin{Bmatrix} \sin \mathbf{n}\varphi \\ c\end{Bmatrix} , \frac{dr}{r} ,$$

where the apparatus will take multiples up to $\mathbf{n} = 3$. The first integral applies in the first derivatives of gravity (horizontal and vertical gravity
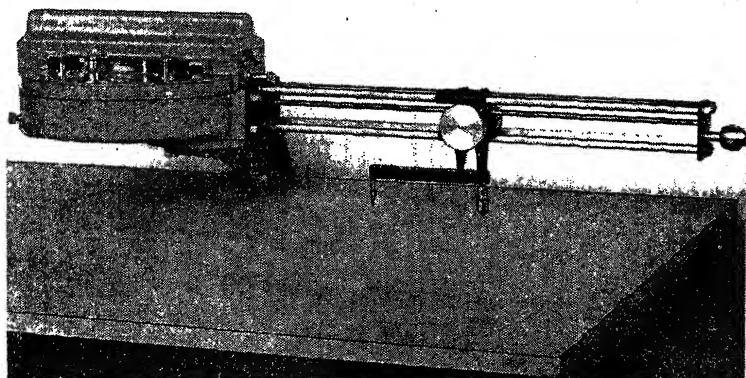
FIG. 7–102b. Torsion balance interpretation integraph.

TABLE 34

APPLICATION OF GRAVITY INTEGRAPH

	dim.	Quantity	dim.	Quantity	dim.	Quantity
Pendulum; Gravimeter	2	$\dfrac{\partial U}{\partial x'} \propto \iint \sin \varphi\, d\varphi\, dr$	3	$\dfrac{\partial U}{\partial z} \propto \iint \sin 2\varphi\, d\varphi\, dr$		
	2	$\dfrac{\partial U}{\partial x'} \propto \iint \cos \varphi\, d\varphi\, dr$	3	$\dfrac{\partial U}{\partial x} \propto \int\int \cos 2\varphi\, d\varphi\, dr$		
Torsion Balance	3	$U_{xz} \propto \iint \sin \varphi\, d\varphi\, \dfrac{dr}{r}$	2	$U_{x'z} \propto \iint \sin 2\varphi\, d\varphi\, \dfrac{dr}{r}$	3	$U_{xz} \propto \iint \sin 3\varphi\, d\varphi\, \dfrac{dr}{r}$
	3	$U_{\Delta} \propto \iint \cos \varphi\, d\varphi\, \dfrac{dr}{r}$	2	$U_{\Delta}{}' \propto \int\int \cos 2\varphi\, d\varphi\, \dfrac{dr}{r}$	3	$U_{\Delta} \propto \iint \cos 3\varphi\, d\varphi\, \dfrac{dr}{r}$

components); the second in the second derivatives (gradients and curvature values). The factor $\mathbf{n}$ depends, among other things, on whether the integral applies to a two- or three-dimensional body as illustrated by Table 34. For three-dimensional bodies the volume integrals are reduced to surface integrals by evaluating the sections of geologic bodies in various azimuths, plotting the effect as a function of azimuth (polar diagram), and evaluating the resulting area with the same integrometer.

With one of the integrations carried out, the gradients and curvatures as measured by this instrument are, therefore, for two-dimensional bodies:

$$\left.\begin{aligned}
U_{x'z} &= 2k\delta \int_{r_1}^{r_2} \int_{\varphi_1}^{\varphi_2} \sin 2\varphi \, d\varphi \, \frac{dr}{r} = k\delta \int_{r_1}^{r_2} \frac{dr}{r} (\cos 2\varphi_1 - \cos 2\varphi_2) \\
U_{\Delta'} &= 2k\delta \int_{r_1}^{r_2} \int_{\varphi_1}^{\varphi_2} \cos 2\varphi \, d\varphi \, \frac{dr}{r} = k\delta \int_{r_1}^{r_2} \frac{dr}{r} (\sin 2\varphi_2 - \sin 2\varphi_1)
\end{aligned}\right\} \quad (7\text{--}96b)$$

and for three-dimensional bodies:

$$\left.\begin{aligned}
U_{xz} &= 3k\delta \int_{\alpha_1}^{\alpha_2} \int_{\varphi_1}^{\varphi_2} \int_{r_1}^{r_2} \cos \alpha \, d\alpha \, (\sin \varphi - \sin^3 \varphi) \, d\varphi \, \frac{dr}{r} \\
&= k\delta \int_{\alpha_1}^{\alpha_2} \cos \alpha \, d\alpha \int_{r_1}^{r_2} \frac{dr}{r} \left(\tfrac{1}{4}\cos 3\varphi_1 + \tfrac{3}{4}\cos \varphi_1 - \tfrac{1}{4}\cos 3\varphi_2 - \tfrac{3}{4}\cos \varphi_2\right) \\
U_{yz} &= \text{same with } \sin \alpha \text{ instead of } \cos \alpha. \\
-U_{\Delta} &= \tfrac{3}{2}k\delta \int_{\alpha_1}^{\alpha_2} \int_{\varphi_1}^{\varphi_2} \int_{r_1}^{r_2} \cos 2\alpha \, d\alpha \cdot \cos^3 \varphi \, d\varphi \cdot \frac{dr}{r} \\
&= \tfrac{1}{2}k\delta \int_{\alpha_1}^{\alpha_2} \cos 2\alpha \, d\alpha \int_{r_1}^{r_2} \frac{dr}{r} \left(\tfrac{9}{4}\sin \varphi_2 + \tfrac{1}{4}\sin 3\varphi_2 - \tfrac{9}{4}\sin \varphi_1 - \tfrac{1}{4}\sin 3\varphi_1\right)
\end{aligned}\right\} (7\text{--}96c)$$

U_{xy} = same with $\sin 2\alpha$ in place of $\cos 2\alpha$.

The mechanism of this integraph is enclosed in a circular case and pivots about a point near the supporting base, this being equivalent to rotation about the angle φ. The variation in the r direction is brought about by radial motion of the pointer touching the board, which by a rack and pinion movement rotates a keyed shaft shown in the center of the arm assembly. This instrument is probably the most advanced means for a rapid determination of torsion balance anomalies and has an accuracy of 1 to 2 per cent. A simple integraph for the evaluation of two-dimensional features has been constructed by Gamburzeff.[126]

G. Discussion of Torsion Balance Results

1. *Measurements on lakes.* The logical approach to the verification of the theory of subsurface effects discussed in the preceding section is a measurement of the anomalies due to *known* subsurface mass distributions. Most suitable for this purpose are frozen lakes, whose bottom contours are usually well known from soundings. Measurements on the ice are readily made. The instrument can be moved from one point to another on skids, and terrain corrections are usually negligible. Eötvös,

[126] Gerl. Beitr., **24**, 83–93 (1929).

himself, was the first to realize the merit of lake measurements.[127]   Even before he had developed his double gradient and curvature variometer, he surveyed thirty-three stations on the ice of Balaton Lake in 1901 and twelve stations in 1903.   Similar measurements were made in 1924 by Holst[128] in the Black Forest on Lake Titi.   This lake is of glacial origin. Its greatest depth is 39 meters, and the bottom formation is gneiss covered
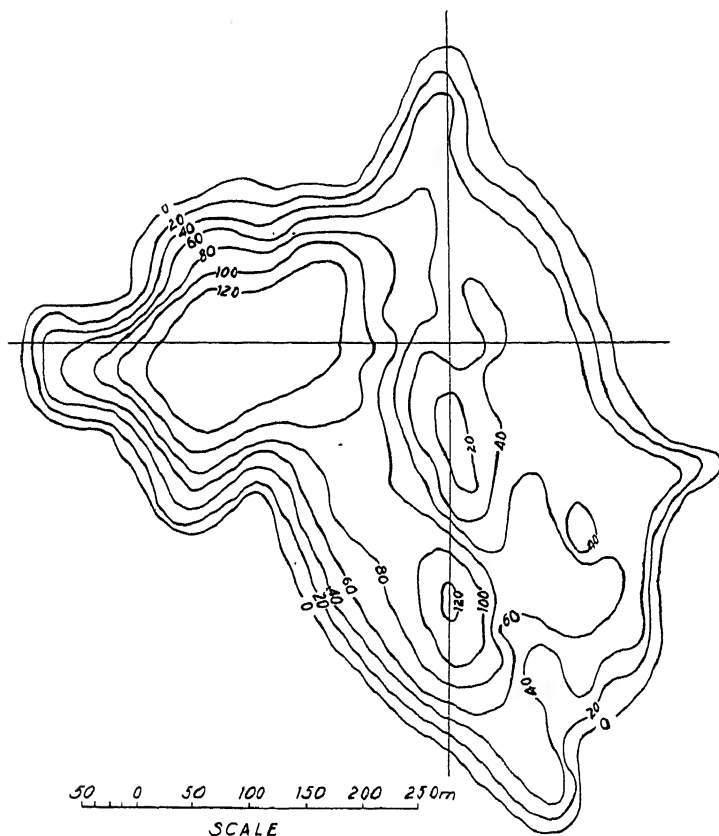
Fig. 7-103a. Bottom contours (in decimeters) of Lake Shuvalovo (after Numerov).

by a thin layer of morainal material. The observed torsion balance anomalies were large because of the large density difference between water and rock (1.7).   Since the lake profile was well known from soundings, the observed indications could be compared with theoretical anomalies (calculated by means of the slope formula [7-93c]).

[127] R. v. Eötvös, *Resull. wiss. Erforsch. Balalonsees*, Vol. I, Geophys. Appendix (1908).
[128] E. Holst, Zeit. Geophys., **1**, 228-237 (1924-1925).

Fig. 7-103 illustrates the results of very careful measurements made by B. Numerov[129] on Lake Shuvalovo near Leningrad, which proved to be a suitable study object since its maximum depth is only 13 meters. In its middle a sand ridge comes within 1 meter of the surface. There is an almost complete identity of the isogams and isobathic lines. Since in the formula $\Delta g = 2k\pi\delta h$, the factor $2\pi k$ is equal to 42 E.U., the variation in
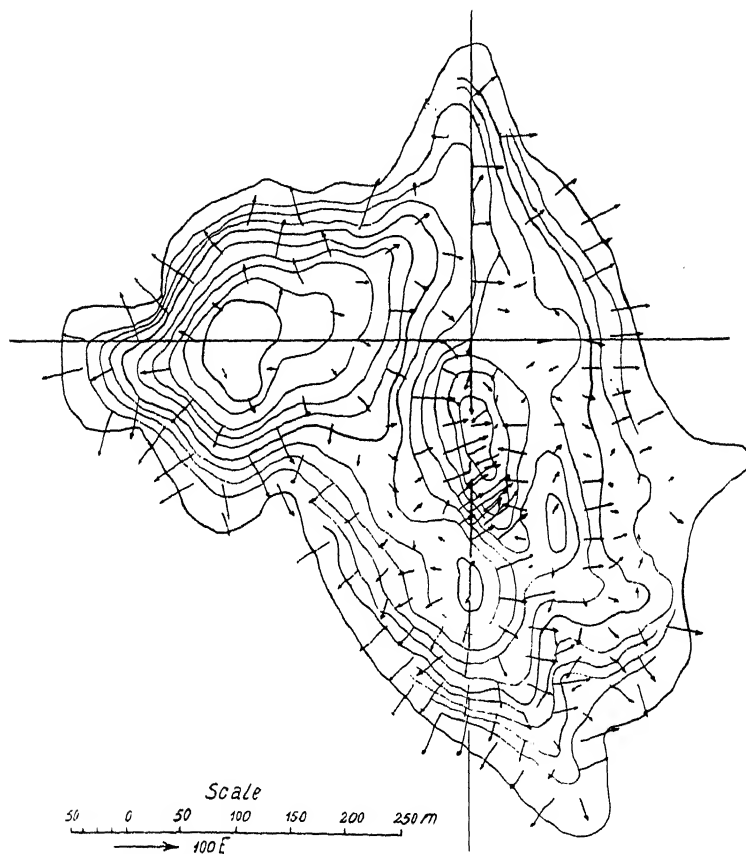
FIG. 7-103b. Isogams and gradients (in 0.01 milligals) on Lake Shuvalovo.

depth of the lake bottom may be predicted from $\Delta h = \Delta\Delta g \cdot 10^8/42\delta$. The density difference was one. An anomaly of 1.37 milligals corresponded to the sand bank previously mentioned.

2. In *oil exploration* the torsion balance has found undoubtedly its greatest commercial application. Its possibilities for mapping subsurface

[129] B. Numerov, Zeit. Geophys., **5**, 276-289 (1929).

geologic structure were realized at an early date by Hugo von Boeckh[130] who gave an interpretation of some of Eötvös' earlier surveys and suggested to him and his assistants the study of oil structures. Fig. 7-104 illustrates relative gravity values calculated from torsion balance measurements for a profile in the Maros Valley in Hungary. It is seen that the
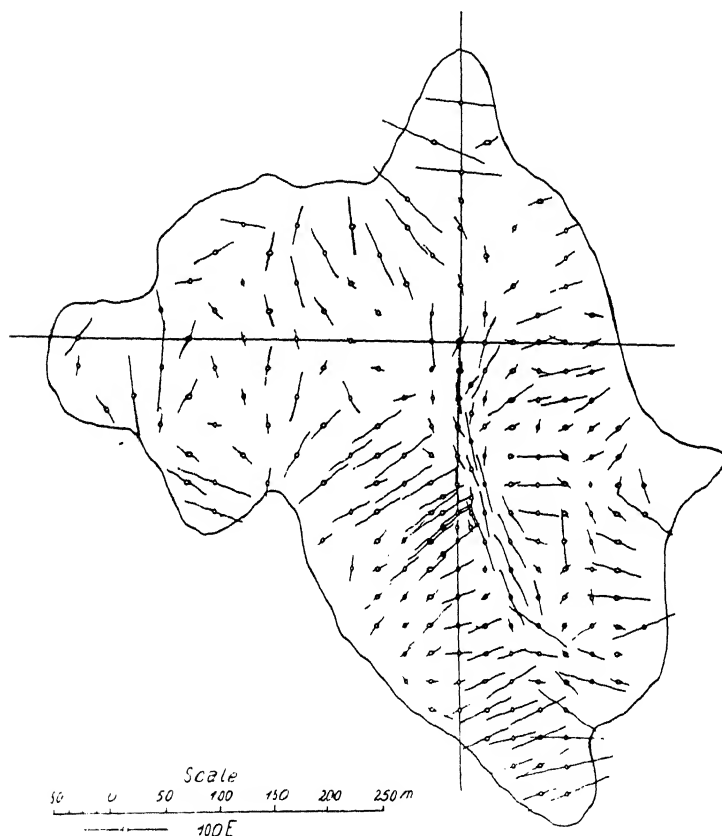
FIG. 7-103c. Curvatures on Lake Shuvalovo.

gravity minima correspond closely to the uplifted positions of the salt beds and to the salt anticlines.

Following Boeckh's publication, attempts were made in other European countries to utilize the torsion balance for the mapping of salt domes and salt anticlines. In 1917 W. Schweydar[131] observed the gravity gradi-

130 H. v. Boeckh, Petroleum, **12(16)**, 817 823 (1917).
131 W. Schweydar, Zeit. Prakt. Geol., **26**, 157 162 (Nov., 1918).

ents on the Nienhagen-Haenigsen salt dome and oil field (northern Germany) and found them to be larger on the west side because of the steep dip of the Mesozoic beds and the overhang of the dome. The Wietze oil field of northern Germany was studied extensively with geophysical methods. Fig. 7–105 shows seismic refraction profiles, the outline of the dome deduced from them, and the results of torsion balance and pendulum measurements. The outline of the dome given by the torsion balance checks closely with that furnished by the seismograph.

Another north German structure studied extensively with seismic-refraction, electrical, magnetic, and torsion balance methods is the Lübtheen salt dome, whose section is well known from borings and potash mines.[132] As shown in Fig. 7–106, the outline of the dome is very well indicated by the gradients and curvature values. Contrary to Gulf coast experience, no gravity maximum occurs, despite a well developed cap rock. The main purpose of the survey was to determine the extent of (potential
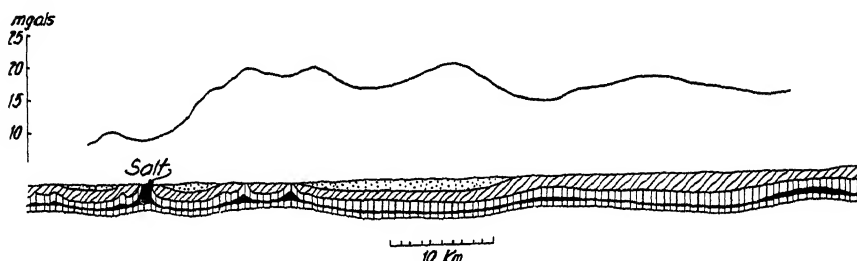
Fig. 7–104. Gravity anomalies on salt anticlines in the Maros Valley v. Boeckh).

oil-bearing) Mesozoic strata around the dome. These strata are well developed on the east flank of the dome, give rise to a reversal of the gradients, and are estimated to be about 500 meters wide there. They broaden on the north flank to 700 meters, increase to 1300 meters width in the northwest, but they are then reduced considerably on the west flank of the dome. Torsion balance work in northern Germany has been continued and supplemented of late by gravimeter observations. Fig. 7 1⁰ shows the torsion balance results for the deep-seated dome of Schneeheide, whose gravimeter anomaly was previously illustrated in Fig. 7 50a.

In Russia, B. Numerov[133] made a study of the salt deposits near Soli kamsk in the northern Urals and correlated the torsion balance anomalic with well data. The variation of gravity anomaly with salt depth Fig. 7–108) was found to be linear. Numerov used an equation derived

[132] H. Seblatnigg, Mecklenb. Geol. L.-A. Mitt., 49–58 (1930).
[133] B. Numerov, Zeit. Geophys., 5(7), 261–265 (1929).

previously in connection with his experiments on Lake Shuvalovo to express the above relation. The difference in density between salt beds and overburden was assumed to be 0.35.

From 1925 to 1928 extensive gravity measurements were made in the Emba district on the northeast shore of the Caspian Sea.[134] Numerous
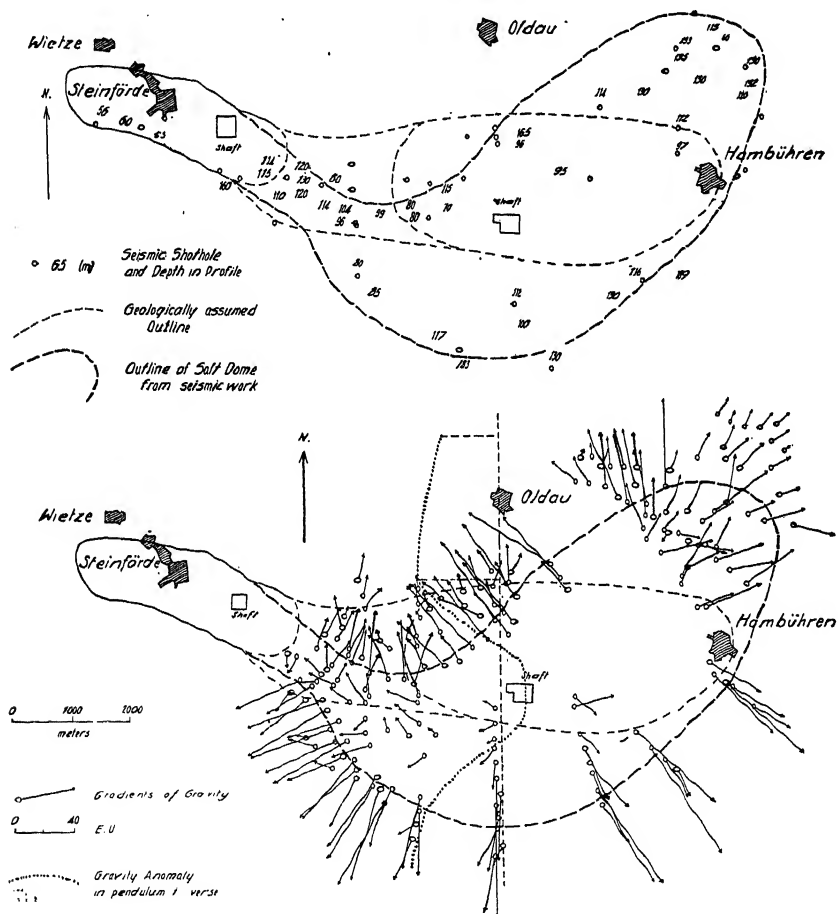
Fig. 7-105. Seismic refraction depths, seismic outline gravity gradients, and gravity profile on Oldau-Hambuehren (Wietze) salt dome in northern Germany.

salt domes have been discovered there by the application of geophysical methods. It appears that the whole region between the Ural and the Volga rivers is fairly studded with salt domes. The Soviets estimated that by 1934 they had discovered more than 400 salt domes by geophysics.

[134] *Ibid.*, 268–270.

Fig. 7–109 shows a small portion of this region between the oil fields of Dossor and Iskin. At Dossor, where the depth to salt is of the order of 400 meters, the gravity anomaly is 31 milligals. Other domes in this area produce anomalies of the order of 15 to 25 milligals. Since 1935, detail

FIG. 7-106. Torsion balance results and geologic section, Lübtheen-Jessenitz salt dome (after Seblatnigg).

work on the geophysically discovered domes has been under way with torsion balance and reflection seismograph.

In another salt dome country, Rumania, the torsion balance has like-wise been very successful. The first measurements there were probably made by W. Schweydar in 1918. Geophysical work of increasing scale was then initiated by commercial companies. In 1928 the Geological

Institute of Rumania began a study of various salt domes and anticlines. The Floreşti salt dome[135] was surveyed with various geophysical methods. It was found to produce a negative magnetic anomaly of the order of 40 gammas and to show distinctly in equiresistivity surveys. Fig. 7–110 represents the gradient and curvature values along a profile across the dome, which is of the mushroom type and is covered with only about 20 meters of terrace gravels of the Prahova River. Further studies of this

Seismos Company
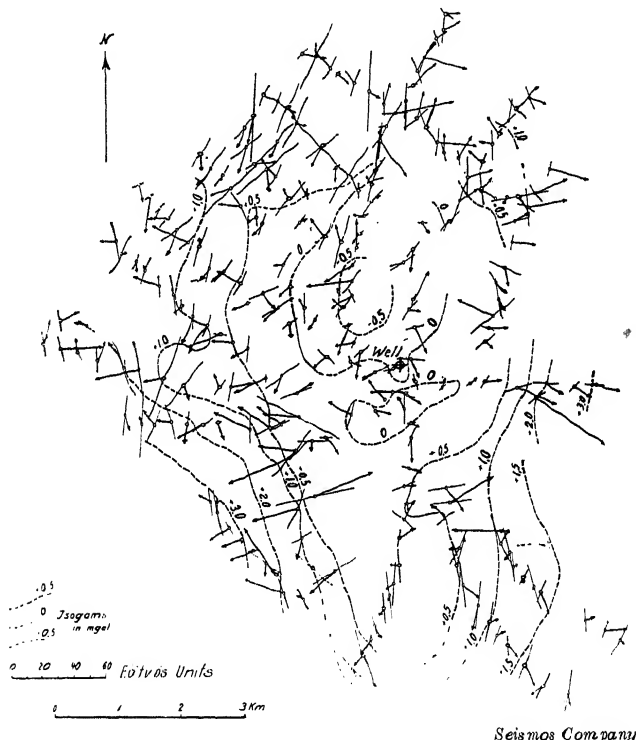
Fig. 7-107. Torsion balance results on (deep-seated) dome of Schneeheide, northern Germany. (Compare with Fig. 7-50a).

and adjacent domes and anticlines were made in subsequent years by the Rumanian Geological Institute.[136] Among those investigated were the domes of Baicoi-Tintea and the anticlines of Bucovul, Filipeşti, Novaceşti, and others between Ploeşti and Targovişte.

The torsion balance was introduced in this country in September, 1922, and used in an experimental survey of the Spindle Top salt dome in December, 1922. The Nash dome was the first to be discovered by the

[135] M. Ghitulesco, 2nd Congr. Internat. de Forage (Paris, 1929).
[136] I. Gavat, Inst. Geol. Roumania Ann., **16**, 683-706 (1934).

torsion balance in the early spring of 1924.   The results of the reconnaissance torsion balance survey were published by Barton.[137]   The dome is of the "shallow" type, its cap coming to within 750 feet of the surface, and it is characterized by a positive gravity anomaly.   In the same year the Long Point dome was found with the torsion balance; in 1925 the Allen, Clemens, and Fannet domes were located.   A study of a previously known dome, Hoskins Mound, was made in 1926 with the object of determining the shape and approximately the sulfur reserves of the cap, which comes within 700 feet of the surface and is about 500 to 600 feet thick.   The interpretation of the torsion balance data (Fig. 7–111) by D. C. Barton[138] is shown for various cap rock sections in Fig. 7–112. The estimated accuracy of prediction was of the order of 10 per cent; larger deviations may occur, since the interpretation furnishes a smooth cap-rock surface while the depth given by drill may correspond to a depression or crevice in the cap.   On the Belle Isle dome, St. Mary's Parish, Louisiana,[139] agreement between prediction and drilling was not nearly so good as at Hoskins Mound because of unfavorable (marshy) terrain. According to Barton, the prediction of depth to top of cap rock was 33 per cent correct and prediction of its thickness only 58 per cent correct.   The specific gravities assumed in the calculations were: 2.2 for the salt and 1.9 to 2.5 for the sediments down to 1600 feet depth; from 1600 to 4400 feet, the density of the salt was assumed to be the same as that of the surrounding sediments.   Torsion balance results have been published for several other *shallow* Gulf coast domes.   The Blue Ridge dome shows the familiar pattern of gradients, indicating a gravity *maximum* over the cap rock, which comes within 100 feet of the surface.[140]   The Moss Bluff dome,[141] whose cap is at a depth of 650 feet while the salt is at a depth of 1170
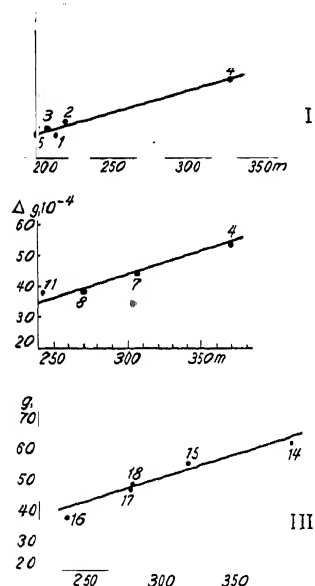
FIG. 7-108. Relation of gravity anomalies and salt depths in Solikamsk district, Russia (after Numerov). I, north of Solikamsk; II, south of Solikamsk; III, near Berezniaky.

[137] D. C. Barton, A.I.M.E. Geophysical Prospecting, 416-466 (1929).
[138] A.I.M.E. Tech. Publ., 719 (1936).
[139] D. C. Barton, A.A.P.G. Bull., 15(11), 1335-1350 (Nov., 1931).
[140] Jack Logan, Oil Weekly, Oct. 11, 1929.
[141] J. B. Eby and R. P. Clark, A.A.P.G. Bull., 19(3), 356-377 (March, 1935).

feet, is indicated by a maximum, surrounded by a minimum, due to the increase in section with depth. Results of fan shooting across this dome are illustrated in Fig. 9-38. Fannet shows a typical maximum but no minimum, and it is assumed to be a dome of nearly vertical sides. The pattern of gradients and curvatures is quite regular; depth to the top of the cap is about 900 feet. Clark and Eby[142] have also illustrated the mag-
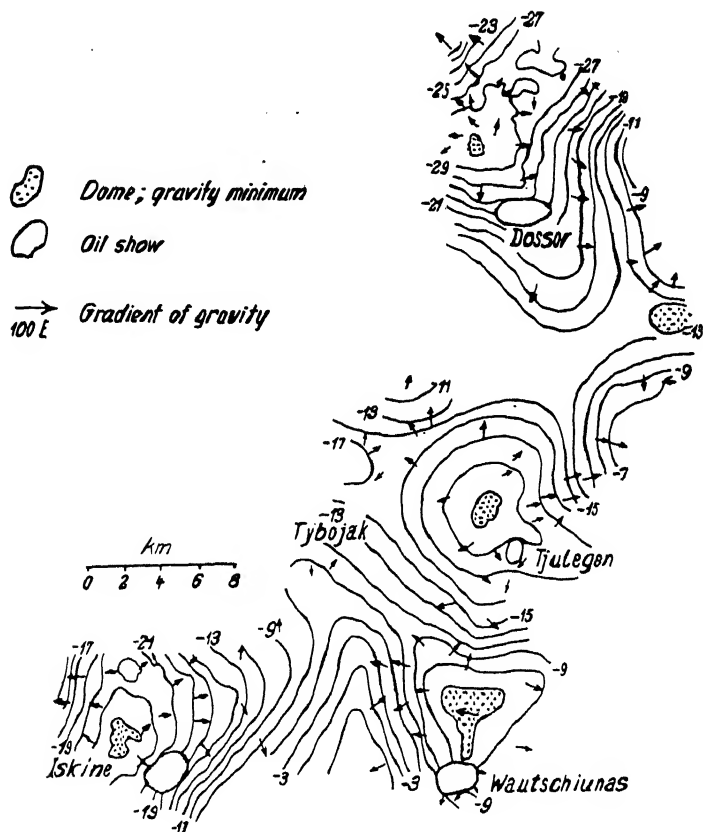
Fig. 7-109. Gravity anomalies between Dossor and Iskin, Emba district, Russia (after Numerov).

netic results for this dome (negative anomaly of about 20 to 25 gammas). The Sugarland dome, for which the torsion balance results have been published by the same authors, is an example of a dome of *moderate* depth, which shows a large minimum and a small maximum. The top of the cap is at a depth of about 3500 feet; salt was encountered at a depth of 4280 feet.

[142] *Ibid.*

Gravity minima *alone* are observed on *deep*-seated domes (depth to cap or salt, 5000 feet or more). An example is the Shepards-Mott dome illustrated in Fig. 7-113. No salt was encountered at depths of 6000 feet. The regional effect is quite large and keeps the gradients from showing the typical reversal. The reflection contour map indicates a closure of 1400 feet. A well-defined gravity minimum has also been found on the Tomball field, showing good closure with and against the regional dip but weak closure in the direction of strike, as is the case in other domes along the Conroe trend. No evidence of salt has been found by drilling.

Fig. 7-114 illustrates the gravity picture of the Esperson dome (discovered by the torsion balance late in 1928[143]) and the geologic section assumed in the interpretation calculations. The gradients are of the order of 2 to 7 E.U.; the gravity minimum on the left is due to the Esperson dome. Because of the interference from the salt mass of the adjoining South Liberty-Dayton dome, a maximum is produced between them. In the calculations, the average density of salt was assumed to be 2.19 and that of the cap rock 2.6. For the sediments the assumptions were: from 0 to 300 feet, 1.9 to 2.05; from 2000 to 4000 feet, 2.20; from
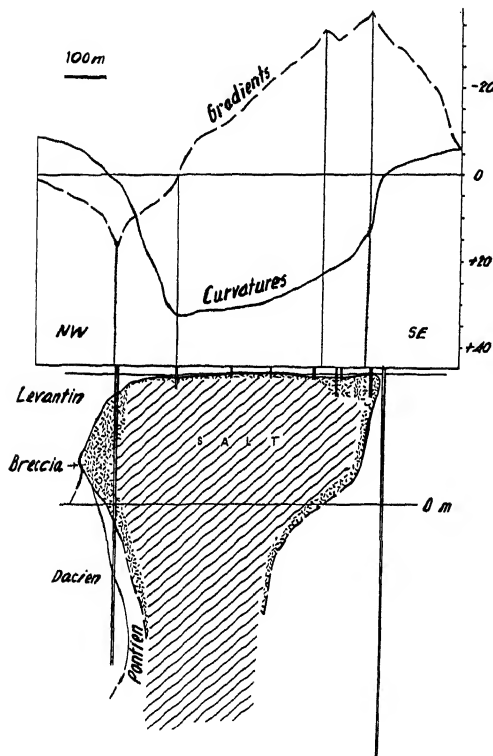
Fig. 7-110. Torsion balance anomalies on Florești salt dome, Rumania (after Ghitulesco).

4000 to 8000 feet, 2.25; from 8000 to 12,000 feet, 2.3. This results in the apparent salt-density differences indicated in the figure. It is seen that a gravity maximum above a dome may be due not only to the effect of the cap but also to that part of the salt which exceeds the density of the surrounding sediments. Such interdomal maxima, as revealed by this survey, may be a source of interpretation difficulties. As a matter of fact, maxima of this

[143] D. C. Barton, A.A.P.G. Bull., **14**(9), 1129–1143 (1930).

type were first confused with the cap effects of moderately deep domes. Drilling these produced only negative results. As shown in Fig. 7–114, interpretation of the Esperson anomaly gave 6000–8000 feet for the top of the salt. It was actually encountered later at a depth of 7000 feet.

In oil exploration the torsion balance has been equally successful in surveys of nonsalt dome-type structures, although fewer results have been published. It was recognized at an early date that *anticlines* and *domes*
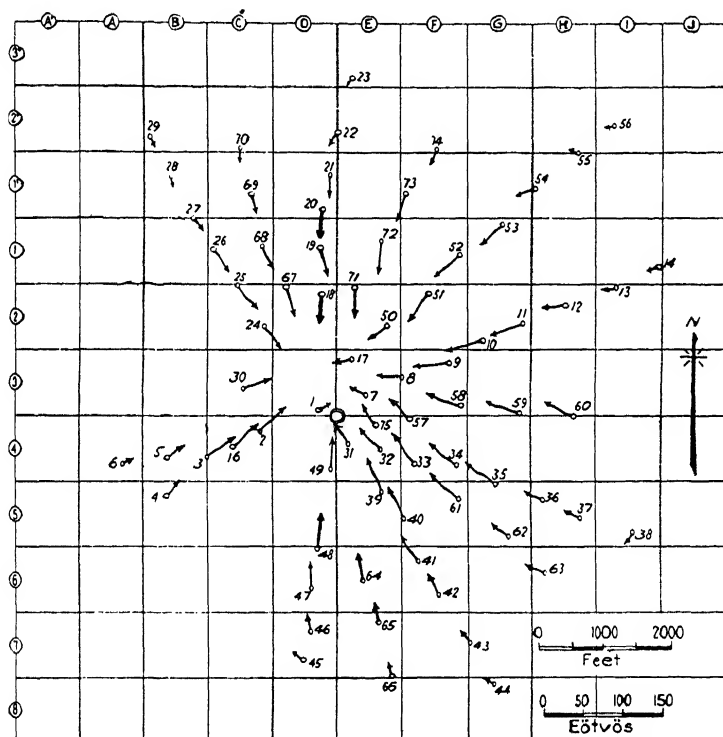
7-111. Torsion balance gradient survey of Hoskins Mound salt dome (after Barton).

with heavier material in their cores would give rise to a positive torsion balance anomaly. Fig. 7–115 shows the results of a survey made in 1915 to 1916 on the Egbell anticline by Eötvös and his associates.[144] The oil occurs in the Sarmatian formations near the surface; denser Eocene and Paleocene formations are assumed in the core of the folds. While the maximum on the Egbell anticline is well defined, the Sasvar dome shows only as a terrace superimposed on the regional gradient. Subsequent

[144] See footnote 130.
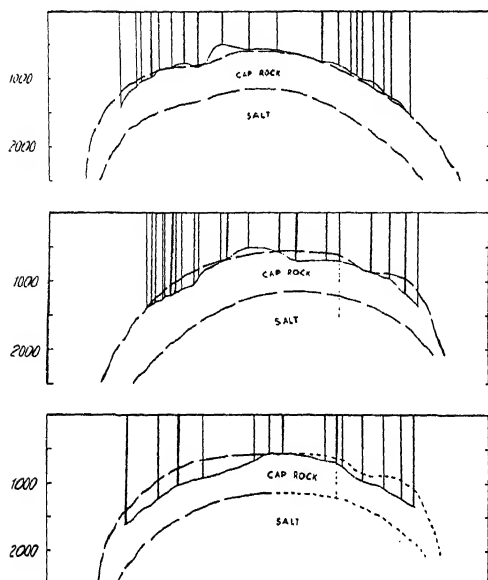
FIG. 7-112. Sections of Hoskins Mound salt dome, showing comparison of torsion balance predictions and results of drilling (after Barton).

torsion balance work on anticlinal structures has been more extensive than the published accounts would indicate. In 1919 and 1920 R. Schumann conducted torsion balance measurements in the Vienna Basin to determine potential oil structure in the Sarmatian formation and to trace the Leopoldsdorf fault.[145] A portion of the torsion balance surveys made on Russian oil structures has been published by Numerov;[146] gravity anomalies in the Grozny oil field (Caucasian fold zone) are shown on the resistivity map of Fig. 10-67. The Grozny and Terek anticlines are indicated by gravity maxima. Results for the Rumanian fields have been discussed
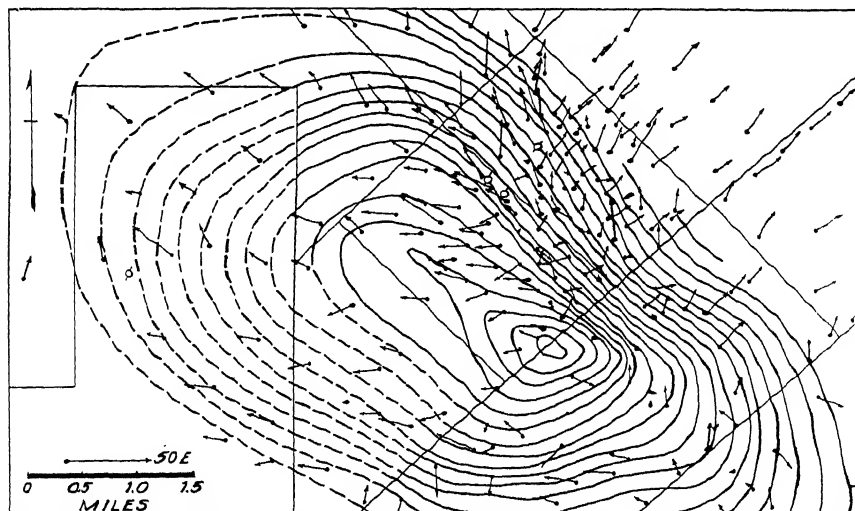
FIG. 7-113. Shepards-Mott dome, reflection seismic and torsion balance survey (after Clark and Eby).

[145] R. Schumann, Montanistische Rundschau, June 1, 1923.
[146] *Op. cit.*, 271.

by Gavat;[147] for anticlines in Persia, by Jones and Davies.[148] A reconnaissance torsion balance survey across the Fort Collins anticline was described by John Wilson.[149]

That the torsion balance is ideally suited for the mapping of the *topography* of *basement* rocks was first recognized by Eötvös himself, whose
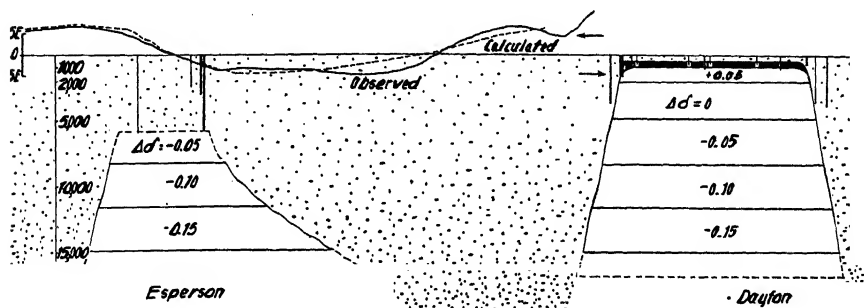
Fig. 7-114. Torsion balance gradient curves (measured and calculated) for the Esperson–South Liberty–Dayton domes, with calculated section (after Barton).
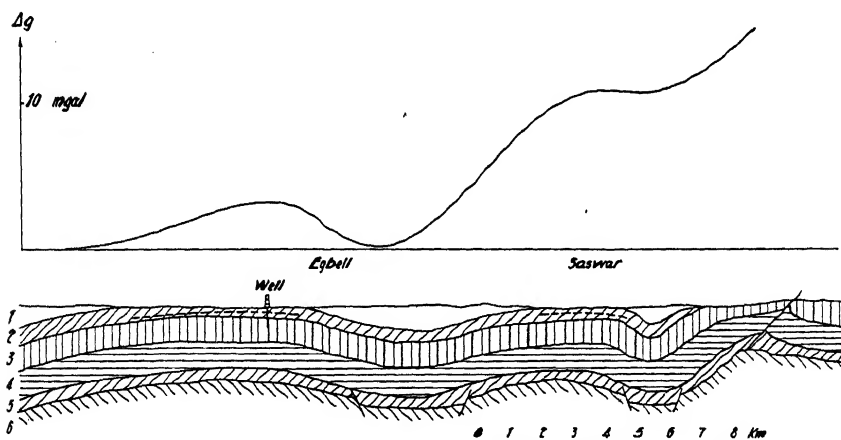
Fig. 7-115. Gravity anomalies (calculated from gravity gradients) on the Egbell and Sasvar domes (Czechoslovakia) (after v. Boeckh). 1. Pontian; 2. Sarmatian; 3. Upper Mediterranean; 4. Schlier; 5. Lower Neocene; 6. Paleocene and Triassic.

classical observations in the Hungarian plain near Arad (begun in 1903 and continued in 1905 and 1906) are too well known to be reproduced in detail. In the Midcontinent fields[150] the torsion balance has been used

[147] See footnote 136.

[148] J. H. Jones and R. Davies, M. N. Roy. Astron. Soc., Geophys. Supp., 11(1), 1–32 (1928).

[149] John Wilson, Colo. School of Mines Magazine, 18(6), 23 (Oct., 1928).

[150] D. C. Barton, A.I.M.E. Geophysical Prospecting, 416–466 (1929).

extensively to map ridges of granite, gneiss, and Cambro-Ordovician rocks.
Examples are the Amarillo granite ridge, the Nocona-Muenster-Bulcher
ridge, the Healdton fields, the Criner hills, the Kansas granite ridges, and
the ridges in Colorado and Nebraska. Some of these appear in the
gravity map of Fig. 7-51b. Barton has reproduced the torsion balance
results for the Muenster-Bulcher ridge,[151] which showed well in the gradient
picture. However, in the Fox area, the Fox and Graham uplifts were
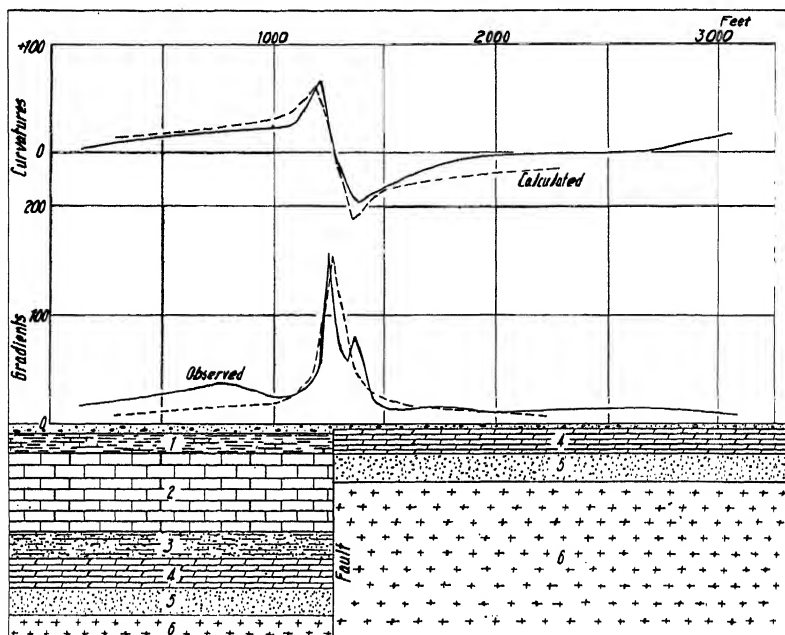
FIG. 7-116. Torsion balance anomalies on Hull-Gloucester fault, Canada (after
A. H. Miller). 1. Shale and limestone under 70' of drift ($\delta = 2.6$); 2. Limestone
($\delta = 2.7$); 3. Chazy shale and sandstone ($\delta = 2.5$); 4. Dolomite ($\delta = 2.8$); 5. Potsdam
sandstone ($\delta = 2.5$); 6. Precambrian ($\delta = 2.8$).

hardly noticeable. Only after considering the regional gradient due to
the adjacent Arbuckle Mountains could a better agreement between struc-
tural and torsion balance data be obtained.

In oil exploration the torsion balance has been widely used for the loca-
tion of *faults*. Eötvös was again first to point out this possibility. The
amount of published data is no measure of the actual scope of work on
fault problems. In 1927 M. Matuyama investigated step faults in Meso-
zoic slate (density 2.5) covered by alluvial material (density 2.0) in the
Kokubu plain near the Sakurazima volcano in Japan.[152] Results obtained

[152] M. Matuyama, Japan. J. Astron. and Geophys., **4**(3), 1–18 (1927).

with torsion balance, magnetic, and electrical methods in an attempt to delineate step-faulted blocks in the Limagne-Graben zone have been published by Geoffroy.[153]

The torsion balance has been rather successful in the Mexia-Luling fault zone. In a profile illustrated by Barton,[154] the Edwards limestone, at a depth of between 1000 and 2400 feet, is in contact with lighter Eagleford, Del Rio, and Austin chalk, while the Eagleford, Del Rio, and Austin are against lighter Taylor and Navarro shales. Hence, the maximum gradient occurs above the subsurface point where this density contrast occurs, that is, down dip in the fault from its surface trace. Two faults in the Paleozoic area near Ottawa were investigated by Miller[155] and
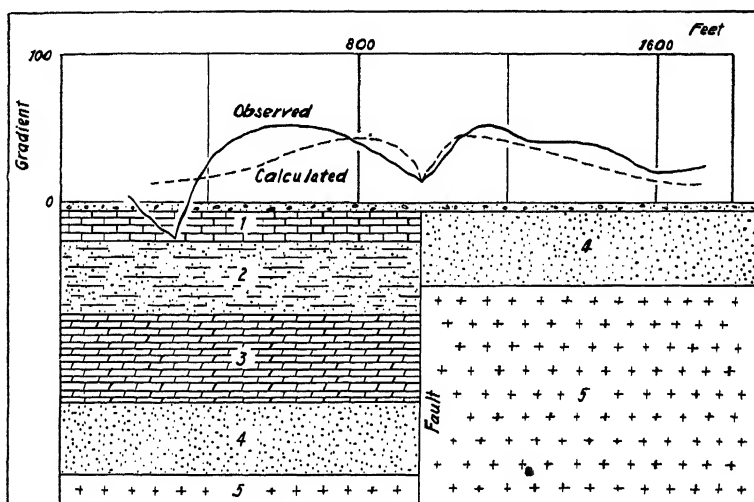
FIG. 7-117. Torsion balance results on Hazeldean fault, Canada (after Miller). 1. Black River, Chazy limestone ($\delta = 2.7$); 2. Chazy shale and sandstone ($\delta = 2.5$); 3. Beekmantown dolomite ($\delta = 2.8$); 4. Potsdam sandstone ($\delta = 2.5$); 5. Precambrian ($\delta = 3.0$).

showed a distinctly different response. The Hull-Gloucester fault near Leitrim (Fig. 7-116) in the Paleozoic and Pre-Cambrian has a 900 foot displacement and produces large gradients (about 150 E.U.) because of a near-surface contrast in density. Theoretical values calculated for an assumed subsurface section agreed well with the experimental results.

In the same Paleozoic section the Hazeldean fault (575 foot displacement) gave a distinctly different picture. A "minimum" gradient was observed, since the effects of the lower beds (density contrast in upthrow direction) are overcompensated by a near-surface effect of density contrast

[153] M. P. Geoffroy, Ann. Office Nat. Comb. Liqu., 4, 617–647 (1929).
[154] D. C. Barton, A.I.M.E. Geophysical Prospecting, 416–466 (1929).
[155] A. H. Miller, Canad. Geol. Survey Mem., 165, 197–208 (1931).

in down-throw direction (Fig. 7–117). The Pentland fault near Porto-
bello in the Edinburgh district was investigated by McLintock and Phem-
ister[156] (Fig. 7–118). This overthrust fault dips toward the west and
separates a series of volcanic beds of 500 feet thickness and of east dip
from the oil shale group of sedimentaries in the east; hence, a westward
tendency of gradients is produced. A satisfactory agreement of theo-
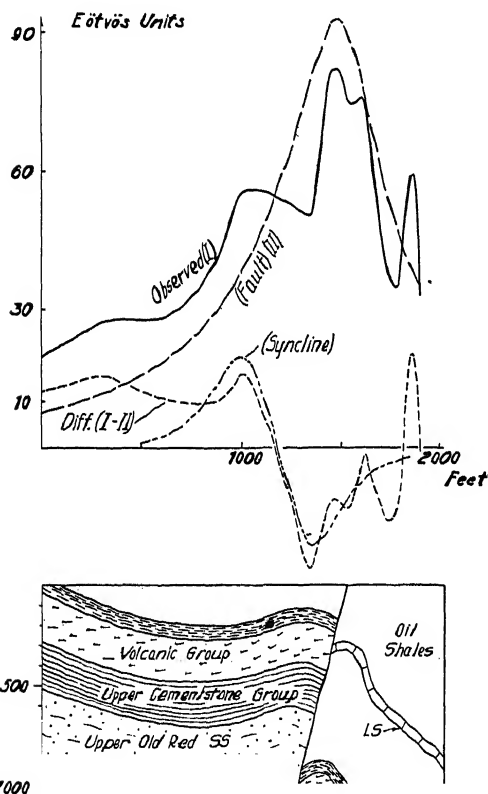
FIG. 7–118. Torsion balance results on Pentland
fault (after McLintock and Phemister).

retical and experimental
values was obtained by
assuming a block with in-
clined face, 0.42 difference
in density, beginning at a
depth of 100 feet, and hav-
ing a superimposed syncline
west of the fault in the lava
beds.

At Dossor (see Numerov,
footnote 134) S. Mironov
investigated a fault on the
west side of the field,
separating the Senonian
from (productive) Jurassic
beds overlying Permo-Tri-
assic and salt formations.[157]
Matuyama and Higasin-
aka[158] determined the tor-
sion balance anomalies of
a fault of 70 meters dis-
placement in the Takumati
oil field, and Vajk[159] dis-
cussed a survey in South
America where a maximum
in the gradients and curva-
tures could be explained
by either an anticline or a
normal fault.

3. *Applications in mining.* Although Eötvös made some experiments
with the torsion balance and magnetic instruments on igneous dikes, it is

[156] W. F. P. McLintock and James Phemister, Great Britain, Geol. Survey, Summ.
of Progr., pt. II, 10–28 (1928).

[157] S. Mironov, Geol. Comm. Vestnic, No. 5 (Leningrad, 1925).

[158] M. Matuyama and H. Higasinaka, Japan. J. Astron. and Geophys., VII(2),
47–81 (1930).

[159] R. Vajk, World Petrol. Congr. Proc. B I, 140–142 (London, 1933).

not known whether he actually investigated any ore deposits. His associate, Stephen Rybar, surveyed the contact-metamorphic iron ore deposits of Banat in Rumania around 1917. In 1919 R. Schumann mapped the area near Zillingdorf north of Vienna to determine the structure of the coal deposits there. In Russia the torsion balance was used by P. Nikiforov, Lasareff, and Gamburzeff in connection with the magnetic survey of the Kursk anomaly.[160] Several torsion balance profiles across this deposit are illustrated in Chapter 8 (Fig. 8-59). The gradients reach a maximum amplitude of 80 and the curvature values an amplitude of 130
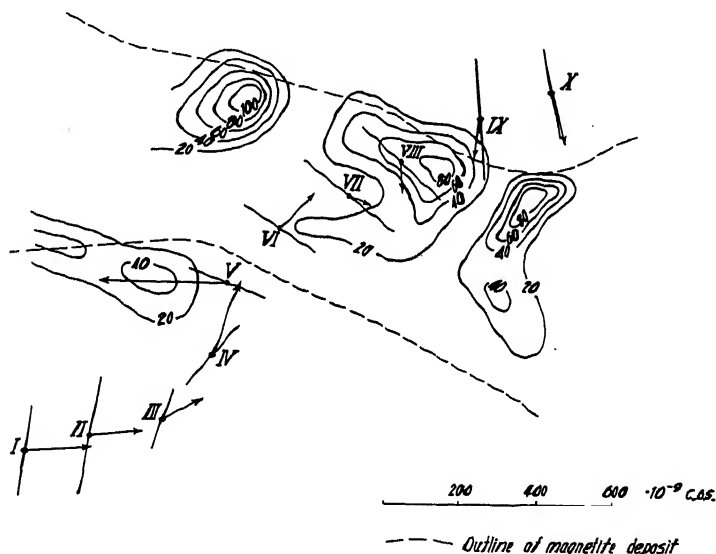
FIG. 7-119. Torsion balance results on Caribou magnetite deposit, Colorado.
(Scale same as in Fig. 7-76)

E.U. and can be explained on the assumption of a density difference of 0.8 between the iron quartzite and the surrounding metamorphic rocks. The Swedish investigators, H. Lundberg, K. Sundberg, and E. Eklund,[161] have used the torsion balance in conjunction with electrical and magnetic surveys and published the results of a reconnaissance survey on Mensträsk Lake.

In Germany the torsion balance was tried at about the same time on some siderite veins of the Siegerland district.[162] Matuyama investigated

[160] P. Lasareff and G. A. Gamburzeff, Gerlands Beitr., **15**(1), 71–89 (1926), **19**(**2/3**), 210–230 (1928).

[161] Sveriges Geol. Unders. Årsbok, **17**(**8**), 86 (1925).

[162] H. Quiring, Glueckauf, **59**, 405–410 (1923).
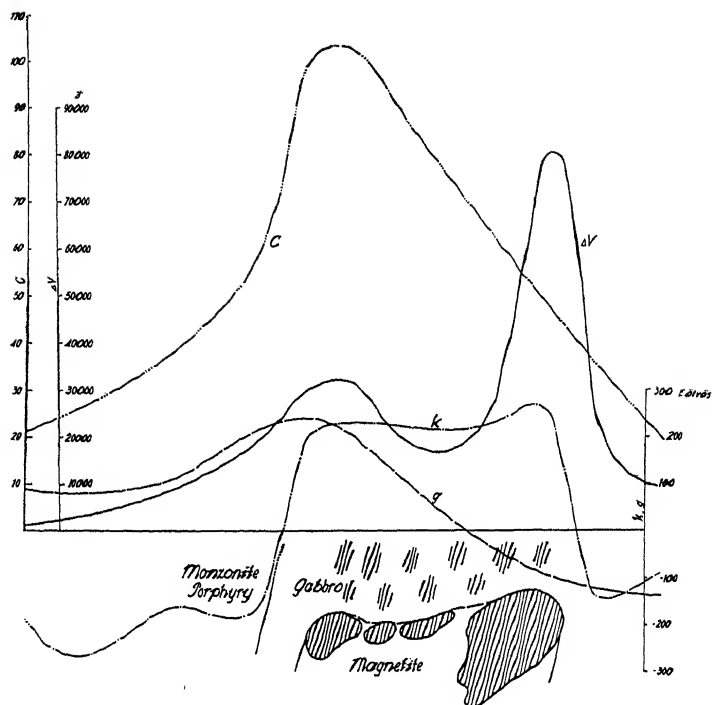
FIG. 7-120. Gravimetric, magnetic, and electrical indications on Caribou magnetite deposit. G, gradients; K, curvature values; ΔV, magnetic vertical intensity; C, rel. conductivity.
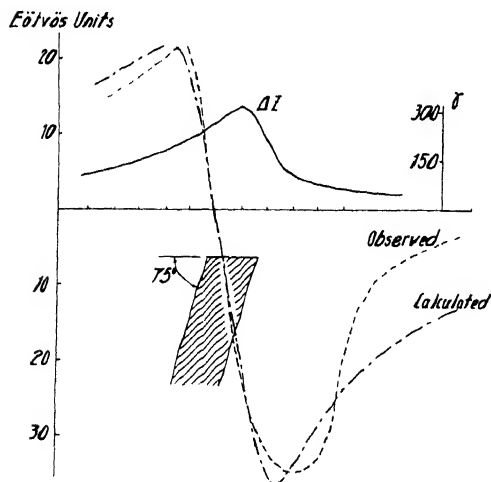
α. 7-121. Torsion balance and magnetic anomaly (ΔZ) on Swynnerton dike (after McLintock and Phemister).

the vicinity of the Fushun Colliery and located a fault separating gneiss from sedimentary rocks.[163] Whether the coal seams were indicated remained doubtful on account of terrain interference. Shaw and Lancaster-Jones conducted a reconnaissance survey across a barite deposit about 50 feet in depth, which was known from underground workings.[164] Mason observed a

[163] Op. cit., 2 (2), 91–106 (1924).
[164] H. Shaw and E. Lancaster-Jones, Mining Mag., Jan. & Feb., 1925.

moderate anomaly of 20 to 30 Eötvös amplitude on the well-known Falconbridge ore body in Canada.[165]   In the Tri-State district the torsion balance was tried with the hope of locating lead-zinc ores directly.[166] However, it was possible only to outline the (lighter) chert pockets in limestone in which the ore bodies occur.

Fig. 7–119 shows torsion balance results obtained by the author at Caribou, Colorado, on a magmatic differentiation type of magnetite deposit in gabbro.   Despite unfavorable terrain conditions indicated in Fig. 7–76, the torsion balance indicates the individual concentrations
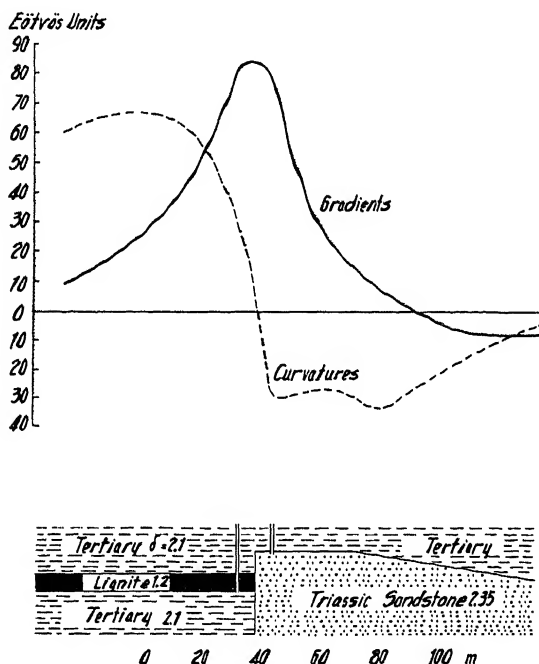
Fig. 7-122. Gradients and curvature values above lignite deposit bounded by sandstone fault block (after Seblatnigg).

(accompanied by magnetic anomalies ranging from 20 to 100,000 gammas) rather satisfactorily.   Fig. 7–120 gives average curves for the gradients and curvatures across this deposit and also illustrates results of magnetic and electrical investigations.   Fig. 7–121 indicates the results of a torsion balance traverse made by McLintock and Phemister[167] across a dike of

[165] M. Mason, Geophysical Exploration for Ores, A.I.M.E. Geophysical Prospecting, 9–36 (1929).

[166] P. W. George, A.I.M.E. Geophysical Prospecting, 561–571 (1929).

[167] W. F. P. McLintock and J. Phemister, Mining Mag., Dec. 1927.

nepheline basalt in Triassic Keuper marls. The vertical intensity anomaly is shown for comparison. In 1926 and 1927 the torsion balance was used in the investigation of magnetite deposits of Krivoj-Rog in southern Russia in connection with magnetic surveys.[168] Two cases are known where the torsion balance has been applied indirectly in the mapping of lignite deposits. The deposit shown in Fig. 7–122 occurs in Tertiary beds[169] (density 2.1) and is bounded on one side by Triassic sandstone (density 2.35). Hence, it was possible to outline it by locating the edge
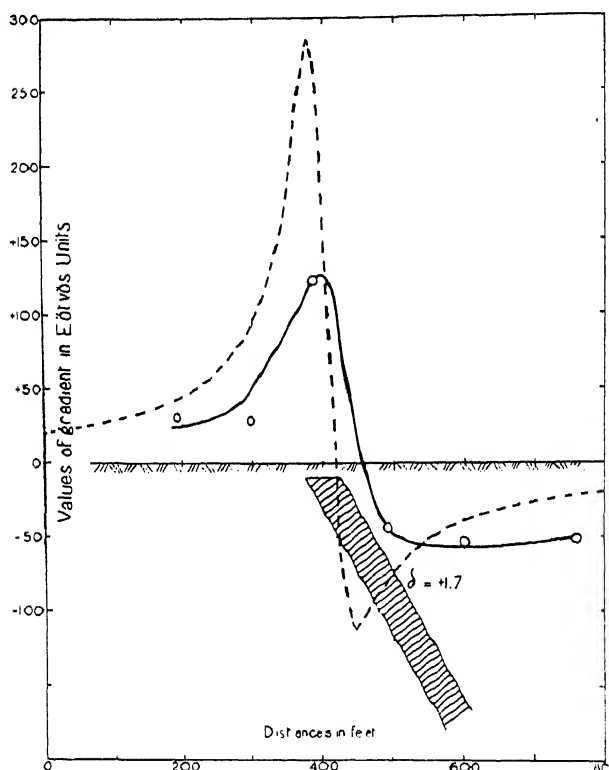
Fig. 7-123. Torsion balance survey of Caldwell pyrite deposit (after Miller). Solid curve, observed; dotted, calculated anomaly.

of the sandstone block. Edge and Laby have published a survey of similar character.[170] In the Gelliondale field in southeast Victoria the lignite bed occurs in horizontal stratification in sandy beds about 100 feet from the surface. Since it is terminated by the sloping surface of

[168] P. Nikiforov and others, Inst. Pract. Geophys. Bull., **4**, 299–307, 315–330 (1928).
[169] H. Seblatnigg, Braunkohle, No. 23 (1929).
[170] Edge and Laby, *Principles and Practice*, etc. (Cambridge Univ. Press, 1931)

denser Jurassic rocks, it could be outlined by mapping bedrock topography. In one of the profiles the lignite did not come up against the edge of bedrock. A *broad* gradient maximum, due to the superimposed effect of the lignite edge and the sloping bedrock surface nearby, was observed.

The torsion balance is also useful for outlining placer channels. Edge and Laby investigated a portion of the Gulgong field in New South Wales with the object of determining the edge of a sloping channel filled with alluvial strata, underlain by granite. (Seismic data for this field are shown in Fig. 9–41.) A similar application of the torsion balance was
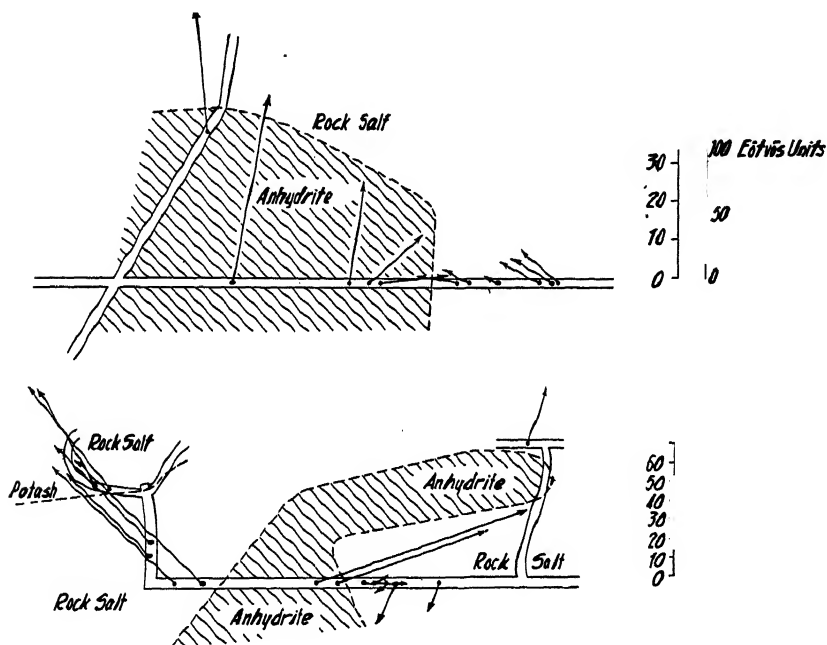
Fig. 7-124. Underground torsion balance observations at Beienrode, Germany (after Birnbaum).

made by McLintock and Phemister[171] who surveyed the buried channel of the Kelvin River near Drumry. Surveys of salt deposits have been made not only in connection with oil exploration but also for mining purposes. An example is A. H. Miller's survey of the Malagash salt deposit,[172] which revealed a dome-shaped anomaly of 3 milligal maximum amplitude. The thickness of the salt is about 300 feet. Fig. 7–123 shows a

---

[171] W. F. P. McLintock and J. Phemister, Roy. Soc. (Edinburgh) Trans., **56**(1), 141–155 (1929).

[172] A. H. Miller and G. W. H. Norman, A.I.M.E. Tech. Publ., No. 737 (1936).

torsion balance survey of the Caldwell (Renfrew Co., Ontario) pyrite deposit.[173] The theoretical curve (based on the assumption of a density difference of 1.7, a thickness of the deposit of 50 feet, depth 20 feet, and dip 60 feet) is likewise shown. Since it is calculated under the assumption of a two-dimensional body, its amplitude exceeds that of the experimental curve.

A number of attempts to use the torsion balance *underground* have been made and published. The earliest survey of this kind was made with a curvature variometer by Brillouin in the Simplon tunnel in 1905. Subsequent experiments indicate that gradient observations are more suitable underground. A. Birnbaum[174] made some torsion balance observations on two levels of the Beienrode potash mine in Germany. As shown in Fig. 7-124, the gradients point toward the anhydrite in the 700 foot level but
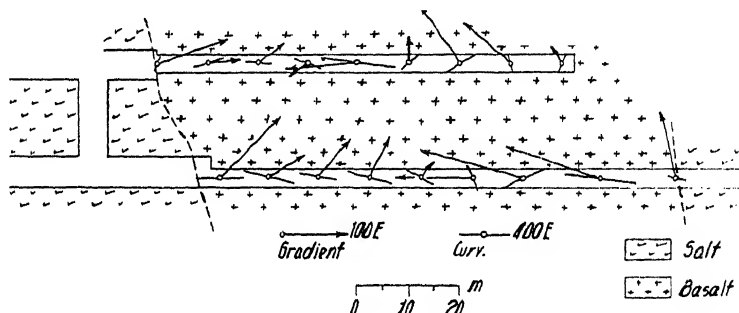
Fig. 7-125. Underground torsion balance measurements on basalt dike in salt (after Meisser and Wolf).

away from it in the 1000 foot level, this indicating that its major portion is located below the 700 and above the 1000 foot level. A rather unusual occurrence of basalt (density 3.0) in salt (density 2.2) was investigated by Meisser and Wolf[175] 700 meters below the surface. Supplementary measurements of magnetic vertical intensity and seismic propagation speed were made at the surface and underground. The thickness of the basalt varied from 0.4 to 90 meters. As Fig. 7-125 indicates, its major portion occurs below the 700 meter level. As has been emphasized by Kumagai,[176] the effects underground are so large that the sensitivity of the instrument must be reduced; otherwise, its starting azimuth must be so selected that the effects of the adjacent tunnel walls are at a minimum.

[173] A. H. Miller, Canad. Geol. Surv. Mem., 170(3), 99-118 (1930).

[174] A. Birnbaum, Kali, 18, 144-148 (1924).

[175] O. Meisser and F. Wolf, Zeit. Geophys., 6(1), 13-21 (1930).

[176] N. Kumagai, Japan. J. Astron. Geophys., 9(3), 141-206 (1932).

8

MAGNETIC METHOD

I. INTRODUCTION

T<small>HE</small> <small>MAGNETIC</small> method of prospecting is one of the oldest geophysical methods. It was applied to the location of ore bodies as early as 1640. Like gravitational methods and in contrast to electrical and seismic methods, it utilizes a natural field of force, consisting of the field of geologic

<center>(a)   (b)</center>
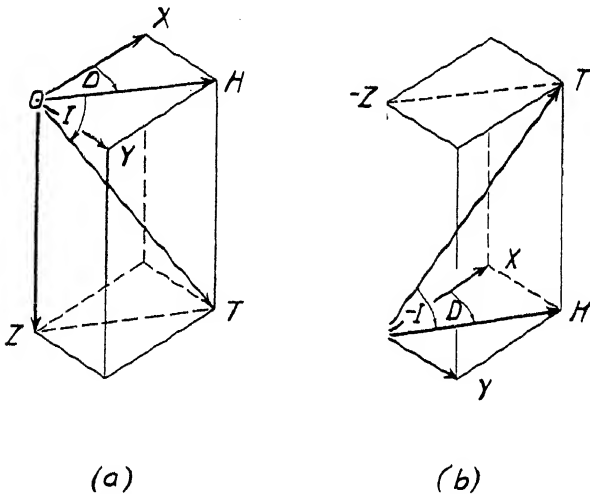
F<small>IG</small>. 8-1. Vector diagram of the earth's magnetic field (a) for the northern hemisphere, (b) for the southern hemisphere.

bodies and the terrestrial magnetic field. Contrary to their gravitational attraction (which exists independently of the earth's gravity field), the magnetic reactions of geologic bodies frequently depend on direction and magnitude of the earth's field. The law controlling magnetic attraction (Coulomb's law) is identical in form with that governing gravitational attraction. Hence, magnetic interpretation problems may often be handled by a simple adaption of the relations which apply in gravitational work. Because of the spontaneous nature of subsurface effects, it is not possible to control the depth of penetration in magnetic prospecting.

<center>293</center>

SYMBOLS USED IN CHAPTER 8

a	distance		
c	constant		
d	diameter, distance, depth		
e	distance		
e/m	specific electron charge		
f	frequency	f	focal length
g	gravity		
h	thickness, height		
i	dip, angle	i	number
k	gravitational constant	k	deflection constant
l	length		
m	mass	m	pole strength
n	revolutions per second	n	number
p	percentage	p	coefficient
		q	coefficient
r	distance	r	reluctance
s	reading	s	direction
t	time	t	thickness
v	volume	v	velocity
x	coordinate	x	force component
y	coordinate	y	force component
z	coordinate	z	force component
		A	magnetization component
		B	induction
C	constant	C	magnetization component
D	couple	D	declination
		E	voltage
F	force	F	field
		G	galvanometer constant
		H	(horizontal) intensity
I	current	I	inclination
		$\mathcal{J}$	intensity of magnetization
L	length		
M	magnetic moment	M	mutual inductance
		$\overline{M}$	magnetomotive force
N	turns		
N_0	turns per unit of length	N	demagnetizing factor
Q	weight	Q	quantity of electricity
R	radius	R	resistance
S	anomaly	S	surface, area
$T.C.$	temperature coefficient	T	total intensity
U	potential		
V	potential		
		X	north component
		Y	east component
		Z	vertical component
α	azimuth		
β	angle		
γ	angle		
γ	10^{-5} gauss	γ	coefficient
Γ	gauss		
δ	angle	δ	density
Δ	anomaly		

SYMBOLS USED IN CHAPTER 8—*Concluded*

ϵ	scale value		
ζ	angle		
η	angle		
θ	angle		
Θ	temperature		
ι	angle		
κ	susceptibility		
λ	angle, longitude		
μ	magnetic temperature coefficient	μ	permeability
ξ	angle		
ρ	distance		
σ	scale unit of level		
τ	torsion coefficient		
φ	angle		
Φ	flux		
ψ	angle		

Further, in order to be detectable, the size of geologic bodies has to increase in proportion to depth.

The magnetic field of the earth and of geologic bodies is uniquely defined by the magnitude and direction of the total intensity vector. In practice it is preferable to resolve the field into its components which, in the direction of the vector, are the *horizontal* and *vertical* intensities. In high or intermediate latitudes of the northern and the southern hemispheres, measurements of the vertical component are most frequently made but are occasionally supplemented by horizontal intensity observations in the magnetic meridian or at right angles to the strike of geologic bodies. Fig. 8–1 is a vector diagram of the earth's magnetic field for both hemispheres. T is the total intensity, H is the horizontal and Z the vertical component; D is the declination and I the inclination. H may be resolved into X (the north) and Y (the east) components. The following relations exist between these components:

$$
\left.
\begin{aligned}
&\mathbf{X} = \mathbf{H} \cos \mathbf{D}; \qquad \mathbf{Y} = \mathbf{H} \sin \mathbf{D}; \qquad \mathbf{Z} = \mathbf{H} \tan \mathbf{I} = \mathbf{T} \sin \mathbf{I}; \\
&\qquad\qquad \mathbf{H} = \sqrt{\mathbf{X}^2 + \mathbf{Y}^2} = \mathbf{T} \cos \mathbf{I}; \\
&\quad \mathbf{T} = \sqrt{\mathbf{X}^2 + \mathbf{Y}^2 + \mathbf{Z}^2} = \sqrt{\mathbf{H}^2 + \mathbf{Z}^2} = \mathbf{H}/\cos \mathbf{I} \\
&\tan \mathbf{I} = \mathbf{Z}/\mathbf{H} = \mathbf{Z}/\sqrt{\mathbf{X}^2 + \mathbf{Y}^2}; \qquad \tan \mathbf{D} = \mathbf{Y}/\mathbf{X}.
\end{aligned}
\right\} \quad (8\text{-}1)
$$

The unit of measurement in magnetic exploration is the gauss[1] (Γ) ($\mathrm{cm}^{-\frac{1}{2}} \cdot \mathrm{g}^{\frac{1}{2}} \cdot \mathrm{sec.}^{-1}$) which, by definition,[2] is numerically equal to 1 dyne.

---

[1] See footnote 3, p. 298.

[2] Field intensity equals force on unit magnetic pole. Another definition for the gauss unit which follows from the discussion on p. 298 is the field strength, or magnetomotive force per unit of length, inside a long coil with 0.796 ampere turns per cm. According to the definitions introduced between eq. (8-3) and (8-4), field intensity in gauss also equals the number of magnetic lines of force per square cm in air.

Magnetic anomalies are frequently expressed in gammas (γ); $1\gamma = 1.10^{-5}$ gauss. There is an immense variety of instruments and methods for the measurement of magnetic field components, both angles and intensities. The intensity measurements are of greater practical importance and are readily made with the required accuracy. In magnetic prospecting this is almost 1/10,000 part of the field while in gravity work it is 1/1,000,000 to 1/10,000,000 part. Therefore, commercially satisfactory magnetic instruments may be designed with comparative ease.

Like many other geophysical methods, magnetic exploration had its origin in methods of observation and research employed in earth physics. While in terrestrial magnetic research the main objective of measurement is the regional distribution of the earth's field and its time variation, magnetic exploration is concerned more with the determination of local variations and their geologic significance. The time variations are merely of secondary importance, since magnetic field observations must be corrected for them to attain sufficient accuracy.

As in other geophysical methods, sufficient contrasts in the physical properties of subsurface formations must exist to make the magnetic method applicable. The properties here involved are the induced and remanent magnetization. Geologic formations are either very strongly or very weakly magnetic; this magnetic classification coincides almost exactly with the divisions of igneous and sedimentary rocks. The magnetization of a rock is usually proportional to its magnetite content. Compared with other physical properties, rock magnetization shows a greater irregularity which is due not only to the bi-polar nature of magnetism but to the frequently unpredictable effects of thermal and mechanical changes in the course of their geologic history.

Since most magnetic anomalies are due to igneous rocks, iron ores, and sedimentary formations which have derived their magnetite content from igneous rocks, magnetic methods can be applied *directly* to the location of magnetic minerals and ores, and *indirectly* to the location of deposits which are associated with magnetic rocks and formations. In oil exploration, applications of magnetic methods in structural investigations include the mapping of *buried hills* usually composed of igneous or metamorphic rocks; the location of *anticlines* where magnetic basement members are uplifted, together with the sedimentaries, and where some of the sediments themselves are magnetic (or contain interbedded members of igneous origin); lastly, the mapping of *salt domes* if they are surrounded by magnetic formations. The location of *faults* is important in both oil and mining applications and is possible if magnetic members are displaced, if the fault fissure contains igneous sheets, or if the adjacent formations have different mag-

netic characteristics. Another structural application which is important in oil and mining exploration is the mapping of igneous intrusions, igneous dikes, and contact-metamorphic zones. In mining, magnetic methods are frequently applied to the location of magnetic *iron ores*, magnetite, and hematite, as well as to *nonmagnetic ores* if they are associated with magnetite or pyrrhotite, or are contained in lava flows. Concentrates of *noble minerals* (gold, platinum) may be found if they are associated with magnetite in placers. In engineering, magnetic prospecting has been used to locate buried magnetic objects, ammunition, pipe lines, and the like.

Experience obtained in the past ten to fifteen years with magnetic prospecting indicates that it is probably the simplest, least expensive, and fastest geophysical method, that it may yield quantitative results provided conditions are suitable, but that it must be supplemented and even replaced by other geophysical methods where the structural consistency of the anomalies is doubtful.

II. MAGNETIC ROCK PROPERTIES

A. DEFINITION

The magnetization of rocks differs from other physical rock properties in one fundamental respect: it is composed of two phases; one remains the same regardless of orientation of a specimen, while the other reverses its sign when the specimen is reversed. The former is called the induced, the latter the remanent magnetization. In rocks the remanent magnetism may be a fraction of the induced magnetization or it may exceed it. Separation of the two magnetizations does not suggest that different physical phenomena are involved. On the contrary, they may both be obtained from a single test involving the tracing of the familiar "hysteresis" curve. Although it is impossible to separate the two magnetizations in the field, their approximate proportions must be known for a complete interpretation of magnetic data.

The strength of the induced magnetization is customarily defined by the *permeability* of the material or a related quantity, the magnetic *susceptibility*. Their physical significance is best understood by the familiar analogy of the magnetic and electrical circuits. The magnetomotive force in a magnetic circuit (measured in gilberts) is analogous to the electromotive force in an electrical circuit. If the magnetomotive force is produced by a solenoid of N turns with I amperes, it is $0.4\pi NI$, and 1 gilbert = 0.796 ampere turns. The current in an electric conductor corresponds, in a magnetic body, to the *flux* Φ, measured in maxwells, or lines of force. The electric resistance is analogous to the magnetic reluctance

(r). The units corresponding to the ohm are the oerstedt[3] (gilberts per maxwell) and the rel (ampere turns per maxwell, or 1.257 oerstedts). The reciprocal of resistivity corresponds, in a magnetic circuit, to the reciprocal of reluctivity (reluctance for unit dimension) and is called "permeability," μ. Hence, for a magnetic conductor of length l and area S, the reluctance

$$\mathbf{r} = \frac{l}{S\mu} \tag{8-2}$$

and the flux $\Phi = \dfrac{\overline{M}S\mu}{l}$ so that

$$\frac{\Phi}{S} = \mu \cdot \frac{\overline{M}}{l}, \tag{8-3}$$

where $\overline{M}$ is magnetomotive force. This equation states that *flux density is equal to permeability times magnetic potential gradient.* It is analogous to equation (10–5), which indicates that electric current density is equal to conductivity times electrical potential gradient.

The magnetic potential gradient is the magnetic field intensity **H**, measured in gilberts per centimeter, or gauss.[4] The flux density Φ/S is called induction, designated by the symbol **B**, and measured in maxwells per cm^2, or also in gauss. Hence from (8–3)

$$\mathbf{B} = \mu\mathbf{H}. \tag{8-4}$$

The permeability in vacuo is 1. Bodies which increase the number of field lines per unit area have permeabilities greater than 1 and are called paramagnetic, while those of permeabilities less than 1 are diamagnetic. Since a unit pole radiates 4π lines of force, $\Phi = 4\pi\mathbf{m}$ where **m** is pole strength. Further, the flux in the magnetized substance may be considered to be the sum of the flux due to the substance alone and the flux in air. Recalling that $\mathbf{B} = \mu\mathbf{H}$ and that for air $\mu = 1$, we have for the flux per unit area

$$\mathbf{B} = \frac{4\pi\mathbf{m}}{S} + \mathbf{H}. \tag{8 5}$$

The ratio $\mathbf{m}/S$ is the surface density of magnetization or *intensity of magnetization* and designated by the script letter $\mathcal{I}$. It is also the *magnetic*

---

[3] As far as the geophysicist is concerned, the ruling of the International Electrotechnical Commission at Oslo in 1930 created no little confusion by adopting the name oerstedt for gauss. Since the gauss unit for field intensity is so firmly entrenched in the geophysical literature, very few geophysical authors since 1930 have adopted the new unit.

[4] See footnote, p. 295.

moment of the unit of volume and proportional to the generating field:

$$\mathfrak{J} = \kappa \mathbf{H} \tag{8-6}$$

where the proportionality factor is the magnetic *susceptibility*. Substituting (8-6) in (8-5) and dividing by H, $\mu = 1 + 4\pi\kappa$ so that

$$\kappa = \frac{\mu - 1}{4\pi}. \tag{8-7}$$

A body has the unit of susceptibility when its unit of volume receives the moment 1 by the field 1. The susceptibility of vacuum is zero. Paramagnetic substances have positive susceptibilities, diamagnetic substances, negative. Since only the strongest magnetic minerals approach the unit of susceptibility, it is customary to employ 1 millionth part of this unit in practical work.

Magnetic susceptibility and permeability are not constants but depend on the strength of the magnetic field. It is customary to plot the induction B or the intensity of magnetization $\mathfrak{J}$ as function of field strength. Flux density is generally measured in maxwells per cm^2 or kilo-lines per square inch (1 kilo-line per square inch = 155 maxwells per square cm, or gauss). It is also obtained from the intensity of magnetization by multiplication with 4π. Field intensity is measured in gauss or ampere turns per inch (1 ampere turn per inch = 0.495 gauss).

A graph showing the magnetization as function of (positive and negative) fields is known as *hysteresis* curve (Fig. 8-2). *OA* is the virgin portion obtained after a specimen has been demagnetized. When the field strength is decreased (after the specimen is magnetized to saturation), this curve is not retraced. Hence when the field strength is zero, the induction is not zero and retains the value *OB*, which is the *remanent* or residual magnetization. The negative field required to reduce the magnetization to zero is the coercive force, *OC*. When the field is further increased in the negative direction, the reflected curve is obtained.

B. Methods of Determining Rock Magnetization

Rock specimens are usually given a preliminary test to determine the proportions of residual and induced magnetization. Next, their susceptibility may be measured at field strengths equal to those of the earth's field components. Further tests involve measurements of susceptibilities at higher field strengths, that is, investigations of complete hysteresis curves.

1. For a *preliminary determination* of the induced and remanent magnetization, the rock sample is placed close to a magnetometer and the deflection at distance r is noted. Then the sample is rotated through 180

degrees (keeping its distance from the magnetometer the same), and the deflection is again observed.

If the specimen is placed in the first Gauss position (that is, the magnetic needle in the extension of the magnet) with respect to the magnetometer, if its equivalent magnetic moment is $M = \mathcal{G}v$, where v is its volume and $\mathcal{G}$ the intensity of magnetization, the apparent change in magnetic intensity is $\epsilon(s - s_0) = \Delta H = 2M/r^3$, so that

$$s - s_0 = c\mathcal{G}, \qquad (8\text{-}7)$$

where $c = 2v/\epsilon r^3$, ϵ is the scale value (see page 323), s_0 is the reading without the specimen, and s the reading with the specimen. If residual magnetism
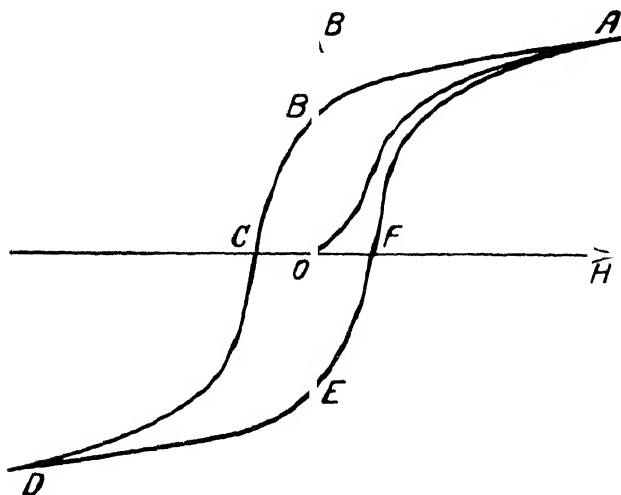
Fig. 8-2. General hysteresis curve.

is present, its component in the longitudinal direction of the specimen will be added to the induced magnetism (reading: s_1). After the specimen has been reversed, the component of permanent magnetization opposes the induced magnetization (reading: s_2). Then with $\mathcal{G}_i$ as the induced, and $\mathcal{G}_r$ as the residual magnetization:

$$c\mathcal{G}_i = \frac{s_1 + s_2}{2} - s_0$$

and

$$c\mathcal{G}_r = \frac{s_1 - s_2}{2}. \qquad \left.\begin{matrix} \\ \\ \\ \\ \\ \end{matrix}\right\} \quad (8\text{-}8)$$

2. *Quantitative determinations of induced magnetization* may be made after residual and induced magnetizations have been separated. It is conven-

ient to determine the induced magnetization and hence the susceptibility in the earth's field since the specimens are then tested in the laboratory under the same conditions as prevail in nature.

In the so-called *test-tube method*, the sample is pulverized, placed into a test tube of known volume, and suspended near the needle of a unifilar magnetometer as shown in Fig. 8–3a or near one of the needles of an astatic magnetometer[5] (see Fig. 8–3b). The deflection measured by a telescope and scale is proportional to the magnetic moment, hence to the intensity of magnetization and the susceptibility of the specimen. Thus $H \tan \varphi = C\kappa$, where H = horizontal intensity; C = a constant depending on the inducing field component, volume, and distance of the tube; and φ = the deflection angle. The deflection may be increased by making H small, that is, by so placing a compensating magnet beneath the magnetometer that its magnetic field opposes and nearly equals the horizontal component of the earth's magnetic field (see Fig. 8–3a).

In *Koenigsberger's method*, specimens are used in solid form at a distance which is small compared with the dimensions of the needle, and with the magnetometer shown in Fig. 8–3a. For field tests, a Schmidt vertical magnetometer is more suitable (after removing the cork cover and placing the sample on the instrument case). Fig. 8–4 shows the arrangement of a specimen with reference to the magnetic

Colorado School of Mines

FIG. 8–3a. Unifilar (Koenigsberger) magnetometer.

system of a vertical magnetometer. It should have the form of a disc (thickness h, diameter d). Its distance a should be less than $1/5l$ (l = *total length* of the system).[5a] The strength of the magnetic pole induced

[5] E. A. Johnson and W. F. Steiner, Rev. Sci. Instr., p. 237 (July, 1937).
[5a] This condition may be met for a laboratory instrument but not for the Schmidt vertical magnetometer.

in the sample at a distance $2a$ from the needle is $\qquad$ $\cdot \mathbf{m}$, where $\mathbf{m}$ is the pole strength of the needle ($= M/l$), $\mathfrak{u}$ is the permeability of the specimen, and $\mathfrak{u}_0$ the permeability of air. The field of the induced pole is pole strength divided by distance squared. Therefore, for a vertical magnetometer:

$$\Delta Z = \frac{\mathfrak{u} - \mathfrak{u}_0}{\mathfrak{u} + \mathfrak{u}_0} \cdot \frac{\mathbf{m}}{4a^2}. \tag{8-9a}$$
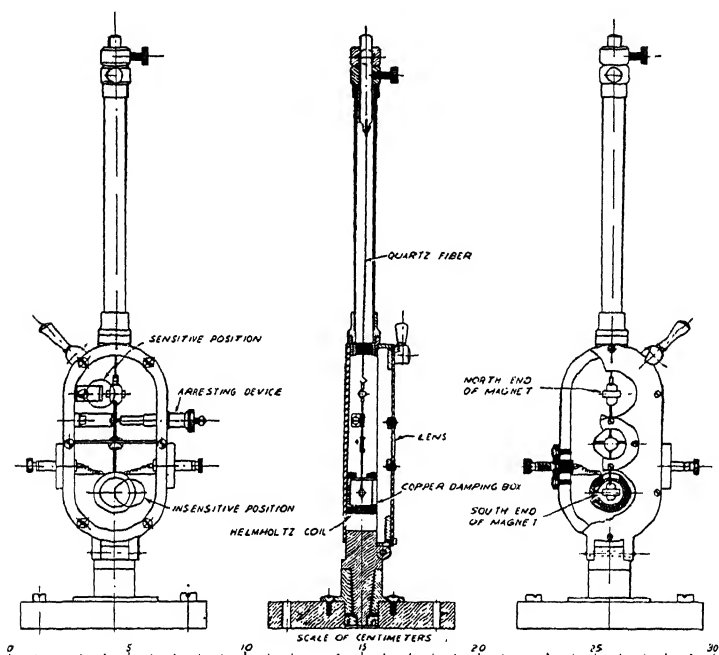
FIG. 8-3b. Astatic magnetometer for susceptibility determination (after E. A. Johnson and W. F. Steiner).

Since $\mathfrak{u} = 4\pi\kappa$ and $\mathfrak{u}_0 = 1$ (air),

$$\Delta Z = \frac{\pi \mathbf{m}\kappa}{2a^2}. \tag{8-9b}$$

The last equation holds for only a very thick specimen. If the thickness is limited and equal to h,

$$\Delta Z = \qquad^{\pi\kappa\mathbf{m}} \tag{8-9c}$$

In practice, it is preferable to use eq. (8-9b) and to correct for thickness and cross section.[6]

[6] J. Koenigsberger, Terr. Mag., **34(3)**, 209 (Sept., 1929).

The effect of remanent magnetization is eliminated by observation in two positions. The apparatus may be calibrated with iron chloride solution whose magnetic susceptibility $\kappa = \delta(88.78p - 0.78)$, where $\delta =$ density, and $p =$ percentage of iron chloride. In a modification of this method, a cast is made of the specimen from a material of known susceptibility, and the comparative effects of sample and cast are measured on an astatic magnetometer.[7] By the use of an astatic system, variations of the earth's magnetic field are eliminated. This method has the advantage of being independent of the shape of the sample.

In the following procedures, susceptibility determinations are made in variable magnetic fields *greater* than that of the earth. These determinations make it possible to trace a complete hysteresis curve. The earliest of these made use of the Coulomb torsion balance (Wiedemann, Curie-Chéneveau, Wilson). The specimen (enclosed in pulverized form, in a small vial) is attached to one end of the balance and exposed to the attraction of a strong electromagnet whose magnetic moment is determined by means of a steel mirror
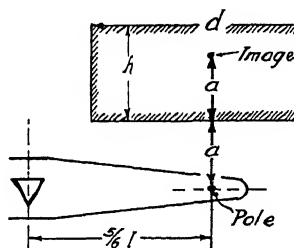
FIG. 8-4. Arrangement of specimen and vertical magnetometer system, for susceptibility determination.

placed at a distance of about 2.5 m. Since the magnetic moment of the specimen is κHv and the torque on a magnet of the moment M in a magnetic field $\mathbf{H}$ is $M H$, the couple acting on the torsion balance is proportional to the square of the field and hence to the square of the current in the electromagnet. In the Curie-Chéneveau and Wilson balances, the specimen is drawn into the gap of a permanent ring-shaped magnet.[8]

FIG. 8-5. Balance method of susceptibility determination (after Haalck).

Very similar in application is the *balance method* of Lord Kelvin, which uses a cylindrical specimen suspended from one end of a scale with its lower end between the poles of a strong electromagnet (see Fig. 8-5). The specimen is first weighed. After current is turned on, balance is re-established by additional weights. If the force of attraction

---

[7] See C. A. Heiland, A.I.M.E. Geophysical Prospecting, 234-236 (1932).

[8] For details see P. Curie and C. Chéneveau, Journ. de phys., 4(2), 796 (1903); Comptes Rendus, 150, 1317 (1910); Phil. Mag., 20, 257 (1910).

$F = \dfrac{\kappa}{2}(\mathbf{H}^2 - \mathbf{H}_1^2)$, $(\mathbf{H} =$ field intensity at lower end of sample; $\mathbf{H}_1 =$ field intensity at upper end of sample) is balanced by Q grams, the susceptibility

$$\kappa = \frac{2Q \cdot 981}{} \qquad (8\text{-}10)$$

in which $\mathbf{H}_1^2$ can be neglected in comparison with $\mathbf{H}^2$ when the specimen is of sufficient length.

The *inductive methods* for susceptibility determinations are based on the fact that the inductance of a coil and the energy transfer in a transformer depend on the magnetic permeability of the core material. In the apparatus designed by Stutzer (Fig. 8-6) the primaries of two air-core transformers are connected in series-aiding to an ammeter, chopper, and battery, while the secondaries are connected in series-opposing through a galvanometer and commutator mounted on the same shaft with the chopper. The coils are accurately balanced so that when pulsating current is sent through both primaries, no current flows in the secondary circuit if no specimen is in the test coil. The balance is disturbed when a sample is inserted in the test coil. The resulting galvanometer deflection is proportional to the susceptibility of the sample.

FIG. 8-6. Stutzer's inductive arrangement for susceptibility determination.

This method is very accurate for minerals of small susceptibility. Strongly magnetic substances should be mixed with quartz sand, and the like, and a corresponding correction should be applied.

Wm. M. Barret,[9] in his inductive method, has employed a single impulse through the primary (or primaries) of one (or two) inductance coils whose secondary (or secondaries) is (or are) connected to a ballistic galvanometer. The circuit is shown schematically in Fig. 8-7. The current from a battery, B, passes through a reversing switch, S_1, to a key, K_1, by which the primary circuit is opened or closed. It then passes through the switches, S_2 and S_3, to the fixed mutual inductance, M_f, the vernier inductance, M_v, and the ammeter, A_2, in one circuit and through the mutual inductance, M_t (containing the sample), and the ammeter, A_3, in

[9] A.I.M.E. Geophysical Prospecting, 216 (1932).

the other circuit in opposite direction. The secondaries of all three inductance coils are connected in series to the ballistic galvanometer, G. Measurements may be made either with one coil, M_t (observing the deflection of the galvanometer), or by balancing the circuits 2 and 3, either inductively or galvanically, so that the deflection of the galvanometer is zero. When working with current balance, the switches S_1, S_2, and S_3 are closed, and the value of I_3 is adjusted according to the desired magnetizing force. After insertion of the sample, I_2 is varied until the galvanometer shows no deflection. Then the susceptibility is given by

$$\kappa = \frac{\mathbf{M}I_2}{C_2 I_3} - C_3, \qquad (8\text{-}11)$$

where $\mathbf{M} =$ the algebraic sum of M_f and M_v in henrys; $C_2 = 4\pi N_2 F S_s \cdot 10^{-8} =$ a constant; $F =$ the effective magnetizing force of 1 amp., so that the field $\mathbf{H}$ is FI_3; $N_2 =$ number of secondary turns on M_t; $S_s =$ cross-sectional area of sample in cm^2; $C_3 = S/4\pi S_s$, with $S =$ cross-sectional area of primary of M_t in cm^2.

In another inductive procedure, Barret has used a modified form of inductance bridge (see Fig. 8-8). Two arms contain the pure resistances R_1 and R_2; the two others contain the variable inductance L_2 and the test inductance L_1 on one side

FIG. 8-7. Schematic circuit of Barret's inductive method.

and the tapped inductance L_3 and the variable L_4 on the other. In operation the bridge is first balanced for D.C. by adjustment of r_5 and rebalanced for A.C., without specimen in L_1, by adjustment of L_4 with L_2 set on zero. The specimen is then inserted and the resulting galvanometer deflection balanced out by adjustment of L_2.

A convenient method of measuring rock susceptibility is afforded by magnetizing a specimen inside a solenoid and observing the corresponding deflection of a magnetometer. Usually two balanced solenoids, S_1 and

S_2 (as in the Ambronn[10] or Stschodro[11] apparatus, Fig. 8-9), are used on both sides of a magnetometer. The specimen is inserted in one solenoid and the corresponding deflection is measured (Stschodro) or neutralized by adjusting the current in an auxiliary winding (Ambronn). In the calculation of susceptibilities in solenoid-deflection tests, it should be noted that the field inside the sample is not the same as the field calculated from the coil dimensions. If the latter is $\mathbf{H}'$, the actual magnetizing field

$$\mathbf{H} = \mathbf{H}' - \mathbf{N}\mathscr{J} \qquad (8\text{-}12)$$

where $\mathbf{N}$ is the "demagnetizing" factor which depends on the shape and dimensions of the specimen. For cylindrical specimens, $\mathbf{N}$ varies from 0.68 to 0.09, for ratios of length to diameter ranging from 5 to 20.

Ballistic methods of susceptibility determinations make use of the fact that the induction current produced in a coil by pulling a magnet rapidly through it is proportional to the moment of the magnet. Ballistic apparatus have been constructed by Stschodro[12] and Puzicha and consist essentially of an induction coil through which the specimen is passed rapidly, connected to a ballistic galvanometer. The induction coil is surrounded by a magnetizing coil so that the susceptibility may be determined as a function of field intensity. In Puzicha's apparatus

FIG. 8-9. Solenoid deflection method for susceptibility determination (after Stschodro). *SN*, magnetometer needle; *A-A'* and A_1-A_1', solenoids; *a*, distance of sample from magnetic needle; *C* and *D*, Helmholtz coils; *R*, distance of rings; Δ, distance of mirror from scale.

[10] See R. Ambronn, Elements of Geophysics, 92, McGraw-Hill (1928).
[11] N. Stschodro, Gerl. Beitr., **17**(**1**), 148-167 (1927).
[12] *Op. cit.*

shown in Fig. 8-10, a transformer with secondary in series opposition with the induction coil was used to compensate for current fluctuations in the magnetizing circuit. The quantity of electricity Q induced in the coil by pulling a specimen of the magnetic moment M through it is given by

$$Q = \qquad\qquad \text{coulombs,} \quad (8\text{--}13)$$

where N_0 is the number of turns per unit length on the ballistic coil, R the resistance of the ballistic circuit, v the volume, and H the reduced magnetizing field in the specimen. A number of hysteresis curves taken in this manner are illustrated in Figs. 8-11 to 8-14.

FIG. 8-10. Arrangement for ballistic susceptibility determination (after Puzicha). A, ammeter; B, ballistic galvanometer; T, transformer; S, magnetizing coil.

Remanent magnetism and *coercive force* may be determined qualitatively in the earth's field and quantitatively from hysteresis loops. The first
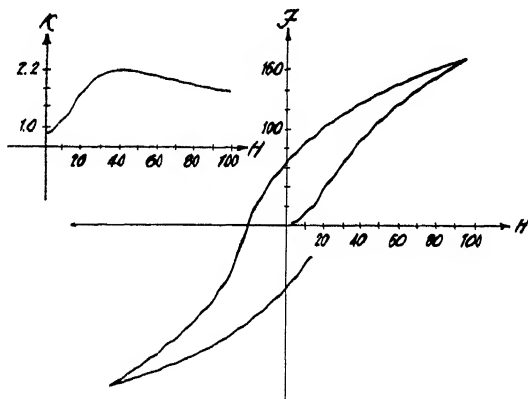
FIG. 8-11. Hysteresis curve of magnetite, Striberg, Sweden (after Puzicha).

method consists of a determination of the difference in the attraction of a specimen when reversed 180° (see page 300). If $\mathcal{I}_r$ is the remanent magnetization and if s_1 and s_2, respectively, are deflections obtained in the two positions of the specimen, the intensity of remanent magnetization (assuming that the two magnetizations can be added algebraically) $\mathcal{I}_r = (s_1 - s_2)/2$. $\mathcal{I}_r$ is often expressed in percentages of $\mathcal{I}_i$. Coercive force and remanent magnetism may be determined directly from the
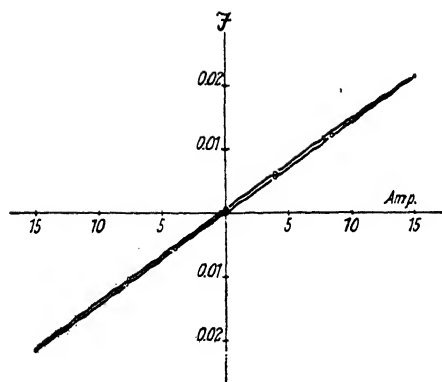
Fig. 8-12. Hysteresis curve for Upper Devonian diabase (no magnetite, Harz mountains, 1 amp. = 29.4 gauss). (After Beyer.)

hysteresis loops obtained by methods previously described. They represent true values (from the physical standpoint) only if the sample has been magnetized to saturation.

Magnetization to saturation has been applied by Puzicha, Loewinson-Lessing, and Mitkevitch. Their fields were of the order of 3 to 5000 gauss. Samples were subjected to hammer blows to insure complete magnetization. Loewinson-Lessing and Mitkevitch found that specimens whose natural magnetism was due to induc-
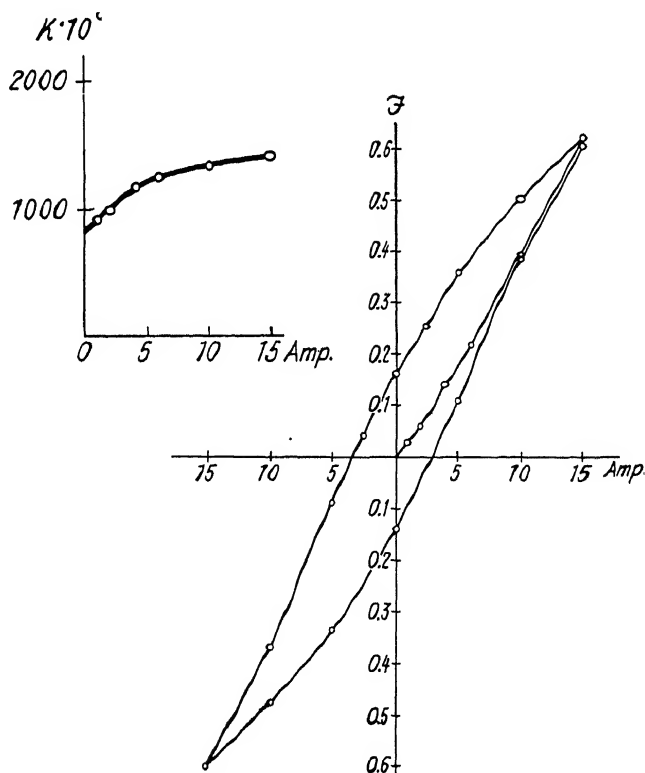
Fig. 8-13. Hysteresis and susceptibility curves for Upper Devonian diabase (containing magnetite, Harz mountains, 1 amp. = 29.4 gauss). (After Beyer.)

tion in the earth's field could be strongly magnetized and that specimens whose magnetism was due to other causes (lightning discharges, and the like) could not be magnetized further.   Hence, magnetizing forces producing strong residual magnetism are great enough to magnetize a rock to saturation; but rocks are not magnetized to saturation by induction in the earth's magnetic field.

C. Numerical Data on Magnetic Properties of Minerals and Rocks[13]

Tables 35 to 40 contain data on susceptibilities, coercive force and remanent magnetism of both minerals and rocks (see also Figs. 8–11 to 8–14).
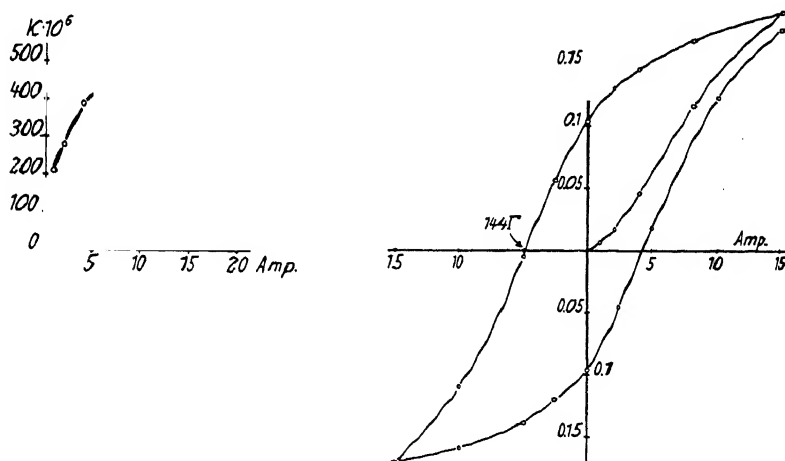
FIG. 8-14. Hysteresis and susceptibility curves for Middle Devonian diabase (containing pyrrhotite but no magnetite, Harz mountains, 1 amp. = 29.4 gauss). (After Beyer.)

[13] Largely after H. Reich, Handb. d. Geophys., VI(1), 58-71 (1931).

TABLE 35
SUSCEPTIBILITIES OF MINERALS

MINERAL	LOCALITY		SUSCEPTIBILITY × 10⁶	FIELD STRENGTH IN GAUSS	REMARKS
			Rock Minerals		
Graphite		Landolt-Börnstein, Phys. Chem. Tab.	−8		
Quartz		" "	−1.07 to −1.2		
Rock salt		" "	−0.9 to −1.3		Calculated from mass-susceptibility
Anhydrite		" "	−1.1		
Sylvite		" "	−0.9 to −1.1		
Calcite		" "	−0.6 to −1.04		Powdered specimen
Dolomite	Gerolstein	F. Stutzer	0.91	220	
Magnesite	Frankenstein	"	2.26-4.53	220	
Serpentine	Snarum	"	10.87	220	
Hornblende	Lukow, Bohemia	"	12.23	220	
Augite	Boreslau	"	133.13	220	
Phlogopite	Norway	Puzicha	184	1	
			196	60	
			207	120	
			212	180	
Serpentine	Harz	"	254	1	
			267	60	
			278	120	
			286	180	
Serpentine	Switzerland	Koenigsberger	1300		
Ilmenite	Egersund	F. Stutzer	30,740	<220	Powdered specimen (estimated)
Franklinite	Franklin	"	35,640	<220	
Ilmenite	Norway	Puzicha	135,000	1	
			252,000	60	
			216,000	120	
			196,000	180	
			Ore Minerals (except iron ores)		
Pyrite	Elba	F. Stutzer	4.53	220	Powdered specimen
Markasite	Brüx	"	5.43	220	" "
Chalcopyrite	Littfeld	"	32.15	220	" "
Malachite	Nischne Tagilsk	"	34.41	220	" "
Azurite	Otavi	"	39.85	220	" "
Cassiterite	Zinnwald	"	88.3	220	" "
Pyrolusite	Thuringia	"	127.69	220	" "
Arsenopyrite	Ontario	"	236.82	220	" "
Wolframite	Zinnwald	"	240.89	220	" "
Chromite	Asia Minor	"	244.51	220	" "
Chalcopyrite	Ural	J. Bahurin	6000	10.3	
Pyrrhotite	Sudbury	L. B. Slichter	125,000	0.5	Calculated from magnetic anomaly
			Iron Minerals (except magnetite)		
Ankerite	Eisenerz	F. Stutzer	23.55	220	Powdered substance
Ankerite		E. Wilson	100	101-160	62.07% FeO

35—*Concluded*

SUSCEPTIBILITIES OF MINERALS

MINERAL	LOCALITY	INVESTIGATOR	SUSCEPTIBILITY $\times 10^6$	FIELD STRENGTH IN GAUSS	REMARKS
Iron minerals (except magnetite)—Concluded					
Hematite	Krivoj-Rog	J. Bahurin	40–100	51.3	
Oxidized brown iron ore	Irthlingborough Distr.	E. Wilson	83	197	44.76% Fe_2O_3
Red iron ore	Oberharz, Germany	Rössiger & Puzicha	90		
Red iron ore	" "	" "	140		
Red iron ore	" "	" "	160		With quartz
Siderite with quartz and chalcopyrite	Siegerland	Koenigsberger	100	No change with H	
Siderite	Siegen	F. Stutzer	331.45	220	Powdered substance
Fine-grained limonite	Melton-Mowbray dist.	E. Wilson	100–105	96–300	53.12% Fe_2O_3
Limonite	Herdorf	F. Stutzer	219.61	220	Powdered substance
Specular hematite	Elba	"	ca. 3200	220	Powdered substance (estimated)
Clayey iron ore from coal measures	Nottinghamshire	E. Wilson	215	48-92	34.28% Fe; 2.32% Fe_2O_3
" "	Derbyshire	"	345	86-108	44.68% FeO; 0.26% Fe_2O_3
Yellow iron ore	Oberharz	Koenigsberger	100–600	400	
Oolitic brown iron ore	Melton-Mowbray dist.	E. Wilson	210–300	92–200	58.88% Fe_2O_3
Iron quartzite	Krivoj-Rog	J. Bahurin	550	10.3	
Magnetite or Magnetite ore					
Magnetite ore	Cornwall	Wilson & Herroun	0.1515 0.204 0.31	10.5 56 368	Max.
Magnetite ore	Kiirunavaara	G. G. Bring	0.32	1280	A. ore 71.1% Fe
Magnetite ore	Gellivaara	"	0.33	1280	
Magnetite ore	Kiirunavaara	Carlheim-Gyllensköld	0.540	70.964	"Staatsrådet II"
Magnetite ore	Urals	A. Turcev	0.718 1.62 0.625	8.7 65.3 522.2	
Magnetite ore	Kiirunavaara	Carlheim-Gyllensköld	1.265	70.964	"Professorn IV"
Magnetite quartz	Kursk	N. Stschodro	0.457 0.150	21.45 858.1	Sample rich in magnetite

TABLE 36

SUSCEPTIBILITIES OF SEDIMENTARY ROCKS

Rock	Locality	Investigator	Susceptibility $\times 10^6$	Field Strength in Gauss	Remarks
Anhydrite & gypsum	N. Germany	Heiland	−1 to −10	0.5	Calculated from anomalies on outcropping cap rocks
Rock salt	"	Koenigsberger	−0.4		
Dolomite	Nottinghamshire	Wilson	1.8	605	
Coal	Waldenburg	Koenigsberger	<2	5	Estimated
Limestone	Leicestershire	Wilson	3.8	200–515	
Sandstone		Koenigsberger	5		
Dolomite	Balaton Lake	Steiner	14	0.5	Calculated
Sandstone	Harz	Puzicha	15.1	180	
			16.2	120	
			16.7	60	
			16.8	1	
Blue clay	Irthlingborough	Wilson	20	94–375	
Blue clay slate	Charnwood Forest	"	39	245–355	
Shales	Texas	Collingwood	44		
Sandy shales	"	"	48		
Shaly sands	"	"	54		

TABLE 37

SUSCEPTIBILITIES OF METAMORPHIC ROCKS

Rock	Locality	Investigator	Susceptibility $\times 10^6$	Field Strength in Gauss	Remarks
Amphibolites	Uri, Switzerland	Koenigsberger	58	0.5–1.0	Tertiary
Magnetite amphibolites	Krivoj-Rog	Bahurin	9000		
Gneiss	Bellinzona	Koenigsberger	10–260	Very low	
Gneiss	Gotthard	"	12–25	" "	
Gneiss	Parana, Brazil	Malamphy, et al.	2000	$H = 0.235$–0.255 $Z = -0.09$–0.06	Average
Metamorphosed slate	Mt. Sorrel	Wilson	61	237–240	
Phyllite	Switzerland	Koenigsberger	130		
Talcous slate	Urals	Bahurin	3000	1.3	
Schist	Oberharz	Rössiger & Puzicha	115		
Serpentine	Harz	Puzicha	254	5–50	
Serpentine	Urals	Bahurin	14,100	30.5	
Iron quartzite	Krivoj-Rog	"	550	10.3	

TABLE 38

SUSCEPTIBILITIES OF IGNEOUS ROCKS

ROCK	LOCALITY	INVESTIGATOR	SUSCEPTIBILITY $\times 10^6$	FIELD STRENGTH IN GAUSS	REMARKS
Plutonic Rocks (arranged in order of increasing basicity)					
Granite	Harz	Puzicha	8	5	
Granite	"	"	28	1	
			27	60	
			26	120	
Gabbro	Skye	Ruecker	2370		
Olivine-gabbro	"	"	5610		
Norite	Harz	Puzicha	52	1	
			89	60	
			107	120	
			106	180	
Harzburgite peridotite	Harz	Puzicha	7600–15600		
Aaregranite	Uri, Switzerland	Koenigsberger	118	0.5–1.0	Metamorphosed
Basic streaks in granite	Italy	Ruecker	400–1810	47–67	
Aaregranite	Uri, Switzerland	Koenigsberger	600	0.5–1.0	Metamorphosed
Granite	Harz	Puzicha	1420–1900	10–100	
Augite-syenite	'	"	2720–3580	10–100	
Diorite	Harz	Puzicha	46.5	1	
			46.8	60	
			47.1	120	
			47.3	180	
Nephrite	"	"	20	1	
			20	60	
			20	120	
			20	180	
Gabbro	"	"	68.0	1	
			68.5	60	
			69.0	120	
			69.5	180	
Volcanic Rocks					
1. *Older Group*					
(a) *Porphyries*					
Porphyry	Harz	Puzicha	40	180	
			42	120	
			45	60	
			47	1	
Enstatite-porphyry	"	"	45	1	
			65	60	
			69	120	
			70	180	
Syenite-porphyry	"	"	48	1	
			64	60	
			95	120	
			120	180	
(b) *Diabases*					
Diabase	Harz	Puzicha	64	180	
			65	120	
			66	60	
			78	1	
"	"	"	80–106	10–100	

<div align="center">

Table 38—*Concluded*

SUSCEPTIBILITIES OF IGNEOUS ROCKS

</div>

Rock	Locality	Investigator	Susceptibility × 10⁶	Field Strength in Gauss	Remarks
			Volcanic Rocks—Concluded		
Diabase	Oberharz	Rössiger & Puzicha	1050		Footwall
Olivine-diabase	Åland, Finland	" "	2000	0.5–1.0	
Diabase	Oberharz	" "	3230		
"	Parana, Brazil	Malamphy, *et al.*	4200	$H = 0.235$–0.255 $Z = -0.09$–-0.067	Might be greater
2. Younger Group					
Dolerite	Nottingham-shire	Wilson	88–130	132–248	
Basalt	Fulda	Koenigsberger	480		
"	"	"	680	1	
			810	60	
			1150	120	
			1500	180	
Basalt	Harz	Puzicha	680–1680	10–100	
Dolerite	Nottingham-shire	Wilson	2790	19.8	
Dolerite	Leicestershire	"	3910–4080	23–39	
Pillow lava	Karadagh	Turcev	4365	26.1	
Nephelite-basalt	Tetschen	Pockels	6070–7170		17.7% magnetite
Basalt	Kassel	Koenigsberger	6300		
Basalt dike	Northumber-land	Ruecker	10090		High value
Peridotite	Petsamo, Fin-land	Koenigsberger	12500	0.5–1.0	

D. Factors Affecting Rock M

Two factors affect rock magnetization: (1) mineral composition, (2) geologic history.

1. *Mineral composition.* At first sight it might be assumed that the magnetization should be dependent upon the iron content. However, the valency of the iron is of far greater importance, since the trivalent iron is more magnetic than the bivalent iron. It is, therefore, more appropriate to state that the *magnetite content* chiefly determines the magnetization of rocks and formations. Next in order is pyrrhotite, then follows ilmenite and titano-magnetite, although data found in the literature regarding the last two are conflicting. Basic rocks (abundant in augite, hornblende, olivine, and magnetite and lacking in quartz) are more magnetic than acidic rocks (rocks abundant in quartz and acidic feldspars, such as orthoclase, with little or no magnetite).

Magnetization depends not only on the type of magnetic mineral but also on the quantity present. Approximate proportionality has been

Table 39

COERCIVE FORCE AND REMANENT MAGNETIZATION OF MINERALS[a]

Mineral or Rock	Locality	Investigator	Coercive Force	Remanent Magnetization	Maximum Field
Magnetite crystal	Traversella	Weiss	−0.5	20	(low)
Magnetite	Sweden	Puzicha	−7	60	4800
Magnetite-lime	Aran	Wilson & Herroun	−12.1		525
Magnetite ore (Fe, 50%)	Lake Champlain	" "	−15.2		525
Magnetite ore (Fe, 66%)	New York	" "	−16.8		525
Magnetite quartzite	Kursk	Stschodro	−19.5	7.5	1073
Magnetite	Sweden	Puzicha	−20	66	100
			−20	70	4800
Magnetite ore (Fe, 55%)	Hey Tor, Devon	Wilson & Herroun	23.8		525
Magnetite ore	Urals	Turcev	−30	72.8	522
Magnetites	Harz	Puzicha	−52	53	90
"	"	"	−80, −96	75, 78	4800
Ilmenite	Norway	"	−19	7	230
			−22	7	4800

[a] With few exceptions, only data for magnetite crystals and magnetite ores are available.   Fields in gauss.

observed on rock powders mixed with known quantities of magnetite (see Fig. 8–15). According to Slichter[14], the deviation from linearity is due to the fact that with an increase in magnetite the demagnetizing influence of the gaps between the magnetite particles decreases.

From experiments made on powders of different fineness, Puzicha concluded that fine-grained powders have a lesser susceptibility than powders of coarse grain. Hence, plutonic rocks are generally more magnetic than volcanic rocks.

2. In the course of the *geologic history* of a formation, a number of physical forces are likely to affect its magnetic properties. They are of a thermal and mechanical nature and occur in connection with igneous intrusions, regional metamorphism, tectonic movements, mechanical and chemical concentration, disintegration, and lightning.

The effect of lightning on rock magnetization is greater than is generally assumed. Current inten-
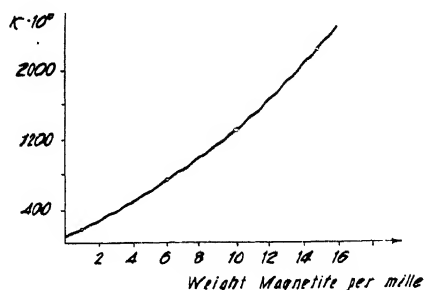
Fig. 8-15. Relation between susceptibility and magnetite content (granite, magnetite powder) (after Puzicha). (Susceptibilities in field of 15 gauss.)

[14] L. B. Slichter, A.I.M.E. Geophysical Prospecting, 247 (1929).

sities in lightning flashes are of the order of 20,000 amperes and give rise to considerable magnetic fields in their vicinity. This explains the irregular magnetic polarities encountered on exposed mountains, hill tops, and the like. Pockels showed by laboratory experiments that

TABLE 40

COERCIVE FORCE AND REMANENT MAGNETIZATION OF ROCKS[a]

Mineral or Rock	Locality	Investigator	Coercive Force	Remanent Magnetization	Maximum Field
Sedimentaries					
Permian sand-stone	Harz	Puzicha	−4	$0.05 \cdot 10^{-3}$	230
			−250	$4.52 \cdot 10^{-3}$	4800
Metamorphics					
Serpentine	Saxony	"	−61	$15.5 \cdot 10^{-3}$	230
			−142	$51.7 \cdot 10^{-3}$	4800
Igneous					
1. *Plutonic*					
Granite	Fichtelgebirge	"	−30	$1.69 \cdot 10^{-3}$	230
			−61	$2.92 \cdot 10^{-3}$	4800
Granite	Harz	"	−18	$0.6 \cdot 10^{-3}$	230
			−161	$3.73 \cdot 10^{-3}$	4800
Augite-diorite	Norway	"	−5	$0.28 \cdot 10^{-3}$	230
			−9.2	$0.56 \cdot 10^{-3}$	4800
Diorite	Sweden	Puzicha	−8	$28 \cdot 10^{-3}$	230
			−11	$34.3 \cdot 10^{-3}$	4800
Augite-syenite	Harz	"	−21	$85 \cdot 10^{-3}$	230
			−32	$110 \cdot 10^{-3}$	4800
Granite powder + 10% pyrrhotite	—	"	−48	0.5	230
Diorite	"	"	−24	$0.140 \cdot 10^{-3}$	230
			−82	$0.502 \cdot 10^{-3}$	4800
Gabbro	Harz	Puzicha	−7	$0.52 \cdot 10^{-3}$	230
			−64	$5.0 \cdot 10^{-3}$	4800
Norite	"	"	−65	$9.15 \cdot 10^{-3}$	230
			−97	$13.2 \cdot 10^{-3}$	4800
2. *Volcanic Rocks*					
(a) *Older Group*					
Enstatite-por-phyrite	Harz	Puzicha	−34	$2.66 \cdot 10^{-3}$	230
			−105	$7.54 \cdot 10^{-3}$	4800
Keratophyre	"	"	−47	0.285	230
			−135	0.920	4800
Syenite-porphyry	"	"	−110	$12.0 \cdot 10^{-3}$	230
			−226	$44.1 \cdot 10^{-3}$	4800
Diabase	"	"	−7	$0.43 \cdot 10^{-3}$	230
			−25	$1.77 \cdot 10^{-3}$	4800
(b) *Younger Group*					
Basalt	Werra	"	−94	$151 \cdot 10^{-3}$	230
			−202	$545 \cdot 10^{-3}$	4800

[a] Fields in gauss.

rocks actually may be magnetized by spark discharges from an induction coil. Columns of basalt erected near lightning rods will eventually show strong permanent magnetizations. The earlier geophysical literature abounds in articles in which authors have attempted to reconstruct the direction of the earth's magnetism in previous geologic periods

from the magnetization of lavas and the like. Such deductions appear hardly justified, since so many factors, such as lightning, contact and dynamic-metamorphic effects, and mechanical stresses, can be of influence. Magnetizations of rocks, taken by and large, offer no positive evidence of changes in direction or intensity of the earth's magnetic field in previous geologic periods.

The remanent magnetism of ferromagnetic substances decreases with an increase in temperature. In fact, all magnetic parameters (coercive force, remanent magnetization, susceptibility) are individually dependent on temperature. A correct analysis of thermal relations is difficult, since the same ferromagnetic body may not exist after changes in temperature, and another body may have been formed with different structural and chemical properties (magnetization of pottery and bricks). The intensity of magnetization decreases first slowly and then more rapidly with temperature until the critical, or "Curie," point is reached ($348°$ for pyrrhotite, $525°$ for magnetite, and $645°$ for hematite). According to these figures, rocks could not be magnetized beyond a depth of about 20 kilometers. On the other hand, it is quite possible that by such extraordinary pressures and temperatures as occur in the earth's interior, unexpected results may be produced. The sun, notwithstanding its high surface temperatures ($5900°C.$) has a strong magnetic field. Further, an analysis of the surface distribution of the earth's magnetism has led to the conclusion that 52 per cent of it originates in the core. When a magnetic rock is heated to the Curie point and then cooled, its magnetism reappears at a much lower temperature. This is known as *temperature hysteresis of magnetization* and occurs particularly in pyrrhotite.

Considerable forces are at work in mountain building, folding, faulting, volcanic intrusions, epeirogenic movements, and earthquakes. They cannot fail to affect the magnetization of rocks and are likely to bring about changes in susceptibility and remanent magnetization. A reciprocal relation exists between deformations caused by magnetization (magnetostriction) and magnetic effects due to deformations such as stretching (Villari effect), bending (reciprocal Guillemin effect), and twisting (Wertheim effect). Different materials have quite different magnetomechanical characteristics.

There is, further, a distinct magnetic hysteresis in mechanical cycles. When the stresses have ceased, the magnetizations never return to their original values. In connection with the possible relation of mechanical stresses and abnormal magnetic polarization, it is of great interest that negative magnetizations may be produced by simultaneous tension and torsion (see Fig. 8-16). Occasional strong magnetizations of drill rods and drill cores may be explained by this effect.
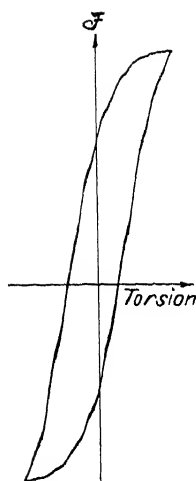
Fig. 8-16. Magneto-mechanical hysteresis loop for nickel (after Steinhaus).

Disintegration of rocks is effective both chemically and mechanically. Since the trivalent iron is more paramagnetic than the bivalent iron, rock magnetization is much reduced when magnetite disintegrates to limonite or hematite. Conversely, in contact and dynamic-metamorphic processes, the iron in sedimentaries and other rocks is transformed from the bivalent into the trivalent form, so that concentrations of magnetic minerals are often found near intrusive bodies. The mechanical effect of disintegration is (1) to break up the magnetite particles and to produce a more fine-grained material, and (2) to increase the spacing of the particles and the path-reluctance. Both result in a decrease of magnetization.

Concentration of magnetic materials has the opposite effect of disintegration. The relations discussed above between susceptibility, grain size, chemical changes, and thermal effects apply accordingly. Examples of an increase in magnetization by concentration are contact-metamorphic zones and magnetite or black sands in gold placers.

Structural forces may change the position of magnetic bodies in the course of their geologic history. When they have acquired remanent magnetization, their overturning may produce apparent abnormal polarization. Similar effects may be expected from a change of position of solidified and magnetized portions of magma and lava flows.

III. MAGNETIC INSTRUMENTS

A. Construction Principles

Instruments for the measurement of magnetic anomalies caused by iron ores were developed at an early date. In the nineteenth century a number of scientific institutions became engaged in the determination of the elements of the earth's magnetic field all over the globe. For this purpose numerous types of instruments have been developed for land, oceanic, and aerial observations. When, fifteen years ago, magnetic prospecting started on its rapid development, extensive design experience was thus available. Although the Schmidt-type magnetometers are in most extensive application, a number of the other designs are employed for the same or different purposes. While preference is given here to the Schmidt magnetometers, other types of magnetic instruments are also discussed in view of their applications in mining and engineering.

Magnetic instruments may be divided into (1) prospecting magnetometers, (2) instruments for regional magnetic surveys, and (3) observatory instruments.

A second classification is based on construction principles and includes the following groups: (1) Instruments for finding the *direction* of the field by determining (*a*) the rest position of a magnet capable of rotation about a vertical axis (declinator, compass), a horizontal axis (inclinator, dip circle, dipping needle), or both horizontal and vertical axes (Swedish mining compass); (*b*) the zero induction position of a rotating coil (the earth induc-
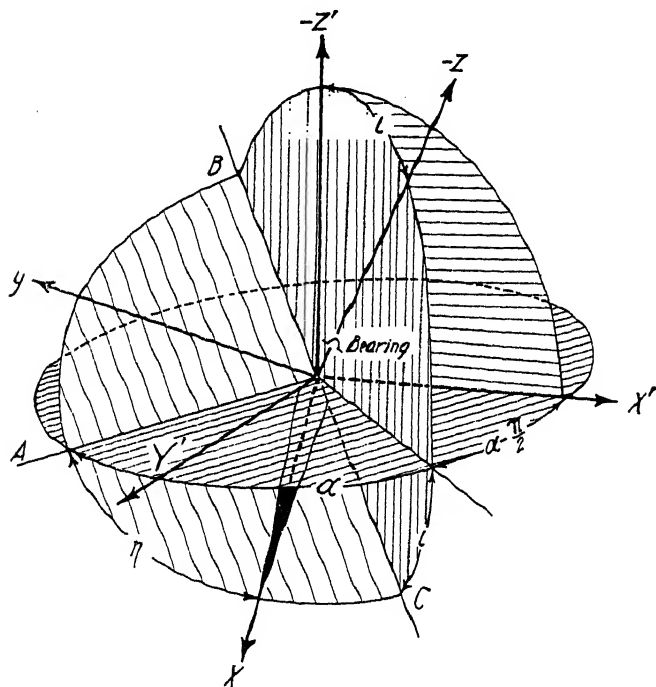
FIG. 8-17. Action of three fixed-force components on moving magnetic system.

tor and earth inductor compass); or (*c*) intensity ratios as in iron-induction inclinometers. (2) In the second group are instruments for the determination of the total *intensity* or its components (*a*) by measuring the period of oscillation of a magnet in a horizontal or vertical plane; (*b*) by measuring the current induced in a rotating coil; (*c*) by measuring the induction in iron bars; or (*d*) by using a comparison force of some kind. These may be produced by (*l*) magnets or coils, (*m*) elastic suspensions, (*n*) gravity, and (*o*) moving electrons.

A *general theory of magnetic instruments* may be derived from the action

of the forces on a magnetic needle free to move in space. Assume a Cartesian system of coordinates oriented in the astronomic directions, north (x'), east (y'), and nadir (z'). Let the components of the earth's magnetic force in these directions be $\mathbf{X'}$, $\mathbf{Y'}$, $\mathbf{Z'}$. Assume the x axis of another system to coincide with the magnetic axis of an imaginary needle free to move in all directions. Then y represents the component acting at right angles to it and z the component in the axis of revolution if the movement of the needle is confined to the plane ABC. The inclination of this plane is given by the angle ι, its intersection with the horizon by the angle (azimuth) α, and the position of the needle on the plane by the angle η (Fig. 8–17). The force acting upon the needle may be expressed by its three components $\mathbf{x}$, $\mathbf{y}$, and $\mathbf{z}$ as function of $\mathbf{X'}$, $\mathbf{Y'}$, and $\mathbf{Z'}$:

$$
\begin{aligned}
\mathbf{x} = \;& \mathbf{X'} (\cos \alpha \cos \eta + \sin \alpha \sin \eta \cos \iota) \\
& + \mathbf{Y'} (\sin \alpha \cos \eta - \cos \alpha \sin \eta \cos \iota) \\
& + \mathbf{Z'} \sin \eta \sin \iota. \\
\mathbf{y} = \;& \mathbf{X'} (\cos \alpha \sin \eta - \sin \alpha \cos \eta \cos \iota) \\
& + \mathbf{Y'} (\sin \alpha \sin \eta + \cos \alpha \cos \eta \cos \iota) \\
& - \mathbf{Z'} \cos \eta \sin \iota. \\
\mathbf{z} = \;& -\mathbf{X'} \sin \alpha \sin \iota + \mathbf{Y'} \cos \alpha \sin \iota + \mathbf{Z'} \cos \iota.
\end{aligned}
\quad (8\text{–}14)
$$

Since all magnetic matter is polarized, the forces acting upon north and south pole balance each other so that $\mathbf{x} = 0$. The three terms in each of the above equations may be reduced to two by revolving the system of coordinates through the angle of declination, so that $\mathbf{X'} \equiv \mathbf{H}$, $\mathbf{Y'} = 0$, $\mathbf{Z'} \equiv \mathbf{Z}$, and $\alpha = $ *magnetic* azimuth. The total force acting upon the needle is $F = \mathbf{m'} \cdot \sqrt{\mathbf{y}^2 + \mathbf{z}^2}$, where $\mathbf{m'}$ is the magnetic pole strength of the needle, and

$$
\begin{aligned}
& [\mathbf{H}(\cos \alpha \sin \eta - \sin \alpha \cos \eta \cos \iota) - \mathbf{Z} \cos \eta \sin \iota]^2 \\
& \quad + [\mathbf{Z} \cos \iota - \mathbf{H} \sin \alpha \sin \iota
\end{aligned}
\quad (8\text{–}15)
$$

This represents the force acting upon a needle free to move in any direction (Swedish mining compass). In all other magnetic instruments the movement of the needle is confined to the xy plane and the z component is neutralized by the pressure of the pivots in the bearings. Then only the y component remains. Its couple is $D_1 = M\mathbf{y}$, where M is the magnetic moment of the magnetic needle. Thus,

$$
D_1 = M[\mathbf{H}(\cos \alpha \sin \eta - \sin \alpha \cos \eta \cos \iota) - \mathbf{Z} \cos \eta \sin \iota]. \quad (8\text{–}16)
$$

If the needle is not suspended in its center of gravity, a moment due to gravity must be added. If e is the distance of the center of gravity from the axis,

$$D_2 = -emg \cos \eta \sin \iota. \tag{8-17a}$$

If e subtends the angle ζ with the x direction and if the horizontal and vertical projections of e are $a = e \cos \zeta$ and $d = -e \sin \zeta$, respectively,

$$D_2 = -mg \sin \iota \, (a \cos \eta + d \sin \eta). \tag{8-17b}$$

In the equilibrium position $D = D_1 + D_2 = 0$ so that

$$\tan \eta = \frac{M\mathbf{H} \sin \alpha \cos \iota + M\mathbf{Z} \sin \iota + mga \sin}{M\mathbf{H} \cos \alpha - mgd \sin} \tag{8-18}$$

This formula is fundamental for all magnetic balances.

B. Prospecting Magnetometers

1. In the *Schmidt vertical magnetometer* (Fig. 8–18) a magnetic system is balanced on a knife edge at right angles to the magnetic meridian. Its inclination is measured by means of a mirror attached to the system, in conjunction with an autocollimation telescope system. The center of gravity is on the south side below the pivot, and is usually readjusted so that the balance system is horizontal in the area under investigation. The balance system is surrounded by an aluminum case containing copper dampers, thermometers, and levels. The case, in turn, is protected by a cork-lined case to reduce the effects of abrupt temperature changes. The magnetic system is supported by a bridge with two quartz bearings. Three points on a movable arm fit three grooves on the underside of the system, the vertical motion of the arm being controlled by an arresting lever from the outside.

The instrument is fastened to the tripod head by means of three pegs on the bottom of the case. In all models up to 1935, deflections were read by observing the relative displacement of two scale images. The scale had forty divisions, of which the 0-, 20-, and 40-scale divisions were marked by heavier lines which were used as "indices." Some users adjusted the system to read 20 at a base station and used this reading as 0 so that subsequent readings gave directly the positive or negative anomalies. In the optical system of the newer models the scale has 60 divisions. Mounted to the side of this scale is a glass plate with 3 index lines; the double scale image is avoided and the range is 120 scale divisions. A teleobjective lens now gives twice the focal length compared with the earlier models. If there is any doubt in which direction the scale of an older type mag-
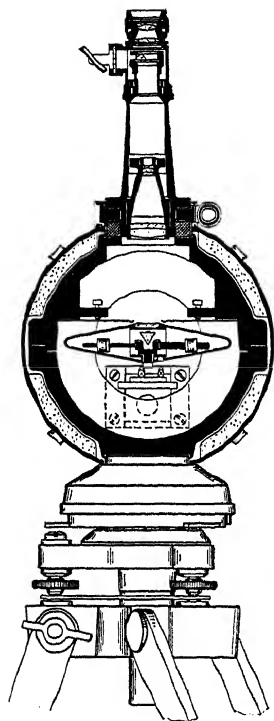
FIG. 8-18a. Section and scale of Askania-Schmidt vertical magnetometer.

netometer should be read, a magnet is placed under the instrument, south pole up. If this causes the readings to increase, the scale is being read in the correct direction.

The magnetic system (earlier type) (see Fig. 8-19) consists of two magnetized bars (tungsten or cobalt steel) attached to an aluminum cube, which carries the knife edge, the mirror, two lateral screws, and one vertical screw. The two lateral screws, provided with counter screws, are for latitude adjustment; the vertical screw is for the scale-value adjustment. In the newer models temperature-compensated magnetic systems with steel frame, compensating aluminum spindle, and invar latitude spindle are used. If large scale values are desired, the brass screw may be replaced by a gold screw.

The top of the tripod is graduated and may be rotated about a vertical axis. A detachable compass is supplied with the instrument for orienting it into the magnetic prime vertical. Below the tripod head is a graduated tube for deflector magnets. In the newer models, stops are provided for the 180° and 90° positions.

Formulas for normal operating conditions are readily derived from eq. (8-18) by writing $\tan 2\eta = (s - s_0)/f$, where s_0 is the reading corresponding to $\eta = 0$ (20 in the older, 30 in the new telescope), s is the reading corresponding to η, and $\mathbf{f}$ the focal length of the objective lens. Neglecting $\tan^2 \eta$ compared with 1, $\tan \eta = (s - s_0)/2f$ so that
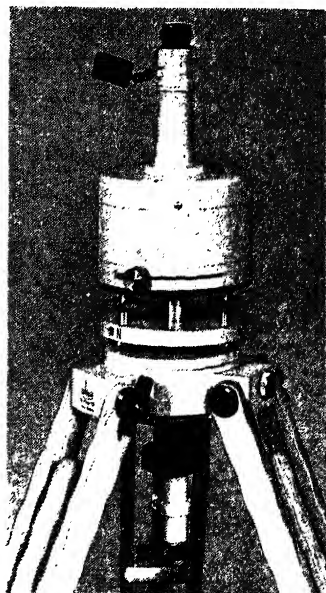
FIG. 8-18b. Simplified Askania magnetometer.

$$s - s_0 = 2f \cdot \frac{MH \sin \alpha \cos \iota + MZ \sin \iota + mga \sin \iota}{MH \cos \alpha - mgd \sin \iota}. \qquad (8\text{-}19)$$

In the normal operating position, $\alpha = \pi/2$ or $3\pi/2$, $\iota = \pi/2$, and d and a are negative. Then

$$s - s_0 = 2f \frac{MZ - mga}{mgd}. \qquad (8\text{-}20)$$

If a reading s corresponding to a vertical intensity Z has been obtained at one locality and a reading s' at another with the vertical intensity Z', the difference in the readings

$$s' - s = \frac{2fM(Z' - Z)}{mgd}. \qquad (8\text{-}21)$$

Hence, $\Delta Z = \Delta s \cdot mgd/2fM = \Delta Z \equiv \Delta s\epsilon$, if

$$\epsilon = \frac{mgd}{2fM} \qquad (8\text{-}22)$$

is the scale value of the instrument. Eq. (8-20) may also be written $(s - s_0) = (2fM/mgd)\left(Z - \dfrac{m}{M} \cdot ga\right)$, so that

$$\epsilon(s - s_0) = Z - \frac{m}{M} \cdot ga = Z - Z_0. \qquad (8\text{-}23)$$

It is seen that $(m/M) \cdot ga$ is the vertical intensity for which the system is adjusted.

If the instrument deviates from the correct azimuth by the angle δ, a change in scale value takes place and

$$\epsilon_\delta = \epsilon_0 \mp \frac{H \sin \delta}{2f}. \qquad (8\text{-}24a)$$

Hence, the deflection decreases when the instrument is rotated to the north of the E-W position and if the reading is greater than 20. For a reading less than 20, the deflection increases. If the instrument is rotated to the south, the readings increase if greater than 20, and decrease when less than 20. For small misorientations (up to 10°) the error cancels out in two diametrically opposite ($\Delta\alpha = 180°$) positions.

If the instrument is tilted, the effect is an optical one in the E-W, and an earth-magnetic one in the N-S direction because the horizontal intensity becomes effective. Whether the errors produced thereby cancel in the mean of the two operating positions depends entirely on whether the tilt is produced by a wrong setup on the tripod head or by an inclination of the axis of rotation of the latter. An E-W component of tilt of the axis
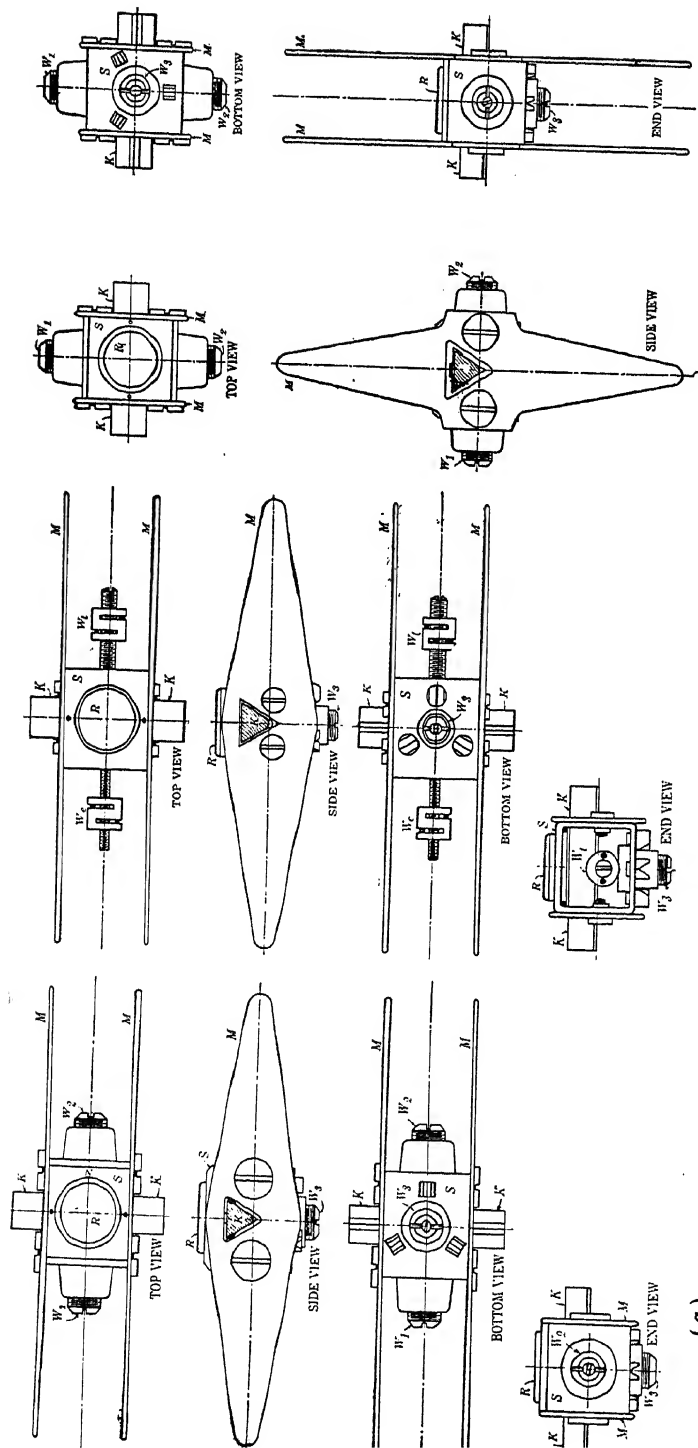
Fig. 8-10. Magnetic systems of Askania-Schmidt magnetometers (after Joyce).

(a) Older type, vertical magnetometer (M, magnets; R, plane mirror; K, knife edges; S, spacer block; W_1 and W_2, latitude adjustment counterweight; W_3, sensitivity adjustment counterweight).

(b) New compensated type, vertical magnetometer (M, magnets; R, plane mirror; S, spacer frame; K, knife edges; W_3, sensitivity adjustment counterweight; W_4, latitude adjustment counterweight; W_4, temperature compensation counterweight).

(c) Older type, horizontal magnetometer (M, magnets; R, plane mirror; K, knife edges; S, spacer frame; W_1 and W_2, latitude adjustment counterweight; W_3, sensitivity adjustment counterweight).

of revolution causes a *difference* in the E and W readings which cancels in the average of the readings. If the case is inclined, if the lid with the telescope is tilted, or if the instrument is so placed on the tripod head that an E-W tilt is produced, a change in reading results, which does not cancel in the mean of the two positions. Therefore, care must be taken to set up the instrument on the tripod head correctly leveled in the E-W direction. The effect of a meridional inclination of the axis of rotation is the *same* for the E and W positions, does not cancel in the mean, requires a
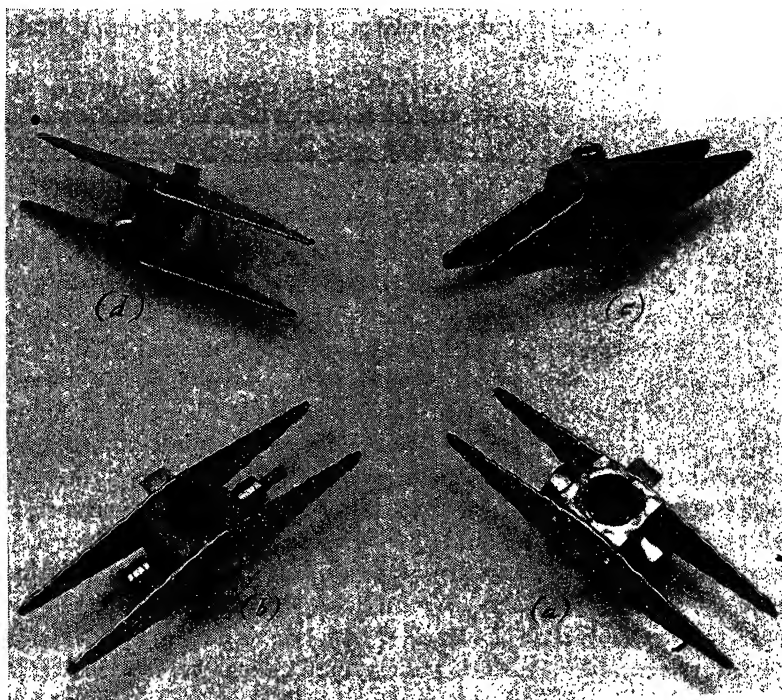
American Askania Corp.

FIG. 8-19b. Views of magnetic systems *a* to *c* of Fig. 8-19a; *d* is compensated horizontal magnetometer system.

correction or very accurate leveling in the N-S direction. Conversely, a N-S inclination of the case, of the bearings, or of the axis of revolution of the *system* cancels in the mean of the two positions, and the difference in readings is $s_W - s_E = 2iH/\epsilon$. It is seen that the tripod axis must be carefully leveled in the direction of the magnetic meridian.

For increasing the range of the magnetometer, auxiliary magnets are used in the extension tube under the tripod head (in first Gauss position). If the scale has disappeared to the left (toward low readings), the magnet

is inserted south pole up; if the scale has disappeared to the right, the magnet is inserted with its north end up. Then the additional field

$$\Delta Z = \pm \frac{2M_a \mathbf{k}}{r^3} \qquad (8\text{-}24b)$$

and therefore the correction in scale divisions

$$\Delta s = \mp \frac{2M_a \mathbf{k}}{\epsilon r^3}, \qquad (8\text{-}24c)$$

where M_a is the moment of the auxiliary magnet, r its distance, and $\mathbf{k}$ is a deflection constant given by

$$\mathbf{k} = 1 + \frac{1}{r^2}\left(\frac{1}{2}L^2 - \frac{3}{4}l^2\right), \qquad (8\text{-}24d)$$

with L as the pole distance of the deflecting magnet and l that of the magnetic system. For the uncompensated Askania system $\frac{3}{4}l^2 = 51.7$. More accurate results are obtained if the correction in scale divisions is determined experimentally on a field station where the scale is about to disappear by taking readings with and without magnet. Since the temperature of the auxiliary magnets is of some influence and their moment and distance may change in transportation, it is advisable to use them only temporarily for large anomalies. When work is being done for any length of time in areas with regionally different vertical intensities, the latitude adjustment screws should be used.

As the Schmidt balances are instruments based upon a comparison of the earth's magnetism with *gravity*, consideration must be given to the problem whether anomalies in gravity or changes of gravity with latitude have any effect. The effect of gravity on the scale value is given by $\epsilon_{g'} = \epsilon_g \cdot g'/g$ so that, if an instrument with 30γ scale value is taken from the pole to the equator, its scale value would change from 30.00 to 30.15. The effect on the reading is approximately $s_g - s_{g'} = \dfrac{Z(g' - g)}{\epsilon g}$, so that a large gravity anomaly of the order of 100 milligals would produce a change of 5.4γ. Hence, in practice, effects of variations in gravity may be disregarded, particularly since most gravity anomalies are accompanied by large magnetic anomalies.

Variations in *temperature* produce probably a greater change in magnetometer readings than any other physical factor; the temperature effect is due to (1) a drop in the magnetic moment of the needle with an increase in temperature, and (2) differential expansion of the metals in the magnetic system, giving rise to displacements of the center of gravity. The first effect may be partially compensated by the second, that is, by a suitable

mass adjustment. In the earlier style magnetic systems the steel blades were so arranged in reference to the aluminum block as to effect a displacement of the center of gravity to the north side, thus offsetting the rise of the system on that side with an increase in temperature. In the new compensated systems steel is used for the frame and compensation is effected by an aluminum spindle on the north side and an invar spindle on the south side, which are both provided with suitable masses.

The drop of the magnetic moment M referred to above with temperature Θ may be written

$$M_\Theta = M_{20}(1 - \mu_s\Theta), \qquad (8\text{-}25a)$$

where μ_s is of the order of 0.00048 for good magnets of the earlier systems and about 0.00014 for the new systems; Θ is the temperature in degrees C, usually referred to a normal temperature of 20°; and M_{20} is the magnetic moment at that temperature. If the above relation is applied to eq. (8-22), it is seen that the magnetic temperature effect on scale value is tolerably small. This is not true for the deflection whose change with temperature is given by $s_\Theta - s_{20} = \dfrac{-2fMZ\mu_s\Theta}{mgd}$. Thus the temperature coefficient,[15] $T.C.$, in gammas is

$$T.C. \equiv \frac{\epsilon(s_\Theta - s_{20})}{\Theta} = -\mu_s Z. \qquad (8\text{-}25b)$$

It follows from the above (considering the magnetic effect *only*) (1) that the reading s_Θ is less than the reading s_{20}, (2) that the temperature coefficient is negative and the temperature correction positive,[15] and (3) that the temperature correction varies with the vertical intensity. It is also seen that an *uncompensated* system with a μ_s of 5.10^{-4} and a normal scale value of 30γ at Golden, Colo., $(Z = 53{,}100\gamma)$ would have a temperature coefficient of -0.85 scale divisions. It is obvious that a compensation must be effected which may be done by a suitable mass distribution. The effect of temperature on the latter may be expressed by the equivalent contraction or expansion of the gravity lever arms a and d in formula (8-20), so that $a_\Theta = a_{20}(1 + p\Theta)$ and $d_\Theta = (1 + q\Theta)$, where p and q are the total expansion coefficients in the horizontal and vertical direction resulting from all metals, their masses, lever arms, and expansion coefficients. Therefore the reading at the temperature Θ is

$$s_\Theta = \frac{2f[MZ(1 - \mu_s\Theta) - mga(1 + p\Theta)]}{mgd(1 - q\Theta)}.$$

[15] The temperature *coefficient* has the opposite sign of the temperature *correction*.

Again, the effect on scale value is small so that $q\theta$ may be neglected; then the temperature coefficient

$$T.C. = \frac{\epsilon(s_\theta - s_{20})}{\theta} = \frac{mga}{M}\cdot(q - p) - Z(\mu_s + q). \qquad (8\text{-}25c)$$

This equation gives two possibilities of compensation for temperature: (1) by making $\mu_s = -q$, and $p = q$, (2) by omitting compensation in the vertical direction and selecting a material for the frame whose expansion coefficient is small. For steel, $\gamma \equiv q = 1.1 \times 10^{-5}$, which is 13 times less than μ_s. Thus, if $q = 0$,

$$T.C. = \frac{\epsilon(s_\theta - s_{20})}{\theta} = -\frac{g}{M}\cdot amp - Z\mu_s. \qquad (8\text{-}25d)$$

Since mga/M is the vertical intensity Z_0 corresponding to the latitude adjustment $(s = 20)$ of the instrument, and since Z may be put equal to Z_0 with reasonable accuracy, the temperature coefficient

$$T.C. = \frac{\epsilon(s_\theta - s_{20})}{\theta} = -Z_0(\mu_s + p). \qquad (8\text{-}25e)$$

For complete compensation, p must be made equal to $-\mu_s$.

For any magnetic system whose mass distribution is known, the coefficient p can be calculated beforehand; details are given in C. A. Heiland's and W. E. Pugh's article on this subject.[16] The μ_s may be determined by deflection observations. Since the temperature coefficient depends on the vertical intensity, a magnetic system compensated for one locality will no longer be compensated at another.

Extreme care should be exercised in the *transportation* of the instrument and in releasing the system, as very slight changes in the horizontal position of the center of gravity produce large changes in reading. From eq. (8-23) the apparent change in vertical intensity equals $d(\epsilon s)/da = -mg/M =$ about 5γ for a displacement of only 10^{-6} cm. The change in scale value due to a vertical displacement of the center of gravity of the same order is $2f$ times less than the change in reading. The magnetometer is also quite sensitive to changes in magnetic moment, for $d(\epsilon s)/dM = mga/M^2$. That is, a drop in the magnetic moment of 1 gauss decreases the reading about 35 gammas. Therefore, it is necessary to keep the instrument away from magnets, power lines, and other demagnetizing effects.

Instrument constants and *corrections*. The purchaser of a magnetometer usually advises the factory where he expects to use his instrument so that

---

[16] A.I.M.E. Geophysical Prospecting, 334–372 (1934).

the magnetic system may be adjusted approximately to the magnetic latitude in his area (by shifting blades). After this adjustment has been made, the steel blades should not be changed by the user, since the temperature correction also depends on their position. On arrival, the magnetometer may require readjusting of the latitude screws so that the reflected

scale is near 20 (or 30 for the new telescopes) at a base station in the area under survey. For two widely separated areas it is advisable to have two properly adjusted systems. Where large anomalies occur, the scale value should be increased or auxiliary magnets should be used.

The scale value of a magnetometer may be determined with (1) magnets, (2) coils, (3) observations in different azimuths. A new instrument should first be tested for uniformity of scale value by measuring and plotting the variation of reading with field changes produced by magnets or coils. Routine scale value tests with magnets are made with a long deflection rod which attaches to the tripod head and carries a slide with pivoted magnet holder. Scale value determinations should be made in the middle of the scale. Readings near 20 may be produced by a magnet set

American Askania Corp.

FIG. 8-20. Deflector-attachments for centering reading and for scale-value determination (Askania).

up on another tripod (in second Gauss position) or by using a deflector attachment especially made for this purpose (see Fig. 8-20). The average scale value should be adjusted to about 30 gammas for the earlier and to 15 gammas for the new systems. It is useless to make the instrument too sensitive, as the errors are increased proportionally. In determining the scale values by magnet deflection, a magnet of known moment M_a is placed at a distance r on the deflecting rod. If the reading without

the magnet is s_0, the reading with the north pole of the magnet down is s_2, and the reading with the north pole up is s_1 (repeated by turning the magnet over two or three times and using two or three distances), the scale value[17]

$$\frac{s_1 + s_2}{2} = s_0 = \text{(check)}, \qquad (8\text{--}26a)$$

where $\mathbf{k}$ is given by eq. (8–24d) and M_a is the moment of the auxiliary magnet. One of the auxiliary magnets should be retained for use as a standard and not be taken into the field. For the determination of the moments of other magnets from the standard, the following formula applies, provided the unknown magnet and the standard are used in the same distance,

$$M_x = M_{st} \cdot \frac{(s_1 - s_2)_x}{(s_1 - s_2)_{st}} \cdot \frac{\mathbf{k}_{st}}{\mathbf{k}}; \qquad (8\text{--}26b)$$

$\mathbf{k}_{st}/\mathbf{k}_x = 1$ if the magnets used for comparison are of the same length.

Since magnets lose their strength with time and must be recalibrated at intervals, Helmholtz coils (Fig. 8–21) are often preferred. Current is supplied from dry cells, controlled by rheostats, and read on a milliammeter. If I is the current in milliamperes, and C the "coil constant" (deflection per mil.), the scale value

$$\epsilon = \frac{2IC}{(s_2 - s_1)}. \qquad \qquad (8\text{--}26c)$$

The Helmholtz coil may also be used for calibrating magnets by producing a number of readings ($s_1 - s_2$) with the magnet first and then with the coil, and by adjusting the current until magnet and coil deflections are equal. Then

$$\epsilon(s_1 - s_2) = 4\frac{M_x \cdot \mathbf{k}}{r^3} = 2IC, \qquad (8\text{--}26d)$$

where r is the distance of the magnet, C the coil constant, I the current. Hence

$$M_x = ICr^3/2\mathbf{k}.$$

Observations in different azimuths are used when deflection magnets or coils are not available. Readings are taken in the E-W and N-S positions of the instrument; then the scale value

$$\epsilon = \frac{s_N \mathbf{H}}{2\mathbf{f}(s_E - s_N)}, \qquad (8\text{--}26e)$$

---

[17] For the vertical magnetometer.

where s_N is the reading in the north, s_E the reading in the east, and **H** the horizontal intensity taken with its approximate value from government maps.

The temperature correction of a magnetometer is found by measuring the variation of reading with temperature. Temperature variations may be produced by setting up the instrument outdoors during periods of temperature rise or fall, by placing it in a box heated by alternating current or hot water, or by inserting a small coil-type heater in the case. Dry

American Askania Corp.

FIG. 8-21. Helmholtz coil for scale-value determination.

ice may be used to chill the instrument but should be applied with caution, since too rapid cooling results in a condensation of water vapor on the knife edge and thus in erratic readings.

A second instrument should be used to observe or record the daily variation and should be kept at constant temperature. Observations on both are taken with magnets permanently released. The instrument to be calibrated is read every five minutes and the corresponding temperature is noted. The temperature coefficient is then given by the mean slope of the curve $s = f(\Theta)$. A least-square adjustment may be applied to im-

prove the accuracy.   Plotting or recording the deflection and temperature
curves separately has the advantage that the time lag between the reaction
of the magnetic system and temperature may be allowed for by shifting
them by the amount of the lag and calculating the temperature correction
from corresponding values of reading and temperature.

The *base correction* allows for gradual or abrupt changes of the instru-
ment in the course of a survey.   It is determined by checking back at a
base station once or twice a day.   If the difference in readings on checking
in on the base is small (1 or 2 scale divi-
sions), and if numerous stations have been
made between base checks, the base cor-
rection applied to any station **p** is

$$-\frac{(s_2 - s_1)}{n} \cdot \mathbf{p}, \qquad (8\text{-}27)$$

where s_1 is the first corrected reading, s_2
the second reading, **n** the number of sta-
tions made between checks, and **p** the
number of the station after the first base
reading.   The application of the formula
is based on the assumption that the change
takes place linearly.   If there is cause to
assume an abrupt change in reading, the
base correction must be applied accord-
ingly.

Magnetic variations are measured and
corrected for as in all other magnetic field
observations; procedures vary with accu-
racy requirements and are discussed on
page 367.   A convenient recorder to use in
connection with Schmidt magnetometers is
illustrated in Fig. 8-22.

American Askania Corp.

Fig. 8-22. Recording arrange-
ment with magnetic system.

The *latitude* correction is a correction for
the normal or planetary change of the in-
tensity and is obtainable from government magnetic maps.   In the verti-
cal and horizontal intensities, the major components of planetary change
are in the N-S direction.   As the vertical intensity increases toward north,
the correction in this direction is negative; for the horizontal intensity
which decreases toward north, the correction is positive.

In the *field operation* of the instrument, the observer must exercise
sufficient care not to have about his person any iron or steel objects, such
as pocket knife, watch, keys and keytainers (if they contain iron), some
makes of belt buckles, pencil clips, some makes of fountain pens, ring-binder

notebooks, and the like. The instrument case, Helmholtz-coil galvanometers, and so on should be set up a sufficient distance from the magnetometer (see page 373). Stations should be sufficiently removed from fences, well casing, pipe lines, derricks, boilers, tanks, mine shafts, bridges, railroads, culverts, and the like, and from electric railways, power stations, magnetic separators, and other mine plants.

The following steps are followed in operating the instrument: (1) Remove instrument from case so that it may acquire the temperature of the air. (2) Set up and level tripod. Orient tripod head with compass into the magnetic prime vertical. Clamp tripod head; read and note position of index. (3) Set up instrument on tripod, level with tube levels. (4) Orient into magnetic prime vertical (N toward E). (5) Adjust eyepiece position and mirror until scale is in focus and evenly lighted. (6) Take several readings (at least three), arresting and releasing the system for each. (7) Read and note time and temperature. (8) Clamp system, rotate to N in W position. (9) Repeat (6) in this position.[18] (10) Clamp magnetic system. Push in safety lock. (11) Dismantle station. Do not jar the instrument when placing it back in its case.

Table 41 is a specimen field record and office calculation. The first occupies the left, the second the right side of a notebook in the corresponding horizontal columns. Anomalies are figured in reference to a base station. The forms given here may be readily modified to suit special conditions.

<div align="center">

TABLE 41
FIELD RECORD

</div>

No.	Location	Date	Time	Tripod	Readings		Av.	Magnets	Temp.
20	NE cor. Sec. 15 R 52 W T 1 S	July 20, 1936	10 A.M. 58 to 11.02	42° (222°)	E 30.0 30.1 30.2		30.1	$M =$ } none $r =$ }	32°
					W 29.8 29.9 30.0		29.9	N $\frac{\text{up}}{\text{down}}$	

<div align="center">

OFFICE RECORD

</div>

s	s_t (γ)	Temp. Corr.	Magnet Corr.	Var. Corr.	Latit. Corr.	Base Corr.	Corr. Read.	Base (γ)	Anomaly (γ)
30.0	900	−12	none	+50	+10	+12	+960	+500	+460

[18] In rapid reconnaissance surveys and when anomalies are large, one or two readings in each azimuth are sufficient. For further increase in speed, other types of magnetometers not requiring a tripod (dip needle, author's Cardan-suspension magnetometer) should be used if they meet the accuracy requirements. In a Schmidt balance the time required for setting up, leveling, and orienting is out of proportion compared to the time consumed in taking the readings.

2. The *Schmidt horizontal balance*[19] is intended for the measurement of horizontal intensity anomalies. It is so designed that it fits the vertical magnetometer tripod. Therefore, vertical intensity measurements may be followed immediately with horizontal intensity determinations at the same station. The first horizontal magnetometers were constructed with a cylindrical case surrounding a vertical magnetic system balanced on a knife edge (see Fig. 8–23). For the later models no special case was made, the round case shown in Fig. 8–18a being adapted to both horizontal and vertical magnetometer systems. This is a simplification from the construction point of view; it is not feasible to use one case and to insert first the vertical and then the horizontal magnetic system.

The construction of the horizontal and the vertical balances is similar. In the earlier type of system illustrated in Fig. 8–19 an aluminum cube carries a knife edge and two magnetized steel blades, mounted in a vertical position so that when the system swings in the magnetic meridian, a deflection will be produced by the horizontal intensity anomaly. The normal horizontal intensity is balanced by unsymmetrical mass distribution; the center of gravity is to the north and above the axis of rotation.[20]

The magnetic system carries a mirror whose deflections can be read on an autocollimational telescope system as in the vertical magnetometer. Thermometers, levels, dampers, and arresting mechanism are likewise provided. In the more recent types, compensated systems and telescopes with teleobjective lenses are em-

Fig. 8-23. Section of Askania-Schmidt horizontal magnetometer.

[19] Heiland, *op. cit.*, 261–313 (1929).
[20] *Ibid.*

ployed. The tripod and compass of this instrument are the same as in the vertical magnetometer except that the auxiliary magnets are used in a horizontal and not in a vertical position.

For a deviation of the theory eq. (8–18) may be used, making allowance for the fact that the zero position of the magnetic system is vertical and that the components a and d of the gravity arm are interchanged because d is now parallel to the magnetic axis.   Then

$$\tan \varphi = \frac{M\mathbf{H} \cos \alpha - mga \sin \iota}{M\mathbf{H} \sin \alpha \cos \iota + MZ \sin \iota + mgd \sin \iota}. \qquad (8\text{–}28a)$$

In the operating positions, $\alpha = 0$ and $\iota = \pi/2$, so that

$$\overline{MZ +} \qquad\qquad (8\text{–}28b)$$

and the reading

$$s - \iota_y - \frac{}{\overline{MZ -}} \qquad\qquad (8\text{–}28c)$$

which may be written

$$s - s_0 = \frac{2\mathrm{f}M}{MZ -} \qquad\qquad (8\text{–}28d)$$

where mga/M is the horizontal intensity $\mathbf{H}_0$ for which the system is adjusted, and

$$\frac{2\mathrm{f}M}{} \qquad 1 \qquad\qquad$$

is the reciprocal scale value of the horizontal magnetometer.

If the instrument is not oriented correctly, an appreciable error may be introduced.   If in eq. (8–28a), $\iota = \pi/2$ and if eq. (8–28c) is substituted, we have for the difference of correct reading, and reading in the azimuth

$$s_\alpha - s = \frac{\mathbf{H}}{\epsilon_\mathbf{H}} (\cos\alpha - 1). \qquad (8\text{–}29)$$

The curve shown in Fig. 8–24 has been calculated for a horizontal intensity of $21{,}790\gamma$ and a scale value of 15γ in Golden, Colorado. An azimuth error of 40′ produces an error of one-tenth of a scale division; hence, the effect of mis-
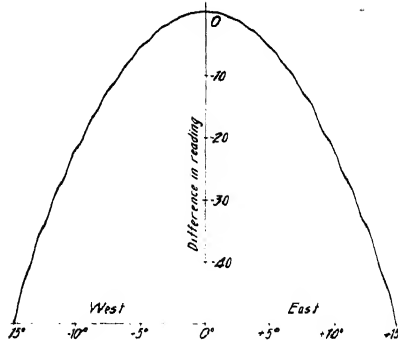
FIG. 8-24. Effect of azimuth changes on horizontal magnetometer.

orientation is much greater on the horizontal than on the vertical field
balance. As it is not customary to apply a correction, the instrument
must be set up accurately before readings are taken; the graduated
circle on the tripod head furnishes the required accuracy.

A tilt of the instrument in any direction may be resolved into a com-
ponent i_N in the N-S and another i_E in the E-W direction. The influence
of the former is of an optical nature, and the change in reading

$$\Delta s = \pm 2f\sigma(n_N - n_0), \qquad (8\text{-}30)$$

where n_0 is the reading of the level bubble (mean of the two ends) in the
horizontal position, n_N the new reading if the instrument is tilted toward
north, and σ the scale value of the level. For an old-style telescope,
$2f\sigma \approx 0.2$. As it is not customary to apply a correction for incomplete
leveling, the instrument should be leveled within one-half a division in
the N-S direction; at right angles thereto, not so much care is necessary.
In comparison with the vertical balance, greater care in leveling is neces-
sary in the plane of oscillation of the system, since two operating positions
to cancel the effect are not available.

As in the vertical instrument, auxiliary magnets are used for determina-
tions of scale value and for increasing the range, and they are applied in
the second principal Gauss position. If the scale has disappeared toward
the south (readings too great), the auxiliary magnet is used with its north
pole toward north. The correction is positive, since the effect of the
magnet is negative, and vice versa. The correction in scale divisions

$$\Delta s = \mp \frac{M_a \mathbf{k}}{\frac{1}{r^2}\left(\frac{3}{2}\, l^2 - \frac{3}{8}\, L^2\right)}$$

Variations in vertical intensity affect the scale value and must be allowed
for. As the horizontal balance is generally used in conjunction with the
vertical instrument, the vertical intensity is known. From eq. (8-28e),

$$\Delta\epsilon = \frac{\Delta Z}{2f}. \qquad (8\text{-}32a)$$

The vertical intensity effect is positive for deflections to one side and
negative for deflections to the other side of 20. Therefore, the correction

$$\Delta H = \Delta\epsilon(s - 20) = \frac{\Delta Z}{2f}(s - 20). \qquad (8\text{-}32b)$$

As differences in $\mathbf{H}$ are figured from the base station, differences in $\mathbf{Z}$
should be taken the same way, provided that the scale-value determina-

tions incorporating the original **Z** are made at the same station. The
diagram shown in Fig. 8-25 represents the vertical intensity correction as
a function of readings from 20 and difference in vertical intensity.

As in the vertical magnetometer, the effect of *gravity variations* is negli-
gible. The influence of *temperature* may be described in the same manner
as for the vertical magnetometer (eq's. [8-25]). Employing the notation
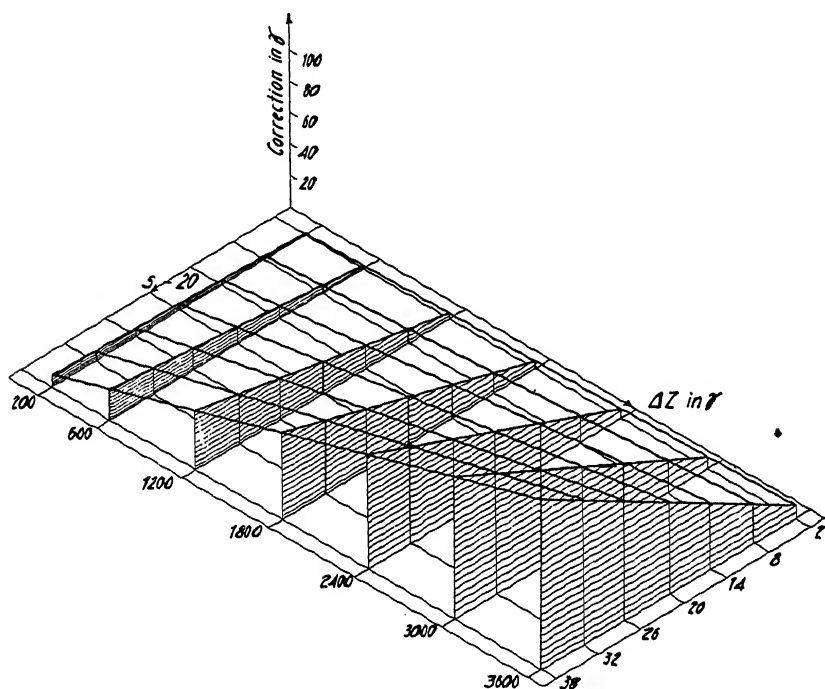
FIG. 8-25. Effect of vertical intensity changes on horizontal magnetometer.

in these equations, the following formula is obtained for the combined
magnetic and mechanical effects of temperature:

$$s_\theta = 2f \left\lfloor \frac{- \mu_s \Theta) - mga(1 -}{MZ(1 - \quad - mgd(1 -} \right. \tag{8-33}$$

For a compensated system,

$$- \mu_s = \mathbf{p} \qquad \text{and} \qquad q = \frac{}{mgd} \tag{8-34}$$

conditions which are effected in the earlier magnetic systems by shifting
the blades and in the newer systems by suitable spindle adjustment. The
effect of temperature on auxiliary magnets is the same as in the vertical

magnetometer and is given by $dH/d\Theta = -H\mu_a$, where **H** is the field and μ_a the temperature coefficient of the auxiliary magnet. Since the absolute sensitivity of a horizontal balance is usually greater than that of a vertical balance, it should be especially well protected against shocks. As before, $d(\epsilon s)/da = -mg/M$; a change of a by 25×10^{-6} mm is sufficient to produce a change of one scale division if $\epsilon_H = 15\gamma$. For changes in magnetic moment the equations for the horizontal and vertical magnetometer are the same.

Procedure in the latitude adjustment of a horizontal magnetometer is the same as in the vertical balance. Scale value determinations may be made (a) with magnets, (b) with coils, (c) by observations in different azimuths. Contrary to the vertical balance, the Helmholtz coils are set up with coil planes vertical, and magnets are used in second instead of first Gauss position. While the coil formula (8-26c) remains the same, the numerical factor and deflection constant, **k**, change in formula (8-26a), so that the scale value

$$\epsilon_H = \frac{2M_a k}{(s_2 - s_1)r^3} \quad \text{where} \quad k = 1 + \frac{1}{r^2}\left(\frac{3}{2}l^2 - \frac{3}{8}L^2\right). \quad (8\text{-}35)$$

Scale values may be obtained from observations in different azimuths where the horizontal intensity is known. From eq. (8-29) $\epsilon_H = \dfrac{H(\cos \alpha - 1)}{(s_\alpha - s)}$, where s_α is the reading in the azimuth α. Observations may be made in various azimuths to increase the accuracy, which, however, is dependent on how accurately the horizontal intensity at the station is known. The azimuth cannot be varied more than 12–13 degrees either way from north.

Moments of auxiliary magnets, temperature correction, base correction, auxiliary magnet correction, and planetary and diurnal variation corrections are applied as in the vertical magnetometer.

Likewise, the operation of the horizontal magnetometer is virtually the same as that of the vertical magnetometer, except that only one operating position is possible. This results in an increased number of readings in this position and greater care in orientation and leveling.

The general directions given previously for the application of the vertical magnetometer apply, especially in regard to the selection of stations. The steps in the operation of the horizontal magnetometer are as follows: (1) Remove instrument from case so that it acquires the temperature of the air. (2) Set up and level tripod. Orient tripod head with compass in the magnetic meridian. Fasten tripod head with screw. Read and note position of index. (3) Set up instrument on tripod; level with tube levels. (4) Orient instrument in magnetic meridian (N toward north).

(5) Adjust eyepiece and mirror until scale is in focus and evenly lighted.
(6) Take a number of readings; arrest and release system between readings. (7) If necessary, use auxiliary magnets. (8) Read and note time and temperature. (9) Clamp magnetic system. Push in safety lock. (10) Dismantle station; avoid jarring instrument when placing it into case. Calculation forms for the horizontal magnetometer (Table 42) are virtually identical with those for the vertical magnetometer except that readings are entered for one operating position only and that a column for vertical intensity correction is added:

TABLE 42
FIELD RECORD

No.	Location	Date	Time	Tripod	Readings s	Magnet	Temp.
20 '	NE cor. Sec. 15 R 52 W T 1 S	July 20, 1936	11 a.m. 04 −12.07	42°	3.8, 3.9, 4.0	$M = 100$ $r = 30$ N in S	32°.0

OFFICE RECORD

$s-20$	$(s-20)$ $\times \epsilon$ (γ)	Temp. Corr. (γ)	Magnet Corr. (γ)	Var. Corr. (γ)	Latit. Corr. (γ)	Vert. Int. Corr. (γ)	Base Corr. (γ)	Corr. Read. (γ)	Base (γ)	Anomaly (γ)
−16.1	−242	−12	−370	−279	−8	−6	−12	−889	−270	−619

3. In *Haalck's universal balance*[21] the magnetic system consists of a "magnetic cross". Horizontal and vertical blades are attached to an aluminum cube which carries a mirror on its side whose deflections are observed by means of a telescope with an autocollimational system. The magnets are fastened to one side only for purposes of temperature compensation. Declination and vertical and horizontal intensity may be measured with this instrument. For this purpose two additional deflector magnets are provided, one mounted above at an angle of 45 degrees (at right angles to the imaginary magnetic axis of the system), the other below in horizontal position. The oblique magnet is used in horizontal intensity measurements; the horizontal magnet in vertical intensity determinations. The latter magnet is permanent while the oblique magnet may be taken out, changed in distance, and reversed in polarity.

With reference to Fig. 8-26, the gravity couple is the same as in the vertical magnetometer, or $D_2 = -mg \sin \iota (a \cos \delta - d \sin \delta)$. The magnetic couple follows from eq. (8-16) by replacing the magnetic cross

[21] For illustrations, see H. Haalck, *Die magnetischen Verfahren der angewandten Geophysik*, Fig. 72, Borntraeger (Berlin, 1927).

by an equivalent magnet of moment M in the symmetry axis of the cross (see Fig. 8-26) and by substitution of $45° + \delta$ for the angle η. Then from $D_1 + D_2 = 0$,

$$\tan \delta \equiv \frac{0.707M[\mathbf{H}(\sin \alpha \cos \iota - \cos \alpha) + \mathbf{Z} \sin \iota] + mga \sin \iota}{0.707M[\mathbf{H}(\sin \alpha \cos \iota + \cos \alpha) + \mathbf{Z} \sin \iota] + mgd \sin \iota}. \quad (8\text{-}36a)$$

Since $\tan \delta = (s' - s_0)/2f$, we have for a horizontal axis of revolution, $(\iota = \pi/2)$,

$$\frac{s - s_0}{2f} = \frac{0.707M(\mathbf{Z} - \mathbf{H} \cos \alpha) + mga}{0.707M(\mathbf{Z} + \mathbf{H} \cos \alpha) + mgd}, \quad (8\text{-}36b)$$

which is the principal equation for the instrument.
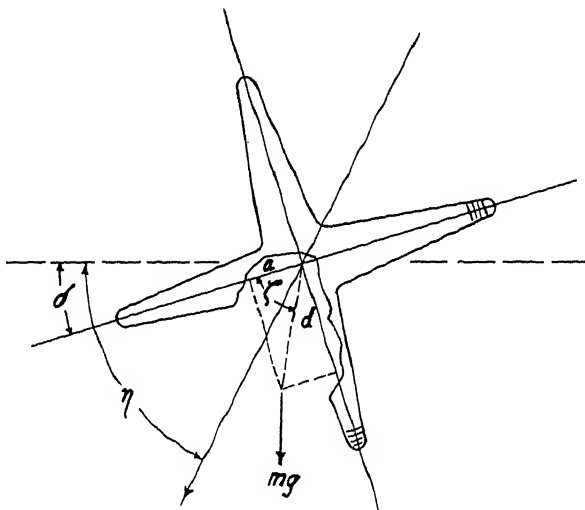
FIG. 8-26. Magnetic system of Haalck universal magnetometer.

After the magnetic meridian has been determined by a compass, the instrument is oriented into the E-W position. If the reflected scale is not in the field, the horizontal deflector underneath is adjusted accordingly. Then

$$\frac{s' - s_0}{2f} = \frac{0.707M\mathbf{Z} \pm mga}{0.707M\mathbf{Z} \pm mgd}. \quad (8\text{-}36c)$$

With sufficient accuracy an average value of $\mathbf{Z} \equiv \mathbf{Z}_0$ may be taken for the $\mathbf{Z}$ in the denominator, so that

$$s = \frac{2fM}{0.707M\mathbf{Z}_0 \pm mgd} \left(0.707\mathbf{Z} \pm \frac{mga}{M} \right), \quad (8\text{-}36d)$$

where $(0.707MZ_0 - mgd)/2fM = \epsilon_Z$, the "vertical-intensity scale value" of the instrument.

For measurements of horizontal intensity, the instrument is used in the magnetic meridian and in two positions. The oblique deflector must be turned about its center when the magnetic system is rotated from $\alpha = 0$ to $\alpha = \pi$. For the two positions, from eq. (8–36a),

$$\left. \begin{aligned} \frac{(s' - s_0)_N}{2f} &= \frac{0.707M(Z - H) \pm mga}{0.707M(Z + H) \pm mgd}, \qquad \text{when } \alpha = 0 \\[2mm] \frac{(s' - s_0)_S}{2f} &= \frac{0.707M(Z + H) \pm mga}{0.707M(Z - H) \pm mgd}, \qquad \text{when } \alpha = \pi. \end{aligned} \right\} \quad (8\text{–}36e)$$

With the following two scale values for the horizontal intensity:

and

$$\left. \begin{aligned} \epsilon_N &= \frac{0.707M(Z_0 + H_0) \pm mgd}{2fM} \\[2mm] \epsilon_S &= \frac{0.707M(Z_0 - H_0) \pm mgd}{2fM}, \end{aligned} \right\} \quad (8\text{–}36f)$$

the readings

$$\left. \begin{aligned} \epsilon_N s_N &= 0.707(Z - H) \pm \frac{mga}{M} \\[2mm] \epsilon_S s_S &= 0.707(Z + H) \pm \frac{mga}{M}, \end{aligned} \right\} \quad (8\text{–}36g)$$

with $s_N = (s' - s_0)_N$ and $s_S = (s' - s_0)_S$.

The difference of the two equations gives the horizontal intensity, so that

$$\frac{1}{1.414}(\epsilon_S s_S - \epsilon_N s_N) = H, \qquad (8\text{–}36h)$$

while their sum gives the vertical intensity

$$\frac{1}{2}(\epsilon_S s_S + \epsilon_N s_N) = 0.707Z \pm \frac{mga}{M}. \qquad (8\text{–}36i)$$

The instrument may theoretically be used for the determination of the magnetic meridian since the latter is situated midway between two directions near S-E and S-W in which the readings are equal. However, the procedure is involved and has been rarely used.

4. *Miscellaneous modifications of Schmidt magnetometers.* In Ambronn's modification of the Schmidt vertical magnetometer the scale is engraved on the end of the magnetic blade and is read on a prism telescope.

The double prism in it admits light from the outside and reflects the reading up to the eyepiece, with which an ocular micrometer is used. The case is provided with a copper mantle and is highly polished on the outside. In the Ostermeier balance the arrangement is essentially the same as in the Schmidt balance, except that the telescope is mounted horizontally on the side of the box. This places the instrument at greater distance from the ground and minimizes terrain effects. The case is likewise highly polished to reduce temperature interference. Watt's and Toepfer's balances differ from the original Schmidt only in construction but not in principle. Koulomzine's balance has a temperature-compensated magnetic system.
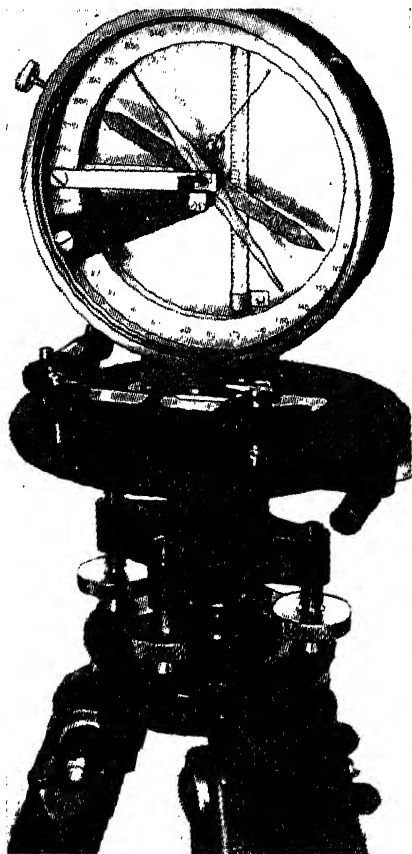
FIG. 8-27. Hotchkiss superdip.

In Koenigsberger's and Angenheister's balances, wire suspension instead of knife edge support is used. If D_1 is the magnetic, D_2 the gravity, and D_3 the torsional couple, two constructions are possible: (1) D_2 may be so adjusted as to nearly compensate D_1, and the residual may be compensated by the torsion of the wire. In such cases the wire needs to have only a small torsional coefficient (1/6 to 1/10 of g). (2) D_2 may be made very small and then may be additive or substractive to D_1. In such a case, D_3 compensates $D_1 - D_2$ or $D_1 + D_2$ and the wire has to be fairly strong. Koenigsberger has used the first, Angenheister the second possibility. The latter suspended a very light magnetic system from heavy tungsten monocrystalline wires. The advantage of wire instruments is that they may be used as universal magnetometers if the suspensions are strong enough.

5. The *Hotchkiss superdip*[22] is intended primarily for measurements of the total intensity and secondarily for dip determinations as shown in Figs. 8-27 and 8-28. A magnet rotates about a horizontal steel axle on agate bearings in the plane of the magnetic meridian. It may be adjusted

---

[22] N. H. Stearn, A.I.M.E. Geophysical Prospecting, 169–186 (1932).

in a position at right angles to the inclination by a counterweight at the end of a nonmagnetic bar fastened symmetrically to the magnet. The angle between the bar and the magnetic axis can be changed. The position of the counterweight changes the "latitude" adjustment, while the angle of the arm with the magnet controls essentially the sensitivity of the instrument. In the construction of the instrument, the centers of gravity of magnet and counterarm are made as nearly coincident with the axis of rotation as possible. During transportation, the swinging assembly is lifted from the bearings and pressed against two confining brackets. Readings in degrees are taken on a graduated circle. Zero of this graduation is up at the highest point of the circle. A trigger is provided to release the magnet from this position. The amplitude of swing from the
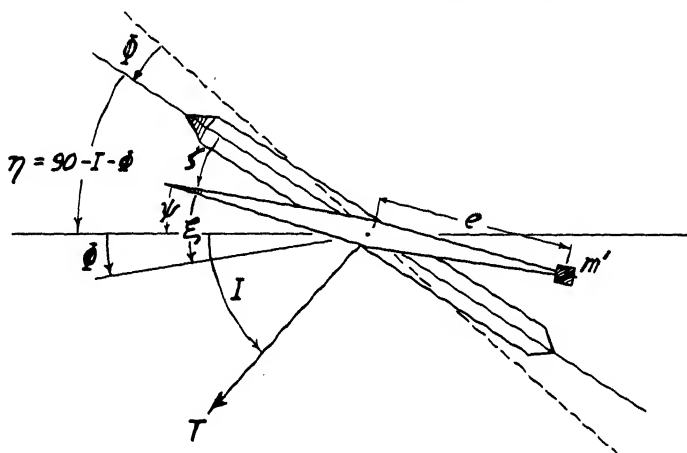
FIG. 8-28. Action of Hotchkiss superdip.

vertical position of the north pole is proportional to twice the deflection angle measured statically as described below. A thermometer is mounted inside the instrument case. For dip determinations, the instrument is oriented in the meridian, the counter weight unscrewed, the counterarm placed parallel to the magnetic axis, and a number of readings taken. In making total-intensity observations, the counterarm is set at an angle ζ determined by the desired sensitivity and the counterweight is so adjusted that the rest position of the system will be at right angles to the direction of inclination. Since it is too laborious to determine both inclination and total intensity (which, moreover, disturbs the constancy of horizontal balance essential for a relative instrument), total intensity alone is generally observed.

The following theory holds for static deflections φ from a rest position normal to the direction of dip when the counterarm is adjusted at the angle ζ.

Substituting $90 - I - \varphi$ for η in eq. (8-16), the magnetic couple for $\alpha = 0$ is

$$D_1 = M\mathbf{H} \sin (90 - I - \varphi) + MZ \cos (90 - I - \varphi). \qquad (8\text{-}37a)$$

When $D_1 = 0$,

$$\tan \varphi = \frac{M\mathbf{H} \cos I + MZ \sin I}{M\mathbf{H} \sin I - MZ \cos I}. \qquad (8\text{-}37b)$$

Substituting $\mathbf{H}/\mathbf{T}$ for $\cos I$ and $\mathbf{Z}/\mathbf{T}$ for $\sin I$, $\tan \varphi = \infty$ and $\varphi = 90°$. Without the counterweight the needle points in the direction of the inclination. For intensity determinations the gravity action due to the counterarm must be considered. It is proportional to the mass m', its arm e, and the angle ψ; hence, the moment $D_2 = -em'g \cos \psi$. Substituting $\psi + \zeta = 90 - I - \varphi$ and $\xi = \psi + \varphi$ (from Fig. 8-28),

$$D_2 = -em'g \cos (\xi - \varphi). \qquad (8\text{-}37c)$$

In the position of equilibrium, $D_1 + D_2 = 0$, or

$$\tan \varphi = \frac{M\mathbf{H} \cos I + MZ \sin I - em'g \cos \xi}{M\mathbf{H} \sin I - MZ \cos I + em'g \sin \xi}. \qquad (8\text{-}37d)$$

Substituting $\cos I = \mathbf{H}/\mathbf{T}$, $\sin I = \mathbf{Z}/\mathbf{T}$, and $(\mathbf{H}^2 + \mathbf{Z}^2)/\mathbf{T} = \mathbf{T}$,

$$\tan \varphi = \frac{M\mathbf{T} - em'g \sin (I + \zeta)}{em'g \cos (I + \zeta)}. \qquad (8\text{-}37e)$$

For a critical angle $\zeta_0 = 90° - I$, φ becomes $90°$ and the system swings into the direction of the inclination. For two total intensities, $\mathbf{T}'$ and $\mathbf{T}$ the two corresponding deflections are given by $\tan \varphi' - \tan \varphi = \dfrac{M(\mathbf{T}' - \mathbf{T})}{em'g \sin \xi}$, which for small angles, is $\Delta \varphi = \epsilon \Delta \mathbf{T}$, where the scale value

$$\epsilon = \frac{em'g \sin \xi}{M}. \qquad (8\text{-}37f)$$

Note the similarity of this scale value and that of the vertical Schmidt balance, $(\epsilon = mgd/2fM)$. The $e \sin \xi$ corresponds to $d = e \sin \zeta$. A diagram showing the sensitivity as a function of angle ξ and further details concerning the operation of the instrument are given in Stearn's article.[28]

6. *Early Swedish and American prospecting instruments.* Of simple construction, these instruments were designed for the rapid measurement of large magnetic anomalies and are still in use for rapid reconnaissance in many mining districts; the use of more accurate instruments there would offer no particular advantage.

---

[28] *Ibid.*

The *Swedish mining compass* is probably the earliest magnetic prospecting instrument,[24] consisting essentially of a light needle in jewel and stirrup suspension, free to move in a horizontal and vertical direction. The case is carried over the ground by three cords tied together above the instrument. To compensate for the vertical component of the earth's field, a small piece of wax may be attached to the south end of the needle.

Not only the vertical component but also the horizontal intensity affects the mining compass. Their action is somewhat involved, since the normal vertical intensity may be compensated by gravity, while the horizontal intensity is not. No actual measurement of H or Z is made. The instrument is used qualitatively. In its practical application, it was soon discovered that the maximum indication is *not* found directly over an ore deposit (if, as is generally done, the vertical intensity is not fully compensated).

The mining compass may be considered a dipping (or dip) needle[25] with automatic meridian adjustment; hence, in eq. (8-15), $\alpha = 0$. Further, since the pivot in the jewel is above the center of gravity, $\iota = \pi/2$ and $D_1 = M(H \sin \eta - Z \cos \eta)$. For the gravity moment, $D_2 = -em'g \sin \iota \cos \eta = em'g \cos \eta$, where m' is the mass of the wax used to place the system approximately horizontal. From $D_1 + D_2 = 0$,

$$\tan \eta = \frac{MZ - em'g}{MH} = \frac{1}{H}\left(Z - \frac{em'g}{M}\right). \qquad (8\text{-}38a)$$

For full compensation of the normal vertical intensity Z_0, $MZ_0 = em'g$, or

$$\tan \eta = \frac{Z - Z_0}{H} = \frac{\Delta Z}{H}. \qquad (8\text{-}38b)$$

The mining compass may therefore be considered a vertical magnetometer with the horizontal intensity as scale value. Since $H = Z \cot \mathrm{an} I$,

$$\tan \eta = \tan I \frac{\Delta Z}{Z}. \qquad (8\text{-}38c)$$

Hence, this instrument furnishes the magnetic inclination multiplied by the "relative" vertical intensity anomaly and therefore acts like the dip needle. As the horizontal intensity may be written: $H = H_0 + \Delta H$,

$$\tan \eta = \frac{\Delta Z}{H_0 + \Delta H}. \qquad (8\text{-}38d)$$

---

[24] For illustrations see Fig. 510 on p. 41 of Fr. J. Berg's catalogue, *Magnetometers*, and Fig. 31 in Eugene Haanel's. *On the Location and Examination of Magnetic Ore Deposits by Magnetometric Measurements*, Dept. Int., (Ottawa, 1904).

[25] For difference between "dip" and "dipping" needle, see p. 346.

This equation illustrates plainly that the greatest deflections will be obtained on the north side of an ore body (for, in the extreme case, $-\Delta H \doteq H_0$, and $\eta = 90°$).

The *American mining compass*, or meridian finder, an improvement of the Swedish mining compass, was produced in the United States in 1860. It was used for a magnetic survey by the Geological Survey of New Jersey in 1880. The needle is free to rotate about a horizontal axis, the bearings being mounted on upright aluminum strips capable of rotation about a vertical axis. A modification of the American mining compass is Prof. Louis' *dipping compass*. In this instrument the needle rotates in both horizontal and vertical directions; the dip of the needle is observed on a semicircular vertical scale which is weighed down and pivoted in line with the axis of revolution of the magnet. The *dial compass* was first described by William Borough in 1581, and is essentially a combination of a sun dial and a compass. In application, the apparent time is determined for the locality and the instrument so turned that the shadow of the dial string falls on the dial division corresponding to this time. The plane of the sighting attachment is then in the meridian and the angle between it and the magnetic needle is the declination. Many magnetic surveys were made with this instrument in the Michigan iron ore region in the early days.

The dip needle should not be confused with the dipping needle. The dipping needle is an inclinator, or an instrument for the determination of the inclination. In its magnetic system, the center of gravity is coincident with the axis of revolution. The dip needle, however, has a counterweight attached to its south side to compensate the inclination and is essentially a vertical intensity instrument. If it were used at right angles to the meridian, the deflections would depend on vertical intensity only. The dip needle has been employed extensively in the Lake Superior iron and copper country. In civil engineering it is frequently used for locating buried pipes and other iron objects. As shown in Fig. 8-29, the dip needle[26] consists of a circular case with graduation in degrees and zero division in the horizontal position. The needle is made of one or more magnetic blades; the pivot is made of steel and supported by two agate, cup-shaped jewels; and the counterweight is a brass rivet or a movable rider. An arresting device is operated by a thumb lever at the top. The meridian is first determined[27] by holding the case horizontal and allowing the needle to adjust itself into the meridian. In this direction the case is turned in the vertical position for the observation of the deflection from

---

[26] N. H. Stearn, A.I.M.E. Geophysical Prospecting, 345–363 (1929).

[27] Fig. 8-29a shows a dip needle with automatic meridian adjustment (gimbal suspension).

horizontal.   Equations previously derived for the mining compass ([8–38a]
and [8–38c]) fully express the action of the dip needle in the magnetic
meridian.
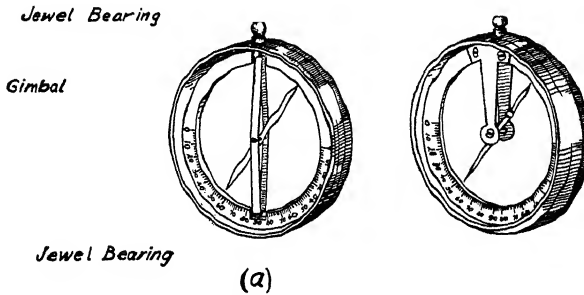
FIG. 8-29. (a) Dip needle in gimbal suspension.   (b) Ordinary dip needle.
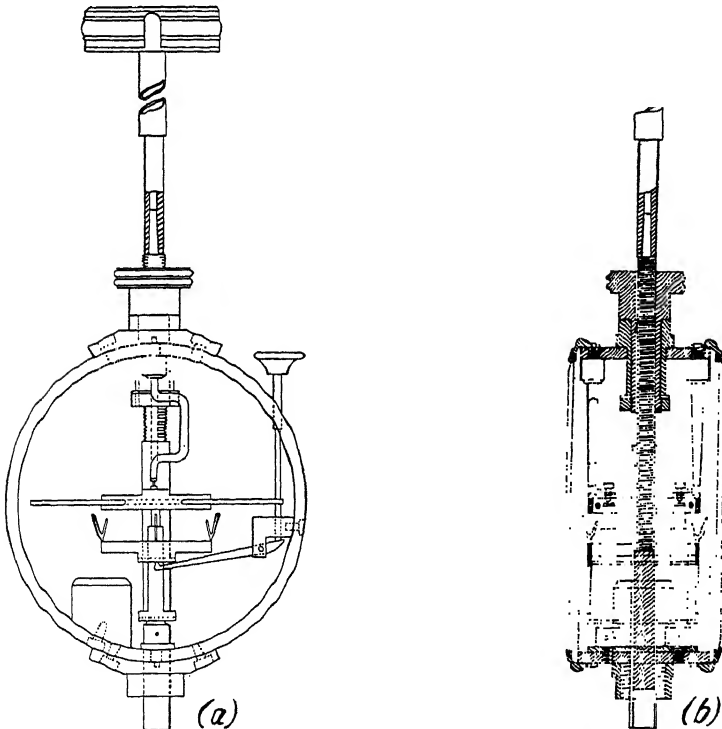
FIG. 8-30. Thomson-Thalén magnetometer (after Haanel).

The *Thomson-Thalén magnetometer* is similar in construction to the
Schmidt vertical balance.   Anomalies in vertical intensity are not read
in terms of deflection angles; they are compensated by changing the posi-
tion of a deflecting magnet beneath the magnetic system.   The differences

in the inverse cubes of the observed readings are, therefore, proportional to the differences in intensities. The instrument shown in (Fig. 8-30[28]), contains a magnetic system consisting of two parallel cylindrical magnetic needles, mounted in a brass ring with like poles in the same direction. This ring is supported in agate, cup-shaped bearings by two pointed hardened steel screws. The arresting mechanism consists of another brass ring below the magnetic system. This ring carries four forks which lift the system off its bearings and press it firmly against two pillars mounted to the upper part of the circular case. The compensating magnet is slightly below the system, north pole up, and is attached to a long spindle, which ends at the top of the case. The spindle may be moved up or down by turning a keyed thumb-nut at the top of the case. This nut is graduated in centimeters, part of the threads being faced off for the divisions. The readings indicate the distance of the upper pole of the magnet from the magnetic system.

The instrument is used at right angles to the magnetic meridian, placed in this direction by a compass mounted permanently on a long staff above the instrument. The deflection of the magnetic system is given by eq. (8-20), or $\tan \eta = (MZ - mga)/mgd$. Contrary to the Schmidt balance, η in this equation is very large, since mga is too small to compensate MZ. Compensation is effected by a magnet producing, in its normal position, a field $\Delta Z_0 = -2M_a k_0/r_0^3$ (which is only approximate for this instrument, as the magnet is very close to the magnetic system). With the effect of the compensator, $\tan \eta = \dfrac{M}{mgd}\left(Z - \dfrac{mga}{M} - \Delta Z_0\right)$. At a point with normal vertical intensity, the compensating magnet is so adjusted that for its distance r_0 the system is horizontal. At another point with the intensity Z, the compensator is moved to a distance r, so that the system is again horizontal. Then $Z' - Z_0 = 2M_a(k_1/r_1^3 - k_0/r_0^3)$. For small differences in distance, $k_0 = k_1 \equiv k$, and

$$\Delta Z = 2M_a k\left(\frac{1}{r_1^3} - \frac{1}{r_0^3}\right). \tag{8-39}$$

This formula is only approximate. A graph showing vertical intensity anomaly as a function of compensator distance based on a more accurate calculation, has been published by Haanel.[29] In practice it would be preferable not to use any calculated effect, but to calibrate with Helmholtz coils or deflecting magnets.

In the *Dahlblom pocket magnetometer* a magnet is suspended in bearings

---

[28] See Haanel (*op. cit.*), Figs. 26 and 27 on pp. 57–58, and plate E; also No. 507 s.e. and No. 509, pp. 30 and 31, Berg's catalogue.

[29] *Op. cit.*, p. 62.

as in a dip needle; however, the comparison force is not gravity but the torsion of a helical spring.

The *Tiberg inclinator*[30] is essentially a compass. The needle rotates on a steel pivot in agate bearings and may be used in either horizontal or vertical plane; the sides of the compass case carry two studs which fit into the standards of the Thalén-Tiberg magnetometer.

The *combined Thalén-Tiberg magnetometer* consists of a tripod head with two uprights to receive the Tiberg inclinator and a horizontal arm with deflecting magnet for the determination of the horizontal or vertical intensity by the tangent method of Gauss or the sine method of Lamont.[31] In the tangent method, the deflection at a base station is given by $\tan \alpha_0 = F/H_0$, where α_0 is a normal angle corresponding to the horizontal intensity H_0 at the base, and F is $2Mk/r^3$. At another station, $H_1 \tan \alpha_1 = F$; therefore,

$$H_1 = \frac{H_0 \tan \alpha_0}{\tan \alpha_1} = \frac{F}{\tan \alpha_1} . \qquad (8\text{-}40a)$$

In the sine method, the needle is deflected and the deflecting arm is rotated until it is at right angles to the needle. Then, $\sin \alpha_0 = F/H_0$; at another station, $H_1 \sin \alpha_1 = F$; thus

$$H_1 = \frac{H_0 \sin \alpha_0}{\sin \alpha_1} = \frac{F}{\sin \alpha_1}. \qquad (8\text{-}40b)$$

Because of the proximity of the deflecting magnet, F is usually large, and conditions may be encountered were H_1 is small compared with $H_0 \sin \alpha_0$. Then the needle cannot be made to occupy a position at right angles to the deflection arm. This defect can be overcome by using the "Dahlblom sine arm," which makes an angle of $30°$ with the original arm. On the arm the distance of the magnet (and therefore F) may be varied by a pulley arrangement. The angle of deflection is kept constant at $30°$. Then, $H_0 \sin 30° = F_0$, $H_1 \sin 30° = F_1$, or $H_0 = 2F_0$ and $H_1 = 2F_1$. Therefore, $H_1 = H_0(r_0/r_1)^3$, where r_0 and r_1 are the distances of the deflector corresponding to the fields F_0 and F_1. Hence, in principle, the Dahlblom sine arm operates like the Thomson-Thalén magnetometer.

7. *Other prospecting magnetometers based on balance or compass principle* include those designed by Kohlrausch, Schmidt, De Collongue, Ostermeier, Wilson, and the author. In the *Kohlrausch deflection magnetometer*, a compass is fastened to a vertical shaft[32] which may be moved up and down by rack and pinion in a tubular extension of a pedestal and may be clamped

---

[30] Illustrated in Figs. 505, 506 s, and 507 s of Berg's catalogue, on pp. 9, 11, 12.

[31] Illustrated in Figs. 507 s, p. 12, and 507 s.d., p. 18, of Berg's catalogue.

[32] See illustration in H. Haalck, *op. cit.*, Fig. 25, p. 29.
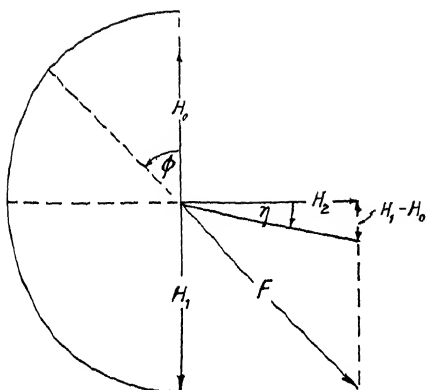
FIG. 8-31. Action of Kohlrausch deflection magnetometer.

field will turn the needle in the E-W direction. After this adjustment has been made in a normal field, everything is left so adjusted, and at another locality, after the meridian has been determined *without* the deflectors, the angle which the needle makes with the E-W position is observed. If the field of the deflectors is F and if its component in the S direction is H_1 and in the E direction H_2, (see Fig. 8-31), then $-H_1 = F \cos \varphi$ and $H_2 = F \sin \varphi$. If, at a base station, the needle is so adjusted that the needle points directly E-W, $H_0 = -H_1$, or $H_0 = F \cos \varphi$. Therefore, $H_2 = H_0 \tan \varphi$. At a locality where $H_1 \neq H_0$, the deflection η from the E-W direction is given by

$$\tan \eta = \frac{H_1 - H_0}{H} . \qquad (8\text{-}41)$$

Schmidt's compensation magnetometer is likewise designed for the determination of horizontal intensity by deflection, and the deflection

in position. The pedestal carries two deflecting magnets which may be rotated horizontally on a turntable into positions 30° west or 30° east of north. The north poles of the magnets are toward north, and the distance of the compass from these deflectors is so adjusted that the north-south component of the deflector field compensates the normal horizontal intensity of the earth's field. Then the E-W component of the deflector
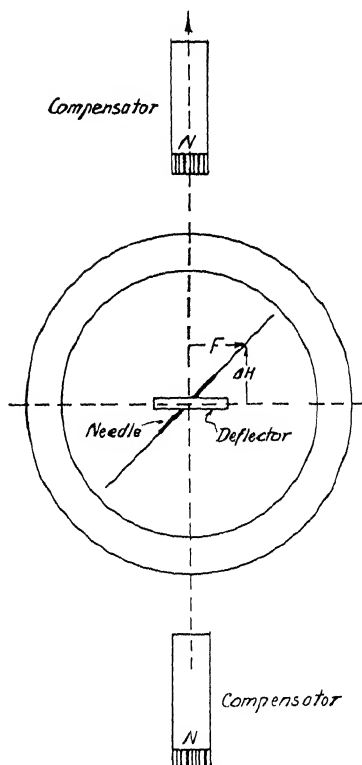
FIG. 8-32. Action of Schmidt compensation horizontal magnetometer.

angle is magnified by compensating most of the horizontal intensity. To obtain **H** with an accuracy of a few gammas by customary methods, it is necessary not only to use a comparison field of comparable magnitude at right angles to **H**, but to observe deflection angles with a high degree of accuracy. Obviously, the same accuracy may be obtained by compensating a portion of **H**, comparing the remainder with only a small field at right angles to **H**, and measuring deflection angles by crude means. The normal horizontal intensity is compensated in this instrument[33] by two magnets north and south of the compass box with their north poles oriented as shown in Fig. 8–32. Above the compass box, in third Gauss position, is a small magnet at right angles to the direction of the compensating field. Then $\Delta \mathbf{H} =$ $\mathbf{H}_1 - \mathbf{H}_0$ and $\tan \varphi = \dfrac{\mathbf{F}}{\mathbf{H}_1 - \mathbf{H}_0}$, so that

$$\tan \varphi = \frac{M_3 \cdot \mathbf{k}_3}{r_3^3 \left[\mathbf{H}_1 - \dfrac{2\mathbf{M}_1 \mathbf{k}_1}{r_1^3} - \dfrac{2M_2 \mathbf{k}_2}{r_2^3} \right]}, \qquad (8\text{–}42)$$

where M_1 and M_2 are the moments of the compensating magnets, M_3 that of the small comparison magnet, r_1, r_2, and r_3 their distances, and $\mathbf{k}_1$, $\mathbf{k}_2$, and $\mathbf{k}_3$ their deflection constants.

De Collongue deflectors have been constructed for horizontal and vertical intensity determination. The horizontal instrument is somewhat similar to the Schmidt compensation magnetometer. It consists of a compass box, a small deflector in the third Gauss and E-W position above the needle, and a large compensator, likewise in the third Gauss position, above the deflector. The compensator is always in the magnetic meridian and is moved up or down until the magnetic needle points E-W. Thus, the inverse cube of its distance is proportional to the horizontal intensity. The vertical intensity deflector is similar to the Thomson-Thalén magnetometer and has been developed primarily for observations on board ship.[34] A compass card is equipped as usual with magnets but is not balanced by a counterweight, and the vertical intensity is compensated by a deflector underneath. As the ship travels from one point to another with a different vertical intensity, the compass card will show an inclination which may be compensated by moving the deflector. Thus, vertical intensity observations are made here *in* the magnetic meridian.

The *Ostermeier universal magnetometer* is, in principle, identical with the Kohlrausch magnetometer. The magnetic system of a Schmidt vertical magnetometer is used as the deflector, and the compass of the same

---

[33] Illustrated in A. Nippoldt, *Erdmagnetismus, Einfuehrung in die Geophysik,* **II,** 37 (Berlin, 1929).
[34] Illustrated in Nippoldt, *op. cit.,* p. 41.

magnetometer is permanently mounted above the magnetometer. The vertical intensity is observed in the customary manner by a telescope mounted on the side of a box; the horizontal intensity is observed as in the Kohlrausch magnetometer; and the declination is determined with the compass alone.

The *Wilson compass attachment* is used with a Brunton compass at an angle of 30° in the same manner as a Dahlblom sine arm.[35]
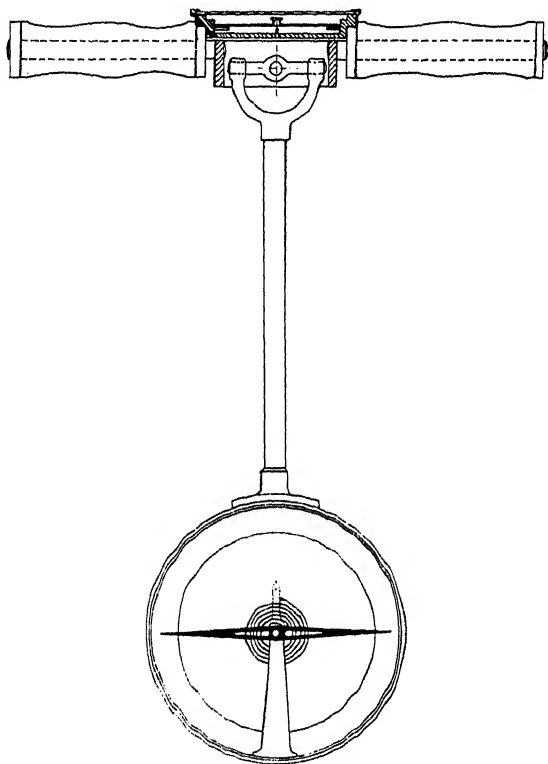
Fig. 8-33. Cardan suspension

The *Cardan suspension magnetometer*, designed by the author, is a vertical-intensity magnetometer similar to a Dahlblom pocket magnetometer, the comparison force being the torsion of a helical spring. The magnetic system is so suspended that the axis of revolution coincides as nearly as possible with its center of gravity. One end of the helical spring is attached to the magnetic system, and the other end is fastened to a movable arm which may be rotated about a horizontal axis by turning a pointer on a

---

[35] Illustration in A.A.P.G. Bull., 1392 (Nov., 1931).

graduated scale on the back of the case. The helical spring is virtually without torsion when the magnetic system is vertical (at right angles to the magnetic meridian). Then the pointer is moved until the magnetic system is in a horizontal position. If τ is the torsional coefficient of the spring, and ψ is the angle through which the pointer was turned to bring the magnetic system into the horizontal position, $MZ_0 = \tau\psi$, where M is the magnetic moment of the needle and Z_0 the "normal" magnetic vertical intensity for which the instrument is adjusted. At another station with the anomaly ΔZ, a deflection φ occurs, so that $M\Delta Z \cos\varphi = \tau\varphi$ or, with sufficient approximation for small angles, $\Delta Z = \varphi \cdot \tau/M$, where τ/M is the scale value of the instrument. The compass case (see Fig. 8–33) is suspended from a fairly long bar terminating in a gimbal suspension on the top. The compass for orienting the case into the magnetic prime vertical is permanently mounted on the upper ring of the Cardan suspension.[36]

8. *Prospecting magnetometers based on other principles* include the magnetrons, the slow-speed cyclotrons, and the magnetic torsion balance. Others, such as the iron-induction magnetometers, compass variometers, and earth inductors, will be treated under the heading of instruments intended for regional magnetic surveys. The earth-inductor gradiometer is discussed in connection with the earth inductors.

The *magnetron*[37] is a special type of diode with a straight axial cathode and a cylindrical anode surrounding it. When a magnetic field is present, the electrons will not travel radially from the cathode to the anode but will be curved into circular paths. After a critical field is reached, the electrons return to the filament without reaching the anode (see Fig. 8–34a). The critical field strength appears as an abrupt drop in plate current (see Fig. 8–34b). In the measurement of a weak field, as that of the earth, a solenoid is placed around the tube coaxially with the filament, and the current through it is so adjusted that the measurements take place on the critical part of the curve. The critical field strength is $H_0 = 6.72 \sqrt{E}/r$, where E is the plate voltage and r the radius of the anode. The magnetron may be used not only for the measurement of the total intensity by adjusting its axis parallel to the lines of force of the earth's field but also for any other component, as only the field in the direction of the axis is effective. The sensitivity of the tube can be increased by regeneration (passing the plate current through an additional solenoid). In practice, the field required to compensate the effect of the unknown field is measured. Rössiger[38] designed an instrument intended for the

[36] Heiland, Physics, **3**(**1**), 18–22 (July, 1932).

[37] See A. W. Hull, Phys. Rev., **3**, 279–292 (Sept., 1923). M. Rössiger, Zeit. Phys., **43**(7), 480–488 (1927). *Idem*, Zeit. Instr., **49**(3), 105–113 (1929).

[38] Zeit. Instr., *loc. cit.*

measurement of magnetic anomalies on a moving support. The accuracy was approximately 40γ.

Slow-speed cyclotrons[39] are designed to measure the time required for an electron to make one complete loop or revolution in the earth's field. Since the path of the electron adjusts itself at right angles to the direction of the field, the total intensity is determined thereby. The present accuracy is only 100 to 300γ. Mechanically, the principle involved is equivalent to a hood with two opposite windows placed over a source of electrons. At a given moment one of the windows is opened and the

(a)
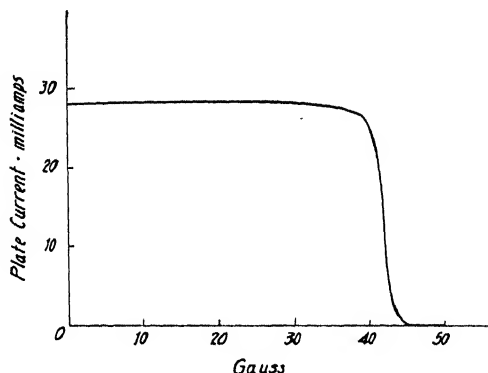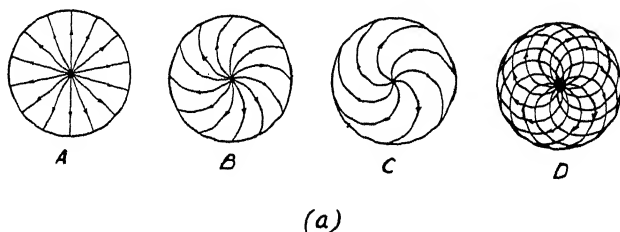
Fig. 8-34. Effect of axial magnetic field (*a*) on paths of electrons, (*b*) on plate current in magnetron. (After Hull.)

electrons are permitted to pass out to complete their loop in the magnetic field and return to the other window. By opening this window at the correct time and by providing means for recording the arriving electrons, the time required for one loop may be determined. In actual operation, the source of electrons is a heated wire, and the opened and closed windows are suppressor grids. They are connected to a tube oscillator and are

[39] See K. H. Stehberger, Terr. Mag., **38(3)**, 184 (Sept., 1933); and Ann. Physik, **17**, 278–292 (1933).

made periodically too negative to allow passage of electrons. The entrance of the electrons is detected by a direct current amplifier. By variation of the frequency of the oscillator, the interval between the emission and return of the electrons can be gauged, since maximum reception is obtained when electrons leave one window on one cycle and enter the other on the next, or another wavepeak. If H is the intensity of the field, v the velocity of the electrons, e/m their specific charge, and r their radius of gyration, $H = \dfrac{v}{e/m \cdot r}$, or $H = \dfrac{2}{e/m} \cdot n$, where n is the number of revolutions per second. Maximum plate current is obtained if the time of revolution is equal to the frequency f of opening or closing of the windows (or equal to a multiple thereof). Hence, $f = in$, or $H = \dfrac{2}{i \cdot e/m} \cdot f$.

A torsion balance for measuring magnetic and gravity gradients was first developed by Eötvös.[40] Berroth[41] perfected an instrument for the determination of gradients of vertical intensity. In the magnetic torsion balance, the hanging weight is replaced by a magnet suspended vertically. Two runs have to be taken, one with north pole up, the other with north pole down, since the magnetic axis of the suspended magnet usually does not coincide with the vertical. Magnetic and gravity gradients must be measured separately, as the magnetic balance is also affected by gravity forces. In Berroth's instrument one balance beam of a double balance is used for the determination of the combined magnetic and gravity effect, while the other measures the gravity effect alone.

This procedure for measuring magnetic gradients is complicated and requires an expensive instrument. Results are not in proportion to time and money expended, considering that the vertical intensity gradient may quite readily be obtained from vertical intensity maps and curves by graphic differentiation.

C. Instruments for Regional Magnetic Surveys

Most of these instruments were developed by government and state magnetic research institutions before the advent of the prospecting magnetometers. Their purpose is a complete determination of the earth's magnetic field, generally at fairly widely separated points. The most suitable magnetic elements are declination, inclination, and horizontal intensity. Instruments for the determination of these elements are called "magnetic theodolites." They include, in addition to an astronomic attachment, (1) an instrument for the determination of the magnetic declination

[40] Ann. Phys., **59**, 354–400 (1896).
[41] Zeit. Geophys., **9**(6/8), 355–368 (1933).

(declinator), (2) an attachment for the determination of the horizontal intensity by oscillation, (3) two bars for horizontal intensity determination by deflection, and (4) a dip circle for the determination of the inclination.
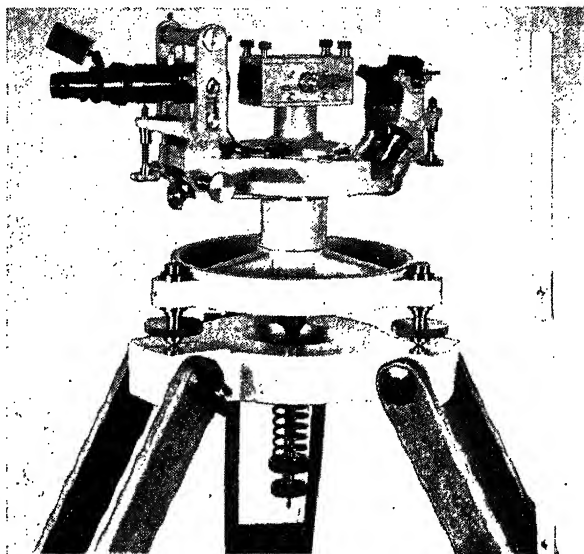
American Askania Corp.

Fig. 8-35a. Magnetic theodolite with declinator attachment.
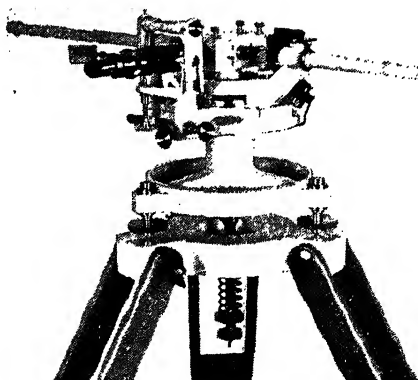
American Askania Corp.

Fig. 8-35b. Magnetic theodolite with deflector attachment.

The accurate determination of inclination has long been a problem in regional magnetic surveying, and the dip circle has gradually been replaced by the earth inductor. This instrument offers great possibilities not only for determining the direction of dip, but also for measuring declination

and horizontal, vertical, and total intensity. These applications will also be discussed in detail below. With perfection in earth inductor technique, it is quite possible that the combination of elements selected for magnetic regional surveys may undergo considerable revision. On the other hand, a simple magnetometer based on the balance principle may easily be substituted for the dip circle, so that a complete determination of the magnetic field would consist of measurements of declination, horizontal intensity (as measured at this time), and vertical intensity.
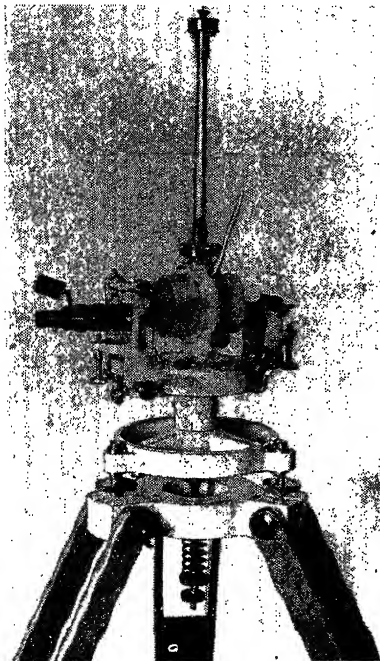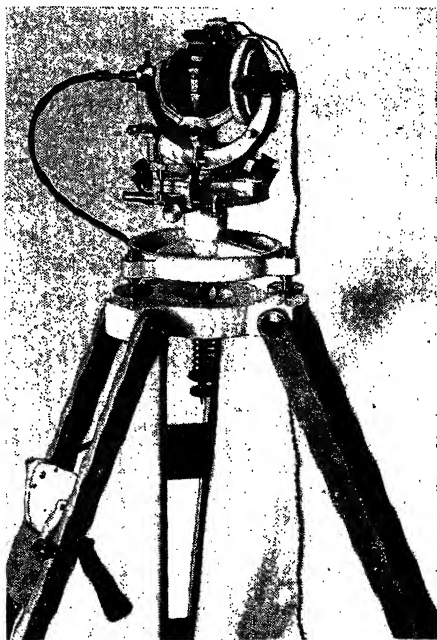
American Askania Corp.

8-35c 836d

Fig. 8-35c. Magnetic theodolite with oscillation box attachment.
Fig. 8-35d. Magnetic theodolite with inductor attachment.

1. *Magnetic theodolites* generally consist of a transit base with horizontal circle and horizontal telescope, to which may be fastened an attachment with standards, telescope, and vertical circle for astronomic observations. For the determination of the magnetic meridian, a small case with short magnetic needle, generally suspended in jewels and provided with a reflecting mirror, is used with the horizontal telescope. For oscillations, a wooden box attachment with torsion tube and thread suspension is substituted for the declinator case. Deflection observations are made with the declinator needle, and two bars with deflecting magnets are attached to

angle of the coil with the normal to the frame (z'' direction), the flux due
to z'' is 0 and that due to y'' is at a maximum when $\varphi = 0$. Hence, the
current due to z'' is max.+ and that due to y'' is 0. If $\varphi = 90°$ (coil
plane in plane of frame), the flux due to z'' is a max. that due to y'' is 0.
The current due to z'' is 0 and that due to y'' is max.+, and so on. In
Fig. 8–37, the e.m.f.'s induced in the coil are indicated by a dotted line.
For the y'' component the maxima occur at 90° and 270°, while for z''
the maxima occur at 0° and 180°. The plane of commutation being at
right angles to the coil, reversals in sign occur at the 90° positions for the
next 180°; therefore, the y'' component is neutralized (provided the gal-
vanometer period is large compared with the commutation period) and
only the e.m.f. due to the z'' component remains. Its value is obtained
from the last equation in (8–14). Changing the astronomic to magnetic
components so that $X' \equiv H$, $Y' = 0$, and $Z' \equiv Z$,

$$z'' = -H \sin \alpha \sin \iota + Z \cos \iota, \qquad (8\text{–}43)$$

where α is the magnetic azimuth of the axis aa' in Fig. 8–36, and ι the
inclination of the axis bb'. If the cross-sectional area of the coil is S and
the number of turns N, the total magnetic flux, when the coil is normal
to the field, is $\Phi = SNz''$. Hence, for any coil position given by the angle
with the y'' direction or "phase" angle, $\delta = 90 - \varphi = \omega t$, the flux $\Phi = SNz''$
$\cos \omega t$ and the induced e.m.f. $E = \dfrac{-d\Phi}{dt} = SNz'' \omega \sin \omega t$. Substituting
$S = \pi r^2$ (in which r is the mean turn radius of the coil) and $\omega = 2\pi n$ (in
which n is the number of revolutions per second),

$$E = 2\pi^2 r^2 Nz'' n \sin \omega t$$
$$I = \frac{2\pi^2 r^2 Nz'' n \sin \omega t}{R}, \qquad \left.\begin{array}{c} \\ \\ \end{array}\right\} \quad (8\text{–}44)$$

where R is the resistance of the coil plus the resistance of the galvanometer.

Instantaneous current values, speed of revolution, and phase angle are
difficult to measure. However, by using a ballistic galvanometer the
quantity of electricity (which is independent of the angular velocity) may
be determined. Since $E = -d\Phi/dt$, $I = (1/R) - d\Phi/dt$. $I dt =$ the quan-
tity of electricity, equals $dQ = -d\Phi/R$. At two instances when the
fluxes are Φ_2 (at the end) and Φ_1 (at the beginning of the motion), $Q =$
$\displaystyle\int_{\Phi_1}^{d} dQ = \frac{(\Phi_2 - \Phi_1)}{R}$. Since $\Phi = SNz'' \cos \delta$ in any position,

$$Q = \frac{\pi r^2 Nz}{R} \; (\cos \delta_1 - \cos \delta_2). \qquad (8\text{–}45)$$

The earth inductor may be used for determinations of declination or inclination, or horizontal, vertical, or total intensity.

To find the magnetic *meridian*, the frame B and therefore the axis of rotation of the coil are set vertical. The azimuth of the horizontal circle A is varied until the current vanishes. (In eq. [8–43], z'' is zero when $\alpha = 0°$ and $\iota = 90°$.) The accuracy of the meridian determination depends on the setting of brushes and commutator. By comparing the direction of zero current with the meridian direction as obtained from a compass, the commutator angle may be determined.

To find the *inclination* with an earth inductor, the axis aa' is oriented in the magnetic prime vertical ($\alpha = 90°; z'' = -\mathbf{H} \sin \iota + \mathbf{Z} \cos \iota$). The plane of the frame is rotated until the deflection of the galvanometer vanishes ($z'' = 0; \mathbf{H} \sin \iota = \mathbf{Z} \cos \iota$, or $\tan \iota = \mathbf{Z}/\mathbf{H} = \tan I$). The axis of rotation is then in the direction of inclination.

For determining the *horizontal intensity*, axis bb' is set vertical and axis aa' in the magnetic prime vertical. Then $\alpha = 90°$ and $\iota = 90°$ so that $z'' = -\mathbf{H}$. For ballistic measurements, substitute this in eq. (8–45) so that $\mathbf{Q_H} = \dfrac{2}{\mathbf{R}} \quad\quad - \cos \delta_2)$. By turning the coil through $180°$, $\delta_1 = 0, \delta_2 = 180°$, and

$$\mathbf{H} = \mathbf{G} \; \mathbf{RQ_H} \qquad\qquad (8\text{–}46a)$$

where $\mathbf{G}$ is the galvanometer constant.

To measure *vertical intensity*, the frame B is placed horizontally with the coil axis toward north, that is, aa' in the magnetic prime vertical. Then, $\alpha = 90°$ and $\iota = 0°$; hence, in eq. (8–43) $z'' = \mathbf{Z}$. Using a similar procedure as outlined before, the vertical intensity as measured on a ballistic galvanometer,

$$\qquad\qquad (8\text{–}46b)$$

$$2\pi r^2 N$$

In some earth inductors a spring switch is provided, which, after the completion of one-half turn, cuts the coil from the galvanometer circuit. Sources of errors in earth inductors are phase shifts due to coil inductance, thermal e.m.f.'s due to brush friction, maladjustment of brushes, and the like. These are discussed in more detail by Dorsey.[44]

As shown by the above theory, the earth inductor is an *almost universal* magnetic instrument and is adapted to the measurements of intensity components and field directions. However, its predominant use at present

[44] N. E. Dorsey, "The Theory of the Earth Inductor as an Inclinometer," Terr. Mag., 18(1), 1–37 (March, 1913).

is in the measurement of the inclination. Standard earth inductors in this country are those of the Coast and Geodetic Survey and the Carnegie Institution of Washington. The instrument of the former is illustrated in Hazard;[45] that of the latter in Dorsey's article.[46] Two types are made in
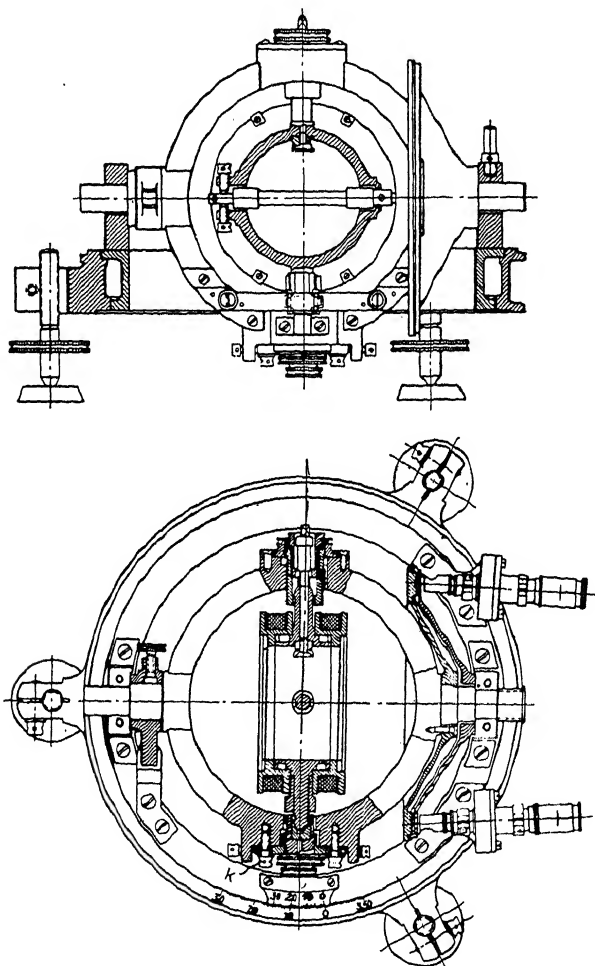
American Askania Corp.

Fig. 8-38. Large earth inductor.

Europe by the Askania Company — a large type for observatory use (see Fig. 8-38) and a small type for field surveys (see Fig. 8-35). Details

---

[45] *Op. cit.*, fig. 10, p. 77.

[46] *Op. cit.*, fig. 2.

of earth inductor observations with record forms are given by Hazard.[47]

The use of the earth inductor as a *compass* is based on its ability to find the magnetic meridian by the zero-induction brush position (see page 361). In application (airplane) the brushes are so set as to make the required course angle with the axis of the ship; the pilot then navigates the ship in such a manner that the galvanometer on the instrument board shows no deflection.

Magnetic *intensities* may be measured with the earth inductor by using the ballistic method previously discussed, by keeping the speed of the coil constant, or by compensating the field so that the speed is no longer of influence. In the constant-speed method the coil is coupled to a synchronous motor driven from a valve-maintained tuning fork, and the e.m.f. induced in the coil is measured with a potentiometer.[48] The compensation principle is applied in an inductor[49] provided with a pair of Helmholtz coils mounted to the frame B in such a manner that the field of the coils opposes the earth magnetic field in the z'' direction. The compensation current is accurately measured by a potentiometer arrangement. A disadvantage is the lack of homogeneity in the inside of the coil. This lack may be overcome by the new form of Helmholtz coils suggested by Fanselau and Bock.[50] In a compensation inductor suggested by the author,[51] a large magnet compensates the major portion of the field and a smaller magnet is moved along a deflection bar for compensation. This instrument is suitable for any intensity component. The possibilities of the compensation inductor are well demonstrated by the fact that it has been proposed as a primary standard in absolute magnetic observatory work.[51a]

The earth inductor gradiometer[52] is intended for the determination of "intensity gradients" in the north and east directions. It consists of a horizontal frame in which two coils rotate about horizontal axes. They are situated on opposite arms of a Kirchhoff-Wheatstone bridge so that the ratio of the e.m.f.'s induced in the coils is observed. The Null instrument is a sensitive galvanometer set up on a separate tripod. When the coil frame is E-W, the axes of the two coils are N-S, which eliminates the

[47] *Op. cit.*, pp. 77–84.

[48] F. M. Soule, Terr. Mag., **35**(2), 103–110 (June, 1930).

[49] W. Uljanin, Terr. Mag., **34**(3), 199–206 (Sept., 1929).

[50] See G. Fanselau, Zeit. Phys., **54**(3/4), 260–269 (1929). F. E. Smith, Phil. Trans., **A223**, 186–191 (1923). R. Bock, Zeit. Phys., **54**, 257–259 (1929). R. H. Bacon, Rev. Sci. Instr., 7(11), 423 (Nov., 1936).

[51] See P. Aguerrevere, Colo. School of Mines Quarterly, **27**(3), 11–29 (July, 1932).

[51a] E. A. Johnson, Terr. Mag., **44**(1), 29-42 (1939).

[52] See I. Roman and T. C. Sermon, "A Magnetic Gradiometer," A.I.M.E. Geophysical Prospecting, 373–390 (1934).

horizontal intensity.   Therefore, the E-W gradient of the vertical intensity
is measured.   When the frame is now turned into the N-S direction, the
axes of rotation are at right angles to the horizontal intensity so that *both*
H and **Z** (that is, the total intensity **T**) are now effective.   Roman actually
measures **T** by setting the brushes at right angles to the field (which
requires a knowledge of the inclination) and calculates **Z** from it.   This
makes the method laborious, but it can be avoided if provision is made to
turn the coils in their frame in such a manner that their axes of rotation
always point north.

3. (*Iron*) *induction instruments* are designed to measure the inclination,
the vertical intensity, and the magnetic meridian.   Induction inclinom-
eters consist of a magnetic needle suspended from a thread or wire, and
two vertical iron bars mounted opposite each end of the magnetic needle.
One bar is up from the plane of the needle; the other is down.   There will
be a south pole induced in the upper end of the lower bar and a north pole
in the lower end of the upper bar.   This deflects the needle from the mag-
netic meridian.   Naturally, opposite poles are also produced in the bars
by the poles of the needle.   This effect can be kept down and is neglected
in the following formulas.   If **F** is the force produced on the suspended
needle from the induction in the bars, the deflection in the Lamont method
is given by $\sin \varphi = F/H$, where $F = 2Zk''/d^2$, k'' is an induction factor,
and d is the distance between needle poles and poles induced in the bars.
Hence,

$$\sin \varphi = \frac{2Z\mathbf{k}}{d^2 \mathbf{H}} \quad \text{or} \quad \tan I =$$

If an astatic magnetic system instead of the magnetic needle is used,
the effect of the horizontal intensity is eliminated, and the torsion of the
suspension wire furnishes the restoring force that opposes the effect of
induction in the bars.   In the vertical intensity magnetometer designed
by McNish,[53] the astatic system is represented by an armature consisting
of two vertical bars mounted on the ends of a nonmagnetic vane (see
Fig. 8-39).

For magnetic meridian determinations, Rieber[54] has designed a micro-
magnetometer consisting of two iron bars mounted end-to-end with a small
gap and the fiber of a string galvanometer between them.   When alter-
nating current of about 100 cycles is passed through the string, and if the
bars are in the magnetic prime vertical, the induction and string deflection
are zero.

[53] Terr. Mag., **41(2)**, 161 (June, 1936).
[54] A.I.M.E. Geophysical Prospecting, 410 (1929).

4. *Sine galvanometers* are combinations of unifilar magnetometers and deflection coils so arranged as to give a horizontal comparison field in the magnetic prime vertical or at right angles to the needle. In the second case, the instrument is used as the "sine" galvanometer proper; in the first, as a "tangent" galvanometer. The horizontal intensity

$$H = \frac{CI}{\tan \varphi} \quad \text{or} \quad H = \frac{CI}{\sin \varphi}, \qquad (8\text{--}48)$$

where C is a coil constant and I the current, measured by standard resistance coil, standard Weston cell, and potentiometer. For field instruments the coil constant may be determined by measuring deflections at an observatory where **H** is known. Large instruments for absolute determinations of the horizontal intensity are described by Barnett[55] and Hazard;[56] a smaller field instrument is illustrated by Nippoldt.[57]

5. *Compass variometers* are instruments intended for the measurement of the horizontal intensity on moving support. They consist of two compasses mounted some distance apart above each other. The force acting on either compass is dependent on the horizontal intensity and the attraction due to the other needle. Generally, the angle of spread between the two compasses is measured, from which the horizontal intensity

Fig. 8-39. Induction vertical magnetometer (after McNish).

$$H = \frac{2Mk}{r^3} \cos \frac{\psi}{2}, \qquad (8\text{--}49)$$

where M is the magnetic moment of each magnetic needle, **k** a deflection constant, ψ the spread angle, and r the distance of the needles. The instrument is well adapted to the measurement of horizontal intensity anomalies on board ship and in aircraft. It may be made into a vertical intensity instrument by using two compasses oscillating in vertical planes side by side with their plane of oscillation in the magnetic prime vertical. Details are given in publications of L. A. Bauer and others,[58] by E. B. Brammer,[59] by G. Angenheister,[60] and by K. Luyken.[61]

[55] Pub. No. 175, Carnegie Institution, 373–394 (Dec., 1921).

[56] *Op. cit.*, p. 38.

[57] Nippoldt, *op. cit.*, p. 33.

[58] Pub. No. 175, Carnegie Institution, V, 339–351 (1926).

[59] Zeit. Instr., **45**(12), 576–579 (Dec., 1925).

[60] Handb. Exper. Phys., **25**(1), 577–578 (1928).

[61] Zeit. f. angew. Geophys., **1**(6), 163–181 (Oct., 1923).

D. Observatory Instruments

Certain instruments now used in observatory practice are also applicable in regional magnetic surveying. Some of these may, by suitable modifications, become of importance for magnetic prospecting. Observatory instruments are employed (1) for the absolute determination of magnetic components, and (2) for recording magnetic variations.

1. *Instruments for absolute determinations are* sine galvanometers, magnetic theodolites, and earth inductors. These require no further discussion here, since their principles have been described before.

2. *Instruments for the recording of magnetic variations* fall into two groups of different design, depending on whether they are intended for permanent observatories or for temporary setups in connection with magnetic exploration. In permanent observatories variation instruments are provided for *declination, horizontal intensity,* and *vertical intensity.* Some observatories prefer to record north and east components of the horizontal intensity. The variometers are usually set up in a straight line in the magnetic prime vertical so that the declination variometer oscillates in the magnetic meridian, the horizontal magnetometer in the prime vertical, and the vertical intensity variometer in the magnetic meridian.[62] For convenience in scale value determinations, Helmholtz coils are permanently installed on the instruments. Temporary observatories in magnetic exploration generally utilize the regular vertical or horizontal intensity magnetometers equipped with a mirror device. This device projects the light reflected from the magnetic system on a recording drum and carries a base-line mirror and a Bourdon tube for recording temperature. A portable recording device using only the magnetic system of a balance magnetometer is illustrated in Fig. 8–22. A method for remote recording of magnetic variations by means of a balanced photoelectric cell arrangement has recently been described by Graf.[62a]

IV. CORRECTIONS

In magnetic prospecting it is necessary to eliminate or correct for temperature, daily variation, planetary variation, base change, influence of iron and steel objects, terrain anomalies, and regional anomalies. These corrections will be discussed in the order indicated.

A. Temperature

1. *Elimination.* The action of temperature may be disregarded in instruments which are well insulated, are compensated for temperature,

---

[62] See Hazard, *op. cit.* (2nd ed.), Fig. 14, and pp. 108–112 for directions for operating a magnetic observatory.

[62a] A. Graf, Beitr. angew. Geophys., **7**(4), 357–365 (1939).

or have low sensitivity. The same is true for recording instruments when they are compensated or used in rooms of constant temperature.

2. Even when a *temperature correction* is applied, magnets and magnetometers are usually well insulated in order to cut down temperature fluctuations and temperature hysteresis. An instrument finish of high reflecting power gives best protection against excessive temperature changes.[63] The procedure in determining temperature coefficients of Schmidt balances was described on page 331. Other magnetometers are treated in a similar manner.

B. MAGNETIC VARIATIONS

Magnetic variations may be divided into periodic (daily or diurnal variation), nonperiodic (magnetic storms), secular variation, and artificial variations due to stray currents, and the like.

1. The *diurnal variation* is closely related to the earth's rotation. It is greater and more irregular during the day than at night; its amplitude and phase varies with season and latitude (see Figs. 8–40 and 8–41). Procedures for elimination or correction are discussed below in ascending order of accuracy.

When large anomalies are encountered or when the sensitivity of the instrument is low, the variation is usually disregarded. Variations may be eliminated by simultaneous observations with two instruments on successive stations. In stationary instruments magnetic variations may be eliminated by the use of astatic systems and by shielding where applicable.

Moderate accuracy in the elimination of the variation is attained by checking back at a base station as often as possible and by considering the daily variation as part of the variation of the base value. If measurements at the base are not possible at regular intervals, it is advisable to select times between which the change is approximately linear.

Curves as shown in Figs. 8–40 and 8–41 can give reliable data for daily variation corrections, particularly when measurements are made fairly near a magnetic observatory for which such curves are available. Allowance must be made for differences in mean local time as shown in the next paragraph.

Greater accuracy is attainable by arranging with magnetic observatories for tracings or photostatic reproductions of their records for specific days. The curve-amplitudes must be multiplied by scale value and must be corrected for temperature (unless the instruments are compensated or are set up in constant temperature rooms) and for difference in local mean time between observatory and area under survey ($\Delta\lambda$ of

[63] For curves on magnetometers of different makes see J. B. Ostermeier, Zeit. Erdoel. Bergbau, etc., June 14, 1930.
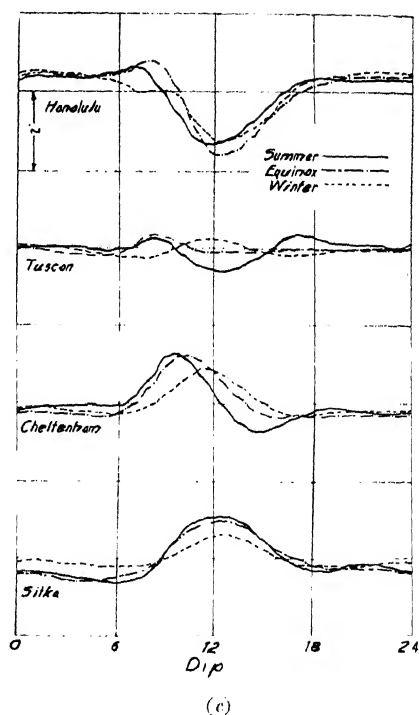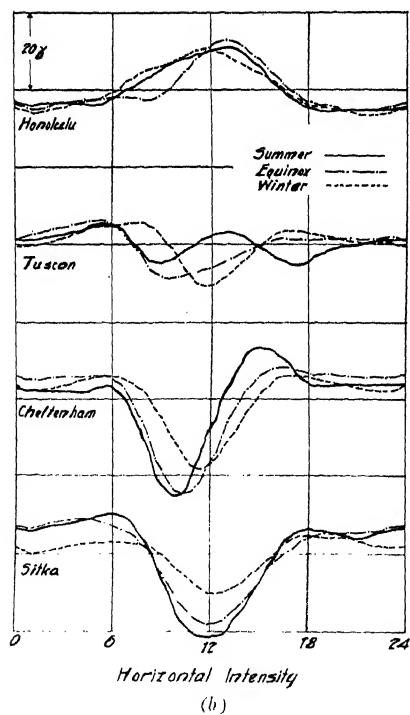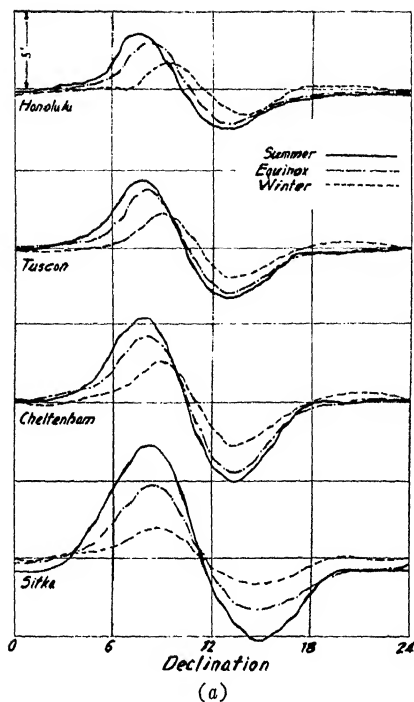
Fig. 8-10. Diurnal variation curves (a) for **D**, (b) for **H**, (c) for **I** (after Hazard).

$15° = 60$ min. of Δt). For some countries formulas are available giving diurnal variation as a function of latitude and longitude. With an increase in distance of the observatory from the area, these calculations decrease in accuracy, since the correction applies only to periodic and not to nonperiodic variations. This has been shown by Soske[64] who found differences between records taken near Pasadena and observatory records of Tucson ($\Delta\lambda = 7°$) amounting to 10–20γ on days of magnetic activity.

To what extent local meteorologic and geologic conditions affect the
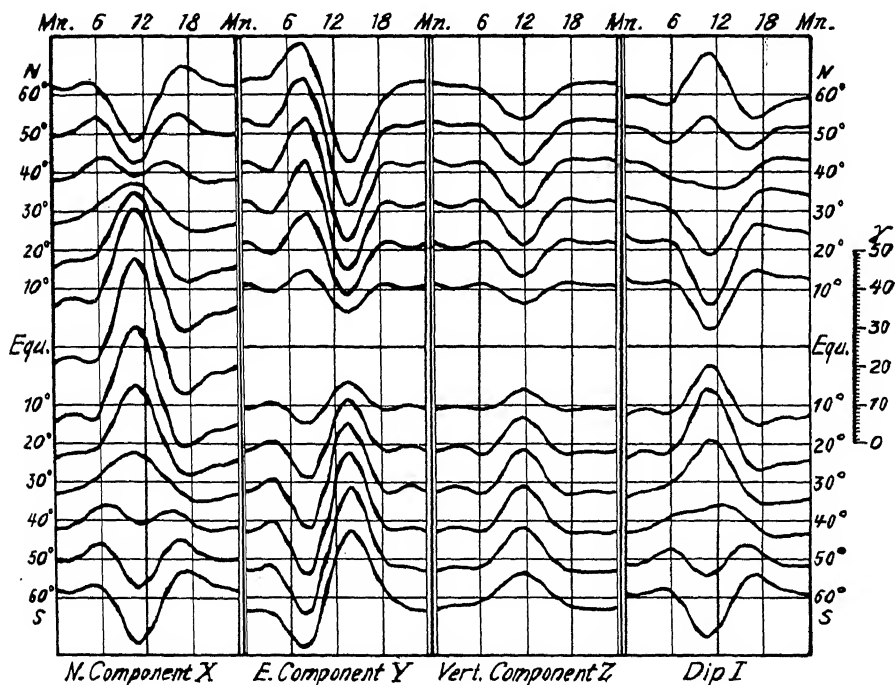
Fig. 8-41. Diurnal variation curves for X, Y, and Z (after Bartels).

magnetic variations has been the object of some discussion. H. Aurand,[65] in an analysis of survey data accumulated between 1928 and 1931 by the Midwest Refining Co., obtained conclusive evidence of the influence of meteorological factors (up to 50γ). Whether variable static charges are produced on magnetic instruments by atmospheric electric fluctuations or whether magnetic fields originating from electrically charged particles in motion are responsible is difficult to decide. Inasmuch as there appears

[64] J. L. Soske, Terr. Mag., 38(2), 109–116 (June, 1933).
[65] Personal communication to the author.

to be a relation between fluctuations of the atmospheric electric potential gradient and magnetic variations, it would seem reasonable that local meteorologic factors can be of influence. Vacquier[66] has shown that, whatever their cause, such local differences exist not only in the variations following local mean time but also in astronomical (nonperiodic, see 2, below) variations as well (see Fig. 8-42).

It is also possible that local geologic conditions (rocks of high magnetic susceptibility) give rise to induction damping and smoothing of the curves. While Soske[67] could not find differences between variations recorded in Tucson and basalt areas in California, with local anomalies up to 3,500γ; Koenigsberger[68] concluded from the rock susceptibilities in two Alpine valleys that variation corrections may be in error by as much as 10–15γ. In such areas, however, his investigations were concerned primarily with nonperiodic variations.

Because of possible discrepancies between observatory records and local magnetic variations, the only procedure which satisfies all accuracy requirements is the local determination of magnetic variations. This requires a second instrument which may be read by another observer at intervals of from 10 to 30 minutes (depending on magnetic activity) or may be provided with a recording attachment as previously described (see also page 356 and footnote 62a). The recording instrument should be free from all magnetic disturbances caused by electric power lines, tramways, automobiles, and the like, and be protected against temperature fluctuations. A recording hut or tent may be used for this purpose, or the instruments may be set up in mine tunnels where available.

2. *Magnetic storms* occur approximately at the same (or astronomic) time all over the earth. Because of their irregular character, rapid time change, and large amplitude, it is difficult to correct for them. To enable observers to distinguish them from possible local effects, announcements of magnetic storms having occurred the week before are published regularly in the *Oil and Gas Journal.*[69] Arrangements may be made with most observatories for collect telegraph report service. During a storm it is advisable to suspend operations, since stations occupied at that time would have to be rechecked in any event.

3. *Secular variation* is the slow change of magnetic elements in the course of centuries. It is not the same all over the earth. Charts of lines of equal secular variation are published by the U. S. Coast and

---

[66] Terr. Mag., **42**(1), 17–28 (March, 1937).

[67] *Loc. cit.*

[68] Zeit. Geophys., **6**(2), 74–78 (1930).

[69] For an illustration of a magnetogram of a magnetic storm, see Oil and Gas Journal, **28**(41), 41 (Feb., 1930).
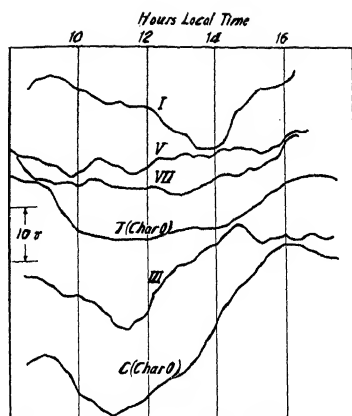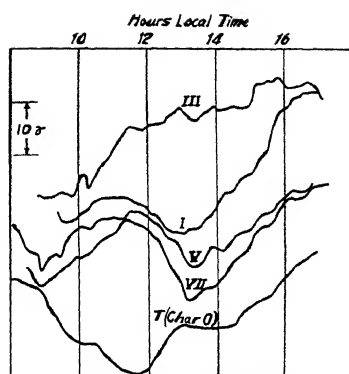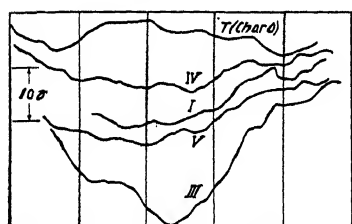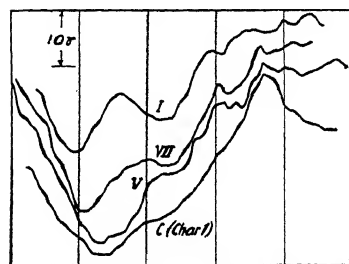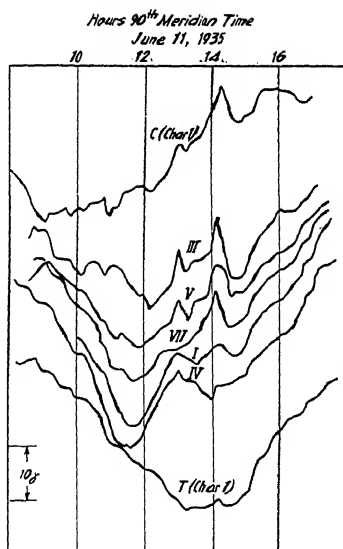
FIG. 8-42. Differences in magnetic variations recorded at various stations (after Vacquier) (a) in local time variations, (b) in astronomical time variations. (T, Tucson; C, Cheltenham; I, Eads (E. Colorado); III, Lumberton, S. Miss.; IV, between Quitaque and Plainview, N. Texas; V, between Millcreek and Randolph, S. Oklahoma; VII, Anadarko, Oklahoma.)

Geodetic Survey. Approximate variation rates are also given on the charts of magnetic elements. This variation does not have to be considered in magnetic surveying except when absolute values in relation to government stations are desired. For calculations of the planetary correction and for adjustments of a magnetometer to a different locality, charts for any year may be used.

4. *"Artificial" variations* are due to both power lines and power plants, surges in A.C. lines, magnetic separators, electric tramways, their return circuit through ground, and anticorrosion currents in pipe lines. A magnetometer should be set up at least 1,500–3,000 feet away from such sources of interference. Near tramways a magnetic station outside the return circuit loop is generally much less disturbed than one inside. There are exceptions to this rule if stray currents are carried to the outside by pipe lines and wires.[70] Abrupt changes in the base value of a magnetometer may occur because of the demagnetizing effect of power lines. Koenigsberger reports displacements as large as 140γ when working near power lines. Transportation of magnetometers on electric tramways caused changes of from -5 to -35γ, while transportation on railroads and automobiles produced little, if any, effect.

C. Planetary Variation

Since the vertical intensity increases and the horizontal intensity decreases toward the magnetic pole, the planetary correction is negative for the former and positive for the latter. The rate of change of magnetic elements with latitude and longitude may be taken from U. S. Coast and Geodetic or other world charts. For a given area an average value may be assumed, or the magnetic lines may be transferred from such charts to the base map of the survey. For small areas and large anomalies (magnetic mine exploration) the planetary correction is generally neglected.

D. Base Change

This correction is applied to allow for changes in the base value of magnetometers between checks on base stations. Before the correction is calculated, base station readings must be corrected for temperature and diurnal variation. If the difference does not exceed 15–20γ in one day, it may be uniformly distributed among stations occupied between base checks. Larger differences indicate abrupt changes and must be corrected for accordingly. The observer is generally in a position to tell from his

---

[70] Much information has been published on leakage currents in connection with corrosion problems. See, for instance, U. S. Bureau of Standards Technologic Papers, No. 63, 75, 127, and so forth.

travelog when such changes (shocks, demagnetizing effects, and so on) are likely to have occurred. Base readings should be plotted against time to separate random from systematic changes (variations, changes in temperature coefficient, and the like).

E. INFLUENCE OF IRON AND STEEL OBJECTS

Since it is impossible to correct for the magnetic fields caused by iron masses, the only remedy is to keep at a distance commensurate with the accuracy of the survey. For objects extending in a vertical direction, the anomaly decreases approximately in proportion to the inverse square of the distance. For predominantly horizontal objects, the attraction is approximately proportional to the inverse first power of distance.

1. Interference from *iron objects about the observer* (watch, knife, key ring, belt buckle, steel frames of glasses, suspender buckles, steel rings in notebooks, and the like) can be avoided since it is a simple matter to determine their influence by approaching a magnetometer from various sides, and from above and below. Objects found to be effective at the customary operating distance should be taken off.

2. The vertical field of the *instrument case* of a magnetometer with compass and auxiliary magnets is about 125γ at 1 yard distance to the north and disappears at 4 or 5 yards.

3. A *bicycle* produces an anomaly of almost -60γ at a distance of 1 meter. An *automobile* has, at 3 yards distance, a vertical field of about -700γ, which disappears at about 25 to 35 yards. It varies somewhat with the direction in which the car is pointed and the position of the instrument with reference to it.

4. The field of a *wire fence* running N-S (the instrument being on the east side) is about -350γ at 1 yard and disappears at about 36 yards.

5. The influence of a *bridge* varies considerably, depending upon construction and material, size and direction, and whether the observer is above or below it.

6. *Pipe lines* can generally be spotted in the field by the overhead telephone lines which follow the course. For a N-S traverse across an 8 inch line buried 4 feet below the surface, running E-W, Barret[71] observed a vertical intensity anomaly of -500γ at about 2 yards (peak in curve) and a disappearance of the anomaly at about 30 yards. From 2 yards to a point directly over the pipe, the anomaly decreases sharply. This interference varies with the direction of the pipe, polarization at the ends, and existence of anticorrosion currents.

---

[71] Oil and Gas Journal, **28**(**22**), 148–150, 245–252 (Oct. 16, 1929); A.A.P.G. Bull., **15**(**11**), 1371–1389 (Nov., 1931).

7. Near a *railroad bed*, running E-W, Barret observed on the south side a negative anomaly up to about 5 yards which then increased to a maximum of 400γ, thence decreased and disappeared at 125 yards.

8. The effect of *buildings* depends entirely upon size and iron and steel content. Brick buildings and brick walls are often magnetic, since the stones acquire magnetism in the process of roasting.

9. The influence of *slag* and *gravel roadbeds*, *drain pipes*, and the like, varies greatly with construction materials; it is difficult to give even approximate figures.

10. The influence of *tank farms* is generally complicated by associated pumping, power, and pipe line equipment; general figures are not available.

11. When magnetic measurements are used for detailing or extending drilled or producing fields, it is necessary to know the effect of *well casing*. The vertical and horizontal intensity anomalies of a tubular casing of uniform diameter may be written[72]

$$\left.\begin{aligned}
\Delta Z &= S\kappa Z_0 \left(\frac{d_1}{r_1^3} - \frac{d_2}{r_2^3} \right) \\
\Delta H &= S\kappa Z_0 \cdot x \left(\frac{1}{r_2^3} - \frac{1}{r_1^3} \right),
\end{aligned}\right\} \qquad (8\text{-}50)$$

where κ is the susceptibility of the casing material, S its cross-sectional area, Z_0 the normal vertical intensity ($S\kappa Z_0$ = pole strength, or magnetic moment divided by the length of the casing), d_1 the depth to the upper and d_2 the depth to the lower pole, r_1 the distance of the point to the upper and r_2 the distance to the lower pole, x the surface distance. This formula corresponds to that for a vertical magnet (formula [8-53]). For a very long magnet the second term in the bracket is negligible and there occurs only a positive anomaly. A short magnet may produce an area of negative anomalies surrounding one with positive anomalies, as illustrated in Table 43. In this example the anomaly disappears at about 200 feet from the well, regardless of the length of the casing. Barret[73] and Clifford[74] conducted surveys in oil fields before and after a change took place in the number of wells and concluded that the picture of the magnetic anomalies was not changed within the limits of accuracy. This is contrary to Van Weelden's[75] contention that cumulative magnetic fields of wells may reach figures sufficient to explain the negative anomalies

[72] Barret, *loc. cit.*

[73] *Loc. cit.*

[74] O. C. Clifford, A.A.P.G. Bull., **16(12)**, 1171-1176 (Dec., 1932).

[75] A. Van Weelden, World Petrol. Congr. Proc., Sec. B. I., 86-90 (1933).

frequently observed on developed fields. The influence of all wells in the
Healdton field was theoretically sufficient to account for its negative
anomaly (-200γ).

TABLE 43[a]
COMPARATIVE VERTICAL ANOMALIES OF A SHORT AND LONG
STRING OF WELL CASING

SURFACE DISTANCE IN FEET	206′ OF 10″ CASING; ΔZ IN GAMMAS	4,609′ OF COMPOSITE CASING; ΔZ IN GAMMAS	SURFACE DISTANCE IN FEET
0	32,400	. . . . .	0
3.2	19,500	35,200	5
6.6	6,700	10,700	10
12.0	2,000	5,500	15
22.0	434	2,990	20
32.1	158	1,220	30
46.0	37	300	50
56.0	−6	. . .	. . .
81.0	−29	53	100
118.5	−29	11	150
147.0	−14	0	200
260.0	0	0	250

[a] After Barret.

12. *Derricks, electric line towers,* and *mine shafts* produce negative mag-
netic anomalies, being above the plane of observation. Depending on size
and amount of steel involved, the fields range from several hundred to
several thousand gammas at nearby points.

F. TERRAIN ANOMALIES

In magnetic prospecting, terrain interference is not nearly so important
as in other lines of geophysical exploration. It is due to (1) a geo-
metric effect resulting in a change of vertical distance, of magnetic
bodies from the plane of observation, (2) magnetic effects caused by
surface rocks.

1. The *geometric effect* is of importance when changes in elevation along
magnetic profiles are comparable with the distance of observation points
from the magnetic body. For a three-dimensional body magnetized by
induction (northern magnetic latitude), whose vertical intensity is nor-
mally at a maximum above the body and whose horizontal intensity has a
maximum and minimum to the south and north, the appearance of the
anomaly curves is almost reversed if the slope is steep enough,[76] since the
lower pole of the body comes closer to the surface. For uniform slopes
the changes in relative position of instrument and subsurface poles may be

[76] See Haalck, *op. cit.*

readily calculated.[77] In the interpretation of the results in irregular terrain, it is necessary to consider the relative position of each station with respect to subsurface bodies. In this case it is advisable to obtain additional data by observations at every station at two heights of the instrument[78] or by the use of a compass variometer[79] which is very sensitive to rapid space changes of intensity.

2. *Magnetic interference* may occur even on a flat terrain surface by locally different weathering, by magnetic rocks in glacial drift, by surface float near iron and nickel deposits, by magnetite stringers in igneous rocks, and by outcrops magnetized by lightning. It is difficult to give even approximate general figures for these effects. On the other hand, the influence of topographic features of simple geometric shape may be estimated[80] by assuming uniform magnetization in the earth's field. If the susceptibility is κ, the greatest vertical intensity field of a hill station (calculated on the assumption of an elongated ellipsoid) is

$$\Delta Z = +4\pi\kappa Z_0 . \qquad (8\text{-}51a)$$

The approximate anomaly near the bottom of a vertical wall (quarry station) is

$$\Delta Z = -\tfrac{4}{3}\pi\kappa Z_0 . \qquad (8\text{-}51b)$$

The vertical field in an elongated depression between walls of uniform slope on either side depends not on the absolute differences in elevation between summits and valleys, but on the degree of slope. For gentle slopes

$$\Delta Z = -2\pi\kappa Z_0 \qquad (8\text{-}51c)$$

approximately, while for steep slopes

$$\Delta Z = -3\pi\kappa Z_0 . \qquad (8\text{-}51d)$$

The anomaly in the interior of a sphere (measurements in caves, tunnels) is

$$\Delta Z = -\tfrac{8}{3}\pi\kappa Z_0 . \qquad (8\text{-}51e)$$

Koenigsberger[81] confirmed these theoretical values by numerous observations. The greatest difference between summit and valley values in gneiss was 130γ; in gneiss quarries the anomalies reached -50γ; in

[77] A. Nippoldt, *Magnetische Mutung*, p. 12 1930.

[78] See A. F. Hallimond, Min. Mag., **41**(1), 16–22 (July, 1929). Nippoldt, *A. Magnetische Mutung*, p. 66. The formulas for platform observations or for different elevations of mine shafts apply (see pp. 407–408).

[79] Phys. Zeit., 176–179 (1907); A. Nippoldt, *Magnetische Mutung*, pp. 68-70.

[80] Koenigsberger, Gerl. Beitr., **20**(3/4), 293-307 (1928).

[81] *Ibid.*

gravel pits they ranged from -13 to -20γ. In valleys of granite, Koenigsberger observed anomalies of from -10 to -25γ; in areas of basic schists, from -50 to -200γ; at the foot of glacio-fluvial terraces the effects varied from -20 to -30γ.

G. Normal Fields

Although interpretation of magnetic anomalies is based mainly on the *shape* of anomaly curves, it is frequently desirable to know the value of the undisturbed intensity in the area under survey. In some interpretation problems it is necessary to differentiate between positive and negative anomalies; in vector and line-of-force interpretation the *sign* of the anomaly, and thus a fairly accurate determination of normal values, is of importance. There is no standard procedure for determining normal values since they depend on the type of anomaly surveyed. For large and locally limited anomalies it is sufficient to select a base station in geologically undisturbed terrain and to consider its intensity as the normal value. Elsewhere it is usually satisfactory to use the U. S. Coast and Geodetic Survey maps. Since regional anomalies are already included in their normal values, anomalies due to local deviations from regional structure appear as excess or deficiencies with respect to these. In extensive surveys conducted for the purpose of obtaining relations between magnetic anomalies and regional structure, it is better to use world charts in which only anomalies of continental order of magnitude remain.

To simply form the average of all magnetic values in an area and designate this as the normal value is not recommended, since a given geologic body may not produce a balanced number of positive and negative anomalies. The selection of a normal value is frequently a trial and error proposition. Its final value can often be chosen only with regard to the shape of the anomaly curve to be expected from theoretical and geological considerations.

V. MAGNETIC FIELDS OF SUBSURFACE BODIES
(INTERPRETATION THEORY)

A. Graphical Representation of Results

For interpretation in geologic terms, magnetic data must be so plotted as to show the *clearest* indication of subsurface bodies. The following representations are in use: (1) lines of equal anomaly; (2) profiles at right angles to strike; (3) peg models, isometric maps; (4) anomalous vectors; and (5) magnetic gradients.

1. *Lines of equal anomaly.* For higher magnetic latitudes lines of equal

vertical intensity anomaly are best suited. Their interval should be two to three times the probable error of the survey; greater intervals are preferred for large anomaly gradients. "Isanomalic" maps are comparable to contour maps; it is helpful to shade areas of equal anomaly, darkest shades corresponding to areas of greatest anomalies. The use of two different colors will be of assistance; red may be used for positive, and blue or green for negative anomalies.

2. *Profiles at right angles to strike* show magnetic values as ordinates and distances as abscissas above a known or inferred geologic section. For geologic features causing negative anomalies, inverted ordinates are used. Where a simple geometric relation between magnetic values and subsurface contours can be assumed, the scale of the magnetic ordinates may be made identical with the vertical scale in the geologic section. Parallel profiles across the same geologic feature may be cut of celluloid strips and mounted on a map (see Fig. 8–72). If horizontal intensity measurements have been made in the plane of the magnetic meridian, the anomalies must be projected upon a direction at right angles to the strike. This projected anomaly is hereinafter designated by the symbol H_p. The conversion may be avoided by orienting a horizontal magnetometer at right angles to the strike or in a profile direction at approximately that angle.

3. *Peg models, isometric maps.* Magnetic anomalies may be represented on maps by pegs of proportionate length (see Fig. 8-71). For areas of small magnetic gradients, better visualization of the magnetic relief can be obtained in this manner. However, negative magnetic anomalies do not show to advantage. Isometric maps are prepared by using the 60° axis for the north, the 120° axis for the east coordinate of the map, and the 0° or vertical axis for the representation of anomalies. A difficulty with isometric maps is that large anomalies may obscure adjacent features and that negative anomalies cannot be shown advantageously.

4. *Anomalous vectors.* Interpretational advantages are often gained by representing the results in the form of anomalous vectors, since they are tangent to the lines of force radiating from the poles of the disturbing objects. Their usefulness, however, depends upon a careful selection of the normal value.

Horizontal vectors may be plotted from anomalies in declination and horizontal intensity. A convenient method is to calculate the north component X and the east component Y from the observations, to subtract X_0 and Y_0, and to plot ΔX and ΔY. The anomalous vector R is the resultant of the two (see Fig. 8-43a). In another method the normal H_0 is plotted in the direction δ_0, and the observed H is plotted at the observed angle (see Fig. 8-43b); the horizontal anomalous vector R is equal to the vectorial difference of H_0 and H. The Tiberg method of the parallelogram

of forces is virtually identical with the method just discussed. Underground measurements are made by stretching a cord between two points, A and B. The line AB may make the angle β with the normal meridian. At each point the actual magnetic meridian referred to AB, and the actual horizontal intensity are measured by using the Dahlblom sine arm. This gives $\mathbf{H}$ and γ and, thus, R (Fig. 8–43c)
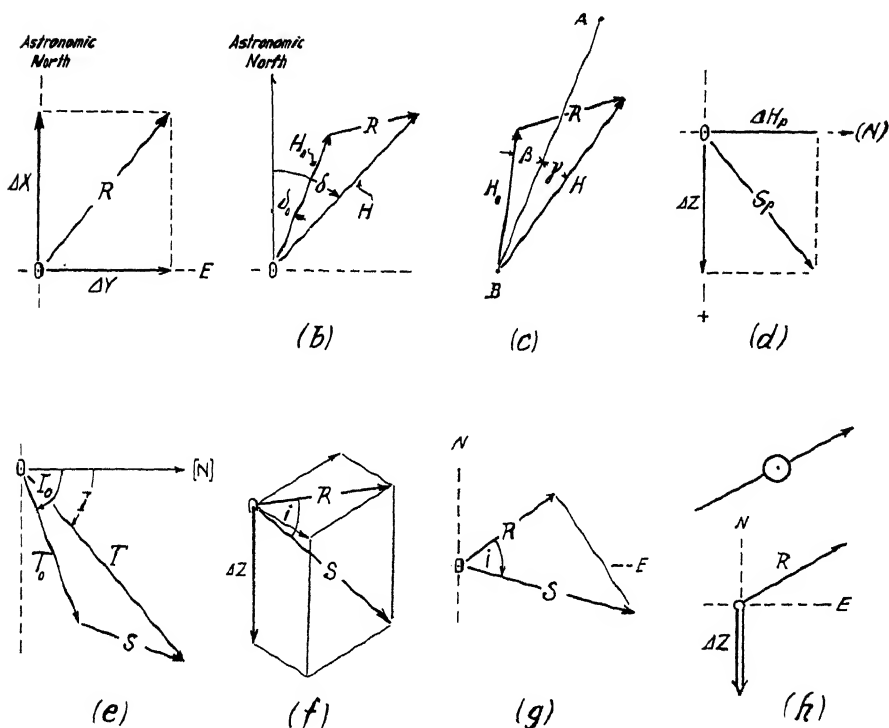
FIG. 8-43. (a) Horizontal anomalous vector from $\mathbf{X}$ and $\mathbf{Y}$. (b) Horizontal anomalous vector from $\mathbf{H_0}$, δ, and $\mathbf{H}$. (c) Tiberg's "arrow" method. (d) Vertical anomalous vector from $\mathbf{H_p}$ and Z. (e) Vertical anomalous vector from $\mathbf{T_0}$, $\mathbf{I_0}$, $\mathbf{T}$, and $\mathbf{I}$. (f) Total anomalous vector in isometric projection. (g) Total anomalous vector in two-dimensional representation (Jenny). (h) Total anomalous vector in two-dimensional representation.

Vertical vectors may be plotted from horizontal and vertical intensity observations with Schmidt balances or from inclination and total intensity observations with the Hotchkiss superdip. If ΔH has been reduced to the direction of the profile, the vertical disturbance vector, $S_p =$

$\,)^2 + (\Delta Z)^2$ is obtained from the construction indicated in Fig.

A positive ΔH_p is plotted toward north, a negative toward south. Inclination $\mathbf{I}$ and total intensity $\mathbf{T}$ observed with the Hotchkiss superdip

are plotted as one vector (see Fig. 8–43e).   A second vector is plotted from the normal inclination I_0 and the normal total intensity T_0.   The vectorial difference between these two vectors is S.[82]   When superimposed on geologic sections, the vertical anomalous vectors point approximately toward the poles of disturbing objects. · They may be used for approximate depth determinations with force-line diagrams.   The accuracy of this method depends on the proper selection of normal values.

Total anomalous vectors may be plotted in isometric projection from the ΔX, ΔY, and ΔZ components as shown in Fig. 8–43f.   Another method of three-dimensional representation is to rotate the total about the horizontal vector and to plot both in the same plane (see Fig. 8–43g).   These procedures have the disadvantage that in plan view the resultant vector does not point in the correct horizontal direction.   Hence, it is better to plot the horizontal vector only and to indicate the size of the vertical vector by the radius of a circle about the station or by a double line (Fig. 8–43h).

· 5. *Magnetic gradients* are obtained by dividing the intensity differences of stations (or contours) to the north and east by their distance.   They may be measured directly with a magnetic torsion balance or inductor gradiometer.   These gradients are expressed in gammas per kilometer, or in 10^{-9} (Eötvös) units per cm (50γ per km equal 5 E.U.).   The direction and length of the resultant gradient follows from the north and east components by vectorial addition.   In interpretation, magnetic gradients are of advantage when torsion balance data are compared with magnetic results.

B. Qualitative and Quantitative Analysis

Most interpretation of magnetic data is of a qualitative nature.   This is due to several factors: (1) the magnetic method lacks depth control; (2) most quantitative interpretation is indirect; (3) magnetic properties of geologic formations, particularly of igneous and metamorphic rocks, are subject to great horizontal and vertical variations and are dependent on the thermal and mechanical history, the effects of which are difficult to evaluate; and (4) magnetism is the only physical rock property which is of a bipolar nature, and variability of polarization adds another unknown. Quantitative interpretation is further handicapped because the proportion of induced and remanent magnetism is rarely known.   Fortunately, in many cases, the remanent magnetism is identical in sign and direction with the induced magnetization, so that interpretations may be based on the assumption that the magnetization is due to induction in the earth's magnetic field, that is, is dependent upon the magnetic latitude.

---

[82] Actually I_0 and I_1 and T_0 and T_1 are in different planes.

The *induction theory* is based upon a relation between the gravitational and the magnetic potential of a body, provided that it is homogeneously magnetized. Since this holds only for bodies bounded by second order surfaces (spheres, ellipsoids of rotation, and the like) which do not occur in nature, the application of the theory to actual forms of geologic bodies (plates, slabs, and so on) results in approximate data only. For these reasons the simpler pole and line theory has been widely used (since about 1870), particularly in magnetic mine exploration. Ore bodies may be considered magnetic poles, doublets, or single and double magnetized lines. Irregular masses, such as igneous intrusions, granite ridges, and the like, can be treated as pole series. The pole theory can be applied regardless of whether magnetic effects are due to induction or any other cause, as long as the positions of the poles are known.

C. POLE AND LINE THEORY

1. *Single pole, depth rules.* Ore bodies may be represented by single poles if they occur in the form of pipes, chimneys, and the like, if their section is lenticular or circular, and if they are small compared with their depth extent so that the lower pole may be assumed to be far away from the upper. The assumption of a single pole is justified if the isanomalic

FIG. 8-44. Single pole.

lines of the vertical intensity are nearly circles or short ellipses, and if only a positive anomaly exists. Assume (Fig. 8-44) a pole[83] of strength $\mathbf{m}$ at depth d below the surface. The magnetic potential of the pole at $P(x, y, d)$[83a] is $V = \mathbf{m}/r$, and the force in the direction of r is $F = dV/dr = -\mathbf{m}/r^2$. Hence, its components:
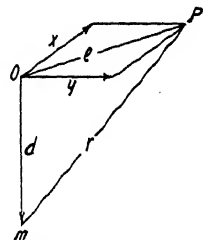
$$\Delta \mathbf{X} = \frac{\partial V}{\partial x} = -\frac{x\mathbf{m}}{r^3}$$

$$\Delta \mathbf{Y} = \frac{\partial V}{\partial y} = -\frac{y\mathbf{m}}{r^3}$$

$$\Delta \mathbf{Z} = \frac{\partial V}{\partial d} = -\frac{d\mathbf{m}}{r^3} \qquad (8\text{-}52a)$$

$$\Delta \mathbf{H} = \frac{\partial V}{\partial e} = -\frac{e\mathbf{m}}{r^3}.$$

---

[83] Contrary to the conventional designation, the South Pole is here positive, so that the vertical intensity anomaly is positive.

[83a] The x is positive toward north (away from $\mathbf{m}$); y is positive toward east (likewise away from $\mathbf{m}$); but d is positive downward (*toward* $\mathbf{m}$, from surface).

Assuming uniform magnetization, the pole strength $\mathbf{m} = \mathcal{G}\mathbf{S}$, where $\mathbf{S}$ is the section of the body and $\mathcal{G}$ is intensity of magnetization. For a vertical body, $\mathcal{G} = \kappa Z_0$, so that

$$\mathbf{m} = \kappa Z_0 \mathbf{S}. \qquad (8\text{--}52b)$$

This relation presupposes that the magnetization is due exclusively to induction. Where an appreciable remanent magnetization exists, the pole strength resulting therefrom is usually greater than that due to induction so that the latter may be neglected, in which case

$$\mathbf{m} = \mathcal{G}_r \mathbf{S}, \qquad (8\text{--}52c)$$

where $\mathcal{G}_r$ is the remanent magnetization. For example, the magnetization intensity resulting from the remanent magnetism of the diabase in Fig. 8-13 is 0.17, whereas the induced magnetization $\mathcal{G} = \kappa Z_0$ is only $5 \cdot 10^{-4}$. This subject is discussed further on pages 400-402.

The vertical intensity reaches a maximum when $r = d$; $\Delta Z_{\text{max.}} = \mathbf{m}/d^2$. If the variable parameter $q \equiv d/r = \sin i$ is introduced,

$$\Delta Z = q^3 \frac{\mathbf{m}}{d^2} \quad \text{and} \quad \Delta H = q^3 \frac{\mathbf{m}}{d^2} \sqrt{\frac{1}{q^2} - 1}. \qquad (8\text{--}52d)$$

For the single pole, horizontal and vertical intensities at any point are *functions of the vertical intensity directly above the pole*:

$$\Delta Z = \Delta Z_{\text{max}} \cdot q^3 \quad \text{and} \quad \Delta H = \Delta Z_{\text{max}} \cdot q^2 \sqrt{1 - q^2}. \qquad (8\text{--}52e)$$

Figure 8-45 shows the horizontal and vertical intensity anomalies as profile curves and isanomalic lines. The horizontal intensity is zero above the pole and has a minimum in the north (positive x) and a maximum in the south (negative x). In horizontal projection, the lines of force for a single pole are straight.

From the above formulas follow a number of relations which are helpful in interpretation:

(a) The highest point of the subsurface (polar) mass lies immediately below the maximum in ΔZ and the zero point in ΔH.

(b) The anomalous vectors intersect in the pole.

(c) The drop of the vertical intensity curve is inversely proportional to the depth of the pole. If c_i is the distance at which the vertical intensity has dropped to one-half of its maximum value, $d = \frac{4}{3}c_i$, and the *distance of the half-value point* from the point of maximum anomaly in Z is equal to $\frac{3}{4}$ *the depth of the pole.*

(d) The distance of a point where ΔZ has dropped to $\frac{1}{3}\Delta Z_{\text{max.}}$ is *equal to the depth of the pole.*

(e) The distance of the point where $\Delta Z = \Delta H$ (where the angle of the
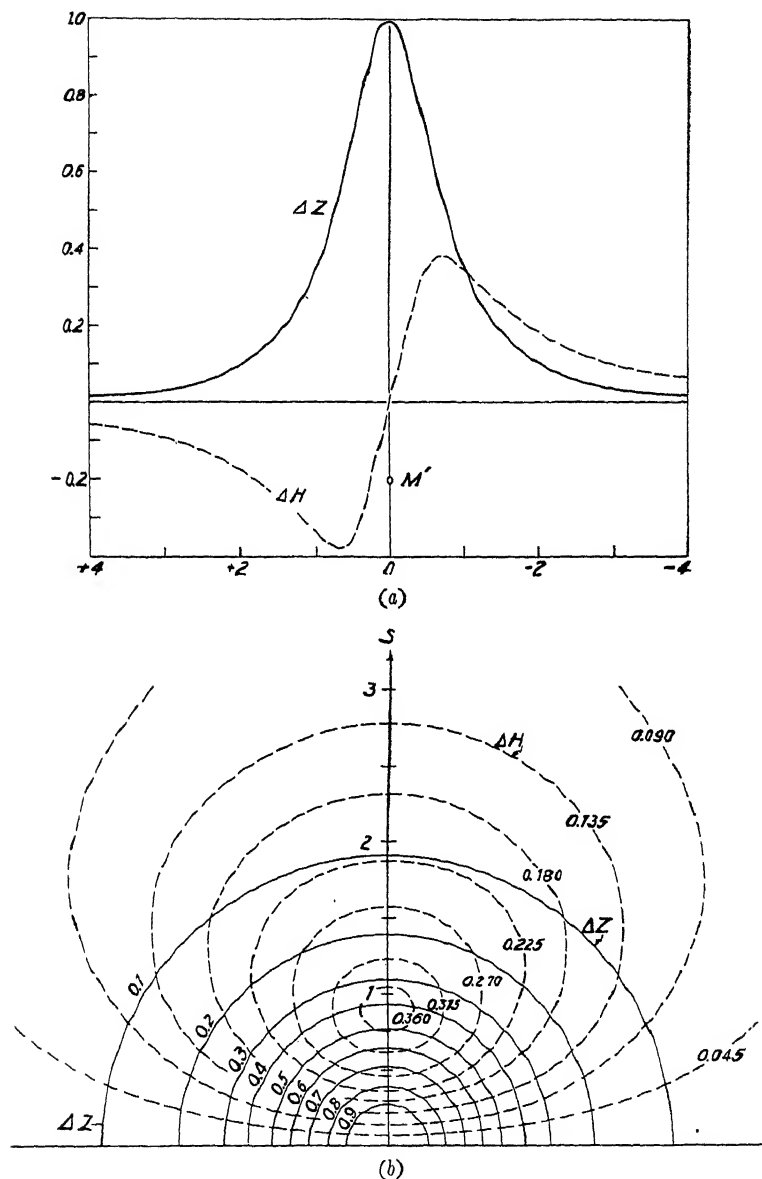
FIG. 8-45. Horizontal and vertical intensity anomalies above a single pole (after Nippoldt): (a) profile curves, (b) isanomalies.

anomalous vector is 45°) is equal to the pole depth, and the ΔH curve intersects the ΔZ curve at a point where $\Delta Z = \frac{1}{3}Z_{max.}$.

(f) The distance between points with maximum and minimum hori-

zontal intensity anomalies is $\frac{3}{2}$ the depth. This obtains for the single pole only.

2. *Vertical magnetic doublets (magnets)* must be assumed in place of single poles if the depth extent of geologic bodies as described on page 381 is small, that is, if a negative anomaly surrounds the area of positive anomaly. If the negative anomaly does not surround the positive anomaly completely, the doublet is inclined and relations shown in the next paragraph are applied. The field of a vertical magnetic doublet follows from an addition of the fields of two poles at different depths. If d_1 is the depth and r_1 the distance from P to the upper (positive) pole, d_2 the depth and r_2 the distance to the lower (negative) pole,

$$\Delta\mathbf{H} = em\left[\frac{1}{(e^2 + d_2^2)^{\frac{3}{2}}} - \frac{1}{(e^2 + d_1^2)^{\frac{3}{2}}}\right]$$

and

$$\Delta\mathbf{Z} = m\left[\frac{1}{(e^2 + d_1^2)^{\frac{3}{2}}} - \frac{1}{(e^2 + d_2^2)^{\frac{3}{2}}}\right].$$

(8-53)

Thalén has given two depth rules for the magnetic doublet which apply when its pole distance $2l$ is greater than three times the depth to the upper pole, d_1 :

(*a*) A line connecting a point of zero vertical intensity (abscissa e_0) with the center of the magnet makes an angle of 54.75° with its axis, so that $\cot 54° = (d_1 + l)/e_0$. This depth rule is not very reliable. If it is applied to Nippoldt's figure 19,[84] the formula gives a depth of 17 instead of 20; in his figure 22 it gives 13.3 instead of 15.

(*b*) The distance between the maximum and minimum in $\Delta\mathbf{H}$ is approximately equal to the depth to the center of the magnet. (This rule is still less reliable; it gives a depth of 14 instead of 20 for Nippoldt's figure 19, and 14 instead of 15 for his figure 22.)

3. *For a dipping magnetic doublet*, the fields of the upper and lower pole are again added (see Fig. 8-46) so that by substitution of $e_2 = 2l \cos i$ and $d_2 = d_1 + 2l \sin i$,

$$\Delta\mathbf{H} = m\left[\frac{-e_1}{r_1^3} + \frac{e_1 - 2l \cos i}{r_2^3}\right]$$

and

$$\Delta\mathbf{Z} = m\left[\frac{d_1}{r_1^3} - \frac{d_1 + 2l \sin i}{r_2^3}\right].$$

(8-54)

[84] A. Nippoldt, *Magnetische Mutung*, pp. 68–70.
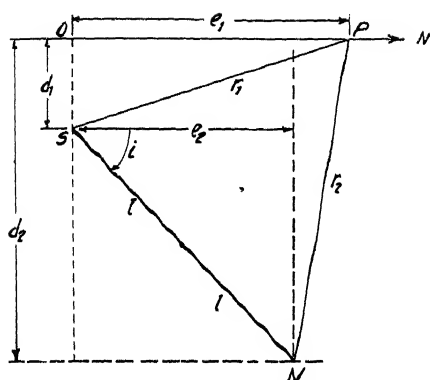
FIG. 8-46. Dipping magnet.

Anomalies for inclined magnets are shown in Fig. 8-47, a to d. The ΔZ curves are unsymmetrical; in the ΔH curves the ratio of maximum to minimum increases with decreasing dip. Dip determinations may be made (a) indirectly, by using diagrams as shown in Fig. 8-47 or force-line diagrams; or (b) directly (for small intervals of dip angle) from the ratio of maximum to minimum in ΔH. For the range of 30° to 60°, Δi is approximately equal to

4. *Magnetized lines* are assumed in the interpretation of the magnetic anomalies of two-dimensional bodies whose extent may be considered infinite in the direction of strike. These bodies include most stratified magnetic formations, iron and nickel ore deposits, intrusive dikes, contact-metamorphic zones, and the like. While the magnetic field of a three-dimensional body is inversely proportional to the square of the distance between it and the point of observation, the field of a two-dimensional body
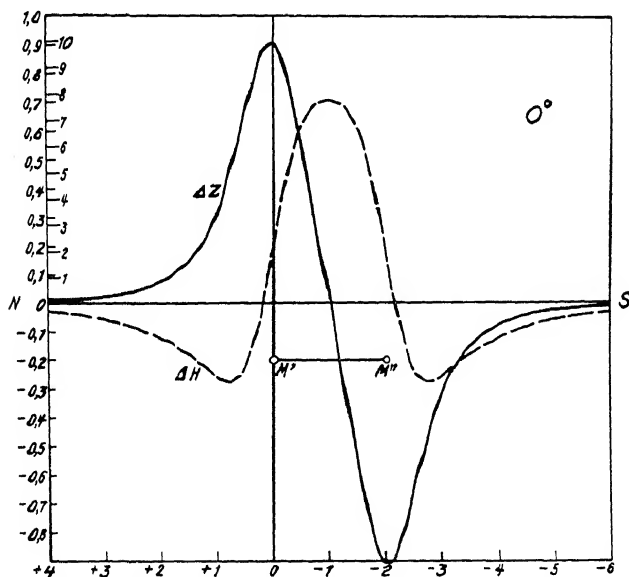
FIG. 8-47a. Anomalies of dipping magnet of 0° dip (after Nippoldt).

depends on the inverse *first power* of the distance.   In practice this makes surprisingly little difference.

For magnetic plates of great depth extent, only the magnetized line at the upper end need be considered.   If the strike of the line is in the y'
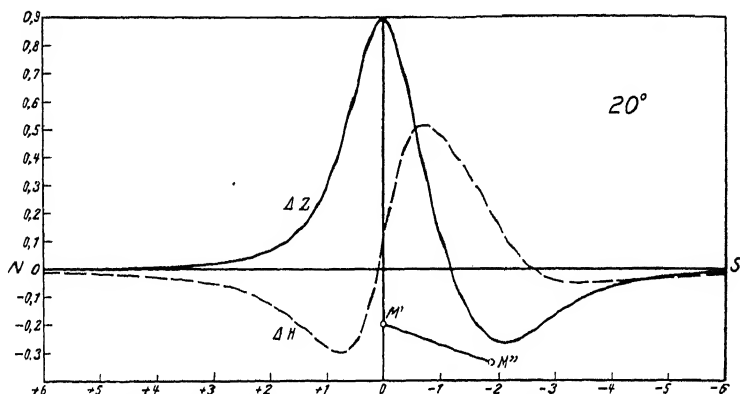
FIG. 8-47b. Anomalies of dipping magnet of 20° dip (after Nippoldt).
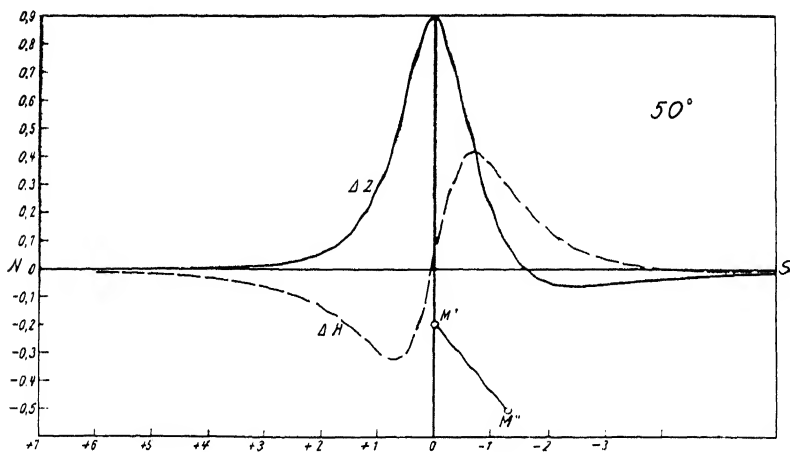
FIG. 8-47c. Anomalies of dipping magnet of 50° dip (after Nippoldt).

direction (Fig. 8-48), ΔY in eq. (8-52a) is zero; $\Delta H = -C \int \dfrac{dy'}{r^3 \cdot x}$, and $\Delta Z = C \int \dfrac{dy'}{r^3 \cdot d}$.   Integrating between the limits of $\pm \infty$,[85]

---

[85] See also A. Banos, Revist. Industrial, **1**(3), 303–310 (Sept., 1933).

For vertical magnetization, the constant $C = \kappa Z_0 b$, where b is the breadth of the magnetized plate, and κ the susceptibility. As in eq. (8–52c), the remanent magnetization $\mathfrak{I}_r$ may again be substituted for κZ_0, where it is appreciably greater than the induced magnetization. The vertical intensity directly above a two-dimensional plate is $\Delta Z_{\text{max.}} = 2C/d$. The

FIG. 8-47d. Anomalies of dipping magnet of 90° dip (after Nippoldt).

following interpretation and depth rules follow from eq. (8–55): (a) The maximum of vertical intensity and the zero of horizontal intensity anomaly occur directly above the plate; (b) the anomalous vectors intersect in the depth of the magnetized line (in the $x'-d$ plane); (c) the *distance* of the point where $\Delta Z = \frac{1}{2}\Delta Z_{\text{max.}}$ from the 0 point is *equal to the depth*; (d) the ΔH curve intersects the ΔZ curve at a distance equal to the depth (where

FIG. 8-48. Magnetized line ($t = b$ in text)

$\Delta Z = \frac{1}{2}\Delta Z_{\text{max.}}$ and where the angle of the anomalous vectors is 45°).

5. *The vertical line doublet* corresponds to a vertical magnetized plate of limited depth extent whose lower end is effective. By adding the anomalies due to two magnetized lines,

$$\Delta H = \qquad\qquad \rho_1^2 \qquad\qquad \text{and} \qquad \Delta Z = \qquad\qquad (8\text{–}56)$$

where d_1, ρ_1 and d_2, ρ_2 are the depths and distances respectively to the upper and lower pole lines.

6. For the *inclined line doublet* the fields of upper and lower pole series are again superimposed as in eq. (8–54). With x' as horizontal distance and d_1 as depth to the upper pole, the anomalies

$$\Delta \mathbf{H} = 2C \left[- \frac{x'}{\rho_1^2} + \frac{x' - 2l \cos i}{\rho_2^2} \right]$$

and

$$\Delta \mathbf{Z} = 2C \left[\frac{d_1}{\rho_1^2} - \frac{d_1 + 2l \cos i}{\rho_2^2} \right],$$

(8–57)

where $2l$ is the length (depth extent) of the plate and i its dip.
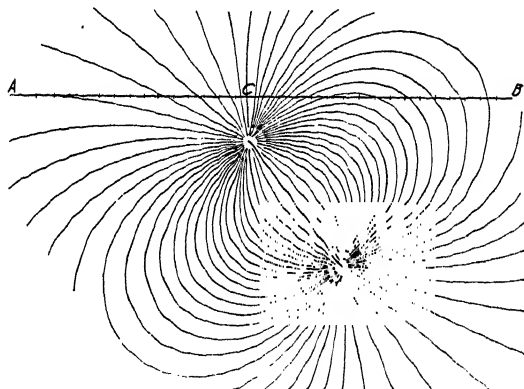
Fig. 8-49. Force-line diagram in application (after Haanel).

7. *The magnetic anomalies of irregular geologic features* may be calculated by assuming a series of poles near the upper surfaces of such features. If the depth extent is limited, vertical magnets are substituted for the single poles. For two-dimensional features with irregular upper or lower surfaces, magnetized lines along the upper and, if necessary, along the lower boundary should be assumed. The spacing of poles or lines does not have to be very close (particularly when the depth is great), since the magnetic method does not have much resolving power.

With the pole and line theory, induction effects (variations with magnetic latitude) may be simulated by placing oblique pole or line doublets into the formation section. Since neither the horizontal nor the vertical intensity anomalies are particularly sensitive to dip, the assumption of oblique magnetization does not afford much advantage except when the magnetic inclination is less than 60°.

9. *With line-of-force diagrams*, depth, dip, and approximate dimensions of ore bodies can be determined from anomalies represented by vectors. The method is applicable to bodies whose effect may be approximated by bar magnets and magnetized plates. Since the vectors are tangent to the lines of force, the diagram is applied by placing the equivalent magnet in such a position beneath the surface that its force-line distribution satisfies the arrangement of the vectors measured at the surface. The construction of force-line diagrams proceeds in accordance with the relation $\cos \alpha - \cos \beta = \mathbf{n} = $ constant, where α and β are the angles between the axis of a magnet and lines drawn from any point on a line of force (given by the constant $\mathbf{n}$) to the north and south pole of the magnet. The diagram shown in Fig. 8–49 may be adapted to equivalent magnets of different lengths by photostatic reduction or enlargement.

D. Induction Theory

The pole and line theory discussed above makes no assumption regarding the origin of the poles or pole series in a magnetized body. It is valid for any strength and direction of magnetization, regardless of origin. On the other hand, certain types of geologic bodies (some iron ores, igneous rocks of medium susceptibility, and magnetic sedimentary rocks) show magnetic anomalies which are obviously related to the strength and direction of the earth's magnetic field. In such cases it is advantageous to apply an interpretation theory which expresses the magnetic anomalies as a function of susceptibility, dimensions, and disposition of geologic bodies and as a function of the strength and direction of the earth's field. Unfortunately, the "induction theory" is handicapped by the fact that the field produced by many types of geologic bodies cannot be calculated accurately, since even bodies of uniform physical composition are not uniformly magnetized except when bounded by second order surfaces. Investigators have, therefore, sought a way out of the difficulty by one of two courses: (1) by approximating the shape of geologic bodies by spheres, infinite cylinders, and ellipsoids of revolution; (2) by dropping the premise of uniform magnetization and calculating the effects of actual bodies as if they were uniformly magnetized, that is, by disregarding the effects of flux concentration on edges and corners.[86] The literature dealing with both phases of the induction theory is fairly extensive; the more important articles are enumerated below:

1. Eötvös, R. v., 15, Allg. Conf. Int. Erdm., 392–394 (Budapest, 1906).
2. Winkelmann, A., Handb. d. Phys., **5**, 140 (1908).

[86] This fundamental limitation of the theory is often overlooked in articles dealing with this phase of the induction theory.

3. Carlheim-Gyllenskiöld, V., Magnetic Survey of Kiirunavaara (Stockholm, 1910).

4. Griesser, R., Diss. Freiburg (1921).

5. Steiner, L., Terr. Mag., **26**, 81 (1921).

6. Haalck, H., Zeit. Geophys., **2**, 1–11 and 49–62 (1926), **4**, 267 (1928); Gerl. Beitr., **22**, 241–255 and 385–399 (1929); Handb. Exper. Phys., **25(3)**, 320–347 (1930); *Die magnetischen Verfahren*, etc. (Berlin, 1927).

7. Bahurin, J., Inst. Pract. Geophys. Bull., **2**, 3 (1926); **3**, 255 (1927); **4**, 3–78 (1928).

8. Koenigsberger, J., Gerl. Beitr., **19(2)**, 241–291 (1928).

9. Gamburzeff, G. A., Gerl. Beitr., **19(2/3)**, 210–230 (1928).

1. *Fields of uniformly magnetized bodies* (spheres, infinite cylinders, ellipsoids of revolution). In Fig. 8–50a let P be a point of observation with the coordinates x and d in the plane of magnetization of a small sphere of susceptibility κ and volume v. The potential V of the doublet with the poles $+\mathbf{m}$ and $-\mathbf{m}$ produced by the earth's field is equal to the sum of the potentials due to each pole. Thus $V = \mathbf{m}/r_1 - \mathbf{m}/r_2 = \mathbf{m}(r_2 - r_1)/r_1 \cdot r_2$. By substituting r^2 for $r_1 \cdot r_2$, $\cos \varphi$ for $(r_2 - r_1)/2R$, and M (magnetic moment) for $2R\mathbf{m}$, the potential

$$V = \frac{M \cos \varphi}{r^2}. \qquad (8\text{–}58a)$$

Since the magnetic moment is the product of intensity of magnetization $\mathcal{I} = \kappa T_0$ (T_0 = total intensity) and volume $v = \frac{4}{3} \pi R^3$, its components due to magnetization by the horizontal and vertical intensities (see Fig. 8–50a)

$$M_x = \tfrac{4}{3} \pi R^3 \kappa \mathbf{H}_0 \qquad \text{and} \qquad M_z = \tfrac{4}{3} \pi R^3 \kappa Z_0. \qquad (8\text{–}58b)$$

This induced magnetization is accompanied by a demagnetization effect; the opposing field, $\mathbf{H}'$, is proportional to the intensity of magnetization $\mathcal{I}$, or $\mathbf{H}' = \mathbf{N}\mathcal{I}$, where $\mathbf{N}$ is the demagnetization factor. The resultant magnetization is therefore $\mathcal{I} = \kappa(T_0 + \mathbf{H}')$, or $\mathcal{I} = \kappa T_0/(1 + \mathbf{N}\kappa)$. For the sphere the demagnetizing factor $\mathbf{N} = 4\pi/3$ and the total intensity $\mathbf{T} = T_0 + \mathbf{H}' = T_0 \cdot 1/(1 + \frac{4}{3}\pi\kappa)$. Therefore, the resultant intensity of magnetization is $\mathcal{I} = T_0/(1 + \frac{4}{3}\pi\kappa)$. If the sphere is imbedded in a medium of the susceptibility κ_0 and if $\Delta\kappa \equiv \kappa - \kappa_0$, $\mathcal{I} = \Delta\kappa T_0/(1 + \frac{4}{3}$ Designating the factor $\Delta\kappa/(1 + \frac{4}{3}\pi\Delta\kappa)$ as κ', the magnetization

$$\mathcal{I} = T_0 \cdot \Delta\kappa'. \qquad (8\text{–}58c)$$

The demagnetizing effect results therefore in reduction of the true to an apparent susceptibility. It is negligible for bodies of low susceptibility. For strongly magnetic bodies, such as magnetite deposits, it may result in an appreciable decrease in susceptibility.
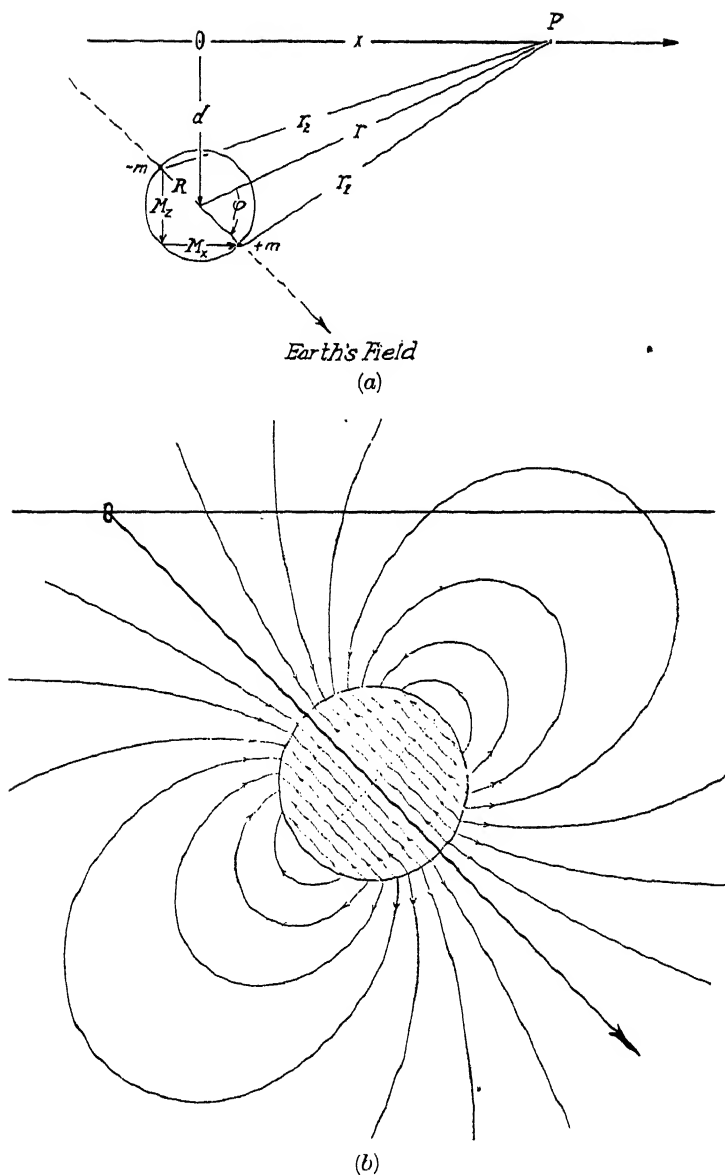
FIG. 8-50. Sphere magnetized by induction in the earth's field.

Returning to eqs. (8–58a) and (8–58b), we find the potentials due to the horizontal and vertical magnetizations to be

and　　　　　　　　　　　　　　　　　　　　　　(8–58d)

which, when differentiated with respect to x and d, give the horizontal and vertical intensity anomalies due to each magnet:

$$\Delta X_x = -\frac{\partial V_x}{\partial x} = -\frac{M_x}{r^3} + \frac{3M_x x^2}{r^5}$$

$$\Delta X_z = -\frac{\partial V_z}{\partial x} = -\frac{3M_z \cdot x \cdot d}{r^5}$$

and   (8-58e)

$$\Delta Z_x = -\frac{\partial V_x}{\partial d} = -\frac{3M_x \cdot x \cdot d}{r^5}$$

$$\Delta Z_z = -\frac{\partial V_z}{\partial d} = -\frac{M_z}{r^3} + \frac{3M_z d^2}{r^5} \cdot$$

By addition of the partial components, the anomalies become

$$\Delta H = -\Delta\kappa' \cdot \frac{v}{r^5}[3Z_0 xd - H_0(2x^2 - d^2)]$$

                                                                       (8-58f)

$$\Delta Z = -\Delta\kappa' \cdot \frac{v}{r^5}[3H_0 xd + Z_0(x^2 - 2d^2)],$$

where v, as before, $= \frac{4}{3}\pi R^3$ and $\Delta\kappa'$ is given by eq. (8-58c). Although spherical bodies are rarely encountered in nature, analysis of this case has the advantage of demonstrating clearly how the magnetic effects of geologic bodies depend on the magnetic latitude (see Fig. 8-51).

For an infinite cylinder the magnetic effects can be cast in simple form when the section S of the cylinder is in the plane of the magnetization, that is, if strike magnetization of the cylinder is zero. Then, according to Haalck:[87]

$$\Delta H = -2\Delta\kappa' \cdot \frac{S}{r^4}[2Z_0 xd - H_0(x^2 - d^2)]$$

and   (8-59)

$$\Delta Z = -2\Delta\kappa' \cdot \frac{S}{r^4}[2H_0 xd + Z_0(x^2 - d^2)].$$

These relations, as is to be expected, are similar to those for the sphere (eq. 8-58f).

Griesser and Koenigsberger[88] have calculated the magnetic anomalies in vertical intensity, horizontal intensity, and declination, for ellipsoids of

[87] *Die magnetischen Verfahren, op. cit.*, p. 54.
        r, Gerl. Beitr., **19(2)**, 241–291 (1928).

rotation with varying proportions of axes and depths. They have also given tabulations for determination of depths and dimensions from relative amplitudes, from distances of positive and negative anomalies, and from distances between the half-, quarter-, and tenth-value points. The formulas for ellipsoids of revolutions are fairly involved and will not be given here.

2. *Relation between magnetic and gravitational anomalies.* Calculations of anomalies due to induction in magnetic bodies have benefited greatly from the fact that a relation exists between the magnetic and gravitational attractions of such bodies. This makes it possible to apply torsion balance
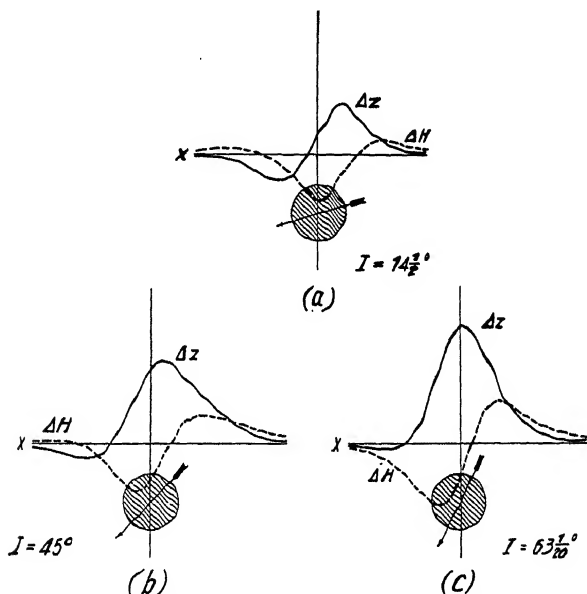
FIG. 8-51. Influence of magnetic latitude on magnetic anomalies (after H. Haalck).

interpretation formulas in connection with a simple conversion. Strictly speaking, this procedure is applicable only to bodies of uniform magnetization. Its use in the calculation of the anomalies of faults, dikes, slabs, plates, and the like, involves approximations, *neglects the influence of edges and corners*, and *disregards the demagnetization*.

A theorem of Poisson states that the *magnetic potential* is *proportional* to the *gravity component in the direction of magnetization*:

$$V = \frac{\mathcal{I}}{k\delta} \frac{\partial U}{\partial i}, \qquad (8\text{-}60a)$$

where V is the magnetic potential, $\mathcal{I}$ the intensity of magnetization, k the gravitational constant ($66 \cdot 10^{-9}$ C.G.S.), δ difference in density, U the

gravity potential, and i the direction of magnetization. From eq. (8–60a) the force in the direction **s**:

$$\frac{\partial V}{\partial s} = \frac{\mathcal{G}}{k\delta} \frac{\partial^2 U}{\partial i \partial s};$$

and therefore, the horizontal and vertical components,

$$\frac{\mathcal{G}}{k\delta} \frac{\partial^2 U}{\partial i \partial x} \quad \text{and} \quad \Delta Z = \frac{\mathcal{G}}{k\delta} \frac{\partial^2 U}{\partial i \partial z}. \qquad (8\text{–}60c)$$

It follows from this formula that (1) for vertical magnetization (high magnetic latitudes) the horizontal intensity anomaly is proportional to the *horizontal gradient of gravity*, and the vertical intensity anomaly is proportional to the *vertical gradient of gravity*; and (2) for horizontal magnetization (near magnetic equator) the horizontal intensity anomaly is proportional to horizontal gradient of horizontal gravity component or proportional to the "curvature" value (for two-dimensional bodies, or to the *negative vertical gravity* gradient), and the vertical intensity anomaly is proportional to the *horizontal gradient of gravity*. For three-dimensional bodies application of formulas (8–60c) leads to equations which are involved and difficult to apply. For two-dimensional bodies these relations remain simple, particularly for extreme cases of dip, dimensions, and magnetic latitudes.

Resolving the magnetization in eq. (8–60b) into a transverse horizontal component (**A**) and a vertical (**C**); assuming that the strike direction is y and the profile direction (at right angles to the strike) is x; and segregating the gravity component $\partial U/\partial i$ into a horizontal and a vertical component, eq. (8–60b) is

$$\frac{\partial V}{\partial s} = \frac{1}{k\delta} \cdot \frac{\partial}{\partial s}\left(\frac{\partial U}{\partial x}\cdot \mathbf{A} + \frac{\partial U}{\partial z}\cdot \mathbf{C}\right),$$

so that the anomalies:

$$\left.\begin{aligned}
\frac{\partial V}{\partial x} = \Delta \mathbf{H} &= \frac{1}{k\delta}\left(\frac{\partial^2 U}{\partial x^2}\cdot \mathbf{A} + \frac{\partial^2 U}{\partial x \partial z}\cdot \mathbf{C}\right) \\
\frac{\partial V}{\partial z} = \Delta Z &= \frac{1}{k\delta}\left(\frac{\partial^2 U}{\partial x \partial z}\cdot \mathbf{A} + \frac{\partial^2 U}{\partial z^2}\cdot \mathbf{C}\right).
\end{aligned}\right\} \qquad (8\text{–}60d)$$

If x' and y' are the magnetic north and east directions, y the direction of strike, and α the angle of strike from north over west (angle between $-y$ and x' direction), the transverse horizontal magnetization and the vertical magnetization are $\mathbf{A} = \kappa \mathbf{H}_0 \sin \alpha$ and $\mathbf{C} = \kappa Z_0$, where κ is the

susceptibility *difference* of the geologic body against the adjacent rock.[89] The torsion balance furnishes the gravity gradients $\partial^2 U/\partial x'\partial z$ and $\partial^2 U/\partial y'\partial z$, and the curvature values $\partial^2 U/\partial y_1^2 - \partial^2 U/\partial x_1^2$ and $\partial^2 U/\partial y'\partial x'$. For two-dimensional bodies $\partial^2 U/\partial y^2 = \partial^2 U/\partial x\partial y = \partial^2 U/\partial y\partial z = 0$, which leaves the gradient $\partial^2 U/\partial x\partial z = U_{xz}$ and the curvature value $\partial^2 U/\partial x^2 = U_{xx}$ in the profile direction. Since $-\partial^2 U/\partial z^2 = \partial^2 U/\partial x^2$,

$$\left.\begin{array}{l} \Delta \mathbf{H} = \dfrac{\kappa}{k\delta}\cdot(\mathbf{H}_0 \sin \alpha U_{xx} + \mathbf{Z}_0 U_{xz}) \\[4mm] \Delta \mathbf{Z} = \dfrac{\kappa}{k\delta}\cdot(\mathbf{H}_0 \sin \alpha U_{xz} - \mathbf{Z}_0 U_{xx}). \end{array}\right\} \quad (8\text{-}60e)$$

In the derivation of these equations uniform magnetization is assumed and demagnetization is disregarded.

3. *Magnetic anomalies of two-dimensional bodies* have been calculated for faults, slabs, vertical and inclined dikes, anticlines, and synclines from the corresponding torsion balance anomalies derived in Chapter 7 on pages 258-65. Angles and distances in the following formulas correspond to the notation used in Fig. 8-52; statements concerning maxima and minima apply mostly to high magnetic latitudes.

For a *vertical fault* (step, cliff, vertical edge of subsurface erosional feature, flank of an intrusion, and the like), the magnetic anomalies are, when both horizontal and vertical magnetizations are considered,

$$\left.\begin{array}{l} \Delta \mathbf{H} = 2\kappa\left[\mathbf{H}_0 \sin \alpha(\varphi_2 - \varphi_1) + \mathbf{Z}_0 \log_e \dfrac{r_2}{r_1}\right] \\[4mm] \Delta \mathbf{Z} = 2\kappa\left[\mathbf{H}_0 \sin \alpha \log_e \dfrac{r_2}{r_1} - \mathbf{Z}_0(\varphi_2 - \varphi_1)\right]. \end{array}\right\} \quad (8\text{-}61a)$$

For N-S strike of the fault the horizontal anomaly is proportional to the gravity gradient and shows a maximum over the fault. The vertical intensity is proportional to the negative curvature value and has a minimum to the south. It is zero over the fault and has a maximum toward north.

---

[89] At this point of the theory it would be possible to introduce the demagnetization by a substitution of apparent for true susceptibility (see p. 390, eq. [8-58c]. The demagnetization factor is *different* for the transverse and the vertical magnetization and depends on the dip. The component magnetizing the body in its longitudinal direction has the smaller demagnetizing factor. For steeply dipping, strongly magnetic bodies, the transverse apparent susceptibility may thus be but a fraction of the actual rock susceptibility. This fact is additional justification for neglecting the transverse horizontal compared with the vertical longitudinal magnetization (see p. 396).

For a *vertical dike of infinite depth extent*, the transverse magnetization may be neglected and the anomalies are:

$$\Delta H = 2\kappa Z_0 \log_e \frac{r_2}{r_1}$$

$$\Delta Z = 2\kappa Z_0 \varphi$$

$$\left.\vphantom{\begin{array}{c}a\\b\end{array}}\right\} \quad (8\text{-}61b)$$

(see Fig. 8-52). The horizontal intensity is proportional to the gravity gradient, has a maximum in the south, and is zero above and at a minimum
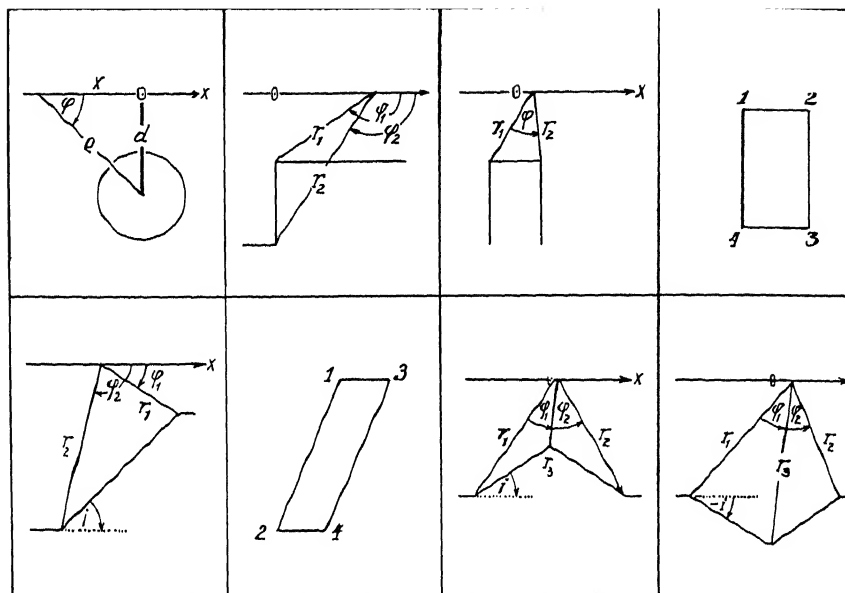
Fig. 8-52. Angles and distances on two-dimensional bodies (from left to right, top row first): cylinder, vertical fault, infinite vertical dike, finite vertical dike, slope, inclined dike, anticline, syncline.

north of the dike. The vertical intensity is proportional to the negative curvature and has a maximum above the dike.[90]

In the case of a *vertical dike of limited depth extent*, the transverse magnetization is likewise negligible and the anomalies

---

[90] Formulas (8-61b) were given in the following form by Smyth as early as 1899:

$$\Delta H = C \log \frac{d^2 + (x+a)^2}{d^2 + (x-a)^2} \qquad \text{and} \qquad \Delta Z = 2C \left(\tan^{-1} \frac{x+a}{d} - \tan^{-1} \frac{x-a}{d} \right),$$

where $2a$ is the width of the dike, C a constant, d the depth to the upper surface, and x the horizontal surface distance from center.

$$\Delta H = 2\kappa Z_0 \log_e \frac{r_2 r_4}{r_1 r_3}$$

$$\Delta Z = 2\kappa Z_0 (\varphi_3 + \varphi_1 - \varphi_4 - \varphi_2).$$

$$\left. \begin{array}{l} \\ \\ \end{array} \right\} \quad (8\text{-}61c)$$

The same rules in respect to maxima, minima, and zero points apply as for the infinite dike. However, since the lower end becomes effective, positive curvature values appear on the sides, and the maximum in vertical intensity is flanked by two minima.

For a *horizontal slab*, the horizontal transverse magnetization is generally not negligible, and the anomalies

$$\Delta H = 2\kappa \left[H_0 \sin \alpha (\varphi_4 - \varphi_3 + \varphi_2 - \varphi_1) + Z_0 \log_e \frac{r_2 r_4}{r_1 r_3} \right]$$

$$\Delta Z = 2\kappa \left[H_0 \sin \alpha \log_e \frac{r_2 r_4}{r_1 r_3} - Z_0 (\varphi_4 - \varphi_3 + \varphi_2 - \varphi_1) \right].$$

$$\left. \begin{array}{l} \\ \\ \\ \end{array} \right\} \quad (8\text{-}61d)$$

The horizontal intensity has a maximum over the southern and a minimum over the northern edge. The maximum in vertical intensity occurs over the middle of the slab and is flanked by two minima in the north and south.

The complete magnetic anomalies of a *slope* are

$$\Delta H = 2\kappa \sin i \left\{ H_0 \sin \alpha \left[\sin i (\varphi_2 - \varphi_1) - \cos i \log_e \frac{r_2}{r_1} \right] \right.$$

$$+ Z_0 \left[\sin i \log_e \frac{r_2}{r_1} + \cos i (\varphi_2 - \varphi_1) \right] \right\}$$

$$\Delta Z = 2\kappa \sin i \left\{ H_0 \sin \alpha \left[\sin i \log_e \frac{r_2}{r_1} + \cos i (\varphi_2 - \varphi_1) \right] \right.$$

$$- Z_0 \left[\sin i (\varphi_2 - \varphi_1) - \cos i \log_e \frac{r_2}{r_1} \right] \right\}.$$

$$\left. \begin{array}{l} \\ \\ \\ \\ \\ \end{array} \right\} \quad (8\text{-}61e)$$

The transverse horizontal magnetization may be neglected when the strike is nearly meridional and in high magnetic latitudes. The horizontal intensity rises gradually to a maximum near the upper edge of the slope and drops rapidly past it if the slope is upward in the x direction, as shown in Fig. 8-52. If the slope is downward in the same direction, the horizontal intensity shows a minimum of the same general character. The vertical intensity rises from a minimum on the south side of the slope through zero to a maximum over the upper edge. Downslope in the x direction the vertical intensity passes from a maximum through zero to a minimum. For very gentle slopes the gradient of gravity and, hence, the horizontal intensity is very nearly constant, particularly for meridional strike or high latitude.

For wide *inclined dikes* or formations of gentle dip, the transverse magnetic effect is generally not negligible, except under favorable conditions of magnetic latitude and strike. For steeply dipping formations and ore deposits whose width is small compared with their depth extent, the anomalies are,[91] when the transverse magnetization is neglected,

$$\Delta \mathbf{H} = 2\kappa \sin i \, \mathbf{Z}_0 \left[\sin i \, \log_e \frac{r_2 r_3}{r_1 r_4} + \cos i(\varphi_2 - \varphi_1 + \varphi_3 - \varphi_4) \right] \left. \right\}$$

$$\Delta \mathbf{Z} = - 2\kappa \sin i \, \mathbf{Z}_0 \left[\sin i(\varphi_2 - \varphi_1 + \varphi_3 - \varphi_4) - \cos i \, \log_e \frac{r_2 r_3}{r_1 r_4} \right]. \left. \right\}$$

$$(8\text{-}61f)$$

Above an inclined dike the horizontal intensity has a maximum in the south and a minimum in the north. The ratio of their amplitude depends on the dip; for a vertical dike they are approximately equal. The smaller amplitude on the hanging wall side rises to a peak above the dike and then drops rapidly on the foot wall side. On the latter a minimum appears which increases in amplitude as the dip decreases. Fig. 8-53 shows the influence of dip for a dike of infinite depth extent and high magnetic latitudes. The anomalies *include* transverse horizontal magnetization.

Figs. 8-54*a* to 8-54*c* illustrate the influence of strike on magnetic anomalies for high, intermediate, and low magnetic latitudes.

Fig. 8-53. Effect of dip on horizontal and vertical intensities for high magnetic latitudes. Strike E-W, $I = 63°$ (after Haalck). Reading down: 90° dip, 45° dip, 0° dip.

[91] Eve (A.I.M.E. Geophysical Prospecting, 204-205 [1932]) gives the following formulas for an inclined dike:

$$\Delta \mathbf{H} = 2\mathrm{m} \, \log_e \frac{r_1 r_4}{r_3 r_2}$$

$$\Delta \mathbf{Z} = 2\mathrm{m}(\varphi_1 - \varphi_3 - \varphi_2 + \varphi_4).$$

These expressions obviously hold for a finite vertical and not for a dipping dike; they correspond to eqs. 8-61*c*.
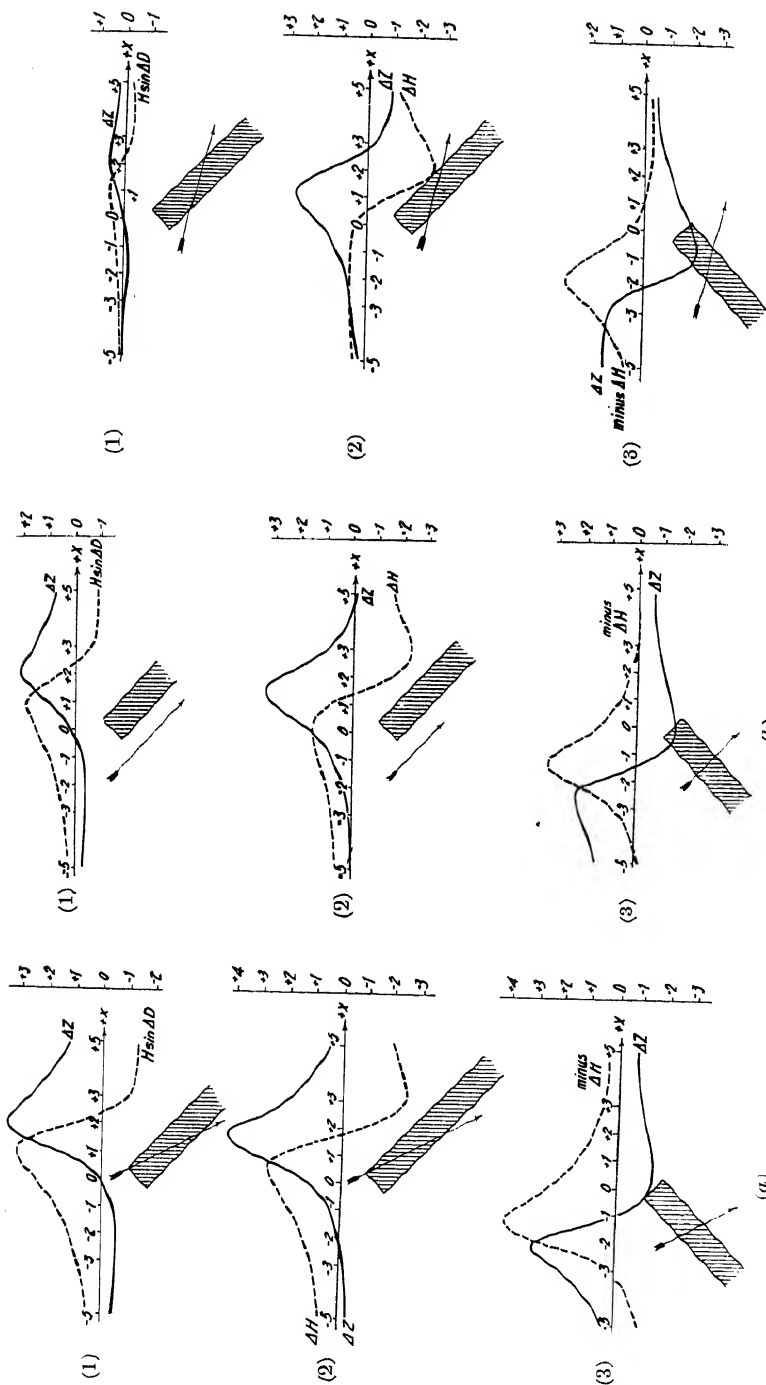
Fig. 8-54. Influence of strike on magnetic anomalies (after Haalck).

(a) In high magnetic latitudes ($I = 63°$): (1) strike, N-S, dip, N; (2) strike, E-W, dip, N; (3) strike, E-W, dip, S.

(b) In intermediate magnetic latitudes ($I = 45°$): (1) strike, N-S, dip, N; (2) strike, E-W, dip, N; (3) strike, E-W, dip, S.

(c) In low magnetic latitudes ($I = 14°$): (1) strike, N-S, dip, N; (2) strike, E-W, dip, N; (3) strike, E-W, dip, S.

For *symmetrical* and *asymmetrical anticlines* and *synclines* the analytical expressions become too complicated even if the transverse magnetization is neglected, and it is simpler to operate with the graphical methods discussed in the next paragraph.

4. *The magnetic anomalies of irregular features* may be calculated by evaluating first their torsion-balance anomalies with graticules, interpretation diagrams, or integraphs, as discussed in detail in Chapter 7, on pages 265–70. If the number of elements comprised by the outline of a geologic body is i in a curvature diagram, and n in a gradient diagram, the gravitational anomalies are $U_{zz} = C'\delta n$ and $U_{xz} = C'\delta i$, where C' is the constant effect of each mass element in E.U. The magnetic anomalies follow by substitution of these expressions in eq. (8–60e): for $\delta = 1$ and $C'/k = C$

$$\left.\begin{aligned}\Delta H &= C\kappa(\mathbf{H}_0 \sin \alpha \cdot \mathbf{i} + \mathbf{Z}_0 \cdot \mathbf{n})\\[2mm]\Delta Z &= C\kappa(\mathbf{H}_0 \sin \alpha \cdot \mathbf{n} - \mathbf{Z}_0 \cdot \mathbf{i}).\end{aligned}\right\} \quad (8\text{--}62a)$$

If the unit effect in the torsion-balance diagrams is 1/10 E.U., the constant C in eq. (8–62a) is 150γ. Diagrams for the direct calculation of magnetic anomalies may be constructed[92] by introducing some simplifications in the last formula.

As shown in Chapter 7, gravitational anomalies may be calculated mechanically with special integraphs. The magnetic anomalies then follow from the surface integrals of the section of subsurface bodies so that, by combination with eq. (8–60e), the horizontal and vertical intensity anomalies

$$\left.\begin{aligned}\Delta H &= 2\kappa T' \iint\limits_{S} \sin \varphi \cos (\varphi - I') \frac{d\rho}{\rho}\\[3mm]\Delta Z &= 2\kappa T' \iint\limits_{S} \cos \varphi \cos (\varphi - I') \frac{d\rho}{\rho},\end{aligned}\right\} \quad (8\text{--}62b)$$

where I' and T' are the apparent total intensity and inclination and ρ and φ the polar coordinates of the elements in the section at right angles to the strike. Gamburzeff[93] has constructed single integraphs for calculations of intensities at one station, and multiple integraphs for simultaneous indication of the surface integral at ten stations.

E. Interpretation Theory Based on Both Permanent and D Magnetization

While the induction theory gives fairly accurate results for formations of low or intermediate susceptibility and furnishes at least the shape of

[92] J. Pirson, A.I.M.E. Contr., 91 (Nov., 1935).

[93] G. A. Gamburzeff, Gerl. Beitr., **24(2/3)**, 83–93 (1929).

the anomaly curve correctly for strongly magnetic rocks, it has been known to fail in several cases as far as the magnitude of the calculated anomalies is concerned. This has led several investigators[94] to assume abnormally high susceptibilities, as in the case of the Kursk, and other magnetic anomalies associated with iron ores. In at least one instance the assumption of high susceptibility could not be maintained after the rock specimen had been tested (Kursk). Hence, it appears that the fault lies with the theory and that susceptibility alone is not sufficient to describe the effects of the surface in all instances. As a comparison of the hysteresis curves of Figs. 8-11 and 8-12 shows, the susceptibility alone would be sufficient in the latter case to express the effect at the surface, whereas in the former, it would not suffice. In the first case, the intensity of magnetization would have to be represented by a function of the form $\mathscr{I} = \mathscr{I}' + \kappa H$ while in the latter the mere product $\mathscr{I} = \kappa H$ as given in the preceding theory expresses the situation satisfactorily. The tabulations given on pages 315-16 for the coercive forces and remanent magnetization $\mathscr{I}'$ of rocks indicate that (1) the ratio of coercive force and maximum susceptibility for rocks is much greater than for commercial iron and steel; (2) for many metamorphic and eruptive igneous rocks the remanent magnetization is *greater* than the product of susceptibility and (earth's) field. Thus, in some instances, the induced magnetization may be neglected in comparison with the remanent magnetization (see formulas on pages 382 and 387).

It is possible to make allowance for such conditions by adding, in the formulas of the preceding section, the remanent magnetization to the induced magnetization. Since the remanent magnetization is a vector whose direction may or may not coincide with the direction of induced magnetization, it must be resolved into its longitudinal and transverse components. For thin ore bodies, igneous sheets, and the like, and for low susceptibilities, the transverse components of both induced and remanent magnetization are usually negligible, so that from formula (8-55):

$$\Delta H = -\frac{2bx}{\rho^2}(\kappa Z_0 \pm \mathscr{I}'_l)$$

$$\Delta Z = -\frac{2bd}{\rho^2}(\kappa Z_0 \pm \mathscr{I}'_l),$$

$$(8\text{-}63a)$$

where $\mathscr{I}'_l$ is the longitudinal remanent magnetization and the $\pm$ sign indicates normal or abnormal polarization, respectively.

For a wider vertical body the transverse components of both induced and remanent magnetization may become important. Hence, the anomalies follow from formula (8-61b) and are, if both the longitudinal ($\mathscr{I}_l$) and

[94] Slichter, *op. cit.*, 250. Haalck, Gerl. Beitr., **22**, 241-255 and 385-399 (1929).

the transverse ($\mathcal{I}_t$) *induced* components are considered,

$$\Delta H = 2 \left(\mathcal{I}_t \log_e \frac{r_2}{r_1} - \mathcal{I}_t \varphi \right) \left. \begin{array}{c} \\ \\ \\ \end{array} \right\}$$

$$\Delta t = 2 \left(\mathcal{I}_t \varphi + \mathcal{I}_t \log_e \frac{r_2}{r_1} \right). \tag{8-63b}$$

By addition of the corresponding components of the remanent magnetization ($\mathcal{I}_l'$ and $\mathcal{I}_t'$), these formulas change to

$$\Delta H = 2 \left[\log_e \frac{r_2}{r_1} (\kappa Z_0 + \mathcal{I}_l') - \varphi \left\{ \left(\frac{\kappa}{1 + \mathbf{N}\kappa} \right) \mathbf{H}_p \pm \mathcal{I}_t' \right\} \right] \left. \begin{array}{c} \\ \\ \\ \end{array} \right\}$$

$$\Delta t = 2 \left[\varphi(\kappa Z_0 \pm \mathcal{I}_l') + \log_e \frac{r_2}{r_1} \left\{ \left(\frac{\kappa}{1 + \mathbf{N}\kappa} \right) \mathbf{H}_p \pm \mathcal{I}_t' \right\} \right], \tag{8-63c}$$

where, for the transverse magnetization also, the demagnetizing effect ($\mathbf{N}$ = demagnetizing factor) has been included. $\mathbf{H}_p$ is the horizontal component perpendicular to the strike. $\mathbf{N}$ and $\mathcal{I}_t'$ are usually important for fairly high susceptibility only. In approximation, formula (8-63c) may also be used for dipping ore bodies provided, of course, that the magnetizations $\mathcal{I}_l'$ and $\mathcal{I}_t'$, as indicated, are reckoned in the longitudinal and transverse direction of the dike or vein.

F. MODEL EXPERIMENTS IN MAGNETIC INTERPRETATION

The value of model experiments in magnetic interpretation lies in the fact that the magnetic fields of geologic bodies can be ascertained with greater accuracy by experiment than they can be calculated. This advantage is enhanced by greater speed and the possibility of simulating irregular distributions of magnetic materials. The earliest application of model experiments was probably made in Sweden, where the use of the magnetic method in the location and depth determination of magnetic ore bodies necessitated accurate interpretation methods. Lundberg and Sundberg state that such experiments have been carried out continuously since 1875 by students of the Royal Institute of Technology in Stockholm.

Probably the first description of model experiments was given by Thalén[95] who used a magnetic bar in a vertical position. Above the bar was a board which he rotated about a vertical axis coincident with the axis of the bar. At intervals of 20°, declination and horizontal intensity were determined with a Thalén magnetometer. Similar model experiments were carried out by Uhlich.[96]

---

[95] In *Jernkontoret's Annaler* (1879), translated by B. Turley (*Untersuchung von Eisenerzfeldern durch magnetische Messungen* [Leipzig, 1879]) p. 56–64.

[96] *Aufsuchung magnetischer Erzlagerstaetten*, pamphlet issued by *Jahrbuch fuer das Berg- und Huettenwesen in Sachsen* (Freiberg, 1902).

Haanel[97] describes an arrangement for magnetic model experiments consisting of a square table about 40 inches high and 65 inches square, brass rails on two sides, on which a bridge could be moved to any desired position. The bridge carried a movable slide to which a magnetometer was attached. Rails and bridge were graduated so that the position of the magnetometer with reference to any stationary object below the table could be accurately determined. The model ore bodies were made of hard cast iron or hardened steel, and they could be magnetized by solenoids. Their distance from the plane of observation was regulated by supports of properly adjusted heights. A vertical adjustment of the position of the magnetometer within small limits made it possible to investigate the effects of topographic irregularities.

Hotchkiss[98] studied the influence of dip and strike of magnetic formations upon a dial compass and a dip needle on a simple drawing board. On the underside of this board a sheet of tin 20 by 28 inches was attached by suspending it on a pair of copper nails in varying distances and at varying angles of dip. For the determination of variations in declination, a compass was fastened to a triangle, and this triangle was moved along a T square. With a more elaborate experiment table adapted to observations with both dial compass and dip needle, he then made measurements of the influence of dip and strike upon both declination and dip.

Rothelius,[99] in 1924 used an elliptical magnet 35 cm long, 7 cm wide at the largest point, and 8.5 mm thick. Eve and Keys[100] experimented with vertical sheets to check methods of determining depths and dimensions of magnetic ore bodies from observations in different levels.[101]

An efficient arrangement for testing magnetic structures, effects of basement rocks, and the like, has been perfected by Barret.[102] The models are made of a plastic substance of variable magnetic susceptibility and are placed in a tray at an adjustable distance from a glass plate representing the earth's surface. The earth's magnetic field is produced by a pair of Helmholtz coils which may be tilted and may be supplied with variable alternating currents to simulate changes in the direction and intensity of the normal earth's magnetic field. The normal field is first measured without the model by a small earth inductor connected to a rectifier and D.C. galvanometer. Then the model is inserted and the measurements are repeated. Since the distance between the glass plate and the model

[97] Op. cit., 95.

[98] Wisconsin Geol. and Nat. Hist. Survey Bull., 44, Chap. IV, "Magnetic Observations," pp. 112–113 (Madison, 1915).

[99] A.I.M.E. Geophysical Prospecting, 210–211 (1932).

[100] A. S. Eve and D. A. Keys, A.I.M.E. Geophysical Prospecting, 206 (1932).

[101] See also Canad. Geol. Survey Mem. 170, 30 ff. (1932).

[102] Oil Weekly, 66(7), 27–30 (Aug. 1, 1932).
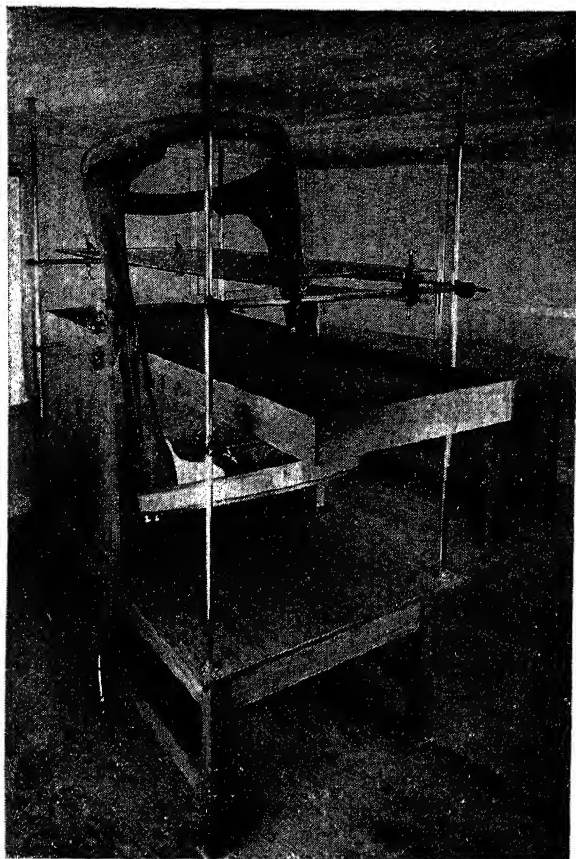
(a)
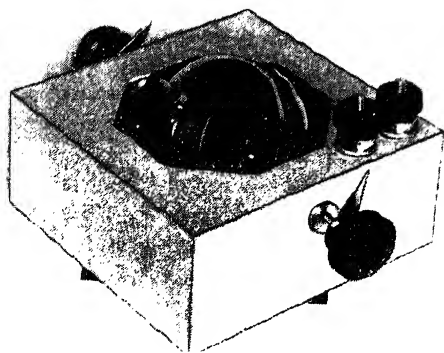
(b)

Fig. 8-55. Arrangement for magnetic model experiments (after Barret). (a) Energizing coil, model tray and inductor platform, (b) inductor.

tray may be changed, rather accurate depth determinations are possible with this method (see Fig. 8–55).

Later Jenny[103] devised an apparatus in which the shape of a structure was represented by bar magnets suspended from pulleys with counterweights. The vector direction was indicated by small dipping needles free to move in vertical and horizontal planes. In place of the bar magnets, glass tubes filled with materials of different susceptibility were suggested to represent the vertical sequence of formations of different magnetizations. In that case the normal terrestrial field was produced by a coil.

G. UNDERGROUND, AERIAL, AND PLATFORM SURVEYS

Since magnetic surveys underground are greatly handicapped by power lines, pipes, and rails, such objects should be removed as far as practicable. Erratic readings may be produced by ore stringers and strongly

magnetic or abnormally polarized rocks on tunnel and shaft faces.　Before an underground survey is contemplated, it is good practice to go through the workings with a compass and determine the spots of irregular attraction. Magnetic measurements underground have been made chiefly with Swedish

δ	α	R	V_I	V_{II}	V_{III}
				normal below	
62°	13°	1.63	-11	+10	+53
69°	28°	0.78	-21	-20	-19
71½°	18½°	1.16	-22	-22½	-21
66½°	13°	1.63	-25	-24	-23
54½°	10½°	2.02	-26	-25	-25
35°	10½°	2.02	-23	-23	-22
24°	11°	1.92	-21	-20	-18
12°	12°	1.76	-18	-17½	-17
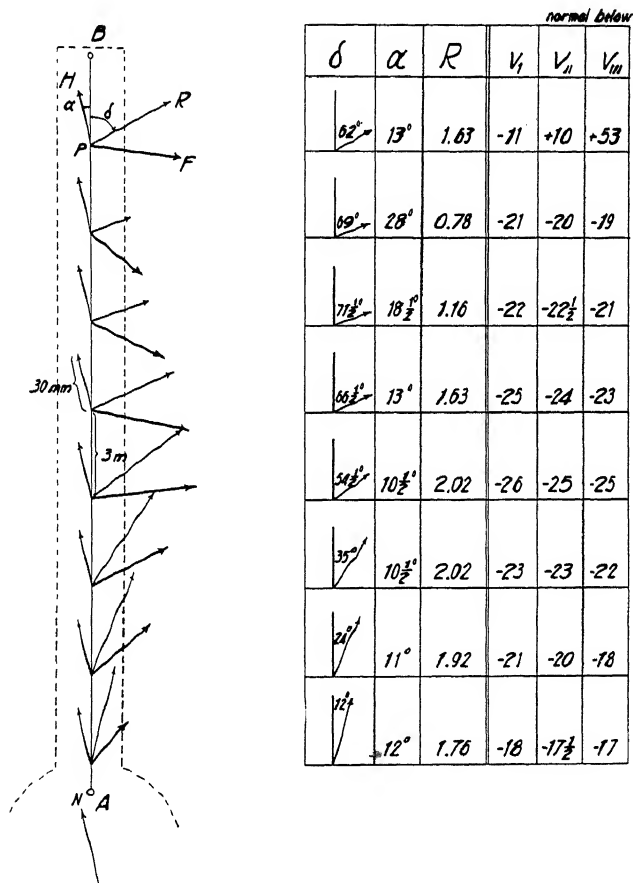
FIG. 8-56. Results of underground observations, by Tiberg method (from Berg Catalogue).

instruments.　However, the more sensitive Schmidt balances have been used in a few cases.　Haalck[104] has published the results of a number of vertical intensity observations in a drift from which rails and pipes had been removed.　Two negative anomalies of about $-200\,\gamma$ were observed. These were due to lenses of serpentine encountered in higher levels of the

[104] Handb. Exper. Phys., 25(III), 386 (1930).

same mine, indicating that ore bodies above the level of observation give rise to negative anomalies (see below). The same phenomenon was observed in the iron ore mines of Berggiesshuebel in Saxony, where measurements were likewise made with the Schmidt balance.

In Swedish mines Tiberg's method of determining vertical intensity as well as direction and length of the horizontal disturbance vector has been widely applied. The procedure was described on page 379. Another method uses a magnetometer with height adjustment on a plane table so that not only the regular stations in the middle of a tunnel but also points horizontally and vertically in line with them may be surveyed. Results of an underground tunnel survey are reproduced in Fig. 8-56, showing the horizontal vectors as well as results of vertical intensity observations in
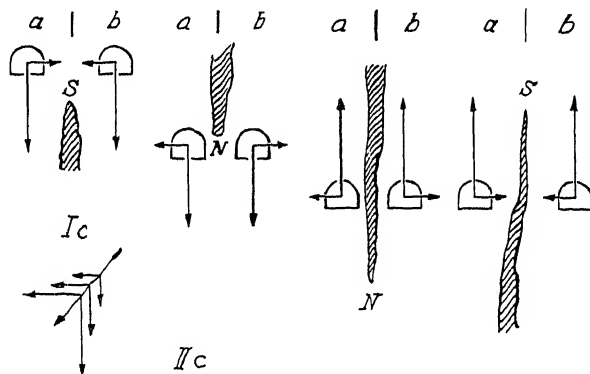
Fig. 8-57. Anomalous vectors for various ore body positions in tunnel surveys. I, Upper end of ore body below tunnel; II, lower end of ore body above tunnel; III, lower end of ore body below tunnel; IV, upper end of ore body above tunnel. Ic, vector gradient at Ib; IIc, vector gradient at IIa.

three levels. The need for vertical intensity measurements arises from the fact that the magnetic bodies may be below or above the instrument.

Four possible combinations are shown schematically in Fig. 8-57: (I) when a south pole, or upper end, of an ore body is below the drift, the horizontal anomalous vectors point toward the pole; (II) if its north pole, or lower end, is above the drift, the horizontal vectors will be directed away from the pole; (III) if its north pole is below, the horizontal vectors point away; and (IV) if its south pole is above, the horizontal vectors will point toward it. If interpretation were based on horizontal vectors alone and a cross cut were driven on the strength of the vector pattern in case IV, the ore body would be found; in case I it would be missed. The addition of vertical intensity measurements overcomes part of the difficulty. If two adits, as shown in Fig. 8-57, were always available, no mistake in interpre-

tation would be possible.   Positive vertical intensities with diverging horizontal vectors could mean a lower end of an ore body above, negative vertical intensities with diverging horizontal vectors a lower end below, positive vertical intensities with converging horizontal vectors an upper end below, and negative vertical intensities with converging patterns an upper end above.   However, such favorable conditions seldom occur and the actual number of combinations of vector directions is not four but eight.

To eliminate the remaining uncertainty, intensity gradients (in vertical or horizontal intensity, or both) may be measured whereby vector gradients, as shown in the figure, may be plotted.   This will correctly indicate the position of the pole, even if the polarization of the ore is abnormal.

Determinations of depth or distance to ore bodies may be made by measuring intensities in different levels of a mine, in different depths of a shaft, at the surface and on a platform (see Fig. 8-58), at the surface and in a balloon, or by airplane in different altitudes.   The first method was proposed by Dahlblom in 1899.   When observations are made at two points directly above an ore body of considerable depth extent, if d is the distance of the lower point of observation from the upper pole of the ore body and if $d + \Delta d$ is the distance of the upper point from this pole, the vertical intensities follow from formulas (8-52a) and are

W. Riddell

Fig. 8-58. Magnetometer observation platform.

$$(\text{above}) \ \Delta Z_2 = \frac{m}{(d + \Delta d)^2} \qquad (\text{below}) \ \Delta Z_1 = \frac{m}{d^2} \ ; \qquad \Delta Z_1 > \Delta Z_2.$$

Hence, from their ratio

$$d = \frac{\Delta d}{\dfrac{\Delta Z_1}{\Delta Z_2} - 1} \qquad (8\text{-}64a)$$

If the ore body is extended in the direction of strike, the relations are (see theory of magnetized line, formulas [8–55]):

$$\text{(above)} \ \Delta Z_2 = \frac{2m}{d + \Delta d} \qquad \text{and} \qquad \text{(below)} \ \Delta Z_1 = \frac{2m}{d},$$

so that

$$\frac{\Delta d}{\dfrac{\Delta Z_1}{\Delta Z_2} - 1} \tag{8–64b}$$

To attain a fair accuracy, it is necessary that Δd be comparable in magnitude with d (about $0.1d$). Haanel[105] and Eve and Keys[106] have given examples of such depth determinations. In Haanel's case, the actual depth of the ore body was about 30 meters; the plane of observation was raised 3 meters and application of eq. (8–64a) gave 30.13 meters. Eve and Keys used a platform 10 feet high on the Falconbridge ore body, whose depth was between 112 and 123 feet; the depth calculated from (8–64b) was 118 feet. Eve and Keys also attempted to determine the depth to the lower pole but were unsuccessful because of the obvious limitations of this method. Where platforms fail to give sufficient change in distance or depth, the geophysicist is forced to "take to the air." Measurements in captive balloons have been used above the Kiiruna ore body.[107] Magnetic measurements by automatic recording devices in airplanes have the advantage not only of direct depth determination but of great speed and applicability to inaccessible country.[108]

VI. MAGNETIC SURVEYS

The following discussion of the results of magnetic exploration is of necessity limited to a number of the more typical cases. In the United States alone the area covered by magnetic surveys is estimated to be close to $\frac{3}{4}$ million square miles and only a fraction of the results has been made public. Nevertheless, the international literature on magnetic surveys is fairly extensive owing to the fact that they are not difficult, that equipment is usually available, that geologic objects for the study of magnetic effects are readily found, and that magnetic exploration has applications in mining, oil exploration, and engineering geology.

---

[105] Haanel, *op. cit.*, 86.
[106] Eve and Keys, *op. cit.*, 201.
[107] H. Lundberg and K. Sundberg, A.I.M.E. Geophysical Prospecting, 209 (1932).
[108] Heiland, Eng. and Min. J., **136**(12), 609–610 (Dec., 1935).

A. MAGNETIC SURVEYS IN MINING

1. *Surveys of iron ore: magnetite, hematite, and brown iron deposits.* Probably the most famous example of magnetic iron ore exploration is the survey of the Kursk magnetic anomaly. This anomaly, near Krjukowa and Bielgorod, was discovered by I. N. Smirnow in 1874; it was further explored by Piltchikow, Sergijevsky, and Rodd, and was briefly discussed by Moureaux in 1896.[109] A systematic magnetic survey was started in 1889 by E. Leyst, who from 1896 to 1909 surveyed some 4500 stations. He left Russia in 1918 and died abroad. The survey data and original maps could not be recovered after his death and a commission was organized in 1919 under the direction of P. Lasareff. Between 1919 and 1926 about 20,000 stations were occupied. In an area of some 500 square kilometers not only were magnetic data collected, but also gravitational anomalies were surveyed by pendulum and torsion balance. In 1923 the first diamond-drill hole at Stschigry reached the ore body at 163 meters. Altogether thirteen holes were put down in this area by 1926, and further drilling revealed additional bodies in the Saltikowsky, Oribuiansky, and Tim districts.

According to a recent notice in the Soviet press, the iron ore reserves proved to date in the Kursk region amount to 290,000 million tons while the quantities of potential deposits are estimated at over 600,000 million tons.

The anomalies have been described by many authors, notably by Lasareff, from 1921 to 1926.[110] They are located east and southeast of Kursk in two parallel strips. One, through Stschigry, is almost 160 km long and 2 to 20 km wide. The other, near Bielgorod, is almost 50 km long and 40 km wide. The strike of the anomalies is NNW-SSE. In the zones mentioned, the vertical intensity anomalies are of the order of 0.5 gauss (that is, the same magnitude as the earth's field), and at some locations they reach 2 gauss. The horizontal intensity anomalies have extremes of $+0.8$ and -0.6 gauss; extremes in declination differ by $180°$. For the vicinity of Stschigry and Stary Oscoe, the magnetic, gravity, and torsion-balance anomalies have been described by Lasareff.[111] In Fig. 8–59, the torsion-balance and magnetic anomalies in the vicinity of Stschigry are reproduced, together with the geologic section as determined by drilling. The sediments in this section are Tertiary, Triassic, and Devonian. At a depth ranging from 152–186 m the basement rocks (gneiss, quartzite)

---

[109] C. R., **122**, 1478, (1896).

[110] For a list of Lasareff's publications see Ambronn, *op. cit.*, Bibl., p. 327, items 910–915.

[111] Gerl. Beitr., **15** (1/2), 71–89, 91–102 (1926).

$$\frac{\partial^2 U}{\partial x'^2}$$

$$\frac{\partial^2 U}{\partial x' \partial z'}$$

(a)

ΔZ

(b)
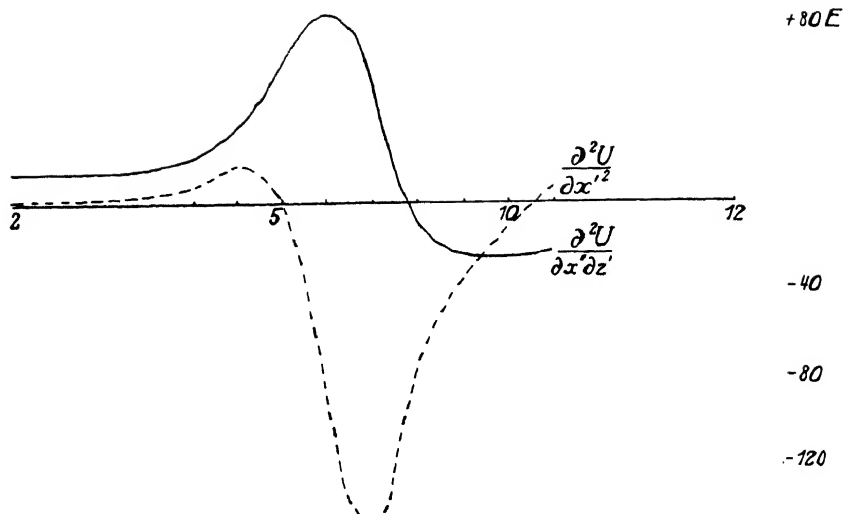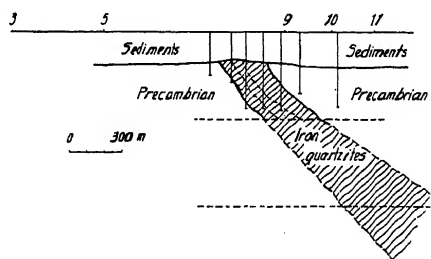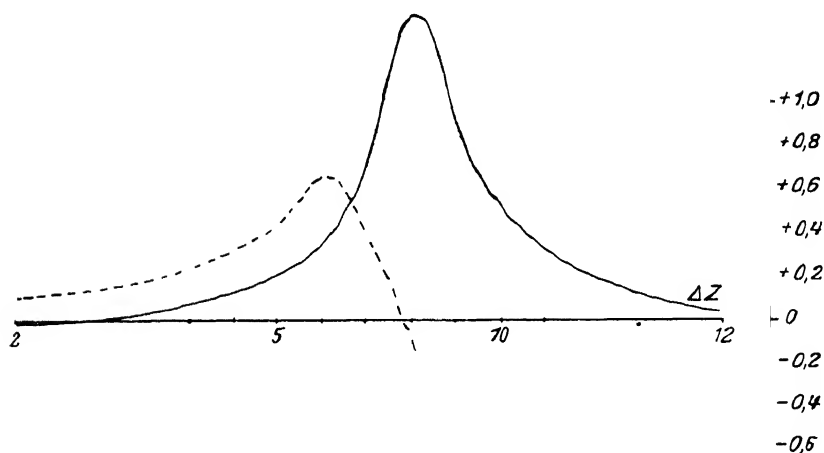
(c)

FIG. 8-59. Torsion-balance and magnetic anomalies in a traverse across the Kursk magnetite deposit, with geologic section (after Haalck): (a) torsion-balance anomalies, (b) magnetic anomalies, (c) geologic section.

were reached, with a bed of magnetite, dipping at an angle of about 60°
and having a thickness of some 220 m. The iron content varies from 26
per cent on the outside to 40 per cent on the inside of the bed. The dip
is likely to decrease and the thickness to increase below the depths reached
by the drill.

In the interpretation of the magnetic anomalies and in the comparison
of the gravitational and magnetic results,[112] difficulties were soon experi-
enced, since the magnitude of the anomaly could not be explained by the
material encountered by the drill. Tests of the quartzites brought to the
surface gave only 0.2 to 0.4 for the susceptibility.

Calculations of the magnetic anomalies by Gamburzeff[113] showed that an
agreement of theoretical and observed values could be obtained for a mag-
netization of 0.7 (which, with $H = 0.5$, corresponds to $\kappa = 1.4$). Haalck[114]
arrived at similar values from a comparison of torsion balance and mag-
netic effects, and Slichter[115] concluded that the susceptibility of the Kursk
ore would have to be of the order of 2.17 to explain the anomalies.[116]

This discrepancy between results of specimen tests and values obtained
from the anomalies leads Haalck to believe that the anomalies are not due
to induction in the earth's field and that their real cause is a mag-
netite deposit of high iron content below the quartzites reached by the
drill.

In another anomaly exceeding the earth's field, a better agreement was
observed between susceptibilities determined in the laboratory and those
obtained from the magnetic observations. Fig. 8-60 shows the magnetic
anomalies at Kiiruna in Sweden. The ore body is magnetite, about 85 m
thick, dips at 55° to the east, comes within 34 m of the surface, and is
known to a depth of about 200 m. The vertical intensity anomaly is
about 0.7 gauss; the horizontal anomaly −0.4 gauss. Carlheim-Gyl-
lensköld[117] determined in the laboratory an average of 0.8 for the sus-
ceptibility of the ore, and Haalck[118] concluded from calculations that induc-
tion in the normal earth's field can sufficiently explain the anomalies if
the susceptibility difference against the adjacent rocks is 0.5 to 0.6. Fig.
8-61 represents an underground survey made in the Kallmerberg district
in Sweden[119] and illustrates the relation between position of ore bodies and
horizontal anomalous vectors.

[112] See discussion on p. 401 in sec. E.
[113] *Op. cit.*, **19**(2/3), 210–230 (1928).
[114] Gerl. Beitr., **22**(3/4), 241–255, 385–399 (1929).
[115] *Op. cit.*, 251.
[116] See discussion on p. 401.
[117] Magnetic Survey of Kiirunavaara (Stockholm, 1910).
[118] Gerl. Beitr., **22**(3/4), 241–255 and 385–399 (1929).
[119] Lehrbuch prakt. Geol., I, 378–381 (1921).

Iron ores of contact-metamorphic origin sometimes show reverse polarization, indicating effects of thermal and mechanical processes. An instance of this sort was observed by the author and H. Seblatnigg on the magnetite deposit of Berggiesshuebel in Saxony.[120] Its western portion shows distinct negative anomalies (max. -1500γ) while the eastern part, offset by a
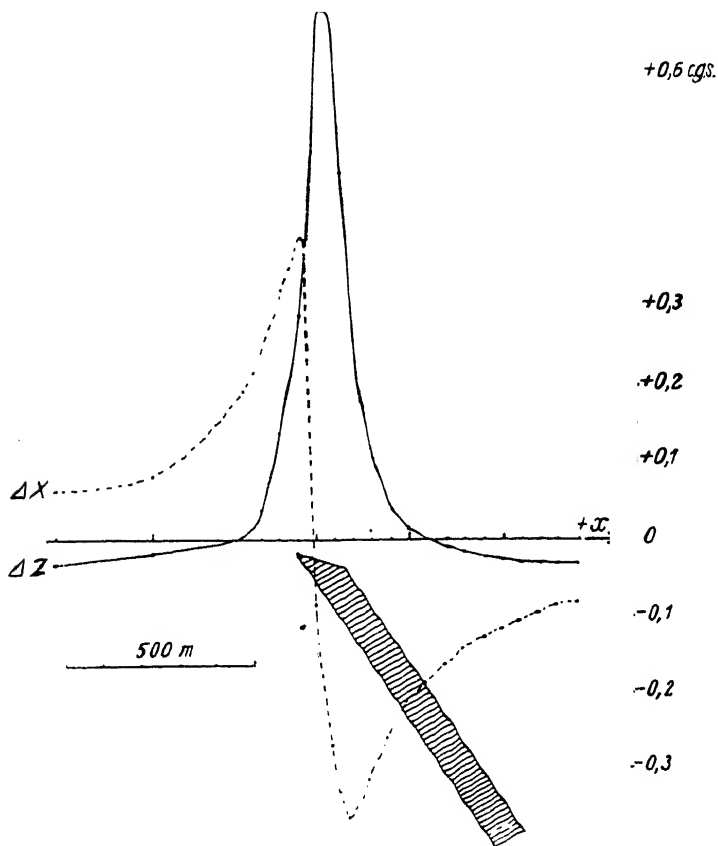
FIG. 8-60. Magnetite anomalies above Kiiruna iron ore body (after Carlheim-Gyllensköld).

fault, reveals positive anomalies of approximately the same magnitude. Another definite instance of reverse polarization was observed by Bahneman (see below) in South Africa. Rapid changes in amplitude, frequently leading to negative anomalies, are found near deposits formed by magmatic differentiation, indicating irregular concentration of magnetite in the process of plastic flow and magnetostriction in the process of cooling.

[120] Beitr. angew. Geophys., **1**(1) 110–116 (1930).

Magnetic anomalies on magnetite deposits formed by contact or dynamo-metamorphism are usually more regular in appearance than on deposits produced by magmatic differentiation.[121]

In this country the iron ore districts of the Lake Superior region were surveyed extensively at an early date.   Field and interpretative technique were described by Smyth[122] and Hotchkiss.[123]   In recent years dip needle surveys have been made in Wisconsin by Aldrich[124] and in Michigan by Stearn[125] and Swanson.[126]   Further studies of magnetic anomalies on iron ore deposits are described by Stratton and Joyce.[127]   Traverses across scattered magnetite veins near the Errington mine in Ontario are described

Ore   Country   Gangue   Magnetic
        Rock   Vector
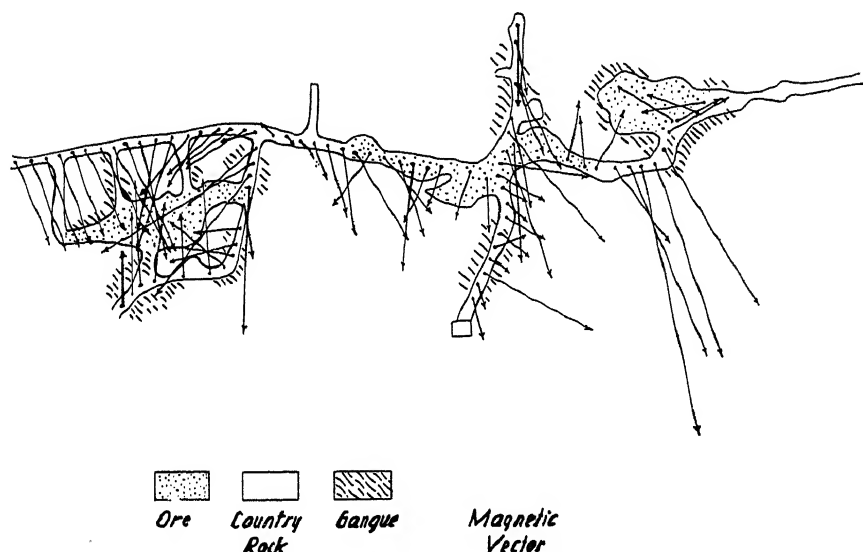
Fig. 8-61.   Underground magnetic vector survey in Kallmerberg mine, Sweden (after Keilhack).

by Eve and Keys[128] with the remark that the anomalies had no relation to the ore sought in this area.   A similar experience was recorded by Edge and Laby[129] who found, at Kadina, South Australia, an anomaly of about

[121] U. S. Bur. Mines Tech. Paper No. 439 (1929).
[122] U.S.G.S. Monograph No. 36, Part II, 336–373 (1899).
[123] Wis. Geol. and Nat. Hist. Survey Bull. No. 44 (1915).
[124] A.I.M.E. Geophysical Prospecting, 393 (1929).
[125] N. H. Stearn, A.I.M.E. Geophysical Prospecting, 361–362 (1929).
[126] A.I.M.E. Geophysical Prospecting, 290–312 (1934).
[127] U. S. Bur. Mines Tech. Paper No. 528 (1932).
[128] Canad. Geol. Survey Mem. 165, 143 (1931).
[129] Edge and Laby, The Principles and Practice of Geophysical Prospecting, p. 192 (1931).

$5500\,\gamma$, several hundred feet long. A shaft sunk at the point of maximum anomaly to a depth of 60 feet encountered much magnetite in the schist country rock but no commercial ore.[130] These are examples of "stray" anomalies produced by magnetite stringers and magnetite slate in areas of contact and dynamo-metamorphism. They often interfere with the effects of commercial ore bodies but may be useful in tracing nonmagnetic ores.

Magnetic anomalies of fairly regular type were observed on hematite and magnetite deposits of the Lahn-Dill district in Germany by Kegel.[131] Rössiger and Puzicha[132] examined the magnetite deposit of the Spitzenberg in the Harz mountains. Correlations of anomalies with susceptibility measurements in the laboratory indicated that the deposit was more
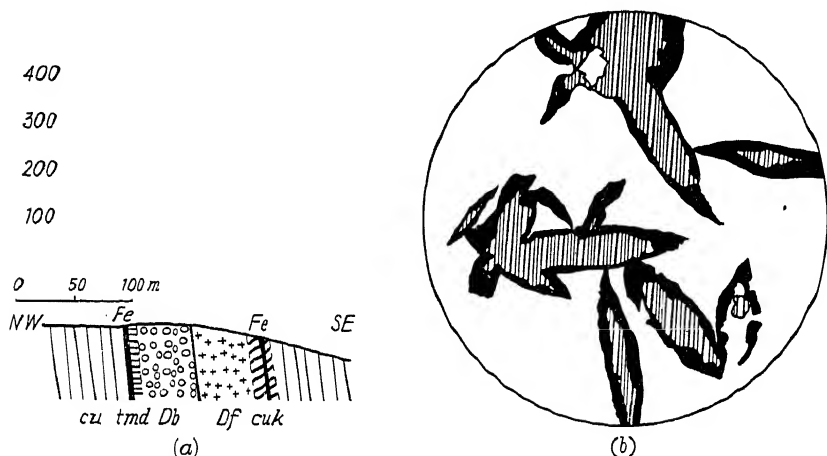
FIG. 8-62. (a) Difference in anomalies on two iron deposits in same section (after Rössiger). (b) Magnetite (black) pseudomorphism after hematite (hatched). (cu, Lower Carboniferous; tmd, Middle Devonian, Stringocephalus beds with hematite; Db and Df, diabase; cuk, lower Carboniferous siliceous slates with hematite.)

strongly magnetized than corresponded to induction in the earth field. The deposits of the Harz mountains originated from contact-metamorphic alteration of hematite and specular hematite to magnetite (see Fig. 8–62b).

Sedimentary iron ores containing hematite and brown iron produce small magnetic anomalies (unless later subjected to contact- or dynamo-metamorphism). Pockets of brown iron ore in basalt, formed by decomposition of basalt, could be located by Meyer[133] (see Fig. 8-63). In Missouri small

[130] The curves indicate a depth of about 80 feet.

[131] Geol. Landesanst. Berlin Sitzungsberichte, 4, 60 (1929).

[132] Beitr. angew. Geophys., 3(1), 45–108. See also G. Beyer, Beitr. angew. Geophys., 3(3), 337–363 (1933).

[133] Beitr. angew. Geophys., 1(4), 420–431 (1937).

and somewhat irregular anomalies were observed by Grohskopf[134] on iron ores in sink holes in sandstone and dolomite. The soft red hematite ore was found to be nonmagnetic, the irregular anomalies being due to blue specular hematite. In Wisconsin Stearn[135] could trace oxidized iron ore by the maximum found on the hanging and foot wall over unoxidized portions of the Cuyuna iron formation. Likewise, Rössiger and Puzicha[136] found that hematite (red iron ore) was virtually nonmagnetic, but that its action changed completely when altered to magnetite. Fig. 8–62a shows a typical example. The iron ore in the N-W of the profile produces little or no effect, whereas the "cuk" formation (a Devonian siliceous slate with
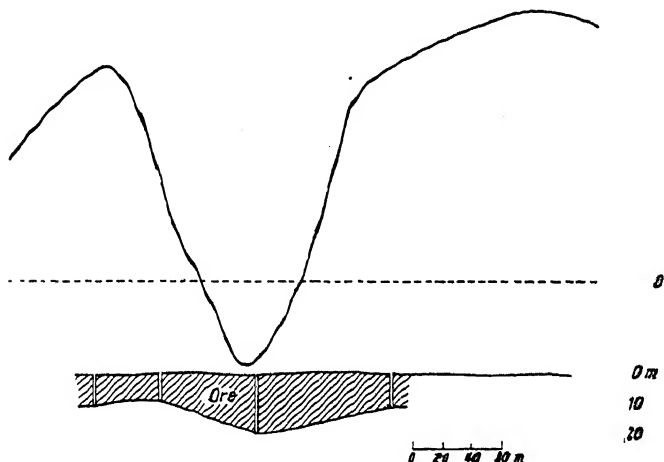
FIG. 8-63. Magnetic anomalies on brown iron ore pockets in basalt (after Meyer).

red iron ore, partially reduced to magnetite [see microphotograph]) is accompanied by a pronounced anomaly.

2. *Surveys of pyrrhotite deposits and of nonmagnetic ores associated with magnetite or pyrrhotite.* The pyrrhotite deposit of Falconbridge (Sudbury, Ontario) has been the subject of intense study with virtually all major geophysical methods—gravitational, electric, magnetic. Various traverses made across the ore body with a dip needle have been published by Slichter[137] and clearly reveal the effect of variations in the thickness of glacial drift.

[134] J. G. Grohskopf and C. O. Reinoehl, Mo. State Geol. Rep., App. III, 146-157 (1931); App. IV, 5-20 (1933).
[135] *Op. cit.*, 188 (1932).
[136] *Loc. cit.*
[137] *Op. cit.*, 254.

In the Zeehan field in Tasmania, Edge and Laby[138] investigated copper-nickel deposits, accompanied by basic dikes. The anomalies were rather indefinite.[139] In the Renison-Bell tin field, flat-lying pyrrhotite bodies containing cassiterite, near the surface and outcropping, were surveyed with the vertical magnetometer, and anomalies as high as $\pm 4000\ \gamma$ were observed. A core hole brought down at the point of greatest magnetic anomaly encountered massive pyrrhotite at a depth of from 8 to 25 feet. Other magnetic indications were confirmed in a similar manner.

In the Lake Superior copper country, magnetic measurements have been used extensively because of the association of magnetite with the copper-bearing lava flows. The copper is found in the brecciated tops of certain of the flows, and the traceability of individual flows within the sequence is due to variations in their magnetite content.[140] In igneous basic rocks an association of magnetite concentration with gold values sometimes is encountered. Where this relation is consistent, magnetic measurements can be useful.[141] Other applications of magnetic measurements to the location of nonmagnetic ores will be discussed under the heading of structural or stratigraphic associations.

3. *Surveys of placer deposits (noble minerals associated with magnetite by mechanical concentration)* have been conducted in California, Colorado, British Columbia, Alaska, and elsewhere. The surveys in British Columbia were described by Laylander,[142] those in Colorado by Heiland and Courtier[143] and by Wantland.[144] On shallow placers, anomalies may be quite large (up to 300 γ) (see Fig. 8-64) which explains why these effects were originally discovered with less sensitive instruments. Recent placer investigations in California and Nevada are described by Jakosky.[145] Magnetic measurements are said to have been applied in platinum placer prospecting in Russia but details are not available. Where placer channels are filled with flows of igneous material they may be located without difficulty, but then the relation between magnetite and gold concentrates is masked and the effect is one of a stratigraphic or structural association.

4. *Surveys of mineral deposits associated structurally or stratigraphically*

---

[138] *Op. cit.*, p. 84.

[139] Authors do not state whether the anomalies are negative or positive. In the southern hemisphere, vertical intensity anomalies are negative when ore bodies are normally magnetized. When plotting anomalies in the same way as in the northern hemisphere, a maximum would indicate abnormal polarization. To avoid confusion, negative anomalies should be plotted upward.

[40] Stearn, *op. cit.*, 187 (1932).

[41] Heiland, Terr. Mag., **37**(3), 343 (Sept., 1932).

[42] Eng. and Min. J., **121**, 325 (1936).

[43] A.I.M.E. Geophysical Prospecting, 369–370 (1929).

[144] Colo. Sch. Mines Quart., **32**(1), 87–115 (1937).

[145] A.I.M.E. Tech. Publ. No. 515, Dec., 1933.

with magnetic formations involve the mapping of intrusions, dikes, magnetic slates, and similar formations.   An example of the first application is the work done on the bauxite deposits in central Arkansas, believed to have been formed by weathering of syenite plugs.   In the Tri-State district[146] lead zinc ores were found to follow the magnetic lows and the flanks of magnetic highs, which in turn reflect topographic highs of the pre-Cambrian porphyry surface.   Apparently the circulation of mineralized solutions was controlled by structure of and faults in the flanks of the buried uplifts. Contact zones with associated ore bodies may be traced by magnetic measurements of igneous intrusions where limonite and hematite com-
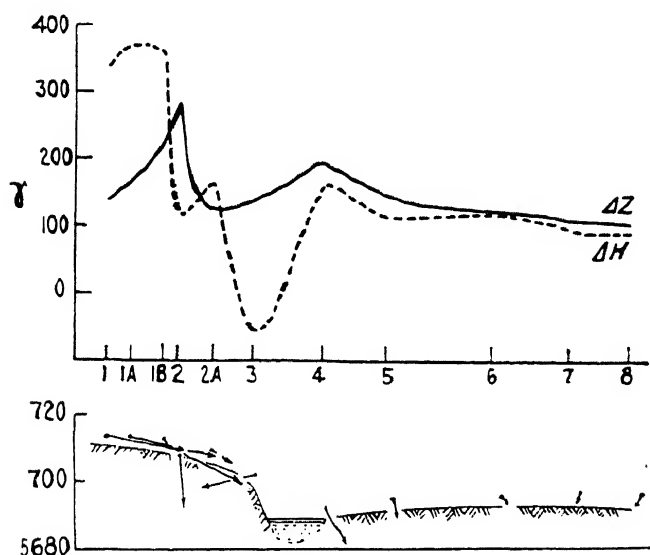
FIG. 8-64. Horizontal and vertical intensity anomalies and anomalous vectors on gold placer near Golden, Colorado.

pounds in adjacent formations have been changed by reduction into mag-netite.   Examples were discussed before.

Frequently the intrusive bodies are magnetic themselves, and ores asso-ciated with intrusives may thus be indirectly located.   Examples are the surveys near the Abana mine, where a quartz diabase dike in the vicinity of sulfide (replacement) deposits was subjected to intensive study with various geophysical methods,[147] and a survey published by Stearn[148] showing the effect of a monzonite dike associated with seams of galena.

[146] Grohskopf and Reinoehl, *loc. cit.*
[147] Canad. Geol. Survey Mem. **170**, 52–73.
[148] *Op. cit.*, 193 (1932).

Surveys of intrusive bodies have been helpful in connection with prospecting for chromite. From the published data it appears that some occurrences of chromite are magnetic and others are not. Deposits in Russia on which magnetic tests were made were definitely magnetic and also showed usable anomalies. Where the chromite is nonmagnetic, a survey of the associated intrusions may, nevertheless, yield useful results.

Intrusive dikes associated with gold values may often be traced by a magnetometer through the use of positive and negative anomalies. Mal-

Fig. 8-65. Section across peridotite plug in Arkansas, showing depth finding by anomalous vectors (after Stearn).

amphy[149] traced gold-bearing pegmatite dikes by their increased magnetization (negative anomalies, Southern Hemisphere), while Stearn[150] surveyed gold-bearing rhyolite dikes that were intruded into monzonite and caused negative anomalies.

In diamond-mine exploration, the magnetometer can be helpful in tracing the igneous plugs or pipes in which the diamonds occur. Stearn[151] applied the magnetic method to the location of peridotite plugs in Arkansas

---

[149] A.I.M.E. Geophysical Prospecting, 325 (1934).

[150] Loc. cit.

[151] Ibid., 197.

(see Fig. 8–65), Krahmann[152] on a Kimberlite pipe in southwestern Transvaal. In this survey the − 1200 gamma (Southern Hemisphere) anomaly followed very closely the outline of the pipe. Strong magnetic anomalies in the contact zone due to magnetized shales were also recorded.

The stratigraphic association of sedimentary nonmagnetic beds of commercial value with magnetic members in the geologic section has been utilized to advantage in the Lake Superior region where strike, dip, and faults of the copper-bearing lava flows have been mapped by tracing magnetic members in the series,[153] and in South Africa in connection with exploration for the gold conglomerates of the Witwatersrand system[154] (see Fig. 8–66). These strata show evidence of considerable metamorphism and consist of quartzites, slates and shales, the gold-bearing conglomerates, and volcanic beds. Several dikes and faults cut through the area. In the west Witwatersrand the accurate stratigraphic relation of the magnetic beds (magnetic slates) to the main reef could be well established. During the experimental period a number of magnetic profiles were run on outcropping sections. Fig. 8–66 shows vertical intensity anomalies for the section near the main reef. The curves are quite irregular because of changes in magnetite content. In the upper profile, at the point of greatest irregularity, magnetic material (extracted by electromagnets) varied from 0 to 80 per cent, and susceptibilities from 0 to $10,000 \cdot 10^{-6}$. When the overburden becomes comparable with the distance of the magnetic shale members, their effects overlap, resulting in one major negative (Southern Hemisphere) anomaly (see Fig. 8–67). While in this particular area the magnetite shales were normally magnetized, syenite, dolerite, and granophyre dikes cutting through the area were abnormally magnetized. In another area[155] abnormal polarization was found on the magnetite shales (anomalies of 20,000 γ for a depth of 477 feet). The susceptibilities determined in the laboratory were not sufficient to explain the magnitude of the anomalies.[156] It has been estimated that as a consequence of the magnetic surveys the potential gold production has been increased by at least one-eighth of its present amount.

In the location of gold placer deposits, the stratigraphic association of placer channels with magnetic formations other than the concentrates can be helpful in locating the channel itself. Edge and Laby[157] have demonstrated this at Gulgong, New South Wales, where the channels are filled with basalt flows, producing positive (Edge-Laby definition) anomalies

[152] Min. and Met., 16, 342 (June, 1935).
[153] Stearn, op. cit., 187.
[154] Krahmann, Geol. Soc. S. Afr. Trans., 39 (1936).
[155] See F. Bahnemann, A.I.M.E. Contrib. No. 79, 1935.
[156] See discussion on p. 401.
[157] Op. cit., 189.
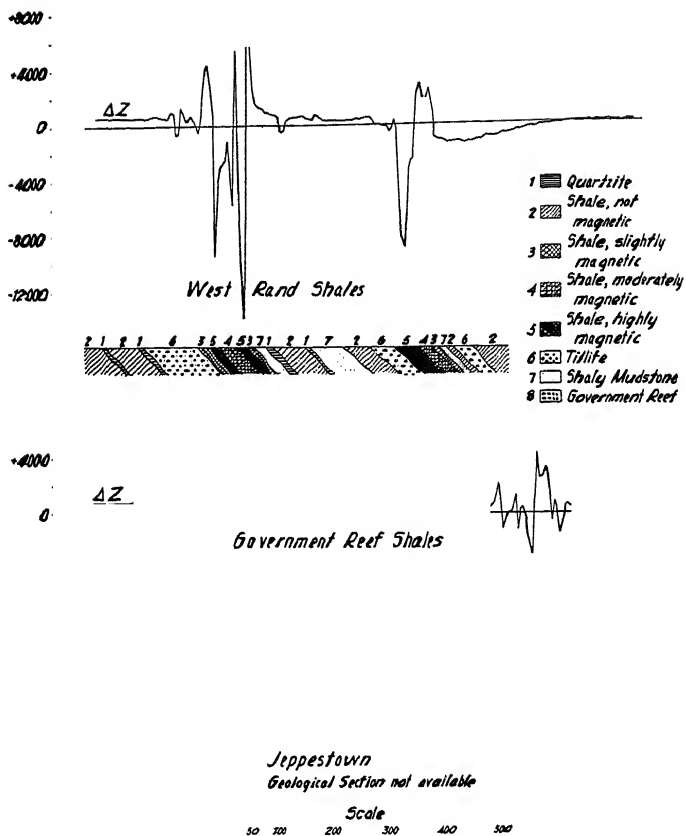
FIG. 8-66. Vertical intensity anomalies on outcrops of sections of lower Witwatersrand system in West Wits area.   The middle profile is 12 miles southwest of Krugersdorp.   (After Krahmann.)
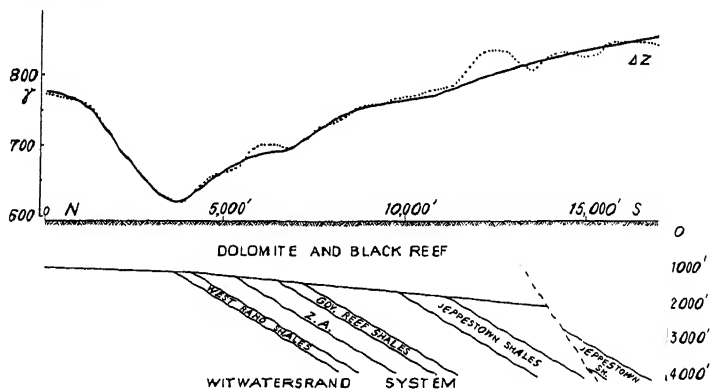
FIG. 8-67. Interpretation of vertical intensity anomalies, western section, West Wits area, 33 miles southwest of Krugersdorp (after Krahmann).

of about 500 γ. Placer channels may also be located structurally if the bedrock is magnetic. Fig. 8–68 shows a negative magnetic anomaly above a bedrock depression corresponding to an auriferous gravel channel in California.

Structural magnetic prospecting has been applied in various countries in coal exploration. Edge and Laby[158] surveyed the brown coal field at Gelliondale, Victoria, with torsion balance and magnetometer. The brown coal is about 400 feet thick and occurs 50 to 100 feet from the
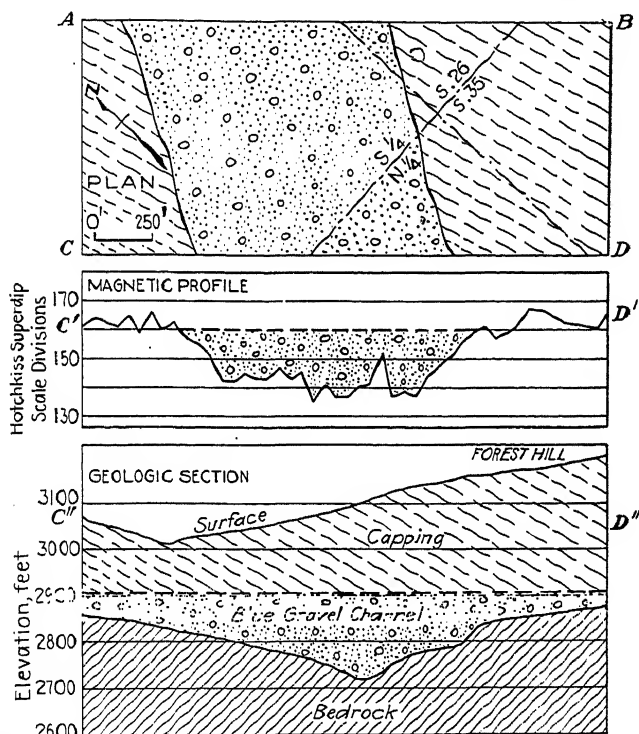
FIG. 8-68. Magnetic lows over placer channels in California (after E. W. Ellsworth).

surface, in troughs of Jurassic sandstone. Magnetic anomalies were caused by this sandstone and basaltic intrusions. Since Carboniferous deposits were formed in geosynclines, the regional depressions of the crystalline basement and therefore negative magnetic anomalies have been found to be characteristic of productive Carboniferous in many areas in Europe (productive belt through Mons, Namur, and Luettich;[159] Ruhr Basin between Muenster, Duesseldorf, Elberfeld, and Soest;[160] Carboniferous areas

[158] *Ibid.*, 158.
[159] Reich, *op. cit.*, I, 20.
[160] *Ibid.*, I, 31.

in northern France, near Aachen, in Hessen, Saxony, and Upper Silesia[161] in Germany).

5. *Surveys for miscellaneous ores* (chromite, manganese, and the like). As stated previously, direct magnetic prospecting for chromite may be successful if the ores are more magnetic than the basic igneous rocks in which they occur. Reference to magnetic work on chromite is made by Krasulin[162] in the Urals, by Bagratuni[163] at Geidara (Kurdistan), and by Snelgrove[164] in Newfoundland. A reference to Lundberg's[165] work mentions magnetic effects of chromite ore in Newfoundland and surveys of chromite-bearing serpentines in Canada. Under favorable conditions, sedimentary manganese ores may be located directly at shallow depth. As shown by a survey made at Nickopol,[166] Russia, the ore, consisting of pyrolusite, psilomelane, polyanite, and wad, occurs at depths of from 20 to 40 meters in clay on granite. Magnetic anomalies were small (of the order of $100\,\gamma$ in Z) and very irregular, corresponding to varying composition of the ore and changes in the granitic bedrock surface.

6. For the *location of meteors*, the use of the magnetometer is, in most cases, uneconomical. An average iron meteorite, buried several feet deep, is not effective beyond a radius of 5 or 10 feet. Unless its location is known within very close limits, magnetic prospecting, even with a dip needle or cardan magnetometer, would require too many stations. When there is an accumulation of a large amount of meteoric material, the magnetic method may be used to locate areas of greatest concentration. For Meteor Crater, Arizona, Jakosky[167] reports anomalies of surprisingly small magnitude (65γ) at the SW portion of the crater and assumes that the magnetic material begins at 200 feet and concentrates with depth.

B. Magnetic Surveys in Oil Exploration

Oil-bearing formations are rarely magnetic, and some other formation of a known structural or stratigraphic relation is mapped. Such associated formations are (1) salt domes, (2) magnetic beds in the sedimentary section, and (3) basement rocks and igneous intrusions. The exceptions where the *oil-bearing formations* themselves *produce magnetic effects* are (*a*) granite wash on the flanks of ridges, (*b*) serpentine plugs and laccoliths, and (*c*) shoe string sands.

[161] Reich, Zeit. Geophys., **2**(7), 273–278 (1927).
[162] Razvedka Nedr., **5/6**, 18–21 (1933).
[163] *Ibid.*, **19**, 19–21 (Dec., 1933).
[164] *Chromite Deposits of Newfoundland*, Dept. of Nat. Res., St. Johns, Nf.
[165] Min. and Met., **16**, 337 (Jan., 1935).
[166] N. Trubiatchinski, Geol. and Prosp. Service, U.S.S.R. Fasc. 166, (1932).
[167] A.I.M.E. Geophysical Prospecting, 69 (1932).

1. The *magnetic location of salt domes* was attempted shortly after the introduction of the Schmidt magnetometer. In northern Germany, salt domes produce negative anomalies by a combination of the following effects: (a) diamagnetism of the salt, (b) diamagnetism of gypsum and anhydrite in the cap rock where present, (c) paramagnetism of glacial strata if salt dome is near surface, and possibly (d) slight paramagnetism of Tertiary and Cretaceous sediments. Magnetic surveys on salt domes
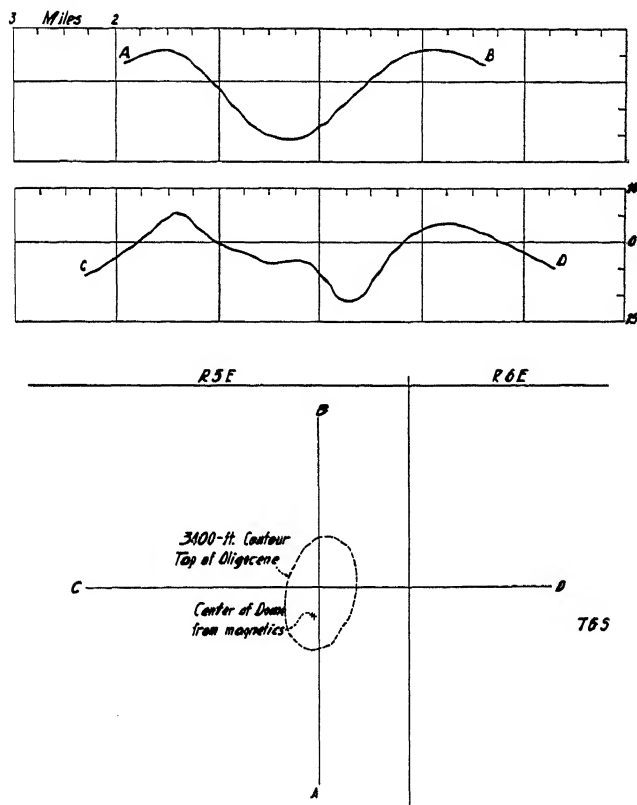
FIG. 8-69. Magnetic anomalies on Port Barre salt dome (after Barret).

were made by Schuh[168] and Moll[169] in Mecklenburg; by the author on the salt domes of Segeberg and Lueneburg; by Haalck and Brinkmeier[170] on the salt dome of Wefensleben; by Kohl and Krahmann[171] on the salt anticlines of Salzgitter and Benthen. Except on outcropping cap rocks,

[168] Mecklenb. Geol. Survey, 32 (1920).
[169] Mecklenb. Geol. Survey, 33 (1922).
[170] Haalck, *Die magnetischen Verfahren*, p. 132.
[171] *Metall und Erz.*, **23**, 583–586 (1926); **25**, 571–582 (1928).

salt dome anomalies seldom exceeded 20 or 30γ in any of the above surveys. On the salt dome of Hettenschlag, in Alsace,[172] the negative anomalies were of the same order. When magnetometers were first introduced on the Gulf coast, experimental surveys were made on a number of known domes. The author ran a number of traverses on the Barbers Hill and Esperson domes in 1925. In the following years the magnetometer found more application for the mapping of basement topography, and it was not until its accuracy was increased that it was used again in salt dome work on the Gulf coast. Surveys have been published by Barret[173] for the Simmsboro area and for the Anse La Butte and Port Barre domes,[174] and by Jenny[175] and Clark and Eby[176] for the Fannet dome. The latter, comparatively near the surface, produces an anomaly of -25γ. The Port Barre dome, at much greater depth, has an anomaly of only -15γ (see Fig. 8–69).

2. *Determination of structure by the mapping of magnetic sedimentary formations.* While most magnetic anomalies in producing or prospective oil territory are due to changes in topography or composition of the basement rocks or to intrusions of igneous rocks, there are certain areas, particularly those distinguished by great thicknesses of sedimentary formations, where the effect of sedimentary beds predominates. The effective magnetic members may be ferruginous shales, sandstones, volcanic tuffs, iron conglomerates, and the like. Uplifts of such formations are characterized by *positive* anomalies except where magnetic members thin out over the crest or have been eroded away. Such conditions occur in California[177] where there is a marked variation in susceptibilities of sedimentary rocks. In the Tertiary formation, susceptibilities vary from $14 \cdot 10^{-6}$ in the Saugus of the Upper Pliocene to $4000 \cdot 10^{-6}$ in the vivianitic sandstone of the McKittrick group in the Pliocene.

The Cretaceous is, on an average, more magnetic than the Tertiary, and the Jurassic (Franciscan) is more magnetic than either Tertiary or Cretaceous. The picture is further complicated by interbedded volcanics, and metamorphic and intrusive rocks. At the Raven Pass anticline with flank dips of $40°$ to $50°$, Cretaceous beds in the center are more magnetic than the Miocene on the flanks, giving rise to positive anomalies of 110γ on the crest. On the other hand, on the White Creek syncline 20 miles northwest of Coalinga with strongly magnetic cretaceous beds on the

[172] P. Geoffroy, Ann. Off. Comb. Liqu., **6**, 1015–1021 (1929).
[173] Barret, Mapping Geologic Structure with the Magnetometric Methods (Shreveport, Feb., 1937).
[174] A.A.P.G. Bull., **19**(7), 1070-1071 (July, 1935).
[175] Oil Weekly, April 27, 1936.
[176] A.A.P.G. Bull., **19**(3), 363 (Mar., 1935).
[177] E. D. Lynton, A.A.P.G. Bull., **15**(11), 1351-1370 (Nov., 1931).

flanks and moderately magnetic Etchegoin beds in the core, a drop in vertical intensity was observed. The Kettleman Hills structure shows a series of highs on the upturned edges of the fold, magnetic lows along the axis of the north dome, and a series of highs on the axis of the middle dome, indicating that the magnetic beds were eroded from the north dome but are continuous across the middle dome. Similar conditions appear to exist on the Dominguez dome.[178]

Erosion of magnetic formations from the crest of anticlines may also be responsible for magnetic lows found above uplifts in other states. The problem of their origin has not been settled and the following explanations have been advanced: (a) effects of well casing and derricks, (b) abnormal polarization, (c) erosion of magnetic formations from crests, and (d) irregular basement magnetization. Negative anomalies have been found in the Healdton, Oklahoma City, and Garber fields.[179] Conversely, Somers[180] believes that positive anomalies may be encountered on anticlines because of uplifts of magnetic sedimentaries as well as on synclines because of an increase in thickness of magnetic sediments.

According to Jenny[181] both effects are in evidence on the Gulf coast. In the northern part of that area magnetic anomalies are presumably caused by structural uplifts, while along the coastal portion they are assumed to be due to changes in thickness of the magnetic strata. The magnetically active beds are assumed to be of Eocene age in the north and of lower Miocene age in the southern portion. In the former, the Conroe field produces a distinct positive anomaly[182] (15 to 20γ) (see Fig. 8-70). When magnetic formations are uplifted by a salt dome, the negative salt effect may be obliterated and replaced by a positive anomaly above the dome (Jenny[183]).

The presence of magnetic members in a sedimentary column gives an opportunity for the location of faults. They may reveal themselves by a transition of higher to lower magnetic values or by abrupt depressions in the curve, all depending on thickness, depth and dip of the magnetic beds, and hade and throw of the fault. Fig. 8-71 (from Lynton[184]) shows a magnetic survey on the San Andreas fault and Fig. 8-72 on the Walnut Creek fault. The trace of the latter is indicated by a sharp drop in the profile curves, high values to the northeast corresponding to the more

[178] California Oil World, April 30, 1931.
[179] Oil and Gas J., Nov. 15, 1928.
    "Anomalies of Vertical Intensity," Colo. Sch. Mines Mag., Aug.-Dec., 1930, Jan.-Feb., 1931.
[181] Oil Weekly, July 16 and 23, 1934.
[182] L. H. Williams, Oil Weekly, Aug. 21, 1934
[183] Oil Weekly, April 27, 1936.
[184] *Loc. cit.*

magnetic Cretaceous sediments and low values to the southwest corresponding to less magnetic Eocene strata. In the Pettus area (Bee

-4990 Contour, top of the Conroe Sand
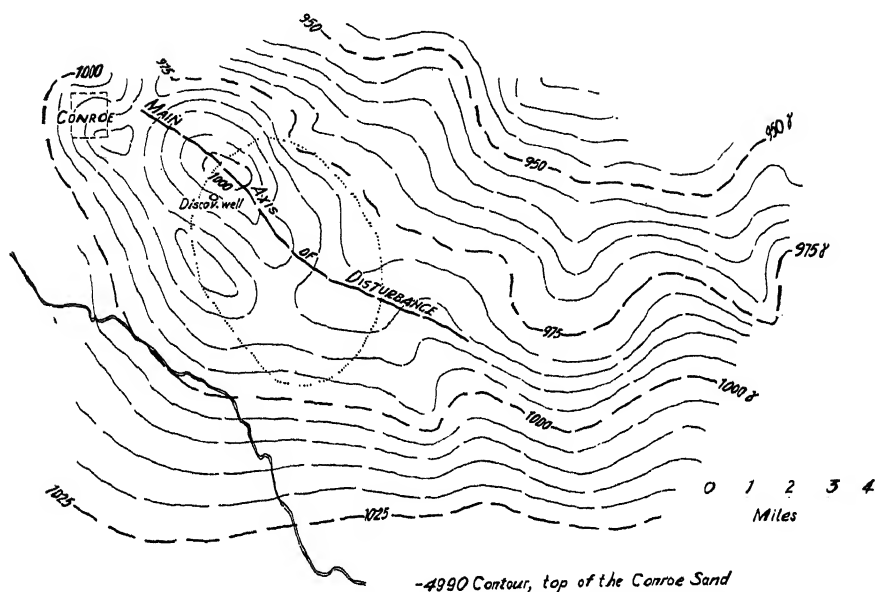
FIG. 8-70. Magnetic survey of Conroe area (after Williams).
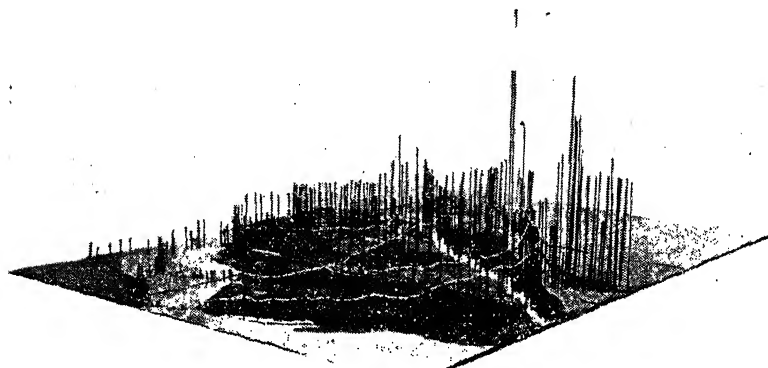
FIG. 8-71. Magnetic survey of San Andreas fault, California (peg model) (after Lynton).

County, Texas) Barret[185] observed a definite minimum on the principal fault whose throw is some 500 feet in the Pettus sand (Eocene, about 4000 feet deep). Magnetic anomalies of faults are often greater than

[185] *Loc. cit.*

anticipated if basement rocks have been affected, if igneous sheets have been intruded into the fault fissure, or if the fault plane has acquired concentrations of magnetic material or has been magnetized by other causes. J. Jung and C. Alexanian[186] made surveys on faults at Allschwill (Meletta against Cyrene marls), at Niederhaslach (Triassic lime against sandstone), at Aubure (granite against sandstone) and at Guewenheim (Meletta marls against shales, and the like), and observed the typical *depression* in the vertical intensity curve also noticed elsewhere. They came to the conclusion that this effect cannot be explained by the susceptibilities and
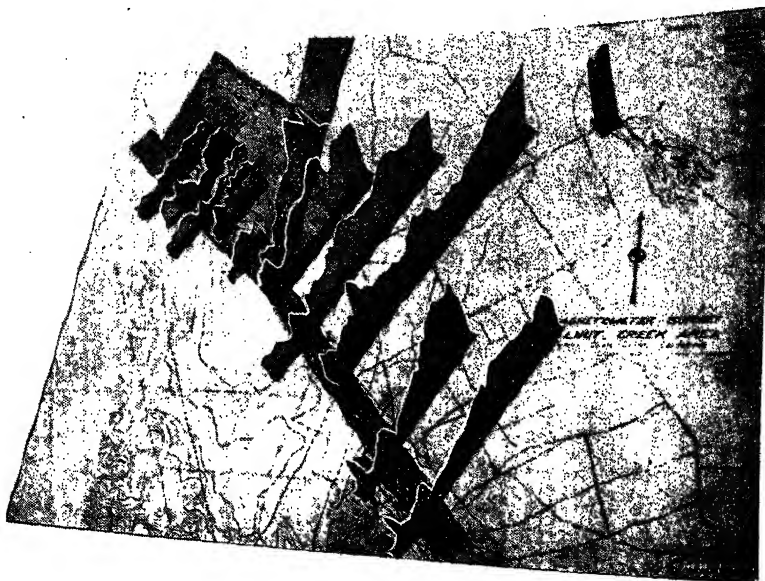
Fig. 8-72. Magnetic survey of Walnut Creek fault, California (celluloid profiles on map) (after Lynton).

disposition of the adjacent formations but must be an effect of the fault plane *itself*. Similar depressions in magnetic curves corresponding to the Leopoldsdorf and Sollenau faults in the Vienna basin were observed by Forberger, John, and Petrascheck.[187]

3. *Mapping of basement topography and of igneous intrusions.* In many oil-producing areas or prospective oil territories, structure in the sedimentaries is controlled by the topography of basement rocks due to deep seated folding or faulting, or by differential settling about pre-existing basement highs. Intrusions of igneous rocks, such as plugs and batholiths,

[186] Ann. Off. Comb. Liqu., 4, 711–720 (1931).
[187] Akad. Wiss. Wien, Sitz. Ber., **143**(**1**), (5–7), 137–145 (1934).

and lateral injections into sediments in the form of laccoliths may produce doming of strata, and their magnetic anomalies will give an indirect indication of structure in the oil-producing section.. Where basement rocks are uniformly magnetized, mapping of topography has resulted in the location of new oil fields and the extension of known ones.

One of the best-known examples is the Hobbs field[188] (Lea County, New Mexico, see Fig. 8-73). It was located in 1926 by a midwest magnetometer party, surveyed by torsion balance, and drilled in 1927. Con-
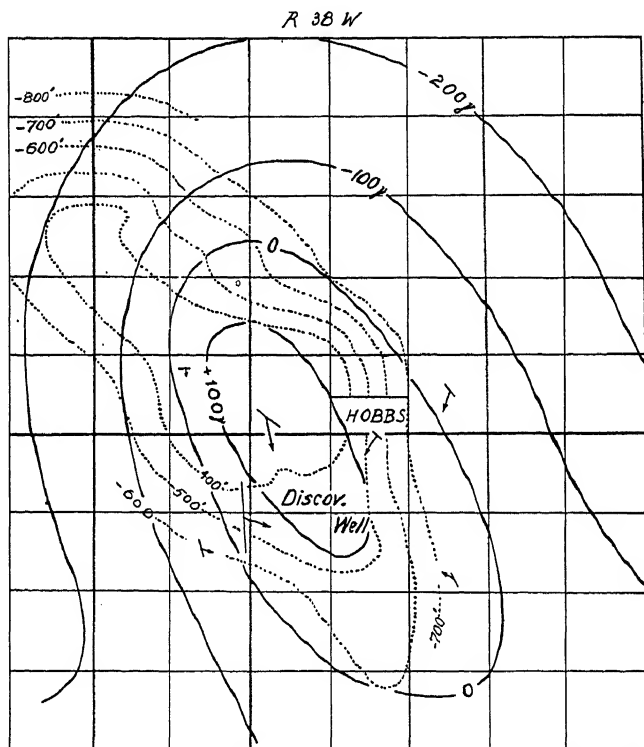
FIG. 8-73. Magnetic contours (after Lahee), structural contours (after DeFord), and torsion-balance data (after Coffin) for Hobbs field, discovered by a magnetic survey.

siderable development followed in 1929. The magnetic contours are shifted in comparison with the structural contours at 4000 feet. According to Barret's interpretation, this is due to the normal induction in the earth's magnetic field which places the maximum in Z south of the highest point of the subsurface feature. On other structures such displacements

of magnetic and structural contours have been found to occur (a) when there is a shift of the structural axis; (b) when an igneous core acts as a buttress against lateral forces which pushed the sedimentaries over the igneous core; and (c) when the basement is not uniformly magnetized, for instance, when a buried hill consists of both sedimentaries and intrusives.

Another instructive example of the successful application of the magnetometer in locating oil structure by mapping basement topography is the survey of the Nocona field (Fig. 8-74).[189]   The magnetometer closure
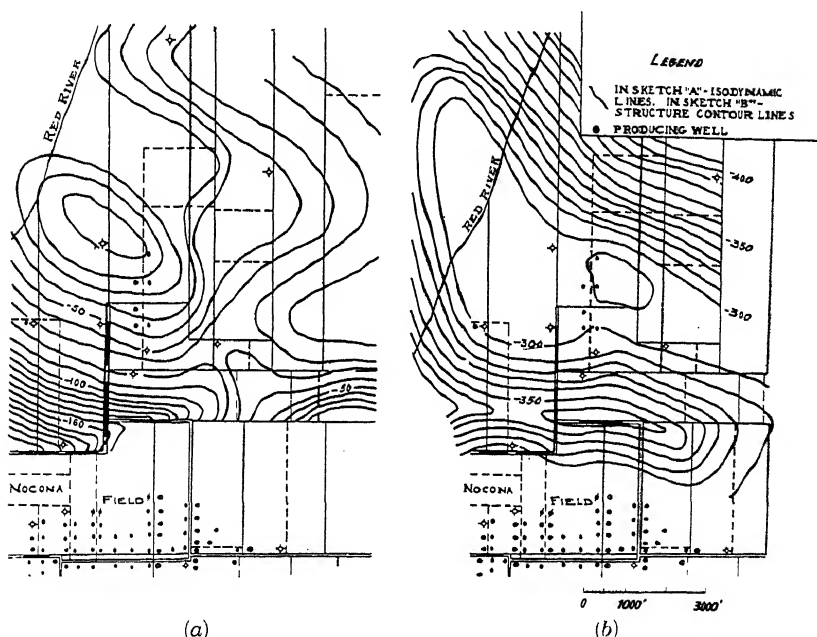
FIG. 8-74. Magnetic and structural contours of Nocona field, Oklahoma. The northern extension of the field was developed as the result of the magnetometer survey. (a) Magnetic contours, (b) structural contours.

is small and the magnetic high is shifted with respect to the structural high.   In the Lucien field a small magnetic anomaly is caused by the granite core of the Ordovician fold.[190]   The buried Amarillo granite ridge has been the object of considerable magnetic study.   Profiles over the ridge were made as early as 1925, and the results were published by Adams[191] and the author.[192]   The granite is about 3000 feet deep at the

[189] Heiland, Terr. Mag., **37**(3), 343-348 (Sept., 1932).

[190] Jenny, Oil Weekly, **72**(13), 16-18 (Mar. 12, 1934).

[191] Oil and Gas J., Feb. 16, 1928.

[192] Colo. Sch. Mines Quart., **24**(1), 64 (Mar., 1929).

highest point, where the magnetic anomaly is some 300γ. In the eastward extension of the Amarillo Ridge, the Wichita and Arbuckle Mountains and their buried forelands have been surveyed in detail by the Shell Oil Co. A portion of their magnetic map is reproduced in Fig. 8-75. The geophysical surveys and subsequent drilling brought out the fact that the Arbuckles form a separate folding system, are not connected with the Wichita Mountains, and are separated from them by the Ardmore basin.[193] The Wichita Mountains continue uninterruptedly as the Walters Arch into the Muenster Arch. The interval of the magnetic isanomalics (obtained with magnetometers) is 100γ. The Arbuckle, Criner, Walters, and Muenster Arches are indicated by magnetic highs approximately corresponding to gravity highs, while the intervening Ardmore and Marietta synclines are magnetic lows. While the magnetic anomalies are, in the main, caused by the contact of the sediments with the pre-Cambrian gneisses, granites, granite porphyries, and the like, changes in the composition of the basement rocks also affect the picture. Sediments appear to have little or no effect on anomalies in this area.

For Alabama, similar regional surveys and interpretations are discussed by Eby and Nicar,[194] and for the coastal plains of North and South Carolina, by McCarthy.[195] Regular trends of highs and lows of considerable amplitude (up to 1200γ) were observed. The actual number of detailed magnetometer surveys made for oil exploration in Texas, Louisiana, Mississippi, Alabama, Oklahoma, Kansas, Colorado, New Mexico, California, Wyoming, and the Dakotas is much greater than these few examples would indicate. The general conclusion to be derived from this work is that the magnetic method can be exceedingly useful in structural oil prospecting of such areas where the basement rocks are of uniform composition and uniformly magnetized and where magnetic sediments, if present, are continuous and conformable to basement topography. Where there are rapid changes of igneous rocks in the basement, intrusions of irregular character, erosion of magnetic sediments, or irregular distributions of magnetic materials within them, magnetic exploration should be replaced by a different geophysical method.

As previously mentioned, faults may be located magnetically where they have affected the basement rocks. In the Amarillo field (N. H. Stearn[196]) the Potter County fault of 1200–1500 foot throw showed by an abrupt drop in Hotchkiss superdip readings. Over the Beckham County fault with a throw of 300–500 feet the intensity dropped about 400γ. The

[193] World Petrol. Congr. Proc., **B(I)**, 174 (1933). See also Fig. 7-51b.
[194] Geol. Survey Ala. Bull., **43** (June, 1936).
[195] Jour. Geol., **44**(3), 396-406 (April-May 1936).
[196] A.I.M.E. Geophysical Prospecting, 189-191 (1932).
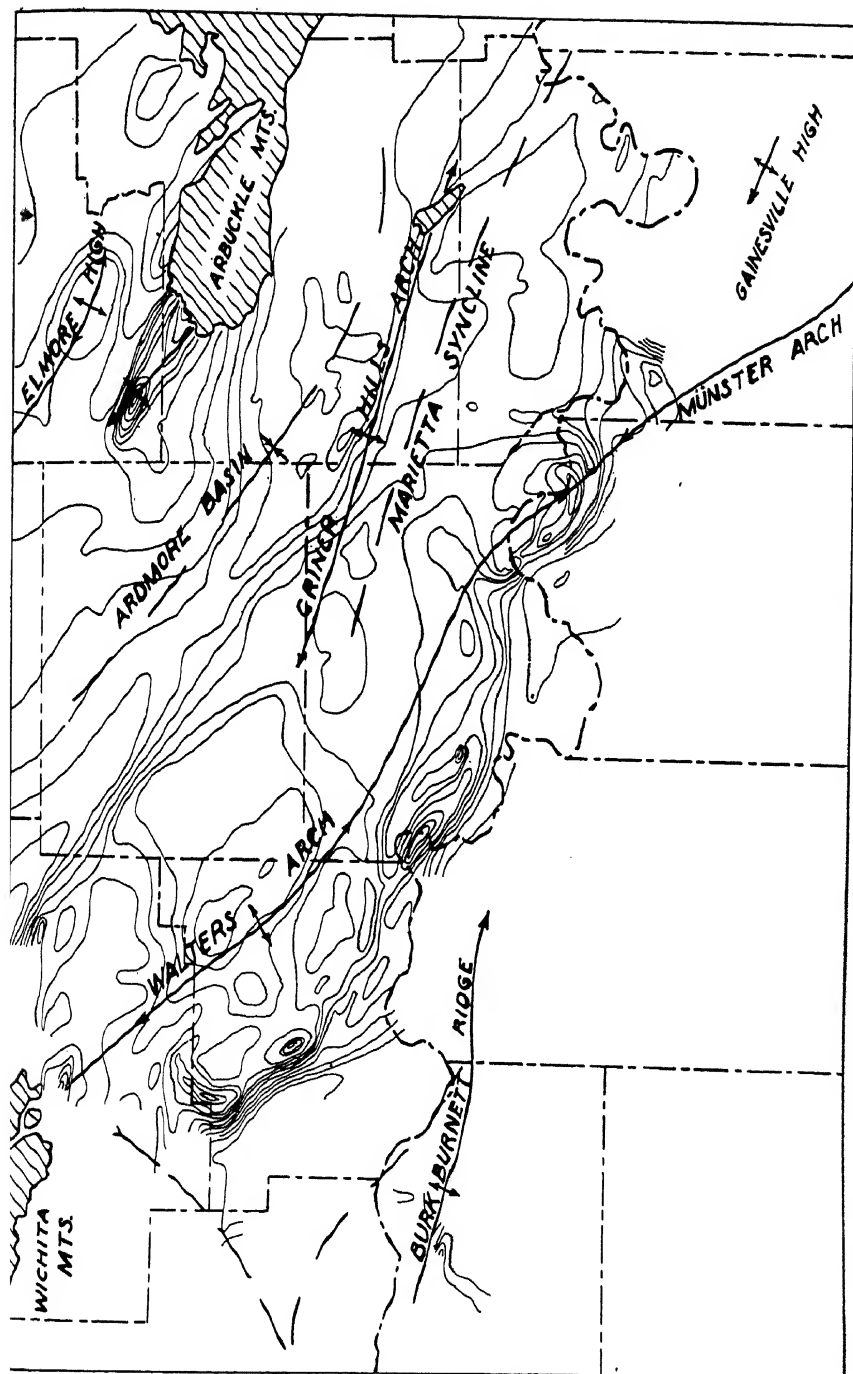
Fig. 8-75. Magnetic map of Wichita and Arbuckle Mountains and of structural trends along the Oklahoma-Texas border (after Van Weelden). Magnetic contour interval: 100 γ.

depth of the basement in the case of the Amarillo fault on the downthrow
side was assumed to be about 4000 feet and the depth of the basement in
the case of the Beckham County fault about 2500 feet.   The Hazeldean
fault (Miller[197]) in the pre-Cambrian, with a throw of 700 feet, caused a
positive peak of about 120γ on the upthrow side and a flatter negative
anomaly of -160γ amplitude on the downthrow side. Theoretical calcula-
tions checked the maximum as to amplitude and position, but gave for
the negative anomaly about half the observed amplitude and a negative
peak much closer to the fault.

Igneous intrusions have been frequently mapped in connection with
magnetic oil exploration.   Extensive batholithic intrusions may give rise
to doming of the oil-bearing strata.   Fracture and fault zones are often
accompanied by intrusions; laccolithic wedges produce warping in the
sedimentary beds.   Examples of magnetic effects of intrusives have been
frequently cited in the literature and but a few examples will suffice.
Lynton[198] reports a number of surveys on basic igneous intrusions from
California whose susceptibility is given as around $7000 \cdot 10^{-6}$ units.   In the
vicinity of Paso Creek in the San Joaquin Valley the magnetometer out-
lined a strong high (anomaly not stated).   A well subsequently drilled
encountered plutonic rocks at 2700 feet.   In the Ventura basin near
Oxnard an anomalous area with peak value of 700γ was outlined, and a
well put down in the high area encountered basalt at 1915 feet.   The
susceptibility of the basalt as determined on well samples was $700 \cdot 10^{-6}$.

On the Jackson uplift in Mississippi an extensive magnetometer survey
was made by Spraragen.[199]   A difference of 900γ in vertical intensity from
the lowest to the highest point corresponds to a difference in depth to the
chalk of 560 feet.   A similar survey was made by Barret[200] on the Caddo-
Shreveport uplift.   The maximum in vertical intensity is 250γ and a
minimum of -250γ occurs to the north.   The structural high is much
broader than the magnetic high, and there appears to be a considerable
shift (to the south) of the place of maximum vertical gradient compared
with the place of maximum structural gradient.   The area of the 600-foot
contour (on top of the producing sand in the Nacatoch formation) is dis-
placed as much as 10 miles to the northwest from the area of the 225γ
contour.   A rather unusual condition exists in the serpentine fields of
southwest Texas (Yoast field, Bastrop County; and Dale field, Caldwell
County) because the oil occurs in the magnetically active formation.
In the Yoast field[201] the serpentine is at a depth of about 1500 feet

[197] Canad. Geol. Survey Mem., **170**, 99–118 (1932).   See also Fig. 7-117.
[198] *Loc. cit.*
[199] Oil and Gas J., **30**(26) (Jan. 21, 1932).
[200] A.A.P.G. Bull., **14**(2), 175–183 (1930).
[201] D. M. Collingwood, A.A.P.G. Bull., **14**(9), 1191–1198 (Sept., 1930).

and produces a positive anomaly of about 25γ. Studies of exposed igneous rocks in Uvalde and Kinney Counties, Texas, were correlated by Liddle[202] with surveys of the Little Fry Pan anticline, where small magnetic anomalies were found. A well located on the highest point of the anticline encountered 150 feet of serpentine at 1000 feet depth. Other serpentine plugs in the same area (Yoast field, Dale field [serpentine at about 2000 feet]; Ellstone structure [serpentine at about 700 feet]; Buchanan field [serpentine at 1800 feet]) were outlined by Spraragen.[203] In the San Pedro area in Brazil, Malamphy[204] studied the effects of laccoliths and sills of basalts, found anomalies of the order of 200γ maximum corresponding to susceptibilities of about $4000 \cdot 10^{-6}$ units, and compared actual depths (350 to 450 feet) with depths calculated from the drop of the vertical intensity curve (which gave from 300 to 400 feet). Where oil production is associated with intrusives along fracture and fault zones, detailed magnetic surveys to locate the igneous sheets will be of considerable help. Examples of such surveys in Mexico have been published by the author.[205]

4. For the *location of shoestring sands*, only one example is known. Stearn[206] has described results obtained on several profiles through the Bush City shoestring in Anderson County, whose depth is from 600 to 800 feet. Anomalies are predominantly negative and of the order of 20 to 40γ. As Stearn indicates, it would be difficult to locate shoestrings magnetically because of the small magnitude and lack of definition of the anomalies.

C. Magnetic Surveys in Civil and Military Engineering

The scarcity of magnetic surveys in civil and military engineering is due not so much to adverse conditions as to lack of information on the part of the civil engineer regarding the possibilities of geophysical exploration. The usefulness of magnetic methods has been demonstrated in a number of cases discussed below.

1. *Water supply and drainage surveys* may derive much assistance from magnetic exploration where water occurs in troughs underlain by crystalline or igneous rocks, where its circulation is controlled by structure of magnetic beds, where water occurs in porous magnetic igneous rocks, or where its circulation is blocked by faults or igneous dikes. An application of this sort is mentioned by Grohskopf and Reinoehl[207] who found that

[202] A.A.P.G. Bull., 14(4), 509–516 (April, 1930).
[203] *Op. cit.*, 28(52) 42 (May 15, 1930).
[204] A.I.M.E. Tech. Publ. No. 696 (Feb., 1936).
[205] Colo. Sch. Mines Quart., 24(1), 61 (1929).
[206] A.I.M.E. Geophysical Prospecting, 192 (1932).
[207] Miss. State Geol. Rep., App. IV (1933).

thinning and tightening of the water-bearing beds occurred on magnetic highs so that chances of increased water supply were greater on the flanks and in the lows. A report by Kelly[208] states that a subsurface
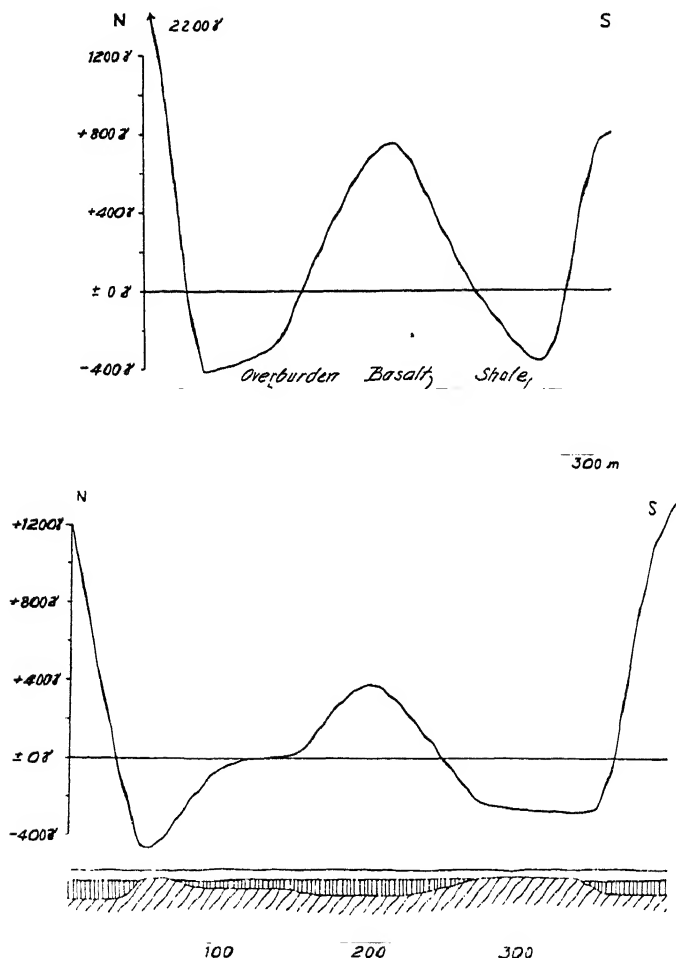
Fig. 8-76. Location and thickness determination of basalt flows for building and road material (after Ahrens).

structural trough was mapped magnetically by Jakosky to investigate water supply conditions on the Kaibab plateau.

2. In the *location of construction materials,* magnetic methods have considerable chance of success in outlining occurrences of igneous rocks suit-

208 Min. and Met., **17,** 10 (Jan., 1936).

able for building stone, such as granite, basalt, and the like. Fig. 8–76 shows the magnetic anomalies of a lava flow above nonmagnetic Tertiary shales. The magnetic anomalies are proportional to the thickness of the lava cover; minima occur where the shales come through to the surface. Ahrens[209] and Schroeder and Reich[210] established by a detailed survey of a basalt quarry that it was possible to differentiate between solid basalt usable for construction purposes and unusable weathered rock, since the anomalies over portions of the latter were much reduced.
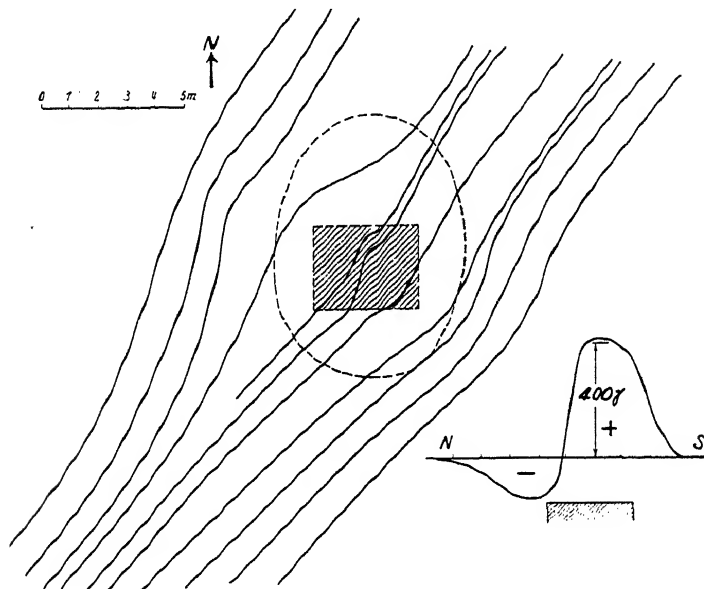
FIG. 8-77. Location of buried ammunition by magnetic and electrical measurements. Anomalies are shown in profile view, together with equipotential lines of an electrical survey. (After Ebert.)

3. *Dam site surveys.* Magnetic surveys can be of much help in determining structural conditions and rock properties on dam sites since they are much less expensive than drilling; at least, their use makes it possible to limit drilling operations to the absolute minimum. How the use of geophysics can reduce excavation and construction costs has been demonstrated in the case of the Bonneville Dam. It is reported that in the geological survey of that area the possibility of igneous intrusions was not recognized and that, after the first excavations encountered basalt, a geophysicist was called in to survey the basalt dikes. This subsequently

[209] Beitr. angew. Geophys., 2(4), 320 (1932).
[210] Beitr. angew. Geophys., 1(4), 432–436 (1931).

changed the construction plans and made it possible to use basalt pillars as foundations for a power house.

4. If the *location of buried metal* (pipe lines, ammunition) is known approximately, it may be readily found by magnetometers adaptable to rapid surveys, such as the dip needle and similar magnetometers. A Keuffel and Esser prospectus describes the location of two pipe lines, and an article by Ebert[211] discusses the location of a buried ammunition magazine by electrical and magnetic measurements (see Fig. 8-77). Vertical intensity anomalies up to 400γ were observed. Two lost magazines were found by combined electrical and magnetic measurements.

---

[211] Beitr. angew. Geophys., 1(1), 9-14 (1930).

SEISMIC METHODS

I. INTRODUCTION

SEISMIC procedures are in the group of "indirect" geophysical methods in which extraneous fields are set up and reactions of subsurface conditions to such fields are measured. Seismic exploration is concerned with the investigation of elastic forces. Contrary to other indirect geophysical methods—such as electrical ones—these fields of elastic forces are not stationary or quasi-stationary but vary and propagate with time. In common with electrical methods, the depth of investigation in seismic exploration may be controlled by varying the spacing between transmission and reception points.[1] This gives both the seismic and electrical methods great interpretational advantages over the gravitational and magnetic methods, since the indications furnished by the latter two represent the integral effects of all masses from great depths up to the surface. Direct and quantitative determinations of depths are the exceptions in gravimetric and magnetic work, but they are common practice in seismic and resistivity methods. A further advantage of seismic methods lies in the fact that not only the depths of geologic bodies but also some of their physical properties may be obtained.

Seismic and resistivity methods are, therefore, particularly well adapted to determinations of horizontal or nearly horizontal formation boundaries. This does not mean that other types of geologic bodies may not be well adapted to seismic exploration. Seismic refraction shooting has attained great practical significance in the location of salt domes because of the distinct geometric disposition and elasticity contrast existing in such domes.

Like most other geophysical methods, seismic methods depend for their successful application on the size of geologic bodies to be located. Both the refraction and resistivity methods depend on the thickness of formations compared with depth. This does not appear to hold for the reflec-

---

[1] With the exception of the reflection method.

SYMBOLS USED IN CHAPTER 9

a	amplitude, distance	**a**	coefficient, factor
b	amplitude, breadth		
c	distance	**c**	constant
d	deflection, distance, diameter, depth	**d**	damping factor
e	distance	**e**	2.718
f	frequency	**f**	friction
(f)	frequency factor		
g	gravity		
h	depth, height, thickness		
i	angle	**i**	number
j	$\sqrt{-1}$		
k	incompressibility factor	**k**	factor, number
l	length		
m	mass	**m**	number
n	tuning factor	**n**	number
p	percentage, proportion, factor	**p**	damping resistance
q	restoration coefficient	**q**	refractive index
r	distance, radius	**r**	ratio
s	distance	**s**	scale reading
t	time	**t**	temperature
u	displacement	**u**	salinity
v	displacement	**v**	velocity
w	displacement		
x	coordinate, displacement		
y	coordinate, displacement		
z	coordinate, depth		
A	distance	**A**	vector amplitude
		B	vector amplitude
C	constant, curvature	**C**	vector amplitude
D	distance, depth	**D**	couple
E	electromotive force	**E**	Young's modulus
F	force, load		
H	height, depth	**H**	field strength
I	current	**I**	intensity
J	sectional moment of inertia	**J**	indicator length
K	moment of inertia	**K**	compressibility
L	length		
M	magnification	**M**	magnetomotive force
N	turns		
P	force, pressure	**P**	power
Q	factor, amplitude		
R	ratio	**R**	resistance
S	factor, amplitude	**S**	surface, area
T	period, time	**T**	transmission constant
U	ultimate stress	**U**	transmission constant
V	volume	**V**	indicator magnification
W	energy density	**W**	dynamic magnification
X	amplitude	**X**	stress component
		Y	stress component
Z	depth	**Z**	stress component
α	angle	**α**	coefficient
β	angle	**β**	coefficient
γ	angle		

SYMBOLS USED IN CHAPTER 9—*Concluded*

δ	angle		$\bar{\delta}$	density
Δ	increment			
ϵ	angle; damping constant		ε	dilation coefficient
ζ	friction factor			
η	damping factor			
			Θ	volume change
λ	wave length		λ	Lamé coefficient
Λ	logarithmic decrement			
μ	(Galitzin) damping factor		μ	rigidity modulus
			ν	velocity ratio
Π	Poisseuille coefficient			
ρ	radius, distance			
σ	Poisson's ratio		δ	factor
τ	torsion coefficient		τ	time
φ	angle			
Φ	flux		Φ	dip angle
ψ	angle			
ω	angular frequency			

tion method, which has been found to be applicable to depths of 20,000 to 30,000 feet without any apparent relation to the thickness of the reflecting formation (provided it exceeds a certain minimum value, such as 25-50 feet). As the principal objective of seismic methods is a depth determination of elastic discontinuities, it is necessary that these properties remain reasonably constant in horizontal direction. This is true for most oil-bearing structures in which formations have been changed comparatively little from their original position, and it is one of the reasons why seismic prospecting has been applied so extensively in oil exploration.

Uses of seismic prospecting in mining have been few. Regions in which ore bodies are found are generally folded, faulted, intruded by igneous bodies, and metamorphosed. The continuity of physical properties that is so prevalent in sedimentary oil-bearing regions rarely exists in mining areas. Further, ore bodies generally do not differ sufficiently in their elastic properties from the surrounding rocks. Exceptions are the seismic determination of overburden thickness, the location of gold-bearing gravel channels, and structural investigations of carboniferous regions and sedimentary ores.

Applications of seismic methods depend on the degree of contrast in elastic properties of geologic bodies with respect to the surrounding media. In seismic exploration, differences in the speed of elastic waves in different formations are measured. These depend on certain combinations of Young's modulus of elasticity, Poisson's ratio, and density. The influence of density counteracts that of the modulus of elasticity. However, with an increasing degree of consolidation, the modulus of elasticity increases at a greater rate than does density so that formations of a greater degree of

consolidation, dynamo-metamorphism, and greater geologic age generally exhibit a greater seismic wave speed.

In regard to physical laws involved, seismic phenomena are comparable to optical phenomena since they deal with a type of energy propagated in the form of waves. Wave propagation may be said to be characterized by velocity, frequency, intensity, direction, and certain associated or derived characteristics and phenomena, such as travel time, wave length, absorption, refraction, reflection, and the like. In optics, only quasi-stationary phenomena are investigated, owing to the rapid rate of propagation of light, whereas in seismic work, virtually all interpretation is based on travel time. Comparatively little quantitative use is made of direction, frequency, and intensity. The chief objective is to determine the distance between the earth's surface and one or more refracting and reflecting surfaces below. Sensitive detection devices are used to record the arrival times of first (refraction) or later (refraction and reflection) impulses. These detectors embody an inert mass which remains (at first) stationary in respect to the ground, and whose movement may be magnified mechanically or electrically. In addition, the instant of the explosion is transferred to the receiving station; accurate time marks are provided on the record so that the time elapsed between the shot and the arrival of the elastic impulses may be found. Together with a determination of distance between shot point and record, this permits of measuring the true and apparent velocities of elastic waves.

The simplest method of seismic prospecting is the *fan-shooting* method. This consists of comparing the travel times from a single shot point to a number of pickups arranged approximately in a circle around it. The existence and sometimes the nature of an intervening medium may be deduced from these data. More detailed information is derived from the *refraction* method, which consists of shooting traverses with one (or two) shot points and a number of seismographs set up in line, and determining the travel time as a function of distance. The time-distance curves give information on the paths of seismic rays below, their refraction, and depths to *refracting* surfaces. In the reflection method, the travel times of *reflected* waves allow depths to reflecting surfaces to be calculated.

Observation methods and instruments in seismic prospecting and earthquake seismology are very similar in respect to time marking, time transmission, and recording procedures. The inductive electromagnetic seismograph, which is now widely used in geophysical exploration, was developed for earthquake seismology by Galitzin more than twenty-five years ago. On the other hand, important differences in instruments were brought about by the needs of adaptation to geological exploration. This resulted in a decrease of size, increase in portability, increase in natural frequency

and magnification, introduction of electrical amplification, increase in photographic recording speed and restriction of the record to the vertical component. However, the theory of wave propagation used in seismic prospecting is again quite similar to the theory developed in earthquake seismology.

In the application of the seismic method to oil exploration, great successes have been obtained in locating salt domes, anticlines and faults, and in mapping the topography of basement rocks. Buried land surfaces and limestone beds are usually good seismic key horizons. While in oil exploration refraction methods dominated the field several years ago both for reconnaissance and detail, the picture has now changed completely. Ever increasing fields of application have been found for the reflection method. It was soon discovered that not only limestone beds but hard shales and other beds with seemingly small differences in elastic properties would give reflections. On occasion, their lack of continuity gave rise to serious difficulties, but these were overcome by the application of the dip-shooting and the continuous-profiling methods.

The field of civil engineering has also seen the application of seismic exploration in late years. Most foundation problems, such as determination of depth to bedrock and investigation of tunnel and dam sites, may be attacked by refraction methods. Another application of seismology in civil engineering (engineering seismology) has as its objective the design of earthquake-proof structures, the determination of dynamic response of models of proposed structures, the investigation of damage done by traffic and blasting vibrations, the determination of the elastic properties of foundation sites, and the analysis of the frequency response of roadbeds, bridges, dams, and buildings. A discussion of the fields of engineering seismology and of acoustic methods is given in Chapter 12.

II. PHYSICAL ROCK PROPERTIES IN SEISMIC EXPLORATION; SELECTED TOPICS ON THE THEORY OF ELASTIC DEFORMATIONS AND WAVE PROPAGATION

A. General

The elastic properties of rocks may be ascertained in the laboratory, and from such data the velocity of the elastic waves in formations may be determined. Direct velocity determinations may be made in the field (1) by shooting on exposed formations; (2) by shooting in or near a well at known depths (average velocity determinations in reflection work); and (3) from the travel-time curve. A direct measurement of velocity on rock samples in the laboratory has not been attempted.

Elastic wave-producing forces are associated with two types of strains:

(1) volume changes, that is, compression or dilation; (2) shearing strains. These two strains propagate in a homogeneous isotropic medium with constant but different velocities. It is true that geologic formations encountered near the surface and in the interior of the earth are far from homogeneous and isotropic. However, this can be allowed for by assuming continuous or discontinuous variations of the physical properties and by applying the theory to small elements of an elastic substance. The derivations given below presuppose, furthermore, a perfectly elastic body, that is, a body in which the stress is proportional to the strain (one to which Hooke's law may be applied), and one in which there is *no elastic hysteresis*.

B. ELEMENTS OF THEORY OF ELASTIC DEFORMATION AND WAVE PROPAGATION[2]

1. *Relation of strain and stress; elastic properties; volume and shear deformations (static problem).* In considering an element of volume of an
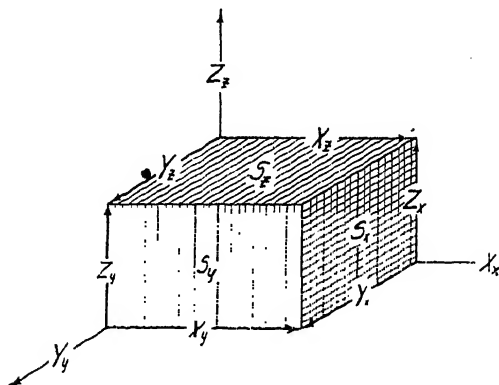
FIG. 9-1. Normal and tangential stress components in elementary parallelopiped.

elastic body subjected to stress (Fig. 9-1), its orientation can be so chosen that the three stress components X_x, Y_y, and Z_z, are at right angles to its surfaces, S_x, S_y, and S_z. These stress components are known as "normal" stresses. Two stress components exist in each surface at right angles to each of the three normal stresses. These components are known as "tangential" stresses and are designated Z_x, X_z; Y_x, X_y; and Z_y, Y_z.

Since the elementary body must be in equilibrium against rotation, the tangential stresses in each pair referred to above are equal to one another.

(a) *Normal stresses.* Under the influence of the normal stresses X_x, Y_y, and Z_z, three sides of the element of volume suffer the displacements u in the x direction, v in the y direction, and w in the z direction. Then the deformations referred to unit length, or the specific strains, are $\partial u/\partial x$, $\partial v/\partial y$, and $\partial w/\partial z$. The change in volume ΔV, resulting from the deformations in the three directions, is equal to the sum of the specific strains:

$$\frac{\Delta V}{V} \equiv \Theta = \frac{\partial u}{\partial x} + \frac{\partial v}{\partial y} + \frac{\partial w}{\partial z}.$$

If Θ is negative, reduction of volume or compression takes place; if positive, extension or dilation. The change in volume is accompanied by a change in shape; when the length is extended, the section is reduced. In this type of deformation, the angles are preserved. Since the strains are proportional to the stresses, the relation between normal stress and the corresponding strain in the x direction may be written[2a]

$$\partial u \tag{9-2}$$

where ε is the dilation coefficient. A more customary definition of this coefficient may be arrived at by writing

$$\frac{1}{\varepsilon} = \frac{X_x}{\dfrac{\partial u}{\partial x}} = \frac{P/S}{\dfrac{\Delta l}{l}},$$

where P/S is the load per unit area, S is area, and $1/\varepsilon$ is *Young's modulus*:

$$E = \frac{P}{S} \cdot \frac{l}{\Delta l}, \tag{9-3}$$

that is, load per unit area divided by relative elongation.

The expansion $\partial u/\partial x$ in the x direction produces a reduction of section in the y–z plane. Assuming the reductions in width, $\partial v/\partial y$ and $\partial w/\partial z$, to be equal and to be a fraction of and proportional to the elongation, we have

$$\frac{\partial v}{\partial y} = \frac{\partial w}{\partial z} = \sigma \frac{\partial u}{\partial x}. \tag{9-4a}$$

The factor σ is called *Poisson's ratio.* From eq. (9-4a), $\sigma = \dfrac{\partial w}{\partial z} \Big/ \dfrac{\partial u}{\partial x}$

[2a] Assuming, for the moment, that X_x alone is effective. The complete expressions are given in eq. (9-6).

or as generally written,

$$= \frac{\Delta d}{d} \Big/ \frac{\Delta l}{l}. \tag{9-4b}$$

Poisson's ratio is the ratio of relative reduction of diameter d and relative elongation. For many substances, σ is in the neighborhood of $\frac{1}{4}$. Substituting (9–2) in (9–4a),

$$\frac{\partial v}{\partial y} = \frac{\partial w}{\partial z} = \sigma \varepsilon X_z. \tag{9-5}$$

The original extension in the x direction given by eq. (9–2) is opposed by a reduction of the x-z section due to the normal stress Y_y. By analogy with (9–5), this reduction is $(\partial u/\partial x) = \sigma \varepsilon Y_y$. A further reduction takes place because of the stress Z_z, which is $\sigma \varepsilon Z_z$. Therefore, the total specific strain is

$$\frac{\partial u}{\partial x} = \varepsilon X_x - \sigma \varepsilon Y_y - \sigma \varepsilon Z_z.$$

Hence,

the strain in the x direction: $\dfrac{\partial u}{\partial x} = \varepsilon[X_x - \sigma(Y_y + Z_z)]$

the strain in the y direction: $\dfrac{\partial v}{\partial y} = \varepsilon[Y_y - \sigma(Z_z + X_x)]$

and

the strain in the z direction: $\dfrac{\partial w}{\partial z} = \varepsilon[Z_z - \sigma(X_x + Y_y)].$

$$\left. \right\} \tag{9-6}$$

Adding these three equations and considering (9–1),

$$\Theta = \varepsilon[(1 - 2\sigma)(X_x + Y_y + Z_z)]. \tag{9-7}$$

Adding to the right side of the first equation of (9–6), $+ X_x \sigma \varepsilon$ and $- X_z \sigma \varepsilon$, the specific strain in the x direction

$$\frac{\partial u}{\partial x} = \varepsilon[X_z(1 + \sigma) - \sigma(X_x + Y_y + Z_z)].$$

Re-substituting eq. (9–7),

$$\frac{\partial u}{\partial x} = \varepsilon\left[X_z(1 + \sigma) - \frac{\sigma \Theta}{(1 - 2\sigma)}\right].$$

Solving for the normal stress and treating all equations of (9-6) in the same manner,

$$
\left.\begin{array}{l}
X_x = \dfrac{\sigma}{\varepsilon}\dfrac{\Theta}{(1+\sigma)(1-2\sigma)} + \dfrac{1}{\varepsilon(1+\sigma)}\dfrac{\partial u}{\partial x} \\[2mm]
Y_v = \dfrac{\sigma}{\varepsilon}\dfrac{\Theta}{(1+\sigma)(1-2\sigma)} + \dfrac{1}{\varepsilon(1+\sigma)}\dfrac{\partial v}{\partial y} \\[2mm]
Z_z = \dfrac{\sigma}{\varepsilon}\dfrac{\Theta}{(1+\sigma)(1-2\sigma)} + \dfrac{1}{\varepsilon(1+\sigma)}\dfrac{\partial w}{\partial z}.
\end{array}\right\} \quad (9\text{-}8)
$$

The two coefficients in these relations are known as the *Lamé* coefficients:

$$
\lambda = \frac{\sigma E}{(1+\sigma)(1-2\sigma)} \quad \text{and} \quad \mu = \frac{E}{2(1+\sigma)}.
$$

If Poisson's ratio is $\frac{1}{4}$, $\lambda = \mu = \frac{2}{5}E$. The quantity μ is also known as the *shear* or *rigidity modulus*.

With these coefficients, eq. (9-8) become

$$
\left.\begin{array}{l}
X_x = \Theta\lambda + 2\mu\dfrac{\partial u}{\partial x} \\[2mm]
Y_v = \Theta\lambda + 2\mu\dfrac{\partial v}{\partial y} \\[2mm]
Z_z = \Theta\lambda + 2\mu\dfrac{\partial w}{\partial z}.
\end{array}\right\} \quad (9\text{-}9)
$$

These are the fundamental equations expressing the normal stresses as functions of the volume changes and of the specific strains in the same directions.

Eqs. (9-9) state that the strains produced by normal stresses depend on both λ and μ whereas the tangential stresses, as shown in the following paragraph, depend on the rigidity modulus μ alone. Eqs. (9-9) indicate further that the normal stresses become equal when the rigidity is zero. In that case all tangential stresses are zero and the normal stress is the hydrostatic pressure. If $X_x = Y_v = Z_z \equiv -P$ in eqs. (9-9), by adding eqs. (9-9) and substituting P we obtain

$$
\left.\begin{array}{l}
-3P = 3\Theta\lambda + 2\mu\Theta; \qquad P = -\Theta(\lambda + \tfrac{2}{3}\mu). \\[2mm]
\text{If } \lambda + \tfrac{2}{3}\mu = k, \text{ then} \\[2mm]
\qquad P = -k\Theta \quad \text{or} \quad -\Theta = P/k \equiv P\mathbf{K}.
\end{array}\right\} \quad (9\text{-}10)
$$

The factor k is the incompressibility factor or *bulk modulus*; its reciprocal, **K**, is the *compressibility*. In terms of Young's modulus:

$$k = \frac{E}{3(1 - 2\sigma)}.$$

If Poisson's ratio σ is $\frac{1}{4}$, $k = \frac{2}{3}E$.

(*b*) *Tangential stresses* produce a change in the angles of an elastic body and preserve the surfaces. In the x-z plane of an elementary parallelo-
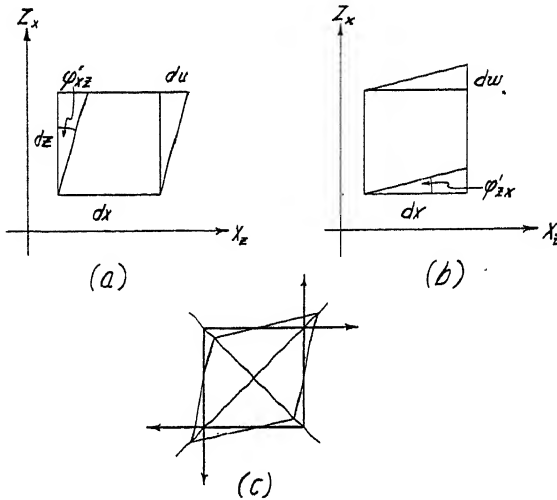
FIG. 9-2. (*a*) Shear deformation by X_z; (*b*) shear deformation by Z_x; (*c*) resultant deformation.

piped, the tangential stresses X_z and Z_x produce the strains du and dw and the "shear" angles φ'_{xz} and φ'_{zx}, which are related to the stresses by a proportionality factor that is the reciprocal of the rigidity, μ. Thus, as shown in Fig. 9–2, $\varphi'_{xz} \approx (1/\mu)X_z$ and $\varphi'_{zx} \approx (1/\mu)Z_x$. Since X_z and Z_x are interchangeable, the resultant change of shape is given by

$$2\varphi_{xz} = \frac{1}{\mu} X_z;$$

and, similarly, for the other planes,

$$2\varphi_{yz} = \frac{1}{\mu} Y_z$$

$$2\varphi_{xy} = \frac{1}{\mu} X_y.$$

(9–11)

As $dz\varphi'_{xz} = du$ and $dx\varphi'_{zx} = dw$, $\varphi'_{xz} + \varphi'_{zx} = \dfrac{du}{dz} + \dfrac{dw}{dx}$ and

$$\left.\begin{aligned}
2\varphi_{xz} &= \frac{\partial u}{\partial z} + \frac{\partial w}{\partial x} \\[2mm]
2\varphi_{yz} &= \frac{\partial v}{\partial z} + \frac{\partial w}{\partial y} \\[2mm]
2\varphi_{xy} &= \frac{\partial u}{\partial y} + \frac{\partial v}{\partial x}.
\end{aligned}\right\} \qquad (9\text{--}12)$$

Combining eqs. (9–11) and (9–12):

$$\left.\begin{aligned}
\mathbf{X}_z(=\mathbf{Z}_x) &= \mathfrak{u}\left(\frac{\partial u}{\partial z} + \frac{\partial w}{\partial x}\right) \\[2mm]
\mathbf{Y}_z(=\mathbf{Z}_y) &= \mathfrak{u}\left(\frac{\partial v}{\partial z} + \frac{\partial w}{\partial y}\right) \\[2mm]
\mathbf{X}_y(=\mathbf{Y}_x) &= \mathfrak{u}\left(\frac{\partial u}{\partial y} + \frac{\partial v}{\partial x}\right).
\end{aligned}\right\} \qquad (9\text{--}13)$$

2. *Propagation of deformations; longitudinal and transverse types of waves (dynamic problem).* For simplification of analysis, consider a plane wave resulting from displacements u in the x direction. Then only the components $\mathbf{X}_x$, $\mathbf{Y}_x$, and $\mathbf{Z}_x$ shown in Fig. 9–1 have to be considered. These forces are referred to unit area and therefore their action on the y-z side of an elementary parallelopiped is given by expressions of the form $\mathbf{X}_x \cdot dy \cdot dz$, or $\partial \mathbf{X}_x/\partial x \cdot dV$. Although the primary deformation is in the x direction, deformations in the y and z directions result from contraction.

The accelerations corresponding to these deformations are $\partial^2 u/\partial t^2$, $\partial^2 v/\partial t^2$, and $\partial^2 w/\partial t^2$. Since the force $(\partial \mathbf{X}_x/\partial x \cdot dV)$ is mass $(dV \cdot \delta$, with $\delta = $ density) times acceleration $(\partial^2 u/\partial t^2)$, the equations for a (plane) wave in the x direction are

$$\left.\begin{aligned}
\delta \cdot \frac{\partial^2 u}{\partial t^2} &= \frac{\partial \mathbf{X}_x}{\partial x} \\[2mm]
\delta \cdot \frac{\partial^2 v}{\partial t^2} &= \frac{\partial \mathbf{Y}_x}{\partial x} \\[2mm]
\delta \cdot \frac{\partial^2 w}{\partial t^2} &= \frac{\partial \mathbf{Z}_x}{\partial x}.
\end{aligned}\right\} \qquad (9\text{--}14)$$

In these equations, $\mathbf{X}_x$, as given by formula (9–9), $= \Theta\lambda + 2\mathfrak{u}\,\partial u/\partial x$. Θ follows from (9–1). Since the initial specific strains in the y and z

directions are 0, $\Theta = \partial u/\partial x$. Hence, $X_x = (\lambda + 2\mu)\ \partial u/\partial x$. Y_x follows from eq. (9-13). Since the problem is limited to propagation in the x direction and the shears in the y and z directions are zero, $Y_x = \mu\ \partial v/\partial x$ and $Z_x = \mu\ \partial w/\partial x$. By differentiation of these components with respect to x as required by (9-14), the following equations are obtained:

$$\left.\begin{array}{l} \dfrac{\partial^2 u}{\partial t^2} = \dfrac{\lambda + 2\mu}{\delta}\dfrac{\partial^2 u}{\partial x^2} \\[3mm] \dfrac{\partial^2 v}{\partial t^2} = \dfrac{\mu}{\delta}\dfrac{\partial^2 v}{\partial x^2} \\[3mm] \dfrac{\partial^2 w}{\partial t^2} = \dfrac{\mu}{\delta}\dfrac{\partial^2 w}{\partial x^2}. \end{array}\right\} \qquad (9\text{-}15)$$

The first equation indicates the *gradient* of the specific strain $\partial u/\partial x$ in the x direction, that is, in the direction of propagation. It is thus the expression for a *compressional* and *longitudinal* wave. The second equation gives the gradient or propagation of the shear $\partial v/\partial x$ in the x direction; and the third equation, the gradient or propagation of the shear $\partial w/\partial x$ in the x direction. This applies to a plane wave traveling in one direction (see Fig. 9-3); however, it can be shown that the equations here derived also hold for space waves.
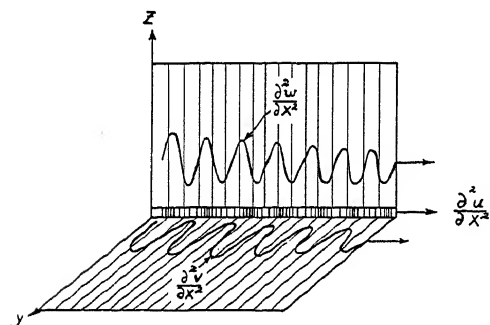
FIG. 9-3. Propagation of longitudinal and shear deformations.

Eqs. (9-15) show that the acceleration in a longitudinal wave (or compression $\partial^2 u/\partial x^2$) is proportional to $(\lambda + 2\mu)/\delta$, while in the second case it is proportional to μ/δ. The two last waves are shear waves; they are not propagated independently. Figure and equations merely indicate the two (z and y) components of the wave whose relative amplitudes determine the *plane of polarization.*

The proportionality factors in the last three equations may be designated by v^2, thus: $v_l^2 = (\lambda + 2\mu)/\delta$ and $v_t^2 = \mu/\delta$. Then $\partial^2 u/\partial t^2 = v_l^2 \cdot \partial^2 u/\partial x^2$; $\partial^2 v/\partial t^2 = v_t^2 \cdot \partial^2 v/\partial x^2$; $\partial^2 w/\partial t^2 = v_t^2 \cdot \partial^2 w/\partial x^2$. The *velocities* of the longitudinal and transverse waves are, therefore,

$$v_l = \sqrt{\frac{\lambda + 2\mu}{\delta}} \quad \text{and} \quad v_t = \sqrt{\frac{\mu}{\delta}}. \qquad (9\text{-}16)$$

When $\sigma = \frac{1}{4}$, $\lambda \equiv \mu$, and $v_l/v_t = \sqrt{3}$; that is, the longitudinal wave moves faster than the transverse wave.

The accelerations on the left side of eq. (9-15) may be set in relation to the ground amplitudes. Since the inertia force, $m \cdot \partial^2 u/\partial t^2$, must equal the restoring force (= force per unit displacement, or spring constant c, times displacement), we have $m \cdot \partial^2 u/\partial t^2 = -cu$ or

$$\frac{\partial^2 u}{\partial t^2} + \frac{c}{m} u = 0. \tag{9-17}$$
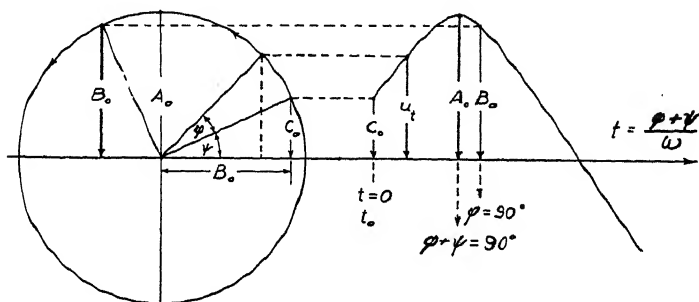
FIG. 9-4. Periodic motion.

In this equation $c/m = \omega^2$; ω is the angular frequency of oscillation or the angular velocity of the motion of a given particle on the circumference of the circle of reference (see Fig. 9-4) or

$$\omega = 2\pi f, \tag{9-18a}$$

where $1/T = f$ is the number of oscillations per second. The solution of eq. (9-17) is

$$u = B_0 \sin \omega t + C_0 \cos \omega t. \tag{9-18b}$$

Substituting for the two arbitrary constants, $A_0^2 = B_0^2 + C_0^2$, $\sin \psi = C_0/A_0$, and $\cos \psi = B_0/A_0$;

$$u = A_0 \sin (\omega t + \psi) = A_0 \sin (\varphi + \psi) = \quad \text{) sin } \langle \tag{9-19}$$

in which φ and ψ are phase angles; $\psi = \omega t_0$ is the starting angle corresponding to the time t_0; and $\varphi = \omega t$ is the phase angle at the time t. The significance of the constants A_0, C_0, and B_0 may be obtained from eq. (9-19) by solving for the limits $\varphi + \psi = 90°$, $\varphi = 0°$, and $\varphi = 90°$. Then, A_0 is seen to be the maximum amplitude (peak amplitude); C_0 is the initial amplitude; and B_0 is the amplitude reached within a quarter period ($\varphi = 90°$) after the start. These relations appear in Fig. 9-4, whose right side shows wave motion plotted against time, while on the left amplitudes are shown as function of phase angles on the reference circle.

3. Earthquake waves. In the preceding section it was stated that in an isotropic elastic body only two types of waves exist, *longitudinal* and *transverse* waves. While the observed waves are actually longitudinal and transverse in character, there are a number of types in addition to the two mentioned. There is virtually but one longitudinal wave and several kinds of transverse waves. The explanation is that the above theory considers a volume element within an unbounded elastic solid and is not strictly valid for surfaces between media. It is readily seen that the transverse waves should be the ones to be influenced by such conditions, since they have an arbitrary direction of oscillation in a plane at right angles to their direction of propagation. This plane should depend, in its orientation and other characteristics, on the orientation and elastic characteristics of a geologic or physical boundary.
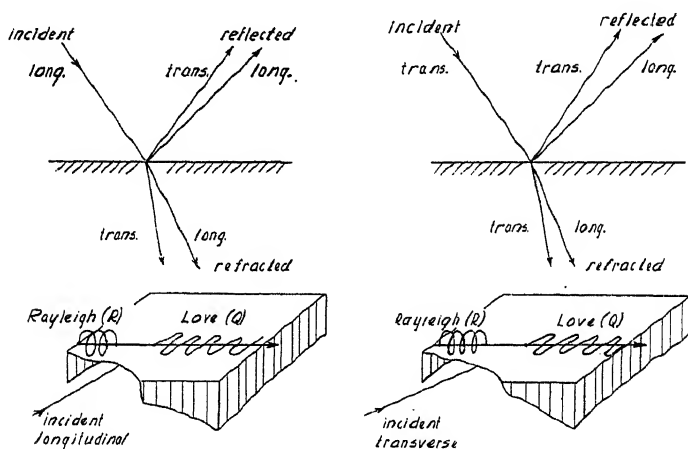
FIG. 9-5. Wave types on boundaries.

When a wave consisting of longitudinal and transverse impulses strikes a boundary, theoretically no less than twelve new wave types are produced. As shown in Fig. 9–5, two refracted (longitudinal and transverse) and two reflected waves are produced by the longitudinal wave. The same is true for the transverse wave, so that in this manner alone eight new waves are accounted for. Further, each wave may generate the Love wave, Q, which is a special type of transverse wave with its plane of oscillation in the formation boundary, and the Rayleigh wave, R, which is a combined longitudinal and transverse wave with plane of oscillation at right angles to the surface and parallel to the direction of the propagation. The last two waves are frequently observed at the earth's surface; it is probable that the so-called "ground roll" observed in reflection seismology is of the Rayleigh type.

Instead of distinguishing between longitudinal and transverse waves it

waves. The preliminary waves, or forerunners, come to a seismic station through the *interior* of the earth, while the surface waves, as their name indicates, propagate along the earth's surface. The forerunners in turn are divided into the longitudinal and transverse preliminary waves, while the surface waves are divided in the same manner into the *Love* waves and the *Rayleigh* waves, named after the investigators who first described and analyzed them.

Usually there are three phases in a long-distance seismogram (see Fig. 9-6): (1) the primae, or normal longitudinal preliminaries, P; (2) the secundae, or transverse preliminaries, S; and (3) the surface waves, L (= longae). Abrupt arrivals are designated by the subscript i (impetus); a gradual appearance is designated by e (emersio). The P waves, as well as the S waves, are divided into the (1) normal, (2) reflected,[3] and (3) refracted waves. Alternating waves, mostly of the reflected type, are designated by the letters PS or SP, depending upon whether they were running first as longitudinal or transverse waves. The subscript n denotes the normal preliminaries; the subscript c designates waves which have passed the core of the earth. Bars above the symbols indicate refractions; double letters, reflections. The main part of a seismogram is generally divided into (1) the arrival of the surface waves, L; (2) the maximum, M; and (3) the coda, C.

An analysis of travel-time curves makes it possible to determine the depth of penetration of seismic waves in the earth's interior, their path, and their velocities along various portions of this path. Obviously, only the preliminary waves can be used for investigations of this character. As the longitudinal waves have the greatest velocity and arrive first, they can be more accurately identified and timed than can later impulses. Travel-time curves for the directly transmitted, for the once and twice reflected,[4] and

[3] Reflected at the surface.
[4] It has been suspected that some unreasonably deep reflections recorded in seismic exploration are of a similar nature, that is, reflected once at the surface and twice
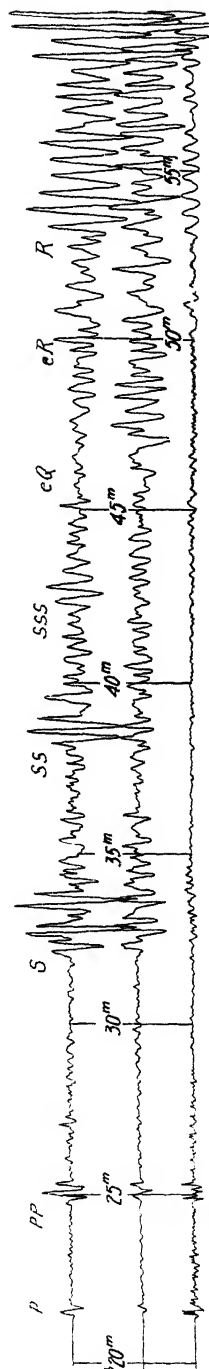
Fig. 9-6. Typical long-range earthquake record (distance, 9800 km; Mexican earthquake, April 15, 1907) (after Gutenberg).

for the first and second preliminary waves have been published in various books on seismology. The time of arrival is not a linear function of the distance traveled. The velocity is not constant but dependent on distance and thus on depth of the strata traversed.

4. *Characteristics of waves observed in seismic exploration.* In seismic exploration one does not have to deal with as many types of waves as in earthquake seismology. This fact is due, first, to the smaller distances and shorter time intervals involved; and second, to the fact that not so many components are recorded, making it impossible to identify transverse waves with certainty. It is true that transverse impulses have been recognized in records of quarry explosions, but in such cases greater distances were involved and horizontal components were also recorded.

Three types of longitudinal waves are observed in seismic exploration: (1) directly transmitted; (2) refracted; and (3) reflected. Longitudinal waves transmitted at the immediate surface are rarely observed; virtually all first breaks, even those recorded close to the shot point, are refracted waves. Surface waves arriving at the end of a record are probably not simple longitudinal but Rayleigh waves. Their frequency is generally low, from 10 to 15 cycles. The frequency of the refracted waves, on the other hand, covers a wide band from around 15 to 60 or 80 cycles, while the frequency of reflected waves is frequently near 50 and covers the range from 30 to 70 cycles.

C. Laboratory and Field Methods for the Determination of Elastic Moduli and Wave Velocities

It was shown in the preceding sections that elastic moduli are the physical parameters relating stresses and deformations and that the elastic wave velocities are functions of these moduli. In the study of the elastic behavior of rocks and formations, it is thus possible to attack the problem in two ways: (1) by measuring elastic moduli in the *laboratory*; (2) by making velocity determinations directly in the *field*. Direct velocity determinations have the advantage that the speed of seismic waves is determined *in situ*, that is, under the natural conditions of moisture, pressure, weathering, and the like. Furthermore, unconsolidated formations cannot be moved and must be tested in the field.

Elastic constants may be expressed in various units. Pounds per square inch is the unit most frequently used in the testing of construction materials in this country. Another technical system uses the atmosphere; scientific publications employ dynes per cm^2, megabars, and baryes. In many articles there is confusion as to the correct usage of the terms bars and baryes. In Europe the normal atmosphere and the technical atmosphere (kg per cm^2), the dyne per cm^2, and kg per mm^2 are preferred.

TABLE 44

NUMERICAL RELATIONS OF PRESSURE UNITS

	DYNE·CM⁻² OR BARYE	ATMOSPHERE	(MEGA) BAR	KG·CM⁻²	KG·MM⁻²	POUNDS PER SQUARE FOOT	POUNDS PER SQUARE INCH
Dyne·cm⁻² or barye.....	1	$9.869 \cdot 10^{-7}$	$1 \cdot 10^{-6}$	$1.02 \cdot 10^{-6}$	$1.02 \cdot 10^{-8}$	$2.089 \cdot 10^{-3}$	$1.450 \cdot 10^{-5}$
Atmosphere................	$1.013 \cdot 10^{6}$	1	1.013	1.033	$1.033 \cdot 10^{-2}$	$2.116 \cdot 10^{3}$	14.696
(Mega) bar...............	$1 \cdot 10^{6}$	0.987	1	1.02	$1.02 \cdot 10^{-2}$	$2.089 \cdot 10^{3}$	14.504
kg·cm⁻²..................	$9.807 \cdot 10^{5}$	0.968	0.981	1	$1 \cdot 10^{-2}$	$2.048 \cdot 10^{3}$	14.223
kg·mm⁻².................	$9.807 \cdot 10^{7}$	96.78	98.07	$1 \cdot 10^{2}$	1	$2.048 \cdot 10^{5}$	$1.422 \cdot 10^{3}$
Pounds per square foot..	478.8	$4.725 \cdot 10^{-4}$	$4.788 \cdot 10^{-4}$	$4.882 \cdot 10^{-4}$	$4.882 \cdot 10^{-6}$	1	$6.944 \cdot 10^{-3}$
Pounds per square inch..	$6.894 \cdot 10^{4}$	$6.805 \cdot 10^{-2}$	$6.895 \cdot 10^{-2}$	$7.03 \cdot 10^{-2}$	$7.03 \cdot 10^{-4}$	144	1

NOTE: Items in separately outlined compartments are nearly equal.

Table 44 is given to aid in the conversion of these units. The units based upon the acceleration of gravity are referred to its value in 45° latitude (980.665 cm-sec^{-2}) by international agreement.

Although, in the technical system of this country, elastic moduli are usually expressed in pounds per square inch, the barye, or dyn cm^{-2}, will be used in the following sections, since the parameters expressed in the C.G.S. system may be more readily converted into velocities of longitudinal and transverse waves. Wave speeds are usually given in meters or kilometers per second, although in seismic prospecting feet per second has been widely adopted. Several of the elastic constants are not independent quantities but may be calculated from one another. If Young's modulus and Poisson's ratio have been determined, the compressibility may be calculated. On the other hand, the compressibility may also be measured directly. If the two values differ, it indicates a deviation from isotropy and homogeneity. Furthermore, a comparison of values determined statically and dynamically in the laboratory, with those calculated from velocity determinations, is of value.

Methods for the determination of elastic constants may be divided into *laboratory* and *field* methods. The latter are dynamic methods, since they involve the measurement of time, while laboratory determinations may be either static or dynamic or both. In the static determinations stress-strain relations are established, while dynamic measurements are based on observations of natural frequencies. Equipment for testing elastic properties of construction materials has been developed to a high degree of perfection.[5] For the measurement of deformations the following devices are used: (1) *extensometers*, (2) *deflectometers*, and (3) *detrusion meters*; they may be (a) mechanical, (b) optical, or (c) electrical.

Mechanical devices are generally not accurate enough for geophysical application. Closest in this respect are some of the more delicate types of Ames gauges, for which an accuracy of 0.000025 inch is claimed.

The simplest *optical devices* for measuring extensions or deflections, microscopes, and cathetometers, are generally not accurate enough for rock testing. Rocking mirror arrangements, however, give satisfactory results. In the Martens mirror extensometer two rocking mirrors are clamped to opposite sides of a specimen. These are rotated when the specimen is extended (see Fig. 9-7) and are observed by separate telescopes. If the arrangement is so modified (Fig. 9-8) that the light travels from one mirror to the other, more magnification is obtained. If A is the distance from scale or telescope to the nearest mirror, D their distance apart, and n

---

[5] Comprehensive descriptions may be found in J. B. Johnson's *Materials of Construction*, Chapter II, John Wiley (1930), and in C. H. Gibbons, *Materials Testing Machines*, Instruments Publishing Co. (Pittsburgh, 1935).

the observed deflection in scale divisions, the deflection angle of each mirror is given by

$$\tan \alpha = \frac{}{4A + 2D} \qquad (9\text{--}20)$$

where A and D are expressed in scale divisions. To obtain the extension of a bar, the angular mirror deflection must be multiplied by the effective lever arm of the rocking mirror. A rocking-mirror arrangement with a powerful telescope 4.5 m away from the scale has been employed by Zisman. He obtained magnifications of the order of one million.

Interference measurements for strain determinations have been applied in two ways. In the interference extensometer of Grueneisen (Fig. 9-9), two tubes are clamped to the sections whose change of distance is to be measured. The ends of the tubes carry two closely spaced polished glass disks, between which interference patterns are produced. If the pattern changes by
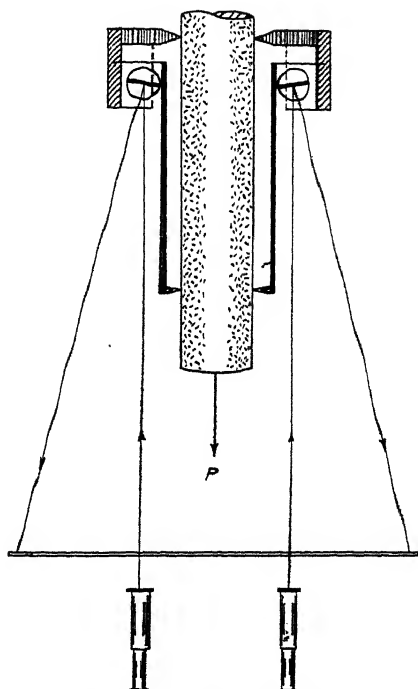
FIG. 9-7. Bauschinger Martens mirror extensometer.
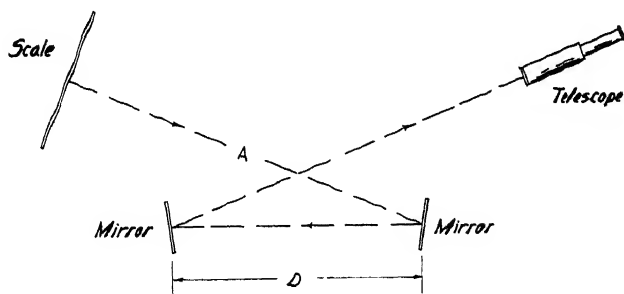
FIG. 9-8. Double mirror reflection arrangement.

one fringe width, the corresponding change in distance is one-half the wave length of the light employed.
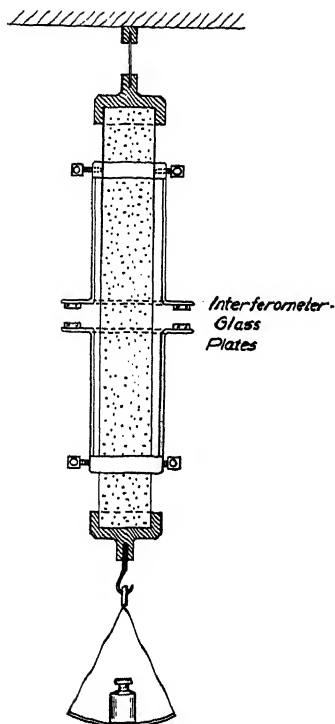
FIG. 9-9. Extension measurement by interferometer (Grueneisen arrangement).

Another interference method has been applied by Richards[6] for testing deformations of rectangular plates. If such plates are subjected to stresses at the ends, they will curve not only in the longitudinal direction but in the transverse as well (see Fig. 9-10). The upper surface of the plate or rock slab under investigation is polished, and interference patterns, as shown schematically in Fig. 9-11, are observed against a fixed plate.

The simplest of the *electrical devices* is the wire-resistance type. An L-shaped lever arm magnifies the extension or deflection of the specimen. Its end acts as the movable arm of a potentiometer which may be placed in any of the well-known bridge circuits to measure resistance or potential changes. An arrangement of this type is used in Zisman's compressibility tester (Fig. 9-13).[6a] In the condenser microphone extensometer,[6b] small variations of distance of two condenser plates are converted into changes of capacity; in the magnetic gauges[6c] the inductance of iron-core solenoids is varied by changes in position of an iron armature. The solenoids may be energized with A.C. of intermediate frequency and may be used in any one of the well-known inductance bridges. Fig. 9-12 shows a Westinghouse extensometer, which, for slow deformations, may be operated from a 60 cycle current source.
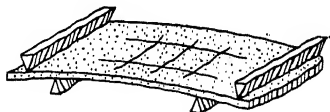
FIG. 9-10. Longitudinal and transverse curvature of bent plate.
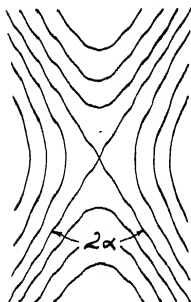
FIG. 9-11. Patterns of interference fringes of rock slab when bent as in Fig. 9-10.

[6] T. C. Richards, Phys. Soc. Proc., **45**(1)(**246**), 70–79 (Jan. 1, 1933).

[6a] W. A. Zisman, Proc. Nat. Acad. Sci., **19**, 653, 666, 680 (1933).

[6b] A detailed discussion of capacitance strain gauges, with literature, is given on pp. 931-932.

[6c] Inductance gauges are discussed further on pp. 932-933.

1. *Laboratory methods.*　　(*a*) *Static determinations* involve measurements of stress-strain relations, utilizing tension, compression, bending, or torsion.

Tension and contraction tests: Samples are used in the form of long bars or drill cores in any of the Olsen, Riehlé, or Emery machines. The strains may be measured by rocking-mirror devices, interferometric gauges, or condenser-microphone attachments. The contraction is obtained by means of a lever device measuring the reduction in diameter with two contact arms, provided with mirror magnification. From the load P, the area S, the original length l, and the change in length Δl, Young's modulus may be calculated:

$$\mathbf{E} = \frac{P}{\mathbf{S}} \cdot \frac{l}{\Delta l}. \qquad [9\text{-}3]$$

Poisson's ratio is:

$$\sigma = \frac{\dfrac{\Delta d}{d}}{\dfrac{\Delta l}{l}}. \qquad [9\text{-}4b]$$

These two constants are sufficient for isotropic media to calculate all other elastic coefficients and, together with the densities, the velocities of the longitudinal and transverse waves.

FIG. 9-12. Westinghouse magnetic strain recorder. (*O*, oscillograph; *R*, rectifier; *P*, potentiometer.)

Compressibility tests: Although the compressibility may be calculated from Young's modulus and Poisson's ratio, it is preferable to measure it separately. For most compressibility tests the sample is used in some liquid which is compressed in a strong steel cylinder. A correction must be applied for the expansion of the steel cylinder and for the compression of the liquid. Bridgman used chrome-vanadium steel for the cylinder; Adams used *n*-butyl-ether for the liquid. A simple way of determining the volume change is to measure the movement of the piston compressing the liquid. The distance the piston should move if the liquid alone were in the cylinder may be calculated from the dimensions of the steel cylinder and the compressibility of the liquid, or it may be measured directly. Since the volume of the sample is also reduced, the difference of the piston movement without sample and the movement with sample gives the volume reduction ΔV of the specimen. Then the compressibility,

$$\mathbf{K} = \frac{\Delta V}{V \cdot P}. \qquad [9\text{-}10]$$

The piston displacement is measured by one of the optical or electrical methods described before; the pressure P is read (Adams)[6d] on a resistance pressure gauge meter immersed in the liquid. Other investigators have used the reduction in length of the specimen for a determination of the cubic compressibility. They measured the pressure of the liquid with a manometer and determined the reduction of length of the specimen by a contact bar whose motion was magnified by optical or electrical means. Amagat carried this rod outside the pressure cylinder and measured its displacement optically; Bridgman magnified its movement by a lever arm acting as the movable arm on a potentiometer; Zisman used the arrangement shown in Fig. 9–13 with the transmission mechanism enclosed in the pressure bomb. If Δl is the reduction of length of the specimen, the linear compressibility may be reduced to the cubic compressibility, since

$$\mathbf{K} = \frac{3\Delta l}{lP}. \qquad (9\text{-}21)$$

Because of the many variables and correction factors entering into such compressibility tests, it has become general practice to use an iron cylinder of known compressibility as a reference standard. Considerable magnification (of the order of one million) is required to measure changes of length accurately.

Bending (transverse) tests: These tests may be divided into two groups. In the first, Young's modulus alone is determined; in the other, both Young's modulus and Poisson's ratio are obtained. Tests in the first group are made with bending (beam testing) ma-

Fig. 9-13. Zisman's resistance extensometer for compressibility tests.

chines. Rock specimens in the form of slabs are clamped on one end or supported on knife edges on both ends. The last procedure is not so favorable as the first because the deflection is only $\frac{1}{16}$ of that observed at the free end of a clamped beam. Deflections are measured optically by mirror devices or by condenser-microphone arrangements. If J is the moment of inertia of the beam section

[6d]F. D. Adams and E. G. Coker, Pub. No. 46, Carnegie Inst., 1906; Gerl. Beitr., **31**, 315–321 (1931). L. H. Adams and R. E. Gibson, Proc. Nat. Acad. Sci., **12**, 275 (1926); **15**, 713 (1929). L. H. Adams and E. D. Williamson, J. Frank. Inst., **195**, 475–529 (1923). L. H. Adams, E. D. Williamson, and J. Johnston, J. Am. Chem. Soc., **237**, 7–18 (Jan., 1939).

under test and if its deflection is d with the load P concentrated at its end,

$$d = \frac{1}{3} \frac{Pl^3}{EJ}. \tag{9-22a}$$

Since the moment of inertia $J = a^3b/12$ for a rectangular section, and $J = r^4\pi/4$ for a circular section, the deflections are:

$$d = \frac{4l^3P}{Ea^3b} \text{ for a rectangular section,} \tag{9-22b}$$

where b = breadth, a = thickness, and

$$d = \frac{4}{3} \frac{l^3P}{Er^4\pi} \text{ for a circular section.} \tag{9-22c}$$

If the specimen is supported on either end by knife edges, the deflection

$$d = \frac{1}{48} \frac{Pl^3}{EJ}. \tag{9-22d}$$

Hence Young's modulus

$$E = \frac{1}{4} \frac{l^3P}{a^3bd} \text{ for a rectangular section and}$$

$$E = \frac{1}{12} \frac{l^3P}{r^4\pi d} \text{ for a circular section.}$$

Deflections may be measured with two mirrors fastened to the ends of the specimen. If the light is reflected from one to the other, the angle is given by eq. (9-20), and Young's modulus

$$E = \frac{3}{4} \frac{l^2}{a^3b} \frac{\dot{P}}{\tan \alpha}. \tag{9-23}$$

Eq. (9-22d) holds for beams supported on knife edges; for fixed ends the factor is $\frac{1}{192}$ instead of $\frac{1}{48}$.

By the second group of flexure tests, both Young's modulus and Poisson's ratio are obtained. A slab is cut from the rock under investigation, supported on either end by knife edges, and a load is applied on the extreme ends, outward from the supporting knife edges (see Fig. 9-10). Both longitudinal and transverse strains are measured with an interferometer. The top of the rock slab is polished, and a plane-parallel glass plate is laid on top of it. Interference fringes resulting from the bending of the beam are observed or photographed. A diagram of the apparatus has been

given by Richards.[7] Poisson's ratio follows from the angle of spread of the asymptotes of the fringe hyperbolas (see Fig. 9–11), $\sigma = \tan^2 \alpha$. The curvatures in the longitudinal and transverse directions may be determined from the fringe patterns, according to the relation

$$C = 4\lambda \mathrm{n}/d_\mathrm{n}^2 , \qquad (9\text{--}24a)$$

where C is the curvature, λ the wave length of the interferometer light, n a given number of the fringe used to calculate C, and d_n is the distance apart of the vertices of the nth pair of fringes. The ratio of the curvatures is Poisson's ratio,

$$\sigma = \frac{C_2}{C_1}; \qquad (9\text{--}24b)$$

and Young's modulus

$$\mathrm{E} = \frac{3\mathrm{D}}{2b\hbar^3 C_1}\frac{1 - \sigma^2}{1 + \sigma^2}, \qquad (9\text{--}24c)$$

where b = width, D = couple, and $2\hbar$ = thickness.

Torsion tests: For static torsion tests, the specimen is clamped in a horizontal position, and a twist is applied to one end in a torsional testing machine. The torsion of two sections with respect to each other is obtained by a detrusion meter provided with mirror multiplication. Since the torsion tests furnish the modulus of rigidity, and since Young's modulus may be obtained from extension tests, Poisson's ratio and all other desired constants may be calculated. The angle of twist between two sections of a bar separated by the length l is

$$\varphi = \frac{\mathrm{D}l}{J_p \mu}, \qquad (9\text{--}25a)$$

where D is the rotational couple and J_p the polar moment of inertia. Hence, the modulus of rigidity for a round bar with the radius r is

$$\mu = \frac{57.3}{\varphi}\cdot\frac{2}{\pi}\cdot\frac{l}{r^4}\,\rho P \qquad (9\text{--}25b)$$

(with ρ = radius of gyration, P = force), when the angle φ is expressed in degrees.

(b) *Dynamic laboratory tests.* Elastic constants of rocks may be determined from the natural frequencies of their transverse, torsional, and longitudinal vibrations. All these determinations are comparatively simple, since only one parameter, time (or its reciprocal, frequency), is

---

[7] *Loc. cit.*

involved. The procedure is to drive the specimen with impulses of continuously varying frequency until maximum amplitude is obtained. With sufficient accuracy, this *resonance* frequency may be considered equal to the natural frequency. Measurements of a complete resonance curve give interesting information on the damping within the specimen.

Transverse vibration tests: These tests[7a] are the dynamic equivalent of the tests referred to on page 459. They may be applied to bars supported on one end or on both ends. As was stated in connection with eq. (9–17), the natural frequency ω_0 of an elastic system oscillating with the load m is given by

$$\omega_0 = \sqrt{\frac{c}{m}} = \sqrt{\frac{P}{dm}}, \qquad (9\text{–}26a)$$

where the spring constant, or force per unit deflection P/d,

$$c = \frac{\frac{1}{4}Eba^3}{l^3} \qquad (9\text{–}26b)$$

for a bar clamped on one end. For slabs suspended between two points, similar relations may be worked out from the formulas previously given for the static deflection.

The above relations hold only if the mass may be considered as concentrated on one end. The transverse frequency of unloaded bars clamped on one end is given by

$$\omega_0 = \frac{r}{2}\left(\frac{n}{l}\right)^2 \sqrt{\frac{E}{\delta}} \quad \text{(for the circular [radius } r\text{])}$$

and

$$\left.\vphantom{\begin{array}{c}1\\1\\1\\1\\1\end{array}}\right\} \qquad (9\text{–}26c)$$

$$\omega_0 = \frac{a}{2\sqrt{3}}\left(\frac{n}{l}\right)^2 \sqrt{\frac{E}{\delta}} \quad \text{(for the rectangular)}$$

sections, a being the dimension of the side in the plane of oscillation. For the fundamental, n is 1.875; for the first harmonic, 4.694; $\sqrt{E/\delta}$ is known as the "bar" velocity (see eq. [9–29a]).

Torsional vibrations: The specimens under tests are suspended in a vertical position and are loaded with a disk whose moment of inertia K is known or may be determined. This method is well adapted to long-drill cores. The general relation for the period of a torsional system is $T = 2\pi\sqrt{Kl/\mu J_p}$, where l is the length of the specimen and J_p the polar

---

[7a] G. Grime, Phil. Mag,, **20**, 304 (1935), **23**, 96 (1937). W. H. Swift, Phil. Mag., **2**, 351–368 (Aug., 1926).

moment of inertia ($\frac{1}{2}\pi r^4$ for a round bar).   Hence, the modulus of rigidity for a round bar

$$\mu = 8\pi \frac{l}{r^4} \frac{K}{T^2}. \tag{9-27}$$

For a round disk attached as a revolving mass, the moment of inertia is $K = \frac{1}{2}\rho^2 m$ (ρ = disk radius).

The torsional frequency of a specimen and thus the modulus of rigidity may also be determined[8] by a resonance method analogous to the one described in the next paragraph.   In a drill core, a saw cut is made on one end and a strip of iron is fastened rigidly in it.   This strip is placed between the poles of two electromagnets.   An identical arrangement is provided at the other end of the specimen.   The electromagnets on one side are excited by a variable-frequency oscillator, while those on the other side are connected to an amplifier and rectifier meter.

The torque produced on one end is transmitted to the other.   Its amplitude is greatest when the natural torsional frequency of the specimen coincides with the driving frequency.   A bar clamped at its center has a node at that point so that its length l is one-half the wave length.   Since the torsional wave velocity is $\sqrt{\mu/\delta}$ and is equal to the product of wave length and frequency,

$$f_0 = \frac{1}{2l} \sqrt{\frac{\mu}{\delta}}, \tag{9-28}$$

where f_0 represents natural frequency, l length, and μ the rigidity modulus as before.

Longitudinal vibrations: The specimen, preferably in the form of a rod or drill core, is arranged horizontally, clamped at its center, and excited to oscillate horizontally.   This may be done by attaching a piece of iron to one of the faces and by exciting this end with an iron-core solenoid supplied with current of variable frequency.   A better arrangement is to attach a light coil to each side of the specimen, each coil being suspended in the field of a dynamic speaker (Fig. 9-14).   One coil is supplied with current of variable frequency and thus drives the specimen.   In the other coil, currents are induced which depend on the frequency and amplitude of motion of the other end.   Resonance is again determined by maximum amplitude.[9]

Another way of setting the specimen into oscillation is by electrostatic coupling.   Fig. 9-15 shows an arrangement proposed by Ide[9a] for such ob-

[8] J. M. Ide, Geophysics, **1**(3), 349 (Oct., 1936).

[9] B. B. Weatherby and L. Y. Faust, A.A.P.G. Bull., **19**(1), 12 (Jan., 1935).

[9a] J. M. Ide, Proc. Nat. Acad. Sci., **22**, 81, 482 (1936); Rev. Sci. Instr., **6**, 296-298 (Oct., 1935); Jour. Geol., **45**, 689-716 (Oct., 1937).

servations. The oscillations of the speci-
men are picked up by a piezo-electric crys-
tal cemented to the specimen (or by a sepa-
rate microphone), are amplified and read on
an output meter.

Longitudinal "bar" vibrations do not de-
pend on Poisson's ratio; their velocity is
given by

$$v_u = \sqrt{\frac{E}{\delta}}. \qquad (9\text{–}29a)$$

Since, as before, for a bar of the length l,
$l = \frac{1}{2}\lambda$ and $v = \lambda f_0$, the longitudinal bar
velocity

FIG. 9-14. Apparatus for
electromagnetic determination
of natural bar frequency (after
Weatherby and Faust). (B,
bar; M, magnet; C, coil; O, os-
cillator; S, supporting knife
edge; A, amplifier; m, meter;
r, rectifier.)

$$v_u = 2lf_0. \qquad (9\text{–}29b)$$

Methods for determining damping from resonance curves are discussed
on page 481.

Rebound observations: Elastic properties of rocks may be determined by
observations of physical parameters related to the rebounding of a steel
ball dropped from a given height. Two methods have been used: (1)
measuring the size of the imprint, and (2) measuring the height of
rebound.[10]

If a steel ball of radius ρ_b, mass m_b, Young's modulus E_b $(= 22 \cdot 10^{11})$,
dropped from a height H on the rock whose surface is blackened, leaves an
imprint of the radius r, then Young's modulus of the rock is given by

$$\frac{1}{E} = \frac{16r^5}{13.5m_b 2gH\rho_b^2} - \frac{1}{E_b}. \qquad (9\text{–}30)$$

FIG. 9-15. Apparatus for electrostatic
determination of natural bar frequency
(after Ide). (O, oscillator; C, con-
denser; D, dielectric; F, foil; B, base
plate; V, polarizing voltage; S, speci-
men; Cr, crystal; A, amplifier; M, out-
put meter.)

If a steel ball is dropped from a
height H on the rock surface and re-
bounds to the height h (see Fig. 9-
16), the so-called "restoration" coeffi-
cient is

$$q = \sqrt{\frac{h}{H}}. \qquad (9\text{–}31)$$

The exact relation between the resto-
ration coefficient and Young's modu-
lus has not been definitely deter-

[10] J. Roess, Union Geod. and Geophys.
Internat. Assoc. Seism. Ser. A, Trav. Sci.,
Fasc., **13,** 3-69 (1935).

mined.   Roess established an empirical relation (Fig. 9–17) by determining both q and E for the same rocks by the two methods described above.

Rebound observations are applicable only to fine-grained materials.   If the ball hits a large mineral grain, the elastic coefficient of the grain and not that of the aggregate is obtained. Another difficulty arises from the fact that the surface constitution of the rock must not deviate from the composition of its interior; otherwise the restitution coefficient would express surface conditions only.   As a matter of fact, rebound observations are used in the metallurgy of steel for hardness determination.
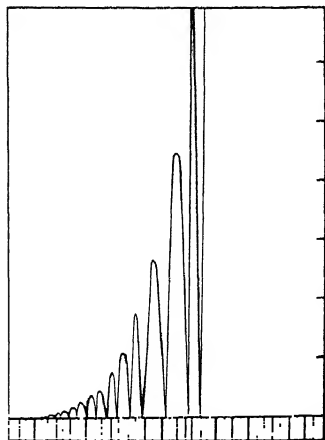
Fig. 9-16.   Record of steel ball rebounding from surface of marble slab (after Roess).

2. *Field methods (velocity determinations)*. Field determinations of *horizontal velocities* are made by measuring the time interval which elapses between the firing of a shot and the arrival of the longitudinal or transverse energy at the location of a detector. A shot point may be used with a number of
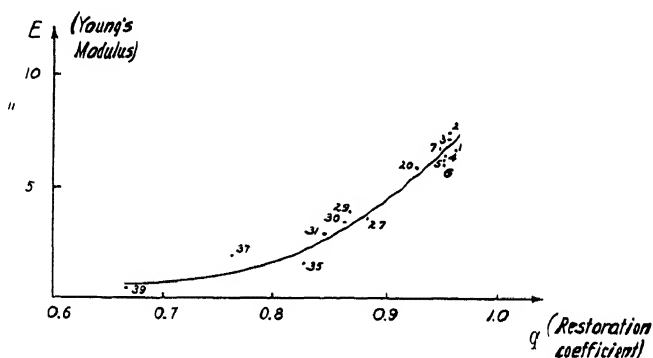
FIG. 9-17.   Young's modulus **E** as a function of restoration coefficient (q) for some homogeneous rocks.   (Numbers refer to tabulation of rock specimens, pp. 11 and 12, Roess' article.)   (After Roess.)

detectors, and the latter may be moved when one spread is not sufficient to cover all desired distances.   Another method is to leave the detectors at their places and to move the shot point.   In practice, the application of this method is not quite so easy as it may appear.   Errors of instrumental and geologic nature occur.   The former arise from (1) inaccuracies in the determination of the exact instant of the shot, (2) errors in the tim-

ing device, and (3) errors in timing the impulses in the record. The shot instant may be transferred to the recorder by wire or radio. For short distances this method is generally not accurate enough; an insensitive seismograph near the shot point is preferable, as it will record the actual time when the energy is impressed on the ground.

Errors in the timing device can generally be kept down sufficiently to make possible time determinations with an accuracy of 1 in 10,000 if necessary. The "timing" of the impulses in the record is generally the most difficult part of the problem (as seen in some of the records published by Weatherby, A.A.P.G. Bull., Jan. 1934). Unless the sharpness of the first impulses can be improved, there is no object in increasing the accuracy of the timer and shot instant transmission to more than $\frac{1}{1000}$ of a second. When a number of seismographs are used, it is necessary to balance their phase shifts and to determine the corresponding parallax corrections.

More serious than these instrumental difficulties are geologic factors which often make it difficult to determine reliable velocities. The surface of the rock whose wave speed is to be determined must be free from cover and reasonably unweathered so that true velocities may be obtained. It is, of course, possible to obtain velocities of inaccessible layers from the travel time curve. However, these velocities are true velocities only if the layers are horizontal. Dip may be eliminated by shooting the profile up and down dip.

Vertical velocity determinations through formation (that is, generally at right angles to the bedding planes) are made in connection with weathered-layer-correction shooting in shallow (25 to 150 foot) holes and in connection with average-velocity determinations in deep wells. For the latter a detector is lowered into the well to various depths and shots are fired either near the well or at a distance corresponding to one-half the general spread distance, to simulate the direction of the ray in its travel to or from the reflecting bed. By means of the travel time to various depths, the average velocity from the surface to the formation in question or the differential velocities between strata are calculated. This method is discussed further in Chapter 11.

Tables 45 through 55 list the elastic moduli and wave velocities for the more important minerals, rocks, and formations. In Table 45 are listed the elastic moduli of minerals, and in Table 46 are given elastic moduli of igneous, metamorphic, and sedimentary rocks.[11] Table 47 shows velocities of longitudinal waves for the formations nearest the surface, particularly the weathered layer; Table 48, the longitudinal wave speeds for alluvium and glacial drift; Table 49, the longitudinal wave velocities for sands,

---

[11] Largely after Adams, Adams and Gibson, Adams and Williamson, Zisman, Richards, Don Leet, Born and Owen.

clays, and marls; Table 50, those for sandstones and shales; Table 51, the velocities in limestones, anhydrite, salt, and the like; and Table 52 represents longitudinal velocities for igneous and metamorphic rocks.   A number of selected values for transverse waves are given in Table 53.   Table 54 shows some values for Rayleigh waves, and Table 55 contains vertical velocities, that is, longitudinal velocities determined by measuring travel times at right angles to the bedding planes in wells.

<div align="center">

Table 45

ELASTIC MODULI OF MINERALS

(at atmospheric pressure)

</div>

Mineral	Compressibility $\times 10^{12}$	Young's Modulus $\times 10^{-11}$
Feldspar:		
Orthoclase	1.68	8.23
Pyroxenes & Amphiboles:		
Augite	1.07	(13)
Olivine	0.85	...
Mica:		
Phlogopite	2.34	5.90
Other Minerals:		
Quartz	2.70	5.12
Pyrite	0.71	19.5
Magnetite	0.54	25.2
Calcite	1.39	9.90
Gypsum	2.5	5.51
Rock salt	4.12	3.35
Ice	13.7	(1)

<div align="center">

Table 46

ELASTIC MODULI OF ROCKS

</div>

Rock	Locality	Investigator	Compressibility $\times 10^{12}$	Young's Modulus $\times 10^{-11}$
		Igneous Rocks		
Quincy granite	Massachusetts	Leet	2.28	4.3
Tishomingo granite	Oklahoma	Born & Harding	1.93	3.29 (field)
				4.55 (lab.)
Diorite		Adams & Williamson	1.62	...
Gabbro		"	1.28	10.8
Norite	Ontario	Zisman	1.65	8.05
Extrusives				
Andesite		Adams & Gibson	4.3	6.9
Diabase	Maine	Zisman	1.45	10.2
Basalt		Adams & Gibson	1.36	10.15
Volcanic Glasses				
Obsidian		"	2.86	(4)
		Metamorphic Rocks		
Quartzitic slate (Archean)		Adams & Gibson	2.08	6.65
Gneiss		Zisman	2.07	3.28
Chloritic slate		Adams & Gibson	1.97	7.0
Quartzite (Triassic)		"	1.88	7.34
Graywacke (Devonian)		"	1.82	7.6

ı 46—*Concluded*

ELASTIC MODULI OF ROCKS

Rock	Locality	Investigator	Compressi- bility $\times 10^{12}$	Young's Modu- lus $\times 10^{-11}$
		Sedimentary Rocks		
Sandstones Sandstone (Triassic)		Adams & Gib- son	13.5	1.02
Sandstone (Tertiary)		"	8.35	1.65
Weathered sandstone (Tertiary)	California	Heiland	. . .	0.25
Limestones and Anhydrite:				
Limestone	S. W. Persia	Richards	2.99	5.3–5.5
Limestone (Devo- nian)		Adams & Gib- son	1.70	8.15
Anhydrite	S. W. Persia	Richards	1.69	7.2–7.4

Rock	Locality	Investigator	Rigidity Modulus $\times 10^{-11}$	Young's Modulus $\times 10^{-11}$	Poisson's Ratio
		Unconsolidated Formations			
Overburden (river de- posits)	Los Angeles, Calif.	Heiland	0.010	0.030	0.45
Loess (dry)	Leine Valley, Germany	Ramspeck	0.011	0.033	0.44
Gravel	Werra Valley, Germany	"	0.0059	0.017	0.47

Tables 47–52

VELOCITIES OF LONGITUDINAL WAVES

Table 47

WEATHERED SURFACE LAYER, AIR, WATER

Formation	Locality	Investigator	Longitudinal Wave Velocity	
			m./sec.	ft./sec.
Weathered surface layer (Pleisto- cene)	E. Alberta, Canada	Heiland	169–305	555–1000
Dry surface sands	California	Rieber	330	1083
Air			$330.8 + 0.66t^a$	$1089 + 0.22t^a$
Weathered layer	E. Colorado	Pugh	335–1690	1099–5545
Loess	Jena, Germany	Meisser & Martin	375–400	1230–1312
Dry surface soil	California	Rieber	600	1969
Weathered surface rocks	Oklahoma	Goldstone	610	2000
Loam (wet)	Australia	Edge & Laby	761	2497
Water (fresh)	. . . . .	. . . . .	1435	4708
Water at 14°C. at 20 m	Germany	Beuerman	1475	4840
Water (sea)	. . . . .	. . . . .	1480–1490	4856–4889

ı $t =$ temper.

TABLE 48

ALLUVIUM, DILUVIUM—GLACIAL DRIFT

FORMATION	LOCALITY	INVESTIGATOR	LONGITUDINAL WAVE VELOCITY	
			m/sec.	ft./sec.
Alluvium				
Alluvium	Spain	Siñeriz	550–650[a]	1805–2133[b]
Tertiary alluvia	Str. Gibraltar	Devaux	800–1500	2625–4921
Alluvium	Diaz Lake, Calif.	Gutenberg	900	2953
Alluvium	Owens Valley, Calif.	Buwalda & Wood	1000	3280
Alluvium at depth	Spain	Siñeriz	1100–2360	3609–7743
Diluvium				
Diluvial sands	Sperenberg, Germany	Reich & Schweydar	855–1011	2805–3317
Diluvial sands (wet)	Kummersdorf, Germany	Reich	1430	4692
Diluvial sands (wet)	San Joaquin Valley, Calif.	Rieber	1650–1950	5414–6398
Glacial Drift				
Glacial drift	E. Alberta	Heiland	484–508	1588–1667
Glacial drift	N. Germany	Barsch & Reich	1700	5578

[a] Round figures such as these indicate values by investigator.
[b] These figures are the equivalent in feet (from conversion tables). Investigators in countries using metric systems usually give velocities in m .sec.$^{-1}$; those in countries using the English system, in ft..sec.$^{-1}$

TABLE 49

SANDS, CLAYS, MARLS

FORMATION		INVESTIGATOR	AVE VELOCITY	
			m/sec.	ft./sec.
Sands and Clays				
Dune sand	Denmark	Brockamp	500	
Cemented sand	Australia	Edge & Laby	852–975	2795–3200
Sandy Clay	"	"	975–1160	3200–3806
Pure sands	Gibraltar	Devaux	1000	3280
Cemented sandy clay	Australia	Edge & Laby	1160–1280	3806–4200
Clayey sands	Gibraltar	Devaux	1400	4593
Miocene sands and clays (wet)	N. Germany	Reich	1600–1700	5250–5578
Oligocene clays	Jueterbog, Germany	Angenheister	1900	6234
Marls				
Eocene marls	N. Germany	Reich	1800	5906
Marl	Gibraltar	Devaux	2000–2500	6562–8202
Marl	Spain	Siñeriz	2000–3800	6562–12467
Eocene marls	Gibraltar	Devaux	2400	7874
Calcareous marl	Spain			

<center>Table 50</center>

<center>SANDSTONES AND SHALES</center>

Formation	Locality	Investigator	Longitudinal Wave Velocity	
			m/sec.	ft./sec.
Ribstone Creek sandstone (Upper Cretaceous)	E. Alberta	Heiland	931–1130	3055–3708
Tertiary sands & shales	Los Angeles Basin	Wood & Richter		
0–200 m			1000±	3280±
200–320 m			1900	6234
320–860 m			2100	6890
860–1650 m			2900	9514
1650–? m			3500	11483
Sandstone	Gibraltar	Devaux	2000	6562
Middle Bunt sandstone (Triassic)	Jena, Germany	Meisser & Martin	2000–2800	6562–9187
Pennsylvanian sandstone, shales, and limes	Oklahoma	Goldstone	2130	6989
Sandstone conglomerate	Australia	Edge & Laby	2400	7874
Upper Miocene (in part)	Texas Gulf coast	Barton	2400–2700	7874–8858
Middle Eocene	Gulf coast	"	4200±	13780±

<center>Table 51</center>

<center>LIMESTONE, GYPSUM, ANHYDRITE, CHALK, SALT</center>

Formation	Locality	Investigator	Longitudinal Wave Velocity	
			m/sec.	ft./sec.
Limestone	Island of Djerba	Ceccaty & Jabiol	1,000–1,103	3,280–3,619
Cretaceous limestone	France	Maurin & Eblé	2,140	7,021
Carboniferous limestone	N. Germany	Barsch & Reich	3,000–3,600	9,841–11,812
Gypsum	Spain	Siñeriz	3,100	10,171
Soft limestone	Gibraltar	Devaux	3,200–3,600	10,500–11,812
Gypsum	Spain	Siñeriz	3,350–3,600	10,991–11,812
Limestone[a] surface velocities	Locations in Miss., La., Tex., N.	Weatherby & Faust		
Cretaceous (Edwards)	Mex., Okla., Kan., Colo.,	"	3,352	11,000
Pennsylvanian (Belle City)	and Penn.	"	4,572	15,000
Mississippian (Mayes)	"	"	3,810	12,500
Devonian (Hunton)	"	"	4,267	14,000

[a] These velocities may be in error as much as 305 m./sec. (or 1000 ft./sec.) because of surface weathering and erosion.

TABLE 51—*Concluded*

LIMESTONE, GYPSUM, ANHYDRITE, CHALK, SALT

FORMATION	LOCALITY	INVESTIGATOR	LONGITUDINAL WAVE VELOCITY	
			m/sec.	ft./sec.
Ordovician (Viola) Cambro-Ordovician (Arbuckle)	Locations in Miss., La. Tex., N. Mex., Okla. Kan., Colo. and Penn.	Weatherby & Faust	5,090 5,303	16,700 17,400
Anhydrite	Spain	Siñeriz	3,400–4,400	11,155–14,436
Zechstein gypsum	Sperenberg, Germany	Schweydar Reich	3,500	11,483
Arbuckle limestone (Cambro-Ordovician)	Tishomingo, Okla.	Weatherby, Born, & Harding	4,090 across bedding plane	13,430
			5,320 along bedding plane	17,430
Leesport lime	Pennsylvania	Ewing	6,400	20,998
Chalk				
Chalk	Denmark	Brockamp		7,218
Pecan Gap chalk (Cretaceous)	Texas	Barton	3,000–3,600	9,843–11,812
Chalk (subsurface)	Texas		3,020–4,200	9,908–13,780
Austin chalk (Cretaceous)	Texas		3,600–4,200	11,812–13,780
Chalk	Austria	Brockamp	4,200	13,780
Salt				
Salt in 710 m depth (= 2,300 ft.)	Rhoen, Germany	Meisser	4,450	14,600
Salt and anhydrite (Triassic)	Jueterbog, Germany	Angenheister	4,500	14,765
Rock salt of domes	Texas	Barton	4,720–5,200	15,486–17,060
Salt beds		Siñeriz	5,000–7,000	16,405–22,967
Salt beds			5,300–6,300	17,388–20,670
Salt beds			5,500	18,045
Salt beds			5,500–5,900	18,045–19,358
Salt beds			5,700–6,950	18,702–22,803
Salt beds			6,200–7,700	20,342–25,264

TABLE 52

IGNEOUS[12] AND METAMORPHIC ROCKS

| FORMATION | LOCALITY | INVESTIGATOR | LONGITUDINAL WAVE VELOCITY | |
			m./sec.	ft./sec.
Igneous Rocks				
Granite	Gibraltar	Devaux	4,000	13,124
Tishomingo gran-ite	Tishomingo, Okla.	Weatherby, Born, & Harding	4,570–5,230	14,880–17,150
Rönne granite	Denmark	Brockamp	4,800	15,749
Quincy granite	Massachusetts	Leet & Ewing	4,960± 20	16,273± 66
Westerly granite	"	"	5,000± 40	16,405± 131
Rockport granite	"	"	5,080± 10	16,667± 33
Granite	Yosemite Val-ley, Calif.	Gutenberg, Buwalda, & Wood	5,100–5,400	16,733–17,717
Rockport granite	Massachusetts	Leet	5,140	16,864
"Gestreifter" granite	Denmark	Brockamp	5,150	16,897
Igneous basement	Venezuela	Allen	5,460	17,914
Crystalline rock	Gibraltar	Devaux	5,500	18,045
Granite	Australia	Edge & Laby	5,630	18,472
Granite facies	San Gabriel Dam to Pasa-dena, Calif.	Wood & Rich-ter	5,670	18,603
Igneous basement (not defined)	Venezuela	Allen	6,510	21,359
Granodiorite	Australia	Edge & Laby	4,570	14,993
Basalt	California	Rieber	3,600	11,811
Metamorphics				
Crystalline gneiss and schist	Alabama Hills, Calif.	Gutenberg, Buwalda, & Wood	3,100	10,170
Hard slate	Australia	Edge & Laby	3,200–3,500	10,500–11,483
Hornfels slate	"	"	3,500–4,420	11,483–14,501
Green slate	Denmark	Brockamp	4,000	13,124
Slates (Cambrian)	Spain	Siñeriz	4,500–5,000	14,764–16,405
Slate and quartz-ite	N. Germany	Barsch & Reich	5,000	16,405
Massive gneiss	Spain	Siñeriz	5,150–7,500	16,896–24,606

[12] Rock types arranged in order of decreasing acidity.

TABLE 53

ELASTIC VELOCITIES OF TRANSVERSE WAVES

| FORMATION | LOCALITY | INVESTIGATOR | TRANSVERSE WAVE VELOCITY | |
			m./sec.	ft./sec.
Tishomingo gran-ite	Tishomingo, Okla.	Weatherby, Born, & Harding	2,130–2,420	7,000–7,950
Rockport granite	Massachusetts	Leet	2,700	8,858

TABLE 53—*Concluded*
ELASTIC VELOCITIES OF TRANSVERSE WAVES

FORMATION	LOCALITY	INVESTIGATOR	TRANSVERSE WAVE VELOCITY	
			m/sec.	ft./sec.
Basement rocks	California	Wood & Richter	3,250	10,663
Sudbury norite	Ontario	Leet	3,490	11,450
Limestone	S. W. Persia	Richards	2,710-2,800-2,930	8,890-9,186-9,613
Leesport lime	Pennsylvania	Ewing	3,260	10,696

TABLE 54
RAYLEIGH WAVE VELOCITIES

FORMATION	LOCALITY	INVESTIGATOR	TRANSVERSE WAVE VELOCITY	
			m/sec.	ft./sec.
Overburden[a]	Los Angeles, Calif.	Heiland	198	650
Gravel[a]	Werra Valley, Germany	Ramspeck	180	590
Loess[a]	Leine Valley, Germany	"	260	860
Sediments (alluvium)	Ventura Basin, Calif.	Gutenberg, Buwalda, & Wood	330	1083
Sediments (alluvium)	Los Angeles Basin, Calif.	"	550	1805
Limestone	S. W. Persia	Richards	2160	7087
Rockport granite	Massachusetts	Leet	2190	7185
Sudbury norite	Ontario	"	2790	9154

[a] From vibrator measurements.

TABLE 55
VERTICAL VELOCITIES OF LONGITUDINAL WAVES[12a]

FORMATION	VELOCITIES (ft·sec.⁻¹) IN SHALES AND SANDSTONES			VELOCITIES (ft·sec.⁻¹) IN LIMESTONES		
	0-2000 ft.	2000-3000 ft.	3000-4000 ft.	At Surface	At Depth (Mean Depth of Section)	
Pleistocene to Oligocene	6,500	7,200	8,100	. . .	. . .	. . .
Eocene	7,100	9,000	10,100	. . .	. . .	. . .
Cretaceous	7,400	9,300	10,700	11,000	13,500	(3,300)
Permian	8,500	10,000	. . .	. . .	15,500	(3,900)
Pennsylvanian	9,500	11,200	11,700	15,000	15,500	(3,000)
Mississippian	. . .	. . .	. . .	12,500	17,000	(4,200)
Devonian	13,300	13,400	13,500	14,000	17,500	(4,500)
Ordovician	. . .	. . .	. . .	16,700	20,000	(4,000)

[12a] Data from fifty wells in Mississippi, Louisiana, Texas, New Mexico, Oklahoma, Kansas, Colorado, and Pennsylvania, from B. Weatherby and L. Y. Faust.

D. Factors Affecting Elastic Properties of Rocks

1. In *igneous rocks*, the rigidity, Young's modulus, and the velocity of longitudinal waves all increase with a decrease in *silica content*; this behavior is in harmony with that of the silicate minerals and holds for both intrusive and extrusive igneous rocks.

Intrusive and coarse-grained rocks generally have a greater elasticity than do extrusive rocks, since they contain less liquo-viscous matter. It is possible that the difference is partially due to differences in porosity. The variation of elasticity with *degree and depth of crystallization* is less pronounced than its variation with silica content.
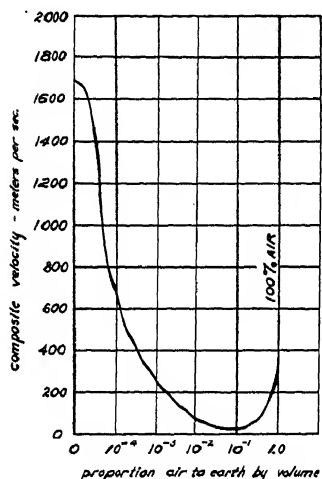
Fig. 9-18. Calculated velocities of sound in air-earth mixtures of various proportions (after Lester).

2. *Sedimentary rocks* show marked differences in elasticity depending on *petrologic composition.* Clastic sediments, such as sands, sandstones, and shales, are less elastic than sediments composed partly or wholly of crystalline matter, such as limestones, dolomites, and the like. Elastic properties of sedimentary rocks depend much more on texture and geologic history than on mineral composition.

The effect of *porosity* and decomposition is to decrease the modulus of elasticity and the wave velocity of a sediment. In areas of great thickness of sedimentary rocks the porosity decreases with depth. Therefore, the modulus of elasticity increases and with it the wave velocity. Related to changes of porosity is the variation of Young's modulus with pressure. For small pressures, rocks appear to be more compressible, since any cavities present have to be closed before the pressure can begin to act on the rock matter itself. Excessive compressibilities resulting from porosity are accompanied by high values of Poisson's ratio. It must be expected that the ratio of longitudinal and transverse wave speeds changes considerably with depth in unconsolidated sediments. The effect of porosity on wave velocity is of practical importance in the near-surface layer, inasmuch as the delay caused by the latter must be eliminated in reflection shooting ("weathered" or "aerated"[13] surface layer). The thickness of this layer is of the order of 5 to 50 feet, and velocities in it range from 500 to 2500 feet per second. Hence, wave speeds less than the speed of

---

[13] O. C. Lester, A.A.P.G. Bull., **16**(12), 1230-1234 (Dec., 1932).

sound in air are possible in this formation. On the assumption that the layer is a liquid mixture of air and earth, the sound velocity

$$\sqrt{} \qquad \frac{E_1 E_2}{(1-p)E_1][p\delta_1 + (1-}} \qquad (9\text{-}32)$$

where E_1 = elasticity of air $(1.2 \cdot 10^6)$; E_2 = elasticity of earth; p = proportion of air to total by volume; δ_1 = density of air (0.0012); δ_2 = density of earth; and $1 - p$ = proportion of earth to total by volume. With a Young's modulus of $5.58 \cdot 10^{10}$ and a density of 1.9, the curve shown in Fig. 9-18 has been computed.

The effect of *moisture*, or water content, on the velocity in sedimentary beds is rather involved. In consolidated beds (sandstones, limestones, slates, schists, porous igneous rocks, and the like) moisture appears to decrease the velocity; in unconsolidated beds moisture increases the velocity appreciably. In reflection work practical use is made of this increase in velocity (and improvement in the transmission characteristics) by
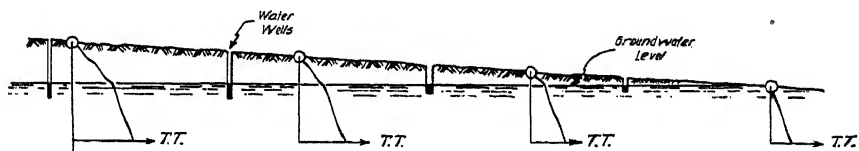
FIG. 9-19. Location of ground water by refraction shooting ($T.T.$ travel time). (After data from Rieber.)

placing the shots in or below the ground-water table.[14] In California Rieber observed distinct breaks in near-surface travel-time curves on the ground-water (see Fig. 9-19).

Many observations of elastic wave speeds appear to indicate a direct relation between geologic age and elasticity. However, the controlling factor is the amount of *diastrophism* to which a formation has been subjected in its geologic history. An increased age merely increases the probability that it has undergone a greater degree of dynamometamorphism. As a consequence velocities in geologic formations change less with depth of burial the greater their geologic age (see Fig. 9-20). Cementation of clastic sediments by mineral solutions during their geologic history is likewise of considerable influence upon their modulus of elasticity.

It follows from the above that metamorphic rocks have an increased elasticity compared with the rocks from which they were derived. Furthermore, their elastic constants are different in the direction of texture

[14] See Lester, *loc. cit.*

than at right angles thereto. In metamorphics the speed of propagation of elastic waves is therefore greater in the direction of strike than at right angles thereto.[15] This *elastic aniso-tropy* also plays a part in sedimentary rocks and accounts for some irregularities encountered occasionally in seismic prospecting. McCollum and Snell[16] found that in shales the velocity parallel to the stratification was as much as 50 per cent higher than at right angles thereto.

FIG. 9-20. Differential velocities (to 2000 feet, from 2000 to 3000 feet, and 3000 to 4000 feet) plotted against mean depths for sections of different ages (after Weatherby and Faust).

With an increase in *depth of burial* the porosities of sedimentary rocks are reduced. This decrease depends on the amount of porosity originally present and the type of sediment concerned. It is caused by the fact that collodial matter in sediments undergoes dehydration with increasing pressure and that their soft mineral grains become granulated.
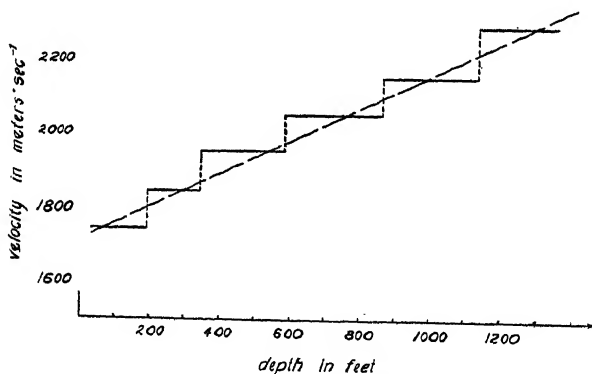
FIG. 9-21. Variation of wave velocity with depth (California). (Adapted from Rieber.)

Fig. 9-21 shows the variation of velocity with depth in the San Joaquin Valley in California for various unconsolidated members of the Tertiary formation (from refraction observations). Not only in sedimentary but

[15] Iso-time curves are elliptical and have the same shape as equipotential curves in anisotropic media (see pp. 700 and 706).

[16] Physics, **2(3)**, 174 (March, 1932).

also in igneous rocks does the velocity of elastic waves change with depth; however, this change is less in the latter than in the former, since igneous rocks have a lesser initial porosity. By laboratory experiments, Adams and Gibson have shown that the compressibility of granites and gabbros drops at first rapidly with an increase in pressure and remains uniform later for greater pressures. The greatest change in compressibility occurs for the first thousand megabaryes, which is equivalent to the first 4 km of depth.

E. Physical Rock Properties Related to Seismic Intensity

To fully characterize the elastic behavior of rocks and formations consideration must be given to the intensity of elastic vibrations in addition to the velocity of propagation. The following physical parameters are significant in this connection: (1) specific acoustic resistance, (2) spreading and dispersion, and (3) absorption and dissipation of energy.

1. *Acoustic (radiation) impedance.* The seismic or acoustic intensity I may be defined as the average rate of flow of energy through a unit section normal to the direction of propagation, or it may be defined as average power transmission per unit area. Power being the flow of energy per second, the intensity is equal to the average energy content, or energy density, W, multiplied by the velocity of an acoustic or seismic wave,

$$I = W \cdot v. \tag{9-33a}$$

Since the kinetic energy is $\frac{1}{2}mv^2$ or, for a simple harmonic motion with the maximum amplitude A and frequency ω, $= \frac{1}{2}mA^2\omega^2$, the energy density per unit volume is $\frac{1}{2}A^2\omega^2\delta$. By substitution of $4\pi^2f^2$ for ω^2, $W = 2\pi^2A^2f^2\delta$, so that eq. (9-33a) becomes

$$I = 2\pi^2A^2v_l \cdot \delta \cdot f^2. \tag{9-33b}$$

If in this equation the factor R is substituted for the product $v_l\delta$, the intensity

$$I = 2\pi^2f^2A^2R. \tag{9-33c}$$

The intensity is thus proportional to the square of the amplitude and to the square of the frequency. Hence, vibrations of high frequency may be accompanied by great intensities, although their amplitude is small. Further, the intensity depends on the factor R, which by analogy with the electrical relation (power $= I^2R$) may be designated as acoustic resistance (in the presence of a reactive component, acoustic impedance). The acoustic resistance referred to unit dimensions is the specific acoustic resistance. Following are the specific acoustic resistances for a number of substances: steel, $390 \cdot 10^4$; rubber, $0.5 \cdot 10^4$; water, $15 \cdot 10^4$; and air, 42.

The acoustic resistance of a medium determines the load or energy output of a sound source within, hence, also, the name radiation resistance or impedance. It also controls the transmission of energy from one medium to another and the ratio of reflected to incident energy. If the specific acoustic resistances of two adjacent media differ considerably, almost no energy is transmitted and nearly perfect reflection occurs. In the case of energy transfer from water to air and vice versa, the amount transmitted is only about 0.12 per cent of the incident energy. The same holds true for the transmission of sound from an orifice or tubing of small diameter to another of larger diameter. The case is analogous to the transmission of sound from a rare to a dense medium.
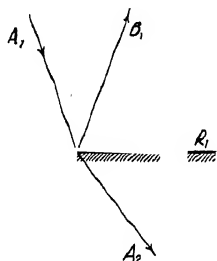
FIG. 9-22. Refracted and reflected rays in two media of different specific acoustic resistances.

In the reverse case, when sound is transmitted from a dense to a rare medium, or from an orifice of large diameter into one of smaller diameter, the transmitted energy is still small as before (most of the incident energy being reflected), and the transmitted amplitude is approximately twice that of the incident amplitude. If a wave passes from a medium with the specific acoustic resistance R_1 to another with the specific acoustic resistance R_2, if A_1 is the amplitude of the direct wave, B_1 the amplitude of the reflected wave in the first medium, and A_2 the amplitude of the energy transmitted into the second medium (see Fig. 9–22) then[17]

$$B_1 = A_1 \frac{R_2 - R_1}{R_2 + R_1} = A_1 \frac{r_{1-2} - 1}{r_{1-2} + 1};$$

$$A_2 = A_1 \frac{2R_1}{R_2 + R_1} = \frac{2}{r_{1-2} + 1},$$

(9-34)

where $r_{1-2} = R_2/R_1$. The power transmission ratio is given by the expression $4/(r_{1-2} + 1)^2$; that is, the energy transmission from one medium into another is poor if the specific acoustic resistances of two adjoining media, such as air and water, differ widely. This may be remedied by placing a third medium of intermediate specific acoustic resistance between

---

[17] See G. W. Stewart and R. B. Lindsay, *Acoustics*, Van Nostrand (1930).

[18] Note the similarity of the coefficient $\frac{R_2 - R_1}{R_2 + R_1}$ with the reflection coefficient $\frac{(\rho_2 - \rho_1)}{(\rho_2 + \rho_1)}$ and the "dimming factor" $2\rho_1/(\rho_2 + \rho_1)$ in the equations involving electrical potentials in media of different resistivities ρ (see p. 712).

them.   If the latter is the geometric mean of the other two specific acoustic resistances and if the thickness of the intermediate layer is one-quarter of the elastic wave length of the intermediate layer, the transmission ratio of energy from water to air may be made equal to unity.   By using rubber for casing materials of listening devices, the intensity of sound reception may be increased considerably; certain types of geophones are not placed in direct contact with the ground but in holes filled with water which acts as an intervening medium to step down the acoustic resistance.

The specific acoustic resistances of the more important rocks and minerals shown in Table 56 have been computed from their velocities and densities.   These values are of interest in connection with reflection shooting, since the ratio of the reflected to the incident amplitude increases with the ratio of the specific acoustic resistances of the formations involved.

<div align="center">

TABLE 56

SPECIFIC ACOUSTIC RESISTANCES

</div>

FORMATION	$R \cdot 10^{-4}$	FORMATION	$R \cdot 10^{-4}$
Basement rocks..............	176	Cretaceous formations........	50
Limestone...................	108	Glacial strata................	20–30
Rock salt....................	100	Top soil.....................	5–10

2. *Spreading, selective scattering, dispersion.*   Since the intensity of sound decreases with the distance from the source, it varies, for spherical waves, inversely as the surface areas of concentric spheres.   For cylindrical waves it varies inversely as the surface areas of concentric cylinders.   Hence, formula (9–33c) becomes, for spherical waves,

$$I = \frac{1}{2}\pi \frac{A^2}{r^2} f^2 R,\qquad\qquad (9\text{-}35a)$$

and, for cylindrical waves,

$$I = \pi \frac{A^2}{r} f^2 R,\qquad\qquad (9\text{-}35b)$$

where R, as before, is specific acoustic resistance, r is distance, f is frequency, and A is amplitude.

Selective scattering is due to reflections and refractions on prominent irregularities.   It is greater for high frequencies than for low frequencies, since the dimensions of the disturbing objects become a controlling factor compared with the wave length.   The amplitude of the scattered waves at any distance from the obstacle is directly proportional to the volume of the obstacle and inversely proportional to the square of the wave length. Hence, the intensity of scattered sound varies inversely as the fourth power of the wave length.   In a medium consisting of numerous small objects,

scattering accentuates the low and attenuates the high frequencies with an increase in distance.

The effects of dispersion on the propagation of seismic waves have been observed in station seismology. The phenomenon is similar to the dispersion of light by refraction. In optics the degree of dispersion depends on the substance and varies inversely as wave length; that is, the index of refraction is greater for small than for large wave lengths. Since light velocity is inversely proportional to the refractive index, the velocity increases with wave length. In other words, both refractive index and dispersion are inversely proportional to wave length, period, and velocity. This is normal dispersion. If the velocity decreases with wave length, abnormal dispersion occurs.

In seismology the effect of dispersion on intensity or amplitude has been observed for longitudinal and transverse waves.[19] In a wave with components having different periods, a maximum will occur at a given station because of interference. If the velocity varies with period because of dispersion, this maximum will travel to another station, not with the velocity of the individual waves, but with greater or less velocity, called the group velocity, C. If no dispersion is present, $C = v$. If the velocity v increases with the wave length (or period), there is normal dispersion, and the group velocity C is less than v. For abnormal dispersion, if the velocity decreases with wave length, the group velocity is greater than the individual wave velocity. Normal dispersion has been observed in the first longitudinal impulses; the occurrence of the *maximum* in this wave group has been found to be *delayed* with increasing epicentral distances.[19a] The effect of dispersion is most pronounced in transverse surface waves; further details are given on page 927.

3. *Absorption and dissipation.* The decrease of seismic intensity with distance, due to geometric spreading, scattering, and dispersion, is accompanied by losses due to energy absorption giving rise to damping. Hence, at the distance r the intensity

$$I_r = I_0 e^{-\alpha r} \qquad (9\text{-}36a)$$

where α is an absorption coefficient or the reciprocal of the distance at which I_0 is reduced to I_0/e. Hence,

$$\alpha = \frac{2.3}{r} \log \frac{I_0}{I_r}, \qquad (9\text{-}36b)$$

where I_r/I_0 may be designated as acoustic transparency and I_0/I_r as acoustic opacity and is measured in decibels: $db = 10 \log I_r/I_0$. Con-

[19] B. Gutenberg, Handb. der Geophys., IV(1), 27–28 (1929).
[19a] *Ibid.*

sidering both spreading and absorption,

$$I_r = \frac{I_0 e^{-\alpha r}}{4\pi r^2} \tag{9-37}$$

for a spherical wave. The absorption coefficient α appears to increase with the second power of the frequency. Hence, high frequencies are largely eliminated with increasing distance from source of vibration and the low frequencies are left over. According to Stewart and Lindsay[20] the following relation exists between absorption coefficient and viscosity:

$$\alpha = \frac{8\pi^2 \Pi f^2}{3\delta v^3} \tag{9-38}$$

where Π is the Poiseuille coefficient of interior friction.

Damping constants may be determined in the field and laboratory from resonance curves. The latter are taken with the apparatus previously described (see pages 462–463), the former with vibrators. In both cases the medium under test is force driven, and its dynamic magnification $\mathbf{W}$ (see page 602) is given by

$$\mathbf{W} = \frac{1}{\sqrt{(1 - n^2)^2 + 4\eta^2 n^2}},$$

where n is the tuning factor or the ratio of impressed and natural frequency ω/ω_0, and η is the relative damping (see page 586) in per cents critical. Substituting in the above formula the resonance tuning factor $n_r = \sqrt{1 - 2\eta^2}$, the magnification at resonance

$$\mathbf{W}_{\text{max.}} = \frac{1}{2\eta\sqrt{1 - \eta^2}} \approx \frac{1}{2\eta}.$$

For the determination of η from a resonance curve it is convenient to measure the frequencies at which, below and above the resonance peak, the maximum amplitude has dropped to $1/\sqrt{2}$ of its peak value. Then a combination of the last two equations gives

$$\left(\frac{\mathbf{W}}{\mathbf{W}_{\text{max.}}}\right)^2 = \frac{4\eta^2}{(1 - n^2)^2 + 4\eta^2 n^2} \quad \text{or} \quad \eta = \frac{1 - n^2}{2\sqrt{\left(\frac{\mathbf{W}_{\text{max.}}}{\mathbf{W}}\right)^2 - n^2}}$$

$$\tag{9-39c}$$

and with $\mathbf{W} = \mathbf{W}_{\text{max.}}/\sqrt{2}$:

$$\eta = \frac{1 - n^2}{2\sqrt{2 - n^2}} = \frac{f_0^2 - f^2}{2f_0\sqrt{2f_0^2 - f^2}}.$$

---

[20] *Loc. cit.*

Since, in approximation, $f^2 \approx f_0^2$ in the denominator, the damping rates become, for two frequencies, f_1 and f_2, at which the dynamic magnification has fallen off to one-half of its maximum value:

$$\eta_1 = \frac{f_0^2 - f_1^2}{2f_0^2} \quad \text{and} \quad \eta_2 = \frac{-(f_0^2 - f_2^2)}{2f_0^2}, \quad \text{so that, since} \quad \frac{f_1 + f_2}{2} \approx f_0,$$

$$\eta = \frac{\eta_1 + \eta_2}{2} = \frac{f_2 - f_1}{2f_0} \tag{9-39d}$$

Since the damping resistance p, or the ratio between driving force and velocity of motion (see page 584), is given by $p = 2m\epsilon$, with m as mass and ϵ equal to $\omega_0\eta$, the damping coefficient ϵ is $\pi\Delta f$; therefore the damping resistance (or dissipative resistance)

$$p = 2\pi m\Delta f. \tag{9-40}$$

(For torsional vibrations the polar moment of inertia is substituted for the mass m). Table 57 gives the damping resistances of a number of substances in bar form at 10 kc (p in kilohms), as found by Wegel and Walther.[21]

TABLE 57

DAMPING RESISTANCES OF SUBSTANCES IN BAR FORM

Lead	117–130	Silver	2.8
Hard rubber	25.5	Glass	2.45
Nickel	10	Steel	0.84
Copper	5.5	Steel (annealed)	0.215

Similar determinations for rocks have not been published, but they would undoubtedly add greatly to our knowledge of dissipation and absorption of seismic energy. From the damping, an equivalent Poisseuille coefficient Π may be derived if the vibrating medium has a simple geometric shape, such as a bar oscillating longitudinally. In such a case the viscosity coefficient is $\Pi = pl/2\pi^2 S$, S being the area of the rod. Substituting $m = \delta l S$ for its mass, $\Pi = pl^2\delta/2\pi^2 m$. Since, from eqs. (9–29a) and (9–29b),

$$l^2\delta = \frac{E}{4f_0^2}, \qquad \Pi = \frac{pE}{8\pi^2 mf_0}; \quad \text{and, since} \quad \eta = \frac{p}{4\pi mf},$$

it is seen that

$$\eta = \frac{\Pi\omega}{E}. \tag{9-41}$$

The relative damping is thus represented by the ratio between a dissipative modulus $\Pi\omega$ and the elastic modulus. Hence, in a complex representa-

[21] Physics, **6**, 141–157 (April, 1935).

tion of Young's modulus (or rigidity modulus) the damping η represents the tangent of a phase angle between elastic ($\mathbf{E}$ or $\boldsymbol{\mu}$) and dissipative moduli ($\Pi_l\omega$ and $\Pi_t\omega$) (see Fig. 9–23). The resulting elastic moduli, $\mathbf{E} = \mathbf{E}_0 + j\omega\Pi_l$ and $\boldsymbol{\mu} = \boldsymbol{\mu}_0 + j\omega\Pi_t$, are thus comparable with the apparent dielectric constant (see Chapter 10, page 641). The reciprocal of the tangent of the

Conditions at Resonance
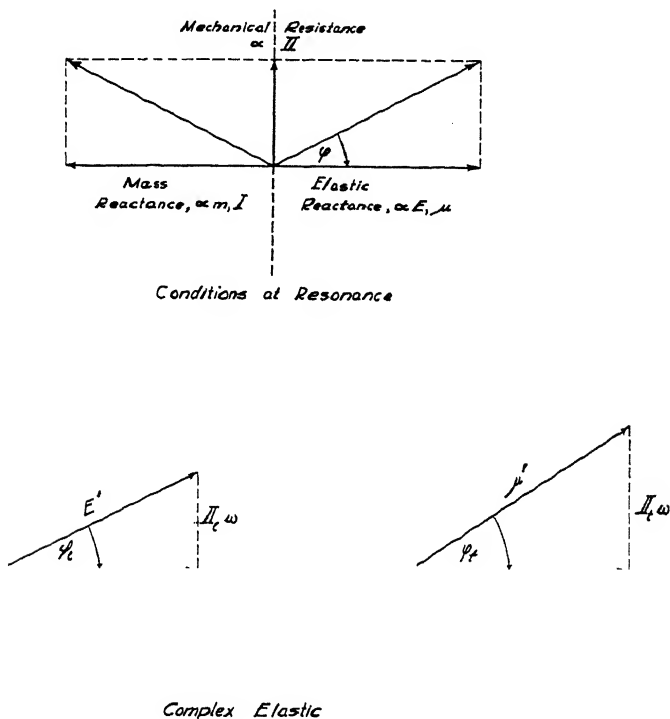
Complex Elastic

Fig. 9–23. Oscillation of elastic systems represented by complex moduli (after Wegel and Walther).

phase angle has also been designated as "dissipation" constant,[22] although this definition does not appear well chosen, since materials with the greatest energy dissipation would have the smallest dissipation constants.

III. METHODS OF SEISMIC PROSPECTING

A. Technique of Shooting; Shot Instant Transmission; Review of Seismic Methods

1. *Source of energy: weights, explosives.* In seismic exploration dynamite is used almost exclusively. However, different energy sources have

[22] H. Walther, Bell Lab. Record, 363–366 (Aug., 1934).

been used or suggested. Fessenden proposed the use of sonic transmitters, as applied in submarine signaling, for the location of ore bodies. Some commercial companies and scientific institutions have experimented occasionally with weights. Hubert,[23] using weights of 20, 50, and 117 kg dropped from heights of 1 to 11 m, could detect reflections from a number of beds down to 5 km in depth by means of a Wiechert seismograph with a magnification of 2 million located at a distance of 125 m from the weight tower. He found that (1) the travel times of seismic impulses generated by falling weights were independent of the masses and of the elevation from which they were dropped, (2) seismograms obtained with different masses and different heights could be correlated phase by phase; (3) the observed amplitudes were proportional to the square root of the height and to the weights of the masses used, hence, the amplitudes were proportional to the square root of the fall energy. Experiments made in this country with falling weights have shown that a 200-pound lead weight dropped from about 20 feet can be detected with a Schweydar seismograph under favorable circumstances up to about 300 feet.

The energy liberated by falling weights is much less than that from a dynamite explosion. To release the same energy produced by a confined buried charge of about 500 pounds of dynamite, an iron ball nine feet in diameter and weighing 75 tons would have to be dropped from a height of one mile. Nevertheless, weights have possibilities in reflection work. Unbalanced flywheel machines (vibrators) have been used for testing the dynamic response of buildings and surface formations. Details are given in Chapter 12.

With the exception of vibration tests of buildings and surface formations, dynamite is used in virtually all commercial seismic exploration. Commercial dynamites fall into two groups:

(A) *Straight dynamites* (dynamites proper). These contain nitroglycerine, in an amount equal to the grade-strength marking, and various absorptive materials.

(B) *Gelatins.* Some of the nitroglycerine is replaced by nitrocotton, forming a gelatin.

(a) *Blasting gelatin:* 91 per cent nitroglycerine, 8 per cent nitrocotton, 1 per cent chalk.

(b) *Straight gelatins:* These are blasting gelatins, diluted with pulp and sodium nitrate. The Du Pont Hi-Velocity Seismic Gelatin and the Atlas and Hercules low-freezing gelatins are in this group.

(c) *Ammonia (or special) gelatins.* These are equal in strength to the straight gelatins, but ammonium nitrate replaces a portion of the nitro-

[23] F. Hubert, Zeit. Geophysik, 1(5), 197 (1924–1925).

glycerine. The Atlas ammonia gelatins, Du Pont's Seismogel A and B, and Du Pont Nitramon are in this group.

For reasons stated later, straight dynamites and blasting gelatin are not so well suited for seismic applications as are ammonia and straight gelatins. Explosives for geophysical as well as other applications are characterized by the following properties:

1. Strength	6. Consistency
2. Density	7. Water resistance
3. Propagation effectiveness	8. Freezing resistance
4. Rate of detonation	9. Safety
5. Cost	10. Inflammability

By *strength* of an explosive is meant the percentage of nitroglycerine in straight dynamites. For any other explosive, regardless of composition, the strength rating is obtained by comparing its effect with that of straight dynamite. The absolute strength of an explosive is of minor importance. While theoretically the effect of an explosion should be independent of the type of explosive used, provided the energy (weight-strength times amount) remains constant, it has been demonstrated in practice that, for the same amount, variations in strength and type of gelatin within the range of 40 to 80 per cent have little effect. Strengths are generally referred to unit weight or unit volume and are thus designated as weight-strength or bulk-strength. High bulk-strength is advantageous for reducing transportation costs and size of shot hole.

Density is of importance in connection with strength. An explosive of both high density and high strength, that is, high weight-strength, is preferable.

Propagation effectiveness is the ability of an explosion to propagate through the explosive itself, as well as through air gaps or other non-explosives, to another portion of explosive or cartridge. A typical indication of ineffective propagation from one cartridge to another is shown in Fig. 2 of an article by N. G. Johnson and G. H. Smith.[24]

Rate of detonation is the speed with which the detonating wave travels through a train of explosives. Experience shows that the percentage of energy converted into ground vibration increases with the rate of detonation and that the latter increases with the degree of confinement. This is caused by the peculiarity of the gelatin dynamites of having two velocities, one around 8500 feet and the other ranging from 13,000 to 20,000 feet, depending upon the grade of the explosive. In ordinary gelatins the high velocity will not be developed in the open but under close confinement in a

[24] Geophysics, 1 (2), 232 (June, 1936).

drill hole; therefore, it is necessary to place shots in as firm ground as possible to insure good confinement and to tamp shot holes with mud or water. Again, high water pressures will prevent the high velocity from appearing in the regular ammonia gelatins. Therefore, both Hercules and Du Pont have developed Hi-Velocity–type gelatins for seismic work which give high unconfined velocities without special priming and withstand such water pressures as occur in the deepest reflection shot holes.

It is obvious that those explosives which will give the greatest explosive energy per dollar expended are the most desirable. In long-range refraction work the *cost* of dynamite amounts to half the cost of operation of a seismic party; consumption of 1200 to 2500 pounds per day is not unusual. In reflection work the cost of hole-drilling exceeds the cost of dynamite. The price of special gelatins is around $17 per 100 pounds in carload and $20 in ton lots.

Commercial dynamites vary in *consistency* from rubber-like constitution (blasting gelatin) to free flowing (Nitramon). For reflection work where charges have to be forced into deep holes, stiff cartridges are required. Therefore, special gelatins in stiff wrappers, or in tin cans (Nitramon) are used in seismic exploration. For special applications where very small charges (1/16 pound) are sufficient, a plastic gelatin of sticky rubber-like consistency, which may be molded around caps, is available. Lack of consistency or excessive obstructions in shot holes can be overcome by the use of tin torpedoes.

Water resistance is one of the most important properties of explosives in geophysical work. Blasting gelatins, straight gelatins, and ammonia gelatins rank highest in water resistance; next follow the straight nitroglycerine dynamites; and lowest are certain types of ammonia dynamites. By wax-dipping of wrappers or use of sealed cans (Nitramon), the water resistance is increased considerably. Both dynamite and caps must be highly resistant to water to be usable in the water-tamped holes required in seismic exploration.

Freezing resistance. Most gelatin dynamites are low-freezing and may be used the year round throughout the United States. For severe cold weather a special low-freezing grade is available.

Safety is one of the prime considerations in any application of explosives. The straight nitroglycerine dynamites are least perfect in this respect; they are too sensitive to shock and friction. Gelatins and ammonia dynamites rank very well. Low-density explosives, because of built-in cushioning effects, are the safest but unsuited for geophysical applications on account of their lack of consistency and low water resistance. Safety of explosives is determined at the factory by impact testers or by dropping an iron ball a distance of about 10 feet on a square section of powder resting on a steel surface.

It is unfortunately true for much of the seismic work that familiarity breeds contempt. The most frequent offense is the storing or transporting of blasting caps with the dynamite, despite repeated warnings by powder companies. Accidents have happened in seismic work. Although remarkably few in number, they were probably more frequent in the days of refraction shooting, owing to the greater quantities of explosives and greater distances involved.

Considerable progress has been made in recent years in solving the problem of storing explosives for seismic parties. Portable magazines have been constructed. Two types are available, one on a two- and the other on a four-wheel chassis. The body is electrically welded steel of a capacity of about one ton. The housing is well ventilated, protected by locks against theft, and coated with aluminum paint (see Fig. 9–24). Since it is illegal to carry dynamite in a trailer or in a car towing a trailer, the dynamite may be transported in one vehicle, the trailer towed by another, and the dynamite transferred on location. Separate steel boxes for caps are also available. These may be chained to a tree in the field.

Inflammability. Straight nitroglycerine dynamites are most easily ignited, but all other grades are of low inflammability. Explosives should be well protected against fire.

Experience collected with various types of explosives in seismic work in this country for over twelve years indicates that the 60 per cent ammonia gelatins, especially the high-velocity types developed for seismic applications, are the most satisfactory. Dynamites for seismic work are manufactured by the Du Pont Powder Company, the Hercules Powder Company, and the Atlas Powder Company. The most popular sizes are: $\frac{1}{2}$-pound sticks, $1\frac{1}{4}$ x 8 inches; 1-pound sticks, 2 x 6 inches; $2\frac{1}{2}$-pound sticks, 2 x 16 inches; 5-pound sticks, 3 x 12 inches; and 70-pound sticks, 8 x 24 inches (for swamp work).

Texas Body and Trailer Co.

FIG. 9-24. Portable dynamite magazine.

For setting off the charge, electric *blasting caps* are used exclusively (Fig. 9–25). These consist of a metal container, two insulated leg wires sealed with a waterproof compound and with sulfur on top, a pressed charge at the lower end of the cap, and a primer charge at the ends of the leg wires where they are connected by a bridge wire. The fusion of this wire detonates the cap. The bridge wire is made of an 80-20 platinum–iridium alloy and is 0.00125 inch in diameter. The priming charge surrounding

FIG. 9-25. Cross section of Hercules electric blasting cap.

the bridge wire is usually mercury fulminate; in the Du Pont "SS" caps it is fulminate chlorate. Instead of having a loose charge around the bridge wire, the Atlas caps have a bead in the form of a matchhead. Caps are usually protected by a shunt clip against accidental discharge due to static or other sources of electricity. This clip is removed immediately before firing.

The time characteristics of electric blasting caps are of great importance in seismic work. Connected to the blasting cap is a circuit for transmitting the instant of the explosion to the seismic record. With the introduction of the reflection method, the requirements of time accuracy went up considerably, for the time of explosion must be transferred to the record with an accuracy of 1 to 2 thousandths of

a second. Ordinary caps are unsuited for this purpose. As shown in Fig. 9–26, the delay for low currents is great. For high currents two breaks occur—one when the bridge wire fuses and the next when the cap fires. In caps especially developed for seismic applications (Du Pont "SSS") not only is the time difference beween bridge break and detonation eliminated but the firing delay is reduced considerably. This type of cap can be fired by any current greater

FIG. 9-26. Firing current vs. firing time for Du Pont seismograph blasting caps (after Burrows). 1 is "SSS" bridge break and total cap lag; 2A, "SS" bridge break; 2B, "SS" total cap lag.

than 2 amperes. At 3 amperes the firing time is about 0.003 second ± 0.0003. Batteries or blasting machines may be used for firing electric blasting caps, the latter being preferable from the point of view of safety. A 50-cap blasting machine furnishes about a 300-volt peak e.m.f.

When dynamite is primed with an electric blasting cap, the latter should be so fastened with its lead wires around the charge that the cap does not pull out when the charge is lowered into a hole. Before shooting, the firing circuit should be tested for resistance to be sure that the current is passing through the blasting cap and through all parts of the line. For this purpose the powder companies furnish test instruments consisting of an ohmmeter and a silver chloride battery which supplies less current than is required to blow up a cap. The resistance of the caps plus the resistance of the leads should be calculated and compared with the results of the test. Both short circuits or high resistance breaks are equally objectionable.

2. *Placement of charges.* In both refraction and reflection work it is necessary to place the charges in the surface in such a manner that maximum energy transfer from the explosive to the ground is obtained. The amount of energy released by the explosion itself is appreciable. It has been estimated[25] that the temperature of the gases liberated by it is of the order of 3000° C., and that pressures of about 50,000 atmospheres (or about 700,000 pounds per square inch) are produced by an explosion of 60 per cent dynamite. However, very little of this energy is likely to be transmitted to the ground. If the charge were placed on the surface without confinement, not only would its rate of detonation be low (unless a high velocity powder is used) but most of the energy would probably be converted into a compressional air wave. Hubert, as early as 1924, demonstrated experimentally that the effect of a buried charge may be from 50 to 100 times greater than the effect of a surface charge. Even then, most of the energy is probably expended in enlarging the hole, in crushing the rock, in moving out water and mud, and in heat. Comparatively little is converted into elastic wave energy.

Charges should be placed as deep as time, terrain, and cost permit, although it may happen that deeper layers have poorer transmission characteristics than do more shallow layers. Firm shales or water-soaked beds are the most effective carriers of seismic energy. Reflection shooting has made it a fairly general practice to place the charge at the depth of the ground-water level if it is not too deep. In long-range refraction shooting, usually a hole 4, 5, or 6 inches in diameter is drilled to a depth of from 12 to 25 feet, and a cavity is blown at the bottom with 4 to 8 pounds of dynamite. The entire charge is then placed in the cavity and the hole is tamped with dirt and water. The large cartridges 8 inches by 24 inches mentioned before are applied in marsh work and are forced down with a wooden tamper as far as they will go. In open water the charges are sacked and primed, and the bags are lashed together and tossed over-

[25] H. E. Nash and J. M. Martin, Geophysics, 1(2), 239-251 (June, 1936).

board at the desired location.   Reflection shot holes are generally of small
diameter, and the primed charge is pushed down with a tamping stick con-
sisting of several sections connected by hook joints.   Several sticks may

FIG. 9-27. Failing seismic shot-hole drill; view of hydraulic.

be taped to a piece of lath, or they may be placed in a tin torpedo.   Nitra-
mon cans are loaded with a spoon attached to the end of the loading pole.
   Shot holes are drilled in various ways, depending upon conditions.   In
easy drilling soil, the use of hand augers is quite feasible, particularly if

local labor is cheap.   In most cases truck-mounted rotary drilling machines
are used (Figs. 9–27 and 9–28). In soft ground holes may be "washed
down" by the use of centrifugal pumps driven by gasoline engines (Fig.
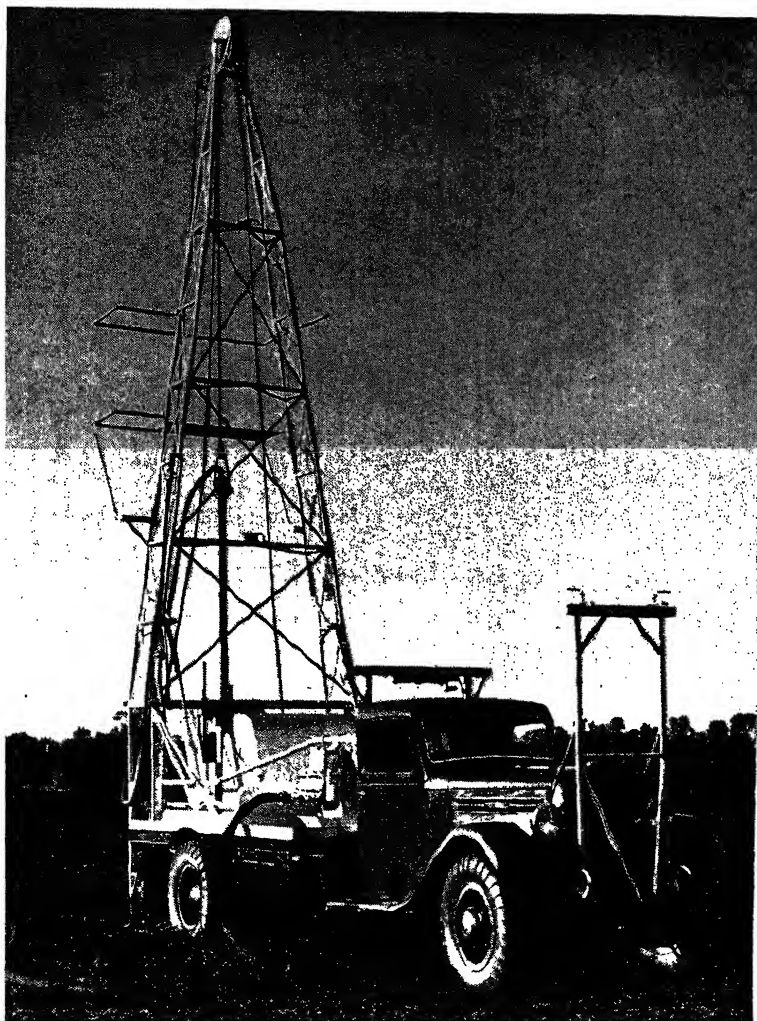
George E. Failing Supply Co.

FIG. 9-28. Failing seismic shot-hole drill; view of entire unit.

9–29).   Hole caving may be prevented by the use of Aquagel or lime, or
by the use of casing[26] which can usually be recovered and used again.

___

[26] A light-weight casing, made of plastic, has recently been put on the market.

Shot holes are tamped with water. Most reflection parties have a water truck following the drilling truck. Drilling costs may range from 25 cents to over a dollar per foot, depending upon conditions. Seismic-hole drilling may be contracted at $1000 to $1500 per month. Charges are generally fired from a shooting truck set up as close to the shot point as practicable.
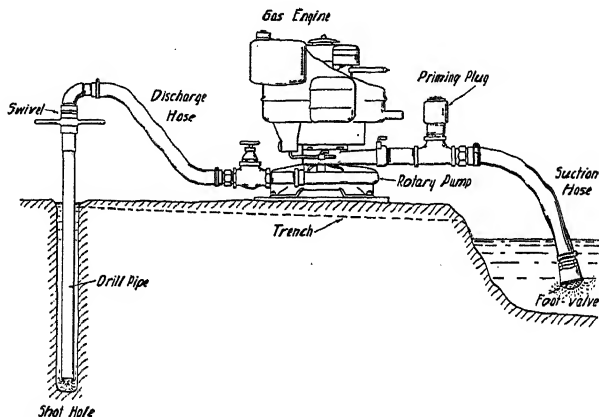
FIG. 9-29. Evinrude centrifugal pump for drilling shot holes in swamps.

In earlier refraction shooting some companies fired charges by radio from great distances but this practice is now abandoned.

It has been demonstrated that no changes in travel times occur when charges are changed as much as ten times in energy, that is, in quantity or in strength. As shown in Fig. 9-30,[27] the amplitudes generally increase in proportion to the square root of the charge.
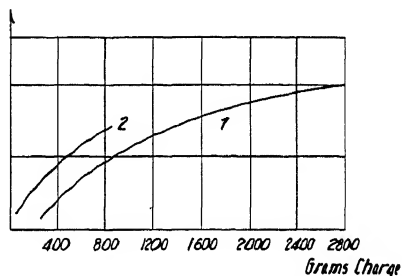
FIG. 9-30. Variation of amplitude with charge (after Rixman). (1) Shots fired in dry sand; (2) shots fired in moist sand; μ, ground amplitude in microns.

3. *Energy transmission and absorption.* It is difficult to determine accurately the relation between distance and record *amplitude*, because such measurements make it necessary to move either shot points or observation points. If the shot point is moved, the energy transferred to the ground changes with local conditions at the shot point. If the re-

[27] F. Rixmann, Zeit. Geophys., 11(4/5), 197-207 (1935).

ceivers are moved, the recorded energy varies with the so-called ground factor, that is, with the dynamic response conditions of the surface strata. Different propagation paths of refracted, reflected, and surface waves further complicate the problem.

In refraction work the amount of dynamite required increases with distance, probably in linear relation. In reflection shooting a relation between charge and depth is hardly recognized, since the recorded amplitudes are predominantly dependent on transmission conditions of surface beds at the shot point. The curves in Fig. 9-31 have been plotted from data published by Barsch and Reich for a number of refraction traverses.
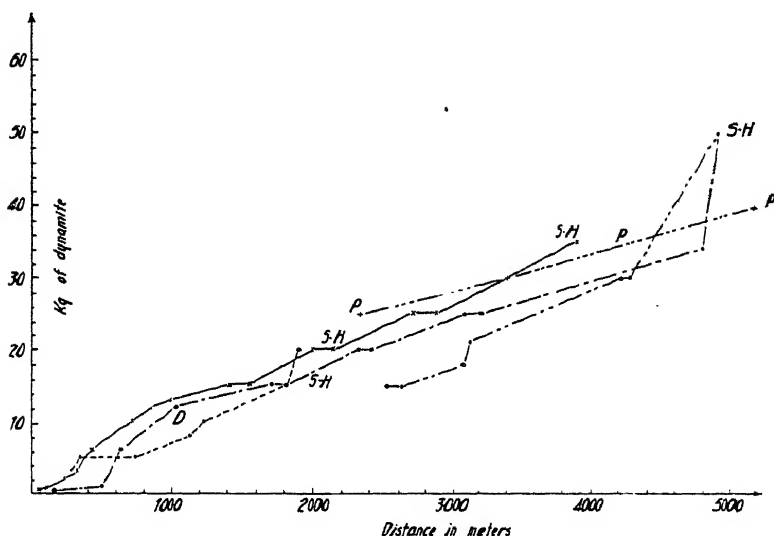
Fig. 9-31. Dynamite charge required to produce legible impulse, as a function of distance (compiled from data by Barsch and Reich). *P*, *S-H*, and *D* indicate localities.

They indicate that the amount of dynamite required varies approximately in direct proportion to distance.

4. *Transmission of shot instant.* The accurate transmission, from the shot point to the receiver, of the instant of the explosion is of importance, since virtually all interpretation methods are based on determination of travel times. In refraction shooting the accuracy in time transmission varies from $\frac{1}{100}$ of a second for short distances to several hundredths of a second for great distances, in reflection work it is of the order of $\frac{1}{1000}$ of a second. The instant of the explosion may be determined (*a*) by its direct effects (sound, light, or temperature), or (*b*) by an indirect effect (electrical current or radiation) released by the explosion.

The instant of explosion may be computed from the time of arrival of the *sound wave*, taking into account the velocity of sound, barometric pressure and temperature, wind direction and velocity, and the distance of seismographs from the firing point. Application of this method decreased when charges were buried at greater depth, but it was later revived for the purpose of determining the distance between firing point and receiver in difficult terrain. In this procedure a "sound" charge is placed on the ground above the buried main charge and a blastophone is used for recording the sound waves. The use of the *light* transmitted by the explosion was mentioned by L. Mintrop in one of his patents. The possibilities of recording an explosion through its heat radiation have never been investigated.

In the transmission of the shot instant by *wire*, a contact in an electrical circuit is made or broken at the instant of the explosion. Double wire or ground return may be used. The indicating devices are electromagnets with mirror armatures, telephone receivers or loudspeaker elements with mirrors attached to their diaphragms, oscillographs, string galvanometers, and the like. These will be discussed in more detail in the article on radio transmission. The transmission circuit (1) may be broken at the instant of firing (a) by wrapping it around the charge, (b) by a series cap, or (c) by a relay in the firing circuit; (2) it may also be closed by a relay, actuated (a) by the firing circuit or (b) by a series cap; or (3) the transmission circuit may be coupled directly to the firing circuit by (a) a resistor or (b) a transformer.

Firing Chamber

sm) spring

cap   piston

American Askania Corp.

FIG. 9-32. Series cap firing relay for wire or radio transmission.

Wrapping the transmission line around the charge has the disadvantage of placing four lines in the shot hole. A series cap is more convenient for breaking the line. For closing the circuit by a series cap, the firing relay shown in Fig. 9–32 has been used in connection with refraction shot-instant transmission. Two field phones are usually connected to the shot-instant transmission line as shown in Fig. 9–33. The first arrangement is actually a three-line circuit. Communication is not interrupted when the shot-instant circuit is broken; the phone current passes through the indicator, which is avoided in the second arrangement. However, the use of a single line requires switching from communication to shot transmission.

Various arrangements are applied (particularly in reflection work) to couple the firing line directly to the transmission line. A small amount of current, not enough to set off the cap but sufficient to attract the armature of the indicator, may be passed from a battery through the

circuit before firing.   At the instant of firing, the circuit is broken and the armature released.   Instead of feeding directly into the transmission line, the firing line may be coupled to it preferably by a transformer, or by a
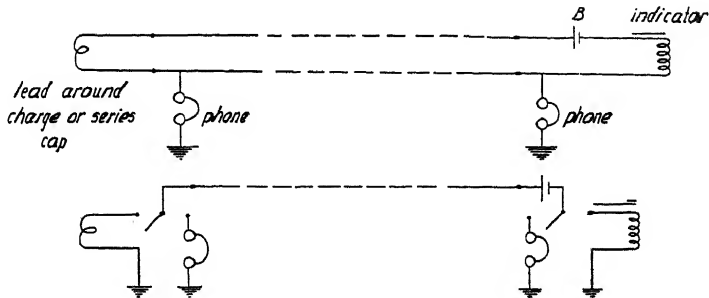
FIG. 9-33. Arrangements for shot-instant transmission by circuits separate from firing line.
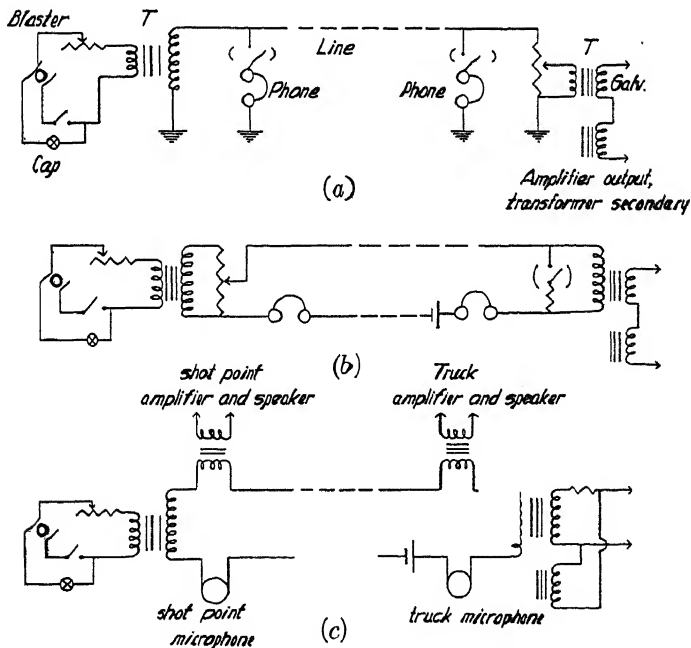
FIG. 9-34. Arrangements for shot-instant transmission over single and double communication lines from firing circuit.

resistor.   This method is the most prevalent.   Fig. 9-34 shows three varieties.   A transformer is connected in parallel to the firing circuit in such a manner that a portion of the firing circuit passes through its primary.

In Fig. 9–34a the phones are in parallel with the secondary of this transformer; in b and c the phones (or the speaker input transformers) are in series with it. In all cases the regular seismograph galvanometer is used for the time break, and the output of the shot-transmission transformer is either in series (a and b) or in parallel (c) with the amplifier output transformer. Arrangement c differs from b by the use of microphones and speakers, which makes for more convenient operation in a recording truck.

Wire transmission of the shot instant is applied in short-range refraction and in most reflection work. In all long-range refraction work and for reflection shooting in areas where distance, type of country (swamps), or topography make laying of lines impracticable, *radio* is used. Transmitters vary from about 40 to 200 meters[27a] in wave length, and from 0.2 to 50 watts in power, which must be great enough to overcome static and to actuate the type of indicator used. Their range may extend to 150 miles or more. Fig. 9–35 shows a portable transmitting and receiving unit. The transfer of the shot instant to the transmitter is generally accomplished by making or breaking the plate circuit. For breaking it, the B battery lead is shot apart; for connecting it, the firing relay shown in Fig. 9–32 is used. Often the transmitter sends some sort of a signal (produced by buzzer or tuning fork) which is either turned off or on by the shot. On the receiving end the signals are picked up as sound and recorded.

A great variety of devices are available for recording. In long-range radio time-signal transmission (deep refraction and pendulum surveys) relays are sometimes applied in connection with less sensitive and, therefore, more rugged indicating devices. These may be mechanical relays or gas-filled tubes (grid-glow tube or thyratron). In the majority of cases relays are avoided, and indicators of special design or oscillograph galvanometers are applied.

A simple recording device may be made from a phone receiver by attaching a mirror to the diaphragm and placing the receiver behind a lens of the same focal length as that used in the (mechanical) seismograph. The receiver is then set up on a stand next to the seismograph. A more effective recorder is made from a magnetic speaker by removing the diaphragm and coupling the driving pin to a light spring fitted with a mirror, or to a mirror suspended on a short platinum-iridium torsion wire. In both cases suitable damping should be used. In refraction work the Askania mirror device has been widely applied (see Fig. 7–24).

All kinds of oscillographs, vibration galvanometers, and string gal-

---

[27a] In this country, the following frequencies have been allotted by the F. C. C. to geophysical work: 1602, 1628, 1652, 1676, and 1700 kilocycles.

vanometers are extensively employed.[28]   They are generally coupled to
the receiver by a suitable step-down transformer; the regular seismic
oscillographs (coil galvanometers or string galvanometers) may be used
when a separate indicator is undesirable.   In that case the output trans-
former of the radio receiver is connected in series or in parallel to the
secondary of the output transformer of the seismic amplifier.   A disad-
vantage of all oscillographs and mirror devices is their inertia, which re-
quires damping.   This is avoided in the glow-tube oscillograph shown in
Fig. 7–25.   The latter ignites with about $2 \cdot 10^{-4}$ amperes for optimum
plate voltage.   Its cathode is a hollow slotted cylinder whose end surrounds
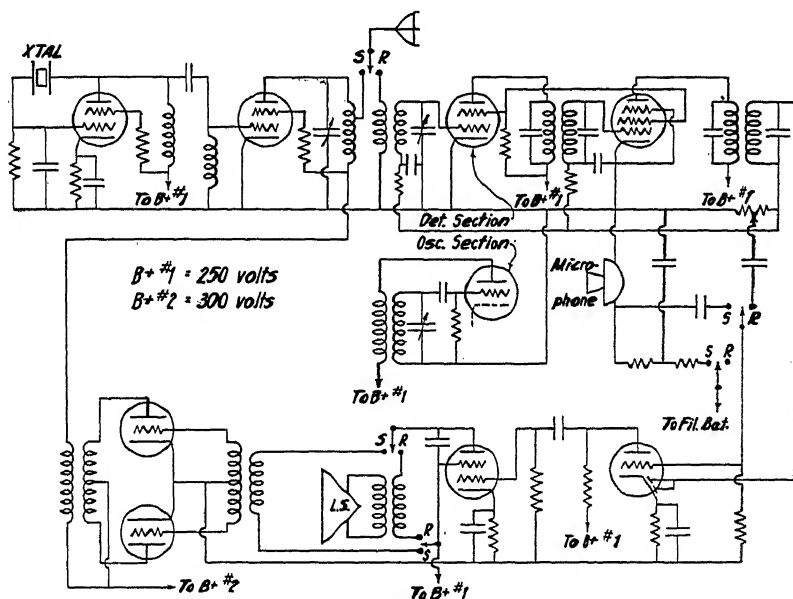
Fig. 9-35. Radio transceiver.

the anode.   The current controls the length of the glow in the slot.   This
glow is projected on the photographic paper.

5. *Review of seismic methods (fan shooting, refraction, reflection).*   All
seismic prospecting methods have in common the generation of an in-
stantaneous shock and the measurement of resultant surface vibrations at
one or more distant points.   The physical parameters which may be deter-
mined for any vibratory motion are (1) frequency; (2) intensity or ampli-
tude; (3) velocity and travel time.   Practical experience has shown that
the first two parameters are too complex to be used for interpretations in

[28] The regular seismic oscillographs are discussed on pp. 552; 598-601.

terms of depth. However, they enter indirectly into the interpretation of a seismogram, since impulses due to any new phase are characterized by a change in both frequency and intensity. The only wave parameter employed for depth calculations in present practice is the time interval elapsed between the instant of the explosion and the arrival of the first or later impulses. According to the type of wave used and the manner in which travel times are observed and analyzed, the following seismic methods are distinguished: (1) fan shooting, (2) refraction, and (3) reflection.

The objective of the first method is to determine whether there is an intervening medium of different velocity between shot point and receiving points. Fan shooting is a reconnaissance method, capable of covering a large area in a comparatively short time. Indications obtained by it may be detailed by the refraction or reflection methods. In many ways the fan shooting method is comparable to resistivity mapping of electrical prospecting. When distances between receivers and shot are kept fairly constant, the depth penetration also remains about the same. In contrast to the fan shooting method, refraction and reflection methods involve absolute determinations of depths to geologic formations. In the refraction method, this determination involves an observation of the variation of travel time with interval between shot point and receiver. Hence, it is comparable with the resistivity-sounding method of electrical prospecting.

While in fan and refraction shooting primarily the first impulses from high-speed beds within the range of the shot distance are evaluated, the reflection method is based on the determination of travel times of impulses arriving subsequently in the seismogram. The interval between shot and receiving points is no longer a factor controlling depth penetration. Were it not for ray curvature and absorption it would be possible to penetrate to any depth with any given spread. This method can be used for both reconnaissance and detail. However, because of difficulties in correlating records through large distances, its main application is to detailed surveying. In refraction shooting, the distance between shot and receiving points is roughly a multiple of the depth penetration (generally from 3 to 5); in reflection shooting, it is a fraction thereof (from $\frac{1}{10}$ to $\frac{1}{2}$).

To obtain depth in refraction shooting, the travel time must be determined as a function of distance. Hence, observations in a number of distances are required. In reflection shooting, one distance would theoretically be sufficient if the velocity is known. In practice, however, more distances are necessary, since it is not possible to differentiate between a refracted and a reflected impulse in a single record.

In field application the distinction between the three seismic methods is not so sharp as it may appear from the above description. To calibrate

the time scale in fan shooting in terms of normal geologic depth-velocity
sequence, a refraction profile is first shot.   There are combinations of fan
and refraction shooting in which absolute instead of relative depths are
obtained; refraction profiles may be tied in with reflection traverses to
obtain average velocities to reflecting beds.   Finally, refraction shooting
for weathered layer corrections is part of everyday reflection practice.

B. FAN-SHOOTING METHOD

1. In *oil exploration* the fan-shooting method was applied extensively
on the Gulf coast for the location of salt domes from 1924 to 1929, which
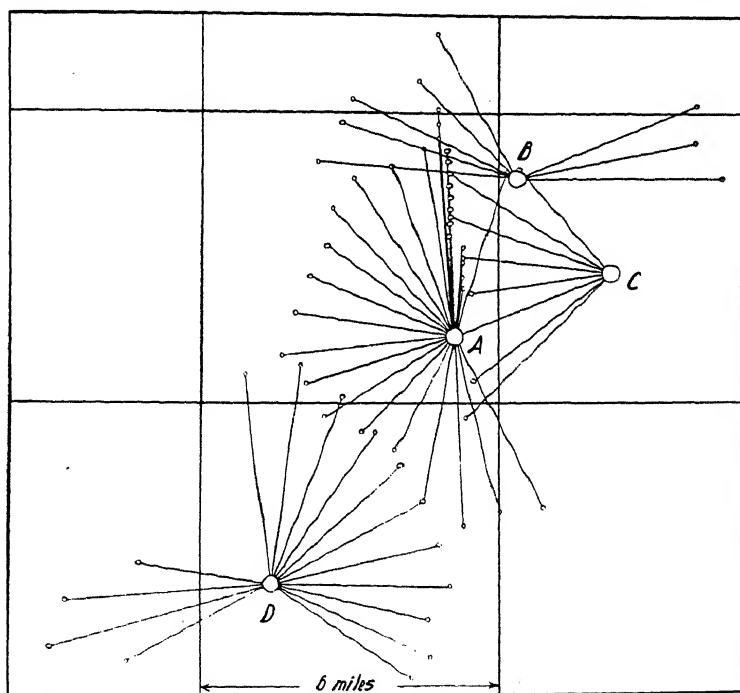
FIG. 9-36. Preliminary profile and fan layouts (after Barton).

are ideally suited for this work, since their velocity differs considerably
from that of the surrounding formations.   The area to be prospected is
covered by a series of overlapping fans (see Fig. 9-36).   Receivers are
grouped, by repeated setups, on the circumference of a circle about the
shot point, at distances varying from four to eight miles.   In a new area
a profile is first shot to determine the normal sequence of beds, that is,
the "normal" travel-time curve (see Fig. 9-37, and profile extending north
from fan shot point *A* in Fig. 9-36).   Travel times observed at the fan
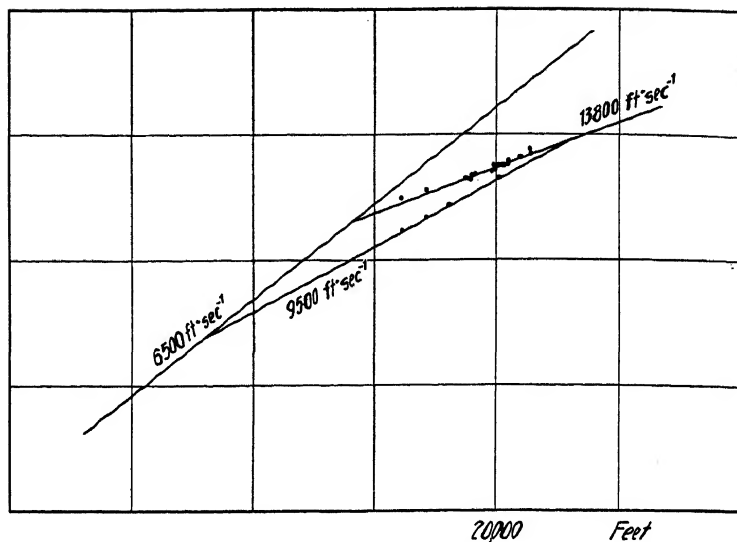
Fig. 9-37. Fan times plotted on preliminary travel-time curve (after Barton).
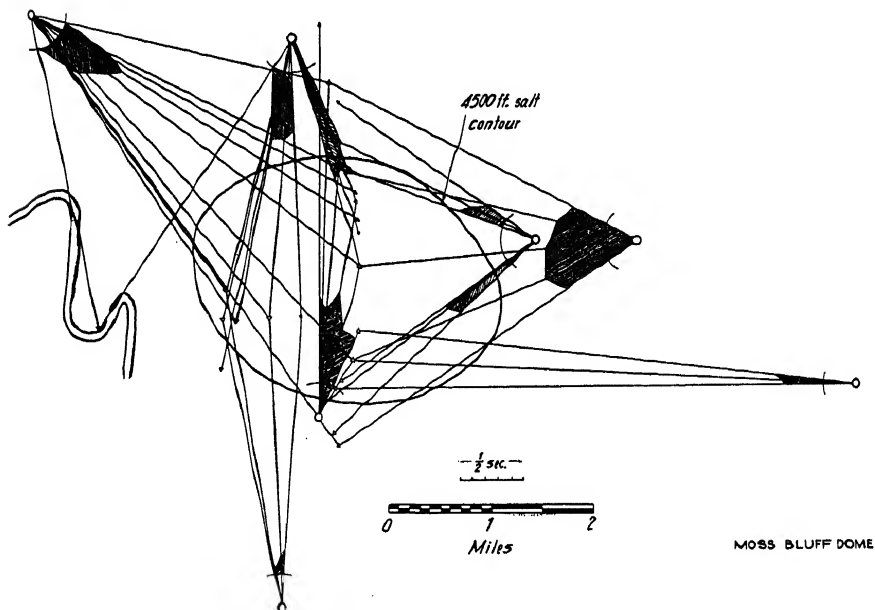
Fig. 9-38. Refraction fans and travel-time anomalies ("accelerations") at Moss Bluff salt dome (after Eby and Clark).

stations are then compared with the corresponding times of the standard curve for the same distance. Fig. 9-37 shows such fan times plotted on

the standard travel-time curve, indicating that there are no media of anomalous velocities within the range of the fan. Time anomalies are plotted for each fan as "accelerations" (in fractions of seconds). Fig. 9-38 shows such fan accelerations for the Moss Bluff salt dome.

An analysis of the length of the acceleration vectors makes it possible to determine approximately the location of the dome. The corresponding travel-time curve for a salt dome is given in Fig. 9-39. After a dome has been located by fan shooting, the company doing the work usually blocks
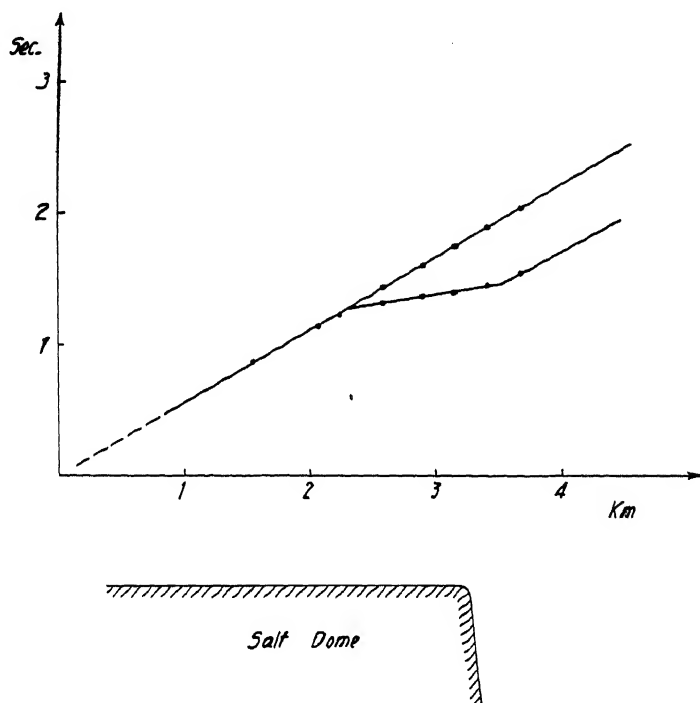
FIG. 9-39. Travel-time curve across salt dome (adapted from Barton).

the prospect as quietly as possible and then returns to the area later to detail the indication by refraction profiling, reflection shooting, or torsion balance to determine the shape of the cap and the attitude of beds above and around the dome. The fan-shooting method has also been applied in the mapping of anticlines[29] (see pages 547-548).

2. In *mining exploration* the fan-shooting method can be used for the location of gold-bearing placer gravel channels and similar problems. Figure 9-40 shows a fan layout as applied in prospecting for gold-bearing

---

[29] J. H. Jones, World Petrol. Congr. B.I., 169-173 (London, 1934).

leads. The receivers are placed at the ends of radial lines at distances of 1000 to 2000 feet. The location of the lead is given by the maximum travel time, and this point is then made the vertex for the next fan. The position of the edge of the channel, as well as the channel depth, may be
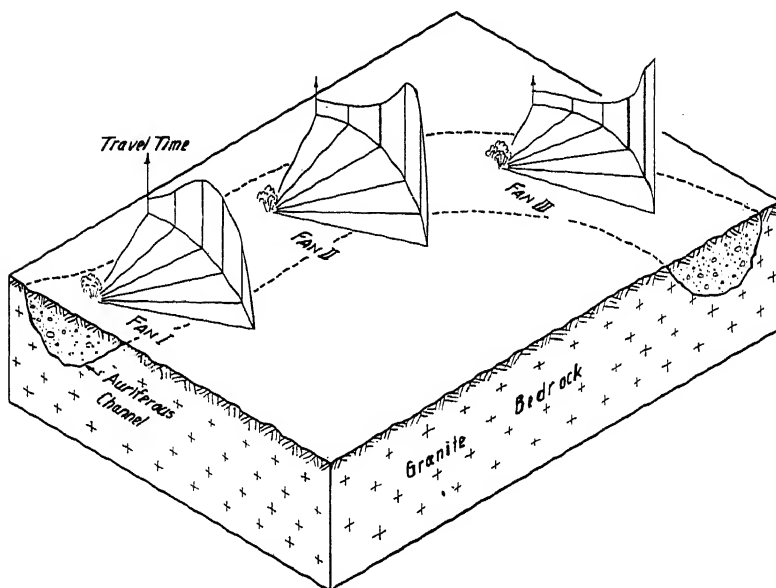
FIG. 9-40. Tracing course of placer channel by fan shooting.
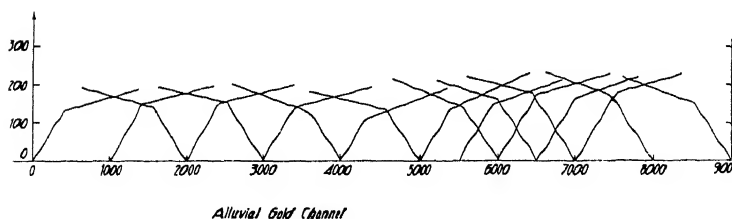
FIG. 9-41. Travel-time curves on two gold-bearing alluvial channels in the Gulgong gold field, New South Wales (after Edge and Laby).

detailed by refraction profiles at right angles to and parallel with the strike of the leads. Fig. 9-41 shows up- and down-lead travel-time curves (to determine *dip* of bedrock surface, see page 525). The depth of the channel is roughly proportional to the ordinate of the break in the travel-time curve.

3. *Fan-shooting equipment.* Equipment and instruments used in fan shooting depend to some extent on the purpose of the survey. Fan-shooting equipment for oil exploration is more elaborate than that employed in mining and engineering applications, since the distances between shot point and receiving points and the distances between individual fan stations are much greater. For this reason, the shooting technique also differs. In oil exploration, where large charges are required for fans three to seven miles in length, a hole is drilled first to a depth of 20 to 25 feet; a large cavity is blown out at the bottom of the hole, and the main charge is placed in it. A surface charge is hooked in with the main charge to transmit the sound of the explosion. The two charges are then fired simultaneously from a shooting truck which is set up at a safe distance and is equipped with a radio transmitter to relay the instant of firing to the receiving points. The latter are individually equipped with either photographically recording mechanical seismographs or with electrical detectors connected to a three- to four-stage amplifier and oscillograph.

The recording camera often contains another oscillograph element for the recording of the sound of the explosion, which is received by an electrical microphone (blastophone). A third element may be used to record the shot-instant signal picked up by the radio receiver, or the shot instant may be recorded on the seismic detector trace. The sound record serves to calculate the distance between shot point and receiving point. Since wind direction, velocity, air temperature, and barometric pressure must be known for an accurate evaluation of the record, the receiving units are usually equipped with meteorological apparatus. Mechanical seismographs are set up in small tents, and electrical detectors are buried in auger holes several feet deep. The radio receivers are equipped with antennas strung out on bamboo poles, one on the recording truck and the other set up some distance from it. The receiving apparatuses with seismic, meteorological, and radio accessories are carried in recording trucks, of which there are usually three to six to each fan party. These operate simultaneously in fan arrangement for one shot and are then moved to the next portion of the fan, the shot being repeated at, or very close to, the original shot location. At the present time the fan-shooting technique in oil exploration is more or less past history in this country, but it is still being applied in foreign oil exploration.

In mining and in engineering applications the dimensions of the fans are small, and therefore multi-channel electrical equipment with a common recording element is much preferred. Four to twelve electrical detectors are connected to a recording truck, recording trailer, or recording tent, which is set up approximately in the middle of the arc of the fan. At this central recording point are the amplifiers and the recording camera

which contains as many galvanometer elements as there are channels. Communication with the shot point is generally maintained by wire and the same wire is used for the transmission of the shot instant. An apparatus that is adapted to extreme requirements of portability and does not necessitate the use of a truck or tent is illustrated in Fig. 9–114.

C. REFRACTION METHODS

1. *General.* The travel of seismic waves in the earth is controlled by the same laws as is the propagation of light rays. Seismic waves are refracted and reflected on any interface at which there is a change in velocity. Therefore, a deviation from normal travel time is observed when media of different velocities occur below. When the variation of travel time with distance has been determined, depths and nature of the refracting beds may be deduced from the *travel-time curves.* If the velocity within a given layer is constant, the seismic rays may be considered straight. The theory of wave propagation is based on Snell's law of refraction and the principle of Fermat which states that seismic energy follows that path which enables it to travel from the shot point to the receiving point in a minimum of time.

In refraction shooting, a charge is placed at one location and a number of seismographs are set up in a straight line, preferably at equal intervals. Profiles may be laid out in the direction of the strike, at right angles thereto, or in both directions. For dipping formations, profiles are shot both up slope and down slope. Depth calculations are based on a time-impulse analysis of the seismogram. Impulses are located which correspond to the arrival of different types of waves; their arrival time is measured from the instant of the shot. In practice, only impulses of longitudinal waves are used. The first impulses or "breaks" are due to the deepest high-speed bed within range. If later impulses (due to shallower beds of lower velocity) are noticed, they may also be timed. However, depth calculations may be based on first impulses only. Travel times are plotted against the distances of the various receiving stations from the shot point. Thus, the travel-time curve is obtained. It consists of one line if only first impulses have been plotted, but it may have several branches if later impulses have been utilized. If the travel time curve is straight and has essentially the same slope for all distances, no higher-speed beds have been reached. When breaks (changes of angles) occur, they may be due to a variety of conditions. Several simple types are discussed below.

2. *Refraction equipment.* Seismic refraction equipment is similar to and in many cases identical in general design with fan-shooting equipment, described on the preceding page. However, in refraction shooting there is greater opportunity to use multielement equipment with a com-

mon recording point.   In oil exploration there are quite a number of problems which can be successfully solved by refraction profiles of moderate detector intervals.   Whereas the detector interval in a four- to six-mile fan is of the order of a mile, a refraction profile shot under similar circumstances would utilize detector spacings of the order of 1000 feet.   In mining applications, such as mapping of the bedrock surface on placer sites, the detector spacing would be of the order of 25 to 100 feet.   In engineering work the detector interval depends largely on the problem and would

In the early days of refraction shooting, mechanical seismographs with individual setups, such as the Mintrop and the Schweydar seismographs (page 608), were widely used.   These were soon superseded by electrical seismographs, such as those described in connection with the fan-shooting equipment for individual setups, and later by multichannel equipment with central-point recording.   Reflection seismograph equipment is well suited for refraction applications; details are discussed on pp. 551–56.   As a matter of fact, reflection equipment is used for refraction work in everyday reflection routine for the determination of the thickness of and the time delay in the weathered layer.   A portable refraction apparatus suited particularly for shallow engineering and mining applications is illustrated in Fig. 9–114a.
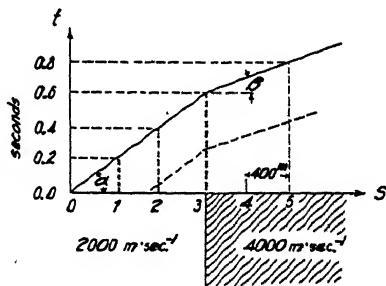
FIG. 9-42. Refraction travel-time curves on vertical boundary.

3. *Travel-time curve for vertical boundary.*   In Fig. 9–42 let $v_1 = 2000$ m per sec. and $v_2 = 4000$ m per sec.   Assume that the shot point is at 0 and that detectors are set up at the points 1 to 5 at 400-m intervals.   The explosion wave will reach point 1, 0.2 sec. after the shot has been fired, point 2 in 0.4 sec., and point 3 in 0.6 sec., point 4 in 0.7 sec., point 5 in 0.8 sec., point 6 in 0.9 sec., and so on.   Plotting these times against distance gives a curve with a break above the contact.   Since a travel-time curve of the same shape is obtained also for a horizontal layer, another shot may be fired some distance away from the first shot point.   In case of a vertical fault at the surface as assumed here, the position of the break remains the same.   If a horizontal boundary occurs at depth, the distance of the break from the shot point remains unchanged.   The slopes of the two parts of the travel-time curve indicate the respective velocities below:

$$\cot \alpha = \frac{ds_1}{dt_1} = \qquad\qquad \cot \beta = \frac{ds_2}{dl} = v_2 .$$

4. *Single horizontal layer.* Equations for this case are obtained by considering the possible longitudinal wave paths through two layers. When a charge is fired at A, waves radiate in all directions. For the wave traveling horizontally to location D, the time is

$$t_1 = \frac{s}{\mathbf{v}_1} \qquad\qquad (9\text{-}42)$$

(see Fig. 9–43), and $\cot \alpha = ds/dt_1 = \mathbf{v}_1$. To find the path of the wave which reaches the receiver through the lower medium, consider the rays impinging on the boundary. If an incident ray subtends the angle φ with the normal to the boundary and the refracted ray subtends the angle ψ, then, according to Snell's law, $\sin \varphi / \sin \psi = \mathbf{q} = \mathbf{v}_1/\mathbf{v}_2$, where $\mathbf{q} =$ index of refraction. For a given index of refraction there occurs an angle φ, for which $\sin \psi = 1$; that is, the refracted beam travels along the boundary surface. If φ becomes greater than this "critical" angle i, total reflection takes place. Hence, $\sin i = \mathbf{v}_1/\mathbf{v}_2 = \mathbf{q}$. Evidently,
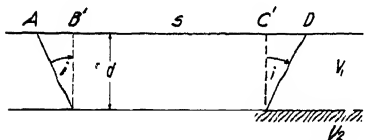
FIG. 9–43. Critical-ray paths, single-layer case.
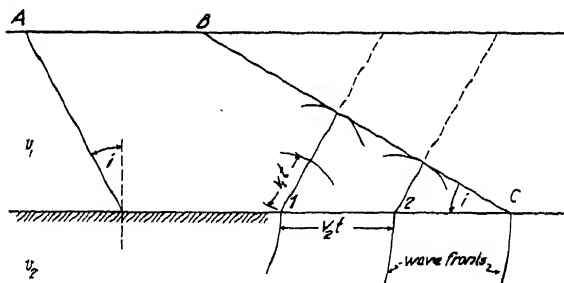
FIG. 9–44. Wave fronts in upper and lower layer.

the only ray which can reach the receiver by refraction will travel horizontally on the boundary of the lower medium. It strikes the boundary at the angle of total reflection and leaves it at the same angle. This statement involves the application of Huygen's principle, since any point of the underlayer wave may be considered a source of new waves.

While this wave proceeds with the velocity of the lower layer, impulses are continually sent upward into the upper medium, where they propagate with the velocity of the latter. In Fig. 9–44 locations 1, 2, and C are considered such source points. Their distance is given by the product $\mathbf{v}_2 \cdot t$, with t as an arbitrary time unit. The "wave fronts" in the lower layer will occupy these positions in successive equal intervals of time. Similar wave fronts may then be drawn for the wave propagating from

points 1, 2, and so on, into the upper medium, their spacing for the same time intervals being $v_1 \cdot t$. Since in the schematic of Fig. 9–44 the velocity in the upper medium was assumed to be half that in the lower medium, the spacing of the fronts in the lower medium is twice that in the upper.

By joining points reached by wave fronts at the same instant, one obtains the front BC in the upper medium, which subtends the angle i with the boundary of the lower layer. Schmidt[30] has coined the expression "traveling reflection" for this phenomenon. He showed that it is analogous to the bow wave which appears when a bullet travels with a velocity greater than that of sound in air (see Fig. 9–45). While the bullet is traveling with the velocity v_2, a compressional wave is produced around the front of the bullet which propagates with the velocity v_1 (sound in air). Hence, the angle of the bow wave with the path of the bullet is given by

sin $i = v_1/v_2$. This wave does not occur if the bullet (or any other compressional impulse) travels with the velocity of sound in air or with less velocity. In the propagation of refraction waves, an analogous phenomenon occurs. In the lower medium the impulses travel with the velocity of that medium, and a bow wave can not occur. It appears, however, in the upper medium, for its velocity is less than the velocity of the lower medium.
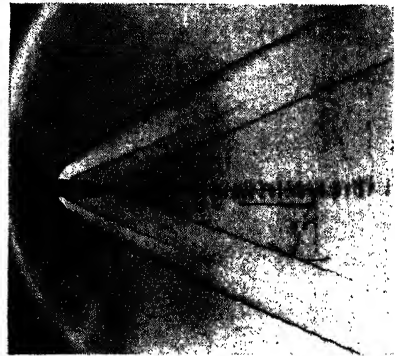
.9-45. Bow wave of bullet (adapted from O. V. Schmidt).

In Fig. 9–43, let ∡ $ABB' = $ ∡ $C'CD = i$, $\overline{AD} = s$, $\overline{B'B} = \overline{C'C} = d$, $\overline{AB'} = \overline{C'D} = d \tan i$ and $\overline{AB} = \overline{CD} = d/\cos i$. Then the travel time for the wave traveling the path $ABCD$ is $t_2 = 2(\overline{AB})/v_1 + \overline{BC}/v_2$; $\overline{BC} = s - 2d \tan i$; therefore,

$$t_2 = \frac{s}{-} + \frac{2d}{-} \cos i. \tag{9-43}$$

Differentiation of this equation gives $ds/dt_2 = v_2 = \cotan \beta$. Without physical contact with the lower layer it is thus possible to obtain the elastic wave velocity in the layer from the slope of the travel-time curve. Near the shot point the wave traveling directly from A to D arrives ahead of the underlayer wave; beginning with the "critical" distance x, it arrives later than the underlayer wave. A break occurs in the travel-time curve at the distance x, that is, for the simultaneous arrival of both waves. By

O. V. Schmidt, Zeit. Geophys., 12(5/6), 199-205 (1936).

equating (9-42) and (9-43), substituting x for s, and multiplying both sides by $v_1/\cos i$,

$$\frac{x}{2}\left(\frac{1 - \dfrac{v_1}{v_2}}{\cos i}\right) = d = \frac{x}{2} \cdot \sqrt{\frac{v_2 - v_1}{v_2 + v_1}}$$

where $C_1 \equiv \frac{1}{2}\sqrt{\dfrac{v_2 - v_1}{v_2 + v_1}}$ is a constant for any area as long as overburden and underlayer velocities remain constant. A number of travel-time
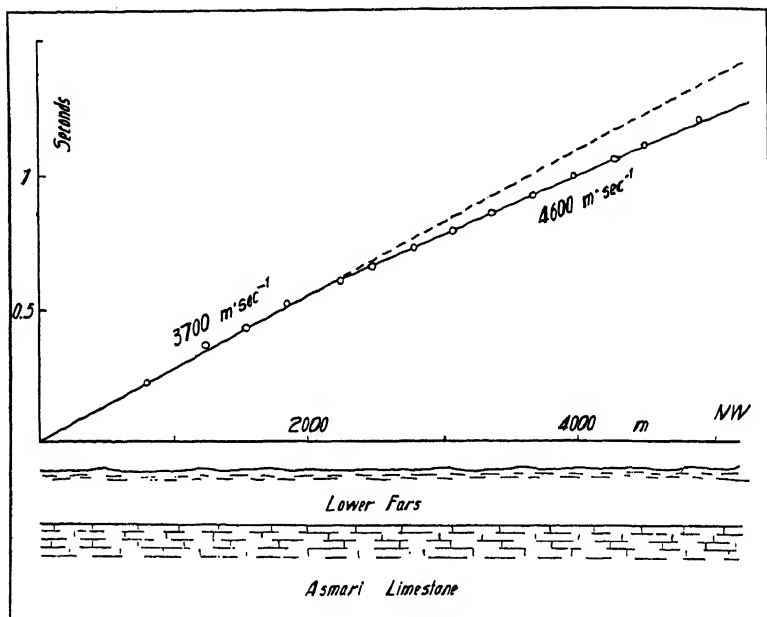
FIG. 9-46. Strike travel-time curve on anticline of Masjid-I-Suleiman, Persia (after Rankine).

curves for a single horizontal bed of varying thickness are given in Fig. 9-41. Fig. 9-46 is a good example of a depth determination in the single-layer case (limestone under shale on crest of anticline).

From eq. (9-44) it is seen that the depth is always less than $x/2$. The break in the travel-time curve occurs at distances at least twice the depth when the velocity contrast is great, but the break moves further out from the shot point as the contrast is reduced. If q is refractive index and r its reciprocal (ratio of velocity in lower and upper medium),

$$x = 2d$$

[31] Examples of depth calculations are given on p. 510.

In another method of depth computation, the second part of the travel-time curve is extended to the intersection with the abscissa, obtaining the distance D. Then

$$d = \frac{D}{2} \tan i. \tag{9-44c}$$

A third method uses the time intercept t_0 on the ordinate:

$$d = \frac{t_0}{2} \cdot v_2 \cdot \tan i = \frac{t_0}{2} \frac{v_1}{\cos i}. \tag{9-44d}$$

A fourth method of depth calculation is based on the time t_x of the intercept:

$$d = \frac{v_1 t_x}{2} \sqrt{\frac{v_2 - v_1}{v_2 + v_1}}. \tag{9-44e}$$

The determination of depth is as accurate as the measurement of distance between shot point and receiver, other things being equal. It depends, further, on the relief (accuracy of elevation correction), on the accuracy of timing of the impulses, and on the difference in velocities. Other refraction methods for the two-layer case, using different interpretation methods and different field technique, are discussed on pages 533 and 546.
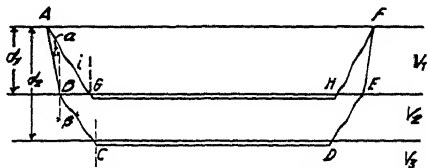
FIG. 9-47. Wave paths, two-layer case.

5. *Two horizontal layers.* In the single-layer case impulses past the first break in the travel-time curve arrive by the path $AGHF$ (see Fig. 9-47). If a third layer is within range, these will be overtaken by waves traveling along the path $ABCDEF$, and the travel-time curve will now have two breaks. Let the velocities of the three media be v_1, v_2, and v_3, and the respective depths of their lower surfaces d_1 and d_2. Then $\sin \beta = v_2/v_3$, since the angle at C is 90°. For the remainder of the path in the upper layer, $\sin \alpha / \sin \beta = v_1/v_2$. Substituting $\sin \beta$, $\sin \alpha = v_1/v_3$.

In the expression for the underlayer travel time, (9-43), the first term represents the underlayer effect and the second that of the overburden. By analogy, the time for the path $ABCDEF$ is composed of one underlayer time and two overburden times, so that

$$t_3 = \frac{s}{v_3} + \frac{2(d_2 - d_1)}{v_2} \cos \beta + \frac{2d_1}{v_1} \cos \alpha. \tag{9-45a}$$

The second part of the travel-time curve gives the velocity through the second layer, and the third part gives that through the third layer. By

differentiation of eq. (9–45a), $\tan \gamma = dt_3/ds = 1/\mathbf{v}_3$. Neither the first nor the second layer is effective after the break x_2 is passed. For determining the depth d_2, let $t_2 = t_3$. By equating eqs. (9–42) and (9–45a), substituting x_2 for s, and proceeding as before,

$$\frac{x_2}{2} \sqrt{\frac{\mathbf{v}_3 - \mathbf{v}_2}{\mathbf{v}_3 + \mathbf{v}_2}} + d_1 \left[1 + \frac{1}{\sin i \cos \beta} (\cos i - \cos \alpha) \right] = d_2. \qquad (9\text{–}45b)$$

All data for the computation of the depth of the lower surface of the second layer are obtainable from the travel-time curve, since $\sin i = \mathbf{v}_1/\mathbf{v}_2$, $\sin \beta = \mathbf{v}_2/\mathbf{v}_3$, and $\sin \alpha = \mathbf{v}_1/\mathbf{v}_3$. The depth to the bottom of the second layer may also be calculated by extending the $\mathbf{v}_1$ and $\mathbf{v}_3$ portions of the travel-time curve to the intersection at the abscissa x_{13} (Fig. 9–48). Then[32]

$$d_2 - d_1 = \frac{x_{13}(1 - \sin \alpha) - 2d_1 \cos \alpha}{2 \sin i \cos \beta}. \qquad (9\text{–}45c)$$

Another convenient depth-calculation method uses the time obtained on the ordinate by extending back the third part of the travel-time curve. Then from eq. (9–45a), with $T_3 \equiv t_3$ for $s = 0$ and h_2 for $d_2 - d_1$,

$$T_3 = \frac{2h_2}{\mathbf{v}_2} \cos \beta + \frac{2d_1}{\mathbf{v}_1} \cos \alpha. \qquad (9\text{–}45d)$$

As an example of depth calculations in the single- and two-layer case, the curves in Fig. 9–48 furnish: $x_1(= x_{12}) = 1000$ m; $x_{23}(= x_2) = 3000$ m; $x_{13} = 1750$ m; $\mathbf{v}_1 = 1000$ m·sec^{-1}; $\mathbf{v}_2 = 2000$ m·sec^{-1}; $\mathbf{v}_3 = 5000$ m·sec^{-1}. Hence, $\sin \alpha = \mathbf{v}_1/\mathbf{v}_3 = 11.5°$; $\sin \beta = \mathbf{v}_2/\mathbf{v}_3 = 23.5°$; $\sin i = \mathbf{v}_1/\mathbf{v}_2 = 30°$.

$$d_1 = \frac{x_1(1 - \sin i)}{2 \cos i} = \frac{500 \cdot 0.5}{0.866} = 289 \text{ m};$$

$$d_2 - d_1 = \frac{x_2}{2} \sqrt{\frac{\mathbf{v}_3 - \mathbf{v}_2}{\mathbf{v}_3 + \mathbf{v}_2}} + d_1 \frac{\cos i - \cos \alpha}{\sin i \cos \beta}$$

$$= 1500 \sqrt{\frac{5000 - 2000}{5000 + 2000}} + 289 \frac{0.866 - 0.979}{0.5 \cdot 0.916} = 911 \text{ m};$$

Also,

$$d_2 - d_1 = \frac{x_{13}(1 - \sin \alpha) - 2d_1 \cos \alpha}{2 \sin i \cos \beta}$$

$$= \frac{1750 \cdot 0.8 - 578 \cdot 0.979}{0.916} = 911 \text{ m}.$$

---

[32] Schmidt, *op. cit.*, **7(1/2)**, 37–56 (1931).
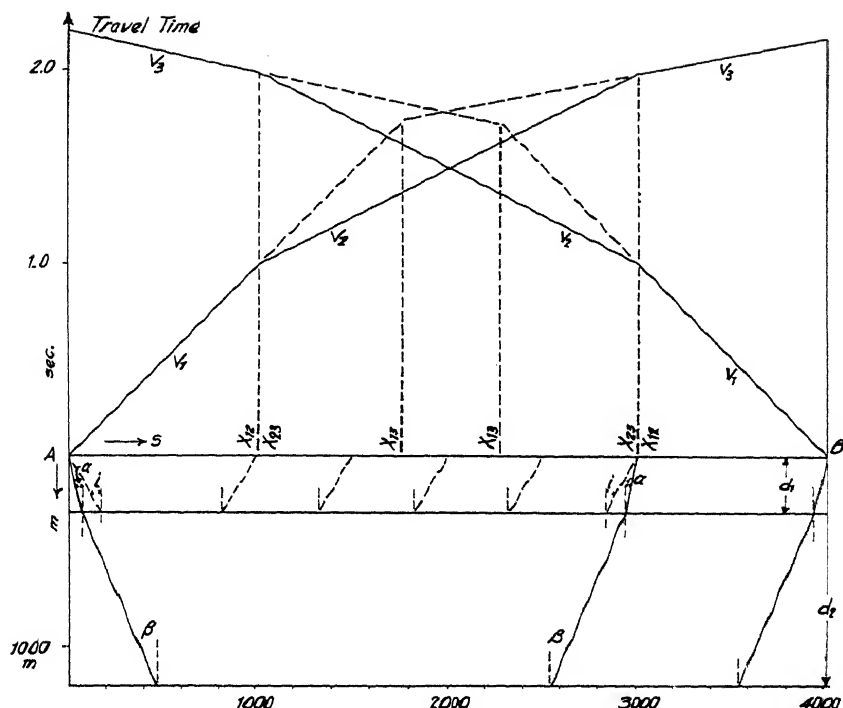
FIG. 9-48. Depth calculation of two layers from intercept distances (after O. v. Schmidt).
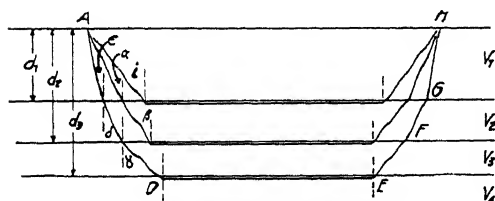
FIG. 9-49. Wave paths, three-layer case.

6. *Three horizontal layers.* The seismic ray follows the path $ABCDEFGH$; the velocities are v_1, v_2, v_3, v_4; the angles at the formation boundaries are ϵ, δ, and γ as shown in Fig. 9-49 in which the two- and three-layer paths have been indicated for comparison. The angle at D is $90°$; hence, $\sin \gamma = v_3/v_4$. Furthermore, $\sin \beta = \sin \delta/\sin \gamma = v_2/v_3$ and $\sin \delta = v_2/v_4$. Also, $\sin i = \sin \epsilon/\sin \delta = v_1/v_2$ and $\sin \epsilon = v_1/v_4$. The travel time

$$t_4 = \frac{s}{v_4} + \frac{2(d_3 - d_2)}{v_3} \cos \gamma + \frac{2(d_2 - d_1)}{v_2} \cos \delta + \frac{2d_1}{v_1} \cos \epsilon. \qquad (9\text{-}46a)$$

The fourth part of the travel-time curve corresponds only to the velocity in the fourth layer, since $dt_4/ds = 1/v_4$. For the simultaneous arrival

of the waves with the travel times t_3 and t_4, a break with the abscissa x_3 occurs, and the depth d_3 may be computed as before:

$$\frac{x_3}{2} \sqrt{\frac{\mathbf{v}_4 - \mathbf{v}_3}{\mathbf{v}_4 + \mathbf{v}_3}} + \frac{d_2 - d_1}{\sin \beta \cos \gamma} (\cos \beta - \cos \delta) + \frac{d_1}{\sin \alpha \cos \gamma} (\cos \alpha - \cos \epsilon)$$

$$(9\text{–}46b)$$
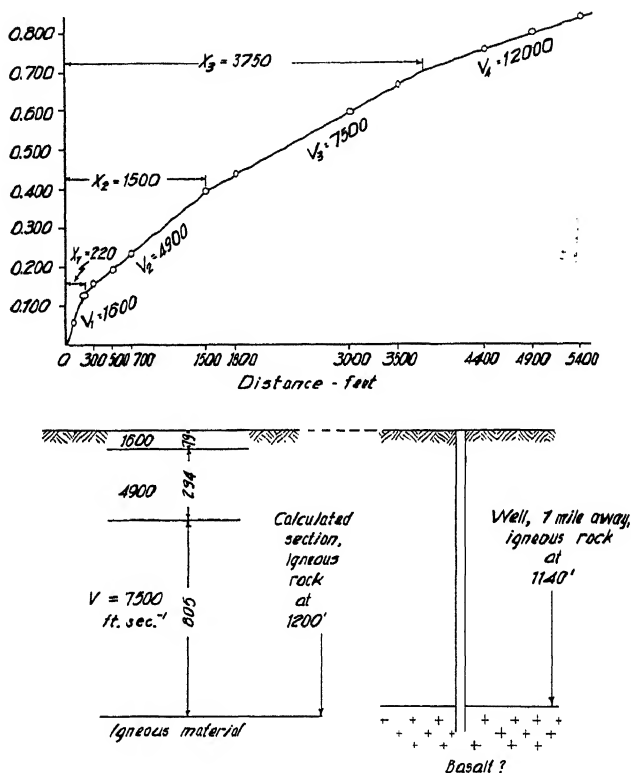
FIG. 9-50. Refraction profile, calculated section, and results of drilling (southern California). (Adapted from F. Rieber.)

Again a more convenient method for depth calculation is the use of the travel time corresponding to the ordinate intercept. Then, from eq.), with $s = 0$, $d_3 - d_2 \equiv h_2$, and so on,

$$\Gamma_4 = \frac{2h_3}{\mathbf{v}_3} \cos \gamma + \frac{2h_2}{\mathbf{v}_2} \cos \delta + \qquad \cos \epsilon. \qquad (9\text{–}46c)$$

Fig. 9–50 gives an example of a travel-time curve in the three-layer case, shot in one direction only. This profile was made in southern California. The sedimentary section is probably Pico formation with sands

and shales of increasing velocity, and the lowest layer is igneous material, probably basalt and basaltic agglomerates. The depth determination based on the travel-time curve gives 1200 feet for this igneous material; a well drilled a mile away from the profile encountered it at 1140 feet.

7. *Multilayer case.* If d_n is the depth to the lower surface of an nth layer, $h_n \equiv d_n - d_{n-1}$ its thickness, v_n its velocity, and α a refraction angle, then the travel time corresponding to the next $(n + 1)$ layer is at the distance s:

$$t_{n+1} = \frac{s}{v_{n+1}} + 2 \sum_1^n \frac{d_n - d_{n-1}}{v_n} \cdot \cos \alpha_n. \qquad (9\text{-}47a)$$

For depth calculations it is more convenient to use eq. (9-47a), as applied to the intercept travel time on the ordinate instead of the distance (x) intercepts. Hence, with T as (ordinate) travel time for $x = 0$:

$$T_{n+1} = 2 \sum_1^n \frac{h_n}{v_n} \cos \alpha_n. \qquad (9\text{-}47b)$$

Likewise convenient for depth calculations is the use of travel times corresponding to the distance intercepts x_n. Substituting x_n for s and solving for the thickness of the deepest layer,

$$2 \frac{h_n}{v_n} \cos i_n = t_{n+1} - \left(\frac{x_n}{v_{n+1}} + 2 \sum_{k=1}^{k=n-1} \frac{h_k}{v_k} \cos \alpha_k \right), \qquad (9\text{-}47c)$$

where i_n is the critical angle in the nth layer.

By comparison with eqs. (9-43), (9-45a), and (9-46a), this is seen to give for the successive thicknesses:

$$\frac{2d_1}{v_1} \cos i_1 = t_2 - \frac{x_1}{v_2};$$

$$\frac{2h_2}{v_2} \cos i_2 = t_3 - \left(\frac{x_2}{v_3} + \frac{2h_1}{v_1} \cos \alpha_1 \right)$$

$$\frac{2h_3}{v_3} \cos i_3 = t_4 - \left(\frac{x_3}{v_4} + \frac{2h_1}{v_1} \cos \alpha_1 + \frac{2h_2}{v_2} \cos \alpha_2 \right),$$

and so on. Application of these formulas to depth calculations of five layers is shown in Fig. 9-51 and the schematic on page 515. Results of a seven-mile shot are shown there, evaluated in the form of velocities, intercept distances, and travel times corresponding to them. These data are entered in columns II, III, and IV. Next is the calculation of all angles of total refraction i_n in columns V through VII. Similarly, the refraction angles α_k (k varies from 0 to $n - 1$) are calculated in columns VIII through X. The procedure is seen to be in accordance with formulas preceding (9-45a)

and (9–46a). Next follows the ratio x/v, and in column XII is given the time spent in all layers above the nth. For successive layers column XII is obtained by multiplying the $2h/v$ values in column XV by the cosine values in column IX. Column XIII is the sum of XI and XII, and XIII in turn is deducted from II, giving $2h/v \cos i$ in column XIV, which is divided by $\cos i_n$ of column VI. Thus, the thickness (XVI) and the total depths (XVII) are obtained.
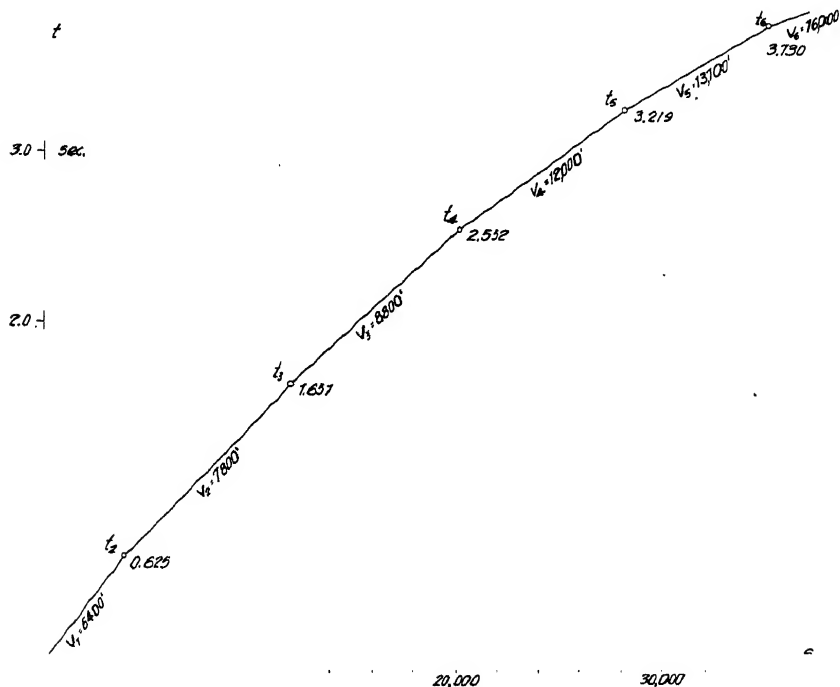
FIG. 9-51. Multiple layer travel-time curve.

8. *Vertical steps and domes.* Travel-time curves obtained on faults, terraces, buried escarpments, salt domes, and igneous intrusions often approach the simple cases discussed in the following section. Contrary to conditions treated previously, formations are not continuous in horizontal direction or are not parallel with the surface for the entire length of the profile. Hence, additional unknowns enter. These can be determined by taking two profiles in opposite directions or by shooting at two shot points at different distances from the detector spread. In the following discussion the direction of shooting is assumed to be at right angles to the strike; however, the same problems may also be handled by shooting parallel with the strike.

n	l_{n+1}	x_n (in feet)	v_n (in feet)	$\dfrac{v_n}{v_{n+1}}$	$\cos i_n$	i_n	$\dfrac{v_k}{v_{n+1}}$	$\cos \alpha_k$	α_k	$\dfrac{x_n}{v_{n+1}}$	$2\sum\dfrac{h_k}{v_k}\cos\alpha$	XI + XII	$2\dfrac{h_n}{v_n}\cos i_n$	$\dfrac{2h_n}{v_n}$	h_n	d_n
1	0.625	4,000	6,400	0.8203	0.572	55°1'	...	...	...	0.5128	...	0.5128	$\left\{\begin{array}{l}0.112\\(\text{II}-\text{XIII})\end{array}\right.$	0.196	626.5	626.5
2	1.851	12,000	7,800	0.8783	0.4782	61°4'	v_1/v_3 ⌇ v_1/v_4 ⌇	0.6926 / 0.846	46°2' / 32°2'	1.351	$\left\{\begin{array}{l}(\text{XV}_1 \times \text{IX}_2)\\0.1357\\0.1656\end{array}\right\}$	1.487	0.164	0.3430	1338	1964
3	2.552	20,000	8,880	0.7400	0.6726	47°7'	v_2/v_4 ⌇ v_1/v_5 ⌇	0.760 / 0.884	40°5' / 27°8'	1.667	$\left\{\begin{array}{l}0.2606\\0.173\end{array}\right\}$	2.0932	0.459	0.6821	3028	4992
4	3.219	28,000	12,000	0.8758	0.4828	61°2'	v_2/v_5 ⌇ v_3/v_5 ⌇	0.822 / 0.761	34°7' / 40°4'	2.044	$\left\{\begin{array}{l}0.2818\\0.5192\end{array}\right\}$	3.018	0.201	0.4162	2497	7489
5	3.730	35,000	13,700	0.8562	0.5165	58°9'	v_1/v_6 ⌇ v_2/v_6 ⌇ v_3/v_6 ⌇ v_4/v_6 ⌇	0.917 / 0.873 / 0.832 / 0.6615	23°6' / 29°2' / 33°7' / 48°6'	2.187	$\left\{\begin{array}{l}0.1795\\0.2993\\0.5070\\0.2753\end{array}\right\}$	3.5081	0.222	0.4297	2943	10432
6	...	...	16,000	...	...	...				...		...	...	...	...	...
I	II	III	IV	V	VI	VII	VIII	IX	X	XI	XII	XIII	XIV	XV	XVI	XVII

$$2\frac{h_n}{v_n}\cos i_n = l_{n+1} - \left(\frac{x_n}{v_{n+1}} + 2\sum_{k=1}^{k=n-1}\frac{h_k}{v_k}\cos\alpha_k\right)$$

In the simple case illustrated in Fig. 9–52,[33] the first part of the curve is given by $t_1 = s/v_1$. Then follows, past the intercept x_1, the travel time t_2 for a single horizontal layer. This is $s/v_2 + 2d/v_1 \cos i$. Beyond the edge of the step the rays travel through the low-velocity medium only. Their path becomes increasingly horizontal with increasing distance so
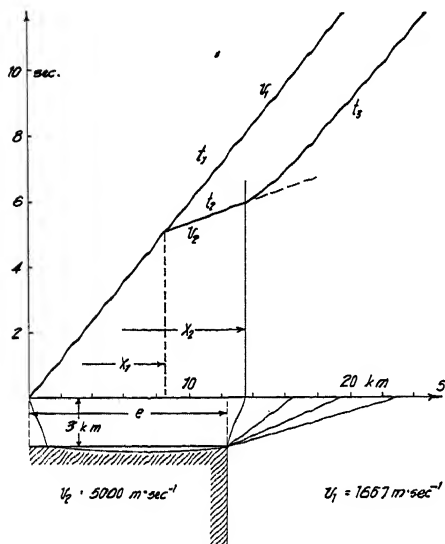
FIG. 9-52. Travel-time curve for deep-seated fault block.
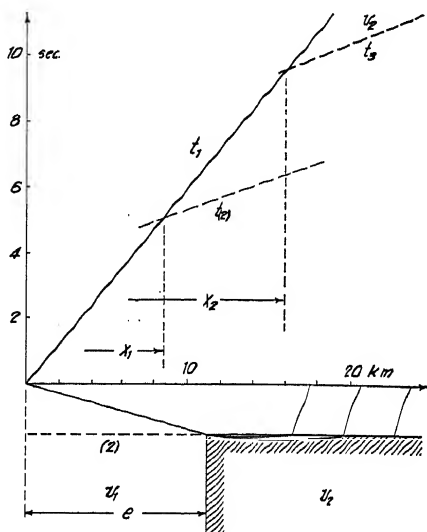
FIG. 9-53. Reverse travel-time curve for deep-seated fault block.

that the travel-time curve past x_2 rapidly approaches the slope corresponding to the overburden velocity v_1. Then the travel time

$$t_3 = \frac{d}{v_1 \cos i} + \frac{e - d \tan i}{v_2} + \frac{\sqrt{d^2 + (s - e)^2}}{v_1}$$

or

$$t_3 = \frac{e}{v_2} + \frac{d \cos i}{v_1} + \frac{\sqrt{d^2 + (s - e)^2}}{v_1}. \qquad (9\text{--}48a)$$

For greater distances the last term approaches $s - e/v_1$, so that $ds/dt_3 \doteq v_1$. The distance of the scarp from the shot point is given by

$$e = x_2 - d \tan i; \qquad (9\text{--}48b)$$

d is calculated from x_1 and i follows from v_1 and v_2. This formula will give only an approximate value, for x_2 cannot be accurately determined.

[33] Travel-time curves in these figures were calculated for long-range shots to determine regional basement structure.

If the same profile is shot in the opposite direction, a travel-time curve identical with the one for a single horizontal layer, but with increased intercept distance, is obtained (Fig. 9-53). Hence, its interpretation alone would give too great a depth unless the same profile is shot in the opposite direction. Together, both travel-time curves furnish an accurate
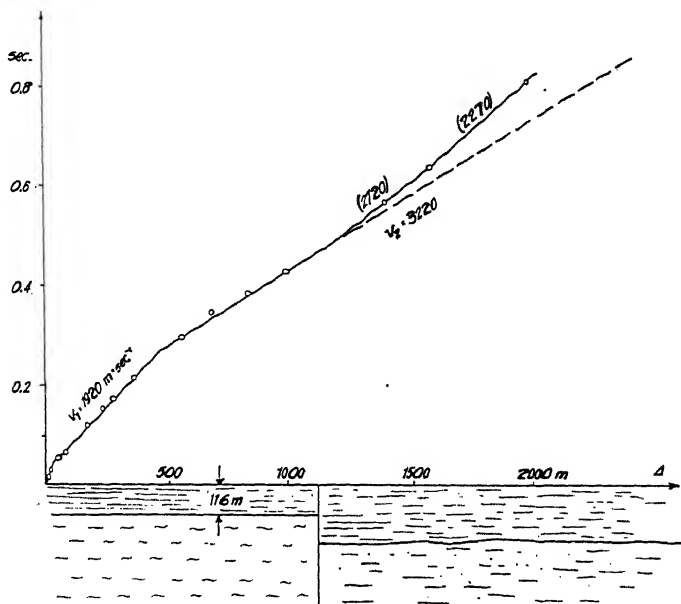
FIG. 9-54. Travel-time curve, Marafael, Venezuela (adapted from O. v. Schmidt).

value for the location of the vertical face. If, from the up-scarp time

$$t_3 = \frac{d}{v_1 \cos i} + \frac{s - e - d \tan i}{v_2} + \frac{\sqrt{e^2 + d^2}}{v_1},$$

the t_2 down-scarp time for the same distance,

$$t_2 = \frac{2d}{v_1 \cos i} + \frac{s - 2d \tan i}{v_2},$$

is deducted, one obtains for e

$$e = \frac{v_1(t_3 - t_2) + d \cos i}{\sqrt{1 + \left(\dfrac{d}{e'}\right)^2} - \sin i}, \qquad (9\text{-}48c)$$

where e' is the approximate distance of the scarp from the shot point calculated from eq. (9-48b).

Combination of two travel-time curves, as in Figs. 9–52 and 9–53, gives the curve for a salt dome or intrusion with vertical flanks (see Fig. 9–39).
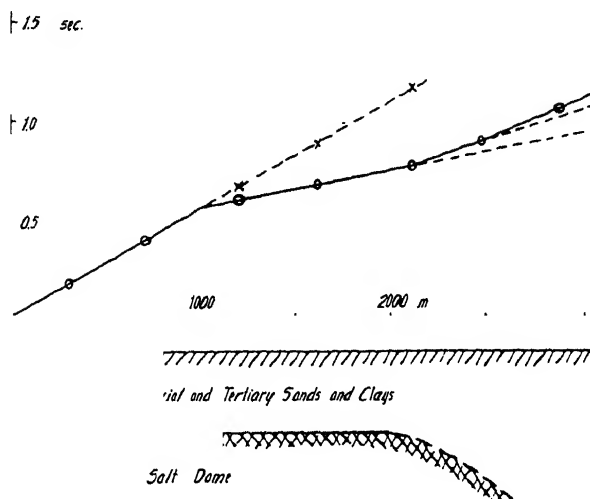
FIG. 9-55. Travel-time curve across salt dome (after Rankine).
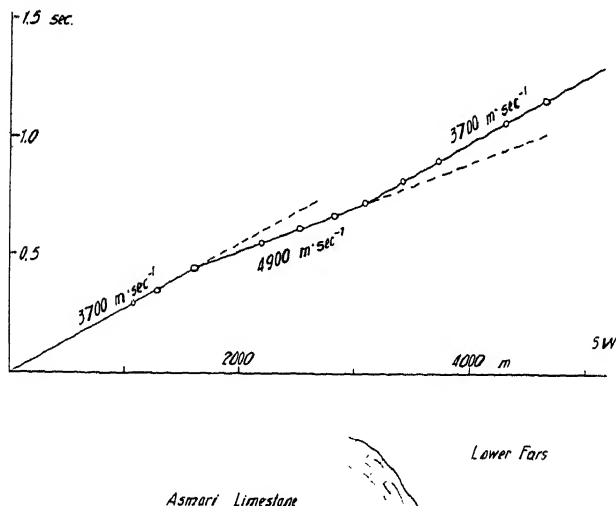
FIG. 9-56. Refraction profile across strike of Masjid-I-Suleiman anticline, Persia (after Rankine).

In some cases the assumption of a homogeneous overburden, as made here, does not furnish the actual travel times accurately enough. Then an assumption of a uniform increase of velocity with depth is required or

the section is split up into individual layers as discussed in the preceding chapter. Data pertaining to the normal section may be obtained from off-dome travel-time curves.[34]

Figs. 9-54, 9-55, and 9-56 are examples of the problem treated here, shooting downward from a faulted block, from the edge of a salt dome, and from a limestone ridge.

When faults, scarps, terraces, and the like, have shapes indicated in Figs. 9-57 and 9-58, additional branches appear at the end of the travel-time curve because the faulted-down portions of the high-speed

FIG. 9-57. Travel-time curve for deep-seated escarpment.

media are within range. Down scarp, the last part of the travel-time curve is given by

$$t_4 = \frac{1}{v_1 \cos i}(d_1 + d_2) + \frac{s - e - d_2 \tan i}{v_2}$$
$$+ \frac{\sqrt{(e - d_1 \tan i)^2 + (d_2 - d_1)^2}}{v_2}. \quad (9\text{-}49a)$$

If the displacement of the fault is small, the sloping path from the point of incidence to the bottom of the scarp may be assumed to be equal to the horizontal path along its surface, so that

$$t_4 = \frac{2d_1 \cos i}{v_1} + \frac{s}{v_2} + \frac{(d_2 - d_1) \cos i}{v_1}. \quad (9\text{-}49b)$$

By differentiation it follows that this part of the travel-time curve has the same slope as the second part. By subtracting t_2 from t_4, we obtain Δt (see Fig. 9-57), which gives the height $(d_2 - d_1)$ of the scarp:

$$d_2 - d_1 = \Delta t v_1 \cos i. \quad (9\text{-}49c)$$

In the reverse direction of shooting, the rays emerging from the top surface on the right are no longer parallel because of the different angles of incidence from below. This causes a deviation of the last part (t_4) of
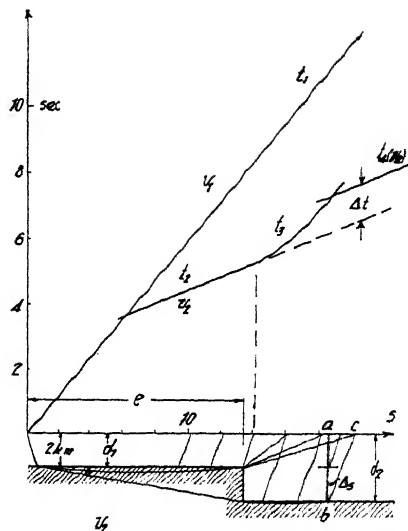
[34] I. Roman, A.I.M.E. Geophys. Pros., 493 (1934).
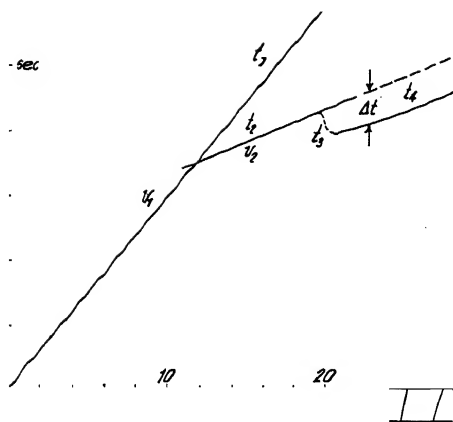
the travel-time curve from a straight line. Where it is nearly enough parallel with the t_2 curve, the time difference Δt may be determined and is again approximately proportional to the displacement $d_2 - d_1$. Fig. 9–59 is an example of the determination of depth of overburden and displacement of a fault at the same time. The first part of the profiles shown are at right angles to a fault, and the second part (profile D) is in the strike of a fault, which had been located by torsion balance observations and by wells. Faults are of commercial importance in this area, as the occurrence of hematite ore in the limestone is associated with the faults. In this case the seismic problem was

G. 9-58. Reverse travel-time curve for deep-seated escarpment.
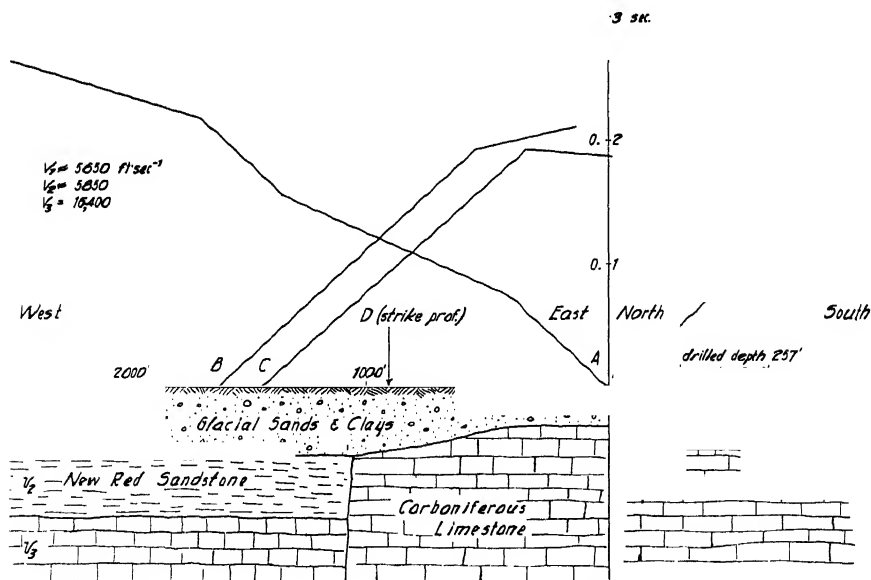
Fig. 9-59. Seismic refraction profiles, hematite district, Millom, Cumberland, England (after Shaw).

comparatively simple, inasmuch as the velocity in the red sandstone was almost identical with the velocity in the overburden. The profile shot down the fault from A is almost the same as the ideal profile of Fig. 9-57. However, in the second part of the travel-time curve the velocity is not a true but an apparent velocity, since the profile is shot down the dip. Therefore, the velocity in the last part of the travel-time curve does not coincide with that in the second part. Furthermore, the third part of the curve is not curved as required by the theory but is straight.

B and C represent the up-fault and also the up-dip profiles, as far as the boundary between overburden and limestone to the east of the fault is concerned. This explains the negative apparent velocity in profile C, second part of the curve. Profile D was shot in the strike, along the line
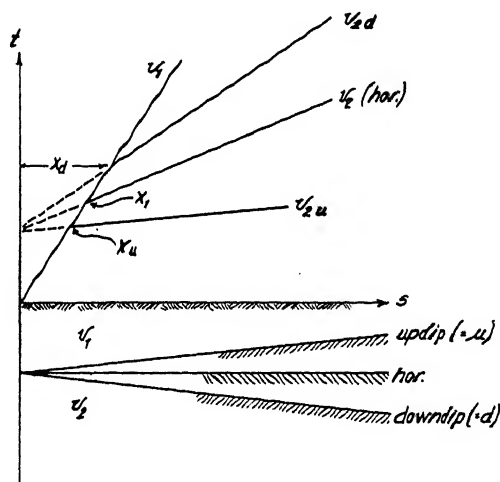
FIG. 9-60. Schematic up- and down-dip travel-time curves.

indicated in the figure. The travel-time curve is that of a single layer; the calculated depth was 245 feet, the actual depth 257 feet. Considering that the dip is 10° and that the depth calculated from the refraction profile is the oblique depth, the discrepancy of 12 feet is reduced to 8 feet.

9. *Single dipping layer.* In the cases previously considered, the travel-time curves gave, with a few exceptions, the true velocities of the subsurface formations. For dipping layers this is no longer true; the slope of the travel-time curve depends upon the dip. Hence, it no longer represents the true underlayer velocity but an apparent velocity which depends on both the dip and the velocity ratio. As seen in Fig. 9-60, the first part of the travel-time curve always corresponds to v_1. If the bed dips away from the origin, the seismic ray travels a greater distance through the upper medium. This results in increased travel time, decreased ap-

parent velocity v_{2d}, and increased intercept distance x_d. When the stratum dips up from the origin, the ray travels a greater distance through the lower high-speed medium. Travel times are reduced; the apparent velocity (v_{2u}) is greater than in the case of a horizontal bed and the intercept distance (x_u) is less. The apparent velocity depends upon both dip and velocity ratio. One profile is not sufficient to determine velocities and dip. Hence, shots are fired at two points on one side of the spread, or else the direction of shooting is reversed and profiles are shot up dip and down dip. This may be accomplished by two shot points on either end of the profile, or by one shot point in the center of two receiver spreads, the former being the preferred procedure.

In Fig. 9-61 let φ be the dip, H the depth vertically below the shot point, and h the depth below the receiving point. Depths normal to the stratum are Z and z. The profile is assumed to be at right angles to the
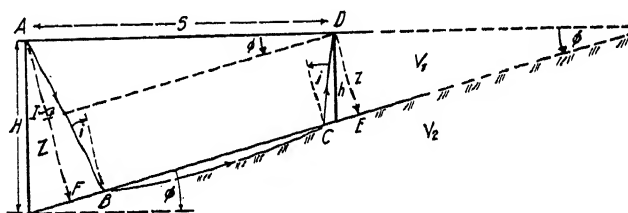
FIG. 9-61. Refraction path in dip shooting.

strike, that is, in the direction of maximum dip. The first part of the travel-time curve is given by $t_1 = s/v_1$. For the second part the time for the path $ABCD = t_2 = (\overline{AB} + \overline{CD})/v_1 + \overline{BC}/v_2$. Since $\overline{AB} = Z/\cos i$, $\overline{DC} = z/\cos i$, $\overline{AD} = s$, $\overline{FE} = \overline{ID} = s \cos \varphi$, $\overline{AI} = s \sin \varphi = Z - z$, $\overline{FB} = Z \tan i$, $\overline{CE} = z \tan i$, and $\overline{BC} = \overline{ID} - \overline{FB} - \overline{CE}$,

$$\frac{Z + z}{\cos i} \qquad \frac{s \cos}{v_2} \qquad (9\text{-}50a)$$

For the up-dip case, substitute for z: $Z - s \sin \varphi$, and $\sin i/v_1$ for $1/v_2$; then

$$t_{2u} \quad \frac{2Z \cos i}{v_1} \quad \frac{s}{v_1} \quad (\quad) \qquad (9\text{-}50b)$$

If for the down-dip case $Z = z + s \sin \varphi$,

$$t_{2d} = \frac{2z \cos i}{v_1} + \frac{s}{v_1} \sin (i + \varphi). \qquad (9\text{-}50c)$$

Since $Z = H \cos \varphi$ and $z = h \cos \varphi$,

$$t_{2u} = \frac{2H \cos \varphi \cos i}{v_1} + \frac{s}{v_1} \sin (i - \varphi)$$

and $\left.\begin{array}{l} \\ \\ \\ \\ \\ \\ \end{array}\right\}$ (9-51)

$$t_{2d} = \frac{2H \cos \varphi \cos i}{v_1} + \frac{s}{v_1} \sin (i + \varphi).$$

The apparent velocities for the up- and down-dip cases are obtained by differentiation of eq. (9-51):

$$v_{2u} = \frac{v_1}{\sin (i - \varphi)} \qquad \text{and} \qquad v_{2d} = \frac{v_1}{\sin (i + \varphi)}. \qquad (9\text{-}52)$$

Hence, eqs. (9-51) become

$$t_{2u} = \frac{2H \cos \varphi \cos i}{v_1} + \frac{s}{v_{2u}}$$

and $\left.\begin{array}{l} \\ \\ \\ \\ \\ \\ \end{array}\right\}$ (9-53a)

$$t_{2d} = \frac{2H \cos \varphi \cos i}{v_1} + \frac{s}{v_{2d}}.$$

The true underlayer velocity is *not* the arithmetic mean of the two apparent velocities. From eq. (9-52)

$$v_2 = 2 \cos \varphi \cdot \frac{v_u \cdot v_d}{v_u + v_d}. \qquad (9\text{-}53b)$$

The true velocity has the same relation to the up-dip and down-dip velocities as a resultant resistance has to its component resistances in parallel. In the example of Fig. 9–63 (where $v_{2u} = 6190$ and $v_{2d} = 2790$), the above formula gives $v_2 = 3795$, whereas the arithmetic mean is 4490. From eq. (9-52) the critical angle i and the dip are calculated as follows:

$$i = \tfrac{1}{2}\left(\sin^{-1}\frac{v_1}{v_{2u}} + \sin^{-1}\frac{v_1}{v_{2d}}\right)$$

$\left.\begin{array}{l} \\ \\ \\ \\ \end{array}\right\}$ (9-54)

$$\varphi = \tfrac{1}{2}\left(\sin^{-1}\frac{v_1}{v_{2d}} - \sin^{-1}\frac{v_1}{v_{2u}}\right),$$

and the true underlayer velocity is obtained from $v_2 = v_1/\sin i$. Fig. 9-62 shows apparent up- and down-dip velocities for dip angles up to $\pm 40°$ and for velocity ratios of four ($i = 15°$) and two ($i = 30°$). The variation is small down dip. On shooting up dip, the velocities change rapidly when the dip angle approaches the critical angle, and they become plus and

minus infinite in this range and negative after dip angles pass the critical range.   The lower layer is not detectable if $i + \varphi$ exceeds 90°; the ray emerging from it does not return to the surface.

The depths of an inclined layer under either shot point may be determined from the overburden velocity, the up- and down-dip velocity, and the distances of the intercepts from the shot points.   For the two directions of shooting, two intercepts are observed, x_u and x_d.   As at the intercept, $t_1 = t_{2u} = t_{2d}$ and $t_1 = x/\mathbf{v}_1$, we have, from eq. (9–51),

$$H_u = x_u \cdot \frac{-\sin(i - \varphi)}{2 \cos \varphi \cos i} \quad \text{and} \quad {}^{\iota} = x_d \cdot \frac{1 - \sin(i + \varphi)}{2 \cos \varphi \cos i}$$

where H_u is the *depth vertically under the shot point* when shooting up dip,
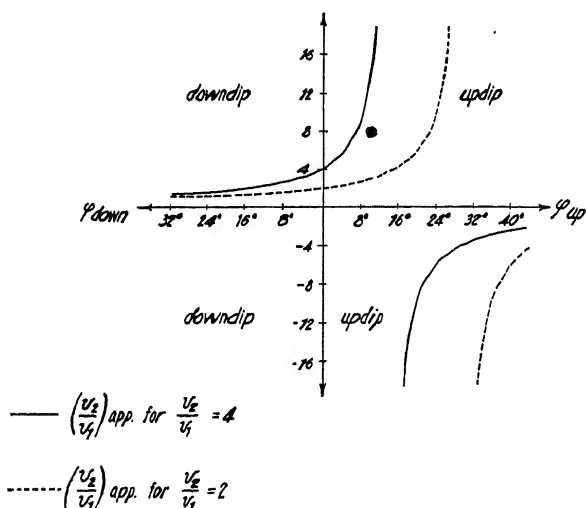
FIG. 9-62. Apparent velocities for up- and down-dip angles from 0° to 40° (after Meisser).

and h_d is the depth under the shot point when shooting down dip.   By substitution of (9–52),

$$H_u = \frac{x_u}{2 \cos \varphi \ \cos i} \cdot \left(1 - \frac{\mathbf{v}_1}{\mathbf{v}_{2u}}\right)$$

and

$$h_d = \frac{x_d}{2 \cos \varphi \ \cos i} \left(1 - \frac{\mathbf{v}_1}{\mathbf{v}_{2d}}\right).$$

$$\left.\begin{array}{r}\\ \\ \\ \\ \\ \\ \\ \end{array}\right\} \quad (9\text{--}55b)$$

Calculation of depth proceeds, therefore, in the following order: (1) plot travel-time curves; (2) determine $\mathbf{v}_{2d}$ and $\mathbf{v}_{2u}$; (3) determine x_u and x_d ;

(4) compute $i + \varphi$, $i - \varphi$, i, and φ; (5) compute v_2; (6) compute H and h; check result with s and φ.

Fig. 9-63 illustrates steps 1 to 3 in the evaluation of two travel-time curves. By step 4, $\sin (i - \varphi) = \frac{1600}{6190} = 0.259$; $i - \varphi = 15°$; $\sin (i + \varphi) =$ = 0.574; $i + \varphi = 35°$; $i = 25°$; $\varphi = 10°$. $v_2 = v_1/\sin i = \frac{160}{0.4\underline{1}}$

$H = 235 (1 - 0.259)/2 \cdot 0.985 \cdot 0.906 = 97.5 \,\mathrm{m}$; $h = 150(1 - 0.574)/$ $1.97 \cdot 0.906 = 35.9 \,\mathrm{m}$; $s = 350 \,\mathrm{m}$; $(H - h)/s = \tan \varphi$; $\frac{61.6}{350} = \tan 10°$. Determination of dip and depth of dipping layers does not necessarily require reversal of direction of shooting. Shots may be fired at two points on the same side of the receiver spread. Shooting down dip, we find that the second part of the travel-time curve is the apparent velocity v_{2d} ;
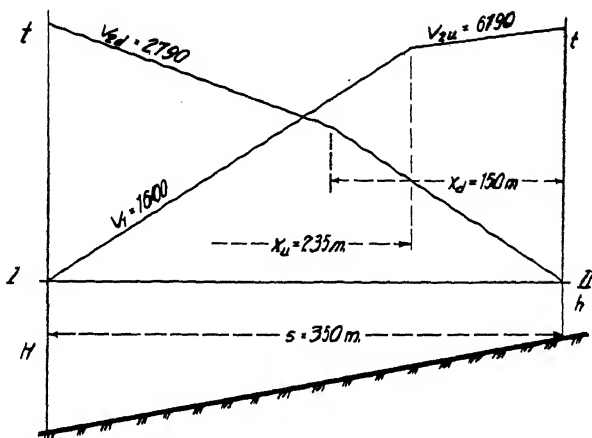
FIG. 9-63. Dip and depth calculation from up- and down-dip refraction profiles.

shooting up dip it is v_{2u} as before. The intercept of t_{2d} with t_1 moves *up* when shooting *down* dip, whereas it moves *down* when shooting *up* dip. Depths h and H may be determined from extended ordinate intercept times.[35]

The relations derived in this section hold only if profiles are shot down or up the *total* dip, that is, at right angles to the strike. If profiles are not shot in this direction, only an *apparent* dip in the direction of the profile is obtained. In Fig. 9-64a[36] the plane $AFED$ is the same as that represented in Fig. 9-61. When this plane is rotated about the shot point A in the direction AD', the rays still travel in a plane at right angles to the dipping bed, $AFE'D'$, whose apparent dip is Φ. If the azimuth of

[35] For formulas, see B. Gutenberg, Lehrb. Geophys., **3**, p. 599.
[36] F. Gassmann, Beitr. angew. Geophys., **4**(3), 358–363 (1934).

the profile AD' is α (from the direction of maximum dip) the relation of apparent and true dip is given by

$$\sin \Phi = \sin \varphi \cos \alpha.$$

The azimuth α may be determined by shooting two profiles each, up and down dip, at right angles to one another (Fig. 9–64b), which give
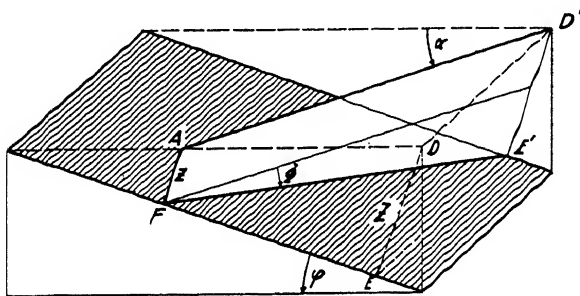
FIG. 9–64a. Relation of apparent dip, true dip, and azimuth (adapted from Gassmann).
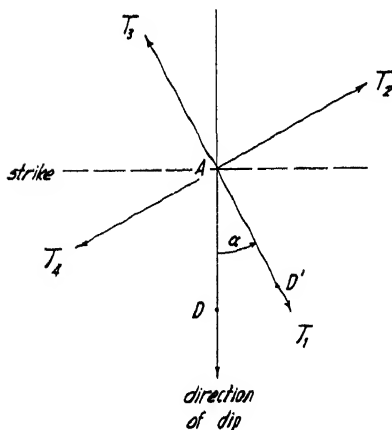
FIG. 9–64b. Two profiles for strike and dip determination (adapted from Gassmann).

four apparent velocities or two groups of up- and down-dip velocities:

$$v'_k = \frac{v_1}{\sin (i + \varphi_k} \qquad (9\text{--}56b)$$

where $k = 1, 2, 3, 4$. The travel-time curves obtained in this case are indicated in Fig. 9–64c, and the azimuth of dip with respect to profile 1 is

$$\frac{v'_1 v'_3}{v'_4 v'_2} \cdot \frac{v'_2 - v'_4}{v'_3 - v'_1} = \tan \alpha. \qquad (9\text{--}56c)$$

If the apparent angle of dip Φ_{1-3} is measured in profile 1–3 and the angle Φ_{4-2} in profile 4–2 by using the relations given in eq. (9–54), then from (9–56a):

$$\frac{\sin \Phi_{4-2}}{\sin \Phi_{1-3}} = \tan \alpha. \qquad (9\text{--}56d)$$

The true dip is then calculated from eq. (9-56a). With the above formulas, relations may readily be set down for two profiles making an arbitrary angle with each other.

10. *Two dipping layers.* Travel times for two inclined layers are derived in the same manner as for the single inclined layer and the double horizontal layer.[37] Thicknesses of layers below the origin will be designated by H for up-dip shooting and by h for down-dip shooting. A profile shot up dip in reference to the upper formation boundary may be down dip in reference to the second boundary. In order to avoid ambiguity, the direc-
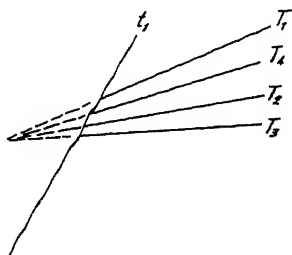
FIG. 9-64c. Travel times for two profiles as in Fig. 9-64b (adapted from Gassmann).
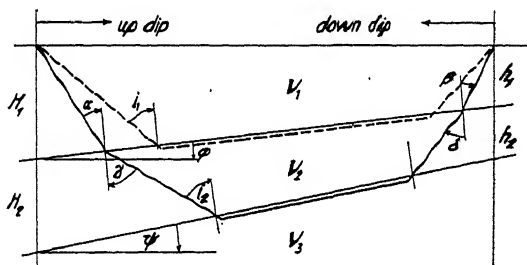
FIG. 9-65. Ray paths in two dipping layers.

tion of shooting will be referred to the upper boundary. With the notations of Fig. 9-65,

$$\sin i_2 = \frac{v_2}{v_3}; \qquad \sin i_1 = \frac{v_1}{v_2}; \qquad \frac{\sin \alpha}{\sin \gamma} = \frac{\sin \beta}{\sin \delta} = \sin i_1 = \frac{v_1}{v_2};$$

$$\gamma = i_2 + (\psi - \varphi) \quad \text{and} \quad \delta = i_2 - (\psi - \varphi).$$

Therefore,

$$\left. \begin{array}{l} \sin \delta = \sin [i_2 - (\psi - \varphi)] = \dfrac{\sin \beta}{\sin i_1} \\[2em] \sin \gamma = \sin [i_2 + (\psi - \varphi)] = \dfrac{\sin \alpha}{\sin i_1} . \end{array} \right\} \qquad (9\text{-}57a)$$

[37] For details see Schmidt, *op. cit.*, **7(1/2)**, 37-56 (1931).

The travel times are:

(a) For up-dip shooting:

$$t_{3u} = \frac{1}{v_1} \{ s_u \sin (\beta - \varphi) + H_{1u}[\cos (\alpha + \varphi) + \cos (\beta - \varphi)]$$

$$+ H_{2u} \cdot 2 \sin i_1 \cos i_2 \cos \psi \}$$

(b) For down-dip shooting:

$$t_{3d} = \frac{1}{v_1} \{ s_d \sin (\alpha + \varphi) + h_{1d}[\cos (\alpha + \varphi) + \cos (\beta - \varphi)]$$

$$+ h_{2d} \cdot 2 \sin i_1 \cos i_2 \cos \psi \}$$

(9-57b)

and the apparent velocities are:

$$v_{3u} = \frac{ds}{dt_{3u}} = \frac{v_1}{\sin (\beta - \varphi)}$$

$$v_{3d} = \frac{ds}{dt_{3d}} = \frac{v_1}{\sin (\alpha + \varphi)}.$$

(9-57c)

Depths may be calculated from intercepts x_1 and x_2 (x_{12}, x_{23}) in the up-dip and down-dip profile. As the relations for x_{12u} and x_{12d} have been given before eq. (9-55), it is assumed that H_1, h_1, and φ are known. For the computation of H_2 and h_2 use is made of the intercepts x_{23u} and x_{23d}; or the first and third parts of the travel-time curve may be extended to the intermediate intercepts x_{13u} and x_{13d}. Then the depths follow from:

(a) The x_{13} intercepts:

$$H_{2u} = \frac{x_{13u}[1 - \sin (\beta - \varphi)] - H_{1u}[\cos (\alpha + \varphi) + \cos (\beta - \varphi)]}{2 \sin i_1 \cos i_2 \cos \psi}$$

and

$$h_{2d} = \frac{x_{13d}[1 - \sin (\alpha + \varphi)] - h_{1d}[\cos (\alpha + \varphi) + \cos (\beta - \varphi)]}{2 \sin i_1 \cos i_2 \cos \psi}$$

(9-58a)

(b) The x_{23} intercepts:

$$H_{2u} = \frac{x_{23u}[\sin (i_1 - \varphi) - \sin (\beta - \varphi)] - H_{1u}[\cos (\alpha + \varphi) + \cos (\beta - \varphi)]}{2 \sin i_1 \cos i_2 \cos \psi}$$

$$+ \frac{H_{1u} 2 \cos i_1 \cos \varphi}{2 \sin i_1 \cos i_2 \cos \psi}$$

$$h_{2d} = \frac{x_{23d}[\sin (i_1 + \varphi) - \sin (\alpha + \varphi)] - h_{1d}[\cos (\alpha + \varphi) + \cos (\beta - \varphi)]}{2 \sin i_1 \cos i_2 \cos \psi}$$

$$+ \frac{h_{1d} 2 \cos i_1 \cos \varphi}{2 \sin i_1 \cos i_2 \cos \psi},$$

(9-58b)

where the substitutions may be made,

$$x_{23u}[\sin (i_1 - \varphi) - \sin (\beta - \varphi)] = \left[\frac{1}{v_{2u}} - \frac{1}{v_{3u}}\right]$$

and

$$\sin (i_1 + \varphi) - \sin (\alpha + \varphi)] = x_{23d} \cdot v_1\left[\frac{1}{v_{2d}} - \frac{1}{v_{3d}}\right].$$

Computation proceeds in the following steps: (1) Compute i_1 and φ from formulas (9-54). (2) Determine $v_2 = v_1/\sin i_1$. (3) Calculate H_1 and

FIG. 9-66. Travel-time curves for two layers of same dip direction (after O. v. Schmidt).

h_1 from eq. (9-55). (4) Find angles α and β from apparent velocities v_{3u} and v_{3d} (formulas [9-57c]). (5) Compute i_2 and $(\psi - \varphi)$ from (9-57a). (6) Find ψ from $(\psi - \varphi)$ and φ. (7) Calculate $v_3 = v_2/\sin i_2$. (8) Find H_2, and (9) h_2 from (9-58).

Two examples are given below, one for boundaries of the same dip direction, the other for boundaries of opposite dips. The corresponding travel-time curves are shown in Figs. 9-66 and 9-67 and furnish the following numerical values:

$$(\text{Fig. 9–66, } \overline{AB} = 2200 \text{ m})$$

<table>
<tr><td align="center">UP-DIP PROFILE</td><td align="center">DOWN-DIP PROFILE</td></tr>
</table>

$$v_1 = 1800 \text{ m} \cdot \text{sec}^{-1} \qquad\qquad \mathbf{v}_1 = 1800 \text{ m} \cdot \text{sec}^{-1}$$

$$v_{2u} = 3415 \text{ m} \cdot \text{sec}^{-1} \qquad\qquad \mathbf{v}_{2d} = 2700 \text{ m} \cdot \text{sec}^{-1}$$

$$v_{3u} = 6530 \text{ m} \cdot \text{sec}^{-1} \qquad\qquad \mathbf{v}_{3d} = 3495 \text{ m} \cdot \text{sec}^{-1}$$

$$\left. \begin{array}{l} x_{12u} = 843 \text{ m} \\ x_{13u} = 1174 \text{ m} \end{array} \right\} \text{from } A \qquad\qquad \left. \begin{array}{l} x_{12d} = 275 \text{ m} \\ x_{13d} = 677 \text{ m} \end{array} \right\} \text{from } B$$

The calculation proceeds as follows:

(1) $\quad \dfrac{\mathbf{v}_1}{\mathbf{v}_{2u}} = [\sin i_1 - \varphi] = \dfrac{1800}{3415} = 0.527 = \sin 31°\,50' \left.\begin{array}{l}\\\\\end{array}\right\rbrace \varphi = 5°$

$\qquad \dfrac{\mathbf{v}_1}{\mathbf{v}_{2d}} = [\sin i_1 + \varphi] = \dfrac{1800}{2700} = 0.667 = \sin 41°\,50' \left.\begin{array}{l}\\\end{array}\right\rbrace i_1 = 36°\,50'$

(2) $\qquad \mathbf{v}_2 = \dfrac{\mathbf{v}_1}{\sin i_1} = \dfrac{1800}{0.6} = 3000 \text{ m} \cdot \text{sec}^{-1}$

(3) $\qquad H_{1u} = \dfrac{x_{12u}[1 - \sin(i_1 - \varphi)]}{2 \cos i_1 \cos \varphi} = \dfrac{843(1 - \sin 31°50')}{2 \cdot 0.8 \cdot 0.996} = 250 \text{ m}$

$\qquad h_{1d} = \dfrac{x_{12d}[1 - \sin(i_1 + \varphi)]}{2 \cos i_1 \cos \varphi} = \dfrac{275(1 - \sin 45°50')}{2 \cdot 0.8 \cdot 0.996} = 57.5 \text{ m}$

(4) $\qquad \dfrac{\mathbf{v}_1}{\mathbf{v}_{3u}} = \sin(\beta - \varphi) = \dfrac{1800}{6530} = 0.2756 = \sin 16° \left.\begin{array}{l}\\\\\end{array}\right\rbrace \beta = 21°$

$\qquad \dfrac{\mathbf{v}_1}{\mathbf{v}_{3d}} = \sin(\alpha + \varphi) = \dfrac{1800}{3495} = 0.5150 = \sin 31° \left.\begin{array}{l}\\\end{array}\right\rbrace \alpha = 26°$

(5) $\quad \dfrac{\sin \alpha}{\sin i_1} = \sin[i_2 + (\psi - \varphi)] = \dfrac{0.438}{0.6} = 0.729 = \sin 46°50'; \ \psi - \varphi = 5°.$

$\qquad \dfrac{\sin \beta}{\sin i_1} = \sin[i_2 - (\psi - \varphi)] = \dfrac{0.3584}{0.6} = 0.598 = \sin 36°50'; \ i_2 = 41°50'$

(6) $\qquad \psi = 10°$

(7) $\qquad \mathbf{v}_3 = \dfrac{\mathbf{v}_2}{\sin i_2} = \dfrac{3000}{0.666} = 4500 \text{ m} \cdot \text{sec}^{-1}$

(8) $$H = \frac{x_{13u}[1 - \sin(\beta - \varphi)] - H_1[\cos(\alpha + \varphi) + \cos(\beta - \varphi)]}{2 \sin i_1 \cos i_2 \cos \psi}$$

$$2 \sin i_2 \cos i_2 \cos \psi = 2 \cdot 0.6 \cdot 0.745 \cdot 0.985 = 0.881$$

$$\cos(\alpha + \varphi) + \cos(\beta - \varphi) = 0.961 + 0.857 = 1.818$$

$$H_2 = \frac{1}{0.881}[1174(1 - 0.2756) - 250 \cdot 1.818] = 450 \text{ m}$$

(9) $$h_{2d} = \frac{- \sin(\alpha + \varphi)] - \qquad (\alpha + \varphi) + \cos(\beta -}{2 \sin i_1 \cos i_2 \cos \psi}$$

$$= \frac{1}{0.881}[677(1 - 0.515) - 57.5 \cdot 1.818] = 252 \text{ m}$$
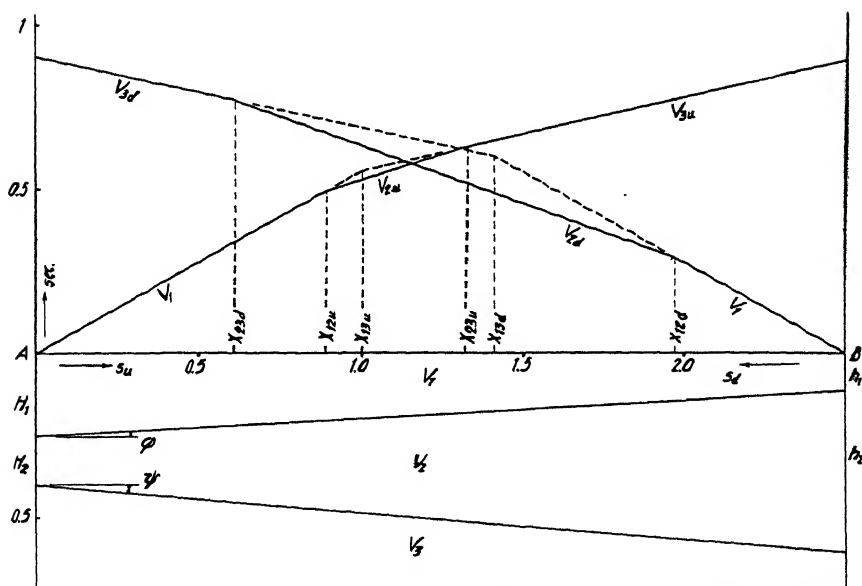
FIG. 9-67. Travel-time curves for two layers of opposite dip direction (after O. v. Schmidt).

For the second example, Fig. 9–67 furnishes the following data:

(Fig. 9-67, $\overline{AB}$ = 2500 m)

UP-DIP PROFILE	DOWN-DIP PROFILE
$v_1 = 1800$ m·sec⁻	$v_1 = 1800$ m·sec⁻
$v_{2u} = 3230$ m·sec⁻	$v_{2d} = 2805$ m·sec⁻
$v_{3u} = 4370$ m·sec⁻	$v_{3d} = 4710$ m·sec⁻

$$x_{13u} = 1006 \text{ m}$$
$$x_{23u} = 1325 \text{ m} \Big\} \text{ from } A$$
$$x_{12u} = 890 \text{ m}$$

$$x_{13d} = 1085 \text{ m}$$
$$x_{23d} = 1890 \text{ m} \Big\} \text{ from } B$$
$$x_{12d} = 525 \text{ m}$$

In the calculation, steps 1 to 3 are carried out as before and give:

$$\varphi = 3°; \quad i = 36°50'; \quad \mathbf{v}_2 = 3000 \text{ m} \cdot \text{sec}^{-1}; \quad H_{1u} = 250 \text{ m}; \quad h_{1d} = 119 \text{ m}.$$

(4) $\quad \dfrac{\mathbf{v}_1}{\mathbf{v}_{3u}} = \sin(\beta - \varphi) = \dfrac{1800}{4370} = 0.412 = \sin 24°20'; \; \beta = 27°20'$

$\quad\quad \dfrac{\mathbf{v}_1}{\mathbf{v}_{3d}} = \sin(\alpha + \varphi) = \dfrac{1800}{4700} = 0.383 = \sin 22°30'; \; \alpha = 19°30'$

(5) $\quad \dfrac{\sin \alpha}{\sin i_1} = \sin[i_2 + (\psi - \varphi)] = \dfrac{0.334}{0.6} = 0.557 = \sin 33°50'$

$\quad\quad \dfrac{\sin \beta}{\sin i_1} = \sin[i_2 - (\psi - \varphi)] = \dfrac{0.459}{0.6} = 0.764 = \sin 49°50'$

$$\psi - \varphi = -8°; \quad i_2 = 41°50'$$

(6) $\quad \psi = -5°$

(7) $\quad \mathbf{v}_3 = \dfrac{\mathbf{v}_2}{\sin i_2} = \dfrac{3000}{0.666} = 4500 \text{ m} \cdot \text{sec}^{-1}$

(8a) $\quad H_{2u} = \dfrac{x_{13u}[1 - \sin(\beta - \varphi)] - H_1[\cos(\alpha + \varphi) + \cos(\beta - \varphi)]}{2 \sin i_1 \cos i_2 \cos \psi}$

$\quad\quad 2 \sin i_1 \cos i_2 \cos \psi = 0.891$

$\quad\quad \cos(\alpha + \varphi) + \cos(\beta - \varphi) = 1.835$

$\quad\quad H_{2u} = \dfrac{1}{0.891}[1006 \cdot 0.588 - 458] = 150 \text{ m}$

(8b) $\quad H_{2u} = \dfrac{x_{23u}[\sin(i_1 - \varphi) - \sin(\beta - \varphi)] - H_{1u}[\cos(\alpha + \varphi) + \cos(\beta - \varphi)]}{2 \sin i_1 \cos i_2 \cos \psi}$

$$+ \dfrac{H_{1u} \cdot 2 \cos i_1 \cos \varphi}{2 \sin i_1 \cos i_2 \cos \psi}$$

$$= \dfrac{1}{0.891}[1325 \cdot 0.145 - 458 + 250 \cdot 2 \cdot 0.8 \cdot 0.997] = 149 \text{ m}.$$

This checks results obtained with different (x_{13u}) intercept.

$$(9) \qquad z_{\cdots} = \frac{x_{13d}[1 - \sin(\alpha + \varphi)] - h_{1d}[\cos(\alpha + \varphi) + \cos(\beta - }{2\sin i_1 \cos i_2 \cos \psi}$$

$$\frac{1085[1 - 0.383] - 119 \cdot 1.835}{0.891} = 508 \text{ m.}$$

For the calculation of depth and dip of several layers it is noted that the travel-time formulas given here for two inclined beds may be written in the same form as those used for depth calculation of horizontal layers. For example, for a single dipping layer the up-dip travel time may be written

$$t_{2u} = \frac{x_u}{v_{2u}} + \frac{2h_1 \cos \varphi}{v_1} \cos i_1.$$

Similarly, for two layers

$$t_{3u} = \frac{x_u}{v_{3u}} + \frac{h_1}{v_1}[\cos(\alpha + \varphi) + \cos(\beta - \varphi)] + \frac{2h_2 \cos \psi}{v_2} \cos i_2,$$

which for $\varphi = 0$ takes the form previously used for depth calculation of three layers:

$$t_3 = \frac{x_2}{v_3} + \frac{2h_1}{v_1} \cos \alpha_1 + \frac{2h_2}{v_2} \cos i_2, \quad \text{and so on.}$$

10. *Variants of refraction method using different interpretation procedures.* The interpretation theory discussed in the preceding sections is based on the assumption that the seismic rays propagate in individual media of constant velocity along straight lines and are refracted in accordance with Snell's law. In addition to the above, there are other interpretation procedures. One uses curved rays resulting from a uniform increase in velocity with depth. Another applies a graphical method involving the pattern of the wave fronts of seismic impulses at progressive time intervals. A third method abandons the assumption of refraction according to Snell's law and operates with vertical incidence upon the underlayer.

(a) Vertical-ray interpretation. This method arose from observations of angles of emergence with a two-component seismometer, which indicated nearly vertical angles close to the origin and led the earlier experimenters to conclude that Fermat's principle did not hold in all cases. It is now known that their results were due to the existence of the weathered layer which causes the emerging ray to be deflected into a practically vertical direction. Nevertheless, vertical-ray theory has a practical application as a simplification of refraction theory where considerable contrast between

formation members exists and where, therefore, the oblique overburden path does not differ sufficiently from the vertical path. In weathered-layer procedure in reflection shooting, interpretation is based almost exclusively on vertical-ray propagation. The following paragraphs contain derivations of vertical-ray formulas for the single and double horizontal layer, and for the single and double inclined layer.

In the case of a single horizontal layer, the wave is assumed to travel vertically to the lower layer, to travel along the interface with the velocity of the lower layer, and to come up vertically. Hence, $t_2 = 2d/\mathbf{v}_1 + s/\mathbf{v}_2$,
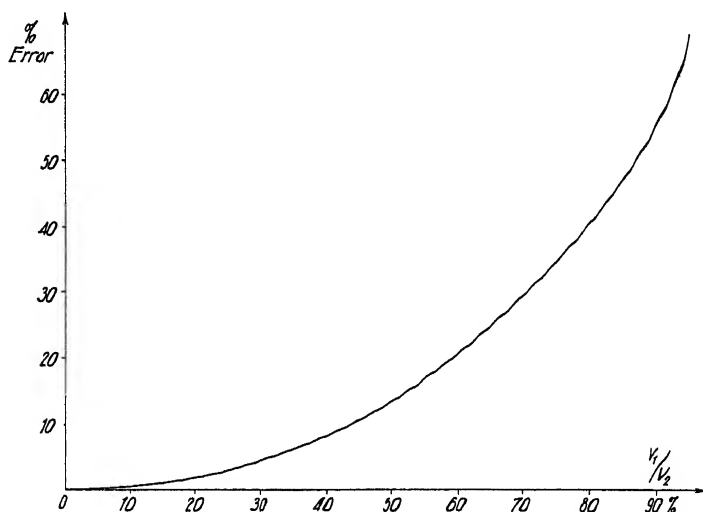
FIG. 9-68. Error of vertical-ray calculation as a function of velocity ratio.

so that the slope of the second part of the travel-time curve $ds/dt_2 = \mathbf{v}_2$
For the intercept, $s \equiv x$, so that

$$d = \frac{x}{2}(1 - \sin i) = \frac{x}{2}\left(1 - \frac{\mathbf{v}_1}{\mathbf{v}_2}\right), \qquad (9\text{-}59a)$$

whereas the application of Fermat's principle gives

$$d = \frac{x}{2}\frac{(1 - \sin i)}{\cos i},$$

which for an angle i of 30° is $d_{\text{Fermat}} = d_{\text{vert.}} \cdot 1.15$. With d_r as depth determined by the refraction interpretation and d_v as depth from vertical-ray interpretation, the error $(d_r - d_v)/d_r = 1 - \cos i$. Fig. 9-68 shows this error as a function of the velocity ratio $\mathbf{v}_1/\mathbf{v}_2$.

In the case of the double horizontal layer we have for the intercept x_{23} :
$-d_1/v_1 + x_{23}/v_2 = 2d_1/v_1 + 2(d_2 - d_1)/v_2 + x_{23}/v_3$, which leads to

$$d_2 = d_1 + \frac{x_{23}}{v_2}\left(1 - \frac{v_2}{v_3}\right). \tag{9-59b}$$

For the refraction path the corresponding depth

$$d_2 = d_1 + \frac{x_{23}\left(1 - \dfrac{v_2}{v_3}\right)}{2\cos i_2} + d_1\,\frac{\cos i_1 - \cos \alpha}{\sin i_1 \cos \beta},$$

that is, the simple cosine ratio previously mentioned applies here only to the first term. The error increases as more layers and less velocity contrast are involved.

In the case of a dipping layer the underlayer travel time for vertical propagation is given by

$$t_2 = \frac{Z + z}{v_1} + \frac{e}{v_2},$$

where the symbols have the same meaning as in formula (9-50a). Substituting $e = s\cos\varphi$, $Z = H\cos\varphi$, $z = h\cos\varphi$,

$$t_{2u} = \frac{1}{v_1}\,(2H_u\cos\varphi - s_u\sin\varphi) + \frac{s_u\cos\varphi}{v_2}$$

$$t_{2d} = \frac{1}{v_1}\,(2h_d\cos\varphi + s_d\sin\varphi) + \frac{s_d\cos\varphi}{v_2}$$

By differentiation,

$$\frac{dt_{2u}}{ds} = -\frac{\sin\varphi}{v_1} + \frac{\cos\varphi}{v_2} = \frac{1}{v_{2u}}$$

and

$$\frac{dt_{2d}}{ds} = \frac{\sin\varphi}{v_1} + \frac{\cos\varphi}{v_2} = \frac{1}{v_{2d}},$$

so that

$$H_u = \frac{x_u\left(1 - \dfrac{v_1}{v_{2u}}\right)}{2\cos\varphi} \quad\text{and}\quad h_d = \frac{x_d\left(1 - \dfrac{v_1}{v_{2d}}\right)}{2\cos\varphi}. \tag{9-59c}$$

These relations differ again by the factor $\cos i$ from those previously given for the depths calculated for the refraction path.

If in the case of the double inclined layer Z'_u and z'_d are the depths

normal to the interface between the two upper formations, and Z_u'' and z_d'' the thicknesses of the second formation (normal to the interface between the second and third formation),

$$t_{3u} = \frac{2Z_u'}{\mathbf{v}_1} + \frac{2z_u''}{\mathbf{v}_2} + \frac{s_u}{\mathbf{v}_{3u}} \quad \text{and} \quad t_{3d} = \frac{2z_d'}{\mathbf{v}_1} + \frac{2Z_d''}{\mathbf{v}_2} + \frac{s_d}{\mathbf{v}_{3d}};$$

hence,

$$Z_u'' = \frac{x_{23u} \cdot \mathbf{v}_2}{2} \left(\frac{1}{\mathbf{v}_{2u}} - \frac{1}{\mathbf{v}_{3u}} \right) \quad \text{and} \quad z_d'' = \frac{x_{23d} \cdot \mathbf{v}_2}{2} \left(\frac{1}{\mathbf{v}_{2d}} + \frac{1}{\mathbf{v}_{3d}} \right). \qquad (9\text{-}59d)$$

(b) *Wave-front diagrams.* In addition to the analytical methods discussed in the preceding paragraphs, graphical methods may be employed in the solution of travel-time problems. They involve the construction of "wave-front diagrams" which have the advantage that the advancement of the seismic wave through geologic formations, both simple and complex, may be more readily visualized. Their principal application is in indirect interpretation. From a preliminary evaluation of a travel-time curve, an approximate geologic profile may be constructed. Then the wave-front diagrams are drawn; travel times obtained from them are compared with the field data; and the geologic section is changed until complete agreement is obtained. Their construction has been described by Thornburg[38] and E. A. Ansel.[39]

A wave front is defined as the surface which a given phase of a seismic impulse occupies at any particular time. A wave-front diagram is a graph showing a number of such surfaces for many successive instants which for convenience are chosen a given constant time-interval apart. In an infinite isotropic medium the wave fronts are spherical shells; their intersection with a vertical plane is represented by circles; their spacing is proportional to the velocity. If the time between consecutive wave fronts is Δt, the spacing is $\Delta s = \mathbf{v} \cdot \Delta t$. However, wave fronts are circular only in such portions of a layer in which the propagation is not disturbed by an adjacent formation (see Fig. 9-69).

The construction of wave-front diagrams for several layers proceeds as follows: Draw a series of concentric circles about the shot point in the upper layer, and calculate their spacing from the above equation. Draw the angles of incidence on the formation boundaries involved (critical and refraction angles). The point of incidence of the critical ray on the first boundary is then determined; wave fronts in the lower layer are drawn about this secondary shot point, their spacing being proportional to the

[38] A.A.P.G. Bull., **14**(2), 185–200 (Feb., 1930).
[39] Gerl. Beit., Erg. Hefte, **1**(2), 117–136 (1930).

velocity in the lower layer. The underlayer fronts are advanced farther than the corresponding overburden fronts. Since there can be no discontinuities, the lower wave front has to be connected to the corresponding
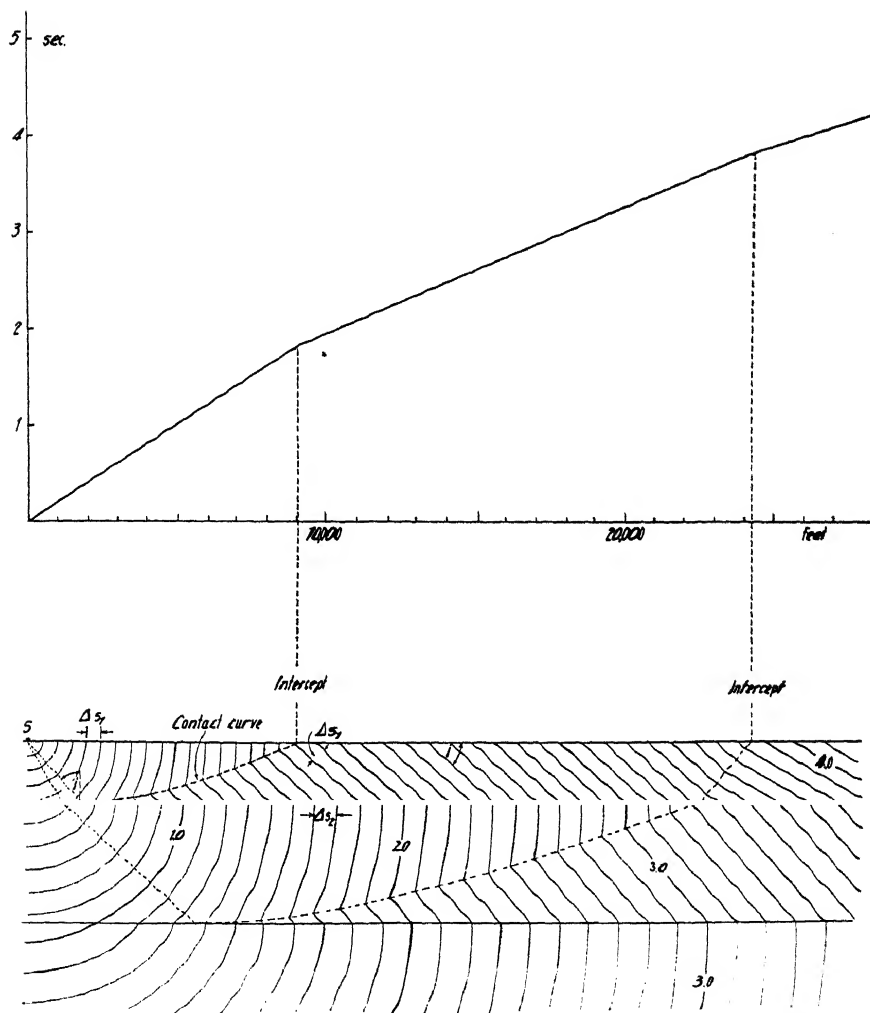
FIG. 9-69. Travel-time curve and corresponding wave fronts in three horizontal layers (adapted from Thornburg).

upper front. This is done by drawing lines through the upper points of the underlayer wave front normal to the critical angle of the emerging ray to intersection with the corresponding wave front in the upper medium.

As seen from Fig. 9-69, a straight wave front (contact front) results,

which moves upward along the contact curve (a parabola) and reaches the surface at the point of the intercept in the travel-time curve. In a two-layer problem, the angle of incidence on the first and the critical angle i_2 on the second interface are determined. Wave fronts in the second layer are completed; the point of incidence on the third layer is determined; and wave fronts in it are drawn with a spacing corresponding to the velocity in the third layer. Connections with the wave fronts in the second layer are made again as before, the second contact front being parallel with the angle of incidence on the third layer (see Fig. 9-69). With increasing distance from the shot point, only contact fronts will be present in the upper layers.

With a wave-front diagram, a depth determination would proceed as follows in the case of one layer: (1) Draw circles with interval $v_1 \Delta t$ about surface shot point. (2) Locate intercept distance. (3) Lay off the angle i from the surface; draw a line through the point of intercept; and draw
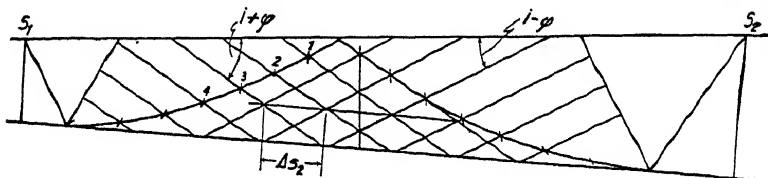
FIG. 9-70. Wave fronts, dipping layer (after Ansel).

parallel lines thereto with a spacing of $v_1 \Delta t$ (spacing in horizontal direction, $v_2 t$). (4) Find intersection with $v_1 \Delta t$ curves and draw contact curve. (5) Determine depth by intersection of ray $(90 - i)$ from shot point and contact curve. For two horizontal layers the procedure begins with the location of the second intercepts after the above steps have been followed and the first interface has been constructed. Then the break x_{23} is lowered down to this interface by using the refraction angles α. Hence, a secondary shot point is established on the interface. From then on the problem is treated like the single-layer problem.

To obtain depths below shot points and dips of inclined layers, the direction of dip is first established from an inspection of velocities and intercepts. Then the construction proceeds as follows: (1) Draw circles at intervals Δs about shot points $S1$ and $S2$ (Fig. 9-70). (2) Locate breaks in travel-time curve. (3) Determine angles $i + \varphi$ and $i - \varphi$ from $\sin(i - \varphi) = v_1/v_{2u}$ and $\sin(i + \varphi) = v_1/v_{2d}$. (4) Lay off angles $(i + \varphi)$ from the down-dip and angles $(i - \varphi)$ at the up-dip shot points, with a spacing (at right angles to the wave front) of Δs_1. (5) Locate intersections of these parallel lines with upper layer wave fronts, thus obtaining

points 1, 2, 3, 4, and so on, on the left and corresponding points on the right (see Fig. 9-70). (6) Draw contact curves on both sides. (7) Draw a tangent to the two contact curves, obtaining depth and dip of stratum. (8) The dip of the lower layer is given by the diagonal of the parallelogram formed by intersection of the two underlayer wave fronts. (9) The velocity and spacing of wave fronts in the lower layer is given by the length of this diagonal.

The case of three inclined layers is treated in a similar manner. As before, the essential point is to lower the surface shot points and x_{23} intercepts to the first formation boundary. A secondary shot point below S_1 is given by the angle α, which follows from $\sin (\alpha + \varphi) = v_1/v$
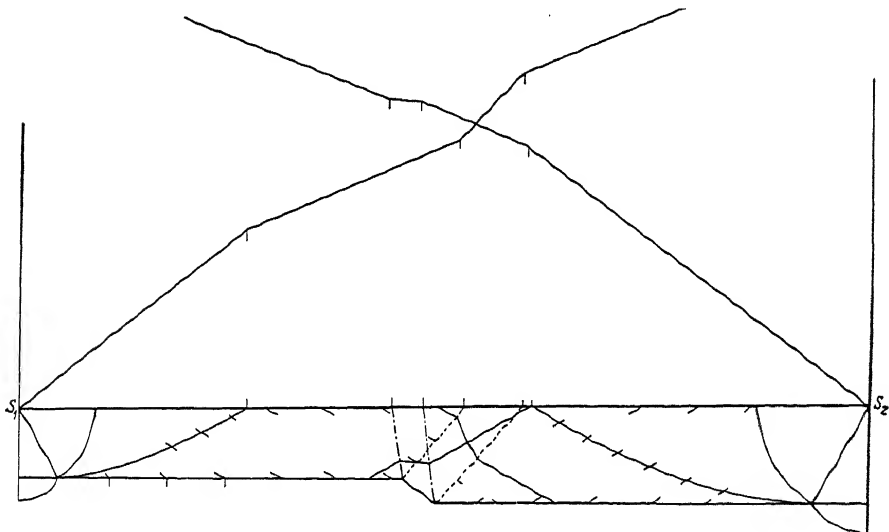
FIG. 9-71. Wave fronts, inclined terrace (after Ansel).

Wave fronts are drawn about this point with the spacing Δs_2, corresponding to the velocity v_2 previously determined. The location of the secondary shot point on the other side is given by the angle of emergence β which follows from $\sin (\beta - \varphi) = v_1/v_3 \text{ up}$. After the shot point has been projected on the lower layer, wave fronts are drawn about it with the spacing Δs_2. After secondary shot points and secondary breaks have been established on the first interface, the construction proceeds as before. Wave fronts of the second contact wave are constructed by drawing parallel lines from the secondary breaks down to intersect with the wave fronts with the velocity v_2. The inclination of the wave front of the second contact wave is given by the angles $i_2 - (\psi - \varphi)$ and $i_2 + (\psi - \varphi)$ (see formula [9-57a]). Contact curves are constructed from the points

of intersection with the v_2 fronts. The second interface is tangent to these two contact curves.

Wave-front interpretation may be used not only for an analysis of simple travel-time curves but also for more complicated types of structures, such as faulted strata, salt domes, and the like. A number of examples of the application of wave-front methods to such types of structures may be found in Thornburgh's and Ansel's articles previously referred to. Fig. 9–71 illustrates travel-time analysis by wave fronts for a sloping terrace.

FIG. 9-72a. Curved-ray paths.

(c) *Curved-ray interpretation.* While vertical-ray and wave-front interpretations are a matter of preference over standard refraction methods, curved-ray interpretation becomes a necessity where the overburden portion of a travel-time curve is not straight. This curvature may also occur on later portions of travel-time curves. However, its presence in the first layer is the predominant condition. Curved rays occur in thick sections of sedimentary beds over basement rocks and in surface-weathered layers above more consolidated formations. In each case, the type of travel-time curve obtained and the interpretation problem resulting therefrom are identical. The mathematical theory has been treated by several authors.[40]

[40] L. B. Slichter, Physics, **3**(6), 273–295 (Dec., 1932). H. M. Rutherford, Amer. Geophys. Union Trans. 1933 (Seism), 289–303; Soc. Petrol. Geophys. Trans., V,

In the following analysis it is assumed (see Fig. 9–72a) that the velocity increases *linearly* from v_0 at the surface to v_1 at the bottom of the top layer, changes abruptly to v_2, and remains constant in the second layer. Then the upper velocity as function of depth is

$$v_h = v_0 + kh. \tag{9–60a}$$

In the upper layer the rays travel in circular paths; their radius of curvature depends on the vertical velocity increase k. The locus for the centers of curvature is a plane whose distance from the surface is given by

$$y = -\frac{v_0}{k}. \tag{9–60b}$$

The travel-time curve is no longer straight and the surface velocity is not constant. By differentiation with respect to distance, an "apparent" velocity is obtained (eq. [9–62]).

For an arbitrary number i of thin parallel horizontal beds, the paths for the incident and emerging rays are identical in the same stratum. The horizontal displacement of the ray due to refraction is

$$x = 2 \sum_{i=1}^{i=n} h_i \tan \alpha_i, \tag{9–61a}$$

since in each bed the distance is decreased by the amount $h_i \tan \alpha_i$. The travel time for the downward and upward (curved) paths is therefore

$$t = 2 \sum_{i=1}^{i=n} \frac{h_i}{v_i \cos \alpha_i}, \tag{9–61b}$$

where $h_i/\cos \alpha_i$ represents the oblique path within each layer. According to Snell's law, $\sin \alpha_i / \sin \alpha_{i+1} = v_i / v_{i+1}$ or $\sin \alpha_i / v_i = \sin \alpha_{i+1} / v_{i+1} = $ constant $\equiv C$ for each ray. Since $\sin \alpha / v = \sin i_0 / v_0$ (where i_0 is the angle of emergence as indicated in Fig. 9–72b, and v_0 is the surface velocity), the constant C may be determined at the surface by graphical differentiation of the travel-time curve. If $\bar{v}$ is the apparent velocity, it is seen from the figure that $\sin i_0 = v_0/\bar{v}$; therefore,
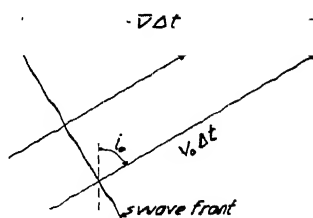
FIG. 9–72b. Apparent and true velocity.

$$\frac{\sin \alpha}{\bar{v}} = C = \frac{1}{\bar{v}}. \tag{9–62}$$

117–120 (March, 1935). M. Ewing and Don L. Leet, A.I.M.E. Geophys. Pros., 245–270 (1932). M. Ewing and A. P. Crary, Soc. Petrol. Geophys. Trans., V, 154–160 (March, 1935). M. M. Slotnick, Geophysics, 1(1), 9–22 (Jan., 1936).

It is further seen that if $\sin \alpha = 1$, the apparent surface velocity is equal to the true velocity in the deepest bed reached, that is, the bed corresponding to the *depth of penetration* (see Fig. 9–72a), which is

$$h_p = \frac{\mathbf{v}_0}{\mathbf{k}} \frac{(1 - \sin i_0)}{\sin i_0} \qquad (9\text{--}63a)$$

This relation applies, of course, only to the part of the travel-time curve ahead of the intercept, that is, to the ray in the overburden. The travel time for a ray corresponding to the distance x with the angle i_0 is

$$t = \frac{1}{\mathbf{k}} \log_e \frac{1 + \cos i_0}{1 - \cos i_0} \qquad (9\text{--}63b)$$

and the distance

$$x = \frac{2\, \mathbf{v}_0 \cot i_0}{\mathbf{k}}. \qquad (9\text{--}63c)$$

Since i_0 may be determined by graphical differentiation of the travel-time curve at any distance x, $\mathbf{k}$ may be obtained from eq. (9–63c). A calculation of this kind is illustrated in Table 57-A. The observed data in the first two columns are distances and travel times; next follow the apparent velocities from which the angles of emergence at these distances are calculated. Application of formula (9–63c) then yields the vertical velocity increase $\mathbf{k}$, which, for an ideal travel-time curve, has to have the same value for any distance. The next set of columns contains a computation of penetration-depth from formula (9–63a), although for bedrock or basement-depth determinations this part may be left out.

The method followed in the calculation of the depth of a high-speed layer of presumably constant velocity beneath an overburden of linear velocity increase will be evident from the following discussion and reference to Fig. 9–72c. In the latter $D = \overline{AE} =$ shot detector separation, $\mathbf{v}_0 =$ speed at surface, $\mathbf{v}_1 =$ speed at base of the overburden, $\mathbf{v}_2 =$ speed of underlayer, $\alpha =$ angle of incidence at contact, $\rho =$ radius of arc AB, and $t =$ travel time of refraction wave from A to E.

Since $\overline{PB} = \mathbf{v}_0/\mathbf{k} + h$, $\mathbf{v}_1 = \mathbf{v}_0 + \mathbf{k}h$, and $h = (\mathbf{v}_1 - \mathbf{v}_0)/\mathbf{k}$, we have $PB = \mathbf{v}_0/\mathbf{k} + (\mathbf{v}_1 - \mathbf{v}_0)/\mathbf{k} = \mathbf{v}_1/\mathbf{k}$. Further, since $\sin \alpha = \mathbf{v}_1/\mathbf{v}_2 = PB/\rho$, $\mathbf{v}_1/\mathbf{v}_2$ is $\mathbf{v}_1/\mathbf{k}\rho$, or $\rho = \mathbf{v}_2/\mathbf{k}$.

The travel time of the trajectory $ABCE$ is $t_{AB} + t_{BC} + t_{CE}$, where $t_{AB} = t_{CD} = \int_0^s ds/\mathbf{v}$. The value of s is $\rho\varphi_1$ and φ is $\alpha - \gamma$; ρ and α are given

by the expressions in the preceding paragraph. $\sin \gamma = \mathbf{v}_0/k\rho = (\mathbf{v} - kh)/k\rho$. Hence, $\sin \varphi = \mathbf{v}/\rho k$ and $s = \rho$ arc sin $\mathbf{v}/\rho k$. Therefore,

$$ds = \frac{\rho d\mathbf{v}}{\sqrt{\rho^2 \mathbf{k}^2 - \mathbf{v}^2}} = \frac{d\mathbf{v}}{\mathbf{k}\sqrt{1 - \dfrac{\mathbf{v}^2}{\rho^2 \mathbf{k}^2}}} \qquad (9\text{-}64a)$$
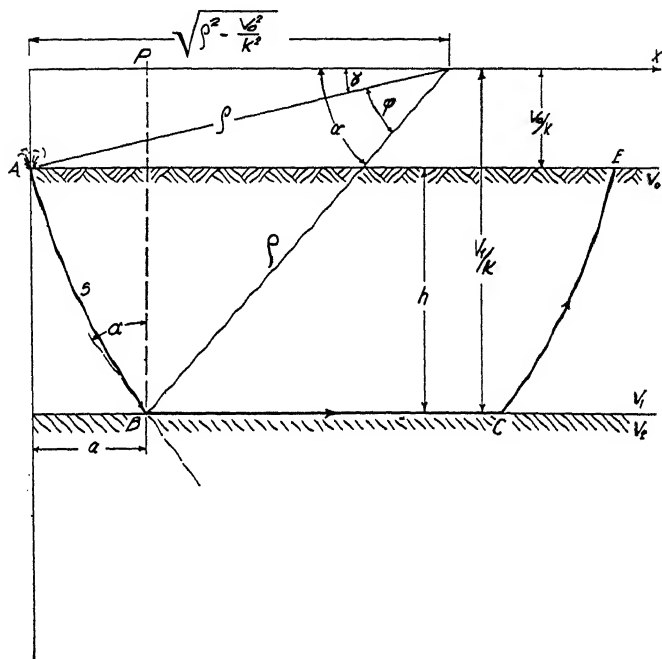
Fig. 9-72c. Depth determination in curved-ray method.

and

$$t_{AB} = \int_{\mathbf{v}_0}^{\mathbf{v}_1} \frac{d\mathbf{v}}{\mathbf{k}\mathbf{v}\sqrt{1 - \dfrac{\mathbf{v}^2}{\rho^2 \mathbf{k}^2}}} = \frac{1}{\mathbf{k}}\left[\cos h^{-1}\left(\frac{\mathbf{v}_2}{\mathbf{v}_0}\right) - \cos h^{-1}\left(\frac{\mathbf{v}_2}{\mathbf{v}_1}\right)\right]. \qquad (9\text{-}64b)$$

The travel time in the underlayer is given by $t_{BC} = (D - 2a)/\mathbf{v}_2$, where $a = \mathbf{v}_2/\mathbf{k}[\sqrt{1 - (\mathbf{v}_0/\mathbf{v}_2)^2} - \sqrt{1 - (\mathbf{v}_1/\mathbf{v}_2)^2}]$. Therefore, the total time

$$t_2 = \frac{2}{\mathbf{k}}\left[\cos h^{-1}(\mathbf{v}_2/\mathbf{v}_0) - \cos h^{-1}(\mathbf{v}_2/\mathbf{v}_1)\right]$$

$$+ \frac{D}{\mathbf{v}_2} - \frac{2}{\mathbf{k}}\left[\sqrt{1 - (\mathbf{v}_0/\mathbf{v}_2)^2} - \sqrt{1 - (\mathbf{v}_1/\mathbf{v}_2)^2}\right]$$

or

$$t_2 = \frac{2}{k}\left\{[\cos h^{-1}(v_2/v_0) - \sqrt{1 - (v_0/v_2)^2}] \right.$$
$$\left. - [\cos h^{-1}(v_2/v_1) - \sqrt{1 - (v_1/v_2)^2}]\right\} + \frac{D}{v_2}. \quad (9\text{-}65)$$

If we let $f(r) = \cosh^{-1}(1/r) - \sqrt{1 - r^2}$, with $r = v_0/v_2$ and $r' = v_1/v_2$ respectively, eq. (9-65) becomes

$$t_2 = \frac{D}{v_2} + \frac{2}{k}[f(r) - f(r')]. \quad (9\text{-}66a)$$

Fig. 9-73a shows the variation of r with $f(r)$ and is valid for any conditions. If

$$\frac{2}{k}[f(v_0/v_2) - f(v_1/v_2)] \equiv T,$$

then

$$= t_2 - \frac{D}{v_2}. \quad (9\text{-}66c)$$
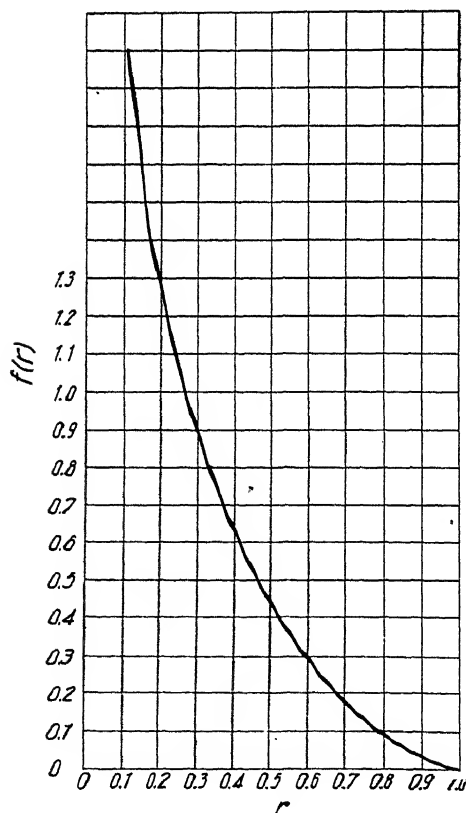
FIG. 9-73a. Graph of $f(r)$ for curved-ray interpretation.

The application of these relations is as follows: Assume k to have been determined from the first part of the travel-time curve, as shown in Table 57-A. If, further, v_2 has been measured in the second part of the travel curve (past the 3000-m intercept in the example), the value of the time function T may be calculated from formula (9-66b) for various depths (and therefore for various values of v_1). In this manner a curve $T = f(h)$ is obtained, as shown in Fig. 9-73b. For the depth determination, T is calculated from the travel-time curve by subtracting, in accordance with formula (9-66c), the value of D/v_2 for each distance as shown in the last set of columns in Table

TABLE 57-A

CALCULATION OF EMERGENCE ANGLE, VERTICAL VELOCITY INCREASE, DEPTH PENETRATION, AND BEDROCK DEPTH FROM TRAVEL-TIME CURVE

OBSERVED DATA		APPARENT VELOCITY; EMERGENCE ANGLE			VERTICAL VELOCITY INCREASE			DEPTH PENETRATION, OVERBURDEN			DEPTH TO BEDROCK		
x m	t sec.	$\dfrac{dx}{dl} = \bar{v} = v_{max}$ m.sec.$^{-1}$	$\dfrac{v_0}{\bar{v}} = \sin i_0$	i_0	cotan i_0	$\dfrac{2v_0}{x}$	$= k$	$v_0(1 - \sin i_0)$	$k \div \sin i_0$	Penetration $= h_p$ m	$\dfrac{D}{v_2}$ sec.	$T = t_2 - \dfrac{D}{v_2}$ sec.	h m
0	0	$(v_0 =$ 1750 m.sec.$^{-1})$											
500	0.286	1763	0.992	82°59'	0.123	7.000	0.86	13.1	0.853	15.3			
1000	0.565	1802	0.971	76°12'	0.246	3.500	0.86	50.6	0.835	60.6			
1500	0.838	1865	0.938	69°46'	0.369	2.333	0.86	108	0.806	133.8			
2000	1.100	1950	0.897	63°50'	0.491	1.750	0.86	179	0.771	231.9			
2500	1.351	2053	0.852	58°26'	0.614	1.400	0.86	259	0.732	353.5			
3000	1.595	2173	0.805	53°37'	0.737	1.167	0.86	341	0.692	492.4			
$D =$ 4000	$t_2 =$ 1.756	$v_2 =$ 6200									0.645	1.111	
5000	1.918	"									0.806	1.112	1375 m
6000	2.079	"									0.968	1.111	
7000	2.240	"									1.129	1.111	

57-A. This gives, for each distance, a constant value of T, from which, in turn, follows the depth by applying the graph of Fig. 9–73b. If, in the example, a uniform velocity (of 1881 m·sec^{-1}) were taken to the 3000-m intercept, the depth would be 1097 m instead of 1375 m.

11. *Variants of refraction method using different field technique.* The methods discussed in the following paragraphs employ such modifications of refraction technique as afford short cuts in the more elaborate methods of depth calculation. These methods are (1) the arc method of structure mapping, and (2) the method of differences (ABC system). They involve a more direct determination of time *differences* which are evaluated in terms of *overburden thickness.*
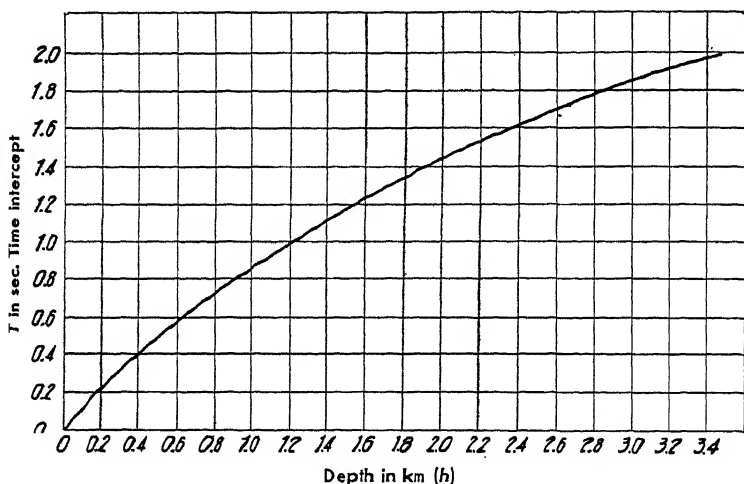
FIG. 9–73b. Graph of $T(h)$ for depth interpretation (basement rocks).

(a) *Arc method of structure mapping.* In this method time differences of fans are correlated with refraction profiles connecting the fan shot points. Thus, a time-contour map of subsurface high-speed beds is obtained and converted to a depth-contour map. The method is applicable to low-dip structures only.[41] The shot points are generally laid out along the strike in a longitudinal traverse (Fig. 9–74a), and reception points are arranged in overlapping fans on the circumference of circles about these shot points (tangential profiles, Fig. 9–74b). Time differences are calculated, as shown below, and plotted for both profiles. With a suitable scale the time curve will indicate the profile of high-speed formations.

Depth calculations are based on simplifications of formulas previously derived. If in eq. (9–50a) the substitution $1/v_1 = 1/v_2 \sin i$ is introduced,

---

[41] Jones, *op. cit.*, 169–173 (1933).

the travel time $t_2 = Z \cotan i/v_2 + s \cos \varphi/v_2 + z \cotan i/v_2$; with $C_0 = Z \cotan i/v_2$ as shot point constant, $C' = \cotan i/v_2$ as depth point constant,

$$\frac{\ldots}{v_2} \quad \cdot C'z \qquad\qquad (9\text{–}67a)$$

(a)

(b)
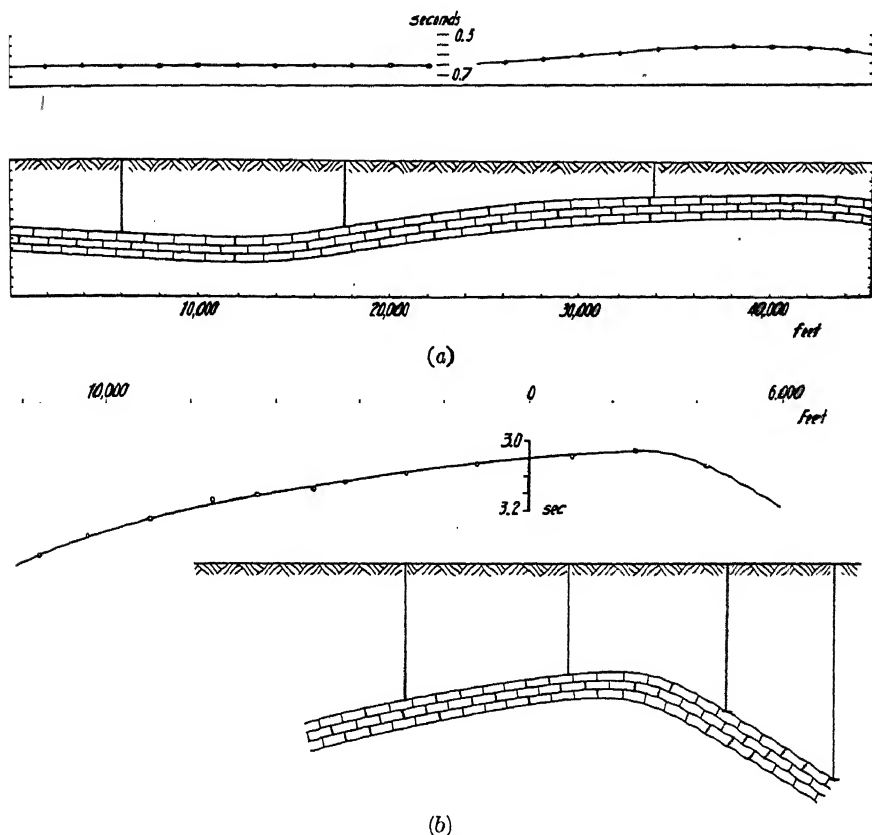
FIG. 9-74. (a) Longitudinal, and (b) transverse profiles, with travel times and lime-stone profile (arc method).   (After Jones.)

Since $\cos \varphi \approx 1$ for small dips, the depth at any point

$$z = \frac{1}{C'}\left(t_2 - \frac{s}{v_2} - C_0\right), \qquad\qquad (9\text{–}67b)$$

which, strictly speaking, is depth normal to formation but for small dips may be taken as vertical depth.   With $t' \equiv t_2 - s/v_2$, eq. (9–67b) may

$$z = \quad t' - C_0) \qquad\qquad (9\text{–}67c)$$

The constants C' and C_0 are obtained from refraction profiles shot at the starting point in two directions. It remains necessary to reduce all shot points to one datum, that is, to eliminate differences in their shot-point constants by referring all times to the C_0 of a reference point. If at a reception point common to two overlapping fans a difference in time of $t'_{01} - t'_{02}$ corresponds to shots from two different points, their difference in shot-point constant is

$$C_{01} - C_{02} = t'_{01} - t'_{02}. \tag{9-67d}$$

Adjusted times are plotted against the location of depth points; points with equal time differences are connected by isochrons which, barring velocity variations and steep dips, give a true picture of the depth contours of the structure.

(b) *Method of differences* (ABC *system*). This method has been applied[42] by the Imperial Geophysical Experimental Survey for the determination of irregular bedrock surface in gold placer channels and is in widespread use in reflection shooting for calculating the delay in the weathered layer. It consists of shooting at A (Fig. 9-75) and receiving at B and C, then
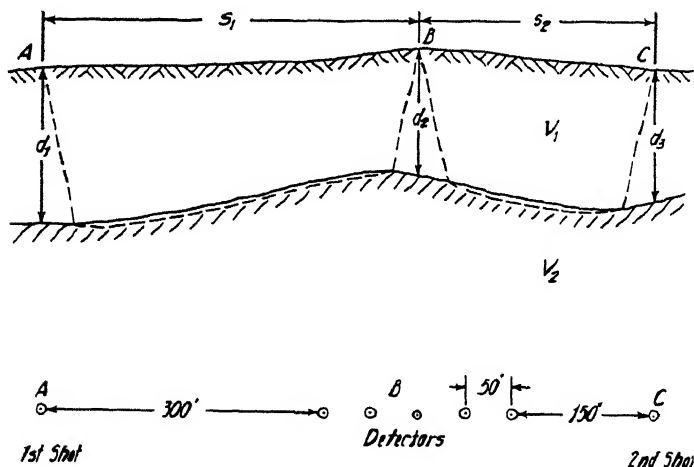
Fig. 9-75. ABC system (method of differences).

shooting at C and receiving at B. This gives the depth under B where one or several receivers may be set up. One receiver is sufficient at A or C. Since in placer and weathered-layer problems, the velocity contrast

[42] A. B. Edge and T. H. Laby, *Principles and Practice of Geophysical Prospecting*, pp. 339-341, Macmillan (1931).

is great, vertical ray propagation may be assumed so that the travel times are:

$$(1) \text{ at } B, \text{ shooting from } A: t_{BA} = \frac{d_1}{v_1} + \frac{s_1}{v_2} + \frac{d_2}{v_1}$$

$$(2) \text{ at } B, \text{ shooting from } C: t_{BC} = \frac{d_3}{v_1} + \frac{s_2}{v_2} + \frac{d_2}{v_1}$$

$$(3) \text{ at } C, \text{ shooting from } A: t_{CA} = \frac{d_1}{v_1} + \frac{s_1 + s_2}{v_2} + \frac{d_3}{v_1}$$

Adding the first two equations and subtracting the third, we get

$$\frac{t_{BA} + t_{BC} - t_{CA}}{2} \cdot v_1 = d_2 . \tag{9-68}$$

The overburden velocity v_1 is determined from *short*-range profiles or (for deep reflection shots) by providing a shot-hole receiver at A. In reflection-correlation shooting, the shot at A is a regular reflection shot with five receivers set up near B and one receiver at C. This receiver is then removed and the second shot placed as shown. In continuous profiling, the reverse reflection shot automatically performs the function of the weathering shot from C.

D. REFLECTION METHODS

1. *General Problems.* Reflection methods differ from refraction procedures in that not the first impulses but *later* impulses are utilized for the depth calculations. Hence, a principal problem in reflection shooting is to separate reflected impulses from *all* others of a different character, that is, not only from the first high-speed refraction impulses but also from low-speed surface waves and other refraction impulses arriving after the first impulses. A *separation* is possible (*a*) in regard to time, and (*b*) in regard to amplitude. In the design and arrangement of detectors, as well as in field technique, various measures are taken to accomplish this.

A universally adopted means for time separation of impulses following in rapid succession is high paper speed (10 to 15 in. sec.$^{-1}$) and near-critical damping of overall channel response. A record taken with an underdamped receiver at refraction-record speed would scarcely show any reflections. An overlap of interfering impulses with reflections may often be eliminated by changing the distance of the entire spread from the shot point. The principal means of segregating refractions from reflections is the use of a multiplicity of receivers (six, eight, or twelve). Interfering impulses (such as refractions or surface waves) will arrive at each receiver

in proportion to the speed of their respective media, whereas the reflected waves (because of their almost vertical incidence) arrive virtually at the same time and have therefore a *high apparent velocity.*

When multiple receivers are connected in series groups, there is an additional possibility of eliminating refractions and reinforcing reflections. In the example illustrated in Fig. 9-76, eight seismometers, connected together, are set up at distances varying from 1000 to 1100 feet from the shot point. When a reflection of 40-cycle frequency with an apparent velocity of 100,000 feet per second strikes the group of receivers, the impulses are virtually in phase and hence reinforced. Conversely, when a
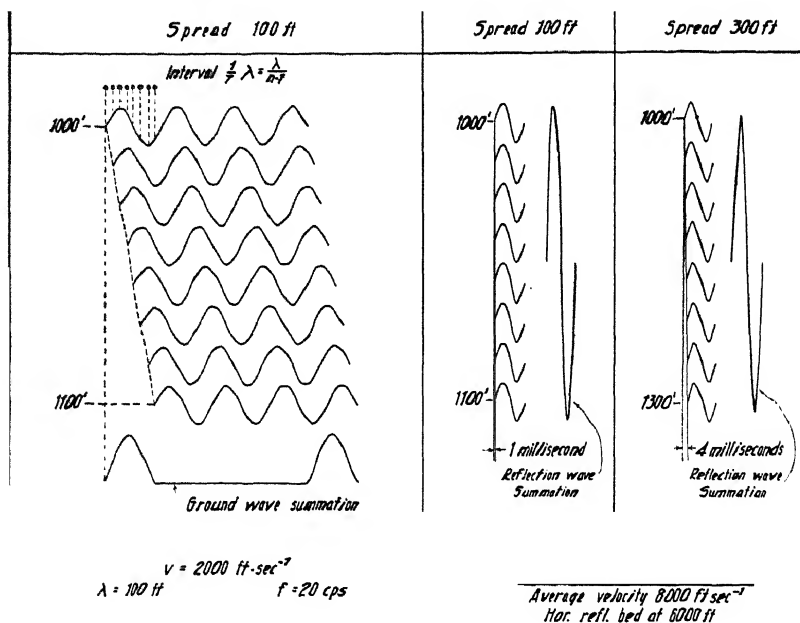
Fig. 9-76. Wave summation in series detectors (after McDermott).

refraction, surface, or "ground roll" wave passes the receivers, the velocity is so low (2000 ft. sec.$^{-1}$ in the example) that the phase difference between each receiver is 1/140 sec., and cancellation occurs except for the beginning and end of the ground wave. The peaks shown in the figure are not serious, as they are much smaller than the amplitude of the reinforced reflected wave.

A decrease in the amplitude of interfering impulses is often made possible by judicious placement of shots and selection of charges. By placing them under the unconsolidated weathered layer, the amplitude of the surface waves at the end of the seismogram (ground roll) is reduced, and

better confinement is obtained. Sometimes the reflection amplitude can be increased, compared with the refraction amplitude, by firing simultaneously two charges one below the other. As the reflected energy comes vertically from below, vertical type seismographs are used. However, this does not minimize refraction impulses, since they likewise come in from an almost vertical direction, nor does it reduce the ground roll (Rayleigh?) waves, since they too possess a strong vertical component. However, if there is a difference in the frequency of undesirable impulses and the frequency of reflected waves, the former may be eliminated or reduced by selective response characteristics of the channels or portions thereof (filters). The first high-speed impulses are generally reduced in amplitude by automatic, semiautomatic, or manually operated volume controls. Finally, a field technique combining suitable drilling depths, charges, and shot distances is the most effective means of obtaining distinct reflection records.

Under favorable surface conditions there is virtually no limit to the possibilities of the reflection method in sedimentary areas of low dip. The range for which it is commonly used extends from 2000 to 10,000 feet; the extremes are 300 feet and about 30,000 feet.[43] Depth penetration is not controlled by the dimensions of the effective beds. Other advantages are small charges, accuracy of depth determinations (0.2 to 0.5 per cent of depth), completeness with which depth information can be obtained without complicated calculations, freedom from terrain effects, and the fact that depth data may be obtained for more than one layer with undiminished accuracy. This is of importance to the geologist, since it makes possible the determination of the displacement of the axes of folds with an increase in depth, the mapping of variations in formation thicknesses, and the determination of the existence and extent of unconformities.

2. *Instruments.*[44] Three primary and two secondary devices are the fundamental constituents of a reflection instrument: (*a*) an electrical detector (phone), (*b*) an amplifier, (*c*) a recording device, (*d*) time-marking mechanism, and (*e*) shot-instant transmission system.

(*a*) *Detector.* The function of the detector is to convert the mechanical ground vibrations into fluctuations of electrical current which are amplified and reconverted into mechanical (rotational) motions of a recording galvanometer. All types of electrical detectors are similar to microphones in construction. The *inductive* type is comparable to the coil microphone,

---

[43] See footnote, p. 451
[44] References to the literature on this subject are given in C. A. Heiland, "Instrument Problems in Reflection Seismology," A.I.M.E. Geophys. Pros., 411-454 (1934). This section gives only a general description of reflection instruments; theory is discussed in section IV.

the *reluctance* type is similar to phonograph pickup, the *capacitive* detector is built in the same manner as a condenser microphone, and the *pressure* detector follows the design of the carbon microphone, or that of the crystal microphone. All electrical pickups have in common a spring-suspended mass whose motion relative to the instrument frame is converted into electrical impulses by some sort of *transducer*. The two component parts of the transducer are attached to the seismograph mass and to the frame. In the *inductive* detector, the transducer is a coil moving in a magnetic field (see Figs. 9-113a and 9-113b). In the reluctance detectors (Fig. 9-115), the transducers consist of iron armatures surrounded by coils and placed close to the poles of a permanent magnet or magnets which usually act as the detector mass. In the capacitive type of seismograph (Fig. 9-116), the transducer is a condenser; the mass is mounted close to a stationary plate so that the two together act as a variable condenser. In the piezoelectric detector (Fig. 9-118), the seismograph mass rests on a stack of quartz plates or a rochelle salt crystal.

(b) *Amplifier.* Virtually all reflection equipment employs, between seismograph and recording device, amplifiers of widely varying construction. At present the preference seems to be for the resistance-coupled type, usually of three stages. The following features are common to most amplifiers: filter systems, input and output transformers for matching the impedance of the pickup and of the indicating device, battery operation, gain and filter controls, A.V.C. systems, and separate volume expanders (companders). A scheme of a seismic amplifier (without A.V.C.) is given in Fig. 9-77.

(c) *Recorder.* The recorder is a combination of recording camera and a bank of galvanometers which may be of the coil, bifilar oscillograph, or string type. The coil galvanometers are modified d'Arsonvals with torsion wire or ribbon instead of jewel suspension and short natural period. Therefore, they are really damped vibration galvanometers, with oil or electromagnetic damping. Bifilar oscillographs are less frequently employed than are coil galvanometers. They combine the advantages of high sensitivity with high natural frequency, but greater care has to be devoted to the design of a good optical system. String galvanometers (harp of strings in a magnetic field) share most of the advantages of the oscillograph but have the drawback of shadow photography (which is somewhat tiring for office work on the records), low sensitivity, and possibility of tangling of the strings.

(d) *Time Marking.* Since for the timing of reflection impulses an accuracy of the order of one one-thousandth of a second is required, it has become general practice to project time lines at one-hundredth of a second intervals on the paper and interpolate to an accuracy of one-tenth line.
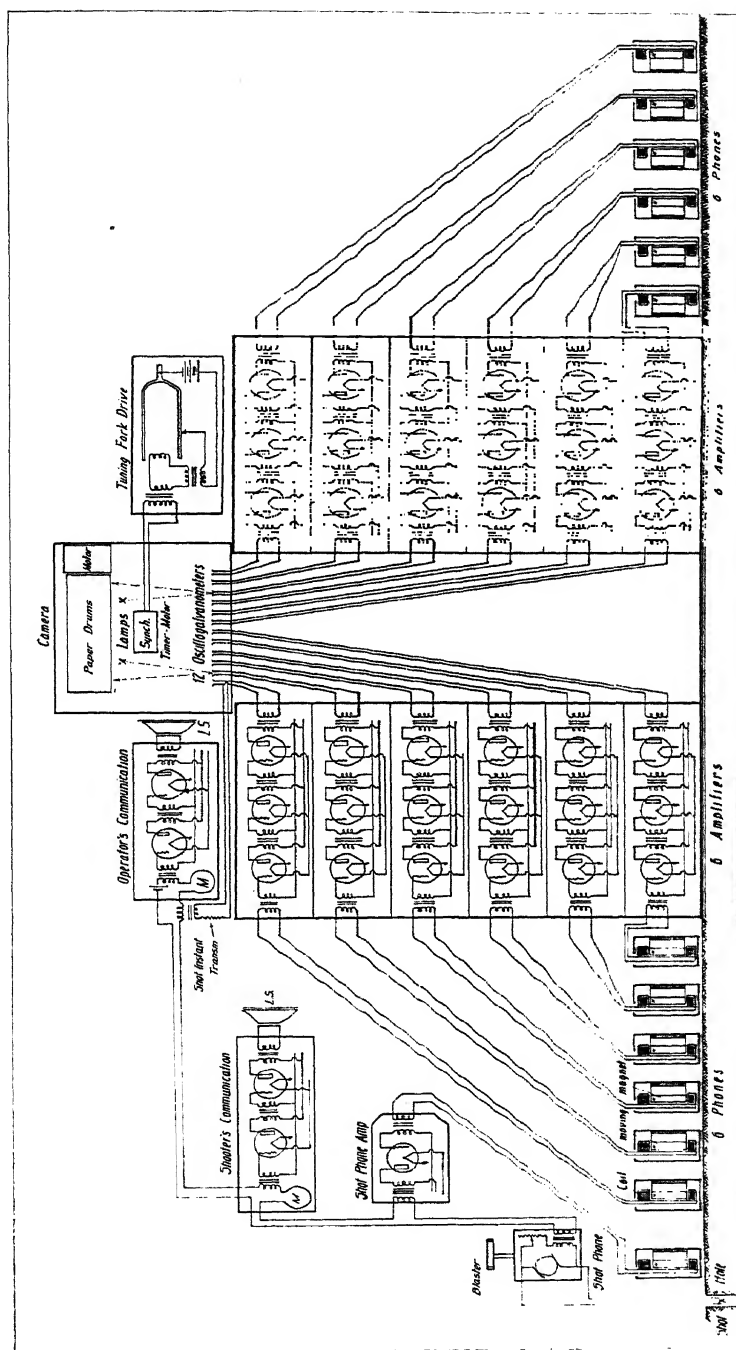
FIG. 9-77. Simplified schematic wiring diagram of a twelve-element seismic reflection apparatus.

553

FIG. 9-78. Twelve-element seismic reflection apparatus in recording truck.

One method employs a hundred-cycle tuning fork which drives a synchronous motor whose shaft carries a wheel with ten spokes, one spoke being heavier to mark tenths of seconds.[44a] This arrangement is used for shadow photography with string galvanometers. For black on white records the spoked wheel is replaced by a disk with the same number of slots.[45] In another arrangement, the prongs of a fifty-cycle tuning fork are provided with slotted diaphragms to project the slot opening every hundredth of a second directly upon the paper.[46] Lastly, vibrating reed timers of fifty-cycle frequency are used, driven by vacuum tube oscillators or tuning forks.

(e) *Shot-instant transmission* is accomplished by wire or radio. The shot-instant line also serves for communication with the shot point. In
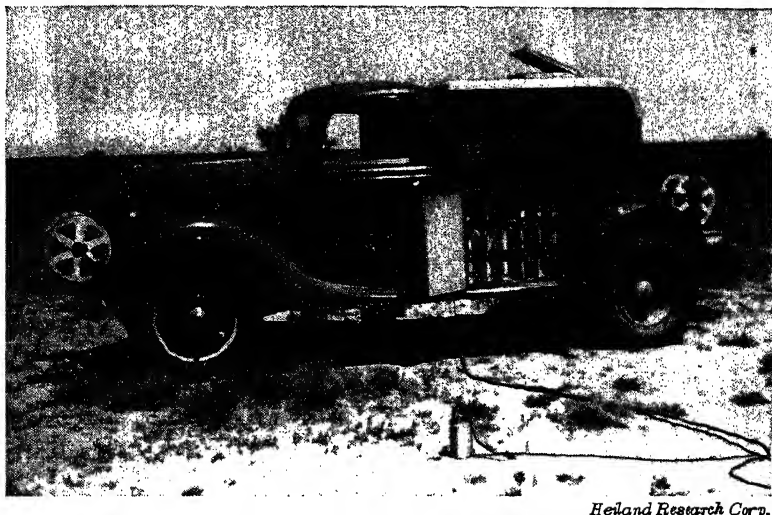
Heiland Research Corp.

FIG. 9-79. Seismic recording truck with detector case and reels.

most reflection equipment the shot instant is recorded on one of the galvanometers as previously described. A second galvanometer may be used to indicate the vertical (or up-hole) time recorded by a shot point detector.

In Fig. 9–77 a schematic and greatly simplified wiring diagram for a twelve-channel seismic apparatus is given, including twelve regular reluctance detectors, one shot-point detector, twelve amplifiers, a twelve-galvanometer camera, synchronous timing arrangement, two-way communica-

[44a] See records Nos. 1 and 2 of Fig. 9–91*a*.

[45] See records Nos. 4 to 8 of Fig. 9–91*b* and *c*.

[46] See record No. 3 of Fig. 9–91*a* with 1/200 sec. time lines from 100 cycle fork.

tion system between shot point and receiving point, and arrangements for transmission of the instant of the shot and the vertical time break. Figs. 9-78 and 9-79 show the interior and exterior of a recording truck for such equipment, with six amplifiers on each side, switch panel and camera between them, communication system on upper left, compander unit in upper center, tuning fork arrangement at upper right. Developing cans are in the rear of the recording compartment within easy reach of the operator, whose position is in a swivel chair in front of the equipment. Fig. 9-80 illustrates a portable six-channel apparatus.
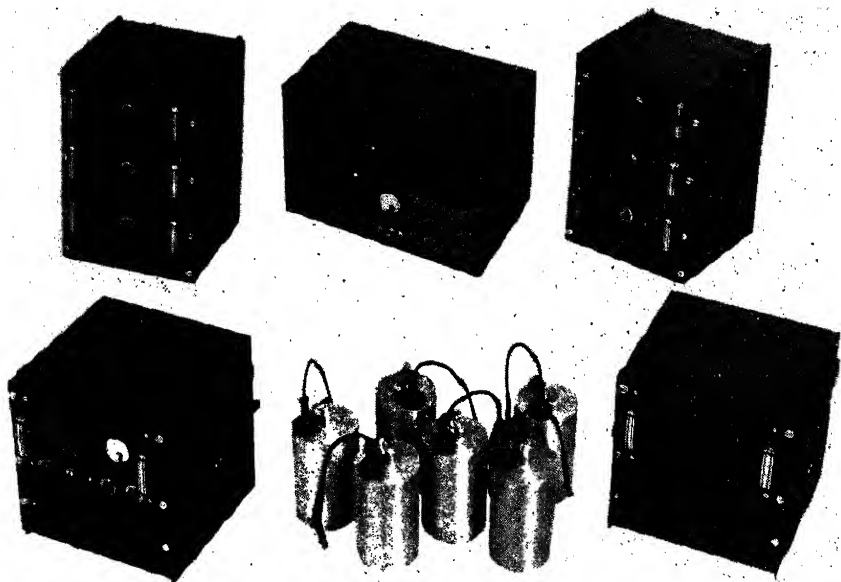
Heiland Research Corp.

Fig. 9-80. Portable seismic reflection equipment. Upper row: two amplifier boxes, each with three amplifiers; camera between them. Lower row (left to right): communication unit, detectors, timing system.

3. *Travel-time relations.* Simple travel-time relations are readily calculated on the assumption that the reflections originate on plane horizontal or inclined surfaces. A further simplification may be introduced by assuming that the rays are straight. Experience indicates that in many cases the curved path may be replaced by the straight path. Another simplification results from a substitution of the straight for the complex path. The latter has offsets due to refractions in reflecting beds higher up in the section.

(*a*) *Horizontal layer.* In Fig. 9-81*a*, let $SR = x$, which is the dis-

tance between the shot point S and any receptor R at the surface. d be the depth, and v_1 the velocity in the section above the reflecting bed. Then the reflection travel time is

$$t_r = \frac{1}{v_1} \sqrt{x^2 + 4d^2}. \tag{9-69a}$$

If x is small compared with d (vertical shooting),

$$t_v = \frac{2d}{v_1}. \tag{9-69b}$$

The travel-time curve represented by eq. (9-69a) is shown in Fig. 9-81b, together with the corresponding travel-time curve for the refracted wave. The reflection-time curve is a hyperbola and is almost horizontal for steep angles of incidence (vertical shooting). For larger distances it rises rapidly
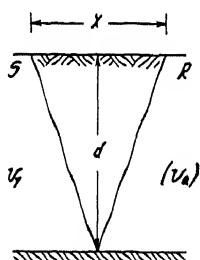
FIG. 9-81a. Reflection path.
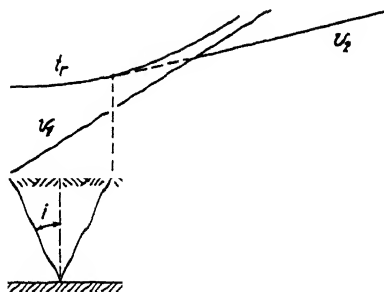
FIG. 9-81b. Relation of refraction and reflection travel-time curves.

until it approaches asymptotically a straight line representing the overburden velocity. If the second part of the refraction travel-time curve is extended toward the shot point, it will be tangent to the reflection travel-time curve at a point corresponding to the critical ray (that is, for which the path in the lower medium is zero). The reflection-time gradient depends on distance as shown by differentiation of eq. (9-69a).

$$\frac{dt_r}{dx} = \frac{x}{v_1 \sqrt{x^2 + 4d^2}} = \frac{x}{v_1^2 t_r} \text{ (see Fig. 9-82).} \tag{9-70}$$

It is often convenient to calculate travel times for vertical incidence and to apply a correction expressed by the ratio of depth and shot distance. $R \equiv d/x$, so that

$$t_r = \frac{2d}{v_1} \sqrt{1 + \left(\frac{x}{2d}\right)^2} \quad \text{or} \quad t_r = t_v \sqrt{1 + \left(\frac{1}{2R}\right)^2}. \tag{9-71a}$$

Also,

$$t_r = \frac{x}{\mathbf{v}_1} \sqrt{1 + \left(\frac{2d}{x}\right)^2}, \qquad (9\text{-}71b)$$

and the time gradient is

$$\frac{dt}{dx} = \frac{1}{\mathbf{v}_1 \sqrt{1 + \left(\frac{2d}{x}\right)^2}}. \qquad (9\text{-}71c)$$
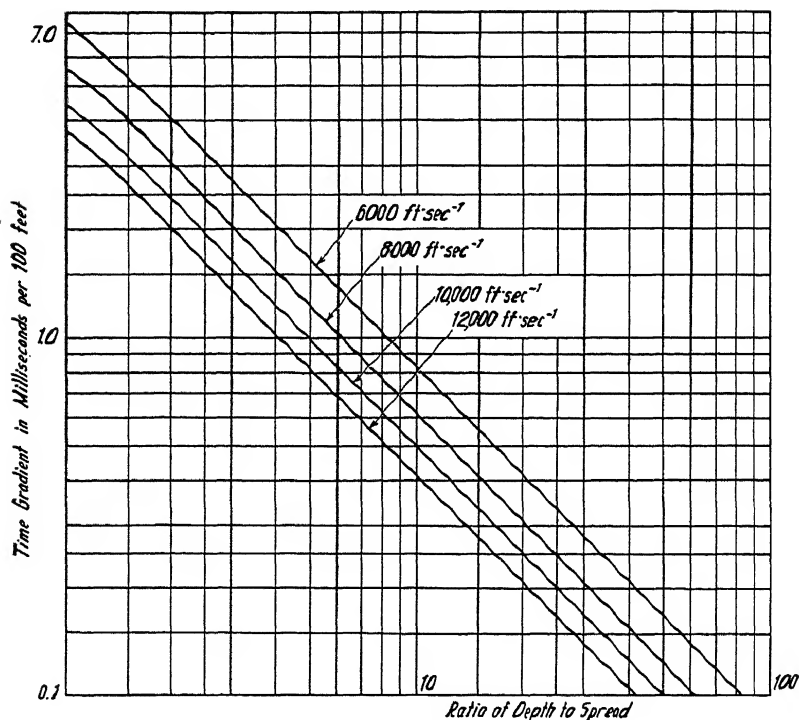
FIG. 9-82. Time gradient of reflection from horizontal bed.

Another correction method is based on an expansion of the second expression in eq. (9-72) into a binomial series. Consideration of only the first two terms gives

$$d = \frac{1}{2}\mathbf{v}_1 t \left(1 - \frac{x}{2\mathbf{v}_1^2 t^2}\right),$$

so that, with t_v as vertical time,

$$d = \tfrac{1}{2}\mathbf{v}_1(t_v - \Delta t),$$

where $\Delta t = x^2/2\mathbf{v}_1^2 t$.
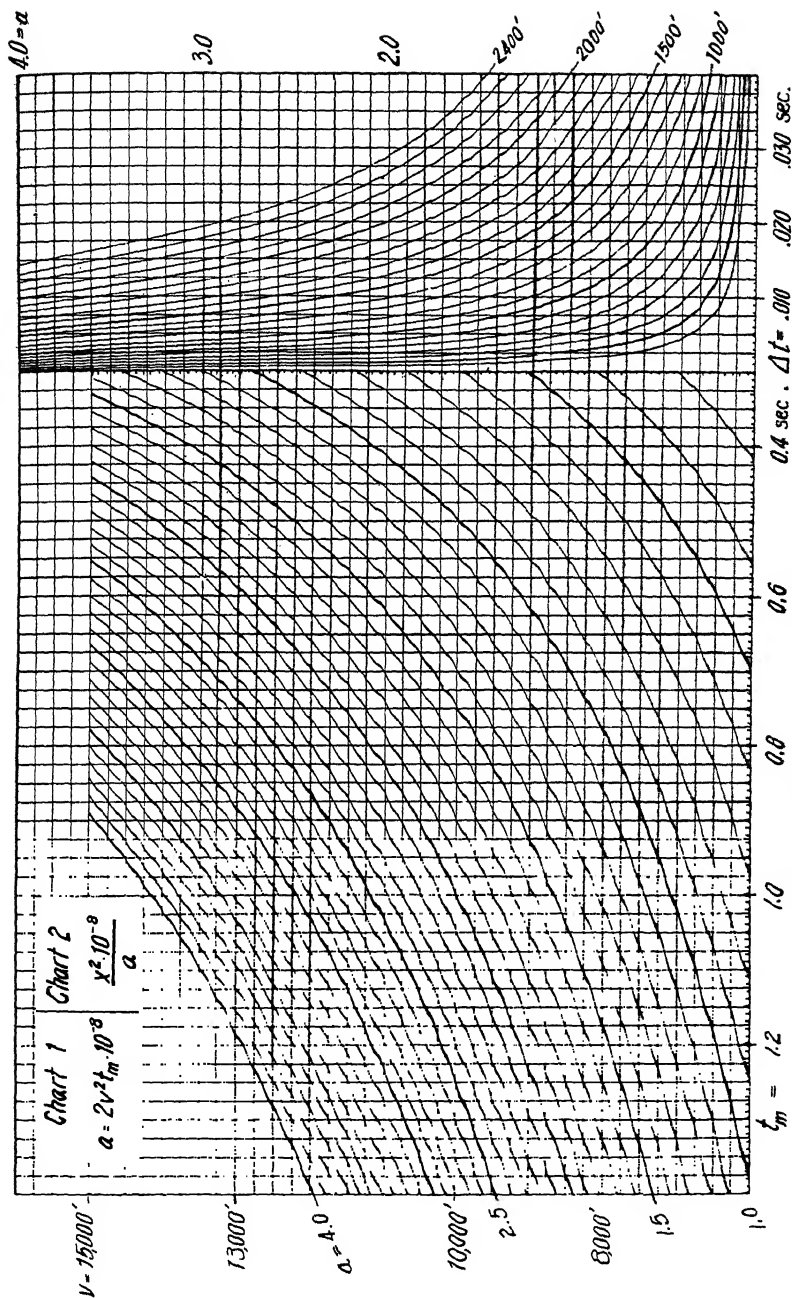
FIG. 9·83. Reduction chart to vertical time (after Pirson).

Fig. 9–83 shows two charts for the calculation of this correction. For any velocity between 6000 and 15,000 feet (ordinate) and any mean reflection time between 0.3 and 1.4 seconds (abscissa), the first chart gives the denominator of the above equation, or the factor $\mathbf{a} = 2\mathbf{v}^2 t \cdot 10^{-8}$. This factor is the ordinate in the second chart on the right. By intersection with the spread distance x (from shot point to center detector), the time correction Δt is located on the abscissa. Thus, this chart carries out the operation $x^2 \cdot 10^{-8}/\mathbf{a}$.

In summary, the following expressions are available for depth calculation from reflection, assuming straight paths:

$$
\left.
\begin{array}{ll}
\text{(general formula)} & d = \tfrac{1}{2}\sqrt{\mathbf{v}_1^2 t^2 - x^2} \\[2mm]
\text{(in terms of vertical time)} & d = \dfrac{1}{2}\mathbf{v}_1 t_v \sqrt{1 - \left(\dfrac{x}{\mathbf{v}_1 t}\right)^2} \\[4mm]
& \equiv \tfrac{1}{2}\mathbf{v}_1(t_v - \Delta t) \\[2mm]
\text{(vertical shooting)} & d = \tfrac{1}{2}\mathbf{v}_1 t_v.
\end{array}
\right\} \quad (9\text{–}72)
$$
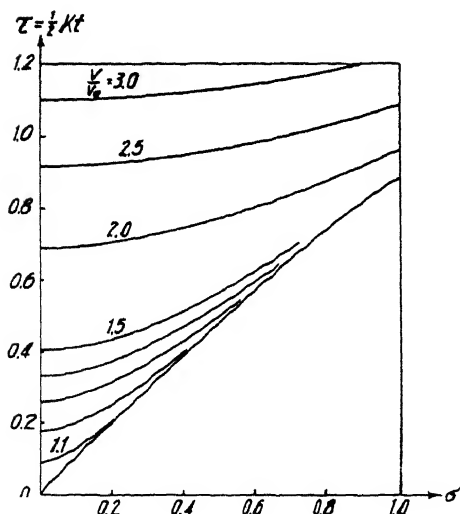
FIG. 9-84. Relative reflection travel time, in a medium of continuous linear velocity increase (after Slotnick).

In eqs. (9–72) the speed of the overburden is assumed to be constant; in practice, an average velocity $\mathbf{v}_a$ is substituted for $\mathbf{v}_1$. For reflections from different depths, different average velocities are generally used. Eqs. (9–72) may be modified for curved ray paths, that is, when there is a variation of the average velocity with depth. Slotnick[47] has calculated the travel-time curves for (1) a linear, and (2) an exponential velocity increase. For a linear increase given by the relation $\mathbf{v}_h = \mathbf{v}_0 + \mathbf{k}h$ (h = depth), the travel time at the distance x is

$$
t = \frac{2}{\mathbf{k}} \log \left[\frac{\mathbf{k}x}{2\mathbf{v}_0} + \sqrt{\left(\frac{\mathbf{k}x}{2\mathbf{v}_0}\right)^2 + 1} \right]
$$

---

[1] Loc. cit.

or

$$= \frac{2}{k} \sin h^{-1} \frac{kx}{2v_0}. \qquad (9\text{-}73a)$$

By introducing the following dimensionless quantities: $\tau = kt/2$; δ ; $v = (v_0 + kh)/v_0 = v_h/v_0$, the travel time may be written

$$\tau = \cos h^{-1} \left[\frac{\delta^2 + 1 + v^2}{2} \right]. \qquad (9\text{-}73b)$$
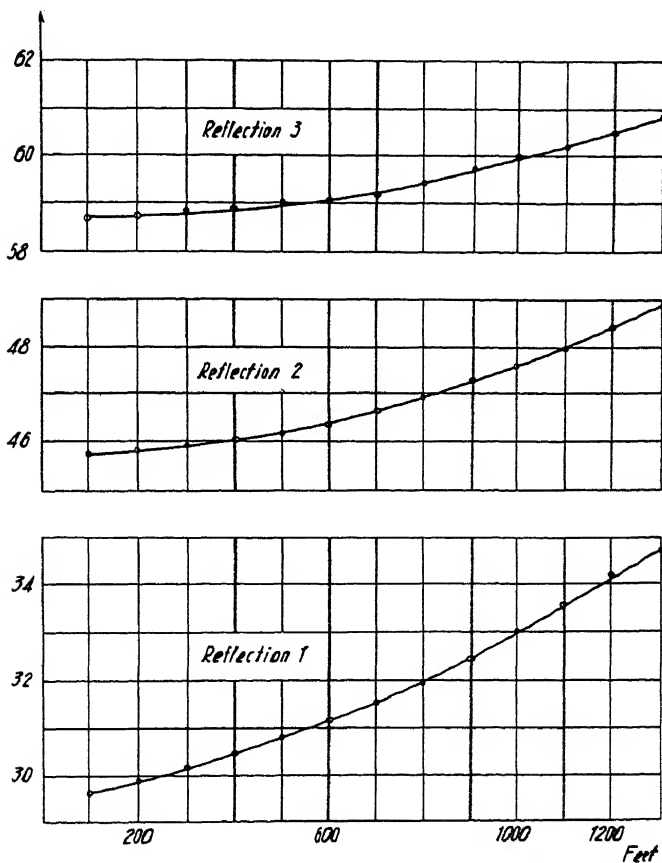
FIG. 9-85. Reflection travel-time curves for three depths.

A graph of reflection travel-time curves for a linear increase of velocity with depth is shown in Fig. 9-84. Fig. 9-85 gives travel-time curves for three reflections originating in a Cretaceous section in Canada. These curves become flatter with depth, which is caused by both the increase in depth and the increase in average velocity with depth.
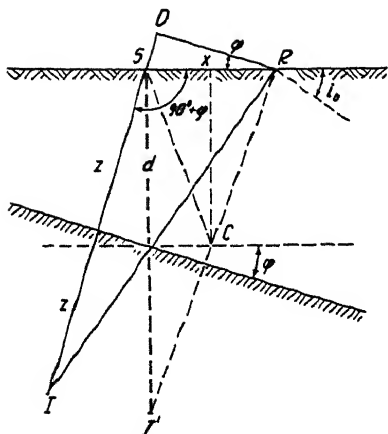
FIG. 9-86. Reflection wave path for dipping bed.

(b) *Dipping bed.* Since in Fig. 9–86 the path $\overline{I'R}$ from the image of the shot point may be substituted for the path to and from the reflection point C on a horizontal bed, it follows that the down-dip travel time for a dipping bed may be written

$$\mathrm{v}t_d = \overline{IR}. \qquad (9\text{--}74)$$

If t_d is varied and x is varied, $\mathrm{v}t_d' = \overline{IR_1}$, $\mathrm{v}t_d'' = \overline{IR_2}$; $\mathrm{v}t_d''' = \overline{IR_3}$, and so on. These relations may be solved graphically for the point I by drawing circles with radii $\mathrm{v}t_n$ about the receiving points which intersect in I. Increased accuracy is obtained by using two sets of receiving points on either side of the shot point. Analytically, the following relations follow from Fig. 9–86:

$$(Down\ Dip)$$

$$\overline{IR}^2 = \overline{DI}^2 + \overline{DR}^2;$$

$$\overline{IR} = \mathrm{v}t_d; \qquad \overline{DS} = x \sin\varphi; \qquad \overline{DI} = 2z + \overline{DS};$$

hence,

$$\mathrm{v}^2 t_d^2 = 4z^2 + 4zx \sin\varphi + x^2. \qquad (9\text{--}75a)$$

$(Up\ Dip)$ (for the *same* distance x):

$$\mathrm{v}^2 t_u^2 = 4z^2 - 4zx \sin\varphi + x^2. \qquad (9\text{--}75b)$$

Subtracting the up-dip from the down-dip time (for the *same* shot distances),

$$\frac{\mathrm{v}^2(t_d^2 - t_u^2)}{8zx} = \sin\varphi, \qquad (9\text{--}75c)$$

and adding,

$$\frac{\mathrm{v}^2(t_d^2 + t_u^2) - 2x^2}{8} = z^2. \qquad (9\text{--}75d)$$

Hence, up- and down-dip times furnish both depth (normal to the bed) and dip, so that the depth d vertically below the shot point becomes

$$d = \frac{z}{\cos\varphi}. \qquad (9\text{--}75e)$$

With the ratio $R = z/x$, formulas (9–75a) and (9–75b) may be written:

$$\frac{\mathbf{v}t_d}{x} = \sqrt{(2R)^2 + 2R\sin\varphi + 1} \qquad (9\text{–}76a)$$

$$\frac{\mathbf{v}t_u}{x} = \sqrt{(2R)^2 - 2R\sin\varphi + 1}. \qquad (9\text{–}76b)$$

The depth under the down-dip shot point is approximately equal to the arithmetic mean of the down-dip and up-dip travel times, multiplied by one-half the velocity. Eqs. (9–75) hold only for equal distances on opposite sides of the shot point. For different distances x_d (down-dip) and x_u (up-dip), we have

$$\mathbf{v}^2 t_d^2 = 4z^2 + 4zx_d\sin\varphi + x_d^2$$

$$\mathbf{v}^2 t_u^2 = 4z^2 - 4zx_u\sin\varphi + x_u^2,$$

so that

$$\frac{\mathbf{v}^2(t_d^2 - t_u^2) + x_u^2 - x_d^2}{4z(x_d + x_u)} = \sin\varphi \qquad (9\text{–}77a)$$

and

$$\frac{\mathbf{v}^2(t_d^2 x_u + t_u^2 x_d) - x_u x_d^2 - x_u^2 x_d}{4(x_d + x_u)} = z^2. \qquad (9\text{–}77b)$$

If dips are determined in two or more distances on the same side of the shot point,

$$\mathbf{v}^2 t_1^2 = 4z^2 + 4zx_1\sin\varphi + x_1^2$$

$$\mathbf{v}^2 t_2^2 = 4z^2 + 4zx_2\sin\varphi + x_2^2,$$

or

$$\frac{\mathbf{v}^2(t_2^2 - t_1^2) - x_2^2 + x_1^2}{4z(x_2 - x_1)} = \sin\varphi \qquad (9\text{–}77c)$$

and

$$\frac{\mathbf{v}^2(t_1^2 x_2 - t_2^2 x_1) - x_2 x_1^2 + x_2^2 x_1}{4(x_2 - x_1)} = z^2, \qquad (9\text{–}77d)$$

if $x_2 > x_1$ and $t_2 > t_1$. In eqs. (9–77a) and (9–77c), an approximate value for z calculated under the assumption of horizontal bedding gives sufficient accuracy for small dips. Formula (9–77c) may be written

$$\sin\varphi = \frac{\mathbf{v}^2}{2z}\left(\frac{t_2 + t_1}{2}\right)\left(\frac{t_2 - t_1}{x_2 - x_1}\right) - \frac{1}{2z}\left(\frac{x_2 + x_1}{2}\right)$$

or

$$\sin \varphi = \frac{\mathbf{v}^2}{2z} \cdot t_m \cdot \frac{\Delta t}{\Delta x} - \frac{1}{2z} \cdot x_m, \qquad (9\text{-}78a)$$

where t_m is the mean time in the mean distance x_m.

In this equation the depth z (normal to the bed) appears. It may be obtained from eq. (9-77d) with its correct value or be calculated from the mean time under the assumption of horizontal bedding. For many dip calculations, other approximations are satisfactory. One of these is to draw a travel-time curve and to extend it toward the shot point. If the shot-point travel time thus obtained is $t_0 = 2z/\mathbf{v}$, eq. (9-78a) becomes

$$\sin \varphi = \frac{\mathbf{v} t_m}{t_0} \cdot \frac{\Delta t}{\Delta x} - \frac{x_m}{\mathbf{v} t_0}. \qquad (9\text{-}78b)$$

In further approximation, let $2z \equiv IR \equiv \mathbf{v} t_m$ (Fig. 9-86). Then (9-78a) becomes

$$\sin \varphi = \mathbf{v} \cdot \frac{\Delta t}{\Delta x} - \frac{x_m}{\mathbf{v} t_m}. \qquad (9\text{-}78c)$$

Finally, the last term of this expression may be dropped so that

$$\sin \varphi = \frac{\Delta t}{\Delta x} \cdot \mathbf{v} \text{ (approx.)}. \qquad (9\text{-}78d)$$

Since $\Delta t/\Delta x$ is equal to the reciprocal of the apparent velocity, eq. (9-78d) is identical with eq. (9-62), and the angle of incidence at the surface, i_0 (at R in Fig. 9-86), is assumed to be equal to the angle of dip. For vertical incidence upon the bed (distances close to shot point) formula (9-78d) is rigorous.

The apparent up-dip and down-dip velocities of reflection impulses may be obtained from a differentiation of the up-dip and down-dip travel times given by eqs. (9-75a) and (9-75b), so that the down-dip gradient (D.G.) is given by

$$\frac{dt_d}{dx_d} = \frac{2z \sin \varphi + x_d}{\mathbf{v}\sqrt{4z^2 + 4zx_d \sin \varphi + x_d^2}} \equiv \text{D.G.}, \qquad (9\text{-}79a)$$

and the up-dip gradient (U.G.) is

$$\frac{dt_u}{dx_u} = \frac{-2z \sin \varphi + x_u}{\mathbf{v}\sqrt{4z^2 - 4zx_u \sin \varphi + x_u^2}} \equiv \text{U.G.}. \qquad (9\text{-}79b)$$

Hence,

$$\frac{dt_d}{dx_d} = \frac{2z \sin \varphi + x_d}{\mathbf{v}^2 t_d} \quad \text{and} \quad \frac{dt_u}{dx_u} = \frac{-2z \sin \varphi + x_u}{\mathbf{v}^2 t_u}. \qquad (9\text{-}79c)$$

These relations are identical with eq. (9-78a). They may be applied in various ways. For a given set of conditions (in an area where the velocity is known and the distance between center of spread and shot point are kept constant), diagrams such as shown in Fig. 9-87 may be prepared, showing, in vertical section, intersecting lines of equal gradient and equal time to center of spread. After the time gradient, or step-out time, has been measured, the point corresponding to these values is located in the diagram, which gives the depth of the reflection point. By connecting
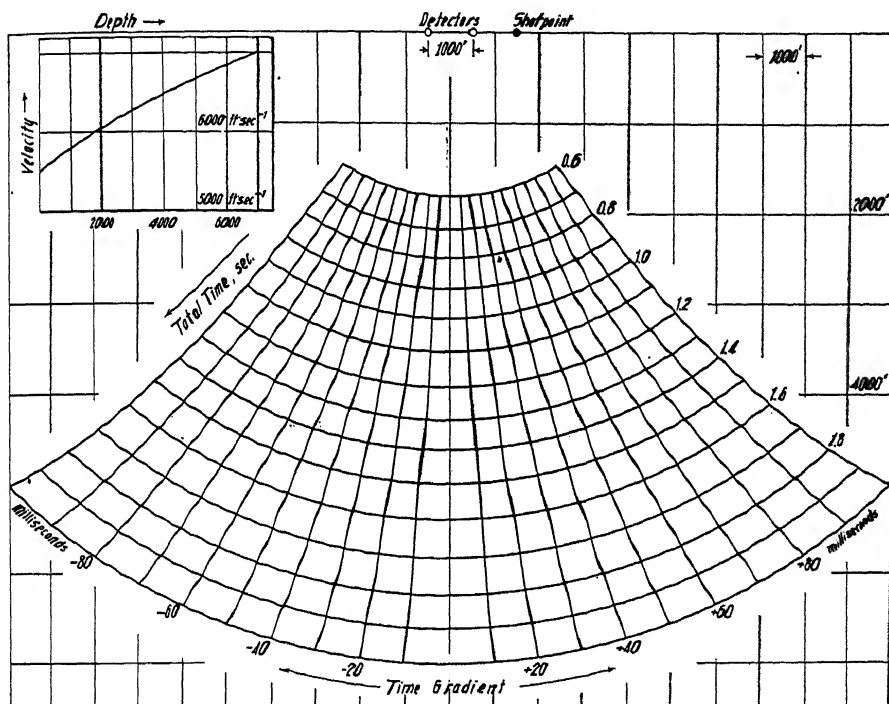
FIG. 9-87. Graph for determining depth and dip from total time and step-out time (after Pirson).

this point with the shot point and drawing a perpendicular, the dip is obtained. A vertical change of velocity may be incorporated in the diagram.

Eqs. (9-79c) may also be utilized for direct dip-calculations. By subtracting the two equations,

$$-^2(\text{D.G.} \cdot t - \text{U.G.} \cdot t_u) - x_d + x_u - \sin \quad (9\text{-}79d)$$

in which the last part of the numerator becomes 0 when equal distances on either side of the shot point are used. Eqs. (9-79a) and (9-79b) are, in

terms of ratios $R = z/x$,

$$\text{D.G.} = \frac{2R_d \sin \varphi + 1}{\mathbf{v}\sqrt{(2R_d)^2 + 4R_d \sin \varphi + 1}}$$

and

$$\text{U.G.} = \frac{-R_u \sin \varphi + 1}{\mathbf{v}\sqrt{(2R_u)^2 - 4R_u \sin \varphi + 1}}. \qquad (9\text{-}79e)$$

Time Gradient
for 100 ft
(at $v_a = 10,000$ ft·sec^{-1})
in milliseconds

$+8.0$

$R=1$

$R=2$

$R=3$

8 4

60

-4.0

Up Dip

Down Dip

$10°$ $30°$ $45°$ $90°$

$R = \frac{z}{x} = \frac{oblique\ depth}{distance}$

-8.0
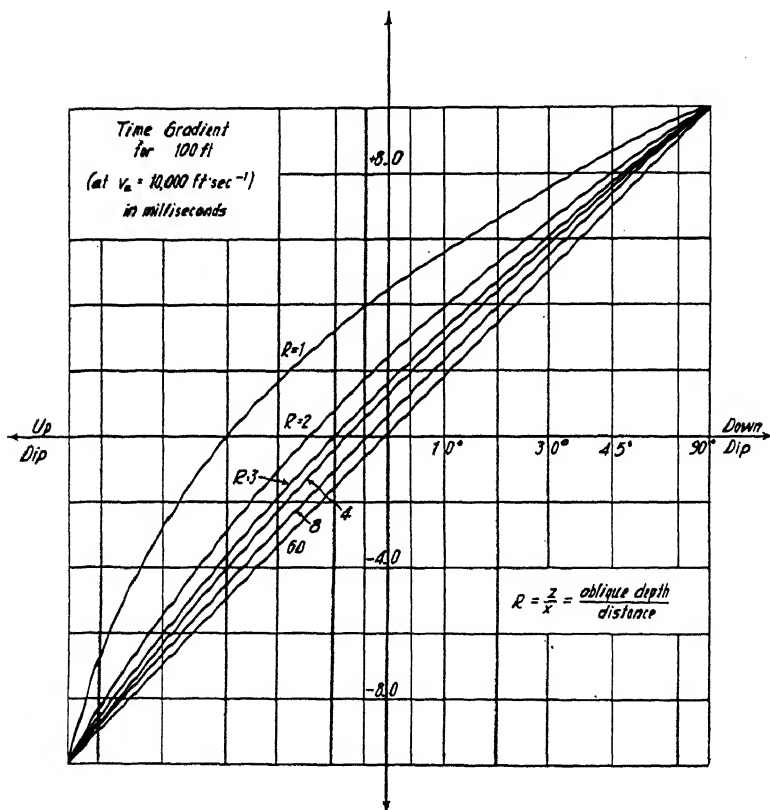
FIG. 9-88. Time gradients for dipping bed.

With these equations the diagram shown in Fig. 9-88 has been constructed. For high ratios of z/x the gradients become negative for comparatively small dip angles, that is, the reflection impulses travel backward in the seismogram. For low angles of dip, travel times of dipping beds are virtually identical with those from horizontal beds; dip shooting becomes applicable if dips exceed about 100 feet to the mile. However, as a means of checking correlations, it is used with lesser angles of dip.

All formulas derived above for dipping beds imply that the traverse is shot up or down in the direction of maximum dip. If the traverse makes the angle α with the direction of dip, the true dip φ follows from the "apparent" dip Φ, as determined along the traverse, from

$$\frac{\sin}{\cos \alpha} = \sin \varphi. \qquad \text{[see 9-56a]}$$

Directions of strike and of total dip may be determined in two reflection profiles at right angles to each other; if the apparent dip angles are Φ and Φ', $\sin \Phi'/\sin \Phi = \tan \alpha$. Another method[48] of determining both dip and strike consists of locating the image of the shot point in three profiles at right angles to one another. At three points of equal distance c from the shot point (see Fig. 9-89) the travel times t_1, t_2, and t_3 are given by

FIG. 9-89. Location of shot-point image from three travel times.

$$v^2 t_1^2 = (x - c)^2 + y^2 + D^2$$

$$v^2 t_2^2 = x^2 + (y - c)^2 + D^2$$

$$v^2 t_3^2 = (x + c)^2 + y^2 + D^2,$$

where x, y, and D are the coordinates of the image point.   Then

$$\left.\begin{aligned} x &= \frac{v^2}{4c} (t_3^2 - t_1^2) \quad \text{(identical with [9-75c])} \\[2mm] y &= \frac{v^2}{4c} (t_3^2 - 2t_2^2 + t_1^2) \\[2mm] D &= \sqrt{v^2 t_1^2 - y^2 - (x - c)^2}. \end{aligned}\right\} \qquad (9\text{-}80)$$

The coordinates of the reflecting point are $x/2$, $y/2$, and $D/2$; the dip is given by $\tan \varphi = \sqrt{x^2 + y^2}/D$, and the strike by $\tan \alpha = y/x$.

The dip-shooting method does not give small dips accurately. This is because of the inherent failure of the travel-time curve to respond to small

---

[8] S. J. Pirson, Oil Weekly, April 26, 1937.

dip angles and errors introduced in the records by surface geological "step outs." The accuracy is probably not greater than 1° or 2°. It can be increased by reducing the station interval, by surveying closed loops, and by adjusting the errors of closure. The most favorable range is from 5° to 30°; in exceptional cases dips of as much as 55° have been recorded.

4. *Average velocity determination.* Notwithstanding the frequent curvature of reflection rays, the assumption of uniform or average velocities to the reflecting bed or beds is generally satisfactory. In the absence of average velocity data, reflection maps may be contoured in reduced time units. In areas where changes of the character of sediments occur, it may be necessary to introduce an average velocity as a function of the geographic coordinates. One or more of the following procedures may be used for the determination of average velocities:

(a) *Calculation from known depth.* Where the geological section is clearly defined so that there is no doubt about the nature and depth of the reflecting formation, a profile is shot near a well and the average velocity is calculated from

$$\mathbf{v}_a = \frac{2d}{t} \sqrt{1 + \left(\frac{x}{2d}\right)^2}. \tag{9-81a}$$

(b) *Well shooting.* A well detector is lowered to various depths and a number of shots are fired at the surface. Usually the distance of the shot locations from the well is made equal to one-half the shot-receptor distance used in the survey, in order to obtain as nearly as possible the velocity along the actual wave path. Well detectors are long seismometers of small diameter, corresponding in design to that of the regular pickups; they have the shape of torpedoes and are well protected against water, mud, and the like. They are lowered on strong steel cables. Average velocities are calculated by dividing the paths from shot point to detector by the respective travel times. Recording of shot instant and accurate time marks are required as in ordinary reflection work. The method is laborious but in most general use at this time.

(c) *Calculation from refraction profiles.* When the thicknesses d_n and the velocities v_n of the strata composing the geologic column are known from refraction profiles, the average velocity to the depth z in the column is

$$\mathbf{v}_a = \frac{z}{\sum \dfrac{d_n}{v_n}}. \tag{9-81b}$$

This method is not particularly accurate, nor is it generally advisable to shoot refraction profiles in an area to obtain average velocity data.

(d) *Calculation from surface profiles.* Since the travel-time equation contains two unknowns—depth and average velocity—a minimum of two equations must be set up to determine both velocity and depth by recording times in at least two distances. Thus (for horizontal beds)

$$v_a = \sqrt{\frac{x_2^2 - x_1^2}{t_2^2 - t_1^2}}. \qquad (9\text{-}81c)$$

In practice many distances are required to give accurate values. Squares of travel times are plotted against squares of the distances. For a reliable determination the curve must be a straight line. The cotangent of its angle α with the abscissa is the square of the average velocity. By differentiating in the travel-time formula ($v^2 t^2 = x^2 + 4d^2$), the square of travel time with respect to the square of the distance, we have $d(t^2)/d(x^2) = 1/v^2$ or $v^2 \equiv \cotan \alpha$. Since $t^2 = x^2/v^2 + 4d^2/v^2$, the velocity squared is the ratio of distance squared divided by times squared. The ordinate at zero distance is $4d^2/v^2$. For this calculation travel times have to be corrected for weathered layer and elevations; they should also be reduced to regional datum.

When the reflecting beds are inclined, it is necessary to shoot an average velocity profile in two directions. In this case the curve representing the squares of travel times as function of the squares of distances is no longer a straight line. Its direction of curvature depends upon whether the profile is shot up dip or down dip. From formulas (9-75a) and (9-75b) we obtain by differentiation

(down dip) $\qquad \tan \alpha_d = \dfrac{d(t_d^2)}{d(x_d^2)} = \dfrac{1}{v^2}\left(1 + \dfrac{2z}{x_d}\sin\varphi\right)$

(up dip) $\qquad \tan \alpha_u = \dfrac{d(t_u^2)}{d(x_u^2)} = \dfrac{1}{v^2}\left(1 - \dfrac{2z}{x_u}\sin\varphi\right),$ $\qquad (9\text{-}81d)$

which indicates that the curvature *decreases* with distance; that is, the time-squared distance-squared curves approach true velocities farthest out from the shot point. The arithmetic mean of two tangents to the curve at identical up- and down-dip distances gives the true velocity to the depth under the shot point:

$$\frac{\tan\alpha_u + \tan\alpha_d}{2} = \frac{1}{v^2}. \qquad (9\text{-}81e)$$

5. *Field practice.* (a) *General procedure.* In a new area where neither transmission characteristics of the near-surface beds nor the subsurface section is known, the most suitable shot depth and arrangement of receivers (shot distance and receiver interval) must be determined by experi-

ment. The best procedure is to select a favorable location (see paragraph *c* below), to drill a hole 25 to 50 feet deep, and to select, from inspection of the well samples, a firm or moist formation for placing the shot. Shots are fired with gradually increased charges and records are taken at 100- to 200-foot intervals, beginning as closely to the shot point as possible. These may be utilized later for average velocity calculations if desired. The distance most favorable for the desired reflections is then selected. Quality of reception may be improved by suitable adjustment of filters, and the like. From the records and from geologic considerations the observer will decide whether dip shooting or continuous profiling may be necessary. Surface geology data will determine the weathered-layer procedure.

(b) *Types of shooting.* When reflecting beds are consistent and of low dip so that no correlation difficulties are experienced, the normal setup with receptor spread to one side of the shot point is used (*correlation shooting*). Shot distances vary from 200 to 2000 feet to the middle receiver and receiver intervals from 20 to 100 feet. If reflecting beds are not consistent or if correlation difficulties arise from other sources, *continuous profiles* are shot.[49] This is a variation of dip shooting. When the spread has been shot in the forward direction, the shot point is moved to the location previously occupied by the last receiver. From this point the first spread is shot in reverse and the next spread in forward direction (Fig. 9-90). Since the paths from I to 6 and from II back to I are identical, the travel times are identical and the two records may be tied in. Within the setup shown in the figure, the reflection points are continuous. The "holes" left under the shot points between successive profiles may be avoided by using more overlap. Receivers are evenly spaced between shot points, generally at 100 to 150 feet.

FIG. 9-90. Arrangement for continuous profiling.

Dip shooting is applied when there is noticeable dip and when reflecting beds are not consistent, so that presence or absence of structure may be

[49] S. J. Pirson, A.I.M.E. Tech. Publ. No. 833, 1937.

established by correlating dips between stations. The following procedures may be followed: (1) shoot twice in the same hole and move the receivers over; (2) leave receivers in place and shoot from both sides of the spread; (3) shoot once in one hole, and use half of the receivers on one side of the shot point, and the other half on the other side; (4) shoot with receivers to one side and determine dip by absolute times and time gradient. These procedures may be applied in two profiles at right angles to each other to determine strike. Structural mapping by small dip angles should be done in closed loops, since the depth errors of closure are considerable and must be distributed by suitable adjustment. Shot distance and receiver interval vary as in correlation shooting.

(c) *Shot placement, surveying, drilling.* Reflection locations should be selected from the point of view of good energy transmission, ease of drilling, and minimum variation of elevation and surface geology along receiver spread. Low places are generally preferred, since water-bearing beds occur closer to the surface. In many cases the selection of reflection locations is a matter of compromise between the above factors. Elevation of shot-point and receiver locations must be determined with an accuracy of about one foot. When dip profiles are shot in more than one direction to determine strike, the direction of the profiles must be recorded.

Holes may be drilled with hand augers in favorable locations or when speed is not an important consideration. However, the more general practice is to use rotary drilling rigs mounted on trucks, as previously described (page 491). In clay, marl, and other soil which is easy to drill, two crews can make as much as 500 to 600 feet of hole a day. For hard formations, coarse gravel, boulder clay, and the like, spudders are used. Caving of shot holes is overcome by the use of "Aquagel," or lime, or by setting casing. In soft marsh ground, holes are washed down with a high pressure pump operated from a small gasoline engine (see Fig. 9–29).

Charges may vary from a single cap to 10 pounds of dynamite. Sixty per cent special gelatin dynamite and Nitramon is most frequently used. Charges are forced down the hole by rods consisting of several sections provided with junctions so made that they do not come apart when lowered into the hole but may be dissembled readily when pulled out. Holes are generally tamped with water; in exceptional cases, with mud. For this purpose a water tank is carried on the shooter's truck.

(d) *Weathered-layer technique.* A near-surface "weathered" or "correction" zone with a considerable reduction in velocity occurs in every area. As this layer is not likely to be identical at all stations it has become general practice to correct for the delay of the reflected wave in this layer. As it has, furthermore, very poor transmission characteristics, shots are placed below it or at least near its lower surface.

The extensiveness of the weathered-layer correction is usually a com-

TABLE 58

SURVEY: Hugo
DATE: May 8, 1939
SHOT POINT NO.: 45A

STATE: Colorado
COUNTY: Lincoln
POSITION: E Center

SECTION: 6
T 11 S R 52 W
DIRECTION: SSW

CALCULATION OF WEATHERING AND DATUM CORRECTION

DISTANCES	200 ft.	1750 ft.	1800 ft.	1850 ft.	1900 ft.	1950 ft.	
ELEVATIONS	5242.2 ft.	5268.4	5268.7	5269.6	5270.5	5271.3	E_r (MEAN) = 5261.7
l_B obs.		9.1	8.2	7.8	6.8	5.9	d_B = 2 ft.
l_B corr.		9.2	8.3	7.9	6.9	6.0	Corr. = +0.1
l_A		26.4	27.0	28.1	28.7	29.2	l_6 = 31.9
Sum		35.6	35.3	36.0	35.6	35.2	
Sum $- l_6$		3.7	3.4	4.1	3.7	3.3	
$\div 2 = l_w$		1.85	1.7	2.05	1.85	1.65	mean = 1.82
$\times v_1 = W_r$							mean = 52.8
$l_A - l_w$		24.55	25.30	26.05	26.85	27.55	$\dfrac{E_r - W_r - D}{v_d} = l_r$

Shot Elev. (E_s) = 5234.6 ft.
Shot Depth (d_s) = 58 ft.
t_v = 2.0
l_{200} corr. = 5.0
$l_{200} + l_v$ = 7.0
$\dfrac{200}{v_2} = t_h$ = 3.0
$(l_{200} + l_v) - t_h$ = 4.0
$\div 2$ = 2.0
$\times v_1 = W_s$ = 58 ft.
$W_s - d_s = t_s$ = 0
$E_s - D - W_s = t_d$ = 2.52

$\dfrac{d_s}{l_v} = v_1$ = 2000 ft. sec.$^{-1}$ v_2 = 6667 ft. sec.$^{-1}$
$= \dfrac{176.6}{v_d}$ v_d = 7000 ft. sec.$^{-1}$

l_r = 3.10
$t_r + t_w$ = 4.02
$t_s + t_d$ = 7.45 +

REFLECTION CALCULATION; CORRELATION

REFL.	VELOCITY	REC. t	CORRECTIONS to Datum	Spread	Sum	CORR. t	$d = \frac{1}{2} v t_c$	$D - d$
T_1 T_2	8000 ft. sec.$^{-1}$ 8000 ft. sec.$^{-1}$	82.2	−7.5	−3.5	−11.0	71.2	2848 ft.	2152 ft.
P_1 P_2	9000 ft. sec.$^{-1}$ …							

572

(1)

(2)

(3)
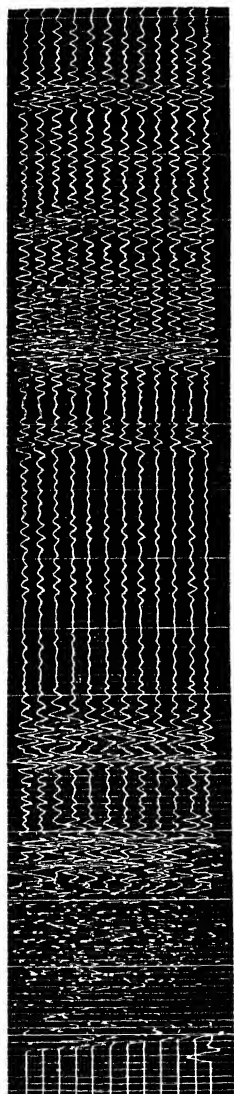
FIG. 9-91a. Seismic reflection records.

(4)

(5)

Heiland Research Corp.

FIG. 9-91b. Seismic reflection records *(continued)*.
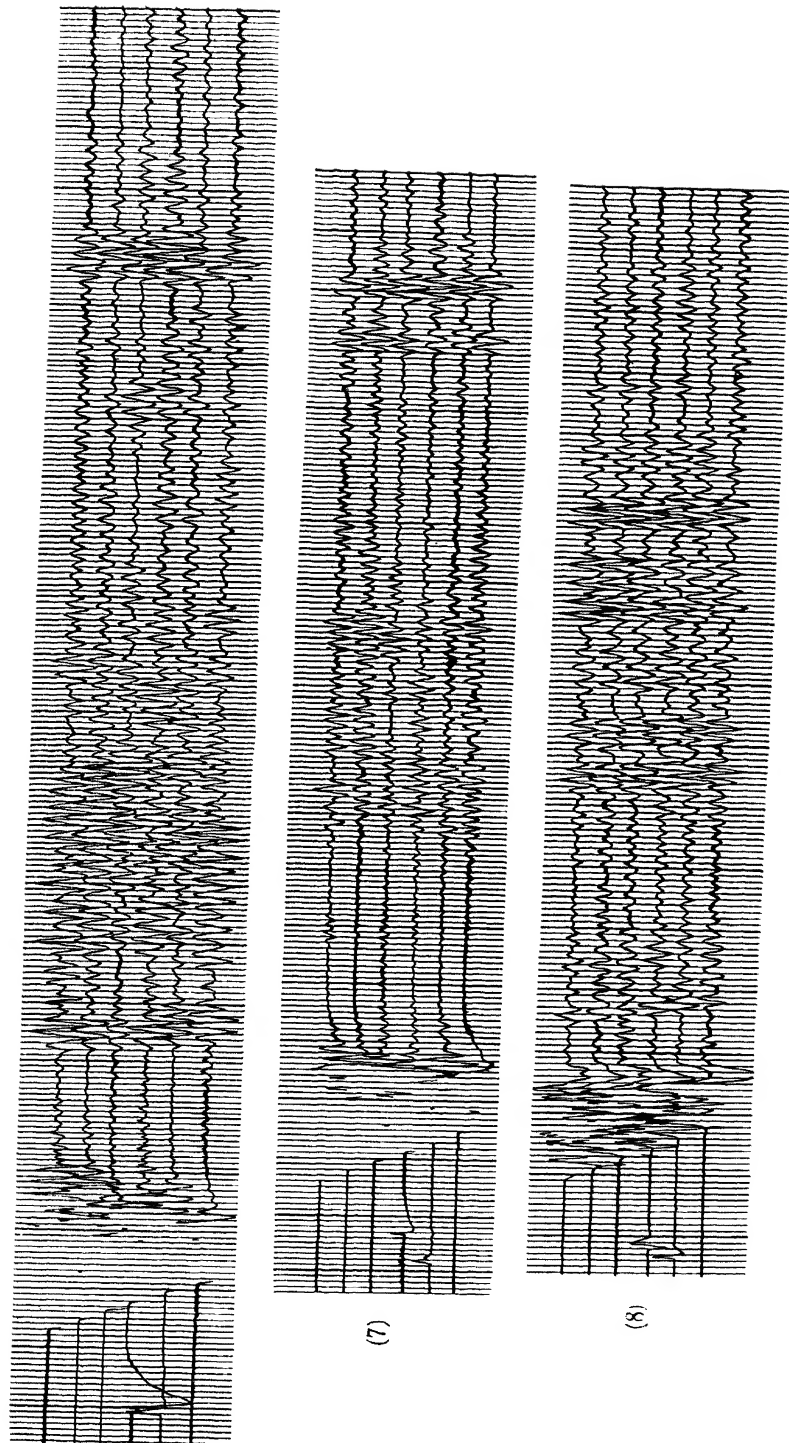
FIG. 9-91c. Seismic reflection records (concluded).

(7)

(8)

promise between accuracy and time available to obtain the correction data in the field. The accuracy need be no greater than that for depth determination. The time required to obtain weathered-layer data in the field depends on the lateral consistency of the layer. Four possibilities exist: (1) conditions may be the same in the entire area; (2) conditions may be the same at the shot and receiving points but vary throughout the area; (3) conditions may differ on shot and receiving points but be the same at the individual receiving locations; (4) conditions may be different at the shot point and differ at the receiving locations.

The first condition prevails in some limited areas so that the correction may be determined once and for all by vertical-time or refraction methods. Assumption of the second condition furnishes sufficient accuracy in many cases. The weathered-layer delay is then most conveniently determined by measuring the vertical-time interval at the shot point with a shot-point detector and correcting to shot level. In the third case (different conditions at shot point and receiving points) the vertical time is measured at the shot point, and a refraction profile is shot at the receptor spread. Finally, when conditions are different at the individual receiving stations, the vertical time is again determined at the shot point and the time delay for each receiver is established by the method of differences (*ABC* system). This is the procedure in most prevalent use. Further details are given in the calculation records (Table 58). The vertical-time phone is usually connected by a separate line to the truck and recorded on the fifth or eleventh trace. A correction to regional datum, from which the average velocity is reckoned, is generally added to the weathering correction.

6. *Calculation, interpretation.* Reflections are not very difficult to spot even in a fair seismogram. They appear with a marked change in amplitude, consist of one to three or four waves (generally with declining amplitude), and reveal themselves primarily by their almost simultaneous appearance on all traces (except when strong dips are present) (see Fig. 9–91). A reflection may be recognized by comparing its time-distance gradient with that of the first impulses. A graphical analysis of records taken in an entirely new area by travel-time curves will identify reflections with certainty, besides offering the advantage of a determination of their average velocity. After reflections have been identified, they are timed, using the trough of the first wave. The mean time, referred to the center of the spread, is entered in the calculation form. In dip shooting, times are read for the closest and the farthest detector. The recorded times are then corrected for weathering to datum and for spread, as described below.

Some reflections may not show very distinct first troughs. In case of doubt, two and sometimes three troughs or "phases" are timed (see Fig. 9–92). Depth errors may readily be committed unless the correct phases

are correlated from point to point. For preliminary depth calculations an average velocity may be assumed or be determined from surface profiles. However, for most areas accurate values derived from well shooting are now available.
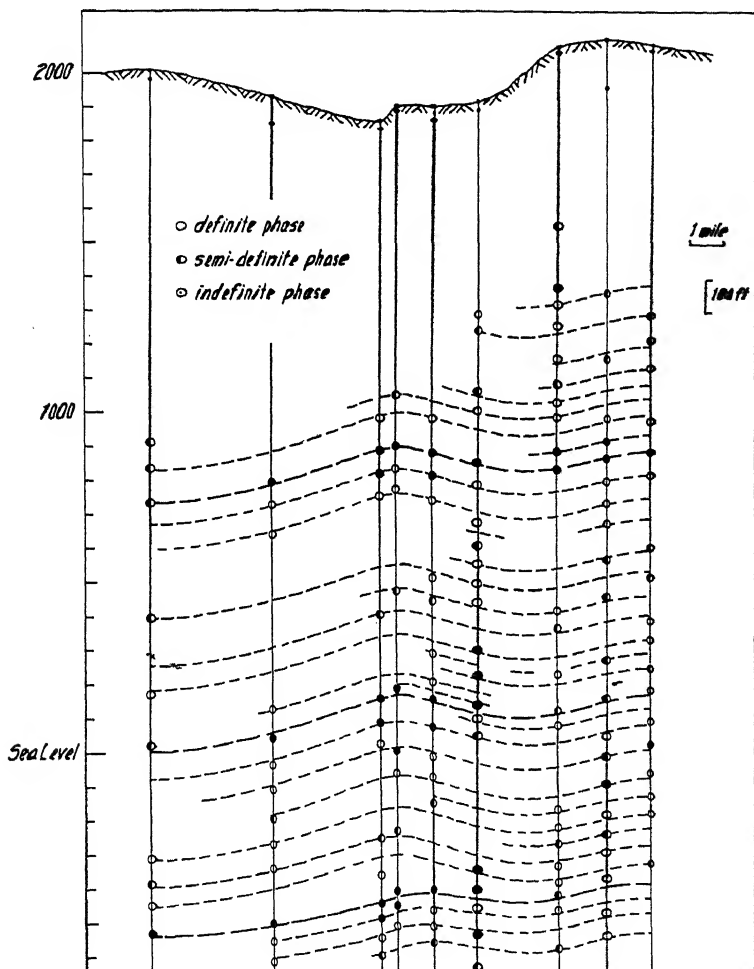
FIG. 9-92. Reflection correlation (phase) logs.

Records are generally calculated in the field office; some companies make it a practice to send duplicate records to headquarters. The field crew keeps the following records and turns them in to the field office at the end of the day's work: (a) Driller's notes, containing data on location of shot holes, formations encountered, depth of hole, depth of casing, and

so on. (*b*) Surveyor's notes, giving locations and elevations of shot holes and receivers, direction of shooting, and the like. (*c*) Observer's notes, consisting of a schedule of records taken, charges and shot depth, distances of receivers, and data pertaining to instrument control and filter settings.

Calculation forms used in the office for the evaluation of seismic records vary greatly in arrangement, depending on company procedure and preference. The form given in Table 58 will be found to be flexible enough to cover most weathering and reflection procedures which are likely to be applied in practice. It contains, in the upper portion, general data on location of shot point and receivers. In the lower part follows a form for calculation of weathering correction by the ABC method. Distances and elevations of receivers are entered first. Of the three main columns, the left pertains to the shot point and a location 200 feet away from it, which is intended to give the depth of weathering W_s under the shot point. In it are entered shot elevation E_s, shot depth d_s, vertical time t_v and time to the 200-foot detector t_{200} corrected for elevation. Depth to weathering at the shot point is obtained by adding the 200-foot time to the vertical time, subtracting the horizontal time t_h, dividing by 2, and multiplying by the overburden velocity v_1 calculated from shot depth and vertical time $(d_s/t_v = v_1)$.

The result will indicate whether the shot is located above or below the weathered layer, and the correction $t_s = (W_s - d_s)/v_1$ is applied accordingly. Added to it is a correction to datum t_d calculated with an (average) velocity v_d of the high-speed bed under the weathered layer. In the middle row of columns are entered the times t_R from the reverse weathering shot which are then corrected for shot depth d_R/v_1. Next follow the times t_4 of the first breaks from the reflection record. They are added; the time t_6 to the sixth receiver (set out as shown in Fig. 9-75) is subtracted; the result $(2t_w)$ is divided by 2; and weathering W_r under each receiver is calculated by multiplication with the overburden velocity. As shown in the form, it is usually sufficient to average the times and calculate a mean weathering depth. Subtracting the weathering times t_w from the forward times t_4 gives accurate times corresponding to the advance of the wave in the high-speed bed underlying the weathered layer. From this, an accurate value for its velocity v_2 may be obtained. An average value v_d (usually close to v_2) determined from refraction profiles or well shooting is used for the calculation of t_d in the first, and of $t_r = (E_r - W_r - D)/v_d$ in the last column for reduction to datum. The total correction $(t_r + t_w + t_s + t_d)$ is entered in the reflection calculation form and added to the spread correction.

In correlation shooting, times corresponding to the various reflections and their phases are entered and corrected, and depths are calculated for

vertical incidence and converted to elevations above sea level. For dip shooting, this form is modified for the calculation of depths and dip from mean times and time gradients (corrected for weathering and to datum).

In correlation shooting, stations are arranged on profiles and cross traverses so that an interlocking pattern is formed. Reflection impulses may be entered by appropriate symbols in the reflection log for each station and may be connected in much the same manner as key beds of adjacent well logs (see Fig. 9–92). In dip shooting, dips may be indicated by a short bar at the reflection depths and correlation may be made on a "phantom" horizon or horizons (see Fig. 9–93). Depth determinations made on this basis are not very reliable, but errors are reduced by conducting the survey in a closed loop and distributing the errors graphically or by calculation.
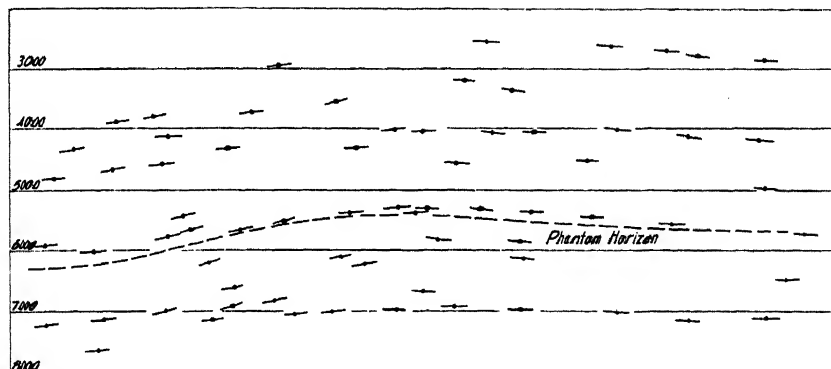
Fig. 9-93. Dip profile across deep-seated salt dome in southern Louisiana (after Goldstone).

IV. ELEMENTARY THEORY AND DESCRIPTION OF SEISMOGRAPHS

A. Classification

Seismographs may be classified according to component recorded or according to application. The first division is customary in station seismology. There we speak of horizontal, vertical, and universal seismographs. Fig. 9–94 shows a number of horizontal seismographs in diagrammatic form. The oldest type is probably the simple pendulum (1). The pendulums in 2, 3, and 4 follow the "swinging door" principle. The Wiechert astatic pendulum (5) is used in most seismological observatories of the world. The torsion seismometer (6) has been installed in many U. S. Coast and Geodetic Survey and Carnegie Institution observatories. The construction of Nos. 7 and 8 is applied in vibrographs and prospecting seismographs.
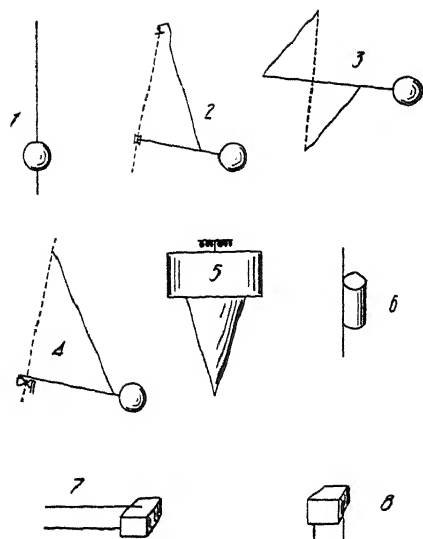
FIG. 9-94. Horizontal seismographs (schematic): (1) Ewing, (2) Rebeur-Paschwitz, (3) Zoellner, (4) Milne, (5) Wiechert-astatic, (6) Wood-Anderson, (7) Galitzin, (8) Schweydar.

According to application, seismometers may be divided into (1) station seismographs, (2) vibrographs, and (3) prospecting seismographs. These differ in respect to mass, magnification, natural frequency, and method of recording, as shown in Table 59.

B. ELEMENTARY THEORY

1. *Geometric and physical characteristics of seismometers.* Assume a simple pendulum seismograph, as shown in Fig. 9-96, its mass m being suspended at a distance l' from the axis. Attached to it is a magnifying lever whose equivalent length is $J - l'$. According to the well-known theory of the mathematical pendulum,

Of the vertical seismographs (Fig. 9-95) the simplest consists of a mass suspended from a coil spring (1). The three seismometers in 2, 3, and 4 use levers with coil springs; the pallograph (4) is employed for the measurement of ship vibrations. The designs in 2, 5, 6, 7, and 8 are used in seismic prospecting detectors.[50] Universal seismographs for the recording of all ground components have been made by combining the coil type (Fig. 9-95, 1) with the Ewing pendulum (Fig. 9-94, 1). This is known as the De Quervain universal seismograph. They have not found application as prospecting detectors.
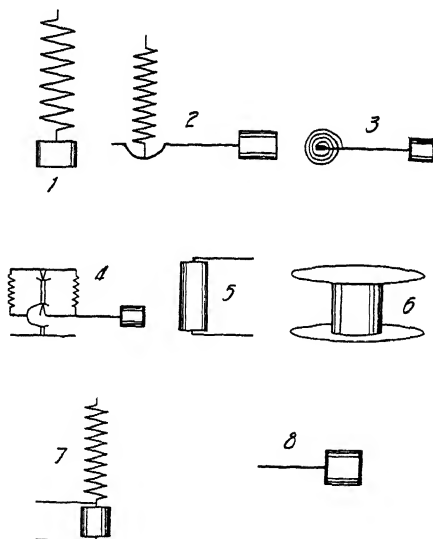
FIG. 9-95. Vertical seismographs (schematic): (1) coil spring, (2) Gray spring-lever, (3) Tanakadate, (4) pallograph, (5) dual spring, (6) geophone, (7) combination of (1) and (5), (8) Vicentini.

[50] Vertical seismographs, particularly the astatic types, are also employed as gravimeters (see pp. 125, 126, 132, and 134).

$$\left(\frac{2\pi}{T_0'}\right)^2 = \frac{g}{l'}, \tag{9-82a}$$

where T_0' is the natural period of the pendulum, g is gravity, l' is pendulum length, and $\mathbf{J}$ is indicator length. If b is the deflection of the mass from

<div align="center">TABLE 59</div>

TYPE	MASS	MAGNIFI-CATION	NATURAL FREQUENCY	RECORDING METHOD
Station seismograph........	large	small	low	mostly mechanical; some optical and electrical
Vibrograph................	small	small	high	mostly optical
Prospecting seismograph...	small	large	intermediate and high	mostly electrical

its rest position and a the corresponding amplitude of the pointer, the indicator or static magnification is

$$\mathbf{V} \equiv \frac{a}{b} \equiv \frac{\mathbf{J}}{l'}. \tag{9-82b}$$

If the suspension point of a seismograph is displaced rapidly, the ground displacement is recorded with the magnification $\mathbf{V}$ in opposite direction, and the negative indicator magnification gives the pendulum displacement for rapid ground movements. In the corresponding physical pendulum

FIG. 9-96. Seismometer as a pendulum.

the period is proportional to the distance of the center of oscillation from the axis of rotation. The reduced or equivalent pendulum length is given by

$$l = g \left(\frac{T_0}{2\pi}\right)^2. \tag{9-82c}$$

Substituting, in eq. (9-82c), ω_0 for $2\pi/T_0$, where ω_0 is the angular frequency of the seismograph, hereafter briefly referred to as natural frequency, ($\omega_0 = 2\pi f_0$, see eq. [9-18a]),

$$\omega_0^2 = \frac{g}{l} = \frac{mgs}{K}, \tag{9-82d}$$

where s is the distance of the center of gravity from the axis of rotation and K the moment of inertia about the same axis. For any type of spring seismograph,

$$\omega_0^2 = \frac{c}{m} = \frac{g}{d}, \tag{9-83}$$

where c is a spring constant and is equal to the ratio of force and spring elongation d (see page 591).

2. *Undamped free oscillations.* In an undamped seismograph, as in a mathematical pendulum (see page 97), the condition of equilibrium of restoring and inertia forces is expressed by $mg \sin \varphi + ml\,(d^2\varphi/dt^2) = 0$ (see Fig. 9-96), so that in abbreviated differential notation after dividing by ml, and letting $\sin \varphi = \varphi$,

$$\ddot{\varphi} + \frac{g}{l}\,\varphi = 0. \tag{9-84a}$$

Substituting $a = \mathbf{J}\varphi$ (Fig. 9-96, where a is the recorded amplitude) and utilizing eq. (9-82d), we have

$$\ddot{a} + \omega_0^2 a = 0, \tag{9-84b}$$

whose solution is

$$a = \mathbf{A}_0 \sin(\omega_0 t + \psi) = \mathbf{A}_0 \sin \omega_0(t + t_0), \tag{9-84c}$$

which is identical in form with eq. 9-19 given on page 449.

3. *Free oscillations with friction.* Actually the last equation does not express completely the motion of the seismograph. Its amplitude decreases with time, since the kinetic energy is consumed and converted into heat. This transformation acts as a brake on the amplitude. The manner in which the amplitude decreases is dependent on the type of braking resistance, of which the following are the more important types: (1) Coulomb's friction, constant during the entire motion, (2) velocity damping, which is proportional to the velocity of motion, and (3) velocity-square damping, proportional to the square of the velocity of motion. Only the first and second will be discussed here. Details on the theory of velocity-square damping may be obtained from the literature.[51]

In early seismograph construction, attempts were made to reduce the natural movement by excessive friction. However, this makes the seismograph inoperative for accelerations equal to or less than the frictional force. It does not return to its zero position, while with velocity damping it always returns.

Although friction is undesirable in a seismograph, it is never possible to avoid it altogether, since there is a certain amount of friction in the suspension springs, electrical wires, and the like. The type of record obtained with a seismograph under the influence of friction only is shown in Fig. 9-97. A line connecting the peaks is straight, while for a damped seis-

---

[51] L. S. Jacobsen, Seis. Soc. Amer. Bull., **20**(3), 160-195 (Sept., 1930); B. Hague, *Alternating Current Bridge Methods* (section on oscillographs), London (Pitman & Sons), 1930.

mograph it is an exponential. The effect of friction may be distinguished from damping by measuring both ratios and differences of successive amplitudes. In a damped curve the ratio is constant (corresponding to a geometric progression), while in a friction curve the difference is constant (representing an arithmetic progression). The vector figure of amplitude progression is an Archimedian spiral for friction and a logarithmic spiral for damping.

As shown in Fig. 9-97, equiphase amplitudes lose the amount 4f within one period so that $a_3 = a_1 - 4f$. Since deflection is force divided by spring constant, the loss of deflection f due to the frictional force is equal to $m'g\zeta/c$, with ζ as Coulomb's friction factor and m' the "equivalent" mass of the seismograph. The period of a seismograph with friction is the same as the period of a seismograph without friction.
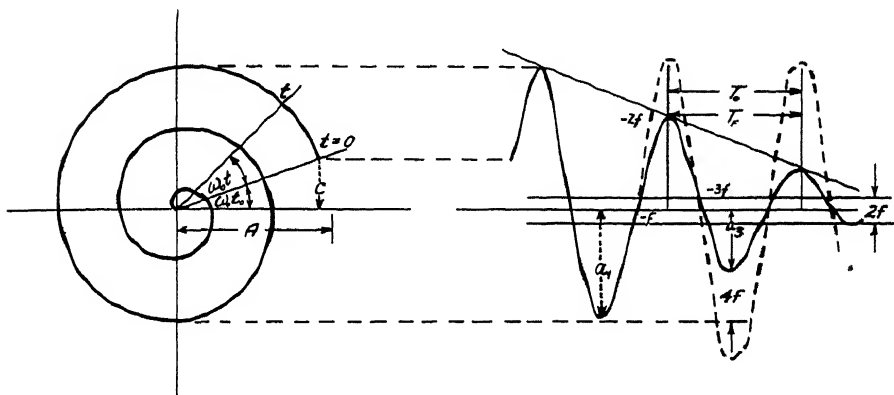
FIG. 9-97. Seismograph oscillations under influence of friction.

4. *Free oscillations with damping.* The type of amplitude decay just discussed may be said to be due to exterior friction. Conversely, interior friction (as in liquids) produces damping in proportion to the first or second power of the velocity of motion. In velocity damping, the closest approach to a correct reproduction of actual ground motion is obtained. Three types of damping are employed in seismic detectors: (1) air, (2) oil, and (3) electromagnetic damping.

Air damping is effective only if the mass of the seismograph is small[52] and the frequency low. Hence, it has found application in condenser-microphone detectors and in some inductive geophones with very light coils. *Oil damping* is most frequently employed. In mechanical seis-

[52] These statements refer to seismic detectors. Air damping can be effective in station seismographs (Wiechert) when used at the end of levers which, however, are usually undesirable on detectors.

mographs a vane may be attached to the end of the magnification cone to be free to move in an oil cup; or a series of vanes may be fastened to the mass directly, arranged between partitions in an oil container. In electrical detectors the receiver cases are generally filled to a level which gives the desired amount of damping. It is preferable to use mineral oils of low temperature coefficient of viscosity (Nujol or automobile oils of various S.A.E. ratings).

Electromagnetic damping is most satisfactory from the point of view of design, clean operation, and independence of temperature. It is most effective in detectors of low natural frequency and light mass. In a Galitzin type seismometer a copper plate at the end of the coil-carrying lever moves between two permanent magnets whose spacing can be adjusted to obtain the desired damping rate. In the Wood-Anderson torsion seismometer the mass moves between the poles of a permanent magnet. In the Wenner seismometer pickups and galvanometer coils are of comparable mass and damp one another; the damping rate may be regulated by a shunt across the line. With an amplifier between pickup and galvanometer the primary of the input transformer produces damping. Additional damping may be produced by short-circuited turns or coil frames of conductive material.

If $\mathbf{p}$ is defined as damping resistance, or damping force on mass of unit velocity, the damping acceleration equals $\mathbf{p}\dot{a}/m$, and

$$\ddot{a} + \frac{\mathbf{p}}{m}\,\dot{a} + \omega_0^2 a = 0. \qquad (9\text{-}85a)$$

Substituting a *damping constant* $\epsilon = \frac{1}{2}\mathbf{p}/m$ (which has the dimension of a frequency),

$$\ddot{a} + 2\epsilon\dot{a} + \omega_0^2 a = 0, \qquad (9\text{-}85b)$$

whose solution $a = \mathbf{B}_0 \cdot e^{\alpha_1 t} + \mathbf{C}_0 \cdot e^{\alpha_2 t}$, or

$$a = \mathbf{B}_0 \cdot e^{-[\epsilon - \sqrt{(\epsilon^2 - \omega_0^2)}\,]t} + \mathbf{C}_0 \cdot e^{-[\epsilon + \sqrt{(\epsilon^2 - \omega_0^2)}\,]t} \qquad (9\text{-}85c)$$

If $\epsilon > \omega_0$, the exponent is negative, the motion overaperiodic, the damping overcritical, and the mass creeps back to the zero position. If $\epsilon = \omega_0$, the mass returns to zero without overswing, and the motion is aperiodic (critical damping). If $\epsilon < \omega_0$, the mass oscillates about the zero position with declining amplitudes. This is referred to as damped free oscillation, comprising damping rates between zero and critical. In this case, the term $\sqrt{\epsilon^2 - \omega_0^2}$ becomes $j\sqrt{\omega_0^2 - \epsilon^2}$, so that by the use of Moivre's theorem

$$a = \mathbf{B}_0 \cdot e^{-\epsilon t} \cdot \sin \sqrt{\omega_0^2 - \epsilon^2}\, t + \mathbf{C}_0 \cdot e^{-\epsilon t} \cdot \cos \sqrt{\omega_0^2 - \epsilon^2}\, t \qquad (9\text{-}86a)$$

Comparing this with eq. (9-18a), we see that $\sqrt{\omega_0^2 - \epsilon^2}$ represents the natural frequency reduced by damping. Hence,

$$\omega_d = \sqrt{\omega_0^2 - \epsilon^2}, \tag{9-86b}$$

the *damped natural frequency*, is always less than the undamped frequency, and approaches zero for critical damping. With (9-86b), eq. (9-86a) may be written

$$a = \mathbf{A} \cdot e^{-\epsilon t} \left[\frac{\mathbf{B}}{\mathbf{A}} \sin \omega_d \cdot t + \frac{\mathbf{C}}{\mathbf{A}} \cos \omega_d t \right],$$

which by substitution of $\mathbf{B}/\mathbf{A} = \cos \psi$ and $\mathbf{C}/\mathbf{A} = \sin \psi$ becomes

$$a \quad {}^{-\epsilon t} \quad \cdot \ ' \quad ' + \psi) \tag{9}$$

and is represented in time-amplitude and vectorial form in Fig. 9-98. The peak amplitudes decrease in geometric progression. A line connecting them is an exponential, since the amplitude at the time t is $\mathbf{A}_t = \mathbf{A}_0 \cdot e^{-\epsilon t}$.
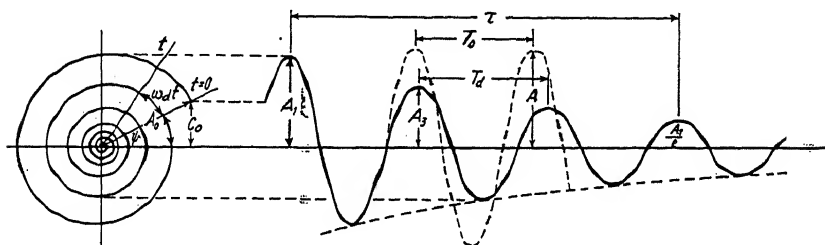
FIG. 9-98. Oscillation of damped seismograph.

Thus, the ratio r of two equiphase peak amplitudes within one period T_d is $r = \dfrac{\mathbf{A}_1}{\mathbf{A}_3} = \dfrac{\mathbf{A}_0 \cdot e^{-\epsilon t}}{\mathbf{A}_0 \cdot e^{-\epsilon(t+T_d)}}$. Hence,

$$r = e^{T_d} = e^{\epsilon/f_d}, \tag{9-87a}$$

where r is the *damping ratio* and $f_d = 1/T_d$ is the damped frequency. In logarithmic form

$$\log_e r = \log_e \frac{\mathbf{A}_1}{\mathbf{A}_3} = \epsilon T_d = \frac{\epsilon}{f_d} = \Lambda_e, \tag{9-87b}$$

with Λ_e as the *natural logarithmic decrement*.

In highly damped seismographs it is difficult to measure accurately the amplitude ratios for one complete period. More suitable is the determination of the *overshoot*, which is the (reciprocal) damping ratio referred to successive amplitudes within one-half of a period. It is expressed as the overswing $\Delta \mathbf{A}$ in terms of the original amplitude $\mathbf{A}$ so that

$$\Delta \mathbf{A} = \mathbf{A}_0 \cdot e^{-\Lambda_e/2}. \tag{9-87c}$$

Another characteristic of damping is the *relaxation* time (Fig. 9-98), that is, the time which elapses until the amplitude has declined to $1/e$ of its initial amount:

$$\tau = \frac{1}{\epsilon} = \frac{T_d}{\Lambda_e}; \qquad \log_e r = \frac{T_d}{\tau}. \tag{9-87d}$$

In seismograph calibration it is convenient to use the relative damping η, which is the ratio of damping constant and natural frequency ω_0 and varies therefore from 0 for no damping to 1 for critical damping. Hence,

$$\frac{\omega_d}{\omega_0} = \frac{f_d}{f_0} = \sqrt{1 - \eta^2}. \tag{9-87e}$$

In Galitzin's publications a damping factor μ is used. This is equal to the ratio of damped and undamped frequency:

$$\mu = \frac{\omega_d}{\omega_0} = \frac{f_d}{f_0} = \sqrt{1 - \eta^2}. \tag{9-87f}$$

5. *Forced oscillations; steady state conditions.* Generally the ground continues to move after the seismograph motion has started. The two motions will be superimposed on each other. Expressions may be derived for the resultant "forced" oscillations, provided that certain simplifications are introduced. Replacing the 0 on the right side of eq. (9-84b) by a term containing the acceleration $\ddot{x}$ of the point of suspension,

$$\ddot{a} + \omega_0^2 a = -V\ddot{x}. \tag{9-88a}$$

It is seen that a seismograph can be made to record the ground motion perfectly if the pointer acceleration equals magnified ground acceleration, that is, if $\ddot{a} = -V\ddot{x}$. This condition can exist only if $\omega_0 = 0$ and if the seismograph has an infinitely long period, that is, if it is astatized. Actually zero frequency is mechanically impossible; however, the lower the natural frequency, the more the second time derivative of the recorded amplitude will correspond to the ground acceleration. The seismograph is essentially a displacement recorder. Conversely, if a seismograph is made with a natural frequency much higher than that of the ground motion, $\ddot{a}$ is negligible compared with $\omega_0^2 a$ and eq. (9-88a) becomes $a = (-V/\omega_0^2)\ddot{x}$. It is seen that the recorded amplitude is proportional to the ground accelerations and that, therefore, the seismograph is an accelerometer. However, the ground accelerations are recorded with a reduced magnification (V/ω_0^2).

A definite solution of eq. (9-88a) can be given if a time function of x is introduced, the simplest assumption being a continuous harmonic function. Hence, if $x = X \sin \omega t$ (where X is the maximum amplitude and ω is ground frequency), $\ddot{x} = -X\omega^2 \sin \omega t$, and eq. (9-88a) becomes

$$\ddot{a} + \omega_0^2 a = VX\omega^2 \sin \omega t, \tag{9-88b}$$

whose solution

$$a = \frac{VX\omega^2}{\omega_0^2 - \omega^2} \sin \omega t = \frac{V\omega^2}{\omega_0^2 - \omega^2} x. \qquad (9\text{-}88c)$$

Substituting the dynamic magnification $\mathbf{W}$ for the ratio a/x, and the "tuning factor" n for the ratio ω/ω_0,

$$\mathbf{W} = \mathbf{V} \cdot \frac{n^2}{1 - n^2}. \qquad (9\text{-}88d)$$

If $\omega = \omega_0$, resonance occurs; $\mathbf{W} = \infty$; and, theoretically, infinite amplitudes are obtained. In practice they do not occur because of a certain amount of friction or damping which is always present. If $\omega \gg \omega_0$, $\mathbf{W} = -\mathbf{V}$; the dynamic magnification is equal to the negative static magnification; and very rapid ground motions are recorded with the indicator magnification. If $\omega \ll \omega_0$, $\mathbf{W} = \mathbf{V}\omega^2/\omega_0^2$; the dynamic magnification is proportional to the square of the ground frequency; and the seismograph acts as an accelerometer.

Undamped seismographs are used in vibration engineering for determining, by resonance, the natural frequency of oscillating shafts, engines, and the like. As a rule, however, seismographs are applied away from the point of resonance. Theoretically, this is possible by a very low or very high natural frequency. Some refraction receivers of the accelerometer type are built in this manner (carbon button and piezoelectric receivers). For the recording of first breaks only, the use of damping offers no particular advantage. Conversely, in station seismometers and reflection seismographs, resonance and continued oscillation after cessation of ground motion are highly undesirable. Therefore, damping is applied.

Forced oscillations of a damped seismograph may be treated by inserting the damping term $2\,\epsilon\dot{a}$ in eq. (9-88b), so that

$$\ddot{a} + 2\,\epsilon\dot{a} + \omega_0^2 a = VX\omega^2 \sin \omega t, \qquad (9\text{-}89a)$$

whose first particular solution $a_1 = A_0 \cdot e^{-\epsilon t} \sin(\omega_d t + \psi)$ is a transient and vanishes with time the more ϵ approaches ω_0. The second particular solution is

$$a_2 = \frac{VX\omega^2 \sin(\omega t - \varphi)}{\sqrt{(\omega_0^2 - \omega^2)^2 + 4\epsilon^2\omega^2}}, \qquad (9\text{-}89b)$$

in which φ is the phase shift between ground motion and record and is given by $\tan \varphi = 2\,\epsilon\omega/(\omega_0^2 - \omega^2)$, with $(\omega_0^2 - \omega^2)^{-1}$ as a frequency factor (f_0) characterizing the reaction of an undamped seismograph and $[(\omega_0^2 - \omega^2)^2 + 4\epsilon^2\omega^2]^{-1/2} \equiv (f_d)$ as a damped frequency factor. For critical damping, the damped frequency factor is $(f_d)_{\eta=1} = (\omega_0^2 + \omega^2)^{-1}$ and for
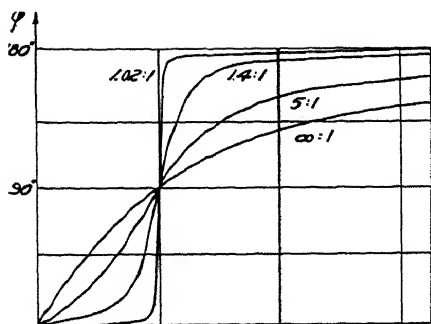
FIG. 9-99. Phase shift of seismograph motion as a function of damping and tuning factor.

0.7 critical it is $(f_{a/\eta}$ $(\omega_0^4 + \omega^4)^{-1/2}$. Fig. 9-99 shows the variation of phase shift with tuning factor n and damping ratio r. For an undamped seismograph (r = 1:1) a phase shift of 180° occurs at the resonance point. This is smoothed out the more the damping approaches critical (r = ∞:1). For small damping ratios and ground frequencies less than instrument frequency, the seismograph moves in the same direction as the ground. At resonance it is 90° out of phase. For ground frequencies greater than the instrument frequency it moves in opposition to the ground. Since in eq. (9-89b) $X \sin(\omega t - \varphi) = x$ = ground movement, the dynamic magnification of a damped seismograph (for sustained oscillations) is $W_d = a_2/x$. The ratio W_d/V is represented in Fig. 9-100 as a function of tuning factors (0-1 up to resonance and inverse factors past resonance) and relative damping η.

It is seen in Fig. 9-100 that, with an increase in damping, the resonance peak moves toward increasing ground frequencies. The resonance frequency for a damped seismograph is

$$\omega_r = \frac{\omega_0^2}{\sqrt{\omega_0^2 - 2\epsilon^2}}. \qquad (9\text{-}89c)$$

If $\epsilon = 0$, $\omega_r = \omega_0$; the resonance frequency is equal to the natural frequency. There is no resonance peak ($\omega_r = \infty$) if $2\epsilon^2 = \omega_0^2$, that is, if $\eta = \sqrt{\frac{1}{2}} = 0.7$ critical. To eliminate resonance, critical damping is therefore not necessary but merely 0.7 critical damping.

The complete solution of the original differential equation (9-89a) is then

$$a = A_0 \cdot e^{-\epsilon t} \sin(\omega_d t + \psi) + \frac{VX\omega^2}{\sqrt{(\omega_0^2 - \omega^2)^2 + 4\epsilon^2\omega^2}} \sin(\omega t - \varphi). \quad (9\text{-}89d)$$

This represents a superposition of a transient and a recurrent phenomenon, the former being the natural oscillation of the instrument set off by the ground impulse, the latter the forced oscillation. The stronger the damping, the more rapidly the natural oscillation dies away. Hence, eq. (9-89b) and Fig. 9-100 describe the phenomenon fully for steady state conditions.

6. *Forced oscillations; onset conditions.* Stationary conditions are gen-

erally reached after the third or fourth peak of a sinusoidal impulse has
been recorded. Before that, the first term in eq. (9-89d) plays an important part. How the seismograph records the "onset" of an impulse
depends on its damping, frequency characteristics, and initial conditions,
that is, the *phase relation* of ground and instrument motion. The simplest
assumption in regard to starting conditions is that at the time $t = 0$, the
amplitudes and velocities of both ground and instrument motion are zero,
and that the ground motion is a train of sinusoidal waves. The corresponding seismograph motion has been calculated by H. A. Wilson.[53]
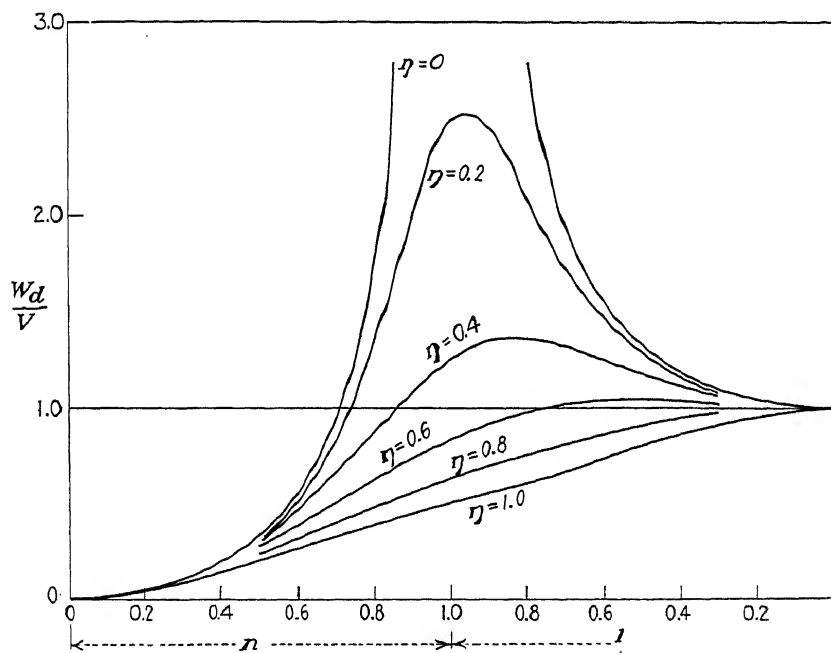
Fig. 9-100. Dynamic response of mechanical seismograph, as a function of tuning
factor and relative damping (after Meisser).

Some of his results are reproduced in Fig. 9-101 for undamped and critically damped seismometers and for various tuning factors.

At *resonance* the onset of a wave train is recorded by an undamped
seismometer with rapidly increasing amplitudes and a phase shift of 90°.
For critical damping, the amplitude is considerably reduced, but the 90°
phase shift in maximum amplitudes remains. In a *station seismometer*
($n = 3$) the reproduction of the ground motion is more faithful. For a
tuning factor of 10, phase shift and amplitude would be still further

[53] Physics, 2(3), 186-199 (March, 1932).

reduced.)   Ground motion and instrument record are here about 180° out of phase.   Critical damping adds no particular advantage; it cuts amplitudes and introduces an additional phase shift.   (In station seismometers, damping is usually less than critical.)   In an undamped *accelerometer* ($n = \frac{1}{3}$) considerable interference is caused by natural oscillations. When damped, the natural oscillations are eliminated.   The instrument record is nearly in phase with the ground motion and much reduced in amplitude.

In the remaining part of Fig. 9-101 the reaction of various seismographs to a single impulse of one-half of a sine wave is indicated.   At the beginning both record and ground amplitude are assumed to be zero.   At *resonance*, the impulse starts a train of waves, the first recorded peak being 90°

Tuning Factor n	Undamped η = 0		Critically Damped η = 1	
n = 1 Resonance				
n₁ = 3 Station Seismometer				
n₄ = ⅓ Accelerometer				
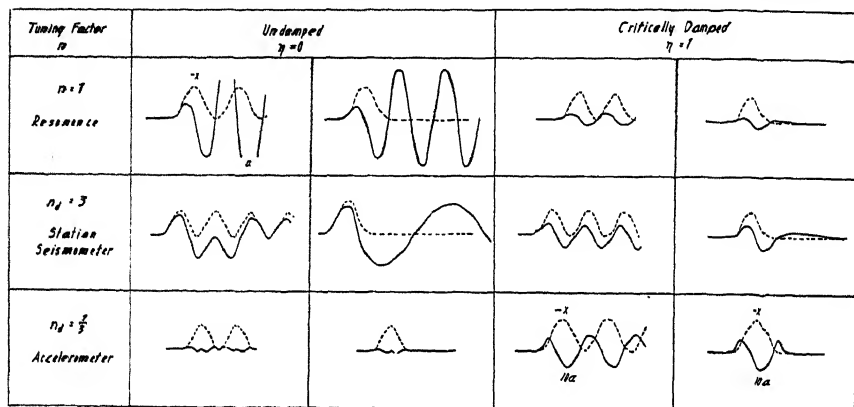
FIG. 9-101. Reactions of damped and undamped seismographs to onsets of periodic and transient vibrations (adapted from Wilson).

out of phase.   With a critically damped seismometer, a double wave is recorded with reduced amplitude, lagging 90° in phase behind the ground impulse.   An undamped *station seismometer* reacts rather unfavorably to a single impulse.   A train of low-frequency oscillations is started.   The first peak coincides with the ground motion peak but is 180° out of phase. With a critically damped instrument, a double instead of a single impulse is recorded, with less than 180° phase shift between peaks.   An undamped *accelerometer* records a single impulse essentially with its own natural oscillation.   When damped, it records three peaks instead of a single one, the main peak being almost in phase with the ground motion.

The behavior of various types of seismometers for an initial phase difference of 90° between ground motion and instrument position has been calculated by H. Martin.[54]   Aside from minor details the response for 90°

Veroeff. Reichsanstalt, **26** (Jena, 1935).

initial phase difference is not much different from that for 0° difference. H. W. Koch and W. Zeller[55] have calculated onset records for ground motions of gradually increasing amplitudes composed of two portions, $X \sin \omega t$ and $-X e^{-\epsilon' t}$, where ϵ' is the damping factor of the ground motion.

C. The Mechanical Seismograph

In principle a mechanical seismograph consists of a mass suspended by a spring. To it may be added a lever or mirror system. This then represents a mechanical seismograph with a mechanical or optical recording system. The mass may also carry inductive, capacitive, or reluctance transducers; it then constitutes a mechanical seismograph with an electrical recording system, sometimes referred to merely as an electrical seismograph, detector, or geophone. Whatever the arrangement for mechanical magnification or electrical transmission, the characteristics of a seismograph are determined in the main by its mechanical design. The following is a brief discussion of suspensions used in their relation to the frequency characteristics of exploration seismographs.

The sensitivity of a seismograph to ground vibrations depends on its deflection for a given load, which is inversely proportional to its natural frequency. It is, therefore, impossible to combine high (mechanical) sensitivity with high natural frequency. The following relations exist between spring constant c (force-producing unit elongation), load on the end of a spring F, natural frequency ω, and deflection a:

$$\omega_0^2 = \frac{c}{m} = \frac{F}{am}; \qquad a = \frac{g}{\omega_0^2}, \qquad (9\text{-}90a)$$

where $\omega_0 = 2\pi f_0$.

For a leaf spring of rectangular section with the length l, breadth b, thickness h, Young's modulus E, and sectional moment of inertia J, the spring constant $c = 3EJ/l^3$. Since $J = bh^3/12$, $c = Eb(h/l)^3/4$, so that the natural frequency

$$2\pi f_0 = \omega_0 = \frac{1}{2} \sqrt{\frac{Eb}{m} \left(\frac{h}{l}\right)^3}. \qquad (9\text{-}90b)$$

When a light mass is suspended at the end of the spring, 30 per cent of the mass of the spring should be added to it. For steel springs Young's modulus is closely enough 2×10^{12} dynes·cm^{-2} (if the geometric dimensions are expressed in cm and masses in g). In horizontal seismometers

[55] Zeit. Geophys., **12(5/6)**, 220–228 (1936).

leaf springs with mass down are sometimes used.   Then the natural frequency

$$\omega_0 = \sqrt{\frac{3\mathbf{E}J}{l^3 m} + \frac{3}{2}\cdot\frac{g}{l}} = \frac{1}{2}\sqrt{\frac{\mathbf{E}bh^3 + 6mgl^2}{ml^3}}.$$ (9-90c)

Hence, when a loaded spring is turned from a horizontal into a vertical position, its natural frequency increases.   For an inverted vertical spring with mass up, the natural frequency is

$$\omega_0 = \sqrt{\frac{3\mathbf{E}J}{l^3 m} - \frac{3}{2}\frac{g}{l}} = \frac{1}{2}\sqrt{\frac{\mathbf{E}bh^3 - 6mgl^2}{ml^3}}.$$ (9-90d)

For a coil spring carrying a mass, the spring constant $\mathbf{c} = d^4\mathbf{u}/64Nr^3$, where d is the thickness of the wire, $\mathbf{u}$ the rigidity modulus (for steel, 8×10^{11} dynes·cm^{-2}), r the radius, and N the number of turns.   Therefore, the natural frequency

$$\omega_0 = \frac{d^2}{8r}\sqrt{\frac{\mathbf{u}}{Nrm}}.$$ (9-90e)

Frequently a seismograph mass is supported by a number of springs in multiple, that is, terminating in the mass.   Their resultant spring constant is equal to the sum of the individual constants, as they act the same as capacitances in multiple.   The natural frequency of a multiple spring suspension is therefore always higher than the frequency of a single spring suspension.

Combinations of levers and springs are used frequently in station seismographs and sometimes in refraction and reflection seismographs, since these give a possibility of lowering the natural frequency of the assembly beyond the frequency obtainable with spring combinations alone.   The natural frequency of a combination of a lever with the length l to which a spring is attached at a distance a from the axis is

$$\omega_0 = \frac{a}{l}\sqrt{\frac{\mathbf{c}}{m}}.$$ (9-90f)

If the spring is attached at a point below the axis so that a line connecting this point with the axis of rotation makes the angle α with the lever,

$$\omega_0 = \frac{a}{l}\sqrt{\frac{\mathbf{c}}{m}\left(\cos^2\alpha - \frac{mgl}{\mathbf{c}a^2}\tan\alpha\right)}.$$ (9-90g)

D. The Electromagnetic Seismograph

In an electrical seismograph a transducer is employed to convert mechanical into electrical impulses.   While the record of a mechanical seis-

mograph furnishes either the ground displacement or the acceleration, depending on frequency adjustment, the effect of the transducer in an electrical seismograph is superimposed on its mechanical action, and the (mechanical) frequency response is modified. It is least changed by a capacitive transducer. In piezoelectric and similar transducers, the conversion of mechanical into electrical energy takes place in proportion to the acceleration, and in electromagnetic transducers in proportion to the velocity of the ground motion. The voltage output of the latter is therefore proportional to the ground frequency, provided the seismograph is adjusted to a low natural frequency. When the natural frequency is so adjusted that the seismograph acts as an accelerometer, its voltage output is proportional to the third power of frequency. Only the theory of the electromagnetic detector is discussed below; little is known at present about the theory of the capacitive and pressure transducers. The theory is applicable to both inductive and reluctance transducers. The overall dynamic response of a seismic channel is dependent on the characteristics of the detector, the amplifier, and the galvanometer, which will be discussed separately.

1. *Theory of the electromagnetic detector.*[56] Assume the transducer in an electrical detector to consist of a circular coil attached to the seismograph mass and to move in the field of an electromagnet. If the amplitude of the mass is a, the induced e.m.f. is

$$E = -\mathbf{H}_s l \frac{da}{dt}, \qquad (9\text{-}91a)$$

where $\mathbf{H}_s$ is the field of the magnet, l the length of wire, and E electromotive force. For an undamped seismograph $a = \mathbf{V}X\omega^2 \sin \omega t / (\omega_0^2 - \omega^2)$, and therefore

$$\frac{da}{dt} = \frac{\mathbf{V} \cdot \omega^2}{\omega_0^2 - \omega^2} X\omega \sin (\omega t \pm 90°).$$

Hence, the e.m.f. generated is

$$E = -\frac{\mathbf{H}_s l \mathbf{V} \omega^2}{\omega_0^2 - \omega^2} \omega X \sin (\omega t \pm 90°). \qquad (9\text{-}91b)$$

For a seismometer adjusted to a low natural frequency,

$$E = \mathbf{H}_s l \mathbf{V} \omega X \sin (\omega t \pm 90°), \qquad (9\text{-}91c)$$

_____

[56] See also F. Sohon, Introduction to Theoretical Seismology, Vol. II: F. Wenner, Bureau of Standards Res. Paper No. 66, (1929); H. Benioff, Seis. Soc. Amer. Bull., **22**, 155–169 (1932); and other references given in Heiland, *op. cit.*, 452–454 (1934).

that is, the voltage output increases linearly with frequency. For a seismometer adjusted to a high natural frequency,

$$E = -\mathbf{H}_s l \frac{\mathbf{V}}{\omega_0^2} \cdot \omega^3 X \sin (\omega t \pm 90°), \qquad (9\text{-}91d)$$

that is, the e.m.f. increases in proportion to the third power of frequency (ground acceleration times frequency). Eq. (9-91b) indicates that the voltage is 90° out of phase compared with the mechanical phase of the seismograph. Fig. 9-102 shows that for a seismograph of low natural frequency the voltage output increases linearly with frequency in the range where the dynamic mechanical magnification is equal to the static
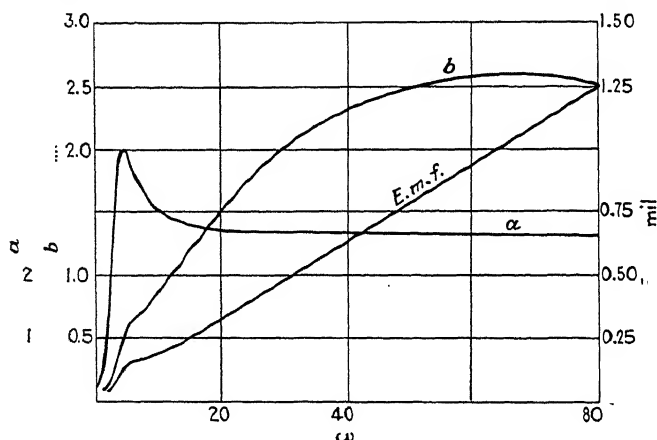
Fig. 9-102. Frequency response of electromagnetic seismograph (after Reutlinger). (a) Mechanical response; (b) galvanometer response.

magnification. The curve b represents the deflection of a galvanometer coupled directly to the seismometer. The deviation from a straight line is caused by the dynamic response of the galvanometer, which decreases with increasing frequency.

For a damped seismograph one obtains by differentiation of the steady state term in eq. (9-89d), and substitution in (9-91a)

$$E = -\mathbf{H}_s l V X \frac{\omega^2}{\sqrt{(\omega_0^2 - \omega^2)^2 + 4\epsilon^2 \omega^2}} \cdot \omega \cdot \sin (\omega t - \varphi \pm 90°). \qquad (9\text{-}92a)$$

With $\mathbf{T}$ as a transmission constant equal to $-\mathbf{H}_s lC$ (where C is a factor introduced by short circuiting the detector through the primary of an impedance matching transformer), the peak e.m.f. $= E_m$ is

$$E_m = \frac{V\omega^3 \mathbf{T} X}{\sqrt{(\omega_0^2 - \omega^2)^2 + 4\epsilon^2 \omega^2}}. \qquad (9\text{-}92b)$$

If the detector is coupled directly to a galvanometer; if the total impedance of detector, external circuit, and galvanometer is Z; and if $\mathbf{U} \equiv - \mathbf{H}_s l/Z$ is a galvanometer transmission constant; the peak value of the current is

$$I_m = \frac{V\omega^3 \mathbf{U}X}{\sqrt{(\omega_0^2 - \omega^2)^2 + 4\epsilon^2\omega^2}}. \tag{9-92c}$$

An electromagnetic seismograph equipped with a coil transducer is known as an inductive detector. If the coil is replaced by an iron armature separated by an air gap from a magnet provided with coils (telephone receiver), the seismograph becomes a reluctance detector or, more specifically, an unbalanced reluctance detector. A station seismometer of this kind has been developed by Benioff.[57] A more advantageous design is afforded by a balanced reluctance detector which is so arranged that the pull of a magnet on two armatures, or the pull of two magnets on one armature, is balanced. The Baldwin telephone receiver, most phonograph pickups, and the seismic detectors shown in Figs. 9–115a and 9–115b are examples of balanced receivers.

Although fundamentally the theory of these receivers is the same as that of the inductive detector as far as voltage output in proportion to the velocity of ground motion is concerned, a modification is introduced because of the dependence of the natural frequency on the magnetic field. The force of attraction of the magnet on the armature F' opposes the elastic-restoring force $F = \mathbf{c}d$ ($\mathbf{c}$ = spring constant, d = deflection). The magnetic force is a function of the field in the air gaps; the field, in turn, is equal to magnetomotive force over reluctance. If, in the schematic reluctance detector shown in Fig. 9-103, $\mathbf{M}$ is the m.m.f. of each magnet, the upper field for two gaps in series is $\mathbf{H}_1 = \mathbf{M}/2(a - d)$ and the lower $\mathbf{H}_2 = \mathbf{M}/2(a + d)$, where a is the normal gap and d the displacement from its position. If $\mathbf{S}$ is the section of the magnet, the force

FIG. 9-103. Scheme of balanced reluctance detector.

$$F' \equiv \frac{\mathbf{H}^2\mathbf{S}}{8\pi} = \frac{\mathbf{S}}{4\pi}(\mathbf{H}_1^2 - \mathbf{H}_2^2) = \frac{\mathbf{S}\mathbf{M}^2 \cdot ad}{4\pi(a^2 - d^2)} \tag{9-93a}$$

Neglecting in the denominator d^2 against a^2, the force $F' = \mathbf{S}\mathbf{M}^2 d/4\pi a^3$. Since, in the position of equilibrium, $\mathbf{c}d - F' = 0$, we have

[57] *Loc. cit.*

$d(c - SM^2/4\pi a^3) = 0$, from which it is seen that the second term represents a negative spring constant, also called negative stiffness:

$$c_m = \frac{SM^2}{} \qquad (9\text{-}93b)$$

The presence of the magnetic field reduces the elastic spring constant and, therefore, the natural frequency is

$$\omega_0 = \sqrt{\frac{c}{m} - \frac{SM^2}{4\pi m a^3}}. \qquad (9\text{-}93c)$$
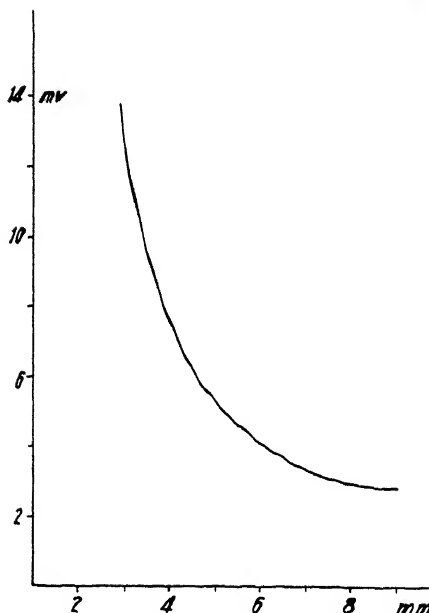
Fig. 9-104. Voltage output of experimental reluctance detector as a function of gap length.

When the armature or magnet moves, the flux $\Phi = SH$ changes, since the gap width and hence the reluctance increases or decreases, respectively. In a balanced detector the two armatures are so wound that opposite flux changes above and below produce an e.m.f. in the same direction. The flux through the upper two gaps (disregarding the deflection d) is SM/a. The same flux passes through the lower gaps, so that $\Phi = 2SM/a$. If N is the total number of turns on the two armatures, the induced e.m.f. $E \propto \dfrac{d\Phi}{dt} \propto \dfrac{d\Phi}{da}\dfrac{da}{dt}$ so that

$$E = -\frac{2NSM}{a^2} \quad dt$$

By substitution of the time derivative of the steady state term in eq. (9-89d),

$$E \qquad NSM \qquad \frac{\omega}{{}^2 \quad \omega^2)^2 + 4\epsilon^2\omega^2} \sin \qquad + \frac{\pi}{2} + \varphi \Big).$$

The voltage output increases, therefore, in inverse proportion to the square of the gap width which is verified by the experiment represented in Fig. 9-104. Analysis of this curve gives $94 \cdot a_{mm}^{-1.77}$ millivolts for the e.m.f. in this case. The deviation from the exponent -2 is probably caused by the fact that in eq. (9-94b) the variation of ω_0 with gap width

is not considered.   Fig. 9–105 shows the response curve of various commercial reluctance detectors and one inductive detector in terms of voltage developed on the first amplifier grids for ground motions of 1μ amplitude.
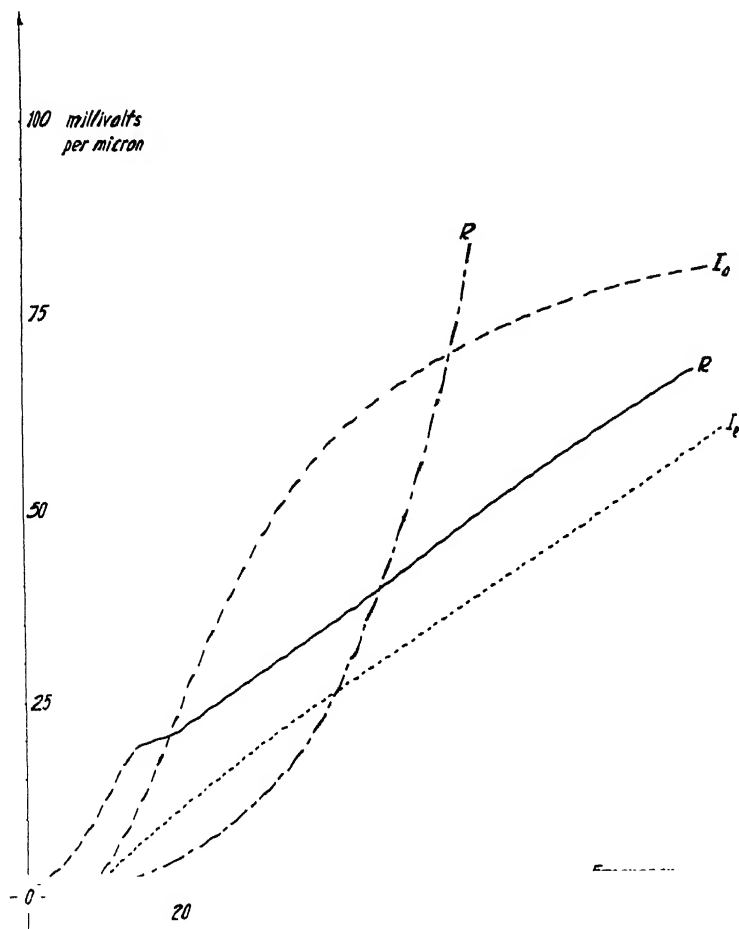
FIG. 9-105. Voltage at grid of first amplifier tube in millivolts per micron ground motion (through impedance matching transformer) of some commercial reflection detectors. R, reluctance detectors; I_o, inductive detector, oil damped; I_e inductive detector, electromagnetically damped.

The difference in the response curves N and S is due to the fact that S is adjusted to a low and N to a high natural frequency.

2. *Amplifier.*   A specific solution for the response of an amplifier is difficult to give because of the complexity and variety of the individual circuits employed.   As a rule, detector and galvanometer are coupled to

the amplifier by transformers which are inefficient in the range from 0 to 20 cycles. Therefore, the response of a seismograph amplifier rises with frequency in this range. Depending on interstage coupling, some amplifiers have an essentially straight response, others keep rising in the range up to a hundred cycles, and still others are peaked. Peaking may be accomplished by filters or by resonant circuits. In view of these differences a general and approximate solution only may be given. The response may be considered equivalent to one obtainable by assuming a definite damping factor and a natural frequency approximately equal to the peak frequency.

In the steady state the general equation for the amplitude of a force-coupled system is

$$y = \mathbf{V}_a \frac{1}{\sqrt{(\omega_a^2 - \omega_0^2)^2 + 4\epsilon_a^2 \omega^2}} \cdot Y \sin(\omega t - \varphi), \qquad (9\text{-}95)$$

where $\mathbf{V}_a$ is the equivalent magnification or gain of the amplifier, ω_a its equivalent natural frequency, ϵ_a the equivalent damping, y the output (current), and Y the peak value of the input voltage. As is shown below, the above expression fits the experimental results, although its simplified form is equivalent to disregarding the action of input and output devices.

3. *Galvanometer.* Three types of galvanometers (Fig. 9–106) may be employed in seismic recording channels: (a) oscillographs, (b) coil galvanometers, and (c) string galvanometers. All have in common a magnetic field and a current-carrying conductor in this field. In a string galvanometer only one conductor is present; its motion in respect to the lines of force is transverse. In coil galvanometers and oscillographs, two conductors are traversed by currents in opposite directions so that a rotational motion results.

In an oscillograph, assume a bifilar loop to be suspended in an air gap of the length L of a magnet with the field strength $\mathbf{H}_g$. The distance of the wires or ribbons is $2d$; its plane of rest is parallel with the lines of force; τ is the equivalent torsional coefficient of the suspension; K the moment of inertia of the wires inclusive of that of the mirror; and φ the deflection. Then the equation of motion for free oscillation is $K\ddot{\varphi} + \tau\varphi = 0$. For the deflection φ produced by a current I, the torque is $-2\mathbf{H}_g I L d \cos \varphi$. Since $2Ld$ is the area $\mathbf{S}$ of the loop between the pole pieces, the current torque is $-\mathbf{H}_g \mathbf{S} I \cos \varphi$. In the equilibrium position this is balanced by the elastic torque of the suspension $\tau\varphi$, so that for static deflections $\tau\varphi = \mathbf{H}\mathbf{S}I \cos \varphi$. For small angles $\cos \varphi \doteq 1$, so that the equilibrium of electrical, elastic, and inertia forces in the state of oscillation is given by

$$K\ddot{\varphi} + \tau\varphi = \mathbf{H}\mathbf{S}I. \qquad (9\text{-}96a)$$
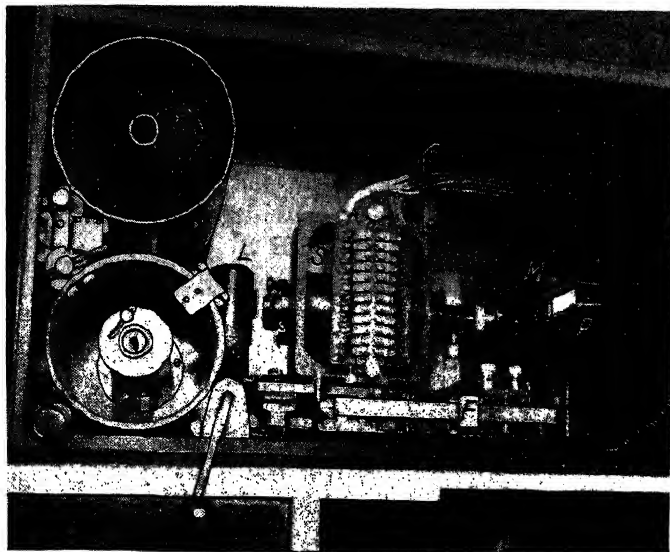
Cambridge Instrument Co.

FIG. 9-106a. Multiple string galvanometer in camera. L, Lamp; S, string harp; M, synchronous timer motor; P, prism; F, fork.
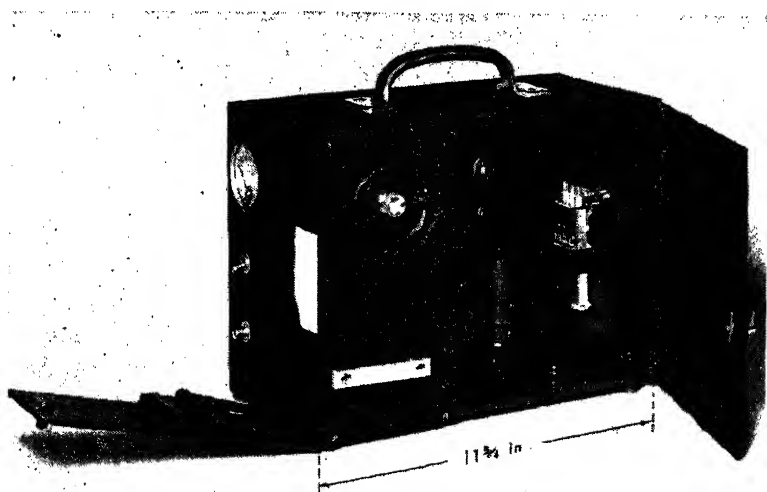
Heiland Research Corp.

FIG. 9-106b. Multiple-coil galvanometer (four channel) in camera. (A twelve-element camera is shown in the center of Fig. 9-78.)

This holds for undamped oscillations. Damping in galvanometers is composed of electromagnetic and viscosity (air or oil) damping. The former results from a counter e.m.f. set up in the coil by its motion when

it is connected to a load. This load may be the seismograph coil or the transformer secondary in the output stage of an amplifier. The counter e.m.f. $E_c = HS\dot{\varphi}$, where $\dot{\varphi}$ is the velocity of motion. The current resulting from it is, for pure D.C. resistances in the circuit, $I_c = \dfrac{\mathbf{H \cdot S}}{\mathbf{R + R'}} \cdot \dot{\varphi}$, where $\mathbf{R}$ is the resistance of the external circuit and $\mathbf{R'}$ the oscillograph resistance. Since the torque of a current, I, passing through the loop, is $\mathbf{H}SI$, the torque due to the counter e.m.f. is $\dfrac{\mathbf{H}^2\mathbf{S}^2}{\mathbf{R + R'}}\dot{\varphi}$, or $\mathbf{d}_e \cdot \dot{\varphi}$, with $\mathbf{d}_e$ as the electromagnetic damping factor. To this may be added a damping factor $\mathbf{d}_m$ resulting from mechanical damping (oil or the like), and their sum $\mathbf{d}_e + \mathbf{d}_m$ may be combined into a resultant galvanometer damping factor $\mathbf{d}_g$. Then eq. (9–96a) is $K\ddot{\varphi} + \mathbf{d}_g\dot{\varphi} + \tau\varphi = \mathbf{H}_gSI$. Dividing by K, and letting $\mathbf{d}_g/K = 2\epsilon_g$ (the damping constant of the galvanometer) and $\tau/K = \omega_g^2$ (the square of the natural frequency of the galvanometer), we get

$$\ddot{\varphi} + 2\epsilon_g \cdot \dot{\varphi} + \omega_g^2\varphi = \frac{\mathbf{H}_g\mathbf{S}}{K} I. \qquad (9\text{–}96b)$$

This may be converted into record amplitudes b by letting $b = 2\varphi D$, with D as focal length of the lens in front of the oscillograph mirror:

$$\ddot{b} + 2\epsilon_g\dot{b} + \omega_g^2 \cdot b = \frac{2D\mathbf{H}_g\mathbf{S}}{K} \cdot I. \qquad (9\text{–}96c)$$

For a coil galvanometer the right side of the last equation is multiplied by N_g, the number of turns in the galvanometer coil, so that

$$\ddot{b} + 2\epsilon_g \cdot \dot{b} + \omega_g^2 \cdot b = \frac{2D\mathbf{H}_g \cdot \mathbf{S} \cdot N_g}{K} \cdot I. \qquad (9\text{–}96d)$$

In a string galvanometer a wire or "harp" of wires of the free length l is suspended between pole pieces of the length L in a field of the strength $\mathbf{H}_g$. The natural frequency of a string (fundamental) is given by

$$\omega_g = \frac{\pi}{l} \sqrt{\frac{P}{a\delta}},$$

where a is its sectional area, P the tension, and δ the density. The free oscillation with combined air and electromagnetic damping and with m as mass of the string is then

$$\ddot{b} + 2\epsilon_g \cdot \dot{b} + \omega_g^2 b = 0,$$

where b is the deflection corresponding to a current I as viewed under a microscope of the magnification M, so that $b = \mathbf{H}LIM$. Hence, the gal-

vanometer equation corresponding to (9–96d) is

$$\ddot{b} + 2\epsilon_g \dot{b} + \omega_g^2 b = \frac{MHL}{m} I.$$ (9–96e)

Eqs. (9–96c, d, and e) may be written in the same general form by denoting the factor of I on the right side as galvanometric magnification factor (static or D.C. sensitivity) V_g, divided by K:

$$\ddot{b} + 2\epsilon_g \dot{b} + \omega_g^2 b = \frac{V_g}{K} \cdot I.$$ (9–97a)

The solution of this equation for a current of the peak value I_m and the frequency ω is

$$b = Ce^{-\epsilon_g t} \sin (\omega_{dg} t + \psi_g) + \frac{I_m V_g}{K} \frac{1}{\sqrt{(\omega_g^2 - \omega^2)^2 + 4\epsilon_g^2 \omega^2}} \sin (\omega t + \varphi_g),$$

(9–97b)

where ω_{dg} is the damped frequency of the galvanometer, ψ_g the initial phase angle, and φ_g the phase shift between galvanometer record and impressed current. Galvanometer response curves for steady state conditions (second term in eq. [9–97b]) are shown in Fig. 9–107 for various damping rates. It is noted that these curves show the opposite behavior compared with the response of a seismograph. While the dynamic magnification of the latter increases to the static level for tuning factors greater than 1, the dynamic response of the former decreases for tuning factors greater than 1 below the (D.C.) static sensitivity. In a seismograph response curve, the resonance frequencies move toward greater tuning factors with increased damping. In a galvanometer response curve they move toward smaller tuning factors. The resonance frequency of a galvanometer is $\omega_{rg} = \sqrt{\omega_g^2 - 2\epsilon_g^2}$.

Fig. 9–108 shows response curves of a number of commercial seismograph galvanometers.

4. *Over-all response.* To obtain the over-all response of a recording channel, that is, the galvanometer deflection for a ground impulse of given amplitude and frequency, the dynamic responses of detector, amplifier, and galvanometer are combined. A similar problem arises in station seismology. Various authors have discussed the reaction of a galvanometer coupled directly to a seismograph. Two extreme cases exist: (1) the seismograph mass is large and the galvanometer mass small, so that the seismograph is essentially the driving and the galvanometer the driven unit, with no energy going back into the seismograph from the galvanometer; (2) seismograph and galvanometer masses are comparable, so that they

represent a coupled system with comparable merits of its members.   The latter leads to fairly complex equations, discussed by Wenner[58] and Schmerwitz.[59]

The first case, involving an energy transfer in one direction only, has been calculated by Galitzin.   When an amplifier representing a unilateral impedance is employed between seismograph and galvanometer, Galitzin's
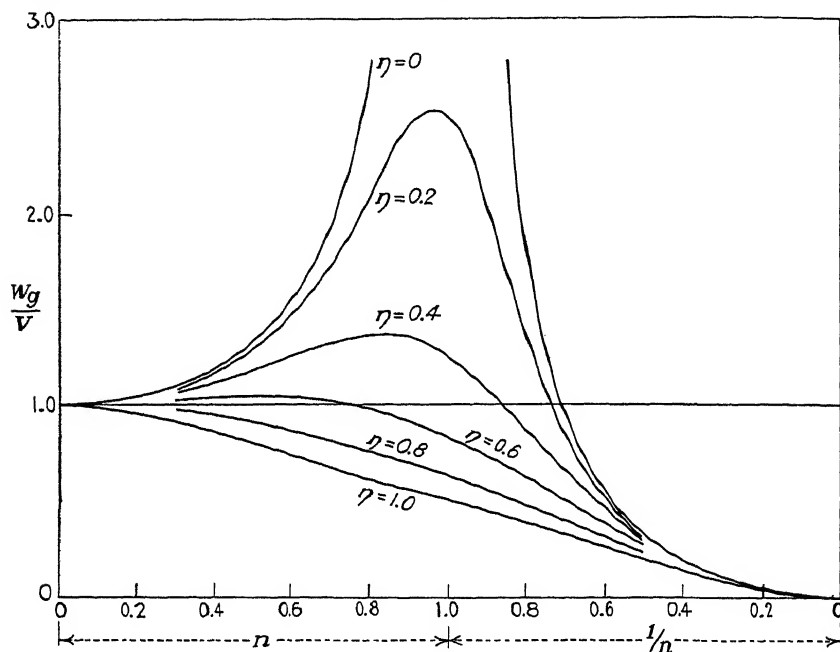
FIG. 9-107. Frequency response of galvanometer, as a function of tuning factor and relative damping.

solution is applicable, provided that the amplifier action is equivalent to that of a system with simple static magnification.

Combining eq. (9-97a) with eq. (9-92c) and lumping all constants, so that $V_g \cdot V \cdot U / K = C$, we obtain

$$\ddot{b} + 2\epsilon_g \dot{b} + \omega_g^2 b = \frac{C\omega^3 X}{\sqrt{(\omega_0^2 - \omega^2)^2 + 4\epsilon^2 \omega^2}} \sin(\omega t \pm 90° + \varphi),$$

of which the *steady state* solution is

$$b = \frac{C}{\sqrt{(\omega_g^2 - \omega^2)^2 + 4\epsilon_g^2 \omega^2}} \cdot \frac{\omega^2}{\sqrt{(\omega_0^2 - \omega^2)^2 + 4\epsilon^2 \omega^2}} \cdot X\omega \sin(\omega t \pm 90° + \varphi + \varphi_g).$$

$$(9\text{-}98a)$$

[58] F. Wenner, *loc. cit.*

[59] G. Schmerwitz, Zeit. Geophys., **12**(5/6), 206–220 (1936).
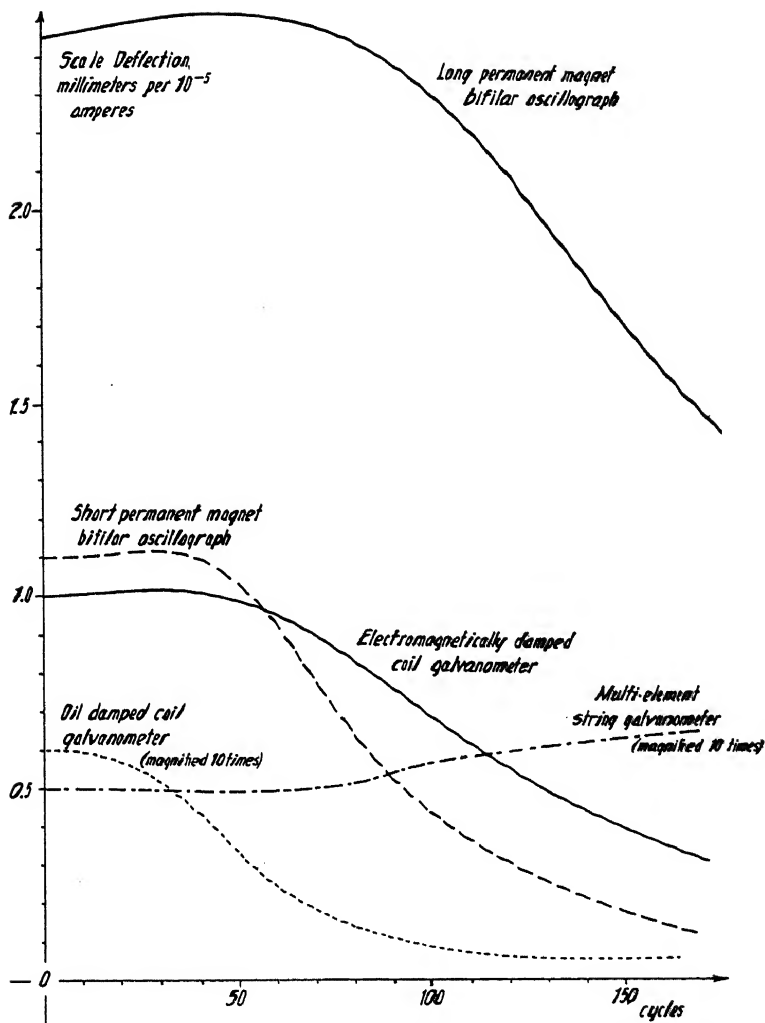
Fig. 9-108. Response of various commercial reflection galvanometers.

Hence, the over-all dynamic magnification $\mathbf{W}'_r$ of a *galvanometer for ground motions of the peak amplitude* X, when coupled directly to a seismometer, may be written in terms of their respective dynamic magnifications:

$$\mathbf{W}'_r = \mathbf{W}_g \cdot \mathbf{W}_d \cdot \frac{\omega \mathbf{U}}{\gamma^2}. \tag{9-98b}$$

Expressions for special cases of over-all magnifications are of interest. When both seismometer and galvanometer are critically damped, the

damped frequency factors (in the denominator of eq. [9–98a]) are

$$(f_g) = \frac{1}{\omega_g^2 + \omega^2} \quad \text{and} \quad (f_d) = \frac{1}{\omega_0^2 + \omega^2}$$

or

$$(f_g) = \frac{1}{\omega_g^2(1 + n_g^2)} \quad \text{and} \quad (f_d) = \frac{1}{\omega_0^2(1 + n_0^2)},$$

where n_g is the tuning factor ($= \omega/\omega_g$) for the galvanometer and $n_0 (= \omega/\omega_0)$ the tuning factor for the seismometer. Therefore, eq. (9–98a) can be greatly simplified by making the two tuning factors equal, that is, making the natural frequency of the galvanometer equal to that of the seismograph. Then the product of the frequency factors (f_g) and (f_d), multiplied by ω^3 in the numerator, is $n^3/\omega_0(1 + n^2)^2$, so that the over-all magnification is

$$\mathbf{W}_r' = \frac{C}{\omega_0} \cdot \frac{n^3}{(1 + n^2)^2}. \tag{9–98c}$$

The function $n^3/(1 + n^2)^2$, given in eq. (9–98c), is shown in Fig. 9–109. It has its maximum at $1/n = 0.577$. When galvanometer and seismograph frequencies are equal and both are critically damped, the response is peaked at a frequency *1.73 times* the natural frequency. Galitzin gives an instructive example showing that one seismometer with a period of 12 seconds was peaked at a period of around 6.9 seconds, while another with a period of 25 seconds was peaked at 14.5 when connected to galvanometers of matched natural frequencies. For 0.7 critical damping the damped frequency factors are

$$(f_g) = \frac{1}{\omega_g^2\sqrt{1 + n^4}} \quad \text{and} \quad (f_d) = \frac{1}{\omega_0^2\sqrt{1 + n^4}}$$

so that for equal frequencies of seismometer and galvanometer the over-all dynamic response is given by

$$\mathbf{W}_r' = \frac{C}{\omega_0} \frac{n^3}{(1 + n^4)}. \tag{9–98d}$$

This curve is shown in Fig. 9–109. The over-all magnification is greater (less damping), the curve peak has moved closer to the tuning factor of 1. The maximum is at $1/n = 0.77$, that is, for a detector and galvanometer which have equal natural frequencies and are 0.7 critically damped, the over-all peak occurs at *1.3 times* their natural frequency. Conversely, a linear response may be produced by making the galvanometer frequency a multiple of the seismometer frequency. Then, for 0.7 critical damping,

$\sqrt{1 + n_0^4}$. If the galvanometer frequency is ten times higher than the seismometer frequency, the product of the frequency factors $(f_g) \cdot (f_d) = 1/\omega_0^4 \sqrt{(10^4 + n_0^4)(1 + n_0^4)}$, which
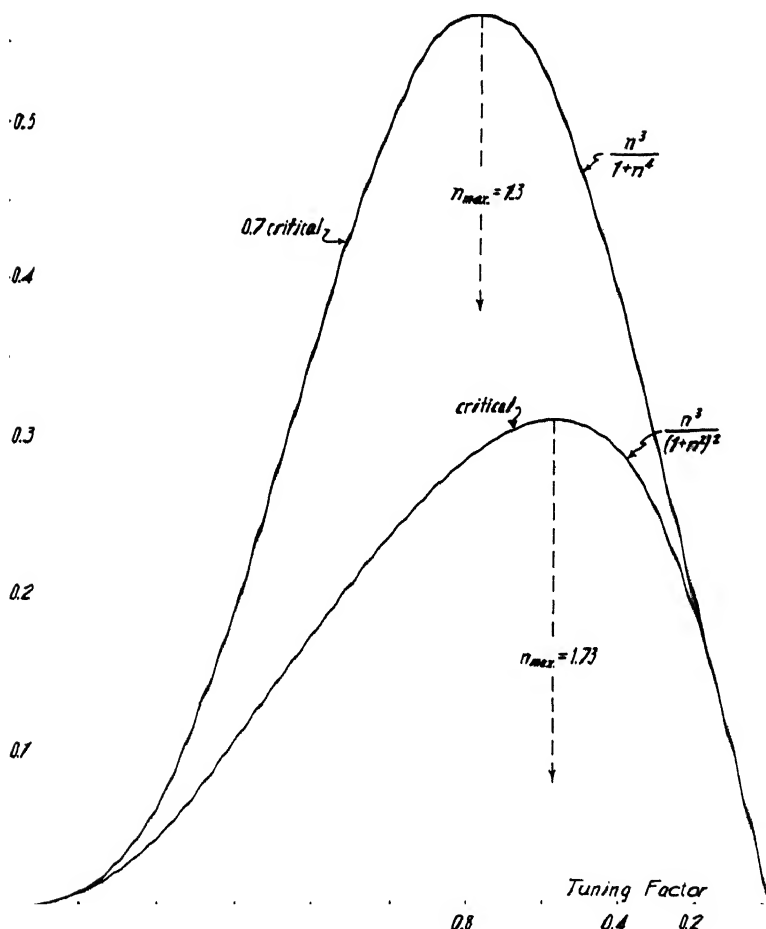
FIG. 9-109. Dynamic response of seismograph and galvanometer of equal natural frequency and equal damping.

is seen to indicate an approximately linear increase of dynamic response with frequency (see Fig. 9-110). In such a case it is comparatively easy to superimpose amplifier-filter characteristics upon the seismometer-galvanometer response and to peak at any desired frequency. The over-all

response $\mathbf{W}_r$ of detector, amplifier, and galvanometer is (from eqs. [9-92b], [9-95], and [9-98a])

$$_d \cdot \mathbf{W}_a \cdot \mathbf{T} \cdot_c \qquad\qquad (9\text{-}99)$$

where $\mathbf{V}_g(f_g)/K = \mathbf{W}_g$.

The resultant dynamic magnification of the entire channel is therefore proportional to the *product of all dynamic magnifications* and to a trans-
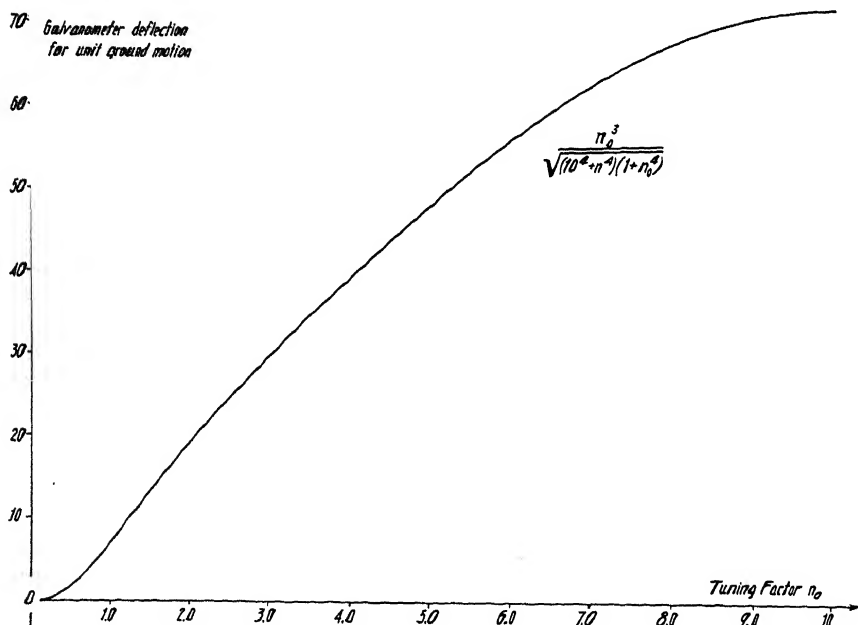
Fig. 9-110. Response of 0.7 critically damped seismograph and galvanometer, if the natural undamped galvanometer frequency is ten times that of the seismograph.

mission constant. Fig. 9-111 shows the characteristics of a peaked amplifier superimposed on the detector-galvanometer curve of Fig. 9-110. The over-all response is calculated for an amplifier peaked at three times the natural frequency of the detector, with an equivalent damping rate of 0.316, so that its damped frequency factor $(f_a) = 1/$ ˆ

Therefore, $\quad = \omega/_a \quad = 3\omega_0$, $\eta_a = 0.316$, and $n_a = n_0/3$, $(f_a) = 1/\omega_0^2\sqrt{81 - 14.4n_0^2 + }$; When multiplied by the factor represented in Fig. 9-110, this gives the theoretical curve shown in Fig. 9-111, which is seen to agree well with the results of test block experiments.

E. Review of Prospecting Seismographs

Prospecting seismographs may be divided into *mechanical* and *electrical* types. The latter, in turn, fall into three groups: electromagnetic, capacitive, and pressure detectors, as was discussed previously in connection with the description of reflection instruments. A reflection detector may be used for refraction work, but not vice versa. Almost all such detectors record the vertical component of the ground motion.
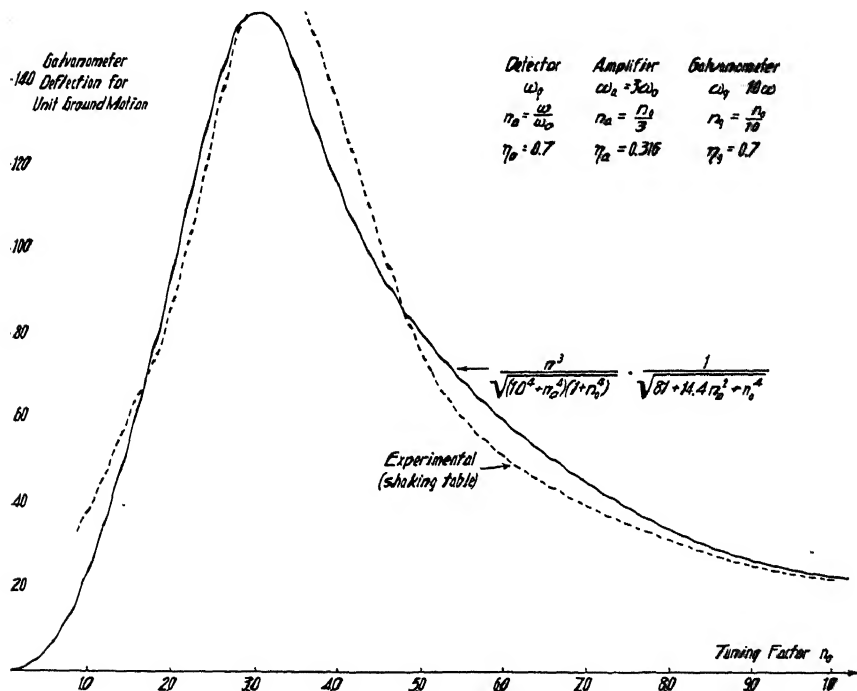
Fig. 9-111. Comparison of calculated and experimental response of detector, amplifier, and galvanometer for given tuning factors and damping ratios.

1. *Mechanical seismographs.* Much of the first refraction work was done with the Mintrop mechanical seismograph[60] (see Fig. 9-112). Pendulum and recorder are separate as in most other mechanical seismographs. The former is a vertical-component instrument, consisting of a spherical mass attached to a leaf spring. The mass carries a long, cone-shaped extension with a thin spring at its end which rubs against a spindle carrying a mirror. The movement of the lever is damped electromagnetically. In the recorder the unexposed paper is housed below and fed through a

[60] C. A. Heiland, Eng. and Min. J., **121**(2), Fig. 18 (Jan. 9, 1926).

number of rollers past a cylindrical lens and a time-marking mechanism. This consists of a pendulum which interrupts a light beam at periodic intervals and projects dashes every 1/10 second on the paper. The paper is started by pressing an idler against one of the rollers driven by the spring motor. By the above combination of mechanical and optical magnification, high over-all magnification is obtained. If V is
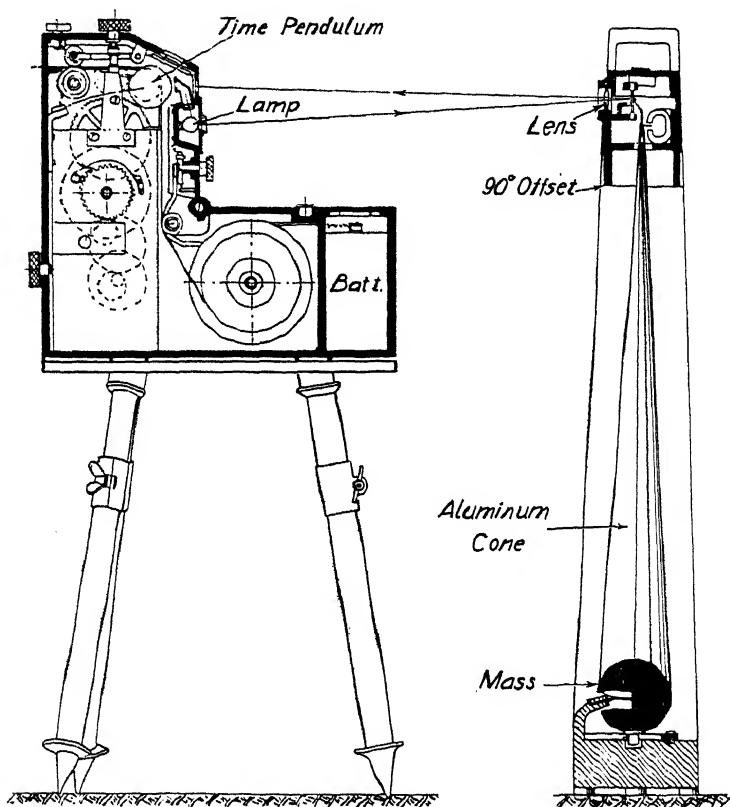
Fig. 9-112. Mintrop mechanical seismograph and recorder.

the geometric magnification of the lever, r the radius of the mirror spindle, and D the focal length of the lens in front of the seismograph mirror, the over-all magnification is $2DV/r$. In this manner magnifications from 15,000 times and up are readily obtained. At a receiving station seismograph and camera are generally set up in a small tent. These are supplemented by a mirror device on a tripod next to the seismograph for the recording of the shot instant transmitted by radio.

Another type of mechanical seismograph that was widely used for refrac-

tion shooting is the Schweydar-Askania two-component seismograph. Descriptions and diagrams of it are given by Edge and Laby.[61] The construction of the vertical seismograph is similar in regard to suspension, mass, and lever, to the Mintrop seismograph. The mass is suspended from a horizontal spring, whereas the horizontal seismograph mass is suspended on a vertical spring. The combined instrument is so set up that the plane of this spring is at right angles to the firing line. In the earlier models a bow-string attachment transferred the movement of the end of the lever to a mirror spindle. The illustrations in Edge and Laby give the details of this arrangement. In later models, a string was tied to the end of the lever, wrapped around the mirror spindle, and kept taut by a spring.

The natural frequency of both seismometers is about 15 cycles. Damping is accomplished by a vane attached near the end of the lever and immersed in an oil chamber. In the models developed subsequently, the masses are cylindrical and the magnifying lever is somewhat shorter than in the first model. Provision is made for attaching a mirror device to the head of the instrument so that the shot instant may be recorded on the same strip as the two components.

Several other mechanical prospecting seismographs were constructed, in the period from 1924 to 1929, by Ricker, Truman, Taylor, and others.

2. *Electrical seismographs.* (a) *Electromagnetic seismographs.* A modification of the Schweydar mechanical seismograph was used extensively at one time as an inductive seismograph. A coil was attached to the end of the magnifying lever. This was free to move in the field of an electromagnet supplied with current from a storage battery. The period of this seismograph was about 0.03 second. It was used without intermediate amplifier with a Zeiss loop galvanometer. Fig. 9-113a shows a dual-coil variant of the original instrument. In the Cambridge

FIG. 9-113a. Dual-coil induction seismograph.

Instrument Company's electromagnetic refraction seismograph, the magnifying lever makes an angle with the horizontal. A string is fastened to its end. This in turn is wound around the shaft of a galvanometer acting as a generator. The seismograph is used in connection with a Cambridge string galvanometer.

---

[61] *Op. cit.*, figs. 158–160 and 255–257.

The Imperial Geophysical Experimental Survey used an inductive seismograph in which the mass consisted of an electromagnet suspended from a diaphragm. The pickup coil was stationary between the poles of this electromagnet (see Fig. 259 of Edge and Laby) and was connected to a Cambridge string galvanometer. Illustrations and diagrams of a multiple-string galvanometer used for refraction shooting by the I.E.G.S. are found in Figs. 153, 154, 156, and 253 of Edge and Laby's book.

Fig. 9-113b illustrates an inductive seismometer with single coil moving in the field of a permanent (pot-type) magnet. Fig. 9-114 represents a portable four-channel refraction seismic apparatus for shallow depth problems in which inductive detectors with electromagnetic damping are employed.
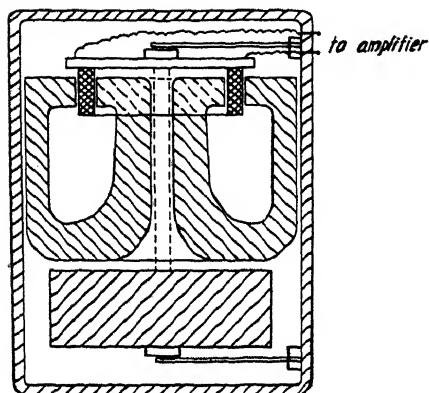
FIG. 9-113b. Inductive seismometer.

Reluctance electromagnetic seismographs have been developed most extensively for reflection shooting. Two balanced-armature types are shown in Fig. 9-115. They are very efficient, well adapted to intermediate and high natural frequencies, and may be used for both refraction and reflection work.

(b) *Capacitive seismographs.* The condenser (or radio) seismograph has been applied in various countries for refraction work, and it is used in this country for reflection work by one or two companies. Various "radio" seismographs have been described by Haeno[62] and Hée.[63] A condenser seismograph, suitable for application in reflection work, is shown diagrammatically in Fig. 9-116. The oscillatory circuit and tube are closed in the detector box, with the seismometer mass acting as the movable plate of a variable condenser. A quadruple cable supplying A and B voltage goes from the detector to a three-stage-resistance coupled amplifier, which is coupled through a transformer to an oscillograph or string galvanometer.

A detailed discussion of the condenser type detectors has been given by Irland.[64] Various mechanical seismometers of the horizontal and vertical type were equipped with a capacitive transducer changing the phase of two coupled oscillators.[65] Simultaneous shaking table and instrument

[62] Japan. J. Astron. and Geophys., **8(2)**, 39–50 (1931).

[63] Union Geophys. Trav. Sci. A(**9**), 1933.

[64] G. A. Irland, *A Study of Some Seismometers*, U. S. Bur. Mines Tech. Paper No. 556 (1934).

[65] U. S. Bur. Mines Tech. Paper No. 518 (1932).
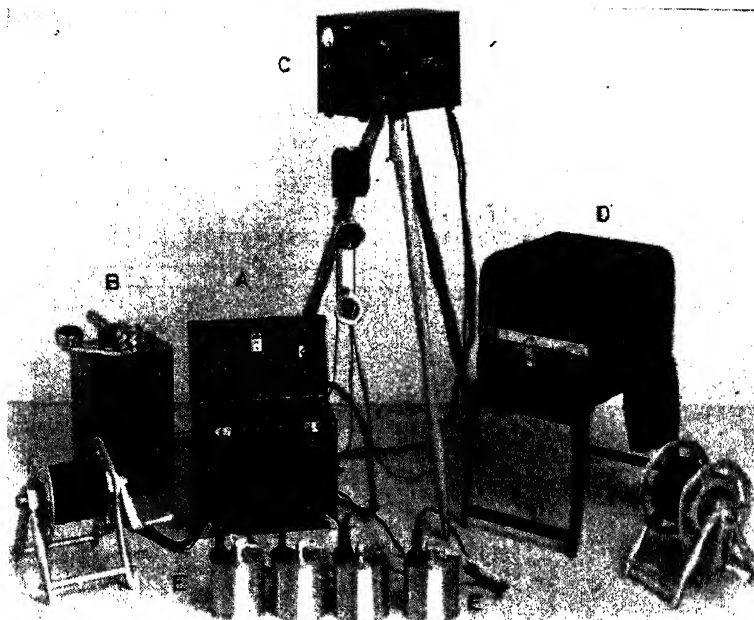
Heiland Research Corp.

FIG. 9-114. Portable seismic four-channel apparatus. A, Four-channel amplifier; B, blaster; C, camera with timer, dry-cell operated; D, daylight developing tank; E, detectors.

(a) (b)
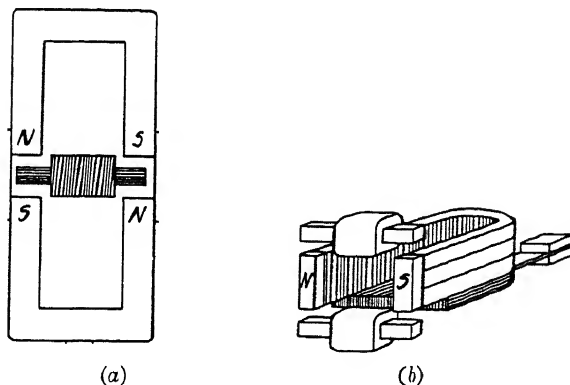
FIG. 9-115. Reluctance detectors.

records showed that a capacitive detector of proper frequency and damping adjustment records sustained ground motion and transients accurately and in proportion to the ground displacement. In the course of the experi-
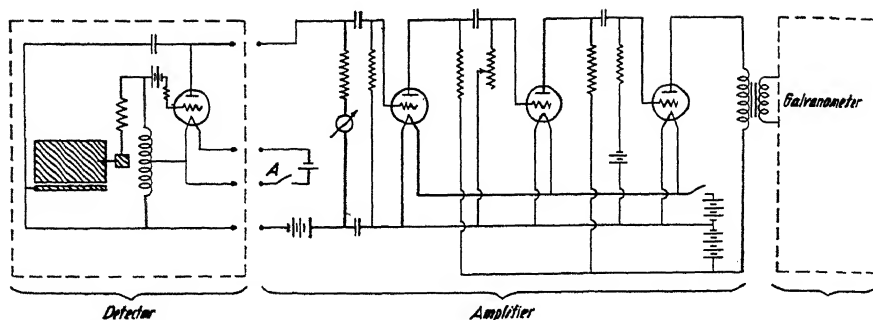
FIG. 9-116. Condenser seismograph.

(a) (b)

(c)
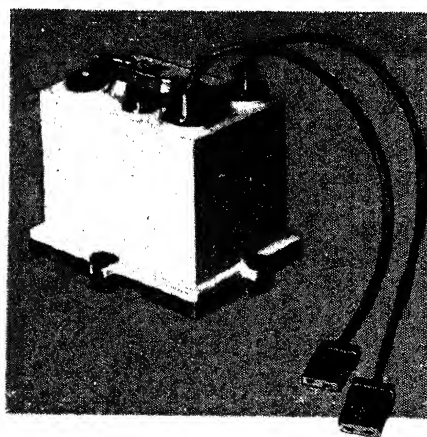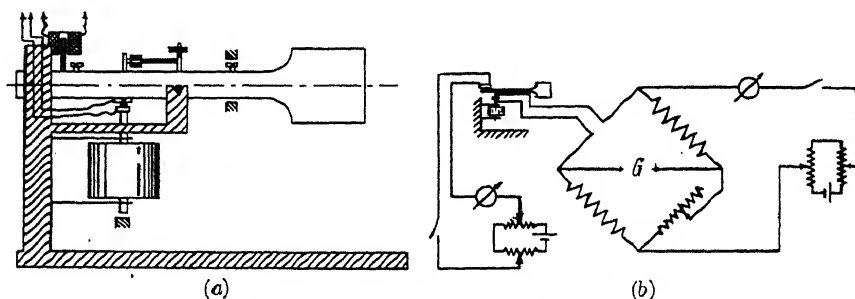
FIG. 9-117. Ambronn accelerometer-refraction sesimograph (partly after Siñeriz).

ments a compensated-spring–type vertical seismometer was developed, which resembles in construction the La Coste[66] instrument.

---

[66] L. J. B. La Coste, Physics, **5**, 178 (1934); and Seis. Soc. Amer. Bull., **25(2)**, 176 (1935).

(c) *Pressure seismographs.* Modifications of the carbon microphone were employed in the days of refraction shooting and are still in use in some civil engineering applications. They have definite limitations because of high noise level and packing. Their use for reflection work has been virtually abandoned. The I.G.E.S. employed a Western Electric mining detector of the carbon type for shallow refraction applications[67] in connection with a string galvanometer recorder. They further used a hot wire seismograph, consisting of a geophone in which the air displaced by the movement of a diaphragm of fairly large diameter is forced through a small orifice. In this orifice a platinum wire heated by a battery is located and is cooled by the air flowing past it. The wire grid is arranged in one arm of a Wheatstone bridge, the indicating device (string galvanometer) is in the center arm of the bridge, the resistance of the wire being varied in proportion to the velocity of the motion of the air.[68]

The Ambronn accelerometer which was used extensively in the earlier refraction work, notably by Siñeriz in Spain (see Fig. 9–117a), is likewise based on variations of a resistance due to ground vibrations. The mass is suspended from two springs; two contact points are arranged on the mass and on a beam balanced on a knife edge. The position of the beam and, therefore, the contact pressure may be controlled from the recording truck by varying the current through a solenoid surrounding an armature on the beam. The contacts are arranged in a Wheatstone bridge, as shown in Fig. 9–117b. Individual string galvanometers of high sensitivity are used at G to record the variations in acceleration. The critical pressure on the contact is adjusted on a control panel in the recording truck by the circuit shown on the left side of Fig. 9–117b. A quadruple cable is required from the truck to each detector.

FIG. 9–118. Crystal detector with preamplifier.

Piezoelectric or crystal detectors have been used for both refraction and reflection applications. A crystal detector with preamplifier is illustrated in Fig. 9–118. A piezoelectric receiver and equipment suitable for refraction and reflection applications was described by Ambronn.[69]

---

[67] See p. 212 of Edge and Laby's report.
[68] See Figs. 152, 260, and 261 in Edge and Laby.
[69] World Petrol. Congr. B.I., 165–168 (London, 1934).

F. Photographic Recording; Time Marking

In station seismographs, most recording is done mechanically by pens writing white lines on blackened paper fastened to a drum. The drum rotates and is shifted sideways by a thread cut on the drum shaft. Time marks are recorded by means of the pens being lifted or shifted by an electromagnet actuated from a contact chronometer. In light-weight station seismometers, such as the Wood-Anderson seismograph, and in galvanometric recording instruments, such as the Benioff and Wenner seismometers, records are taken photographically on sensitized paper. Time marks are provided by interrupting the light beam with a shutter actuated from an electromagnet or by deflecting the trace for a short interval by a mirror or prism mounted on a relay connected to the contact chronometer. Both mechanical and photographic recording is used in vibrographs, depending on the sensitivity of the instrument. In some types the record is made on celluloid strips by a pointed needle and is inspected under a microscope. Disk recording has not been applied in seismology. In high-speed recorders time marks are projected by mechanically started vibrating reeds with shutters, or by electrically sustained indicators (galvanometers, reeds, oscillographs) driven from tuning forks or V.T. oscillators.

In virtually all prospecting seismographs, records are taken photographically on rapidly moving paper varying in width from 2 to 6 inches. To obtain good quality of reproduction, attention must be paid in the field to the proper concentration, temperature, and freshness of the developing and fixing solutions.[70] The speed at which the paper travels is about 3 to 10 centimeters per second in refraction recording and 30 to 40 centimeters per second in reflection recording. Provision is usually made for simultaneous visual observation and photographic recording. This may be done by splitting the reflected light beam, by providing separate incident and reflected beams for the visual and photographic system, or by viewing the light spots from the rear of the camera through paper. Even paper speed increases the accuracy of record evaluation; hence, the recorder drive is usually equipped with a fairly elaborate governor.

Time marking may be accomplished in various ways. In recorders used with mechanical seismographs, a small pendulum provided with a shutter arrangement is set in motion at the instant of firing. In reflection cameras, a reed of higher frequency (50 cycles) electrically sustained from a tuning fork or vacuum tube oscillator may be used. This has a shutter arrangement to project dashes on the paper (if the reed is mounted close to the paper), or to project time lines across its entire width (by reflecting light

---

[70] F. A. Tompkins, Geophysics, **1**(1), 107–114 (Jan., 1936).

from a mirror attached to the reed to a stationary mirror and thence to the cylindrical lens). Instead of a reed a regular galvanometer may be used to project a time wave on the record. This is the method used for calibrating time lines with a standard fork (see below). Another convenient way of projecting time lines across a record of almost any width is to mount a neon tube close to the paper and to connect it to an electrically driven tuning fork through a high tension step-up transformer. An arrangement now in very common use is a synchronous motor driven by a tuning fork. To its shaft is attached a spoked wheel for shadow recording, or a slotted drum for black on white recording. This gives the possibility of making every fifth and tenth time line heavier, which simplifies evaluation of the record. Finally, a tuning fork alone may be used to project time lines across the paper by attaching shutters to its tines and projecting a light beam through them onto the cylindrical lens.

In all timing devices, reeds and forks must be compensated for temperature or be made of metals of low temperature coefficient of elasticity. Timing devices in field recorders should be checked once a month against a standard tuning fork which should be so arranged that it may be readily connected to one of the regular galvanometers in the recording camera.

G. CALIBRATION OF SEISMOGRAPHS

In station seismology, the calibration of instruments is a comparatively simple matter and involves determinations of natural period, friction, and damping. Natural frequency and friction may be obtained from free vibration records with damping disconnected; damping is determined from the ratio of consecutive amplitudes with damping mechanism connected. The static magnification V of a seismograph may be obtained by adding a known mass m, and measuring the deflection a of the pen. Then $V = am_0\omega_0^2/mg$, where m_0 is the mass and ω_0 the natural frequency of the seismograph. For electrically recording instruments, determination of galvanometer characteristics and transmission constant is necessary in addition to the calibration of the seismometer. Galitzin[71] has described this procedure in detail.

The calibration of the mechanical prospecting seismograph proceeds in essentially the same manner as calibration of station seismometers. Natural frequency, friction, damping, and magnification are determined as discussed above. Calibration of electrical prospecting seismographs is rendered more elaborate because it has to extend not merely to one, but to as many units as there are recording channels. Further, requirements

[71] B. Galitzin, *Vorlesungen ueber Seismometrie*, Chaps. 6 and 7, Teubner, (Leipzig, 1914). See also F. W. Sohon, *Introduction to Theoretical Seismology*, Wiley (1932).

for reflection seismographs are more rigorous than for refraction seismographs because not merely the first but later impulses have to be recorded as faithfully as the particular geologic situation requires and must be balanced in regard to both amplitude and phase. The following section deals chiefly with the calibration of electrical reflection seismographs, that is, calibration of pick-ups, amplifiers, and galvanometers and determination of over-all response.

1. *Detectors.* Both mechanical and electrical characteristics must be determined. The former include: (a) natural frequency, (b) deflection (geometric magnification), (c) friction, and (d) damping.

The natural frequency of the detector may be determined in a number of ways. A *mirror device*[72] may be attached to the mass of the seismograph, and its free vibration may be recorded on a laboratory camera provided with a timing mechanism. For this test damping must be eliminated. If electromagnetic damping is applied it should be disconnected. From the record, natural frequency and friction may be determined as previously described. The natural frequency may also be obtained from the *resonance frequency* by (a) driving the seismograph with an electrical oscillator, or (b) by observing its mechanical or undamped electrical response on a shaking table.

Mechanical deflection tests make it possible to determine the static sensitivity and thus the static magnification of detectors. A small mass is placed on the seismograph mass. Its deflection is observed as stated above, or the deflection of the magnification lever is observed by a microscope or mirror device.

For the determination of damping, overshoot records are best suited, since the detectors are usually critically or near-critically damped. Damping may be determined also from the shape of the dynamic response curve of a detector taken on a shaking table. Possibly simpler is the procedure of driving the detector from a beat oscillator with constant input at varying frequencies. This will result in a dynamic response curve of a force-driven device, from which the damping rate may be determined. Damping tests should be made for various oils and various temperatures unless an electromagnetically damped detector is used.

Virtually the only important electrical characteristic of a detector is its output for a given ground amplitude and frequency. It is best defined in units of open-circuit volts per micron ground motion (see Fig. 9–105). Since it depends on the impedance of generator and load, detectors of different impedances can be compared only by using a matching transformer whose secondary may be coupled directly to a vacuum tube volt-

---

[72] For the details of these and other seismograph calibration methods see Heiland, *op. cit.*, 434–454 (1934).

meter grid to give open circuit voltage. With a shaking table, the variation of voltage output with ground frequency may be obtained; the amplitude of the table may be measured by various means described in the literature on shaking tables.[73]

A quantity related to the voltage output is the electrical sensitivity of a detector when it is used as a motor. This is the mechanical deflection for a given current input and is thus proportional to Galitzin's transmission constant, inasmuch as it includes the circuit characteristics and the strength of the magnetic field in the detector. However, this is a test that will give only qualitative comparisons of detectors with similar circuit characteristics. Being a static determination, it is inferior to a shaking-table test.

2. *Amplifiers.* In radio practice it is customary to rate amplifiers in terms of decibel gain. A test to determine gain can also be applied to seismograph amplifiers by using a fixed voltage input and determining the output on a vacuum tube voltmeter. Output should be measured in the plate circuit of the last tube, inasmuch as with most galvanometers a stepdown transformer is used. The gain so measured is useful for relative comparisons only; for seismograph amplifiers it is more convenient to measure gain together with galvanometer response as described below.

3. *Galvanometers.* Quantities characterizing the action of seismic galvanometers are natural frequency and damping and static (D.C.) sensitivity. Together they determine the dynamic response. The natural frequency of the galvanometer may be determined from free oscillations by plucking it or giving it an electrical impulse after removing or disconnecting the damping. This test may be made in the regular camera. Possibly simpler is a determination of the resonance frequency by using a beat frequency oscillator. Damping is obtained from overshoot records or from a dynamic response curve. The static sensitivity of a galvanometer is determined by observing the scale deflection for a given current, visually or photographically. If an even rating of galvanometers of different construction is desired, their natural frequency, impedance, and optical lever must also be considered. The D.C. test of a galvanometer will generally show whether the unit is performing properly and whether friction is present without requiring a separate friction test.

4. *Combined amplifier and galvanometer response.* This test has several advantages over separate amplifier and galvanometer tests: (a) the resultant response can be obtained more nearly quantitatively and in terms more closely related to the practical application (galvanometer deflection for a given voltage input of a given frequency); (b) tests for quiet operation

---

[73] Heiland, *op. cit.*, 454 (1934), (bibliography on shaking tables).

are readily made; (c) tests can be made in the recording truck to determine whether coupling with timing or shot instance transmission circuits, and the like, is present.

The combined amplifier and galvanometer response is measured in terms of galvanometer deflection for constant signal input. By varying the frequency of the signal, the combined amplifier and galvanometer dynamic response is obtained. This test should be made for all possible filter positions.

5. *Over-all response.* The over-all response of an entire seismic channel is measured by placing the detector on a shaking table, connecting it to its amplifier and galvanometer, and measuring the galvanometer deflection for a given ground amplitude at varying frequencies. Measurements are made for the various filter positions and for various settings of gain controls in amplifier and galvanometers to determine effects of automatic volume control devices, if these are incorporated.

6. *Various other tests of seismic equipment* include tests of the timing system by standard forks, parallax tests to determine time lag between shot instant record and galvanometric record, and phase tests. When all component parts of a recording channel have been balanced properly in respect to their mechanical and electrical characteristics, phase differences should not occur. Whether and to what extent they exist may be determined by a phase shot, that is, a reflection shot taken with all receivers set together closely at the same location. Fig. 9-119 shows a phase shot made with a 12-channel apparatus.
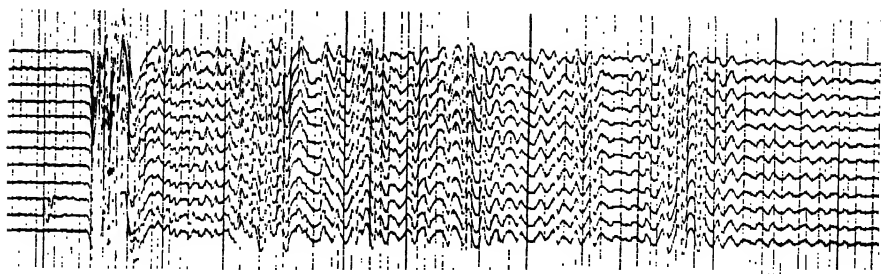
Fig. 9-119. Twelve-element alignment record.

I O

ELECTRICAL METHODS

I. INTRODUCTION

A. Fundamentals

ELECTRICAL PROSPECTING in the most general sense may be defined as prospecting by electricity for mineral deposits and geologic structures. Contrary to geophysical methods previously discussed, each of which makes use essentially of one field of force—gravitational, magnetic, or elastic—there is much greater variety in the type of electrical fields and in methods of observation employed in electrical prospecting. First, an ore body may act as a battery and furnish its own electrical field; second, the ground under test may be energized by extraneous fields and the reaction of subsurface conductors to such fields may be measured. Both direct current and alternating current are used; the latter gives not only greater sensitivity but additional physical quantities, which helps in the interpretation of the results. Direct current can be introduced into the ground only by galvanic contact, but alternating current can be applied by both contact and inductive coupling. The resulting fields are measured by instruments making contact with the ground by electrodes, or by employing inductive coupling with reception frames. Thus, in reference to observation methods, electrical methods may be divided into *potential* and *electromagnetic* methods.

Electrical exploration uses a wide range of frequencies. Those from 5 to about 100 will be referred to herein as low frequencies, from about 200 to 1000 cycles as intermediate, from 10 to 80 kilocycles as high, and from about 100 kilocycles to several megacycles as radio frequencies. Low frequencies are applied in potential methods, intermediate frequencies in both potential and electromagnetic methods, high frequencies in electromagnetic methods, and radio frequencies in radio methods. Since depth penetration decreases rapidly with frequency, the practical utility of high and radio frequencies is limited.

With the exception of the self-potential method, electrical prospecting falls in the group of indirect geophysical procedures which involve an

SYMBOLS USED IN CHAPTER 10

a	distance, radius, semiaxis	a	factor
b	distance, semiaxis	b	coefficient
c	constant	c	light velocity
d	distance, depth		
e	electrical charge	e	2.718
f	frequency		
		g	conductance
h	height, depth, thickness	h	capacitive susceptance
i	current density	i	number
j	$\sqrt{-1}$		
k	reflection factor	k	number; factor
l	distance, length	l	ion mobility
m	electrical, magnetic moment	m	factor
n	valency	n	number
p	adsorption potential	p	factor
q	ratio	q	factor
r	radius, distance	r	ratio
s	distance, thickness	s	specific heat
t	time	t	absolute temperature
		u	ratio
v	volume	v	velocity
		w	viscosity
x	coordinate	x	reading
y	coordinate	y	reading
z	coordinate		
		A	factor
		B	factor
C	capacity	C	ion concentration
D	difference	D	displacement
E	electromotive force	E	electrical field strength
F	Faraday constant	F	field
G	gravitational constant		
		H	magnetic field strength
I	current		
K	diffusivity (of heat)		
L	inductance	L	factor
M	mutual inductance	M	factor
N	turns	N	factor
P	(solution) pressure	P	polarization
Q	quantity (of heat)	Q	factor
R	resistance	R	radius, distance
		R	gas constant
		S	surface, area
T	time constant	T	total field
U	vector potential	U	factor
V	potential		
X	reactance	X	horizontal field component
		Y	horizontal field component
Z	impedance	Z	vertical field component
α	angle	α	dissociation
		β	coefficient
		γ	coefficient
δ	angle	δ	density
ϵ	ellipticity	ε	electrical susceptibility

SYMBOLS USED IN CHAPTER 10—*Concluded*

θ	angle	θ	temperature
η	anisotropy		
ι	dip		
κ	dielectric constant		
λ	wave length		
Λ	decrement		
μ	micro-	μ	permeability
π	3.141		
ρ	resistivity	ϱ	distance, radius
σ	conductivity		
φ	(phase) angle		
ψ	angle		
ω	angular frequency		

excitation and consequent reaction of subsurface bodies and are not based on spontaneous effects like the magnetic and gravity methods. It is a common characteristic of these indirect methods that the depth from which reactions are obtained can be controlled by the spacing of the transmitting and receiving points. Most potential methods (resistivity and potential-drop–ratio methods in particular) have distinct depth control and are in many ways comparable to seismic refraction methods. Electromagnetic, most inductive, and equipotential methods have comparatively little depth control. The spontaneous polarization method lacks depth control completely.

Physical quantities measured in electrical exploration vary greatly and depend largely on the method applied. In the self-potential, equipotential, resistivity, and potential-drop-ratio methods, results are obtained in the form of electrical potentials or potential differences (sometimes referred to the primary field in regard to amplitude and phase) and in the form of ratios of adjacent potential differences. In electromagnetic methods the magnetic field produced by the currents flowing beneath the surface is determined either semiabsolutely (in reference to the phase and amplitude of the excitation current) or in the form of ratios and phase differences of the fields on successive points. Essentially, therefore, the purpose of potential methods is a determination of direction and intensity of the *electrical* field, whereas in electromagnetic methods direction and intensity of the *electromagnetic* field is measured. Measurements of electrical and electromagnetic fields are made by contact probes and coils. Null methods and bridge arrangements are employed extensively for the determination of the direction of current flow, of voltages, voltage ratios, intensities, and intensity ratios.

Potentials and potential gradients are expressed in volts or millivolts absolute or in volts or millivolts per unit distance. Results of resistivity

measurements are given in units of ohm-meters or ohm-feet. Potential ratios are plotted against horizontal distance or equivalent depth. Electromagnetic fields are measured absolutely in microgauss (1.10^{-6} gauss) or semiabsolutely in units of microgauss per ampere primary (loop) current. The fields are represented by their in-phase and quadrature components or by the value of the total vector and its phase. Ratio measurements likewise furnish the in-phase and quadrature components of the electromagnetic field or its amplitude and phase by successive multiplication or addition respectively along a continuous traverse.

In electrical prospecting, as in other geophysical methods, the distinctness of surface indications depends on the contrasts in the physical properties of geologic bodies and their surroundings. The following properties are involved: electrochemical activity, conductivity, dielectric constant, and permeability. Comparatively little is known about electrochemical and dielectric rock properties and geologic factors controlling them; more extensive information is available on rock conductivities. While in most other geophysical methods the distinctness of surface indications increases in linear proportion with differences (or ratios) of the rock properties involved, this is not true for all electrical prospecting methods. In potential methods, a saturation effect is encountered, so that indications from large differences in conductivity are not proportionately stronger than indications obtained from small differences. Therefore, potential methods are particularly suitable for the detection of small differences in conductivity. The same appears to hold for electromagnetic methods with galvanic power supply. Inductive methods, on the other hand, are controlled by absolute conductivities and are therefore best suited for the detection of very good conductors.

Continuity of physical properties is an essential characteristic for the usability of any geophysical method. In those electrical methods that are used for the purpose of determining depths of horizontal formations (resistivity, potential-drop–ratio, and inductive methods), it is necessary that these physical properties remain continuous in a horizontal direction since the spacing of transmitting and receiving units is changed horizontally to obtain increased depth penetration. In the application of electrical methods to ore location, these requirements are not, and need not be, fulfilled since horizontal discontinuities in conductivity are the object of detection. To obtain distinct results it is, of course, desirable that the physical properties remain fairly continuous vertically and in the strike of an ore body.

As in other geophysical methods the uniqueness of interpretation of electrical prospecting results depends on the ease with which interfering factors can be eliminated. Terrain, for instance, affects the surface potential methods much more than it does the electromagnetic methods. High

frequency and radio work is greatly handicapped by terrain because of the refraction of the wave front on the ground surface. There is no satisfactory way of correcting for terrain effects in potential, high frequency, and radio methods except by small-scale model experiments. Electromagnetic and inductive methods are comparatively free from terrain effects. Field components can be measured in reference to the terrain surface, and its disposition relative to subsurface conductors can be taken care of geometrically in the interpretation of the results. Interferences of a geologic nature that may seriously affect the interpretability of electrical results include mineralized solutions in formations and on fissures, and rocks impregnated with noncommercial minerals, such as graphite and pyrite.   .

In some electrical methods (such as the spontaneous potential, the equipotential-line, and those electromagnetic methods in which only the direction of the field is determined) interpretation is merely of a qualitative nature; that is, it is concerned only with locating areas of anomalous indications. Depth determinations with these methods are generally not possible except in simple cases where the depth may be estimated or calculated from the shape of the anomaly curve. However, absolute depth determinations are possible where vertical changes in conductivity are obtained by varying the spacing between transmitting and receiving units (resistivity and potential-drop-ratio methods). In some inductive methods, depth calculations are made indirectly by comparing the field data with type curves calculated for various possible depths of subsurface conductors. More often, however, recourse is had in the interpretation of electrical results to small-scale model experiments.

Progress and development in most geophysical methods have been largely the result of preceding developments in geophysical science. In gravitational, magnetic, and seismic methods field procedure and methods of observation are closely allied to those used in pure geophysics. Electrical methods lacking this background have followed their own course of development.   .

Electrical prospecting methods have three fields of application: oil exploration, mining, and engineering geology. In oil exploration, surface potential, resistivity, potential-drop-ratio, "Eltran," inductive, and electrochemical methods have been used to delineate structure. The most widespread use of electrical methods is made in oil exploration in the process of "electrical logging." This is a modified resistivity method and involves running a continuous resistivity record in uncased wells with an electrode assembly of fixed spacing.

Since their early stages of development, electrical methods have been applied in mining exploration. At first this work was almost entirely

confined to the location of sulfide ores.   Soon this was supplemented by structural investigations.   Lately the field has been extended to the location of such poor conductors as gold quartz veins and the determination of gold content in placer deposits.   In the field of civil engineering, applications of electrical methods have been ever increasing in number, applications including determinations of depth to bedrock on dam and tunnel sites; harbor investigations; location of materials for highway, railroad, and dam construction; location of water-bearing formations and of buried metallic objects, pipes, corrosion, ammunition, and the like.

B. CLASSIFICATION OF ELECTRICAL METHODS

The classification adopted here distinguishes three groups of methods. In the first, ground potentials and, in the second, the electromagnetic fields of the ground currents are determined.   A third group includes radio methods and treasure finders.

1. *Potential methods* may be divided into (*a*) self-potential, (*b*) D.C. and A.C. equipotential-line and potential-profile, (*c*) resistivity, (*d*) potential-drop–ratio, and (*e*) electrical-transient methods.

(*a*) In the *self-potential* method the electrical field is furnished by the electrochemical polarization of ore bodies and other geologic formations. The electrical field is investigated by surveying lines of equal-potential or potential profiles.   It has been found that not only sulfide ore bodies but also metals in placer deposits, faults, corroded pipe lines, and the migration of subsurface waters cause such electrochemical phenomena.   Spontaneous potentials likewise occur when solutions of different character (for example, drilling fluid and formation water) come in contact with one another.   Electrofiltration potentials are produced by the movement of water in porous formations and are used, together with the concentration potentials just mentioned, to indicate the porosity of beds in electrical logging.

(*b*) In this group direct or alternating current is impressed on the ground. The primary electrodes may be pointed or linear.   The potential distribution between them is studied by measuring *equipotential lines* or by surveying potential profiles.   D.C. methods require the use of depolarized electrodes and potentiometers.   In A.C. methods equipotential lines, strictly speaking, do not exist but can be surveyed when out-of-phase components are not too large.   A more exact method is the determination of potential differences according to magnitude and phase by a bridge compensator in which a reference voltage is carried to the instrument from the generator, is varied in phase and amplitude, and is balanced against the unknown voltage difference.   Sulfide ores may be located and structural and stratigraphic conditions may be studied by these methods.

(c) In *resistivity* methods current is supplied to the ground at two points and the potential is measured between two additional points whose spacing or distance from the primary electrodes is varied. The ratio of voltage and current, multiplied by a spacing factor, gives what is known as apparent resistivity as a function of spacing and, hence, as a function of depth penetration. This application makes possible a determination of depth to bedrock, to sulfide ore bodies, to water level, and to beds of stratigraphic significance. If the spacing (and therefore the depth penetration) is kept constant and the arrangement as a whole is moved, horizontal variations in character or in depth of a given formation may be determined. An adaptation of this procedure is the process of electrical logging discussed in further detail in Chapter 11.

(d) The *potential-drop-ratio* method involves a comparison of voltage differences with reference to magnitude and phase in successive ground intervals. This method is also applied to a determination of depth of horizontal and vertical formation boundaries. Although the potential-drop-ratio method has greater resolving power in determination of stratified formations than the resistivity method has, it is best adapted to an investigation of vertical formation boundaries, that is, to the location of ore bodies, quartz veins, and the like.

(e) *Eltran* (transient) methods derive their name from the fact that, not quasistationary fields, but transients are studied. The so-called electrochemical method measures the time that elapses between the application of a current impulse and the peak of the polarization current released by the primary impulse. This time interval is said to be dependent on the electrolytic properties of the formations affected. In the "Eltran" methods proper, a current impulse is impressed on the ground, and the time decay of the corresponding potential impulse is determined. The time constant is primarily dependent on the resistance characteristics of the ground circuit.

2. *Electromagnetic methods* may be classified according to the manner in which the currents, whose electromagnetic field is measured, are caused to flow in the ground. In electromagnetic *galvanic* methods, current is supplied by grounded electrodes. In electromagnetic *inductive* processes, currents are induced to flow in subsurface conductors by insulated loops or cables. A sharp line cannot be drawn between these methods because there are some that employ either power supply. It is difficult to classify the various electromagnetic methods except to enumerate them by name:

(a) The *Lundberg-Sundberg* methods involve the measurement of horizontal and vertical field components with compensator devices giving their in-phase and quadrature constituents in reference to the primary field supply. (b) *Ambronn's* method employs a similar arrangement, except that the compensator gives the phase and magnitude of three field

components. (*c*) In the *Müller* method the out-of-phase components are made negligible by the use of 60-cycle power, so that the vector amplitude may be measured without reference to its phase by a vacuum tube voltmeter arrangement connected to the pickup coil. (*d*) The *Elbof* method measures merely the direction of strike and dip of the ellipse of polarization.

The next three methods are closely related: (*e*) *Bieler* and *Watson* use two coils in fixed arrangement. One is vertical, the other horizontal; the latter picks up the vertical field component produced by the primary loop, whereas the vertical coil responds to the horizontal out-of-phase component produced by subsurface current concentrations. (*f*) Some of the electromagnetic-*ratio* methods utilize two independent coils connected in series through an amplifier detector. One coil remains fixed in direction on one station while the other, at a second location, is rotated until balance is obtained, the angle of rotation corresponding to the difference in intensity and phase angle. Other electromagnetic-ratio methods make use of ratio bridges by which the voltages induced in two coils (usually held horizontally to measure the vertical component) are balanced for phase and amplitude.

The four remaining procedures are generally referred to as truly inductive: (*g*) In the *Sundberg* method a large rectangular loop is laid out, and the horizontal component is measured across one cable. Due to the "reflection" of the cable on subsurface conductors, the depth of the latter can be determined from the shape of the anomaly curve. The real and imaginary components of the horizontal field components are measured with a compensator. This method is primarily applicable to structural studies. (*h*) Another procedure known as the *ring induction* method uses a circular primary loop of small diameter laid out concentrically with a smaller secondary horizontal coil. The effect of the primary coil on it is compensated by an auxiliary coil, and the secondary fields are measured according to phase and amplitude. By varying the radius of the ring it is possible to reach different depths and to calculate the resistivities of formations at these depths. (*i*) In the *Mason* method the primary field is produced by a vertical loop, and strike and dip of the secondary field are measured with a search coil. (*j*) The high-frequency *Radiore* method utilizes a similar arrangement, except that the primary field is produced by a circular loop of comparatively small diameter. The dip of the field resulting from a combination of the primary and secondary components is determined with a search coil.

With the exception of the Sundberg-inductive, the Müller, and the ring-induction methods, electromagnetic methods are applied principally in the location of sulfide ore bodies. The methods mentioned as exceptions have been used chiefly for structural and stratigraphic studies.

3. *Radio methods and "treasure finders."*   Radio measurements fall into two natural groups.   In the first, the reaction of a transmitter to changes in surrounding media is determined.   Methods in the second group measure the effect of the media, situated between transmitter and receiver, upon the latter's reception characteristics.   The *quarter wave* method is based on the fact that when a reflecting surface is at a distance of one quarter of the wave length from the transmitter, a maximum of the emission occurs.   Hence, the depth of such reflecting surfaces as water under dry surface beds, or flat-lying ore bodies in dry formations, may be found by varying the frequency and observing the antenna current.   Inasmuch as the antenna *capacity* is affected by the proximity of conductors, they may be located by changes in wave length and damping.   This method has no depth control and, therefore, interpretation of results is difficult except when geologic conditions are simple and interferences from noncommercial conductors are absent.

Application of radio methods in the second group requires a transmitter and receiver, and measurements are made on the receiving side.   By *absorption* measurements, ore bodies in dry country rock have been outlined from underground workings.   With the *interference* method depths to reflecting surfaces may be determined by observing the change of intensity of reception with horizontal distance.   The direction of the incident beam is measured in the *reflection* method by a search coil.

Treasure finders may be divided into low and high frequency devices. The former are modifications of induction balances.   In one of these, one energizing coil and two pickup coils are arranged on the same coil frame. Presence of metallic bodies changes the mutual inductance between the lower pickup coil and the primary coil.   Instruments of this type have been found useful in locating fairly small buried metallic objects such as bombs.   In another device two search coils a few feet apart are in a balanced bridge circuit and energized with current of intermediate frequency.   The inductance change resulting from metallic bodies near one coil is measured.   The depth range of low-frequency treasure finders does not extend far beyond five feet.

High frequency treasure finders are (1) beat frequency oscillators, and (2) combinations of transmitters and receivers.   In the former the frequency of one oscillating circuit remains fixed; that of the other varies with the proximity of conductive bodies.   This changes the beat note or the plate current in a third circuit.   The depth penetration of these devices does not exceed fifteen feet.   In treasure finders consisting of a transmitter and receiver combination, intensity of reception is indicated by a plate current meter, and a compensating circuit is provided so that for barren ground the normal intensity gives a zero reading.   The reading changes

with the presence of conductive bodies. Two commercial treasure finders, the "metallascope" (Fisher) and the "terrometer" (Barret), operate on this principle. The terrometer is reported to be sensitive enough to detect mineral disseminations in shallow placers to a depth of fifteen or twenty feet.

II. ELECTRICAL PROPERTIES OF ROCKS

It is the function of electrical prospecting methods to measure the distribution of natural and artificial potentials, of electromagnetic fields, and of the propagation of radio waves. This variety of electrical phenomena causes not merely one but a number of physical properties of geologic bodies to be significant. They are: (1) *electrochemical properties*, giving rise to (a) spontaneous and (b) polarization potentials; (2) *electrical conductivity*; (3) *dielectric constant*; and (4) *magnetic permeability*. Of these, the electrical conductivity is undoubtedly the most important. Strictly speaking, none of the above properties are constants but depend on other factors, mainly *frequency*.

A. ELECTROCHEMICAL PROPERTIES

Electrochemical effects are responsible for the electrical field surrounding chemically polarized ore bodies; they give rise to interference potentials when metallic electrodes are placed in contact with moist ground; they produce electrical potentials when solutions of different concentrations come in contact with one another in wells or when a solution is forced through a porous medium; and, lastly, they give rise to counter e.m.f.'s when current is applied to the ground. The first three of these effects do not depend on extraneous electrical fields and are therefore called *spontaneous potentials*, or, more specifically, (a) electrode potentials, (b) diffusion potentials, and (c) electrofiltration potentials. Potentials caused by the application of an electrical field are called *polarization potentials*.

1. *Spontaneous potentials.* (a) *Electrode potentials.* When a metallic electrode is placed in a solution it acquires a potential difference against the solution which, however, cannot be measured except by placing a second electrode in the liquid. If the metals of the two electrodes are alike and if the concentrations of the solution at the two contact points are the same, no potential difference between the two electrodes is observed. A potential difference occurs, however, if either the metals or the concentrations are different. Practical application of this principle is made in electrical prospecting (1) in the so-called activity of ore bodies, which is due (a) to their contact with solutions of different character and concen-

tration near the surface and below, and (b) to differences in ore material above and below; (2) in the interference potentials which originate on metal electrodes when the latter make contact with the ground at points where the concentrations of electrolytic solutions are different; (3) in the construction of nonpolarizable electrodes.

Potential differences resulting from the contact of two electrodes with solutions of different concentration may be calculated from the potential of a metal against a solution, which is dependent only on the concentration of the ions of the particular metal. The potential difference of solution minus metal is

$$E = \frac{\mathsf{R}}{F} \cdot \frac{\mathsf{t}}{n} \cdot \log_e \frac{P'}{\mathsf{C}} \qquad (10\text{--}1a)$$

where R is the gas constant, or 8.309 joule per degree C.; n is the valency; F is Faraday's constant of electrolysis, that is, the quantity of electricity liberating one gram equivalent, or 96,494 coulombs (so that the ratio R/F is 8,610 e.m.u.'s or $0.861 \cdot 10^{-4}$ volts); t is the absolute temperature, or $273° + \theta$, P' is constant for the metal involved (its electrolytic solution pressure); and C is the ion concentration. If two electrodes of the same metal are immersed in two solutions of different concentration, $\mathsf{C_2}$ and $\mathsf{C_1}$ (which may be connected by a syphon bridge to afford a return circuit with negligible diffusion potential), the potential difference between the two electrodes is

$$\Delta E = 1.98 \cdot 10^{-4} \cdot \frac{\mathsf{t}}{n} \log_{10} \frac{\mathsf{C_2}}{\mathsf{C_1}} \text{ volts}, \qquad (10\text{--}1b)$$

where the numerical factor contains the ratio R/F, the modulus of the natural logarithms, and the conversion of e.m.u.'s into volts. An evaluation of the above equation shows that for $\theta = 18°$C. the voltage difference is $\Delta E = 1/n \cdot 0.0577 \cdot \log_{10} \mathsf{C_2}/\mathsf{C_1}$ volts, so that for $n = 1$ and a concentration ratio of 10, the voltage difference is 0.058 volts and, for a ratio of 100, 0.115 volts.

The voltage gradients observed on polarized ore bodies are normally from 1 to 2 millivolts per foot, which amounts to anomalies of the order of 0.1 volt to a maximum of 1.5 volts. This is comparable to the voltage delivered from a wet cell; it is, therefore, probable that not only differences in concentration but differences in the composition of the ore near the surface (gossan!) and unoxidized portions below, where the solutions are less acid and poorer in H ions, play a part in causing such potentials. To explain the phenomenon on ore bodies showing spontaneous polarization, equation (10–1b) should be written in a form allowing for (1) electrode

potentials due to differences in solution pressure P' and (2) differences in concentration:

$$\Delta E = 1.98 \cdot 10^{-4} \cdot \frac{t}{n} \log_{10} \frac{P'_1 \cdot C_2}{C_1 \cdot P'_2} \text{ volts.} \qquad (10\text{-}1c)$$

With this equation, voltages are calculated which are in better agreement with those actually observed. Under the assumption that there are no appreciable differences in concentration of solution between the upper and the lower parts of the ore body, eq. (10-1c) retains the form $\Delta E = c \cdot \log_{10} P'_1/P'_2$, which gives potentials sufficient to account for the anomalies measured at the surface. Pyrite in undisintegrated form is likely to have a solution pressure of around 10^7 atm. and in altered form (such as limonite, and the like, in the gossan) probably not more than 10^{-30} atm. The equation in its last form makes it possible to allow for equivalent series connections of altered and unaltered portions of an ore body.

Electrode potentials occur when metal probes are placed in contact with the ground in order to measure potential differences between them. Contact potentials amounting to several millivolts and even several tens of millivolts may be observed and may be avoided by the use of so-called nonpolarizable electrodes. The latter consist of electrodes (of the same metal for a pair) immersed in a saturated solution of one of its salts (copper in copper sulfate, zinc in zinc sulfate, and so on). The solutions are carried in vessels made of a permeable substance (porous clay or beef gut) so that they may filter through and make contact with the ground solutions. Inasmuch as identical metals and identical solutions are used for both electrodes, the electrode potentials are of equal sign and cancel when no current is flowing.

Potentials arising from direct contact of metal with soil solutions of different concentrations are avoided by the interposition of a concentrated solution. To obviate diffusion potentials (see paragraph b), some investigators have proposed the use of two chambers, an inner one with the saturated solution and an outer chamber with a more dilute solution. Upon the passage of current, the polarization (see paragraph 2) of these electrodes is negligible; since metals in solutions containing their ions belong to the "reversible" systems, a passage of current will form no new chemical compounds. What polarization occurs is due merely to concentration changes in the solution near the electrodes. In the practice of electrical prospecting this concentration polarization is small because of the small current densities involved. Nonpolarizable electrodes are necessary in all D.C. methods of electrical exploration; in A.C. procedures ordinary metal electrodes are satisfactory.

(b) *Diffusion (osmotic) potentials* occur in wells in connection with po-

rosity measurements. They are produced by the contact of fresh-water drilling mud with the saline connate water solutions in sandy or other porous layers. Theoretically, the e.m.f. generated between two solutions of the ion concentrations C_1 and C_2 is given by

$$\frac{l_1}{l} \text{ volts}.$$

$$(10\text{-}2)$$

where l_c and l_A are the mobilities of the cation and anion, and n is their valency. For a NaCl solution, for instance, $n = 1$, $l_c/(l_c + l_A) = 0.4$ and $l_A/(l_c + l_A) = 0.6$. Therefore, the diffusion potential at standard temperature $E = 11.6 \log_{10} C_1/C_2$ millivolts. If $C_1 = 10C_2$, the potential difference is 11.6 millivolts. Inasmuch as the concentrations are inversely proportional to the resistivities of the drilling mud (ρ_2) and the formation water (ρ_1), ρ_2/ρ_1 may be substituted for C_1/C_2, and therefore $\Delta E = 11.6 \cdot \log_{10} \rho_2/\rho_1$ millivolts.

(c) *Electrofiltration potentials* are likewise important in the measurement of porosities in wells. They occur when a solution of the conductivity σ and the viscosity w is forced with a difference in pressure P through a porous medium (or a number of capillaries) with the adsorption potential p (potential of double layer on wall of capillaries, depending on concentration) and the dielectric constant κ, so that the potential difference

$$= \frac{pP\kappa}{4\pi w \cdot \sigma}.$$

$$(10\text{-}3)$$

It is seen that the potential increases with the fluidity of the liquid and with pressure and, therefore, with the speed with which the ions can be transported. In wells the diffusion potentials are due to the penetration of drilling fluid into porous formations; and they are usually negative and of the order of 0.1 to 0.2 volts. When the drilling mud is of the same composition as the formation solution, electrofiltration potentials are the only ones giving rise to spontaneous polarization. If, however, the ion concentrations of the two liquids are different, both effects are superimposed on each other, and it is possible that the diffusion potentials overshadow the electrofiltration potentials in such cases.

2. *Polarization potentials* are produced by applying an electric field to an electrolyte. They are of importance in some "Eltran" methods, in the determination of rock resistivities with D.C., in some applications of the D.C. equipotential-line method, and in connection with the corrosion of pipes.

If an electrical field is applied to an electrolyte or rock containing molecules in dissociated form, the ions move to the electrodes of opposite

polarity, and the liquid becomes polarized. Since matter is transported, differences in concentration result, which in turn give rise to a potential difference. This opposes the potential difference causing the electrical field and is known as the polarization counter e.m.f., E'. Hence, Ohm's law, as applied to the passage of D.C. through polarized electrolytes, is often written in the form $I = (E - E')/R$.

Owing to the slow speed with which the ions travel, the counter e.m.f. reaches its maximum value but gradually. After the concentration gradient between the electrodes has become linear, stationary conditions are reached. The time required for its establishment depends on the distance between the electrodes and the diffusion constant of the electrolyte. The counter e.m.f. cannot exceed definite values for given conditions and solutions, but the electrical field can be increased. Hence, in determining resistivities of rocks containing electrolytes, more reliable values can be obtained with high fields.[1] The difficulty mentioned may, of course, be avoided by alternating current.

B. METALLIC AND ELECTROLYTIC CURRENT CONDUCTION

From the viewpoint of molecular physics the following kinds of current conduction may be distinguished: (1) *electronic* conduction, (2) *electrolytic* conduction, and (3) *dielectric* conduction. The first is identical with metallic conduction and is due to the movement of free electrons; the second results from the transport of ions in electrolytes. In the third no free electrons are available. Under the influence of an electrical field the effective centers of electrons and nuclei are displaced. Current propagation results from changes of this polarization or changes in the electrical flux with time and is called displacement current. It will be discussed separately in section c.

Metallic conductivity is associated with virtually all minerals of *metallic luster*, ores composed of those minerals, and impregnations of metallic minerals in crystalline and metamorphic rocks. The best conductors are the sulfides, a few of the oxides, and graphite. The conductivity of ores and mineral deposits depends largely on the continuity of the conducting particles. Details are given below. Numerical values for the conductivities of minerals and ores will be found in section G.

The fundamental difference between electronic and electrolytic conduction lies in the fact that in the solids no matter is transferred whereas in the electrolytes the current propagation is invariably accompanied by a transport of matter and hence by chemical transformation. In solids

---

[1] See B. McCollum and K. H. Logan, Bur. Stand. Tech. Paper, **25** (1914); M. W. Pullen, U.S. Bur. Mines Circ. No. 6141 (1929).

conduction of current is accomplished by the "free" electrons in the outermost orbits of the atoms. In gases and liquids, current conduction is associated with ions, that is, molecules combined with electrons or those having a deficiency of electrons, or a positive charge. Because of this association, matter is transferred, that is, deposited at one electrode and dissolved at the other. Hence the name *electrolytic* (= solvent) phenomena. Current conduction in electrolytes depends not only on the mobility but also on the number of ions. The latter, in turn, depends on the concentration and degree of dissociation, which increases with the *dielectric constant* of the solvent. Hence, water with the highest dielectric constant (about 80) is of great importance in enhancing conductivity.

For D.C., conduction in both metallic and electrolytic conductors is governed by Ohm's law. By it a conductor is defined as having a unit of resistance if the potential difference 1 produces the current 1. Its resistivity ρ is defined as resistance R referred to unit dimensions. If the length of the conductor is l, and S its section,

$$R = \rho \cdot \frac{l}{S}.$$

Although the resistance of a body of unit dimensions is numerically equal to the resistance of a centimeter cubed, resistivity should not be expressed in ohms per centimeter cubed. Since $\rho = SR/l$, and the square of dimensions appears in the numerator and the first power in the denominator, the dimension of resistivity is *ohm-centimeter*. In the practice of electrical prospecting, the use of this unit often results in comparatively high figures, and the ohm-meter (ohm-cm$\cdot 10^{-2}$) is frequently employed, in addition to ohm-inch (ohm-cm$\cdot 0.3937$), ohm-foot (ohm-cm$\cdot 0.0328$) and kilohm-cm (ohm-cm$\cdot 10^{-3}$). In certain electrical problems it is necessary to convert the practical into electromagnetic or electrostatic units: 1 ohm = 10^9 e.m.u. = $1.111 \cdot 10^{-?}$ e.s.u. The reciprocal of resistivity is designated as conductivity σ:

$$\sigma = \frac{}{} = \frac{l}{SR}. \tag{10-4b}$$

The unit is the reciprocal ohm-cm or mho-cm. Conductivity is the ratio of current density and electric field strength E:

$$\sigma = \frac{i}{E}. \tag{10-5}$$

This relation follows directly from Ohm's law. Since $V = IR$ and $R = \rho l/S$, $dV/dl =$ (potential gradient or field strength) $= E = (I/S) \cdot 1/\sigma$, with $I/S =$ current density i.

In alternating electrical fields the current is not in phase with the e.m.f. Current conduction is controlled by the resultant modulus of resistance and reactance, which is known as impedance. Impedances are customarily represented by conjugate numbers with the resistive component on the real axis, the reactance on the imaginary axis, and the phase shift as the argument of the complex quantity.

Although most rock-forming minerals are insulators, it does not follow that most rocks are poor conductors. This is true only if they are solid throughout (such as some igneous rocks and chemical sediments). The majority of rocks and formations are porous, are filled with more or less conductive moisture, and act as electrolytes. Their conductivity depends on four factors: (1) pore volume; (2) disposition of pores (grain packing); (3) portion of pores filled with water; and (4) conductivity of the water, which is composed of (a) a primary conductivity (that is, conductivity of the water as it enters the pores), and (b) a secondary conductivity (acquired by solution of mineral matter and therefore dependent on duration of contact [stagnation]). These relations may be expressed by the following formula:

$$\rho_x = \frac{c}{v_1} \cdot \rho_1 \quad \text{or} \quad \sigma_x = \frac{v_1}{c} \cdot \sigma_1, \qquad (10\text{-}6)$$

where ρ_x is the resistivity and σ_x the conductivity of the rock, c a constant depending on the arrangement of the pores, v_1 the pore volume, ρ_1 the resistivity and σ_1 the conductivity of the water or other medium filling the pores.

For specific arrangements of mineral grains of regular geometric shape, it is possible to calculate not only the pore volume and thus the resistivity as a function of the resistivity of the water filling the pores, but also the relative effect of the conductivity of the grains compared with the effect of the medium in which they are imbedded. Maxwell has derived a general relation for the conductivity σ_x of an aggregate consisting of a medium with the conductivity σ_1, in which spherical grains of the conductivity σ_2 are imbedded in regular arrangement and in such a manner that their distance is large compared with their radius.[1a] If the total volume of the aggregate is v_x and the total volume of the grains v_2, and if the ratio of these two volumes $v_2/v_x = r$, then the following relation obtains:

$$\sigma_x = \frac{2\sigma_1 + \sigma_2 - 2r(\sigma_1 - \sigma_2)}{2\sigma_1 + \sigma_2 + r(\sigma_1 - \sigma_2)} \cdot \sigma_1. \qquad (10\text{-}7a)$$

Hence, in terms of the (pore) volume v_1 (if the pores are filled completely with the medium of the conductivity σ_1),

---

[1a] See also J. N. Hummel, Beitr. angew. Geophys., **5**(1), 32–132 (1935).

$$\tau_x = \frac{3\sigma_2 + 2v_1(\sigma_1 - \sigma_2)}{3\sigma_1 - v_1(\sigma_1 - \sigma_2)} \cdot \sigma_1. \tag{10-7b}$$

Assuming now that $v_1 = r$ (or $2v_1 = v_x$, a porosity of 50 per cent), we obtain from eq. (10-7b): $\sigma_x = \dfrac{2\sigma_1 + 4\sigma_2}{5\sigma_1 + \sigma_2}$ and therefore, for the ratio,

$$\frac{\sigma_x}{\sigma_2} = \frac{\sigma_1}{\sigma_2} \cdot \frac{2\dfrac{\sigma_1}{\sigma_2} + 4}{5\dfrac{\sigma_1}{\sigma_2} + 1}. \tag{10-7c}$$

From this it follows that, for a conductivity of the pore filling medium very much greater than that of the grains, or for $\sigma_1 \gg \sigma_2$, we have $\sigma_x \doteq \frac{2}{5}\sigma_1$, and for $\sigma_2 \gg \sigma_1$, $\sigma_x \doteq 4\sigma_1$.

Fig. 10-1 is a graph of eq. (10-7c). For a porosity of 50 per cent, the conductivity of the aggregate increases almost in direct proportion to the conductivity of the medium filling the pores (assuming all pores to be filled with the medium of the conductivity σ_1). For virtually all porous rocks we are, therefore, justified in disregarding the conductivity of the mineral grains and operating only with

FIG. 10-1. Rock resistivity as a function of resistivity of pore-filling medium, for 50 per cent porosity (after Hummel).

the conductivity of the medium filling the pores. Thus, letting $\sigma_2 = 0$ in formula (10-7b), we get

$$\sigma_x = \frac{}{3 -} \qquad \text{or} \qquad \cdot \rho_1. \tag{10-7d}$$

Eq. (10-7d) can be further simplified for porosities less than 25 per cent by assuming that the pore volume is equivalent to a system of cylindrical tubes of identical radius r, not touching one another, traversing the substances in the three directions. If there are n tubes per square centimeter, their area on one side of a cube (or one-third of the pore volume) is $r/3 =$

n. Since the resistance in the direction of the tube is inversely proportional to its area, $\frac{\rho_x}{\rho_1} = \frac{1}{\pi r^2 \mathbf{n}}$, so that

$$\frac{\rho_x}{\rho_1} \quad \frac{3}{v_1}. \qquad\qquad (10\text{-}7e)$$
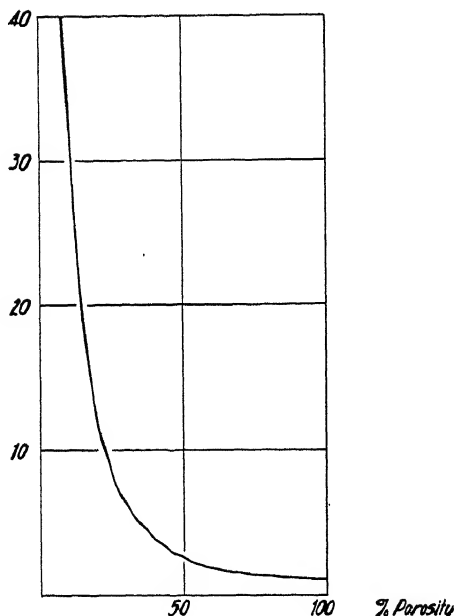
Fig. 10-2. Relation between resistivity ratio and porosity (after Sundberg).

The relation (10-7d) is shown graphically in Fig. 10-2. Resistivities determined by this diagram are in good agreement with resistivities actually observed.

Table 60 gives some values for the porosities of various types of rocks, formations, and soils, and for the corresponding values for the resistivity ratio ρ_x/ρ_1.

In the derivation of preceding equations, no assumption was made in regard to the spacing of the mineral grains or pore spaces, respectively. For definite ratios of spacing to size of the grains, it is possible to determine the pore volume and therefore the resistivity ratio ρ_x/ρ_1. Table 61 (largely from Sundberg) gives these values for various grain arrangements. This tabulation brings out the fact that the resistivity may in certain cases depend on the direction of current with respect to the arrangement of the particles. Materials of such nature are called *anisotropic*. Anisotropy of resistivity plays an important part in all stratified formations where resistivities in the bedding planes are generally quite different from those at right angles thereto.

It was shown before that the resistivity of a rock can be found if the pore volume, the pore arrangement, and the resistivity of the water filling the pores is known. The latter may be determined by experiment if specimens of well or formation water have been taken. If the specimen itself is not available, but only its analysis is, the conductivity can still be calculated. For this purpose it is first necessary to recalculate the

constituents in terms of gram (or better milligram) equivalents per liter. From the concentration C thus expressed, the degree of dissociation is obtained. Sundberg[2] has given diagrams showing dissociation as a function of concentration of a number of salts. Only the curves for NaCl are of practical importance. If the dissociation of a solution is α, the number of anions per cc is $\alpha \cdot C$ gram equivalents. With a charge F per gram equivalent ($= 96500$ coulombs), the quantity of electricity carried by the anions is $F \cdot \alpha \cdot C \cdot v_A$, and $F \cdot \alpha \cdot C \cdot v_C$ is that carried by the cations, if v is their velocity for a potential gradient of 1 volt per cm. Hence, the

TABLE 60

Rock or Formation	Porosity	Ratio $\frac{\rho_2}{\rho_1}$
	%	
Igneous and metamorphic rocks	$\frac{1}{2}$– 2	100
Dense limestones and sandstones	3– 4	50 –100
Clays and sands in general	8–15	20 – 40
Porous clays, sands, sandstones, cellular limestones, and dolomites	15–40	3 – 20
Marl, loess, clay, and sandy soil	40–75	1.5– 4
Peat, diatomaceous earth	80-90	1.0– 1.5

TABLE 61

Grain Arrangement	Porosity	Ratio $\frac{\rho_2}{\rho_1}$
Spheres of radius r, distance $r/2$	73.2	1.37
Spheres in cubic arrangement	47.6	2.64
Spheres in rhombic arrangement	39.5	3.38–4.40 depending on direction
Spheres in hexagonal arrangement	26.2	5.81 in direction perpendicular to base

total quantity per second, the current strength, and thus the conductivity per cm^3 is $\sigma = F \cdot \alpha \cdot C(v_A + v_C)$. For infinite dilution, α is 1 and the velocities are $v_{A\infty}$ and $v_{C\infty}$. If we designate the quantities $l_A = Fv_A$ and $l_C = F \cdot v_{C\infty}$, as ion mobilities, the resistivity for any number of salts in solution is $\rho = 1/(\Sigma \alpha C[l_A + l_C])$. For very diluted solutions in which all salts are completely dissociated (C less than 0.5 mg per liter), $\alpha \doteq 1$ and the resistivity in terms of concentration expressed in milligram equivalents per liter is $\rho = 1000/(\Sigma C[l_A + l_C])$. Theoretically, the sum of the concentrations and ion mobilities should be taken for all salts in solution.

[2] K. Sundberg, A.I.M.E. Geophys. Pros., 381 (1932).

A comparison of analyses of water from different sources with the results of theoretical calculations has shown, however, that for waters of less than 1000 ohm-cm, the resistivity can be determined closely enough from their chlorine content alone. The curves in Fig. 10–3 show resistivities of NaCl solutions as a function of concentration.
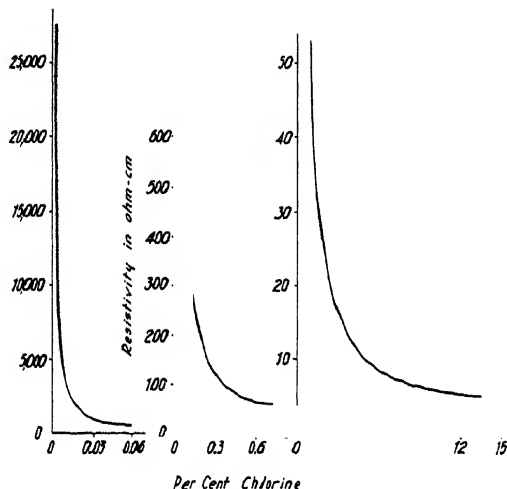
FIG. 10-3. Resistivities of salt solutions as a function of chlorine content (after Sundberg).

The composition of natural waters varies widely, depending on origin and on geologic occurrence. They may be classified as follows:

1. Meteoric waters, derived from precipitation: $\rho = 3000 - 100,000$ ohm-cm.

2. Surface waters (lakes, rivers, and the like) vary from 300,000 ohm-cm for very pure water to as little as 10 ohm-cm for salt lakes. Surface waters in districts of igneous rock are estimated to range from 3000 to 50,000 ohm-cm; surface waters in areas of sedimentary rock from 1000 to 10,000 ohm-cm.

3. Soil waters (discharged into the atmosphere by evaporation) may be as low as 10 ohm-cm, but their average is around 10,000 ohm-cm.

4. Normal ground water in areas of igneous rock is of the order of 3000 to 15,000 ohm-cm and in areas of sedimentary rocks as low as 100 ohm-cm.

5. Subsurface (connate) waters (Na, K, Ca, and Mg chlorides) are generally good conductors and are between 3 and 10 ohm-cm.

6. Mine waters (usually copper, and zinc, and so on, sulfates) are likewise of low resistivity, generally not exceeding 30 ohm-cm.

Contrary to metals, the conductivity of electrolytes increases with an increase in temperature, so that

$$\sigma_\theta = \sigma_{18}[1 + \beta(\theta - 18° \text{ C.})]. \tag{10-8}$$

While in metals the temperature coefficient of resistivity is the reciprocal of the absolute temperature, the temperature coefficient of electrolytes (being the increase in ion mobility due to a reduction in the viscosity of the solvent) is approximately equal to the temperature coefficient of viscosity of water. For NaCl solutions the coefficient is 0.022; for an increase in temperature of 35° C. the conductivity is about doubled (see Fig. 10-4).

Metals and electrolytes also show a difference in alternating current conduction. In electrolytic solutions voltage and current are generally not in phase, particularly when the polarization e.m.f. is comparable with the applied e.m.f.[3] The phase shift is reduced as the voltage is increased. If P is a "polarization constant" (ratio of polarization e.m.f. and quantity of electrolysis products deposited per unit surface of electrode), the impedance of an electrolytic solution is
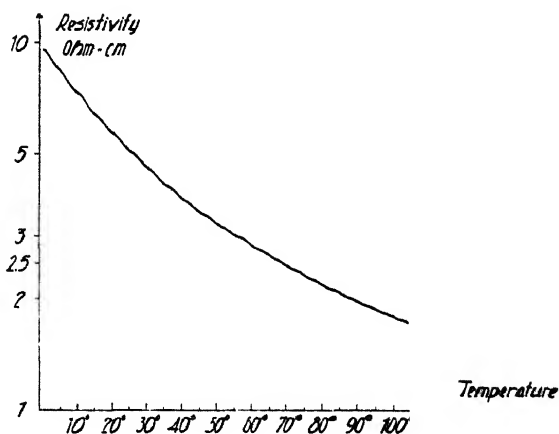
Fig. 10-4. Decrease of resistivity of an NaCl solution with temperature (after Sundberg).

$$Z = R\sqrt{1 + \frac{P^2}{\omega^2 R^2}}. \tag{10-9a}$$

Substituting $1/C_p$ for P, eq. (10-9a) takes the form

$$Z = \frac{1}{\omega C_p}\sqrt{1 + \omega^2 C_p R^2}, \tag{10-9b}$$

which is seen to be identical with the formula for the impedance of a circuit consisting of a resistance with a capacity in series. The phase

[3] See oscillograms in W. R. Cooper, *Electrolysis as Applied to Engineering*, p. 16 (New York, 1923).

shift in a circuit consisting of an electrolyte with the polarization **P** is

$$= -\tan^{-1} \frac{\mathbf{P}}{-} \tag{10-9c}$$

C. DIELECTRIC CURRENT CONDUCTION

In most nonmetallic, solid, and isotropic media the number of free electrons is too small to permit free passage of direct current. Alternating current, however, will be transmitted, since the electrical field produces a displacement of the nuclear and electron patterns (*dielectric polarization*) which is propagated when the field changes with time. The polarization **P** (electric moment of the unit of volume) is proportional to the electrical field. **P** = ε**E**, where ε is the *electric susceptibility*. Treating the electrical flux in the same manner that the magnetic flux was treated in Chapter 8, the flux per unit area or the electric *displacement* **D** = **E** + 4π**P**. Substituting for **P**: ε**E**, the displacement becomes **D** = (1 + 4πε)**E**, where 1 + 4πε =
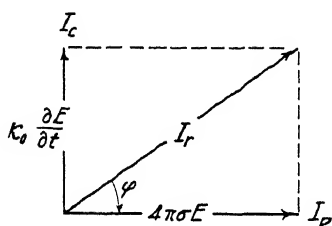
FIG. 10-5a. Relation between conduction current and displacement current.

κ is the *dielectric constant*. Hence the displacement is **D** = κ·**E**.

An alternating electrical field produces a current in a dielectric equal to ∂**D**/∂t or = κ·∂**E**/∂t, which is known as the *displacement current*. Considering the conduction current and recalling from eq. (10-5) that the current density $i = 4\pi\sigma\mathbf{E}$, we get, for the total current (see Fig. 10-5a),

FIG. 10-5b. Relation between conductivity and true and apparent dielectric constant.

$$I_r = \kappa \frac{\partial \mathbf{E}}{\partial t} + 4\pi\sigma\mathbf{E}. \tag{10-10a}$$

For a sinusoidal e.m.f. of the angular frequency ω, the differentiation gives an e.m.f. 90° out of phase with the last term of the equation, so that the peak value of the displacement current becomes κω**E**. Therefore

$$I_r = 4\pi\sigma\mathbf{E} + j\kappa\omega\mathbf{E}, \tag{10-10b}$$

so that the *phase shift* between conduction component and resultant current

$$\varphi = \tan^{-1} \frac{\kappa\omega}{4\pi\sigma}. \tag{10-10c}$$

In terms of the displacement current and by substituting $\partial E / \partial t = j\omega E$, or $E = \dfrac{-j}{\omega} \cdot \dfrac{\partial E}{\partial t}$, eq. (10-10a) may be written:

$$I_r = \kappa \frac{\partial E}{\partial t} - j\frac{4\pi\sigma}{\omega} \cdot \frac{\partial E}{\partial t} = \frac{\partial E}{\partial t}\left(\kappa - \cdot\, 4\pi\sigma\right.$$

so that

$$I_r = \kappa' \frac{\partial E}{\partial t}, \tag{10-10d}$$

where $\kappa' = \kappa - j4\pi\sigma/\omega$ is the *apparent* dielectric constant (see Fig. 10-5b).
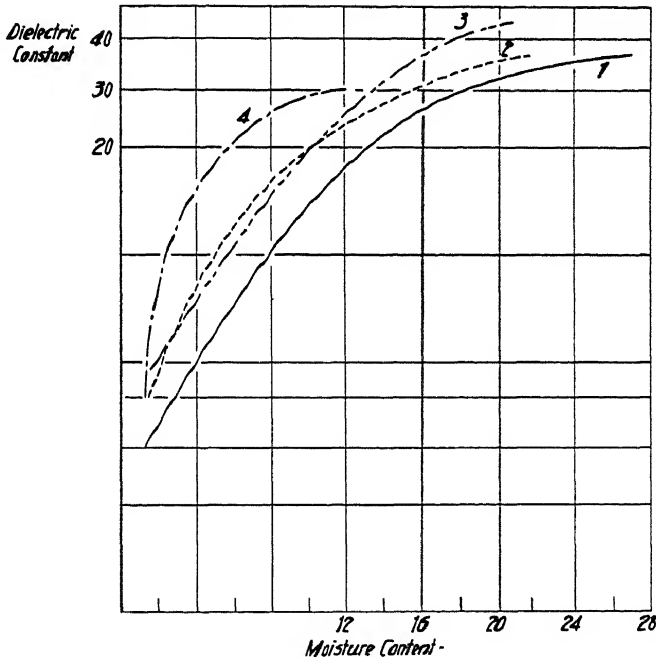
FIG. 10-6. Apparent dielectric constant as a function of moisture content (after Smith-Rose).

Like the conductivity, the dielectric constant of an aggregate increases with water content, owing to the large dielectric constant of water. Smith-Rose gives as dielectric constants for *dry soils*, 2.6 to 2.8; for soils with 3.6 per cent *moisture*, 2.3 to 5.6; and for soils with 16 to 30 per cent *water*, 18 to 30. Fig. 10-6 shows the change of dielectric constant with moisture for a frequency of 1200 kc.

D. The Effects of Magnetic Permeability

As was shown in the introduction to Chapter 8, magnetic permeability is the ratio of magnetostatic induction to field strength. It plays a part in all electric induction phenomena. In accordance with Faraday's law, the e.m.f. induced in a conductive body depends on the time rate of change of the field: $E = - d\mathbf{H}/dt$. If the field change occurs in a medium of the permeability $\mathbf{u}$, the induced e.m.f. $E = - \mathbf{u}\, d\mathbf{H}/dt$. Theoretically this relation should be expected to find application in electrical prospecting methods where current is induced in subsurface conductors by insulated loops. In practice, however, it is of limited importance since with few exceptions, good conductors (sulfide ores) to which inductive methods are applied chiefly are not very magnetic, while very magnetic (iron) ores, on the other hand, are usually poor conductors, making potential methods more suitable.

E. Methods for the Determination of Rock Resistivity

Methods for determining rock resistivity may be divided into two groups: (1) laboratory determinations (on rock specimens) and (2) measurements *in situ* (at the ground surface, outcrops, and the like). Laboratory determination has the disadvantage that only small specimens are tested, that the effects of unhomogeneities in the specimen not characteristic of the entire formation may be exaggerated, and that conditions in nature may not be exactly duplicated. By making measurements on location, these disadvantages are overcome, but their limitation is that unknown near-surface strata differing in conductivity may affect the results; hence an "apparent" instead of the true resistivity of the surface formation may be determined. In regard to technique, two major groups may be distinguished: one that uses direct current and the other that uses alternating current (commutated D.C., low-frequency A.C., intermediate-frequency A.C., and high-frequency A.C.). Measurements at radio frequencies are discussed in the next section in connection with determinations of the dielectric constant.

1. *Preparation of specimens; electrodes.* For resistivity determination in the laboratory the sample should be cut to regular shape so that its resistivity may be readily calculated from resistance and dimensions. Rock saws with carborundum or diamond discs are suitable. The length of the specimen should be at least four times its diameter. High contact resistances may be overcome by the use of a frame shown in Fig. 10-7. Between the metal plates and the specimen various layers of tinfoil should be inserted. Contact resistance is likewise reduced with mercury electrodes. Two arrangements are shown in Figs. 10-8 and 10-9, the latter

being suitable for testing drill cores. Drill cores may be dipped in solder of low melting point to reduce contact resistance. Specimens suspected of being anisotropic should be measured in more than one direction. In any event, it is a good policy to reverse the specimen and to make at least two determinations.

Fig. 10-7. Clamp for rock resistivity determinations (after Sundberg).

Effects of polarization are difficult to eliminate. In D.C. measurements the direction of current should be reversed in as brief periods as possible and high voltages should be used. Owing to the difficulties with direct current, A.C. methods are now in more prevalent use.

2. *Continuous D.C. methods.* For moderate requirements of accuracy, the direct reading ohmmeters of radio and universal testing sets are quite satisfactory; they are conveniently carried in the field for rapid checks on unprepared specimens of approximately regular shape. For measurements on outcrops, the Shepard earth resistivity tester may be applied. This consists of two long steel electrodes with the ohmmeter and self-contained battery

Fig. 10-8. Substitution method of resistivity determination with mercury electrodes (after Pullen).

mounted on one of the rods. The surface of the rod acting as the cathode is greater than that of the anode, in order to reduce polarization. As may be expected, Wheatstone bridge methods are widely applied for resistivity determinations by continuous or commutated D.C. and low-frequency A.C. Well suited for measurement of high resistance is the bridge shown in Fig. 10-10. R_2 is a comparison resistance of high order, from 10,000 to 1,000,000 ohms; the ratio r_1/r_2 is adjusted in steps up to 1:1000. Then $R_x = R_2 \cdot r_1/r_2$. Resistances up to 10^9 ohms may be measured with this bridge.

Likewise convenient for rock resistivity measurement

Fig. 10-9. Mercury electrode for drill cores (after Pullen).
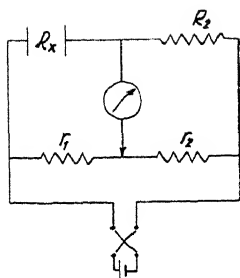
FIG. 10-10. Wheatstone bridge arrangement for rock-resistivity determination.

is the "substitution" method illustrated in Fig. 10-8. A galvanometer deflection is first observed and adjusted by means of the shunt to give a suitable deflection with the unknown resistance in series. Then the switch is thrown over to the known resistance, which is adjusted until the same galvanometer deflection is obtained. The use of this method with A.C. is shown in Fig. 10-12.

For a determination of the resistance of bodies of arbitrary shape, separate measurements of current and voltage are made. Four connections are then necessary for the current and voltage leads. As H. v. Helmholtz pointed out as early as 1853, the current leads may be interchanged with the potential leads without altering the resistance. This value is equal to the ratio of voltage difference and current, multiplied by a factor controlled by the spacing of the electrodes; the method is particularly suitable for measurements of resistivities *in situ*. Since it employs commutated D.C., this procedure will be discussed in the next paragraph.

3. *Methods using commutated D.C.* have attained great practical importance for the determination of resistivity in the laboratory and in the field. One reason is simplicity of technique. D.C. instruments may be used throughout, since the current through the ground may be commutated in synchronism with the current through the meters. In this category are the well-known Wenner-Gish-Rooney and the "Megger" instruments.
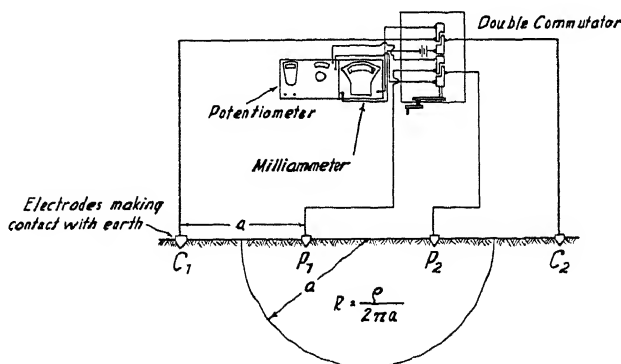
FIG. 10-11. Resistivity determination by four-terminal (Gish-Rooney) method.

The Wenner-Gish-Rooney method is illustrated in Fig. 10-11. It consists of a set of B batteries, a double commutator, four electrodes, a milliammeter, and a potentiometer. Current from the batteries passes through

the milliammeter to the two external electrodes and through the commutator in such a manner that the direction of the current through the ground is reversed periodically while it is passing in the same direction through the milliammeter. The potential difference set up between the internal pair of potential electrodes is likewise of an alternating nature but is "rectified" by the double commutator, so that D.C. potentials are read on the potentiometer. The ratio of voltage and current, multiplied by a spacing factor, gives the resistivity

$$\rho = 2\pi a \cdot \frac{V}{I}. \tag{10-11}$$

The derivation of this formula is given on pages 709-710. If R is substituted for V/I, the formula takes the form $R = \rho/2\pi a$, which is seen to be the resistivity of a hemisphere with the radius a (length of current path $= a$, surface $= 2\pi a^2$) (see Fig. 10-11). On this relation is based the thumb rule that the depth penetration of the Gish-Rooney arrangement is equal to the electrode separation.

The "Megger" differs from the Gish-Rooney arrangement in that a direct reading ohmmeter (cross-coil instrument, giving the ratio of V/I) is substituted for the ammeter and potentiometer and that power is supplied by a hand-cranked generator instead of by batteries (see Fig. 10-60).

4. *Low-frequency A.C. methods.* These methods are well suited for laboratory measurements because low-frequency A.C. is readily available, no commutation device is required, and disadvantages of continuous D.C. are avoided. For high-resistance specimens 110 volt A.C. may be used directly. For lower resistances it should be stepped down by a lamp bank, a carbon resistor, or a transformer. As an indicating instrument, a D.C. current meter of high sensitivity together with a copper oxide rectifier, a vibration galvanometer, or any other oscillographic instrument of high current sensitivity, will be satisfactory. A Wheatstone bridge circuit or the substitution method are applicable (see Fig. 10-12).

Ground resistivity may be determined directly with a Wheatstone bridge, using *two* electrodes only. If their radius is a, if l is the distance between their centers, and R is the resistance measured on the bridge, the resistivity $\rho = \dfrac{2R}{\dfrac{1}{a} + \dfrac{0.8a}{l^2} - \dfrac{0.85}{l}}$. If the distance is a multiple of the electrode radius so that $a = l/n$ the resistivity is

$$\rho = \frac{2R}{n \quad \dfrac{0.8}{nl} \quad 0.85},$$

in which the middle term in the denominator is negligible, so that

$$\rho = \frac{2R}{n - 0.85},$$ (10–12)

which for large electrode separations is equal to $\rho = 2Ra$. This shows that the resistivity between two electrodes depends largely on their radii and therefore on the material in immediate contact with them. In the double electrode setup as described, Koenigsberger used iron discs about $\frac{1}{4}$ inch thick and 10 inches in diameter, with a contact substance of clay or soil soaked with either $FeCl_3$ and $FeSO_4$ or $NaCl$ solution.[4] He applied frequencies between 100 and 400 cycles.

5. *Intermediate-frequency methods.* The use of audio-frequencies from 500 to 1000 cycles facilitates the field technique of resistivity measurements, since phones may be employed as indicating instruments. In the
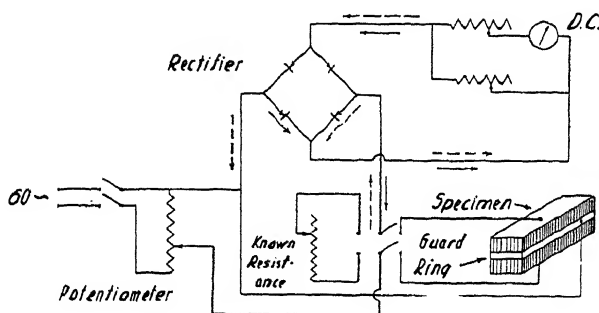
Fig. 10–12. Determination of rock resistivity using 60 cycles (after Pullen).

lower frequency range, effects of inductance and capacitance are generally negligible and some of the arrangements are used as D.C. bridges. Intermediate frequency methods are applied (1) galvanically (by contact with the specimen) or (2) inductively (by measuring the mutual inductance between two loops). The latter are best suited for resistivity measurements on outcrops or horizontally stratified ground, since they function better on comparatively large volumes of earth.

As an example of the galvanic application of intermediate frequency methods, the soil resistivity bridge of the U. S. Department of Agriculture is illustrated in Fig. 10–13.[5] Current is supplied from a battery-operated induction coil or buzzer. A container for the soil sample is in one arm of the bridge, a multiplier resistance in the opposite arm; two sides of a slide-

J. Koenigsberger, A.I.M.E. Geophys. Pros., 221 (1929).
R. O. E. Davis, U.S. Dept. Agr. Circ. No. 423 (July, 1927).
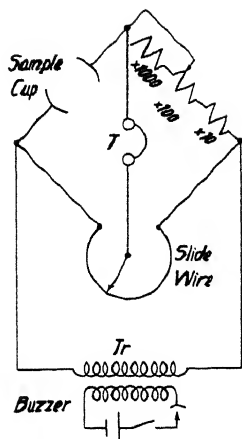
FIG. 10-13. Soil resistivity bridge (adapted from Davis).

wire rheostat comprise the remaining bridge arms. A telephone is used as null indicator. This instrument is primarily a low-resistance device and may be used not only for soils but also for electrolytic solutions. The entire apparatus is portable and is illustrated in the article referred to.

The Zuschlag instrument for rock resistivity determinations (see Fig. 10-14) is a regular A.C. (frequency) bridge, and provision is made to determine both the resistance and the capacitance of the specimen. Power of comparatively low voltage is supplied from a beat-frequency oscillator or buzzer of constant frequency. If in this bridge pure resistances are in three arms and an inductance and capacity in the other, the phone will remain silent if
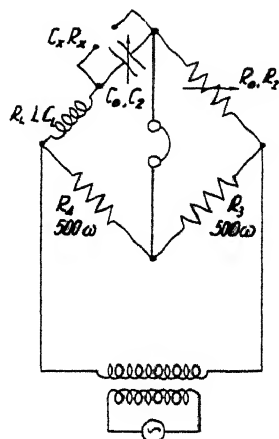
FIG. 10-14. Zuschlag impedance bridge.

$$\frac{R_L}{R_0} = \frac{R_4}{\overline{}} \qquad \text{and if} \qquad \omega = \frac{1}{\sqrt{L(C_0 - \tilde{}}}, \qquad (10\text{-}13a)$$

where C_L is the distributed capacity, R_L the resistance and L the inductance of the coil, C_0 the setting of the condenser, and R_0 the setting of the resistance in the other side of the bridge when balance is obtained. If a high resistance specimen is now connected across the variable condenser, the balance is disturbed and re-established by adjustment of the condenser and resistance. Assuming that the new values to obtain balance are C_2 and R_2, the resistance of the specimen R_x and its capacity C_x are given by

$$R_x = \frac{1 + [\omega C_0 (R_2 - R_0)]^2}{\omega^2 C_0^2 (R_2 - R_0)}$$

and

$$C_x = \frac{C_0}{1 + [\omega C_0 (R_2 - R_0)]^2} - C_2.$$

$$(10\text{-}13b)$$

If R_x is too low to obtain a balance, the specimen may be connected in series with the induction coil and condenser. If C_3 and R_3 are the capaci-

ties and resistances to obtain balance,

$$R_x = \left[\frac{1}{\omega C_0} - \frac{1}{\omega C_3} \right]^2 \cdot \frac{1}{R_3 - R_0} + R_3 - R_0 , \qquad (10\text{--}13c)$$

so that if $C_x = 0$, $R_x = R_3 - R_0$. Also,

$$C_x = \omega \, \frac{\dfrac{1}{C_0} - \dfrac{C_0}{C_3}}{\left(\dfrac{1}{C_0} - \dfrac{1}{C_3} \right)^2 + \omega^2 (R_3 - R_0)^2} . \qquad (10\text{--}13d)$$

A method for determining the ground resistivities by induction is arranged as follows.[6] A circular loop is laid out flat on the ground in such a manner that its radius may be varied. In its center a pick-up coil is set up, likewise in a horizontal position. The e.m.f. induced in it is measured, in respect to amplitude and phase, with a compensator whose pickup coil is connected to the primary loop. An amplifier and phone, or meter, indicates the balance between induced current and compensation current. The e.m.f. induced in the pickup coil (and therefore the field **H**) is dependent on the current I of the frequency f flowing in the primary loop with the radius **R**. If ρ is the resistivity of the medium within range,

$$\frac{\mathbf{H}}{I} = \frac{cf\mathbf{R}}{\rho} , \qquad (10\text{--}14)$$

where c is a constant. The depth penetration is assumed to be equal to the diameter of the loop; hence, the resistivity measured may not be a true but an *apparent* resistivity. Further details will be given in the section on inductive methods (page 797).

6. *High-frequency methods.* The frequencies employed here range from 10 to 100 kilocycles. Several years ago when this frequency band was used extensively, the Radiore Company developed a bridge in which the impedance of the specimen in one arm of the bridge was measured by comparison with a known resistance with capacitance in parallel in the other arm.

Measurements of the ground characteristics at high frequencies *in situ* may be made with a double wire Lecher system[7] or with the single ground wire of a high-frequency generator, buried at a shallow depth parallel with the surface. The current (measured at various points with a thermo-milliammeter) decreases with distance from the source since the waves die out because of space damping. If the wire is long enough so that no re-

[6] J. Koenigsberger, Beitr. angew. Geophys., **3**(4), 392 (1933); 4(2), 201 (1934). See also pp. 782 and 796, this chapter.

[7] M. Abraham, *et al.*, Phys. Zeit., **20**(7), 145 (1919).

flection occurs at the end, the decrease of the current with distance is given by

$$I_x = I_0 \cdot e^{-\gamma x}. \qquad (10\text{--}15a)$$

Assuming further that the displacement current is negligible, the damping coefficient may be written

$$\gamma = 2\pi \sqrt{f\sigma}, \qquad (10\text{--}15b)$$

that is, damping increases with frequency f and ground conductivity σ. It is seen that $I_x = I_0/e$ when $x_e = 1/\gamma$. Hence, $x_e = \dfrac{1}{2\pi}\sqrt{\dfrac{1}{f\sigma}}$, so that

$$\sigma = \frac{1}{4\pi^2 x_e^2 f}, \qquad (10\text{--}15c)$$

if x_e denotes the distance at which the current has dropped to $\dfrac{1}{2.7}$ of its value at the source.

F. Methods for the Determination of Dielectric Constants

Since the capacity of a condenser is proportional to the dielectric constant of the medium within, most laboratory methods for the determination of the dielectric constant make use of the difference in the capacity of a condenser with and without the substance.   (1) The change in capacity may be measured directly by the *resonance* method.   (2) The more common procedure, however, is to determine the impedance of a specimen by a *substitution* method.   (3) The ratio of the reactive and conductive components may be determined by the *phase-shift* method.   (4) Dielectric soil properties may be studied by an analysis of the ellipse of *polarization* of surface radio waves.

1. *Resonance method.*   In all laboratory methods for the determination of soil properties at radio frequencies, a soil condenser is applied, consisting of two concentric cylinders separated by an insulator (Fig. 10-15a). Most measurements consist of, or are equivalent to, determining the geometric capacity C_0 of this condenser and comparing it with its capacity when filled with soil (C_s).

In the resonance method (Fig. 10-15b) a source of RF is coupled to a circuit containing the secondary of a mutual inductance in parallel with a variable condenser C_A and the soil condenser C_s.   The voltmeter V indicates a maximum at the point of resonance.   The soil condenser is first removed and the condenser C_A is so adjusted that resonance is obtained. Assume that its capacity is then C'.   The soil condenser is then inserted

and the air condenser is re-adjusted to the value C'' to give voltage resonance. Since $C_s = C'' - C'$, the dielectric constant is given by $\kappa = (C'' - C')/C_0$, where C_0 is the geometric capacity of C_s. This method also furnishes the conductance component or the equivalent damping factor by an analysis of the shape of the resonance curve, by varying the condenser C_A in steps and observing the corresponding voltages on either side of and at the resonance point. If C_1 and C_2 are two condenser readings obtained on either side of the resonance point where the voltage is $\frac{1}{2}$ of the maximum e.m.f., and if ΔC is the difference of these two readings, the phase shift of the resultant in respect to the conductive component is given by

$$\tan \varphi = \frac{2C_s}{\Delta C}. \tag{10-16}$$

According to eq. (10-10c) the phase shift is $\tan \varphi = \kappa\omega/4\pi\sigma$. In the equivalent circuit (Fig. 10-15c) the reactance component of the current
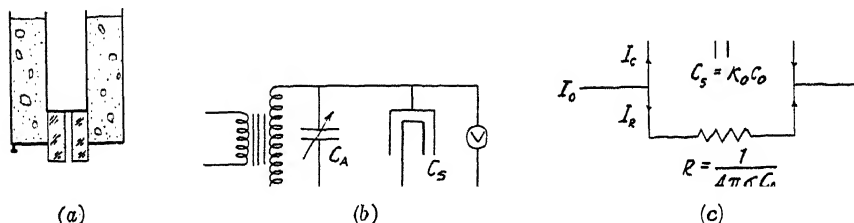
FIG. 10-15. (a) Soil condenser. (b) Resonance method of determining dielectric constants of soils. (c) Reactive and conductive components through soil condenser. (Adapted from Ratcliffe and White.)

I_c is controlled by the effective capacity of the soil condenser, or $C_s = \kappa C_0$, whereas the conductive component is given by the resistance $R = 1/4\pi\sigma C_0$. Hence, by substitution, $R = 2/\omega\Delta C$. The method of determining the conductive component from the decrement of the response curve furnishes good results only for comparatively high frequencies, of the order of 0.2 to 5 megacycles.[8]

2. *Substitution method.* In this method the impedance of the soil specimen is determined[9] by substituting for the coil condenser a simulating unit consisting of a resistance with a condenser in parallel. These are varied until the same resonant output voltage is obtained. A tuned circuit loosely coupled to an oscillator and provided with a beat oscillator and low-frequency detecting unit may be used in these measurements as shown in Fig. 10-16. From the resistance and capacitance components

[8] J. A. Ratcliffe and F. W. G. White, Phil. Mag., **10**, 667 (1930).

[9] C. B. Feldman, I.R.E. Proc., **21**, 764-801 (June, 1933).

read on the simulating unit, the resistivity and dielectric constants can be calculated as in the resonance method (see paragraph 1).

3. *Phase-shift method.* The phase shift between the resultant current and the conductance component can be determined directly in the following manner (Fig. 10–17): A perfect air condenser C_p without appreciable loss angle is connected in series with the soil condenser C_s. Both are placed in a high-frequency circuit and the voltages across the soil condenser and across the perfect condenser are compared on a cathode ray oscilloscope. The current through the soil condenser I_r makes the phase angle φ with the pure conductance component. If a perfect condenser is now placed in series with the soil condenser, the e.m.f. across it will be 90° out of phase with respect to this current and, therefore, have a phase shift of $90 - \varphi$ compared with the e.m.f. across the condenser.
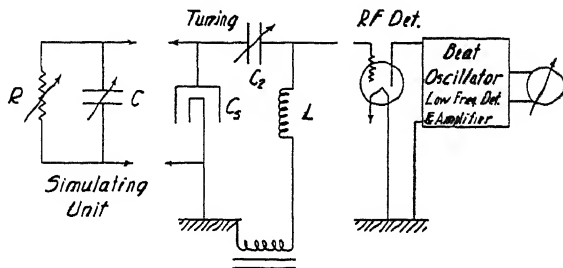
Fig. 10-16. Determination of reactive and conductive components of soils at radio frequencies (adapted from Feldman).

If the condenser terminals are then connected to the four plates of a cathode-ray oscilloscope as shown in Fig. 10–17c, the light spot will trace the resultant of the two voltage components and thus give their phase shift directly.[10]

4. *Polarization measurements.* In this connection, the term "polarization" refers to the polarization of radio waves in the course of their propagation over the earth. This is brought about in the following manner: The radiation from an antenna may be considered as consisting of three component parts: (a) a *space wave,* whose amplitude decreases *inversely with the distance* from the source because of a geometric spreading; (b) a *surface wave,* decreasing in amplitude *inversely with the square root of distance*; and (c) a *ground wave* of a depth penetration generally smaller

[10] C. B. Feldman, Bell Lab. Rec., **12**(12) (Aug., 1934). Ratcliffe and White, loc cit. R. L. Smith-Rose, Roy. Soc. Proc., **A130**, 359 (1933).

than the wave length. Because of the differences in the variations with distance, the radiation in the vicinity of the antenna consists almost entirely of space waves, while at greater distances it approaches more and more the character of a surface wave. In addition to geometric spreading, the amplitude decreases because of absorption. The change from space to surface wave occurs more rapidly the shorter the wave and the lower the conductivity and dielectric constant of the surface and near-surface
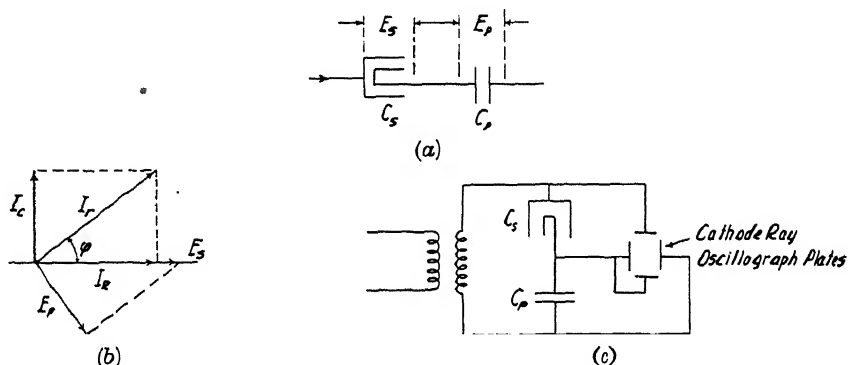
FIG. 10-17. Measurement of phase shift in soil specimen by cathode-ray method (after Ratcliffe and White).

beds. Thus, the variation of the electric and magnetic fields of the radiation may be expressed by the relations:

$$\left.\begin{array}{l} E_r = 120\,\dfrac{\pi ah}{\lambda} \cdot \dfrac{I_0\,(\text{amp})}{r(\text{cm})} \cdot e^{-\beta r}\,(\text{volts cm}^{-1}); \\[3mm] H_r = 4\pi\,\dfrac{ah}{\lambda} \cdot \dfrac{I_0}{r} \cdot e^{-\beta r}\,\text{C.G.S.,} \end{array}\right\} \quad (10\text{--}17)$$

where E is the electric and H the magnetic field, a is the form factor and h the height of the antenna, r the distance from the source, β an absorption coefficient, I_0 the current in the antinode of the antenna, and λ the wave length.

If the earth were a perfect conductor, the electrical field would be at right angles and the magnetic field parallel with the earth's surface, and the electrical and magnetic fields would be in phase. For finite conductivity at the surface or at shallow depth, a forward inclination of the electrical wave front is produced, while the magnetic field remains substantially parallel with the surface. In other words, the electrical field now consists of a vertical component Z and a small horizontal component which are out of phase with respect to each other. The ratio of the peak

amplitudes of the horizontal and the vertical components, as well as their relative phase shift, are functions of the effective conductivity and dielectric constants of the near-surface formations.   According to Zenneck,

$$\frac{X^2}{Z^2} = \frac{jm_0}{1 + jm_1} \quad \text{or} \quad \frac{X}{Z} = \sqrt{\frac{m_0}{\sqrt{1 + m_1^2}}} \cdot e^{j\varphi}, \quad (10\text{--}18a)$$

where the factor $m_0 = f\kappa_0\rho_0/18 \cdot 10^{11}$ (κ_0 = dielectric constant, f = frequency, and ρ = resistivity in ohm-cm) refers to air, and the factor $m_1 = f\kappa_1\rho_1/18 \cdot 10^{11}$ refers to the effective ground properties.   The phase
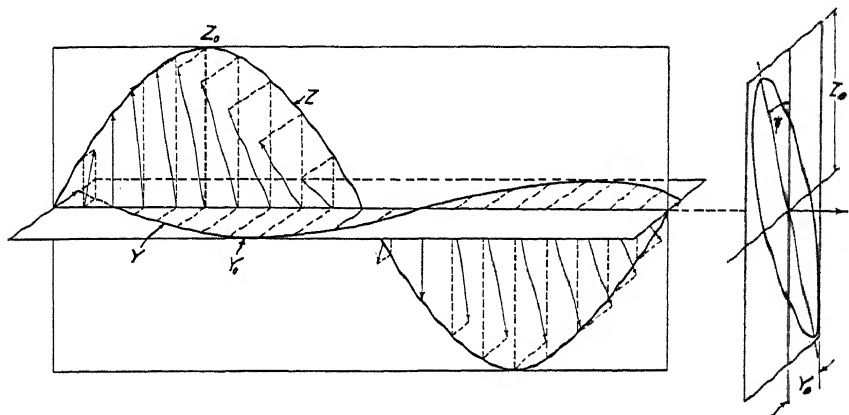
Fig. 10-18. Elliptical polarization resulting from composition of a horizontal and a vertical component which are out-of-phase.

shift between the two components is proportional to the reciprocal of the factor m_1 , so that

$$\tan 2\varphi = \frac{18 \cdot 10^{11}}{} \qquad\qquad (10\text{--}18b)$$

Curves giving the ratio X/Z and their phase shift as functions of dielectric constant and conductivity of the ground have been calculated by Zenneck[11] and Feldman.[12]

Because of the out-of-phase condition of the horizontal with reference to the vertical component, the resultant electrical field vector describes an *ellipse*; this phenomenon is referred to as *elliptical polarization* and plays an important part in all electrical prospecting methods using intermediate and high frequencies.   In Fig. 10-18 a large vertical component is shown as one wave train, and a horizontal component as another, with

[11] *Wireless Telegraphy* (1915), Fig. 300, curves for 670-meter wave length.
[12] I.R.E. Proc., **21**, 790 (June, 1933), Fig. 22, for 16-meter wave length.

a phase shift of $2\pi/10$. For the sake of illustration, the horizontal component is shown at right angles to the direction of propagation (Y) while actually, in the radio surface wave, the horizontal component is in the plane of propagation (X). This, however, does not change the resulting phenomenon or the equations given later.

If for each instant the position of the resultant vector is constructed and then the ends of the vectors are projected on one plane, they lie on the circumference of an ellipse. The maximum vertical and horizontal components are tangents to this ellipse, and its tilt angle depends on the ratio of the two components as well as their relative phase shift. As shown below, the ratio of major and minor axes of this ellipse may be measured conveniently in the field. If their ratio (see Fig. 10–19) b/a
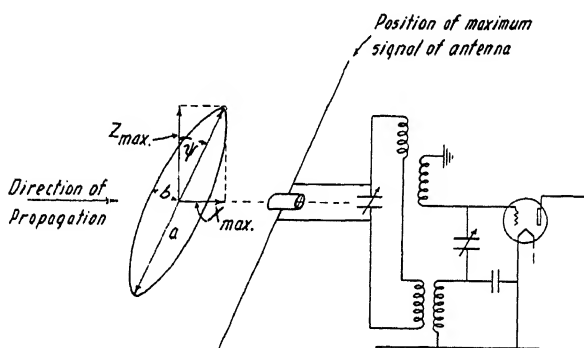
Fig. 10-19. Ellipse of polarization and receptor with rotatable antenna to measure compression and obliquity of this ellipse (adapted from Feldman).

is designated by r, the ratio of the horizontal and vertical components is given by

$$\left(\frac{X}{Z}\right)^2 = \frac{(r^2 - 1)\sin^2\psi + 1}{(r^2 - 1)\cos^2\psi + 1},\qquad (10\text{–}18c)$$

where ψ is the tilt angle of the ellipse.

The following equation[13] for the relation between phase shift φ, tilt angle ψ, and intensity ratio, follows from the geometry of the ellipse:

$$\cos\varphi = \tfrac{1}{2}\tan 2\psi\left(\frac{Z}{X} - \frac{X}{Z}\right).\qquad (10\text{–}18d)$$

An apparatus for the determination of these quantities is illustrated in Fig. 10–19. It consists of a receiver with a rotatable double L antenna

---

[13] Derived on p. 690.

which is first oriented in the plane of polarization and then rotated until minimum signal is obtained.   The axis of the double antenna is then in the direction of the minor axis of the ellipse.   Ninety degrees from this position a maximum signal will be observed.   The ratio of the maximum and minimum signals gives the ratio r.   The inclination of the antenna in the position of minimum signal gives the tilt angle of the ellipse and, therefore, the ratios of the horizontal and vertical components and the phase shift between them.   From these, the effective ground conductivities and dielectric constants may be determined by trial and error with
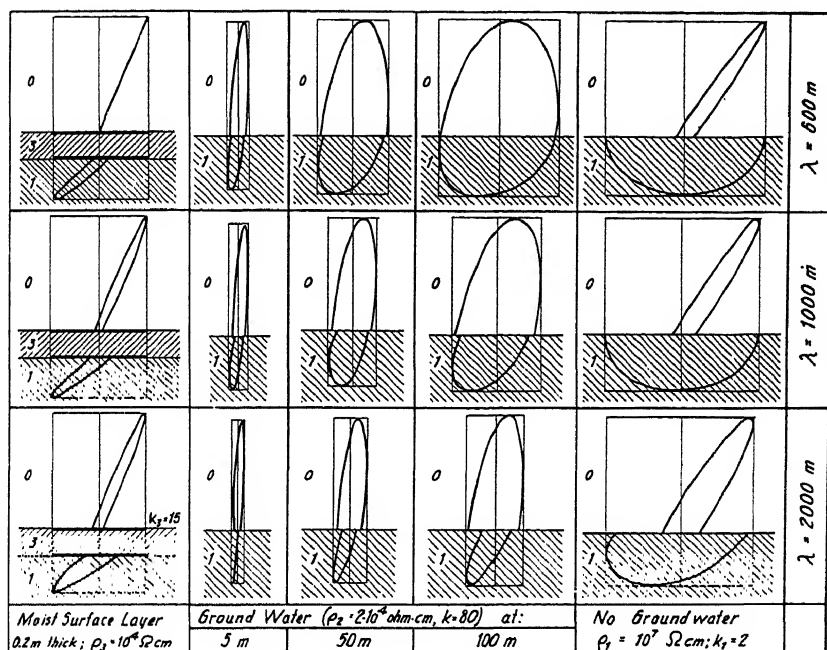
FIG. 10-20. Ellipses of polarization for surface and ground waves, for various frequencies, and for various conductivities and dielectric constants (after F. Hack).

the help of curves referred to in the last footnote.   Changes in dielectric constants are of less effect than changes in conductivity.   For both long and short waves it is observed that with an *increase* in *conductivity* the *horizontal component vanishes* and that the *phase* shift *approaches 45°*. The ground wave referred to before may be considered as a surface wave having penetrated into the ground, with concomitant modification of wave front and polarization due to the electrical properties of the surface strata.   The ellipse of polarization takes different forms, depending on whether the surface beds are dry to the depth of penetration, a moist

surface layer is present, or a ground water level exists. These conditions affect not only the ground wave but the surface wave as well. Both are shown schematically in Fig. 10–20.[14]

G. RESISTIVITIES AND DIELECTRIC CONSTANTS OF MINERALS, ORES, ROCKS, AND FORMATIONS

Resistivities of minerals, ores, rocks, and formations vary within much wider limits than their other physical properties. For instance, the density may vary between the limits of 1 and 8 for minerals and between 1.5 and 4 for rocks and formations. The range of elastic wave speeds in formations is from about 150 to 7000 meters per second; magnetic susceptibilities vary from 2 to 1×10^{-6}. Extremes in electrical resistivity are represented by silver with 1×10^{-6} ohm-cm and by sulfur with 10^{18} ohm-cm. This range is not encountered in practice. It is probably greatest in ore prospecting and lies between 10^{-2} and 10^{7} ohms, which corresponds to 10 powers. For comparisons of resistivities it is therefore advantageous to apply a logarithmic scale.

Minerals and rocks may be divided according to resistivity into three groups, each of which comprises a range of 8 powers:

1. Minerals of *good conductivity*, in the range of 10^{-6} to 10 ohm-cm.

2. Minerals and rocks of *intermediate conductivity*, covering the range from 10^{2} to 10^{9} ohm-cm.

3. Minerals and rocks of *poor conductivity*, in the range of 10^{10} to 10^{17} ohm-cm.

In the first group are the metallic elements and graphite, the arsenides, the tellurides, the sulfides with the exception of sphalerite, cinnabar, and stibnite. The group also includes a few of the oxides, such as specularite, magnetite, pyrolusite, and ilmenite, although these are on the border line between the first and the second group. In the second and largest group of intermediate conductors are the oxide minerals except those mentioned above, most ores, virtually all rocks possessing electrolytic conductivity, and anthracite. Most minerals, particularly the rock-forming types, such as all silicate minerals, the phosphates, and the haloids, belong in the third group of poor conductors, as do also the hydrates, borates, nitrates, carbonates, sulfates, chromates, and molybdates.

In Tables 62 through 70 resistivities are given in the following order: elements, arsenides, tellurides, sulfides, oxides, haloids, various rock-forming minerals, and miscellaneous commercial minerals. Then follow the ores and rocks with impregnations of conductive minerals. Next is a tabulation of resistivities of igneous and metamorphic rocks, determined

---

[14] F. Hack, Ann. Phys., **27**, 43–63 (1908).

TABLE 62

RESISTIVITIES OF ELEMENTS AND MINERALS

RESISTIVITY IN OHM-CM

MINERAL	INVESTIGATOR	Good Conductors						Intermediate Conductors								
		10^{-6}	10^{-5}	10^{-3}	10^{-2}	1	10	10^2	10^3	10^4	10^5	10^6	10^7	10^8	10^9
Elements															
Graphite, C	Sundberg				3										
Arsenides															
Nicollite, NiAs	Reich			2											
Tellurides	"			7--3											
Sulfides															
Covellite, CuS					3										
Galena, PbS	Sundberg					5--5									
Pyrrhotite, Fe_6S_n	"						5								
Pyrite, FeS_2	"					1									
Chalcopyrite	Edge & Laby					1.2									
Bornite, Cu_3FeS_3	" "					3									
Marcasite, FeS_2	Sundberg						1--1								
Molybdenite, MoS_2	"						8								
Cinnabar, HgS	Löwy													5	
Stibnite, Sb_2S_3	"														
Sphalerite, ZnS	Sundberg												1		
Oxides															
Specularite, Fe_2O_3	Koenigsberger					4-8									
Magnetite, Fe_3O_4	Sundberg					6--1									
Pyrolusite, MnO_2	Löwy							5--5							
Ilmenite, $FeTiO_3$	"							5--5							

RESISTIVITY IN OHM-CM

MINERAL	INVESTIGATOR	Good Conductors	Intermediate Conductors								Poor Conductors						
		10	10^2	10^3	10^4	10^5	10^6	10^7	10^8	10^9	10^{10}	10^{11}	10^{12}	10^{13}	10^{14}	10^{15}	10
Hematite, Fe_2O_3	Löwy						4--------1										
Limonite, $2Fe_2O_3 \cdot 3H_2O$	"						1										
Wolframite, (Fe, Mn)(WO_4)	"			1													

Table 62—Concluded

RESISTIVITIES OF ELEMENTS AND MINERALS

RESISTIVITY IN OHM-CM

Mineral	Investigator	Good Conductors	Intermediate Conductors								Poor Conductors						
		10	10^2	10^3	10^4	10^5	10^6	10^7	10^8	10^9	10^{10}	10^{11}	10^{12}	10^{13}	10^{14}	10^{15}	10^{16}
Halides																	
Impure rock salt	Koenigsberger			3	—	5											
Various Rock-Forming Minerals																	
Serpentine	"				2												
Hornblende	"									1							
Mica	Sundberg										1.5	—					9	
Quartz, SiO_2	"												3.8	—	1.2			
Calcite, $CaCO_3$	"														5.5			
Misc. Commercial Minerals																	
Sulfur	Curtis & Thornton														10^{14}		10^{17}
Bituminous coal	Ewing	6—	–1														
Anthracite	"		1-2														
Coal	Koenigsberger					2–	–5										
Coal, dry & CO_2	"								1								
Fire clay	Hawkins			1.9													
Coal seam	Schlumberger				4–	1.0											

RESISTIVITY IN OHM-CM

Mineral	Investigator	Good Conductors								Intermediate Conductors						
		10^{-6}	10^{-5}	10^{-4}	10^{-3}	10^{-2}	10^{-1}	1	10	10^2	10^3	10^4	10^5	10^6	10^7	10^8 10^9
Carbonates												7.1					
Siderite, $Fe_2(CO_3)_3$	Sundberg										7.1					
Waters[a]																
Saline water, 20%	Edge & Laby						5.1									
Saline water, 10%	" "						8.2									
Saline water, 3%	" "							1.5								
River water (Montana)	Erdmann										5.5					

[a] For average values of waters in different geologic provinces, see p. 638.

TABLE 63

RESISTIVITIES OF ORES

ORE	LOCALITY	INVESTIGATOR	Good Conductors				Intermediate Conductors							
			10^{-2}	10^{-1}	1	10	10^2	10^3	10^4	10^5	10^6	10^7	10^8	10^9
Chalcopyrite	Quebec	Gilchrist	2.1											
Pyrite	Sweden	Lundberg, et. al.	1											
Native copper	Arizona	Sundberg	1											
Cong. with Cu	Michigan	"	2											
Galena	Joplin, Mo.	"	1											
Sphalerite, dry, & +10% pyrite	Quebec	Gilchrist				4.95	—	—	1.4					
Blende ore (no iron)	Missouri	Sundberg									5			
Zincite	Franklin Furnace, N. J.	"		3										
Chalcocite	Butte, Mont.	Sundberg				6								
Pyrrhotite	"	"		7										
Chromite	Canada	Gilchrist								1.3				
Chromite	New York	Lee											1.7	
Hard graphite	Sweden	Hunkel	2-4											
Magnetic ore	Sweden	Sundberg			1—		—1							
Magnetite	New York	Lee										7.5		
Brown hematite ore	Sweden	Sundberg											1	

TABLE 64

RESISTIVITIES OF ROCKS WITH CONDUCTIVE MINERAL IMPREGNATIONS

ROCK	LOCALITY	INVESTIGATOR	Good Conductors				Intermediate Conductors							
			10^{-2}	10^{-1}	1	10	10^2	10^3	10^4	10^5	10^6	10^7	10^8	10^9
Graphite slate	Sweden	Lundberg, Sundberg		5—	—	—	3.5							
Rock with disseminated pyrrhotite	Falconbridge, Ont.	Gilchrist				1—	—	—	—	—	.85			
Volcanic rock with chalcopyrite and sphalerite—sulfides equal 20% of specimen	"	"					1.7							

TABLE 64—*Concluded*

RESISTIVITIES OF ROCKS WITH CONDUCTIVE MINERAL IMPREGNATIONS

Rock	Locality	Investigator	Good Conductors				Intermediate Conductors							
			10^{-2}	10^{-1}	1	10	10^2	10^3	10^4	10^5	10^6	10^7	10^8	10^9
Limestone with lenses of hematite	Algeria	Schlumberger							1.2 to 4					
Sericite slate with pyrite	Quebec	Gilchrist									3.5			
Hornblende with graphite and pyrite	Bavaria	Hunkel									8	—	1	
Hornblende syenite with magnetite	"	"											1	

TABLE 65

RESISTIVITIES OF IGNEOUS & METAMORPHIC ROCKS

Rock	Locality	Investigator	Dir.	Freq.	Intermediate Conductors							
					10^3	10^4	10^5	10^6	10^7	10^8	10^9	10^{10}
Specimens												
Diabase	Idaho	Sundberg	3				3.1					
Granite	Bavaria	Hunkel	3							1		
Devonian slate	Harz	Ebert					2					
" "	"	"						6.5				
Porphyry, schistose	S. Australia	Edge & Laby		100			3					
Serpentine		Eve & Keys					3-	-2				
Diorite	Bavaria	Hunkel	3					1				
Gabbro	Mineville	Lee & Boyer		D.C.					1.0	——	1.4	
Garnet gneiss	Bavaria	Hunkel	3						2			
Hornblende gneiss	Mineville	Lee		D.C.						1-6		
Gray biotite gneiss	"	Lee & Boyer		D.C.						4		
Syenite	Bavaria	Hunkel	3							1		
In Situ												
Graphitic schist	Normandy	Schlumberger		16	1-	1						
Schists	Missouri	Poldini			2-	6						
Hard calc. schist	Belgian Congo	Geoffroy & Charrin				2-	1.1					
Mica schist (hard packed)	Washington, D. C.	Gish & Rooney		16			1.3					
Quartz porphyry (slightly altered)	Newfoundland	Kihlstedt				3.4						

Table 65—*Concluded*

RESISTIVITIES OF IGNEOUS & METAMORPHIC ROCKS

Rock	Locality	Investigator	Dir.	Freq.	Resistivity in ohm-cm Intermediate Conductors							
					10^3	10^4	10^5	10^6	10^7	10^8	10^9	10^{10}
Keweenawan lavas	Michigan	Hotchkiss, et. al.		10–15		1.2	—	4.4				
Greenstone	"	Rooney		16			1.1					
Porous trap-rock	"	"		16		1.6						
Pre-Cambrian	Sweden	Sundberg					3–6					
Granite	Washington, D. C.	Gish & Rooney		16			5					
Slightly altered syenite	Ontario	Kihlstedt		200			2.4 3.7					
Massive vein quartz	"	"		200				2				
Diabase	Michigan	Rooney		16		4.5						
Serpentine	Ontario	Kihlstedt		200		2.1 5.3						

Table 66

RESISTIVITIES OF CONSOLIDATED SEDIMENTS[15]

Rock	Locality	Investigator	Dir.	Freq.	Resistivity in ohm-cm			
					10^2	10^3	10^4	10^5
Shales and Slates								
Chattanooga shale (Dev.)	Cent. & south Illinois	Hubbert		50				1.4
Shale & glacial drift				50				
Nonesuch shale	Houghton Co., Mich.	Hotchkiss, et. al.		10–15			1.8	
Shale	W. Hancock, Mich.	Rooney		60				
Slate		Lee, Joyce, & Boyer		0			6.4	
Clay (wet)	Jugoslavia	Loehnberg & Stern		D.C.		2.1		

[a] Electrode spacing in four-terminal method, in feet.

[15] Determined in the field.

TABLE 66—*Continued*

RESISTIVITIES OF CONSOLIDATED SEDIMENTS

ROCK	LOCALITY	INVESTIGATOR	DIR.	FREQ.	a^a	RESISTIVITY IN OHM-CM					
						10^2	10^3	10^4	10^5	10^6	10^7
Grinneld argillite	N½ sec. 23, T32N R20W, Flathead Co., Montana	Erdmann	dip 32°	16							
					10			1.7			
			‖ to stratification		20		9.6				
					20			1.1			
					30			1.0			
			⊥ to strike		10		8.7				
					20		7.4				
					40			1.1			
Grinneld argillite	" (Water's Edge)	"	dip 32°	16				1.3			
			‖ to strike		15			1.4			
					30		8.0				
		.					8.2				
					10		7.7				
Argillite (Missoula group); pre-Cambrian, thin-bedded, platy argillite; resembles Grinneld	Sec. 27, T 32N R20W, Flathead Co., Montana	"	dip 31°	16							
					10			1.4			
					20			1.6			
			⊥ to strike		30			1.5			
		.			40			1.4			
					50			1.5			
									1.1		
Conglomerates											
Great conglomerate outcrop	Eagle Harbor, Mich.	Hotchkiss, et. al.		10–15							
Calumet & Hecla conglomerates	Michigan	Rooney		60					2	1.3	
Sandstone											
Eastern sandstone	Michigan	Hotchkiss, et. al.		10–15				3.5–1.2			
Eastern sandstone	"	Rooney		16				4.3			
Muschelkalk ss. (Triassic)	Lorraine	Schlumberger		16				7			
Sandstone (Tertiary Oligocene); soft, friable; extremely fine grained ss.; pale green to yellowish and buff; contains thin beds of lignite	Coal Creek Road, Flathead Co., Montana	Erdmann	dip = almost 0	16	10			8.8			
								9.8			
					20			6.2			
								6.7			
					30			4.8			

TABLE 66—*Concluded*

RESISTIVITIES OF CONSOLIDATED SEDIMENTS

ROCK	LOCALITY	INVESTIGATOR	DIR.	FREQ.	a^a	RESISTIVITY IN OHM-CM					
						10^3	10^4	10^5	10^6	10^7	10^8
Armorican ss. compact Siliceous-Ordovician	Normandy	Schlumberger						1			
Ferruginous sandstone (Jurassic)	Switzerland	Koenigsberger						·4			
Limestone											
Muschelkalk ls. (Triassic)	Lorraine	Schlumberger		16		6					
Limestone with lenses of hematite	Algeria	"					1.2–4				
Muschelkalk oolitic ls. (Triassic)	Lorraine	"		16			1.8				
Limestone	Mississippian (Missouri)	Poldini					3–4				
Siyeh ls., hard homogeneous, dark bluish-gray, siliceous magnesium ls.; pre-Camb.	SW cor. sec. 5 T29N R18W Flathead Co., Montana	Erdmann	dip 54°　∥ to strike　⊥ to strike	16	10 20 30 10 20 30 50		6.8　　3.6 5.4 7.9 6.6 6.9 6.1 8.1	–1.4 1.5 1.4			

TABLE 67

RESISTIVITIES OF UNCONSOLIDATED FORMATIONS (MOSTLY QUARTERNARY)

FORMATION	LOCALITY	INVESTIGATOR	a^a	FREQ.	RESISTIVITY IN OHM-CM					
					10^2	10^3	10^4	10^5	10^6	10^7
Marls										
Marl & gypsum	Germany	Schlumberger		16	3–	1.2				
Marl & gypsum	Algeria	"		16		1–3				
Jarnisy marls	Lorraine	"		16		5				
Marls	"	Geoffroy				7				

^{a} Electrode spacing in four-terminal method, in feet.

TABLE 67—*Concluded*

RESISTIVITIES OF UNCONSOLIDATED FORMATIONS (MOSTLY QUARTERNARY)

FORMATION	LOCALITY	INVESTIGATOR	a^a	FREQ.	RESISTIVITY IN OHM-CM					
					10^2	10^3	10^4	10^5	10^6	10^7
Clay										
Clays with Mg salts	Australia	Rooney		16	1-2					
Clay (wet)	Palestine	Loehnberg		D.C.	5-	-4				
Boulder clay (no gravel)	Montana	Erdmann	10				2.1			
			20				2.3			
Marine clay	Ontario	Hawkins					3.6			
Dry clay	New Jersey	Feldman		40 mc.[b]			5.1			
Wet clay	" "	"					8			
Boulder clay (wet)	Montana	Erdmann	20					1.1		
Alluvium and Silt										
Alluvium (moist)	Montana	"	10				2.3			
Silt (dry)	"	"	5				2.0			
			10				1.3			
			20				1.4			
Glacial out-wash (dry)	Washington (state)	"	10					1.3		
" "	"	"	10					1.6		
" "	"	"	10					2.1		
Fluvio glacial till (wet)	"	"	20					8.4		
			40					5.7		
			60					4.9		
			100					3.9		
Glacial	Connecticut	Leonardon						5		
River gravel (wet)	Montana	Erdmann	10					1.2		
" " "	"	"	10					1.4		
Yellow river sand (3.3% moisture)		Sundberg						1.7		
Yellow river sand (0.86% moisture)		"						8.3		
Stream gravel (wet)	Montana	Erdmann	10					3.3		
			15					3.3		
			20					3.2		
River gravel (wet)	Colorado	"	10					4.8		
			10					6.5		
			10					4.8		
			10					8.9		

[b] mc. = megacycles = 10^6 cycles.

on specimens in the laboratory; this is followed by a tabulation of resistivities determined on the same group of rocks *in situ*. The remaining tabulations give resistivities of consolidated and unconsolidated sedimentary rocks, determined in the field, and of oil bearing formations, most of them measured by electrical logs.

<div align="center">TABLE 68</div>
<div align="center">RESISTIVITIES OF OIL FORMATIONS[16]</div>

FORMATION	LOCALITY	INVESTIGATOR	RESISTIVITY IN OHM-CM									
			10^2	10^3	10^4	10^5	10^6	10^7	10^8	10^9	10^{10}	10^{11}
Oil sand—fair	Salt Dome, Hull, Texas	Deussen & Leonardon	4									
Oil sand—good	" "	"		1.8								
Lower oil formation (daily av. 30 tons)	Tintea	Koenigsberger	6									
Upper oil formation (2000 to 60 tons)	"	"		1.5-7								
Heavy saturated oil sand	Seminole field, Oklahoma	Schlumberger & Leonardon		9-	1.1							
Associated beds	" "	" "	5.6									
Very productive sands	Maracaibo Dist., Venezuela	" "		7.6								
Same ss.; no oil, H_2O saturated	" "	" "	5									
Oil sands, much oil	Grozny Dist., Russia	" "				2.2						
Sand (dry)	" "	" "		2.5								
Productive formations	" "	Koenigsberger "			5-8							
Same, with shows	" "	"		6								
Oil horizon, 320 tons per day	Dacian field, Rumania	Deussen & Leonardon		4								
Oil horizon, 110 tons per day	" "	" "		2								

[16] Most of these were measured by electrical logs.

<div align="center">TABLE 69</div>
<div align="center">DIELECTRIC CONSTANTS—MINERALS AND OTHER SUBSTANCES</div>
<div align="center">κ' = apparent dielectric constants; κ_0 = true dielectric constants, e.s.u.</div>

MATERIAL	LOCALITY	INVESTIGATOR	FREQ. CYCLES	DIR.	κ'	κ_0
Elements or Substances						
Ice		Pohl				3.2
Petroleum		Various authors				2.07-2.14
Water		" "				81
Minerals						
Sulfur		Schmidt	4×10^8	3 cryst. axes		3.60; 3.9-4.7
Quartz		"	4×10^8	$\perp$; ∥ 3 cryst. axes		4.3-46
Gypsum		"	4×10^8	3 cryst. axes		5.0; 5.1; 9.9

<div align="center">Table 69—Concluded</div>

DIELECTRIC CONSTANTS—MINERALS AND OTHER SUBSTANCES

κ' = apparent dielectric constants; κ_0 = true dielectric constants, e.s.u.

MATERIAL	LOCAL-ITY	INVESTI-GATOR	FREQ. CYCLES	DIR.	κ'	κ_0
Rock salt		Schmidt	4×10^8			5.6
Anthracite		Ambronn				5.6–6.3
Anhydrite		"				6–7
Dolomite		Schmidt	4×10^8	‖; ⊥ cryst. axes		6.8; 7.0
Siderite		"	4×10^8	" "		6.9; 7.9
Barite		"	4×10^8	3 cryst. axes		7.7; 7.6; 12.2
Augite		"	4×10^8	" "		6.9; 7.1; 8.6
Calcite		"	4×10^8	‖; ⊥ cryst. axes		8.0; 8.5
Sphalerite		Rubens				8.3
Muscovite		Poole				9
Limonite		Löwy				10–11
Cassiterite		Rubens	4×10^8			12.7
Hematite		Löwy				25

<div align="center">Table 70</div>

DIELECTRIC CONSTANTS—ROCKS AND FORMATIONS

= apparent dielectric constants; κ_0 = true dielectric constants, e.s.u.

MATERIAL	LOCALITY	INVESTIGATOR	FREQ.	DIR.	κ'	κ_0
Marble		Fleming				6
Granite (dry)	Germany	Löwy				8
Limestone	"	Stern				8–12
Diorite	"	Löwy				8.5
Sandstone (dry)	"	"				9–11
Syenite	"	"				12
Basalt		"				12
Porphyry	"	"				9–10
Gneiss	France	"				14
Mica schist	Germany	Stern				16
Schist	"	Löwy				16–17
Chalk (mois. 24%)	Baldock, Eng.	Smith-Rose	10 mc.[a]		21	
Dark fibrous loam (mois. 60%)	Rugby, Eng.	"	10 mc.		54	
Soil (mois. 3.6%)	Teddington, Eng.	"	10 mc.		1	
Dry river sand		Fleming				2–3
Dry clay		"	long wave			2–5
Dry clay (stone chips)	Netcong, N. J.	Feldman	20 mc.			7–10
			30 mc.		1.5	7–10
			40 mc.			7–10
Soil (mois. 11%)	Teddington, Eng.	Smith-Rose	10 mc.			8–10
Sandy loam	Holmdel, N. J.	Feldman	10 mc.			11
Sandy loam	" "	"	20 mc.			11
Dry topsoil	" "	"	10 mc.			15

[a] mc. = megacycles

TABLE 70—*Concluded*

DIELECTRIC CONSTANTS—ROCKS AND FORMATIONS

κ' = apparent dielectric constants; κ_0 = true dielectric constants, e.s.u.

MATERIAL	LOCALITY	INVESTIGATOR	FREQ.	DIR.	κ'	κ_0
Dry topsoil	Holmdel, N. J.	Feldman	40 mc.			12
			30 mc.			13
			20 mc.			14.5
Soil (mois. 17%)	Teddington, Eng.	Smith-Rose	10 mc.		17–20	
Dry clay	Holmdel, N. J.	Feldman	40 mc.			19.5
			30 mc.			22
			20 mc.		0.5	23.5
			10 mc.			26.5
Loam & clay (mois. 15%)	Rugby, Eng.	Smith-Rose	10 mc.		21	
Chalk (mois. 26%)	Baldock, Eng.		10 mc.		38	
Wet topsoil	Holmdel, N. J.	Feldman	20 mc.			23
			30 mc.			23
			40 mc.			23
Subsoil (wet)	" "	"	20 mc.			28
			30 mc.			28
			40 mc.			28
Wet clay	" "	"	20 mc.			29
			10 mc.			32
Blue clay (mois. 23%)	Rugby, Eng.	Smith-Rose	10 mc.		29	
Blue clay (mois. 25%)	" "	"	10 mc.		46	
Daventry soil (moist)	Daventry, Eng.	Ratcliffe & White	3 mc.			39
Clay and sand (mois. 21%)	Rugby, Eng.	Smith-Rose	10 mc.		42	
Cambridge soil (moist)	Daventry, Eng.	Ratcliffe & White	2 mc.			43
Loam & clay (mois. 33%)	Rugby, Eng.	Smith-Rose	10 mc.		43	
Clay & sand (mois. 26%)	" "	"	10 mc.		48	

III. SELF-POTENTIAL METHOD

A. GENERAL

The self-potential method is the only electrical method which uses a *natural* field, that is, one supplied by *spontaneous* electrochemical phenomena. All other electrical methods use artificial electric fields.

The electrical activity of ore bodies and the potentials associated with (1) concentrations of metals in placers, (2) the corrosion of pipe lines, (3) the movement of underground waters, and (4) foundation boundaries all arise from concentration differences of electrolytic solutions in contact

with metallic objects, from chemical differences of the materials coming in contact with solutions, and (in exceptional cases) from electrofiltration. These phenomena were discussed in detail in section II. In eq. (10-1a) a relation was given between the potential and the ratio of the solution pressures of two different substances in electrolytic solutions of different concentration; eq. (10-3) stated the conditions responsible for electrofiltration potentials.

In the spontaneous polarization of ore bodies, the potentials arising from differences in solutions and from differences in materials appear to be related to one another as cause and effect. Differences in the solutions contacting different portions of an ore body (which probably consisted at first of the same material throughout) have brought about, largely through the medium of oxidation, a condition of unbalance which in turn is responsible for the potentials observed. Near the surface, the atmospheric agencies form an aerated zone *rich in oxygen*, while at the lower portion of the ore body the solutions are either poor in oxygen or are even of a *reducing* nature. The oxidation of the pyrite at the top proceeds in accordance with the relation

$$FeS_2 + 7O + H_2O = FeSO_4 + H_2SO_4 .$$
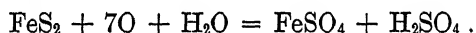
The ferrous sulfate is readily transformed to ferric sulfate since

$$2FeSO_4 + H_2SO_4 + O = Fe_2(SO_4)_3 + H_2O.$$

Ferric sulfate in turn changes by hydrolysis to hydrous ferric oxide (limonite):

$$Fe_2(SO_4)_3 + 6H_2O = Fe_2O_3 \cdot 3H_2O + 3H_2SO_4 .$$

The sulfuric acid formed in this process is mostly neutralized by the carbonates (calcite, limestones, and the like) in the adjacent formations. The last relation explains the formation of the gossan in the zone of oxidation. Minerals contained in it have a lower solution pressure than the unaltered ones in the lower end of the ore body. Hence, in accordance with eq. (10-1c), a potential difference is set up between the upper end and the lower end of the ore body. A current is then flowing downward in the ore body as well as around it outside; the zones of ingress of this current are above the top of the body and are indicated by a negative potential center (see Fig. 10-21).

Although pyrite shows the strongest spontaneous polarization, it is not the only mineral exhibiting this property. Activity has been observed also on *pyrrhotite, magnetite, cobalt ore, graphite,* and *anthrazite*; on formation boundaries; and in connection with the corrosion of iron pipes.
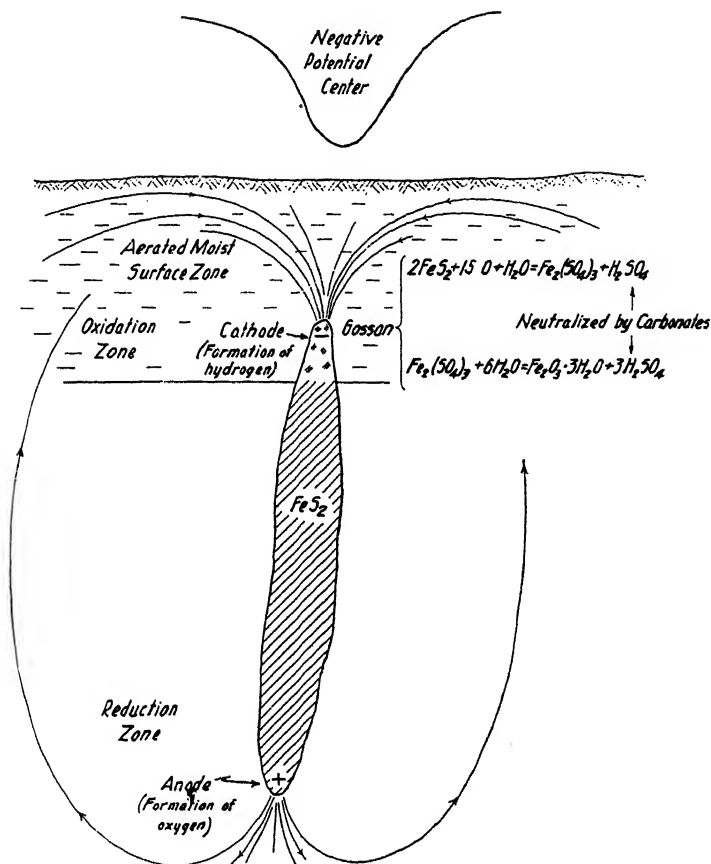
FIG. 10-21. Chemical reaction and electrical activity on pyrite ore body.

B. EQUIPMENT; ELECTRODES; SURVEYING PROCEDURE

The object of a spontaneous polarization survey in mining is the localization of negative centers. This may be done by surveying (a) *equipotential lines*, or (b) *potential profiles*. In either case nonpolarizable electrodes ("porous pots") are employed. The theory of these was discussed in section II (page 630). Special attention is given to an *identity* of *electrode potentials* (that is, maintenance of a *saturated* solution). Polarization (and current density) is kept at a minimum by making the electrode *surfaces* in contact with the copper sulfate as *large* as possible. All electrode metals are usable that act reversibly, that is, metals in their salt solutions, (Cu in $CuSO_4$, Zn in $ZnSO_4$, and so on). In practice, Cu in $CuSO_4$ electrodes are most widely employed. The electrodes are satisfactory when the voltage between a pair does not exceed 1.10^{-3} volts.

Details on construction and operation have been given by Edge and Laby[17] (see also Fig. 10–22).

Lines of equal potential are measured by locating points between which no current flows. This is a null method and requires only a sensitive galvanometer. A *high-resistance milliammeter*, zero center, with a range of 300 to 400 milliamperes and reading to an accuracy of $\frac{1}{2}$ milliampere, is most suitable. Potential differences along "potential profiles" are measured with a potentiometer whose accuracy should be about 1 milli-volt, and which should read up to 1 volt. Extensively used for both self-potential and resistivity measurements is the Leeds and Northrup pH potentiometer, which is described in more detail in section v on resistivity methods[18] (see page 724, Fig. 10–59a).

In a new area, the field procedure is largely determined by terrain conditions. If the area is accessible, fairly level, and reasonably moist to give good contact, the equipotential lines can be traced directly. In more difficult terrain straight-line traverses are first laid out with tape and compass perpendicularly to the supposed strike, so as to intersect such surface indications as may be available. Numbered wooden pegs are fixed along them at from 20 to 100 foot intervals. Having determined and noted the potential difference between the two electrodes placed at the first two pegs on the traverse, and noted the polarity of the forward station, the operator moves the forward electrode and potentiometer to the next peg forward while the assistant moves the rear electrode to the position just vacated by the operator. Readings are plotted in the form of potential gradients (referred to unit distance) or in the form of potentials calculated by progressive addition of potential gradients. Potential differences recorded on (normal) ground free from minerals are usually small and irregular. Ore bodies produce large and steady gradients which are readily recognized. If the reconnaissance shows a well-defined gradient of the order of $\frac{1}{2}$ of a millivolt or more per foot, which persists over distances of several tens or hundreds of feet, time may often be saved by mapping equipotential lines.

FIG. 10-22. Porous pot electrodes (*Heiland Research Corp.*).

In this procedure, the potentiometer (or a milliammeter, which is faster

[17] A. B. Edge and T. H. Laby, *Principles and Practice*, etc., pp. 208-240.
[18] See also *ibid.*, pp. 236-237.

in this particular procedure) and one electrode are placed at a point on the reconnaissance traverse at which the gradient is steep and regular. The assistant then takes the second electrode, connected to the potentiometer or milliammeter by a 50- to 100-foot length of insulated wire and applies it to the ground in a succession of trial points situated approximately on the circumference of a circle, the radius of which is determined by the length of the wire. The operator, in watching the direction and the amount of deflection of the galvanometer[19] or milliammeter for each of the trial contacts, will be able to direct the assistant to the point of equal potential at which no deflection is observed. A stake is driven at this point and the operator moves up to it while the assistant moves forward to locate the third equipotential point. With a type of electrode to which a small milliammeter is permanently fastened, the survey may be expedited by leaving one electrode stationary with the assistant while the operator moves the other to a point of zero current. Equipotential-line surveys should be closed back to the starting point. As soon as an equipotential line has been traced, the disposition of the electric field and the approximate location of a negative center will be known. Its precise position is established by surveying other equipotential lines at arbitrary intervals of constant potential difference which may be spaced with the potentiometer.

With a milliammeter, potential differences may be determined as follows: Two resistors are placed in series with the electrodes, one of unknown resistance R_0 (resistance of milliammeter included) and the other of variable resistance R. First, a reading I_1 is taken with only R_0 in the circuit, so that $I_1 = (V_A - V_B)/R_0$, where V_A and V_B are the electrode potentials. Then R is inserted and adjusted until one-half of the former reading is obtained, so that $I_2 = \dfrac{V_A - V_B}{R_0 + R}$. Hence, $R_0 = R$ and, therefore, the potential difference $V_A - V_B = RI_1$.

C. Interpretation

The spontaneous polarization method is one of the few electrical methods in which the depth of penetration cannot be controlled. Hence, any quantitative interpretation must necessarily be of an indirect nature. Anomaly curves may be calculated for bodies of simple geometric shape; depth and dip can then be determined approximately from them by interpolation. Such calculations may be readily made for spheres with vertical or inclined polarization and for bars and sheets. These calculations give

---

[19] If the galvanometer of the potentiometer is used, the slide wire dial must be set at zero.

curves of a degree of approximation which is satisfactory in practice. It is evident, of course, that actual ore bodies are far from having the shapes assumed here.

Assume that the electrical field distribution is equivalent to that of a vertically polarized doublet and that E is the potential difference between its terminals, corresponding to the electrical charges e and $-e$ (Fig. 10–23). Then the potential at a point P is $V_p = e/r_1 - e/r_2 = e(r_2 - r_1)/r_1 r_2$. If the diameter $2R$ is assumed to be small compared with r, then $\cos$
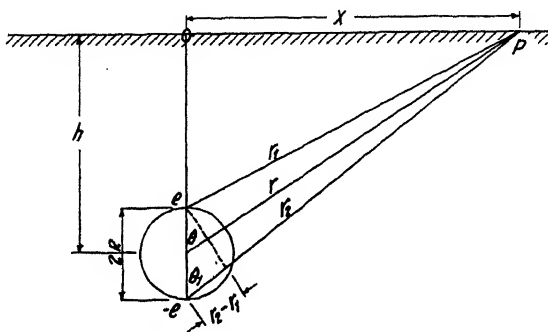
FIG. 10–23. Vertically polarized sphere.

$(r_2 - r_1)/2R \approx \cos \theta$, and $r_2 - r_1 = 2R \cos \theta$, so that $V_p = \cos \theta / r_1 r_2$. As $r_1 \approx r_2$,

$$V_p = \frac{2eR \cos \theta}{r^2}. \qquad (10\text{--}19a)$$

Since the moment of the electric doublet is $2eR = m$, $V_p = m \cos \theta / r^2$. The potential on the sphere[20] for an angle θ is $\dfrac{E}{2} \cdot \cos \theta$; therefore, $\dfrac{E}{2} \cdot \cos \theta = m \cos \theta / R^2$, so that $m = ER^2/2$. The expression for V_p then becomes[21] $V_p = \dfrac{ER^2}{2r^2} \cos \theta$ or, since $\cos \theta = h/\sqrt{x^2 + h^2}$,

$$V_p = \frac{ER^2 h}{\ } \qquad (10\text{--}19b)$$

To find the maximum potential, differentiate (10-19b) with respect to x:

$$\frac{dV_p}{dx} = -\tfrac{3}{2} ER^2 hx(x^2 + h^2)^{-5/2}. \qquad (10\text{--}19c)$$

[20] See A. Petrowsky, Inst. Prakt. Geophys. Bull. No. 1, 87 (1925).
[21] Eq. (10-19b) is obtained also by applying the theory of images, that is, by assuming a reflected sphere above the earth's surface. See E. Poldini, Univ. de Lausanne Bull. No. 61, 21 (1938).

This expression is zero when x is zero, so that, from (10–19b),

$$V = \frac{ER^2}{} \qquad\qquad (10\text{–}19d)$$

An approximate calculation of the depth of the doublet may be made by determining the distance of the "half-value" point of the curve from the point of the maximum. Equating the general expression for the potential in (10–19b) to one-half the maximum value given by (10–19d), we get $\left(x^2_{1/2} + h^2\right)^{3/2} = 2h^3$, which gives

$$x_{1/2} = h\sqrt{2^{2/3} - 1} = 0.767h. \qquad (10\text{–}19e)$$

The expression in eq. (10–19c) signifies current density. An analysis of the curve representing the variation of this quantity with distance is
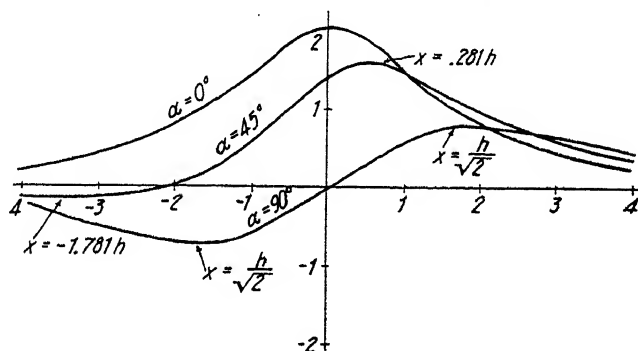
FIG. 10-24a. Potential curves for polarized spheres of various angles of inclination (depth $h = 2$).

useful for depth determinations as follows: Differentiating (10–19c) again with respect to x and equating the result to zero, we find that a maximum occurs when

$$x = h \qquad\qquad (10\text{–}19f)$$

It follows from (10–19c) and (10–19f) that the current density above the vertically polarized sphere is zero and that on either side a maximum and minimum occur whose distance is equal to the depth to the center of the sphere (see Fig. 10-24b). It should be recalled that current density and therefore potential gradient is obtainable directly in the field from voltage readings with constant electrode separation.

A dipping ore body may be considered equivalent to a polarized sphere whose axis of polarization makes an angle α with the vertical. Resolving this inclined doublet into two doublets of the respective moments $m \cos \alpha$

and $m \sin \alpha$, we note that $m \cos \alpha$ acts at P as a vertically polarized sphere. Hence, the potential at P, according to eq. (10–19b), is

$$V_1 = \frac{ER^2}{2} \frac{h \cos \alpha}{(x^2 + h^2)^{3/2}}.$$

The horizontal doublet $m \sin \alpha$ is the equivalent of a horizontally polarized sphere. With x instead of h as its distance from the surface, we have for the potential of this doublet at P

$$V_2 = \frac{ER^2}{2} \frac{x \sin \alpha}{(x^2 + h^2)^{3/2}}.$$

The total potential at P is the sum of the potentials due to the components of the dipole:

$$V = \frac{ER^2}{2} \cdot \frac{(h \cos \alpha + x \sin \alpha)}{(x^2 + h^2)^{3/2}}. \qquad (10\text{–}20a)$$

For $\alpha = 45°$, $V = \frac{ER^2}{2\sqrt{2}} \cdot \frac{(h + x)}{\qquad}$; and for $\alpha = 90°$, $V = \frac{ER^2}{2} \cdot \frac{x}{\cdot\; h^2)^{3/2}}.$

The point of maximum potential for $\alpha = 45°$ is given by $x = h(\pm\sqrt{17} - 3)/4$; $0.281h$ is a maximum and $-1.781h$ a minimum point.

At both points the current density is zero (see Fig. 10–24a). By repeated differentiation, the points of maximum and minimum current density are found at $x = 0.55h$ (max.), $x = -0.425h$ (min.), and $x = -2.1h$ (max.) (see Fig. 10–24b). For $\alpha = 90°$, the point of maximum potential is at $x = \pm h/\sqrt{2}$; and the current density at $x = 0$ is a minimum and at $x = \pm1.22h$ is a maximum.
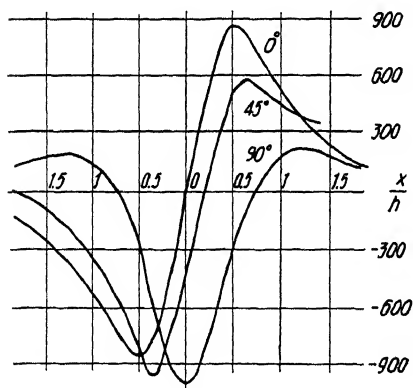
FIG. 10-24b. Current density curves for polarized spheres of various angles of polarization.

Simple relations may be derived for the self-potential of an ore body considered as a polarized bar with a negative current source on its upper end and a positive source on its lower end. Assume the ore body to be located in the xz plane, so that the vertical distance of its upper end from the surface is h_1, that of its lower end is h_2, its projection on the x axis is a, and the distances of its ends from a surface point are r_1 and r_2. The coordinates of this point are x and y and the 0-point of the system is assumed to be directly above the

upper end. Then the potential for the upper (negative) source or sink is $V_1 = - \rho I/2\pi r_1$ and that for the lower source is $V_2 = \rho I/2\pi r_2$, so that the total potential

$$V = - \frac{\rho I}{2\pi}\left(\frac{1}{r_1} - \frac{1}{r_2}\right). \tag{10-20b}$$

Substituting

$$r_1 = \sqrt{x^2 + y^2 + h_1^2} \quad \text{and} \quad r_2 = \sqrt{(x - a)^2 + y^2 + h_2^2},$$

the potential is

$$V = - \frac{\rho I}{2\pi}\{(x^2 + y^2 + h_1^2)^{-1/2} - [(x - a)^2 + y^2 + h_2^2]^{-1/2}\}. \tag{10-20c}$$

.To what extent the second term is effective depends on the length of the ore body. The negative center becomes displaced from a position above the negative pole in proportion as the body becomes shorter and the dip becomes less; until, for a flat-lying body, a positive and negative anomaly of equal strength will be observed. As before, depth rules can be calculated for various angles of dip of the bar. Such calculations are simplified by moving the point P into the xz plane $(y = 0)$.

The effect of a dipping polarized sheet may be derived from the one previously treated by assuming polarized lines instead of point sources at the upper and lower ends of the body. Calculations and curves are given by Edge and Laby.[21a]

D. CORRECTIONS

Compared with other electrical methods, few corrections and interferences occur in self-potential surveying. (1) For very accurate surveys a correction for polarization of electrodes may be determined and deducted. (2) In hilly country, corrections may arise from uphill currents (due to the fact that in the earth's electrical field, localities of higher elevation are at a different potential). The topographic effect is not so pronounced in the self-potential as in the equipotential-line method (in which the entire ground is energized and, therefore, the distribution of potential is influenced by topography).

E. RESULTS

The self-potential method has been applied to the location of: (1) sulfide ore, (2) anthracite coal, (3) metals in placer deposits, (4) formation

[21a] *Op. cit.*, p. 244.

boundaries, and (5) pipe corrosion. Since Schlumberger made his famous measurements on the Sain Bel pyrite ore body in France in 1913, numerous sulfide ore bodies and mine prospects have been surveyed by the self-potential method in all parts of the world.

A discussion of two examples will suffice. One is the survey of the Hope Mine in British Columbia (see Fig. 10-25) (about eighty miles from Vancouver). Nickeliferous pyrrhotites with a proved tonnage exceeding 500,000 tons occur in the vicinity of a pyroxenite dike in granodiorites. In 1930 a self-potential survey showed a prominent indication near the mine where ore was not suspected. The potential anomalies exceeded 300 millivolts. A trench dug at the indication (see figure) revealed an ore body of pyrrhotite about 40 feet wide. One of two inclined drill holes traversed a mineralized zone about 70 feet wide, leaving it at a depth of 176 feet.

Self-potential phenomena are not necessarily limited to large and very massive ore bodies. They have also been observed on "stringer" types of mineralizations. Fig. 10-26 shows a self-potential survey made in the Pallières region in the Département du Gard in France. The
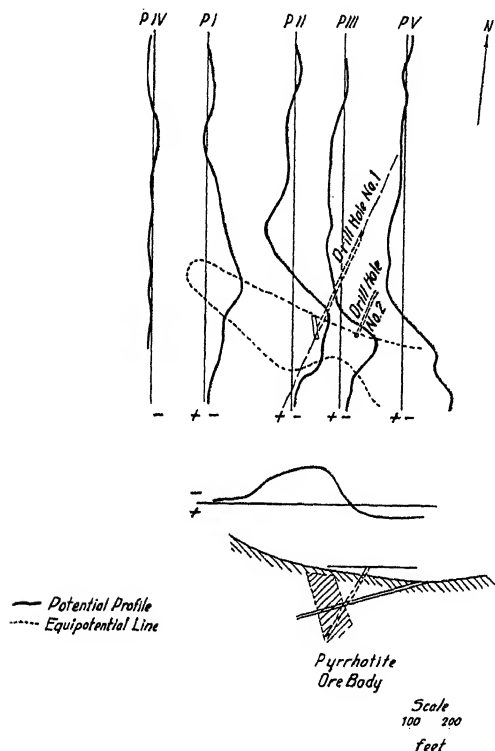
FIG. 10-25. Self-potential profiles at Hope Mine, British Columbia (after Geoffroy).

geologic section is characterized by an extended contact zone with Paleozoic granites on the east and Triassic arkose and Rhetian shales on the west. Resting unconformably on the shales are limestones and dolomites of Hettangian age. The mineral solutions have been forced into the contact zone from below and have followed the bedding planes and shattered zones in the sandstone and shales as well as in the limestones, thus giving rise to the pattern shown in the figure. The self-potential survey clearly reveals the areas of greatest mineral concentration (mostly pyrite).

Anthracite coal is a good conductor of electricity and also shows strong spontaneous polarization. A positive potential center, instead of a negative one, is found on the upper part of anthracite beds.[22]

It was found by Ostermeier[23] that metal concentrations in placer deposits may show spontaneous polarization. In the rivers of the bight of
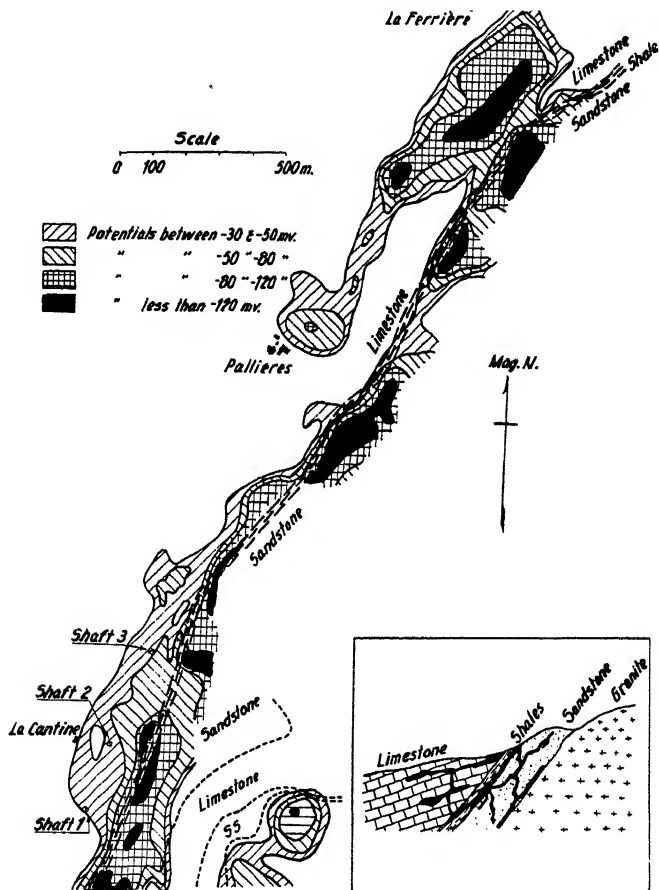
FIG. 10-26. Self-potential survey on mineral stringers in the Pallières contact zone, Département du Gard, France (after Poldini).

Cienaga in Colombia, conditions appear to be favorable because the river gravels contain boulders with impregnations of pyrrhotite which are probably in the immediate vicinity of the mother lodes partially eroded by

[22] See S. F. Kelly, Eng. and Min. J., 114(15), 1922.
[23] Metall und Erz, 30(2), 21–24 (1933).

the river bed. A cane provided with two electrodes at its end and a simple potentiometer consisting of a rheostat, galvanometer, and dry cell was sufficient to locate the eroded veins and boulders in the river bed (see Fig. 10-27).

By accurate spontaneous polarization measurements, taken at short intervals, small potential differences have been established on formation boundaries.[24] At five-meter intervals the potential differences are of the order of several tenths of a millivolt, whereas in undisturbed terrain their value is generally but one-tenth of this magnitude. Boundary potentials are probably caused by differences in the conductivity of solutions filling the pores, so that "concentration elements" are formed (see II, A, page 631).
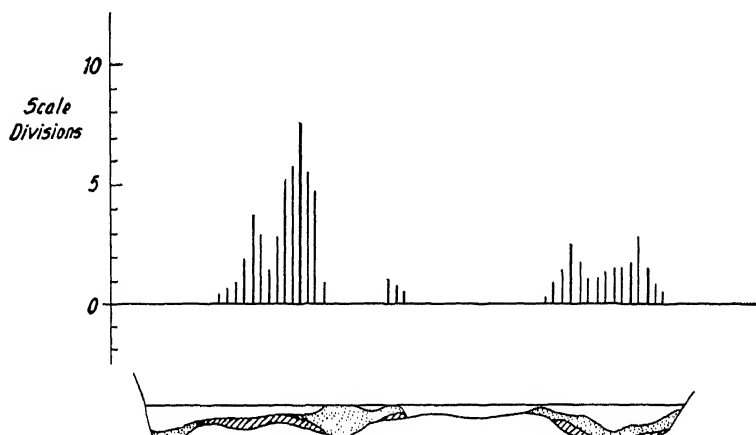
Fig. 10-27. Spontaneous polarizations obtained on ore placers and eroded veins in Colombia (after Ostermeier).

In Fig. 10-28, curve b shows the potential gradients; curve b' shows the potentials, and the section below indicates a formation boundary between granite and gneiss which was located on the basis of the potential measurements by four auger holes.

In areas of metamorphosed sediments it is sometimes possible not only to locate formation boundaries but also to make more detailed studies of geologic structure. Conditions shown in Fig. 10-29 made the self-potential method applicable because graphite occurred in some of the key beds. In the copper district of Katanga the ore occurs in anticlines of the so-called mine series of the Kundelungu formation, made up largely of slates and dolomites and containing a graphitic horizon. Another similar horizon occurs in the so-called Muaslira series, immediately beneath the Great

[24] H. Hunkel, Zeit. Prakt. Geol., 36(7 and 9) (July and Oct., 1928).

Kundelungu conglomerate.   It was possible to determine the boundary of the area occupied by the conglomerate and to locate the uplifted portions of the beds in the mine series.   The extreme right of Fig. 10–29 shows plainly the rela-
tion between the loca-
tion of a mine and the
maxima in the self-
potential anomaly.

The problem of pipe line corrosion is one of great commercial importance.   Extensive studies have been made in recent years to determine its cause and to devise remedies.   Various electrical prospecting methods and modifications thereof have been instrumental in making possible a better understanding of the phenomena involved.

When a metal is immersed in a conductive liquid it emits positive ions and takes on a negative charge.   Under normal conditions an equilibrium is established, since the positive ions are held near the metal by the negative charge.   Two agents will disturb this equilibrium:

1. *Acid solutions* (rich in oxygen, sulfate, and chloride ions).   These have a tendency to elimi-

Fig. 10-28. Potential gradients, potential profile, and geologic section uncovered on the basis of the survey (after Hunkel).

nate the metallic ions as soon as they appear, and the metal will therefore be strongly attacked.   Destruction will occur at the points of lowest potential, that is, in the anodic zones or zones of positive potential.

2. *Stray currents.*   Metallic conductors attract currents in certain zones

in the vicinity of power plants, trolley lines, and the like, and discharge them again in others. Current is collected in the negative zones and leaves the conductor in the anodic or positive zones. It is again in the latter that the destruction of metal occurs. The effects described are related as cause and effect. In the former, chemical action is the cause
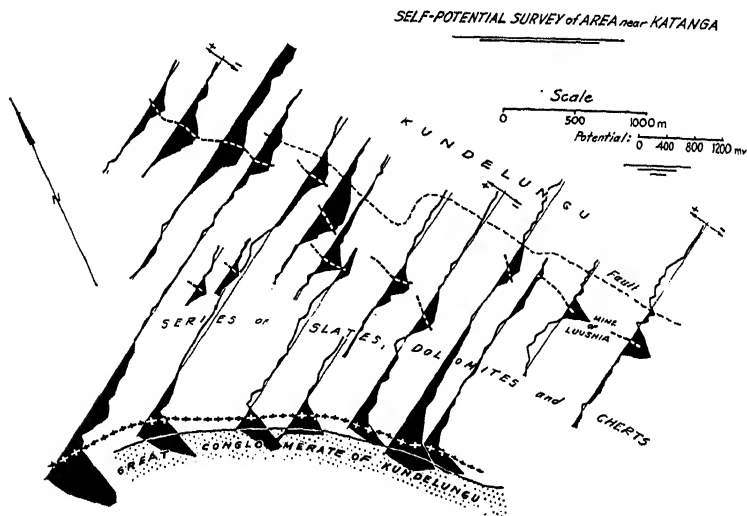
Fig. 10-29. Location of folds of graphitic slates in Katanga (after Poldini).
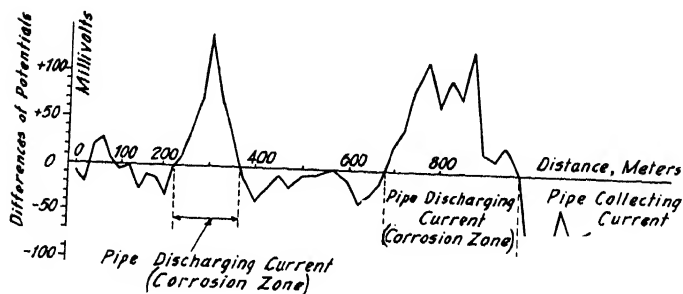
Fig. 10-30. Location of corrosion zones in pipes by self-potential measurements (after Schlumberger).

of the current; in the latter, extraneous currents produce the chemical reactions.

Since anodic zones are generally located in areas of low resistivity, systematic studies of the resistivity of soils around pipe lines have been made. Another line of attack is to measure the acidity of soils to determine their corrosiveness. Self-potential methods are used for the determination of

the zones of egress when the corrosion is of a chemical nature or is produced by stray currents not due to industrial plants. Measurements are made in the customary manner with nonpolarizable electrodes at short intervals to locate zones of positive potential. Fig. 10–30 shows measurements made in this manner along 2300 feet of pipe line in Paris, at intervals of some 65 feet, establishing two corrosion zones by their positive potential. C. and M. Schlumberger[25] have described these and other methods for the location of corrosive zones in more detail.

IV. EQUIPOTENTIAL-LINE AND POTENTIAL-PROFILE METHODS

A. CONDITIONS IN STATIONARY FIELDS

When electric energy is applied to two points at the ground surface, an electric current will flow between them because of their difference in potential. If the medium between the two electrodes is homogeneous, the current and potential distribution is regular and may be calculated. When good or poor conductors are imbedded in this homogeneous medium, a distortion of the electrical field occurs. Good conductors have a tendency to attract the current lines toward them while poor conductors force them away. Theoretically it should be possible to detect bodies of different conductivity by measuring the geometric disposition of these current lines. In practice this cannot be done with sufficient accuracy; it is necessary to determine the direction in which no current flows by locating points which have no potential difference. Using a null method has the advantage of both accuracy and ease of procedure. Quantitative measurements of potential difference are not required when the lines of identical potential, or "equipotential lines," are traced. For homogeneous ground the potential variation in both a horizontal and a vertical plane is illustrated in Fig. 10–31. The potential gradient is not uniform; it is greatest in the vicinity of the electrodes. The "current lines" are concave to the surface because of the repulsion of adjacent current fibers. Equipotential lines, at right angles to the current lines, are circles only in the immediate vicinity of the electrodes. Elsewhere in the horizontal plane and vertical section, they are curves of the fourth degree.

For a stationary field the potential distribution in homogeneous ground can be calculated. By a stationary field is meant here a field which does not change with time and is produced by direct current after equilibrium has been reached. The results obtained apply also to A.C. fields if skin effect and elliptical polarization are neglected (quasi-stationary fields). A

---

[25] A.I.M.E. Tech. Pub. No. 476. The trade journals covering oil and gas transportation currently carry articles dealing with pipe corrosion.

FIG. 10-31. Potential and current distributions in vertical and horizontal plane (partly after Schlumberger).
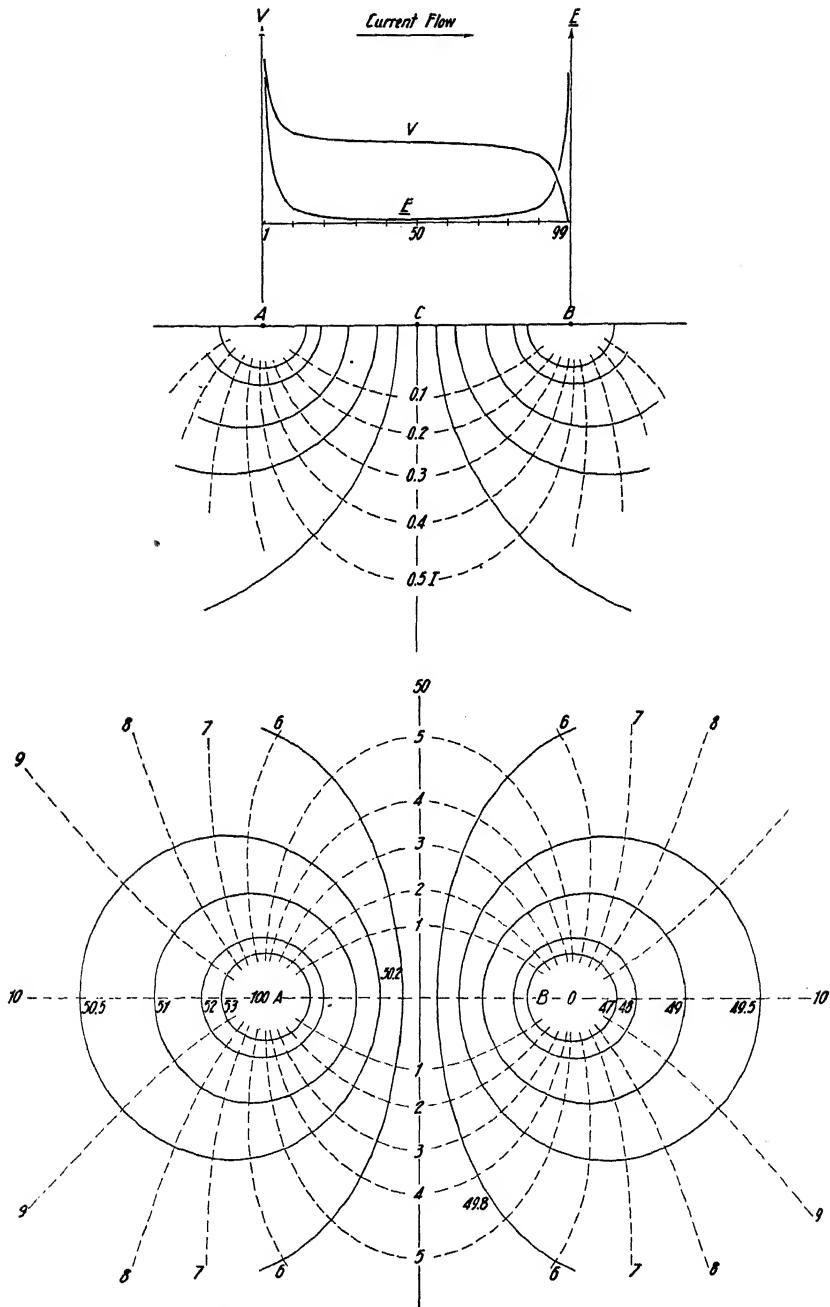
determination of the potential distribution for the horizontal or vertical plane is possible by calculating the potentials of each electrode separately from Ohm's law for the semi-infinite space and by combining them for any given point.   The resistance of a hemispherical shell with the radius r, the thickness dr, and the resistivity ρ is $dR = \rho\, dr/2\pi r^2$, and the potential drops from the inside of the shell to the outside by the amount $-dV = IdR$. Therefore, from an integration of this expression and a similar one for the second electrode, the potential at any point is

$$V = \frac{\rho I}{2\pi}\left(\frac{1}{r} - \frac{1}{r'}\right). \tag{10--21a}$$

The "equipotential surfaces" are defined by the expression $1/r - 1/r' =$ constant and are surfaces of revolution of the fourth order about the base AB.   In the vicinity of either electrode $1/r'$ is negligible compared with $1/r$ and the equipotential surfaces are nearly spherical.   The potential gradient or electrical field strength is proportional to the inverse square of the distance, or

$$\mathbf{E} = \frac{-dV}{dr} = \frac{\rho I}{2\pi}\left(\left|\frac{1}{r^2}\right| + \left|\frac{1}{r_1^2}\right|\right). \tag{10--21b}$$

The addition is vectorial.   As applied to the surface, this becomes

$$\mathbf{E} = \frac{\rho I}{2\pi}\left(\frac{1}{r^2} + \frac{1}{(b-r)^2}\right) \tag{10--21c}$$

(algebraic addition).   In the center between two points of the distance (base length) b,

$$\mathbf{E}_c = \rho i_0 = \rho\,\frac{4I}{\pi b^2},$$

and the current density i at any point below the center in the vertical plane is

$$i_d = i_0 \cdot \cos^3 \varphi, \tag{10--21e}$$

where φ is the angle subtended by a ray from the electrode to this point with the horizontal plane.

   For given fractions of the current density at depth d in terms of the density at the surface center, the corresponding depths can be determined. C. H. Knaebel[26] and W. Weaver[27] have calculated the portion of the current penetrating below a depth d through a section at right angles to the electrode basis (see Fig. 10–32).

[26] Mich. Coll. Min. Bull., NS, 5(2) (Jan., 1932).
[27] W. Weaver, A.I.M.E. Geophys. Pros., 70 (1929).
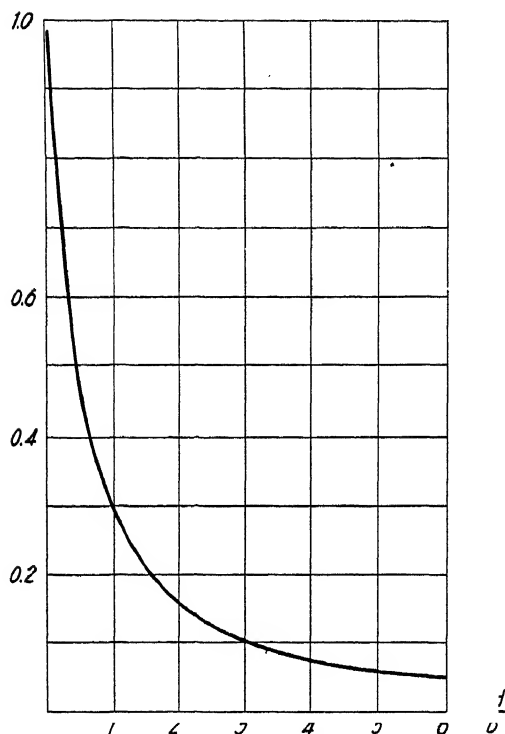
FIG. 10-32. Fraction of current penetrating below depth d, as a function of the ratio of depth and base length (after Knaebel).

As previously stated, a determination of the direction of current lines is impracticable since there is but little change in potential away from the direction of maximum current (see Fig. 10-33). In the direction x of maximum potential difference, the electrical field is $-dV/dx$. In any other direction r, it is $-dV/dr$. Since $r = x/\cos \alpha$,

$$-\frac{dV}{dr} = \mathbf{E} = \mathbf{E}_x \cos \alpha, \quad (10\text{-}22)$$

so that the vector, for all values of α, is represented by a figure eight. This explains the sharpness of the nulls observed in the location of equipotential lines, a condition which is strictly true for direct current only.
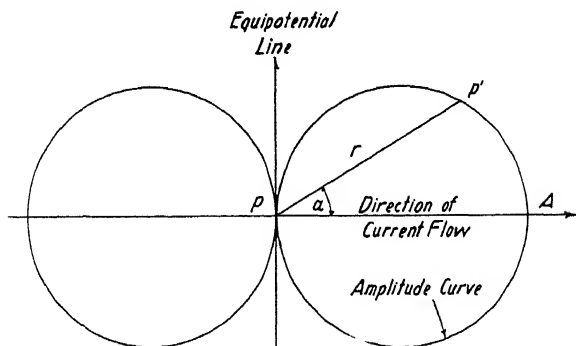
FIG. 10-33. Relation of amplitude curve, and directions of equipotential and current lines.

B. CONDITIONS FOR A.C. FIELDS

The use of alternating current for potential investigation introduces two limitations which may prove to be severe if experimental conditions are unfavorable: (1) reduced depth penetration and (2) elliptical polarization.

Contrary to direct current, the passage of alternating current is controlled by the capacitive and inductive reactance as well as by the resistance of the circuit. For a conductor of sufficient section the inductance of the current fibers in the interior is greater than that at the surface. Thus the current has a tendency to flow nearer the surface. For very high frequencies the current is confined to the outermost "skin."

Relations governing the depth penetration of A.C. such as used in equipotential-line methods (300 to 1000 cycles) may be derived from the laws of electromagnetic wave propagation by introducing certain simplifications. Since for the above frequencies the displacement current may be neglected, the current density at a depth d from the surface of a conductor (where the current density is i_0) may be written

$$i_d = i_0 \cdot e^{-\frac{2\pi d}{c}\sqrt{\mu f \sigma}} \cdot \sin\left(2ft - \frac{2\pi d}{c}\sqrt{\mu f \sigma}\right), \qquad (10\text{--}23a)$$

where the depth is in centimeters, f is frequency, μ is permeability, σ is conductivity (in e.s.u.), c is light velocity, and t is time. The equation states that an attenuation of amplitude and a phase shift between surface and depth current occurs. The attenuation for the peak values of the current is therefore

$$I_d = I_0 \cdot e^{-\frac{2\pi d}{c}\sqrt{f\sigma}}, \qquad (10\text{--}23b)$$

where the permeability has been assumed to be equal to 1. Hence, the depth at which the surface-current density has dropped to $1/e$ of its value, with ρ as resistivity, is

$$d = \frac{c}{2\pi}\sqrt{\frac{\rho}{f}}. \qquad (10\text{--}23c)$$

Since the presence of good conductors at the surface or near the surface reduces the depth of penetration, provision is made in some A.C. methods to lower the frequency when greater penetration is desired. Fig. 10-34 shows the depth penetration of alternating currents of the frequencies 1, 25, 60, and 500, as a function of resistivity, in double logarithmic scale. For any other frequency the penetration may be read off on the frequency scale, which is half that of the depth scale, since the penetration is inversely proportional to the square root of frequency.

In a single A.C. field, the voltage oscillates between its extreme positive and negative values on a current line. The projection of its amplitude variation with time on a horizontal plane is a straight line. The voltage drop is a maximum along this line. At right angles thereto a true equipotential line is present. Conditions are therefore the same as in the D.C. fields. If another A.C. electrical field, or fields, interferes, one of the two following phenomena will occur. If there is no phase shift between the
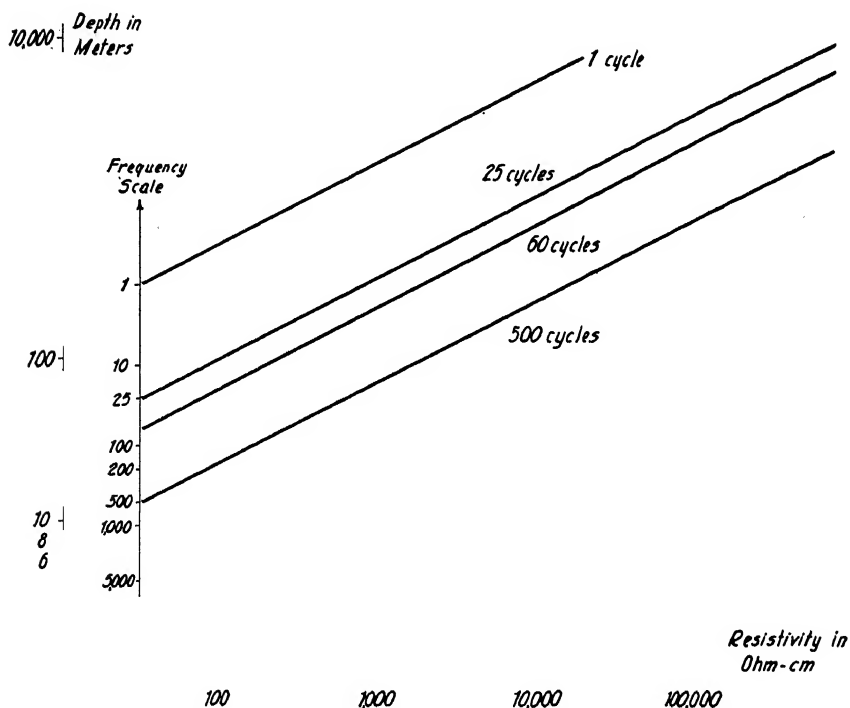
FIG. 10-34. Depth penetration (d at I_0/e) for alternating current of various frequencies, as a function of resistivity (permeability $= 1$; displacement current neglected).

fields, conditions remain as before. The maximum amplitude of the vector is the resultant of the maximum amplitudes of its components. The projection of its time variation on a plane will still be a straight line. If, however, the other field or fields are shifted in phase with respect to the field considered, elliptical polarization of the resultant field occurs. This occurrence derives its name from the fact that the projection of the time variation of the resultant vector upon a plane is an ellipse. The out-of-phase field may differ from the original field in direction or in coordinate.

Elliptical polarization may be readily demonstrated if it is assumed that the additional field differs from the original field in respect to both direction and phase by 90°. If the time variation of the two fields is represented in two vertical planes at right angles to each other (Fig. 10-35) and if the main field is assumed to have the larger amplitude and the interfering field the smaller one, the length of the resultant vector I will be equal to the maximum amplitude A of the larger field at the instant 1, since the amplitude of the second field is zero. At the instant 2 the amplitude of
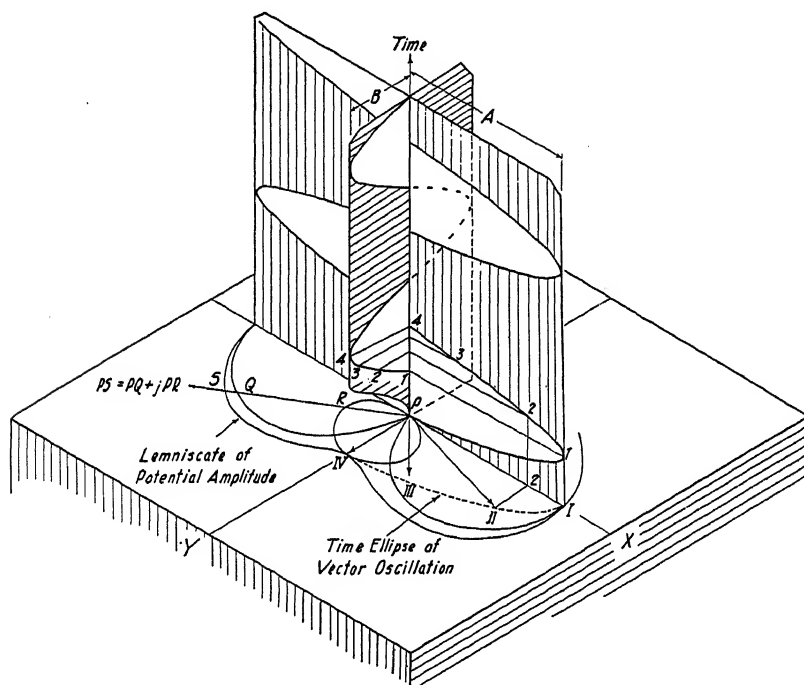
FIG. 10-35. Elliptical polarization of an electric field when its components are 90° out-of-phase and differ in direction by 90°.

the larger field has decreased; the amplitude of the smaller field has increased; and their resultant is given by the length and direction of the vector II. At the instant 3, the resultant field is given by the length of vector III. At the instant 4, the amplitude of the larger field is zero. Hence, the vector IV has the length B and is at right angles to the vector I. The same phenomenon recurs in the three remaining quadrants. A line connecting the ends of the vectors is an ellipse.

The variation of the field amplitude with horizontal direction was previously represented by two adjoining circles (Fig. 10-33). If this pro-

cedure is applied to both fields considered here, two figures eight result, rotated 90° in respect to their larger axes. Amplitudes resulting from each are superimposed. If in any given direction the amplitude of the large field is $\overline{PQ}$ and that of the smaller field $\overline{PR}$, the resulting amplitude is $\overline{PS} = \overline{PQ} + j\,\overline{PR}$. Plotting the amplitude of the PS vector for the entire horizontal plane, we get a lemniscate. If the small out-of-phase field were not present, a single figure eight would represent the amplitude variation. An absolute zero would be obtained in the direction of the equipotential line. With an interfering field, however, the sound never vanishes. Only a minimum is observed, whose sharpness depends on the amplitude of the out-of-phase field.

Out-of-phase fields in electrical prospecting may be due to a variety of causes. Currents traversing media of different conductivity, capacitance, and inductance, will be shifted in phase. Further, ground currents and electrode leads will induce out-of-phase currents in adjacent conductors.

For two field components at an arbitrary angle with one another and with a phase shift of 90°, polarization conditions are the same as for two components at right angles to each other but with an arbitrary phase shift. Two adjacent currents with a phase shift of 90° produce a transverse component with a phase shift depending on the respective amplitudes of the currents. If the one component is $\mathbf{X}$ and the other transverse component is $\mathbf{Y}$, we have, therefore, for the general case of two out-of-phase components at right angles to each other:

$$\mathbf{X} = \mathbf{A} \sin \omega t$$

$$\mathbf{Y} = \mathbf{B} \sin (\omega t - \varphi), \qquad\qquad (10\text{--}24a)$$

where ω is the angular frequency and φ is the phase shift. Since $\sin \omega t = \mathbf{X}/\mathbf{A}$, and $\mathbf{Y} = \mathbf{B}\,(\sin \omega t \cos \varphi - \cos \omega t \sin \varphi)$, $\mathbf{Y}$ becomes equal to

$$\mathbf{B}\left(\frac{\mathbf{X}}{\mathbf{A}}\cdot \cos \varphi - \sqrt{1 - \frac{\mathbf{X}^2}{\mathbf{A}^2}}\cdot \sin \varphi\right); \quad \text{or,}$$

$$\mathbf{Y} - \mathbf{B}\frac{\mathbf{X}}{\mathbf{A}}\cdot \cos \varphi = -\mathbf{B}\sqrt{1 - \frac{\mathbf{X}^2}{\mathbf{A}^2}}\cdot \sin \varphi.$$

Squaring both sides and dividing by $\mathbf{B}^2$ gives

$$\frac{\mathbf{Y}^2}{\mathbf{B}^2} - \frac{2\mathbf{X}\mathbf{Y}}{\mathbf{A}\mathbf{B}} \cos \varphi + \frac{\mathbf{Y}^2}{\mathbf{A}^2} = \sin^2 \varphi. \qquad\qquad (10\text{--}24b)$$

Dividing by $\sin^2 \varphi$,

$$\frac{\mathbf{Y}^2}{\mathbf{B}^2 \sin^2 \varphi} - \frac{2\mathbf{X}\mathbf{Y}\cos \varphi}{\mathbf{A}\mathbf{B}\,\sin^2 \varphi} + \frac{\mathbf{X}^2}{\mathbf{A}^2 \sin^2 \varphi} = 1,$$

which has the form

$$Lx^2 + 2Mxy + Ny^2 = 1 \qquad (10\text{--}24c)$$

and is the expression for an inclined ellipse whose major axis is tilted in reference to the x axis. In this equation,

$$L \equiv \frac{1}{A^2 \sin^2 \varphi}; \quad M \equiv \frac{-\cos \varphi}{AB \sin^2 \varphi}; \quad N \equiv \frac{1}{B^2 \sin^2 \varphi}.$$

If the phase shift is 90°, it is seen that the major axis of the ellipse coincides with the x axis, so that

$$\frac{Y^2}{A^2} + \frac{Y^2}{B^2} = 1,$$

which is the standard form of the ellipse. To determine the angle of deviation ψ of the ellipse (given by eq. [10–24c]) from the x axis, rotate the system of coordinates so that $x = x_1 \cos \psi - y_1 \sin \psi$ and $y = x_1 \sin \psi + y_1 \cos \psi$.

By substitution in (10–24c),

$$\begin{aligned}
x_1^2[L \cos^2 \psi &+ N \sin^2 \psi + 2M \sin \psi \cos \psi] \\
&+ y_1^2[L \sin^2 \psi + N \cos^2 \psi - 2M \sin \psi \cos \psi] \\
&+ 2x_1 y_1[(N - L) \sin \psi \cos \psi + M(\cos^2 \psi - \sin^2 \psi)] = 1.
\end{aligned} \qquad (10\text{--}24e)$$

In this new system an equation of the form of (10–24d) must obtain, and therefore the coefficient of $2x_1 y_1$ must be zero. This leads to

$$\tan 2\psi = \frac{2M}{L - N}. \qquad (10\text{--}24f)$$

By substituting for L, M, and N their values given before,

$$\frac{1}{2} \tan 2\psi = \frac{\cos \varphi}{\dfrac{A}{B} - \dfrac{B}{A}}, \qquad (10\text{--}24g)$$

which is the same as eq. (10–18d) given in connection with the discussion of the elliptical polarization of radio waves (there the tilt angle was measured from the Y and not from the X axis).

The axes of the ellipse may be determined from eq. (10–24e) by casting it in the form of the standard ellipse as in eq. (10–24d). Designating the coefficient of x_1^2 by U and that of y_1^2 by Q,

$$Ux_1^2 + Qy_1^2 = 1, \qquad (10\text{--}24h)$$

where

$$\mathbf{U} \equiv \mathbf{L} \cos^2 \psi + \mathbf{N} \sin^2 \psi + 2\mathbf{M} \sin \psi \cos \psi$$

$$\mathbf{Q} \equiv \mathbf{L} \sin^2 \psi + \mathbf{N} \cos^2 \psi - 2\mathbf{M} \sin \psi \cos \psi$$

$$(10\text{--}24i)$$

Forming the difference D, we have

$$D \equiv \mathbf{U} - \mathbf{Q} = (\mathbf{L} - \mathbf{N}) \cos 2\psi + 2\mathbf{M} \sin \,\colon$$

and substituting eq. (10–24f) we get

$$\sin 2\psi = \pm \frac{2\mathbf{M}}{\sqrt{4\mathbf{M}^2 + (\mathbf{L} - \mathbf{N})^2}} \quad \text{and} \quad \cos 2\psi = \pm \frac{\mathbf{L} - \mathbf{N}}{\sqrt{4\mathbf{M}^2 + (\mathbf{L} - \mathbf{N})^2}}.$$

The difference is

$$D \equiv \mathbf{U} - \mathbf{Q} = \pm\sqrt{4\mathbf{M}^2 + (\mathbf{L} - \mathbf{N})^2}. \qquad (10\text{--}25a)$$

Since from eq. (10–24i) the sum $\mathbf{U} + \mathbf{Q} = \mathbf{L} + \mathbf{N}$, and $\mathbf{U} - \mathbf{Q} = D$, the coefficients are $\mathbf{U} = (\mathbf{L} + \mathbf{N} + D)/2$ and $\mathbf{Q} = (\mathbf{L} + \mathbf{N} - D)/2$. In the standard form of the ellipse, ($\mathbf{X}^2/\mathbf{A}^2 + \mathbf{Y}^2/\mathbf{B}^2 = 1$), $\mathbf{A}$ is the major semiaxis and $\mathbf{B}$ the minor semiaxis. By comparison with eq. (10-24h) the squares of the semiaxes of the ellipse in the $x'y'$ direction are $a^2 \equiv 1/\mathbf{U}$ and $b^2 \equiv 1/\mathbf{Q}$, so that

$$a^2 = \frac{2}{\mathbf{L} + \mathbf{N} - \sqrt{4\mathbf{M}^2 + (\mathbf{L} - \mathbf{N})^2}}$$

and

$$b^2 = \frac{2}{\mathbf{L} + \mathbf{N} + \sqrt{4\mathbf{M}^2 + (\mathbf{L} - \mathbf{N})^2}}.$$

$$(10\text{--}25b)$$

The sign before the radical determines which is the major and which the minor axis. By substituting the values for $\mathbf{L}$, $\mathbf{M}$, and $\mathbf{N}$ from eq. (10-24c), the square of either semiaxis is

$$a^2, b^2 = \frac{2\mathbf{A}^2\mathbf{B}^2 \sin^2 \varphi}{\mathbf{B}^2 + \mathbf{A}^2 \mp \sqrt{4\mathbf{A}^2\mathbf{B}^2 \cos^2 \varphi + (\mathbf{B}^2 - \mathbf{A}^2)^2}}. \qquad (10\text{--}25c)$$

By substituting the ratio major axis/minor axis $= a/b \equiv \mathbf{r}$, and by further substituting the tilt angle relation given in eq. (10–24g), formula (10–18c) is obtained, allowing for the fact that the tilt angle is reckoned from the $\mathbf{Y}$ (vertical) component.

Two fields 90° out of phase, forming an arbitrary angle with each other likewise give rise to elliptical polarization. The theory is treated in section VIII (page 787), as it is of importance in electromagnetic and inductive electrical prospecting methods.

The amplitude variation of the electrical field in a horizontal plane, in the case of elliptical polarization, differs from that for D.C. which was previously represented by two circles (Fig. 10-33). Since elliptical polarization may be assumed to result from a combination of two fields at right angles to each other, their combined amplitude variation follows from a superposition of two amplitude circles at right angles to each other. Since in each circle the amplitude variation is represented by a cosine law, the resultant amplitude in a line connecting the probes $\overline{OA}$ (in Fig. 10-36) is

$$\overline{OA} = \sqrt{a^2 \cos^2 \alpha + b^2 \sin^2 \alpha}. \qquad (10\text{--}26a)$$

Numerical Values:
$$\frac{b}{a} = 0.444$$
$$\alpha = 39°$$
$$\delta = 36\tfrac{1}{2}°$$
$$\frac{x^2}{201.6} + \frac{y^2}{39.7} = 1$$
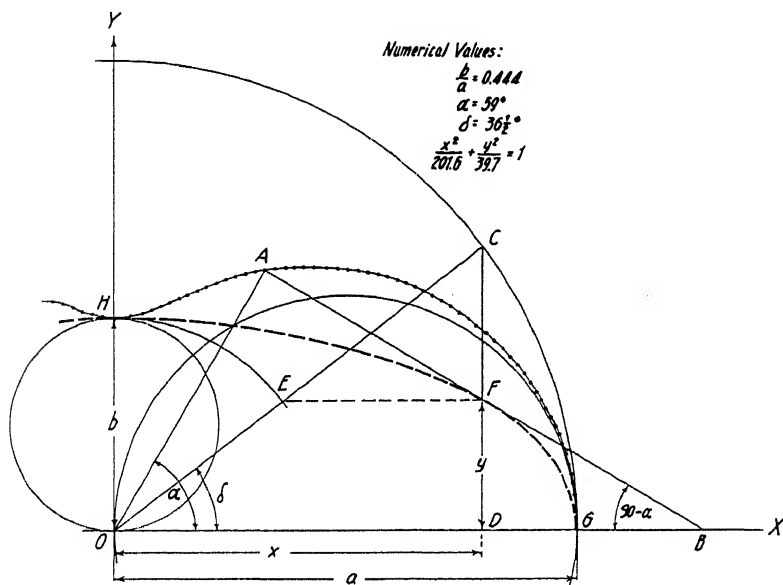
FIG. 10-36. Relations of amplitude, direction, phase, ellipse- and lemniscate characteristics in A.C. potential fields (adapted from Ambronn).

The phase δ in the line $\overline{OA}$ with respect to the phase in the direction of the major axis may be calculated, though in practice the procedure is reversed, since the phase difference is measured and the characteristics of the ellipse are obtained from it. Assuming the ellipse to be known, a tangent drawn from the point A will give points F and B. The normal to the x axis through F intersects a circle drawn about O with the radius a in the point C. The direction of $\overline{OC}$ with respect to the x axis is the phase angle in the line OA. These geometric relations may be expressed by the following equations:

(1) $\qquad x = a \cos \delta;$ $\qquad$ (2) $\qquad y = b \sin \delta.$

Since the inclination of the tangent to the ellipse is given by $\tan (90 - \alpha) = \dfrac{b^2}{a^2} \cdot \dfrac{x}{y}$, we have

$$(3) \quad \tan \alpha = \frac{a^2}{b^2} \cdot \frac{y}{x}.$$

Dividing eq. (2) by eq. (1) and substituting in (3), we obtain the following relation between the azimuth of the line and phase angle

$$\tan \alpha = \frac{a}{b} \cdot \tan \delta. \tag{10–26b}$$

If we substitute eq. (10–26b) in eq. (10–26a), the amplitude in the line $\overline{OA}$ as a function of phase angle and ellipse axes is

$$|\overline{OA}|^2 = \frac{a^2 b^2}{b^2 \cos^2 \delta + a^2 \sin^2 \delta}. \tag{10–26c}$$

In the mapping of the A.C. ground-potential distribution, it is not customary to survey the ellipse and deduce the ratio of major and minor axes and ratio of in-phase and out-of-phase field components, as is done in the determination of propagation characteristics of radio waves. When elliptical polarization is noticeable, potentials are generally determined with a compensator which measures their amplitude and phase with reference to those of the primary supply; or else the in-phase and quadrature potentials are determined, and equipotential lines are drawn separately for each. These procedures are discussed in the following section.

C. Field Procedure; Equipment

Direct or alternating current may be used for surveying equipotential lines. Direct current has the advantage that the equipotential points can be located with greater precision and that the galvanometer gives a clear indication of the direction in which to move the electrode. A disadvantage is the necessity for porous pots and the interference from polarization and other D.C. effects. Alternating current has the advantage of portability and convenience of the movable circuit, possibility of amplification of signals, and freedom from commercial current interference. Disadvantages may arise from its use in highly conductive regions because out-of-phase components prevent a location of equipotential points.

For mapping D.C. equipotential lines, a small D.C. generator (1 KVA, 200 volts) driven by a gasoline engine (of ample power margin for higher altitudes) is generally employed. Current electrodes are iron pegs, coils of copper wire, or copper screens. Equipotential lines are traced with non-polarized electrodes connected by a wire to a galvanometer. The primary

electrodes are laid out up to a mile or more apart so that the equipotential lines over the section of ground under consideration will be approximately straight and parallel to one another. In the planning of the survey, the general geology of the region should be considered and electrodes should be so laid out that the equipotential lines will be at right angles to the strike. Modifications may be necessary to suit special conditions. For instance, for determining the outline of partly accessible ore bodies, the primary electrode may be connected *to the ore body* thus making its outline an equipotential surface. In a similar technique one electrode is connected to a formation in a well so that its strike and dip near the surface is revealed by its equipotential pattern. Because of an increased conductivity in the direction of the bedding planes, equipotential lines surrounding one electrode in a stratified medium are elliptical, with the major axis in the direction of strike.

It is possible to number equipotential surfaces and to determine their interval by the following arrangement: Near the primary electrodes two auxiliary electrodes are placed in the ground in such a manner that their potential difference is nearly the same as that between the primary electrodes. These are connected to the ends of a high resistance slide wire. To find the potential of a given point or line, the point or line is connected through a galvanometer to the sliding contact, which is changed in position until the galvanometer deflection vanishes. If the resistance on one side of the tap is R_1 and on the other R_2, $R_1/R_2 = V_1/V_2$, which may also be written $R_1/(R_1 + R_2) = V_1/(V_1 + V_2)$, since both the total resistance and the total potential difference between the points A' and B' are known.

For subtracting from the measured potentials the normal potential variation due to the primary electrodes, formula (10–21a) is applied. Substituting, for the center line connecting the two electrodes, the value b for the base length and designating by x the distance of a point P from the center, the potential at that point is $V = \pm 8x/(b^2 - 4x^2)$, the sign depending on whether the point is closer to the left or right electrode.

A.C. equipotential-line methods may be divided into two groups: (1) methods applicable when elliptical polarization is negligible and (2) methods for the determination of potentials in respect to amplitude and phase (or by their in-phase and quadrature components). *Point* or *line* electrodes may be used; their arrangement is the same in both methods. Point electrodes should be laid out with their base line parallel to the supposed strike. Line electrodes are laid out at right angles to the strike and have the advantage that the "normal" equipotential lines are parallel with the primary electrodes; therefore, distortions are more readily interpreted. Line electrodes are usually bare stranded copper wire and are

tacked to the ground at numerous points by steel pegs. In ore prospecting their distance is 2000 feet to a half mile and their length of the same order or greater. To cover large areas, the electrodes are leapfrogged, since too great a distance between electrodes reduces the distinctiveness of response.

The *normal field* of line electrodes is no longer given by formula (10–21a) and may be derived as follows. With reference to Fig. 10–37 the potential at the point P is given by

$$V_p = E\left(\int \frac{dl}{\varrho_1} - \int \frac{dl}{\varrho_2}\right) = E\left(\int_{-l_2}^{l_1} \frac{dy}{\sqrt{r_1^2 + y^2}} - \int_{-l_2}^{l_1} \frac{dy}{\sqrt{r_2^2 + y^2}}\right),$$

where E is one half the potential difference between the electrodes. Hence,

$$V_p = E \log_e \frac{(l_1 + \sqrt{r_1^2 + l_1^2})(l_2 + \sqrt{r_1^2 + l_2^2})r_2^2}{(l_1 + \sqrt{r_2^2 + l_1^2})(l_2 + \sqrt{r_2^2 + l_2^2})r_1^2}.$$

On a line of symmetry where $l_1 = l_2 \equiv l$, the potential is

$$V_p = 2E \log_e \frac{\sqrt{l^2 + (a - }}{(a - x)(l + \sqrt{l^2 + (a}} \tag{10–27}$$
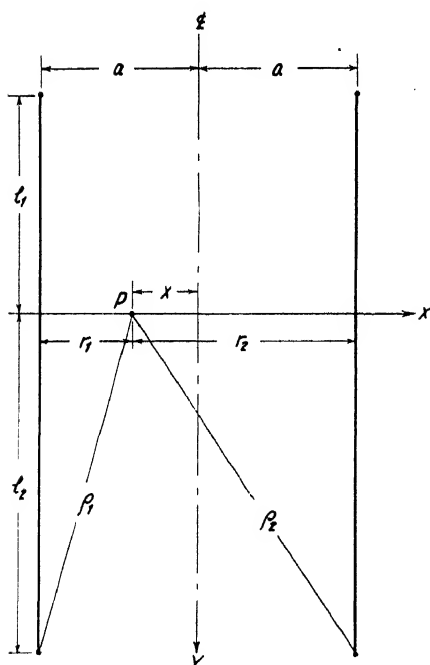
Fig. 10-37. Line electrodes (adapted from Heine).

The electrical (field and, therefore, the current density) is greater with line electrodes than it is with point electrodes.

In most equipotential, electromagnetic, and inductive surveys, portable gasoline-engine driven alternators of a frequency of 500 to 1000 cycles are used, furnishing from 200–1000 KVA at 110 or 220 volts.

The equipment for surveying equipotential lines consists of two search electrodes, an amplifier, and headphones when out-of-phase fields are negligible. It is supplemented by more elaborate bridge arrangements when a complete determination of A.C. potentials in regard to phase and amplitude becomes necessary. In many cases, even if out-of-phase fields exist,

the minima in the amplitude curve can be determined with sufficient accuracy for the mapping of equipotential lines. The search electrodes are usually copper-jacketed steel rods. For dry ground the Imperial Geophysical Experimental Survey found a "self-watering" electrode helpful.[28] Almost any kind of a two- or three-stage amplifier may be used for equipotential-line surveying, provided that it is light, small, and does not depend on storage batteries for filament supply. Circuit diagrams and descriptions will be found in the reports published by the I.G.E.S. In conducting equipotential-line surveys, several parties may work concurrently. At least two parties can work in two sections of the area covered by one electrode layout and more can be kept busy with two or more simultaneous electrode arrangements, which may in many cases be supplied from the same power source. Two men are required to map equipotential lines, which should be marked with stakes and be surveyed with a compass (in areas where large declination anomalies are absent) and a 100-foot tape.

More quantitative surveys of the potential field require A.C. bridge arrangements. With one of these the voltage ratio and phase difference of adjacent portions of ground are measured. Details are given in section VI. Another type makes possible a determination of complex potentials in reference to the potential and phase of the generator; it therefore requires a "reference" lead from the bridge to the generator. The voltage difference and its phase are measured directly or the potential is split up into its in-phase and quadrature components; thus, in-phase and quadrature equipotential lines may be mapped. In the compensator illustrated in Fig. 10–38, the generator is coupled through a power transformer to the primary electrodes and through a phase transformer to the reference lead. The reference voltage is then supplied to the four coils of a variometer in such a manner that two of them (V_1 and V_2) are provided with current *in phase* with the generator current whereas the other pair (V_3 and V_4), coupled to the reference lead through an air-core transformer, receive current in *quadrature*. The resultant field is picked up by the secondary coil of the variometer whose position determines the phase of the reference voltage that is taken off on the terminals of the potentiometer P. No sound will be heard in the headphones if the ground potential is compensated, in regard to amplitude (potentiometer adjustment) and phase (variometer adjustment) by the reference potential. If this compensator is used for the determination of electromagnetic fields in reference to amplitude and phase of the generator potential, a search coil is substituted for the ground probes. Data obtained with this compensator may be

---

[28] See Edge and Laby, *op. cit.*, p. 265, Fig. 197.

represented by lines of equal potential, by equiphase lines, or by in-phase and quadrature equipotential lines.

The compensator shown in Fig. 10–39 permits of determining the real and imaginary components directly. The generator side is connected, as before, to the reference lead; the reference voltage is split up into its com-
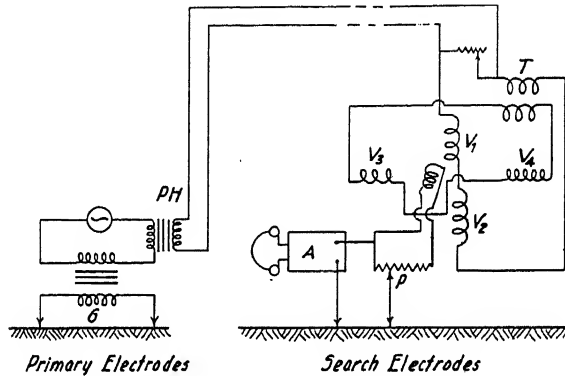
FIG. 10-38. Arrangement for determining amplitude and phase of ground potentials (adapted from Ludwiger). PH, phase transformer; G, ground transformer; A, amplifier; T, air-core transformer; P, potentiometer; V_{1-4} variometer coils.
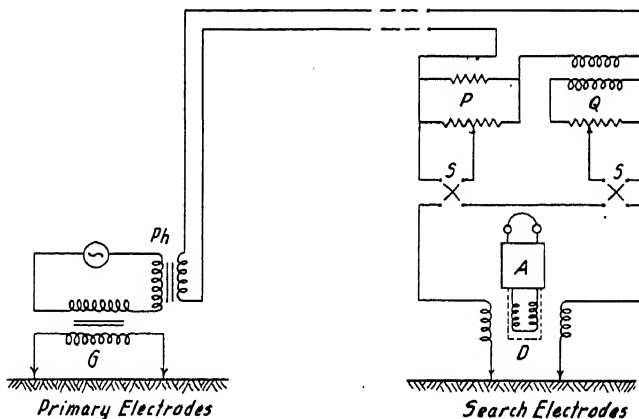
FIG. 10-39. Bridge arrangement for determining in-phase and quadrature potentials (adapted from D. C. Gall).

ponents which are applied to the in-phase potentiometer P and quadrature potentiometer Q. These are connected to the search electrodes through two switches, SS, which permit of changing the sign of the reference components. Current null is determined by a differential transformer, D, connected to an amplifier, A.

D. INTERPRETATION

The interpretation of an equipotential-line survey is empirical and is based largely on previous experience with the method as well as on a satisfactory knowledge of the geological features of the area under consideration. Owing to its speed, this method is of value for general reconnaissance. However, it is advisable to re-examine conductive zones thus located with other electrical methods. In many cases it is relatively simple to make a general qualitative interpretation of an equipotential-line survey by marking off the axes of the conductive zones indicated by the greatest line distortions.

1. *Equipotential-line anomalies of simple geometric bodies.* Depth estimates are sometimes possible by measuring the displacement of the equipotential lines from their normal position. What may be expected in the way of displacement may be calculated by assuming, for simplicity, that a subsurface body has the shape of a sphere and is traversed (in the x direction) by a current paralleled to the earth's surface, so that it is equivalent to a horizontally polarized doublet. In eq. (10–19a) the potential of a charged sphere at a surface point P was given as $V_1 = m \cos \theta / r^2$, in which the electrical moment is proportional to the electrical field $\mathbf{E}$ so that $m \equiv \mathbf{p}\mathbf{E}$ and $-V_2 = \mathbf{p}\mathbf{E} \cos \theta / r^2$. Since the undisturbed potential at the point P is $-x\mathbf{E}$, the resultant total surface potential is

$$V_r = - r\mathbf{E} \cos \theta - \frac{\mathbf{p}\mathbf{E} \cos \theta}{r^2}. \qquad (10\text{–}28a)$$

The value of the factor $\mathbf{p}$ may be determined from the boundary conditions at the surface of the sphere, where the current densities (ρ_2 = resistivity of the sphere, ρ_1 = resistivity of the surrounding medium) are given by

$$\frac{1}{\rho_1} \cdot \frac{dV_r}{d\mathbf{R}} = \frac{1}{\rho_2} \cdot \frac{dV_\mathbf{R}}{d\mathbf{R}}. \qquad (10\text{–}28b)$$

Since it follows from eq. (10–28a) that at the surface of the sphere ($r \equiv \mathbf{R}$)

$$-V_\mathbf{R} = \mathbf{E} \cos \theta \left(\mathbf{R} - \frac{\mathbf{p}}{2\mathbf{R}^2} \right), \qquad (10\text{–}28c)$$

substitution of eqs. (10–28a) and (10–28c) in (10–28b) gives

$$\mathbf{p} = \frac{\rho_2 - \rho_1}{2\rho_2 + \rho_1} \cdot \mathbf{R}^3. \qquad (10\text{–}28d)$$

Substituting this in eq. (10–28a),

$$V_r = - i\rho_1 x \left(1 + \frac{\rho_2 - \rho_1}{2\rho_2 + \rho_1} \cdot \frac{\mathbf{R}^3}{r^3} \right), \qquad (10\text{–}28e)$$

with $x = r \cos \theta$, and $\mathbf{E} = i\rho_1$. If the resistivity ratio $k = \rho_1/\rho_2$, the factor

$$c = \frac{\rho_2 - \rho_1}{2\rho_2 + \rho_1} - \frac{k - 1}{k} \qquad (10\text{--}28f)$$

expresses the effect of good or poor conductors imbedded in another medium on the surface potential (see Fig. 10-40). A "saturation effect" occurs since, for *poor* conductors, *one-half* of the maximum effect is reached for a (inverse) conductivity ratio of 2.5, whereas for *good* conductors *one-half* of the maximum effect occurs already at a ratio of 4.
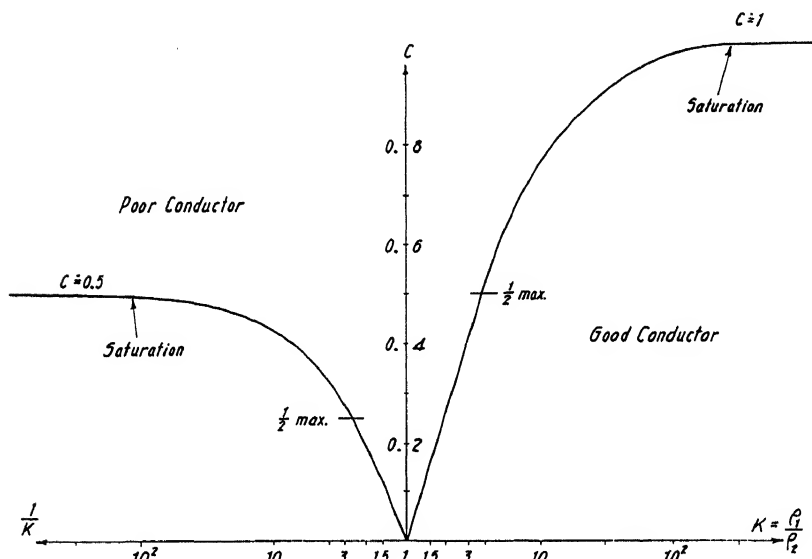
FIG. 10-40. Saturation effect in potential methods, for poor and good (approximately spherical) conductors.

These relations hold for spherical or nearly spherical bodies. For elongated bodies the effect depends essentially on the extent of the body in the direction of current flow compared with the extent at right angles thereto. For elliptical bodies of various ratios of major/minor axis ($\epsilon = a/b$) traversed by current in the direction of the major axis, Hummel[29] has calculated the ratio of current density in the body to that in undisturbed ground (Fig. 10-41). Only in a body which is very extended in the direction of current is the current density ratio equal to the resistivity ratio.

It is noted in eq. (10-28e) that the anomalous potential of a sphere is inversely proportional to the cube of its distance, and that it increases in

[29] J. N. Hummel, Zeit. Geophys., **4(2)**, 73 (1928).

proportion to its volume. The second derivative of the potential with respect to x indicates that the current density is a minimum directly over the sphere and that a maximum occurs at $x = \pm 1.22h$, (where h is the depth to the center of the sphere). If the sphere were not present, the equipotential lines would be parallel to one another (for line electrodes). The potential of a line at a distance x' would be $-\mathbf{E}x'$. With the sphere, the line is shifted to a position x with the potential given by eq. (10–28e), so that

$$x' - x \equiv \Delta x = c \cdot \qquad\qquad (10\text{–}29)$$
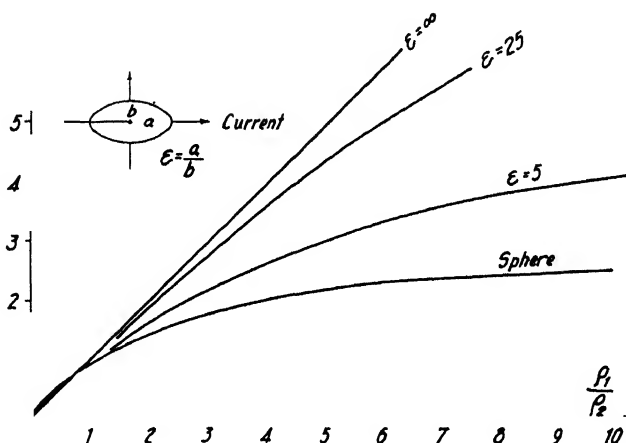
FIG. 10-41. Current densities in conductors of various relative dimensions (ϵ = axis ratio) as functions of resistivity ratio (adapted from Hummel).

By differentiation of this expression with respect to x it can be shown that the maximum displacement of the equipotential lines occurs at a distance $x = 0.707h$.

The effect of other bodies on the distribution of equipotential lines may be calculated if they are of simple geometric shape.[30] However, in most cases, it is more convenient to determine the effects of such bodies by model experiments as discussed below.

2. *Equipotential-line anomalies in stratified ground.* Horizontally stratified formations do not permit the application of equipotential-line methods. Other potential methods must be used, the most important ones being the resistivity and potential-drop–ratio methods discussed in sections V and VI.

---

[30] See J. N. Hummel, Zeit. Geophys., **4(2)** 67–75 (1928); Gerl. Beitr., **21(2/3)**, 204–214 (1929).

However, in the case of dipping formations, equipotential-line surveys can give useful information on dip and strike because of the electrical anisotropy of stratified media. Schlumberger has designated the ratio of the transverse and longitudinal resistivities as "anisotropy coefficient." For vertically stratified ground, the influence of anisotropy on the shape of the equipotential lines is most noticeable. The equipotential surfaces are no longer spherical about one electrode but are ellipsoids of revolution with the major axis in the direction of stratification. In plan view the trace of the equipotential surface will likewise be an ellipse, with the major axis in the direction of strike. The ratio of the axes is proportional to the ratio of the square roots of the conductivity in the direction of strike and that at right angles to the strike.

When stratified ground is covered with glacial drift or other unconformable layers, it is necessary that the equipotential surfaces reach deeply into the stratified portion to make the deformations detectable. Hence, large equipotential ellipses whose minor axes are at least twice as great as the assumed cover thickness should be traced. Dips may also be determined directly from the displacement of the ellipses if contact can be made underground with the formation under test.

There occurs a refraction of the equipotential surfaces on formation boundaries. If a given line approaches the boundary in a medium with the resistivity ρ by the angle α, and if it is refracted into the second medium (resistivity ρ') by the angle α', the relation obtains:

$$\rho \tan \alpha = \rho' \tan \alpha'. \tag{10-30}$$

The maximum refraction is obtained if the bisecting direction makes an angle of 45° with the formation boundary. Hence, it is advantageous to lay out the electrode basis at an angle of 45° with the boundary to be located.

3. In virtually all electrical methods, *model experiments* play an important part because of difficulties encountered in the calculation of the electrical anomalies of geologic bodies. These experiments are made on a small scale in the laboratory where it is possible to simulate a number of conditions difficult of evaluation, such as topography, irregular shape of the ore body, and so on. In duplicating actual conditions on a small scale it is necessary to pay close attention to the fundamental equations controlling the electrical anomalies of subsurface bodies, since it may be necessary to change the conductivity scale when the geometric scale is changed. In accordance with formula (10-28e), the potential of a sphere depends on the *relative* dimensions and on the conductivity ratio in reference to that of the country rock. Hence, if both are duplicated in the laboratory, the observed potential anomalies may be expected to be dupli-

cates of those occurring in nature.   Model experiments with equipotential lines and potential profiles are usually made in tanks filled with a weakly electrolytic solution.   Model ore bodies are generally made of some readily available metal.   Fujita[31] used a vacuum tube oscillator, line electrodes of bare copper wire, a copper sulfate solution (33 mg copper per 100 cm^3), and phones (no amplifier).   The secondary electrodes were made of glass tubes filled with mercury in which a coiled platinum wire was immersed and made contact with the surface of the solution.   The model ore body consisted of a copper sheet 5 mm thick and 100 mm square.

Fujita's results may be summarized as follows: (1) The field between the line electrodes was uniform only in the central third portion.   (2) For a conductive body the maximum distortion was observed when its strike was at right angles to the electrodes.   (3) For a nonconductive body the maximum distortion resulted when its strike was parallel with the line electrodes.   (4) The dip of a model ore body could be determined from the difference in the disturbed area on either side of the suboutcrop. (5) The position most favorable for indications was in the center between the electrodes.   (6) The greatest area of distortion was obtained when the length of the line electrodes was five times the length of the ore body and their distance three times.   (7) The depth reached increased in direct proportion to the length of the ore body, the detectable depth being about 63 per cent of the length.   (8) Thickness of an ore body was effective only up to a certain point; a saturation effect was soon reached.   (9) Detectability increased distinctly with dip.

Considerable experimental work on model ore bodies has been done by Lundberg and Sundberg.[32]   Fig. 10-42 shows equipotential lines as traced by the ordinary method (phones), in contrast with the in-phase equipotential lines located with a compensator.   Out-of-phase equipotential lines appear to be of equal diagnostic value, as shown by Gall[33] in some model experiments (where, however, the out-of-phase potentials were introduced artificially by feeding an out-of-phase current into the arrangement at right angles to the main current).

4. *Distortions of equipotential lines due to power leads.*   Generator leads often cause induction currents which are 90° out of phase with respect to the currents produced by contact.   These induction currents deflect the equipotential lines from their regular position, and elliptical polarization occurs.   Since it is not possible to apply a correction for the effect of the cable (in the ordinary procedure of mapping with amplifier and phones), the leads are generally so laid out that the interference is at a minimum.

[31] Proc. World Eng. Congr. (Tokio, 1929), Part 5, Paper No. 436, pp. 143-281.

[32] Beitr. angew. Geophys., **1**(3), 298-361 (1931)..

[33] J. Sci. Instr., **8**(10), 311 (Oct., 1931).

When complete observations are made by resolving the potential into its in-phase and out-of-phase components, the effect of the leads is readily recognized and may be separated from the in-phase anomalies. As a matter of fact, the out-of-phase potentials near the cable may be of great diagnostic value (see page 801).

5. *Effect of topography.* Barring the existence of highly conductive layers of irregular composition or thickness near the surface, the interpretation of equipotential line surveys in level terrain is generally not too difficult. However, with the exception of northern glaciated countries such as Canada or Sweden, ore prospecting work is usually carried on in mountainous areas where considerable interference may result from changes in topographic conditions.
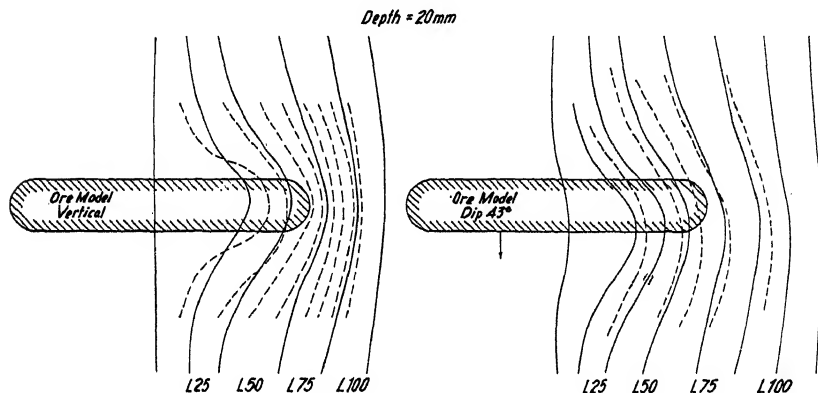
FIG. 10-42. Potential anomalies on model ore bodies (after Sundberg). Solid lines: equipotential lines, traced by phones. Dotted lines: in-phase equipotential lines, constructed from amplitude and phase measurements.

Topography is, first, of geometric influence. If a line connecting the two electrodes is not parallel with the surface, the ore bodies are not located vertically below their surface indications but are on a normal to the line connecting the electrodes.[34] The second effect of topography is of an electrical nature. The earth's surface represents the boundary between a conductive and a nonconductive medium; hence, the current lines, tending to follow the surface of the conductive medium will reflect, in vertical section, the contours of the surface, and the equipotential lines will show corresponding distortions.

To correct for topography by analytical methods is not practicable. The usual procedure is to plot topographic contours, together with equipotential lines, and to eliminate from consideration equipotential lines

[34] W. Heine, *Elektrische Bodenforschung*, p. 107, Fig. 53 (1928).

tending at right angles to the topographic contours (see **Fig. 10–43**). Where this would involve discarding an entire survey, the only procedure left is a model experiment. Notwithstanding the marked effects of topographic irregularities, it is observed in most applications of the equipotential line method that irregularities in surface geological features are of remarkably little effect. The only exceptions appear to be areas where highly saline beds occur at or near the surface.
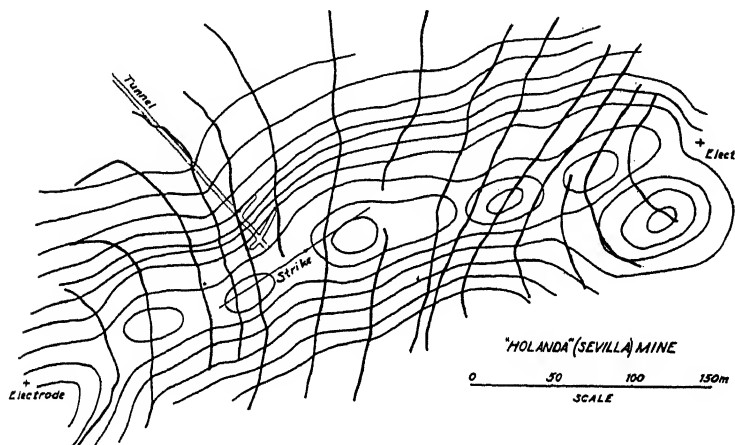
FIG. 10–43. Equipotential line survey in which most distortions are caused by topography (after Heine).

E. DISCUSSION OF RESULTS

Equipotential-line and potential-profile methods have been applied to (1) location of ore, (2) structural studies, and (3) military and civil engineering problems.

1. *Ore location.* Probably the most extensive work with equipotential-line and potential-profile methods has been done in the Skellefte district in northern Sweden. Close to 120 square miles have been surveyed there systematically with electrical methods and more than twenty ore fields have been found. Conditions for electrical prospecting are exceedingly favorable because of a comparatively shallow blanket of glacial moraine and frequent ore indications in the form of ore boulders and float. Although these had been known for centuries, it was not until 1918 that systematic electrical prospecting was started.

The ores in the Skellefte district occur in a leptite formation which corresponds in age to the Keewatin. It consists largely of volcanic rocks which were intruded, in Archean times, by large bodies of granite; this led to considerable metasomatic alteration and to deposition of ore. The

more important ores occur in the form of large lenses in the leptite formation. Others, likewise in the form of lenses, are found in black slates.
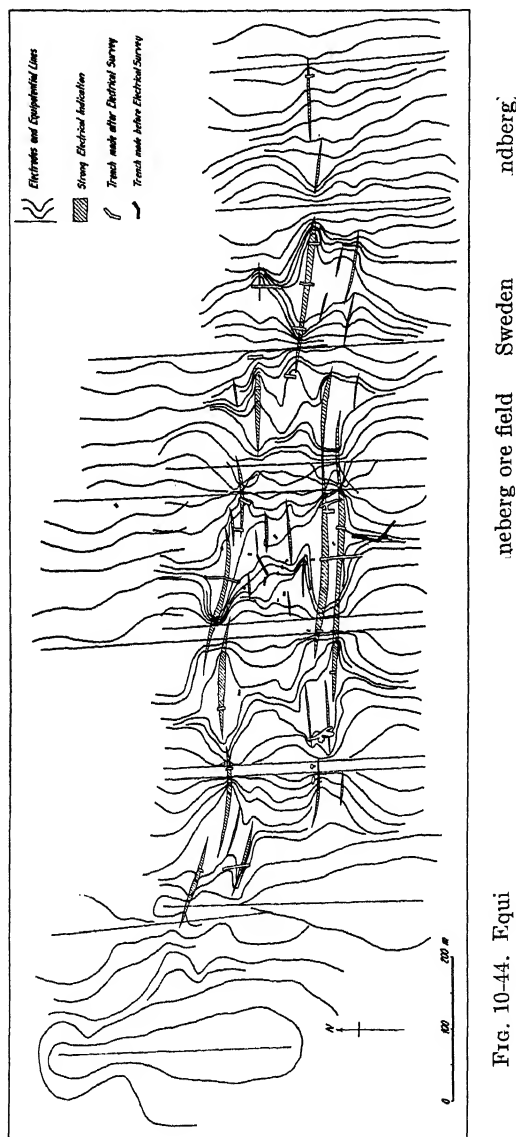
FIG. 10-44. Equineberg ore field Sweden ndberg.

The ore contains pyrite, chalcopyrite, pyrrhotite, arsenopyrite, and gold. The ore bodies are from 40 to 600 m long, from 5 to 30 m wide, and are covered by glacial moraine which has an average thickness of 7 to 8 m.

The more important ore discoveries resulting from the application of equipotential-line methods were at Kristineberg, Bjurfors, and Bjurliden. (The Boliden gold and arsenic deposit was located largely by electromagnetic methods and is discussed in that connection.) The equipotential survey in the Kristineberg field is illustrated in Fig. 10-44. Intervals between the primary electrodes were of the order of 150 to 200 m. Ore boulders had been found early in this field, and numerous test pits and trenches had been sunk. The distribution of these boulders first gave rise to the assumption that the strike of the deposits was north-south but no ore was found by these prospecting activities. An equipotential-line survey was made in 1918, and in the same year two important ore bodies were located. By 1919 the entire field had been outlined. Out of eight prospecting trenches dug to test the indications, five encountered ore. The ore

bodies averaged 6 to 7 m in width and contained from 70 to 80 per cent ore.

The field at Bjurfors has had a similar history. At first much trenching was done because of the abundance of ore boulders in the area, but no ore was found. The equipotential-line survey, started in 1918, was at first unsuccessful. The work was taken up again in 1922 when a party consisting of both geologists and geophysicists made a detailed survey of the area and located some strong equipotential-line distortions. The indications were confirmed by diamond drilling, and commercial mineralization was encountered in the eastern and central portions of the field. In the eastern part the ores were about 5 to 9 m deep while in the western portion the ores ran from 16 to 20 m in depth.

East of Bjurfors an extended zone more than 3 km long and over 1 km wide was surveyed in order to locate more ore bodies in the direction of strike. Numerous very distinct indications were obtained, some of them accompanied by magnetic effects. The presence of wet gravels in this area made trenching difficult, and exploration by drilling proved these indications to be largely due to graphitic and pyritic slates and noncommercial mineral impregnations. This survey is an example of extensive and distinct indications which are not due to commercial ore. In cases of this kind only repeat measurements with other electrical and magnetic methods, accompanied by as much geological mapping as applicable, will lead to correct interpretations.

In the glaciated areas of the northern United States and particularly in Canada, where conditions are very similar to those in Sweden, the equipotential-line methods have been applied successfully. In Newfoundland an extensive equipotential survey was made covering an area about 2 miles long and 1 mile wide, following the location of lead-zinc ore at the Buchans mine in the center of the area. The ore, consisting of lead-zinc copper sulfides in a baryte gangue, occurs in lenticular masses in bedded tuffs and porphyritic lava flows of Archean age. The thickness of the glacial overburden varies from a very few to 60 feet. East of the Buchans mine large indications were found at Oriental; two of these were drilled and found to be high grade lead-zinc ore. West of the Buchans mine a large area of indications was encountered and was confirmed by a number of trenches. Subsequent drilling and underground work has indicated more than 3 million tons of high-grade ore. A number of equipotential surveys for ore exploration were made by Edge and Laby[35] in the eastern part of Australia (Queensland, New South Wales, Victoria, and Tasmania).

' *Op. cit.*, pp. 75, 78, 83, 85, 86, 92, 122, 123, 124, 129, 132.
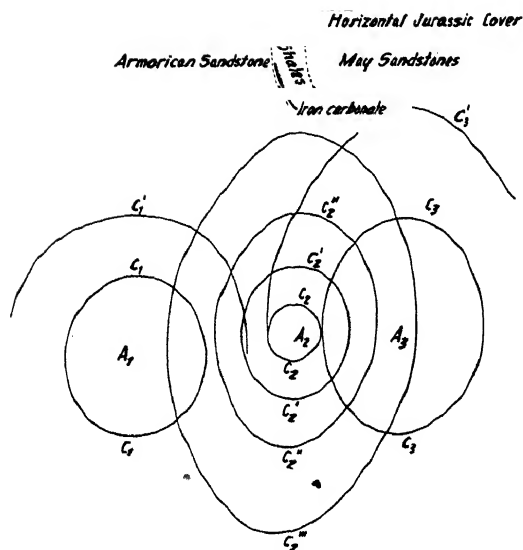
FIG. 10-45. Determination of strike of steeply dipping shale beds in Normandy, France (after Schlumberger).

2. *Structural studies.* Equipotential-line studies have been applied to structural problems for determining strike of formations under over-burden. Fig. 10–45 shows elliptical equipotential surfaces on dipping Silurian shales, interbedded between Armorican and May sandstones, and covered by Jurassic beds 200 to 300 feet thick. This survey was made to determine strike and to trace a siderite deposit on the footwall of the Silurian shales.

3. *Military applications.* The equipotential-line method may be useful for the location of iron and steel objects in civil and military engineering problems. Fig. 10–46 shows an application of this kind to the location of a buried ammunition magazine whose depth was about five feet.

Following his model experiments with equipotential-line methods, Fujita conducted extensive studies of the potential distribution on the Suwa mine, 100 miles northeast of Tokyo. This mine is operating a large vein of cupriferous pyrite in schists on six levels at 100-foot intervals to a depth of 700 feet below the surface. The experiments were chiefly concerned with various arrangements of the line electrodes and attempts to derive the dip of the ore body (70°) from the relative disposition of the anomalous areas.
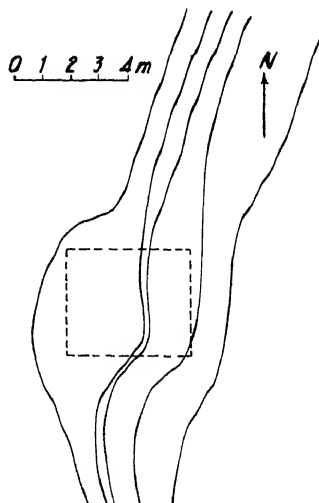
FIG. 10-46. Location of a buried ammunition magazine by equipotential methods (after Ebert).

V. RESISTIVITY METHODS

A. General

The equipotential-line methods discussed in the preceding section are best suited to the location of laterally limited geologic bodies, that is, bodies with vertical or nearly vertical boundaries. If they are used on horizontally stratified ground, only the spacing, but not the direction of the lines, is affected. To determine differences in spacing, potential gradients must be measured, that is, potential differences must be determined at no less than two points. If such measurements are supplemented by observations of current in the circuit, they are referred to as *resistivity* methods because (as stated on page 644) current measurements at two points
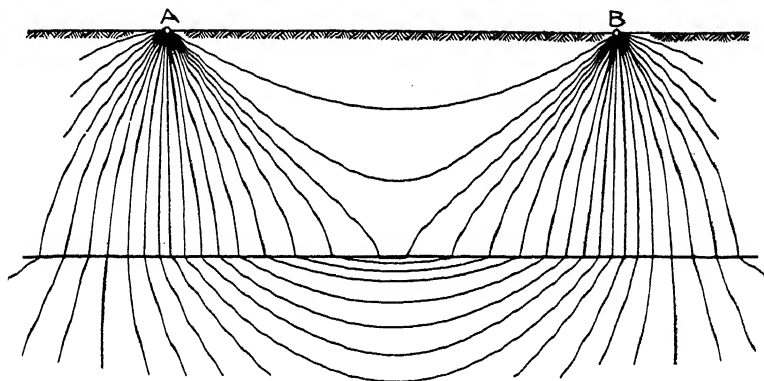
Fig. 10-47. Lines of current flow in layered section. (Conductivity of lower medium is fifty times greater than that of upper.) (After W. Weaver.)

and potential measurements at two others will give the resistivity of bodies of almost any shape.

The effect of vertical changes in conductivity on surface potentials is illustrated in Figs. 10-47 and 10-48. The more conductive lower medium (Fig. 10-47) results in an attraction of the current lines toward it. The current density in the upper medium is less than in the lower. Since the equipotential lines are at right angles to the current lines, their spacing, and hence the potential gradient, is likewise affected by the presence of layers of different conductivity. As shown in Fig. 10-48, the effect on the gradient varies with the conductivity, but it does not vary uniformly as far as conductivity ratio is concerned. The effect of a layer a hundred times as conductive as the surface layer is only about twice as much as that of a layer five times as conductive (*saturation effect*).

Measurements of potential differences in the vicinity of one power elec-

trode, or between two power electrodes, can therefore give information
in respect to the presence of subsurface formations of different conduc-
tivities. When these measurements are supplemented by measurements
of current, it is possible to determine the resistance of the circuit. By
applying a factor depending on the spacing of the electrodes, the ground
resistivity can be obtained. This is a true resistivity only if the medium
is homogeneous; if layers of different conductivities are present, it is an
apparent resistivity. It is customary to calculate the apparent resistivity
by the same formula that applies to homogeneous ground.

The depth to which the resistivity is measured can be controlled by
varying the *spacing* between the electrodes. This gives rise to two appli-
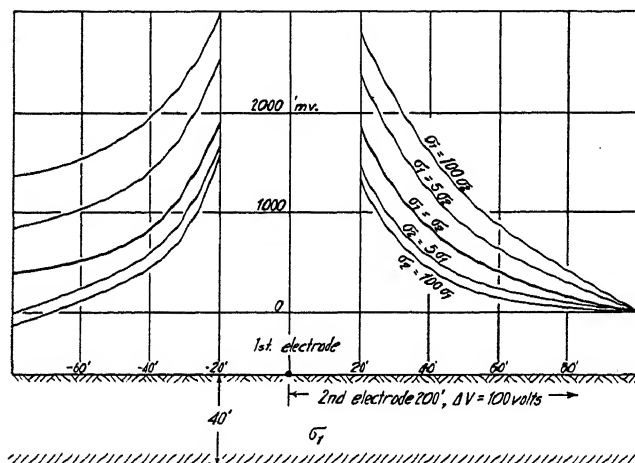
FIG. 10-48. Potential variations near electrode (outside and inside spread) for layers
of different conductivity, at 40 feet depth (after W. Weaver).

cations of the method. In the first, the spacing is kept constant and the
arrangement as a whole is moved over the ground (resistivity mapping).
In the second, measurements are made at one location which is the center
of the measuring arrangement. From this center the spacing of the elec-
trodes is gradually increased. Thus, the depth penetration is increased
and the apparent resistivity is obtained as a function of depth (vertical
electrical drilling).

While four equally spaced electrodes are the arrangement most gen-
erally used, other arrangements can be and have been applied. A deriva-
tion of the formulas for the more common arrangements is given in the
next article.

B. Electrode Arrangements

If, at the surface of the (homogeneous and isotropic) ground of the conductivity σ, an electric current I is introduced by means of two point electrodes, A and B, and if the current flows from A to B, the potential at any point P on the surface is $V_p = \dfrac{I}{2\pi\sigma}(1/r_1 - 1/r_2)$, where r_1 and r_2 are the distances of a point P from the electrodes A and B, respectively. The potential difference between *two* points P and R, which have the distances r_1, r_2, and $\mathbf{R}_1$ and $\mathbf{R}_2$, respectively, from the electrodes is

$$V_P - V_R \equiv V = \frac{I}{2\pi\sigma}\left(\frac{1}{r_1} - \frac{1}{r_2} - \frac{1}{\mathbf{R}_1} + \frac{1}{\mathbf{R}_2}\right). \qquad (10\text{-}31a)$$

Hence, the resistivity

$$\rho = \frac{1}{\sigma} = 2\pi\,\frac{V}{I}\,\frac{1}{\left(\dfrac{1}{r_1} - \dfrac{1}{r_2} - \dfrac{1}{\mathbf{R}_1} + \dfrac{1}{\mathbf{R}_2}\right)}. \qquad (10\text{-}31b)$$

This equation holds for any position of the current electrodes A and B and the search electrodes P and R, and does not change when current and potential electrodes are interchanged. Differences in the position of the search electrodes with respect to the current electrodes give rise to various resistivity methods. By selecting definite dispositions, it is possible to simplify the field procedure or to give the expression for resistivity a form that will simplify the interpretation of the results.

Seven different electrode systems are discussed below. They may be classified as follows:

Group I
Electrode Arrangements with Finite Distance of Power Electrodes

1	2	3	4
Symmetrical Wenner-Gish-Rooney method (four terminal)	Lee partitioning method	Asymmetrical double probe method	Asymmetrical single probe method

Group II
Measurements Near One Power Electrode; Second Power Electrode in Infinity

Double equidistant probe method	Double probe method with unequal probe spacing	Single probe method

1. In the *Wenner-Gish-Rooney method* the two potential electrodes are placed on a line with the two current electrodes, so that all four electrodes are situated at equal distances from one another. With a as the distance between the electrodes, $r_1 = R_2 = a$ and r_2 and $R_1 = 2a$. Then the expression for the resistivity, from eq. (10–31b) is

$$\rho = 2\pi a \frac{V}{I} . \qquad (10\text{–}31c)$$

2. In the *Lee partitioning method* an additional potential electrode is provided halfway between P and R. Two potential measurements are made, one for the left and another for the right interval. With $r_1 = a$, $r_2 = 2a$, $R_1 = \frac{3}{2}a$, and $R_2 = \frac{3}{2}a$, the resistivity

$$\rho = 4\pi a \frac{V_{PC}}{I} , \qquad (10\text{–}31d)$$

where $V_{PC} \equiv V_{PR}$ is the potential difference between the center stake and the adjacent potential stake.

3. The *asymmetrical double probe method* is an arrangement with the two potential probes placed at equal intervals from one power electrode but unsymmetrically placed in respect to the center. If l is the distance between the current electrodes and a the potential-electrode interval, $r_1 = a$, $r_2 = l - a$, $R_1 = 2a$, and $R_2 = l - 2a$, and the resistivity

$$\rho = 2\pi \frac{V}{I} \frac{2a(l - a)(l - 2a)}{(l - 2a)^2 + al} . \qquad (10\text{–}31e)$$

Eq. (10–31e) gives the Wenner formula when $l = 3a$.

4. The *asymmetrical single probe method* results from the last by leaving out one potential electrode and measuring the potential of the remaining electrode against that of the next power electrode. Then $r_1 = 0$, $r_2 = l$, $R_1 = a$, and $R_2 = l - a$, so that with V_e as half the potential difference between the power electrodes

$$\rho = 2\pi \frac{(V_e - V)}{I} \cdot \frac{a(l - a)}{(l - 2a)} . \qquad (10\text{–}31f)$$

5. The *double equidistant probe method* is a modification of arrangement 3, with the second power electrode far removed. With $r_1 = a$, $r_2 = \infty$, $R_1 = 2a$, and $R_2 = \infty$,

$$\rho = 4\pi a \frac{V}{I} . \qquad (10\text{–}31g)$$

6. The *double probe method with unequal probe spacing* differs from the last by an unequal probe spacing and is generally used with a potential

profile at right angles to the power electrode base. If $r_1 = a$ is the distance to the first potential electrode and $R_1 = b$ the distance to the second one, and $R_2 = r_2 = \infty$,

$$\rho = \frac{2\pi ab}{(b-a)} \cdot \frac{V}{I}.$$

(10-31h)

7. The *single probe method* corresponds to arrangement 4, with one power electrode in infinity. Since $r_1 = 0$, $r_2 = \infty$, $R_1 = a$, and $R_2 = \infty$,

$$\rho = 2\pi a \frac{(V_e - V)}{I}.$$

(10-31i)

Arrangement 1 is most frequently employed, for both vertical electrical drilling and resistivity mapping. Next in order is probably 2, then follows 4. Arrangements 5 and 6 are convenient for vertical electrical drilling and are used in the potential-drop-ratio procedures with one additional potential electrode. Arrangement 5 is also applied in electrical logging.

C. Potential Functions for Layered Media

1. *General.*[36] If a difference in resistivity exists on a formation boundary (see Fig. 10-49) its effect may be represented by placing a plate with definite transmission and reflection characteristics in the boundary. Assume a source at P above the

Fig. 10-49. Conditions on boundary between two media of different resistivity.

plate. Considering the phenomenon for the moment as one of light transmission, an observer at A facing the plate would see the point P by looking at its image I. The light at A would be that received directly from P plus the amount reflected by the plate and appearing to come from the image I. If the dimming of the apparent source at I, due to reflection, be indicated by a factor k, the light and by analogy the potential at A is equal to its amount at the source diminished by the geometric effect of distance $(1/r)$ plus the amount reflected, so that

$$V_A = \frac{\rho_1 I}{4\pi}\left(\frac{1}{r_1} + \frac{k}{r_2}\right).$$

(10-32a)

[36] For a more rigorous discussion of the theory of images than the one given here to illustrate merely its elements, see J. H. Jeans, *Mathematical Theory of Electricity and Magnetism*, 4th ed., Cambridge U. Press, 1923, pp. 200–201.

An observer facing the plate at B sees the source P at an intensity reduced by transmission through the plate. The amount transmitted is the original intensity minus the amount lost through reflection, which in turn is proportional to k times the original intensity. Therefore, the light and by analogy the potential at B is

$$V_B = \frac{\rho_2 I}{4} (1 - k).$$ (10-32b)

Continuity of the potential requires that in the boundary plane where $r_1 = r_2 = r_3$, V_A and V_B be equal, so that $\frac{\rho_1 I}{4\pi r} (1 + k) = \frac{\rho_2 I}{4\pi r} (1 \quad k)$. Hence,

$$k = \frac{\rho_2 - \rho_1}{\rho_2 + \rho_1},$$ (10-32c)

so that in eq. (10-32b)

$$1 - k = \frac{2\rho_1}{\rho_2 + \rho_1} \quad \text{and} \quad 1 + k = \frac{2\rho_2}{\rho_2 + \rho_1}.$$ (10-32d)
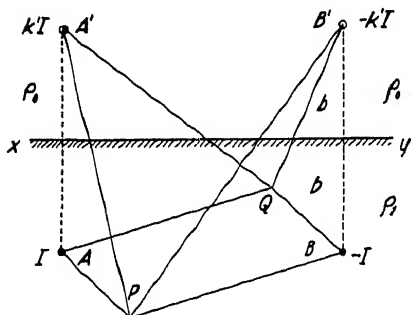
Fig. 10-50. Four points and images on boundary.

The factor k expresses the "electrification" of a plane between two media of different resistivities due to a point source and its image. The application of this principle is illustrated by a calculation of the potential distribution resulting from two current electrodes near the ground surface, corresponding to a Wenner-Gish-Rooney arrangement with buried electrodes (Fig. 10-50). If the point A is considered as current source (I) and B as the corresponding "sink" $(-I)$, the potential distribution at the surface is obtained by considering the effects of both sources, A and B, and their images, A' and B'. The intensities of the images are $k'I$ and $-k'I$, respectively. Applying eq. (10-32c), k' is seen to be equal to 1, since $\rho_2 = \infty$ (air). Hence, the images have the strength I and $-I$, respectively. The potential difference between P and Q due to a source I at A is $\Delta V = \frac{\rho_1 I}{4\pi} \left(\frac{1}{AP} - \frac{1}{AQ} \right)$, and that due to an image I at A' is $\frac{\rho_1 I}{4\pi} \left(\frac{1}{A'P} - \frac{1}{A'Q} \right)$ Similar relations apply to the potential difference at

the same points resulting from the source at B and its image at B'. If the electrodes are at equal intervals a in a straight line and at a depth b below the surface, the potential difference is

$$\Delta V = \frac{\rho_1 I}{4\pi}\left(\frac{1}{a} + \frac{2}{\sqrt{a^2 + 4b^2}} - \frac{1}{\sqrt{a^2 + b^2}}\right)$$

$$= \frac{\rho_1 I}{4\pi a}\left(1 + \frac{2}{\sqrt{1 + 4q^2}} - \frac{1}{\sqrt{1 + q^2}}\right), \qquad (10\text{-}33)$$

where $q = b/a$.
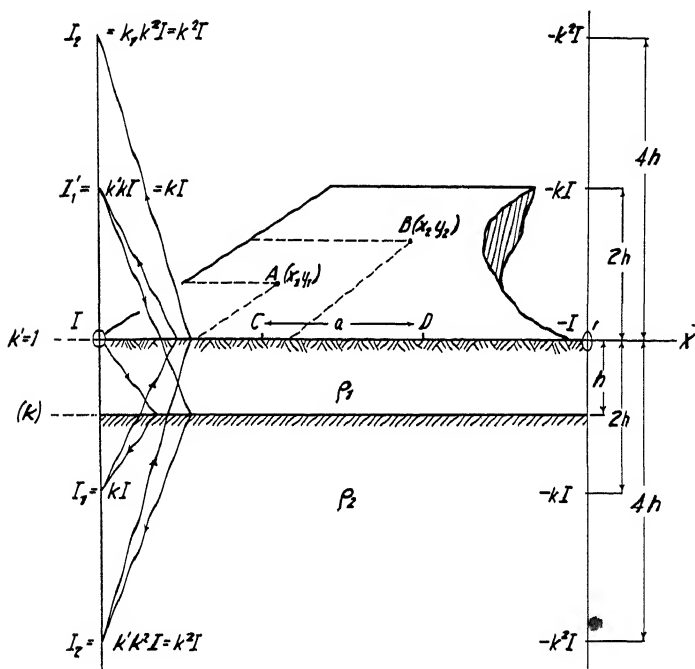
FIG. 10-51. Image distribution in two-layer potential problem.

When q is large (depth great compared with the electrode separation), $\Delta V = \rho_1 I/4\pi a$ (potential for an infinite homogeneous medium). When $q = 0$ (electrodes on ground surface), $\Delta V = \rho_1 I/2\pi a$ (potential for the semi-infinite medium).

2. *Two horizontal layers.* Assume two semi-infinite media with resistivities ρ_1 and ρ_2, as in Fig. 10-51. The upper layer is bounded by air (resistivity $\rho_0 = \infty$). If current is supplied at two points, O and O', the potential distribution at the surface can be calculated by considering a source I at O, a sink $-I$ at O', and the images of this source and sink

that are produced by reflection on the formation boundary and the earth's surface. The source I is reflected at the formation boundary and produces the image kI. The value of k is given by eq. (10-32c) and is equal to $(\rho_2 - \rho_1)/(\rho_2 + \rho_1)$, since it applies to the formation boundary $(\rho_2 \rho_1)$. The image $I_1 = kI$ is now reflected at the earth's surface and produces the image $I_1' = k'kI$ above. In this case k' as applied to the boundary between the upper medium and air is 1, since $\rho_0 = \infty$. Hence, the image $I_1' = kI$. The potential at any surface point will therefore result from a summation of an infinite series of images. Thus, $I_1 = kI$ at a depth $2h$; $I_1' = kI$ at a height $2h$; $I_2 = k^2I$ at a depth $4h$; $I_2' = k^2I$ at a height $4h$; so that $I_n = k^nI$ at a depth $2nh$, and $I_n' = k^nI$ at a height $2nh$. Since $I_n = I_n'$, $I_n + I_n' = 2k^nI$, and the potential at any point on the surface is

$$V = \frac{\rho_1}{2\pi}\left[\frac{I}{r} + \sum_{n=1}^{n=\infty} \frac{2k^nI}{r_n}\right]. \qquad (10\text{-}34)$$

The potential at a point $A(x_1 y_1)$ due to a source I at O and its series of images is therefore

$$V_{AO} = \frac{I\rho_1}{2\pi}\left[\frac{1}{\sqrt{x_1^2 + y_1^2}} + 2\sum_{n=1}^{n=\infty} \frac{k^n}{\sqrt{x_1^2 + y_1^2 + (2nh)^2}}\right], \qquad (10\text{-}35a)$$

and the potential due to an equal sink at O' at the same point is

$$V_{AO'} = -\frac{I\rho_1}{2\pi}\left[\frac{1}{\sqrt{(l - x_1)^2 + y_1^2}} + 2\sum_{n=1}^{n=\infty} \frac{k^n}{\sqrt{(l - x_1)^2 + y_1^2 + (2nh)^2}}\right], \qquad (10\text{-}35b)$$

where l is the distance between the electrodes so that the resulting potential is

$$V_A = \frac{I\rho_1}{2\pi}\left[\frac{1}{\sqrt{x_1^2 + y_1^2}} - \frac{1}{\sqrt{(l - x_1)^2 + y_1^2}} + 2\sum_{n=1}^{n=\infty} \frac{k^n}{\sqrt{x_1^2 + y_1^2 + (2nh)^2}}\right.$$
$$\left. - 2\sum_{n=1}^{n=\infty} \frac{k^n}{\sqrt{(l - x_1)^2 + y_1^2 + (2nh)^2}}\right]. \qquad (10\text{-}36a)$$

Similarly for another point $B(x_2 y_2)$,

$$V_B = \frac{I\rho_1}{2\pi}\left[\frac{1}{\sqrt{x_2^2 + y_2^2}} - \frac{1}{\sqrt{(l - x_2)^2 + y_2^2}}\right.$$
$$+ 2\sum_{n=1}^{n=\infty} \frac{k^n}{\sqrt{x_2^2 + y_2^2 + (2nh)^2}}$$
$$\left. - 2\sum_{n=1}^{n=\infty} \frac{k^n}{\sqrt{(l - x_2)^2 + y_2^2 + (2nh)^2}}\right]. \qquad (10\text{-}36b)$$

Hence, the difference of potential between the point A and B is

$$
\begin{aligned}
V_A - V_B = \frac{I\rho_1}{2\pi}\Bigg[& \frac{1}{\sqrt{x_1^2 + y_1^2}} - \frac{1}{\sqrt{(l - x_1)^2 + y_1^2}} \\
& + 2\sum_{n=1}^{n=\infty} \frac{k^n}{\sqrt{x_1^2 + y_1^2 + (2nh)^2}} \\
& - 2\sum_{n=1}^{n=\infty} \frac{k^n}{\sqrt{(l - x_1)^2 + y_1^2 + (2nh)^2}} - \frac{1}{\sqrt{x_2^2 + y_2^2}} \\
& + \frac{1}{\sqrt{(l - x_2)^2 + y_2^2}} - 2\sum_{n=1}^{n=\infty} \frac{k^n}{\sqrt{x_2^2 + y_2^2 + (2nh)^2}} \\
& + 2\sum_{n=1}^{n=\infty} \frac{k^n}{\sqrt{(l - x_2)^2 + y_2^2 + (2nh)^2}} \Bigg].
\end{aligned}
\tag{10-37a}
$$

From this general formula the potential difference between any two points may be determined.[37]

For the electrode arrangement in the Wenner-Gish-Rooney method, $x_1 = a$, $y_1 = 0$, $x_2 = 2a$, $y_2 = 0$, $l = 3a$, so that

$$
\begin{aligned}
V_A - V_B = \frac{I\rho_1}{2\pi}\Bigg[& \frac{1}{a} - \frac{1}{2a} + 2\sum_{n=1}^{n=\infty} \frac{k^n}{\sqrt{a^2 + (2nh)^2}} \\
& - 2\sum_{n=1}^{n=\infty} \frac{k^n}{\sqrt{(2a)^2 + (2nh)^2}} - \frac{1}{2a} + \frac{1}{a} \\
& - 2\sum_{n=1}^{n=\infty} \frac{k^n}{\sqrt{(2a)^2 + (2nh)^2}} + 2\sum_{n=1}^{n=\infty} \frac{k^n}{\sqrt{a^2 + (2nh)^2}} \Bigg],
\end{aligned}
$$

or

$$
V_A - V_B = \frac{I\rho_1}{2\pi a}\left[1 + 4\sum_{n=1}^{n=\infty} \frac{k^n}{\sqrt{1 + \left(\dfrac{2nh}{a}\right)^2}} - 4\sum_{n=1}^{n=\infty} \frac{k^n}{\sqrt{4 + \left(\dfrac{2nh}{a}\right)^2}} \right];
$$

$$
V_A - V_B \equiv \frac{I\rho_1}{2\pi a}[1 + 4\mathbf{F}].
\tag{10-37b}
$$

The quantity $\rho_1(1 + 4\mathbf{F})$ is an apparent resistivity. If $k = 0$ (homogeneous ground) the formula becomes $V_A - V_B = I\rho_1/2\pi a$. Hence the

[37] See J. N. Hummel, A.I.M.E. Tech. Publ. No. 418.

ratio of apparent resistivity, ρ_s, and true resistivity, ρ_1, is

$$\rho_1 \left[1 + 4 \sum_{n=1}^{n=\infty} \frac{k^n}{\sqrt{1 + \left(\frac{2nh}{a}\right)^2}} - 4 \right] \qquad (10\text{-}38)$$

where $u \equiv a/h$, the ratio of electrode separation and depth.
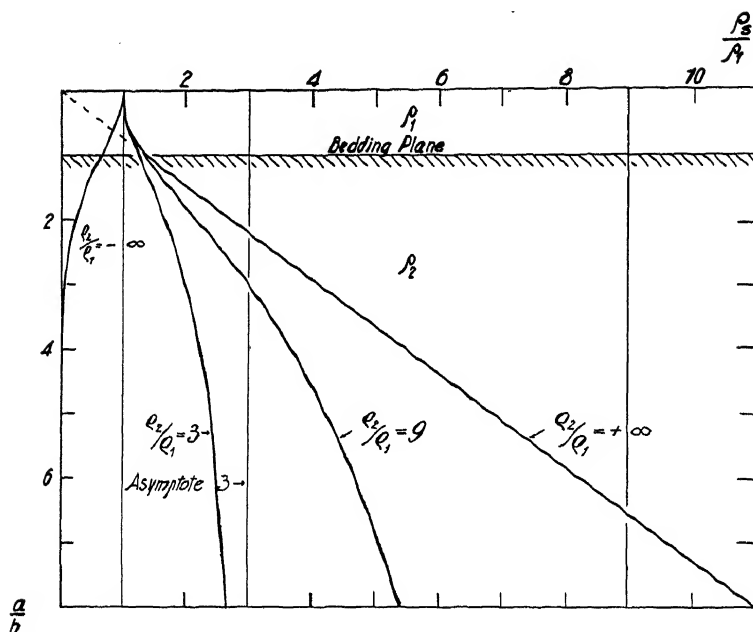
Fig. 10-52. Apparent resistivity ratio as a function of electrode separation in terms of depth, for various true resistivity ratios (after Hummel).

Fig. 10-52 shows the ratio of apparent and top-layer resistivity as a function of the ratio of electrode separation and depth, for various resistivity contrasts. If the resistivities are equal, the apparent resistivity is equal to the true resistivity. If $k = 1$ (lower layer of infinite resistivity), the apparent resistivity increases in direct proportion to the electrode separation, the proportionality factor being about 1.386. (with a/h). The apparent resistivity ratios for the k-values between 0 and 1 approach asymptotically the true resistivity ratios for large electrode separations.

If conductivity ratios are reversed (good conductor below), the apparent resistivity ratio lies between values of 0 and 1 and approaches 0.

3. *Three horizontal layers.* The theoretical treatment of this case proceeds along the same lines as that for the two-layer case. The mathematical relations become more complex, however, because images of sources and sinks are produced by reflection on two boundary surfaces. The calculation has been carried out by Hummel[38] for the general case and for a special condition where the thickness of the two top layers is the same ($h = h_1$) and the bottom layer is infinite in extent and of infinite resistivity. Results obtained for the latter case indicate that (for large electrode separations) the apparent resistances follow Kirchhoff's law for two resistances connected in parallel, so that the average resistivity of two infinite layers, of resistivity ρ_1 and ρ_2 and respective thickness h_1 and h_2, is given by

$$\frac{h_1 + h_2}{\rho_{av.}} = \frac{h_1}{\rho_1} + \frac{h_2}{\rho_2}. \qquad (10\text{-}39)$$

Fig. 10-53. Three-layer case (after Hummel).

This relation may be extended to cover the case of more than two layers of any thickness and makes possible a graphic approximation in the interpretation of resistivity curves. Fig. 10-53 illustrates the apparent resistivity curve for three layers with resistivities ρ, ρ_1, and ρ_2 and of thickness h, h_1, and ∞, with $h = h_1$. The shape of the curve for distances large in comparison with the depths of the upper layers is almost independent of the properties of these upper layers. For large spacings it is asymptotic to the line $\rho_s/\rho = 2$, since the resistivity of the lower infinite medium is twice that of the surface layer. Curves b and c are the "approximation" curves obtained by combining the upper two layers and considering the resultant layer with the bottom layer as a two-layer problem (curve b). Similarly, curve c follows by combination of the middle and bottom layer.

In Fig. 10-54 the middle layer has a high and the bottom layer a low resistivity. This curve is commonly obtained in water table determinations.

The theoretical curves prove that even for large differences in conductivity there is *no abrupt change* in apparent resistivity measured at the surface. If irregular curves and "breaks" are obtained in the field, they

---

[38] *Ibid.*, p. 409-414.

are due to local conditions, usually at the contact of the electrodes with the ground, and must be eliminated before any interpretation can be attempted.

4. *Effects of vertical contacts.* In Fig. 10-55, let AB be the surface of the ground and DE a fault plane dividing the region into two parts, of

resistivities ρ_1 and ρ_2. If a four-electrode system is moved as a whole or if the separation is increased, a resistivity curve consisting of five portions is obtained (Fig. 10-56). These, in turn, result from five possible positions of the arrangement in reference to the fault plane: (1) all electrodes in the first medium; (2) only one electrode across the fault line; (3) two electrodes in each medium; (4) three electrodes in the second medium; (5) all electrodes in the second medium. A sixth case arises

FIG. 10-54. Three-layer case (adapted from Hummel).

when measurements are made in either medium parallel to the strike of the contact.

(a) *Case 1* (four electrodes in one medium) corresponds to the condition $a < 2d/3$, if a is the electrode separation and d the distance from the center
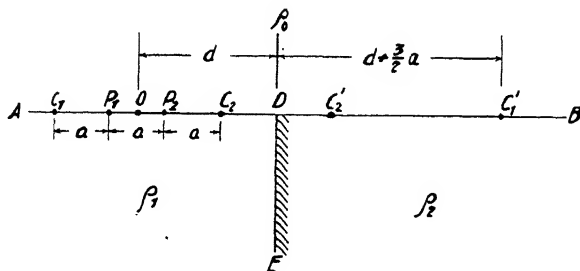
FIG. 10-55. Four-terminal electrode arrangement on contact plane.

of the electrode system to the contact. Assume a source of current I at C_1 and a sink $-I$ at C_2. The potential at points P_1 and P_2 will depend on the strength of I and $-I$ and of their images at C_1' and C_2' resulting from reflection on the interface DE. The potential at P_1 due to the source I at C_1 is $I\rho_1/2\pi a$; that at P_1 due to the sink $-I$ at C_2 is $-I\rho_1/4\pi a$. The potential resulting from the image at C_1' is $kI\rho_1/2\pi(2d-2a)$ and that

due to the image of $-I$ at C_2' is $kI\rho_1/2\pi(2d-a)$, where $k = (\rho_2 - \rho_1)/(\rho_2 + \rho_1)$. The total potential at P_1 is therefore

$$V_1 = \frac{I\rho_1}{2\pi}\left[\left(\frac{1}{a} - \frac{1}{2a}\right) + k\left(\frac{1}{2d+2a} - \frac{1}{2d-a}\right)\right]. \quad (10\text{-}40a)$$

Similarly, the potential at P_2 is

$$V_2 = \frac{I\rho_1}{2\pi}\left[\left(\frac{1}{2a} - \frac{1}{a}\right) + k\left(\frac{1}{2d+a} - \frac{1}{2d-2a}\right)\right]. \quad (10\text{-}40b)$$

Hence we have for the potential difference:

$$V_1 - V_2 = \frac{I\rho_1}{2\pi a}\left[1 + 4k\frac{d}{a}\left(\frac{1}{4\dfrac{d^2}{a^2} - 4} - \frac{1}{4\dfrac{d^2}{a^2} - 1}\right)\right], \quad (10\text{-}40c)$$

so that the apparent resistivity becomes

$$\rho_s = \rho_1\left[1 + 4k\frac{d}{a}\left(\frac{1}{4\dfrac{d^2}{a^2} - 4} - \frac{1}{4\dfrac{d^2}{a^2} - 1}\right)\right]. \quad (10\text{-}40d)$$

(b) In *case 2* (one current electrode in the second medium) the potential difference $V_1 - V_2$ due to the source I at C_1 and its image at C_1' will be the same as in case 1. However, the potential in medium (ρ_1) due to the sink $-I$ at C_2 in medium (ρ_2) must be considered as being due to a source $-2\rho_1 I/(\rho_2 + \rho_1)$ (see eq. (10–32d)), and the potential at P_1 will be the sum of the potentials due to a source I at C_1, to an image kI at C_1', and to a source $(k-1)I$ at C_2:

$$V_1 = \frac{I}{2\pi}\left[\rho_1\left(\frac{1}{a} + \frac{k}{2d+2a}\right) + \frac{\rho_2(k-1)}{2a}\right].$$

The potential at P_2 is accordingly

$$V_2 = \frac{I}{2\pi}\left[\rho_1\left(\frac{1}{2a} + \frac{k}{2d+a}\right) + \frac{\rho_2(k-1)}{a}\right].$$

$\left.\rule{0pt}{60pt}\right\} \quad (10\text{-}40e)$

From the difference the apparent resistivity is

$$\rho_s = \rho_1\left[1 + \frac{k}{2}\left(1 + \frac{1}{\dfrac{d}{a}+1} - \frac{2}{\dfrac{2d}{a}+1}\right)\right]. \quad (10\text{-}40f)$$

(c) In *case 3* (two electrodes in each medium) the potential at P_1 is due to the source I at C_1, kI at C_1', and $-2\rho_1 I/(\rho_2 + \rho_1) = (k-1)I$ at

C_2. Similar conditions apply to the potential at P_2, so that

$$\left.\begin{aligned} V_1 &= \frac{I}{2\pi}\left[\rho_1\left(\frac{1}{a} + \frac{k}{2d + 2a}\right) + \frac{\rho_2(k-1)}{2a}\right] \\ V_2 &= \frac{I}{2\pi}\left[\rho_2\left(\frac{1}{a} + \frac{k}{2a - 2d}\right) + \frac{\rho_1(k-1)}{2a}\right]. \end{aligned}\right\} \quad (10\text{–}40g)$$

Then the apparent resistivity becomes

$$\rho_s = \frac{\rho_1}{1-k}\left[1 + k^2 - k\left(\frac{k + \dfrac{d}{a}}{1 - \dfrac{d^2}{a^2}}\right)\right]. \qquad (10\text{–}40h)$$

(d) In *case 4* (three electrodes in second medium) we have for the apparent resistivity

$$\rho_s = \rho_1\frac{k+1}{1-k}\left[1 - k\left(\frac{1}{2} - \frac{1}{\dfrac{2d}{a}+1} + \frac{1}{\dfrac{2d}{a}+2}\right)\right]. \qquad (10\text{–}40i)$$

(e) In *case 5* (four electrodes in second medium) it is

$$\rho_s = \rho_1\frac{1+k}{1-k}\left[1 + k\left(\frac{4\dfrac{d}{a}}{4\dfrac{d^2}{a^2}-1} - \frac{\dfrac{d}{a}}{\dfrac{d^2}{a^2}-1}\right)\right]. \qquad (10\text{–}40j)$$

Figs. 10–56a and 10–56b show curves of apparent resistivity on contacts calculated for various k values. These curves are valid for the four-terminal Wenner-Gish-Rooney electrode arrangement, and they express the observed quantities as a function of spread distance from fault plane. It is seen that the apparent resistivities approach the true resistivities as the distances of the arrangement from the fault plane increase. Abrupt changes occur when $d/a = 0.5$ and 1.5, that is, when electrodes cross the contact plane.

An application of the above theory is made in electrical logging. This method involves the location of formation boundaries in wells by means of a system of fixed spacing electrodes (see Chapter 11).

When the electrode arrangement is used parallel to the strike of a fault, formula (10–33) may be applied to the contact (ρ_2, ρ_1), so that

$$V_1 - V_2 = \frac{I\rho_1}{2\pi}\left[\frac{1}{a} + \frac{2k}{\sqrt{4d^2 + a^2}} - \frac{2k}{\sqrt{4d^2 + 4a^2}}\right] \qquad (10\text{–}41a)$$

which gives for the apparent resistivity

$$\rho_s = \rho_1 \quad 1 + 2k \left(\frac{1}{\sqrt{4\dfrac{d^2}{a^2} + 1}} - \frac{-}{\sqrt{4\dfrac{d^2}{a^2} + 4}} \right) \qquad (10\text{--}41b)$$

Tagg[39] has published a series of curves showing for various k values the apparent resistivity as a function of distance from the contact. These
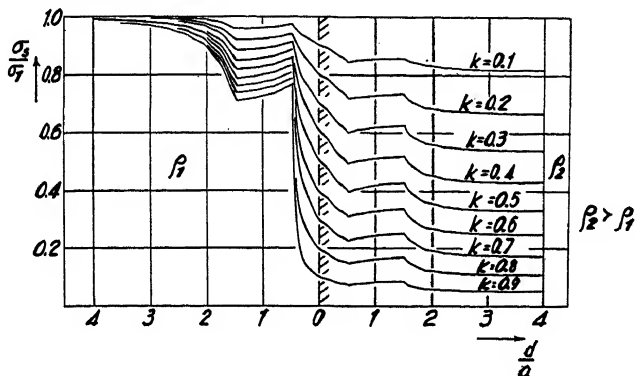
FIG. 10-56a. Apparent conductivities obtained with four-terminal electrode arrangements on contact (after Tagg).
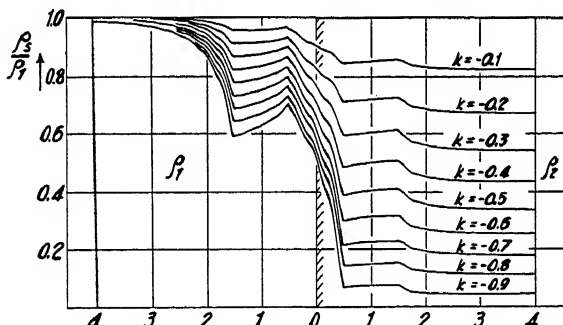
FIG. 10-56b. Apparent resistivities obtained with four-terminal electrode arrangements on contact, as a function of distance of center of spread from contact plane (in terms of electrode separation) (after Tagg).

indicate that if the distance of the electrode system from the fault is four times the electrode separation, its influence is practically negligible.

5. *Effects of dipping beds.* For dipping beds, apparent resistivities may

---

[39] G. F. Tagg, A.I.M.E. Geophys. Pros., 135–145 (1934).

be calculated in the same manner as for horizontal beds and by using the theory of images. In this case the number of images is no longer infinite.[40] The images lie on the circumference of circles with radii equal to the distances of source or sink from a hypothetical point of intersection of the interface with the surface. The number of effective images is $\pi/2\theta$, where θ is the dip. Fig. 10-57 shows a number of curves calculated for various dip angles for a constant resistivity ratio. The abscissa is the ratio of apparent and true surface-layer resistivity, the ordinate the ratio of electrode separation and depth (under the down-dip power electrode,
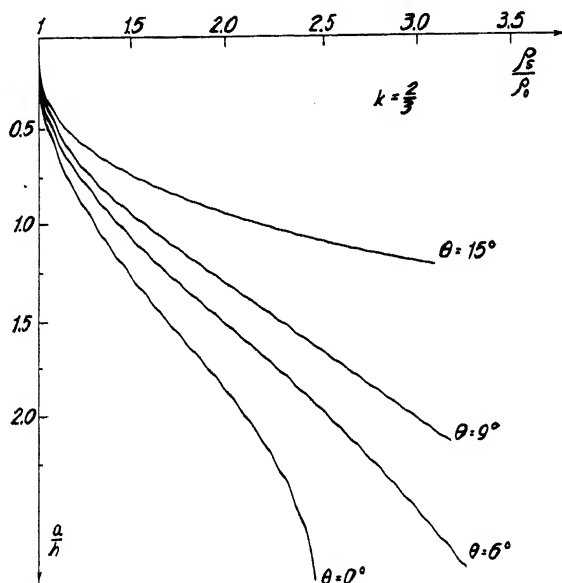
Fig. 10-57. Effect of dip on apparent resistivity ($k = 2/3$) (after Aldredge).

normal to the bed). For electrode separations less than one-half the depth, the influence of dip is very small and is approximately proportional to the sine of the dip angle. For large ratios of a/h, the curves straighten out appreciably. Since it is difficult to calculate dip analytically from up-dip and down-dip profiles, it is better to determine dip indirectly by profiles parallel to the strike.

6. *Effects of three-dimensional geologic bodies.* The effects of ore bodies, lenticular conductors, and the like, can be calculated by considering them as the equivalents of electrical doublets. The calculation is simplified by assuming that the doublet is situated below the midpoint of the electrode

[40] R. F. Aldredge, Colo. Sch. Mines Quart., **32**(1), 171-186 (Jan., 1937).

basis. Fig. 10–58 shows the ratio of apparent and true resistivity as a function of the ratio of electrode separation and length of spread for a polarized doublet. A distinct change in ρ_s/ρ occurs. This is of interest because the potential curve along the same line exhibits a smaller variation.
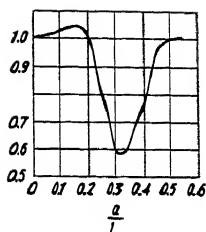
Fig. 10-58. Curve of apparent resistivity over polarized doublet (after Hummel).

D. Procedure; Equipment

For measurement of apparent resistivity, widely different procedures, electrode arrangements, and equipment are used. The latter fall into the following groups: (1) D.C. commutator method (Wenner-Gish-Rooney) with separate measurement of voltage and current; (2) Megger method, likewise with commutator and with direct resistance measurement by dual-coil indicators; (3) D.C. measurement with nonpolarizable electrodes; (4) A.C. method.

1. *D.C. commutator (Gish-Rooney) method.* A scheme of the equipment is given in Fig. 10-11. C_1 and C_2 are the external or current electrodes; P_1 and P_2 the potential electrodes. Current is measured with a milliammeter between C_1 and C_2, while the potential difference is observed between P_1 and P_2 on a potentiometer. A section of a double commutator is interposed in each circuit so that the current flows in the same direction through the measuring instruments while it is reversed periodically in the ground (about sixteen times a second). Much care must be devoted to the proper design of the commutator to insure correct and steady meter readings. Inasmuch as it takes the current a certain amount of time to build up to its equilibrium value (an effect which increases with increasing electrode separation, see formula [10-45a]), the segments on the potentiometer commutator are offset with respect to those on the current commutator.

Because of the insulating segments, the current read on the milliammeter is lower and hence the resistance is greater than its actual value. This difference may be corrected out by determining the value of a known resistance with commutator in motion and with commutator at rest (commutator factor). Unsteadiness of the galvanometer needle of the potentiometer can be avoided by placing a condenser of large capacity in series with one of the potential leads. Leakage between high- and low-voltage circuits in the instrument may be eliminated by the use of a grounded guard ring between the two sections of the commutator. A customary commutator design is shown in Fig. 10-59b.

2. *Megger method.* The "Megger" (abbreviation for "megohmer") instrument was developed primarily for the use of power and communication

companies to test the grounds of power stations and transmission towers, and the like. The Megger differs from the Gish-Rooney arrangement in two respects: (1) power is supplied from a generator mounted with the commutator on the same shaft; (2) measurements of voltage and current are made with cross-coil instruments so that automatically the ratio of
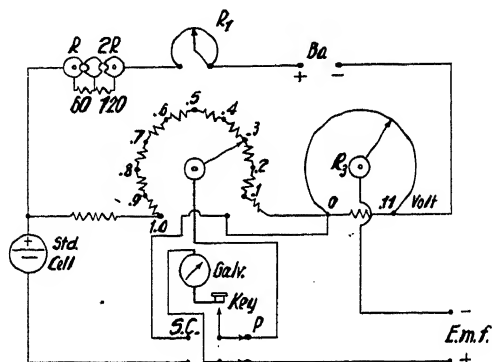
Fig. 10-59a. Circuit of Leeds and Northrup potentiometer.
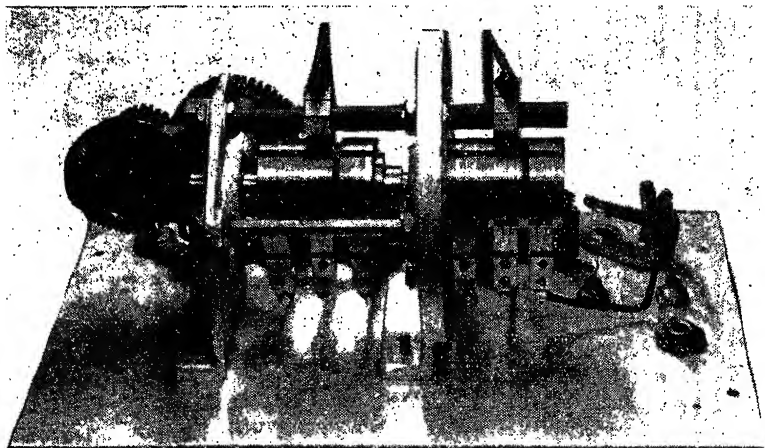
Colorado School of Mines

Fig. 10-59b. Close-up of double commutator.

voltage and current and therefore the resistance is determined. In the scheme of Fig. 10-60 the cross formed by the current and potential coil is not shown. The current coil is in series with the current or external leads, while the potential coil is across the internal or potential pair of electrodes. Although the potential coil is in series with a high resistance, this is generally not sufficient to give the same accuracy as the potentiometer method. Therefore, resistivities determined with the Megger are generally lower

than the resistivities determined with either the Gish-Rooney commutator or porous-pot resistivity equipment.

3. *D.C. resistivity measurements with porous pots.* By the use of porous pots, polarization on the potential electrodes and hence the commutator can be eliminated, although it is still necessary to provide for a reversing switch to eliminate effects of stray currents and leaks from the current into
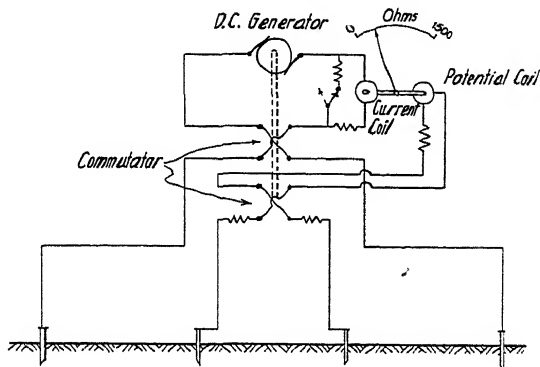
James G. Biddle Co.

FIG. 10-60. Schematic Megger circuit.
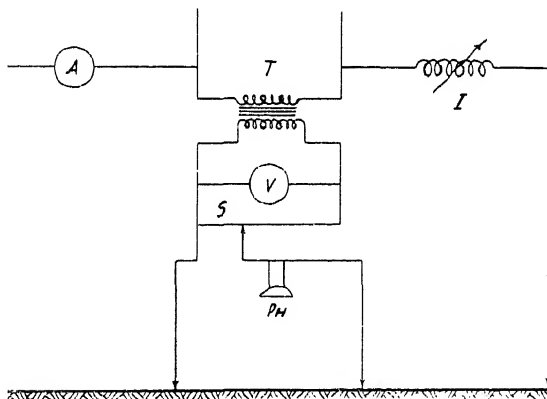
FIG. 10-61. Measurement of apparent resistivity with four-terminal A.C. method (adapted from Wenner).

the potential circuit. The Shepard earth resistivity meter and the Lee "geoscope" are representative of instruments using porous-pot electrodes. In the latter the galvanometer of the potentiometer is used with resistances in such a manner that the current is kept adjusted to a predetermined value. This value is made numerically equal to $2\pi a$, ($= 191$, if a is in feet) so that the potentiometer readings give directly the value of the apparent resistivity.

4. *A.C. resistivity method.* An arrangement for measuring resistivity with A.C. by compensation is illustrated in Fig. 10-61, in which A is an ammeter in the current circuit, I a variable inductance, T a transformer
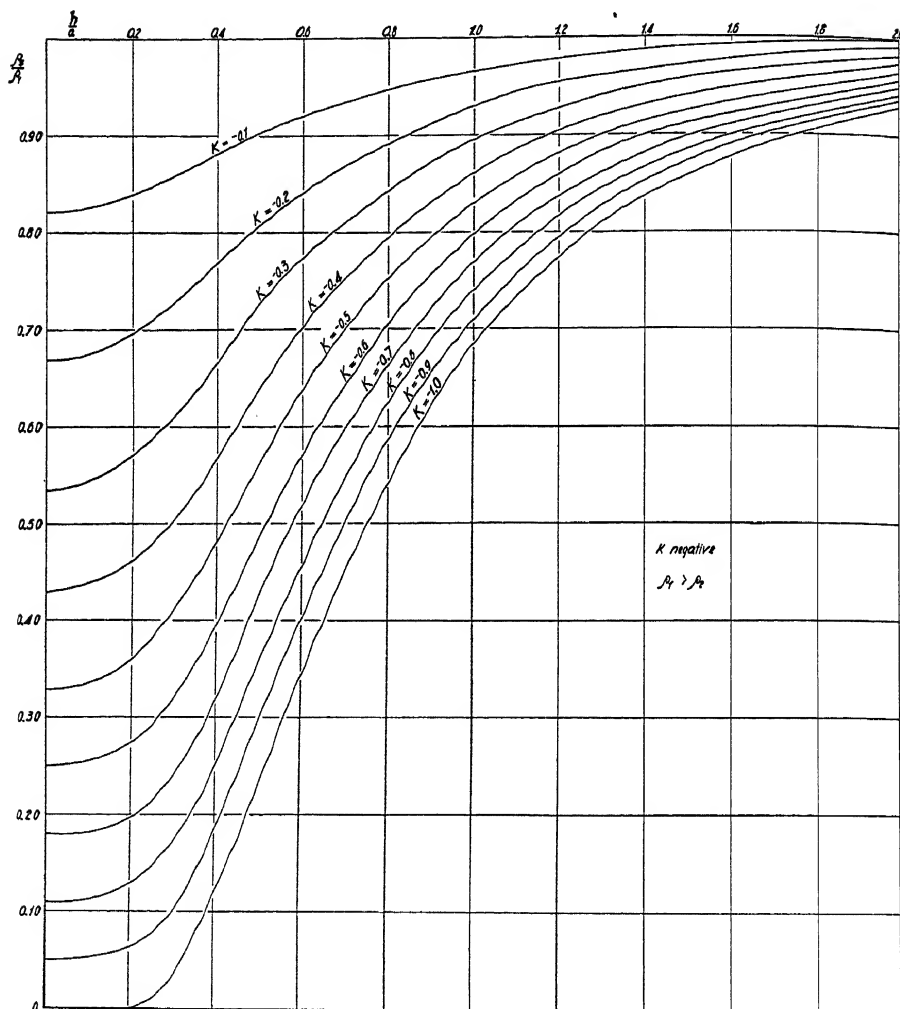
FIG. 10-62a. Tagg interpretation diagram (k negative).

used to supply a reference voltage to the potentiometer, V a voltmeter, S a slide wire, and PH a phone for detecting balance. Another A.C. indicator must be substituted for the phone if currents of lower frequency and hence greater depth penetration are applied.

E. INTERPRETATION

Interpretation of data, obtained with resistivity mapping or resistivity sounding, may be made (1) qualitatively (using the appearance of the curves); (2) quantitatively, by analytical interpretation methods; (3)
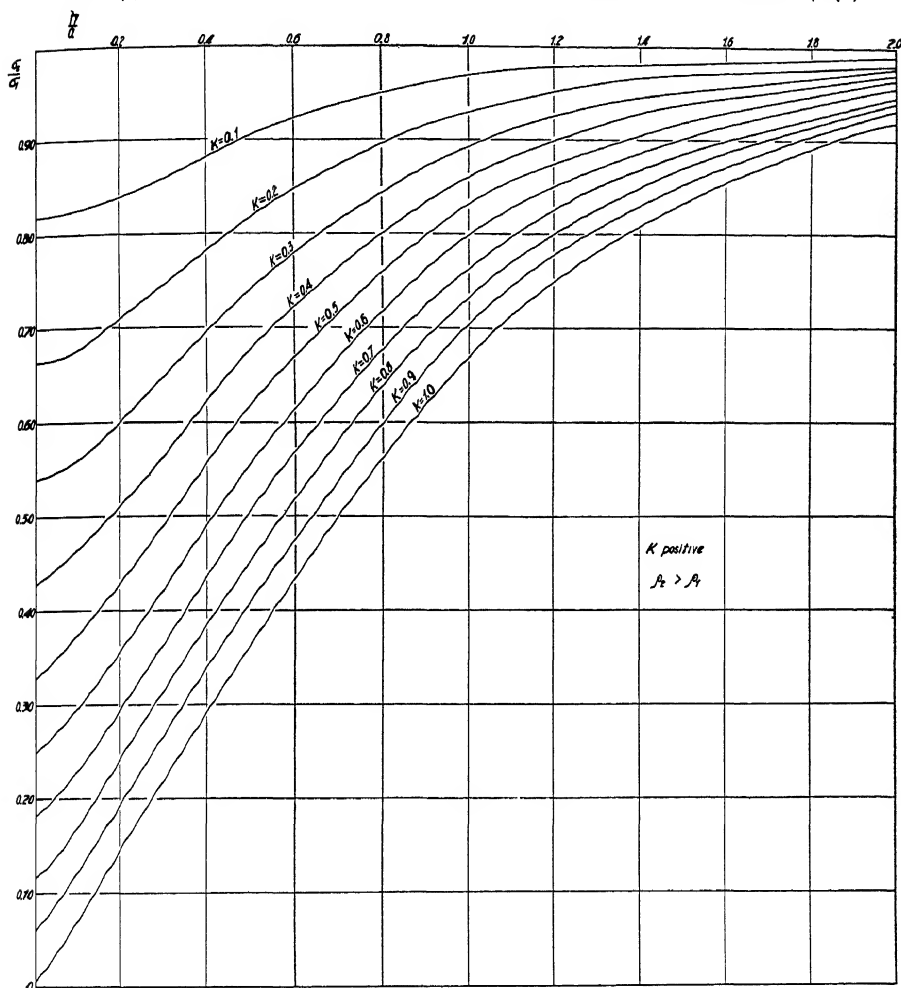
FIG. 10-62b. Tagg interpretation diagram (k positive).

quantitatively, using "type" curves calculated for given conditions; (4) with the help of model experiments.

1. *Qualitative methods.* Qualitative interpretation has a definite place in resistivity mapping. High apparent resistivities indicate the presence of bodies or formations of high resistivity within the depth range and

vice versa. Examples are given below in section F. In some instances it is possible (especially with the help of borings) to represent the lateral variations of apparent resistivity on such a scale that they may be translated directly into changes of depth of formations of different resistivity (bedrock profiles, and the like). Qualitative methods are also frequently used in a preliminary interpretation of resistivity depth curves although, as stated below, complete reliance on such methods may lead to serious misinterpretation, since the apparent resistivity continues to change with electrode separation long after the true resistivities have ceased to change with depth.

2. *Quantitative interpretation (analytical).* Analytical, direct methods of depth interpretation are primarily applicable to simple two- and three-layer conditions. One most frequently used is known as *Tagg's* method. This method establishes a number of simultaneous equations, giving depth h as a function of resistivity factor k. Hence, a family of curves giving ρ_s/ρ_1 as a function of h/a must be prepared (see Fig. 10–62). Since the apparent resistivity, for a given electrode separation, is only a function of the depth and the k value of a contact, theoretically two resistivity values for two electrode separations are sufficient to obtain both h and k. In practice, several equations are set up for various electrode separations, and depths are calculated numerically or graphically. It is convenient to use two diagrams: one for resistivity ratios (when the resistivity of the underlayer is less than that of the upper layer) and the other for conductivity ratios (when the resistivity of the underlayer is greater). Each diagram contains ten curves for k from -0.1 to -1 and from 0.1 to 1. Since a is known, h values as functions of k may be tabulated or plotted for each electrode separation. The correct depth is indicated by the intersection of the curves or by h values, which do not vary with k (see example). From the k value thus determined, the resistivity of the lower layer is obtained from $\rho_2 = \rho_1(k + 1)/(1 - k)$. If necessary, field curves are smoothed out for small electrode separations in order to obtain a reasonable average value for the surface resistivity.

The results in Table 71[41] were obtained from Fig. 10–63a to determine depth to limestone, overlain by loam, sand, and clay. For separations of less than 70 feet, the resistivities were averaged, obtaining a surface resistivity of $\rho_1 = 6703$ ohm-in.

Since $\rho_s/\rho_1 > 1$, the "conductivity" curves will be used for interpretation. In Table 72 the vertical columns contain ten values of h/a for 10 values of k. This is repeated for all electrode separations and corresponding σ_s/σ_1 values.

---

[41] Tagg, *op. cit.*

It is noted that, for the value $k = 0.7$, the depth h remains practically constant; $h = 142$ may be taken as the depth to the surface of separation between limestone and clay or sand. If the h values are plotted as a function of k (Fig. 10-63b), the curves intersect at about 140 feet. The most probable value of k is 0.702. The true depth in this case ranged from 145 to 150 feet.

Tagg's method of interpretation may be extended to the three-layer case, provided the infinite third layer does not influence the first part of the curve too much. This requirement is satisfied when the thickness of the second layer is two to three times the thickness of the top layer. The procedure followed is equivalent to a reduction of the three-layer to a two-layer problem, that is, it is equivalent to the construction and evaluation of the approximation curves shown in Figs. 10–53 and 10–54.[42] The order to be followed is as follows: (1) Average the surface resistivities for
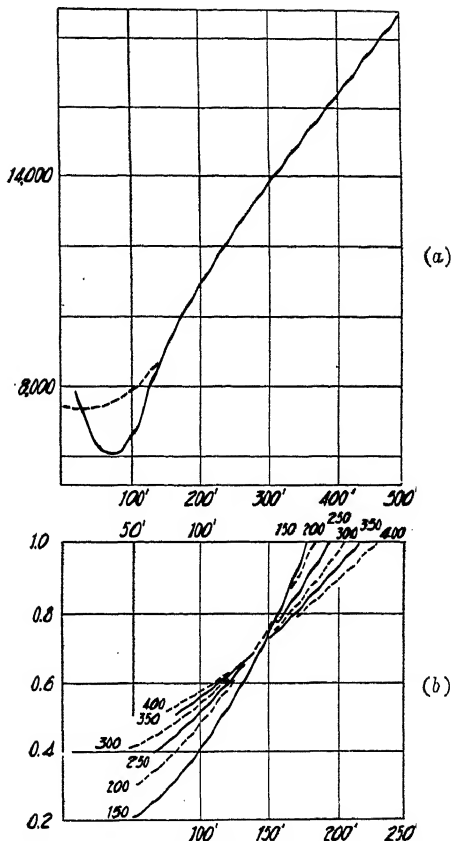
FIG. 10-63. Resistivity curve (a) and graphical depth interpretation (b) (after Tagg).

TABLE 71

ELECTRODE SEPARATION	RESISTIVITY (ohm-in.)	ρ_s/ρ_1	σ_s/σ_1
150 feet	8,960	1.338	0.748
200	10,740	1.601	0.625
250	12,320	1.840	0.544
300	13,860	2.068	0.483
350	15,220	2.270	0.441
400	16,480	2.460	0.407

[42] See also Sundberg, A.I.M.E. Geophys. Pros., 146 (1934); and S. J. Pirson, A.I.M.E. Geophys. Pros., 148–158 (1934).

spacings from 5 to 20 feet, thus obtaining the resistivity (ρ_1).   (2) Plot ρ_1 to scale on the resistivity axis and draw a line from ρ_1 to meet tangentially the first part of the curve.   (3) Read resistivities at six or eight points on the curve just drawn and apply Tagg's method to that part of the curve.

TABLE 72

ELEC-TRODE SPACING	150 FEET		200 FEET		250 FEET		300 FEET		350 FEET		400 FEET	
σ_2/σ_1	0.748		0.625		0.544		0.483		0.441		0.407	
k	h/a	h	h/a	h	h/a	h	h/a	h	h/a	h	h/a	h
1	1.19	179	0.915	183	0.770	193	0.675	202	0.61	214	0.560	224
0.9	1.12	168	0.850	170	0.705	176	0.610	183	0.545	191	0.500	200
0.8	1.045	157	0.775	155	0.640	160	0.545	163	0.485	170	0.435	174
0.7	0.96	144	0.700	140	0.565	141	0.478	143	0.41	144	0.36	144
0.6	0.87	130.5	0.620	124	0.485	121	0.390	117	0.325	114	0.28	112
0.5	0.785	118	0.525	105	0.39	97.5	0.295	74	0.226	78	0.17	68
0.4	0.66	99	0.42	84	0.27	67.5	0.16	40	0.06	21	...	...
0.3	0.525	79	0.26	52	0.03	7.5	...	...	...	...	...	...
0.2	0.315	47	...	...	...	...	...	...	...	...	...	...
0.1	...	...	...	...	...	...	...	...	...	...	...	...

TABLE 73

a	ρ_a
5	106
10	120
15	140
20	154
25	165
30	166
40	158
50	120
60	87
70	65
80	49
90	35
100	26
110	18
120	12

This procedure yields ρ_2, and h_1, as well as $k_1 = \dfrac{\rho_2 - \rho_1}{\rho_2 + \rho_1}$.   (4) Estimate the depth to the third layer by applying the approximation $h_1 + h_2 = \frac{2}{3}d$, where d is the distance to the inflection point (between the two points of maximum curvature).   (5) Calculate the apparent resistivity ρ_1' of the two upper layers (ρ_1 and ρ_2) in parallel from $(h_1 + h_2)/\rho_1' = h_1/\rho_1 + h_2/\rho_2$.

(6) Apply Tagg's method to the bottom part of the curve between the lowest two points of maximum curvature.   A more accurate value is then

obtained for the depth $(h_1 + h_2)$. Determine the resistivity of the bottom layer ρ_3 from $k_2 = \dfrac{\rho_3 - \rho_2}{\rho_2 + \rho_3}$. (7) Repeat the above with better values of ρ_1' to obtain a more accurate figure for $(h_1 + h_2)$, and so on. As an example of the application of the above procedure, the curve of Fig. 10-54 (a typical water indication) may be selected, with resistivity values of $\rho_1 = 100$, $\rho_2 = 300$, and $\rho_3 = 0$ ohm-foot. The first point of the resistivity curve at depth 0 is 100. Multiplying the vertical scale by 10 (if $h_1 = 10$) gives the apparent resistivity values in Table 73.

Since a theoretical curve is analyzed here, steps (1) and (2) may be disregarded. Proceeding directly to the analysis of the first part of the curve (from 5 to 25 feet), we obtain the data in Table 74.

TABLE 74

$1/\rho_i$	0.945		0.835		0.715		0.65		0.607	
a $\diagdown$ k_1	5		10		15		20		25	
	h/a	h	h/a	h	h/a	h	h/a	h	h/a	h
0.1	0.76	3.8	0.17	1.7	...	...	...	...	...	...
0.2	1.13	5.65	0.55	5.5	0.21	3.16	...	...	...	...
0.3	1.4	7.0	0.77	7.7	0.44	6.6	0.3	6	...	...
0.4	1.6	8	0.9	9	0.58	8.62	0.45	9	0.21	5.25
0.5	1.77	8.9	1.1	11.0	0.70	10.5	0.56	11.2	0.37	9.25
0.6	1.88	9.4	1.13	11.3	0.79	11.85	0.665	13.3	0.475	11.19
0.7	1.98	9.8	1.23	12.3	0.88	13.2	0.75	15	0.585	14.6
0.8	...	...	1.33	13.3	0.96	14.4	0.82	16.4	0.66	16.5
0.9	...	...	1.42	14.2	1.025	15.4	0.89	17.8	0.74	18.5
1.0	...	...	1.51	15.1	1.105	16.6	0.965	19.3	0.81	20.6

The best agreement of depth values prevails in the row $k_1 = 0.5$. The average there is 10 feet. This gives 300 ohm-feet for ρ_2. The inflection point in the curve indicative of the second interface is at 60 feet. Hence, $h_1 + h_2 = \frac{2}{3} \cdot 60 = 40$ feet, and $40/\rho_1' = \frac{10}{100} + \frac{30}{300}$. Thus $\rho_1' = 200$ ohm-feet. The approximation curve is then traced, starting with $\rho_1' = 200$, tangent to the resistivity curve at the lower inflection point. The points chosen for applying Tagg's method to the bottom part appear in Table 75, which gives the best agreement of depth values in the lowest row for $k = 1$. The average of the depth values in this row is 40.1, which is in close enough agreement with the depth assumed in the construction of the theoretical curve.

3. *Quantitative interpretation (type curves)*, based on an interpolation of theoretical curves, is used almost exclusively by Schlumberger and his associates. Curves are calculated for given k values with layer thickness

TABLE 75

THREE-LAYER INTERPRETATION, DETERMINATION OF DEPTH TO SECOND LAYER

(Curve of Fig. 10-54)

ρ_s'/ρ_1	$\frac{166}{200}=0.83$		$\frac{128}{200}=0.64$		$\frac{108}{200}=0.54$		$\frac{84}{200}=0.42$		$\frac{65}{200}=0.325$		$\frac{49}{200}=0.245$		$\frac{35}{200}=0.17$	
a/h_2	30		40		50		60		70		80		90	
	$\frac{h_1+h_2'}{a}$	h_1+h_2'	$\frac{h_1+h'_2}{a}$	h_1+h	$\frac{h_1+h_2'}{a}$	h_1+h_2'	$\frac{h_1+h_2'}{a}$	h_1+h_2'	$\frac{h_1+h_2'}{a}$	h_1+h_2'	$\frac{h_1+h'_2}{a}$	h_1+h_2'	$\frac{h_1+h_2'}{a}$	h_1+h_2'
0.1	0.13													
0.2	0.565	*												
0.3	0.76		0.36		0.08									
0.4	0.90		0.5		0.36									
0.5	1.0		0.605		0.475		0.31	18.6						
0.6	1.05		0.7		0.565		0.43	25.6	0.31	21.7				
0.7	1.18		0.77		0.63		0.49	29.4	0.41	28.7	0.31	24.8		
0.8	1.25		0.825		0.69	34.5	0.56	33.6	0.47	32.9	0.39	31.2	0.31	27.9
0.9	1.32		0.88		0.745	37.3	0.62	37.2	0.525	36.8	0.45	36.0	0.395	35.5
1.0	1.38	41.4	0.93	37.2	0.8	40	0.67	40.2	0.58	40.6	0.51	40.8	0.455	40.9

as variable. Fig. 10–64 shows a diagram prepared for a two-layer case in which the resistivity of the upper formation is 480 ohm-m while the resistivity of the lower formation is infinite. Apparent resistivities are shown for top-layer thickness varying from 5 to 125 m. The former are plotted as ordinates, and the lengths of the electrode arrangement ($l = 3a$) as abscissas. In the two-layer case several of such diagrams are available for various k values; and it is not difficult to select approximately the right diagram, since the resistivity of the upper medium may be determined fairly closely.
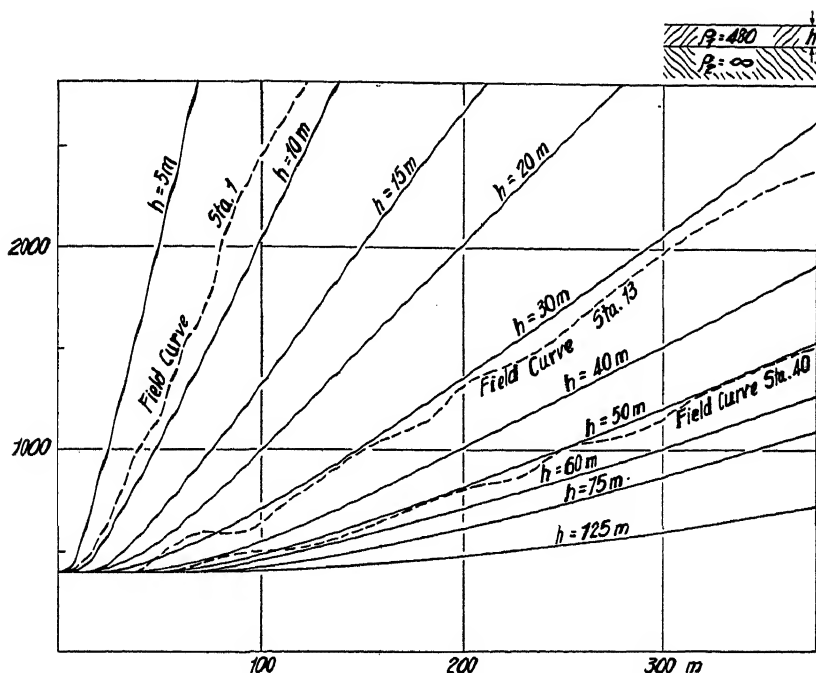
FIG. 10-64. Schlumberger two-layer interpretation diagram, with field curves (after Poldini).

Interpretation consists of placing the field curves over the theoretical curves and determining the depth by interpolation. For instance, in the curve for station 1 the depth obtained from the curve was 8 m while the depth reached by drilling was 8.75 m. In the curve for station 13 the depth read by interpolation was 32 m and the depth found by drilling was 31.05 m. In the curve for station 40 the interpolated depth was 51 m and actual depth was 51.05 m. The results under discussion were obtained in a resistivity survey on a dam site at Littleton, New Hampshire, where the upper layer consisted of Quarternary sands, gravel, and clay, underlain by

crystalline, highly metamorphosed rocks of 10,000 ohm-m resistivity. Curves of the type under discussion may likewise be constructed for the three-layer case. These are divided into an upper two-layer portion and a three-layer curve proper, to interpret the lower part of the curve. It is evident that in this case the number of combinations of k values for which such diagrams must be available is much greater.

The Schlumberger method has the obvious advantage that depth determinations can be made directly in the field without any calculation—at
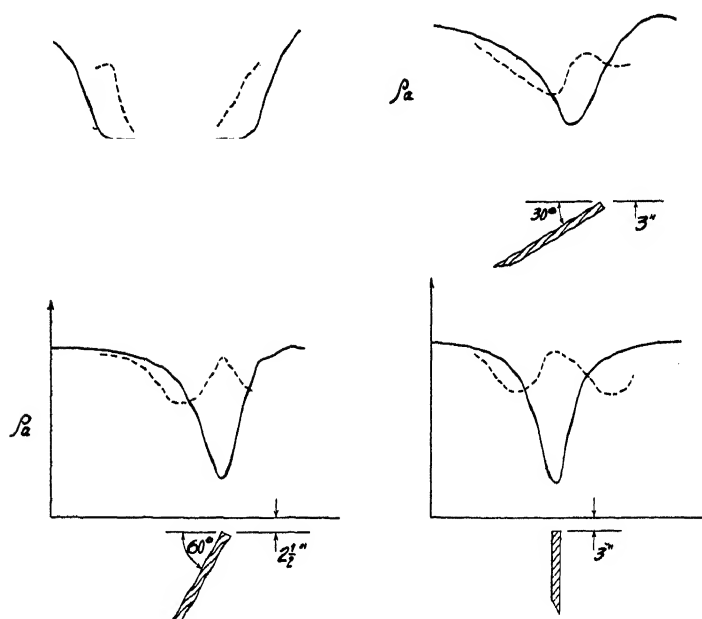
FIG. 10-65. Studies of the effect of dip of model formations in a water tank, using a four-terminal contacting arrangement with constant electrode separation of 8 inches.

the expense, however, of a great amount of office calculation beforehand to meet various conditions. This method increases in value the more field data are obtained and interpreted.

4. *Model experiments.* Small-scale experiments are of twofold value in the interpretation of resistivity measurements: (1) for checking theoretical calculations, and (2) for simulating geologic bodies whose effects cannot be calculated. These experiments are usually made in tanks, filled with water to simulate the country rock (or top layer), whereas ore bodies are represented by metal plates, and stratified ground by layers of sand (ρ large),

clay (ρ small), or water (ρ intermediate).   The conductivity of these substances may be altered by adding electrolytes (NaCl or $CuSO_4$).   Tanks should be compensated to eliminate wall effects.

Model experiments are of value in determining the anomalies of ore bodies whose calculation would be too time consuming.   The curves reproduced in Fig. 10-65 show that a dipping conductive formation may produce a negative anomaly in resistivity when the electrodes are parallel to the strike; but that it produces a maximum, flanked by two minima, when the electrodes are perpendicular to the strike.   These experiments were made in 1929-1930 at the Colorado School of Mines to study the possibility of locating fluorspar deposits associated with faults, rendered conductive by circulation of mineralized solutions.   They were confirmed later in the field.   Similar results were published by Hubbert in 1932,[43] who also supplemented his field data with model tank experiments.[44]   Further experiments were contributed by N. H. Johnson,[45] with a theoretical discussion by Howell.[45a]   Other model experiments were made by T. A. Manhart[46] and R. J. Watson.[47]

F. Results Obtained by Resistivity Surveying

Resistivity methods have been applied (1) in structural investigations for the purpose of locating potential oil structure, that is, anticlines, salt domes, faults, and the like; (2) in mining (a) in connection with structural investigations, (b) for the location of ore bodies, of brown coal, anthracite, and salt, (c) for the determination of thickness of overburden in proposed shaft and tunnel sites and of depth to bedrock in placer projects; (3) in civil engineering (a) in foundation problems, (b) in determining depth to bedrock or rock consistency in proposed dam and tunnel sites, and (c) in highway engineering for the location of construction materials, sand and gravel, and the like; (4) in prospecting for water.

1. *Structural investigations in oil exploration.*   For comparatively shallow problems (to 2000 feet or so) resistivity mapping has been found fairly useful in oil exploration.   Fig. 10-66 shows a curve of apparent resistivity across an anticline of Devonian limestone flanked by Mississippian shales and sandstone and concealed by glacial formations, boulder clay, and the like.   This traverse was run with an electrode separation of 200 feet.   Ow-

[43] M. K. Hubbert, A.I.M.E. Geophys. Pros., 9 (1934).

[44] *Ibid.*, 14.

[45] , 35.

[46] Colo. Sch. Mines Quart., **32(1)**, 141-168 (Jan., 1937).

[47] A.I.M.E. Geophys. Pros., 222-232 (1934).

ing to the high resistivity of the lime, this anticline appears as a peak of high apparent resistivity. The variations in the curve are probably due to small irregularities in the surface of the glacial till.

Not all anticlines can be expected to appear as resistivity highs. Frequently the overburden is of high resistivity and the anticlines are made up of shale formations with lower resistivity. In such cases an anticline will appear as a resistivity low. The Caucasian foothill zone, extending from the vicinity of the well-known field of Grozny to Vladicavcas, shown in Fig. 10-67, is an example. All anticlines appear as elongated zones of low resistivity. The depth of penetration and electrode separation in this survey was about 820 feet.
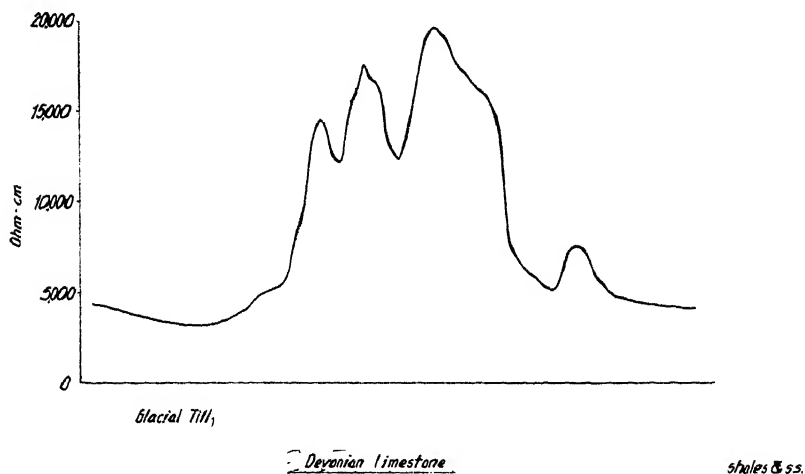
FIG. 10-66. Resistivity profile across buried anticline, taken with an electrode spacing of 200 feet (after Hubbert).

The survey represented in Fig. 10–68 is of interest because of the excellent correlation possible between resistivity profiles. The section (New Mexico) is made up of gypsum, red beds, shales, and limestone with salt underneath, at a depth of 400 to 500 feet. The red bed and shale section (with the exception of the near-surface portion) appears as a good conductor. The first downbreak of the curve is readily correlated, the characteristics of the first four curves being similar in all details. The correlation of the troughs of these curves gives a picture closely related to the surface of the salt beds several hundred feet down. It would be difficult, however, to find a direct indication of salt in the lower portion of the curves. This results from the screening effect of the good conductors above.
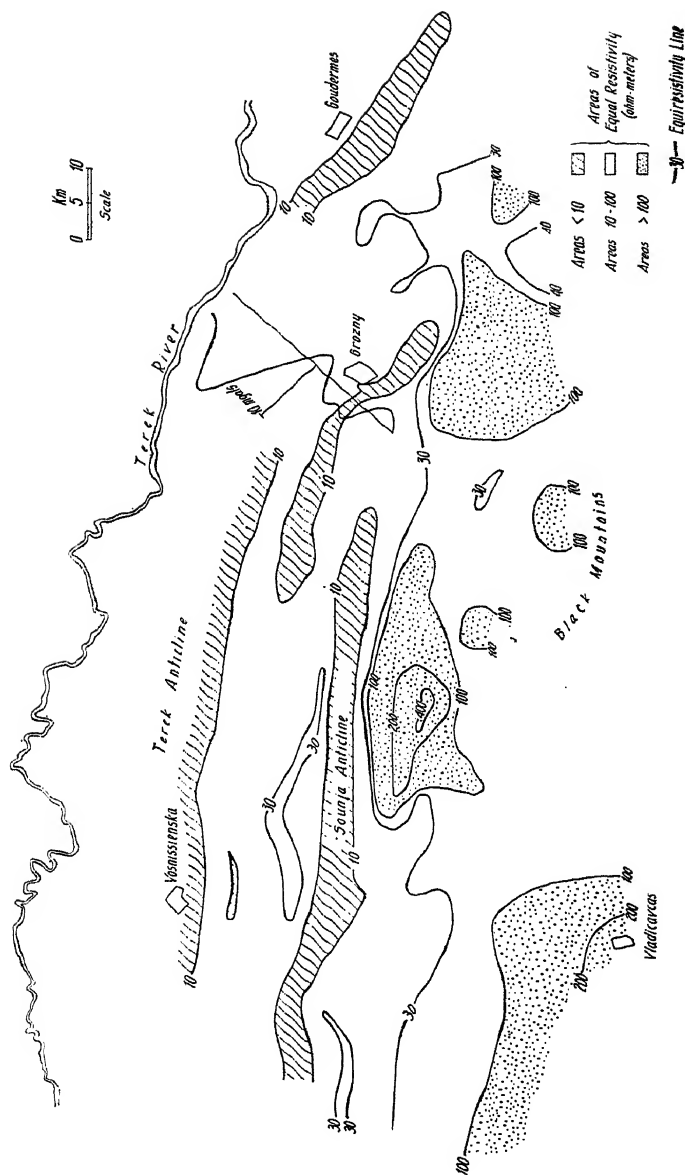
Fig. 10-67. Equiresistivity map of Caucasian foothill zone (after Schlumberger). Depth of penetration = 820 feet. Note gravity profile near Grozny.

737

In many instances faults have been located by the resistivity contrast of the formations on either side, or by the effect of the fault itself resulting from highly mineralized waters in the fault plane.[48] Structural investigations with resistivity methods are often facilitated by tracing certain key beds of high or low resistivity. An example is the survey of the Bibi-
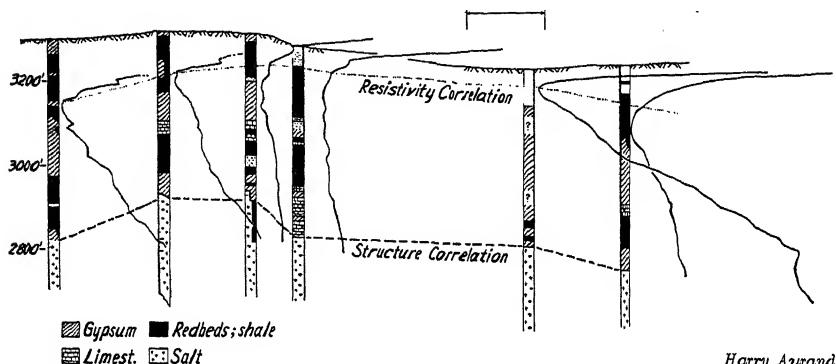
FIG. 10-68. Results of electrical vertical drilling with single-probe method, and corresponding geologic section in an area in New Mexico.
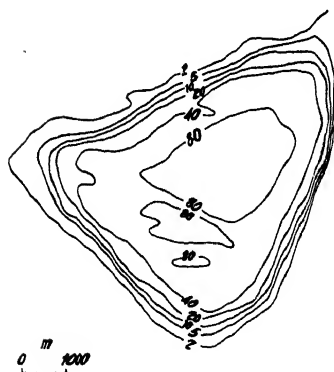
FIG. 10-69. Equiresistivity contours (ohm-meters) on a salt dome in the Emba District, Russia (after Schlumberger).

Eibat[49] anticline near Baku and is of interest because measurements were made at the bottom of the sea. A tri-conductor cable with three electrodes was dragged along the sea bottom, the fourth electrode being a fixed ground on land. The key bed in this area (Apsheron limestone) could be clearly noted in the resistivity curve.

The possibility of electrical salt dome location was demonstrated at an early date by Schlumberger and his associates.[50] In 1926 and 1927 the salt domes of Meyenheim and Hettenschlag in Alsace-Lorraine were found by resistivity mapping. They appeared as resistivity lows, contrary to what would be expected. The lows result from the occurrence of highly conductive marls above the salt which in turn are cov-

48 Hubbert, op. cit., 40-47.
49 A.I.M.E. Geophys. Pros., 127 (1934).
50 G. Carrette and S. F. Kelly, A.I.M.E. Geophys. Pros., 211-220 (1929).

ered by alluvial beds of high resistivity. The latter thin out where the marls have been forced up by the salt intrusion. Conversely, the salt uplift shown in Fig. 10-69 shows as a resistivity high. It is located at Tschernaja Rieschka and is one of the numerous domes found by geophysical methods in the Emba district in Russia.

2. *Applications in mining and mining geology.* General structure in mining districts can be outlined by means of resistivity mapping, provided that key beds with greatly differing resistivities exist in the section. Faults may be located if the beds on either side differ in resistivity or if mineralized solutions circulate along the fault plane. In this manner, nonconductive minerals accumulated on the fault planes may be found indirectly (fluorspar veins in Illinois, see footnote 43, page 735).

Resistivity methods have been used extensively in the location of sulfide ore bodies, both at the surface and underground. Fig. 10-70 illustrates electrical results at the Abana mine. The resistivity curves were obtained by surveying with constant electrode spacing. The ore body is indicated by a resistivity low. Fig. 10-71 shows resistivity-depth curves for a dip-

FIG. 10-70. Resistivity curves and self-potential profiles across Abana ore body (after Schlumberger [Eve & Keys]).

ping vein taken along three profiles, laid out 15° off strike, at increasing distances from the outcrop. The lows in the curves move out to greater distances (or depths) as the distances of the traverse from the outcrop are increased. In this instance these distances were found to correspond to depth to the dipping vein, although they would be expected to be reckoned perpendicular to the bed.

Several attempts have been made to apply resistivity methods in lignite prospecting. If the lignite beds are soaked with mineralized waters and overburden formations are poor conductors, fairly definite results may be obtained (see Fig. 10-72). However, if conditions are less favorable

(clayey overburden, small conductivity contrast, varying water content), the data may become very unreliable, as indicated by Stern's measurements in the Niederlausitz and Hawkins'[51] observations in Ontario. Extensive resistivity measurements have been made by Ewing and Crary on anthracite coal beds. Further references to geophysical results on coal measures are given in an article by the author.[52] In the prospecting for salt, potash,
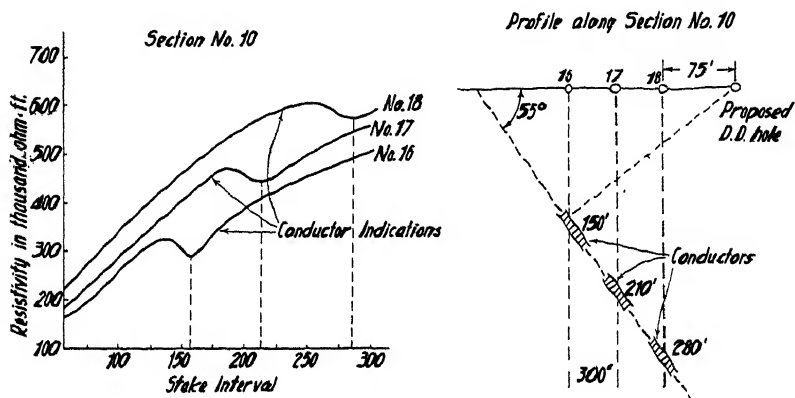
Fig. 10-71. Apparent resistivity curves on three traverses (15° off strike) above Peach Bottom Vein, Alleghany County, North Carolina (after Griswold).
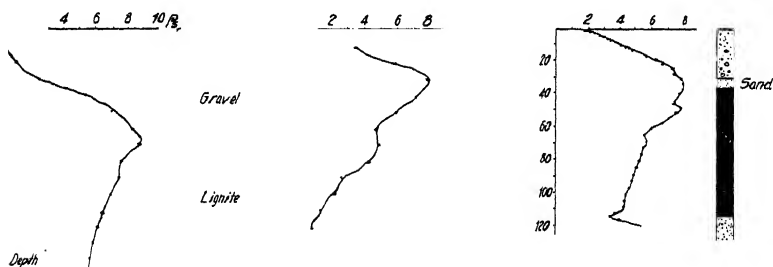
Fig. 10-72. Apparent resistivity curves on lignite beds, Ville, Germany (after Stern).

or sulfur for mining purposes, the geologic problems are the same as in the location of salt domes in oil exploration.

Determination of overburden thickness, a problem frequently encountered in mining operations in connection with sinking shafts, driving tunnels, and excavations from surface, has been accomplished successfully by

[51] R. H. Hawkins, A.I.M.E. Geophys. Pros., 76-120 (1934).

[52] "Geophysics in the Non-Metallic Field," A.I.M.E. Geophys. Pros., 546-577 (1934).

both resistivity mapping and sounding.   Fig. 10–73 shows the application of resistivity mapping in a section consisting of glacial drift at the surface and limestone with ore bodies below.   The limestone is underlain by conglomerates.   The three curves represent: (*solid* curve) actual subdrift topography; (*dotted* curve) apparent conductivity obtained with 40-foot electrode separation; (*dashed* curve) apparent conductivity with 120-foot electrode separation.   The conductivity curve obtained with the 40-foot separation does not give a true picture of the subdrift topography because the average thickness of the glacial drift is greater than this separation, and the results also reflect irregularities in the composition of the drift. The closest relation between subdrift topography and apparent conductivity was obtained with 120-foot electrode separation, which is the greatest thickness of the drift encountered in the area investigated.
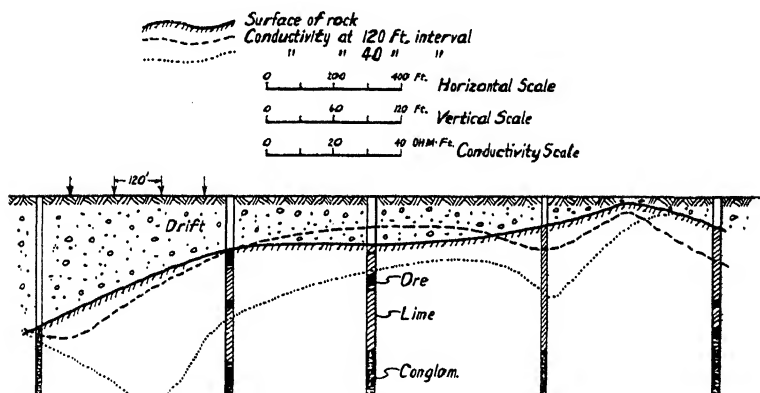
FIG. 10-73. Apparent resistivity curves, with different electrode separations to determine subdrift topography (after Lancaster-Jones).

Location and depth determination of placer deposits is closely related to the problem of determining depth to bedrock in foundation problems, discussed in the next paragraph.

3. *Applications in civil engineering (foundation and highway problems).* Application of resistivity methods in this field is threefold: (a) determination of depth to bedrock; (b) determination of physical rock characteristics for dams, structures, tunnels, and the like; and (c) location of construction materials.

Bedrock depth determinations by resistivity methods have been made on numerous occasions.   Many of these have been carried out by Schlumberger and his associates.[53]   An example was illustrated in Fig. 10–64. In this particular survey, predictions could be verified within 1 to 2 meters

[53] Leonardon and Crosby, A.I.M.E. Geophys. Pros., 199–210 (1929).

(10 per cent of depth); only two wells showed discrepancies.   Where bed-
rock consists of unaltered crystallines and the overburden is glacial drift,
the conductivity contrast is great enough to assume an infinite bedrock
resistivity in the interpretation.   On the other hand, when altered crystal-
lines or sediments are overlain by river gravels traversed by water, the
opposite type of resistivity indication (good conductor below) may be
observed.

Fig. 10-74 shows the results of a resistivity survey made for a determina-
tion of physical rock characteristics at the site of a proposed aqueduct.
It revealed a fault zone 350 feet wide in which the crystalline rocks were
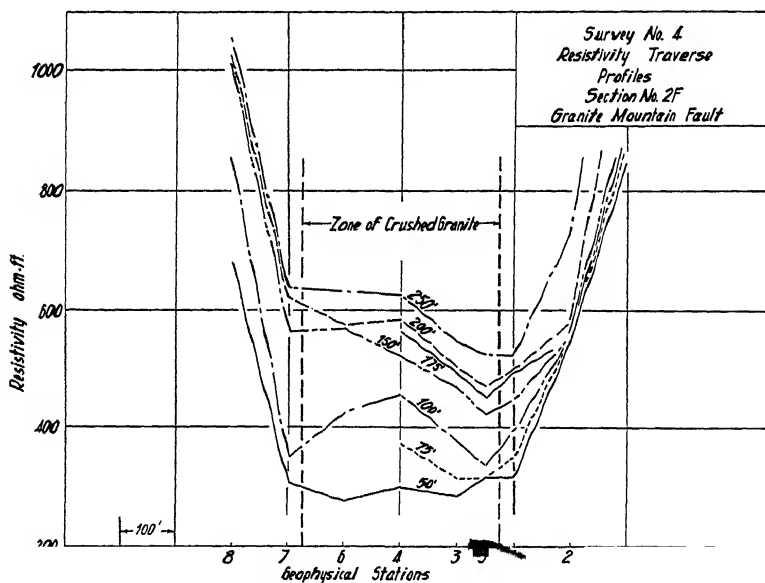
FIG. 10-74. Location of fault zone by resistivity mapping (after Henderson).

crushed and waterlogged (reduced resistivities), making it necessary to
reject the site for the proposed structure.

In highway construction, resistivity surveys can be of considerable help
by locating construction materials.   There are still many projects where
sand and gravel are hauled for considerable distances, while sources of
near-by supply might be located by resistivity measurements without much
trouble.   The curves reproduced in Fig. 10-75 show how effectively a
gravel and sand lens in a clay bed can be mapped.   Many more examples
of this type are given by Kurtenacker in an article dealing especially with
the applications of geophysics to highway problems.[54]

[54] K. S. Kurtenacker, A.I.M.E. Geophys. Pros., 49–59 (1934).

4. *Location of water.*   Resistivity and related surface-potential measurements are probably the most promising geophysical methods for the location of water.   The problem is not simple and requires a careful study of the stratigraphic situation since the occurrence of groundwater is quite variable and the conductivity of water itself may vary.   The manifold conditions applying in electrical water prospecting have been discussed in detail by Heiland[55] and Tattam.[56]

Experience has shown that in many cases the water itself, though potable, is conductive and occurs at the bottom of a dry layer, which in turn is covered by a surface medium of intermediate conductivity (see Fig.
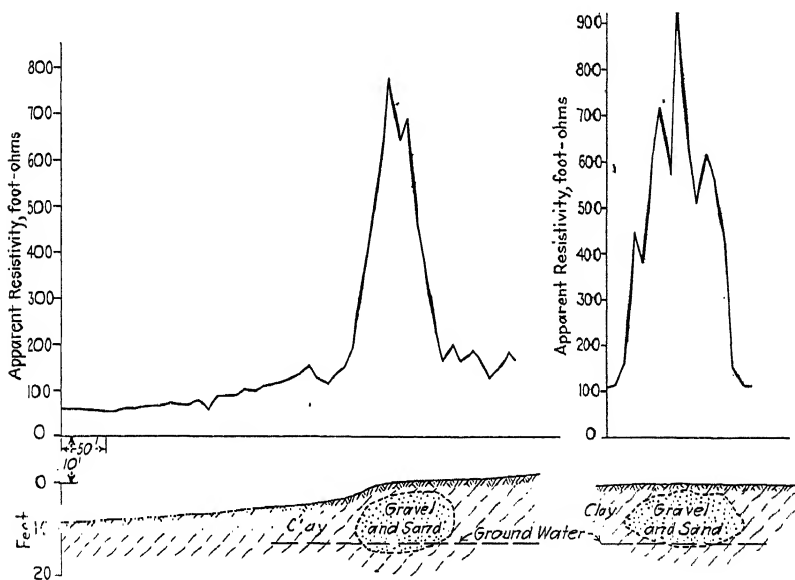
FIG. 10-75. Location of gravel lenses by resistivity mapping (after Wilcox).

10-76, diagram [a]).   Conversely, the bottom layer may have a high resistivity (crystalline bedrock, and the like) and the water may occur as an intermediate layer of good conductivity above it (b).   The typical three-layer curves so obtained may degenerate into the extreme curve ([a], e) when the top layer is of very good conductivity, and into (c), e when the top layer has poor conductivity.   Water subject to rapid circulation in beds of large pore volume and permeability often acts as a nonconductor compared with other beds (curve [c]).   Curve (d) is less frequently observed and occurs when

[55] Amer. Geophys. Union Trans. (Hydrology), 574-588 (1937).
[56] C. M. Tattam, Colo. Sch. Mines Quart., **32**(1), 118-138 (Jan., 1937).

moist layers of different capillarity occur above one another. It is seen that three-layer curves encountered in water prospecting require a careful analysis of near-surface stratigraphic conditions and that the same resistivity curve may indicate totally different conditions.
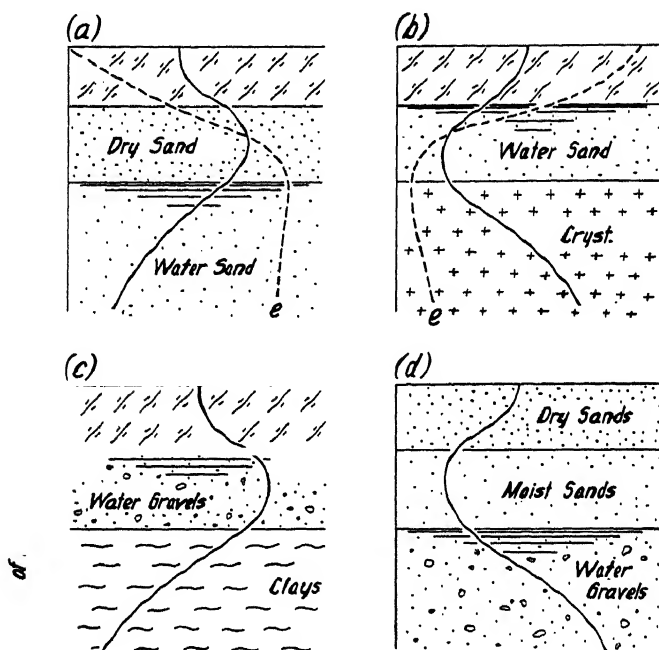
Fig. 10-76. Various resistivity indications on conductive and nonconductive ground waters.

G. Electrical Logging

Electrical logging is the application of resistivity mapping with fixed electrode separation to the location of formation boundaries in uncased wells. Methods and equipment, theory and results are discussed in Chapter 11.

VI. POTENTIAL-DROP-RATIO METHODS

A. General

Compared with resistivity methods, the advantages of potential-drop-ratio procedures are that sharper indications are obtained on vertical formation boundaries, and that in favorable cases of horizontally stratified ground the indications are more directly related to depth. The P.D.R.

method is also superior in resolving power because potential differences are not measured absolutely but in the form of a ratio of successive differences. However, this increase in precision frequently results in increased near-surface interference, and special precautions are necessary to reduce it. P.D.R. arrangements consist essentially of Wheatstone bridge circuits with adjacent stake intervals in two arms, known resistances in the other two arms, and an indicating instrument in the center arm, connected to the center stake (see Fig. 10–82). Hence, for a D.C. circuit, the ratio of the two voltage differences is equal to the ratio of the two resistances when adjusted for balance.

B. THEORY

1. *Horizontal layers.* In all applications of P.D.R. method for the exploration of stratified ground, measurements are made outside the elec-
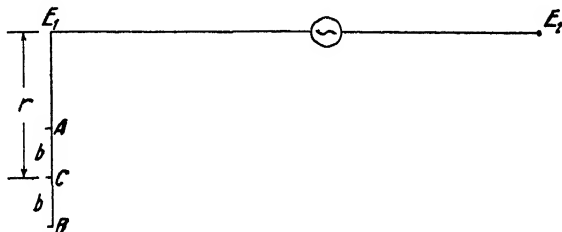
FIG. 10-77a. Electrode arrangement for constant spacing.

trode basis and usually at right angles to it. By this means the effect of the second electrode is virtually eliminated (Fig. 10–77a). For two layers of arbitrary conductivity ratio, with a lower layer of infinite depth extent, the P.D.R. may be calculated from the potentials at three surface points, using the equations previously derived. According to eq. (10–35a), in the vicinity of one power electrode

$$V_p = \frac{I\rho_1}{2\pi}\left[\frac{1}{r} + 2\sum_{n=1}^{n=\infty} \frac{k^n}{\sqrt{r^2 + (2nh)^2}}\right].$$

Applying this to three equidistant points with the interval b, and with a center distance r from the power electrode (see Fig. 10–77a), we get

$$V_A = \frac{I\rho_1}{2\pi}\left[\frac{1}{r-b} + 2\sum_{n=1}^{n=\infty} \frac{k^n}{\sqrt{(r-b)^2 + (2nh)^2}}\right]$$

$$V_B = \frac{I\rho_1}{2\pi}\left[\frac{1}{r+b} + 2\sum_{n=1}^{n=\infty} \frac{k^n}{\sqrt{(r+b^2) + (2nh)^2}}\right] \Bigg\} \quad (10\text{--}42a)$$

$$V_C = \frac{I\rho_1}{2\pi}\left[\frac{1}{r} + 2\sum_{n=1}^{n=\infty} \frac{k^n}{\sqrt{r^2 + (2nh)^2}}\right].$$

By introducing the ratios $x \equiv r/h$ and $c \equiv b/h$, we obtain the following equations:

$$
\left.
\begin{aligned}
V_A &= \frac{I\rho_1}{2\pi h}\left[\frac{1}{(x-c)} + 2\sum_{n=1}^{n=\infty}\frac{k^n}{\sqrt{(x-c)^2+4n^2}}\right] \\
V_B &= \frac{I\rho_1}{2\pi h}\left[\frac{1}{(x+c)} + 2\sum_{n=1}^{n=\infty}\frac{k^n}{\sqrt{(x+c)^2+4n^2}}\right] \\
V_C &= \frac{I\rho_1}{2\pi h}\left[\frac{1}{x} + 2\sum_{n=1}^{n=\infty}\frac{k^n}{\sqrt{x^2+4n^2}}\right].
\end{aligned}
\right\} \quad (10\text{–}42b)
$$

Therefore, the potential differences are:

$$
\left.
\begin{aligned}
V_A - V_C &= \frac{I\rho_1}{2\pi h}\left\{\frac{c}{x(x-c)}\right. \\
&\quad + \left. 2\sum_{n=1}^{n=\infty}k^n\left[\frac{1}{\sqrt{(x-c)^2+4n^2}} - \frac{1}{\sqrt{x^2+4n^2}}\right]\right\} \\
V_C - V_B &= \frac{I\rho_1}{2\pi h}\left\{\frac{c}{x(x+c)}\right. \\
&\quad + \left. 2\sum_{n=1}^{n=\infty}k^n\left[\frac{1}{\sqrt{x^2+4n^2}} - \frac{1}{\sqrt{(x+c)^2+4n^2}}\right]\right\}.
\end{aligned}
\right\} \quad (10\text{–}42c)
$$

If we let

$$
\sqrt{(x-c)^2+4n^2} = \sqrt{A}
$$
$$
\sqrt{x^2+4n^2} = \sqrt{B}
$$
$$
\sqrt{(x+c)^2+4n^2} = \sqrt{C},
$$

the potential ratio is given by

$$
\frac{V_A - V_C}{V_C - V_B} = \frac{\dfrac{c}{x(x-c)} + 2\sum\limits_{n=1}^{n=\infty}k^n\left[\dfrac{1}{\sqrt{A}} - \dfrac{1}{\sqrt{B}}\right]}{\dfrac{c}{x(x+c)} + 2\sum\limits_{n=1}^{n=\infty}k^n\left[\dfrac{1}{\sqrt{B}} - \dfrac{1}{\sqrt{C}}\right]}. \quad (10\text{–}42d)
$$

When $k = 0$ (homogeneous ground), the series in both numerator and denominator vanish and the P.D.R. becomes

$$
\frac{V_A}{V_B} = \frac{x+c}{x-c}. \quad (10\text{–}42e)
$$

The P.D.R.'s measured in the field must be referred to a "normal" ratio, that is, the ratio for homogeneous ground. To this end, they are

multiplied by the reciprocal of the ratio in eq. (10–42e). Hence, the correction factor is $(r - b)/(r + b)$, and it is always less than and gradually approaches 1 (for ratios figured in terms of V_A/V_B) as the separation becomes smaller in comparison with distance. Ratios expressed in terms of V_B/V_A are reduced with the reciprocal of the above correction factor.

In stratified ground either a constant-spacing or an expanding-electrode system is applied. As shown in Fig. 10–77b, the spacing b may be increased in proportion to the center stake distance. A convenient electrode separation is one-third of the center stake distance. Then, if $EA:EC:EB = 2:3:4$, c equals $x/3$, so that eq. (10–42d) becomes

$$\frac{V_A - V_C}{V_C - V_B} = \frac{\dfrac{1}{2x} + \displaystyle\sum_{n=1}^{n=\infty} k^n \left[\dfrac{1}{\sqrt{\left(\dfrac{x}{3}\right)^2 + n^2}} - \dfrac{1}{\sqrt{\left(\dfrac{x}{2}\right)^2 + n^2}} \right]}{\dfrac{1}{4x} + \displaystyle\sum_{n=1}^{n=\infty} k^n \left[\dfrac{1}{\sqrt{\left(\dfrac{x}{2}\right)^2 + n^2}} - \dfrac{1}{\sqrt{\left(\dfrac{2x}{3}\right)^2 + n^2}} \right]} .$$

$$(10\text{–}42f)$$
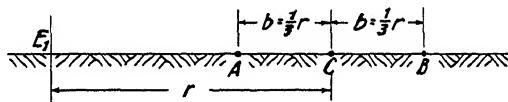
FIG. 10-77b. Expanding electrode system.

With the expanding system, the normal P.D.R. for homogeneous ground ($k = 0$) is $V_A/V_B = 2$. Hence, the correction factor is then constant and equals $\frac{1}{2}$. In comparison with the constant electrode system, the expanding system has the advantage that the P.D.R.'s are larger and less influenced by near-surface variations.

For positive values of k, the series in eq. (10–42f) converge rapidly. When a good conductor is underlain by a very poor conductor ($k = 1$), the extreme ratio is about 1.3 for a constant electrode spacing of one half the depth. This ratio occurs at a center stake distance of $1\frac{1}{2}$ times the depth (see Fig. 10-77c). The same relation prevails for lesser resistivity contrasts, although the curves become flatter and the peaks shift toward values slightly greater than $1\frac{1}{2}$. The simple relation between depth and peak distance makes it possible to interpret measured P.D.R. values more readily than resistivity values, provided that (1) a poor conductor occurs beneath a good conductor, (2) only two layers are effective, (3) surface interference is carefully eliminated, and (4) the observed ratios are reduced for normal ratio.

Curves like those illustrated in Fig. 10-77c may also be calculated for an
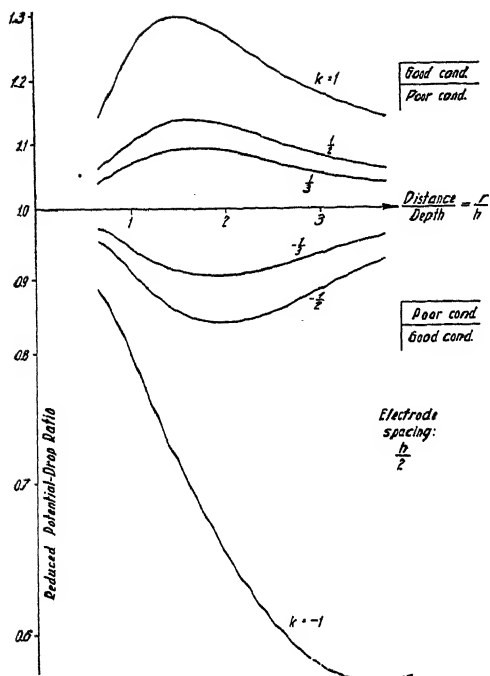
FIG. 10-77c. Potential-drop ratios for two layers as functions of distance, for constant electrode separation (adapted from Baird).

expanding electrode system. If the electrode interval is one-half the distance to the first (A) stake (which is the same as one-third of the center stake distance), the curves peak at a depth closely equal to the A stake distance (for positive k values).

When a good conductor occurs below a poor conductor, k is negative and the series terms in eq. (10–42f) become alternatingly positive and negative. The series converge less rapidly and the peaks are located at center stake distances nearly twice the depth (for constant electrode spacing equal to one-half the depth). For extreme conductivity contrasts, the convergence of the series is very slow and the ratio drops rapidly. Preliminary calculations[57] indicate a ratio peak at about $3\frac{1}{2}$ times the depth.

2. *Dipping layers.* The effect of dip on P.D.R. may be calculated from the corresponding apparent resistivity relations. Only one set of images is required for one source, since the other electrode may be assumed to be at infinity. The potentials must be figured for three instead of two points and their difference and the difference ratio must be formed.[58] P.D.R.'s so calculated are shown in Fig. 10–78 for various angles of dip of a single layer. It was assumed in all cases that the near-power electrode was so located as to make the depth, normal to the dipping bed, 18.5, regardless of dip. Calculations were carried out for one resistivity ratio only ($k = 1$). The results are valid for an electrode system moved downward in the direction of maximum dip. Results in Fig. 10–78a are for a constant electrode separation and in Fig. 10–78b for an expanding system.

3. *Vertical contacts.* A determination of the effects of vertical boundaries is of practical importance for the location of contact zones, faults,

---

[57] John Baird, Doctor's Thesis, Colorado School of Mines, May, 1940.
[58] M. Jameson, Master's Thesis, Colorado School of Mines, 1937.

and veins.   The P.D.R.'s for simple contacts with resistivities of ρ_1 on one side and ρ_2 on the other may be calculated from eqs. (10–40a) to (10–40j), which can be simplified, since only one source has to be considered. Details of the calculations depend on whether the source is moved or kept stationary with respect to the fault plane.   The theory of this case has
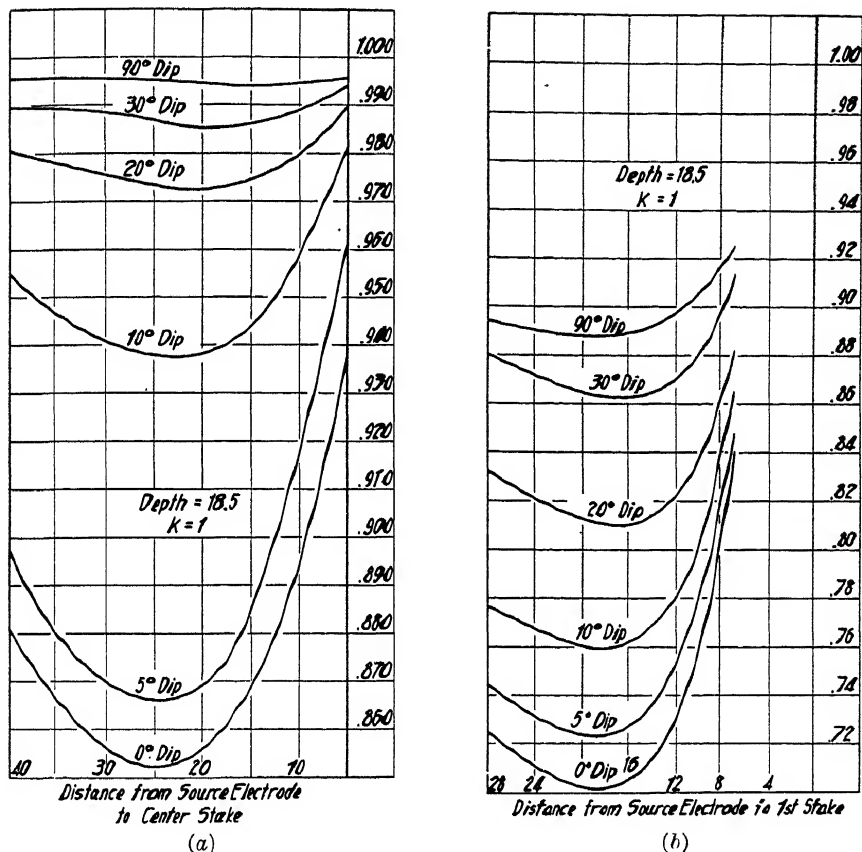
FIG. 10-78. Potential-drop–ratio curves for dipping bed: (a) constant spacing, (b) expanding system. Depth is reckoned perpendicularly to bed. (After Jameson.)

been discussed by Hedstrom.[59]   Curves have been published by Hedstrom and T. Zuschlag.[60]   Some of these are reproduced in Fig. 10–79.   When the power electrode is stationary, the greatest P.D.R. is obtained when the center stake crosses the boundary.   When the good conductor is the me-

[59] H. Hedstrom, Min. Mag., April, 1932.
[60] A.I.M.E. Geophys. Pros., 48 (1932).

dium on the left, the P.D.R. (in terms of V_B/V_A), is greater than 1; if the poor conductor is on the left, the ratio is less than 1.

For vertical veins the calculation of theoretical P.D.R.'s can be made in three ways. In the first, the assumption is made that the vein is very wide and that for the left side of the vein the effect shown in Fig. 10-79a can be compounded with that shown in Fig. 10-79b. This procedure is
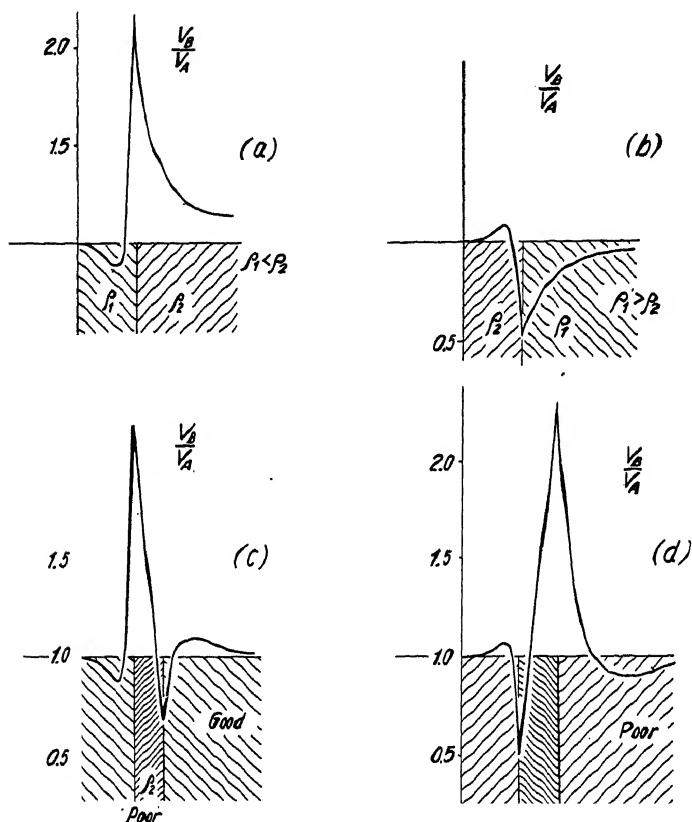
FIG. 10-79. Potential-drop–ratio curves for contacts and vertical dikes (after Zuschlag).

permissible only when the vein is so wide that the effect of the electrification of one side on the other side can be neglected. The more rigorous procedure is to figure with a reflection of the source not only on the boundary close to the power electrode but also on that away from the electrode. In this manner the curves shown in Fig. 10-79c and d were obtained. They show the effect of a poorly conductive vein in a medium of good conductivity as well as the effect of a vein of good conductivity imbedded in a

medium of poor conductivity. Another procedure is to consider a vein as a sheet of negligible thickness, that is, equivalent to a plane of ideal reflecting characteristics. If the plane is a good conductor, its effect is equivalent to producing an image of opposite sign, while an insulating sheet, assumed to be so thin that charges do not collect on it, produces an image of a source of like sign. In this manner both resistivity and P.D.R. distributions can be calculated.[61]

4. *Ore bodies.* The method by which anomalies of ore bodies are calculated depends entirely on their shape and geometric disposition. For ores in horizontal or nearly horizontal stratification (certain types of lead-zinc and lead-silver ores) the treatment is the same as for horizontal beds. For vein-type deposits in vertical positions the P.D.R.'s may be calculated by assuming two adjacent contacts or a thin conductive or insulating sheet. This procedure is applicable when the depth of overburden is small; if such is not the case, the problem can be treated as a two-layer case with a vertical vein in the lower medium that reaches up to the interface. Dipping ore bodies may be considered as two contacts of equal dip or as thin sheets, as the case may be. Lenticular bodies of limited dimensions may be assumed to be equivalent to polarized doublets. The more complicated cases are best treated by model experiments.

5. *Surface geologic features.* Owing to the great sensitivity of the P.D.R. method to horizontal resistivity variations, considerable anomalies will be produced by slight changes in the composition and structure of surface and near-surface formations. In regard to *vertical* contacts, the theory holds only if beds are infinite in *vertical* direction; for *horizontal* formation boundaries, the theory assumes that they remain the same in a *horizontal* direction. The field technique described below is intended to eliminate surface geologic features which are characterized by a limited extent in either horizontal or vertical direction, or both.

In Fig. 10–80, A', C', and B' are the three potential stakes and E the next power electrode. The arrangement is moved over a conductive body of limited depth extent, with an electrode separation equal to the width of the body. Assume as unit of length one-half of the electrode separation and let the depth extent of the conductive body vary from one to eight units. The corresponding ratio curves become more unsymmetrical with increasing depth extent. Therefore, to detect bodies of great depth extent and to eliminate near-surface interference, it is but necessary to take a reverse profile. Upon averaging the two curves, one obtains curves with amplitudes proportional to depth extent, and anomaly peaks over the center of the body.[61a]

[61] Howell, *op. cit.*, 34–37 (1932).
[61a] F. Kihlstedt, A.I.M.E. Geophys. Pros., 62–74 (1934).

C. EQUIPMENT; PROCEDURE

Various types of equipment have been developed for P.D.R. surveying. D.C. bridges have been used for recording corrosion effects on pipes (Schlumberger). Alternating current bridges are operated with audio frequencies of from 250 to 900 cycles, which has the advantage that phones can be used as indicating instruments.

In the Imperial Geophysical Experimental Survey series-capacity ratiometer, each arm consists of a condenser and a resistance in series.
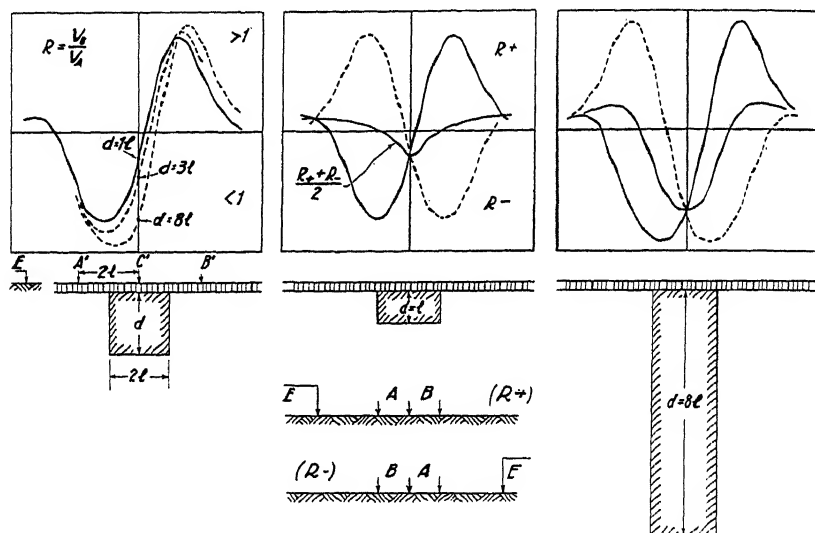
FIG. 10-80. Elimination of surface geologic anomalies by ratio curves taken in opposite directions (after Kihlstedt).

The ratio of the potential drops V_1 and V_2 between the equidistant pairs of contacts AB and BC, and their phase differences are determined by adjusting the capacities and resistances in each arm to balance. Thus $V_2 = (Z_2/Z_1) V_1$, where $Z_2 = \sqrt{R_2^2 + X_2^2}$ and $Z_1 = \sqrt{R_1^2 + X_1^2}$, Z_1 and Z_2 are the total impedances in the arms of the bridge, R_1 and R_2 resistances, and X_1 and X_2 are capacitive reactances, with $X_1 = 1/2\pi f C_1$ and $X_2 = 1/2\pi f C_2$. Hence,

$$\frac{V_2}{V_1} = \frac{R_2 \cos \tan^{-1} \dfrac{X_1}{R_1}}{R_1 \cos \tan^{-1} \dfrac{X_2}{R_2}} \tag{10-43a}$$

and the phase difference

$$\theta = \tan^{-1} \frac{X_1}{R_1} - \tan^{-1} \frac{X_2}{R_2}.$$

In a modification of the original ratiometer, the I.G.E.S. used condensers in parallel with the resistances. Then the admittance $1/Z$ in each arm is

$$\frac{1}{Z} = \frac{1}{R} + \frac{1}{\frac{1}{1}} = \frac{1}{R} + j2\pi fC.$$

If $1/R \equiv \mathbf{g}$, the conductance and $2\pi fC \equiv \mathbf{h}$, the capacitative susceptance of the circuit, then the admittance is $\mathbf{g} + j\mathbf{h}$, and the ratio is

$$\frac{V_2}{V_1} = \frac{\mathbf{g}_1 + j\mathbf{h}_1}{\mathbf{g}_2 + j\mathbf{h}_2}. \tag{10-43b}$$

In the parallel ratio-arm instrument (see Fig. 10-81) the variable capacities and resistances are so graduated that the conductances $\mathbf{g}_1$ and $\mathbf{g}_2$ and the susceptances $\mathbf{h}_1$ and $\mathbf{h}_2$ are in the same units, the unit being the conductance of a 300,000 ohm resistance. When the frequency is 535 cycles per second, this is approximately equal to the susceptance of a condenser of a 0.001 microfarad capacity, and the various portions of the variable capacity come out as whole numbers.

In the *Swedish-American Racom* (*ratio compensator*) bridge, inductive reactances take the place of the capacitive reactances; phase differences are not read but merely compensated by the use of a variable mutual inductance. A schematic circuit diagram is given in Fig. 10-82. The P.D.R., as computed from the resistance ratio, represents the ratio of the in-phase components of the potential drops. With R_A and R_B

FIG. 10-81. Parallel capacity ratiometer (after Edge and Laby).

as contact resistances of the stakes A and B, and R_{L_A} and R_{L_B} as resistances of coils L_A and L_B, the ratio is (approximately)

$$\frac{V_{AC}}{V_{CB}} = \frac{R_A + R_{L_A} + R_1}{R_2 + R_{L_B} + R_B}. \tag{10-44a}$$

The contact resistances may be determined and eliminated by a second setting of the resistances R_1' and R_2'. Then

$$\frac{V_{AC}}{V_{CB}} = \frac{R_A + R_{L_A} + R_1'}{R_2' + R_{L_B} + R_B}. \tag{10-44b}$$

Hence, by combination,

$$\frac{V_{AC}}{V_{BC}} = \frac{R_1 - R_1'}{R_2 - R_2'}. \tag{10-44c}$$

Field procedure in P.D.R. surveys depends entirely on their purpose. In prospecting for ore bodies, veins, contacts, and faults, field practice differs somewhat from that used in stratigraphic investigations. A third procedure is applied in corrosion surveys. In mining exploration, the P.D.R. traverse is usually run along a line between the two power electrodes and, if possible, in the vicinity of *one* of them. The electrode separation is kept constant, and observed P.D.R.'s are corrected for normal ratio. If ratio stations have been taken with 50 per cent overlap, the potential gradient per unit distance may be obtained by assuming an arbitrary potential gradient (usually 1) in the first *A–B* interval and by calculating the gradients for all other intervals by successive multiplication. Potential gradient (electric field intensity) values are then plotted against the center of the respective intervals.

A continuous phase curve may be plotted by starting in the first interval with an arbitrary phase angle and by calculating subsequent phase angles
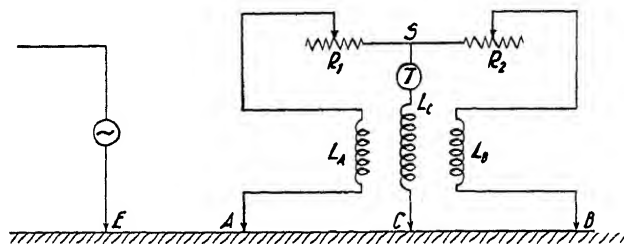
Fig. 10-82. Schematic of Swedish-American Racom.

by successive addition. As seen in Fig. 10-84, ore bodies are indicated by zones of low potential gradient and maximum phase anomaly. For the elimination of surface anomalies, ratio curves are surveyed in opposite directions from two power electrodes which may be switched on alternatingly so that two ratio readings are taken at each setup.

In determining depths to horizontal formations, measurements are usually made in the vicinity of one electrode; the other is kept at a distance from five to ten times the depth to be reached. Profiles are run out from the close electrode at right angles to the base. Then the power electrode is moved to another position and a second profile is run again normal to the base. The potential ratios thus obtained must be corrected for normal ratio. From a survey made with constant electrode interval and overlap, potential gradients and apparent resistivities may be calculated. In certain problems, expanding electrode systems are preferred. Profiles radiating out from the power electrode in different directions are useful for determination of dip. An electrode arrangement in which the power elec-

trodes are close together and the spacing of the secondary electrodes is a function of the base length, has been proposed by Koenigsberger.[62]

In corrosion surveys, the potential ratiometer has been used to determine zones of positive potential (where the greatest destruction is likely to occur), and to record fluctuations in corrosion potential. In the latter, the bridge is set at a fixed ratio, and galvanometer fluctuations with time are recorded.[63]

D. Results

P.D.R. methods have been applied in mining, in oil exploration, and in civil engineering. Applications in mining fall into two groups: (1) structural and stratigraphic investigations and (2) prospecting for ore bodies. The former include location of faults, shear zones, and quartz veins. Mineralization may accompany such zones or may be related to it in some

way. F. Kihlstedt[64] has published a number of examples where the P.D.R. method was supplemented by magnetic tests. Extensive use has been made of the potential-ratio method in search for (gold bearing) quartz veins. Fig. 10-83 is reproduced from an article by Hedstrom[65] and shows the P.D.R. curve above an andesite dike, flanked by volcanic conglomerates on one side and slate on the other, obtained near the Lebong Donok mine in Sumatra. Since the andesite is a poor conductor with respect to the conglomerates and the slate, the observed ratio curve (in terms of B/A) is in accord with the theoretical curve shown in Fig. 10-79c. Edge and Laby have published a number of ratiometer curves, largely for known deposits. In comparison with curves by other investigators it should be noted that measurements were made between two electrodes and that no
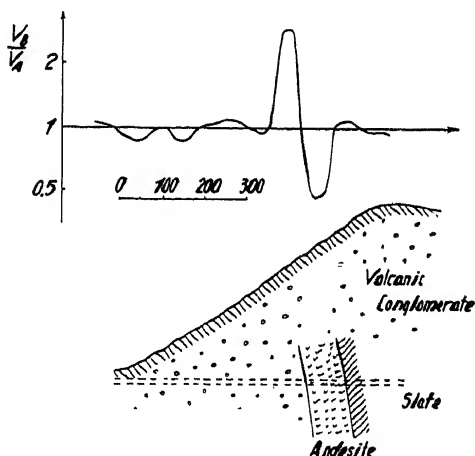
Fig. 10-83. Potential-ratio curve on andesite dike in Sumatra (after Hedstrom).

[62] Beitr. angew. Geophys., 1(1) 57 (1930).

[63] C. and M. Schlumberger, A.I.M.E. Tech. Publ. No 476 (1932).

[64] Loc. cit.

[65] H. Hedstrom, *loc. cit.*

correction for normal ratio was applied. Observed ratios were generally converted to a potential "variation" curve, the latter being identical with the potential gradient referred to above. Fig. 10–84 shows a profile taken in the Uley graphite area near Port Lincoln, South Australia. The graphites are believed to have originated from a metamorphism of Precambrian rocks, probably consisting originally of magnesium limestones. The potential gradient curve shows a minimum in the middle of the profile, indicating a good conductor; the small peaks on either side signify a crowding of the equipotential lines. The phase curve has a maximum, corresponding to out-of-phase currents induced in the conductor.

FIG. 10–84. Potential gradient and phase curve on graphite deposit at Port Lincoln, South Australia (after Edge and Laby).

On the basis of the electrical survey, a graphite body about fifty feet in width was located, dipping about 45–50° to the NW.

Application of P.D.R. surveys in oil exploration has been made to determine depth to key beds and to locate structure. Those known to date do not involve depths exceeding several hundred feet. In some P.D.R. surveys in Alberta,[66] depth interpretation was first based on peaks in the reduced ratio logs and was later supplemented by an evaluation of apparent resistivity curves calculated from the P.D.R. readings.[67] To what extent the simple two-layer relations between the distance of the peak in the P.D.R. curve and depth hold for more than one interface has not been determined, although it is probable that peaks in opposite directions appear near the upper and lower boundaries.

P.D.R. methods offer a rapid means of measuring depth to bedrock in foundation problems, of locating faults and shear zones, of determining the general characteristics of formations, and of locating water. The survey shown in Fig. 10–85 was made near the Oriental ore body at Buchans in Newfoundland, where glacial drift occurs above arkose bedrock. The potential-ratio (B/A) curves are plotted in such a manner that

[66] Lundberg and Zuschlag, A.I.M.E. Geophys. Pros., 61 (1932).
[67] Kihlstedt, op. cit., 199.

ratios greater than 1 are to the right, and those less than 1 to the left. A peak to the right signifies a transition from a good to a poor conductor, and a peak to the left a transition from a poor to a good conductor.   The
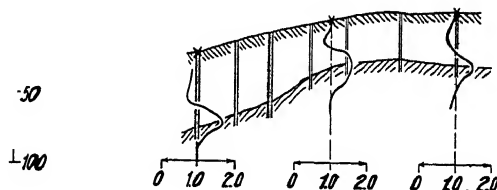
FIG. 10-85. Potential-drop-ratio curves indicating water level in glacial moraine and bedrock, Newfoundland (after Lundberg and Zuschlag).

electrical indications were interpreted as showing the effects of both water and bedrock, the dry upper portion of the moraine being the poor, and its water-bearing portion above bedrock being the good conductor.

VII. ELECTRICAL TRANSIENT ("ELTRAN") METHODS

Electrical methods previously discussed involve the measurement of stationary potentials or potential differences.   In electrical transient methods, on the other hand, their variation with time is observed.   The recorded time constants of the ground are primarily related to the resistance of the ground circuit; it is likely that capacitive and electrolytic-polarization effects introduce a reactive component.

When a ground circuit is closed or opened, the equilibrium values of voltage and current are not reached immediately.   Because of the change of the current with time, induction currents are generated.   The greater inductance of the lower paths causes the current to flow at first near the surface (skin effect).   The variation of the e.m.f. with time may be expressed by a relation of the form

$$E_t - E_0 = (E_{max.} - E_0)e^{-\frac{t\rho}{c\mu b^2}}, \tag{10-45a}$$

where $E_{max.}$ is the maximum initial potential difference between the ground electrodes when the circuit is closed, E_0 is the steady state value, t is time, ρ is resistivity in ohm-cm, μ is permeability, b is the distance between the electrodes, and c is a constant[68] equal to $2.32 \cdot 10^{-6}$.   With $\mu = 1$, the time required for the difference $E_{max.} - E_0$ to drop to $1/e$ of its value (time constant T) is given by

$$T = \frac{cb^2}{\rho}. \tag{10-45b}$$

---

[68] T. M. Pearson, A.I.M.E. Geophys. Pros., 34 (1934); C. and M. Schlumberger, *ibid.*, 139 (1932).

Since the time constant depends on electrode separation and resistivity, methods have been proposed to measure the time variation in the ground circuit, either with only two electrodes[69] or between two potential electrodes in the Wenner-Gish-Rooney or similar arrangements.[70]

In most Eltran arrangements used at present, the transients are measured in a separate potential circuit. It has also been found that the Wenner-Gish-Rooney setup is not so suitable for Eltran work because of the large voltages that may be induced by the current circuit into the potential circuit. Therefore, most arrangements now provide for observations outside the current basis in a potential circuit of about 1000 feet electrode separation. The interval between adjacent electrodes of the current and potential circuits varies between one thousand and several thousand feet.

Various techniques have been used to record electrical transients. They are: (1) direct oscillographic recording, (2) neutralization of transients by two opposing generating circuits, (3) compensation of the transient by a reference signal furnished by the power generator or by a locally synchronized generator, and (4) controlled alteration of the received transient to give a predetermined (saw-tooth) wave form.

Direct oscillographic recording was probably first used by Karcher and McDermott.[71] These investigators employed in the primary circuit two electrodes about a half mile apart, supplied through a switch from a storage battery of several hundred volts with currents of 10–20 amperes. Measurements were made half to three-quarters of a mile away in the extension of the primary electrode basis with two nonpolarizable electrodes about 0.1 to 0.2 mile apart, connected to a calibrated D.C. amplifier and oscillograph. The time constant was represented in the form of an "inductance function" which, according to the foregoing, is the apparent inductance due to the skin effect and therefore chiefly dependent on electrode base length and resistivity. Hence, the similarity in Karcher's "inductance" and "resistivity-slope-function" curves at the same locality.

In a method described by White,[72] power is supplied by a 60-cycle generator through a rectifier capable of delivering several thousand volts on open circuit. The rectifier charges a bank of condensers totaling 10 to 15 microfarads in capacity. The condensors are discharged by a fast mechanical switch which is released by a radio signal received from a transmitter synchronized with the sweep of the cathode-ray oscillograph on the receiving end. In this method the records are evaluated by taking

[69] L. W. Blau and L. Statham, U. S. Patent No. 2,079,103.
[70] L. W. Blau, U.S. Patent No. 1,911,137.
[71] J. C. Karcher and E. McDermott, A.A.P.G. Bull., 19(1), 64–77 (Jan., 1935).
[72] G. White, A.I.M.E. Tech. Publ. No. 1216, 4 (Feb., 1940).

the time gradient of the surge or by measuring the maximum height of
the transient and dividing it by the total charge of the current surge.
These transient voltage maxima, when contoured across a structure, give
a picture very similar to a resistivity contour map.

The difficulties encountered in the evaluation of oscillographic records
lead to the adoption of neutralization and compensation methods to deter-
mine magnitude and shape
of the transients. Statham[73]
developed a method based
on a comparison of tran-
sients in adjacent ground
intervals. In Fig. 10-86a,
I and III are the two pri-
mary circuits of opposing
polarity energized simulta-
neously through two screen-
grid thyratrons by closing
the switch S in their parallel
grid circuits. II is the
potential circuit connected
through a two-stage direct-
coupled amplifier to the
vertical plates of a cathode-
ray oscillograph on which
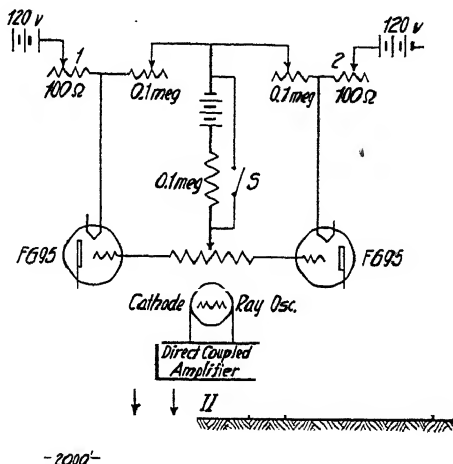
FIG. 10-86a. Circuit for comparison of electrical
transients (after Statham).

a 4-inch deflection corresponds to a (ground) potential difference of 4
millivolts, while the horizontal plates are actuated by a tuning-fork–con-
trolled linear sweep circuit. With currents flowing in circuits I and III,
resistors 1 and 2 are first adjusted so that no steady potential occurs
in circuit II. If the switch S is then closed and the transients due to
circuits I and III are equal, no transient will be recorded in circuit II.
When transients appear, they are compensated by moving the potential
electrodes. The direction and distance required for cancellation are in-
dicative of direction and rate of increase in effective conductivity.
Statham has published a map showing the effect of a deep-seated Gulf
coast oil field on the conductivity vectors thus determined.

Another group of Eltran methods involves a determination of the shape
of the transient by compensation with a simulating network. This net-
work may be synchronized by using a reference lead to the generator.
For large electrode separations, a local oscillator feeding the simulating

[73] Louis Statham, Geophysics, 1(2), 271–277 (June, 1936), and U. S. Patent No.
2,113,749.

network is synchronized by the received transient itself. Fig. 10–86b shows an arrangement developed by West,[74] in which the primary impulses of 50-cycle frequency and rectangular wave form are supplied by a thyratron relaxation oscillator controlled by a tuning fork. In the figure the synchronization of a reference signal by this oscillator is indicated; the reference lead may be dispensed with by synchronizing a local oscillator with the transient of the potential circuit.

In still another Eltran method, the technique is based on the assumption that the ground circuit has capacitive reactance in addition to resistance. The transient potential feeds two parallel circuits. One portion is amplified to actuate the sweep while the other is mixed in a double triode with the reference signal, after it has passed through an adjustable network.
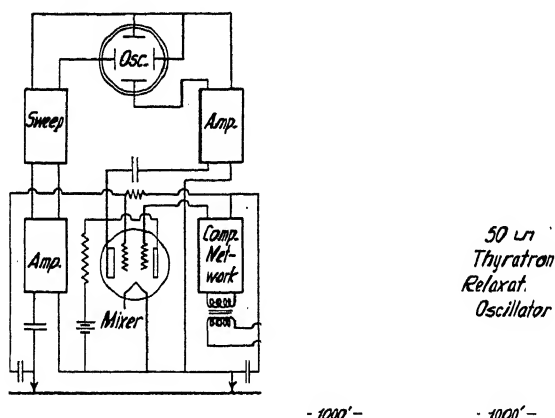
FIG. 10–86b. Arrangement for comparison of transients with simulating network (after West).

From the mixer the signal goes through an amplifier and thence to the vertical plates of a cathode-ray oscillograph. Time constants of transients are then expressed in terms of the value of the variable element in the compensating network required for balance (probably RC) and maps are contoured in units of reciprocal time constants. Fig. 10–87 shows such contours for the Sandy Point oil field in Brazoria County, Texas. The productive area coincides with contours of high reciprocal time constants.

Recent developments in mixing, synchronizing and simulating circuits have been discussed by Klipsch.[75] In the mixing of the reference signal with the received impulse, a bridge circuit has been found advantageous. The potential transient and the reference signal produced by an oscillator

[74] S. S. West, Geophysics, III(4), 306–314 (Oct., 1938).
[75] P. W. Klipsch, Geophysics, IV(4), 283–291 (Oct., 1939).

and distortion network are in opposite arms of the bridge, the former synchronizing the latter. An amplifier and oscilloscope are connected to the detector arm. Two potentiometers in series are connected across the input to the distortion network. The tapped portion of one potentiometer carries a resistance and a capacitance in parallel, while the tapped portion of the other potentiometer has a capacitance in series and a resistance in parallel. Transients can be simulated with sufficient accuracy by the four variable resistances in this network.

A technique referred to under (4) above, that uses a controlled distortion of the received impulse to produce a linear saw-tooth transient (Saw-tran), has likewise been described by Klipsch. In this case the distortion network consists simply of a tapped resistance with capacitance in series, both across the input line. By adjusting the sliding contact on the resistor until the resultant wave consists of a straight-line saw tooth, the time constant (RC) of the transient can be determined.

Opinions in the literature differ concerning the superiority of the transient over standard resistivity methods. Some authors claim that transient indications cannot be duplicated by resistivity measurements, that data

FIG. 10-87. Eltran contours, Sandy Point oil field, Brazoria County, Texas (after Rosaire).

on hitherto unobservable rock properties may be obtained, and that depth penetration is much greater. Others contend that the depth penetration is no greater than for other electrical methods under similar field conditions and that the observed anomalies are essentially due to shallow stratigraphic variations.[76] It is possible that the Eltran method and related electrical methods designed to measure ground circuit reactance, will reveal formation properties of diagnostic value not obtainable with the straight resistivity method. As was stated on page 639, the capacitive reactance of the ground is probably related to its electrolytic polarization properties.

An attempt has been made to measure this polarization directly by a so-called "electrochemical" method,[77] likewise based on the observation

[76] E. E. Rosaire, Geophysics, III (2), 96–115 (March, 1938).
[77] M. Müller, Beitr. angew. Geophys., 4(3), 302–315 (1932).

of transients. When current is sent into the ground, there result changes
in the concentration of electrolytic solutions which in turn give rise to a
counter (or polarization) e.m.f. It was noted before that this phenomenon
is responsible for corrosion potentials and that it is utilized in stimulating
the "activity" of ore bodies by passing current into the ground before a
self-potential survey.

An arrangement for measuring these counter e.m.f.'s is shown in Fig.
10-88.[78] The upper portion represents a beat oscillator furnishing fre-
quencies of the order of
1-5 cycles. The output
is coupled to the ground
circuit through the trans-
former T and is recti-
fied on the secondary
side, so that impulses in
only one direction pass
through the ground.
The potential difference
between the electrodes
E_1 and E_2, as well as
their time variation, is
recorded on the string
galvanometer or oscillo-
graph G_1. In parallel
with this circuit is an-
other one, consisting of
a second rectifier with
condenser in parallel,
going into the grid of an
amplifier with record-
ing galvanometer in
the plate circuit. With
proper selection of the
capacity C in parallel

FIG. 10-88. Circuit in electrochemical polarization
method (adapted from Müller).

with the second rectifier, the galvanometer G_2 will record only the return
impulses because of the unilateral impedance of the rectifier tube. The
fluctuations of both the input e.m.f. and the polarization e.m.f. are recorded
on the same film with time marks every hundredth of a second. The
ratio of charging time to discharge time is always greater than 1 and is
a function of the electrolytic polarization properties of sub-surface forma-

[78] *Ibid.*

tions reached by the action of the electrodes. It is claimed that the depth penetration is the same as the electrode separation. Since the ability of formations to furnish polarization e.m.f.'s is closely related to their electrolytic content and hence to their resistivity, there is some question as to whether an altogether different physical property is recorded in these measurements. Although the power supply to the ground is small (1–2 watts) the question arises further how much polarization e.m.f. is produced in the nonpolarizable electrodes.

VIII. ELECTROMAGNETIC METHODS

Electromagnetic methods constitute one of the largest and most diversified groups of electrical prospecting. They differ from the potential methods in that the electromagnetic field and not the surface potential of the ground currents is measured. Electromagnetic methods are divided into two groups. In the first, energy is supplied to the ground by contact; in the second group, energy is supplied inductively, that is, by insulated loops. The first group is sometimes called electromagnetic, and the second inductive.

A frequency of 500 cycles is most commonly used in electromagnetic methods. When a simpler technique is desired, when phase shifts are to be kept to negligible values, where a substantial depth has to be reached (as in Schlumberger's method of electromagnetic dip determination or in Koenigsberger's ring induction method), low frequencies of the order of 25–60 cycles are preferred. More than one operating frequency may be required when highly conductive layers near the surface are to be penetrated. Electromagnetic methods using frequencies of the order of tens of kilocycles are referred to as "high frequency" methods. Such frequencies are likely to energize noncommercial conductors and to produce excessive terrain effects. A band between 300 and 900 cycles is a practical compromise. Lower frequencies would make energy transmission too inefficient and would eliminate the telephone as a practical null detector. Higher frequencies lack depth penetration and produce too much interference.

Transmission units are: long cables, connected to a generator and grounded at both ends; rectangular or square loops; or circular coils. They are fed by generators driven by gasoline engines, storage battery operated buzzers, commercial lighting plants, or vacuum-tube oscillators.

Receiving devices are of widely diversified construction, depending on quantities measured. Their two fundamental constituents are a reception frame with several hundred turns of wire and an amplifier. Use is made of null methods wherever possible, with telephones as null indicators.

The more complex arrangements measure the field components by amplitude and phase, or as in-phase (real) and out-of-phase (imaginary) components. Fields at successive points may also be measured relatively in regard to amplitude ratio and phase difference. Following is a summary of observed electromagnetic field parameters:

Strike and dip of the ellipse of polarization.

Absolute values of intensity and intensity components.

Semi-absolute determination of intensity components in reference to amplitude and phase of the primary current.

Out-of-phase field components in terms of corresponding in-phase components.

Field ratios and phase differences in successive intervals.

Ratios of in-phase components at successive points.

Potential methods of electrical prospecting are preferred whenever primary power may be readily applied by contact and when the objects sought are not very good conductors. Electromagnetic-galvanic methods are suitable where bodies of good conductivity are to be located, where surface beds of good conductivity would produce too much screening effect on potential methods,[79] where requirements of depth penetration are not too great, and where contact of the primary electrodes with ground is readily possible. When this is difficult (as in deserts, on the ice of lakes, and the like) inductive methods must be applied.

A. ELECTROMAGNETIC METHODS WITH GALVANIC POWER SUPPLY

1. *Electrode arrangements* are like those used in equipotential-line or potential-profile methods. Line electrodes are laid out at right angles to the strike so that maximum distortion of the current lines occurs; profiles are run at right angles to the strike. Where large amounts of ground are to be covered and where the uniformity of the primary field does not play an important part (as in field-ratiometer measurements), point electrodes are preferred.

A long cable is laid out each way from the generator and grounded at the ends with a number of pins or wire screens. The line must be in the direction of strike so that profiles can be measured at right angles thereto. The field produced by the line connecting the electrodes to the generator may be reduced by carrying the leads around the area in a square or rectangle or by taking the measurements on the outside of a short current basis. For the simpler layouts, the field due to the leads may be calcu-

---

[79] See J. N. Hummel, Zeit. Geophys., **7**(**5/6**), 258 (1931).

lated and corrected for. Corrections need not be applied when compensators are used with inductive field excitation, since the loop field appears in the in-phase component, whereas the field induced in an ore body will generally affect most strongly the out-of-phase component.

2. *Receiving equipment* used in electromagnetic methods is virtually identical with that in inductive methods and is discussed in that connection. A piece of equipment not described there is the *Darley pipe locator*, since it is a direct application of the electromagnetic method with galvanic current supply. One pole of a small A.C. generator (buzzer) is connected to an accessible point of a system of pipes; the other pole is grounded. The receiving device is a small rectangular coil (carried in horizontal position over the ground), connected to an amplifier with phones. As such a coil will respond to the vertical component, which is zero directly over a conductor (see Fig. 10-92a), the point of minimum or zero signal will indicate the position of the pipe. In other types of pipe locators where the coil is carried in a vertical position, the horizontal component is received and therefore the pipe is indicated by a maximum.

A method not strictly classifiable under the groups tabulated on page 764 has been proposed by Haalck.[80] It is based on a comparison of the horizontal field of the ground currents with the field produced by the electrode leads. The latter are predominantly vertical; the former predominantly horizontal, at least on the electrode base. The receiving arrangement is set up in the center of the electrode base and the cable is carried around this location in a half rectangle. If the current flows in the cable from front to back, the cable field Z_0 is upward and that of the ground return current is to the left. The two fields are approximately in-phase. If the reception frame is set up with its horizontal axis of rotation parallel with the electrode base, a minimum of sound will be observed in the headphones when its plane is in the resultant direction of the two fields, that is, if tan $\varphi = Z_0/H$.

The sensitivity may be increased by using two frames, one stationary and the other rotatable (Fig. 10-96). In investigating stratified ground with this method, the electrode separation is increased in steps and the change in tilt angle is observed. If the ground is homogeneous, the horizontal field will decrease with an increased electrode separation due to greater depth penetration of the current. Hence, the tilt of the frame will increase. If bodies or strata of different conductivity are present, the depths of the effective current concentration will change; therefore, changes in the regular trend of tilt variation will occur. There is a definite relation between electrode separation and depth, the factor being $2\frac{1}{2}$ to 3, depending on conductivity contrasts involved.

¹ H. Haalck, and A. Ebert, Zeit. Geophys., 8(8), 409–419 (1932).

3. *Interpretation* procedures applied in electromagnetic-galvanic prospecting vary with the completeness and nature of observed field parameters. If only the direction of the field is measured (Elbof method), interpretation has to be largely qualitative. The direction of the field obtained with a vertical pickup coil, or the strike and dip of the ellipse of polarization determined with a coil rotatable about both a horizontal and a vertical axis, is a function of (a) the normal ground field due to the regular current distribution between two point or line electrodes, (b) the field produced by subsurface current concentrations, and (c) the field of the generator leads. The normal field can be calculated from relations previously given for the potential field. It is expressed by[81] $H = \sqrt{X^2 + Y^2} = I(1/r_1 - 1/r_2) \cdot 10^{-3}$ (Gauss), where the total current I is in amperes and r is in meters (see Fig. 10-89). The field direction is given by $\tan \alpha = Y/X$ in the horizontal plane and by $\tan \varphi = Z/H$ in the vertical plane, where the components due to subsurface conductors follow from eq. (10-46a). A similar relation applies if the field of the cable is used for comparison as in the Haalck method (see page 765).

Fig. 10-89. Magnetic field due to currents between two electrodes.

When the field intensities are measured at low frequency, phase shifts are small and the observed anomalies may be compared to advantage with fields calculated for simple geometric bodies as shown below. This procedure is likewise applicable when the components have been measured separately with a compensator and normal fields and cable effects have been deducted.

The electromagnetic anomalies of subsurface bodies may be determined with sufficient approximation by assuming equivalent current concentrations in such bodies. Hence, if the width of an ore body is small compared with its depth, the total field is $T = 2I'/r$ (see Fig. 10-92a), where r is the distance to any point at the surface and I' is the current in the conductor. In the following equations, let d be the depth of a current concentration and $X, Y,$ and Z be the components of the electromagnetic field (where X is the horizontal strike component, Y the horizontal component at right angles to the strike, and Z the vertical component). Further, let y be in the direction at right angles to the strike, x in the direction parallel with the strike, and φ be the angle between y and r. Then the

[81] J. Koenigsberger, Phys. Zeit., **28**, 342 (1937). A. Graf, Zeit. Geophys., **5**(8), 331 (1929); and Beitr. angew. Geophys., **1**(3), 286 (1931).

$\mathbf{X}$ component is zero and the other components are given by $\mathbf{Y} = \mathbf{T}\sin\varphi$ and $\mathbf{Z} = \mathbf{T}\cos\varphi$. Since $\cos\varphi = y/r$ and $\sin\varphi = d/r$, we have

$$\mathbf{Y} = \frac{2I'd}{r^2} = \frac{2I'd}{y^2 + d^2}$$

and

$$\mathbf{Z} = \frac{2I'y}{r^2} = \frac{2I'y}{y^2 + d^2}.$$

$$\left.\begin{array}{c}\\\\\\\\\end{array}\right\} \quad (10\text{-}46a)$$

Since $\partial\mathbf{Y}/\partial y = 0$ if $y = 0$; $\partial\mathbf{Z}/\partial y = 0$ for $y = \pm d, \mathbf{Z} = 0$ if $y = 0$ and $\partial^2\mathbf{Z}/\partial y^2 = 0$ for $y = 0$.

The horizontal component has a maximum directly over the current concentration ($y = 0$) and the maximum intensity is $\mathbf{Y}_{max.} = 2I'/d$. The maximum gradient in vertical intensity is directly over the ore body where the vertical intensity itself is zero. A maximum in vertical intensity occurs on either side at a distance from the zero point equal to the depth. The distance between the maximum and minimum vertical intensity anomalies is therefore equal to $2d$. For an ore body of definite width and infinite depth extent which can no longer be considered equivalent to a current concentration (see Fig. 10-92c),

$$\mathbf{Z} = 2I' \cdot \log_e \frac{r_2}{r_1}$$

$$\mathbf{Y} = 2I' \left(\varphi_2 \pm \varphi_1\right).$$

$$\left.\begin{array}{c}\\\\\\\end{array}\right\} \quad (10\text{-}46b)$$

Curves for bodies of various dimensions, dip, and depths have been published by Mueller.[82] Heine has calculated the electromagnetic field for rectangular sections of various dimensions, at right angles to the direction of current flow.[83] He assumed that the current density throughout the section was uniform which is permissible within the conductor itself. It is necessary, however, to allow also for the decrease of current density with depth, which was previously discussed (see Fig. 10-32 and eq. [10-21e]).

Belluigi has compiled a set of curves, showing the variation of current in the median plane between two electrodes as a function of base length.[84] When the current density for a given depth has been found, the electromagnetic field components may be determined[85] for a conductive body of

[82] Gerl. Beitr., **21**(23), 249-261 (1929).

[83] W. Heine, *Elektrische Bodenforschung*, 137, Bornträger (Berlin, 1928).

[84] A. Belluigi, Beitr. angew. Geophys., **1**(4), 370 (1931).

[85] *Ibid.*

arbitrary section by the use of gratings similar to those applied in gravimetric interpretation (see page 154). Since the magnetic field is proportional to the section of an element in which the current density is uniform, the field components are, for an element $dy\,dz$ traversed by a current in the x direction:

$$\left.\begin{aligned}
\mathbf{Y} &= -2I' \iint \frac{z}{y^2 + z^2}\, dy\, dz \\
\mathbf{Z} &= -2I' \iint \frac{y}{y^2 + z^2}\, dy\, dz.
\end{aligned}\right\} \quad (10\text{-}47a)$$

Substituting $y = \mathbf{R}\cos\theta$, $z = \mathbf{R}\sin\theta$, and $dy\,dz = \mathbf{R}\cdot d\theta\,d\mathbf{R}$, we have for the same components

$$\left.\begin{aligned}
\mathbf{Y} &= -2I' \iint \sin\theta d\theta\, d\mathbf{R} \\
\mathbf{Z} &= -2I' \iint \cos\theta d\theta\, d\mathbf{R}.
\end{aligned}\right\} \quad (10\text{-}47b)$$
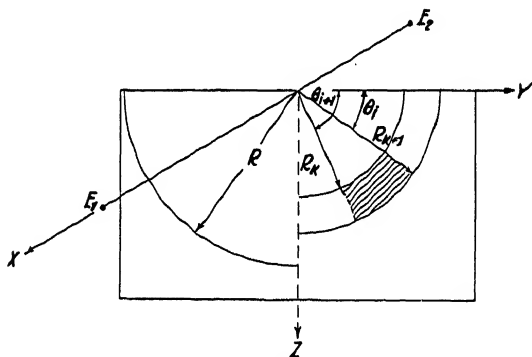
Fig. 10-90. Subsurface element traversed by current between two electrodes.

Hence, for a plane element, as in Fig. 10–90, the intensities are given by

$$\mathbf{Y}_{i,k} = -2I' \int_{\theta_i}^{\theta_{i+1}} \sin\theta\, d\theta \int_{\mathbf{R}_k}^{\mathbf{R}_{k+1}} d\mathbf{R}$$

and

$$\mathbf{Z}_{i,k} = -2I' \int_{\theta_i}^{\theta_{i+1}} \cos\theta\, d\theta \int_{\mathbf{R}_k}^{\mathbf{R}_{k+1}} d\mathbf{R}.$$

$$(10\text{-}47c)$$

The fields of all elements in the section are therefore

$$\left.\begin{aligned}
\mathbf{Y} &= \sum 2I'\, (\cos\theta_{i+1} - \cos\theta_i)(\mathbf{R}_{k+1} - \mathbf{R}_k) \\
\mathbf{Z} &= \sum -2I'\, (\sin\theta_{i+1} - \sin\theta_i)(\mathbf{R}_{k+1} - \mathbf{R}_k).
\end{aligned}\right\} \quad (10\text{-}47d)$$

For a current density of 1 amp./100 m², a unit effect ($H_{i,k} = 1.10^{-4}$ Gauss) is produced when $\cos \theta_{i+1} - \cos \theta_i = 0.1$ and $R_{k+1} = 10$ m. This applies to both horizontal and vertical components; for the latter, the diagram is rotated 90° (see Fig. 10–91).

Grounded electrodes cause currents to flow not only by galvanic action, but by inductive action as well. Since the ore body, with the cable or loop, acts as a transformer with a short-circuited turn, eddy currents are produced along the edges of the ore body, and flow down the dip as well as around its upper edge. The latter cause the greatest portion of the field observed at the surface. The field may be calculated from formula (10–46a)

Fig. 10–91. Interpretation grating for electromagnetic-galvanic methods (after Belluigi). Each compartment, when it is traversed by current at right angles to its section, produces the same effect on the horizontal component of the electromagnetic field. For calculations of the vertical component, the diagram is rotated 90°.

by adding the effects of the two current concentrations. With $2a$ as the width of the ore body, we have for the components

$$
\left.
\begin{aligned}
\mathbf{Z} &= 2I_i \left(\frac{a + y}{r_1^2} + \frac{a - y}{r_2^2} \right) \\
\mathbf{Y} &= 2I_i d \left(\frac{1}{r_1^2} - \frac{1}{r_2^2} \right),
\end{aligned}
\right\} \tag{10–48}
$$

where I_i is the induced current.

Use of grounded cables results in a superposition of currents produced by galvanic and inductive action. Considerable phase shifts may occur between the currents, so that in the absence of definite phase data only approximate curves can be given for the resulting fields (see Fig. 10–92c). Since one side of an ore body is usually much closer to the primary cable than the other is, the maximum on that side is greater than the minimum on the far side. The latter can be brought out by reversing the position of the primary cable or loop. The curves shown in Fig. 10–92d represent the variation of the X and Y vectors compounded from fields with greatly differing phase angles produced by both galvanic and inductive action. Separate measurement or calculation of in-phase and quadrature components has the advantage of segregating the induced from the galvanic and

FIG. 10-92. Horizontal and vertical field components due to galvanic and inductive action of vertical ore bodies.
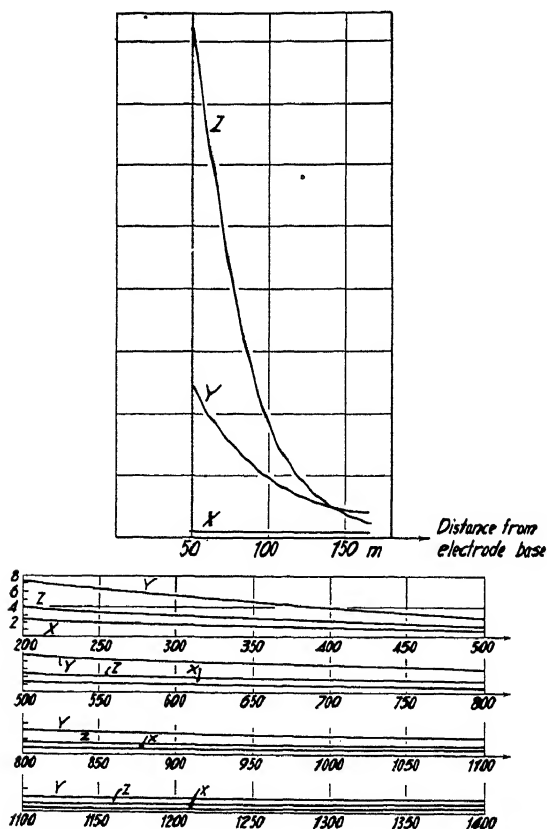
FIG. 10-93a. Normal field components for profile, at right angles to electrode basis of 200 m length, taken with 30 cycles (after Müeller).

normal fields. A further advantage is gained by using insulated loops whenever possible, because the galvanic effects are then eliminated. Since conditions in the field are not so simple as those assumed in the theory, interpretation is simplified by such applications of primary energy and observation methods as will produce the clearest type of indication.

In electromagnetic-galvanic methods, *corrections* are required for: (*a*) cable leads, (*b*) topography, and (*c*) normal field. The field of the cable depends on the position of the point of observation with reference to the cable. It can be calculated for all three intensity components (see page 777). The topographic effect may be of an electrical or geometric

nature. The former is due to a distortion of current lines on the ground surface (see page 702) and may be determined by small-scale experiments. The geometric influence is due to a change in relative position of ore body and plane of observation. A correction for the normal field is necessary in order to obtain the best picture of anomalies due to subsurface bodies. The normal field distribution may be calculated from the formula previously given (see page 766). A better procedure is to measure actually all field components in a location known to be free from outstanding anomalies

Fig. 10-93b. Horizontal and vertical intensity anomalies on parallel ore bodies (after Lundberg and Sundberg).

(see Fig. 10-93a). In the interpretation of electromagnetic survey data, considerable help may be expected from model experiments.[86]

4. *Results.* Electromagnetic-galvanic methods have been used for the location of ore bodies and structural investigation.

Fig. 10-93b shows two sets of curves on parallel bodies of steep dip, observed in Sweden. The horizontal and vertical components are those of a thin sheet as illustrated schematically in Fig. 10-92a. Fig. 10-94 shows the variation in the dip of a reception frame for minimum sound (Elbof method) for a profile near the Horne mine in Rouyn, Quebec. The range in the angles is 50°, undoubtedly because the ore bodies are very near the surface.

Various electromagnetic methods have been used for structural studies.

[86] K. Sundberg, Beitr. angew. Geophys., **1**(3), 335 (1931). Heine, *op. cit.*, 141–145.

Fig. 10–95 shows a syncline of slates of upper Devonian age near Meggen (Sauerland, Germany).   Results obtained there demonstrate the importance of corrections for cable and topography.   If a third correction had
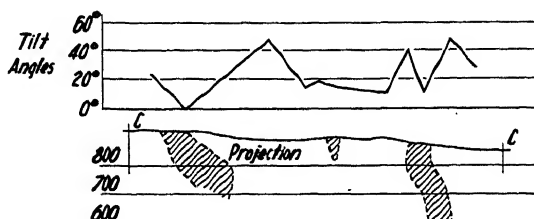
FIG. 10-94. Curve showing dip of polarization ellipse on Horne ore bodies, Rouyn, Quebec (after Mueser).
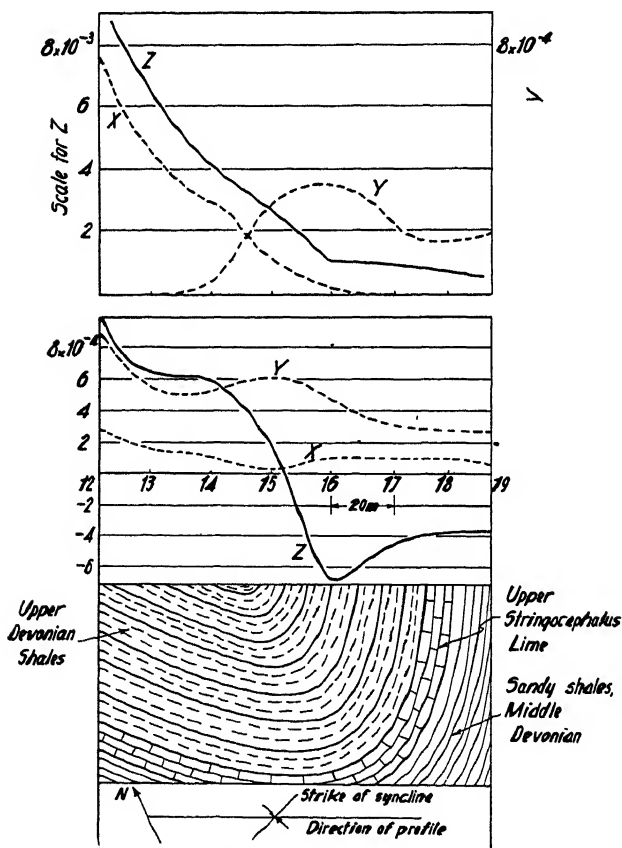
FIG. 10-95. Upper curves: electromagnetic field components (in Gauss) as measured.   Lower curves: same, corrected for cable and topographic influence, showing influence of Devonian syncline (after Dieckmann).

been applied for the normal field, the curves might have been improved further.   The maximum in the **Y** component and the trend of the **Z** curve indicates that the syncline acts as a current concentration, probably because the shales in the center of the syncline are of good conductivity. The Haalck electromagnetic method (see page 765) was used for depth determination of lignite beds in the Ville area by observing changes in the tilt angle of the detection coil with changes in spacing of the primary electrodes (Fig. 10-96).   For the same area, resistivity-depth curves were illustrated in Fig. 10–72.
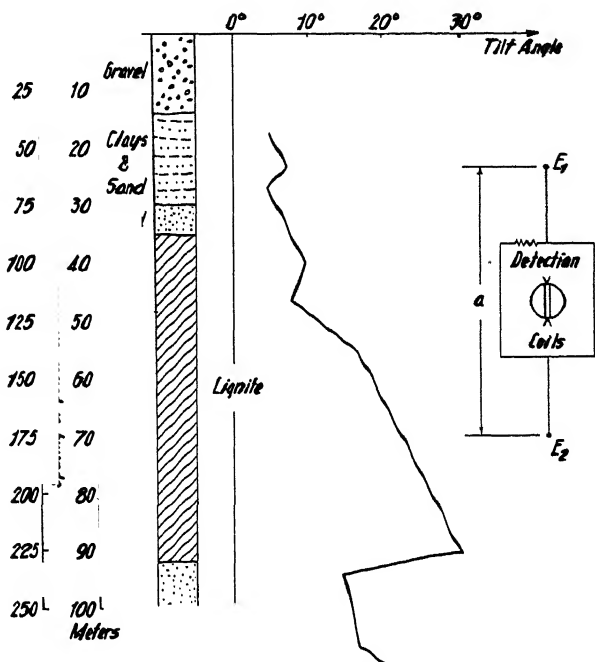
FIG. 10-96. Effect of electrode separation on tilt angle of electromagnetic field in determining thickness of lignite beds at Ville, Germany (adapted from Haalck). Left scale, electrode spacing; right scale, depth.

B. ELECTROMAGNETIC METHODS WITH INDUCTIVE POWER SUPPLY

The application of primary energy by insulated loops gives the electromagnetic-inductive methods a number of advantages over the electromagnetic-galvanic methods.   First, power can be transferred to the ground without great loss, particularly in areas of poorly conductive surface beds. While galvanic methods appear to be better adapted to massive geologic bodies, inductive methods are more suited for sheet-like deposits.   Good conductors may be reached when covered by poor conductors; depth penetration can be regulated by using different frequencies.

Electromagnetic-inductive methods may be divided into *horizontal-* and *vertical-*loop methods. The choice between them should theoretically be controlled by the closeness of coupling (loop and geologic body in parallel planes). For instance, in exploration of stratified ground, the loops should be horizontal; in prospecting for vertical or steeply dipping ore bodies, the loops should be vertical. However, a limitation is placed on this procedure, since large vertical loops are difficult to handle and since, with practical sizes, their range is comparatively small. Hence, horizontal loops are used more extensively. The following frequency ranges are applied in inductive methods: (1) low frequencies (30 to 100 cycles), (2) audio frequencies (250 to 1000 cycles), and (3) high frequencies (several tens of kilocycles).

1. *Horizontal-loop methods.* (a) *Power supply.* A large variety of transmission and generating equipment is available for use with insulated loops. A simple procedure is to feed the loop from the industrial power network through a suitable rheostat and transformer. This method has been applied where ore veins, fault conditions, and the like, were investigated in or near electrically operated mines. As a rule it is preferable to employ frequencies that are removed from the commercial frequencies to avoid interference. Gasoline-engine driven generators provide ample power ($\frac{1}{4}$ to $\frac{1}{2}$ kw.) for this purpose. It is desirable to provide them with a frequency meter or frequency bridge.[87] For absolute intensity measurements with a vacuum tube voltmeter, great constancy of output[88] and frequency are required.

Although of low power (15 to 20 watts), storage battery operated buzzers are satisfactory for moderate depths. Two types are illustrated in Fig. 10–97. Motor generators have been applied with storage battery driven (6 or 12 volt) D.C. motors and A.C. generators of low or audio frequency. Vacuum tube oscillators are used where both constancy of a given frequency and adjustability of frequency are desirable. Their output can be increased to about 80 watts when they are used with a power amplifier. The oscillator shown in Fig. 10–98 may be adjusted in frequency between 5 and several hundred cycles and has an output of several watts. In the power amplifier shown in the same figure, the plate supply is furnished from an A.C. generator, rectified, filtered, and connected to the center tap of the output transformer and the cathodes of six screen-grid tubes.

(b) *Transmission units.* Transmission units in inductive prospecting have the form of extended lines, rectangles, or circles. Single cables and rectangles are arranged parallel to the strike and profiles are surveyed at right angles to the strike.

[87] Canad. Geol. Survey Mem., **165**, 150.
[88] Müller, Gerl. Beitr., **21(2/3)**, 241 (1929).
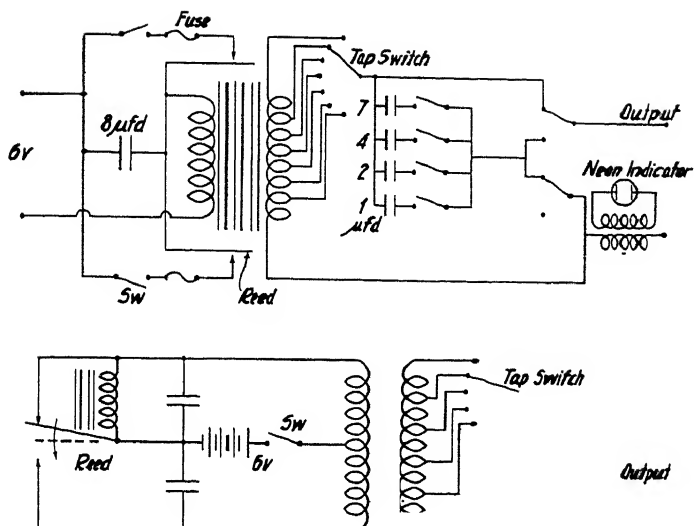
FIG. 10-97. Buzzers for electromagnetic prospecting.
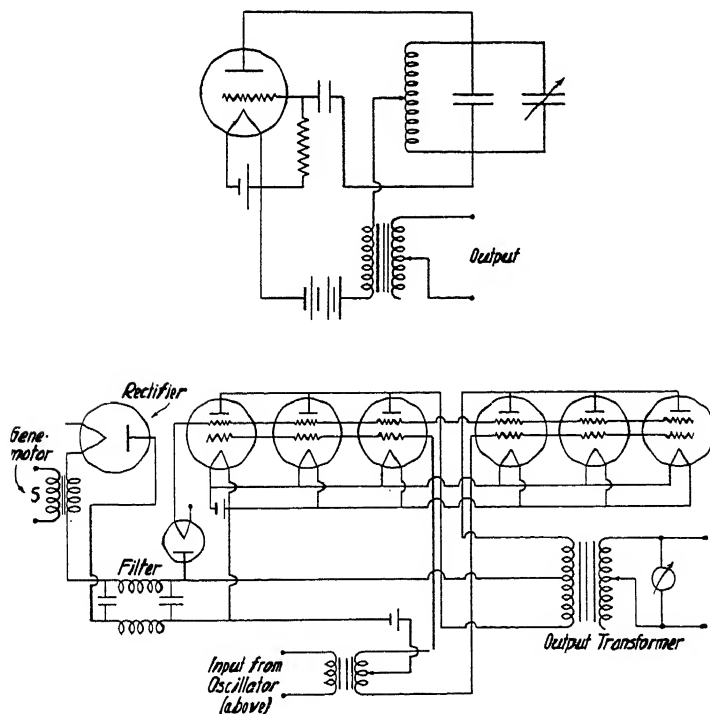
. 10-98. Vacuum tube oscillator and power amplifier for electromagnetic methods
(adapted from Müller).

The electromagnetic fields of cables or loops are readily calculated. For a long cable the field some distance away is practically vertical if the observation points are located at the same elevation. Since the magnetic intensity of a current element ds at a point P having the polar coordinates $\mathbf{R}$ and α is equal to $Ids \sin \alpha/\mathbf{R}^2$, the normal field is

$$\mathbf{Z}_0 = \frac{I}{10\,r} (\sin \alpha_2 \pm \sin \alpha_1),$$

where r is the distance normal to the line, and the current I is in amperes (see Fig. 10-99a). The minus sign applies if P is below E_1. If P, E_1,
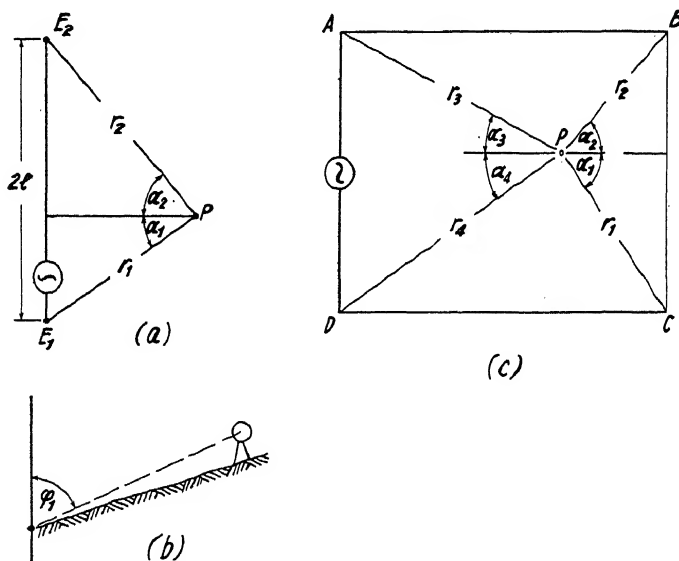
FIG. 10-99. Horizontal cables and loops.

and E_2 are all at the same elevation, the horizontal components are zero. If P is halfway between E_1 and E_2, $\alpha_1 = \alpha_2$ and

$$\mathbf{Z}_0 = \frac{I}{5\,r} \frac{l}{\sqrt{l^2 + r^2}}, \tag{10-49b}$$

where $2l$ is the distance between E_1 and E_2.

If the point P is not at the same elevation with the cable and if a line connecting the center of the search coil and the line E_1-E_2 makes an angle φ_1 with the vertical (Fig. 10-99b), a horizontal component is produced in

addition to the vertical, and

$$
\left.
\begin{aligned}
Z_0 &= \frac{I}{10r} \left(\sin \alpha_2 \pm \sin \alpha_1\right) \sin \varphi_1 \\[2mm]
Y_0 &= \frac{I}{10r} \left(\sin \alpha_2 \pm \sin \alpha_1\right) \cos \varphi_1 \\[2mm]
X_0 &= 0,
\end{aligned}
\right\} \quad (10\text{-}49c)
$$

where Y_0 is the horizontal component at right angles to the line E_1-E_2, and X_0 is the component parallel with it.

If the line E_1-E_2 is inclined at an angle φ_2 from the horizontal, all components are effective and

$$
\left.
\begin{aligned}
Z_0 &= \frac{I}{10r} \left(\sin \alpha_2 \pm \sin \alpha_1\right) \sin \varphi_1 \cos \varphi_2 \\[2mm]
Y_0 &= \frac{I}{10r} \left(\sin \alpha_2 \pm \sin \alpha_1\right) \cos \varphi_1 \\[2mm]
X_0 &= \frac{I}{10r} \left(\sin \alpha_2 \pm \sin \alpha_1\right) \sin \varphi_1 \sin \varphi_2 .
\end{aligned}
\right\} \quad (10\text{-}49d)
$$

The field of a horizontal loop (see **Fig. 10-99c**) may be calculated by adding the fields of its straight portions, so that

$$
Z_0 = \frac{I}{5} \left[\frac{1}{r_1 \sin 2\alpha_1} + \frac{1}{r_2 \sin 2\alpha_2} + \frac{1}{r_3 \sin 2\alpha_3} + \frac{1}{r_4 \sin 2\alpha_4} \right]. \quad (10\text{-}49e)
$$

At the *center* of a *square* loop with sides a, $r_1 = r_2 = r_3 = r_4 \equiv r = a/\sqrt{2}$. Then the sum in the bracket is $4\sqrt{2}/a$, and the intensity

$$
Z_0 = \frac{4I\sqrt{2}}{5a}. \quad (10\text{-}49f)
$$

In the central portion the field is very nearly uniform. Hence, formula (10-49f) may be applied in a fairly large area. In hilly country these formulas remain the same, provided the loop is laid out in a plane on a slope and the vertical component is measured at right angles to the ground surface. The field in the *center* of a *rectangle* with the sides a and b is, by application of eq. (10-49e),

$$
Z_0 = \frac{I}{5} \sqrt{a^2 + b^2} \left(\frac{1}{a} + \frac{1}{b}\right)^2 . \quad (10\text{-}49g)
$$

Müller[89] has measured the field outside a rectangle 200 meters in length and 150 meters in width and found a decrease approximately proportional to the third power of distance. This is also true for the space outside a circular loop (see below) and is in accordance with the well-known fact that a closed loop is equivalent to a magnetic doublet with the moment IS (S = area).

For a circular loop of the radius R, the (axial) component Z and the (radial) component Y_r are given by

$$
\left.
\begin{aligned}
Z &= \frac{I\pi}{R}\left[2 + \frac{3}{2}\left(\frac{r}{R}\right)^2 - 3\frac{z^2}{R^2}\right.\\
&\qquad\left. + \frac{45}{32}\left(\frac{r}{R}\right)^4 - \frac{45}{4}\frac{r^2 z^2}{R^4} + \frac{15}{4}\frac{z^4}{R} + \cdots\right]\\
Y_r &= \frac{I\pi r z}{R^3}\left[3 + \frac{45}{8}\left(\frac{r}{R}\right)^2 - \frac{15}{2}z^2\right.\\
&\qquad\left. + \frac{525}{64}\left(\frac{r}{R}\right)^4 - \frac{525}{16}\frac{z^2}{R^4} + \frac{105}{8}\left(\frac{z}{r}\right)^4 + \cdots\right],
\end{aligned}
\right\} \quad (10\text{--}50a)
$$

where I is in abamperes. The radial component becomes zero both in the axis ($r = 0$) and in the plane of the loop ($z = 0$). In the center ($r = 0$, $z = 0$), the vertical component

$$
Z_0 = \frac{2\pi I}{R} \ (I \text{ in abamps.}) \qquad \text{or} \qquad \frac{\pi I}{5R} \ (I \text{ in amps.}). \quad (10\text{--}50b)
$$

The variation of Z inside and outside a circular loop is shown in Fig. 10-100. For outside points, the vertical component is

$$
Z_0 = \frac{IR^2\pi}{r^3}\left[1 + \frac{9}{8}\left(\frac{R}{r}\right)^2 + \frac{75}{64}\left(\frac{R}{r}\right)^4 + \cdots\right]. \quad (10\text{--}50c)
$$

For large distances the series terms approach zero and the vertical component is $Z_0 = IR^2\pi/r^3 \equiv m/r^3$, that is, the vertical component is proportional to the magnetic moment m of the loop and inversely proportional to the cube of distance.

(c) *Reception equipment.* Reception equipment in electromagnetic prospecting varies from the simplest to the most complex, depending on what information about the field is sought. If only the strike and dip of the ellipse of polarization is desired, a simple coil with amplifier and phones is sufficient. For intensity measurements without reference to phase, a vacuum-tube voltmeter is used in the output stage of the amplifier. In-

[89] Müller, *op. cit.*, **30**(1/2), 185 (1931).

tensities and phases are determined in reference to the loop current by compensator arrangements. The out-of-phase component (generally due to subsurface conductors) may be obtained in reference to the in-phase field (usually due to the loop) by the Bieler-Watson method. Fields in successive intervals may be determined relatively by measuring the ratio of the field vectors and their phase difference. Finally, the in-phase components on successive stations may be compared (field ratiometer).

With a reception coil of round or square shape the orientation of the plane of polarization of the ellipse and its projections can be determined. When elliptical polarization is small, this is equivalent to a measurement of the direction of the resultant horizontal field and the inclination of the field. The reception coil must be capable of rotation about a vertical and a horizontal axis. Transit bases are frequently used for this purpose.
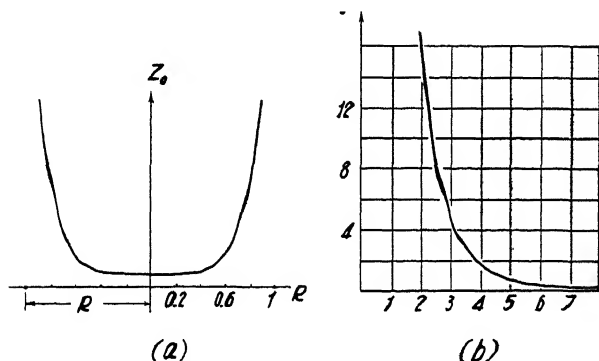
FIG. 10-100. Fields of circular loops: (a) inside of loop, (b) outside of loop
(adapted from Müller).

The standards are changed to a semicircular support in which the reception frame can be rotated about a horizontal axis. A small vertical circle is usually provided so that the tilt angle of the frame in the minimum position may be determined. The horizontal azimuth on the horizontal circle is read in respect to markers on the base line or in respect to magnetic north.

The Swedish investigators have used a long staff with a horizontal crossbar, about which a square frame may be rotated. The crossbar is provided with peepsights and a clinometer so that both horizontal azimuth and tilt angle of the frame can be determined. Coils are generally wound on wooden or aluminum frames. They have a diameter of 40 to 50 centimeters, from 500 to 1000 turns of wire, a D.C. resistance from 75 to 150 ohms, and an inductance of from $\frac{1}{4}$ to $\frac{1}{2}$ henry. The amplifiers are usually transformer coupled; they have two to three stages; and carry headphones

in the output circuit. Reception coils and amplifiers are common to all receiving arrangements discussed below.

When the frequency is too low for audio detection, the telephone is replaced by a galvanometer in the plate circuit of the output stage (see Fig. 10-101). The sensitivity of the galvanometer is 10^{-6} to 10^{-7} amperes
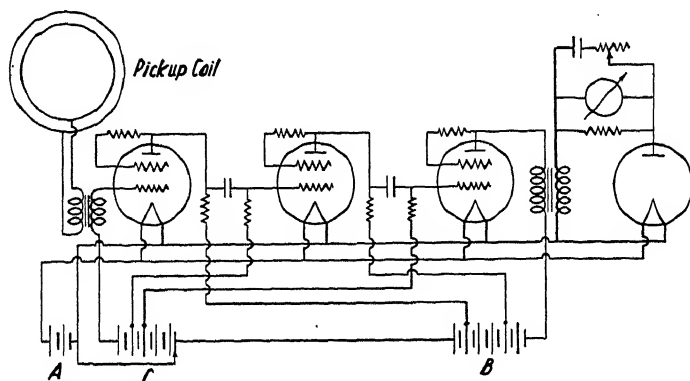
FIG. 10-101a. Resistance-coupled amplifier for electromagnetic prospecting, with output meter (adapted from Müller).
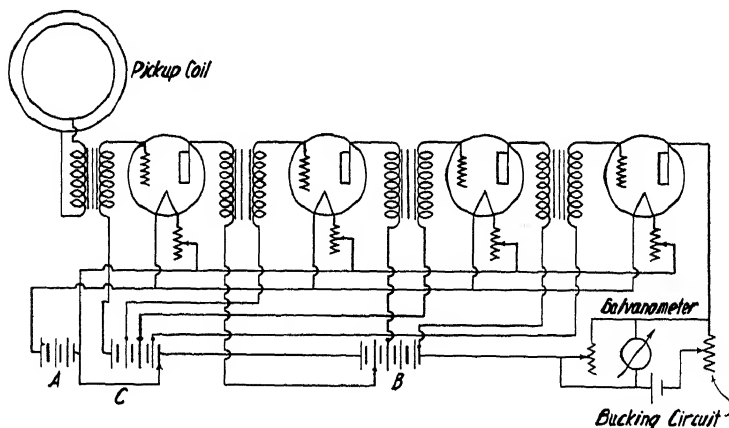
FIG. 10-101b. Transformer-coupled amplifier for electromagnetic prospecting, with output meter (adapted from Müller).

per scale division; that of the reception arrangement, of the order of 10^{-8} gauss. The amplifiers should remain in good calibration and should have constant gain. The latter may be expressed as galvanometer deflection for a given input voltage. The corresponding field is then

$$H = \frac{E\sqrt{2}}{\omega SN} \ 10^8 \text{ gauss,} \tag{10-51}$$

where E is the e.m.f. induced in the coil of the area S and turn number N, and ω is the angular frequency.

Absolute measurements of field intensity have the disadvantage of depending on generator voltage and frequency. Hence, it has become more general practice to measure A.C. fields semiabsolutely, that is, in reference
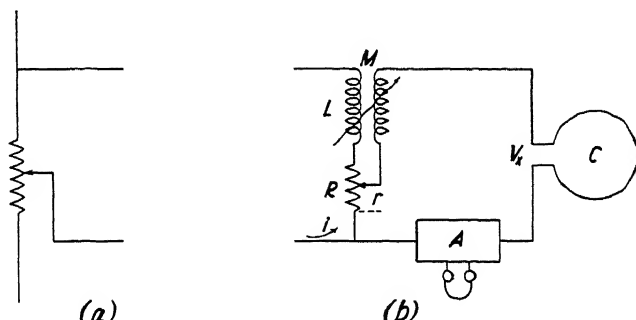
FIG. 10-102. Larsen compensator with (a) resistance coupled reference, and (b) inductively coupled reference.
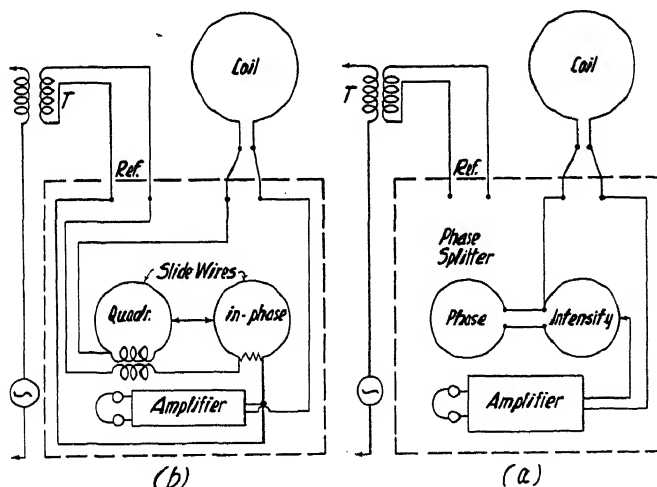
FIG. 10-103. Compensators giving (a) intensity and phase of field and (b) in-phase and quadrature field.

to generator voltage and phase. With a voltage divider or a transformer (see Fig. 10-102) a portion of the generator voltage is carried to the field-measuring network by a separate cable. Two compensators for the measurement of potentials with reference to generator amplitude and phase are described on page 696. Adaptations of these to electromagnetic measurements are shown in Fig. 10-102 and 10-103. The Larsen compensator

gives the in-phase and quadrature components of the field, the former being obtained by adjustment of the slide wire, the latter on the secondary of a variometer. When the bridge is balanced, the in-phase voltage drop ri on the resistor R, plus the quadrature e.m.f. induced in the secondary of the mutual inductance M, is equal to the voltage V_x induced in the pickup coil:

$$M \frac{di}{dt} + ri = V_x \qquad (10\text{-}52)$$

Heiland Research Corp.

Fig. 10-104. Compensator with amplifier and receiving coil.

with $i = V/(R + jL\omega)$. A complete compensator arrangement with coil on tripod and instrument case containing network and amplifier is shown in Fig. 10-104.

In the *ring-induction* method[90] compensation is accomplished by creating in-phase and out-of-phase fields outside the detector coil. When alternating current is passed through the primary loop in Fig. 10-105, a quadra-

[90] J. Koenigsberger, Phys. Zeit., **31**, 487–498 (1930), **35**(1), 6–8 (1934); Beitr. angew. Geophys., **3**(4), 392–407 (1933), 4(2), 201–216 (1934), **7**(2), 112–161 (1937). W. Nunier, Beitr. angew. Geophys., **3**(4), 370–391 (1933); Phys. Zeit., **35**(1), 8–10 (1934). A. Graf, Beitr. angew. Geophys., **4**(1), 1–75 (1934). S. Stefanescu, Beitr. angew. Geophys., **5**(2), 182–192 (1935), **6**(2), 168–201 (1936).

ture field is caused by currents induced in subsurface conductors. The field depends on frequency, radius of the primary coil, current strength, and the apparent conductivity of the subsurface section. It is measured by a compensator coil which is connected to the primary coil through a "reference" transformer and mounted in the same level (h) with the detector coil, while the effect of the in-phase (primary) field is compensated by a neutralizing coil laid out on the ground. The detector coil is connected to an amplifier with a vacuum-tube voltmeter circuit.

A receiving arrangement involving the determination of (horizontal) out-of-phase components in terms of (vertical) in-phase fields is known as the *Bieler-Watson* method.[91] It makes use of a dual coil receiver, consisting of a large rectangular frame rigidly connected to another smaller
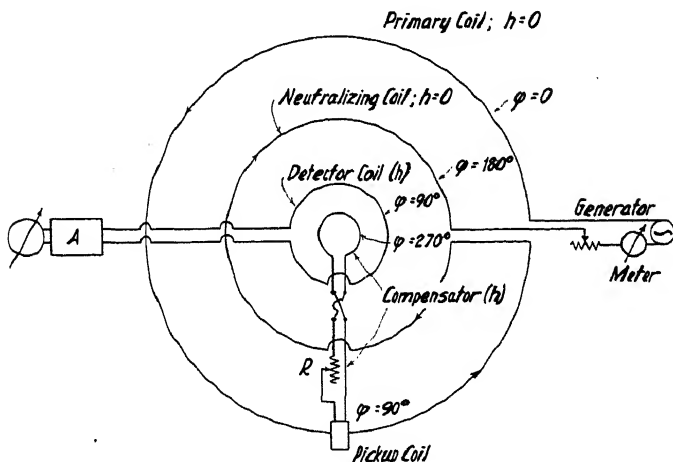
FIG. 10-105. Compensator and primary loop arrangement in Koenigsberger ring induction method.

one at right angles to it. The purpose of the small frame is to pick up the field corresponding to the major axis of the ellipse of polarization (almost vertical, due to the in-phase loop field), while the large frame will pick up the field in the direction of the minor axis of the ellipse (Fig. 10-106a). This field is usually horizontal, and is in quadrature with the loop field. The e.m.f.'s induced in the coils are pulled back into phase by a condenser across the vertical coil and connected in opposition to a detector. The number of turns in the horizontal coil is changed until balance is obtained. The detector is a three-stage, transformer coupled,

[91] Edge and Laby, *op. cit.*, pp. 64–67, 283–286.   H. G. I. Watson, Canad. Geol. Survey Mem. **165**, 144–151.   J. McG. Bruckshaw, Phys. Soc. Proc., **46**, 350 (1934).

plane-tuned amplifier with phones. At each station the observer records
the number of turns in the horizontal coil required to obtain a balance,
holding the axis of the double coil vertical with the plane of the large coil
first in a north and south, and then in an east and west direction. Com-
pounding of the two readings yields the ratio of the quadrature horizontal
to the vertical in-phase field and gives, therefore, approximately the ratio
of the axes of the ellipse of polarization. This resultant may be plotted
as an arrow whose direction points toward the conductor and whose length
is greatest near its edges. Points of equal vector amplitude may be joined
by lines of equal intensity of the out-of-phase component.
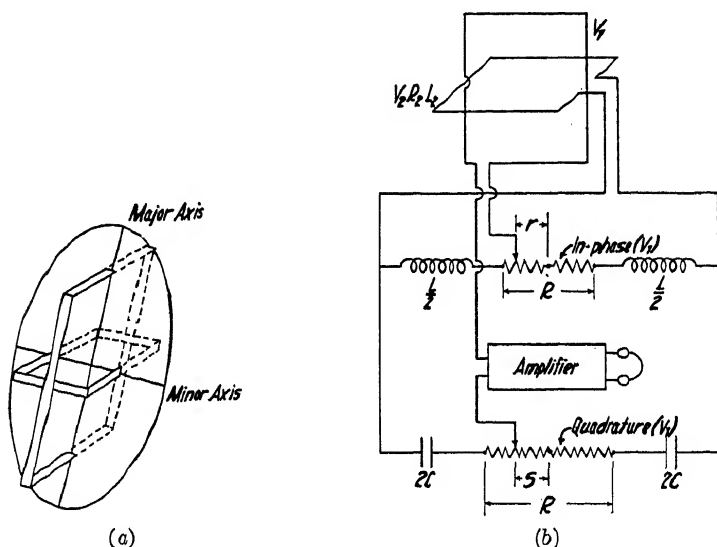
FIG. 10-106. (a) Double-coil arrangement in reference to polarization ellipse (after
Edge and Laby). (b) Bruckshaw's modification of Bieler-Watson system.

With the simple Bieler-Watson system sharp nulls are often unobtain-
able. If the ellipse is not vertical, an in-phase e.m.f. appears in the
vertical coil and a quadrature e.m.f. appears in the horizontal coil. Fur-
thermore, the phase shift between the vertical and horizontal components
is not always 90°. An instrument designed to measure any phase shift
between the vertical and horizontal components has been constructed by
Bruckshaw[92] (Fig. 10-106b). The circuit is comparable with that of a
compensator if one considers the horizontal frame as "reference" coil. An
inductance with resistance, as well as a capacitance with resistance, are
connected in two parallel branches to this coil and its (reference) e.m.f.

[92] Loc. cit.

is split up into its in-phase and quadrature components. The currents in these two branches differ by 90° if $L = CR^2$. To measure the in-phase and quadrature components of the e.m.f. induced in the vertical coil, the latter is connected across two slide-wire resistances as shown in Fig. 10–103. Equal sensitivity for in-phase and quadrature components may be obtained by making the currents in both branches equal to each other and $\pm 45°$ different in phase from the main current. This is true when $L\omega = 1/\omega C = R$. If, further, $L_2\omega = R + R_2$, and if $\mathbf{r}$ is the setting of the potentiometer in the upper branch (in-phase with V_1) and $\mathbf{s}$ is the setting of the potentiometer in the lower branch (in quadrature with V_1), the condition for balance is given by

$$\frac{V_1}{V_2} = -\frac{1}{2(R + R_2)}\,(\mathbf{s} + j\mathbf{r}). \qquad (10\text{–}53a)$$

Relative determination of electromagnetic fields may be made by measuring field *ratios* and phase *differences* in successive ground intervals. In other words, the field at one location serves as a reference for that at an adjacent location. In the application of this procedure to the vertical component, two coils are laid flat on the ground in horizontal position or are carried by two surveyors with straps around their waists (see Fig. 10–107b). For horizontal-intensity determinations, two coils are held in a vertical position; their direction is kept parallel with the direction of strike if the primary cable has been laid out parallel with the strike. Instruments for the relative measurement of intensity ratios and phase differences have been constructed as adaptations of potential ratiometers and compensator bridges. The type shown in Fig. 10–107a is an

FIG. 10-107a. Dual-coil instrument for measuring intensity ratios and phase differences. Adaptation of capacity ratiometer.

adaptation of the parallel capacity ratiometer of Fig. 10–81. Other compensator bridges are likewise adaptable to dual-coil ratiometer construction.

Comparison of *in-phase components* at *successive stations* may likewise be made with two coils, but this process does not require a compensator.

The coils are connected in series opposition to a detector. One coil is laid flat on the ground at one location; the second is placed at another location. With the second coil, the plane of the ellipse of polarization is determined first on the second location. The axis of rotation of the coil is then so oriented as to be in the plane of the ellipse. After this, the coils are connected and the coil on the second location is rotated about a

J. E. Hawkins

Fig. 10-107b. Colorado School of Mines dual-coil field ratiometer.

horizontal axis until a null is obtained. If the phase difference between successive locations is small, this method will give the ratio of the in-phase components at the two locations with sufficient accuracy. For a complete determination of intensity ratios and phase differences between two points, a three-frame arrangement must be used.[93]

(d) *Elliptical polarization.* In the discussion of potential methods

[93] Sundberg, A.I.M.E. Geophys. Pros., 134 (1929).

(page 687) it was shown that elliptical polarization results from a combination of two vectors which differ in coordinate and phase. The combination of two vectors that differ in direction and are in quadrature, likewise results in elliptical polarization. This combination applies in electromagnetic methods. As illustrated in Fig. 10–108, a horizontal loop laid on the ground surface induces a current to flow in opposite direction along the upper edge of an ore body whose magnetic field at the distance r from the current concentration is given by the vector $\mathbf{T}$. This vector combines with the vertical loop field Z_0 and is in approximate quadrature with it. The components of $\mathbf{T}$ are: $Y = \mathbf{T} \cos \theta$, and $Z = \mathbf{T} \sin \theta$. The difference
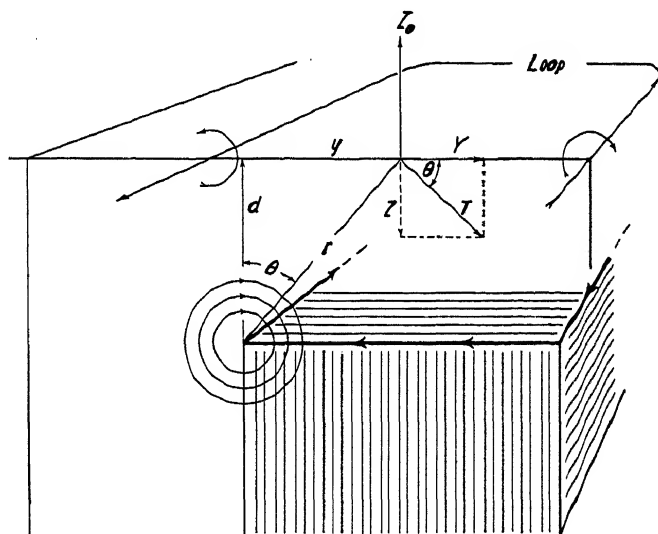
FIG. 10-108. Composition of loop field and eddy current field.

in the vertical components is $Z_1 \equiv Z_0 - Z$. If all vectors oscillate with the same frequency and $\mathbf{T} = \mathbf{B} \cos \omega t$ is in quadrature with $Z_0 = \mathbf{A} \sin \omega t$, then

$$Z_1 = \mathbf{A} \sin \omega t - \mathbf{B} \cos \omega t \sin \theta$$

and   (10-53b)

$$Y = \mathbf{B} \cos \omega t \cos \theta.$$

Since, in the second equation, $\sin \omega t = \sqrt{1 - \cos^2 \omega t} = \dfrac{\sqrt{\mathbf{B}^2 \cos^2 \theta - \mathbf{Y}^2}}{\mathbf{B} \cos \theta}$, the first equation becomes, by substitution, $Z_1\mathbf{B} \cos \theta + \mathbf{BY} \sin \theta =$

$A \sqrt{B^2 \cos^2 \theta - Y^2}$. Squaring and dividing by $A^2 B^2$ and $\cos^2 \theta$ give

$$Z_1^2 \left(\frac{1}{A^2}\right) + 2Z_1 Y \left(\frac{\tan \theta}{A^2}\right) + Y^2 \left(\frac{B^2 \sin^2 \theta + A^2}{A^2 B^2 \cos^2 \theta}\right) = 1. \quad (10\text{–}53c)$$

This equation has the standard form of an inclined ellipse (see eq. [10–24c]), so that $L \equiv 1/A^2$; $M \equiv \tan \theta/A^2$; $N \equiv (A^2 + B^2 \sin^2 \theta)/A^2 B^2 \cos^2 \theta$. The tilt angle ψ from vertical is then

$$\tan 2\psi = \frac{2M}{N - L} = \frac{2 \tan \theta}{\dfrac{A^2 + B^2 \sin^2 \theta}{B^2 \cos^2 \theta} - 1} = \frac{B^2 \sin 2\theta}{A^2 - B^2 \cos 2\theta}. \quad (10\text{–}53d)$$
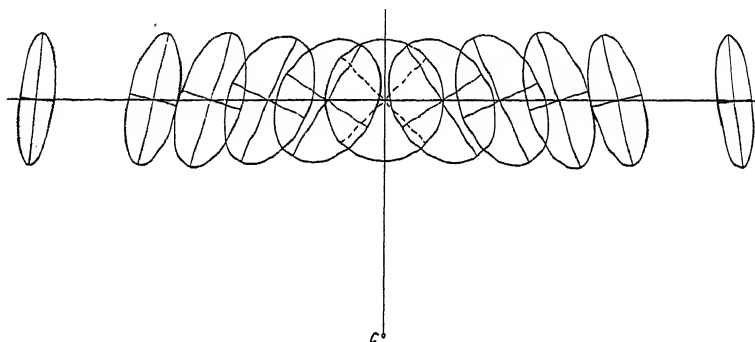
FIG. 10-109. Elliptical polarization resulting from a quadrature field (produced by a conductor at C), which is equal to the in-phase (loop) field above C (after Edge and Laby).

The squares of the major and minor semiaxes of the ellipse are, in accordance with eq. (10-25b),

$$a^2, b^2 = \frac{2}{L + N \mp \sqrt{4M^2 + (L - N)^2}}$$

$$= \frac{2A^2 B^2 \cos^2 \theta}{A^2 + B^2 \mp \sqrt{[A^2 - B^2 \cos 2\theta]^2 + [B^2 \sin 2\theta]^2}}. \quad (10\text{-}53e)$$

For two fields of equal maximum amplitude, $A \equiv B$ and $\tan 2\psi = \sin 2\theta/(1 - \cos 2\theta) = \tan (\pi/2 - \theta)$, so that $\psi = \pi/4 - \theta/2$. Eq. (10-53e) is then $a, b = B \cos \theta/\sqrt{1 \mp \sin \theta}$.

Fig. 10–109 shows the variation of compression and tilt angle of the polarization ellipse with distance for a conductor carrying a quadrature current at depth d. If the out-of-phase field is directly above the conductor, it is equal to the in-phase field ($A \equiv B$), and if T declines from there in proportion to d/r (since $T_{max} = 2I'/d$ and $T = 2I'/r$), it is seen

that $\mathbf{B}$ declines in the same proportion, so that $\mathbf{B} = \mathbf{B}_{max}.\ d/r$. Since $\mathbf{B}_{max}. \equiv \mathbf{A}, \mathbf{B} = \mathbf{A}\cos\theta$, so that by substitution of the above and of $\tan\theta = y/d$ in eq. (10–53d),

$$\tan 2\psi = \frac{\sin 2\theta}{\cos 2\theta - \tan^2\theta - 1}. \qquad (10\text{–}54a)$$

The axes of the ellipse follow by substituting $\mathbf{B} = \mathbf{A}\cos\theta$ in eq. (10–53e) and by dividing the result by $\mathbf{B}^2$:

$$a^2,\ b^2 = \frac{2\mathbf{B}^2}{2 + \tan^2\theta \mp \dfrac{1}{\cos^2\theta}\sqrt{1 - 2\cos^2\theta - 3\cos^4\theta}}. \qquad (10\text{–}54b)$$

Further relations for elliptical polarization may be developed by considering different surface variations of the quadrature fields and different ratios of their maximum amplitude to the loop field.

(*e*) *Theory of interpretation.* Although, for complete definition, the electromagnetic field theoretically requires six quantities (three components and their phases), it is seldom necessary to determine all of them. If the primary loop has been laid out parallel with the strike, the $\mathbf{X}$ component is generally negligible, and measurements are concerned with the in-phase and quadrature constituents of the $\mathbf{Y}$ and $\mathbf{Z}$ components only. Of these, the vertical and horizontal quadrature components are of greatest diagnostic value.

From the theoretical relations given below for the out-of-phase fields produced by various geologic bodies, the requisite formulas for any other electromagnetic method not directly measuring these components may be deduced. For instance, the horizontal and vertical direction of the field determined with a simple induction coil follows from the characteristics of the ellipse of polarization, that is, by compounding the in-phase loop field with the quadrature field of subsurface bodies. Intensity ratios and phase differences (as determined by ratiometers) may be calculated by compounding the loop field with the subsurface fields and their correct phases for successive points.[94]

Interpretation of results obtained by inductive-electromagnetic methods in mining differs greatly from procedures applied in the investigation of stratified ground. Absolute values for the magnetic fields of subsurface currents may be calculated if the strength of the induced current is known. It is difficult to determine these currents theoretically. However, since most inductive procedures measure the magnetic field relatively, it is suffi-

---

[94] If long *grounded* cables are used, the observed fields result from a combination of in-phase components (due to conduction) with quadrature fields (due to induction), and the phase shifts are calculated accordingly.

cient to consider the induced current as a constant parameter as far as applications in mining are concerned. For stratified ground, expressions for the relation of induced and primary current will be given later.

The type of indication produced by current concentrations in subsurface ore bodies depends primarily on their geometric disposition. The magnetic fields follow from relations previously given (eq. [10–46]). As shown in Fig. 10–110, relations are identical for electromagnetic and inductive methods for a single current concentration (thin vertical ore body). In this case the eddy currents flow in a vertical plane around the sheet. The effect of the return circuit at the bottom and at the sides can be disregarded, and formulas (10–46a) then apply.

In a wide ore body the induced current flows in opposite directions on opposite sides. Disregarding the effect of current concentrations on the
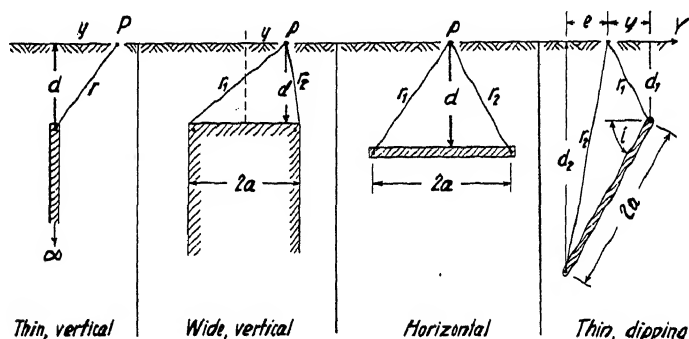
Fig. 10–110. Calculation of electromagnetic fields produced by currents induced in various types of ore bodies (current concentrations indicated by dots).

bottom of the body, the horizontal component due to the upper concentrations is

$$\mathbf{Y} = 2I_i d\left(\frac{1}{r_2^2} - \frac{1}{r_1^2}\right) = \frac{8I_i yad}{(y^2 + a^2 + d^2)^2 - 4a^2 y^2}. \qquad (10\text{–}55a)$$

The vertical components are additive, so that

$$\mathbf{Z} = 2I_i\left(\frac{a+y}{r_1^2} + \frac{a-y}{r_2^2}\right) = \frac{4I_i a(a^2 + d^2 - y^2)}{(y^2 + a^2 + d^2)^2 - 4a^2 y^2}, \qquad (10\text{–}55b)$$

if the zero point of the coordinate system is above the center of the ore body.

In a thin horizontal bed the current distribution is the same as in the upper surface of a wide vertical ore body. Therefore, the horizontal and vertical components are given by the preceding formulas. In a dipping thin ore body the eddy current will be concentrated along the upper and

lower edges. When the sheet is short, the lower current concentration is effective. If we place the zero point of the system of coordinates above the upper edge of the ore body, we have, with the notations of Fig. 10–110,

$$Y = 2I_i\left(\frac{d_1}{r_1^2} - \frac{d_2}{r_2^2}\right) = 2I_i\left(\frac{d_1}{r_1^2} - \frac{2a\sin\iota + d_1}{r_2^2}\right) \qquad (10\text{–}55c)$$

and

$$Z = 2I_i\left(\frac{y}{r_1^2} - \frac{e}{r_2^2}\right) = 2I_i\left(\frac{y}{r_1^2} + \frac{2a\cos\iota - y}{r_2^2}\right). \qquad (10\text{–}55d)$$

In structural and stratigraphic investigations, both fixed loops and expanding loops are applied. The former procedure is known as the Sundberg inductive, and the latter as the central ring induction (Koenigsberger) method. Interpretation theory in the first is based on an evaluation of the fields of thin layers of good conductivity in a section considered a poor conductor. In the second, the effect of a section of progressively increasing thickness is evaluated as the radius of the primary loop is expanded. The theory of the first method has been developed by Levi-Civita, Sundberg, Rostagni, Hummel, Hedstrom, Focken, and others. A list of pertinent literature is found in Focken's article.[95]
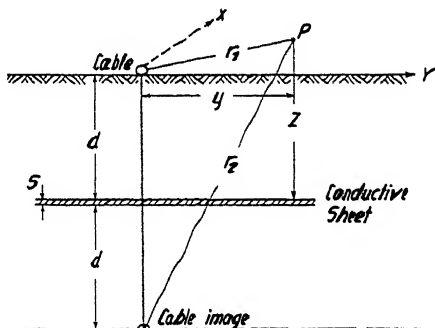
FIG. 10-111. Electromagnetic field in P resulting from cable and cable image.

Assume that a long cable is laid out on the ground surface in the x direction (Fig. 10–111). A formation, whose thickness s is small compared with its depth d, is parallel to the surface and extends to infinity in the x and y directions. The electromagnetic field is measured at a point P, whose horizontal distance from the cable is y and whose vertical distance from the sheet is z. If the point P is sensibly in the surface and if no sheet is present, a horizontal component does not exist and the vertical component is due only to the primary cable. The action of a sheet of *very good conductivity* is to reflect the cable and to produce, at twice the depth of the sheet, an image current concentration with a phase shift of 180°. In that case, the total vector at P can be readily calculated (see below). Its vertical component is subtracted from the component due to the primary cable; its horizontal com-

[95] Colo. Sch. Mines Quart., **32**(1), 225-252 (Jan., 1937).

ponent is likewise readily obtainable; and a phase shift beyond 180° does not occur (disregarding absorption through the overburden). As a rule, however, conditions are complicated by the finite conductivity of the sheet. The fundamental equations for the potentials of the electrical and electromagnetic fields of a cable in the presence of a conductive sheet have been derived by Levi-Civita. The electrical forces are virtually intercepted by the sheet and need not be considered. The potential U of the electromagnetic field is given by

$$U = -2I_0 e^{i\left(\omega t - \frac{\pi}{2}\right)} \left[\left(\log \frac{1}{r_1} - \log \frac{1}{r_2} \right) + \frac{j}{\mathsf{q}} \frac{\partial}{\partial z} \left(\log_e \frac{1}{r_2} \right) \right], \qquad (10\text{-}56)$$

in which $I_0 \sin \omega t$ is the current in the primary cable, r_1 and r_2 are distances (as in Fig. 10–111), and q is an induction factor. The first part of this expression indicates the direct effect of the cable at the point P if the sheet is not present; the second is the effect of a perfectly conductive sheet, equivalent to a field 180° out of phase caused by the cable image; the third is a quadrature term indicating the phase shift resulting from finite conductivity.

The induction factor q is defined by

$$\mathsf{q} \equiv \frac{4\pi^2 f}{R} = \frac{4\pi^2 f s}{\rho_{\text{ohm–cm}}} \cdot 10^{-9}, \qquad (10\text{-}57)$$

where f is the frequency in cycles per second and R is the resistance of 1 cm^2 of the sheet. With s as the thickness of the sheet and ρ as the resistivity, $R = \rho/s$. The horizontal and vertical field components are then obtained by differentiation of the potential given in eq. (10–56). There is no strike component; $\mathbf{X} = 0$, $\mathbf{Y} = -\partial U/\partial z$, and $\mathbf{Z} = \partial U/\partial y$. Hence,

$$\left.\begin{aligned}
\mathbf{Y} &= 2I_0 e^{i\left(\omega t - \frac{\pi}{2}\right)} \left[\frac{\partial}{\partial z} \left(\log \frac{1}{r_1} - \log \frac{1}{r_2} \right) + \frac{j}{\mathsf{q}} \frac{\partial^2}{\partial z^2} \left(\log \frac{1}{r_2} \right) \right] \\
\mathbf{Z} &= -2I_0 e^{i\left(\omega t - \frac{\pi}{2}\right)} \left[\frac{\partial}{\partial y} \left(\log \frac{1}{r_1} - \log \frac{1}{r_2} \right) + \frac{j}{\mathsf{q}} \frac{\partial^2}{\partial y\, \partial z} \left(\log \frac{1}{r_2} \right) \right].
\end{aligned}\right\} \quad (10\text{-}58a)$$

Since $r_1^2 = y^2 + (z - d)^2$ and $r_2^2 = y^2 + (z + d)^2$ for $z > 0$,

$$\left.\begin{aligned}
\mathbf{Y} &= 2I_0 \sin \omega t \left(\frac{z + d}{r_2^2} - \frac{z - d}{r_1^2} \right) - 2I_0 \cos \omega t \left(\frac{(z + d)^2 - y^2}{\mathsf{q} r_2^4} \right) \\
\mathbf{Z} &= 2I_0 \sin \omega t \left(\frac{y}{r_2^2} - \frac{y}{r_1^2} \right) + 2I_0 \cos \omega t \left(\frac{2y(z + d)}{\mathsf{q} r_2^4} \right).
\end{aligned}\right\} \quad (10\text{-}58b)$$

For the field at the earth's surface, where z is always closely enough equal to d in level terrain,

$$\mathbf{Y} = \frac{4I_0 d}{4d^2 + y^2}\left(\sin \omega t + \frac{1}{2d\mathsf{q}}\cdot\frac{4d^2 - y^2}{4d^2 + y^2}\cos \omega t\right)$$

and

$$\mathbf{Z} = -\frac{8I_0 d^2}{4d^2 + y^2}\left(\frac{1}{y}\sin \omega t - \frac{1}{d\mathsf{q}}\cdot\frac{y}{4d^2 + y^2}\cos \omega t\right). \tag{10–58c}$$

From eq. (10–58c) the phase shift in the horizontal component is

$$\tan \varphi_{\mathbf{Y}} = \frac{1}{2d\mathsf{q}}\cdot\frac{4d^2 - y^2}{4d^2 + y^2} \tag{10–58d}$$

and that in the vertical component is

$$\tan \varphi_{\mathbf{Z}} = -\frac{1}{d\mathsf{q}}\cdot\frac{y^2}{4d^2 + y^2}. \tag{10–58e}$$

Their difference is

$$\tan \varphi_{\mathbf{Y}} - \tan \varphi_{\mathbf{Z}} = \frac{1}{2d\mathsf{q}}. \tag{10–58f}$$

Depth and induction factor of a conductive sheet are calculated by diagrams as shown in Figs. 10–112a and 10–112b. A large loop (about 6000 by 2500 feet) is laid out (longitudinal direction parallel with assumed strike) and a number of parallel profiles are run at right angles to the cable. Along each profile the in-phase and quadrature components of both the vertical and the horizontal fields are measured at a number of distances. Theoretically, one distance on each profile is sufficient to calculate both depth and induction factor. Assume this distance to be $y = 100$ m, for which the diagrams of Fig. 10–112 have been calculated. These diagrams contain, for both vertical and horizontal component, lines of equal depth (solid) and lines of equal reciprocal induction factor ($1/\mathsf{q}$, dotted). If at 100 m distance from the cable one has observed an in-phase vertical component of $17\frac{1}{2}$ microgauss per ampere primary current, and a quadrature component of $1\frac{1}{2}$ microgauss, the depth as read from the diagram is 100 m and the induction factor is 100 (meters, since the reciprocal induction factor has the dimension of length). For the horizontal field the in-phase component would be 7 microgauss per ampere and the out-of-phase component -2 microgauss per ampere.

For horizontal beds the in-phase horizontal component has a maximum directly above the cable. For a dipping bed the image point moves to

one side and the corresponding maximum is displaced by $\Delta y = 2h \sin \iota$, where h is the depth perpendicular to the bed and ι the dip. Relations readily understood in their geometric significance may be obtained from Fig. 10–113 by considering a perfectly conductive layer, for which $\rho = 0$, $\mathbf{q} = \infty$ (see eq. [10–57]). Since the quadrature components cancel,

$$\mathbf{Y} = \frac{4I_0 d}{4d^2 + } \quad \text{and} \quad \mathbf{Z} = - \tag{10–59}$$
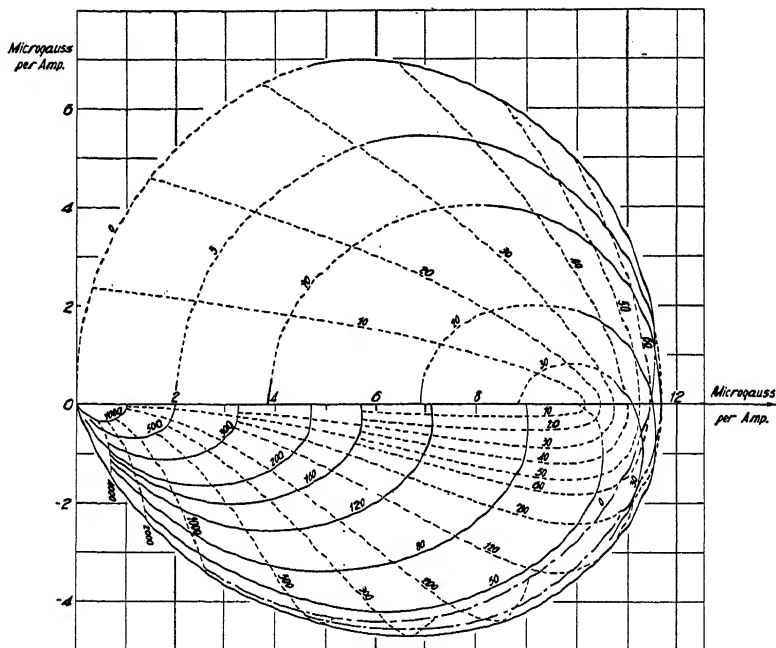
Fig. 10-112a. Sundberg interpretation diagram for inductive methods, vertical component, 100 meters from cable. Solid lines represent depth; broken lines, $1/\mathbf{q}$ (reciprocal induction factor).

These relations follow likewise by combining the primary field (Fig. 10–113, dotted circle) with the image field (solid circle). At P the horizontal component of the primary field is zero and that of the secondary field $\mathbf{T}$ is $\mathbf{Y} = 2I_i d'/r^2$. With perfect reflection, $I_i \equiv I_0$; $d' \equiv 2d$; $r \equiv r_2 \equiv \sqrt{4d^2 + y^2}$; and, therefore, $\mathbf{Y} = 4I_0 d/(4d^2 + y^2)$. The vertical component of $\mathbf{T}$ due to the image is (eq. [10–46a]) $\mathbf{Z} = 2I_i' y/r^2$ or, with the present notation, $\mathbf{Z} = 2I_0 y/(4d^2 + y^2)$. The field of the cable at the same point is $\mathbf{Z}_0 = -2I_0/y$, since $r \equiv y$. Hence, the resultant vertical component equals

$$-\frac{2I_0}{y}\left(1 - \frac{y^2}{4d^2 + y^2}\right) \text{ or } \frac{-8I_0 d^2}{y(4d^2 + y^2)}.$$
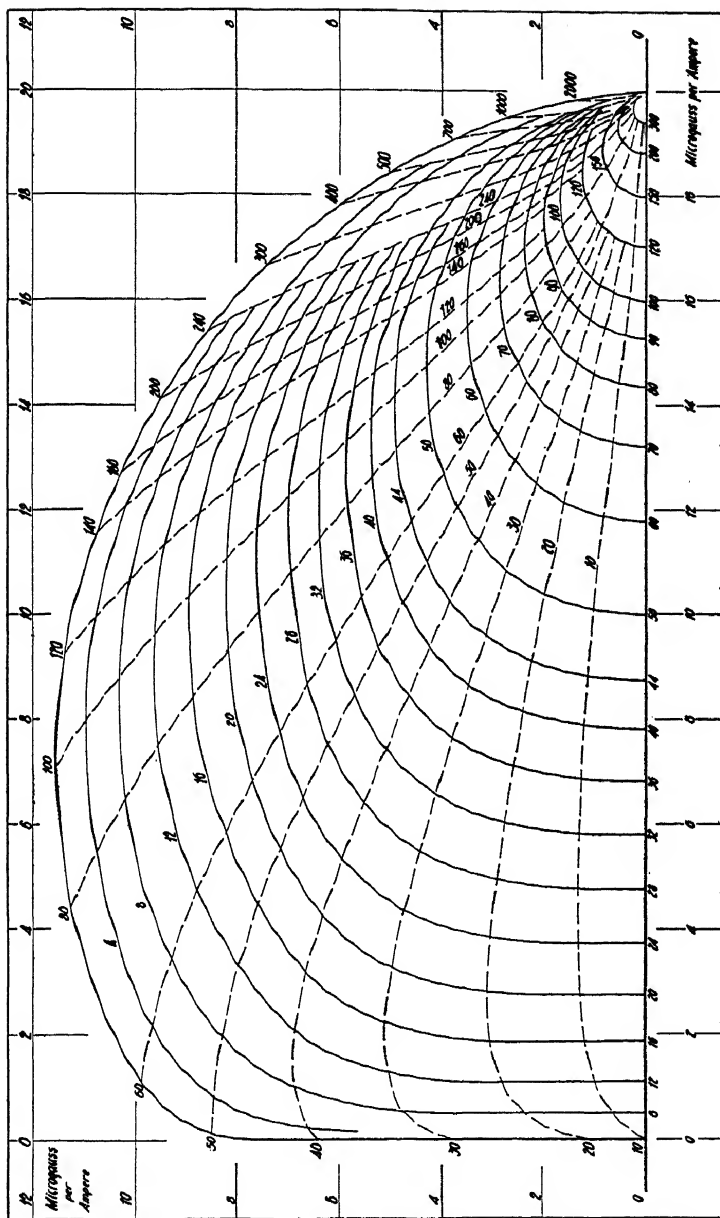
Fig. 10-112b. Sundberg interpretation diagram for inductive methods, horizontal component, 100 meters from cable. Solid lines represent depth; broken lines, 1/q (reciprocal induction factor).

If more than one conductive sheet is present, the interpretation procedure makes use of the fact (proved by experiment) that the electromagnetic field beneath one conductive sheet is independent of its position. Hence, when two sheets occur, their effect is equivalent to one sheet, produced by dropping the upper sheet on the lower. The field of the combined sheet is therefore given by the depth of the lower sheet and the *sum* of the induction factors. The procedure of depth determination has been described in detail by Sundberg and Hedstrom.[96]

In the central-ring induction method the fundamental theory is the same as that discussed above, except that the 180° component practically vanishes and the quadrature component predominates. The magnetic field inside the loop is proportional to the conductivity of a portion of
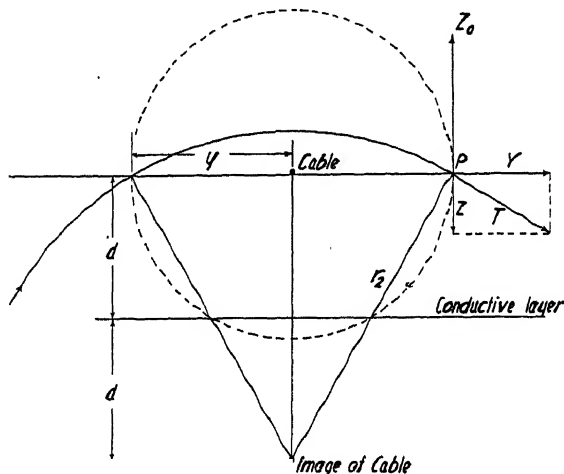
FIG. 10-113. Combination of primary and secondary fields for perfect conductor.

ground whose depth is *roughly equal to the radius* **R** of the loop. The arrangement used by Koenigsberger and his associates is illustrated in Fig. 10-105, and references to the pertinent literature are given on page 782. Only the vertical component is measured. The magnetic field in the loop is affected by the ground conductivity and differs from the field of a loop suspended in air.

As shown in eq. (10-58), the field near a straight cable is composed of (1) the direct vector, (2) the vector due to the image of the cable, and (3) a vector arising from finite conductivity of the bed. Since the first two are in opposition and in quadrature with the third vector, the vertical component for any medium below may be written $Z = Z_P + jZ_Q$, where

[96] Sundberg and Hedstrom, World Petrol. Congr. Proc., **B(I)**, 107 (1934).

Z_P is the combined in-phase component and Z_Q the quadrature component. According to Stefanescu,[97] the 180° component is negligible for low frequencies, and $Z_P = 2\pi I_0/R$ (field in air, see eq. [10-50b]). The quadrature component is $Z_Q = \frac{1}{2}\pi I_0 k^2 R$, where I_0 is the loop current, R its radius, and k^2 an induction factor similar in significance to the factor q previously defined by eq. (10-57). Since $k^2 = 4\pi\sigma\omega$ (ω = frequency, σ = conductivity), the quadrature component is

$$Z_Q = 2\pi^2 I_0 \sigma\omega R = \frac{4\pi^3 I_0 fR}{\rho} = \frac{12.4 \cdot 10^{-9} fRI_0}{\rho}, \qquad (10\text{-}60a)$$

where I_0 is in amp., R in cm, f in c.p.s., and ρ in ohm-cm.

As a rule, the ground is not homogeneous, so that when the loop radius is increased, beds of different conductivities affect the magnetic field. As in the resistivity method, formula (10-60a) is still applicable, provided that ρ is understood to represent now an apparent resistivity, ρ_a, which in accordance with (10-60a) follows from the observed parameter, Z_Q/I (quadrature field in gauss/amp. primary current):

$$\rho_a = 12.4 \cdot 10^{-9} fR \cdot \frac{1}{Z_Q/I}. \qquad (10\text{-}60b)$$

In resistivity methods the effect of layers of different conductivity is calculated by reflecting the source on the formation boundaries. The same procedure is applicable here, with the significant difference that, for each interface, only one image is required.[98] The analysis is simplified considerably by considering low frequencies only, in which case the 180° field is always zero and the quadrature field is given by $Z_Q' = -\lim_{f=0} \partial Z_Q/\partial f$.

If a circular loop energized by low-frequency current is suspended at an elevation d above an interface (for example, the surface of the ground), the magnetic field at any point $P(z)$ in its axis is *equal to the gravity potential of a disk at a depth $2d$* (see Fig. 10-114) of thickness 1 and density $2\pi^2 I_0\sigma_1$, if σ_1 is the conductivity of the medium above which the loop is suspended. The gravity potential above a disk at a distance h from its center is given by $U = 2\pi G\delta\, dh(r - h)$, where G is gravitational constant and δ is density. If $dh = 1$, $G\delta \equiv \delta'$, $h = 2d - z$, and $r^2 = R^2 + (2d - z)^2$, the magnetic field at the point P is

$$Z_Q' = 2\pi\delta_1[\sqrt{R^2 + (2d - z)^2} - (2d - z)], \qquad (10\text{-}61a)$$

so that when P is moved up to the center of the loop ($z = 0$),

$$Z_Q' = 2\pi\delta_1[\sqrt{R^2 + 4d^2} - 2d]. \qquad (10\text{-}61b)$$

---

[97] Beitr. angew. Geophys., **5**(2), 188 (1935).
[98] *Ibid.*

When the loop is laid out on the surface of the ground $(d = 0)$, $Z'_Q = 2\pi\delta_1 R$. Substituting the electrical density $2\pi^2 I_0 \sigma_1$,

$$Z'_Q = 4\pi^3 I_0 \sigma_1 R. \tag{10-61c}$$
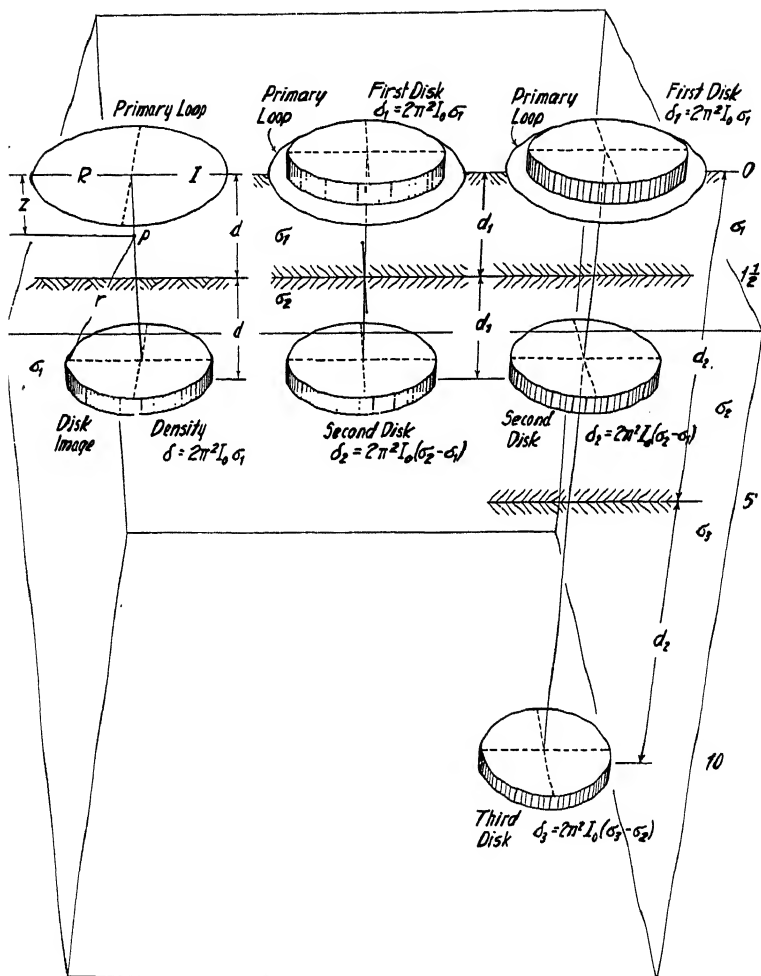
Fig. 10-114. Representation of magnetic fields of loops by potentials of disks and disk images of equivalent densities.

This is obviously the same as eq. (10-60a), differentiated with respect to f. When the ground is not homogeneous, the same relation can again be used for an apparent conductivity, so that, analogously to eq. (10-60b),

$$\sigma_a = \frac{Z'_Q}{4\pi^3 I_0 R}. \tag{10-61d}$$

By analogy with the gravitational potential, the magnetic field for two layers with conductivities σ_1 and σ_2 is readily obtained (see Fig. 10-114). As the loop is on the ground surface, the magnetic field due to the effect of the upper layer is equal to the potential of a disk with the density $\delta_1 = 2\pi^2 I_0 \sigma_1$ in its own plane. The effect of the interface below is given by the potential of a disk at twice the depth of the interface d_1 with the density $\delta_2 = 2\pi^2 I_0(\sigma_2 - \sigma_1)$. The magnetic field due to the latter is therefore, according to eq. (10-61b),

$$Z_Q' = 2\pi \delta_2 [\sqrt{R^2 + 4d_1^2} - 2d_1],$$

to which must be added the field of the disk inside the loop, so that

$$Z_Q' = 4\pi^3 I_0 \{\sigma_1 R + (\sigma_2 - \sigma_1)[\sqrt{R^2 + 4d_1^2} - 2d_1]\}, \quad (10\text{-}62a)$$

from which the apparent conductivity is

$$\sigma_a = \sigma_1 + \frac{\sigma_2 - \sigma_1}{R}[\sqrt{R^2 + 4d_1^2} - 2d_1]. \quad (10\text{-}62b)$$

For small values of R, or *small depth* penetration, the second term in eq. (10-62b) approaches zero, and therefore the apparent conductivity approaches the conductivity in the upper layer. On the other hand, if $d_1 \ll R$ (large loop radius), the apparent conductivity approaches σ_2.

If two interfaces exist (see Fig. 10-114), the magnetic field is composed of three potentials: (1) due to the surface disk with density δ_1, (2) due to the disk image of density δ_2, and (3) due to the disk image with density $\delta_3 = 2\pi^2 I_0(\sigma_3 - \sigma_2)$. Hence, the magnetic field

$$Z_Q' = 4\pi^3 I_0 \{\sigma_1 R + (\sigma_2 - \sigma_1)[\sqrt{R^2 + 4d_1^2} - 2d_1]$$
$$+ (\sigma_3 - \sigma_2)[\sqrt{R^2 + 4d_2^2} - 2d_2]\}. \quad (10\text{-}63a)$$

The apparent conductivity in this case is

$$\sigma_a = \sigma_1 + \frac{\sigma_2 - \sigma_1}{R}[\sqrt{R^2 + 4d_1^2} - 2d_1]$$
$$+ \frac{\sigma_3 - \sigma_2}{R}[\sqrt{R^2 + 4d_2^2} - 2d_2]. \quad (10\text{-}63b)$$

It follows from eq. (10-63b) that the effect of the nth interface on the apparent conductivity is given by

$$\sigma_{a,n} = \frac{\sigma_{n+1} - \sigma_n}{R}[\sqrt{R^2 + 4d_n^2} - 2d_n].$$

Substituting the ratio $r_n = R/2d_n$,

$$\sigma_{a,n} = \frac{\sigma_{n+1} - \sigma_n}{r}[\sqrt{r^2 + 1} - 1]. \quad (10\text{-}64)$$

Fig. 10–115 shows in double logarithmic scale a diagram for the calculation of the function of eq. (10-64).

(*f*) *Model experiments.* In the interpretation of field data obtained by horizontal loops, experiments with small-scale models play an important part. They are applicable to both mining (ore bodies) and oil exploration problems (stratified ground). To obtain perfect similitude, it is necessary to change the physical properties of the materials as well as the frequency.[99] If the fields are expressed in terms of primary current and the model scale is reduced n times, it is necessary to increase *both* frequency and conductivity n times. If the conductivity cannot be increased n times, it is necessary to increase the frequency n^2 times.
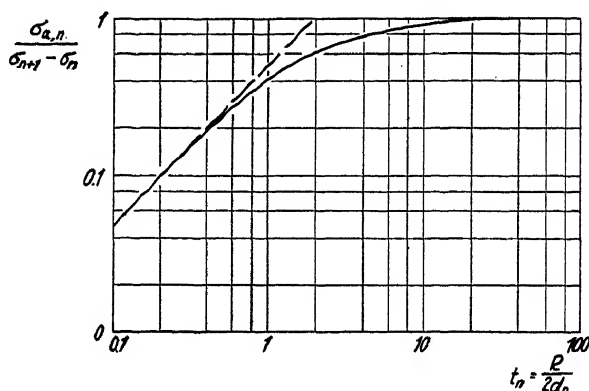
FIG. 10-115. Diagram for the calculation of apparent conductivity as a function of conductivity contrast on the n th layer, and of the ratio of loop radius ($= R$) and layer depth ($= d_n$) (after Stefanescu). (Note: for t_n, read r_n.)

Extensive experiments with model ore bodies have been made by Lundberg, Sundberg, Hedstrom, and their associates. Some of the results are reproduced in Figs. 10–116 to 10–118. Fig. 10–116*a* represents the distribution of the vertical primary field inside the loop as well as the vertical and horizontal components of the (combined primary and secondary) fields without regard to phase, for a vertical ore body. The anomalies are symmetrical, the vertical intensity having a maximum over the center of the body, the horizontal intensity two maxima over the edges. When the ore body is dipping (Fig. 10–116*b*), the maximum in vertical intensity over the up-dip edge of the ore body is greater than the anomaly over the down-dip edge. A clearer picture of conditions is obtained when the field vectors are split up into their in-phase (P) and quadrature (Q) components

[99] Sundberg, Beitr. angew. Geophys., **1**(**3**), 334 (1931). L. B. Slichter, A.I.M.E. Geophys. Pros., 446 (1934).

(Fig. 10-117). It should be noted that these experiments represent a *combination* of electromagnetic and inductive methods, excitation being produced by a long *grounded* cable. Hence, the effects of current concentration due to *conduction* are superimposed upon those due to *induction*.
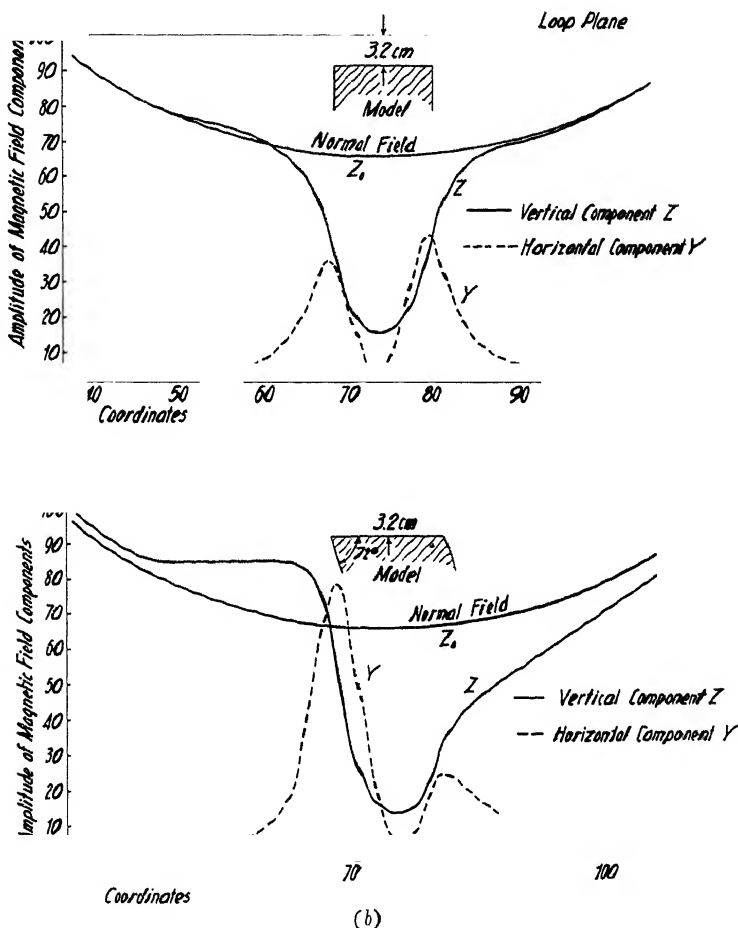
FIG. 10-116. Vertical and horizontal components (without regard to phase) of induced electromagnetic field for: (a) vertical ore body, and (b) dipping ore body, in center of rectangular loop (after Sundberg).

The former produce largely the in-phase (*P*) component, while the latter give rise to the quadrature (*Q*) component. The current concentrations for the *Q* component are near the edge of the conductor (skin effect), while those responsible for the *P* component are more toward the interior of the conductor.

Fig. 10–118 shows the effect of a plate on both the amplitude and the phase of the horizontal component measured across the cable. The gradient of both amplitude and phase decreases with the depth of the plate. This example represents one of the earlier applications of the Sundberg method; in later surveys, in-phase and quadrature components were measured at definite distances.[100]

(g) *Results obtained by horizontal loop methods.* Inductive methods were used at an early date in the Skellefte district in northern Sweden, where the overburden is relatively thin, and fairly ideal conditions exist. The general geology of this district has been previously described (page 703). A number of typical indications obtained in several ore fields have been published by Lundberg, Sundberg, and Eklund.[101] The profile shown in Fig. 10–119 was surveyed on the ice of Lake Mensträsk. Geologic and electrical prospecting was begun in 1921 and continued through 1923–1924, but drilling was not started until 1923–1924. The ore bodies occur in two zones, the principal zone passing beneath the lake. The country rocks are quartz-porphyritic or brecciated hälleflintas; layers of slate are common. The ore bodies are partly in graphitic slate containing disseminations of pyrite and pyrrhotite and partly on the contacts of slates and hälleflinta. They consist chiefly of pyrite, but copper is also present. About 150,000 electrical observations were made in this field, supplemented by torsion-balance observations to differentiate between impregnations and ore bodies. While most of the drilling located ore under the electrical indications, nothing but black slate was encountered in one part of the field.

FIG. 10-117. In-phase (subscript P) and quadrature (subscript Q) components of electromagnetic fields produced by galvanic and inductive action of a long grounded cable on dipping (model) ore body (after Hedstrom).

[100] Sundberg, World Petrol. Congr. Proc., B(I), 107 (1934).
[101] H. Lundberg, K. Sundberg, and E. Eklund, "Electrical Prospecting in Sweden," Sveriges Geol. Unders. Årsb., **17**(8), 37–73 (1925).
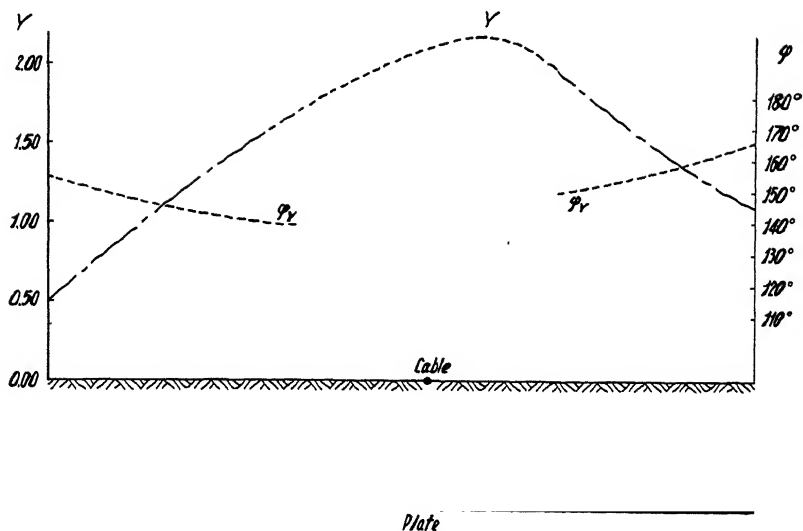
Fig. 10-118. Model experiment on horizontal plate, showing variation of amplitude and phase of horizontal component across cable (after Friedl).

By the same technique as that illustrated in Fig. 10–119, numerous ore bodies have been located in the Swedish fields, among them being the large gold (arsenic copper) deposit of Boliden. In northern Canada and Newfoundland electromagnetic-inductive methods have likewise been very successful. Fig. 10–120 shows the results of a dual coil ratiometer survey.[102] Amplitude ratios and phase differences of the vertical field were measured at successive locations 20 meters apart. The position of the conductor is indicated by the peaks in the ratio and phase gradient curves. A method

Fig. 10-119. Electromagnetic indications on Mensträsk Lake, verified by diamond drilling (after Sundberg, Lundberg, and Eklund).

of calculating the in-phase and quadrature components of the vertical intensity (Z_P and Z_Q) from the phase differences and amplitude ratios is indicated in the calculation form. By combining electromagnetic

[102] H. Hedstrom, A.I.M.E. Tech. Publ. No. 827, 1937.

and the inductive methods as here discussed and using phase difference and amplitude ratio for interpretation, it has been possible to locate not only good but also poor conductors.

The Imperial Geophysical Experimental Survey carried out a number of surveys with the Bieler-Watson method. Fig. 10–121 shows direction and amplitude of the horizontal quadrature field for a survey at Leadville, N.S.W. The ore bodies, 100–200 feet long by 15–20 feet wide, consist of pyrite, chalcopyrite, galena, and zincblende, and occur on the contact of porphyry and highly altered sedimentary rocks. Oxidation is fairly

40 N	60	80	100 N	120	140	150	160	170	180	190	200	220	240	260	280

Ratio $\frac{Z_2}{Z_1}$

$Δφ_z$

-10 — $Δφ_z$

Ratio Scale — 1.10 / 1.00

$φ_z$ Ratio:　+0.4 | +0.5 | -0.8 | -6.6 | -14.5 | -11.6 | -5.3 | -0.4 | +3.6 | +2.8 | +1.9 | +0.7

0.2 | 0.5 | 0.9 | 1.4 | 1.6 | -5.8 | -20.3 | -31.9 | -37.2 | -37.6 | -31.2 | -29.3 | -28.6

0.970 | 0.975 | 1.165 | 1.250 | 1.185 | 1.110 | 1.020 | 0.935 | 0.945 | 0.975

100 | 102 | 105 | 108 | 107.7 | 72 | 80.7 | 54.7 | 51.2 | 61.0 | 64.5 | 66.3

$Z \cos$:　101% | 105 | 104.5 | 67.0 | 51.0 | 43.3 | 42.5 | 47.5 | 52.0 | 58.3

+0.9% | +1.33 | +2.56 | +3.0 | +1.47 | -9.1 | -25.0 | -32.0 | -33.0 | -32.8 | -31.2 | -30.5 | -31.5 | -31.7

-60

Scale for — Z_P — Z_Q — -30

Scale Z_Q

Fig. 10-120. Observations of phase differences and vertical intensity ratios with calculations of in-phase (Z_P) and quadrature (Z_Q) components across a conductor (adapted from Hedstrom).

deep. At the Grosvenor workings, the depth is from 80–100 feet; in the Extended Workings, about 70 feet. The most pronounced indication was obtained over the Eastern Lode (60 feet wide) of the Extended Workings. A similar survey was conducted at Renison Bell, Tasmania, on flatlying, outcropping lodes of pyrrhotite on the contact of tuffs and slates.

Figs. 10–122 and 10–123 illustrate the application of the Sundberg inductive method in stratigraphic investigations. Fig. 10–122 represents results obtained with the earlier technique when amplitude and phase profiles of the horizontal component were measured. They demonstrate clearly the effects of differences in depth on the gradients of intensity and

phase curves. Fig. 10–123 indicates the position of an equivalent deep conductor on the Hawkinsville salt dome. By the mapping of such beds, the outline of a salt plug, in addition to the structure of the flank formations, may be determined. Sundberg[103] has further described the results obtained at the Moore's Field dome, Ft. Bend Co., Texas, illustrating the usefulness of the inductive method for mapping details of formations around a dome, and for locating faults. A survey of the Bruner field, near Luling, Caldwell Co., Texas, (Balcones fault zone), has been discussed by Zuschlag.[104]
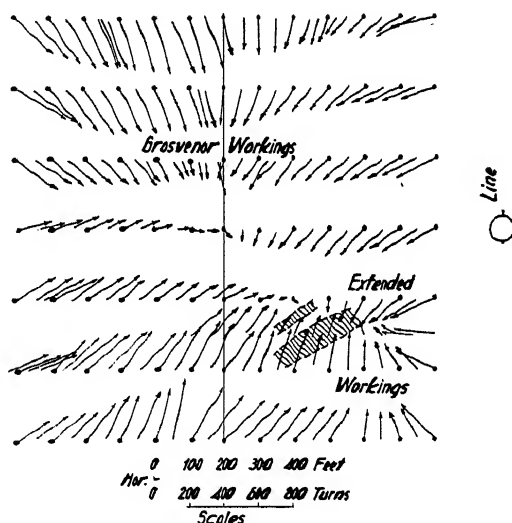
FIG. 10-121. Bieler-Watson vectors of quadrature horizontal component at Lead-ville, New South Wales (after Edge and Laby).

2. *Vertical-loop methods.* Vertical transmission loops are used in some inductive methods with audio- and high-frequency excitation. As was previously stated, they afford a closer coupling with vertical or steeply dipping ore bodies, as well as reduction of interference from highly conductive surface beds. This advantage is offset by the difficulty of erecting low-frequency vertical loops in the field and by their lack of magnetic field strength. The range of vertical audio-frequency loops is limited and of the order of 500 feet. Triangular loops were used by the I.G.E.S. (height

[103] Inst. Petrol. Technol. J., 17(**92**), 376-380 (June, 1931).
[104] A.I.M.E. Geophys. Pros., 156-157 (1932).
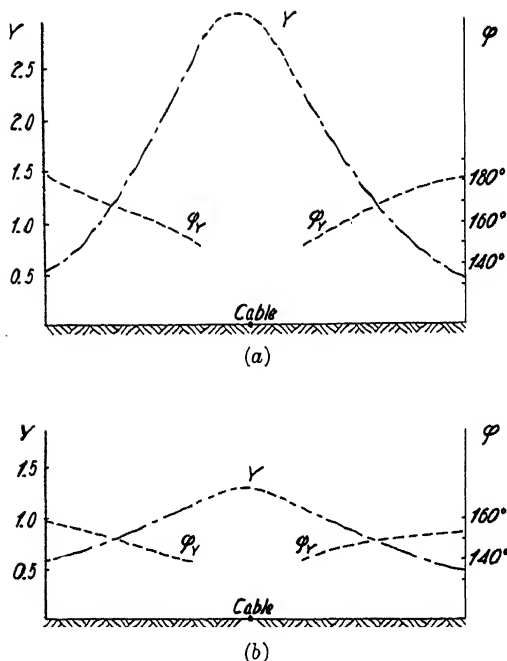
Fig. 10-122. Horizontal component and phase of horizontal component for beds of different depths in Vienna basin (after Friedl).

45 feet; base 133 feet) and by Mason,[105] with their plane parallel with the assumed strike. The I.G.E.S. employed a Bieler-Watson coil to determine the quadrature field in terms of the loop field.

The lack of penetration associated with the use of audio frequency in vertical loops may be overcome by excitation with higher frequency. The I.G.E.S. employed frequencies around 60 kc., the Radiore Company about 50 kc. On the other hand, there is a definite upper limit to frequency, due to the tendency of noncommercial conductors (water-bearing fissures, and the like) at shallow depths to become energized.

In application, a vertical transmitting loop is set up with its plane approximately parallel with, and (if possible) directly above a suspected conductivity zone. A certain distance away a receiving coil is placed with its axis of rotation horizontal, pointing toward the transmitting loop. The field of the transmitting loop at the location of the receiving coil is horizontal if the centers of both are at the same elevation. The magnetic field of the transmitter induces currents along the edge of a subsurface conductor. These currents, in turn, are surrounded by an electromagnetic field. This field combines with the loop field into a resultant vector, whose direction may be determined by tilting the re-

[105] A.I.M.E. Geophys. Pros., 13 (1929).
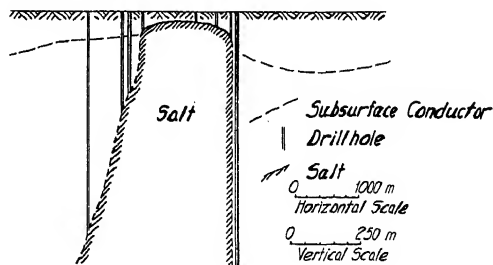
Fig. 10-123. Equivalent conductor determined by application of inductive methods at Hawkinsville salt dome, Texas (after Sundberg).

ception coil about a horizontal axis until a minimum is obtained. The current concentration may thus be located by measuring dip angles along a profile at right angles to the strike. Contrary to low-frequency vertical-loop methods, the loop field and the subsurface field are very nearly in phase; elliptical polarization is negligible and sharp minima are obtainable when the reception coil is tilted. The Radiore Company employed a portable transmitter in the form of a circular coil with the oscillator built into its base, supplied with plate voltage by a hand-cranked alternator.[106] Receiving coils consisted of several tens of turns of wire wound on bakelite hoops 1 to 2 feet in diameter, mounted on transit heads in place of the telescope.

If the magnetic field surrounding a subsurface current concentration alone were present, its direction at any point A on a profile (see Fig. 10-124)
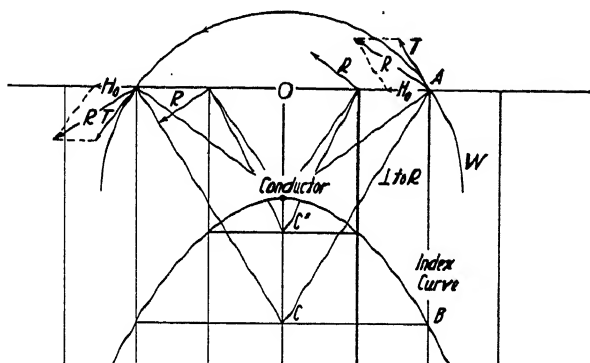
Fig. 10-124. Construction of index curve.

would be given by the vector **T**, and would coincide with the direction of the plane of the detection coil in the minimum position. If normals were drawn to this position at all points, they would intersect in the subsurface conductor. However, the horizontal field **H₀** of the transmission loop combines with the subsurface field **T** to form the resultant field vector **R**, whose direction is that of the detection coil in the minimum position. Therefore, the normals to the direction of the coil will intersect the vertical at progressively deeper points CC' as the distance of points A from the point 0 increases. The conductor may nevertheless be located by the procedure of drawing an index curve: At any point (A) the normal to the vector **R** or to the plane of the detection coil is drawn to the intersection with the vertical at the point C. Through C a horizontal line is drawn to

[106] Illustrated in J. Jakosky, I.R.E. Proc., **16**(10), 1344 (Oct., 1928).

the intersection with the vertical from A in B. B is then a point on the index curve. Other points are similarly located. The apex of the index curve is the conductor. Actually, index curves are more complex, de-
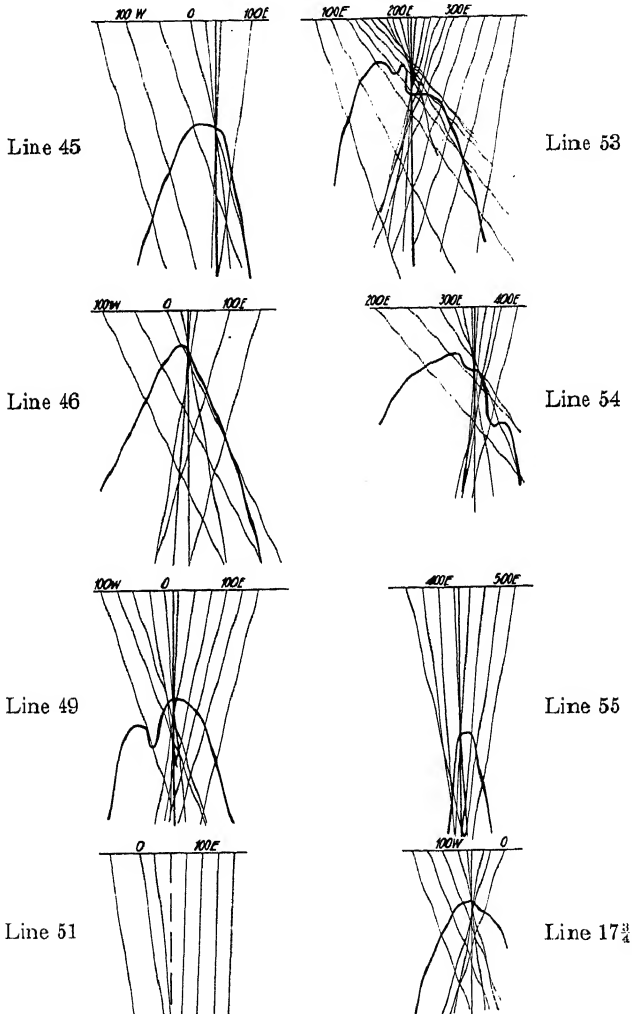
Fig. 10-125. Index curves obtained in Zeehan copper-nickel field (Tasmania) by the high-frequency method (after Edge and Laby).

pending on the shape of the conductor. Furthermore, a considerable modification is introduced because a refraction of the wavefront W occurs at the earth's surface.[107]

[107] *Ibid.*

Considerable ground was covered with high-frequency methods about ten years ago in Canada and elsewhere, and numerous conductive zones were located. Some proved to be commercial ore bodies; but others, and probably the majority, did not. Because of this experience the trend in inductive methods has been consistently toward lower frequencies. On the other hand, the I.G.E.S. has reported fair success with high frequencies. An example is shown in Fig. 10-125. This survey was made in the Zeehan copper-nickel field where the ore occurs near the peridotite and pyroxenite portions of basic dikes intruded into Cambro-Ordovician slates. The ore is a mixture of pyrrhotite, pentlandite, and chalcopyrite. The more uniform indications were obtained in the southern part of the area (lines 45, 46, and 49). The three remaining profiles are located in the northeastern part of the area where the trend of the dike is northeast instead of north. The effect of differences in the depth (and width) of the ore bodies is clearly recognized. Indications in the northeastern portion of the area were verified by trenching.

IX. RADIO METHODS

A. GENERAL

"Radio" methods of electrical prospecting make use of frequencies ordinarily employed in wireless communication. They range from several hundred kilocycles to several megacycles (corresponding to a wave length of several kilometers to several hundred meters). In regard to their mineral-locating possibilities, radio methods have been fertile soil for the imagination of laymen, radio amateurs, and even physicists. While theoretically the conditions for locating ore bodies or oil by radio waves appear to be very simple, there are, in practice, innumerable interferences from topography and near-surface variations in moisture and mineralization. Further, the depth penetration is very limited in the type of ground occurring in temperate climates. Where indications from deep ore bodies or oil deposits have been obtained, it has not been definitely proved that the indications did *not* come from *shallow* petrographic or structural variations genetically related to the subsurface mineralization.

In the application of radio methods to
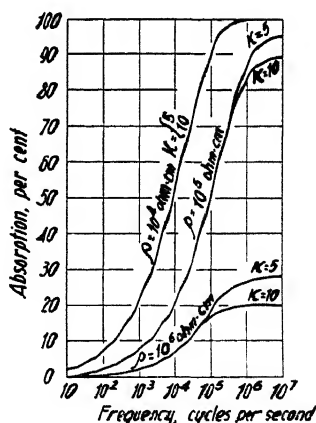
FIG. 10-126. Attenuation in sheet 124 feet thick, for various resistivities and dielectric constants (after Joyce).

geologic problems, the theoretical assumption of a simple radiation wave is frequently not justified and all field components must be considered, particularly at points close to the source. Assume a radiating doublet source of pole distance l, in a medium of the dielectric constant $\kappa = 1$, the permeability $\mu = 1$, and the conductivity $\sigma = 0$. At a point P in the vicinity of this doublet, with the polar coordinates r and φ in reference to the center of the doublet, the magnetic and electrical field intensities due to a periodic charge $e = e_0 \sin \omega t$ are given by the following equations:[108]

$$
\left.
\begin{aligned}
\mathbf{H} &= -\frac{e_0 l}{r\mathbf{c}} \sin \varphi \left(\frac{\mathbf{c}}{r} \omega \cos \omega t - \omega^2 \sin \omega t \right) \\[2mm]
\mathbf{E}_\varphi &= -\frac{e_0 l}{r} \sin \varphi \left(\frac{\mathbf{c}^2}{r^2} \sin \omega t + \frac{\mathbf{c}}{r} \omega \cos \omega t - \omega^2 \sin \omega t \right) \\[2mm]
\mathbf{E}_r &= -2 \frac{e_0 l}{r} \cos \varphi \left(\frac{\mathbf{c}^2}{r^2} \sin \omega t + \frac{\mathbf{c}}{r} \omega \cos \omega t \right),
\end{aligned}
\right\} \quad (10\text{-}65)
$$

where $\mathbf{H}$ is the magnetic field, $\mathbf{E}_\varphi$ the tangential and $\mathbf{E}_r$ the radial electrical field, and $\mathbf{c}$ is the light velocity. The first term in the electrical field expressions $[(\mathbf{c}^2/r^2) \sin \omega t]$ represents the electrostatic component of the doublet, decreasing with the inverse cube of distance. It is independent of frequency and important only in the immediate vicinity of the source. The second term $[(\mathbf{c}/r)\omega \cos \omega t]$ is the induction effect, inversely proportional to the square of distance and proportional to frequency. The third term $(\omega^2 \sin \omega t)$ represents the radiation component, which is inversely proportional to the first power of distance and directly proportional to the square of the frequency. The last term is the only one important in long-range radio communication. If the distance r has reached the value of $\lambda/2\pi$, the first and second terms (static and inductive) have dropped to the amount of the radiation term at that point. The electrical field strength $\mathbf{E}_\varphi$ is of particular interest in the equatorial plane ($\varphi = 90°$). With the phase shift $\psi = r\omega/\mathbf{c}$, the equatorial electrical field strength

$$
\mathbf{E} = -\frac{e_0 l}{r} \left[\left(\frac{\mathbf{c}^2}{r^2} - \omega^2 \right) \sin \omega \left(t - \frac{\mathbf{r}}{c} \right) + \frac{\mathbf{c}}{r} \omega \cos \omega \left(t - \frac{r}{\mathbf{c}} \right) \right]. \quad (10\text{-}66)
$$

Substituting $\omega = 2\pi\mathbf{c}/\lambda$ and $r/\lambda \equiv x$, the relative field in terms of wave length is

$$
-\frac{\mathbf{E}\lambda^3}{e_0 l \mathbf{c}^2} \equiv -\mathbf{F}' = \frac{1}{x} \left[\left(\frac{1}{x^2} - 4r^2 \right) \sin 2\pi \left(\frac{\mathbf{c}}{\lambda} t - x \right) + \frac{2\pi}{x} \cos 2\pi \left(\frac{\mathbf{c}}{\lambda} t - x \right) \right]
$$

$$
(10\text{-}67a)
$$

[108] Hummel, Zeit. Geophys., 5(3–4), 109 (1929).

whose root-mean-square value is

$$\mathbf{F}' = \frac{1}{x} \sqrt{\frac{1}{2}\left[\left(\frac{1}{x^2} - 4\pi^2\right)^2 + \frac{4\pi^2}{x^2}\right]}. \qquad (10\text{-}67b)$$

This expression is virtually the same as the radiation component from a distance of $\lambda/2\pi$ (or $x = 0.159$) and outward, but in the near-zone this field is very much greater than the radiation component. Hence, the static and inductive field components must be considered in problems involving distances from the conductor of less than $\frac{1}{2}$ to $\frac{1}{4}$ wave length. In all electrical methods previously discussed, only the induction component of the magnetic field (eq. [10-65]) is measured, and the radiation component is neglected.

If the source of radiation is in or beside a conductive medium, the electrical and magnetic field components decrease more rapidly than stated in eq. (10-65). This attenuation is largely due to the skin effect (see page 652 and 685). In the formulas previously given, the displacement current was neglected. If this is now considered, the "transmission factor" may be written

$$\text{T.F.} = e^{-\frac{2\pi f d}{c} \sqrt{\frac{\mu}{2}\sqrt{x^2 + \frac{4\sigma^2}{f^2}} - \kappa}}, \qquad (10\text{-}68a)$$

where d is depth, $\mathbf{c}$ light velocity, κ the dielectric constant, f frequency, μ permeability, σ conductivity, and lengths are in cm and physical constants in e.s.u.'s. Usually, the ground permeability is unity, and the transmission factor becomes

$$e^{-\frac{2\pi f d}{c}\sqrt{\sqrt{\left(\frac{\kappa}{2}\right)^2 - \left(\frac{\sigma}{f}\right)^2} - \frac{\kappa}{2}}}, \qquad (10\text{-}68b)$$

which for $\kappa = 0$ is identical with formula (10-23b). For a layer 124 feet thick, Joyce[109] has calculated the attenuation for various resistivities and dielectric constants (Fig. 10-126). The dielectric constant is effective only when it is accompanied by high resistivities; it causes the curves to branch at the higher frequencies only (10^4 to 10^5). For most geophysical applications, the simpler formulas are therefore sufficient. The depths at which a wave with horizontal front decreases to one-half of its initial amplitude may be obtained from Fig. 10-127. It is evident that application of radio methods is limited to dry climates, dry overburden formations, interiors of salt mines, and geologic problems where subsurface structures are reflected in conductivity changes very near the surface. Eve and Keys[110] made extensive measurements in the Mammoth cave in

[109] J. W. Joyce, Bur. Mines Tech. Publ. No. 497. See also A. S. Eve, and D. A. Keys, A.I.M.E. Tech. Publ. No. 316.

[110] *Loc. cit.*

Kentucky and found that radio broadcast waves could not be picked up through more than 100 feet of overburden with a loop aerial, and through no more than 300 feet with a long antenna. Reception dropped almost to zero past 20 or 30 kilocycles.

Radio methods fall into two groups: (1) methods in which subsurface effects are measured by their reaction on antenna emission; (2) methods involving a determination of signal strength, that is, measurement at the receiving end.
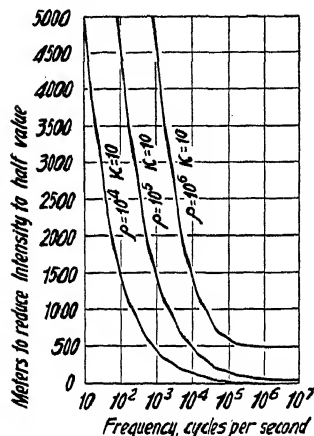
FIG. 10-127. Half-value thicknesses of absorption, for various resistivities and dielectric constants (after Joyce).

B. TRANSMISSION MEASUREMENTS

1. The *quarter-wave method* makes use of the effect of wave reflection on the emission characteristics of the antenna. If the reflected wave is in phase with the transmitted wave, the antenna has maximum emission and the antenna current is at a maximum. This occurs when the distance of a reflecting surface is equal to one-quarter of the wave length or an odd multiple thereof $[d = (2n + 1)\lambda/4]$. The depth can therefore be determined by varying the frequency of the transmitter and by plotting the antenna current as a function of f. Hummel has pointed out[111] that the maxima and minima in the transmission intensity are not so sharp as would be expected from this simple scheme, since, near the antenna, the static and induction portions of the field cannot be neglected. The effect of a sheet of good conductivity in a poorly conductive medium upon the antenna emission is equivalent to the action of a reflected doublet at twice the depth obtainable from eq. (10-67a).

A theoretical curve expressing the variation of effective field strength with variation of the distance of the reflecting bed is shown in Fig. 10-128a. Contrary to the *simplified* theory, the peak at $\lambda/4$ is very indistinct, and the minimum at $2 \cdot \lambda/4$ and the maximum at $3 \cdot \lambda/4$ are more pronounced. Theory and experiment are in very good agreement, as is shown by Fig. 10-128b. The quarter-wave method is reported to have been tried in Southwest Africa for the location of ground water in desert areas. These experiments were interrupted by the World War in 1914, and little has become known since then about the application of the method in prospect-

---

[111] Zeit. Geophys., *loc. cit.*

ing for water. In Russia, Petrowsky tried the quarter-wave procedure for the location of ore bodies but nothing definite is known about results obtained. It is noted that neither theory nor the model experiments discussed above make allowance for the absorption; therefore, the reflected energy may be less than assumed, which would make the maxima and minima less distinct. The absorption would increase with an increase in conductivity and frequency.

FIG. 10-128a. Theoretical variation of electrical field strength with distance of reflecting sheet (after Hummel).

2. The *capacity method* is based on the fact that the capacity of an antenna and therefore the natural frequency of an oscillator is dependent on the distance and electrical properties of bodies in its vicinity. Assume a long cylindrical conductor of the length l and radius r in a medium with the dielectric constant κ_0, stretched out parallel with the surface of an infinite medium of the dielectric constant κ at the distance d. Then the antenna capacity is

$$ C = \frac{\kappa_0 l}{2\left(\log_e \dfrac{l}{r} + \dfrac{\kappa - \kappa_0}{\kappa + \kappa_0}\log_e \dfrac{l}{2d}\right)}. \qquad (10\text{-}69a) $$

This expression is composed of the c, an image at depth $2d$, the reflection factor being $(\kappa - \kappa_0)/(\kappa + \kappa_0)$. For $\kappa = 0$, and $\kappa_0 = 1$ (antenna in air), eq. (10-69a) becomes

$$ C = \qquad l \qquad (10\text{-}69b) $$

It is seen that the elevation of the antenna above the interface is the predominant factor; hence, this method has been proposed for the measurement of the height of planes and dirigibles. Changes in

FIG. 10-128b. Experimental curve, determined by varying distance of sheet (after Hummel). See also preceding figure.

depth are more effective the greater the length of the antenna. Changes in antenna capacity are determined by measuring its wave length or natural frequency by (1) a resonance (Fig. 10–129a) or (2) a heterodyne method (Fig. 10-129b).

In the first method, a push-pull oscillator of variable frequency and a measuring circuit M with rectifier meter are coupled to the antenna circuit. If the antenna is in resonance with the oscillator circuit, maximum energy transfer occurs and the meter will indicate maximum current. The accuracy obtainable with this circuit is $d\lambda = 0.1$ m and $dC = 0.1$ cm.
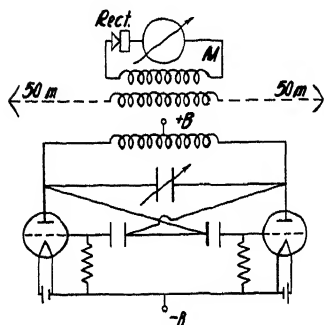
FIG. 10-129a. Oscillator circuit in capacity-resonance method (after Stern).
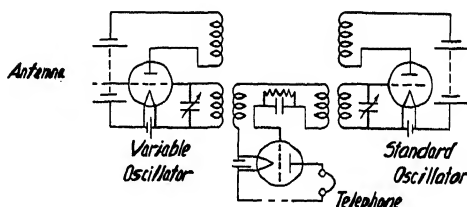
FIG. 10-129b. Beat method for measuring changes in antenna capacity (after Stern).

More accurate is the heterodyne method illustrated in Fig. 10–129b. The frequency of the beat note may be determined by comparison with a fork or other frequency standard. The measurement consists of determining the capacity of the standard oscillator to bring about a definite beat note. Its sensitivity may be adjusted to almost any desired value. Since the beat note is $\Delta f \equiv f_s - f_x$, (with either frequency given by $f = 1/2\pi\sqrt{LC}$), where f_s is the frequency of the standard oscillator and f_x the frequency of the antenna circuit, it is seen that with $1/2\pi\sqrt{L} = \mathbf{p}$, the change in frequency with change in capacity is $df = -\frac{1}{2}\mathbf{p}C^{-3/2}\,dC$. Therefore, since $\mathbf{p} = fC^{1/2}$, the sensitivity is given by $df = -\frac{1}{2}f\,dC/C$. It can be increased by using a high frequency and a low capacity. However, it is preferable to increase the accuracy in the determination of the beat frequency. Stern[112] states that with the circuit shown in Fig. 10-129b the accuracy was ±0.03 cm in dC, which corresponds to an accuracy of several decimeters for depths varying from 10 to 30 m. He applied the capacity method to the measurement of thickness of glaciers. Considerable difficulties were experienced in the field because of changes produced

---

[112] Gerl. Beitr., **23**(3), 292-333 (1929).

by variations in the observer's position and because of formation of a conductive surface layer on the ice during daytime. Hence all observations had to be made at night. To minimize surface effects and to give the method some degree of depth resolution, apparent capacities for different antenna elevations may be observed. Fritsch[113] has published a number of curves obtained in this manner on a siderite mine and on caves. While the presence of two caves could be predicted correctly, there was too much interference from surface moisture, topography, and rails and pipes in tunnels, to make the method reliable in all cases.

3. *Measurements of antenna damping.* Both the natural frequency and the damping of an antenna depend on the electrical properties of the surrounding media. These properties may be determined from the sharpness of the resonance peak; for example, from the natural frequencies corresponding to half of the maximum resonance amplitude. If C_r is the capacity for resonance (maximum current) and C_1 and C_2, respectively, two capacities giving half the antenna current on either side of the resonance point, the decrement of damping is given by $\Lambda = \frac{\pi}{2} \cdot (C_2 - C_1)/C_r$. It decreases with the ratio of conductivity and dielectric constant.

C. FIELD-STRENGTH MEASUREMENTS

In this group of methods both a transmitter and a receiver are required, and measurements are made exclusively on the receiving end. The transmitter is left untouched except for frequency alteration where called for. Broadcasting stations and amateur and other transmitters are sometimes used, particularly for purely scientific studies. For mine examinations, and the like, where different positions of the transmitter are necessary, a unit specially built for this purpose is required. This unit has the form of an antenna or loop transmitter. On the receiving end a direction-finding coil is used, that may be rotated about a vertical and horizontal axis. Fig. 10–130 shows a heterodyne receiver used by Stern for field-strength measurements. In the plate circuit of the output stage is a sensitive galvanometer provided with a circuit for bucking normal plate current. Petrowsky[114] has used and described a number of transmitters and receivers of similar construction.

1. *Absorption method. Related methods of intensity mapping.* Measurements of reception intensity as a function of the characteristics of intervening media have been made to determine the depth penetration of radio waves, to map faults, and to locate intervening ore bodies, cavities, or

---

[113] Beitr. angew. Geophys., **6**(1), 100–119 (1936).

[114] A. Petrowsky, Beitr. angew. Geophys., **3**(2), 149–204 (1933).

brines in mines. Fritsch[115] found that broadcast signals could be received in subterranean cavities, that reception and penetration was better for waves above 600 m wave length than for waves of 200 m or less, that the propagation of radio waves was controlled more by geologic factors than by the length of the path, and that the absorption in the direction of strike was greater than at right angles thereto. E. Cloos[116] noted dead spots of radio reception on faults and observed reception anomalies on formation contacts. Such contacts may act as carriers or shields for the radiation, depending on their conductivity and geometric disposition.
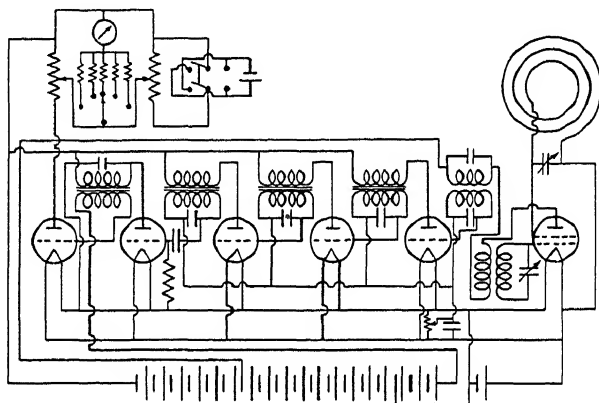
FIG. 10-130. Heterodyne receiver for measuring relative field strength (after Stern).

Quantitative measurements of intensity, with constant frequency and constant amplitude excitation across faults, have indicated a characteristic anomaly. If a transmitter is set up on the down-dip side of a normal fault with the antenna slightly sloping toward the fault, the anomalous intensity shows a maximum near the suboutcrop, flanked by two minima.[117] On quartz veins a similar phenomenon has been observed, the steep gradient portion of the curve between the intensity maximum and the far minimum corresponding to the vein intersection with the surface. This indicates that a shallow phenomenon is involved. Frequencies used in this work were around 1900 kc. (158 m wave length); according to the theory discussed on page 811 their depth penetration is rather small. It can happen, of course, that fissures and beds of good conductivity act as carriers, thus making energy available at more remote points horizontally and vertically.

[115] *Loc. cit.*
[116] Amer. J. Sci., **28(166)**, 255 (1934).
[117] Wm. M. Barret, U.S. Patent No. 2,172,6

It is difficult to say just what type of electrical field or current distribution causes the observed type of anomaly. It probably results from distortions of equipotential lines of the electrical field induced in the near-surface strata. These distortions occur near the boundaries of good and poor conductors. Similar anomalies, observed near subsurface salt water contacts in oil fields and above salt domes and igneous intrusions, are believed to reflect near-surface resistivity variations sometimes associated with such geologic features.[118] Otherwise (with the exception of fissures, and the like, acting as carriers) it appears impossible to reconcile the apparent depth penetration of this method with the limited range postulated by the theory.

Petrowsky[119] observed that radio waves in salt mines had about the same range as in air, and that waves of from 50–250 m in length could be transmitted through quartz porphyry rocks, tuffs, and conglomerates in a pyrite mine. In one case it was definitely possible to locate a pyrite stock by its "shadow."

2. In the *interference methods*, variations in signal strength due to interference of waves which travel by different routes are utilized to determine the difference in path and, if possible, the path itself. Interferences may be measured (*a*) by leaving the wave length constant and varying the position of the receiver, and (*b*) by leaving the receiver constant and varying the wave length of the transmitter.[120] If the path difference between two waves is Δr, a minimum in reception will result when $\Delta r = \lambda/2$ or $\Delta r = (2n + 1) \lambda/2$. When the wave length is held constant and the receiver is moved at the surface, the distance between successive minima in reception will be λ, or twice the path difference. If, on the other hand, the receiver is left constant and if two wave lengths, λ_1 and λ_2, produce successive reception minima, the path difference is

$$\Delta r = \frac{\lambda_2 \cdot \lambda_1}{\lambda_2 - \lambda_1}. \tag{10-70a}$$

Since $4d^2 = 4r^2 + a^2$ and $\Delta r = 2r - a$, the distance of a reflecting surface follows from the path difference Δr and is given by

$$d = \tfrac{1}{2} \sqrt{(\Delta r)^2 + 2a(\Delta r)}. \tag{10-70b}$$

[118] The apparent reaction of the Eltran methods to deep structures and fields, at first unexplainable, is now believed to result from near-surface resistivity variations accompanying such features. See E. E. Rosaire, Geophysics, **3**(2), 96–121 (Mar., 1938), and E. E. Blondeau, Geophysics, **4**(4), 271–278 (Oct., 1939).

[119] *Loc. cit.*

[120] A third possibility, that of producing interference by varying the distance of a reflecting surface, is used in radio-altimeters but not in geophysics.

If the receiver has been kept constant and two wave lengths, λ_1 and λ_2, have been found to produce successive minima in reception, then the depth

$$d = \tfrac{1}{2} \sqrt{\left(\frac{\lambda_2 \cdot \lambda_1}{\lambda_2 - \lambda_1}\right)^2 + 2a\frac{\lambda_2 \cdot \lambda_1}{\lambda_2 - \lambda_1}}. \qquad (10\text{--}70c)$$

For practical applications, the above formulas are only approximate, since the wave lengths in air and in rock are not the same. The two paths are usually traversed with different speeds and different wave lengths. This leads to more complex formulas, which have been derived by Petrowsky.[121]

The depth to a horizontal reflection surface can lastly be determined by taking a "bearing" of the image of the antenna with a coil-aerial receiver, so that $d = (a \tan \varphi)/2$.

3. The *polarization* of radio waves and its relation to the electrical properties and disposition of near-surface beds was discussed on page 653. The ratio of major and minor axis of the ellipse and its tilt angle may be measured by a receiving set with rotatable double L antenna. The polarization is chiefly dependent on depth of ground water level near surface moisture and varies with wave length (see Fig. 10-20). With the exception of Feldman's recent studies,[122] little has been done along this line since Hack's fundamental investigations in 1908.[123] Measurements of polarization, when combined with relative or semiabsolute determinations of electrical and magnetic field components, are likely to place the radio methods of electrical prospecting on a more quantitative basis and to make them more usable than they are at present.

X. TREASURE AND PIPE FINDERS

These devices and methods utilize electrical prospecting procedures for locating objects buried at shallow depth. Obviously they can be applied only if differences in conductivity exist, that is, if buried objects are conductive or enclosed in metal cases. Often the duration of burial makes considerable difference in detectability, since the chemical action of the surface waters creates a zone of low resistivity around the conductor, which increases its effective electrical size.

A. TREASURE AND PIPE FINDERS WITH SEPARATE EXCITATION

A method for locating pipe by separate excitation, that is, an adaptation of the electromagnetic method, was mentioned on page 765 (Darley pipe

---

[121] *Loc. cit.*
[122] I.R.E. Proc., **21**, 790 (June, 1933).
[123] Ann. Phys., **27**, 43-63 (1908).

locator).   If the detection coil is carried in horizontal position above the
ground, the sound will increase as the pipe is approached and will be null
immediately above the pipe.   With a vertical coil (plane parallel with the
pipe) the sound will be at a maximum above the pipe.   If no contact can
be made with a pipe system, it may still be located by grounding both
terminals of a buzzer.   Since depth penetration is not important, fre-
quencies of the order of 1000–1500 may be used, for which the human ear
is most sensitive.

For small metallic objects (boxes, chests, safes) inductive excitation by
an insulated horizontal loop about 50–100 feet square is preferable.   For
detection, a vertical reception coil is best suited, since the normal loop field
(with the exception of a narrow area near the wire) is vertical, while the
field of metallic bodies (due to eddy currents induced to flow along their
edges) is horizontal above them and is thus picked up full strength.   When
a signal is detected, the coil should be used in two positions at right angles
to each other to determine the direction of the horizontal field.   The
vertical frame may also be tilted until minimum sound is obtained.   In
this manner metallic masses may be located by indications of anomalous
field direction.   The frequency in this application is again of the order of
1000–1500 cycles.   However, the higher frequencies also have been em-
ployed with small vertical transmission loops and receiving coils in hori-
zontal position to eliminate the primary field.   A transmitter and receiver
built by the Fisher Research Laboratories for such work is illustrated in
Fig. 10–135b.

B. (SELF-CONTAINED) TREASURE FINDERS

Self-contained treasure finders contain their own source of power or
energizer.   They may be divided into low- and high-frequency instruments.

1. *Low-frequency instruments* operate in the range of 500–2000 cycles.
A device commonly used is the induction balance, that is, an instrument
or bridge intended for the comparison of the self-inductances of two coils.
The principle was first proposed by Dove in 1841 and further perfected by
Hughes in 1879.   When applied in prospecting for metallic objects, it is
made with two similar coils in opposite arms of a bridge, which is balanced
when the inductances are balanced.   The two coils may be carried over
the ground at the ends of a carrying frame.   As one of them comes above
a conductive or magnetic body its inductance changes, upsetting the bridge
balance.   It is also possible to use only one coil and to enclose the other in
a shielded case with the remainder of the equipment.   Power is derived
from a 500- to 1000-cycle buzzer.   The two detection coils are connected
to the opposing primary windings, P_1 and P_2, of a differential transformer

(see Fig. 10-131a) whose secondary does not respond until the detection coils become unbalanced from the presence of conductive or magnetic material near them.
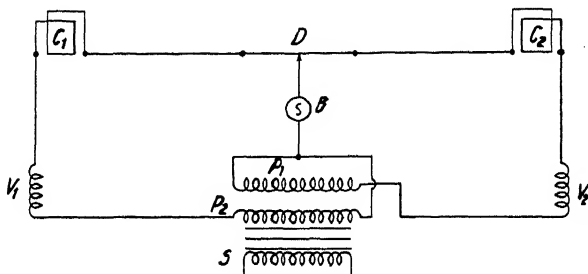
Fig. 10-131a. Hughes induction balance. (P_1, P_2, primaries of differential transformer; S, secondary; B, buzzer; C_1, C_2, detection coils; V_1, V_2, service coils; D, slide wire.)
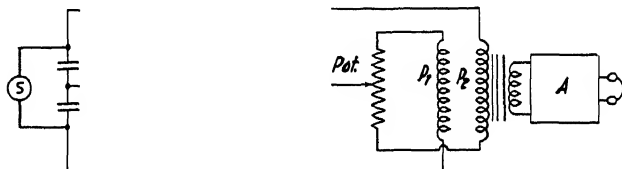
Fig. 10-131b. Modified induction balance. For symbols see Fig. 10-131a.

Fig. 10-131b shows a somewhat improved arrangement, with a potentiometer to facilitate adjustment of the bridge, and an amplifier following the secondary of the differential transformer. In the instrument illustrated in Fig. 10-131c, the inductances are replaced by mutual inductances, with one variable mutual inductance and two small resistors for adjustments. This bridge, developed by the Bureau of Standards during 1917–1918, is said to have encountered

U. S. Bureau of Standards

Fig. 10-131c. Mutual-inductance balance (after Theodorsen).

practical difficulties because the primaries and secondaries of the mutual inductances were too closely coupled.

Another group of low-frequency treasure finders employs a transmitting coil and one or two receiving coils close to them. In the arrangements shown in Figs. 10-132 and 10-133, the receiving coil is in the axis of the transmitter coil, so that no induction occurs above barren ground. Transmitter and receiver may be interchanged. Fig. 10-132 shows a hori-

zontal and a vertical transmitter with closely coupled receiving coil.   The distance between the coils may be increased to allow the operator to walk between them, as in Fig. 10–133.   This arrangement is customary in high-frequency treasure finders.

Two receiving coils are used in the detector shown in Fig. 10–134a, which was applied successfully by Theodorsen for the location of unexploded bombs several feet below the ground.[124]   It consists of a cylinder with three coaxial coils.   The middle coil is the transmitter, or energizer; the upper and lower coils are the receiving coils, in series opposition. On barren ground the induced fields are equal.   With a metallic or magnetic body present, the lines of force are distorted, chiefly in the lower coil.   This results in an unbalanced e.m.f., which is detected in the head phones. In Theodorsen's original instrument the coils were 3 feet in outside diameter and about 7 inches distant from each other.   Undoubtedly the diameter of the coils can be reduced, if the sensitivity is increased by tuning the transmitter coil and using

FIG. 10-132. Single energizer (T) and pickup coil (R), with schematic circuit diagram (after Joyce).

an amplifier on the receiving side (see Fig. 10–134b).

2. *High-frequency treasure finders* include *beat-frequency instruments* and combined transmitter-receiver arrangements.   The former utilize the change in the inductance of a coil produced by the presence of metal, a principle that was used very much during and after the last war in munitions factories and is now applied in mints and penal institutions to prevent

[124] Jour. Frank. Inst., **210**, 311–326 (1930).

coins or weapons from being carried in or out by workers or visitors. These installations use large coils, through which the persons under examination have to pass. The great sensitivity of these devices is made possible by beating the frequency of the search coil circuit (which is slightly changed by the presence of metal) against a fixed frequency and
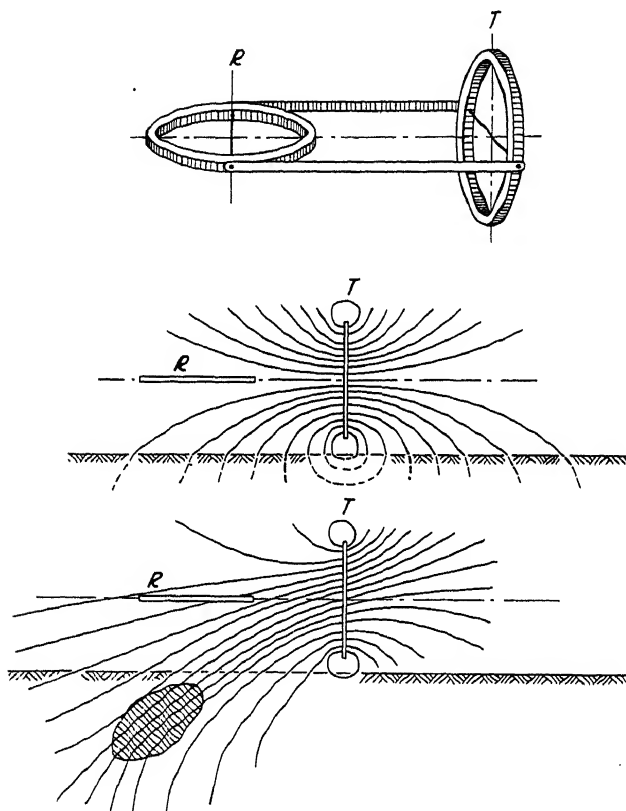
FIG. 10-133. Single energizer (T) and pickup coil (R) combination; reaction to subsurface metal object (after Joyce).

by detecting the beat frequency. This may be considered as a modification of the induction balance, since the inductance in one circuit remains fixed while the other is being varied. The same idea has been used in treasure finders, one coil being carried over the ground, the other being housed in a shielded box with the fixed oscillator. An instrument of this kind was constructed by Joyce.[125]

---

[125] U. S. Bur. Mines Circ. Inf. No. 6854, Oct., 1935.

Probably the majority of present-time treasure finders employ fixed combinations of high-frequency transmitters and receivers. Arrangement and operating principle are the same as in the low-frequency transmitter and receiver combinations, except that an R.F. carrier is used for
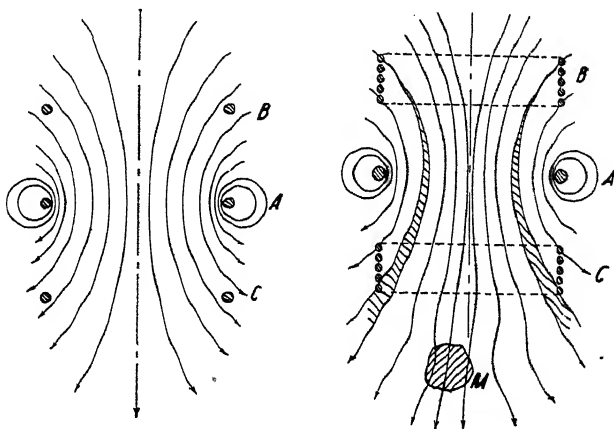
FIG. 10-134a. Single energizer, double pickup coil detector (after Theodorsen).
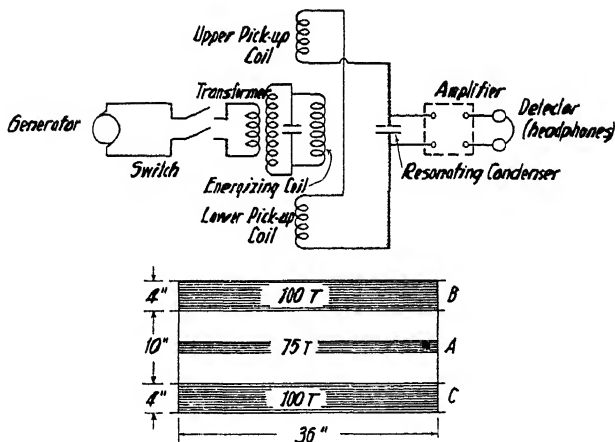
3. 10-134b. Modification of metal detector of Fig. 10-134a (after Joyce).

the 1000 cycles. In the Fisher Metallascope and the Barret Terrometer the transmitter and receiver are arranged as on the lower right of Fig. 10-135a. A circuit diagram of the Metallascope is given in Fig. 10-135a. Fig. 10-135b shows a more elaborate type of the Fisher Metallascope for operation as separate transmitter and receiver. In the Barret Terrometer the trans-

mitter is behind the operator and emits an approximately vertical field. The receiver, equipped with a sensitive galvanometer, is forward and so adjusted that either a maximum- or medium-size scale deflection is ob-
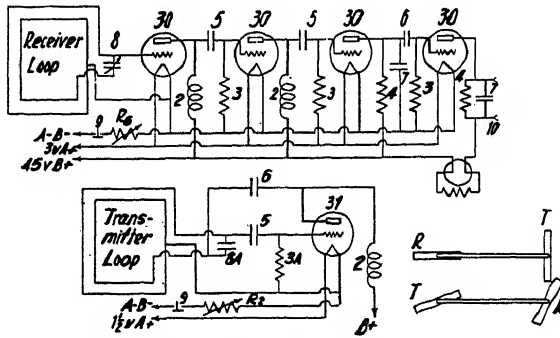
Fig. 10-135a. Circuit of Fisher Metallascope, with combined transmitter and receiver (after Chapel). (R_2, 5 ohms, 1 W.; R_6, 2 ohms, 1 W.; 1, milliammeter (0-1); 2, R.F. choke, 1500 turns No. 34ECC; 3, 1 megohm; 3A, 3 megohms; 4, 0.1 megohm; 5, 0.0005 mfd., fixed; 6, 0.006 mfd., fixed; 7, 0.001 mfd., fixed; 8, 0 to 0.0005 mfd., trimmer adjuster; 8A, 0.00025 mfd., fixed; 9, push-pull switches; 10, phonetip jacks.)
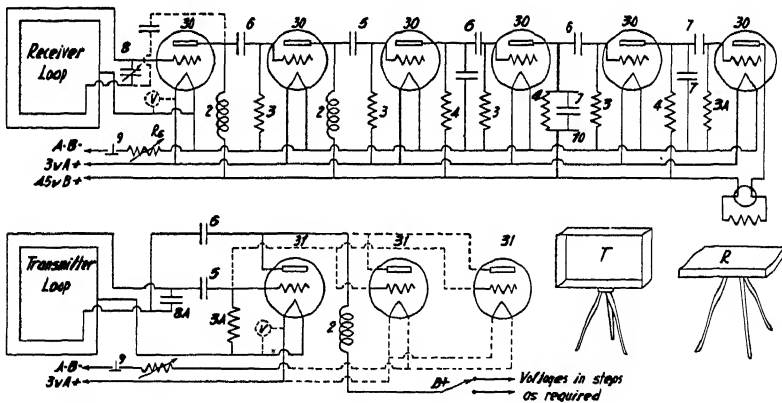
Fig. 10-135b. Circuit of Fisher Metallascope, separate transmitter, and receiver (after Chapel). R_2, 5 ohms, 1 W.; R_6, 2 ohms, 1 W.; 1, milliammeter; 2, R.F. choke, 1500 turns, No. 34ECC; 3, 1 meg. resistor; 3A, 3 meg. resistor; 4, 0.1 meg. resistor; 5, 0.0005 mfd., 1 W., fixed; 6, 0.006 mfd., 1 W., fixed; 7, 0.001 mfd., 1 W., fixed; 8, 0 to 0.0005 mfd. trimmer adjuster; 8A, 0.00025 mfd., 1 W., fixed; 9, push-pull switches; 10, tip jacks for phones.)

tained on barren ground. A decrease in scale deflection then indicates the presence of a metallic body. The depth penetration of the high-frequency treasure finders, for a medium-size metal chest, is probably not in excess of 6 to 7 feet.

I I

GEOPHYSICAL WELL TESTING[1]

The essence of geophysical well testing is a determination of *physical rock properties in situ.* Its purpose is (1) to correlate wells by using physical formation characteristics which either are more significant or can be obtained more readily than their petrographic and geologic characteristics; (2) to detect commercial minerals (oil, gas, coal) or other media which are of significance in the process of drilling (water, cement, and the like); (3) to determine data required in the interpretation of geophysical surface measurements (seismic wave velocities and the like). Somewhat removed from our field is a fourth application, the determination of crookedness of holes (by seismic measurements).

In regard to procedure, geophysical well-testing methods may be divided into (I) electrical logging, (II) temperature measurements, (III) seismic measurements, and (IV) miscellaneous measurements (magnetic, radioactive, and so on).

I. ELECTRICAL LOGGING

Electrical logging in the most general sense is the examination of the electrical properties, electrical reaction, and geometric disposition of subsurface formations by electrical measurements in wells. It involves a determination of the following quantities, in order of present commercial importance: (A) resistance or impedance of formations, (B) spontaneous potentials (porosities), (C) resistance of drilling mud, (D) dip and strike, and (E) casing depth.

A. Determination of Resistance or Impedance of Formations

In respect to the determination of impedance or resistance in (uncased) wells, electrical logging is equivalent to *resistivity mapping* with fixed electrode separation (see page 708). Hence, a variety of electrode arrangements is possible. In fact, most of those described at pages 710-711 have

---

[1] The symbols in this chapter are the same as in Chapter 10, except where otherwise noted.
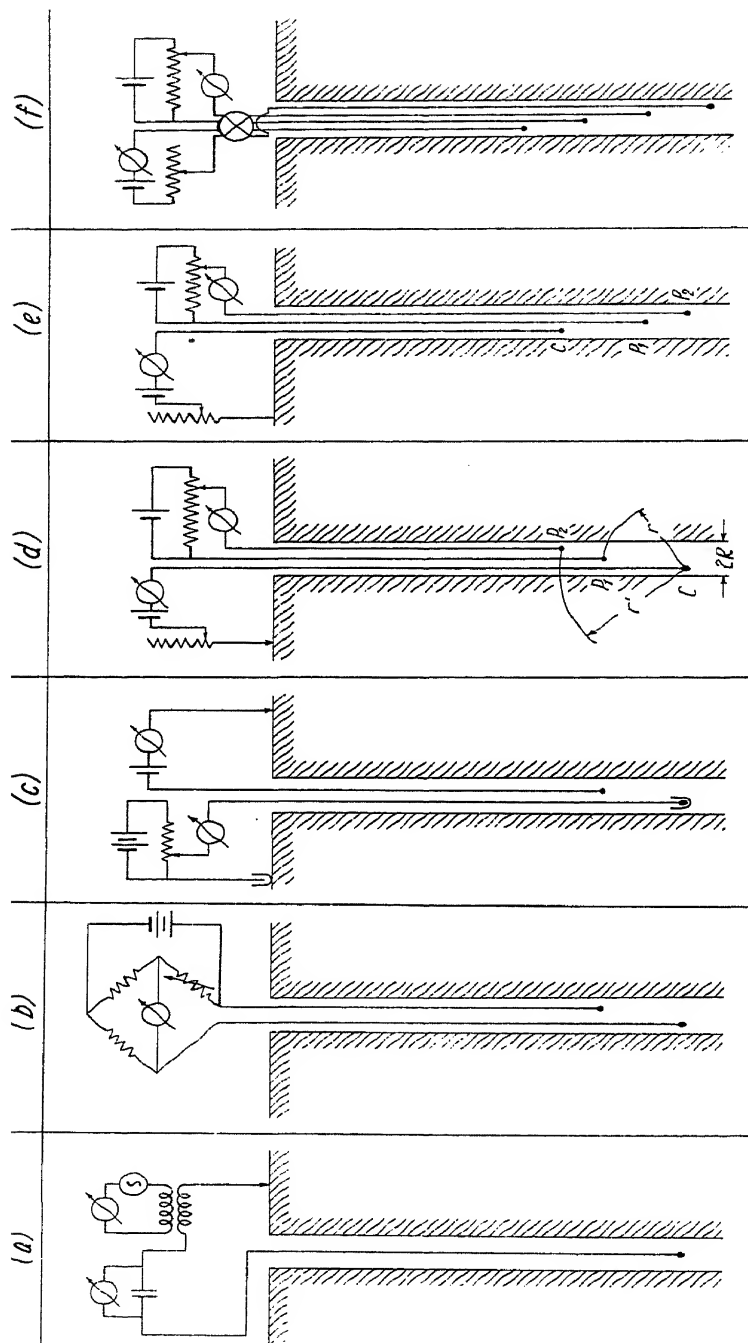
FIG. 11-1. Electrode arrangements and schematic circuits in electrical logging

been used or proposed. While in resistivity surface mapping a simple circuit with but two electrodes would not be suitable because of the preponderance of the contact resistance at the terminals, such an arrangement is permissible in electrical coring, since the distance between electrode and wall is small enough for the formation resistivity to affect the contact resistance of an electrode suspended in drilling mud of generally uniform resistivity.

Fig. 11–1 illustrates various electrode arrangements in increasing order of electrode number. The measuring devices indicated are not necessarily limited to the electrode arrangement with which they are shown and may be interchanged. Scheme a is used by the Halliburton Oil-Well Cementing Company (Blau patent) and in the Karcher system. In the latter, the electrode is the (insulated) bit at the end of the drill pipe. Scheme (b) is a Wheatstone bridge arrangement; it is used by Lane-Wells in a modified form, the upper electrode being represented by the cable sheath. The two-electrode scheme of Fig. 11–1c is well suited for separate self-potential and resistivity measurements. The three-electrode arrangement shown in Fig. 11–1d (Schlumberger) is now in most extensive use. The D.C. source indicated in the current circuit may be replaced by an A.C. generator, or a commutator may be provided, together with an A.C. meter in the potential circuit to record resistivity. One of the potential electrodes is then switched by a second commutator to a D.C. meter and a grounded electrode as in scheme (c) to give the self-potential record. Fig. 11–1e (Hummel) shows a modification with potential electrodes down; Fig. 11–1f is the conventional four-terminal arrangement with commutator, adapted to well surveying.

The spacing of the electrodes in schemes b and c is usually ten to twenty times the diameter of the hole; in schemes d and e, the distance CP_1 is ordinarily about 60 feet and P_1P_2 is about 15 feet. These distances may be decreased and increased to obtain two curves of different side penetration. Because of the uniform constitution of the drilling fluid, it is generally satisfactory to use ordinary metal electrodes in the hole; however, some companies use porous-pot electrodes. Two- or three-electrode arrangements usually have the form of a weighted insulated bar, the weight at the bottom representing the energizing electrode and the rings at the other end representing the potential electrodes. The electrode assemblies are lowered on cables that contain as many heavily insulated conductors as there are electrodes, and that protected by stranded flexible steel wire and surrounded by a steel sheath on the outside.

Current is straight D.C., commutated D.C., or, most often, low-frequency A.C. (20 to 100 cycles) as indicated above. The current can be held sufficiently constant so that a recording potentiometer, whose drum

or camera drive is coupled to the cable winch, gives a direct graph of *apparent resistivity* against depth. Resistivities and self-potentials are usually recorded simultaneously as indicated schematically in Fig. 2–15.

In homogeneous ground, the relation between resistivity and potential readings given at pages 710–711, apply. Since the electrodes are buried in an infinite and not a semi-infinite medium, the spacing factors given in these formulas change from $2\pi a$ to $4\pi a$, so that, for the Schlumberger arrangement, with the notation of Fig. 11–1d,

$$\rho = \frac{4\pi r r'}{r' - r} \cdot \frac{\Delta V}{I},\qquad (11\text{--}1)$$

which follows directly from eq. (10–31h). Since r, r', and I are kept constant, it is seen that the resistivities are directly proportional to the potential difference recorded. Formula (11–1) holds for homogeneous ground only. In the presence of layers of different resistivity, an *apparent* instead of a true resistivity is recorded. The relation of apparent and true resistivities for given formation thicknesses and resistivities can be calculated in the same manner as on page 719 since by rotating the geologic section 90° the bedding planes are equivalent to the vertical formation contacts treated in resistivity mapping, assuming for the moment that the effect of the drilling fluid is negligible.

When a formation contact is passed with the four-electrode system (Fig. 11–1f), an apparent resistivity variation as in Fig. 10–56 is obtained with four breaks near the formation boundary instead of one. As the number of electrodes is reduced, the number of peaks decreases, as illustrated in Fig. 11–2 for the Schlumberger electrode arrangement. The two upper diagrams are for one formation boundary and the two lower diagrams for two boundaries. The distance of the breaks is uneven and corresponds to $\overline{CP_1}$ in one and $\overline{P_1P_2}$ in the second case. The resistivity of the second medium is approached in steps and not all at once. For formations whose thickness is large compared with the electrode separation, the corresponding apparent resistivity curves may be derived by joining curves such as those given in Fig. 11–2 (upper part).[2] For thin formations, the images of the current electrode, due to reflections on *both* formation boundaries, must be considered, which means that resistivities must be calculated as in a three-layer case. Results of such calculations are illustrated in Fig. 11–2. It is seen that a formation whose thickness is less than the distance of one potential electrode from the next current electrode will not allow the apparent resistivity to come up to the value of the true resistivity. This is possible only when the electrode separation is smaller than the formation thickness.

---

[2] J. N. Hummel, Beitr. angew. Geophys., 6(1), 89–99 (1936).

The influence of the drilling fluid on the apparent resistivity can be calculated[3] by assuming the mud-filled hole to represent the "cover" of resistivity ρ_1 on a layer of uniform resistivity ρ (two-layer case, page 714). As may be expected from the similarity of electrical logging and resistivity mapping, the drilling fluid decreases in effectiveness with an increase in electrode separation. If the resistivity of the formation is ten times greater than that of the drilling fluid, and if the electrode interval $\overline{CP_1}$ is ten times the hole diameter, the apparent resistivity is 75 per cent of the true re-

Fig. 11-2. Variation of apparent resistivity with true resistivity and electrode separation in electrical logging (after Hummel).

sistivity. If the drilling fluid is of high resistivity compared with the formation, the electrode spacing need be but two to three times the hole diameter, to produce an apparent resistivity virtually equal to the formation resistivity (Fig. 11-3).

Conversely, for measuring mud resistivity, it is necessary to reduce the electrode separation and make the electrode interval *less* than the diameter of the hole. In that case the electrode intervals are made equal. To suppress any possible wall influence, the electrodes may be enclosed in a nonconductive cylinder, open at both ends. For a still closer approach to true conditions, a third layer representing a zone flooded by drilling mud, may be interposed between the formation and the drill hole in the above calculations.

As a matter of fact, the replacement of formation water by well water near the hole may be so pronounced as to obliterate formation resistivities and to require the so-called "third" curve, which is a resistivity curve taken with larger electrode spacing and, therefore, greater depth penetration.

[3] J. N. Hummel and O. Rülke, Beitr. angew. Geophys., **6**(3), 265–270 (1937).
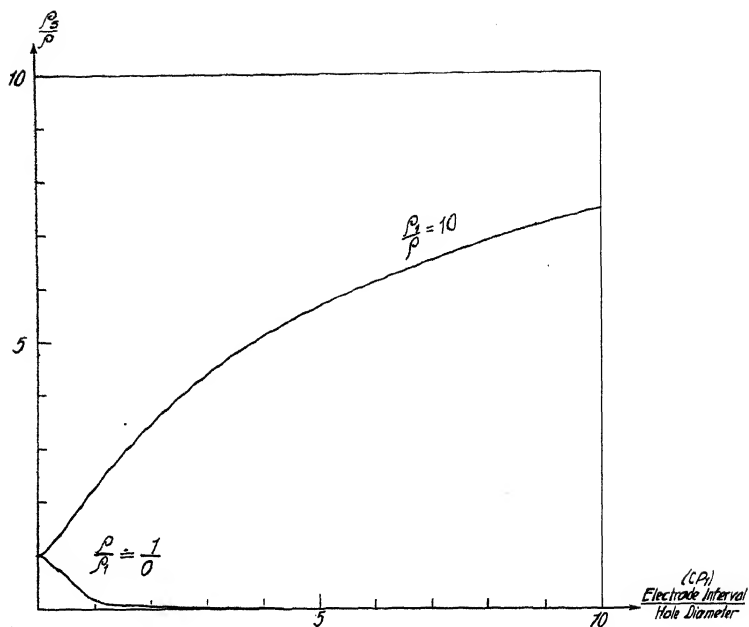
FIG. 11-3. Variation of apparent resistivity with ratio of electrode spacing and hole diameter for two resistivity ratios $\dfrac{\text{formation } (\rho_1)}{\text{drilling mud } (\rho)}$ (after Hummel). The electrode interval CP_1 is as shown in Fig. 11-1d.
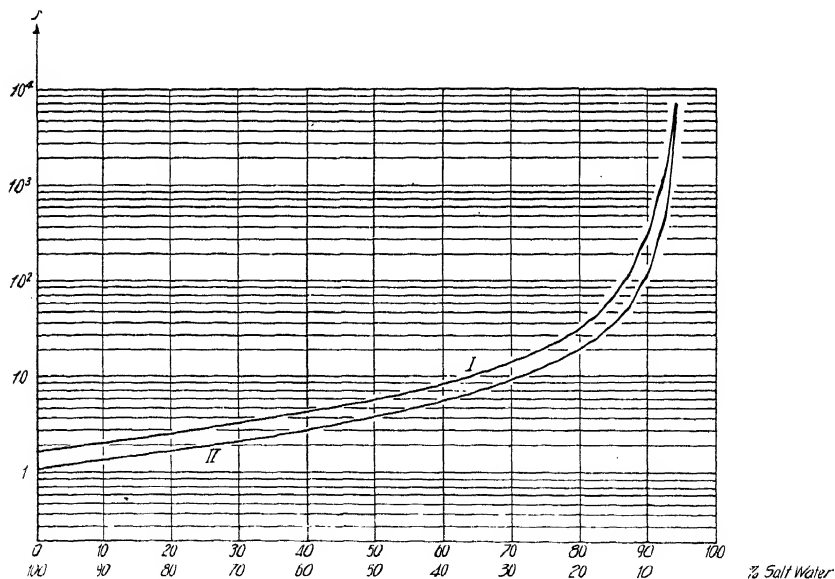
FIG. 11-4. Variation of formation resistivity with oil and water content (after Martin, Murray, and Gillingham). (I, porosity 45 per cent; II, porosity 20 per cent; resistivity in ohm-meter.)

Of considerable practical interest is the problem of how the *true* formation resistivity changes with the proportion of salt water and oil. Such experiments have been conducted by Martin, Murray, and Gillingham[4] (see Fig. 11–4). Oil contents up to 60 per cent increase the formation resistivity about ten times. As was stated before, (see page 665), this ratio between the resistivities of productive and barren formations is frequently encountered in the practice of electrical logging. It is further seen in Fig. 11–4 that oil contents exceeding 70 per cent bring about a sharp increase in formation resistivity, of the order of one hundred to several thousand times.

B. Determination of Spontaneous Potentials (Porosities)

When porous formations are penetrated by the drill, they give rise to spontaneous potentials in two ways: (1) by movement of liquids through the formation into or from the hole (electrofiltration potential), and (2) by differences in concentration between formation water and drilling fluid (diffusion potential). The former, discussed on page 631, is practically the only source of spontaneous potentials in the absence of concentration differences between formation water and drilling fluid. These potentials are positive when water is discharged into the hole but negative when water flows from the hole into the formation. Hence, the magnitude of the potential anomaly depends on the pressure or height of the mud column in the hole. The extreme potential anomaly in the well illustrated in Fig. 11–5 was ±20 millivolts. No diffusion potential was present, since the mud contained about 2 g NaCl per liter and the formation water about 3 g NaCl per liter. Usually the electrofiltration potentials are negative in sign, since the drilling fluid penetrates the porous formation under excess pressure.

Diffusion potentials are produced by porous formations because the (fresh water) drilling fluid is generally lower in ion concentration than is the (connate) formation water. As shown in Fig. 11–6, currents flow from the drill hole into the layer and cause negative potential peaks which may amount to 100 to 200 millivolts. This phenomenon was discussed on page 631. The theoretical potential difference, according to eq. (10–2), is $E = 11.6 \log_{10} \rho_2/\rho_1$ millivolts, so that, for a formation water of 0.5 ohm-m and a drilling fluid of 5 ohm-m resistivity, the potential difference would be 11.6 millivolts. However, because of an additional potential difference set up along the return circuits at the points CB and $C'B'$, respectively, the potential difference is actually greater than for only one boundary, so

that the factor in eq. (10–2) is about 17 instead of 11.6 for the contact of clay and siliceous sand. Hence, in an experiment where ρ_2 was 24 ohm-m and ρ_1 varied from 17 to 0.04 ohm-m, the potentials varied from 2.5 to 46
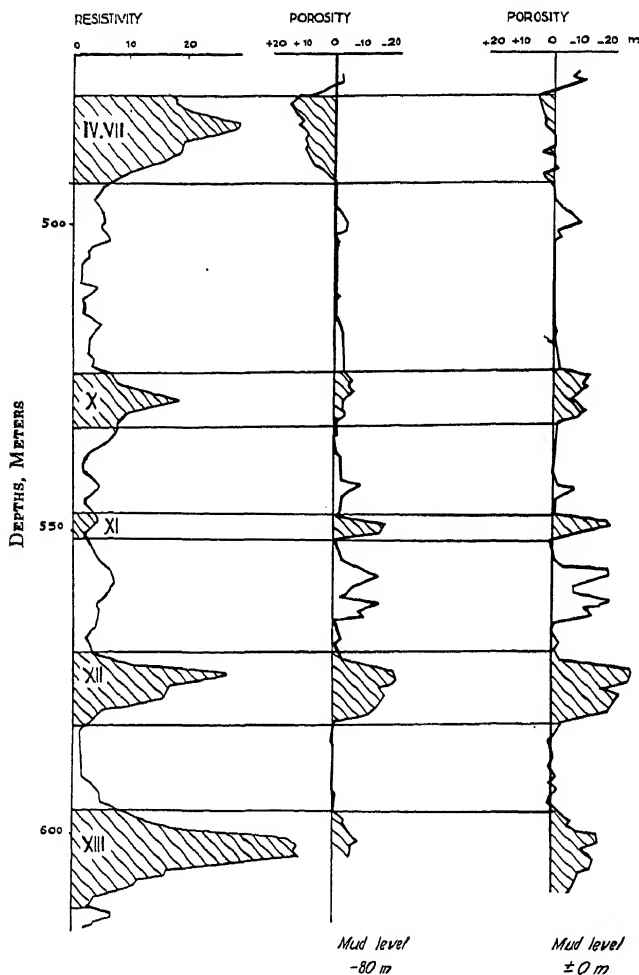
FIG. 11-5. Variation of self-potential effects in drill holes (electrofiltration phenomenon) with pressure of mud column, in Grozny field (after Schlumberger).

millivolts.[5] Fig. 11-7 shows results of some trials made with drilling muds of three different resistivities.

[5] C. and M. Schlumberger and E. G. Leonardon, A.I.M.E. Geophys. Pros., 278 (1934).

Frequently, the electrofiltration and diffusion potentials reinforce each other. Hence, self-potential records (taken with the electrode arrangement illustrated schematically in Fig. 11-1c) give a good indication of the porosity of a formation and furnish valuable information supplementary to resistivity data. Since a low-resistivity indication may be interpreted as a salt-water sand or clay bed, the porosity indication would decide which interpretation is correct. The same is true for high-resistivity indications which could mean a limestone bed or an oil sand, unless a porosity record is available.
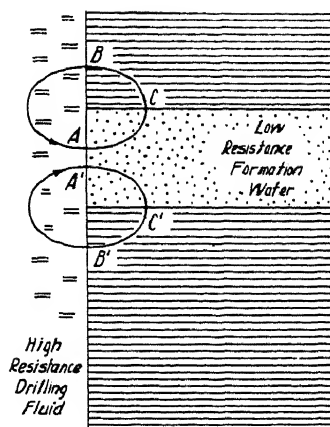
FIG. 11-6. Origin of diffusion potentials in drill holes (adapted from Schlumberger).
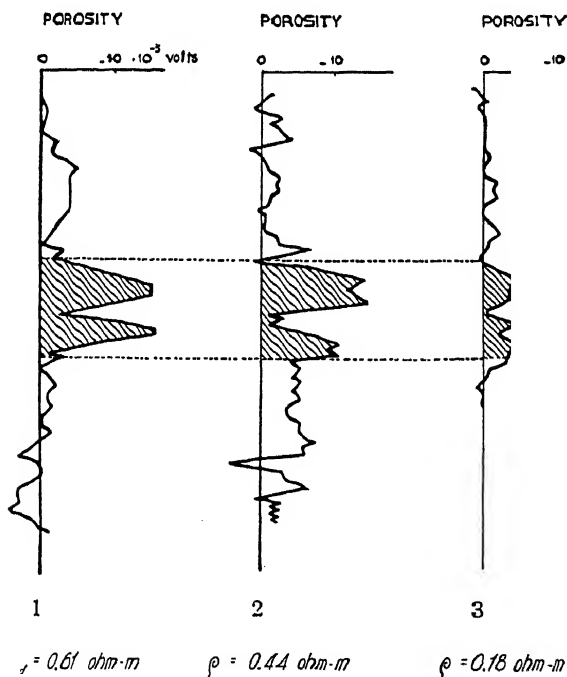
FIG. 11-7. Variation of diffusion potential with resistivity of drilling mud (after Schlumberger).

C. DETERMINATION OF RESISTIVITY OF DRILLING MUD

The resistivity of the drilling fluid is determined with closely spaced electrodes. Its practical importance lies in the location of water flows. To this end, the hole is first conditioned by washing with fresh-water mud, and the first run indicated in Fig. 11–8 is taken immediately afterward. The level of the mud is then lowered, allowing formation water to penetrate the hole. Another run (second curve in Fig. 11–8) is taken, which indicates the portion of the hole filled with (low-resistivity) formation water.
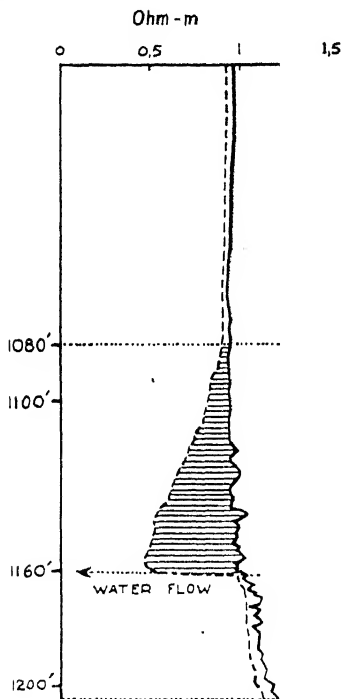
FIG. 11-8. Location of water flow by measuring resistivities of drilling mud (after Schlumberger).
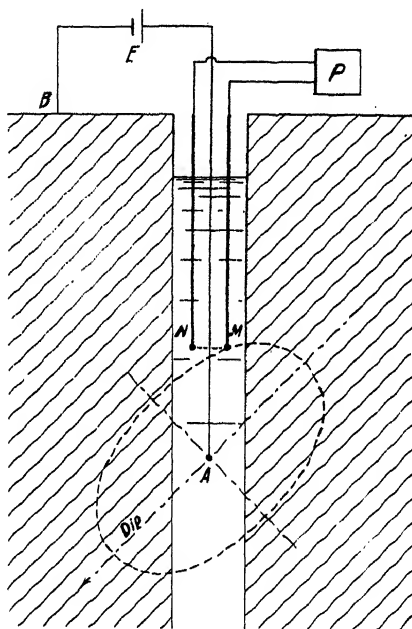
FIG. 11-9. Electrode arrangement for measuring dip and strike in wells (after (Schlumberger).

D. MEASUREMENT OF DIP AND STRIKE

Since in stratified formations the conductivity in the bedding planes is greater than at right angles thereto, the equipotential surfaces about a source are not spheres but ellipsoids of revolution. These ellipsoids are tilted when the strata dip. If an electrode configuration, as illustrated in Fig. 11–9, is lowered into the hole with a rigid rotatable connection between

N and M, a maximum potential difference, proportional to dip, will occur between the electrodes when they are in the position shown. When the configuration is then rotated to a position at right angles to the plane of the paper, the potential difference vanishes, whereby the direction of strike is established. In practice, the two directions are determined with reference to magnetic north, which may be established with an earth inductor well compass.[6]

E. DETERMINATION OF CASING DEPTH

Since the casing is a much better conductor than the mud or the adjacent rocks, its depth can be established from the abrupt change in apparent resistivity when the electrodes pass through the casing shoe. Inside the casing, the resistivity is zero. For these measurements, intermediate and small electrode separations are used.

F. DISCUSSION OF RESULTS

How closely electrical logging data may coincide with results of core analysis is illustrated in Fig. 11-10. The section represents the oil zone
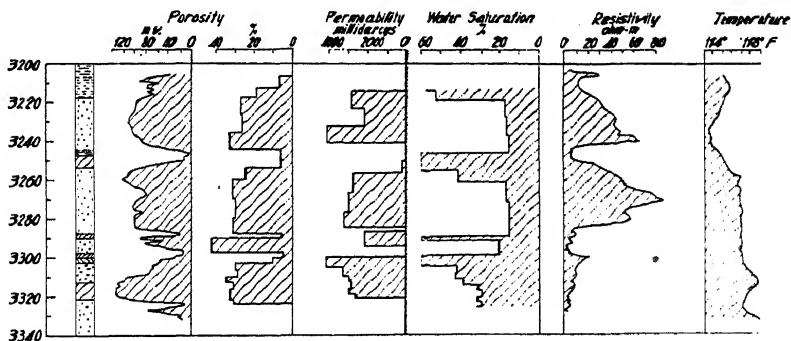
FIG. 11-10. Comparison of core analyses with results of electrical logging (after Schilthuis).

of the Woodbine sand in the east Texas field. Porosities were determined by the Washburn-Bunting method,[7] permeabilities in accordance with A.P.I. Code No. 27,[8] and connate water and oil by vaporization and combustion.[9] Porosities indicated by the self-potential curve are closely paral-

---

[6] Schlumberger and Leonardon, *loc. cit.*

[7] Amer. Ceramic Soc. J., **4**, 983-989 (1921).

[8] Barnes, A.P.I. Drilling and Production Practice, 191-203 (1935).

[9] R. J. Schilthuis, A.I.M.E. Tech. Publ. No. 869, 1937.

leled by the permeabilities and porosities measured on cores, the resistivity and water-analysis curves are quite similar.

The main value of electrical logs lies in the possibility of well correlation by the "character" of the indication. A structural correlation can be made, regardless of whether the geologic significance of an indication is known or not. Small changes in moisture and lithologic character are detected much more readily and with more continuity in an electrical log than is possible by any mechanical coring process. Even if formations do not appear to be differentiated in respect to lithologic and paleontologic characteristics, the electrical log can usually be depended on to segregate them.

Fig. 11-11 shows correlation on the basis of resistivity logs between two wells three-quarters of a mile apart in the Oklahoma City field. The water sands there are quite readily distinguished by their low resistivities. The jagged peaks indicate limestones (Tonkawa lime at II) or sandy shales; the smooth portions (I and III) represent fairly homogeneous shales and clays. In some oil fields, such as in Rumania, correlations have been possible over considerable distances.

Fig. 11-11. Electrical log correlation between two wells in Oklahoma City field (after Schlumberger).

Fig. 11-12 shows well logs taken in the Gorgoteni field. The wavy appearance of both porosity and resistivity logs in the Dacian formation (composed of alternating sands and marls) is in striking contrast to their smooth character in the Pontian, which consists of argillaceous marls. The sandy

section of the Maeotic below is again indicated by the irregular saw-toothed appearance of porosity and resistivity curves. In this section, correlations have been made over distances of the order of 50 miles. In some areas in this country, long-distance correlations are likewise possible.[10] Very good correlations are the rule in the mid-continent fields.[10a]

Fig. 11–13 is an outstanding example of how electrical logging may be applied to indicate productive horizons. In this section of the Maracaibo field, the three important oil horizons are very well indicated, as are the depths to correct water shutoff and the low-resistivity clay formations. In some fields a direct proportionality has been established between resistivity and productivity of oil horizons. At Grozny, for instance (Fig. 11–14), a high resistivity of the H horizon corresponds to gusher produc-
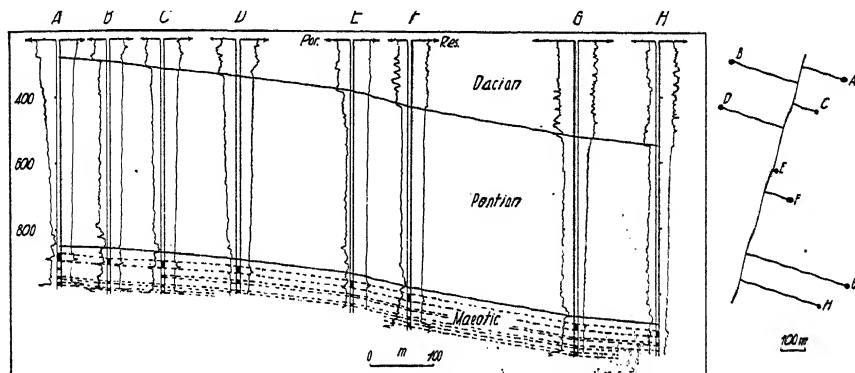
Fig. 11-12. Resistivity and porosity correlation of eight wells in the Gorgoteni field, Rumania (after Schlumberger).

tion and an intermediate resistivity (well 2), to oil shows with water. In well 3, where the amplitude is about the same as that of other beds, the horizon is dry.

Electrical logging has become daily routine in many oil-producing fields and wildcat wells. Results are accumulated at a much more extensive rate than the few examples given above indicate.

II. TEMPERATURE MEASUREMENTS

It is an age-old belief that the interior of the earth is hot, and it is a matter of long-standing experience that ground temperature increases with

[10] A.A.P.G. Bull. No. 23 (11), 1622-1626 (Nov., 1939).
[10a] Personal communication from H. Guyod.
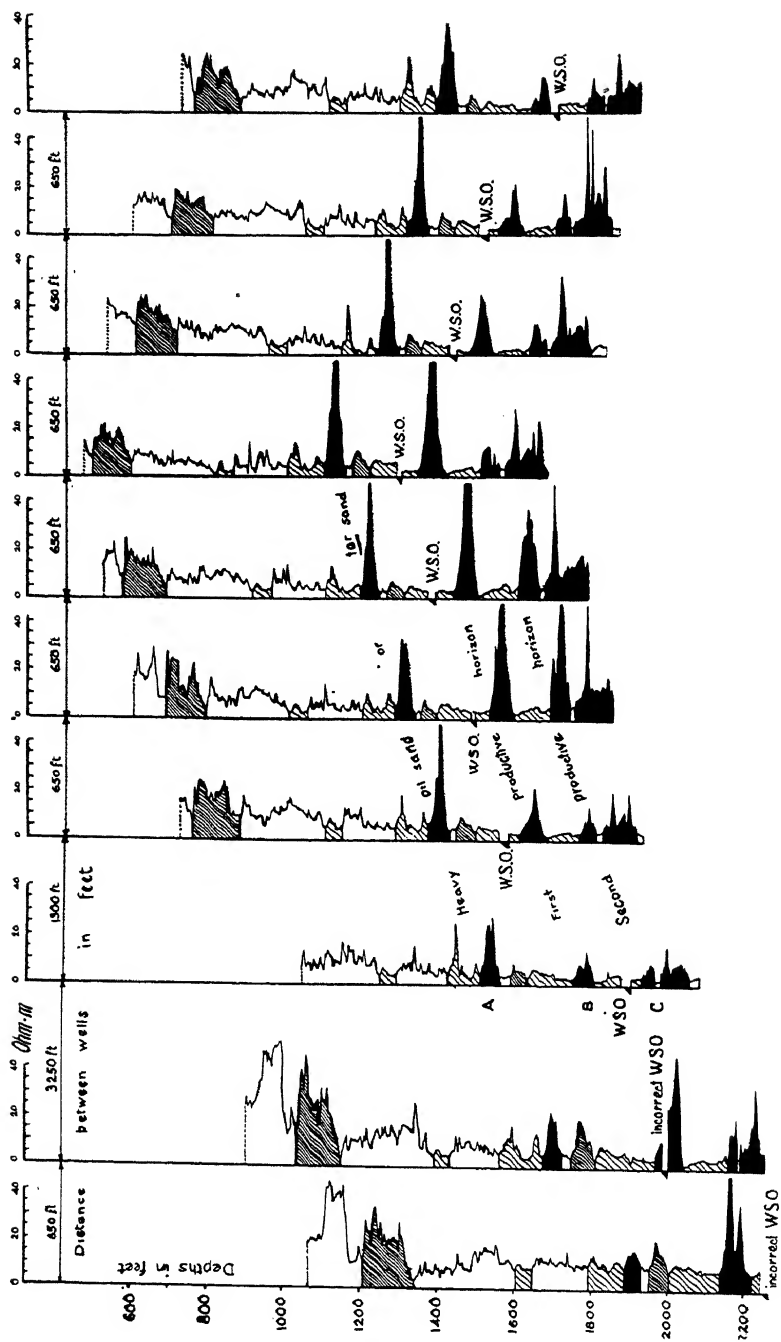
FIG. 11-13. Electrical log correlation between wells in Maracaibo field, Venezuela (after Schlumberger).

depth.   One of the earliest accounts of rock temperatures in mine workings was given by Athanasius Kircher in 1665, but about 150 years elapsed before systematic underground observations were conducted in England, Germany, and France.   Reliable temperature measurements in wells were
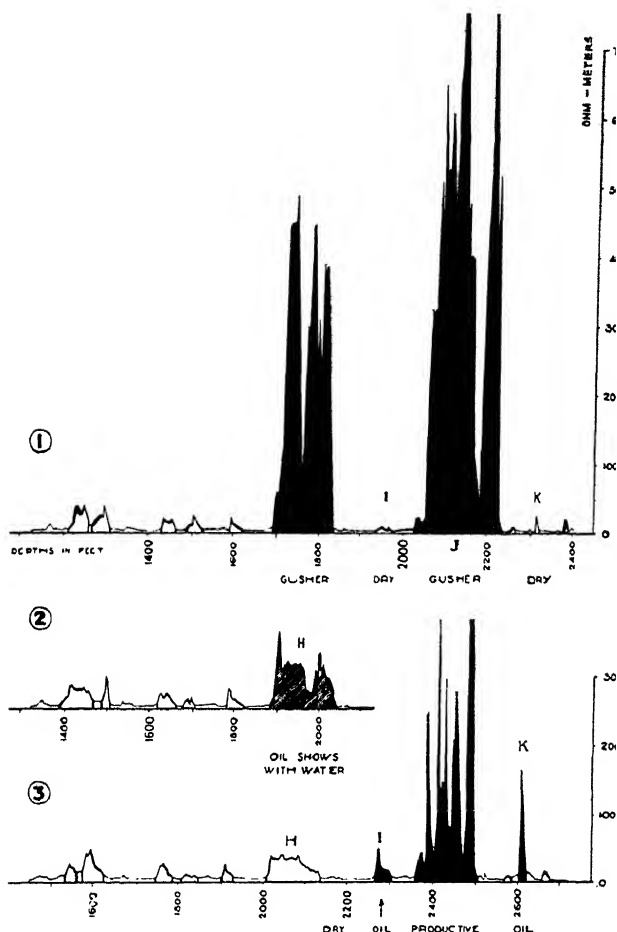
Fig. 11-14. Correlation between productivity of oil horizons and electrical resistivities in the Grozny field, Russia (after Schlumberger).

made possible by the development of overflow thermometers in 1830.   In the eighties, this was followed by a systematic inquiry into the influence of rock conductivities and of other factors.   With progress in well drilling (see Fig. 11-15), much material was accumulated after the turn of the century and was made the object of exhaustive studies by Van Orstrand,

Koenigsberger, Heald, and others. The development of the electrical logging process in the past five years has made it possible to obtain detailed and continuous records of well temperatures and to study their relation to geologic conditions and production technique.

A. Apparatus; Procedure

Apparatus used in geothermal well testing depends entirely on the purpose for which the test is undertaken. In present practice measurements are made (1) in shallow holes for the location of near-surface formations,
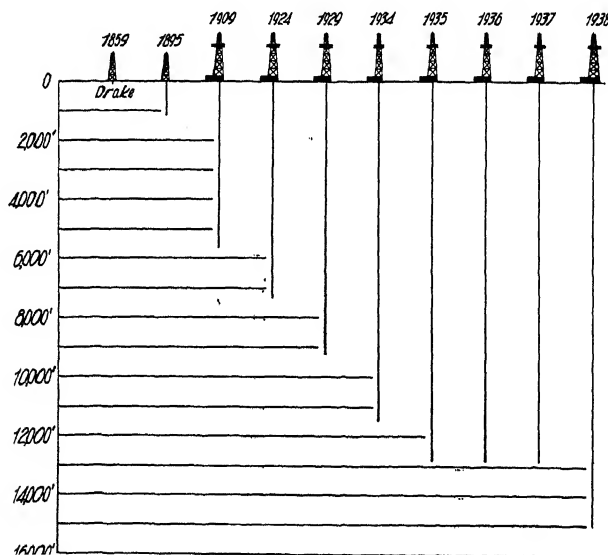
Fig. 11-15. Trend of drilling depths in the United States in the past eighty years (from *Union Oil Bulletin*).

near-surface structure, spring waters, and the like; (2) in deep wells for correlating the mean gradient between wells with geologic structure; and (3) in deep wells individually, for locating gas, oil, and water flows, and for determining cementation depth.

For shallow well testing, ordinary thermometers are suitable, if they are provided with some sort of a cover (paraffine, rubber, or the like) to slow down rapid temperature fluctuations. If they are so protected and are hauled up rapidly, they will give the true bottom-hole temperature. Resistance thermometers and thermocouples have the advantage that two of them may be so connected as to give the difference in temperature of adjacent holes. Thereby, the daily or any other temperature variation is

eliminated, since it affects adjoining holes alike. Thermocouples may be used with the hot junction in the hole and with the cold junction in a liquid kept at constant temperature. Van den Bouwhuijsen[11] used a Moll galvanometer of 2.7×10^{-7} volt sensitivity with a thermocouple supplying $4 \cdot 10^{-5}$ volt e.m.f. for a temperature difference of 1° C.

In underground workings, ordinary mercury thermometers are suitable if they are properly protected. A thermometer constructed by L. R. Ingersoll[12] maintained its temperature for about one minute by being inclosed in a bakelite tube; the bulb was insulated with vulcanite and paper. In seven-foot holes sunk from rock faces but a few days old, measurements were made with sets of two or three thermometers in tandem. These were read about every two hours for one day and the readings were repeated after two or three days. This made it possible to determine the cooling of the walls in drifts, tunnels, or shafts, and to calculate the virgin rock temperatures.

The mean temperature gradients in deep holes are generally determined by maximum thermometers. Their use is predicated on the fact that the temperature in deep holes is greater than the mean annual temperature. (Maximum thermometers may also be used at shallow depths provided they are chilled with ice before and after the run.) An overflow type of maximum thermometer is illustrated by R. Ambronn.[13] In it, the maximum temperature has to be determined by a separate testing operation and by measuring the temperature at which the mercury overflows. In another type of maximum thermometer, the upper 2–3 mm of mercury are separated from the main stem by an air bubble. The most extensive application has been made of the constriction type of maximum thermometer which requires resetting in some sort of centrifugal device after each use. The thermometer used by the U.S. Geological Survey has a length of about 20 cm, a stem diameter of 6–7 mm, and an accuracy of 0.1°–0.2° F.; and it is divided in Fahrenheit degree intervals between 32° and 212° over a length of 17–18 cm. Usually two or three thermometers are employed for each run to increase the accuracy and to reduce errors due to jarring of the assembly in hoisting and lowering.

Fig. 11–16 shows a number of thermometer carriers[14] with their containers adapted to various types of wells. Fig. 11–16A' is a holder for three thermometers which fits the container B' for use at the end of a rope in shallow wells; C' is a container suitable for clamping to a piano-wire line; D' is a steel container for use, at the end of a wire line, in oil or water wells.

[11] Eng. and Min. J., **135**(8), 342-344 (Aug., 1934).
[12] Physics, **2**(3), 154-159 (March, 1932).
[13] *Elements of Geophysics*, p. 275.
[14] C. E. Van Orstrand, Econ. Geol., **19**(3), 229-248 (1924).

Several containers may be arranged in tandem with the T joint. The open containers are applied in dry, open holes. In wells filled with water, drilling fluid, or oil, the use of the closed containers (A–C) prevents the pressure of the liquid from reaching the thermometers and altering the reading. Thermometers in European equipment are enclosed in cotton-packed and capped steel cylinders, which are arranged in tandem in a tube of larger diameter. Leather diaphragms are provided around the ends of the large tube to reduce circulation.

The thermometers may be lowered into the well on the end of the sand line, inside or outside the bailer, or on a separate line, using an apparatus developed especially for this purpose, illustrated in Fig. 11–17. This ma-
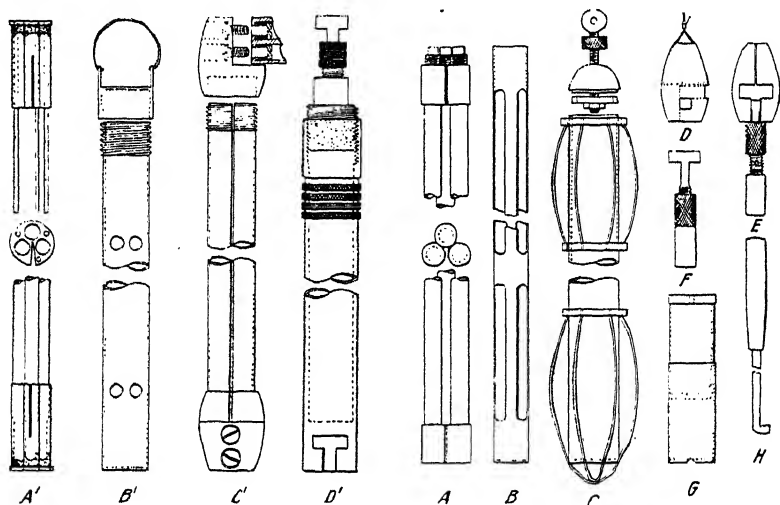
FIG. 11-16. Holders and containers for maximum-thermometers (after Van Orstrand).

chine holds 9000 feet of No. 19 or No. 20 piano wire and is equipped with a spooling and depth indicating mechanism.

The use of maximum thermometers requires that the well be in temperature equilibrium and that jars and other sources of error be carefully avoided. Since this technique is intended for structural correlations, disturbances arising from an influx of oil, water, and gas into the well are considered sources of error and are carefully avoided if possible. Drilling with a standard rig should be discontinued for at least twenty-four hours before a test is begun. For a rotary outfit the time required for temperature equilibrium is much greater and may be several days. When measurements between 100–1000 feet are taken with maximum thermometers, outside temperatures may be higher than the well temperatures, and the

thermometers must therefore be chilled before and after the run. Otherwise they may be left in the well over night and be hauled up in the early morning hours. The time required for the thermometers to acquire formation temperature is about $1\frac{1}{4}$ hours in air and $\frac{3}{4}$ hour in water. Since the reading at 100 feet is from 1° to 4° F. higher than annual mean temperature, the latter provides a convenient check on the upper portion of the depth-temperature curve and may be obtained from the volume on *Climatological Data for the U. S. by Sections*, published by the U. S. Weather Bureau. With maximum thermometers, readings are taken at intervals of 250–500 feet. Such thermometer assemblies are lowered at the rate of 200 feet per minute maximum and removed at the rate of 100 feet per minute maximum. Readings are taken with a telescope and corrections for constant and stem deviation are applied.
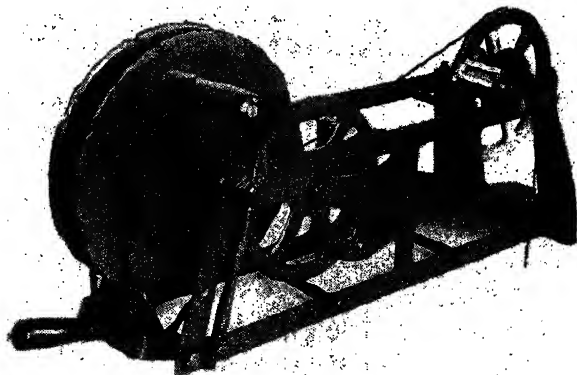
FIG. 11-17. Device for well-temperature measurements (after Van Orstrand).

For detailed temperature investigations required in connection with production tests, continuously recording thermometers are more suitable than maximum thermometers, since they do not require hoisting after every reading. The following thermometers are suitable: (1) bimetallic thermometers, (2) thermocouples, and (3) resistance thermometers. The former require a recording mechanism inside a water-tight case and do not require wires for remote surface indication. Thermocouples and resistance thermometers are widely used, since cables are usually available in connection with electrical logging.

Fig. 11–18 shows three arrangements of resistance thermometers. Fig. 11–18a represents a Wheatstone bridge circuit with Siemens lead-resistance compensation. Fig. 11–18b shows a customary method of measuring resistance variations by galvanometer deflection. For recording, the switch S is in position 2; for calibration (by adjusting R to a predetermined

galvanometer deflection), it is in position 1.   In the arrangement of Fig.
11–18c, the resistance of the thermoelement is determined by measuring
the potential drop across it, with the switch to the left, and determining
the current in the circuit from the potential drop across the known resistor
r, with the switch to the right.   During a run the current measurement
can be dispensed with, and an automatic self-balancing potentiometer can
be used to record the temperature.   In the Schlumberger apparatus,
measurements are taken with an accuracy of 0.25° F., and the thermometers
are lowered at the rate of about 1000 feet per hour.
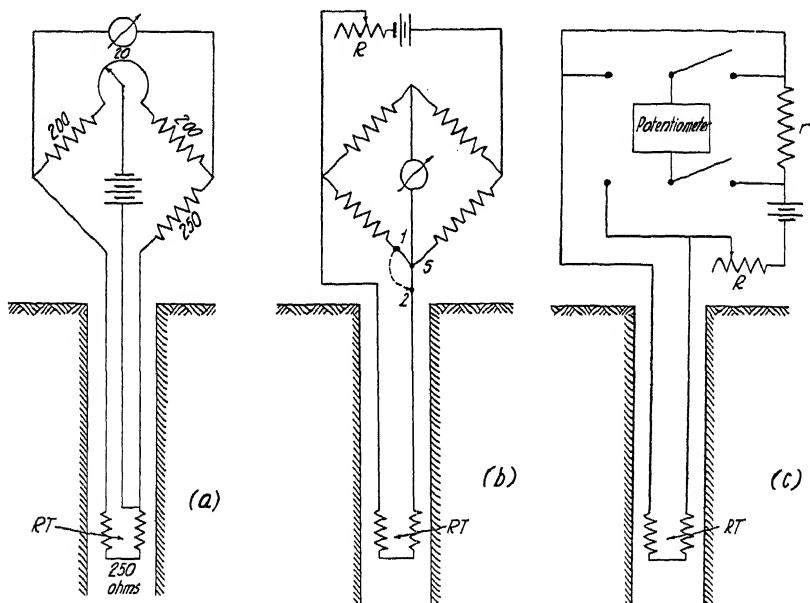
FIG. 11-18. Resistance thermometer arrangements for well-temperature recording.
(a) Wheatstone bridge with Siemens lead-resistance compensation (adapted from
Johnston and Adams); (b) deflection bridge; (c) potentiometer method.

For general structure correlation of deep wells, temperatures are meas-
ured and plotted beginning with a depth of about 100 feet.   From this
curve a mean temperature gradient can be calculated by assumption of a
straight-line function $\theta_d = \theta_0 + bd$, where θ_d is the temperature at depth
d, θ_0 is the mean annual temperature, and b the mean slope of the curve,
or the temperature-depth gradient.   The gradient can be measured di-
rectly by recording the difference in temperature between two thermome-
ters mounted a definite distance apart.   In some cases, gradient records
have advantages over the direct temperature records.   The *reciprocal
gradient* $1/b$ is the number of feet or meters one has to advance in vertical

direction to obtain an increase in temperature of 1° C. or F. For a detailed analysis of individual wells, the slope or gradient is taken over limited portions of the temperature-depth curve. Areal temperature distribution is represented by lines of equal reciprocal gradient for a given depth, or by contour lines of equal temperature. In profile view equi-temperature lines or "isogeothermal surfaces" are useful for correlation with regional and local dip. Temperature measurements, made in connection with electrical logging for purposes of production engineering, are represented in the form of a temperature curve, deviations from the (normal or regional) gradient being shaded to indicate the anomalies. Results of shallow-well investigations are plotted by showing lines of equal temperature for a given depth of investigation. When temperature differences have been measured with two thermometers between adjacent wells, temperature gradients are plotted in profile or plan view.

B. The Universal Geothermal Gradient

Wherever great depths have been reached, an increase of temperature has been observed. In the Simplon tunnel (maximum cover under mountain crest, 7000 feet) the highest rock temperature was 132° F. In the Robinson Deep mine in the Rand of South Africa, the temperature was (only) 103° F.[14a] at a depth of about 8500 feet. The Wasco well in the San Joaquin Valley, California (15,004 feet deep), revealed a bottom temperature of 268° F.,[15] which is higher than the boiling point of water. Yet, the greatest depth reached to date is but a $1\frac{1}{2}$ thousandth part of the earth's radius. This makes any deductions in regard to the temperature in the earth's interior and the age of the earth highly speculative, to say the least.

Of the many approaches to the problem of temperatures in the earth's interior, the so-called Kelvin theorem is probably the best known. It gives the temperature at any depth as a function of an initial temperature, time of cooling and an absorption coefficient, for an infinite slab heated at one face while the other is kept at 0° temperature. The solution appears in the form of a probability integral[16] which, when differentiated with respect to depth, gives the geothermal gradient

$$\frac{\partial \theta}{\partial d} = \frac{\theta_0}{\sqrt{\pi k t}} \cdot e^{-\frac{d^2}{4kt}}, \qquad (11\text{-}2)$$

[14a] Other mining districts have shown reciprocal gradients of the order of 175–375 feet per degree F.

[15] Probably mud temperature. Actual formation temperature was probably around 300°. (Personal communication from H. Guyod.)

[16] H. Cecil Spicer, Geol. Soc. Am. Bull., **48**, 75–92 (1937).

in which θ is temperature, d is depth, θ_0 is initial temperature, t is time since beginning of cooling, and $\mathbf{k}$ is thermal diffusivity. Therefore, for the earth's surface, $\partial\theta/\partial d = \theta_0/\sqrt{\pi \mathbf{k} t}$. Substituting a value of 1° F. per 50 feet for the temperature gradient and a value of $64 \cdot 10^{-4}$ C.G.S. for $\mathbf{k}$, and assuming further a temperature of 7000° F. for the initial condition, it follows that the time elapsed since the beginning of the cooling is about 175 million years. This is generally considered too low for the age of the earth, yet it is nearly of the right order of magnitude. An earth with the temperature distribution postulated by the Kelvin theorem has been claimed to be unstable against tidal and similar forces. Therefore, the assumption has been made that the cooling process is partly compensated
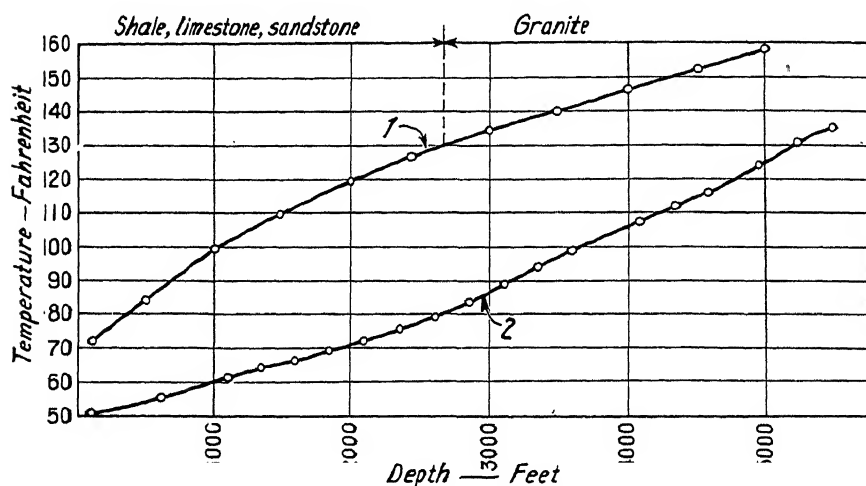
FIG. 11-19. Trends of temperature depth curves (1) near basement rocks, and (2) in sedimentary areas (after Van Orstrand).

by the heat generated at moderate depth by a layer of constant or exponentially decreasing radioactivity.

Whatever the cause of the earth's heat, the amount of heat transmitted to the surface is exceedingly small and barely sufficient to melt a layer of ice $\frac{5}{16}$ of an inch thick in one year. The heat quantity Q transmitted in the time t between the faces of surface S and distance l of a slab of the conductivity c is given by

$$Q = cSt\frac{\Delta\theta}{l}. \tag{11-3}$$

If for $l/\Delta\theta$ the normal reciprocal gradient, or 50 feet for 1° F., is substituted, it follows that the amount transmitted is only 200 B.t.u.'s per square foot in one year.

As was stated above, the normal reciprocal gradient varies from about 27.5 meters per degree C. (or 50 feet per degree F.) to about 35 meters per degree C. (or 64 feet per degree F.) in normal areas. Regionally, the observed reciprocal gradients may be quite different from these values, depending on geologic structure.[17] In wells where the drill has penetrated uplifts of basement rocks, the temperature–depth curve is concave toward the depth axis; that is, the reciprocal gradient increases with depth. This is because of the better heat conductivity of the basement rocks (see Fig. 11–19). Conversely, in areas of sedimentary beds of great thickness the reciprocal gradient decreases with depth (Fig. 11–19). This may be caused by the decrease of porosity[18] (hence, water content[19] and thermal conductivity) with depth, or by the compression of the isogeothermal surfaces as the basement rocks are approached. However, when the basement is entered, these types of curves turn again toward the depth axis. According to Van Orstrand,[20] only 5 per cent of 400 wells investigated up to 1932, had a linear depth-temperature curve; 26 per cent were concave, and 59 per cent were convex to the depth axis.

C. Thermal Properties of Rocks

The thermal behavior of rocks and formations is characterized by three properties. They are: (1) the *thermal conductivity*, or the heat current traversing the unit section for the unit of heat gradient, expressed in cal. cm.$^{-1}$ sec.$^{-1}$ centigrade^{-1}; (2) the *specific heat*, which is the quantity of heat required to raise the unit of mass by the unit of temperature, in cal. gram^{-1} centigrade^{-1}, or B.t.u. per pound per degree F.; and (3) the *diffusivity* K, a property derived from the first two, and given by

$$K = \frac{c}{s\delta}, \tag{11-4}$$

where c is thermal conductivity, s is specific heat, and δ is density. A fourth property, the heat given off in certain chemical reactions, is likewise of importance. However, it is difficult to define and is discussed in the next section.

Since diffusivity is a derived property, this discussion will be confined to specific heat and thermal conductivity. The specific heat of most minerals

---

[17] Van Orstrand, A.A.P.G. Bull., **19**(1), 78–115 (Jan., 1935).

[18] For correlations of depth-temperature with depth-porosity curves see Van Orstrand, *ibid.*, **18**(1), 19 (Jan., 1934).

[19] Depths to boiling point of water are 7000 feet or less in one-third of the locations investigated by Spicer (A.A.P.G. Bull., **20**(3), 279 [March, 1936]). In the remaining two-thirds, they are 10,000 feet or less.

[20] Physics, **2**(3), 139 (March, 1932).

and rocks is in the neighborhood of 0.2 for dry rocks, but it may increase to 0.5 to 0.7 for moist formations. Wet peat, with 0.9, approaches the specific heat of water. Table 76 gives a few representative values, in cal. gram^{-1} centigrade^{-1}.

TABLE 76

SPECIFIC HEATS

MINERALS

Feldspar	0.21	Calcite	0.20
Dolomite	0.22	Quartz	0.21
Gypsum	0.26		

SEDIMENTARY ROCKS

Sandstone	0.22	Loam (wet)	0.51
Slate	0.22	Sandy loam (dry)	0.49
Clay	0.22	Sandy loam (wet)	0.75
Quartz sand	0.19	Humus soil	0.44
Chalk	0.21	River sand (moist)	0.32
Coal	0.31	Peat (dry)	0.15
Loam (dry)	0.31	Peat (wet)	0.9

IGNEOUS ROCKS

Granite	0.19	Andesite	0.20
Gneiss	0.20	Basalt	0.21
Porphyry	0.20	Syenite	0.20

Specific heat of rocks is determined by any one of the calorimetric methods used for other solids. For instance, the specimen may be heated to a given temperature, and then be dropped in a calorimeter. The quantity of heat given off until both specimen and bath have reached the same temperature is dependent on the specific heat of the specimen.

Compared with the metals whose conductivity, when expressed in units of cal. cm.$^{-1}$ sec.$^{-1}$ centigrade^{-1}, may be as much as 1 unit (silver), most rocks have only a conductivity of third decimal value. Most sedimentary and some metamorphic rocks are distinctly anisotropic with respect to heat conduction. The anisotropy ratio is about $1\frac{1}{2}$:1 (gneiss) to 3:1 (schists). Table 77 gives heat conductivities for a few minerals and rocks in 10^{-3} C.G.S. units.

TABLE 77

HEAT CONDUCTIVITIES

MINERALS

Coal	0.3–0.8	Calcite	10
Petroleum	0.3	Graphite	12
Mica	0.9	Rock salt	17[a]
Water	1.4	Quartz $\perp$	17
Ice	2–6	Fluorite	25
Gypsum	3	Magnetite	30
Feldspar	5	Quartz $\parallel$	32

[a] This value is for crystals and is probably too high for salt formation. Leonardon (Geophysics, 1[1], 115, [Jan., 1936]) gives 6.6, which value is also quoted by Alexanian.

SEDIMENTARY ROCKS[21]

Very dry sand	0.8	Molasse sandstone, $\delta = 2.57$	8.1
Sand with 11.3% moisture	2.7	Alpine limes	4.9
Quartz sand (dry)	1.0	Limestone	5.2
Quartz sand (moist)	8.2	Clayey lime, $\delta = 2.59$	6.7
Red sandstone (dry)	2.5	Clayey lime, $\delta = 2.71$	8.1
Red sandstone (moist)	6.0	Lime	8.8
Clays (dry)	2.5	"Nagelflue," $\delta = 2.03$	5.9
Clays (moist)	3.5	"Nagelflue," $\delta = 2.73$	9.0
Molasse sandstone, $\delta = 2.06$	3.0		

IGNEOUS AND METAMORPHIC ROCKS

Granite, $\delta = 2.66$	7.6	Slate	5.7
Granite, $\delta = 2.6$	9.8	Phyllite	7.0
Granite, $\delta = 2.66$	8.1	Lava, $\delta = 2.62$	4.0
Basalt, $\delta = 2.97$	6.7	Traprock, Calumet & Hecla	3.4
Aare granite	4.0	Porphyry	8.4
Rofna porphyry	5.5	Andesite	6.9
Serpentine	8.4	Trachyte, $\delta = 2.55$	4.6
Gneiss	5.3	Trachyte, $\delta = 2.4$	3.0
Andesite	3.1	Garnet schist	6.5
Obsidian	1.9	Calcareous phyllite	4.7
Marble	5.2	Lava, $\delta = 2.83$	4.6

The values for sedimentary, igneous, and metamorphic rocks indicate that the thermal conductivity is greatly dependent on porosity[22] and moisture. From molecular theory, the following relation has been deduced,[23] in which c is thermal conductivity, v_l is longitudinal wave velocity, and δ is density:

$$c \cdot 10^3 = v_l^2 \cdot \delta^2 \cdot 10^{-11}.$$

Since approximately $v_l = \sqrt{E/\delta}$, the conductivity

$$c = E \cdot \delta \cdot 10^{-14}, \tag{11-5}$$

where E is Young's modulus. This relation has probably not been tested experimentally on rocks. However, calculations made for various homogeneous rocks and for representative values of E and δ, give reasonable figures for the heat conductivity. The high heat conductivities of igneous and metamorphic rocks are in good agreement with high elastic moduli and densities.

Thermal rock conductivities may be measured in the laboratory by absolute or relative procedures. An absolute method, illustrated in Fig. 11-20a, provides a heater and a plate of constant temperature on both sides of a specimen. Holes of small diameter are drilled into it and are

---

[21] Largely after H. Reich, Handb. Exper. Phys., 25(3).

[22] See also Van Orstrand, A.A.P.G. Bull., 18(1), 19 (Jan., 1934).

[23] N. M. Thornton, Phil. Mag., 6, 38, 705, 707 (1919).

fitted with thermocouples or resistance thermometers. If **S** is the surface of the plate and $(\theta_2 - \theta_1)/x$ is the temperature gradient, the thermal conductivity

$$c = \frac{x}{S} \cdot \frac{Q}{\theta_2 - \theta_1},$$

(11-6)

where Q (cal. sec.$^{-1}$) is the heat current which may be calculated from the current and the resistance of the heater circuit. Another absolute method[24]
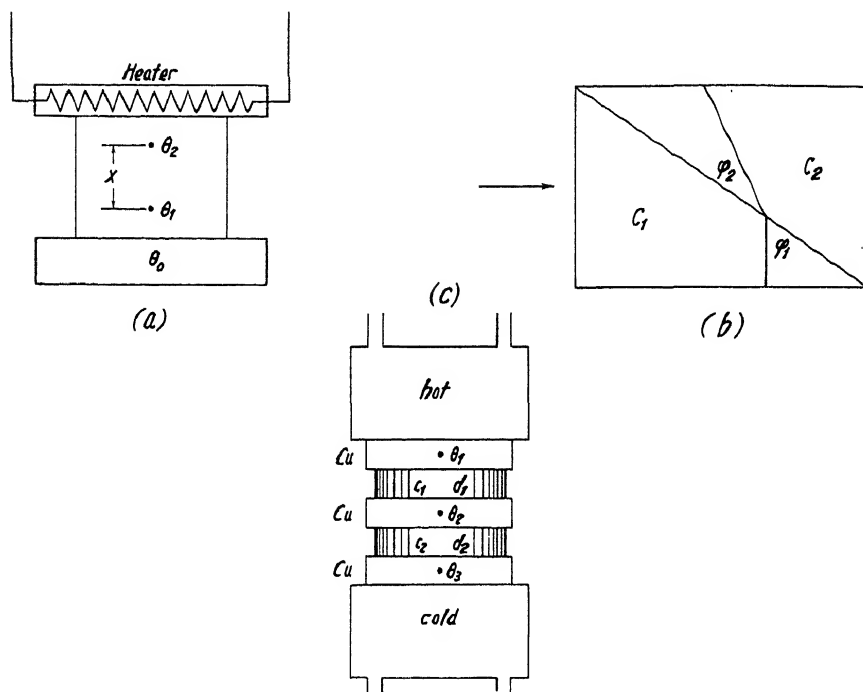
FIG. 11-20. Arrangements for measuring thermal conductivities of rocks: (a) absolute method, (b) and (c) relative methods.

uses a thermocouple in the center of a slab whose two faces are exposed to constant temperature for twenty-four hours and then abruptly chilled to and kept at 0° C. The conductivity is calculated from the time required for the center temperature to fall to its half-value.

A simple relative method for comparison with a material of known conductivity is shown in Fig. 11-20b. Two plates of triangular shape are joined with their hypotenuses and covered with a wax film. If heat is

[24] Ingersoll, Phys. Rev.. **24**, 92 (1924).

applied on one side, the wax will melt along a broken line which makes the angles φ_1 and φ_2 respectively, with the diagonal. Then $c_1 = c_2 \tan \varphi_1 / \tan \varphi_2$, where the subscripts 2 refer to the standard material. Another convenient relative method,[25] shown in Fig. 11-20c, places the specimen, of the conductivity c_1 and thickness d_1, in series with a standard of the conductivity c_2 and thickness d_2, with a copper plate between them. If a thermal gradient is now produced by heating one side and cooling the other, the conductivity of the specimen follows from that of the standard and from the respective thermal gradients:

$$c_1 = \tag{11-7}$$

Anisotropy of heat conduction may be determined by covering the surface of a specimen with wax, applying heat at one point, and measuring the axes of the melting ellipse.

Variations in thermal conductivity of rocks and formations are of profound influence upon the thermal gradient. Since the heat current, that is, the quantity of heat transferred in the unit of time through a plate of section S and thickness d, is given by

$$\theta = \frac{c(\theta_2 - \theta_1)S}{}$$

and since $d/(\theta_2 - \theta_1)$ is the reciprocal temperature gradient, or $1/b$ (see page 844), it is seen that

Fig. 11-21. Depth-temperature curve, showing effect of change in thermal conductivity (15 miles southeast of Thompsons, Grand County, Utah). (After Van Orstrand.)

$$\frac{1}{b} \quad \frac{S}{Q} \cdot c. \tag{11-8b}$$

Hence, the reciprocal gradient is directly proportional to the heat conductivity of a formation. This is well illustrated in Fig. 11-19 and particularly in Fig. 11-21, where a reduced slope (large reciprocal gradient) corresponds to the increased conductivity of the salt. With the value of

[25] C. Christiansen, Ann. Physik., 14, 23-33 (1881).

6.6 given on page 848, the conductivity should be about 2.8 units for the overlying sediments, which agrees with the values for sands and clays given on page 849. An increase in the reciprocal gradient in salt is also evident in Fig. 11-22 from the arrangement of the isogeothermal surfaces. Usually the contrast on the contact of two media is not so sharp as that indicated in Fig. 11-21 but is more gradual because of the crowding of the lines near a medium of better heat conductivity.[26]

Where formations are definitely anisotropic in respect to heat conductivity,[27] the reciprocal gradient changes with dip. If **b** is the (normal)
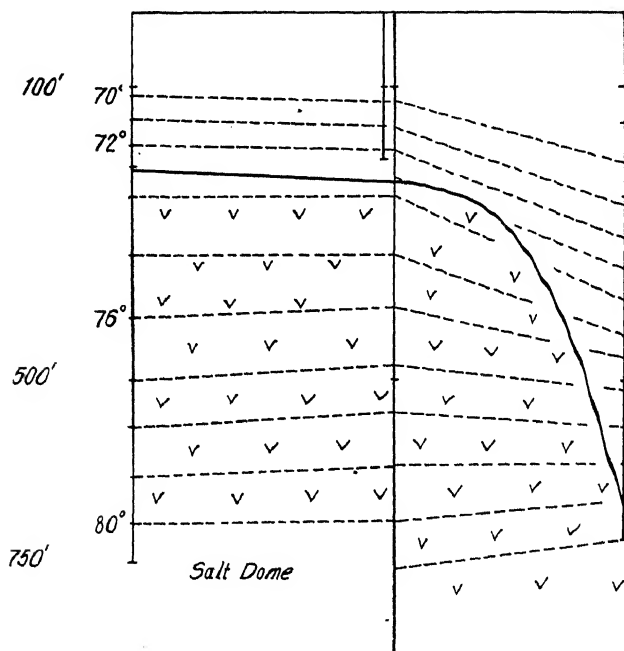
FIG. 11-22. Isothermal lines through Grand Saline salt dome, showing increased interval in the salt and a decrease in interval above it (after Hawtof).

vertical gradient, c_1 the conductivity in the bedding planes, c_2 the conductivity normal thereto, and η the thermal anisotropy that is equal to $\langle$ then the normal gradient is reduced in the ratio

$$r = \frac{1}{\sqrt{\sin^2 \varphi + \cos^2}} \qquad (11\text{-}9)$$

[26] Mathematically, the problem is similar to the calculation of electrical potential distribution about a conductive body. See, for instance, J. Koenigsberger, Gerl. Beitr., **18(1/2)**, 115-126 (1927).

[27] Van Orstrand, Amer. J. Sci., **15**, 507 (June, 1928).

where φ is dip. The normal reciprocal gradient of $1°$ F. in 50 feet changes, therefore, with dip to the extent shown in Table 78, if the anisotropy is 1.765 (slate).

TABLE 78

	1/b		1/b
	50.0 feet	$20°$.............	54.5 feet
$5°$.	50.3	$25°$.............	56.8
$10°$.	51.2	$30°$.............	59.6
$15°$.	52.5		

The influence of dip can be so pronounced as to make the isogeothermal surfaces almost parallel with the structural contours. Two well-known examples are the Salt Creek field (Fig. 11–23) and the section from Oklahoma City to Sapulpa (Fig. 11–24). The A.P.I. report on geothermal investigations[28] contains many more instances of this character. Faults may be indicated in geothermal maps: (1) by a slight deflection of the isogeothermal surfaces if the fault has thrown blocks of different conductivity against one another;[29] and (2) by a peak in the temperature curve, as shown in Fig. 11–25, if waters of different temperature circulate in the fault plane.
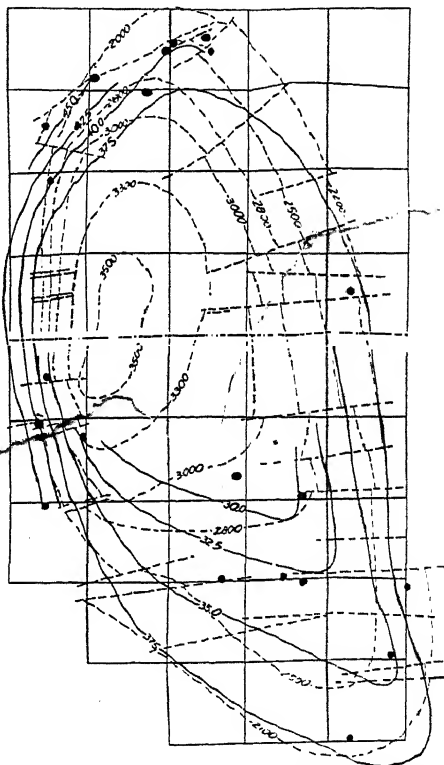
FIG. 11-23. Lines of equal reciprocal temperature gradient and contours on second Wall Creek sand in Salt Creek dome, Wyoming (after Van Orstrand).

D. HEAT GENERATING PROCESSES; CAUSES OF TRANSIENT TEMPERATURES

As shown in the preceding section, static distribution of temperatures is a function of the variations in the heat conductivities of rocks and formations. With the exception of factors of geologic periodicity (such as volcanism, glaciation, and radioactivity) most of the heat-generating proc-

[28] Am. Petrol. Inst. Prod. Bull. No. 205 (Oct., 1930).
[29] I. O. Haas and C. R. Hoffmann, A.A.P.G. Bull., 13(10), 1257–1273 (Oct., 1929).

esses discussed below produce transient temperature conditions of widely varying duration. When such processes are to be detected by geophysical well investigation, it is, of course, not necessary to wait until temperature equilibrium has been established, as was the case in the structural applications described in the preceding section.

1. *Radioactivity.* Much has been written about the part played by radioactivity in the retardation of the cooling of our planet. It is impossible to deal with this problem extensively here from the theoretical viewpoint. Reference is made to the review and bibliography by Van Orstrand.[30] It is noteworthy that virtually no verification of the
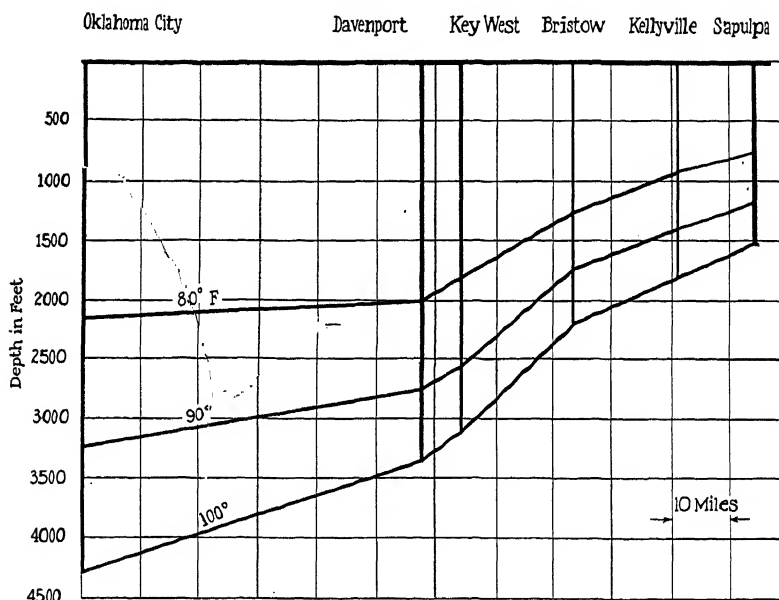
FIG. 11-24. Isogeothermal surfaces and depth to granite between Oklahoma City and Tulsa (after McCutchin).

theory has been obtainable, the outstanding observation being that[31] the pitchblende deposit in Joachimstal, which is in one of the richest radium localities, does not exhibit abnormally high temperatures.

2. *Volcanism.* In volcanic areas large anomalies in geothermal gradients may arise (a) from rapid changes in conductivities of formations (intercalation of highly porous lavas, and the like), or (b) from circulating hot waters. In Oregon, Van Orstrand[32] observed reciprocal gradients as small

---

[30] A.A.P.G. Bull., 18(1), 13-38 (1934).

[31] J. Koenigsberger, Inst. Min. Eng. Trans., 39, 1-28 (1910).

[32] Van Orstrand, Am. J. Sci., 35, 22-46 (1938).

as 3.3 feet per degree F. and as large as 20–21 feet per degree F.　In such cases, the depth-temperature curves may consist of both extremely flat and abnormally steep portions.　High rock temperatures should naturally be expected in areas of volcanic activity even without the presence of circulating waters.　There is frequent evidence of this condition in mines located in volcanic areas.　Underground workings in ores deposited by thermal waters will show high temperatures if deposition is still going on.
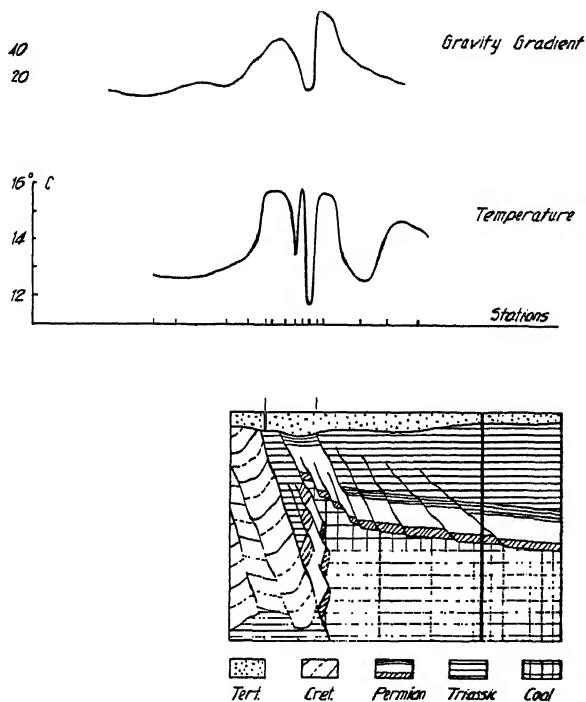
Fig. 11-25. Torsion-balance and geothermal indication of fault near Winterswijk, Holland (after Van den Bowhuijsen).

3. *Glaciation.*　As shown below (section E), any change of temperature at the earth's surface is propagated downward in the form of a wave. Short-periodic changes, such as the diurnal temperature variation, are damped out within a few feet.　Long-periodic variations, such as those occurring during glacial and interglacial periods, may be expected to have affected the thermal gradient down to several thousand feet of depth.[33] With sufficient data on geologic section and heat conductivities, the effect of temperature changes of given periodicity on the depth-temperature

[33] A. C. Lane, Geol. Soc. Amer. Bull. No. 34, 711 (1923).

curve may be calculated. In this manner, Ingersoll, *et al.*,[34] estimated that 30,000 years have elapsed since the last glacial period.

4. *Oil.* Opinions were expressed in the earlier literature that chemical processes associated with the formation of oil deposits (polymerization, and the like) should have given rise to geothermal anomalies. However, no definite evidence of such anomalies has yet been found. Of particular significance have been (*a*) the measurements in the Burbank pool[35] where no rock deformation is in evidence and where no temperature anomaly is found, in spite of extensive oil accumulation, and (*b*) observations on salt domes, whose geothermal reaction appears to be the same regardless of the presence or absence of oil. Even in oil deposits which occur so near the surface that they are mined by shafts, as in Pechelbronn,[36] there is no evidence of a direct heat influence of the oil. On the other hand, it is possible to determine the influx of oil into a well by a slight drop in the temperature curve,[37] which is probably caused by the expansion of the gas dissolved in the oil. In drilling wells, the well is conditioned with a light mud, and the survey is made several hours after circulation. In producing wells, it is preferable to swab the well down and to take the temperature run while it is filling up.

5. *Gases* in subsurface formations are generally confined under considerable pressure. When they are tapped and liberated by a well, the reduction in pressure produces a decrease in temperature in accordance with the relation

$$\Delta\theta = c \cdot \Delta P \left(\frac{273° \text{ C.}}{} \right.$$

where c is a constant depending on the gas, ΔP is the difference in pressure, and θ is the temperature at which the gas escaped. As Fig. 11-26 shows, the effect is quite noticeable and may readily amount to several degrees (F.) drop in temperature. The location of the base of a gas formation is of considerable practical importance for determining the depth at which to set casing. If it is set too low, part or all of the oil formation may be cased off; if too high, a well with a high gas-oil ratio, or even a practically dry gas well, will result. In some areas, such as West Texas, temperature well surveys for gas are an indispensable adjunct to electrical logging.

6. The location of *water* in wells is likewise of importance in connection with shutoff and cementation depth control. The interaction of formation

[34] A.I.M.E. Tech. Publ. No. 481, Feb., 1932.
[35] K. C. Heald, A.P.I. Proc. Bull. No. 205,
[36] Haas and Hoffmann, *loc. cit.*
[37] W. J. Gillingham and W. B. Steward, Petroleum Engineer, **9**(**7**), 52–55 (April, 1938), and **9**(**8**), 84–92 (May, 1938).

water and drilling fluid will produce quite different geothermal effects, depending on relative temperatures, hydrostatic head, and agitation. As shown in Fig. 11–27, the trend of temperatures in static condition may be as in curve *a*. Drilling will result in cooling the lower portion of the well by the drilling fluid, and in heating the upper portion in comparison.
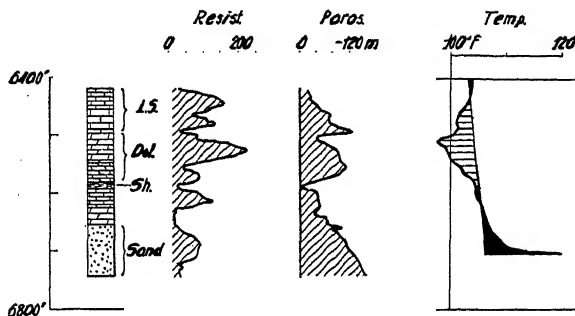
FIG. 11-26. Anomaly in depth-temperature curve due to escaping gas (after Leonardon).

When the well is left idle, the lower portion will again tend to take the temperature of the surrounding formations and cool the upper portions further. A gradual approach to static conditions takes place. In practice, the order of events is reversed when several runs are taken for locating water flows. If the well has been idle for a time and a first run is taken, curve *c* is obtained. If, then, the mud is circulated for a few hours, a second run will give curve *b*.[37a] Following this, the hydrostatic head of the mud is generally reduced by bailing to allow (warm) water to flow into the hole. This will give rise to a definite peak in the curve.

FIG. 11-27. Depth-temperature curves in idle drilling, and flowing wells (after French).

Fig. 11–28 shows a series of water sands with their corresponding temperature peaks recorded through the casing. Note the

[37a] R. W. French, Oil and Gas J., April 27, 1939.

similarity of the temperature and the self-potential curves taken before the casing was run.

Close supervision of temperature conditions in a well is valuable in connection with water encroachment problems. It is frequently observed that the temperature of oil flowing into a well remains fairly uniform until the well turns to water; then a rapid increase in temperature of the flow is noted. This may be explained on the basis of the difference in heat conductivity of oil and water. The temperature of the latter is likely to be higher than that of the former but not felt until the oil envelope separating it from the well becomes too thin.

FIG. 11-28. Temperature Anomalies of water sands (after Guyod). (Note similarity of temperature and self-potential curves.)

In shallow wells water does not always produce an increase in temperature; descending surface waters may produce negative deflections of the temperature-depth curve. In areas of volcanic activity circulation of thermal waters may produce unpredictable anomalies in the records (see paragraph 1). Since water-bearing beds are better heat conductors than dry formations, depth-temperature curves flatten at times near the surface (increase in reciprocal gradient) as the groundwater level is approached.[38]

In some instances, temperature curves indicate that water leaves a well at one level and enters it at another. In such cases, virtually uniform temperatures may be maintained for appreciable depth intervals.

7. *Cementation* problems are successfully handled by well-temperature surveys. To seal off water-bearing formations effectively, it is important to know at what point behind the casing the cement ring begins (Fig. 11-29). There is an appreciable rise in temperature during the setting period of the cement. For most Portland cements the temperature rise,

---

ʼ Van Orstrand, *Problems of Petroleum Geology*, p. 999 (1934).
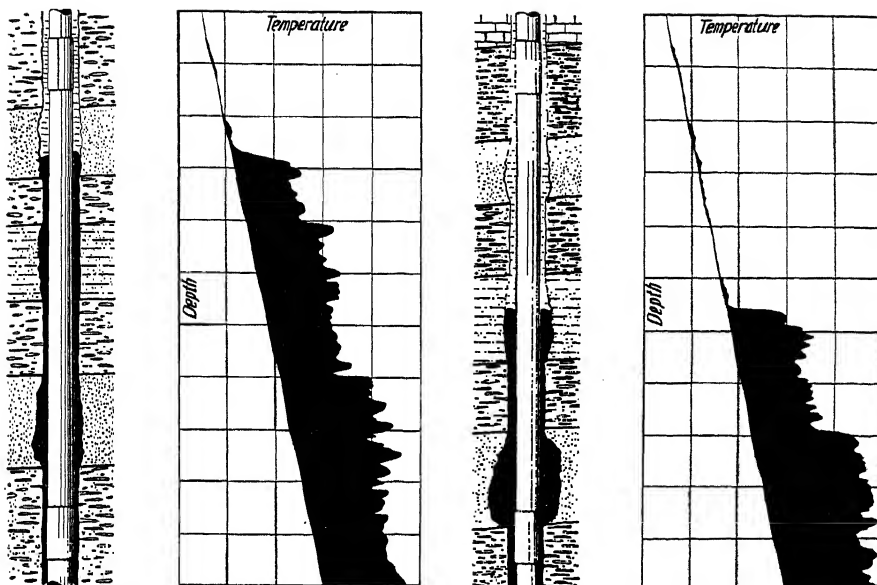
Fig. 11-29. Location of top of cement collar by temperature measurements (after Schlumberger).
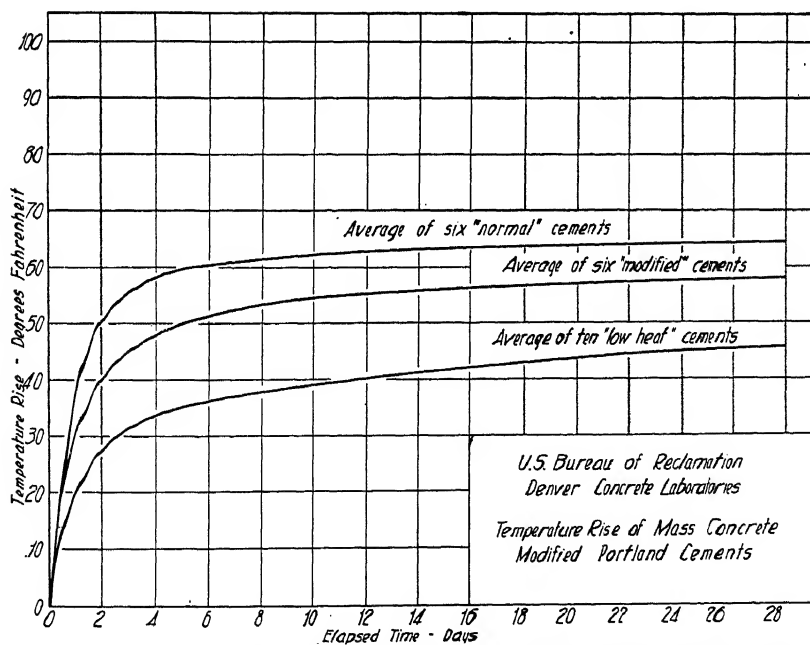
Fig. 11-30. Temperature rise during setting time of various cements (after Savage)

approached asymtotically within about one month (Fig. 11–30), is between 40° and 65° F. The corresponding temperature variation through well casing is of the order of 10°–20° F. and therefore quite readily detected.

8. *Other chemical transformations* affect well and underground temperatures when the reactions are of an exothermic nature. Well known in mining are such sources of heat as: active fires of broken sulfurous ores, or of coal, carbonaceous shales, and timber; the decay and oxidation of timber, aided by bacteriological action; and oxidation of sulfurous ores, coal, and shales (not sufficient to raise the temperature to the point of ignition). An example of this kind is the pyrite deposit of Sain Bel in France. Evidence of its oxidation is a zone of strong self-potentials above it (see page 676). In workings 100–150 meters deep, the temperature is as high as in other mines at depths of around 1000 feet. Although some increase of temperature occurs in the transformation of anhydrite to gypsum, the main reason for the high temperatures of salt domes is probably the high thermal conductivity of the salt.

E. EFFECT OF SURFACE RELIEF AND SURFACE TEMPERATURE

Since the earth's surface may be considered, in very close approximation, an isothermal surface, and since all irregularities due to near-surface distributions of conductivity and topography must be expected to be equalized at a certain depth (geothermal "isostasy"), it follows that the isothermal surfaces must be compressed under the depressions and expanded under topographic highs.[39] The deflections of the isothermal surfaces due to topographic irregularities may be calculated for a medium of constant diffusivity if the topographic profile and the gradients under the apex of a hill and the adjacent plane are known. This calculation is readily made for ridges of two-dimensional configuration.[40] Fig. 11–31*a* shows such theoretical isothermal surfaces for the topography at the Long Beach field, and Fig. 11–31*b* represents actual rock temperatures in the Moffat Tunnel near Denver.

Temperature variations at the surface of the earth penetrate into the ground to a depth which can be calculated from their periodicity. The diurnal variation is relatively unimportant for well measurements; its penetration is of the order of 3 to 4 feet. The annual variation, however, penetrates to a depth of about 80 feet in high and 50 to 65 feet in intermediate latitudes. For deep well measurements this variation is not important if observations are started below 100 feet. The variation must be

---

[39] This phenomenon is analogous (and mathematically almost identical) to the effect of topography on the equipotential surfaces in an electrical field (see p. 702).

[40] Van Orstrand, Physics, **2**(3), 144 (1932).

considered in shallow holes unless temperature differences between adjacent holes are measured. The temperature $\theta_{d,t}$ at a given depth d and
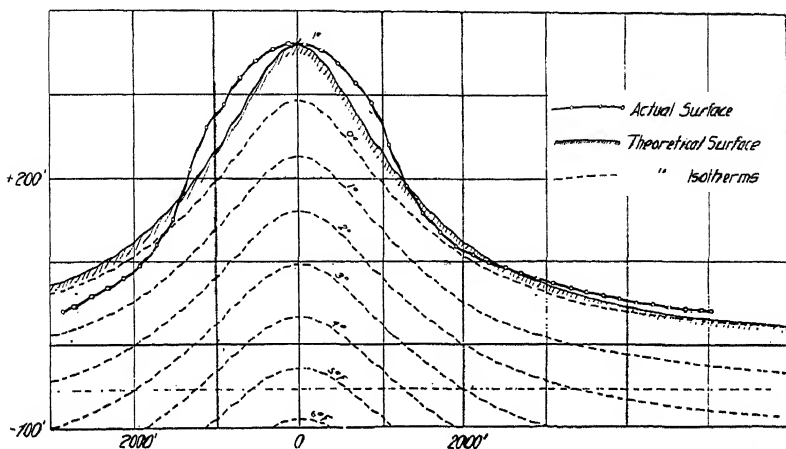
11-31a. Topographic effect (calculated) of Long Beach dome on isothermal surfaces (after Van Orstrand).
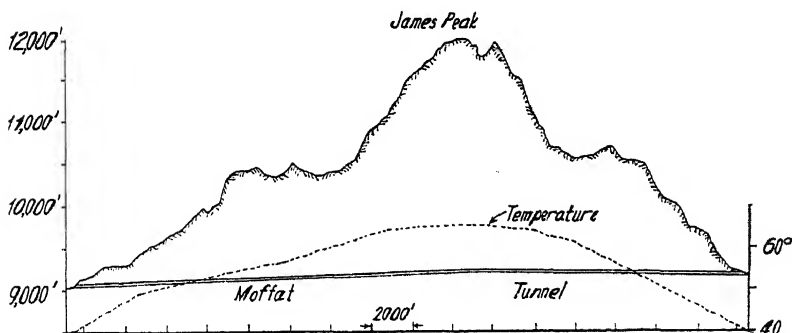
Fig. 11-31b. Observed temperatures in Moffat Tunnel near Denver (after Van Orstrand).

time t (in days, from a reference instant) may be calculated for ground of known diffusivity K from

$$\theta_{d,t} = \theta_m + \frac{\Delta\theta_a}{2}\cdot e^{-d\sqrt{\frac{\pi}{KT}}}\left(\cos\frac{2\pi t}{T} - d\sqrt{\frac{\pi}{KT}}\right), \qquad (11\text{--}11)$$

where θ_m is the mean annual temperature, $\Delta\theta_a$ is the annual range, and T is the period (365 days) of the variation. The exponential indicates the penetration, and the bracket term indicates the phase shift; K follows from eq. (11-4) and is expressed in m^2 per day, if depth is in meters and

time in days.   It follows from this equation that the depth penetration of the daily variation is $1/\sqrt{365}$, or 1/19, of that of the annual variation.

III. SEISMIC MEASUREMENTS

Seismic measurements in wells are made (1) to determine the vertical velocity distribution, (2) to extend the range of refraction exploration vertically and laterally, and (3) to determine crookedness of holes.

Seismic (*deep*) well shooting is applied widely to secure data on velocities along refraction and reflection paths.   To this end, shots are fired a certain distance away from the top of a well, detectors are lowered to successive depths, and travel times are recorded.   This method was mentioned on page 465 in connection with total and differential vertical velocity determinations.   On page 568 its relation to average reflection velocities was discussed.   Seismic well shooting detectors are usually reluctance seismographs of small diameter.[41]   Several units may be arranged in tandem to increase the sensitivity.   Precautions are required to protect their interior from the pressure of the drilling fluid.   Shot instant and travel times are recorded as usual; over-all or differential velocities can then be readily calculated if the depth to the detector or detectors is known.   For distances from the top of the well comparable to the detector depths (oblique incidence) more elaborate calculations are necessary[42] in order to obtain the vertical velocity distribution from travel-time records (see Fig. 11-32).

In *shallow* holes the procedure is reversed and shots are fired at the bottom of the hole while the detectors are set up at the surface.   This is the present practice in connection with weathered–layer procedure and for securing average vertical travel times and velocities at the shot point (see page 576).

In the vicinity of salt domes, faults, and other vertical contacts which are difficult to delineate by surface refraction measurements, deep wells can be used to advantage to extend the vertical range of refraction observations.[43]   Detectors lowered into wells on the outside of a dome will help to obtain more data on the flank formations.   Wells used with shot points on the opposite side of the dome are useful for determining overhang. The velocities in the salt and surrounding formations at various depths are usually well enough known to determine proportionate paths in the salt and in the sediments.

The crookedness of drill holes may be measured by seismic procedures

[41] C. A. Heiland, Explosives Engineer, Dec., 1935, Fig. 14.
[42] C. H. Dix, Geophysics, **4**(1), 24–32 (1939).
[43] B. McCollum and W. W. LaRue, Oil Weekly, June, 1931.

in areas of simple stratigraphic and structural conditions.   If a detector
is lowered to the bottom of a well, and if shots are fired at three or four
equidistant points (with reference to the top of the well), the travel times
are equal, provided the bottom of the well is located exactly below the
top.   If the travel times differ, the corresponding hole deviation may be
calculated from the geometric relations involved.[44]   The accuracy of this
method is not comparable to that of standard well surveying procedures.
In addition, its application is limited to areas in which the velocity distri-
bution around a well is absolutely uniform.
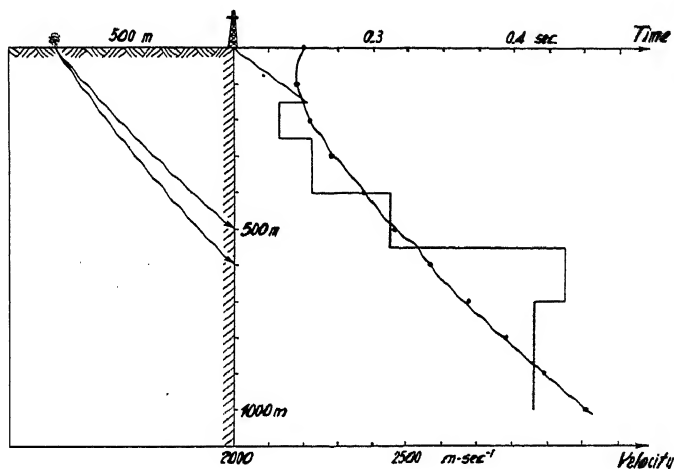
FIG. 11-32. Travel times (heavy curve) to various well depths from a point 500
meters off well top, with calculated velocity distribution (light curve) (after Dix).

IV. MISCELLANEOUS MEASUREMENTS IN WELLS

A. DETERMINATION OF RADIOACTIVITY

Measurements of radioactivity of rock samples taken from wells, mine
workings, and tunnels have been made (since about 1905) by various
investigators; the literature has been compiled by Ambronn.[45]   In most
instances the α radiation was examined, and radioactivity and type of
formation could be correlated.   Continuous measurements in *deep* wells
by the wire-activation method were suggested by B. Ostermeier.[46]

   Interest in radioactive well examination was recently revived, inasmuch
as the penetrating γ radiation is about the only rock property permitting

[44] D. C. Barton, A.I.M.E. Geophys. Pros., 587 (1929).

[45] *Elements of Geophysics*, pp. 125–126.

[46] Zeit. Tech. Phys., 7, 196–198 (1926).

of well logging through casing.[47]　A radioactive well logging arrangement
is shown in Fig. 11-33.　Two Geiger counters[48] (to eliminate chance varia-
tions) are connected separately through two low-impedance secondary
transformers to two A.C. amplifiers feeding into thyratron-controlled fre-
quency meters.　The latter are provided with a tank circuit (12 micro-

farads across 1 megohm) to
smooth out the current varia-
tions, so that the galvanometer
indication is proportional to
an average pulse frequency.
The measuring cylinder may
be lowered and records may
be taken at a rate of about
1500 feet per hour.　As Fig.
11-34 indicates, the γ-ray in-
dication is markedly parallel
to the potential and to the
impedance record of the elec-
trical log.　High porosity sands
are indicated by radioactivity
lows, shales by radioactivity
highs.[49]　The sand indications
do not appear to be affected
by variations in oil content.
While α-ray determinations
made on oil sand cores show
an increase of radioactivity,
γ-ray logging does not seem to
be sensitive to the presence of
oil.　However, it has been
found that gamma rays will
pick up readily the presence
of unconformities, which is
probably due to the concen-
tration of radioactive materials
on such surfaces.　Comparison

FIG. 11-33. Geiger-Mueller tube arrangement
for gamma-ray well logging (after Howell and
Frosch).

of the two lower curves in Fig. 11-34 gives an idea of the absorption of
gamma radiation in the well casing.

[47] L. G. Howell and A. Frosch, Geophysics, 4 (2), 106–114 (1939).

[48] See pp. 881–883.

[49] The high radioactivity of shales is due largely to the ability of colloids to absorb
radioactive substances and possibly to the presence of potassium compounds
(see p. 875).

Measurements of radioactivity in *shallow* holes are made in connection with the mapping of faults, contacts, dikes, radioactive ores, and the like. In this case the emanation method is applied. This involves the withdrawal of soil air from the hole into an emanation chamber, as described on pages 880–881.

B. MAGNETIC MEASUREMENTS

Most magnetic well investigations involve laboratory tests of cores after removal from the well. Procedures for determining magnetic susceptibilities, remanent magnetization, and hysteresis curves of cores were described on pages 300–309. In the magnetic core orientation method devised by Lynton[50] (Sperry-Sun), the direction of dip is determined by locating the direction of magnetization in a well sample. With the exception of
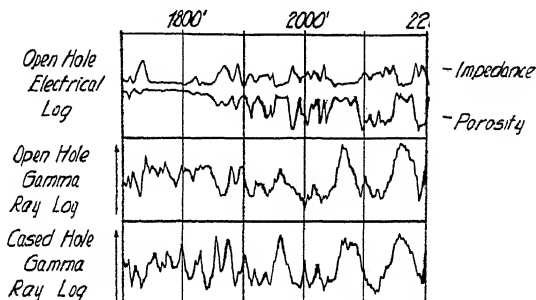
FIG. 11-34. Comparison of electrical (impedance and potential) logs with gamma-ray logs in open and cased hole (after Howell and Frosch).

limestones, anhydrites, and dolomites, cores with distinct bedding planes generally retain a sufficient amount of magnetism after removal and shipment. As shown in Fig. 11-35, the core, with axis horizontal, is placed close to the lower needle of an astatic magnetic system which, with the core, is shielded by a steel cylinder. The core is revolved slowly through 360°, and the deflection of the system is recorded photographically. The record will show a sine wave whose extreme amplitudes are proportional to twice the remanent magnetization. The effect of induced magnetization which shows no reversal with rotation[51] may be eliminated by taking a second run in reverse direction and forming the difference of the two curves. To obtain absolute dip, a correction for the crookedness of hole must be made.

Magnetic measurements have also been used in wells to determine their

---

[50] A.A.P.G. Bull., **21**(5), 580–615 (1937); Geophysics, **3**(2), 122–129 (1938).
[51] See Chapter 8, section II B, p. 300.

deviation from vertical and the azimuth of deviation. For this purpose, an earth inductor with vertical axis of rotation has been applied. As in the earth inductor compass,[52] the e.m.f. induced in the coil depends on the orientation of the brushes, and, therefore, on the orientation of the apparatus with respect to the magnetic meridian. By suspending a pendulum (which can be magnetized at will from the surface) in a universal joint vertically above the coil, an e.m.f. is produced when the apparatus (and the hole) is not vertical. An accuracy of 0.5° is claimed.[53] This apparatus can naturally be used only in an open hole.

It appears possible that earth-inductor measurements can be used to determine the magnetization of subsurface formations in open hole.
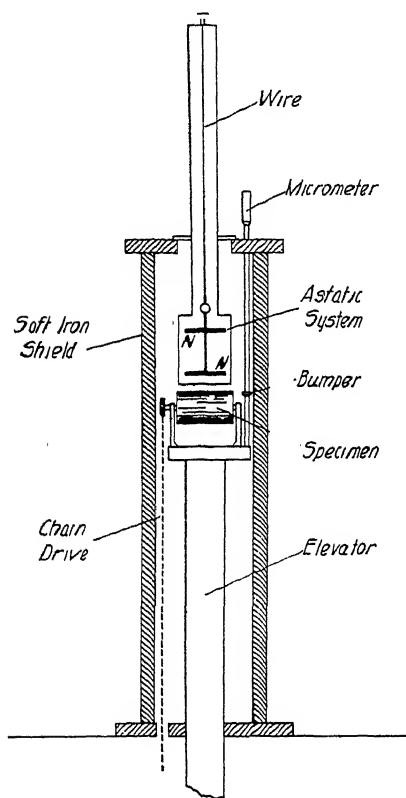
FIG. 11-35. Magnetic core orientation apparatus (after Roberts and Webb).

C. ACOUSTIC MEASUREMENTS

Water flows in *deep* wells and gases escaping from formations, or from behind the casing, may be detected by acoustic measurements. Geophones of high frequency (about 1000 cycles) are lowered into the well in the same manner as are seismic detectors.

In *shallow* holes (maximum of several feet) acoustic measurements are applied in the location of leaks in water pipes under pavement, sidewalks, and the like. A rod provided with a directional vibration pickup may be lowered into the hole so that (since the approximate course of a buried pipe is generally known) the longitudinal component in the direction of the pipe, as well as the transverse component of vibration produced by a leak, may be measured.[54] Since the transverse component is much more

[52] See Chapter 8, section III c, p. 363.

[53] C. and M. Schlumberger and E. G. Leonardon, A.I.M.E. Geophys. Pros., 269, (1934).

[54] Known as vibration differentiation method, Western Instrument Company (see also p. 962).

rapidly damped out than the longitudinal component which follows the pipe, the ratio of the two components at different frequencies (tuned amplifier) as a function of distance gives a clue to the location of the leak.

D. FLUID-LEVEL MEASUREMENTS BY SOUND REFLECTION

The depth to the fluid level in a deep well may be measured by recording the reflection travel time of an acoustic wave. The wave may be initiated by the release of compressed gas from a tank or by the firing of a cartridge. In the latter case the higher frequencies are filtered out mechanically by a tube which may be combined with a flame arrester.[55] The reflections from the fluid level and other obstructions in the well (such as tubing collars, tubing catcher, and the like) are picked up by a microphone, stepped up by a selective amplifier provided with automatic volume control, and are recorded photographically, or by a pen and ink recorder. The sound velocity is not constant under all conditions and depends on the composition of the gas mixture in the hole. An incremental velocity arises from the expansion of the gas used for initiating the impulse. The record may be readily calibrated, however, (1) by an auxiliary (coiled) tube of known length, (2) by the reflections from tubing collars of known depth, or (3) by the reflection from the tubing catcher or other reflector purposely placed at a known depth.

E. HIGH-FREQUENCY MEASUREMENTS IN OPEN HOLES

In the earlier days of geophysical exploration, much thought was devoted to the possibilities of high-frequency methods for determining the characteristics of formations in an open hole. These ideas probably received their impetus from the demand for some method of ascertaining wall thickness in connection with the freezing method of shaft sinking. Small leaks in the freezing pipes, spreading of the freezing pipes at the bottom, and other causes leading to a break in the ice wall were known to produce disastrous results. It was thought that the measurement of the damping of an antenna lowered into the shaft would give good leak indications, owing to the considerable difference in the conductivity of brine, and ice or frozen ground. The method was then extended to measure antenna capacity in open holes, with the object of determining the dielectric constant of the surrounding formations. These procedures were covered by a number of patents, since expired. Beyond a few brief references in the literature[56] nothing further has been published about them.

---

[55] J. J. Jakosky, Petrol. Tech., **2**(2) (May, 1939).

[56] G. Leimbach, Phys. Zeit., **14**, 447–457 (1913). H. Löwy, Phys. Zeit., **12**, 1001–1004 (1911); **20**, 416–420 (1919).

F. GAS DETECTION

In *shallow* holes, gas detection methods have been used to locate gas leaks in buried mains and pipes. A bar of small diameter is driven through the topsoil or pavement at closely spaced points, the sampling pipe shown in Fig. 11–36 is inserted, and the soil air is passed through a combustible gas detector, either by an aspirator or by open flow.[57] The detector consists of a sampling system and a hot wire detecting circuit. The sampling system is essentially a gas chamber with two platinum filaments; one of these is exposed to the gas sample, and the other is sealed in air. The filaments form two branches of a Wheatstone bridge that becomes unbalanced when the temperature (and, therefore, the resistance of the gas
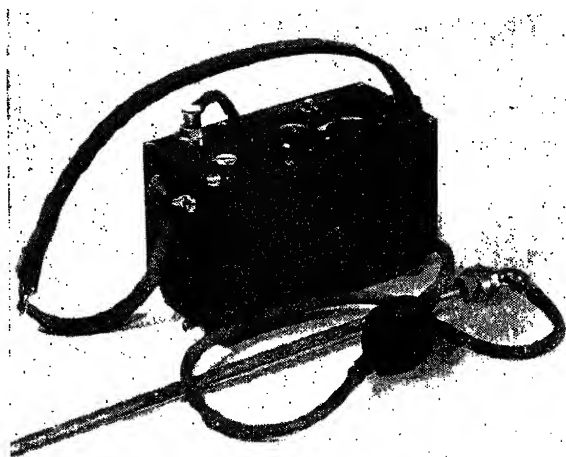
Heiland Research Corp.

FIG. 11-36. Combustible gas detector with sampling tube and aspirator.

filament) increases as the result of gas combustion. A triple-screen explosion check surrounds the filaments inside the gas chamber. By systematic reconnaissance and detail surveys it has been found possible to locate leaks correctly in 90 per cent of the surveys made.

Gas surveys for the location of subsurface oil and gas accumulations are likewise made in shallow holes. These methods require detectors of much greater sensitivity, as described on pages 892-898. The double filament detector previously mentioned may be used in a deep well provided the hole is uncased and dry. During drilling, the gas content of drilling fluid

---

[57] P. C. Dixon, Gas-Age Record, **76(24)**, 517 (Dec. 14, 1935).

can be logged continuously by connecting a gas detector to the discharge system in a suitable manner.

G. PHOTOELECTRIC MEASUREMENTS

When formation water is discharged into a well, the transparency of the drilling fluid increases. This change may be measured by a photoelectric detector. This unit contains a light source which projects a beam through a portion of the drilling mud to a photoelectric cell connected to a pre-amplifier. The resulting current fluctuations are further amplified and are recorded at the surface. In operation, the well is first conditioned with a light mud and then bailed out sufficiently to allow formation water to enter the hole.[58]

H. SIDE-WALL SAMPLER BULLETS

These bullets are short cylindrical shells fastened to two retaining wires and are shot electrically into the sides of an open hole. The cores thus recovered are analyzed in the laboratory for porosity, permeability, salinity, and content in colloids and organic matter. This procedure is useful for correlation with electrical resistivity and porosity (self-potential) logs; but, strictly speaking, it is not a geophysical method. Details are given in the paper by E. G. Leonardon and D. C. McCann.[59]

---

[58] Gillingham and Steward, *loc. cit.*
[59] Petrol. Tech., **2**(**2**) (May, 1939).

I 2

MISCELLANEOUS GEOPHYSICAL METHODS[1]

I. RADIOACTIVITY MEASUREMENTS

A. GENERAL

APPLICATIONS OF radioactivity measurements in geophysical exploration are concerned with the location of concentrations of radioactive material and radioactive rocks. Other applications of radioactivity in geology, such as its possible contribution to the earth's temperature and its use in the measurement of ages of rocks, are not discussed in this chapter. As a whole, radioactive substances are fairly uniformly distributed all over the earth and are present in the atmosphere, the water, and the solid earth. Local enrichments occur by association with certain rocks (mostly acidic igneous rocks), absorption in certain liquids (radon in water and oil), and confinement to predetermined transportation channels (faults, crevices, dikes, and the like).

As is well known, radioactivity is a group of phenomena characteristic of substances with high atomic weight (except potassium and rubidium), of which the best-known examples are uranium, radium, and thorium. Probably tremendous energies were required to build up and hold these atoms together in the very early stages of the earth's history. Since these conditions no longer prevail, they are now in a process of spontaneous decomposition. This process affects almost entirely the nucleus of the atom and is therefore unaffected by ordinary physical and chemical processes such as heat, electrical and magnetic fields, and mechanical pressure. It can be changed and produced, however, by bombardment of the nucleus with particles comparable with, or identical in velocity and nature to, those released by radioactive atoms. If it were possible to produce such nuclear changes by thermal energy, temperatures of the order of 10^{10} degrees C. would be necessary (Nernst). While in chemical transforma-

---

[1] The symbols in this chapter are the same as in Chapter 9, except where otherwise noted.

tions and combinations the nuclear properties, such as mass and charge, remain unchanged, the radioactive decomposition of the nucleus alters its mass and charge and, therefore, alters the number of electrons in the outer orbit and usually its chemical properties.[2]

Nuclear transformations in radioactive substances are accompanied by a release of energy in the form of corpuscular emission, heat, and other electromagnetic radiation. The corpuscular emission may be positive electrically, analogous to "canal" rays. It is then referred to as alpha radiation. If it is negative (analogous to "cathode" rays), it is called beta radiation. The electromagnetic radiation may be at the low-frequency end of the spectrum. Then it is noted as heat and will not be further discussed here. It may also be at the very high-frequency end of the spectrum. If so, it is more penetrating than X rays and is spoken of as gamma radiation. As the decomposition of radioactive products proceeds and new elements are formed, the character of these radiations changes. Some of them emit only alpha, others only beta and gamma, and still others all three radiations. As a rule, their velocities (and for the gamma rays, their absorption) are characteristic for the element present. In other words, it is possible to identify radioactive elements by their radiation. Moreover, the radiation *intensity* is found to be proportional to the *quantity* of radioactive matter present. As a matter of fact, radioactivity measurements are virtually the only means of quantitative study of radioactive elements, since approach by chemical analysis is not only difficult but frequently impossible.

Very schematically, the origin and relation of the various radiations is as follows: Within the nucleus there is probably a central nucleus (Rutherford) which carries virtually all the mass of the atom. Its number of positive charges is equal to the atomic order number (92 for U, 88 for Ra, 82 for lead, and so on). This central nucleus may be assumed to be surrounded by neutral helium satellites (possibly on internuclear quantum orbits) consisting of alpha particles with two electrons. When these electrons are lost, a doubly positive alpha particle is expelled with tremendous energy by repulsion from the central nucleus. The alpha particles have the greatest individual energy of any particle known to science. They are identical in mass for all types of radioactive elements emitting them and have velocities approaching 10,000 miles per second. Each radioactive substance produces alpha particles of characteristic speed. The shorter the period of transformation of a radioactive element, the greater is the velocity of the alpha particle. One gram of radium emits

---

[2] This chemical change is most striking in the case of radium, which is a solid resembling barium, then changes into a chemically inert gas (radon) which in turn changes to a solid (Ra A).

alpha particles at the rate of 3.6 x 10^{10} per second. These particles are assumed to consist of two neutrons and two protrons ($= H$ nucleus, mass $=$ 1 unit,[3] charge 1 unit positive). Therefore, when an alpha particle is released, the *atom number decreases two units* and the *atomic weight four units.*

Despite their great velocities, alpha particles are readily stopped, the fastest (of thorium C′, $\mathbf{v} = 2$ x 10^9 cm·sec.$^{-1}$) being absorbed by air of 8.62 cm thickness. An aluminum foil of 0.05 mm thickness is sufficient to keep the apha radiation out of an ionization chamber. In different elements the range of the apha particles is proportional to the square root of their atomic weights. Nevertheless, it is probably the *most important* radiation for the measurement of radioactivity, particularly in connection with *emanation* measurements. In a chamber of 10 cm side length, the ionizing effects of alpha, beta, and gamma radiations are as 10,000:100:1.

When an alpha particle is released, two electrons become available and may be captured by the central nucleus or shot off as beta particles. Only one of the radioactive elements (radium C) emits beta particles simultaneously with alpha particles. The others alternate, by themselves or in groups, between emitting alpha and beta particles. The release of a beta particle (charge $- e$) raises the atomic number by one unit, but it is not believed to affect the atomic weight (since $m = 1/2000$ unit). The velocity of beta rays may be as much as 99.8 per cent of light velocity. The harder components are very penetrating. An aluminum sheet of 0.5 mm thickness absorbs about one-half of the uranium beta rays. This radiation possesses much less energy than does the alpha radiation. More than half of the beta radiation incident on a metal plate is reflected and dispersed; when it passes through matter, X rays are generated.

Similar in nature is the emission of *gamma* ("penetrating") rays from the nucleus of the radioactive atom. Since gamma rays never occur by themselves but always in conjunction with alpha or beta radiations, it is probable that they are produced by internuclear orbit rearrangements following the emission of beta particles Some of the softer radiation possibly originates outside the nucleus by changes in the inner electron orbits. The wave length of gamma rays is of the order of 10^{-9} to 10^{-11} cm. Their penetrating power is so great that 55 mm of aluminum or 12 mm of lead is required to reduce the gamma radiation of radium by one-half. Gamma rays produce a secondary beta radiation (whose penetrating power is almost as great as that of the primary radiation) not only when they pass through other materials but also in their own atoms by releasing electrons from the inner extranuclear orbits. The absorption of

---

[3] The unit of mass is 1/10 of the weight of the oxygen atom or approximately equal to the atomic weight of hydrogen.

gamma rays depends on the density of the substance traversed and is, therefore, usually expressed in terms of a "mass-absorption-coefficient."

It is seen that all radioactive radiations are analogous to tube discharges in high electrical fields. For instance, the energy of an alpha particle of Ra C' is 8 million electron-volts. To produce electrons having the same velocity as the beta rays from Ra C', 3 million volts would be required. To excite X rays of the frequency of gamma rays (10^{19} to 10^{20} cycles), a tube with 2–3 million volts would be necessary. Incidentally, the voltages employed in atom-smashing machines are of this magnitude.

It was mentioned before that radium breaks up into one atom of (ionized) helium and another of radon (radium emanation). This gas is of special importance in the technique of radioactivity measurements, since its alpha radiation and the quantity of radium in radioactive equilibrium with it can be readily determined. At normal pressure and temperature, 0.6 mm^3 of radon weighing $6 \cdot 10^{-6}$ grams is in equilibrium with 1 gram of Ra and is called a *curie*. For radioactivity tests of liquids, the Mache unit (1 M.U. $= 4 \cdot 10^{-10}$ curie units) is often used. This represents the amount of radon in one liter producing a "saturation" current[4] of $1 \cdot 10^{-3}$ e.s.u., that is, 1 curie produces a saturation current of $2.5 \cdot 10^5$ e.s.u.'s. Compared with radon, the corresponding gases in the thorium and actinium series are unimportant because of their rapid decay. The half-value period of thoron is 54 seconds, that of actinon 3.9 seconds, and that of radon 3.82 days.

B. RADIOACTIVITY OF ROCKS

The radioactive elements and decay products, respectively, of uranium, thorium, actinium, rubidium, and potassium are, geologically, of very unequal distribution and importance. Rubidium and actinium are so rare that they may be disregarded completely. Although potassium occurs abundantly and often rather uniformly throughout geologic formations, its radiation is of low intensity and noticeable only where rocks contain potassium compounds in chemically recoverable quantities.[5] Of the two remaining radioactive elements, uranium is geologically more important. Its decomposition series contains a greater number of products of long life and strong radiation than does the thorium series. In the uranium series, radium and associated products are most readily detected in quantities much beyond the reach of the analytical chemist. It is customary to express the radioactivity of rocks in units of 10^{-12} grams per gram (or

---

[4] See p. 880.
[5] G. Kirsch, Handb. Exper. Phys., **25**(2), 32 (1931).

cm^3) of substance.   The radioactivity of gases is generally characterized by the amount of Ra-emanation present.

Table 79 gives a few representative figures for the radioactivities of soil, water, and air.   Table 80 gives a number of average values for the radium and thorium contents of igneous and metamorphic rocks.

The radioactivity of igneous rocks increases with an increase in SiO_2 content.   Basic rocks are generally less radioactive than are acidic rocks, although there are considerable regional and local variations.   The average

TABLE 79

REPRESENTATIVE FIGURES FOR THE RADIOACTIVITIES OF SOIL, WATER, AND AIR

	U (g/cm^3)	Ra /	Th (g/cm^3)	EM. (Curie/ cm^3)	PENETRATING RADIATION (ions/cm^3/sec.)
Soil.		$2.3 \cdot 10^{-12}$			3–5 I[a] (up to 20 I on radium deposits)
Water......		10^{-14} to 10^{-16}	10^{-7} to 10^{-8}		
Soil air.....				2·1	
Atmos. air.				10^{-16}	about 4 I on land
				10^{-18}	0–2 I at sea

[a] I = ions.

TABLE 80

AVERAGE RADIOACTIVITIES OF IGNEOUS ROCKS[6]

ROCK	Ra (10^{-12} g/g^{-1})	Th (10^{-6} g/g^{-1})	ROCK	Ra (10^{-12} g/g^{-1})	Th (10^{-6} g/g^{-1})
Granites	2.7	20	Gabbro, norite	1.3	5.0
Quartz-porphyry	3.9	22	Diabase, dolerite	1.0	2.2
Syenite	2.4	17	Basalt	1.4	5.6
Diorite	1.6	9.9	Basalt, high values	5	15
Trachyte	3.0	17.9	Basalt, low values	0.5	4
Porphyrite	2.8	15.4	Recent lavas	2–20	
			Gneiss	2.1	8.7

[6] After Kirsch, *loc. cit;* A. Born, Lehrb. Geophys, p. 26.

for acidic igneous rocks is about $3 \cdot 10^{-12}$ g Ra g^{-1}; for basic rocks the average is about $1 \cdot 10^{-12}$ and may reach $0.5 \cdot 10^{-12}$ for extremely basic constituents.   Effusive rocks are more radioactive than are plutonic rocks; the radioactivity of metamorphic rocks is largely dependent on whether they are derived from igneous or sedimentary rocks.

The average radioactivity of sediments is comparable to that of the basic igneous rocks, as shown in Table 81.   This tabulation does not include the (recent) deep-sea sediments which range from about 10 to $40 \cdot 10^{-12}$ g Ra.

Radioactive mineral concentrations, not only in sedimentary but also in igneous rocks, may exceed their surroundings in radioactivity by 1000 to 100,000 times. Radioactive ores low in uranium oxide (from 0.3 to 0.5 per cent) have a radium content of the order of 10^{-9} g Ra g^{-1}, while those of high concentration (80 per cent uranium oxide) reach 10^{-7} g Ra g^{-1}. Of interest is the observation of Béhounek that the range of a radium deposit is fairly limited.[8] The pitchblende deposit in Joachimstal could not be detected at distances exceeding 1000 feet. It is further significant that the anomalies caused by local concentrations of radioactive products (faults, and the like, see below) may exceed those due to radioactive ores. Hence, radioactivity prospecting is more useful for detailing local concentrations than for finding radioactive ores by reconnaissance.

Likewise, the delineation of rocks of different radioactivities, the separation of sedimentary from igneous rocks, and similar applications based on the data given in Tables 80 and 81 will be possible only in exceptional cases because of interferences from such local concentrations. On the

TABLE 81
RADIOACTIVITIES OF SEDIMENTARY ROCKS[7]

Rock	Ra (10^{-12} g g^{-1})	Rock	Ra (10^{-12} g g^{-1})
Slates	3–8	Limestones	2–3
Quartzite	5	Gypsum	7
Sandstones	2–4	Dolomites	8

[7] Largely after Born, *loc. cit.*

other hand, radioactivity methods can be quite useful for locating faults, fissures, and other openings along which radioactive products have been deposited or radioactive waters are circulating. Radon is readily absorbed by water much in the same manner as is carbon dioxide; it also has a tendency to accumulate in porous and shattered rocks, that is, in and near fractured and faulted zones. Experiments indicate that, to be radioactive, it is not necessary for such concentration channels to remain open; mineral dikes deposited in fault zones exhibit as much and sometimes more radioactivity than do open fracture zones. Organic matter appears to have a considerable affinity for radon. For instance, oil absorbs from 40–50 times as much radon as does water (at temperatures from 20°–60°C.). Certain spring sediments containing vegetable matter are more radioactive than are the rocks on which they are deposited. Deep-sea ooze rich in animal remains is more radioactive than are ordinary sediments. Radioactive ores are frequently found in beds rich in carbonaceous matter and

[8] Fr. Béhounek, Phys. Zeit., **28**, 333–342 (1927).

plant remains. In some localities carnotite is associated with fossil wood. An increased radioactivity of oil sands has been observed when the drill cores were tested by the alpha-ray method. However, gamma-ray logging has failed to indicate an increase in this radiation.[9]

Radioactivities of minerals and rocks may be determined in the laboratory in three ways: (1) by measuring the total radiation of a given weight of substance in an ionization chamber, (2) by preparing a solution and measuring the radiation of the radon contained in it, (3) by measuring the
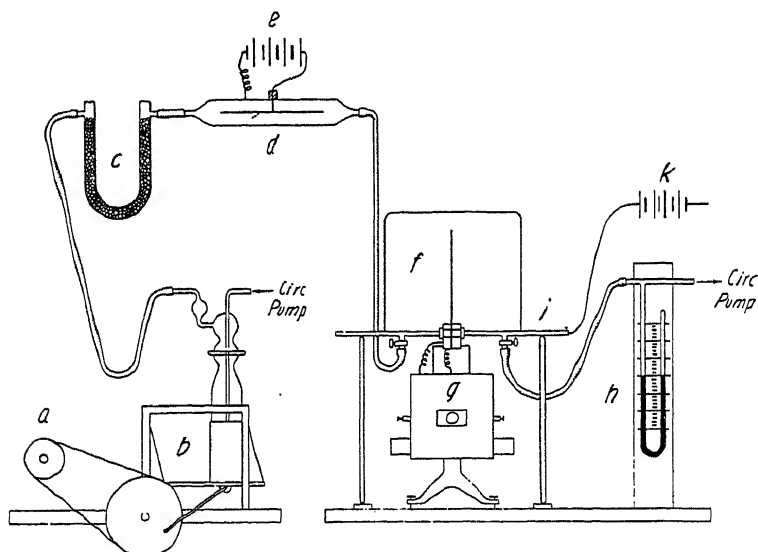
FIG. 12-1. Measurement of rock radioactivity by emanation method (Mache and Bamberger, after Kirsch). (a) Motor, (b) shaking table, (c) drying tube, (d) ion trap, (e) dry-cell battery, (f) ionization chamber, (g) electroscope, (h) manometer, (i) guard ring, (k) battery.

penetrating (gamma) radiation of a given weight of substance with a Geiger counter or gamma-ray electroscope.

Measurements under (1) are made as follows: The specimen is ground, dried, and weighed; and a definite amount (say 2 g) is placed in the tray of the ionization chamber of an electroscope whose scale value (volts per scale division) and normal dispersion rate are known. Assume the former to be 51 volts per scale division and the latter 3.5 millivolts per second. Then, if a 2-g specimen produces a total decay of 10 scale divisions in 8 minutes, 50 seconds, the reduced decay is $96.2 - 3.5 = 92.7$ millivolts per second, and the decay per unit weight is proportional to $46.4 \cdot 10^{-3}$

---

[9] See p. 864.

volts·sec^{-1}. The equivalent Ra content is obtained by comparison with a standard powder of identical thickness. If the standard weighs 3 g and produces a decay of 10 scale divisions in 1 minute, 8 seconds, the reduced decay is $(750 - 3.5)/3 = 238.8·10^{-3}$ volts·sec^{-1} per gram of substance. Assuming the standard to contain $2.5·10^{-8}$ g Ra g^{-1}, the equivalent radium content of the specimen is $(46.3/238.8)·2.5·10^{-8} = 4.86·10^{-9}$ g Ra g^{-1}. In this method, therefore, the entire radiation (inclusive of that of thorium) is expressed by the equivalent Ra content.

Measurement of the activity of the emanation under (2) gives the Ra content alone.[10] The specimen is ground up and about $\frac{1}{2}$ g is fused with
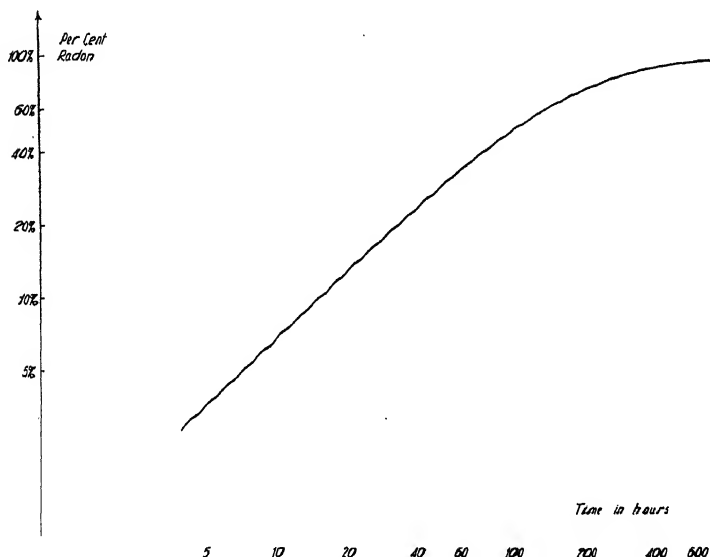
Fig. 12-2. Percentage of radon (developed in confined space) as a function of time

sodium carbonate. The alkaline and basic solutions are kept separately in two sealed flasks for about twenty-five days. Within this time a maximum amount of radon has developed and is in radioactive "equilibrium" with the Ra in the solution, since, from then on, as much radon is formed as in turn decomposes. For strongly radioactive solutions it is not necessary to wait twenty-five days, since the amount of radon present at any time may be calculated in relation to the maximum amount developed (see Fig. 12-2). One of the flasks is then placed on a shaking platform as shown in Fig. 12-1, and air is forced through the solution by a pump or aspirator whose intake connects to the ionization chamber outlet so that

---

[10] Within the time required for this experiment, the short-lived thoron (54 sec. half-value time) has decayed completely.

air is continuously circulated through the apparatus. The air-radon mixture then passes through a drying tube and ion trap, and then into the ionization chamber.

The calculation of the equivalent radium content is done as follows, after a standard Ra solution has been treated in the same manner as the acid and alkaline solutions of the sample. If $\frac{1}{2}$ g of rock was treated and the acid solution was left alone for 26 hours, 17.9 per cent of the maximum radon was formed. When the air-gas mixture was forced through the ionization chamber, the dispersion was 10 scale divisions in 2 minutes, 22 seconds. With a scale value of 51 volts and a normal dispersion of 3.5 millivolt·sec^{-1}, this is $359 - 3.5 = 355.5 \cdot 10^{-3}$ volts·sec^{-1} and, reduced to maximum emanation emission, $1985 \cdot 10^{-3}$ volts·sec^{-1}. The alkaline solution was kept more than thirty days and produced, in 8 minutes, 10 seconds, a decay of 10 scale divisions. This yields, with the above scale value and normal dispersion, $104 - 3.5 = 101.5 \cdot 10^{-3}$ volts·sec^{-1}. If this is added to the decay of the acid solution and reduced to 1 g of substance, the emanation yield of the specimen is proportional $4173 \cdot 10^{-3}$ volts·sec^{-1}. To obtain the equivalent Ra content, the specimen is now compared with a standard solution of, say, $1.19 \cdot 10^{-9}$ g Ra, which, when treated in the same manner as the two sample solutions, produces a dispersion of $200 \cdot 10^{-3}$ volts·sec^{-1}. Hence, the specimen contained $(1.19 \cdot 10^{-9} \cdot 4173)/200$ or $2.29 \cdot 10^{-8}$ g Ra g^{-1}.

In method (3) the radium content of a specimen is determined from its penetrating radiation. The specimen is set up at a fixed distance from the electroscope, which may be protected from the alpha and beta rays by a lead screen about $\frac{1}{4}$ inch thick. The equivalent Ra content may be determined by comparison with a standard. The electroscope method is suitable only for strongly radioactive minerals and rocks; more universally applicable are Geiger counters (see section c). The specimen is placed at a fixed distance from the counter and its radiation is compared with that of a standard preparation. It is advantageous to surround the lower half of the counter (axis horizontal) with a heavy lead shield and to expose only the upper half of the counter tube[11] to the radiation so that the effective counter area is the section of the tube. The ionization of the gamma radiation from a milligram of Ra at a distance of 1 m amounts to about 120 impulses[12] per cm^2 per minute of the effective counter area, and it decreases with the square of the distance.

C. Instruments and Procedure in Radioactivity Exploration

Radioactivity exploration may be carried out in two ways: (1) by taking soil samples and testing them in the laboratory for their radioactive prop-

[11] A. K. Das and K. Wölcken, Phys. Zeit., **31**, 136–139 (1930).
[12] *Ibid.*

erties, or (2) by determining the activity of formations *in situ* with portable ionization chambers. The first exploration procedure is identical with the methods described in the preceding section; the second group of procedures includes: (*a*) measurement of the entire radiation with *open-bottom* ionization chambers, (*b*) measurement of the soil-air *emanation* (mostly radon), and (*c*) measurement of the *penetrating* (gamma) radiation.

(*a*) An *open-bottom* ionization chamber is illustrated in Fig. 12-3. It consists of a metal box with insulated dispersion rod and double-leaf electroscope. The latter is detachable (as in most other chamber-electroscope combinations). The dispersion rod may be charged by a rubber rod or small dry-cell battery. The charge is so dimensioned that approximately the same leaf deflection is obtained for every measurement. The instrument is first tested in a room where no radioactive substances are present, and the normal dispersion rate is determined. When the chamber is placed on the ground (after the surface vegetation and top soil have been cleared off), the radioactivity of the surface formations and soil air will ionize the air in the chamber (mostly by alpha radiation) and produce a corresponding decay of the charge. In a calibrated[13] electroscope the potential difference corresponding to a scale division is known, and therefore the decay or dispersion dE/dt may be expressed in volts (or millivolts)

FIG. 12-3. Open-bottom ionization chamber (schematic, after Hummel). (1) Case, (2) electrometer, (3) leaf, (4) insulator, (5) dispersion rod, (6) charging rod.

per second. The latter is proportional to the conductivity of, and therefore to the (saturation) current, I, in the chamber:

$$I = C \cdot \frac{dE}{dt} \qquad (12\text{-}1)$$

C is the capacity of the chamber (in centimeters) and dE/dt is the dispersion (in statvolts = (volts/300) sec^{-1}). Current in amperes is obtained by multiplication by $1/9 \times 10^{-11}$ instead of by $1/300$. The current is proportional to the number (**n**) of ions formed, so that

$$n = \frac{C}{300 \cdot e \cdot V} \cdot \frac{dE}{dt}, \qquad (12\text{-}2)$$

[13] By a dry battery and precision high-resistance voltmeter.

where e is the elementary quantum of electricity or $4.77 \cdot 10^{-10}$ e.s.u.'s, V the volume of the chamber in cm³, and dE/dt is in volts·sec⁻¹.

In the calibration of the equipment, it is first necessary to be certain that saturation current is measured at all times. For this purpose the voltage loss dE/dt is determined for a given ionization and for various voltages. This gives the voltage range for which the current is constant. According to Kohlhoerster,[14] a 4-liter chamber has its saturation current for potentials exceeding 100 volts and a 2-liter chamber for potentials greater than 80 volts. If these measurements are to be made accurately, the air in the chamber must be completely dry. The same is required of the field observations. The volume V is determined by filling the chamber with water and weighing it. The capacity C may be obtained by calibrating the chamber with a standard U_3O_8 preparation of known dispersion, usually rated for 1 cm capacity and 1 cm² radiating surface. To avoid infesting the chamber with radioactive decay products, a duplicate chamber may be tested instead. Another method of measuring the capacity uses a U_3O_8 preparation and an additional condenser of known capacity.[15]

It has also been suggested that bore holes be used as ionization chambers and that a dispersion rod with electroscope be introduced after stationary conditions have been established.[16]

(b) The activity of the soil-air emanation (mostly radon) may be measured with the instrument shown in Fig. 12–4.[17] A hole several feet deep and about $1-1\frac{1}{2}$ inches in diameter is pounded down in the surface soil with a steel bar. A pipe having a bulge midway of its length to prevent the influx of atmospheric air is inserted in the hole. This pipe is connected to the intake of a suction pump whose outlet in turn connects by a rubber hose to the dryer and filter tube of the instrument. The soil air is thus forced under pressure through the chamber. After several strokes of the pump, the chamber is shut off by two cocks, and the measurement is made in the usual manner by observing the dispersion rate. An alcohol lamp is provided to obviate insulation difficulties resulting from moisture. It is necessary to sample the soil air always at the same depth; if possible, soils of nearly identical consistency should be used and observations should be taken within the same time interval after the air has been pumped into the chamber.

[14] W. Kohlhoerster, Phys. Zeit., **27**, 62 (1926); **31**, 280-288 (1930).

[15] Kohlhoerster, loc. cit.; V. F. Hess and A. Reitz, Phys. Zeit., **31**, 284 (1930); R. A. Millikan and G. H. Cameron, Phys. Rev., **31**, 921 (1928); and A. Lomakin, Inst. Pract. Geophys. Bull. 4, 151-156 (1928).

[16] J. Koenigsberger, Zeit. Prakt. Geol., **34**, 187–190 (1926).

[17] R. Ambronn, Phys. Zeit., **28(12)**, 444–446 (1927). A similar apparatus is described by A. Lomakin, op. cit., **3**, 124–136 (1927).

The type of emanometer described here may be applied also in measuring the activity of spring and soil waters ("fontactometer"). The water is placed in a bottle similar in construction to that shown on the shaking table of Fig. 12–1 and connected to a rubber bulb aspirator in such a manner that the air circulates continuously through the water and the ionization chamber. After the bottle has been shaken for about 1 or 2 minutes and the air been circulated for about the same time, the cocks of the chamber are closed and the electroscope is read in the usual manner.

The dispersion is referred to a water volume of 1 liter, and the current is calculated from formula (12–1) (in e.s.u.'s); multiplication by 1000 gives the activity in Mache units.[18]

(c) The *penetrating radiation* is measured with an ionization chamber which is shielded above and on its sides against the "softer" radiations.[19] Theoretically, a minimum thickness of 2.93 inches of (inactive) lead is required. Bogoiavlensky used a chamber with brass walls 3 mm thick and lead shields 10 mm thick. The bottom is closed off by filters of varying thicknesses, which make it possible to determine the absorption coefficient and therefore the wave length of the radiation. It is probable that the radiation increases in hardness with the depth of the source. In Bogoiavlensky's apparatus the filters were each 2.5 mm thick, the volume was 1650 cm^3, the capacity 0.725 cm, and the sensitivity 0.65 volts per division.

Fig. 12-4. Ambronn emanometer. (1) Ionization chamber, (2) electrometer, (3) microscope, (4) charging peg, (5) drying tube, (6) alcohol burner, (7) tripod.

Another convenient method of measuring gamma radiation is the use of a *Geiger counter*. In its most widely used form it consists of a wire surrounded by a cylindrical metal tube, sealed in a glass tube in an atmosphere of argon under about 8 mm pressure. The cylinder is usually at a negative potential with respect to the wire. Alpha and beta radiation is almost completely rejected by this type of counter. The gamma radiation, however, passes readily through the glass and liberates electrons

---

[18] Since one M.U. produces a saturation current of 1/1000 e.s.u.'s, see p. 873.

[19] L. N. Bogoiavlensky and A. Lomakin, Zeit. Geophys., **3**, 87-92 (1927); U. S. Bur. Mines, Circ. Inf. No. 6072, 1928; Inst. Pract. Geophys. Bull. **1**, 57, 69, 184 (1925), **2**, 184-195 (1926), **3**, 87-112 (1927), **4**, 165-178 (1928).

from the metal.   These electrons, in rushing toward the wire, form positive ions and new electrons, building up the current exponentially until the potential difference drops to a point where ionization by collison can no longer occur.   Thence, the potential recovers at a rate depending on the time constant of the circuit (current "pulse").   The current is practically independent of the number of ions formed by the original electron;[20] the same is true for open counters sensitive to alpha particles and beta rays. The pulses may be counted by an arrangement shown in Fig. 12–5 in
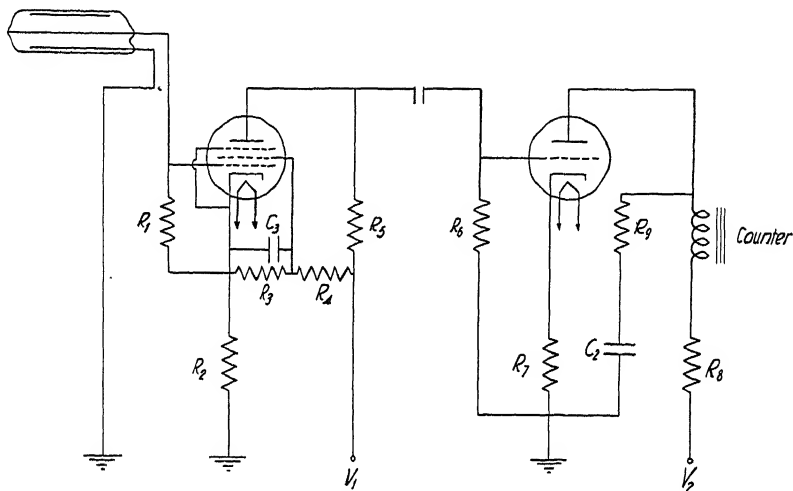
FIG. 12–5. Geiger–Mueller tube, with amplifier and counter (after Neher). R_1 = 5 meg.; R_2 = 1 meg.; R_3 = R_4 = R_6 = $\frac{1}{2}$ meg.; R_5 = $\frac{1}{4}$ meg.; R_7 =,10,000 ohms; R_8 = current-limiting resistor; R_9 = 80,000 ohms; C_1 = 50 $\mu\mu f$; C_2 = 0.2 μf; C_3 = 0.1 μf; V_1 = 100 volts; V_2 = 250 volts.   The tube following the counter is a 57 and the output tube an 885.

which the cathode, grid, and screen of the 57 tube and the wire of the counter are all at a high positive potential.   When a rush of electrons passes the counter, the grid goes negative, blocking the current through the tube.   Cathode, grid, and so forth, drop rapidly to ground potential. When the counter potential drops below the threshold value, the current ceases.   The negative charges leak off the grid; and the tube, counter, and associated circuit are recovered for another count.   The positive pulse thus produced gives rise to a gas discharge in the 885 tube, actuating the recorder K and charging the condenser C_2 which, by its effect on the bias, stops the discharge in the tube.   In a portable instrument, the high voltage batteries required for a counter are annoying and may be elimi-

---

[20] H. V. Neher, in J. Strong, *Procedures in Experimental Physics*, p. 259, Prentice-Hall, 1938).

nated by employing a V.T. oscillator, as shown in Fig. 12-6. Another feature of this apparatus is an output stage in which the pulses are rectified and passed into a tank circuit containing two 40-μf condensers and a counting-rate meter. The Geiger counter and first amplifier tube are carried in an extension handle connected to the remainder of the instrument, so that the ground radiation at any point may be readily investigated.
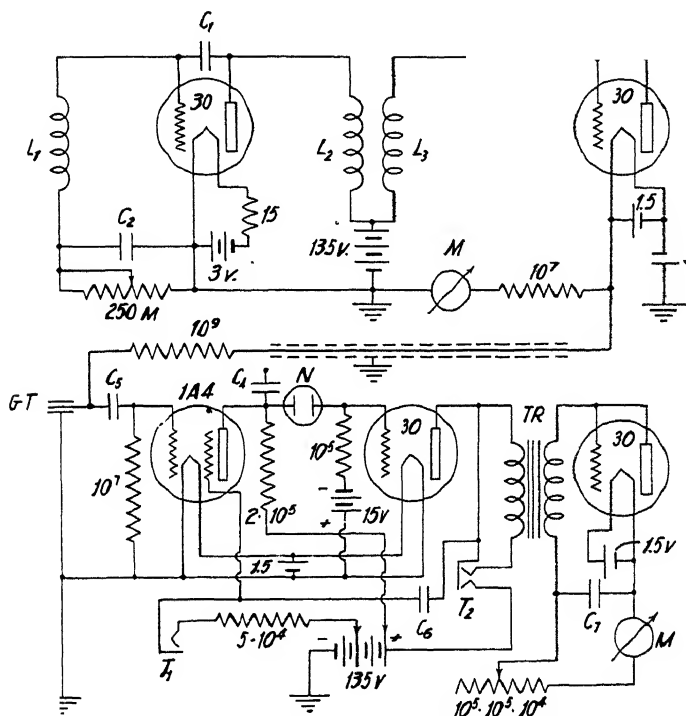
Fig. 12-6. Portable Geiger counter detector, with oscillator replacing high-voltage batteries (after Kaiser). $C_1 = 500\mu\mu f$; $C_2 = 0.01\ \mu f$; $C_3 = 0.02\ \mu f$; $C_4 = 0.01$ μf; $C_5 = 5\ \mu\mu f$; $C_6 = 0.5\ \mu f$; $C_7 = 80\ \mu f$ (midget electrolytic); N = G.E.-CD-1010-C1 neon lamp, 40 milliwatt; T_1, T_2 = telephone jacks; TR = output transformer, 1:6; GT = Geiger-Mueller tube; M = 0-200 or 0-100 microammeters; L_1, L_2, L_3 = oscillator air-core transformers.

D. Results and Interpretation of Radioactivity Measurements

Measurements of radioactivity have been made (1) in wells, to indicate oil sands or formation boundaries; (2) underground, to locate concentrations of radioactive ores; (3) at the surface, to locate radioactive ores; (4) to locate radioactive springs; (5) to locate oil; (6) to map faults and contacts; and (7) to locate mineral veins. These measurements have been

made by taking and testing samples, by open-bottom chambers, by emanometers, and by Geiger-Mueller counters.

Results of radioactivity tests of *oil well samples* have been published and discussed by Ambronn.[21]   In one of these, an increase of activity (alpha radiation) immediately below an oil sand was noted.   Because of the high absorbing power of oil for radon, a peak of alpha-ray activity should be expected to coincide with the sand.   As stated in Chapter 11,[22] there is no noticeable increase in gamma radiation in oil sands.   *Underground* observations of radioactivity for locating *pitchblende* seams have been reported by von dem Borne[23] and Béhounek.[24]   At a distance of 6 meters from a pitchblende seam, the latter observed an activity of 200 M.U. (per liter air, taken from drill holes) while at 17 meters distance the activity had dropped to about 3 M.U., and at 29 meters to about 2 M.U.   It is likely that measurements have been made at the surface for the same purpose in the more recently discovered radium districts of the Belgian Congo and in Canada, although definite reports have not been published. In balneological work, the activity of spring waters is tested in routine fashion.   The rather extensive literature on the subject has been reviewed by Ambronn.[25]   Location of oil by surface measurement of the penetrating radiation appears possible only on shallow deposits, according to Bogoiavlensky and Lomakin, who published the results of some experimental profiles across the Maikop field in Russia.[26]   Above these shallow deposits, the radiation increased only 1 or 2 ions, the error being of the order of 0.2 ions.

Radioactivity measurements seem best adapted to the location of faults, fissures, contacts, and some types of mineral veins.   An increased activity (alpha radiation) was first observed by Ambronn on some faults near Blankenburg and above an iron ore vein near Ilfeld in the Harz Mountains.[27]   Similar observations on fracture zones in the Black Forest (near Wildbad) were reported by Link and Schober.[28]   Mueller[29] verified these results on mineralized veins and contact zones in the Siegerland.   Some of his results are reproduced in Fig. 12–7.   Patriciu surveyed a number of profiles across the Leine graben near Goettingen and located some hitherto unknown fault zones through an alluvial cover of 20 or 30 feet.[30]

[21] *Elements of Geophysics*, p. 125, McGraw-Hill (1928).

[22] P. 864

[23] *Habilitationsschrift* (Breslau, 1905).

[24] *Loc. cit.*

[25] *Elements of Geophysics*, p. 131.

[26] *Op. cit.*, see p. 881.

[27] Jahrb. Hall. Verb, **3**(2), 21 (1921).

[28] Gas und Wasserfach, **69**, 225–28 (1926).

[29] F. Mueller, Zeit. Geophys., **3**(7), 330–36 (1927).

[30] Preuss. Geol. L.-A. N. F., 116 (1930); curves reproduced by J. N. Hummel, Handb. Exper. Phys., **25** (3), 537 (1930).

All the measurements discussed above were made by testing the activity of soil air.   According to Lane, a fracture zone could be located in Michigan by an analysis of the radioactivity of well waters.[31]   Measurements of the penetrating radiation are reported to show fault zones much less distinctly than do observations of the alpha radiation.[32]

If a fault is covered by a layer of alluvium, the thickness of cover may be calculated[33] by assuming a linear source of concentration, C_0, located
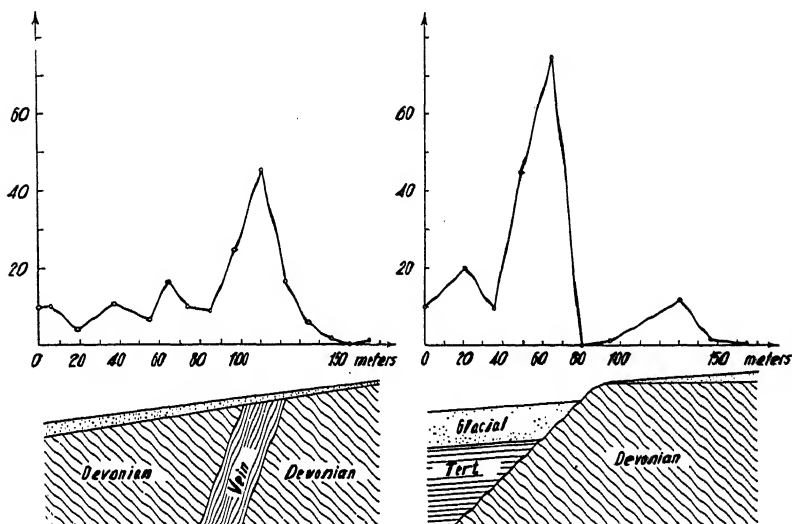
Fig. 12-7. Effect of mineralized dike and contact zone on radon content of soil air (after Mueller).

in the boundary between impervious rock and cover.   The gas ascends through the latter by diffusion.   A maximum concentration, C_m, is located directly above the source and is given by

$$C_m = C_0 \cdot \frac{d\pi}{2h}, \qquad (12\text{--}3)$$

where d is the sampling depth and h the thickness of the cover.   At a distance $x = 0.76\,h$ from the maximum, the concentration (activity) has dropped to one-half its maximum value.

II. HYDROCARBON (SOIL AND GAS) ANALYSIS

Methods for the detection of hydrocarbons in the surface soil are designated in the literature either as geochemical or geophysical.   Their classifi-

[31] Science, **79**, No. 2040, 34 (Feb., 1934).
[32] Ambronn, *op. cit.*, p. 131.
[33] Koenigsberger, Zeit. Geophys., 4(2), 76–83 (1928).

cation as a chemical method results from the fact that certain characteristic chemical compounds are the object of separation and quantitative detection, whereas their inclusion among geophysical methods is justified on the grounds that they constitute a definite prospecting method and that procedures of detection and analysis are physico-chemical if not entirely physical.

A. MACROSCOPIC AND MICROSCOPIC METHODS

Soil analysis, in principle, is a refinement of the observation methods used for some time by the geologist in his quest for indications of subsurface oil accumulations. Although these indications have always been present and some of them were well known to the ancients,[34] their significance was then not appreciated[35] and thus the vast subterranean reservoirs of oil and gas remained untapped up to the middle of the past century.

Surface indications of oil deposits may be of a direct nature, for example, emanations of hydrocarbons in the form of oil seeps, gas exhalations, oil impregnations, asphalt deposits, earth wax (ozokerite), iridescent oil films, or gas bubbles in water. Indirect indications are: shows of characteristic inorganic compounds, such as hydrogen sulfide ("sour" dirt, "sour" waters), sulfur bacteria, brines, and bromine and iodine waters; characteristic vegetation; or signs of mechanical displacements associated with gas emanations, such as mud "volcanoes," gas mounds, sandstone dikes, brecciated clay dikes, and mud flows. Careful observations of these phenomena have led to considerable success in recent years. In the Gulf coast salt dome province alone, 75 out of 219 domes discovered prior to February, 1936, were located by the application of such "macroscopic" detection methods.[36]

These methods have the disadvantage, however, that the indications are not always unique. For instance, methane may be formed by decaying vegetation in swampy areas (and in coal and lignite seams), and salt

---

[34] Examples: the oil seeps near Cuba in southwest New York, used by the Seneca Indians for medicinal purposes; the St. Quirinus spring on Tegern Lake in Bavaria, known to the monks since the fifteenth century; the asphalt deposits near the Dead Sea (Genesis 14:10) and between Babylon and Nineveh; those at Apsheron, at Sakhalin, and in Trinidad (Sir Walter Raleigh, 1595); and, further, the "eternal fires" of the Chimaira in Lycia, as described by Herodotus about 450 B.C., and the fires of Burma, Mesopotamia, and Baku, the latter well known from the fire-worshipping Zoroastrians or Parsis.

[35] Plutarch relates that the Macedonian warriors of Alexander the Great found, in 328 B.C., oil oozing out of the rock on the banks of the Oxus (Amu-Darya) River (near Bukhara, U.S.S.R.) and were much surprised since in the vicinity "no olive trees" were in evidence.

[36] G. Sawtelle, A.A.P.G. Bull. **20** (6), 728 (June, 1936). Another table in the same article gives 35 out of 141 domes.

waters may originate from the leaching of salt deposits. Further, active seepages indicate a depletion of a subsurface reservoir and there is always doubt as to whether it is in its initial or final stages. Conversely, many of the best sealed (mid-continent, Paleozoic) fields have no seepage indications at all. Even when they are accompanied by structural and stratigraphic observations, the use of surface indications has the obvious limitation that it is impossible to determine the length and direction of the supply channel from the visible surface concentrations. The surface evidence may be far removed from a commercial subsurface accumulation. In this respect, microscopic methods of observation and analysis are more

TABLE 82

DETECTION OF HYDROCARBONS AND ASSOCIATED INORGANIC COMPOUNDS

I. Macroscopic Methods
   A. Direct Indications
      1. Oil seepages
      2. Gas emanations
      3. Asphalt deposits
      4. Oil impregnations
      5. Wax (ozokerite)
   B. Indirect Indications
      1. Salt, sulfur
      2. Bromine and iodine waters
      3. Gas mounds
      4. Mud volcanoes
      5. Sandstone and clay-breccia dikes
II. Microscopic Methods
   A. Gas Detection
      (volatile constituents in interstitial soil air)
   B. Soil Analysis for Occluded Constituents
      1. Volatilizable fraction
         Hydrogen, methane, ethane, propane, butane
      2. Extractable fraction
         Organic liquids, waxes, inorganic solids

successful, since they locate not only concentrations on outcropping fissures, faults, and the like, but also accumulations resulting from the continuous flow by diffusion from the reservoir through the overlying strata. The pattern of indications furnished by the microscopic methods is therefore more uniform and has been found to show certain characteristic patterns in the fields thus far investigated.

The micro methods fall into two groups: gas detection and soil analysis. In the former the concentration of gases in the interstitial soil air is determined by withdrawing it from shallow holes and passing it through a portable detector, usually of the "hot wire" type. Soil-analysis methods, on the other hand, require an analysis of soil samples for their content of hydrocarbons and other significant constituents. There are two main pro-

cedures of soil analysis, one depending on a determination of the volatilizable components—usually methane, ethane (propane, butane), and hydrogen—and the other involving the extraction of organic liquids and waxes and inorganic constituents. The quantities investigated are exceedingly small and, therefore, the accuracy requirements are high. The *gaseous* paraffin hydrocarbons occur in quantities ranging from 10 to 1000 parts per *billion* by weight. The *solids* (waxes) vary between several tens to several thousand parts per *million* by weight, and the *liquid* organics from 1000 to 10,000 parts per *million* by weight. Table 82 shows the relation of the more important gas and soil analysis methods, compared with the older macroscopic procedures.

B. Significant Hydrocarbons; Occurrence

The question arises as to which of the hydrocarbons present in and detachable from a subsurface oil concentration are the most significant, the most unique, and lend themselves most readily to observation and analysis. Crude oil is an exceedingly complex mixture of hydrocarbons; the composition varies greatly with locality and therefore with the original constitution of the organic source materials. It is assumed that they were converted by anaerobic fermentation of cellulose and proteins to methane and unsaturated fatty acids, probably in the presence of bacteria and salt water; these presumably changed by polymerization, aided by pressure and moderate temperatures, to the compounds of the naphthene series. D. C. Barton has assumed that the originally naphthenic petroleums were transformed to the more paraffinic types with time and depth.[37] According to Brooks,[38] "no petroleum has ever been found which contains unsaturated hydrocarbons of the olefine type, at least in the lighter fractions which can be separated by distillations without decomposition."

Table 83 illustrates schematically the relation and variety of the various groups of the natural hydrocarbons. In crude oil the aliphatic group is the most important; in coal and its derived products the aromatic compounds predominate, although they are also found in certain types of crudes. The saturated open-chain aliphatics (paraffins) are the chief constituents of the *paraffin*-base oils; the saturated closed-chain aliphatics (naphthenes) occur chiefly in the *asphalt*-base crudes. The monolefin and diolefin groups, both open- and closed-chain, are represented chiefly in cracked oils and artificial products. Table 84 gives the composition of some of the crude oils, (*a*) in the low-temperature range from 60°–95° C.,

---

[37] *Problems of Petroleum Geology*, p. 109 (1934).
[38] Dunstan, A. E., *et al.* (eds.), *Science of Petroleum*, I, 48, Oxford (New York, 1938).

TABLE 83

RELATION OF THE NATURAL HYDROCARBON GROUPS

ALIPHATIC							AROMATIC	
Acyclic (open chain)				Cyclic (closed chain)			Cyclic	
Saturated	Unsaturated			Saturated	Unsaturated			
Paraffins (Alkanes)	Olefins (Alkenes)	Acetylenes (Alkynes)	Diolefins (Alkadienes)	Cycloparaffins (Cycloalkanes) (Naphthenes)	Cycloolefins (Cycloalkenes)	Cyclodiolefins (Cycloalkadienes)	Benzenes	Naphthalenes
C_nH_{2n+2}	C_nH_{2n}	C_nH_{2n-2}	C_nH_{2n-2}	C_nH_{2n}	C_nH_{2n-2}	C_nH_{2n-4}	C_nH_{2n-6}	C_nH_{2n-12}
Methane Ethane Propane Butane etc.	.... Ethylene Propylene n-Butylene etc.	.... Acetylene Allylene Ethylacetylene	.... Allene Erythrene	.... Cycloethane Cyclopropane Cyclobutane etc.	... Cycloethylene Cyclo-propylene etc.	.... Cycloacetylene etc.	Benzene Toluene Xylene etc.	Naphthalene etc.
Paraffin-base oils; natural gas (methane, ethane); gasoline (pentane to dodecane); natural gasoline (butane to pentane)	Cracked oils	...	Cracked oil, coal tar benzene; mostly synthetic	Asphalt-base oils	Only synthetic	Lubricating oils	Coal tar distillates; some in crude oils	

which incidentally corresponds approximately to the temperature range at the depths where most of these oils are found, and (b) for the 250°–300° fraction.

In natural gases, methane predominates, then follow ethane, propane, butane, and pentane. Contents generally decrease with molecular weight (Table 85). Other gases present may include oxygen, hydrogen, helium, nitrogen, and carbon dioxide. According to this table, therefore, the most significant hydrocarbons of the crudes and natural gases are the paraffins,

TABLE 84
COMPOSITION OF SOME CRUDE OILS[39]

Type	60°–90°C.			250°–300°C.		
	Paraf-fins	Naph-thenes	Aro-matics	Paraf-fins	Naph-thenes	Aro-matics
Grozny, high paraffin............	72%	25%	3%			17%
Grozny, paraffin free............	69	26	5	35	37	28
Texas (Mexia)...................	54	17	29	59	29	12
Oklahoma (Davenport)..........	73	21	5	51	32	17
California (Huntington Beach)..	65	31	4	31	40	29

[39] From G. Egloff, *Reactions of Pure Hydrocarbons* (Reinhold, 1937).

TABLE 85
SOME U. S. GAS ANALYSES[40]

Field	Well	Pres-sure (lb. per in.$^{-2}$)	Meth-ane %	Eth-ane %	Pro-pane %	Bu-tane %	Pen-tane %	Source
Oklahoma City	D	265	87.3	7.9	3.0	1.8	...	Separator gas
Oklahoma City	D	16	60.4	16.9	13.8	6.3	2.6	Oil gas
Kettleman Hills	F	1672	85.6	8.2	3.6	1.6	1.0	Free gas
Kettleman Hills	F	52	51.2	18.5	15.1	9.7	5.5	Gas in solution

[40] A. R. Bowen, *Science of Petroleum, op. cit.*, Vol. II, p. 1504.

naphthenes, and aromatics. Of these, the aromatics take last place, are not present in all crudes, and would probably not be a unique indicator at the surface. Of the naphthenes and paraffins, the latter are unquestionably the more important for gas detection and soil analysis, since at least the first members of the series are more readily isolated and determined quantitatively.

It must be remembered that the determination of the constituents in a hydrocarbon mixture is a very difficult and sometimes impossible procedure. Bowen[41] refers to an analysis of one oil by eight Bureau of Standards investigators who isolated in one fraction twenty-three paraffinic, eighteen naphthenic, and six benzenoid hydrocarbons. This work

[41] *Ibid.*

took several years.   Even a qualitative approach of this sort would not
be possible in soil analysis where hundreds of samples must be analyzed
in the course of one survey.   This narrows most of the analytical work
down to the paraffin series whose first members, at least, can be isolated
satisfactorily.   From butane upward, however, isolation by fractional dis-
tillation is difficult because the number of isomers of different boiling and
melting points increases considerably toward the end of the series.   In one
phase of soil analysis (for liquid and solid "pseudo"-hydrocarbons) isola-
tion is not attempted, and these constituents are determined collectively
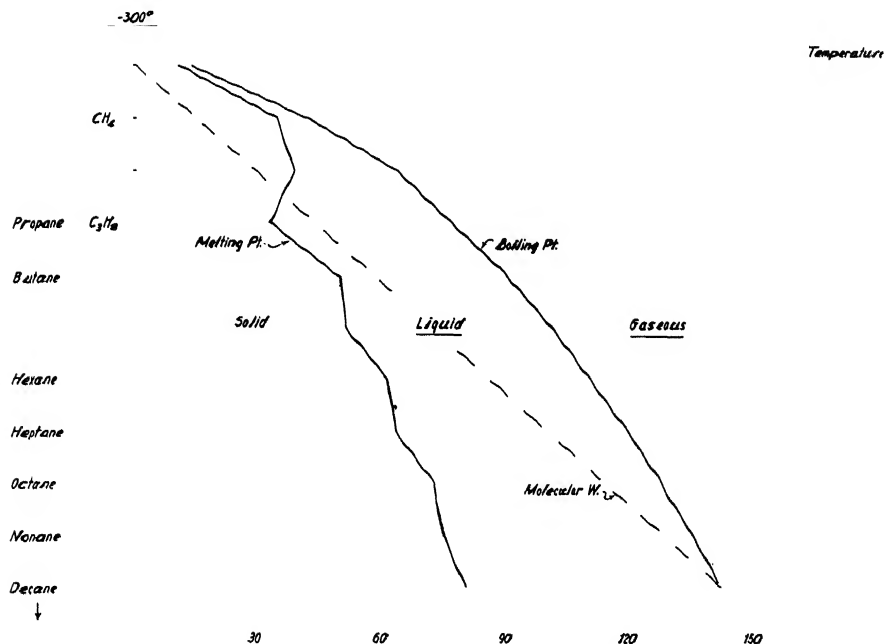
FIG. 12-8. Melting points, boiling points, and molecular weights of some of the
paraffin hydrocarbons.

by extraction with certain solvents.   In the "gas method," using the
hot-wire type of detector, no differentiation in the type of combustible
hydrocarbon molecule is made.

Fig. 12-8 shows the variation of the melting points, boiling points, and
molecular weights for the first members of the paraffin series up to decane
and inclusive of hydrogen.   The variation of the molecular weight is
linear; that of the boiling point, being a function of the molecular weight,
is regular but not linear; and that of the melting point is irregular, particu-
larly at the beginning of the series.   At ordinary temperature and pressure,
methane, ethane, propane, and butane are gaseous.   The differences in

melting and boiling points of the earlier members in the paraffin series are utilized for their isolation by low-temperature fractionation, as shown below.

C. GAS-DETECTION METHODS

Gas-detection methods are aimed at the measurement of the content of combustible gases of the interstitial soil air near the surface. For this purpose, portable detectors of the hot-filament type may be employed. Samples of the soil are not taken. In these detectors no differentiation
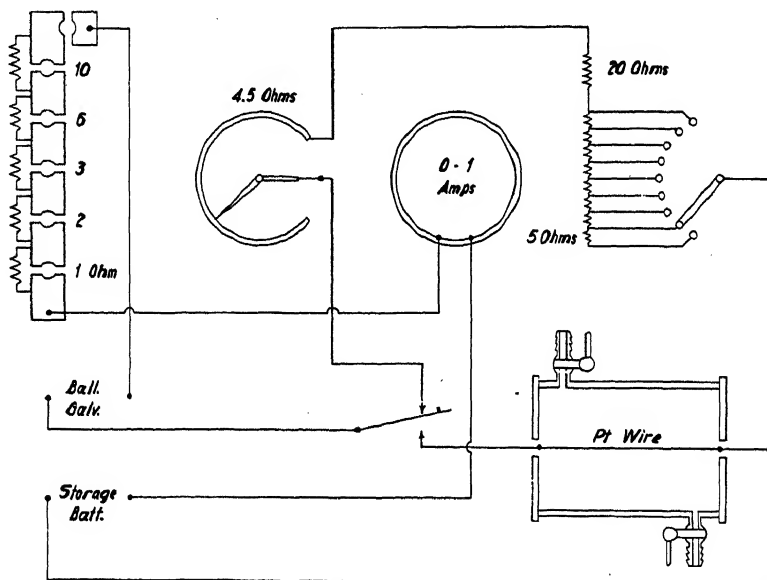
American Askania Corp.

FIG. 12-9. Original Laubmeyer gas apparatus.

between ethane and methane is made; the effective amount of ethane depends somewhat on the technique of evacuation of the drill hole (because of the different densities and diffusion rates of ethane and methane). The air is sampled from shallow holes. These are drilled to a depth of about five feet, and are then sealed off with a lid provided with two concentric cylinders of large radius and a piece of tubing ending in a stop cock.[42]

The hole is left alone for twelve to twenty-four hours before the air is pumped into the combustion chamber, shown in Fig. 12-9. Because of their natural agitation, the gas molecules in this chamber come into contact with

the heated platinum filament and are burned with the oxygen of the air, thereby raising the temperature of the platinum filament which in turn increases its resistance.   To attain sufficient sensitivity, the measurements must be made with the gas mixture at rest, and the current must be turned on after the gas has been introduced into the chamber   Hence, a ballistic galvanometer is best suited for the purpose.   The instrument is calibrated by a mixture of air and methane and is said to be sensitive to one part in 10 million.   However, at the smaller dilutions the sensitivity drops rapidly. For instance, in one of the original Laubmeyer instruments, the deflection was 2.8 scale divisions for a dilution of $1:10^6$, and 2.0 scale divisions for a
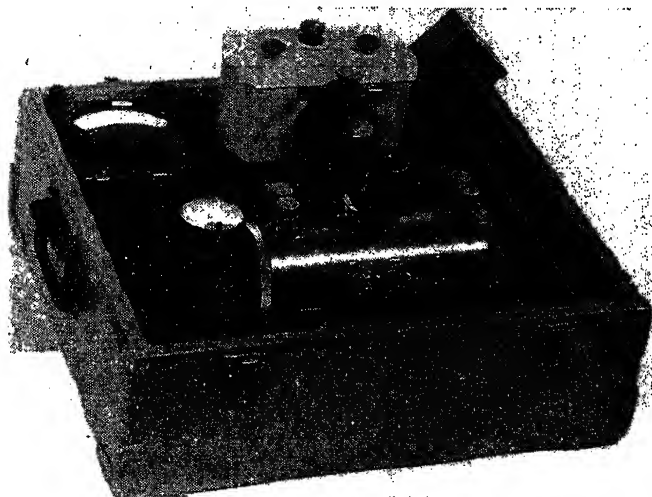
American Askania Corp.

FIG. 12-10. Graf-Askania double-chamber combustible gas detector.

dilution of $1:10^7$.   The measurements are made by comparing the reaction of the galvanometer in an empty combustion chamber with that in one filled with the gas-air mixture.   Difficulties arise from the fact that the voltage of the battery supplying the filament current cannot be kept sufficiently constant.

This is avoided in the double-chamber instrument[43] shown in Fig. 12-10 in which the two combustion chambers are arranged in opposite arms of a bridge circuit, much in the same manner as in the regular double-filament combustible gas detector (see Fig. 11-35).   The zero instrument is a Zeiss loop galvanometer which may be used also for photographic recording. The bridge is first balanced for air in both chambers, and the bridge

[43] A. Graf, Oel und Kohle, **11(36)**, 644-648 (Sept. 22, 1935).

current is fixed for the desired ignition temperature of the wire. Then
the sample is introduced into one chamber and the (ballistic) galvanometer
deflection is observed. A mixture of gases may be analyzed by raising or
lowering, in steps, the temperature of the wire, that is, by changing the
bridge current. This has been demonstrated successfully for mixtures of
methane, carbon monoxide, and hydrogen; but it would be difficult to
accomplish it for a mixture of methane and ethane. Nevertheless, the
same apparatus is usable for a separate quantitative analysis of air-
methane and air-ethane mixtures if the ethane and methane have been
separated from each other by some other means (such as low temperature
fractionation, see page 900).
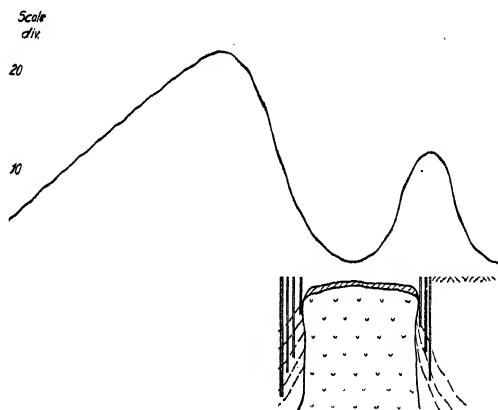
FIG. 12-11a. Gas indications (methane-ethane) measured with Laubmeyer apparatus
on Pierce Junction Salt Dome. (N. Gella).

In its application as described, the bridge apparatus proposed by Graf
measures the content of combustible gases in the same manner as the Laub-
meyer instrument, without differentiation between methane and ethane.
Fig. 12-11a shows the results obtained with a combustible gas detector on
the Pierce Junction salt dome near Houston, Texas, in units of galvanom-
eter scale deflections. The anomalies are most pronounced on the flanks,
are unsymmetrical, and are almost zero above the top of the dome.

Another type of gas detector[44] measures the amount of carbon dioxide
liberated upon the combustion of the gaseous hydrocarbons pumped from
a well into the apparatus. Again, no differentiation is made between
methane, ethane, and heavier hydrocarbons. The hydrocarbons are

[44] V. A. Sokolov, Neftianoe Hoziaistvo, **27(5)**, 28–34 (May, 1935).

burned, in the presence of (purified) air (or oxygen), to water and carbon dioxide. The volume of the latter and, therefore, the reduction of the original volume bears a definite relation to each other if the number of hydrocarbons present and their molecular formulas are known. This procedure (combustion and volumetric carbon dioxide determination) is also widely used in those soil-analysis methods in which gaseous members of the paraffin series are measured.
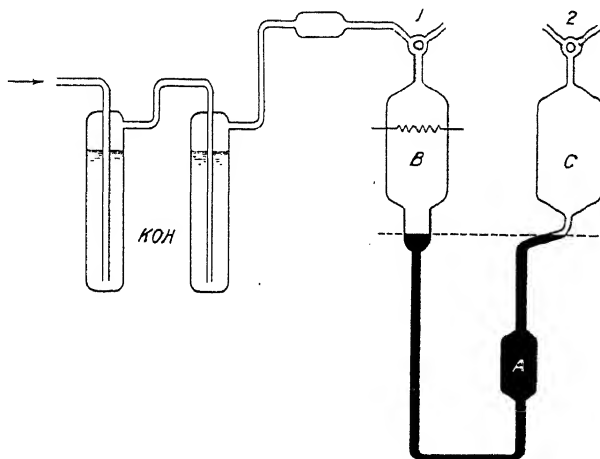
Fig. 12-11b. Apparatus for measuring volume contraction in the combustion of hydrocarbons (partly after Sokolov).

The combustion of hydrocarbon gases[45] of the molecular formula C_nH_{2n+2k} (where n is the number of carbon atoms and k may vary from -3 to $+1$) is governed by the relation

$$C_nH_{2n+2k} + \frac{3n+k}{2} \cdot O_2 = n \cdot CO_2 + (n+k)H_2O, \qquad (12\text{-}4)$$
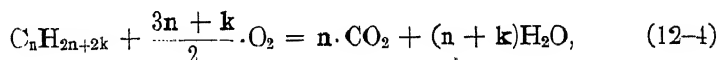
so that

$$O_2 = \frac{3n+k}{2} \cdot V, \quad CO_2 = nV, \quad \text{and} \quad \Delta V = \frac{2+n+k}{2} \cdot V, \qquad (12\text{-}5)$$

with V as the original volume, ΔV as volume reduction due to combustion, and O_2 and CO_2 representing the volumes of these gases. For the members of the paraffin series, $k = 1$ and n takes values from 0 to 4, since soil

[45] And of CO, CO_2, O_2, and H_2, according to L. M. Dennis, *Gas Analysis*, Chapter XI.

analysis is concerned only with the members from hydrogen to butane. With $k = 1$, eqs. (12-4) and (12-5) take the form

$$C_n H_{2n+2} + \frac{3n+1}{2} \cdot O_2 = nCO_2 + (n+1)H_2O$$

and

$$O_2 = \frac{3n+1}{2} \cdot V, \quad CO_2 = nV, \quad \Delta V = \frac{n+3}{2} \cdot V,$$

(12-6)

so that, for methane, $CH_4 + 2O_2 = CO_2 + 2H_2O$, and, for ethane, $C_2H_6 + \frac{7}{2}O_2 = 2CO_2 + 3H_2O$, and similarly for the other paraffin hydrocarbons (see Table 86).

TABLE 86
COMBUSTION OF PARAFFIN HYDROCARBONS

HYDROCARBON	COMBUSTION EQUATION				CONTRACTION IN HC VOLUME UNITS	
	HC	+ Oxygen =	CO₂ +	Water	with CO₂ absorption = HC vol. + O₂ vol.	without CO₂ absorption = HC vol. + O₂ vol. − CO₂ vol.
Methane	CH_4	2	1	2	3	2
Ethane	C_2H_6	3.5	2	3	4.5	2.5
Propane	C_3H_8	5	3	4	6	3
Butane	C_4H_{10}	6.5	4	5	7.5	3.5
	I	II	III	IV	(I + II)	(I + II − III)

The volume contraction may be measured by an apparatus of the type illustrated in Fig. 12-11b, fashioned after the Burrell methane indicator and consisting of a combustion bulb, B, connected through an equalizing vessel, A, with a capillary and compensator, C. The latter is provided to obviate changes in reading due to changes in volume resulting from variation of temperature. The gas is introduced through the bubbling tubes and burned by heating the platinum filament. The corresponding volume contraction follows from readings of the capillary before and after combustion. The sensitivity of the apparatus can be increased by using, in place of water, potassium hydroxide, which has the property of absorbing the carbon dioxide and which, therefore, raises the contraction, as shown in Table 86. If methane alone is present, its quantity follows directly from the amount of carbon dioxide developed and, therefore, from the contraction. However, admixtures of heavier hydrocarbons will contribute proportionately greater amounts of contraction, since the volumes of carbon dioxide are equal to the numbers of carbon atoms. This type of apparatus, like the second Sokolov field instrument to be described next,

does not differentiate between the hydrocarbons contained in the soil air and gives greater indications for the heavier constituents.

Difficulties experienced with instability of the capillary induced Sokolov to design another combustion instrument, illustrated in Fig. 12–12. Its action is based on a determination of the amount of air which must be burned to liberate a minimum detectable volume of carbon dioxide. Detection is made by the turbidity produced by the passage of the gas mixture through a barium hydroxide solution after combustion. A carbon dioxide content of about 0.03 per cent is required to cause turbidity. The corresponding volume of air may be read on a burette and is called the apparatus constant C. If air containing hydrocarbons is then burned and carbon dioxide is liberated, and if V is the volume of air required to
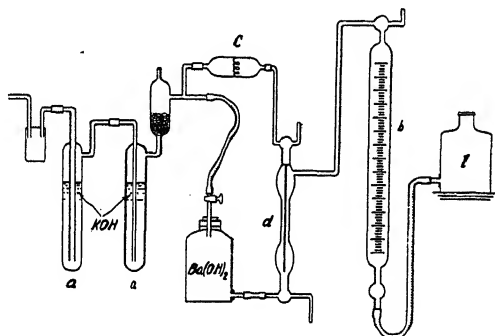
Fig. 12–12. Portable (combustion–absorption) gas detector (after Sokolov). (a) Caustic potash tubes for removal of carbon-dioxide; (b) burette; (c) combustion tube; (d) absorption capillary; (l) leveling flask.

start turbidity, then the content of carbon dioxide in percentage is $0.03 \times C/V$. The smaller the hydrocarbon content, the greater therefore is the volume required to cause turbidity. Hence, it is a virtue of this apparatus that the readings increase as the hydrocarbon content decreases. It is obvious that the air must be well cleaned of carbon dioxide before being injected into the apparatus. For this purpose the two bubble tubes a filled with caustic potash are provided. In application, the soil air is first passed through these tubes, and through the combustion chamber c (cold filament), the turbidity capillary d (constructed like the Hankus type of Orsat pipette), and the burette b. Then the capillary pipette d is filled from a jar with $(N/10)\,Ba(OH)_2$ solution, the filament turned on, the stopcocks closed, and the burette read. As soon as turbidity appears, the burette is read again, the filament turned off, and the capillary tube washed. The apparatus is calibrated by known volumes of CO_2 or CH_4 and is reported to be accurate to $1 \cdot 10^{-5}$ to $1 \cdot 10^{-6}$.

Sokolov[46] also developed an apparatus for the separate determination of methane and heavier hydrocarbons by low-temperature fractionation, combustion with air, and volumetric determination of the carbon dioxide thus formed. This procedure is very similar to that applied in soil analysis and will be discussed in section D.

An adaptation of the mass spectrograph to gas and soil analysis was recently proposed by H. Hoover, Jr., and H. Washburn.[47] The mass spectrograph is an electron gun for determining the mass of positive ions (canal rays) by deflection in a combined electrical and magnetic field. It consists of an ionization chamber in which gas molecules are bombarded by electrons. The positive ions thus formed pass through a small slit, are accelerated to a high velocity by a potential of several hundred to a thousand volts, and then pass through another slit into a semicircular evacuated tube placed in a magnetic field. At the end of the tube is a slit through which only ions of a predetermined radius of path curvature can pass. Behind the slit is a collector for measuring the number of arriving ions. The ion current is stepped up by an amplifier and recorded as a proportionate plate current by an oscillograph galvanometer. If the magnetic field H is held constant, the only quantity determining the radius of curvature r of the ion path is the accelerating voltage E, since for a given ion $m/e = r^2H^2/2E$. A mixture of gases can therefore be analyzed by slowly varying the accelerating voltage so that ions with various masses are admitted successively by the exit slit, where their number is recorded. It is claimed that an accuracy of 0.2 parts per billion by weight is readily obtainable and that an analysis for the first members of the paraffin series in a gas mixture takes only a few minutes.

Other methods of gas analysis which have been proposed include: (1) infrared absorption spectroscopy, (2) Ramann effect spectrography, and (3) low-voltage excitation and observation of resonance radiation. Although some of these methods may also be applicable to laboratory procedure, none of them has found, as yet, practicable application in gas and soil analysis work.

D. SOIL ANALYSIS

As the name indicates, soil analysis differs from gas detection in that soil samples and not gas samples are analyzed. By breaking down the mineral grains mechanically and, if necessary, chemically, it is possible to obtain access to the entrained and occluded hydrocarbon constituents instead of depending solely on the interstitial air. Otherwise, in some phases

---

[46] *Loc. cit.*
[47] A. I.M.E. Tech. Publ. No. 1205, May, 1940.

of the work, the analytical procedures are similar if not actually alike. For instance, for an analytical determination of methane and ethane, it makes no difference whether the sample introduced into the apparatus is pumped out of the ground or is obtained by boiling a soil sample with water and solvents. While such analytical procedures in which the volatilizable fraction is determined are therefore equivalent to gas-analytical methods (see Table 82), there are other soil-analysis methods relying on the fractions which are extractable by solvents (so-called liquid pseudo-hydrocarbons and soil waxes).

For an analysis of the volatilizable components—hydrogen, methane, ethane (plus propane and butane if present)—soil samples are taken usually by hand augers or light machine drills at depths varying from 5 to 15 feet. Where practicable, they should be secured below the ground-water level or below the surface-weathered layer. Contact with any oil- or grease-contaminated soil, vicinity of pipe lines or roads, and the like, must, of course, be avoided. Duplicate samples are usually taken at each location and are shipped to the laboratory in mason jars. They are then freed of moisture, and definite quantities are weighed out and transferred to a degassing apparatus. Some companies liberate the occluded gases from pulverized specimens at fairly high temperatures. Others prefer to boil them off from an aqueous solution to which, if necessary, certain solvents may be added to accelerate the degassing process.

After the gas has been driven out of the soil sample, it is passed to an analytical apparatus consisting essentially of low-temperature condensation, combustion, and pressure-measuring components Descriptions and illustrations of such apparatus or procedures, respectively, have been given by V. A. Sokolov,[48] L. Horvitz,[49] E. E. Rosaire,[50] and D. H. Stormont.[51] The diagram of Fig. 12–13 is a simplified scheme incorporating the more important features of these descriptions. The pressure in the component parts may be indicated by a compression manometer of the Arago-McLeod type, as shown, or by some other low-pressure gauge. The vacuum is generally produced by rotary Gaede or Cenco pumps working in conjunction with a mercury diffusion pump. More than the two condensers shown in the scheme may be employed to increase the number of fractionation components.

To produce low temperatures, liquid oxygen ($-183°$ C.) or liquid nitrogen

ι is   The number of purification stages is subject to varia-

[48] V. A. Sokolov, *loc. cit.*

[49] L. Horvitz, Geophysics, **4**(3), 212 (1939).

[50] E. E. Rosaire, Handbook of Geochemical Prospecting, fig. 4, p. 20, Subterrex (Houston, 1939).

[51] D. H. Stormont, Oil and Gas J., 53 (Sept. 14, 1939).

tion. Additional purifiers of solid caustic potash and absorption tubes with sulfuric acid may be added to take out unsaturates and aromatics. In operation, the entire apparatus is evacuated, the Dewar flask containing the liquid air or nitrogen is moved up to the condenser C_1, and the gas sample is admitted at a. As the sample passes through C_1, ethane and the heaviest hydrocarbons are retained and the remaining noncondensable fraction (methane and hydrogen) are allowed to pass through C_2 into the combustion tube T.

Upon isolation from the rest of the apparatus, hydrogen and methane are burned with the oxygen of the air to carbon dioxide and water, which are frozen out in condenser C_2. The remainder of the air is then pumped out, the Dewar flask is withdrawn from C_2, and readings are taken on the compression manometer, M, at various temperatures. This allows calcu-
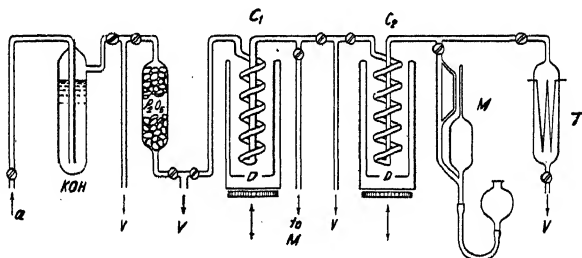
FIG. 12-13. Scheme of laboratory apparatus for gas and soil analysis (partly after Sokolov). (a) Inlet from degassing apparatus; (V) vacuum; (C) condensers; (M) manometer; (D) Dewar flask; (T) combustion bulb.

lation of the partial pressures and, therefore, of the relative amounts of water vapor and carbon dioxide. Assuming that the volume of the CO_2 formed upon combustion equals that of the methane, the content of the latter in terms of volume or weight of the sample can be calculated. The hydrogen content follows[52] (in approximation) from the excess of water over that to be expected in accordance with eq. (12-6). After condenser C_2, manometer M, and combustion tube T have been evacuated, they may be used in the described manner for the determination of the heavy fraction retained in C_1, which may be passed over into T upon warming of C_1; its combustion products may be condensed as before in C_2. In practice, it may be necessary to deviate from this simple procedure to increase the efficiency of combustion in this fraction and to narrow down the number of hydrocarbons in one fraction by additional condensers and smaller steps in the distillation temperatures. With increasing molecular weight of the

---

[52] Horvitz, *op. cit.*, p. 212.

constituents, the difficulties of isolation increase because of isomerism. Even for a mixture of normal homologues of one series, the calculation of the constituents from the carbon dioxide and water formed in the combustion is difficult if their number is greater than two.[53]

The second group of soil-analysis methods (see Table 82) is concerned with the determination of extractable liquids and organic and inorganic solids. Since these occur in proportionately larger quantities than the gaseous hydrocarbons, this determination is much easier and requires less complicated apparatus. The so-called "liquid hydrocarbons" and "soil waxes" are not members of the paraffin series, as has been stated in some articles, but are probably more or less complex fatty acids. They may be extracted by a variety of solvents, such as carbon tetrachloride, chloroform, ether, benzene, and so forth. Since these liquid organics and soil waxes are found in their greatest concentration at the immediate surface, the samples are taken (at undisturbed locations) with the grass roots and are air dried. Definite quantities are weighed out and placed in an extraction apparatus. The Soxhlet type or a modified form of the Bailey-Walker apparatus, or some other form of extractor, preferably permitting continuous operation, is suitable.

The liquid containing the waxes, and the like, is then placed in a distillation apparatus; the solvent is distilled off through a condenser; and the residue, in liquid or semisolid form, is determined by weighing. The range encountered in soil analysis (from 0.01 to 1 per cent by weight) is quite within the reach of ordinary accurate analytical procedure and therefore requires no special apparatus. An extraction method used in conjunction with semiquantitative colorimetric analysis is briefly mentioned by Rosaire.[54] While the soil wax samples are taken at the immediate surface (depth $\frac{1}{2}$ inch), the specimens for colorimetric analysis are collected at the depth of supposedly greatest bacterial action (about 6 inches). Naturally, any topsoil samples must be taken at locations undisturbed by wind or water erosion, agriculture, and so on.

Inorganic constituents, likewise determined by extraction, include halides, sulfates, and carbonates; more rarely there are bromides, iodides, bicarbonates, and the like. Inasmuch as some of these constituents may also be determined by their physical (for example, electrical resistivity) expression, it is seen that a close relation must exist between results obtainable by certain soil analysis and geophysical (resistivity, Eltran, and similar) methods.

[53] L. M. Dennis, *Gas Analysis*, Chapter XII (Macmillan, 1929).
[54] *Op. cit.*, p. 10.

E. Interpretation and Results of Gas and Soil Analysis

Gas and soil analysis in its present form is of comparatively recent development. There is still some dispute over its merits. Divergent opinions have been expressed regarding the type of organic compounds to be considered significant and the relation of their surface distribution to subsurface accumulations of oil and gas. More information is needed, particularly about the variation of organic and inorganic constituents with depth in wells, and on known fields. In any event, whatever interpretation procedure is developed will not be the equivalent in physical and mathematical rigorousness to procedures currently employed in other geophysical methods. The fundamental problem is, in principle, no different from that which faced the surface geologist a number of years ago, namely, that of locating subsurface oil and gas accumulations from the surface distribution of seeps. Factors which have made possible an advance in his interpretation methods are: (1) the greater areal completeness of sampling points and greater independence of random indications; (2) a segregation of the surface materials by physico-chemical analysis, in regard to geologic significance; (3) information on their variation with depth, by the analysis of well samples; and (4) data on geologic structure, by simultaneous application of other geophysical methods to a given problem.

Any attempt to deduce from the surface or near-surface accumulations of organic products the existence, location, or depth of a subsurface oil deposit must, of necessity, involve some definite assumption regarding the mechanism of their migration. Various ideas have been advanced on the basis of observed horizontal and vertical distribution and theoretical possibilities.

What little data have been released on the variation in organic and inorganic constituents at the surface and in wells suggests a picture indicated schematically in Fig. 12–14. Above an oil deposit, the heavier gaseous hydrocarbons of the paraffin series show the most significant indications; they appear to be the most reliable indicator of subsurface oil deposits, since they are not known to be associated with near-surface decomposition of organic materials. The heavy hydrocarbon content (ethane, propane, and the like) of rocks overlying an oil deposit decreases toward the surface, although that decrease is far less regular than the scheme suggests and varies with the permeability and related characteristics of the individual formations. Methane appears to be more irregular in its vertical distribution, since decomposition processes within formations tend to be superimposed on the regular decrease away from the deposit. This is particularly true near the surface where anaerobic decomposition resulting from fermentation of vegetable matter (as in marshes, peat, lignite) may

produce large quantities of methane without relation to the underlying oil deposit (last curve in Fig. 12–14).

The role played by hydrogen is still somewhat obscure. It appears to reach its maximum somewhere above and at the sides of an oil deposit;[55] in some areas its surface distribution is conformable with that of methane and the heavier gaseous paraffin hydrocarbons.[56] In wells it may go somewhat parallel with methane. The greatest concentrations of the heavy gaseous hydrocarbons and of methane may or may not coincide at the
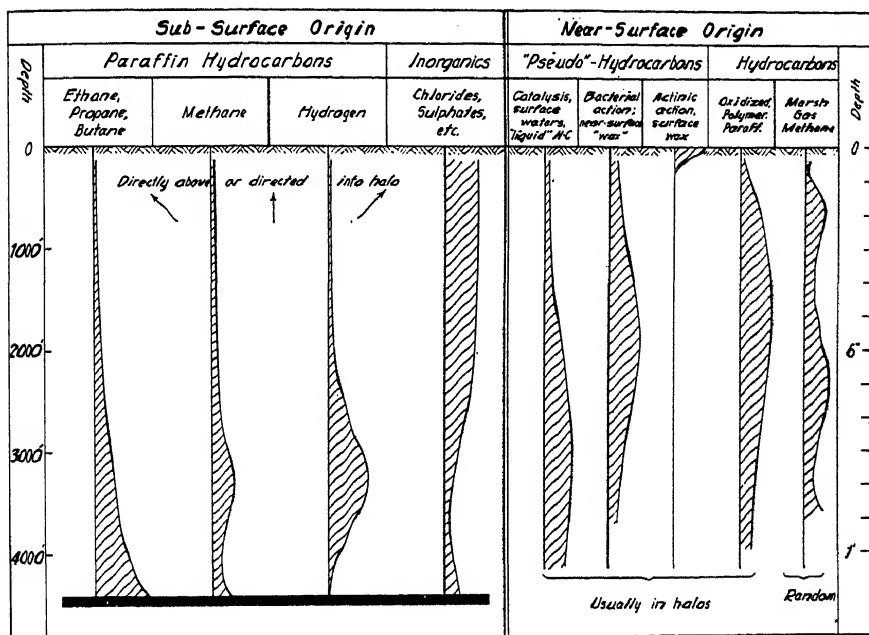
FIG. 12-14. Scheme showing variation of several organic and inorganic constituents in the subsurface section and near the surface above an oil deposit.

surface and may occur directly above an oil deposit. More often, however, the heavier hydrocarbons and sometimes the methane have a maximum in the form of a halo surrounding the deposit. Possibilities of origin of such halos will be discussed below.

The same appears to be true for some of the significant inorganic minerals, such as chlorides and sulfates, and for the four secondary products of near-surface agents indicated on the right side of Fig. 12–14, namely, the so-called liquid and solid pseudohydrocarbons and oxidized and poly-

[55] Personal communication from E. E. Rosaire.
[56] Horvitz, loc. cit.

merized paraffin hydrocarbons   Most of these are assumed to be reaction products of organic materials and inorganic agents.   In the case of the liquid and visco-solid pseudohydrocarbons, the organic materials are probably furnished by surface vegetation.   The solutions carrying the substances (chlorides?) with which they enter into (catalytic?) reactions are assumed to come from below.   Since the significant inorganics have their greatest concentration usually in halo fashion, the pseudohydrocarbon reaction products are likewise arranged in the form of halos.[57]

The depth at which the maximum amounts of these reaction products occur varies greatly.   The maximum of the "liquid" hydrocarbons may be found several inches to several feet deep.   One kind of "wax," assumed to be caused largely by bacterial action, occurs in greatest concentration about six inches from the surface,[58] whereas another, resulting from oxidation and actinic effects, has its maximum at the immediate surface.   The chemical nature of these pseudohydrocarbons has not been definitely determined; they are assumed to be fatty acids.   In the second case conditions are reversed.   The organic materials are assumed to come from below and are changed near the surface not so much by catalytic reactions as by oxidation and polymerization.   The product so formed is a heavy paraffin hydrocarbon[59] and occurs in much smaller quantities than do the pseudohydrocarbons.

This very generalized scheme of the distribution of hydrocarbons and pseudohydrocarbons is subject to revision as more field data are accumulated and the chemical nature of the substances mapped becomes better known.   It is but partially in accord with what should be expected theoretically from the laws controlling the migration of gases and liquids through homogeneous media.   According to Pirson,[60] there are three ways in which gases emanating from a subsurface source may reach the surface: (1) by permeation, (2) by effusion, and (3) by diffusion.

Permeation takes place by virtue of the porosity, or better, the permeability of rocks; it is governed by d'Arcy's law which states that the velocity of gas flow is proportional to the pressure gradient, multiplied by the ratio of permeability times density, divided by the viscosity of the gas.   Limes, slates, and moist strata have litte permeability; therefore, migration by permeation is hardly to be expected across the bedding planes of stratified formations (except sands and sandstones) and is confined to loose overburden, faults, and fissures.   Assuming, therefore, that a fracture zone of high permeability crosses a series of impermeable forma-

---

[57] Rosaire, *op. cit.* p. 8.

[58] *Ibid.*

[59] "Pseudohexane," Horvitz, *loc. cit.*

[60] Oil Weekly, Oct. 10, 1938.

tions covered by overburden of uniform permeability, the depth of the suboutcrop of the fault can be determined from the variation of the gas concentration along the surface. Formulas for the effect of a linear source of infinite strike extent have been derived by Antonov, Sokolov, and Pirson.[61] Those of the first author were derived under the assumption of diffusion through the overburden, are equally valid for migration by permeation, and are identical in form with those given by Koenigsberger for the effect of a source of radium emanation (eq. [12-3]). Very simple in application is a modification of Sokolov's formulas for the gas concentration C at a station with the distance x from a point directly above the center of a linear source of finite width and depth, h:

$$C = \frac{c}{h} \cdot \varphi, \qquad (12\text{-}7)$$

where c is a constant involving permeability, pressure at the source, and viscosity of the gas, and φ the angle under which the edges of the source appear from the station.

Effusion of gas takes place through very small capillaries whose diameter is less than the mean free path of the molecules; the rate of flow is proportional to the pressure differential and inversely proportional to the square root of the molecular weight of the gas involved. This phenomenon would account for the greater ease with which the lighter paraffin hydrocarbons (hydrogen and methane) are carried to the surface.

However, the greater portion of the available gases may be expected to travel across the bedding planes of seemingly impervious rocks by *diffusion*, that is, by penetration of gas molecules through the intermolecular space of solid substances. Diffusion of light gases (for example, helium) through metals is well known in vacuum technique; hence, a phenomenon observable over a short period of time must be expected to assume correspondingly larger proportions in the course of millions of years that elapsed since the oil deposits were laid down. The diffusion laws are similar in form to those controlling permeation, and they indicate that the velocity of flow is dependent on the diffused medium, the size of the diffusing molecules, and the pressure gradient. Gases diffuse readily through liquids; therefore, diffusion of gases through moist formations should take place with comparative ease. Since the lighter gases diffuse more readily, it is understandable why hydrogen (expected to be associated with gaseous hydrocarbons) occurs in comparatively small quantities, probably having made its escape much ahead of methane.

In addition to migration of gases by permeation, effusion, and diffusion,

[61] References in *idem*.

it is likely that some of them have been carried in solution by circulating waters along fissures, and the like, or up the dip in formations. Modifications may occur along the path because of adsorption on colloidal matter; they do occur near the surface in the aerated zone because of oxidation, polymerization, and actinic action. Besides, changes must be expected from one formation to another when there is a difference in diffusion constants.

If the process of diffusion of gases through formations *without* lateral variations were alone responsible for the distribution of hydrocarbons and related organics at the surface, their maximum concentration should in all cases occur directly above the source, since the migration may be assumed to take place from it in essentially a vertical direction. As a matter of fact, this has been found to be true in many cases, particularly above faults and fracture zones. It has also been claimed, particularly by the Russian investigators, that maximum concentrations of methane should be formed above gas fields, and those of the heavy hydrocarbons above oil fields. Further, it has been stated that in a given field where both oil and gas are found, the maximum methane concentration should occur over the highest point of a dome or monoclinal trap where the gas occurs, and the heavy hydrocarbons should occur above the oil accumulations at the flanks. The Russians' own data do not bear out this conclusion in all cases.

To begin with, natural gas is not pure methane but is frequently associated with ethane and other heavy hydrocarbons (Table 85). Conversely, methane is often absorbed in and liberated by oil deposits. Hence, a clean-cut separation of oil and gas occurring in the same structural or stratigraphic trap appears hardly possible by surface measurements. Furthermore, the process of diffusion is not so simple as theoretically indicated, and the surface expression of subsurface hydrocarbon distribution is modified considerably by lateral variations in the permeability and diffusion characteristics of the overlying formations. For this reason, the simple explanation given by Pirson,[62] that heavy hydrocarbon halos are due to the marginal arrangement of oil below the gas on the flanks of an anticlinal or domal trap does not appear tenable, besides being in discord with the observation that in many cases production is found *under the bare spot* in the center of a halo and not under the halo itself.

It is evident, therefore, that other causes besides uniform diffusion must be responsible for the halo formation or must at least interfere with the process of normal diffusion. The solution of the problem is rendered difficult because the published data frequently lack information about

---

[62] *Ibid.*

geologic structure and nature of hydrocarbons mapped; besides, there is confusion in some of the recent articles in regard to geologic significance of the earlier data on the subject. The claim is certainly unjustified that in regard to halos, different results are obtained by the free-gas analysis (using the Sokolov or Laubmeyer techniques) and the soil analysis (mapping adsorbed and entrained constituents).

Laubmeyer definitely states in his publication that a sharp drop above production was observed in the Oberg field and attempts to explain the phenomenon by the withdrawal of gas from the productive formations by the wells in the center of the field. A survey of the Nienhagen field[63] revealed a maximum gas concentration above the western part of the field, while the eastern portion shows nearly normal concentration. On the north side of the Wietze dome[63] the gas maximum is forced northward or away from the productive zone, and the same trend is indicated by the gas measurements on the Pierce Junction dome (see Fig. 12-11a). It may be argued that in the vicinity of salt domes, the indications are related to fracture zones; however, this still leaves it unexplained why the indications should be forced consistently outward and away from them. On the other hand, this argument shows the necessity for considering closely the geologic structure associated with a halo. It is evident that a halo around a salt dome is not directly comparable with a halo around production above a stratigraphic trap because in the former we deal with steeply dipping beds around an impervious core (unless production occurs above the dome) while in the latter any evidence of folding or faulting is absent. Macroscopic halos have been reported for several Gulf coast fields,[64] such as Goose Creek, Humble, and Sour Lake.

The true halos, then, may be assumed to occur in regions of gentle folding and above stratigraphic traps. They have been variously explained, the prevalent assumption being that some sort of clogging occurs near the center of the productive structure. McDermott[55] believes that because of the tendency of oil and gas to migrate to the highest point of a fold, monocline, or lenticular deposit, these become clogged first, the sealing action working its way down the dip. This clogging is not noticeable at the surface if subsequent folding has developed cracks in the caprock and thus provided an avenue of escape for the gases near the top. The surface effect is thus similar to that of a buried fault (linear source). Rosaire,[66] on the other hand, assumes that such clogging occurs fairly near

[63] G. Laubmeyer, unpublished reports.
[64] Rosaire, Geophysics, III(2), 107 (March, 1938).
[65] Geophysics, IV(3), 1-15 (July, 1939).
[66] Handbook of Geochemical Prospecting, *op. cit.*, p. 22.

the surface because of the action of ascending mineralized[67] solutions along minute fissures and cracks developed in the overlying formation by differential settling over a fold or lenticular deposit. He points out that surface formations above oil deposits are frequently indurated, due to
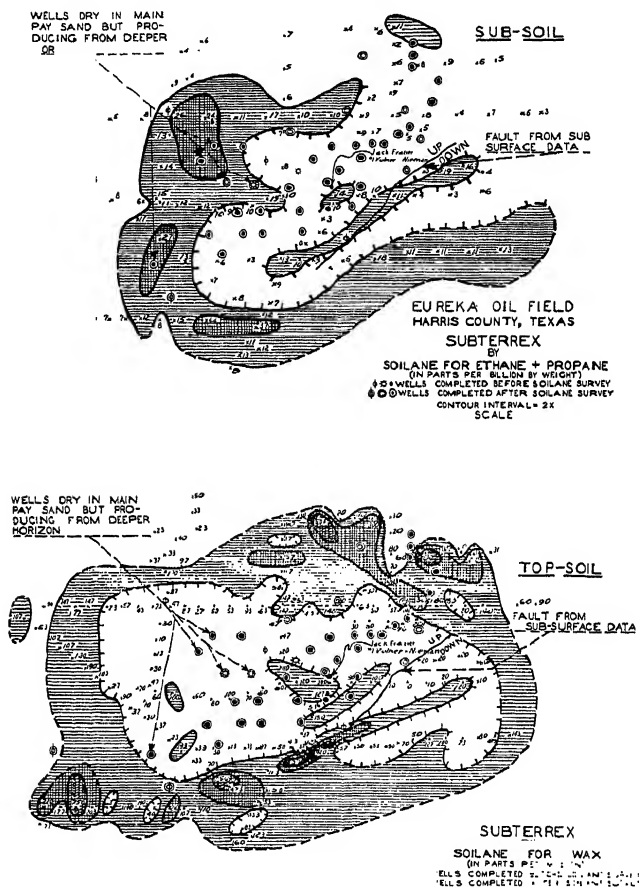
FIG. 12-15. Ethane and surface-wax halos in Eureka field (after Rosaire)

silification and calcification, and that this has been verified by low drilling rates ("dome digging"), high seismic refraction speeds, erroneous dips in reflection shooting, and high resistivities mapped in Eltran surveys.[68]

[67] McDermott (A.A.P.G. Bull., 24[5], 859–881 [May, 1940]) assumes that the mineral waters are carried upward by the gases escaping from oil deposits below.
[68] P. 817.

Since this induration works progressively outward from a point above the field, the mineralized solutions are diverted toward the edge of the field. This is in harmony with the halo arrangement of both characteristic minerals (see Fig. 12–15) and pseudohydrocarbons, presumably formed by the reaction between these solutions (chlorides?) and organic materials, and with processes occurring near the surface. Methane, hydrogen, ethane, and the heavier paraffin hydrocarbons are diverted in the same manner by the near-surface "plug" into halo arrangement.

The observations and interpretation of soil and gas analysis surveys may, therefore, be summarized thus: *The maximum concentrations of (significant) hydrocarbons occur above the suboutcrop of fissures or high points of subsurface oil and gas traps except where clogging of the reservoir or near-surface formations has diverted them.* This diversion is generally outward from the high-point, that is, in down-dip direction. Virtually all results published to date can be explained in this manner. Laubmeyer was first to measure gas concentrations (mostly methane) on the proved German fields of Oberg, Nienhagen, and Wietze, whose maxima, as pointed out before, were shifted outward, away from the centers of known production. Laubmeyer also found maxima (in both hydrocarbon and radioactivity curves) above the suboutcrop of faults. Graf likewise obtained a maximum near the suboutcrop of a fault in the Oberg field with a down-dip shift, and maxima with outward shift surrounding the Pierce Junction dome in Texas. Pirson observed maxima in ethane above fault outcrops in the Woodhull gas field in New York. Sokolov observed that the maxima in methane and heavy hydrocarbons were, in some cases, shifted away from the axis of the anticline of the Malgobek field in Russia. Although Antonov's results appear to indicate a definite tendency to halo arrangement, the latter considers the maxima as being directly related to the suboutcrops of the gas formations and faults in this area. He claims to have obtained fairly good agreement between drilling data and calculation, but details on the actual geologic situation are too meager in his article to decide his evidence for or against the halo theory.

In the Ishimbaev field, however, the area of greatest concentration definitely surrounds the productive area in halo fashion, as pointed out by Sokolov.[69] The same is true for the Turkiana and the Kala fields.[70] McDermott reports that in the Big Lake field (Reagan County, Texas) not only the significant heavy hydrocarbons, but also the pseudohydrocarbons and significant minerals show a maximum directly above the field, which is explained by the existence of a fissure zone in the axis of

---

[69] *Loc. cit.*

[70] Located on the Apsheron Peninsula (east of Baku), the scene of extensive electrical and gravity work.

the fold developed by subsequent folding. In all other cases reported by McDermott (La Rosa field, Refugio County, Texas; Cedar Lake field, Gaines County, Texas; Monument field near Hobbs, New Mexico; Riverside area, Nueces County, Texas; Atlanta area, Columbia County, Arkansas; Coles-Levee, Canal, and Ten Section fields in Kern County, California; and the East Texas field, Fig. 12–16), the halo (in significant gases, pseudohydrocarbons, and minerals) is associated with a producing area. Only halos are described by Rosaire for the Ramsey (Payne County, Oklahoma), Griffin (Gibson County, Indiana), Hastings (Brazoria County, Texas), Lopez (south Texas) and Eureka (Harris County, Texas) fields (see Fig. 12–15).
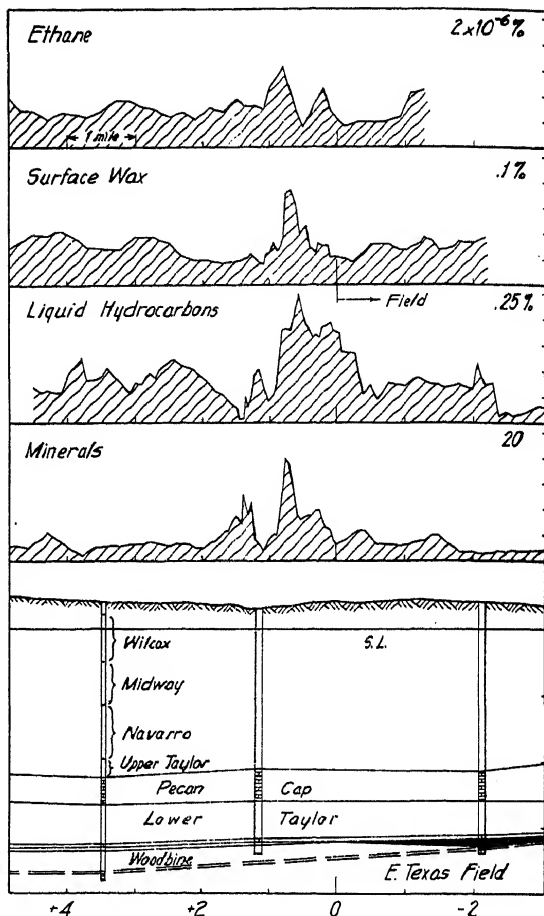
FIG. 12-16. Variation of ethane, surface wax, liquid pseudohydrocarbons, and mineralization near edge of East Texas field (after McDermott).

III. VIBRATION RECORDING, DYNAMIC TESTING, AND STRAIN GAUGING

The following section is concerned with various geophysical methods which find application in structural, transportation, and mining engineering. Collectively, they constitute the major portion of the field of engineering seismology which has as its main objective the reduction (if not elimination) of the damage done to structures by earthquakes and industrial vibrations. Most fruitful in this field has been the recognition that

damage should be considered not in the light of static, but of dynamic, phenomena. Specifically, the damage depends on the frequency response of a structure and therefore on its interaction with the ground, whose response to earthquakes and industrial vibrations, in turn, is likewise a function of its frequency characteristics. Damage is therefore primarily a local phenomenon, depending individually on the design of the structure and the surface geologic conditions. It is the function of vibration-recording and dynamic-testing methods to determine the frequency response of both structure and ground and to devise means by which resonance between the two can be avoided.

In both cases, the significant characteristics of ground and structure are natural frequency and damping. They may be determined by observations of (1) free vibrations, and (2) forced vibrations. In the first case, the ground or building is subjected to a static deflection and is released. From the free vibration that follows, natural frequency and damping may be calculated. Deflections leading to free vibrations may be due to natural causes, such as wind, or they may be produced at will by blasts, mechanical shocks, and so on. To obtain the vibration characteristics of buildings before construction, it is convenient to use models. Methods of measuring free vibrations are briefly referred to here as *vibration recording*.

In *dynamic investigations*, the building or ground under test is set into forced oscillation by vibrators (also called oscillators or agitators) whose frequency is varied during the experiment. Thus the frequency (or dynamic) response of the structure is obtained, from which natural frequency and damping may be calculated. For proposed structures, similar tests are made on models before construction. Dynamic ground tests furnish the frequency response of the foundation and thus, indirectly, its bearing capacity and vibration absorption characteristics. Since the speeds of the sustained waves produced by a vibrator may be determined from measurements in various distances, it is possible to arrive at depths of formation members and their elastic moduli. For complex geologic sections whose geometric dimensions and elastic characteristics have been determined previously by other geophysical methods, it may be convenient to supplement the *in situ* work by model experiments, particularly if the natural setup is likely to be disturbed by later excavations.

Strain gauging, discussed at the end of this section, is concerned with the measurement of displacements in structures and rocks under the influence of natural or artificial loads, static or transient. Structural tests are made on bridges, road beds, dams, and the like, after completion, or on models. Strains in rocks are measured in connection with underground operations in transportation, hydraulic, and mining engineering. Closely related to this application is the observation of rock bursts and fault activity.

A. VIBRATION RECORDING (FREE VIBRATIONS)

1. *Vibrations of buildings and other structures.* Free vibrations occur in buildings and other structures (bridges, water tanks, dams) as a result of wind gusts, earthquakes, traffic vibrations, blasting, and other industrial activity. Observations of free vibrations usually have to depend on the random occurrence of such agencies; only when the structures are small (water tanks, bridge models) may the initial deflections be produced by pullbacks with predetermined load. Vibrations are recorded with vibrographs or seismographs of moderate magnification, equipped with mechanical or optical recorders. It is advantageous to make measurements on various portions of a structure in both horizontal and vertical directions, so that various vibration modes in the planes of symmetry and the variation of amplitude with height may be obtained. When a multiplicity of records has to be secured simultaneously, electrical seismographs with central recording are preferred to mechanical instruments. In this work, moderate magnifications ranging from 200 to 1500 are sufficient; natural instrument periods vary from 1 to 3 seconds; damping should be nearly critical. Observations are arranged to yield natural frequencies and damping (in at least two directions) and variation of vibration amplitude with height.

For buildings whose ratio of height to width is great, flexural vibrations are most important. In the opposite case, where the width is much greater than the height, flexure is unimportant and shear predominates. When the ratio of height to width is between 3 and 4, both kinds of vibrations will be encountered. Torsional vibrations may also occur. In addition to the fundamental, several harmonics are generally observed. If shear predominates,[71] the ratios of the translational and torsional fundamental periods to higher mode periods should be near 3, 5, and 7 (for a building on rigid foundation). When flexure predominates, the translational period ratios should be near 6.2, 17.5, 34.6, and so on. Observations on completed buildings are of value in establishing a reference file for future use, particularly when such measurements have been made on buildings that have been through an earthquake. In this manner, the damage done may be correlated with the frequency response of both building and ground.

Before construction is commenced, the natural frequency of a building may be calculated if it has a simple geometric form. It is more satisfactory, however, to determine the natural frequency on a model by a pullback test (free vibration) or from the response on a shaking table (forced vibration).

2. *Free ground vibrations.* Free ground vibrations are produced by

---

[71] U. S. Coast & Geod. Surv., Spec. Pub. No. 201, 51 (1936).

blasts, traffic, various industrial activities, earthquakes, wind, surf, and the like. They are largely responsible for the phenomenon known as seismic unrest. Since there are, at almost every locality, well-defined geologic formations that are capable of oscillation and impress their frequency characteristics on microseismic and earthquake records,[72] the action of the ground and its constituent parts may be considered like that of a seismograph and may be characterized by a single or by several natural frequencies and damping ratios. Harmonics of such frequencies, where recorded, are in the ratio of $1:3:5$.[73] The frequency characteristics of the ground determine its response to external impulses, this reaction being defined in seismology by the so-called "station factor." The presence of formation members capable of free oscillation accounts for the observation of identical predominant frequencies in the microseismic unrest in earthquake and in explosion records, and these usually agree with the resonance frequencies excited by vibrators. Statistical analyses of earthquake records have been made by various investigators to determine predominant ground frequencies. Examples are the investigations carried out recently by B. Gutenberg[74] as part of a U. S. Coast and Geodetic Survey earthquake research program in California.

As stated before, the damage done by earthquakes and artificial vibrations depends (1) on the dynamic response of a given building or structure to the ground vibrations, and (2), although to a lesser extent, on the reaction of the ground to incoming earthquake waves. The frequencies of distant quakes are usually so low as to be completely out of resonance with the natural ground frequencies. Therefore, such quakes rarely do any damage;[75] besides, their amplitudes would probably be too small even if resonance did occur. Greater damage may be expected from near-quakes and industrial vibrations, since they have greater amplitudes and their frequency is likely closer to the predominant ground frequencies. In some instances it has been possible to correlate prevalent frequency with formation thickness, which is approximately equal to one-quarter of the transverse wave length. Hence, $d \approx v/4f_0$ where v is the velocity of the transverse waves and f_0 is the natural frequency of free-layer oscillation. How earthquake damages to structures may be evaluated approximately when natural frequencies and damping of ground and structure are known, will be discussed below.

Related to the problem of recording free ground vibration is that of

[72] R. Koehler, Nachr. Ges. Wiss. Goettingen, Math. Phys. Klasse 1, (2), 11–42 (1934).
[73] Koehler, Zeit. Geophys., 6(2), 123–126 (1930).
[74] U. S. Coast & Geod. Surv., Spec. Bull. No. 201, 163–224 (1936).
[75] Koehler, Nachr. Ges. Wiss. Goettingen, loc. cit.

rock-burst investigation. Rock bursts are miniature earthquakes of the displacement type and result from the release of rock stresses. These stresses may be due to natural orogenic forces, that is, folding or faulting, or may be caused by the removal of rock material in underground mining operations. At times these rock bursts are of no small intensity; they have been recorded by seismic stations several hundred miles away. Continuous rock-burst records in areas subjected to faulting and mining may not only help in the interpretation of the records of distant earthquake stations, but may be expected to be helpful in predicting fault quakes, cave-ins, and roof failures. This subject is discussed further in the section on strain gauging (page 929). Statistical analyses of rock-burst records appear to indicate a triggering effect of variations in atmospheric pressure.[76] There may also be a parallelism with sun spot cycles and bodily tides. Therefore, the possibility of predicting earthquakes, at least those of the displacement type, is probably not so remote as some seismologists appear to believe.

Most of the measurements of free ground vibrations published to date have been made with regular seismic station equipment. For proposed building sites, dam foundations, and the like, it is necessary to employ recording mechanical or electrical vibrographs. The vibration produced by traffic or industrial plants in the vicinity may be sufficient; otherwise, blasting will be required. However, it is much more satisfactory to use a vibrator and to record a complete response curve. In the interpretation of the field data much help may be obtained from an investigation of models of the surface formation.[77] If the actual geologic conditions have been duplicated with sufficient accuracy on the model (for instance, by securing data on the thicknesses and elastic characteristics of surface formations from refraction surveys), and if the elastic properties of the model material have been scaled down in keeping with dimensional analysis, field data and model results will be in good agreement.

B. Dynamic Testing

In various fields of material testing it has been recognized for some time that dynamic tests give better and more complete data on the properties of materials than do static tests. The limitations of static methods are obvious in the testing of soils *in situ*: with a given load, the area covered is small; the lateral and vertical compression ranges are limited; and the weight sizes that have to be used to obtain sufficient penetration become impracticable even for moderate depth ranges. On the other hand, a

---

[76] C. Mainka, Forsch. & Fortschr., **14(28)**, 314–321 (1938).
[77] C. A. Heiland, A.I.M.E. Tech. Publ. No. 1054, Feb., 1939.

vibrator with revolving eccentric masses permits the forces to be stepped up considerably.   With sensitive detectors, vertical and horizontal ranges extend to several hundred feet and, in some cases, to several thousand feet. Furthermore, the measurement of travel-time and amplitude–distance relations gives an opportunity to test formations not exposed at the surface. Vibrations recorded near a variable frequency vibrator indicate a number of parameters not obtainable by other means, such as natural frequency, damping, energy consumption, ground compaction, and phase shift between impressed force and ground vibrations.

Vibrators may be applied in testing not only the ground but structures as well.   As a matter of fact, vibrators were constructed first for use in structural engineering and for the dynamic investigation of bridges, trusses, framework, conveyors, skyscrapers, shaft houses, cranes, dams, and so on.   Such tests were extended to include all kinds of conveyances such as ships, trucks, automobiles, locomotives, dirigibles, and airplanes.   Investigations of road beds and machine foundations, made in connection with structural tests, led quite naturally to their application in soil testing.[78]

For some of these applications an agitator made of a bicycle wheel with a weight attached to its rim is quite satisfactory.   This wheel is brought up to speed and allowed to run down.   For more accurate work, it is better to apply a vibrator whose frequency is held constant, yet is adjustable in definite intervals.   The usual construction employs two eccentrically loaded wheels or drums that are geared together and revolve in opposition. If the two cylinders are mounted side by side, the vertical components of their centrifugal forces will add and the horizontal components will cancel. By turning the entire assembly 90 degrees (so that the two cylinders are now above each other) the vertical components cancel and the horizontal components remain.   For the agitation of structures, the vibrator is applied in the latter position, since vibration damage to structures results generally from horizontal forces.   In soil testing, the vibrator is laid flat on the ground (so that vertical forces are produced) and is weighed down with ballast.   In some vibrators, four disks are arranged with their axes in the four principal horizontal directions.   The disks are then geared to produce torsional forces.

The total eccentric masses of vibrators range from a few ounces to several pounds and the radius arm from a few inches to about one foot.   Centrifugal forces may thus be varied between several hundred and several thousand pounds.   Some vibrators are so constructed that a given centrifugal force may be produced by a small mass on a large radius arm, or by a larger mass on a smaller arm.   The simplest arrangement is to provide a

---

[78] Koehler, Nachr. Ges. Wiss. Goettingen, *loc. cit.*

number of tubular openings on the circumference of the vibrator drums into which cylindrical masses of various sizes can be fitted. A soil test vibrator must be capable of producing vertical forces up to 40 to 50 cycles (2400 to 3000 r.p.m.). The larger commercial vibrators weigh from a few hundred to 1000 pounds (without ballast) and are equipped with shunt-wound D.C. motors to permit accurate speed control. The smaller vibrators are driven by gasoline engines or motors supplied from storage batteries; the more primitive models are merely brought up to speed manually and are allowed to run down.

Undoubtedly, the greatest flexibility is obtained by a D.C. motor supplied from a gasoline-engine driven D.C. generator, in which case the
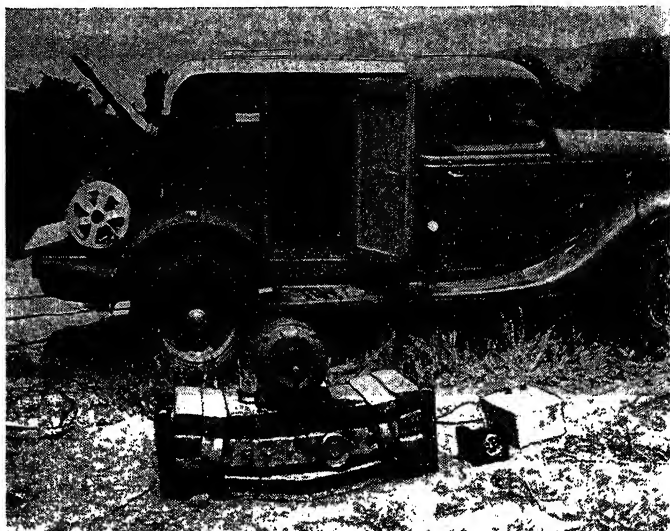
Heiland Research Corp.

Fig. 12-17. Vibrator and recording truck.

speed may be accurately controlled by varying the fields of both the generator and the motor. The frequency is adjusted by a tachometer and evaluated accurately by timing the vibration records. For the measurement of the phase shift between force and displacement it is convenient to provide an electrical impulse transmitter on one of the revolving drums. This will record the vibrator phase, together with the oscillations picked up by one or more vibration detectors. A vibrator with recording truck in the background is shown in Fig. 12-17. For certain applications it may be convenient to insert a wattmeter in the vibrator-motor circuit for the measurement of power consumption. As shown below, the power taken from the vibrator is at a maximum near the resonance point of the ground.

For testing *models* of buildings, bridges, dams, and the like, miniature vibrators or electromagnetic drivers are applied. If size permits, an entire model may be tested on a shaking table.

Vibrations may be recorded with a variety of instruments. For testing larger structures and buildings, mechanical vibrographs are generally quite satisfactory. Their magnifications range from 200 in the simpler types to 1500 in the Wood-Anderson seismograph. For model experiments, miniature microphones of the electromagnetic or piezoelectric variety are required.

In dynamic soil testing, the sensitivity of the mechanical vibrograph is not sufficient, and more delicate seismographs must be used, equipped with mechanical, optical, or electrical magnification, ranging from 10,000 to 50,000 times.[79] The ground vibrations may be recorded in three directions, one being the vertical and the others the two horizontal directions through the station and at right angles to the base line. Although a vibrator may produce only vertical forces, the horizontal components are quite noticeable. Since, however, the maximum response in the horizontal components appears to occur at the same frequency as in the vertical component, vertical seismographs usually suffice. If a multiplicity of seismographs is on hand, it is better to use them at different distances rather than for different components. Vertical seismographs or detectors with electrical transducers are available in any event where seismic refraction work is combined with the dynamic tests. Lastly, it is easier to evaluate the results when vibrations from several stations are recorded on one film (see Fig. 12–19). In order to convert record amplitude to ground amplitude in terms of impressed force, the recording channels must be calibrated. With the larger vibrators, the regular phones used in seismic refraction or reflection equipment work satisfactorily without amplifiers. Where a large number of soil tests have to be made, it may be more convenient to record with (calibrated) amplifiers and to cut down the weight of the vibrator to make it more portable.

When the variation of vibration amplitude with depth is measured, a hole is dug with a hand auger, and a vibration pickup is placed at its bottom at the desired depth or depths. In some cases, steel rods are driven into the bottom of the hole, to which the detectors are fastened.

1. *Dynamic building tests.* To test buildings or structures for earthquake or other vibration damage, a vibrator is set up on, or clamped to, the actual structure or to a model thereof (model structures require a very light vibrator, see above). Usually, the vibrator is so oriented that horizontal forces are produced. The frequency of the vibrator is then varied

[79] R. Koehler and A. Ramspeck, Zeit. Tech. Phys., 14(11), 512–514 (1933).

and the response of the structure (or model) is recorded at one or several points. The records give the variation of amplitude with frequency and (when several detectors are used) the variation of amplitude with vertical elevation and horizontal direction. Buildings and other structures may have different frequencies in different directions. Different harmonics may appear for different modes of vibration (see page 912). In dynamic investigations, harmonics are more readily segregated than in free vibration records and may not even appear when outside the range of the vibrator. Evaluation of the vibration records yields resonance frequency, natural frequency, damping, and magnification for any point. These quantities are usually combined by plotting the response curve, that is, a curve giving relative amplitude (and magnification) as a function of frequency. Earthquake or vibration damage for a given structure is dependent on its response function[80] and therefore on its degree of tuning in respect to prevalent ground frequencies. Hence, the damage is larger if the ratio of building to ground frequency is near 1 and if damping is small. Since, in turn, the response of the ground to earthquake waves increases with the ability of layers to oscillate, earthquake damage is controlled largely by local geologic factors. This is well illustrated by the example of two Japanese earthquakes[81] which, though originating about 1100 km apart, caused maximum damage in virtually the same area.

The vertical component of earthquake or other vibrations is believed to be comparatively ineffective; most structures are damaged primarily by horizontal motion. For the duration of a vibration, a structure is subjected to a strain whose magnitude depends on the vibration amplitude at the particular point, and damage results when the ultimate stress of the building material is exceeded. This has been verified by dynamic building tests in areas where earthquakes of known intensity had occurred and where, therefore, the building amplitude (which follows from the response function of the building for an earthquake of given strength) could be correlated with the observed damage. Calculations[82] showed that the ultimate stress of the material actually had been exceeded where destruction occurred. The importance of resonance between building and ground may be seen from the fact that for a brick house the critical ground amplitude (just causing damage) is 53 microns at resonance and as much as 75 centimeters off resonance.

The *seismic resistance* of a structure may be calculated for sinusoidal ground motion and for simple modes of vibration, provided the response

[80] Ramspeck, Zeit. Geophys., **9**(1/2), 44–59 (1933).
[81] H. Martin, Zeit. Geophys., **12**(7/8), 335 (1936).
[82] Ramspeck, *loc. cit.*

function of the structure has been determined.[83]   Seismic resistance may be defined as the ratio of ultimate stress U to the stress $\mathbf{X}$ corresponding to an amplitude x at a given point.   For example, in a low structure where shear predominates over flexure, the stress is approximately $\mathbf{X} = \mu x_H / H$, where μ is rigidity and x_H is the amplitude at the elevation H.   The building amplitude x is a function of the static magnification $\mathbf{V}$, the ground amplitude a, and the frequency factor f.   In other words, x is dependent on the magnification function of the building.   Therefore, the seismic resistance $\mathbf{R} = U / \mathbf{X}$, where $U = \mu(x_H)_u / H$, with $(x_H)_u$ as the critical building amplitude at the elevation H.   Since $\mathbf{X} = \mu x_H / H$ and $x_H = \mathbf{V} \omega^2 a(f_d)$, where $(f_d) = \dfrac{1}{\sqrt{(\omega_0^2 - \omega^2)^2 + 4\epsilon^2 \omega^2}}$ is a damped frequency factor, the seismic resistance becomes

$$\mathbf{R} = \frac{UH}{\mu \mathbf{V} a \omega^2} \cdot \sqrt{(\omega_0^2 - \omega^2)^2 + 4\epsilon^2 \omega^2}. \tag{12-8}$$

Determination of static magnifications appears to have been made hitherto only on low buildings.   On such structures the static magnifications ranged from 0.8 to 2 and the dynamic magnifications (at resonance) from 2 to 20, the high figures indicating that the buildings were poorly damped.

Dynamic vibration tests are of practical value in industrial plants where large machines are used in connection with a light framework.   Structures of this kind may eventually be shaken to pieces when the machine vibrations resonate with the building and particularly when machine, structure, and ground are in resonance.   It is sometimes possible to avert damage by a slight change in the speed of the machine.   Koehler[84] describes investigations of a coal dressing plant whose vibration amplitude could be reduced 77 per cent by increasing the speed of a screening machine by only 11 per cent.

2. *Dynamic ground tests.*   In a dynamic ground test the site under investigation is set into forced oscillation by a vibrator and the vibrations are recorded either at the source or at one or several points some distance away.   The shakers are fairly heavy, cover a surface of about 10 square feet, and are arranged for reinforcement of the vertical and cancellation of the horizontal components of the centrifugal force.   Vibrations are recorded by the usual electromagnetic vertical component seismographs employed in seismic exploration.   Other possibilities, in respect to vibrators and detectors, are discussed on pp. 915-917.   Higher frequency agitators

[83] Heiland, *loc. cit.*
[84] Zeit. Geophys., 12(4), 148-166 (1936).

do not belong in the category of ground tests and are discussed in connection with geoacoustic methods on page 958.

The reaction of the ground to the vibrator may be described by a simple expression if it is assumed that the vibrator is force-coupled to a semi-infinite medium (with a definite stiffness and velocity damping) whose displacement x is controlled only by Hooke's law.[85] Let m_0 be the mass of the vibrator, plus whatever portion of ground partakes in the motion, $\omega_0 = \sqrt{c_0/m_0}$ the natural frequency of the ground, ω the impressed frequency, c_0 a stiffness coefficient of the ground and ϵ_0 a damping coefficient, and $x = X \sin(\omega t - \varphi)$ the ground displacement having a maximum amplitude X and a phase shift φ in reference to the agitator. Then the centrifugal force referred to unit mass is

$$F = \frac{m' r \omega^2}{m_0}, \qquad (12\text{-}9)$$

where m' is the eccentric mass with a radius r on the vibrator of the mass m_0 . The equation of motion of the ground is therefore given by

$$\ddot{x} + 2\epsilon_0 \dot{x} + \omega_0^2 x = F \sin \omega t. \qquad (12\text{-}10)$$

This leads to a maximum ground amplitude of

$$X = \frac{F}{\sqrt{(\omega_0^2 - \omega^2)^2 + 4\epsilon_0^2 \omega^2}}, \qquad (12\text{-}11a)$$

whose phase shift in reference to the application of the maximum force is given by

$$\tan \varphi = \frac{2\epsilon_0 \omega}{\epsilon_0^2 - \omega^2}. \qquad (12\text{-}11b)$$

The power transferred to the ground is then

$$\mathbf{P} = \frac{m_0 F X \omega}{2} \sin \varphi, \qquad (12\text{-}11c)$$

so that, by substitution of eq. (12-9) in (12-11a) and (12-11b),

$$X = \frac{m' r \omega^2}{m_0 \sqrt{(\omega_0^2 - \omega^2)^2 + 4\epsilon_0^2 \omega^2}} \qquad (12\text{-}11d)$$

and

$$\mathbf{P} = \frac{m' r}{2} \cdot X \omega^3 \sin \varphi. \qquad (12\text{-}11e)$$

---

[85] A. Hertwig, G. Früh, and H. Lorenz, Veröff. Deut. Ges. Boden-Mechanik Heft 1, 44 pp. (Berlin, 1933).

Measurements of the response characteristics of the ground may be made (1) at the vibrator itself (for which purpose a vibration detector may be set up on the vibrator), and (2) at one or more outside points. The observations under (1) are intended to give several quantities, all as functions of frequency: (a) amplitude, (b) phase shift, (c) power, and (d) compaction. Lastly, the variation of natural frequency and damping of the ground with a change in mass (ballast) may be measured. Observations at points removed from the vibrator determine the following quantities: (a) amplitude as a function of frequency, (b) amplitude as a function of distance (and, therefore, the existence of reflections and refractions), (c) phase or travel time as a function of distance, and, finally, (d) phase speed as a function of frequency (dispersion).

The *variation of amplitude with frequency* is measured with a detector mounted on the vibrator, or with one or several detectors some distance away. The frequency response may be taken from a continuous record by getting the shaker up to top speed and allowing it to run down, or by adjusting its frequency in steps of two cycles and taking individual records for each frequency interval. The record amplitude is converted to true ground amplitude by means of the calibration curve of the recording instrument or recording channel and is further reduced to constant impressed force by correcting for the variation of the centrifugal force with frequency. By plotting the reduced amplitude against frequency, a peaked curve (see Fig. 12-20) is obtained. The location of the peak indicates the resonance frequency; the steepness of the slope away from the resonance peak varies inversely with the damping. The damping factor ϵ or the relative damping η, which is equal to the ratio ϵ/ω_0, may be calculated from the frequencies ahead of and past the resonance point at which the amplitude has dropped to one-half of the resonance amplitude. The natural undamped frequency is then computed from the resonance frequency and the damping (see Chapter 9, section IV).

Natural frequency and damping are important characteristics of the surface soil and are closely related to its bearing capacity and compaction. Soils having a natural frequency of from 25 to 32 cycles may be loaded with 2.5 to 5 kilograms per square centimeter.[86] From the natural ground frequency and the mass of the vibrator (plus a certain amount of ground, see below) the equivalent spring constant of the ground can be calculated. Upon repetition of vibrator experiments, it will be found that both resonance frequency and damping are slightly greater the second time, owing to compaction resulting from the ground vibration. The resonance frequency also increases somewhat with the surface of the vibrator, corresponding to a larger spring area, that is, to a stiffer spring. The damping

[86] *Ibid.*

factor is proportional to what is known in soil mechanics as the "friction angle." Soils with large damping (or friction) factors are desirable as foundation materials since they lessen not only the amplitude and the corresponding stress in case of resonance with extraneous vibrations, but also the range of vibratory impulses (due to increased absorption).

A second quantity which may be determined from vibrator measurements at the source is the *phase shift* between impressed force and displacement. At low frequencies this phase shift is nearly zero, increases at resonance to 90°, and gradually approaches 180° at the higher frequencies (see Fig. 12-18). It is possible to calculate damping from the phase-frequency curve (see Fig. 9-99).

The variation of *power* with frequency may be measured with a wattmeter in the circuit of the vibrator motor. The power rises rapidly with frequency (see Fig. 12-18) and shows a peak at resonance, since at maximum amplitude the ground draws the greatest power. The measured value should be corrected for the no-load variation of power with frequency which can be determined by running the vibrator with balanced masses.[87]

The *compaction*, or setting, of the ground is obtainable from readings of a strain gauge inserted between a tripod and the vibrator underneath.[88] The variation of compaction with frequency runs parallel with the phase curve (see Fig. 12-18), the gradient being a maximum at resonance.

FIG. 12-18. Variation of amplitude, phase shift, power, and compaction with frequency for a resonant surface formation (after Späth).

Natural ground frequency and damping show a slight decrease with an increase in the mass of the vibrator. The mass partaking in the oscillation includes a portion of the surface soil and is slightly greater than the vibrator mass. This equivalent mass

[87] *Ibid.*

may, therefore, be determined by running two tests with different amounts of ballast.

Although the more important soil characteristics may be obtained from measurements at the vibrator as described, it is advantageous to supplement these measurements with observations at a number of points a short distance away. The additional information gained thereby is, chiefly, the variation of amplitude with distance and the velocity of the elastic waves transmitted by the vibrator. Since such measurements involve a determination of the variation of amplitude with frequency, it is now the more common procedure to omit measurements at the vibrator and to confine the observations to points generally arranged in a straight line through the vibrator. Several such profiles may be made, radiating from the location of the source.
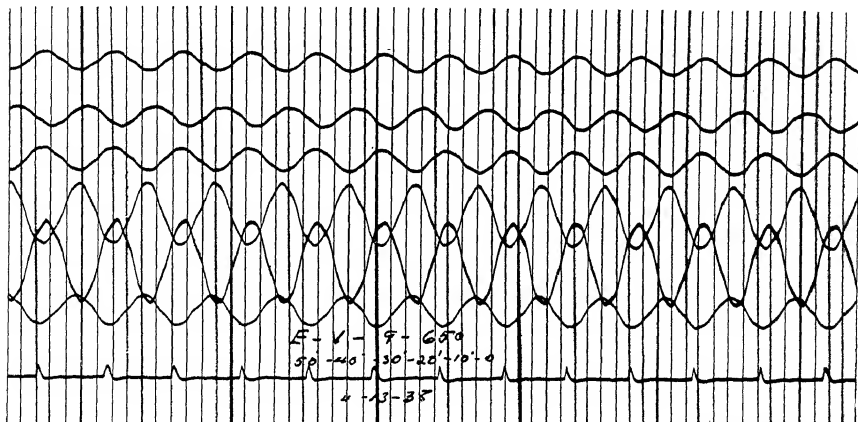
FIG. 12-19. Record of ground response test.

Measuring the *variation of amplitude with frequency* involves the same technique as previously described, with the exception that now as many amplitude-frequency curves are plotted as there are detectors. Fig. 12-19 shows a typical record taken at constant frequency, and Fig. 12-20 is a graph giving the amplitudes as functions of frequency for the distances involved. From such curves the variation of *amplitude with distance* may be plotted, as is seen in Fig. 12-21. In this case the resonance amplitude was chosen for the graph; however, amplitudes at different frequencies may be plotted as well, since the variation of amplitude with distance is dependent on frequency, as shown below.

In a homogeneous medium, the vibration amplitude decreases inversely with distance for space waves, and inversely with the square of the distance for surface waves. Further, there is an exponential decrease due to

absorption (see eqs. [9–35] and [9–37]). In a stratified medium the directly transmitted waves interfere with refracted and reflected waves because of their path and phase difference. The amplitude-distance curve is, therefore, not uniform, as in a homogeneous medium, but shows a series

VERTICAL GROUND RESPONSE

IN

5 DISTANCES FROM VIBRATOR
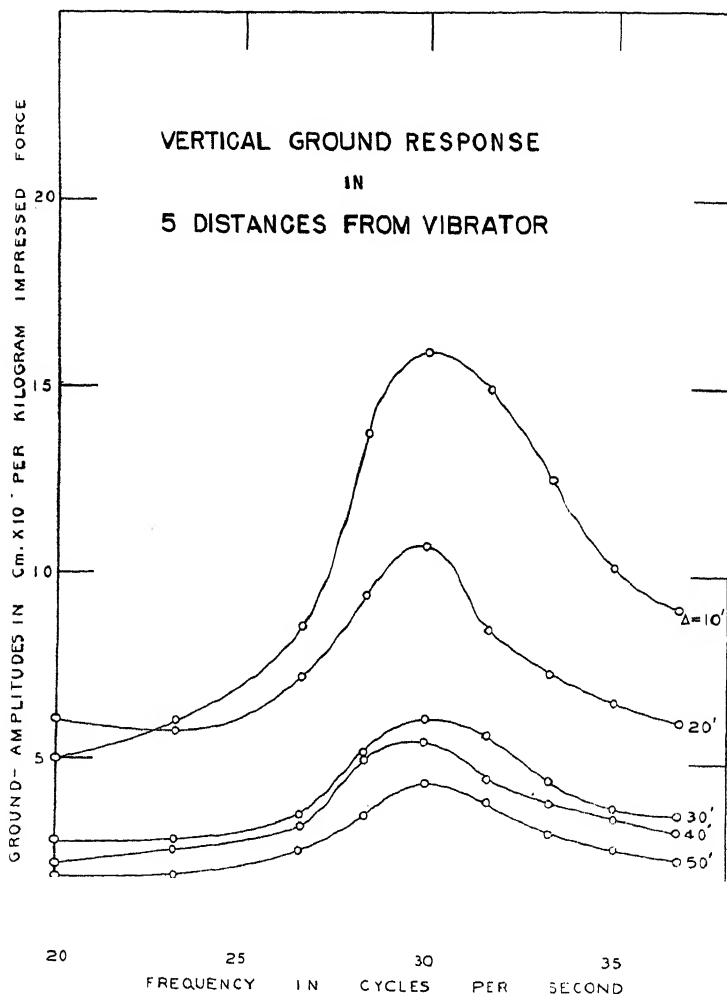
Fig. 12-20. Resonance curves of surface soil at various distances.

of minima and maxima. Conditions for the occurrence of minima and maxima have been discussed by Koehler and Ramspeck.[89] If the surface

[89] Degebo. Veröff., **4**, 1–38 (1936).

distance between the vibrator and a given detector is s, if a surface layer with the wave velocity v_1 is underlain by another layer with the velocity v_2 at the depth d, and if the assumption is made that the waves travel
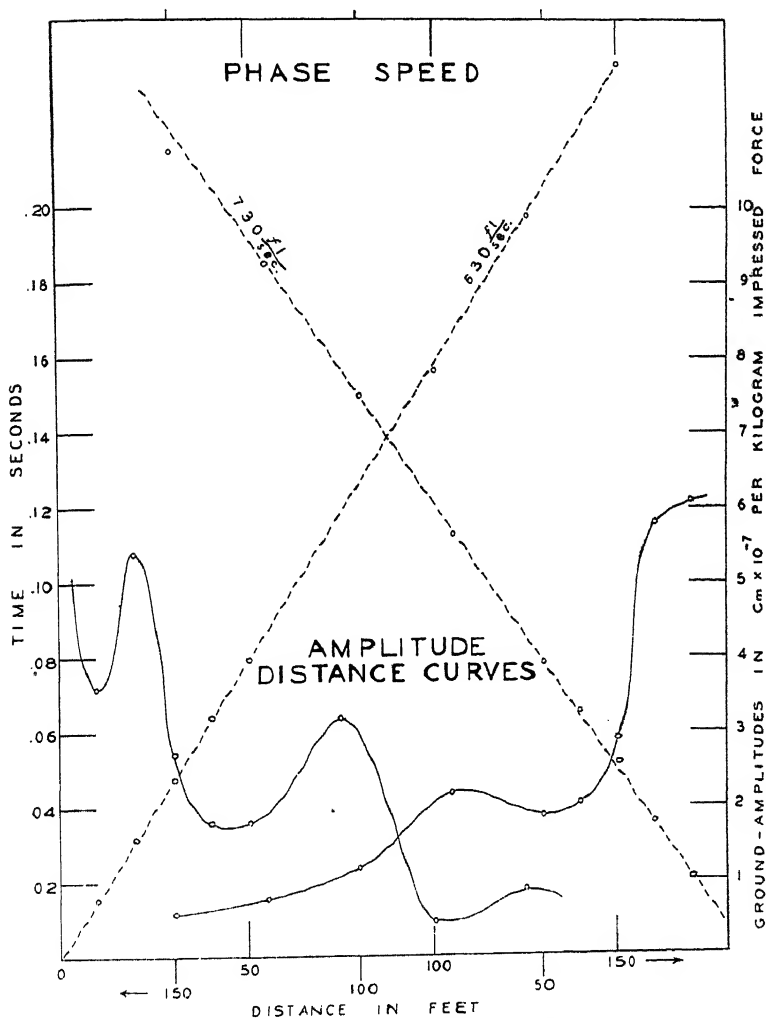
Fig. 12-21. Phase-speed and amplitude-distance curves.

vertically to and from the second layer, the phase difference between the surface wave and underlayer wave is

$$= \frac{2d}{v_1} + s\left(\frac{1}{v_2} - \frac{1}{v_1}\right). \tag{12-12}$$

Therefore, a maximum in amplitude occurs when

$$\pm\omega\left[\frac{2d}{v_1} + s\left(\frac{1}{v_2} - \frac{1}{v_1}\right)\right] = 2i\pi, \qquad (12\text{-}13a)$$

and a minimum occurs when

$$\pm\omega\left[\frac{2d}{v_1} + s\left(\frac{1}{v_2} - \frac{1}{v_1}\right)\right] = (2i \pm 1)\pi, \qquad (12\text{-}13b)$$

where ω is the angular frequency and $i = 0, 1, 2, 3, 4 \cdots$. It is noted that the amplitude has to be considered as a function not only of distance but of frequency as well. Taking, first, the variation of amplitude with frequency at a given distance s, we see that the ratio of two frequencies at which successive minima occur is equal to the ratio of two successive uneven numerals (or $= [2i - 1]/[2i + 1]$), whereas the frequency ratio corresponding to two successive maxima is equal to the ratio of two successive numbers, or $i/(i + 1)$.) On the other hand, if the frequency f is held constant, the distance Δs between two adjacent minima is given by

$$\Delta s = \frac{\pm 1}{f\left(\dfrac{1}{v_1} - \dfrac{1}{v_2}\right)}. \qquad (12\text{-}13c)$$

Similar relations may be written for the interference of the reflected with the directly transmitted waves.

Measurement of vibrations at various distances from the source has the advantage that the *speed of propagation* of the waves may be measured. This is done by observing the time of occurrence of equiphase amplitudes, usually the troughs, and by plotting these times as functions of distance (see Fig. 12-21). The speed of vibrator waves is much less than that of first impulse (longitudinal) waves generated by explosion. The nature of vibrator waves is still a matter of speculation; it is fairly certain, however, that they are transverse waves. Ramspeck[90] assumes that they are Love waves. In any event, it is permissible to state their velocity of propagation by an expression of the form $v_t^2 = \mu/\delta$, where μ is the modulus of rigidity and δ the density. Therefore, when vibrator measurements are made in conjunction with seismic refraction observations, all important elastic properties of the surface layers may be calculated, provided density determinations are available. Thus, the modulus of rigidity μ, Poisson's ratio

[90] A. Ramspeck, and G. A. Schulze, Degebo Veröff., **6**, 1-27 (1938).

σ, and Young's modulus E follow from a combination of the longitudinal and transverse wave speeds:

$$\mu = v_t^2 \cdot \delta \qquad \sigma = \frac{1 - 2\left(\dfrac{v_t}{v_l}\right)^2}{2 - 2\left(\dfrac{v_t}{v_l}\right)^2} \qquad E = 2\mu(1 + \sigma). \qquad (12\text{-}14)$$

In homogeneous or nearly homogeneous ground the phase-speed travel-time curves are straight lines of constant slope, that is, they indicate constant velocities which in turn depend solely on the elastic properties and the densities of the formations. In stratified media there occurs a change of velocity with frequency known as *dispersion*. Where there is an underlayer of higher velocity, the apparent velocity will decrease with frequency, first slowly, and then more rapidly. Generally, therefore, the presence of an underlayer will not be indicated by two true velocities and a break between them, as in the longitudinal wave travel-time curves. Only in such cases where dispersion is not possible, that is, when the frequency is less than the overburden velocity divided by four times the depth to the interface, will there be a break in the travel-time curve. Then, velocities will be recorded that are independent of frequency.

This means that for obtaining travel-time curves with true velocities, one should operate with low frequencies, since in that case no nodal point will develop at the interface and the underlayer will partake in the oscillation. Simple expressions[91] may be written for the apparent velocity, $\bar{v}$, measured at the surface, and for the depth, d, to the interface when there is a considerable contrast between the rigidity moduli and, therefore, the velocities v_1 and v_2 of the two layers. In that case,

$$\bar{v} = \frac{4f v_1 d}{\sqrt{16 f^2 d^2 - v_1^2}} \qquad (12\text{-}15a)$$

and

$$d = \frac{\lambda}{4\sqrt{\dfrac{\bar{v}^2}{v_1^2} - 1}}, \qquad (12\text{-}15b)$$

where λ is the wave length and f is frequency.

Owing to the considerable amount of information on surface and sub-surface formations that can be obtained by comparatively simple means from dynamic soil tests, these tests have found increasing application in various engineering fields. Such applications include: determination of

[91] *Ibid.*

bearing strength, compaction, rigidity and general stability of foundations, seismic resistance of foundations and dams, effectiveness of compaction in earth dams in horizontal and vertical direction, solidity of road beds and road surfaces, determination of the thickness of cement slabs, and the like.

C. STRAIN GAUGING

Strain gauging, in the general sense, involves the measurement of small displacements of mechanical parts under static or transient loading. Secondarily, strain gauging devices are useful for the recording of vibrations and for a comparison of the dimensions of machined parts with those of standards. Strain gauging finds widespread application in the fields of automotive, railroad, pipe-line, highway, and related fields of transportation engineering; in the testing of all kinds of industrial machinery requiring an analysis of performance under transient loads and measurements of ambient pressures; and in automatic dimension control in the machining of matched parts.

Application in the mechanical engineering field includes the measurement of strain (and usually vibrations) in airplanes, airships, locomotives, steamships; the testing of railway and trolley tracks, railway and highway bridges and beds, and transmission towers; the determination of pressure and vibrations in pipe lines; and measurement of impact and vibration stresses in all kinds of industrial machines, such as punch presses, rolling mills, steam and water turbines, internal combustion engines, elevators, mine hoists, and the like.

Although most of these applications of strain gauging are rather remote from our field, geophysical problems arise where mechanical structures are tested in relation to, or in connection with, their foundations. Examples are railway and highway road beds and bridges, irrigation and flood control dams, foundations for industrial machines, and similar structures. Another application of a purely geological nature is the measurement of rock displacements in faults, shear zones, active earthquake areas, mine workings, and railroad and drainage tunnels, and the investigation of rock bursts and the subsidence of the surface of the ground and the roofs of mines.

Methods and instruments for the measurement of strains or displacements cover the entire range from ordinary length and elevation measurements to measurements as precise as one one-millionth of an inch. Ordinary procedures for measuring lengths and the regular methods of leveling are often satisfactory for observing the changes on very active faults, particularly in earthquake areas, for checking the movement of formations along major faults or fissures underground, and for keeping track of

surface subsidence.   Surface subsidence occurs, first, as a natural process in consequence of the leaching of salt beds, domes and other rocks or formations which may be removed by the action of subsurface waters. More frequently ground subsidence is encountered above underground workings, particularly coal mines; sometimes it results from the excavation of subway tunnels in cities; it has been observed in oil fields as a consequence of the removal of oil, gas, salt water, and sand from wells. An example is the Goose Creek field in Texas in which the ground subsidence over the center was as much as 3.25 feet in 8 years.[92]   Subsidence may be due also to the removal of artesian water from large basins and the pumping dry of sands and sandy clays in the process of subway or building excavation.   It may, finally, result from the sanding up and accumulation of sediments in large reservoirs, although the latter is a slow process requiring most delicate means of observation.

Next in accuracy to the simple leveling devices discussed above are mechanical gauges.   They come equipped with more or less intricate lever arrangements and with dials for reading the displacement, or with a pen or stylus for continuous recording.   The latter are useful in the surveillance of active faults, shear zones and fissures, mine roof subsidence, and tunnel movements.   For it is only by the continuous and systematic study of the time variation of such displacements that we can hope to predict roof and wall failure underground and possibly the occurrence of tectonic earthquakes.   An instructive example has been published by Landsberg[93] showing that the rate of roof subsidence changed in a definite manner (approximately in inverse proportion to the distance of the pillar retreat line) until a cave-in occurred.

For attaining the ultimate objective, that is, the ability to predict the time at which a roof or wall is likely to fail or a fault is likely to slip, it would be necessary to study not only the time variation of the relative displacements along mine walls or faults, but to record simultaneously the variation of as many other factors as may be suspected of accumulating tensions and contributing to such failures.   In addition to processes under human control, such as the removal of rock, and shocks produced by blasting, the following phenomena should be observed continually: natural earthquakes, rock bursts, variations in barometric pressure, variations in moisture, and possibly the bodily tides produced by sun and moon (see page 164).   Most of these phenomena may be recorded by a single instrument and may possibly be combined with the displacement record by using a gauge that is sensitive to both displacement and vibration.   It should be added that rock bursts and roof and wall displacements may be mutually

[92] W. T. Thom, A.I.M.E. Tech. Publ. No. 17, 9 pp. (Sept., 1927).
[93] A.I.M.E. Tech. Publ. No. 685, 5 (Feb., 1936).

related. It is possible that abrupt displacements give rise to audible vibrations, and rock bursts of sufficient strength in turn may be responsible for the release of tension elsewhere in the vicinity.

For recording roof subsidence, Landsberg[94] applied a simple recorder consisting of two telescoping steel tubes. The lower of these rested on the mine floor, while the upper was pressed against the roof by a coil spring and connected to the pen of a recorder supported by the base. The displacements resulting from mining by retreating pillars may amount to several centimeters in a day's time.

The sensitivity of mechanical strain gauges may be increased by the addition of an optical lever. Such gauges have been described by Tuckerman.[95] A sensitive optical gauge can be made by combining a Martens lozenge extensometer with an autocollimation telescope (used in magnetometers, see Fig. 8–18a). The fixed pin of this extensometer rests on one part of the member to be tested and the lozenge, to which a mirror is attached, rests on another part a few inches away. Displacements as small as 1/250,000 inch may be detected. Interferometer gauges, while very sensitive, are too intricate for field applications.

Compared with mechanical and optical gauges, electrical devices have the advantage of smaller dimension and possibility of remote indication and recording. These gauges are used chiefly in the testing of conveyances, railway tracks, bridges, pipe lines, dams, and foundations. They are applicable also in the investigation of ground and roof subsidence and of rock bursts as discussed above. Generally speaking, an electric strain gauge is a device by which an electric current is controlled or modulated according to the relative position of two of its parts. The current modulation, in turn, may be accomplished by variations in (1) resistance, (2) capacitance, and (3) inductance.

A simple resistance gauge is made from a potentiometer whose sliding contact is actuated by the magnification lever of a displacement meter (see Fig. 9–13). Another resistance gauge, known as the telemeter,[96] employs a stack of carbon disks held by a metal frame under an initial pressure of about 180 lb. in^{-2}. Variations in resistance of the stack result from small deformations of the metal frame and are recorded by a Duddell-type oscillograph. The telemeter unit may be used in a water-tight cartridge for sealing into the concrete walls of dams or similar structures whose internal stresses are to be checked periodically. Because of its

---

[94] *Ibid.*, with bibliography.

[95] L. B. Tuckerman, Am. Soc. Test. Mat. Proc., **23**(II), 602–610 (1923).

[96] B. McCollum and O. S. Peters, U. S. Bur. Stand. Tech. Paper, **17** (No. 247), 737–777 (Jan., 1924). O. S. Peters and R. S. Johnson, Am. Soc. Test. Mat. Proc., **23**(II), 892–901 (1923). O. S. Peters, Am. Soc. Test. Mat. Proc., **27**(II), 522–533 (1927).

small size, the unit would also be suited for diamond-drill holes issuing from mine drifts, cross cuts, raises, and the like, where it may be left to record variations in roof or wall stresses as mining operations proceed. With a high-speed oscillograph, these elements may also serve to record rock bursts and blasting vibrations. Several elements in suitable geometric arrangement would permit the taking of travel-time records in connection with blasting operations. From such records the velocity of seismic waves and their variation with time may be calculated. This will furnish data on the variation of rock pressure with time (see discussion at end of this section, page 934).

Single-stack carbon gauges have the disadvantage that their current characteristics are not linear. This may be overcome by mounting two stacks in one frame, with a tongue projecting between them from the frame. The tongue is actuated by a thrust rod free to move through the frame, the end of the rod being connected to that part of the member whose displacement is to be measured. The two stacks are arranged in opposite arms of a Wheatstone bridge containing an oscillograph in the center arm. This arrangement has the advantage of greater sensitivity and of balanced setup, since the resistance of one stack increases while the other decreases when the thrust rod moves in a given direction. The double unit is well suited for clamping to structural members of bridges, foundations, pipe lines, rails, and the like.

A unique type of resistance strain gauge has been described by R. Gunn.[96a] It consists of a vacuum tube with the cathode filament between two anodes that are mounted together on a rod passing outward through a flexible diaphragm. A displacement of the rod decreases the plate resistance of the tube on one side and increases it on the other. The plates are connected to a balanced bridge circuit with microammeter. The magnification is of the order of 10,000.

Strain gauges depending on variations in capacitance to indicate displacement are known as ultramicrometers.[97] Various circuits and methods have been proposed for the measurement of minute changes in capacity. These are: (1) the Dowling method, using a grid-tuned or plate-tuned circuit with variable capacity in a Hartley, Colpitt, or similar oscillator;

[96a] Rev. Sci. Instr., 11(6), 204 (June, 1940).
[97] J. J. Dowling, Phil. Mag., 46(27), 81-100 (July, 1923). C. B. Bazzoni, J. Frank. Inst., 202, 35-50 (July, 1926). S. Ekelöf, J. Opt. Soc. Amer., 18(4), 337-341 (April, 1929). J. Obata, J. Opt. Soc. Amer., 16(6), 419-432 (June, 1928). H. Olken, Instruments, 5(2), 33-36 (Feb., 1932); Electronics, 3, 144 (1931). H. Thoma, V.D.I. Zeit., 73, 639 (1929). R. W. Whiddington, Phil. Mag., 40(139), 634-639 (1920). W. W. Loebe and C. Samson, Zeit. Tech. Phys., 9(10), 414-419 (1928). H. Gerdien, Wiss. Veröff. Siemens Konzern, 8, 2 (1929). H. Riegger and R. Boedecker, Wiss. Veröff. Siemens Konzern, 1, 126 (1920). S. Reisch, Zeit. Hochfrequenztech., 38, 101 (1931). G. Gustafson, Ann. Phys., Sec. 5, 22(5), 507-512 (Mar. 21, 1935).

(2) the Gerdien-Thoma resonance circuit; (3) the Whiddington heterodyne method; and (4) capacitance bridges. The simplest of these arrangements is probably the Dowling circuit which contains the variable capacitance in the grid circuit, the corresponding plate current variation being read on a sensitive meter provided with a bucking circuit. Obata used this method in a seismograph accelerometer and a pressure gauge. The disadvantage of this circuit is its nonlinear characteristic, the sensitivity decreasing in inverse proportion to the condenser spacing.

In the resonance method a V.T. oscillator is coupled through a condenser to a measuring circuit that is so tuned as to nearly resonate with the former. The measuring circuit contains the variable capacitance, amplitude variations being read on a thermocouple-millivoltmeter. Several commercial machines for matched production control have been developed along this line. In Whiddington's heterodyne ultramicrometer two oscillators are employed; one contains the variable capacitance (and is therefore variable in frequency), whereas the frequency of the other oscillator is fixed. In Whiddington's setup, the beat frequency is observed directly in a detector circuit by means of a speaker. In a modification by Loebe and Samson, the beat frequency, converted into amplitude variation in a nearly resonant circuit, is then amplified and read on a meter. The capacity-bridge ultramicrometer developed by Reisch has the advantage of a linear relation between reading and displacement. It employs a movable plate between two fixed condenser plates, and stray effects are eliminated by a balanced circuit.

Ultramicrometer capacitance gauges are exceedingly sensitive. It is not difficult to measure changes in length to a millionth of a centimeter. However, there is frequent interference because of stray capacitances, temperature changes, and the like. This probably accounts for the fact that these gauges are used chiefly in plants and laboratories and are not so desirable as the resistance and inductance gauges for use in the field.

An inductance-bridge strain gauge is essentially a Wheatstone bridge with iron core reactors in opposite arms. The iron core coils are provided with armatures, and the gap between them remains fixed in one of the reactors whereas the other changes with the displacement to be measured. In another form of the inductance gauge there is but one armature with two coils on opposite sides, so that a displacement of the armature increases one gap and decreases the other.[98] In still another form of this bridge, two balanced armature coils are in one arm of the bridge while two balancing coils, wound on a transformer core, are in the other arm.

---

[98] A. V. Mershon, Gen. Elec. Rev., **31**(10), 526–531 (Oct., 1928); **35**(3), 139–144 (March, 1932). C. M. Hathaway and E. S. Lee, Mech. Eng., **59**(9), 653–658 (Sept., 1937). M. A. Rusher, Am. Ceram. Soc. Bull., **14**(11), 365–367 (Nov., 1935).

The supply frequency of inductance bridges is usually 60 cycles, but it may be increased to 500 and 2000 cycles for certain applications. In gauges intended for thickness measurements and similar uses in controlled plant production, the indicators are rectifier meters. When time variations of displacements or vibrations are to be recorded, measurements are made with oscilloscopes or oscillographs.

General Electric Company has developed several commercial models for the inspection of outside and inside tolerances of machined parts, spacing of holes, and the like, and for the automatic control of machining operations. (A balanced armature inductance gauge of similar construction is illustrated in Fig. 9–12). Inductance gauges are suitable for the measurement of strains in foundations, bridges, and dams, and for recording stresses, roof subsidence, and wall and fault displacements in underground workings. In application, the fixed and variable air gaps in the reactors are first adjusted to bring the bridge into balance. Then the variable reactor is taken apart, transferred to the member to be tested, and again adjusted for air gap length to obtain bridge balance. The magnification of inductance gauges is of the order of 100,000 and may be combined with trouble-free operation.

Various seismologists have attempted to measure displacements between points at the earth's surface. Milne[99] determined the motion between two piers 3 feet apart by attaching a thrust rod to one of them and recording the motion of the free end of the rod with respect to the other. This arrangement is therefore similar to the convergence recorder previously described (see page 930) operating in a horizontal instead of a vertical direction. Milne's arrangement was modified and increased in sensitivity by various investigators, such as E. Oddone,[100] R. Takahashi,[101] and H. Benioff.[102] Benioff used two piers 60 feet apart, with a thrust rod connected to one of them. The free end of the thrust rod was provided with a balanced armature reluctance transducer. The currents induced by the movement of the piers with respect to each other were proportional to the displacement velocity; hence, the apparatus functioned essentially as a seismograph and not as a strain gauge. However, it could readily be converted into a displacement meter by an adaptation of the inductance bridge previously described.

A number of the strain gauges described above, when reproduced on smaller scale, may be applied in experiments with models of proposed structures, tunnels, or underground workings. It is true that much valu-

[99] Trans. Seis. Soc. Japan, **12**, 63 (1888).
[100] Bull. Soc. Seis. Ital., **11**, 168 (1900).
    Bull. Earthq. Res. Inst., **12**(4), 760–775 (1934).
[102] Bull. Seis. Soc. Amer., **25**(4), 283–309 (Oct., 1935).

able information on strain distribution in structures can be obtained by photoelastic studies.   However, the fact that only relatively thin sections can be used limits the validity of the conclusions to a single plane.   If actual conditions are to be duplicated in three dimensions, it is necessary to resort to reduced scale models and test them with miniature strain gauges placed at suitable points.   Attention must be given to model scale factors, and the elastic properties of the model material must be scaled down in keeping with the requisite dimensional relations.

In concluding this section on strain gauging, it should be pointed out that a strain gauge will indicate merely the variation of stress or strain with time and not the absolute stress that may be present in the member to be tested.   To a certain extent this difficulty may be circumvented by imbedding strain gauges into a structure in the process of construction, or by relieving the stress at suitable points after the installation of the gauges. There is a possibility of obtaining absolute pressures in rocks (*in situ*) by measuring velocities of elastic waves.   As was shown in Chapter 9 (see page 474), the elastic modulus and therefore the elastic wave speed of porous rocks change with pressure.   The variation is not linear; it is fairly large for small pressures but decreases for larger pressures as a limiting value is approached.   It is assumed that the pores are first closed up by the lower pressures, after which the stress begins to work on the mineral grains themselves.   Hence, the variation of elastic modulus with pressure is different for every type of rock and is dependent on porosity, moisture, crystalline structure, and anisotropy.   The variation of elastic wave speed with pressure for various types of rocks has been determined recently by L. Obert.[103]   At reasonably shallow depths, where the pressure is not so great that the flat part of the pressure-velocity curve is approached, stresses in underground workings may therefore be determinable by seismi c velocity observations.

IV. ACOUSTIC METHODS

Acoustic methods are included here in the discussion of geophysical exploration since, by definition, geophysics is concerned with the three acoustic transmission media: the earth, the water, and the atmosphere. Although we are inclined to associate the transmission of sound with the latter only, sound passes with equal and often greater ease through the media of water and solid ground.   Transmission of infra-acoustic frequency earthquake waves of natural or artificial origin is usually referred to as *seismic* wave propagation, whereas sound transmission through air and water, ranging in frequency from single impulses to supersonics, as well

---

[103] U. S. Bur. Mines Rep. of Invest. No. 3444, April, 1939.

as the transmission of audio-frequency vibrations through the ground, is termed "acoustic" transmission. With this in mind, we divide the following discussion into (a) atmospheric-acoustic, (b) marine-acoustic, and (c) geoacoustic methods.

The principal applications of acoustic methods are: (1) communication (*signaling*); (2) location of sound sources (acoustic triangulation, *position-finding*, or *sound-ranging*) by measurements of time and distance; (3) determination of the direction and characteristics of a source (*direction-finding* and *noise-detection*); (4) location of intervening media (*transmission measurements*); (5) determination of distances of sound-reflecting objects (*echosounding*); (6) *noise-prevention*.

A. ATMOSPHERIC-ACOUSTIC METHODS

1. *Velocity and absorption of sound in air.*   Of the three possible sound transmitting media—air, water, and earth (inclusive of solids)—the atmospheric air is, of necessity, the one most widely used and yet probably the least efficient of the three.   Sound propagates in air more slowly than in liquid or solid media.   If the ratio of the specific heats for constant temperature and pressure be designated by k (= 1.405 for dry air), if P is the pressure (1.013 megadynes cm^{-2}) and δ (= 0.29·10^{-3}) the density of air at 0° C., the sound velocity (at that temperature) is given by

$$v_0 = \sqrt{k \frac{P}{\delta}}, \qquad (12\text{-}16)$$

or, with the above numerical values, = 331.8 meters per second. The velocity increases with the absolute temperature, $t_{ab.}$, or $v =$ ∕   ·sec.$^{-1}$, which for centigrade temperatures t above zero is usually written $v_\theta = 331.4_m + 0.66\ t°$.

Other factors which affect the sound velocity in air are humidity, wind direction, and velocity.   Near intensive sources, velocity increases have been observed.   For long ranges the sound does not always propagate along straight paths through the atmosphere.   From the source the sound rays may curve upward because of a decrease in atmospheric temperature with height, up to about 15-20 km.   Temperatures are likely to remain uniform and then to increase again at heights of 30-40 km in the ozone layer where sound velocities may reach values of 350-360 m·sec^{-1}. The vertical increase in velocity results in an advance of the upper portion of the wave front and a bending back of the sound rays to the earth's surface.   For a uniform vertical velocity gradient $\partial v/\partial z$, the ray curvature is given by $-(1/v)·\partial v/\partial z$.   The bending of the sound rays in the high velocity layer gives rise to the well-known "silence zones" in sound-ranging

and explosion observations and is similar in principle to the "reflection" of radio waves from the Kennelly-Heaviside layer. Another cause of ray curvature may be the increase of wind velocity with altitude.

Sound is absorbed in air because of viscosity, heat conduction, and scattering on small particles. The effect of viscosity and heat conduction may be expressed by

$$I_x = I_0 \cdot e^{-2\alpha x},$$

where I is intensity at distance x and α is an amplitude attenuation coefficient, that is, the reciprocal of the distance at which the amplitude has dropped to $1/e$ of its initial value. If internal friction alone is considered, the coefficient

$$\alpha = \frac{8}{3} \frac{\pi^2 \Pi f^2}{v^3 \delta}, \qquad (12\text{--}17)$$

where Π/δ is the static mass-viscosity coefficient, v is the sound velocity, and f is the frequency. The coefficient of absorption due to heat conduction is about one-third of that due to internal friction. The absorption increases in proportion to the square of the frequency; hence, the range of audio signals in air is much less (30 kilometers maximum for the band of 300 to 600 cycles) for audio frequencies than that of explosion sounds (which have been recorded by microphones up to 400 to 500 km at 5 to 10 cycles). However, there are so many possible interferences with sound transmission, due to variations in meteorologic factors (humidity, wind, clouds, fog, and the like) that these ranges are not always reached; sound transmission through air is, therefore, much less reliable than through water. Some of the very large ranges observed for explosions are no doubt caused by the so-called "abnormal" sound propagation, that is, repeated reflections on the (ozone) layer and the earth's surface. For very high (supersonic) frequencies the absorption and scattering on small particles become so strong that their range is very small. The scattering effect is inversely proportional to the volume of the particles concerned and directly proportional to the fourth power of frequency.

2. *Sound transmitters.* The design and construction of sound transmitters and receivers for atmospheric acoustic work depends entirely on the purpose for which the sound transmission is intended. When sound originates without control by the listener (explosions, gun fire, airplane propeller noise) the technical problem is, of course, confined to the construction of suitable receivers. In atmospheric acoustic signaling, position-finding, and echo-sounding, the transmitters vary in construction, but the emphasis is usually on the low-frequency end of the spectrum. The Behm airplane echo sounder and the "Echometer" for measuring the depth of fluid levels in wells employ simple gunpowder cartridges as transmitters.

In radio-acoustic atmospheric position-finding and communication, the transmitting devices are, in increasing order of range, bells, horns, whistles, sirens, diaphragm-whistle combinations, and "group" transmitters of the latter.   For controlled communication, sound telegraphy, and the like, 300–600 c.p.s. appears to be the most suitable frequency band; it is more or less a compromise between a frequency to which the ear is most sensitive, one having a practical range, and one giving directional properties when necessary.   The latter increase with the ratio of diameter and sound wave length $(2\pi/\lambda, \approx 2\pi f)$.[104]   In this frequency range, electromagnetically driven diaphragms combined with quarter-wave whistles or exponential horns seem to be most efficient.

If directional transmission is desired, a group of horn transmitters may be arranged vertically above one another.   For nondirectional transmission, Hecht[105] has designed a double diaphragm transmitter of 500-cycle frequency, about 33 cm in diameter (= half wave length to resonate the air cavity to the diaphragm), with diaphragms in horizontal position, four of these being arranged vertically (at a distance of half the wave length) above one another.   The (acoustic) power is about 2000 watts and the range is of the order of 15 miles.

3. *Sound receivers.*   In a number of applications of atmospheric acoustics, signals are received unaided by the human ear.   This is particularly true for short-range communication.   The sensitivity of the ear is greatest in the frequency range of 1500 to 3000 cycles; the corresponding detectable pressure variation at the ear drum being of the order of $6 \cdot 10^{-4}$ dynes·cm^{-2}. The sensitivity of the ear may be increased by various mechanical and electrical devices, particularly if arrival times of sounds are to be recorded. Mechanically this may be accomplished by increasing the area of reception and by narrowing it down to the ear passage, that is, by the use of horns. More effective is a combination of such horns with diaphragms whose motion can be recorded photographically by transferring it by a bow-string mechanism to a rotating mirror ("Undograph")[106] or electrically by the use of transducers (carbon, crystal, reluctance, or coil microphones).[107]   Of these, the carbon microphone is least suitable.   Crystal and reluctance phones are better adapted to marine use, which leaves the coil microphone as the most advantageous.   It is virtually the only kind that can be used

[104] Considering that the radiation from a diaphragm of radius r is confined to a cone, and designating one-half of the apex angle by α, the (approximate) relation that obtains is $\sin \alpha = 0.6\lambda/r$.

[105] H. Hecht, Handb. Exper. Phys., 17(2), 409 (1934).

[106] This mechanism resembles that applied in the Schweydar mechanical seismograph (p. 609).   See also C. A. Heiland, A.I.M.E. Geophys. Pros., 242 (1932).

[107] Regarding arrangement of transducers, see notes on construction of hydrophones, p. 948.

when quantitative reproductions of sound intensity and phase are required (as in electrical direction-finding compensators).

For detection purposes, receivers are generally arranged in groups either along a horizontal base line, along a vertical line, on the surface of a sphere, or on the circumference of a circle, all depending on the purpose of the detection apparatus. For detecting low-frequency sounds (gun reports, and the like) the hot-wire microphone (or "thermophone") is given preference over the types just mentioned. It consists of a grid of platinum wires of about $6 \cdot 10^{-4}$ cm thickness, heated by an electrical current, and placed in the neck of a Helmholtz resonator or in the passage between two resonators. At these points the amplitude of the air moving to and fro is greatest and produces variations in the temperature and therefore the resistance of the platinum filament. When the microphone is arranged in one of the arms of a Wheatstone bridge with an oscillograph in the detector arm, it is possible to obtain a linear relation between oscillograph amplitude and resistance variation and, therefore, the sound amplitude.

The direction of sound is determined by the binaural effect, that is, the ability to detect (subconsciously) very small differences in arrival time at each ear. If the incoming sound makes the angle α with the connecting (base) line of both ears and if d is their distance, the corresponding phase shift is[108]

$$\Delta\varphi = \frac{2\pi d}{\lambda}\cos\alpha \qquad \text{or} \qquad \Delta t = \frac{d}{\mathbf{v}}\cos\alpha \qquad (12\text{-}18)$$

where λ is wave length and $\mathbf{v}$ is velocity.

In other words, the directional sensitivity of the ear depends on the ratio d/λ (which also controls the directional properties of transmitters) and amounts to about $3°$, or a time difference of 30 microseconds.

It is obvious that the directional accuracy can be increased by a binaural device of larger base, as in airplane detectors. The direction of sound is then determined by rotating the device until the base coincides with the wave front. For airplane detection, two sets of "ears" (microphones in parabolic reflectors or in horns) are required, one pair rotatable about a vertical axis to determine the horizontal azimuth, the other rotated about a horizontal axis to obtain the vertical angle.

If apparatus of this type is impracticable because of size, the phase shift in the sound impulses received by a pair of detectors may be ascertained by insertion of time-delaying arrangements. These may be mechanical (extension tubes) or electrical (compensators). Fig. 12-22 shows a compensator employed in connection with a number of microphones

---

[108] This relation is identical with that relating time and apparent surface velocity to emergence angle in seismology, see p. 541.

arranged on the surface of a sphere.   The microphones are associated with
a network consisting of an equal number of series inductances, L, and
parallel capacities, C.   The latter are connected by two sets of contact
brushes in such a way that the
time differences are balanced.
Then the position of the two sets
of brushes gives the direction of
the sound ray in space.   The
delay for each filter is $\sqrt{LC}$.
The total delay is $n\sqrt{LC}$, if
there are n receivers to the diam-
eter d of the sphere.   The total
delay must equal the time re-
quired for the sound to pass
through this distance, so that[109]

$$\frac{d}{\mathbf{v}} \qquad (12\text{--}19)$$

In automatic compensators the
position of the contact brushes
is · continually adjusted to the
direction of the sound, which
makes it possible to aim search-
lights   and   anti-aircraft   guns
automatically at the target.

4.   *Atmospheric-acoustic com-
munication.*   Sound signaling in
air to warn approaching vehicles
and vessels is applied in every-
day life more extensively than is
probably realized, the automobile
horn, the factory whistle, the
fire bell or siren, the fog horn,
bells and whistles on buoys and
lighthouses and lightships being
familiar examples.   For trans-
mission   of   messages,   special

FIG. 12-22. Electrical direction compen-
sator for acoustic airplane detection (after
Hecht).

audio-frequency transmitters have been constructed (see page 937).

5.   *Atmospheric-acoustic position-finding and sound-ranging.*   By *position-
finding* is meant the procedure of determining one's location by distance

---

[109] H. Hecht, *loc. cit.*

measurement from one or two acoustic *sources* of *known position* which transmit a controlled impulse or, as in radio-acoustic position-finding, a simultaneous radio and acoustic impulse. Conversely, *sound-ranging* is a method of locating a source by acoustic triangulation, that is, by recording its sound impulses on a number of receivers of known position. When a lighthouse or lightship transmits simultaneous light (or radio) and acoustic signals, an approaching vessel may readily determine its distance. Assuming that both impulses travel by the same path and that Δt is the time difference of arrival, v_l the light velocity, v_s the velocity of sound in air, and Δv the difference in the velocities, the distance from the source is

$$s = \frac{\Delta t}{\Delta v} \cdot v_l \cdot v_s \approx t \cdot v_s , \qquad (12\text{--}20)$$

since $\Delta v \approx v_l = 3 \cdot 10^8$ m, whereas $v_s = 3 \cdot 10^2$ m. Therefore, the distance in kilometers is readily obtained by dividing 3 into the time interval (in seconds) between reception of radio and acoustic signal. Measurement of distances from two sources of known position gives the true position of the receiver. In seismic refraction work, use is made of this method to obtain the distances of the seismic receivers from the shot point by recording the shot instant by radio and the sound of the explosion by a blastophone on the same film.

The object of *sound-ranging* is to locate enemy guns by recording the sound of their detonation. Records of arrival time are taken at a number of receiving stations spread out along a base behind one's own lines. To minimize errors due to local variations in sound velocity, the length of the base is made as great as practicable and of the order of 15,000 to 25,000 feet. It is generally about 10,000 feet behind the lines. From six to twelve microphones are arranged at equal intervals along the lines and are connected through amplifiers to a six- or twelve-element oscillograph camera constructed like the seismic cameras used in refraction or reflection recording.[110] To be sensitive only to the low-frequency sounds transmitted by the firing of a gun and to reject other sounds produced by the activities of one's own or enemy troops, the microphones are coupled to Helmholtz resonators tuned to about 12 cycles. The microphones are usually of the hot-wire type, although experiments with moving-coil microphones have also been very successful.

Since the enemy batteries may be 15,000 to 50,000 feet away from the microphones and must be located with an accuracy of about 100 feet, the position of the microphones must be surveyed with an accuracy of 1 to 3 feet. Records must be taken with an accuracy of 1/100 of a second and

---

[110] See p. 556.

the sound velocity must be known to about 1 per cent or better. It is in regard to the latter that the chief difficulties arise, since the effects of wind, temperature, and humidity, their rate of change in vertical direction, and the corresponding curvature of the sound rays are not known. To eliminate this uncertainty as much as possible, another sound-ranging station may be set up between the front and the main base line, with microphones arranged in a circle about a point at which small charges are exploded from time to time and meteorological elements are recorded simultaneously. In this manner, the relation between sound velocity and meteorological data is established empirically.

The location of the sound source is established by measuring the time differences in the arrival of the sound at the various stations 0, 1, 2, 3, and so on.[111] If the sound arrives at station 0 in t_0 (unknown) seconds after its initiation at the source, in t_1 seconds at station 1, in t_2 seconds at station 2, and so on, circles may be drawn about station 1 with the radius $v(t_1 - t_0)$, about station 2 with the radius $v(t_2 - t_0)$, and so on, with v the velocity of sound corrected for wind velocity, temperature, and humidity, or determined experimentally by the auxiliary ranging setup described above. The source is the center of a circle with radius vt_0 passing through 0 and touching the circles about stations 1, 2, 3, and so on. In practice, the source is located by the intersection of hyperbolas drawn about the receiving station as foci.

To eliminate calculations, a series of hyperbolas are plotted previously on a large map with the time differences to be expected, and the source is located by interpolation. The recording apparatus and amplifiers are started by a sentry located between the front lines and the base, when he hears the sound of the gun, or they are set in motion automatically by a microphone in forward location. With some practice it is possible to identify the type of gun from the character of the record; if shell bursts from the same gun have been recorded, its range and thus its caliber can be deduced.

6. *Direction-finding, noise-detection.* Atmospheric-acoustic direction-finding is concerned largely with the detection of enemy scouting or bombing planes when unfavorable weather or light conditions preclude other ways of detection. The sound emitted by a flying plane is composed of the exhaust noise, the ship's vibration, and the propeller noise (the latter being the most predominant), and comprises a wide range of frequencies. Most suitable for detection is probably the band from 300 to 600 cycles, corresponding to a wave length of 1 to $\frac{1}{2}$ meters. Since the

---

[111] The appearance of the record is much similar to that of a seismic refraction record (see Fig. 9-91, first part of record) except that the impulses are of shorter duration. See also plate on p. 16 (article: "Sound") Ency. Brit., 14th ed.

unaided ears have a directional sensitivity of about 3 per cent, corresponding to a time difference of 30 microseconds, it follows that to attain an accuracy of $\frac{1}{2}°$ or better, as required in plane detection, an artificial pair of ears should have a base length of six times that of the ears, or of 1.2 meters.   Airplane detectors have base lengths of this order, consist of two pairs of large "ears," and have the shape of reflectors, horns, or funnels which can be aimed independently by two operators to locate the target by horizontal and vertical angle adjustments.   If such detectors are too bulky, compensators with mechanical or electrical time delay mechanisms are used in conjunction with a cluster of (coil) microphones in circular or spherical arrangement (see Fig. 12–22) and may be arranged to operate anti-aircraft batteries and searchlights mechanically or electrically.

Noise analysis, or determination of type of source by the character of sound emitted, is often associated with direction-finding and sometimes with sound-ranging.   An analogy familiar from everyday life is the physician's method of diagnosing heart and lung diseases by the use of the stethoscope.   Another acoustic diagnostic procedure applied in medicine, the determination of the condition of certain organs by tapping and listening to the sound with the stethoscope, is without analogy in atmospheric-acoustic transmission measurements.

7. *Atmospheric echo-sounding.*   In primitive form, echo-sounding in air has been employed for a long time in the navigation of narrow channels during foggy weather by skippers, who estimate the distance to shore by the length of time required to receive the echo from the ship's whistle. Another application of atmospheric echo-sounding is made in the Behm ground-distance meter.   A pistol is fired on one side of an airplane and the reflection from the ground is received on the other side by a microphone.   The firing of the pistol sets in motion a disk carrying a mirror which projects the image of a light source on a scale.   The light passes through a small lens which is deflected electromagnetically at the instant when the sound is received by the microphone.   The Behm airplane echo-sounder is not usable for distances much in excess of 500 feet and has been superseded by an electromagnetic terrain-clearance indicator using frequency-modulated short-wave radio transmission.[112]

Finally, atmospheric echo-sounding is applied in geophysical research concerned with the constitution of the upper atmosphere (investigation of the so-called "anomalous" sound propagation, see page 936) and in the measurement of depth to fluid level in oil wells.[113]   The sound is generated in the last method by the firing of a cartridge in a chamber attached to

[112] Bell Sys. Tech. J., **18**(1), 222–234 (1939).
[113] J. J. Jakosky, Petrol. Tech., **2**(2), 1–23 (May, 1939).

the casing head of an oil well.   Reflections are recorded from any kind of obstacle in the well, that is, not only from the oil level, but also from tubing catchers, liner tops, and tubing collars.   These echos are picked up by a microphone and are recorded oscillographically on rapidly moving film.   Because of the variation of the sound velocity with the nature and temperature of gas admixtures in the well, the lesser reflections from tube collars of known depth-interval are used as a means of calibrating the time scale when necessary.

8. *Noise prevention.*   Noise prevention or noise reduction becomes increasingly important with the growth in the use of industrial machinery. In respect to vehicle traffic, noise prevention methods extend to the reduction of sounds and noises from horns, engines, exhausts, automobile tires, and tram wheels; in construction work they involve decreasing the noise of riveting, and the like; in mechanical and electrical processing, these methods aim at sound-proofing and vibration-insulation of foundations. One important phase of this work is the reduction of reverberations in offices and auditoriums and the improvement in their acoustics generally speaking; another phase, of military significance, is the design of airplane, submarine, and battleship engines, shafts, and propellers in such a manner that noise and noise transmission is reduced as much as possible.

B. Marine-Acoustic Methods

1. *Velocity and absorption of sound in water.*   Compared with air, water is a much more suitable medium for the transmission of sound.   Its *velocity* is $4\frac{1}{2}$ times as great, its absorption more than thousand times less. Like the velocity of atmospheric sound, the velocity of sounds in a liquid changes with temperature.   In marine transmission, significant variations occur with changes in salinity.   Following are two useful relations expressing the velocity in water as a function of temperature t (in degrees C.) and salinity u in *permille* (at 0° C.):

(1) Metric (Maurer) formula:

$$V_{m.sec^{-1}} = 1445 + 4.46t - 0.0615t^2 + (1.2 - 0.015t)(u - 35)$$

$$(12\text{--}21)$$

(2) English formula:

$$V_{ft..sec^{-1}} = 4626 + 13.8t - 0.12t^2 + 3.73u.$$

Unlike sound in air, sound in water is not much affected by the movement of the transmission medium; in other words, oceanic, tidal, and similar currents are ineffective.   However, as in air, refraction and reflection occur because of vertical variations in salinity and temperature.   The

vertical velocity variation in water is often much the same as that in air but it occurs on a smaller scale. In some experiments described by Swainson,[114] the velocity decreased rapidly for the first 50–100 fathoms, then leveled off, and increased again from about 500 fathoms on down (1 fathom = 6 feet). The temperature decreased from 14° to 9° C. to 100 fathoms and stayed constant at about 4° from 500 fathoms on down. The salinity increased from 33 to 34.2 thousandths as far as about 200 fathoms and stayed constant from that depth on down. These levels change to a certain extent with the seasons. The result of such velocity variations is that the sound rays are first bent away from the horizontal and curve toward it again at greater depth.

Contrary to air, the energy does not return to the surface by refraction but only by reflection at the ocean floor. Long-range transmission does not occur by the direct path but by multiple reflections on both the ocean bottom and water surface. According to Swainson's observations,[115] the direct ray was recorded up to 20 km, once-reflected waves up to 70 km, twice- to five-times-reflected waves up to 85 km (and possibly more). At that distance the travel time was about 1 minute. These ranges hold for bomb explosions and not for continuous waves. When the depth is small compared with distance (as in most marine-acoustic communication problems, except echo-sounding) the time "delay" τ due to the reflection is small compared with the total travel time. According to Swainson,[116] the time difference between the first and fifth reflections at 85 km distance was about 1 second; thus, the delay for each reflection was $\frac{1}{4}$ second. Although the delay is, strictly speaking, dependent on distance (since the travel-time curves are hyperbolas, see page 557) and varies in value from one reflection to another, it is satisfactory to write

$$s = \mathbf{v}(t - \mathbf{n}\tau) \qquad (12\text{-}22)$$

for distance determinations from the travel time, for $\mathbf{n}$ reflections.

The velocity of sound waves in water increases somewhat near the source and decreases slightly with an increase in frequency (in the supersonic range).

The *attenuation* of sound waves in water and air is governed by the same relation (formula [12-17]) as far as viscosity damping is concerned. The coefficient α/f^2 is $1.45 \cdot 10^{-13}$ cm·sec.$^{-1}$ for air, and $8.5 \cdot 10^{-17}$ cm·sec.$^{-1}$ for water. For the latter, the attenuation is therefore about 1700 times less.[117]

[114] O. W. Swainson, "Velocity of Sound Waves in Sea Water," U. S. Coast & Geod. Surv., Spec. Rep., Feb. 28, 1936.

[115] *Ibid.*

[116] *Ibid.*

[117] L. Bergmann, *Ultrasonics*, Wiley (1939).

In water, the losses due to heat conduction are negligible. Contrary to air, water is suitable for both audio- and high-frequency transmission. Theoretically, for 1000 cycles the sound intensity decreases to 0.81 of its initial value at a distance of one kilometer in air, whereas in water approximately the same ratio (0.75) obtains for *ten times* the range (10 km) at *ten times* the frequency (10 kc.). Ultrasonic frequencies are, therefore, a highly suitable means of signaling. A wave of 100-kc. frequency travels in air but 5 m to its I_0/e value while in water the same wave would travel 3.6 km, or more than 700 times the distance.[118] Actually, the ranges are very much less than the theoretical values because of scattering, refraction, and reflection. H. Hecht[119] places the average practical range of subaqueous (audio-frequency) signaling at 20 km with 150 km as the maximum possibility.

2. *Marine sound transmitters.* Sources of sound in marine transmission vary greatly with application. Their construction depends primarily on the directional characteristics desired. As pointed out on page 937, the latter depend on the ratio of transmitter diameter and wave length. Since in water the wave lengths, for the same frequencies, are $4\frac{1}{2}$ times greater than in air, it is seen that correspondingly greater transmitter dimensions are required to obtain the same directional characteristics as in air. Such dimensions are usually impracticable; therefore, transmitters intended for signaling are built for high or ultrasonic frequencies. Where directional characteristics offer no advantage, low frequencies are satisfactory. Hence, the frequency range of subaqueous transmitters covers the entire band from detonations to ultrasonics, depending on purpose. Detonations may be produced by depth bombs (as in radio–acoustic position-finding) or by the firing of cartridges (as in the Behm echo-sounder). For submarine telegraphy, a frequency is selected which is sufficiently removed from the noise produced by the propellers, shafts, engines, and the like.

When transmitters are used in conjunction with direct listening devices, this frequency is usually close to the frequency for which the human ear is most sensitive. Originally, the transmitters in the audio range between 500 and 1000 cycles were simple bells or sirens driven by jets of water. They were later abandoned in favor of electromagnetically driven diaphragm transmitters. On lightships, two or more twin-diaphragm transmitters are employed. They are rotated with respect to one another for uniformity of directional coverage and are mounted one above another with diaphragms vertical. These transmitters are lowered through a shaft in the vessel to a point 10 to 15 feet below its keel. A transmitter of this type (frequency, 525 c.p.s.; power, 800 watts; efficiency, 63 per cent) has

[118] E. Grossmann, Handb. Exp. Phys., **17** (**1**), 498 (1934).
[119] *Loc. cit.*

been described by Hecht.[120]   In echo-sounding, single units may be made to do double duty as transmitter and receiver.   These are then mounted on the keel of the ship with diaphragm in horizontal position.   Where separate units are preferred for transmission and reception, the transmitter is on one side of the ship and the receiver is on the other side and slightly forward from the transmitter.

An electrical transmitter of high efficiency, designed like a dynamic speaker, has been constructed by Fessenden.[121]   There are two fields at each end of the electromagnet; the diaphragm is a steel plate; and the moving coil is a copper cylinder in which eddy currents are induced by two stationary windings in push-pull arrangement.   The range of this transmitter is about 30 miles for telegraphy and one-half mile for speech. Another widely used transmitter of unique construction is the Hahnemann "Tonpilz."   Since, in a subaqueous transmitter, one part of the vibrating system is actuated in air whereas the other vibrates in contact with water, it is advantageous to employ a mechanical step-up transformer because of the considerable difference in radiation impedance between water and air. This is realized by converting the large displacement and low-pressure oscillation of the electromagnetic driver into the small displacement and high-pressure oscillation of the water-bounded diaphragm.   Mechanically, the transformation is effected by coupling a heavy diaphragm to a driver of small mass by means of a solid elastic rod.

Ultrasonic transmitters are less useful in position-finding and sound-ranging but are well suited for communication and echo-sounding because of their directional characteristics.   Three types are in predominant use: electromagnetic, piezoelectric, and magnetostrictive.   The electromagnetic transmitters follow in design the Fessenden or Hahnemann type previously discussed and cover the lower ultrasonic range (10,000 to 20,000 cycles).   A transmitter consisting of six elements about 15 cm in diameter, mounted one above another on a vertical tube which can be withdrawn by a hydraulic lift into the ship's hull, is described by Hecht.[122]   An echo-sounding transceiver operating electromagnetically at a frequency of 17,500 cycles is illustrated in Fig. 12-23.   The piezoelectric (crystal type) transmitters are generally used at between 30 and 40 kc., which gives ample range (10 to 20 km) and sufficient directional discrimination (about 25° to 30°, see footnote on page 937) for signaling between shore stations and ships and between ships in motion, and also for echo-sounding.   Since a large radiation area would not be obtainable with thin quartz plates,

---

[120] *Ibid.*, p. 413.
[121] Illustration in G. W. Stewart and R. B. Lindsay, *Acoustics*, p. 249, Van Nostrand (1930).
[122] *Op cit.*, p. 413.

mosaics of such plates between two steel plates are used.   In the Langevin-Florisson transmitter,[123] the quartz plates are 2 mm and the steel plates each 3 mm thick.   The diameter is 25 cm, the frequency 38 kc.   Virtually the same transmitter has been built in England and Germany for the purpose of echo-sounding (37.5 kc., driven by peak voltages of 6000 volts, transmitting damped impulses of about 1/1000 second duration).

Magnetostrictive transmitters make use of the Joule effect, that is, changes in length of a rod when it is magnetized longitudinally.   The drivers are solenoids (see Fig. 12-24) or iron yokes, surrounded by coils and used with a biasing field.   The armatures are nickel rods, coupled to aluminum diaphragms.   Driving power is supplied by V.T. oscillators in regenerative arrangement or by high-tension generators discharging through a condenser into the field coils surrounding the rods.   The latter scheme is used in the (20 to 30 kc.) echo-sounding transmitters built by Atlas-Werke and by the Electroacoustic Company[124] and in the Hughes echo-sounder (Fig. 12-24).

3. *Submarine sound receivers (hydrophones).* Subaqueous sound receivers fall into two groups: (1) stethoscopic listening devices, and (2) electrical microphones.   In the former, the application of the stethoscopic principle (amplification by reducing the section of a receiving chamber to that of an ear tube) is necessitated by the energy loss occasioned by the tremendous contrast in the acoustic resistivities of water and air.   Were the sound to pass directly from water to air, only 0.12 per cent of the incident amount would be transmitted.   A stethoscope with a 15:1 ratio of base to tube diameters raises this to 2.4 per cent,[125] that is, it effects a twentyfold improvement.   To obtain unit yield, a 60:1 ratio in the base to tube diameters would have to be realized.   This means that with the normal ear-tube size, hydrophones of impracticably large diameters would have to be built.

The difficulty may be overcome by interposing another medium between air and water.   Unit transmission may be accomplished if the acoustic resistivity of this medium is the geometric mean of the acoustic resistivities of air and water and if its thickness is one-quarter of the wave length of the sound in it.   This has led to the adoption of listening devices with rubber shells fashioned in the form of a Broca tube, that is, a spherical receiver attached to an ear tube.   On small vessels such receivers have been used on both sides of the ship, and the direction of sound has been determined by aiming the ship for equal sound intensity or phase, making use of the binaural effect.   For larger vessels, mechanical or electrical

[123] Illustrated in Bergmann, *op. cit.*, p. 196.

[124] Illustrated in Bergmann, *op. cit.*, p. 198.

[125] Stewart and Lindsay, *loc. cit.*

compensators take the place of the rotatable receiver system. In stethoscopic devices, mechanical compensation may be accomplished by varying the length of the ear tubes in trombone fashion, or by inserting a rotatable capsule which has variable air passages inside[126] and allows the direction of sound to be read directly. Greater accuracy in direction-finding is possible by the use of multiple receivers. As many as twelve to eighteen have been used on each side of the ship.

Stethoscopic listening devices have been largely superseded by electrical receivers. The latter consist in the main of diaphragms provided with carbon-microphone, electromagnetic, piezoelectric, or magnetostrictive transducers. Carbon microphones have been applied mainly in inertia-coupled form as described below. Electromagnetic hydrophones are of the inductive (moving coil) or reluctance (variable air gap) variety. Representatives of the former are the Fessenden oscillator (see page 946) and the Electroacoustic Co. detector.[127] In this, the diaphragm carries a piston, moving in a closely fitted ring, with oil in the gap to achieve damping. Reluctance receivers are constructed very much like the reluctance seismographs described in Chapter 9.[128] One example is the Hahnemann Tonpilz transmitter (when used as a receiver), another the ordinary headphone receiver, and a third is the balanced armature (Baldwin or Westinghouse) speaker when suitably coupled to the diaphragm as discussed below. The piezoelectric and magnetostrictive receivers are usually identical in construction with the transmitters previously described.

Hydrophones may be readily constructed with available microphone or speaker units. Three arrangements are possible: (1) mounting the microphone to the orifice of a stethoscopic air chamber behind the diaphragm;[129] (2) combining the diaphragm with the moving coil of a dynamic speaker or of a coil microphone, or with the armature of a reluctance phone, the magnet unit being rigidly fastened to the case; (3) suspending the reproducer in inertia or Tonpilz fashion from the diaphragm. The first arrangement lends itself best to hot-wire, condenser, electromagnetic, and other available microphones or diaphragm reproducers, but it is the least efficient of the three. The second method is best suited for velocity (inductive and reluctance) transducers and for quantitative reproduction, particularly in connection with compensators. The third is probably the most effective and is used with reproducers of light weight, such as crystal and carbon button microphones.

---

[126] Illustrated in Stewart and Lindsay, *op. cit.*, p. 276.
[127] Illustrated in Hecht, *op. cit.*, p. 429.
[128] See p. 611.
[129] Such a use of Baldwin balanced armature reproducers is described by H. G. Dorsey, U. S. Coast and Geod. Surv., Field Eng. Bull. No. 12, 212 (Dec., 1938).

Electrical receivers may be combined with electrical compensators for directional reception. The design of the delay network is the same as in the atmospheric sound compensators previously discussed (see page 939). However, determination of vertical angles is rarely required; and, therefore, the hydrophones and the delay elements in the compensators are arranged as nearly in a circle as the ship's outline will permit. A compensator for submarine detection, corresponding in construction to that illustrated in Fig. 12-22, is described by Hecht.[130]

4. *Marine-acoustic communication.* The frequencies used for marine communication depend greatly on purpose, location of the receiver, relative stability of the positions of the communicating parties, as well as range, directional selectivity, and secrecy desired. Since receivers are usually located on ships in motion, interfering noise frequencies due to engines, propellers, and the like, must be suppressed. This requirement sets the lower frequency limit at about 500 cycles. For direct reception, the upper limit is determined by the sensitivity of the ear. As a practical compromise, a frequency of 1050 cycles has been adopted in most merchant marines for some time. In the navy, where directional transmission is desirable, communication frequencies are higher and extend into the ultrasonic range. Speech transmission, direct or by modulating a high-frequency carrier, has been successful for short distances only (one-half to one mile). Audio-frequency transmitters and receivers are generally of the electromagnetic type. Ultrasonic receivers are arranged in groups and are mounted on tubes which may be lowered from the ship's keel and rotated about a vertical axis. The purpose is to confine the beam to the direction of communicating shore stations, surface ships, or submarines. Because of its directional properties, acoustic communication is often superior to radio. When used between ships of the same fleet in combat, it is less vulnerable than radio.

5. *Marine-acoustic position-finding and sound-ranging.* In its simplest form, marine-acoustic position-finding consists of a determination of the bearing of two sources of sound of known position, such as buoys, light vessels, and shore stations equipped with identifiable transmitters. Strictly speaking, this method comes under the heading of direction-finding; hence, this discussion will be confined to the more quantitative methods of position-finding and sound-ranging by measurement of travel times.

The distance of a ship from a source transmitting both an air and water signal at the same time, such as light vessels and buoys, may be determined by application of formula (12-20). If v_l is the velocity of sound in

[130] *Op. cit.*, p. 428-429.

water and v_s that in air, the formula gives a factor of 0.42 with which the time difference in seconds is multiplied to obtain the distance in kilometers. Capable of greater range is distance determination by the use of radio and sound signals transmitted simultaneously from shore stations and light vessels. In that case (by application of formula [12–20]) the distance in kilometers is approximately equal to one and one-half times the observed time difference in seconds. By receiving signals from two radio and underwater sound transmitters of known position, the ship's position may be found without difficulty. Conversely, a ship firing a depth charge and transmitting a radio signal at the same time to two shore stations equipped with hydrophones may be given its position by radio. This is of considerable help to navigation in fog; a ship forty miles away from the transmitters may thus locate itself within about 2000 feet.

A similar procedure is applied in the "RAR" (radio-acoustic-ranging) system of the U. S. Coast and Geodetic Survey to determine the position of echo-sounding vessels. From the latter, a depth bomb is fired electrically at the desired location, and the sound wave is picked up by two Sono-radio-buoys anchored at known positions. The buoys are equipped with short-wave transmitters which radio the instant of reception back to the surveying vessel where the radio signals are recorded on a chronograph. For this purpose, a hydrophone is suspended half way down the anchor line of the buoy. The phone is connected to a tuned three-stage transformer-coupled amplifier which, through a gas tube, trips the grid of a 4 megacycle (2 to 5 watt) transmitter.[131] This arrangement removes the carrier between signals and makes for a longer life of the transmitter batteries. The maximum hydrophone range to trip the transmitter is 80 to 100 km; the range of the radio transmitter in terms of signal required to work the recording chronometer is about twice as great. The accuracy of the RAR system depends, naturally, on how well the velocity of the sound in sea water is known; and this in turn changes with refractions, reflections, and variations in temperature and salinity (see page 944). For a given area, velocities can be determined by RAR observations with known vessel positions obtained from geodetic triangulation or astronomic measurements.

Marine sound-ranging methods are used for the location of mine explosions and depth charges, and for determining the range of a ship's shell fire. The hydrophones are placed along a base line about twelve miles long and are connected to a shore recorder similar to the type used in atmospheric sound-ranging. If the secrecy of the installation is of no

[131] A. M. Vincent, U. S. Coast and Geod. Surv., Field Eng. Bull. No. 11, 73, (Dec., 1937). A slightly different circuit is described by H. G. Dorsey, *op. cit.*, p. 99.

consequence, the hydrophones are suspended from radio-equipped buoys which communicate the impulses to a shore recording station or recording vessel.

Explosions of mines and torpedoes or shell hits may be located by submarine sound-ranging equipment up to distances of 100 km.

6. *Direction-finding and noise-detection.* Marine noise-detection and direction-finding are applied (1) in navigation, to determine a ship's position by taking bearings of one or two sound sources of known position (submarine transmitters on buoys, lighthouses, shore stations); (2) in the detection of enemy craft from surface ships and submarines, and in detecting the approach of friendly ships to avert collisions with emerging submarines; (3) in the surveillance of straits and harbors during periods of poor visibility. With the exception of the last application, the detecting devices are mounted on board ship and therefore an immediate difficulty arises from the high noise level caused by the ship's engines, propellers, rush of water, and activities on board ship. This interference may be partially reduced by sound insulation and electric or mechanical filtering; however, the only really effective means of separating the noises to be detected from these accidental noises is by directional hearing.

Among the noises produced by other ships, most important is probably that caused by the propeller as the result of the collapse of air bubbles. This noise is so characteristic that a practiced listener may determine the number of propellers and blades, the type of engine, and therefore the type of ship to which he is listening. Other noises are produced by the ship's engines, by pumps, and by generators, and are transmitted through the hull to the water unless special precautions are taken. The frequency range of a ship's noises is considerable; for practical purposes, the band from 500 to 2000 is most suitable.

In the early days of marine direction-finding, two receivers of the Broca type were used with a rotatable base of comparatively small length. Later this was replaced by two or more receivers on both sides of the ship, connected to a mechanical time-delay compensator of the trombone type previously described. This system has recently been superseded by electrical coil microphones with electrical compensators, as described on page 939.

7. *Echo-sounding.* Echo-sounding is undoubtedly the most widely used marine-acoustic method. Its advantages in speed and accuracy over the mechanical wire-sounding method are obvious. The method is more than a mere means of measuring depth. Because of the speed and completeness with which the topography of the ocean floor may be mapped, it is an aid in navigation since in many cases the ship's position may be determined accurately from a bottom contour map. Echo-sounding has been applied

in the location of shipwrecks and submarines on the bottom, the determination of the character of the ocean floor, and the detection of fish shoals. Echo-sounding was tried at an early date on icebergs; Fessenden found at the time that (on account of the irregular surface of the berg under water) the ice echoes were much more feeble than the sea-bottom echoes. This may possibly be overcome by the use of high-frequency sounds and horizontally directed beams. In this manner ranges of at least several hundred yards may be obtained. It has been reported[132] that greater ranges (up to three miles) are obtainable by listening to the bursts which apparently develop in the iceberg from its cracking under water.

Marine echo-sounding methods involve the principle of distance determination by measuring (1) the direction of the return ray, and (2) the time interval that elapses between the initiation of a sound impulse and the arrival of the echo. The first system requires that the depth be comparable with the length of the triangulation base, that is, the length of the ship. Therefore, this method is applicable only at shallow depths, to about 100 fathoms. As originally applied, this method utilized the propeller noise as sound. A group of submarine detectors was mounted forward on the ship and connected to a compensator, whereby the direction of the incoming sound could be determined. If φ is the angle which the sound, reflected from the sea bottom, makes with the horizontal, and if $2a$ is the distance of the detector group from the propellers, the depth to bottom is given by $d = a \tan \varphi$. This method is not particularly fast nor is it very accurate.

In all other echo-sounding procedures, the time interval that elapses between the initiation of a sound impulse and the arrival of the echo is measured. The reflection of a sound impulse generated by striking a bell may be perceived by the human ear. However, the intensity of such an impulse would not be sufficient to actuate an automatic indicating device, nor would this timing method be accurate enough. Large intensities may be generated by crowding the available energy into a short space of time, for example, by the detonation of an explosive, or by a condenser discharge into an electromagnetic or magnetostriction oscillator. A wide frequency range has been utilized. High frequencies, although subject to great absorption, offer definite advantages in regard to directional selectivity. In shallow water they are the only ones applicable. Since, for a depth accuracy of five feet, a time interval of 2 milliseconds must be measured, the length of the initial impulse cannot be more than 1/10 of this interval. Inasmuch as, for moderately damped transmitters, the impulse dies out after about 10 oscillations,[133] frequencies ranging from 10 to 50 kc. are

[132] H. T. Barnes, Nature, **124**, 337 (Aug. 31, 1929).
[133] H. Hecht and F. A. Fischer, Handb. Exp. Phys., 17(2), 433-439 (1934).

required for shallow echo-sounding. Ultrasonic receivers and transmitters of the electromagnetic, piezoelectric, or magnetostrictive type, previously discussed (see pages 946 and 948), are mounted on opposite sides of the ship, usually in water-filled tanks on the inside of the hull. In many installations, only one device is used for both transmitting and receiving.

In regard to construction and operation, three different kinds of echo-sounders may be distinguished: (1) phase shifters, (2) dial indicators, and (3) automatic recorders. An example in the first group is the British Admiralty depth finder, in which the transmitter is a 2000 cycle diaphragm that is struck a hard blow with an electromagnetic hammer to start the sound impulse. The electrical impulses are transmitted to the oscillator three times a second from a contactor switch rotating at uniform speed. This commutator carries two segments which are connected to the receiving phones and which put a short circuit on the phones except for a brief instant. The brushes making contact with the transmission segments are fixed, whereas the receiving brushes may be revolved with respect to the former. The operator adjusts the angle between the two sets of brushes until he can hear the echo distinctly, the angular rotation then being a measure for the echo time and therefore for the depth. In one of the sonic depth finders developed by the U. S. Navy, the above principle is reversed and the time interval between successive impulses is changed until transmitted and received impulses are heard simultaneously. This will be the case if the transmission interval is an integral multiple of the echo time. The transmission interval is controlled by varying the distance of a friction wheel from the center of a driver disk rotated at constant speed. Further details on this method will be found in Stewart and Lindsay.[134]

In the second group of echo-sounding devices, depth readings are taken on rotating dials or pointers that are started by the sound impulse and stopped by the echo. The earliest of these is the "microtimer" invented by Behm.[135] It is essentially an electrically operated stop watch and consists of a disk with a steel projection which is held in the starting position by an electromagnet. When an underwater cartridge is fired, a nearby microphone picks up the sound impulse and by a relay disconnects the starter electromagnet from the circuit. The disk is then set in motion by a leaf spring which engages a projection on the outside of the disk. A second microphone, when struck by the echo, disconnects a second or brake electromagnet, thus releasing its armature which is fastened to a brake

---

[134] *Op. cit.*, p. 283-286.

[135] Literature will be found in: B. Schulz, Ann. Hydro., **52**, 254-271, 289-300 (1924). H. Maurer, Ann. Hydro., **52**, 75 (1924), **54**, 336-340, 391 (1926), **56**, 347-352 (1928); Zeit. Ges. Erdk. Berlin, **62**, 371-377 (1927), **63**, 248-249 (1928); Erg. H., III, 130-218 (1928). Hecht and Fisher, *loc. cit.*

shoe. At that instant the disk is stopped, its graduation giving the depth directly. The accuracy of this device is claimed to be 1/10,000 of a second.

In the "echometer" designed by Hecht, a steel disk connected to a pointer is situated between two electromagnets. One of these is stationary and the other is revolved continuously by a synchronous motor. Before the sound impulse is sent, both electromagnets are energized and the steel disk is held by the stationary electromagnet in such a manner that the pointer is on the zero point of the dial. The sending of the impulse disconnects the stationary electromagnet so that the moving electromagnet is free to take the disk along with it. When the echo arrives, the rotating magnet is disconnected and the stationary magnet is energized so that the disk and the pointer stop at an angular position corresponding to the echo time and, therefore, the depth. The pointer is held in this position for a few seconds, permitting a reading to be taken. It is then returned automatically to its starting position.

Another dial-indicating instrument is the "fathometer" developed by the Submarine Signal Corporation. A modification for shallow depths by Dorsey[136] is illustrated in Fig. 12–23. In this instrument the pointer is represented by a slot in a disk attached to the rotor of a synchronous motor driven by a 1025-cycle tuning fork. In front of the revolving disk is a frosted glass dial and behind it is a circular neon tube which lights up instantaneously when the echo strikes the receiver, thus illuminating the depth reading on the stationary dial. The sound impulse is dispatched by the action of a photoelectric cell which receives a flash of light from a mirror attached to the rotor when the latter passes through its zero position.

Recently, the recording type of echo-sounding device has come into increased use. It is a simple matter to record oscillographically the reflected impulse, together with what motion may be produced by the direct wave which travels from the source to the receiver through or around the hull of the ship. Records of this kind resemble those taken in reflection seismic exploration.[137] However, such oscillograph records are required only in connection with experimentation and research. Because of the relative strength of the reflected impulse, its well-defined character, and the absence of interference from other refractions or reflections, a complete record can be dispensed with. The echo-depth recorders now used work automatically and record continuously both impulse transmission and echo depth; in other words, they trace the water surface and the bottom contour.

An automatic recorder developed by the British Admiralty[138] is illus-

[136] H. G. Dorsey, J. Wash. Acad. Sci., **25**(11), 469–476 (Nov., 1935).
[137] See records in B. Gutenberg, Lehrb. Geophys., **3**, 585 (1926).
[138] J. S. Slee, J. Inst. El. Eng. (London) **70**, 269–280 (1932).

trated in Fig. 12–24. Both transmitter and receiver are high-frequency
(16,000 cycles) magnetostriction units and are mounted on opposite sides
of the ship in water-filled tanks. The sound impulse is initiated by dis-
charging a high tension generator through a condenser into the windings
of a submarine oscillator, the transmission key being actuated by the
recorder itself when it reaches the zero position. The recording unit is
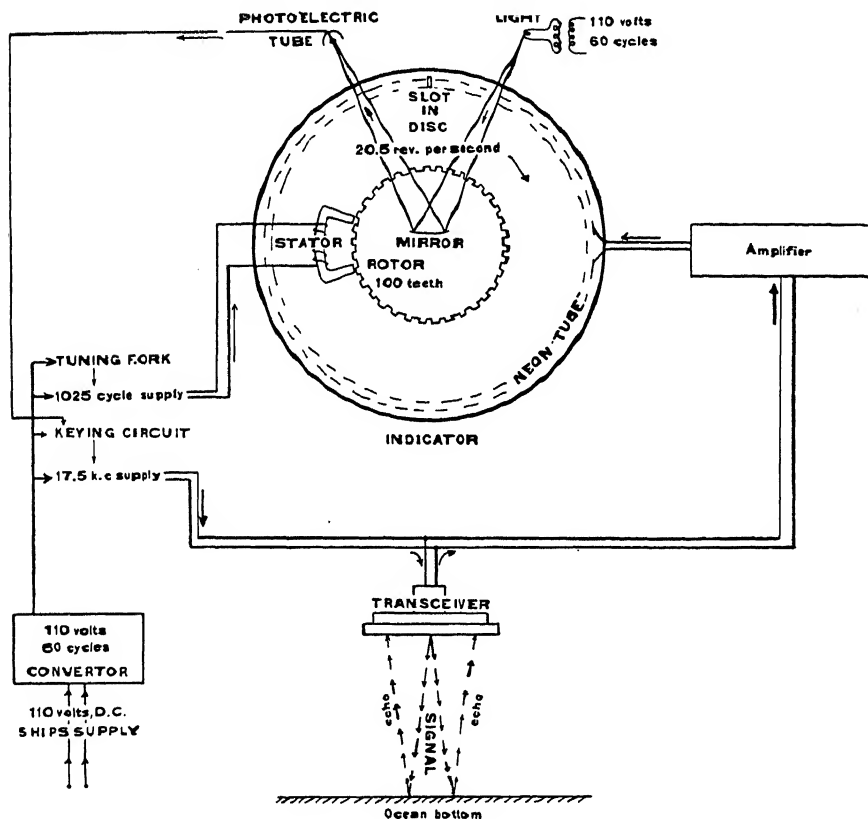
FIG. 12-23. Schematic circuit of Dorsey fathometer.

essentially a spiral drive which moves a stylus back and forth across re-
cording paper impregnated with starch iodide. An imprint is produced by
liberating iodine when current passes through the stylus and the paper to
a metal roller beneath the paper. When the stylus is at the edge of the
paper, the transmission key is closed and current passes through the stylus,
thus marking the instant when the signal is dispatched. On arrival of the
echo, current is again passed, thus producing a continuous record of the
ocean bottom. With these high-frequency recorders it is possible to dif-
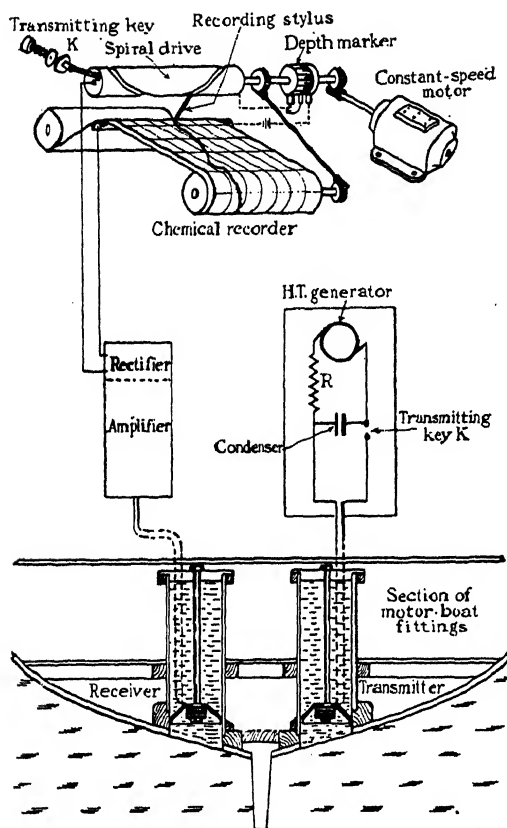
FIG. 12-24.   Automatic magnetostriction echo depth-recorder (after Slee).

ferentiate between the surface of the silt and the solid rock on the bottom of the ocean, and to pick up fish shoals, determining their depth and their concentration in relation to the topography of the ocean floor (Fig. 12-25). The ability of high-frequency echo-sounders to furnish this information in addition to ocean bottom contour has made them invaluable in commercial fishing.[139]

C. GEOACOUSTIC METHODS

Geoacoustic procedures are essentially short-wave (or high-frequency) seismic methods. They are distinguished from seismic methods[140] in that they involve audio-frequency communication and direction finding and not direct measurement of travel times. At present, geoacoustic methods are applied in mine safety, mine rescue, mine surveying, location of water pipes and water leaks, and location of enemy sappers in trench warfare.

1. *Velocity and absorption of sound waves in the ground.*   Since travel times are not measured in geoacoustic methods, few direct data on the ground velocities of audio-frequency sounds are available.   However, there is no reason to assume that they differ from the velocities of seismic waves of lower frequencies, as discussed in Chapter 9, pages 468-472.

Of the three sound-transmitting media—air, water, and earth—the latter, particularly consolidated rock, shows the highest velocities.   Com-

[139] O. Sund, Nature, **135**(3423), 953 (June, 1935).

[140] In respect to transmission frequency, dynamic soil-testing (discussed in section III of this chapter) occupies an intermediate place between seismic and geotic methods.

pared with water and air, the ground is a rather poor sound-transmission medium. Attenuation of audio-frequency elastic waves in the ground is much greater than the attenuation of seismic waves. Many factors are responsible, such as refraction, reflection, scattering, absorption, and damping. To begin with, more energy is lost in audio-frequency than in seismic-frequency transmission because of scattering, since the wave length of audio-frequency sounds is comparable with the dimensions of the interfering objects. In seismic exploration, the wave length of reflected waves of an average speed of 10,000 feet per second is 200 feet at a
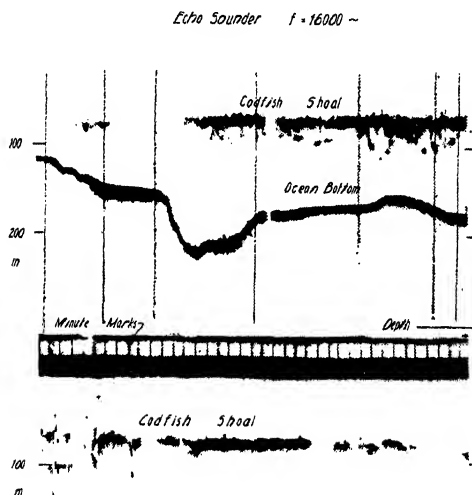
FIG. 12-25. Fish-shoal detection by sonic depth finder.

frequency of 50 cycles, and the wave length of ground-roll waves of a velocity of 1000 feet per second is 100 feet at a frequency of 10 cycles. On the other hand, the length of geoacoustic waves of a velocity of 6000 feet per second is only 3 feet at a frequency of 2000 cycles. Since the intensity of sound scattered by an obstacle is proportional to the volume of the obstacle and inversely proportional to the fourth power of the wave length, it follows that high-frequency sounds may readily be scattered several hundred thousand times more than low-frequency seismic waves, other conditions being equal. This accounts for the limited range of high-frequency sound waves in the ground. The relative range of seismic and

acoustic waves in the ground is therefore comparable with the ranges of audio-frequency and supersonic waves in air.

Another cause of attenuation is loss of amplitude due to internal friction. In a viscous medium, the distance traveled by an elastic wave until its amplitude is diminished to $1/e$ of the initial amplitude is the reciprocal of the absorption coefficient, or $3v\delta\lambda^2/8\pi^2\Pi$, where Π is the static viscosity coefficient, v the velocity, δ the density, and λ the wave length. The range is thus inversely proportional to the square of the frequency. With increasing distance, the higher frequencies drop out and the lower-frequency components of the initial impulse remain. The range increases further in direct proportion to the radiation impedance (product of velocity and density). Hence, the waves travel farther in firm and consolidated than in loose and unconsolidated rocks (see page 478). Leighton[141] has given the following values for distances at which the pounding of a sledge hammer could be detected with a 1000-cycle geophone through various formations: 3000 feet through hard rock, 2000 feet through coal, 400 feet through clay, and 550 feet through the mine cover. For vertical propagation down to 400 feet, Howell, Kean, and Thompson obtained half-value distances of 900-cycle waves ranging from 78 to 640 feet.[142] It follows from the above that geoacoustic methods are well suited for the location of highly absorptive formations underground, such as clay seams, faults, and shear zones.

2. *Geoacoustic sound transmitters.* More than twenty years ago Fessenden suggested the use of submarine transmitters in wells as a source of elastic waves for the exploration of mineral deposits.[143] Such transmitters were not wholly successful because of the limitations of the high frequencies just discussed. Comparing 400-cycle propagation with explosion-generated waves in a profile across the Hawkinsville salt dome, L. G. Howell, *et al*,[144] found shorter travel times for the explosion waves, which would indicate that the latter penetrated the cap rock whereas the audio-frequency waves tended to travel near the surface. It is probable, therefore, that for exploration purposes the lower frequencies, such as those used in dynamic soil-testing vibrators, have better possibilities.

In mine rescue work and trench warfare there is, naturally, no choice in regard to the frequency characteristics of the sound source. As a matter of fact, the higher frequency components have to be utilized if the drilling or digging tools and associated activities are to be identified. The

[141] A. Leighton, U. S. Bur. Mines Tech. Paper No. 277 (1922).

[142] L. G. Howell, C. H. Kean, and R. R. Thompson, Geophysics, **5**(1), 1–14 (Jan., 1940).

[143] U. S. Patent 1,240,328.

[144] *Loc. cit.*

same applies in the location of water leaks, whose characteristic sounds are caused by the impact of the escaping water on the surrounding formations. In underground communication and mine rescue operations it has been found that the most effective way of transmitting sounds is to strike a hard rock surface with a sledge hammer.

3. *Geoacoustic receivers.* The unaided ear would be a rather ineffective means of detecting earth sounds. A marked improvement may be attained by the simple means of using a canteen almost full of water, and by placing the ear as closely as possible to its orifice. The principle involved here is that the contrast in radiation impedance between ground and air is stepped down by the insertion of water (see page 947). Another way of detecting sounds transmitted through the earth is to resonate a mechanical detector or seismograph to the predominant ground frequency and to connect this detector with the ear by a stethoscopic amplification device. A detector of this kind is known as a *geophone* and is illustrated in Fig. 12–26.
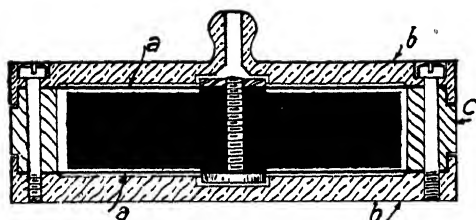
Fig. 12–26.   Geoacoustic detector (geophone) (after Leighton).   (a) Diaphragm, (b) cap plate, (c) iron ring; lead weight in solid black.

In it a lead mass weighing about one pound is suspended between two nickel diaphragms about $\frac{25}{1000}$ inch thick. The space above the upper diaphragm is about 3 inches in diameter and connects to an orifice of about $\frac{1}{4}$ inch in diameter. From the orifice the sound passes into the rubber hose of a stethoscope whose end fits snugly into the ear. Geophones are generally used in pairs for directional hearing. To obviate phase differences, the rubber hoses must be of equal length.

The reduction of diameter of the geophone in its orifice results in an increase of amplitude. Since the transmission of sound from a large to a small tube is equivalent to the transmission from a dense to a rare medium, eqs. 9–34 (see page 478) apply. Substituting, for the radiation impedance, the products of velocity and density, considering the velocities equal on both sides, and setting the densities proportional to the cross-sectional areas, the transmitted amplitude is $2S_1/(S_2 + S_1)$ times greater than the amplitude of the diaphragm. For a standard geophone in which the ratio of the cross-sectional areas of diaphragm and orifice is of the order of 120,

the amplitude of the air in the rubber hose is therefore about twice the amplitude of the diaphragm.

Thus, the gain resulting from a reduction of the cross-sectional area is rather small. It may be increased by the use of electro-mechanical transducers coupled to the geophone mass. Ackley and Ralph[145] have reported that the minimum audible distance could be doubled by using a standard geophone with an unbalanced reluctance transducer and a three-stage triode amplifier. Undoubtedly this sensitivity can be further increased by crystal transducers and higher gain amplifiers. Carbon microphones and hot-wire microphones have been proposed for this application but are probably not so good as crystal microphones.

4. *Geoacoustic communication.* Geoacoustic methods are used as a means of communication of rescue parties with entombed miners and with other parties located at the surface or in near-by mine openings. Signals are transmitted by striking the wall at short intervals with a sledge hammer or other available tool. Transmission is better in the direction of the strike of formations than at right angles thereto, and it may be cut off occasionally by faults or shear zones. Communication is possible in this manner through distances of 2000 to 3000 feet in rock and through about 500 feet of overburden. Speech may be picked up through distances of several hundred feet, although the standard geophone, being undamped, is not particularly suited to a faithful reproduction of speech. It is probable that an adaptation of the crystal microphone would be better adapted to direct speech transmission.

5. *Geoacoustic position-finding and sound-ranging.* From the discussion of these topics in connection with marine-acoustic methods, it will be recalled that position-finding is defined as the determination of one's position by timing the sound from one or two sources of known location, and that sound-ranging involves the location of a source by acoustic triangulation. Both of these procedures involve the measurement of travel times and have therefore no direct parallel in geoacoustic work with present equipment. A related seismic application is the determination of crookedness of drill holes by measuring the travel time from surface shot points to a phone located in the hole (see page 863). Geoacoustic triangulation is possible only by an application of direction-finding methods discussed in the next paragraph.

6. *Direction-finding, noise-detection.* These methods are applied in mine rescue, mine safety, and mine surveying work for locating entombed miners, detecting and locating underground fires, determining the approach of tunnels and drifts and bringing together raises and stopes (thereby pre-

---

[145] W. T. Ackley and C. M. Ralph, U. S. Bur. Mines Rep. Invest., Ser. No. 2639, Sept., 1924.

venting accidents in blasting through), and locating and measuring the drift of boreholes sunk from the surface with the intention of reaching a definite point of the subsurface workings. Military application includes the detection and location of enemy galleries in trench warfare and the surveillance of underground sapping activities for escaping enemy blasts and directing counterblasts.

In the latter application, the object of acoustic observations is to detect, identify, and locate mining operations by the noise of mining tools such as hammers, picks, drills, shovels, and other machinery. Sounds transmitted by mining tools are characteristic and permit definite identification, despite the distortion occurring in the intervening media and an undamped tuned receiver. Underground fires are identified by a typical hissing sound produced by air drafts, by cracking of timber, and by the fall of rock from the mine roof.

Civil engineering application of geoacoustic methods includes the location of pipes and pipe leaks. Water, gas, and oil pipes can often be found by the typical noise of the gas or liquid passing through them, that is, by the vibration set up in the pipe, although the use of an electromagnetic detector (see page 819) is preferable if the pipe itself is to be located. Leaks in water pipes can be found by the noise of the water impinging on sand, gravel, or rock in the cavity surrounding the leak, and by the vibration produced in the pipe by the water issuing from the leak.

Geoacoustic direction-finding makes use of the binaural effect discussed on page 938. Two geophones are shifted in position until a line connecting them is at right angles to the direction of the sound. The phones may also be used in fixed position, when they are provided with a compensator to determine direction by adjusting the phase difference. In application of the first method, the two phones are first set out with their base approximately at right angles to the direction of sound. One phone is left stationary and the other is moved toward the sound source so that the sound appears to come from the right. Then this phone is moved back in the opposite direction from the base line until the sound appears to come from the left. In this manner an intermediate position can be established in which the sound comes from neither the left nor the right.[146] A source is then located by making direction determinations at a number of points and by finding the intersection of the rays. Pipe leaks are usually not located by direction-finding but by following the course of the pipe and by observing changes in sound intensity. The location of a leak is indicated by the point of maximum intensity. This point may be considerably removed from the surface evidence of the leak, since the liquid issuing from

[146] Leighton, *loc. cit.*

it may travel along the pipe or follow subsurface cavities of an unpredictable course. Noise measurements for the detection of leaks should be made in the early morning hours when traffic is at a minimum.

Another method of leak detection developed by the Western Instrument Company requires contact between the pipe and a probe carrying a crystal pickup at its end. The pickup is oriented in two directions, one parallel with, and the other at right angles to, the pipe. Intensity of vibration is measured in both directions and also as a function of frequency if necessary. It is claimed that the ratio of longitudinal to transverse vibration intensity shows significant variations when a leak is approached.

Geoacoustic direction-finding is not so reliable nor is it applicable at such great distances as marine-acoustic methods. Transmission is limited, not only in range but in direction as well, by rapid changes in the elastic wave speeds, particularly near the earth's surface. When underground workings are situated in a district of complex geology, it may be quite difficult to establish consistent directions from geoacoustic observations.

7. *Transmission measurements.* Occasionally, valuable information may be obtained in underground mining operations from the location of faults, fissures, shear zones, clay seams, and the like. This may be done by producing sounds at a given location and observing the intensity of reception at a number of points so arranged in adjacent drifts, tunnels, or shafts that the presence and approximate disposition of sound-absorbing media may be determined. With electrical geophones, direct measurements of intensity may be made by the use of a calibrated amplifier with output meter.[147] Indirect measurements of intensity may be made by swinging a hammer through a predetermined arc in a mechanism especially made for this purpose. By gradually reducing the arc, the minimum transmission intensity necessary to produce an audible signal is obtained. As a rule, however, quantitative intensity measurements are not made, and the presence or absence of sound-absorbing media is ascertained by merely noting at which points the sound reception is poor or entirely absent.[148]

8. *Geoacoustic-reflection methods.* Reflection of sound waves in the ground is determined (1) by noting the direction of the return ray, and (2) by measuring the time interval between the initiation of a sound impulse and the arrival of the echo.

Distance of reflecting surfaces has been measured underground by adjusting the position of two geophones in a vertical plane for equal reception. This is not possible at the earth's surface, and it is necessary to use a compensator to establish the direction of the return ray. Attempts have

---

[147] A suitable instrument (sound-level meter) is manufactured by the General Radio Company, Cambridge, Massachusetts.

[148] Leighton, *loc. cit.*

been made to locate ground-water levels and bedrock surfaces in this
manner, but they have not been wholly successful. This is because the
sound rays may be diverted in a quite unpredictable manner by the in-
tervention of different formations. This is particularly true of the near-
surface weathered layer which deflects the return ray into an almost verti-
cal direction, thus virtually obliterating any significant variations in the
direction of the reflected ray. A measurement of reflection travel time
would undoubtedly obviate the difficulties mentioned, since it is then pos-
sible to correct for the low-velocity surface layer.

Unquestionably one of the reasons for the lack of progress in geoacoustic-
reflection methods is the superiority of explosion-generated impulses as
used in seismic reflection procedure over audio-frequency impulses. As
far as principle is concerned, there is, of course, very little difference be-
tween acoustic echo-sounding and seismic-reflection methods. The dif-
ference is primarily one of frequency. As a matter of fact, the use of
low-frequency sustained oscillations (as applied in dynamic soil testing)
has been proposed for the location of shallow formations, since the seismic-
reflection method, at present, cannot be used successfully for that purpose.
In practice, this limitation is not too serious, inasmuch as shallow forma-
tions may be readily mapped by the seismic-refraction method.

SUBJECT INDEX

---

[1] Geographical names will be found in the Name and Place Index.

NAME AND PLACE INDEX